Advances in Photosynthesis and Respiration
Volume 25

Chlorophylls and Bacteriochlorophylls

Biochemistry, Biophysics, Functions and Applications

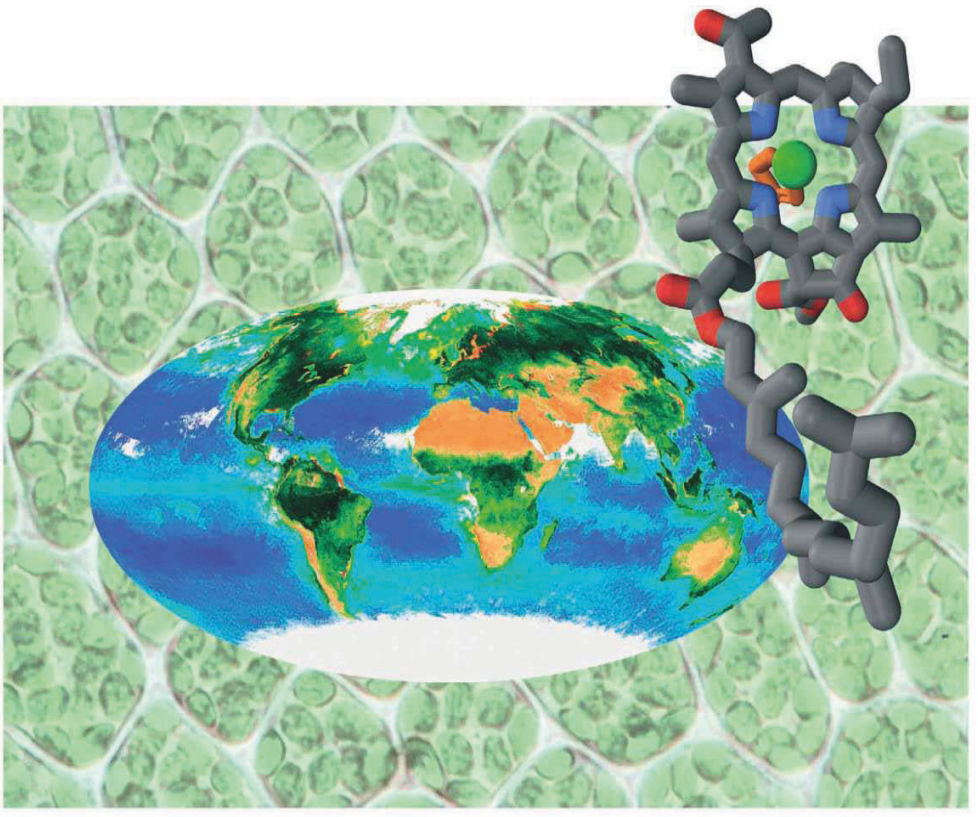

Edited by
Bernhard Grimm, Robert J. Porra,
Wolfhart Rüdiger and Hugo Scheer

Springer

Chlorophylls and Bacteriochlorophylls

Advances in Photosynthesis and Respiration

VOLUME 25

The scope of our series, beginning with volume 11, reflects the concept that photosynthesis and respiration are intertwined with respect to both the protein complexes involved and to the entire bioenergetic machinery of all life. *Advances in Photosynthesis and Respiration* is a book series that provides a comprehensive and state-of-the-art account of research in photosynthesis and respiration. Photosynthesis is the process by which higher plants, algae, and certain species of bacteria transform and store solar energy in the form of energy-rich organic molecules. These compounds are in turn used as the energy source for all growth and reproduction in these and almost all other organisms. As such, virtually all life on the planet ultimately depends on photosynthetic energy conversion. Respiration, which occurs in mitochondrial and bacterial membranes, utilizes energy present in organic molecules to fuel a wide range of metabolic reactions critical for cell growth and development. In addition, many photosynthetic organisms engage in energetically wasteful photorespiration that begins in the chloroplast with an oxygenation reaction catalyzed by the same enzyme responsible for capturing carbon dioxide in photosynthesis. This series of books spans topics from physics to agronomy and medicine, from femtosecond processes to season long production, from the photophysics of reaction centers, through the electrochemistry of intermediate electron transfer, to the physiology of whole orgamisms, and from X-ray crystallography of proteins to the morphology or organelles and intact organisms. The goal of the series is to offer beginning researchers, advanced undergraduate students, graduate students, and even research specialists, a comprehensive, up-to-date picture of the remarkable advances across the full scope of research on photosynthesis, respiration and related processes.

The titles published in the Series are listed at on p. v/vi, those forthcoming volumes on p. 8. A complete list is also provided at the end of book following p. 603.

Chlorophylls and Bacteriochlorophylls

Biochemistry, Biophysics, Functions and Applications

Edited by

Bernhard Grimm
Humboldt University, Berlin, Germany

Robert J. Porra
CSIRO Plant Industry, Canberra, Australia

Wolfhart Rüdiger
Ludwig-Maximilians-Universität München Germany

and

Hugo Scheer
Ludwig-Maximilians-Universität München Germany

Springer

A C.I.P. Catalogue record for this book is available from the Library of Congress.

ISBN-10 1-4020-4515-8 (HB)
ISBN-13 978-1-4020-4515-8 (HB)
ISBN-10 1-4020-4516-6 (e-book)
ISBN-13 978-1-4020-4516-5 (e-book)

Published by Springer,
P.O. Box 17, 3300 AA Dordrecht, The Netherlands.

www.springer.com

Cover illustration: Molecular structure that is characteristic of chlorophylls, with the central Mg (green), to which an extra ligand (orange) is bound from the *α*- or back side, together with an image of the Earth from outer space showing the chlorophyll distribution on the continents and in the oceans. The background shows maize tissue with the chloroplasts in green, where photosynthesis takes place. The structure is bacteriochlorophyll BChl3 from the reaction center of *Rhodobacter sphaeroides* (H. Komiya, T.O. Yeates, A.J. Chirino, D.C. Rees, J.P. Allen, G. Feher, Proc. Natl. Acad. Sci. USA 85, 7993, 1988, pdb entry 4RCR, structure prepared with DS ViewerPro V. 4.0, Accelrys). We thank Compton Tucker and Norman Kuring from NASA, USA, for granting the use of the SeaWiFS image of the Earth (July 1999, Hammer projection), and Gerhard Wanner (University of München, Germany) for granting the use of the maize micrograph. The color-coding for the SeaWIFS image can be found in the supplementary material at http://epub.ub.uni-muenchen.de/archive/00000776/

The camera ready text was prepared by Lawrence A. Orr, Center for the Study of Early Events in Photosynthesis, Arizona State University, Tempe, Arizona 85287-1604, U.S.A.

Printed on acid-free paper

From the Series Editor

Advances in Photosynthesis and Respiration

Volume 25: Chlorophylls and Bacteriochlorophylls: Biochemistry, Biophysics, Functions and Applications

I am delighted to announce the publication, in the *Advances in Photosynthesis and Respiration* (AIPH) Series, of ***Chlorophylls and Bacteriochlorophylls: Biochemistry, Biophysics, Functions and Applications,*** a book covering the key pigments that play many crucial roles at the heart of both oxygenic and anoxygenic photosynthesis. This volume was edited by four distinguished authorities: Bernhard Grimm (Berlin, Germany), Robert (Bob) Porra, (Canberra, Australia), Wolfhart Rüdiger (Munich, Germany) and Hugo Scheer (Munich, Germany). Several earlier AIPH volumes did include, by necessity, functions of chlorophylls and the bacteriochlorophylls acting as antenna and as key reaction center components, but none of the volumes focused on all the aspects of the properties and of the roles played by these key pigments not only in the natural process of photosynthesis but also in such applications as photodynamic treatment of cancerous tumors and the detection and measurement of chlorophyll-bearing phytoplankton from satellites in outer space. This book integrates all the knowledge on these pigments essential for life on earth. The current volume follows the 24 volumes listed below.

Published Volumes

- *Volume 1*: ***Molecular Biology of Cyanobacteria*** (28 Chapters; 881 pages; 1994; edited by Donald A. Bryant, from USA);
- *Volume 2:* ***Anoxygenic Photosynthetic Bacteria*** (62 Chapters; 1331 pages; 1995; edited by Robert E. Blankenship, Michael T. Madigan and Carl E. Bauer, from USA);
- *Volume 3:* ***Biophysical Techniques in Photosynthesis*** (24 Chapters; 411 pages; 1996; edited by the late Jan Amesz and the late Arnold J. Hoff, from The Netherlands);
- *Volume 4:* ***Oxygenic Photosynthesis: The Light Reactions*** (34 Chapters; 682 pages; 1996; edited by Donald R. Ort and Charles F. Yocum, from USA);
- *Volume 5:* ***Photosynthesis and the Environment*** (20 Chapters; 491 pages; 1996; edited by Neil R. Baker, from UK);
- *Volume 6:* ***Lipids in Photosynthesis: Structure, Function and Genetics*** (15 Chapters; 321 pages; 1998; edited by Paul-André Siegenthaler and Norio Murata, from Switzerland and Japan);
- *Volume 7:* ***The Molecular Biology of Chloroplasts and Mitochondria in Chlamydomonas*** (36 Chapters; 733 pages; 1998; edited by Jean David Rochaix, Michel Goldschmidt-Clermont and Sabeeha Merchant, from Switzerland and USA);
- *Volume 8:* ***The Photochemistry of Carotenoids*** (20 Chapters; 399 pages; 1999; edited by Harry A. Frank, Andrew J. Young, George Britton and Richard J. Cogdell, from USA and UK);
- *Volume 9:* ***Photosynthesis: Physiology and Metabolism*** (24 Chapters; 624 pages; 2000; edited by Richard C. Leegood, Thomas D. Sharkey and Susanne von Caemmerer, from UK, USA and Australia);
- *Volume 10:* ***Photosynthesis: Photobiochemistry and Photobiophysics*** (36 Chapters; 763 pages; 2001; authored by Bacon Ke, from USA);
- *Volume 11:* ***Regulation of Photosynthesis*** (32 Chapters; 613 pages; 2001; edited by Eva-Mari Aro and Bertil Andersson, from Finland and Sweden);
- *Volume 12:* ***Photosynthetic Nitrogen Assimilation and Associated Carbon and Respiratory Metabolism*** (16 Chapters; 284 pages; 2002; edited by Christine Foyer and Graham Noctor, from UK and France);
- *Volume 13:* ***Light Harvesting Antennas*** (17

Chapters; 513 pages; 2003; edited by Beverley Green and William Parson, from Canada and USA);

- *Volume 14:* ***Photosynthesis in Algae*** (19 Chapters; 479 pages; 2003; edited by Anthony Larkum, Susan Douglas and John Raven, from Australia, Canada and UK);
- *Volume 15:* ***Respiration in Archaea and Bacteria: Diversity of Prokaryotic Electron Transport Carriers*** (13 Chapters; 326 pages; 2004; edited by Davide Zannoni, from Italy);
- *Volume 16:* ***Respiration in Archaea and Bacteria: Diversity of Prokaryotic Respiratory Systems*** (13 chapters; 310 pages; 2004; edited by Davide Zannoni, from Italy);
- *Volume 17:* ***Plant Mitochondria: From Genome to Function*** (14 Chapters; 325 pages; 2004; edited by David A. Day, A. Harvey Millar and James Whelan, from Australia);
- *Volume 18:* ***Plant Respiration: From Cell to Ecosystem*** (13 Chapters; 250 pages; 2005; edited by Hans Lambers and Miquel Ribas-Carbo, from Australia and Spain).
- *Volume 19:* ***Chlorophyll a Fluorescence: A Signature of Photosynthesis*** (31 Chapters; 817 pages; 2004; edited by George C. Papageorgiou and Govindjee, from Greece and USA);
- *Volume 20:* ***Discoveries in Photosynthesis*** (111 Chapters, 1262 pages; 2005; edited by Govindjee, J. Thomas Beatty, Howard Gest and John F. Allen, from USA, Canada and Sweden (& UK));
- *Volume 21:* ***Photoprotection, Photoinhibition, Gene Regulation and Environment*** (21 Chapters, 378 pages; 2006; edited by Barbara Demmig-Adams, William Adams III and Autar K. Mattoo, all from USA);
- *Volume 22:* ***Photosystem II: The Light-Induced Water:Plastoquinone Oxidoreductase*** (34 Chapters; 826 pages; 2005; edited by Thomas J. Wydrzynski and Kimiyuki Satoh, from Australia and Japan);
- *Volume 23:* ***Structure and Function of the Plastids*** (27 Chapters; 2006; edited by Robert Wise and J. Kenneth Hoober, both from USA);
- *Volume 24:* ***Photosystem I: The Light-Induced Plastocyanin:Ferredoxin Oxidoreductase*** (40 Chapters; 2006; edited by John H. Golbeck from USA).

Further information on these books and ordering instructions can be found at <www.springeronline.com> under the Book Series 'Advances in Photosynthesis and Respiration.' Tables of Contents of volumes 1–24 can be found at <www.life.uiuc.edu/govindjee/photosynSeries/ttocs.html>. Special discounts are available for members of the International Society of Photosynthesis Research, ISPR (<http://www.photosynthesisresearch.org>).

About Volume 25: Chlorophylls and Bacteriochlorophylls: Biochemistry, Biophysics, Functions and Applications

Chlorophylls are the most obvious natural pigments on Earth being observable, as they are, from outerspace; they also sustain all life on Earth via their involvement in photosynthesis. With 37 concise chapters, this book reviews recent progress and current status of studies of the chemistry, metabolism and spectroscopy of chlorophylls and chlorophyll-protein complexes. Also discussed is progress on the applications of the chlorophylls as photosensitizers in photodynamic therapy of cancerous tumors, as molecular probes, and as reporters on the physiological status of whole plants and ecosystems. The last book, dedicated to chlorophylls, was published in 1991, and has been out of print since 1995; thus, this book fills a gap by summarizing the chemical, physical, biological and medical aspects of chlorophyll research and development with a focus on the tremendous progress achieved over the past 15 years. The book is aimed equally at advanced students and both novice and experienced researchers: each of the five sections has an up-to-date introductory overview which is followed by a series of concise well-focused and fully-referenced chapters written by chemists, biochemists, biophysicists, photobiologists and pharmacologists.

This book has 37 authoritative Chapters written by 70 international authorities from 18 countries (Australia, Austria, Belarus, Czech Republic, Denmark, France, Germany, Indonesia, Israel, Japan, Malaysia, Mexico, The Netherlands, Russia, Spain, Switzerland, United Kingdom and the United States of America). It is, therefore, a truly international book and the editors deserve our thanks and our congratulations for giving this gift for our future. It was a Herculean task that Hugo Scheer and his co-editors, Bernhard Grimm, Bob Porra and Wolfhart Rüdiger, have accomplished. I remain in awe at the encyclopedic knowledge provided in this Bible of chlorophylls and bacteriochlorophylls (their structures; chemistry and

analysis (9 chapters); their metabolism (9 chapters); their native environment (9 chapters); their functions (4 chapters); and finally their applications (6 chapters). The readers can easily find the titles and the authors of the individual chapters in the Table of Contents of this book. Instead of repeating this information here, I prefer to thank each and every author by name (listed in alphabetical order) that reads like a 'Who's Who in Chlorophyll and Bacteriochlorophyll research':

Thijs J. Aartsma; Machiko Akiyama; James P. Allen; Idan Ashur; Samuel I.Beale; Christoph F. Beck; Robert E. Blankenship; Alexander S. Brandis; Paula Braun; Donald A. Bryant; Aline G. M. Chew; Ido de Boer; Huub J.M. de Groot; P. Leslie Dutton; Patrick W. Fowler; Niels-Ulrik Frigaard; Ritsuko Fujii; Adela Garcia-Martin; José L. Garrido; Bernhard Grimm; Dirk W. Heinz; Stefan Hörtensteiner; C. Neil Hunter; Dieter Jahn; Shirley W. Jeffrey; Yoshinori Kakitani; Hiromi Kano; Brendan J. Keely; Hideo Kise; Masami Kobayashi; Michal Koblizek; Jürgen Köhler; Yasushi Koyama; Bernhard Kräutler; Frithjof C. Küpper; Hendrik Küpper; Lee-Gyan Kwa; Anthony W.D. Larkum; Dieter Leupold; Leenawaty Limantara; Heiko Lokstein; Julia A. Maresca; Alexander N. Melkozernov; André Morel; Christopher C. Moser; Jürgen Moser; Mamuro Nango; Ladislav Nedbal; Dror Noy; Harald Paulsen; Robert (Bob) J. Porra; Wolfhart Rüdiger; Claudia Ryppa; Yoram Salomon; Hugo Scheer; Avidgor Scherz; Wolf-Dieter Schubert; Mathias O. Senge; Yuzo Shioi; Martin Spiller; Erich Steiner; Matthias von Jan; Josef Wachtveitl; Tadashi Watanabe; Arno Wiehe; JoAnn C. Williams, Elena Yaronskaya; Roie Yerushalmi; Manuel Zapata, and Wolfgang Zinth.

The Web Site for the Book

A unique innovation introduced by the editors for this book has been the construction of a web site that hosts the supplementary material including several colored figures. It is located at <http://epub.ub.uni-muenchen.de/archive/00000776/>. Our readers will really appreciate this contribution by the editors.

A Brief History—From Then till Now

Discoveries

- In 1818, two French scientists Pierre Joseph Pelletier (1788–1842) and Joseph Bienaimé Caventou (1795–1877) named the green plant pigment chlorophyll ('green of leaf ').
- In 1877, the Russian physiologist Climent A. Timiriazeff (1843–1920) established the red maximum of the absorption spectrum of chlorophyll and showed that red light absorbed by chlorophyll is the most efficient for photosynthesis. On the basis of this experiment, he claimed that chlorophyll is an optical and chemical photosensitizer of photosynthesis. He proposed that light absorption by chlorophyll causes its chemical transformation, which induces further reactions leading to photosynthesis.
- In 1906, the Russian botanist Mikhail Semenovich Tswett (1872–1919) separated the plant pigments (chlorophylls and carotenoids) by passing a solution containing the natural pigment mixture through glass columns packed with finely-divided calcium carbonate, thereby inventing a new technique termed appropriately chromatography ('color representation' or 'color writing').
- In 1915, Richard Martin Willstätter (1872–1942), of Munich, Germany, received the Nobel Prize in Chemistry for his detailed chemical investigations on chlorophyll, including its chemical nature; he suggested that chlorophylls play an active role in photosynthesis. Willstätter's close collaborator in these studies was Arthur Stoll (1887–1971) of Switzerland.
- In 1930, Hans Fischer (1881–1945), also of Munich, Germany, received the Nobel Prize in Chemistry: he had made new inroads in the chemistry of chlorophyll, whose structure he elucidated in the subsequent 12 years. The award recognized his researches into the constitution of porphyrins, hemins and chlorophylls.
- In 1965, Robert Burns Woodward (1917-1979), of Harvard, USA, received the Nobel Prize in Chemistry for the synthesis of many organic compounds including chlorophyll, the topic of this book.
- Shortly after, in 1966, the terpenoid specialist Basil C.C. Weedon of Imperial College, London,

published a full record of the synthesis of phytol, the esterifying alcohol of most chlorophylls that comprises about 1/3 of their mass.

The Books

The appearance over the past 100 years of several books dedicated to chlorophylls, emphasizes the importance of and continuing interest in the subject.

- In 1913, a first concise account of chlorophyll research was published in a 423 page book *Untersuchungen über Chlorophyll* by Richard Willstätter and Arthur Stoll (Verlag von Julius Springer, Berlin).
- Between 1934 and 1940, Hans Fischer and Hans Orth published a monumental work *Die Chemie des Pyrrols* (Akademische Verlagsgesellschaft, Leipzig). The 2nd half of volume 2, by Hans Fischer and Adolf Stern, published in 1940, was entirely dedicated to chlorophylls. The relevance of this book is witnessed by its repeated reprinting, first in 1943 (Edwards Brothers, Ann Arbor, Michigan) and again in 1968 (Johnson Reprint Corporation, New York and London).
- In 1966, Leo P. Vernon and Gilbert R. Seely, both from USA, edited a 679 page book *The Chlorophylls* (Academic Press, New York); they had 22 authors, but none are in the current Grimm et al. book.
- In 1991, one of the editors of the current book, Hugo Scheer from Munich, Germany, edited a 1,257 page detailed and beautiful *opus* (*Chlorophylls*, CRC Press, Boca Raton). This book had 72 authors and 42 chapters. I am delighted to see that among these 72 authors, Sam Beale; Masami Kobayashi; Tony Larkum; Bob Porra; Wolfhart Rüdiger; Hugo Scheer; Avigdor Scherz; Yuzo Shioi; and Tadashi Watanabe are also authors in the current book.

For a time-line on oxygenic photosynthesis, see Govindjee and David Krogmann (2004) *Photosynthesis Research* 80: 15–57, and on anoxygenic photosynthesis, see H. Gest and R. E. Blankenship (2004) *Photosynthesis Research* 80: 59–70. Jack Fajer (2004) has provided a personal perspective on chlorophyll chemistry in *Photosynthesis Research* 80: 165–172.

Future AIPH Books

The readers of the current series are encouraged to watch for the publication of the forthcoming books (not necessarily arranged in the order of future appearance):

- ***Biophysical Techniques in Photosynthesis II*** **(**Editors: Thijs J. Aartsma and Jörg Matisyk**);**
- ***Photosynthesis: A Comprehensive Treatise; Biochemistry, Biophysics, Physiology and Molecular Biology, Part 1*** (Editors: Julian Eaton-Rye and Baishnab Tripathy); and
- ***Photosynthesis: A Comprehensive Treatise; Biochemistry, Biophysics, Physiology and Molecular Biology, Part 2*** (Editors: Baishnab Tripathy and Julian Eaton-Rye).

In addition to these contracted books, we are in touch with prospective Editors for the following books:

- Chloroplast Bioengineering
- Molecular Biology of Cyanobacteria II.
- ATP Synthase
- Genomics and Proteomics
- Anoxygenic Photosynthetic Bacteria II
- Hydrogen Evolution
- Sulfur Metabolism in Photosynthetic Systems
- Global Aspects, Parts 1 and 2
- Artificial Photosynthesis

Readers are encouraged to send their suggestions for future volumes (topics, names of future editors, and of future authors) to me by E-mail (gov@uiuc.edu) or fax (+1-217-244-7246).

In view of the interdisciplinary character of research in photosynthesis and respiration, it is my earnest hope that this series of books will be used in educating students and researchers not only in Plant Sciences, Molecular and Cell Biology, Integrative Biology, Biotechnology, Agricultural Sciences, Microbiology, Biochemistry, and Biophysics, but also in Bioengineering, Chemistry, and Physics.

I take this opportunity to thank and congratulate Hugo Scheer (corresponding editor), Robert Porra, Bernhard Grimm and Wolfhart Rüdiger for their outstanding and painstaking editorial work. I thank all the 70 authors (listed above) of volume 25 of the AIPH Series: without their authoritative chapters, there would be no such volume. I especially thank Larry Orr for typesetting this book: his expertise has been crucial in bringing this book to completion. We are grateful to Jacco Flipsen and Noeline

Gibson (both of Springer) for their friendly working relationship with us during the production of this book. I also thank Jeff Haas (Director of Information Technology, Life Sciences, University of Illinois at Urbana-Champaign, UIUC), Evan DeLucia (Head, Department of Plant Biology, UIUC) and my dear wife Rajni Govindjee for constant support.

February 15, 2006

Govindjee
Series Editor, *Advances in Photosynthesis and Respiration*
University of Illinois at Urbana-Champaign
Department of Plant Biology
Urbana, IL 61801-3707, USA
E-mail: gov@uiuc.edu
URL: http://www.life.uiuc.edu/govindjee

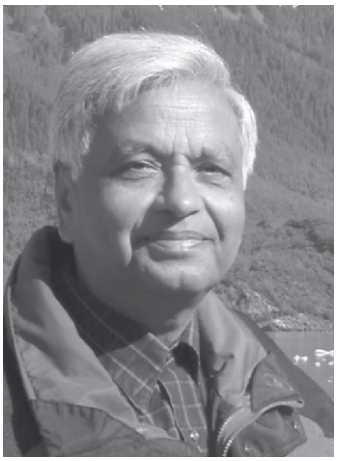

Govindjee

Govindjee, born in 1932, obtained his BSc (Chemistry, Biology) and MSc (Botany) in 1952 and 1954, from the University of Allahabad, India. He was a student of Robert Emerson and of Eugene Rabinowitch, receiving his PhD (Biophysics), in 1960, from the University of Illinois at Urbana-Champaign (UIUC), IL. He has focused mainly on "*Photosystem II*" (PS II, water:plastoquinone oxidoreductase) throughout his career. His early research included the discovery of a short-wavelength form of chlorophyll (Chl) *a* functioning in the Chl *b*-containing system, now called PS II (in 1960, with Eugene Rabinowitch); of the two-light effect in Chl *a* fluorescence (1960); and of the two-light effect (Emerson Enhancement) in NADP-reduction in chloroplasts (1962–1964, with Rajni Govindjee and George Hoch). In collaboration with his ~25 graduate students and postdoctoral associates, he has worked on the origins of the different spectral fluorescing forms of Chl *a* and the temperature dependence of excitation energy transfer down to 4 K (1963–1970); established basic relationships between Chl *a* fluorescence and photosynthetic reactions (1968–1988); discovered a unique role of bicarbonate on the acceptor side of PS II, particularly in protonation events involving the Q_B binding region (1970–1998); formulated the theory of thermoluminescence in plants (1983, with Don DeVault); made the first picosecond measurement on the primary photochemistry of PS II (1989–1997, with Michael Seibert and Michael Wasielewski); and pioneered the use of the lifetime of Chl *a* fluorescence in understanding photoprotection against excess light (with Adam Gilmore). His current focus, however, is on the "*History of Photosynthesis Research*" and in '*Photosynthesis Education.*' He has served the UIUC as an Assistant Professor, Associate Professor and Professor (1961–1999). Since 1999, he has been Professor Emeritus of Biochemistry, Biophysics and Plant Biology at the UIUC. His honors include: Fellow of the American Association of Advancement of Science (1976); Distinguished Lecturer of the School of Life Sciences, UIUC (1978); Fellow and Life Member of the National Academy of Sciences, India (Allahabad, 1978); President of the American Society of Photobiology (1980-1981); Fulbright Senior Lecturer (1996–1997); and Honorary President of the 13th International Photosynthesis Congress (Montréal, 2004).

Contents

Functions

Applications

Preface

Chlorophylls (from the Greek: *chloros*-green and *phyllon*-leaf) are, beyond any doubt, the most visible and most abundant organic pigments on Earth. Indeed, as beautifully illustrated on the cover of the book, they are clearly visible from outer-space. It has been estimated that between 10^9 and 10^{12} tons of chlorophylls are produced annually on Earth. Much of this synthesis, if not most, occurs in the oceans where marine algae and photosynthetic bacteria of lakes and tidal flats, with their shorter life cycles than terrestrial plants, abound. But it is not only because of their abundance that chlorophylls are important. Chlorophylls derive their ultimate importance from their role as the key pigments which capture radiant energy from the sun for plant, algal and bacterial photosynthesis, a process which supports life on Earth, even non-photosynthesizing life forms such as animals, including ourselves. This knowledge seems inherent to man after the invention of agriculture as it is expressed widely in our general and religious literature alike: in the great Aton-Hymn we hear the Egyptians praise the sun: 'your rays nourish every garden…'; in the biblical quote we are informed 'all flesh is grass'; and, in Ingeborg Bachmann's poem 'To the Sun' we read 'more beautiful…. than other celestial bodies, as your and my life depend on it day by day…'

While the importance of light for plant growth has been realized since the beginning of agriculture, a role for the chlorophylls in this process was proposed less than 130 years ago in 1877 by the Russian plant physiologist, Climent Timiriazoff. It was 1913, however, before the first concise chemists' account of chlorophyll research was published by Richard Willstätter and Arthur Stoll in their book *Untersuchungen über Chlorophyll* (Investigations on Chlorophylls). Since then three more books on chlorophylls have appeared testifying not only to their importance in photosynthesis, but increasingly to the useful applications being discovered for them. The second book devoted entirely to chlorophylls is Part 2 of Volume 2 of *Die Chemie des Pyrrols* (The Chemistry of Pyrroles) published by Hans Fischer and Adolf Stern in 1940: this book highlighted the research of the Fischer school, and of other chlorophyll researchers like Henry Conant, which culminated in the elucidation of the structures of chlorophylls *a* and *b*, and suggested the structure of bacteriochlorophyll *a*. This book was reproduced in the USA in both 1943 and 1968 and is still cited today because of the wealth of information it provided. The next book, *The Chlorophylls*, edited by Leo P. Vernon and Gilbert R. Seely appeared in 1966 by which time many more chlorophylls were known and the emphasis changed from the chemistry to the biochemical and physiological roles of these pigments in photosynthesis. The fourth book, *Chlorophylls*, edited by one of the current authors (H.S.) and published in 1991, described the tremendous broadening of the subject which occurred in the intervening years. It described the rapid progress in the biosynthesis of chlorophylls and its regulation, the development and applications of new analytical and spectroscopic techniques, the progress in structure elucidation of new chlorophylls, their chemistry, and their evolution over geological timescales; also, the isolation of several chlorophyll-protein complexes, the crystallization of two of them, and the emerging molecular details of their native protein environments were described, and the applications of chlorophylls in medicine were summarized.

The now completed fifth book on chlorophylls is aimed at summarizing our current knowledge on plant, bacterial and algal chlorophylls, with a focus on the many advances made over the past 15 years. Many new chlorophylls have been isolated following, mainly, the development of new chromatographic techniques, and their novel structures have been determined. New bacteriochlorophylls have been isolated from phototrophic bacteria and, from marine algae, new chlorophylls have been found with increasingly complex structures: one is esterified to a glycolipid. Probably many more await discovery. Besides the obvious plant chlorophylls, bacteriochlorophylls are increasingly cited in the modern photosynthesis literature. In attempting to understand photosynthesis in molecular detail, not only plants but also photosynthetic bacteria have been exploited by photosynthesis researchers for the obvious advantages of their rapid growth in defined media and controlled environments, and also for the relative simplicity of their photosynthetic apparatus. Most chlorophylls found in living organisms occur in chlorophyll-protein complexes, containing up to 100 chlorophylls; their structures, therefore, hold the key to the safe and efficient harvesting of light but their elucidation also presented a formidable challenge. However, the organization of chlorosomes, the light-harvesting complexes of green bacteria, relies mainly on chlorophyll-chlorophyll

interactions, thereby reviving older concepts of, for example, Joseph J. Katz and coworkers.

Since the first high-resolution crystal structure of a membrane protein, the reaction center of photosynthetic purple bacteria, was published in 1984, examples of the crystal structures of most of the relevant classes of chlorophyll-protein complexes have become available. These advances were complemented by methods to selectively modify the pigments and the proteins. By using increasingly sophisticated spectroscopic techniques, such studies served as a base for advancing our understanding, on the molecular level, of the function of these pigment-protein complexes. As the first multi-chromophore complexes of known atomic structure were examined by advanced steady-state and kinetic spectroscopy, the results have challenged experimental and theoretical physicists to critically test existing theories of electron and energy transfer. These studies of the complexes have equally challenged the chemists: since the true understanding of structures always implies the capacity to rebuild functional structures *de novo,* and several groups have successfully pursued the fabrication of synthetic chlorophyll-binding proteins. Eventually, this combined knowledge may help to harvest the sun on a technical scale.

Already, the intimate knowledge of chlorophyll functions has led to diagnostic and therapeutic applications. The possibility now exists to use chlorophyll spectroscopy for remote, non-invasive monitoring of the physiological status of individual plants, of ecosystems or of the whole Earth, or to use chlorophyll derivatives to detect and treat cancer, monitor oxygen tension, or measure partial electron flow from ligands to coordinating metals. An important aspect in modern research is the stress which can be imposed on the plant system by excess or changing light and by low temperatures: chlorophyll proteins, almost always, contain carotenoids which function as protectants against photodynamic (i.e., light- and- oxygen-induced) damage by chlorophylls. These potentially deleterious effects on chlorophylls are associated with their intense absorption and long excited-state lifetimes, which have been selected during the evolution of photosynthesis. Since animals lack such efficient photoprotection, the phototoxicity of chlorophylls has also attracted the medical interest and they have shown particular promise in the selective damage of tumors at the cellular or vascular level.

This book is aimed at a broad audience from advanced students to experienced scientists in basic and applied research, in chemistry, physics, physiology, medicine and geosciences. It has five sections, covering structures, properties and the analysis of chlorophylls (part 1), their metabolism (part 2), their native environment (part 3), their functions (part 4) and their applications (part 5). In each section, an overview is followed by a series of chapters focused on the basic concepts and including recent developments. We are grateful to the 70 authors who contributed to this group effort extending over several years: we hope that the result proves worthy of these efforts.

December 24, 2005

Bernhard Grimm
Institut für Biologie/Pflanzenphysiologie
Humboldt Universität Berlin
Unter den Linden 6
D-10999 Berlin
Germany
Tel.: +49-30-2093-6119
Fax: +49-30-2093-6337
Email: bernhard.grimm@rz.hu-berlin.de

Robert Porra
CSIRO Plant Industry
GPO Box 1600
Canberra ACT 2601
Australia
Tel.: +61-262-814653
Fax: +61-262-465000
Email: Robert.Porra@csiro.au

Wolfhart Rüdiger
Dept. Biologie I – Botanik
Ludwig-Maximilians-Universität München
Menzinger Str. 67
D-80638 München
Germany
Tel.: +49-89-17861-280
Fax: +49-89-17861-185
Email: ruediger@lrz.uni-muenchen.de

Hugo Scheer
Dept. Biologie I – Botanik
Ludwig-Maximilians-Universität München
Menzinger Str. 67
D-80638 München
Germany
Tel.: +49-89-17861-295
Fax: +49-89-17861-171
Email: hugo.scheer@lmu.de

Bernhard Grimm

Bernhard Grimm is Professor of Plant Physiology in the Institute of Biology at the Humboldt University in Berlin, Germany. He studied Biology at the University of Hannover from 1978 to 1984 and received his PhD for his thesis on 'Early light inducible proteins' under the supervision of Klaus Kloppstech at the Institute of Botany in 1987. He continued as a postdoctoral fellow at the Carlsberg Laboratory, Copenhagen, Denmark, in the department of Diter von Wettstein and studied 5-aminolevulinate and chlorophyll biosyntheses with Gamini Kannangara and Simon Gough. During his PhD and postdoctoral studies, visits to the laboratories of Itzhak Ohad, Jersualem and Hans Jansonius, Basel, proved most rewarding. Bernhard accepted a position as research group leader at the re-formed Institute of Plant Genetics and Crop Plant Research (IPK), Gatersleben, in the Eastern part of Germany. While he previously used biochemical techniques for analysis of various enzymatic steps in chlorophyll biosynthesis at the Carlsberg Laboratory, he continued to explore the regulation mechanisms of this pathway by introducing transgenic and mutant plants with deregulated expression of many enzymes in the tetrapyrrole pathway. In 1993, he completed his Habilitation in Plant Physiology at the University of Hannover before accepting, in 2001, his present Professorial position at the Humboldt University. The expertise of his group includes methods in molecular genetics and biology, tissue culture work, biochemical analysis of proteins, porphyrin intermediates and photosynthesis. Current research in tetrapyrrole biosynthesis includes studies on the control of Mg porphyrin biosynthesis and on the rate limiting step, 5-aminolevulinate formation, as well as the cellular response to photoreactive porphyrins. His studies were facilitated by the enthusiastic collaboration of students and postdoctoral fellows in his group and with many research groups. The latter include productive studies: on oxidative stress with Heinrich Sandermann (Munich); on X-ray crystallography of glutamate-semialdehyde amino transferase structure with Hans Jansonius (Basel) and of uroporphyrinogen decarboxylase structure with Robert Huber (Munich); on porphyrin mutants of *Chlamydomonas* with Christoph Beck (Freiburg); on geranyl-geraniol reductase with Wolfhart Rüdiger (Munich); on photoprotection with Paul Hoffmann (Berlin); and, on circadian rhythm with Klaus Kloppstech (Hannover), on control of chlorophyll synthesis with Nicolai Shalygo and Elena Yaronskaja (Minsk), on tocopherol biosynthesis with Michel Havaux (Cadarache), on tetrapyrrole synthesis in *Physcomitrella* with Ralf Reski (Freiburg), on plastid derived signaling with Thomas Börner (Berlin), on nucleotide transporters with Ekkehard Neuhaus (Kaiserslautern), and on peroxidizing herbicide resistant mutants with Tatjana Ezhova (Moscow) and Kyoungwhan Back (Gwangju, Korea). Bernhard acknowledges the contributions of his own research team and of all his colleagues: these studies have contributed to the better understanding of the regulation and physiology of tetrapyrrole metabolism.

Robert J. Porra

Robert (Bob) Porra has been 45-years in Canberra (Australia) with Plant Industry-Commonwealth Scientific and Industrial Research Organization (PI-CSIRO) where, following retirement in 1993, he remains an Honorary Research Fellow. Born in 1931 in Adelaide (Australia), he graduated with a BSc (Honors) in Biochemistry at the University of Adelaide in 1958 and PhD at the Australian National University, Canberra, in 1963, for research on heme biosynthesis at PI-CSIRO with John Falk. Post-doctoral research in 1964 with the late June Lascelles (1924–2004) at the University of Oxford (UK) extended studies of Fe^{2+}-ion incorporation into hemes by mammalian-mitochondrial ferrochelatases to the ferrochelatases of photosynthetic bacteria. Later, at PI-CSIRO, ferrochelatases were studied in higher-plant mitochondria, proplastids and chloroplasts. In 1969–1971, with David Griffiths (University of Warwick, UK) and Owen Jones (University of Bristol, UK), research switched to the regulation of 5-aminolevulinate (ALA) and heme biosynthesis. Later at PI-CSIRO, with Horst Grimme from Bremen University (Germany), regulation of ALA and chlorophyll (Chl) biosynthesis was studied in regreening, nitrogen-starved *Chlorella fusca*: the difficulty of pigment extraction from these cells kindled an enduring fascination with the extraction and determination of Chl *a* and Chl *b* in plant and algal cells. Studies of ALA biosynthesis, by the succinate-glycine (Shemin) pathway in *Rhodobacter sphaeroides* and the glutamyl-tRNA-mediated (C_5) pathway in greening maize, started in 1979 with Horst Senger (University of Marburg, Germany) and culminated in 1981 with ^{13}C-NMR experiments at PI-CSIRO, with Peter Wright (Sydney University, Australia) and Otto Klein (Marburg), which unequivocally demonstrated that Chls formed in greening maize were derived entirely from ALA generated by the C_5 pathway. Bob has enjoyed many visits to the University of Munich (Germany), during a 17-year (1989–2006) association with Hugo Scheer. Together, they conducted experiments on greening maize and various photosynthetic bacteria, using ^{18}O-labelling coupled to mass spectrometry and unequivocally established the origin of all oxygen-bearing side chains of Chls *a* and *b*, and of bacteriochlorophyll *a,* by determining which arose from O_2 or from H_2O by oxygenase- or hydratase-mechanisms, respectively. These Munich studies were supported by the Deutcher Akademischer Austauschdienst and Deutsche Forschungsgemeinschaft.

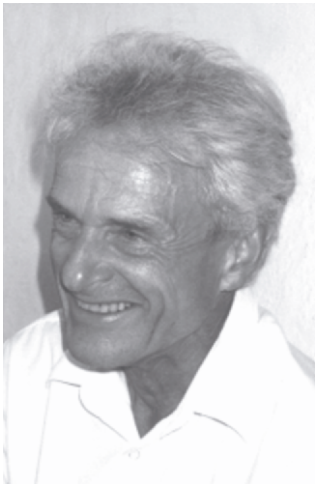

Wolfhart Rüdiger

Wolfhart Rüdiger was Professor of Phytochemistry at the 'Botanisches Institut' of the University of Munich for 32 years. After his retirement in 2001, he became Professor Emeritus at the same institute. Born in 1933 in Stolp (Germany), he graduated in Chemistry (Dipl.-Chem. in 1958, and doctorate in 1961) for research on chlorophyll (Chl) biosynthesis at the University of Würzburg (Germany) with Franz-Gottwalt Fischer. His post-doctoral research was with Hans-Joachim Bielig (Max-Planck-Institut, Heidelberg, and Marine Biological Station, Naples, Italy); he worked on vanadium metabolism in tunicates. In 1963, he moved to the University of Saarbrücken (Germany) and started research on bile pigments in animals and plants; it led to the elucidation of the chromophore structures of phycobiliproteins in 1967 (with Pádraig Ó Carra, Galway, Ireland) and of the photoreceptor phytochrome in 1969 (with David Correll, Washington). In 1971, he was appointed professor in Munich where he continued this research that culminated, in 1983, in the detection of *cis-trans*-isomerization as the primary reaction of the phytochrome chromophore. Other research interests included the plant photoreceptor for phototropism, phototropin; the photoreaction of the latter was established in 2001 as photo-addition of cysteine to the flavin chromophore. However, his major research, throughout the years in Munich, was concerned with Chl biosynthesis. Continuing research included: in 1980, the detection and study of Chl synthase activity which catalyses the phytylation of Chl; in 1994, the demonstration with John Mullet (Texas Agricultural and Mechanical University, College Station, USA) of its role in stabilizing Chl a-binding proteins; and, in 1977, with Carl Bauer (Indiana University, Bloomington, USA) a substrate specificity study of the recombinant enzyme. Later, the substrate specificity of protochlorophyllide oxidoreductase was studied by Wolfhart in cooperation with Margareta Ryberg and Christer Sundqvist (Gotenburg, Sweden). Studies with Christoph Beck (Freiburg, Germany) revealed, in 1997, that the Chl precursor, magnesium-protoporphyrin, is a plastid signal for the regulation of the expression of nuclear genes. In 2000, cooperation with Ayumi Tanaka (Sapporo, Japan) resulted in the first in vitro synthesis of Chl *b*, mediated by recombinant chlorophyllide a oxygenase. In 1994, Wolfhart Rüdiger received an Honorary Doctorate (Dr.h.c.) from the University of Gotenburg (Sweden).

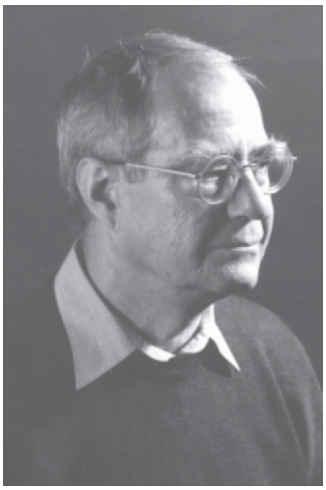

Hugo Scheer

Hugo Scheer is Professor of Plant Biochemistry and Biophysics at the University of Munich, Germany. Born in 1942 in Berlin, Germany, he received his diploma (1968) and doctorate (1970) in chemistry at the Technical University of Braunschweig, Germany, for studies on the stereochemistry and spectroscopy of tetrapyrrole pigments. He became interested in photosynthesis during his post-doctoral research (1973–1975) with Joseph J. Katz and James R. Norris at Argonne National Laboratory, Chicago, USA, while researching the redox and aggregation chemistry of chlorophylls. In 1975, Hugo joined the Botanisches Institut, University of Munich, where he completed his Habilitation in 1978, and was appointed Professor in 1980. Initially, in Munich, he worked on linear tetrapyrroles, and their adaptation to diverse functions by static and dynamic interactions with the apoproteins and other chromophores. He extended this work to chlorophyll and carotenoid proteins, where there are, in addition, pronounced pigment-pigment interactions. In bili- and chlorophyll-protein complexes, absorption energies, excited state lifetimes or redox potentials of chromophores were changed by directed chemical modification, and the effects on energy- and electron transfer studied. Recently, these studies have involved transmetallated bacteriochlorophylls, and their medical applications in photodynamic therapy of tumors. This work, and related studies by other Munich research groups, has led to a DFG-funded Collaborative Research Center (Sonderforschungsbereich 533) 'Light-induced dynamics of biopolymers,' chaired by Hugo Scheer since 1997. During his career, Hugo has visited: Avigdor Scherz (Weizmann Institute, Rehovot, Israel) studying chlorophyll aggregation and chlorophylls in photodynamic therapy; Robert Porra (CSIRO-Division of Plant Industry, Canberra, Australia) working on the reduction of chlorophyll protein complexes by borohydrides; Tomas Gillbro (University of Umea, Sweden) where he studied the bleaching of biliproteins; and, Ken Sauer (University of California, Berkeley, USA) investigating energy transfer in biliproteins. More recently, he was introduced to genetic engineering by Nicole Tandeau de Marsac (Institut Pasteur, Paris, France) and Jean Houmard (École National Superieur, Paris, France). In China, he worked with Kai-Hong Zhao (Huazhong University, Wuhan, China) on enzymatic chromophore ligation in biliproteins and also with Gen-Xi Li (University of Nanjing, China) where Hugo received an Honorary Professorship. Hugo is grateful for the friendship and for all the scientific contributions of his students and colleagues, both in Germany and overseas, and also for the very generous funding of his research by the Alexander von Humboldt Foundation (Bonn), Deutsche Akademischer Austauschdienst (DAAD, Bonn), Deutsche Forschungsgemeinschaft (DFG, Bonn), German Ministry of Science and Technology (Bonn and Berlin), German-Israel Foundation (GIF, Jerusalem), European Community (Brussels), Hans Fischer Gesellschaft (München), INTAS (New York), NEDO (Tokyo) and the VW Foundation (Hannover).

Author Index

Color Plates

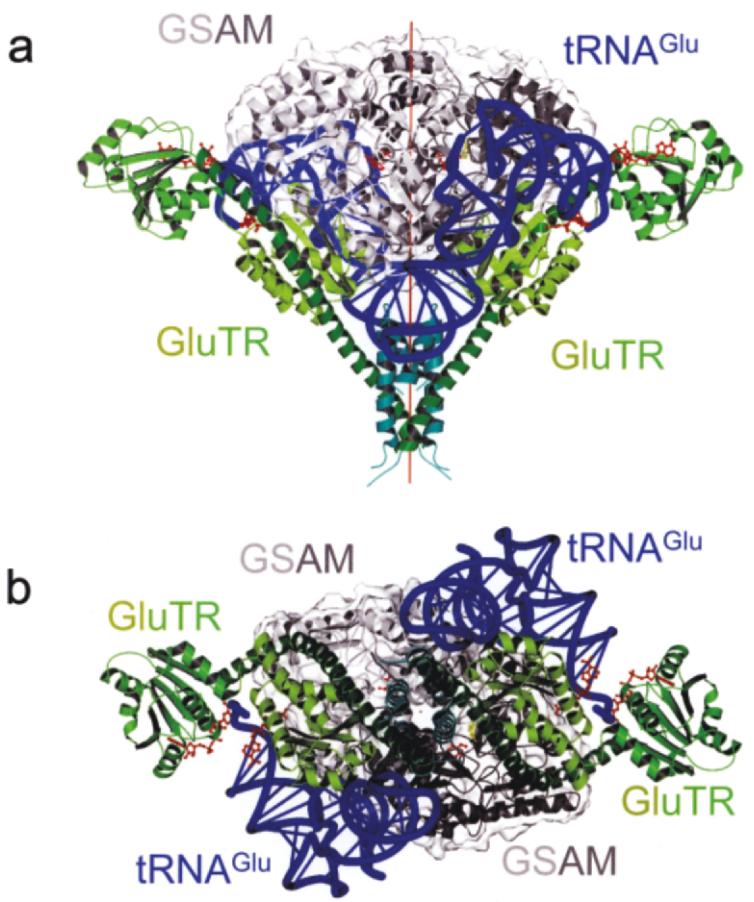

Fig. 1 . The proposed ternary complex of glutamyl-tRNA-reductase (GluTR)/glutamyl transfer RNA ($tRNA^{Glu}$)/glutamate-1-semialdehyde-aminomutase (GSAM) viewed (a) perpendicular to the common two-fold axis and (b) along this axis from the dimerization domain of GluTR (opposite direction to Fig. 3a shown in Chapter 12, p. 165). The ribbon depiction of GluTR is rendered in shades of green. $tRNA^{Glu}$ is represented as a backbone model (purple), while GSAM is shown by a transparent surface covering a gray and white ribbon diagram. (Produced as Fig. 1 in Chapter 12, p. 161.) See Chapter 12, p. 168.

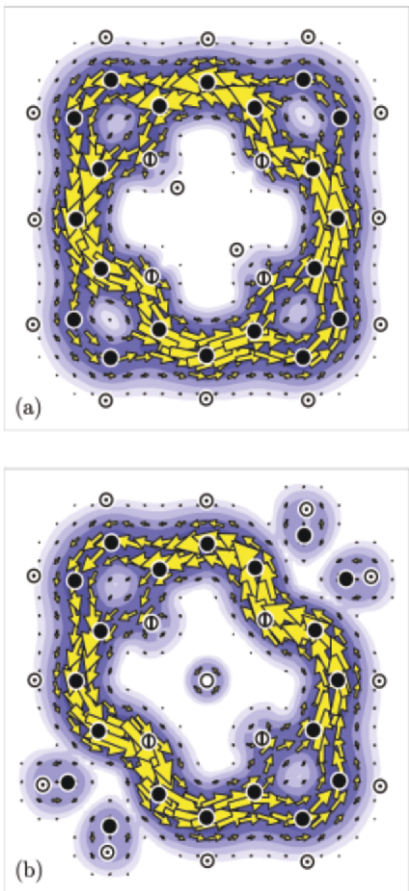

Fig. 2. Global ring currents, induced by a perpendicular magnetic field, in the π–electron distributions of (a) free-base porphin and (b) magnesium bacteriochlorin are rationalized, as are the electronic spectra, by a four-orbital model. Plotting conventions are given in the legend to Fig. 5 shown in Chapter 23, p. 343. See Chapter 23, p. 344.

Bernhard Grimm, Robert J. Porra, Wolfhart Rüdiger and Hugo Scheer (eds): Chlorophylls and Bacteriochlorophylls: Biochemistry, Biophysics, Functions and Applications, pp. CP1–CP8. © 2006 Springer. Printed in The Netherlands.

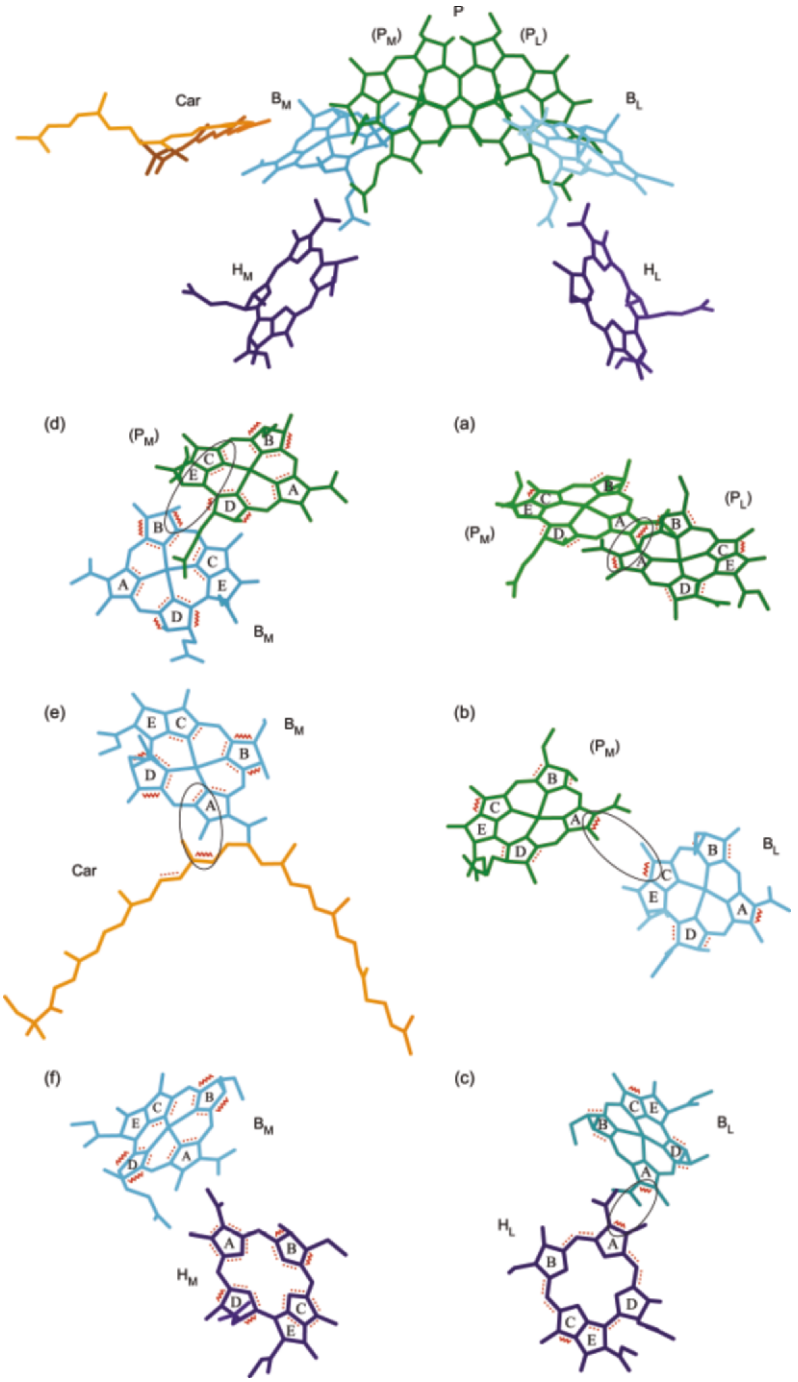

Fig. 1. Spatial arrangement of the special pair bacteriochlophylls (P, tentatively named 'P_L' and 'P_M'), the accessory bacteriochlophylls (B_L and B_M), the bacteriopheophytins (H_L and H_M) and the carotenoid (Car) molecules in the RC from *Rhodobacter sphaeroides* strain AM260W (Richard J. Cogdell, personal communication). The regions where the largest and the second-largest changes in bond order take place (where the highest occupied molecular orbital (HOMO) and/or the lowest unoccupied molecular orbital (LUMO) are/is expected to be most or second-most localized) are indicated by wavy and dotted red lines in each pigment molecule (see Fig. 4, Chapter 22, p. 330); further, overlap of those regions is indicated by a black circle for each pigment pair. See Chapter 22, p. 332.

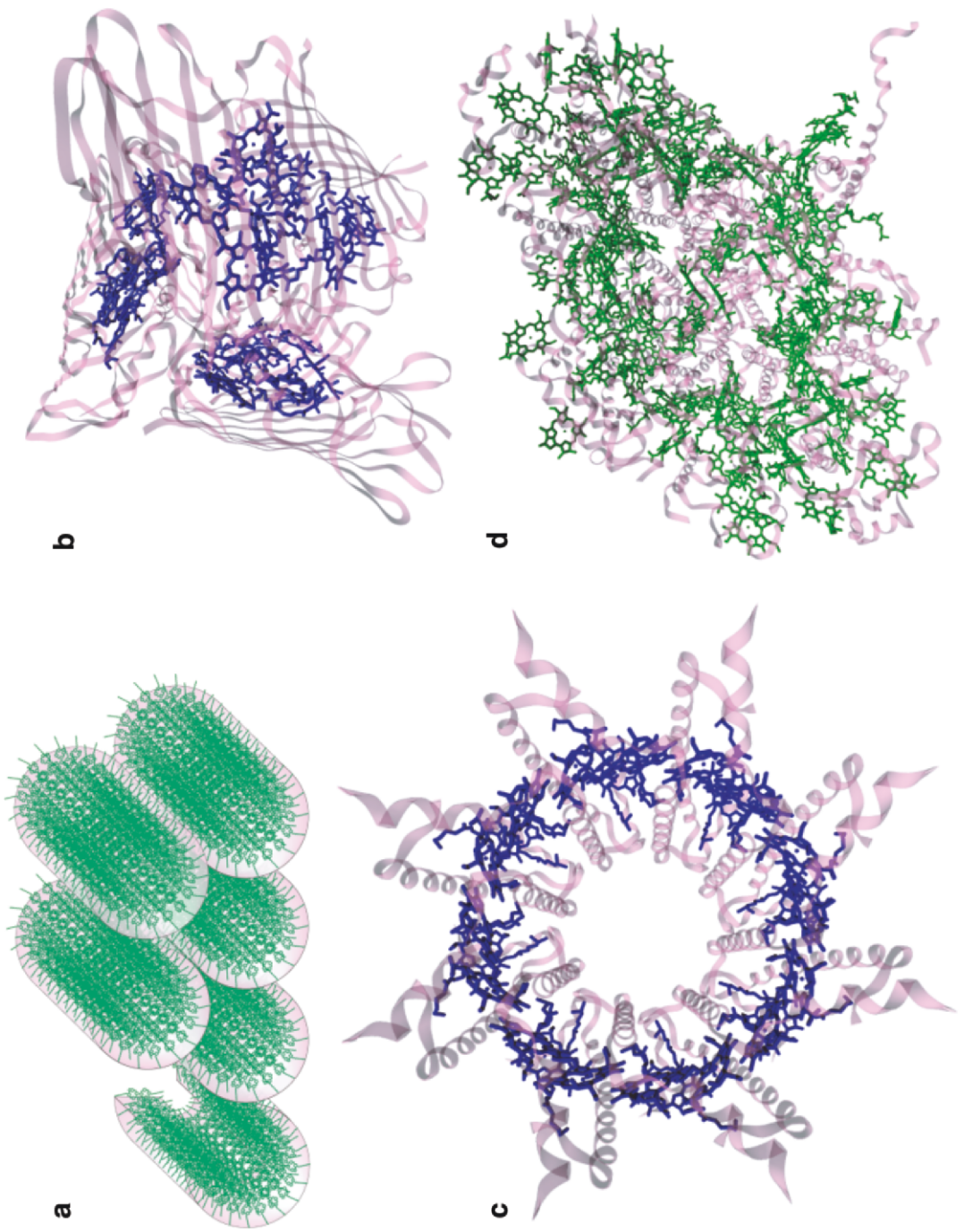

Fig. 1. Examples of various pigment/protein architectures of chlorophyll- and bacteriochlorophyll-protein complexes. (a) Rod like bacteriochlophyll *c* aggregate in chlorosomes of green sulfur bacteria (scheme based on models suggested by van Rossum et al., 2001). (b) Fenna-Matthew-Olson (FMO) protein from *Chlorobium tepidum* (PDB reference 4BCL). (c) Light harvesting complex 2 from *Rhodospirillum molischianum* (PDB reference 1LGH). (d) Reaction center and core light harvesting complex of Photosystem I (PDB reference 1JBO). Images b, c, and d were created with the software VMD (Humphrey et al., 1996). See Chapter 24, p. 351.

(A) Peripheral membrane antennas

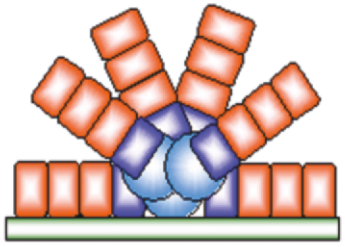

Phycobilisomes

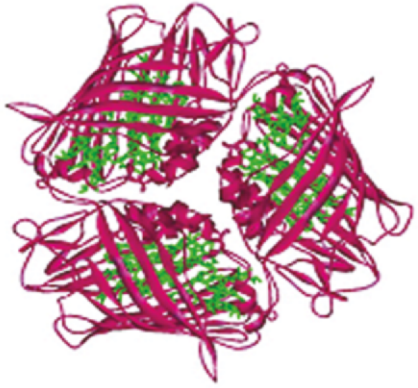

Fenna-Matthew-Olson protein

(B) Fused PSI type RC

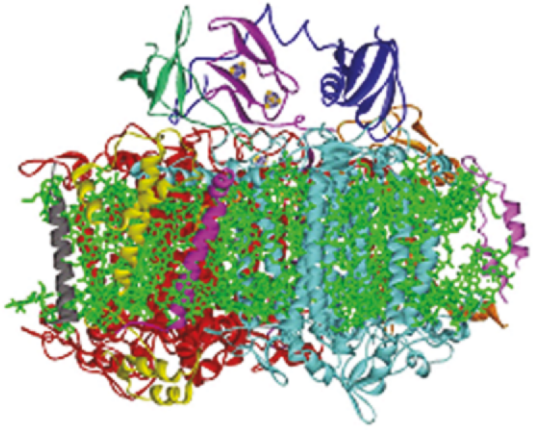

Photosystem I core

(C) Core antennas

CP43 and CP47 from PSII

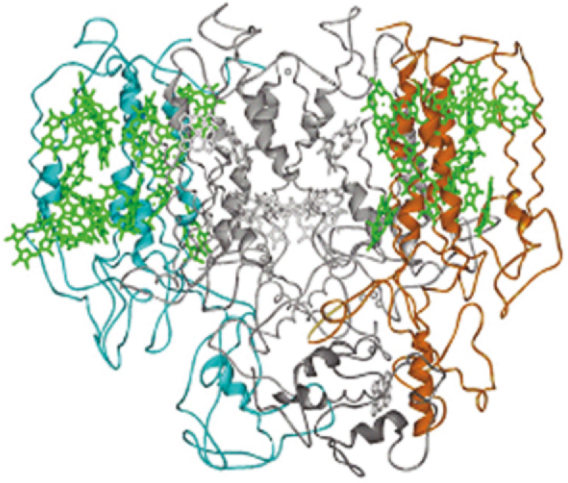

LH1 core

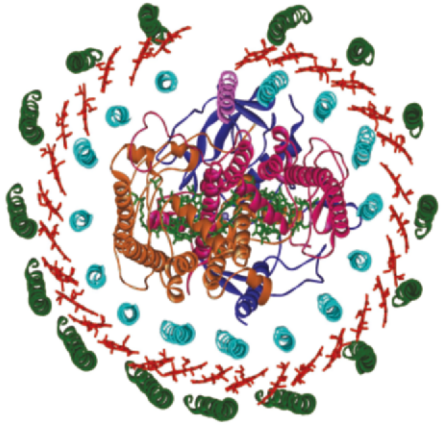

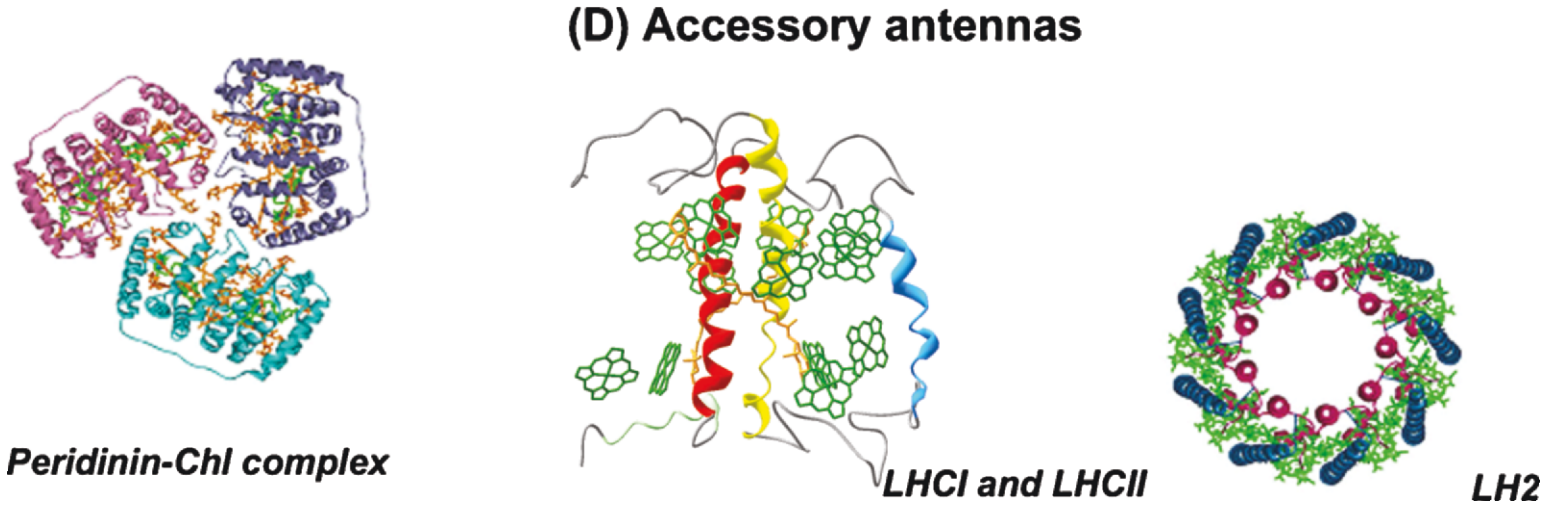

Fig. 1. Classes of light-harvesting antenna complexes. (A) Peripheral antennas: phycobilisomes from cyanobacteria and red algae (schematic); Fenna-Matthew-Olson protein from a green sulphur bacterium *Prosthecochloris aestuarii* (pdb code 4BCL, Tronrud et al., 1986) and peridinin-chlorophyll complex from a dinoflagellate *Amphidinium carterae* (pdb code 1PPR, Hofmann et al., 1996); (B) fused Photosystem I type reaction center from a cyanobacterium *Synechococcus elongatus* (pdb code 1JB0, Jordan et al., 2001); (C) Core antennas: CP43 and CP47 from the Photosystem II of cyanobacterium *Synechococcus elongatus* (pdb code 1FE1, Zouni et al., 2001) and light-harvesting complex 1 core from purple bacterium *Rhodopseudomonas palustris* (1PYH, Roszak et al., 2003); (D) Peripheral antennas: light-harvesting complex I and light-harvesting complex II from algae and higher plants (pdb file of light-harvesting complex II provided by Werner Kühlbrandt, Kühlbrandt et al., 1994) and light-harvesting complex 2 from *Rhodopseudomonas acidophila* (pdb code 1KZU, Prince et al., 1997). Molecular graphics rendered using Web Lab Viewer from Molecular Simulations, Inc. See Chapter 28, p. 403.

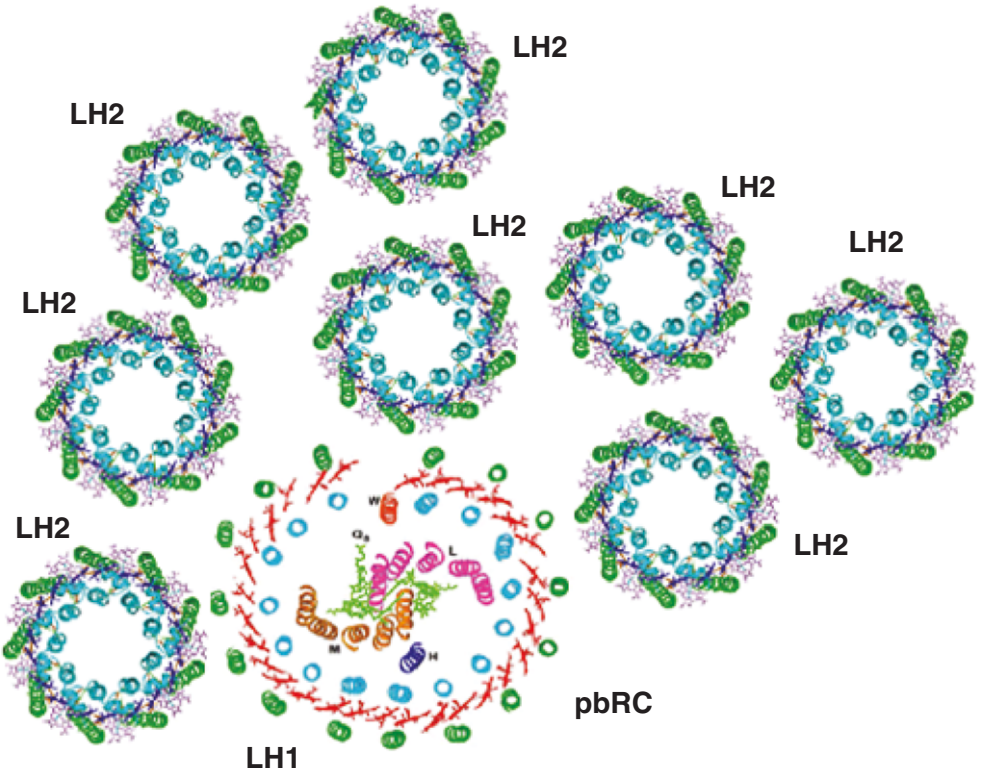

Fig. 1. Structural model of the photosynthetic unit from the purple photosynthetic bacterium *Rhodopseudomonas palustris* (pdb file 1PYH, Roszak et al., 2003*).* See Chapter 28, p. 407.

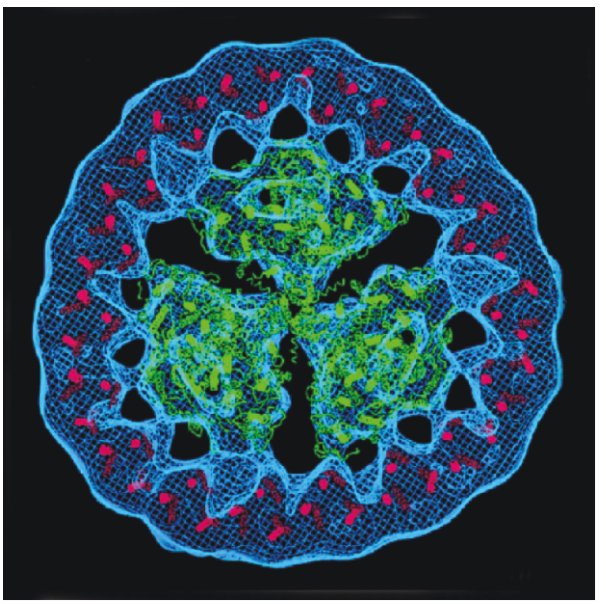

Fig. 2. Structural model of the Photosystem I supercomplex from iron-depleted cyanobacteria. The complex consists of the Photosystem I trimer surrounded by 18 copies of the iron-stress induced CP43-like antenna pigment protein. Figure used with permission from Bibby et al., 2001b. See Chapter 28, p. 407.

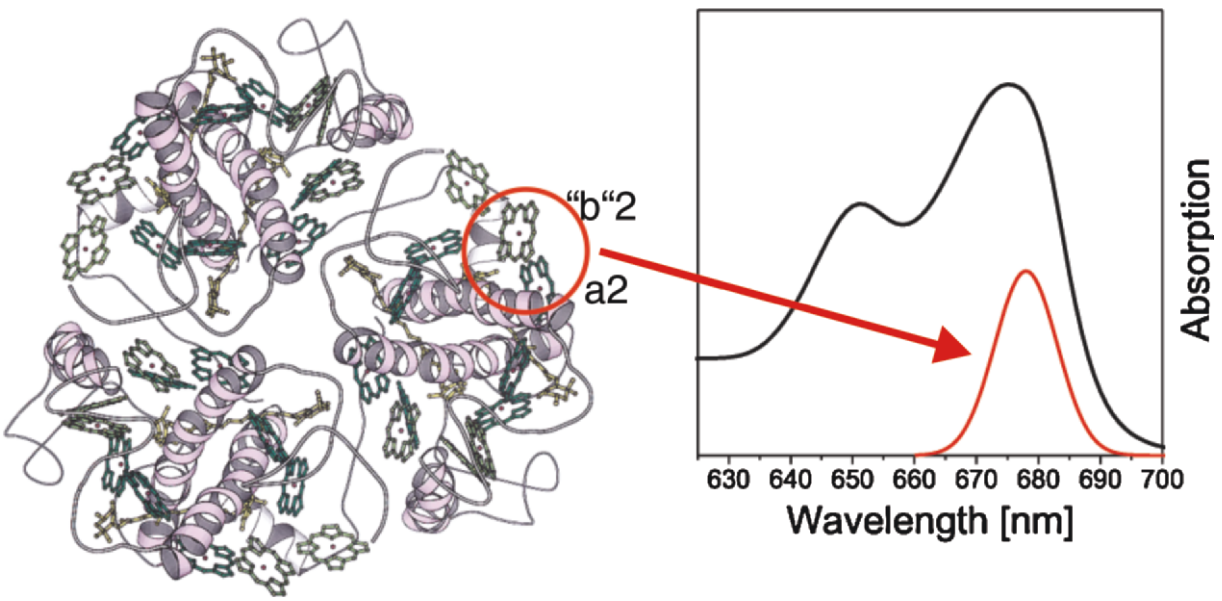

Fig. 1. Structure (left as adapted from Rogl et al., 2002) and its absorption spectrum (right, black line) of light-harvesting complex II. The red-most excitonic transition (peaking at 678 nm, right, red line) can be assigned to a cluster involving the pigment binding sites a2 and "b"2 in the structural model of LHC II (but compare also the recent, refined structure of Liu et al., 2004). See Chapter 29, p. 422.

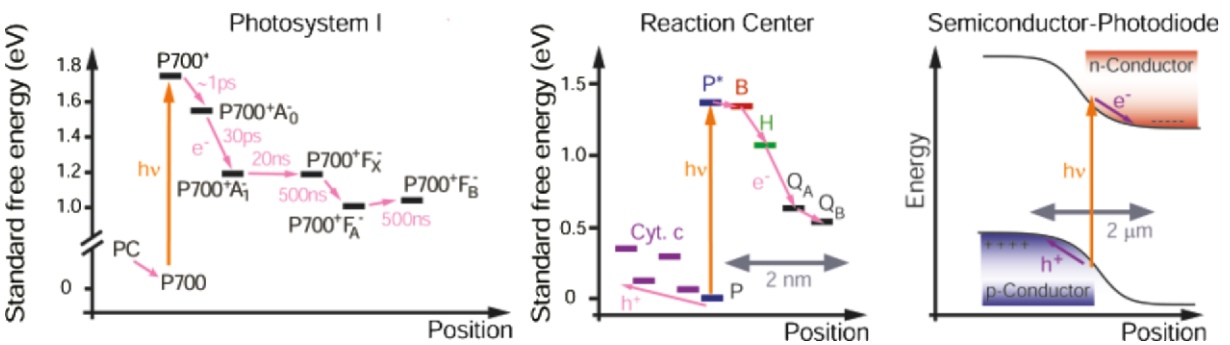

Fig. 2. Energetics of electron transfer (ET) systems. Left: Photosystem I (PS I); middle: bacterial reaction center (RC); right: semiconductor photodiode. For PS I the ET kinetics, electron pathways and energetics of ET intermediates are still under debate: depicted on the left is the schematic arrangement and the energetic positions of the cofactors, as recently discussed in Brettel and Leibl (2001), is depicted on the left. The primary electron donor P700 is a dimer of chlorophyll (Chl) *a* and the chain of electron acceptors consists of a Chl *a* monomer (A_0), a phylloquinone (A_1) and three [4Fe-4S] clusters (F_x, F_A and F_B). The ET steps for purple bacterial RC from *Blastochloris viridis* (center) are discussed in detail in the text. The photoprocesses taking place in the reaction centers resemble those in a photodiode (right). In all systems, light absorption is followed by fast charge separation processes involving both electron and hole transfer. See Chapter 31, p. 447.

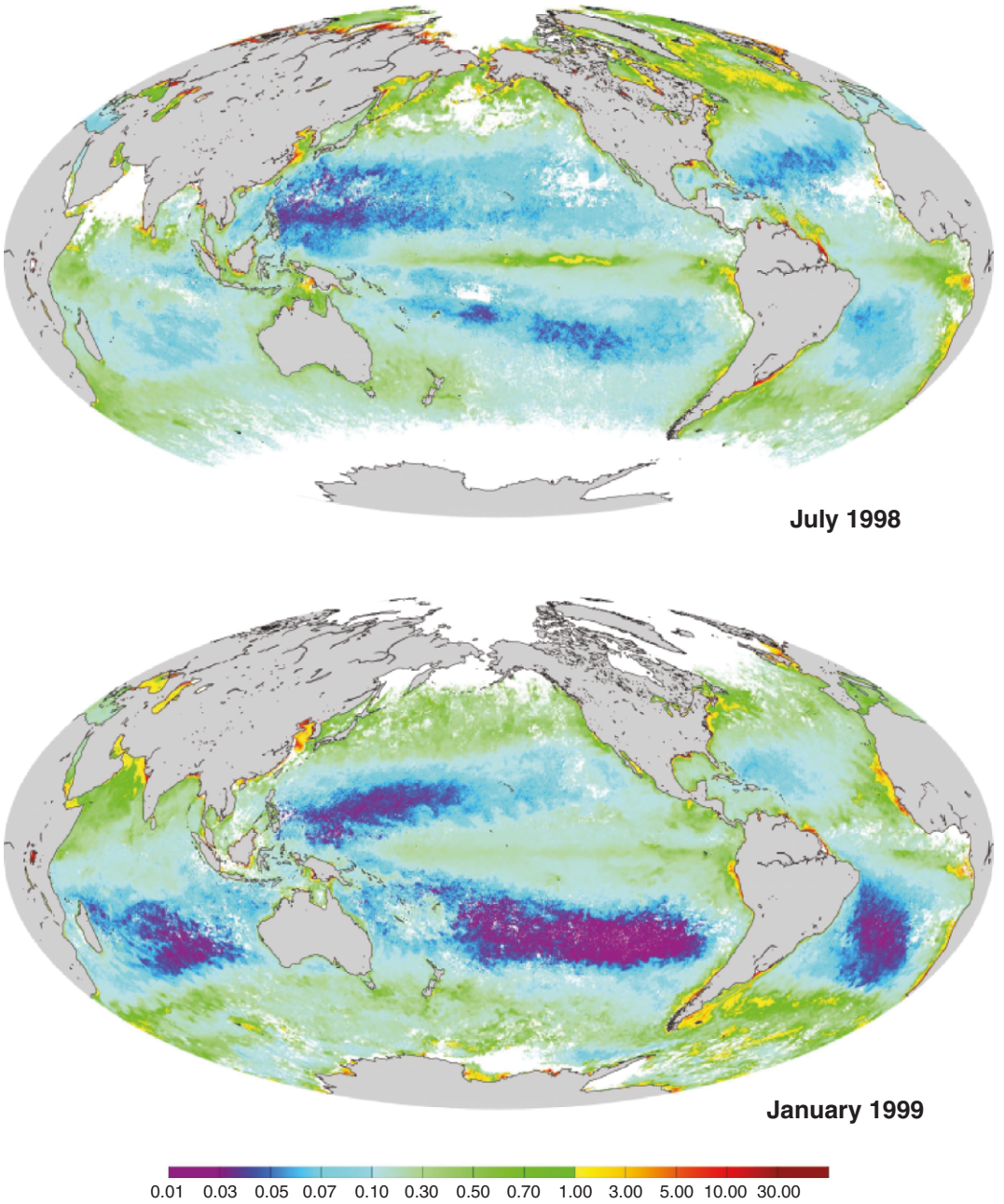

Fig. 1. Examples of global maps of chlorophyll concentration (color encoding indicated) within the oceanic upper layer, as derived from observations by the SeaWiFS sensor. Similar maps are produced on a daily basis; they are, however, incomplete, because of coverage limitations and presence of clouds. By merging daily maps, weekly, monthly, and yearly averages can be produced. Shown here are monthly averaged maps for two opposite seasons, July 1998 and January 1999. Even over one month, some areas remain unseen (clouds masked in white). The high latitude zones, alternatively in the Northern (January) or Southern (July) hemispheres, which are either ice covered or too dark (in the polar night), are also masked in white. These maps show the permanence and extension of the oligotrophic deep blue subtropical gyres and, in-between, of the equatorial divergence which sustains an enhanced algal biomass. Spring-early summer blooms occur alternatively in both hemispheres at latitudes beyond 40°. The upwelling systems, induced by the trade winds, support high biomasses along the coasts of South Africa, Angola, Mauritania, Senegal, Chile and Peru. In the northeast Indian ocean sector, probably one of the most productive zones of the ocean, the situation is more complex because of the alternation of opposite monsoons in summer and winter. See Chapter 36, p. 530.

Chapter 1

An Overview of Chlorophylls and Bacteriochlorophylls: Biochemistry, Biophysics, Functions and Applications

Hugo Scheer*
Department Biologie I – Botanik der Ludwig-Maximilians-Universität, Menzinger Str. 67, D – 80638 München, Germany

Summary

The chlorophylls are a structurally and functionally distinct group of macrocyclic tetrapyrrole pigments that may occur at the porphyrin, chlorin or bacteriochlorin oxidation levels. Biosynthetically, they are derived from protoporphyrin IX. Structurally, they are characterized by the presence of a fifth ring, isocyclic ring E, which confers the prefix 'phyto' to the porphyrin and chlorin type molecules. Chlorophylls generally have Mg as the central metal and a long-chain esterifying alcohol at C-17[3]. Chemically, they are unstable to both acids and bases, to oxidation and light, and have a pronounced tendency for aggregation and/or interaction with their

*Email: hugo.scheer@lmu.de

Bernhard Grimm, Robert J. Porra, Wolfhart Rüdiger and Hugo Scheer (eds): Chlorophylls and Bacteriochlorophylls: Biochemistry, Biophysics, Functions and Applications, pp. 1–26.

molecular environments. Physically, they are characterized by long-lived excited states and by intense absorptions covering, in mono-disperse solutions, the spectral range from 330 to 800 nm, extending in aggregates or in vivo to 1020 nm.

Due to their high absorption and long-lived excited states, chlorophylls are powerful photosensitizers. The efficient, yet safe transduction of this excited state into chemical energy is the basis of photosynthesis. It requires not only a careful balance between productive energy transduction and excess energy degradation processes, but also tight control of the metabolism of chlorophylls. Interference with these controls is the basis of several herbicides. Chlorophylls can also be applied as natural biocides to non-photosynthetic organisms: the subsequent irradiation with light allows for a spatial and temporal control of phototoxicity, for example in photodynamic therapy of cancer.

Chlorophylls have evolved to fulfill several functions in photosynthesis: incorporated into light-harvesting complexes, they strongly absorb light and transfer the excitation energy with quantum efficiencies near 100% to the photosynthetic reaction center complexes where specialized chlorophylls are active in primary charge separation and energy transduction processes. In both complexes, chlorophylls contribute to the stabilization and regulation of the photosynthetic apparatus; also, there is evidence that they may be directly involved in the degradation of excess energy to heat. Chlorophyll precursors also serve as signals in the regulation of photosynthesis and of plastid-nucleus interactions. The functional relevance of the structural features is discussed.

Content and composition of chlorophylls are important physiological and taxonomic parameters of photosynthetic organisms. Critical physiological parameters can be derived from their absorption and, in particular, fluorescence. Both can be remotely monitored from the cellular level to the global scale from outer space.

I. Introduction

Chlorophylls (Chls) are probably the most abundant and certainly the most obvious biological pigments. Widespread in eubacteria and ubiquitous in plants, they are clearly visible from outer space (Chapter 36, Morel). This relatively small group of cyclic tetrapyrroles performs three major functions in photosynthesis which, by using solar energy, drives the fixation of CO_2 into carbohydrates and provides the energetic basis for the global ecosystem. Firstly, in the light-harvesting complexes or antennas, Chls absorb light efficiently and, secondly, they transfer the excitation energy with high quantum efficiency to the reaction centers where, thirdly, the Chls perform the primary charge separation across the photosynthetic membrane: this separation eventually leads to the generation of reductants and also ATP via a simultaneously generated membrane potential. Only few Chls are found unassociated with the photosynthetic light reactions. A Chl *a* molecule with unknown function is present in the electrogenic cytochrome b_6f complex located between the two photosystems in oxygenic organisms (Pierre et al., 1997; Peterman et al., 1998; Kurisu et al., 2003; Stroebel et al., 2003), and several plant species contain non-photosynthetic, water-soluble Chl proteins which may serve for storage or transport of the pigments (Noguchi et al., 1999; Horigome et al., 2003; K. Schmidt et al., 2003), but are also involved in Chl degradation (K. Watanabe et al., 1999). Likewise, Chl-related structures are relatively rare in nature, which is probably due to the high photodynamic potential of these pigments. They include bonellin, the sex-determining pigment of the marine worm *Bonella viridis* (Dhere, 1932; Pelter et al., 1978; Montforts et al., 1990), a visual pigment of dietary origin in certain deep-sea fish (Campbell and Herring, 1987; Douglas et al., 2000), and bioluminescent pigments in *Euphausid* shrimps (Shimomura, 1980; Topalov and Kishi, 2001). Several chlorophyll metabolites have been identified from animal sources (Ma and Dolphin, 1998) including a

Abbreviations: Acc. – Acariochloris; BChl(s) – bacteriochlorophyll(s); BPhe – bacteriopheophytin; B_X, B_y – higher energy absorption bands of tetrapyrroles in the Vis/UV spectral range, also termed Soret band(s); Chl(s) – chlorophyll(s); Chlide(s) – chlorophyllide(s); FMO – Fenna-Mathews-Olson LHC; GG – geranyl-geraniol; GGPP – geranyl-geranyl pyrophosphate; IC – internal conversion; ISC – intersystem crossing; LHC – light-harvesting complex; NIR – near infra-red spectral range (700–1200 nm); NMR – nuclear magnetic resonance; NUV – near ultraviolet spectral range (300–400 nm); P – phytol; Phe(s) – pheophytin(s); PPP – phytyl pyrophosphate; Proto – protoporphyrin IX; PS – Photosystem; Q_x, Q_y – low energy absorption bands of tetrapyrroles in the Vis/NIR spectral range; RC – reaction center (type I and type II relate to the homologies with PS I and PS II, respectively); *Rsp. – Rhodospirillum*; UV – ultraviolet spectral range (200–400 nm); Vis – visible spectral range (400 – 700 nm); ε – molar extinction coefficient [M^{-1} cm^{-1}]; λ – wavelength [nm]

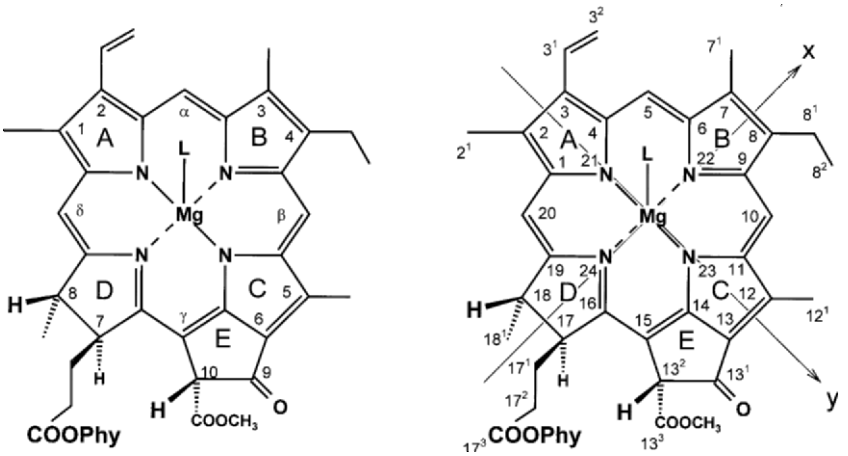

Fig. 1. Chlorophyll *a*: Numbering of rings, C and N-atoms according to Fischer's nomenclature (left) and IUPAC-IUB nomenclature (Moss, 1988) (right). The ligand (L) to the central Mg is shown in the β-position (e.g., above the macrocycle), when it is oriented as shown, with the numbering running clockwise (see footnote). The diagonal arrows in the right structure indicate directions of the two polarization axes, x and y.

variety of pigments with (dark) antioxidant potential from dinoflagellates and marine animals (Karuso et al., 1986; N. Watanabe et al., 1993; Harradine and Maxwell, 1998; Harradine et al., 1996). The tolyporphins are dioxo-bacteriochlorins, lacking the isocyclic ring of Chl, from the cyanobacterium *Tolypothrix tenuis* (*Calothrix* PCC 7601); they may serve a photodynamic defense role (Prinsep et al., 1992, 1998; Minehan and Kishi, 1999). The tunicate *Trididemnum solidum* contains Ni-phytochlorins lacking the 13^2-$COOCH_3$ group and bearing a 3-CH_2OH group that is acylated with a variety of fatty acid alcohols (Bible et al., 1988; Sings et al., 1996): these tunichlorins are clearly derived from chlorophylls. The excited state lifetimes of [Ni]-Chls are so short that photosensitization seems unlikely (Musewald et al., 1999; Fiedor et al., 2000). Chlorophyllous products are also geochemical markers (Chapter 37, Keely). The degradation of chlorophylls in photosynthetic organisms is reviewed in Chapter 17 (Kräutler and Hörtensteiner).

When the photosynthetic apparatus is light saturated, or when the chlorophylls are disconnected from it, the intense absorptions and the long-lived excited states render both Chls and their tetrapyrrole precursors powerful photodynamic agents: when irradiated with visible (vis) or near-infrared (NIR) light in the presence of oxygen, both are capable of generating highly cytotoxic reactive oxygen species. Biosynthesis and degradation of Chls are therefore tightly controlled and co-regulated with the other parts of the photosynthetic apparatus, and several precursors have, vice versa, been directly implicated in affecting regulatory processes (Chapter 10, Grimm and Rüdiger; Chapter 11, Beale; Chapter 12, Jahn et al.; Chapter 13, Yaronskaya and Grimm; Chapter 16, Beck and Grimm). When present in excessive concentrations in photosynthetic organisms, or when incorporated into non-photosynthetic organisms, the photodynamic activities of Chls and their tetrapyrrole precursors can be exploited, for example, as herbicides (Rebeiz et al., 1990), insecticides (Rebeiz et al., 1995) or anti-tumor agents (Chapters 32, 33, Brandis et al.).

Most Chls and bacteriochlorophylls (BChls) are bound to proteins, where they contribute to the

**The nomenclature and numbering system* used throughout this book is that recommended by the Joint Commission on Biochemical Nomenclature (JCBN) of the International Union of Pure and Applied Chemistry and International Union of Biochemistry (IUPAC-IUB) which is described by Moss (1988). The recommended but cumbersome omission-resubstitution nomenclature is not used: substitutions are indicated by placing the modified group in square brackets [ ]; thus, 3-devinyl-3-acetyl-Chl *a* becomes [3-acetyl]-Chl *a*. The esterifying alcohol is generally indicated as a subscript, so that BChl *a* esterified with phytol (P) becomes BChl a_p and BChl *b* esterified with phyta-2,10-dienol becomes BChl $b_{\Delta 2,10}$. The central Mg is always ligated and ligation from above the macrocycle, when it is orientated with the numbering running clockwise, is denoted 'β' and indicated by a solid line (see Fig. 1) while α ligation, from the bottom, is indicated with a dashed line (Moss, 1988; Balaban, 2002).

folding and stabilization of the polypeptide chain. Chl-proteins are unusual in the number of cofactor molecules they can bind; for example, 14 Chls plus 4 carotenoids are bound to only 250 amino acids in LHC II (Chapter 26, Paulsen). In the green bacteria, capable of growing at exceedingly low light intensities (Overmann and Schubert, 2002; Blankenship and Matsuura, 2003), this concentration has reached an extreme, since current models even suggest that no protein is directly involved in the short-range organisation of their peripheral antenna, the chlorosome (Chapter 20, de Boer and de Groot). The driving forces for such a dense packing are twofold: firstly, it ensures a high light absorption per unit volume and, secondly, it reduces the amount of protein needed per chromophore thus saving energy input into protein biosynthesis which becomes the more advantageous at the lower light intensities where the cells are growing. A potential danger of dense packing, however, is the so-called 'concentration quenching.' This quenching can be imagined as a statistical process. There is a certain chance that a pigment molecule is defective such that its excited state is very short-lived and relaxes by rapid internal conversion to the ground state. If this pigment is isolated, the effect is negligible but when this defective pigment molecule is tightly coupled to others, it will act as a sink and degrade any excitation of the entire coupled unit to heat, in a time that corresponds to the (average) transfer time from any pigment of the unit to the defective molecule. Therefore, chlorophyll aggregates generally show negligible fluorescence and an extreme shortening of excited state lifetimes (Sauer, 1975, Katz et al., 1976; Scherz et al., 1991). Expanding on this scenario, the photosynthetic apparatus can be viewed as an assembly of pigments in which concentration quenching has evolved from a random to a tightly controlled process where the reaction centers are the productive sinks, leading to 'photochemical quenching' of the excitation: other centers, in particular certain carotenoids, act as safety valves by 'non-photochemical quenching' (Chapter 36, Nedbal and Koblizek).

II. Structures

A. Structures and Distribution

The term chlorophyll, the green (Greek *chloros*) of leaves (Greek *phyllos*), was introduced in 1818 (Pelletier and Caventou, 1818) for the pigment(s) extracted from leaves with organic solvents. It was recognized as a mixture of pigments by (partly undisclosed) spectroscopic and solvent partition techniques (Stokes, 1864; Fremy, 1877), but made most obvious perhaps by Tswett's chromatography (Greek *chromos* = color, *graphein* = to write) that separated the blue Chl *a*, the green Chl *b* and several yellow to orange carotenoids (Tswett, 1906). The structural relationship of the tetrapyrrole moiety of Chls *a* and *b* to that of heme, the structure of which was elucidated in 1928 by Hans Fischer's group (Fischer and Stangler, 1927), was suggested early (Verdeil, 1851) although it was based on false evidence. The structural similarity was verified later (Hoppe-Seyler, 1880; Marchlewski, 1909; Willstätter and Stoll, 1913). The latter two books summarized Chl chemistry for the first time. Important aspects of the hydrophobic part of the molecule, phytol, were first identified by Willstätter (1907), including its likely relationship to the isoprenoids. The structure of Chl *a* was established in 1942 (Fischer and Strell, 1947), as the result of more than ten years of work mainly by the groups of Hans Fischer and James Conant (summarized in Fischer and Orth, 1940). The total synthesis of the tetrapyrrole moiety was completed by the groups of Strell in 1962 (Strell and Kalojanoff, 1962) and of Woodward in 1960 using a more rigorous approach (Woodward, 1961). The total synthesis of phytol, the isoprenoid moiety of Chl *a,* was completed a year earlier (Burrell et al., 1959). Chl *a* contains six asymmetric centers: the absolute stereochemistry (Fig. 2A) of the asymmetric C-13[2], C-17 and C-18 of the tetrapyrrole macrocycle was elucidated by Fleming (1967), and those of the asymmetric C-7 and C-11 of phytol by Burrell et al. (1959) and Crabbe et al. (1959). Addition of a single or two different extra ligands to the central Mg creates a sixth asymmetric center, which is of importance in Chl proteins (Balaban et al., 2002; Oba and Tamiaki, 2002).

Based on these structures, nearly 100 Chls are known today, with the majority of structures occurring in anoxygenic bacteria, in particular, in the green bacteria. Chls are now defined as cyclic tetrapyrroles carrying a characteristic isocyclic five-membered ring, that are functional in light-harvesting or in charge separation in photosynthesis. The IUPAC-IUB numbering of Chl *a* (Fig. 1) reflects the fact that the isocyclic ring is derived from the C-13 propionic acid side-chain of the common heme and Chl precursor, protoporphyrin IX (Proto) (Moss, 1988). The Chls

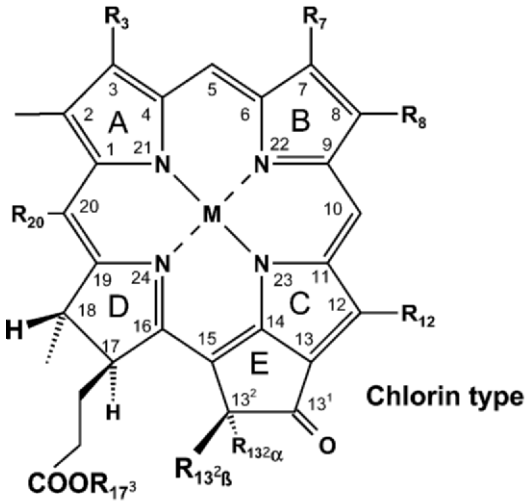

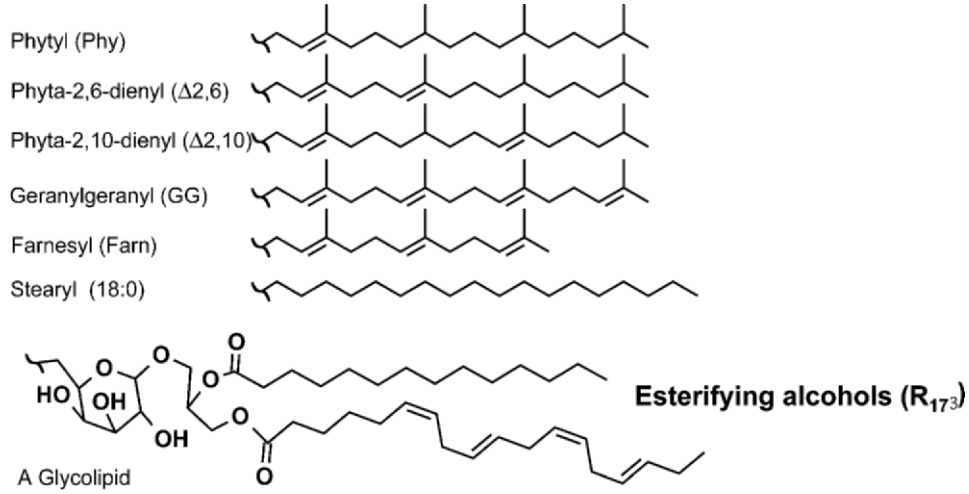

Pigment	Abbreviation	R_3	R_7	R_8	R_{12}	$R_{13}^2{}_\alpha$	$R_{13}^2{}_\beta$	R_{17}^3	R_{20}	M	Rem.
Chlorophyll a	Chl a	C_2H_3	CH_3	C_2H_5	CH_3	$COOCH_3$	H	Phy	H	Mg	a)
Chlorophyll a'	Chl a'	C_2H_3	CH_3	C_2H_5	CH_3	H	$COOCH_3$	Phy	H	Mg	
[8-Vinyl]-chlorophyll a	[8-Vinyl]-Chl a	C_2H_3	CH_3	C_2H_3	CH_3	$COOCH_3$	H	Phy	H	Mg	b)
[8-Hydroxyethyl]-chlorophyll a_F	[8-Hydroxyethyl]-Chl a_F	C_2H_3	CH_3	C_2H_4OH	CH_3	$COOCH_3$	H	Farn	H	Mg	
Chlorophyll b	Chl b	C_2H_3	CHO	C_2H_5	CH_3	$COOCH_3$	H	Phy	H	Mg	
[8-Vinyl]-chlorophyll b	[8-Vinyl]-Chl b	C_2H_3	CHO	C_2H_3	CH_3	$COOCH_3$	H	Phy	H	Mg	b)
Chlorophyll d	Chl d	CHO	CH_3	C_2H_5	CH_3	$COOCH_3$	H	Phy	H	Mg	
Chlorophyll d'	Chl d'	CHO	CH_3	C_2H_5	CH_3	H	$COOCH_3$	Phy	H	Mg	
Pheophytin a	Phe a	C_2H_3	CH_3	C_2H_5	CH_3	$COOCH_3$	H	Phy	H	H_2	
Bacteriochlorophyll c	BChl c	CHOH-CH_3	CH_3	$CH_2CH_n(CH_3)_{3-n}$	CH_3/C_2H_5	H	H	Farn/others	CH_3	Mg	c)
Bacteriochlorophyll d	BChl d	CHOH-CH_3	CH_3	$CH_2CH_n(CH_3)_{3-n}$	CH_3/C_2H_5	H	H	Farn/others	H	Mg	c)
Bacteriochlorophyll e	BChl e	CHOH-CH_3	CHO	$CH_2CH_n(CH_3)_{3-n}$	CH_3/C_2H_5	H	H	Farn/others	CH_3	Mg	c)
Bacteriochlorophyll f	BChl f	CHOH-CH_3	CHO	$CH_2CH_n(CH_3)_{3-n}$	CH_3/C_2H_5	H	H	Farn/others	H	Mg	d)

Fig. 2. A: Phytochlorin-type chlorophylls (single bond between C-17/C-18) and esterifying alcohols of chlorophylls. Numbering according to IUPAC-IUB (Moss, 1988). Note that pheophytins lack the central Mg. Footnotes: a) Chl a_F esterified with farnesol has been identified in green sulfur bacteria (see Chapter 4, Kobayashi et al.) b) Pigment is often also termed divinyl-chlorophyll *a* (DV-Chl *a*) to distinguish it from 'normal' (= monovinyl (MV-)) Chl *a*. c) Complex mixture of pigments with varying substituents at C-8 (= R_3), C-12 (= R_4), C-17^3 (= R_7) and epimers at the asymmetric C-3^1. The prevailing sterochemistry at C-3^1 changes from R to S with increasing size of the C-8 substituent R_3. d) Hypothetical

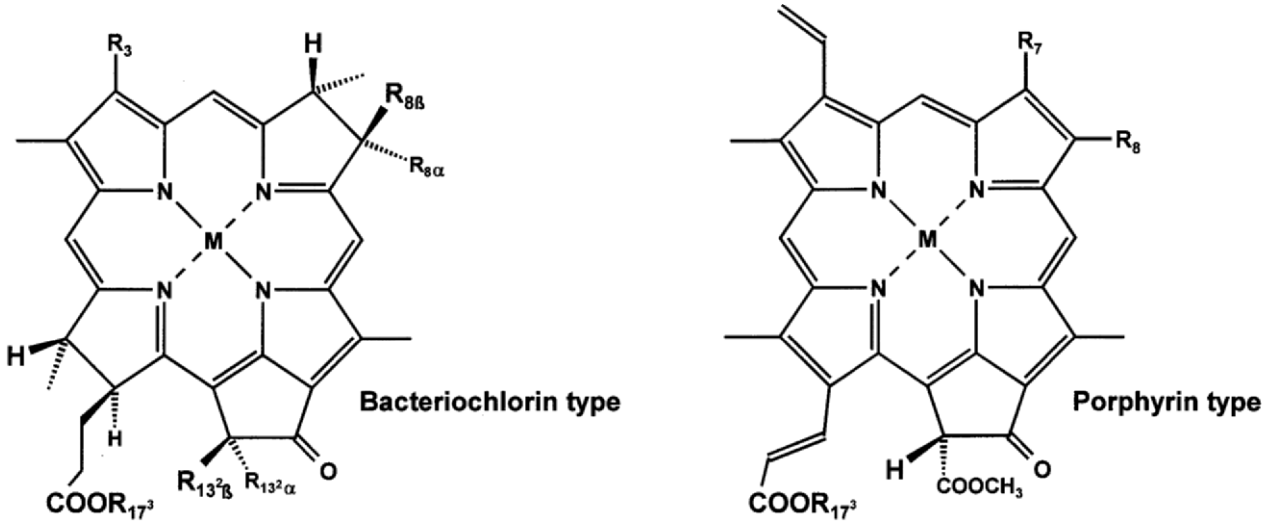

Pigment	Abbreviation	R_3	R_7	$R_{8\alpha}/R_{8ß}$	$R_{13^2\alpha}$	$R_{13^2ß}$	R_{17^3}	M	Rem.
Bacteriochlorophyll a	BChl a	$COCH_3$		H/C_2H_5	$COOCH_3$	H	Phy	Mg	a)
Bacteriochlorophyll a'	BChl a'	$COCH_3$		H/C_2H_5	H	$COOCH_3$	Phy	Mg	a)
Bacteriochlorophyll a_{GG}	BChl a_{GG}	$COCH_3$		H/C_2H_5	$COOCH_3$	H	GG	Mg	a,c)
[Zn]-Bacteriochlorophyll a	Zn-BChl a	$COCH_3$		H/C_2H_5	$COOCH_3$	H	Phy	Zn	a)
Bacteriochlorophyll b	BChl b	$COCH_3$		$=CH-CH_3$	$COOCH_3$	H	Phy	Mg	a)
Bacteriochlorophyll $b_{\Delta 2,10}$	BChl $b_{\Delta 2,10}$	$COCH_3$		$=CH-CH_3$	$COOCH_3$	H	Δ2,10	Mg	a,c)
Bacteriochlorophyll g	BChl g	C_2H_3		$=CH-CH_3$	$COOCH_3$	H	GG	Mg	a)
Bacteriochlorophyll g'	BChl g'	C_2H_3		$=CH-CH_3$	H	$COOCH_3$	GG	Mg	a)
Bacteriopheophytin a	BPhe a	$COCH_3$		H/C_2H_5	$COOCH_3$	H	Phy	H_2	a)
Bacteriopheophytin b	BPhe b	$COCH_3$		$=CH-CH_3$	$COOCH_3$	H	Phy	H_2	a)
Chlorophyll(ide) c_1	Chl(ide) c_1		CH_3	C_2H_5			H	Mg	b,d,e)
Chlorophyll(ide) c_2	Chl(ide) c_2		CH_3	C_2H_3			H	Mg	b,d,e)
Chlorophyll(ide) c_3	Chl(ide) c_3		$COOCH_3$	C_2H_5			H	Mg	b,d,e,f)
Protochlorophyll(ide) a	PChl(ide) a		CH_3	C_2H_5			H	Mg	b,d,g)
[8-Vinyl]-Protochlorophyll(ide) a	[8-Vinyl]-PChl(ide) a		CH_3	C_2H_3			H	Mg	b,d,g)

Fig. 2. B. Bacteriochlorin-type chlorophylls (single bonds between C7/C8 and C-17/C-18, left) and phytoporphyrin-type chlorophylls (right). Numbering according to IUPAC-IUB (Moss, 1988). Note the distinction between chlorophylls (Chl, esterified at C-17^3, R_3 = esterifying alcohol) and chlorophyllides (Chlide, free C-17^3 acid group, R_3 = H), which is often blurred in the literature, in particular on Chls *c*. Footnotes: a) Bacteriochlorin. b) Porphyrin. c) Sometimes esterified with other alcohols. d) Generally free acid, esters found as minor pigments. An extreme case is the glycolipid shown in Fig. 2A . e) Sterochemistry at C-13^2 uncertain. f) Probably mixture with $R_3 = C_2H_3$ and C_2H_5. g) No $17^1/17^2$ double bond.

generally carry Mg as the central metal and, further, a sesqui- (C_{15}) or di-terpenoid (C_{20}) alcohol esterified to the C-17 propionic acid side chain (Fig. 2A), but there are exceptions to both of these characteristics. There are tetrapyrrolic pigments which function in electron or energy transfer, but do not have the central Mg: the central metal is *either* lacking as in the pheophytins, which are involved in electron transfer in type II reaction centers (Satoh, 1993; Dimagno and Norris, 1993), *or* is replaced by Zn in a group of acidophilic purple bacteria (Wakao et al., 1996) (Chapter 4, Kobayashi et al.). Further, large variations in the esterifying alcohols are found in bacteriochlorophylls (BChls) *c, d* and *e* (Fig. 2A; Chapter 15, Friegaard et al.), and most of the *c*-type Chls lack an esterifying alcohol (Fig. 2B; Chapter 3, Zapata et al.).

A major distinction among the various classes of Chls which defines very characteristic spectral features is the degree of unsaturation of the macrocycle (see Fig. 3; Weiss, 1978; Hanson, 1991; Scheer, 2003). The fully unsaturated phytoporphyrin macrocycle, present in the *c*-type chlorophylls of chromophyte algae and some prokaryotes (Fig. 2B), is characterized by an intense absorption in the blue spectral region (Soret or B-bands, $\varepsilon \approx 150{,}000$) and only a moderate absorption in the region around 620 nm (Q_y-bands $\varepsilon \approx 20{,}000$). The phytochlorin system, which is a 17,18-*trans*-dihydrophytoporphyrin, is present in Chls *a, b* and *d* of oxygenic organisms and also in BChls *c, d* and *e* of green anoxygenic bacteria (Fig. 2A). These pigments have (in organic solvents) absorption bands around 440 and 660 nm of equal intensity ($\varepsilon \approx 100{,}000$), with a conspicuous gap in the green spectral region. The bacteriochlorin macrocycle is a 7,8-*trans*,17,18-*trans*-tetrahydrophytoporphyrin system found in BChl *a, b* and *g* of anoxygenic bacteria (Fig. 2B). Here the two major bands ($\varepsilon \approx 100{,}000$) have even moved farther apart into the near ultraviolet (NUV, 350–400 nm) and near infrared (NIR) spectral regions. These pigments also have an appreciably strong absorption in the visible range (Q_x, $\varepsilon \approx 15{,}000$), which has been recognized as a marker band for the state of ligation and H-bonding (T. A. Evans and Katz, 1975; Chapter 34, Yerushalmi et al.). Obviously, the generic nomenclature of the Chls does not relate in a unique way to their degree of unsaturation nor does it necessarily reflect their origin since bacteriochlorophylls include both bacteriochlorins and phytochlorins, while the cyanobacteria also contain the same phytochlorin type Chls as possessed by green plants.

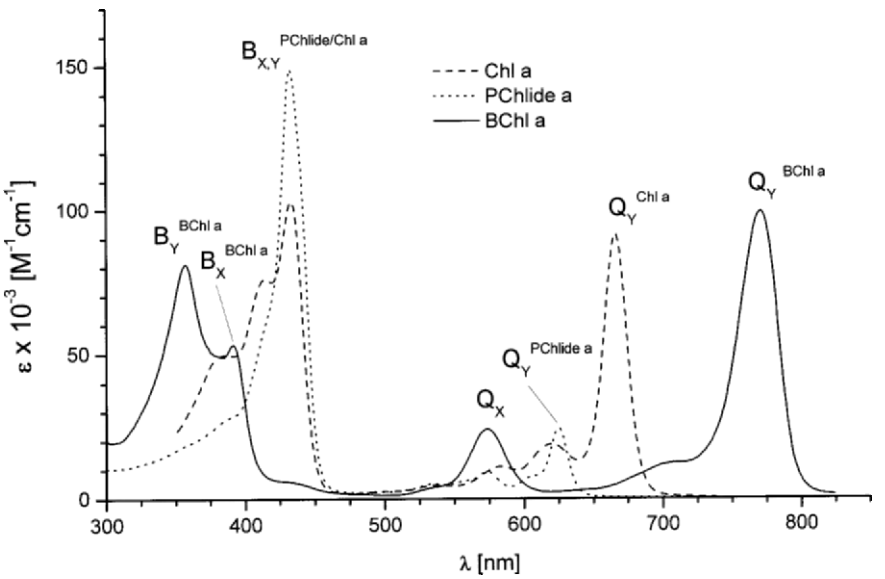

Fig. 3. Absorption spectra of chlorophylls in monodisperse solutions showing the influence of the conjugation system on spectra. Shown are type-spectra of the phytoporphyrin type (PChlide *a* = protochlorophyllide *a*), the phytochlorin type (Chl *a* = chlorophyll *a*) and the bacteriochlorin type (BChl *a* = bacteriochlorophyll *a*) and the assignments of the major absorption bands according to the four-orbital model (Weiss, 1978; L.K. Hanson, 1991). The author is indebted to M. Kobayashi for providing a concise list of extinction coefficients of chlorophylls.

B. 'Green' Chlorophylls of Oxygenic Organisms: Chlorophylls a, b, and d

The most abundant Chl, Chl *a* (Figs. 1, 2A), is present in the reaction centers and the core antennas of almost all oxygenic organisms (Tables 1 and 2). In green algae and plants it is the major pigment of the peripheral antenna complexes and, in a slightly modified form carrying a second vinyl group at C-8 (see Fig. 2A), also occurs in the type II cyanobacteria, sometimes referred to as prochlorophytes (Goericke and Repeta, 1992; Chapter 4, Kobayashi et al.). Its absorption maxima are intense, but restricted to two narrow bands at the edges of the visible spectrum (≈430 and ≈680 nm); it is, therefore, almost always accompanied by other pigments to broaden the absorption range for photosynthetically active radiation. These supplementary pigments are in many cases other Chls. The type II cyanobacteria and the green photosynthetic eukaryotes (green algae, plants) contain Chl *b* (Fig. 2A). With absorption maxima at $\lambda_{max} \approx 460$ and $\lambda_{max} \approx 650$ nm, Chl *b* reduces the green absorption gap to the spectral region between 500 and 600 nm. Chl *d*, a relatively rare pigment of the phytochlorin-type (see Fig. 2A), has distinctly red-shifted absorption maxima as compared to Chl *a*. Originally reported in red algae (Allen, 1966), Chl *d* has now been identified as the major pigment in several oxygenic prokaryotes, including *Acaryochloris* (*Acc.*) *marina* (Miyashita et al., 1997), which also contain Chl *c* (Chapter 4, Kobayashi et al.; Chapter 18, Larkum). Chl *d* largely replaces Chl *a*, including in the primary donor of PS I (Hu et al., 1998), while the pheophytin acceptor and possibly (part of) the primary donor remain Phe *a* and Chl *a*, respectively (Itoh et al., 2001; Mimuro et al., 2004; Chen et al., 2005; Tomo et al., 2005).

Table 1. Occurrence and functions of major chlorophylls (majaor pigments bold, minor pigments in brackets). 'A' denotes antenna or light-harvesting pigments, 'R' reaction center pigments. See Figs. 2 A,B for structures, and Chapter 4 for occurrence and functions of minor chlorophylls.

Pigment / Organism[a]	Chloroflexaceae	Chlorobiaceae	Heliobacteria	Purple bacteria	Cyanophyta I[b], Glaucophyta	Cyanophyta II[b]	Rhodophyta	Heterokonts	Bacillariophyceae (Diatoms)	Cryptophyta	Dinophyta (Dinoflagellates)[c]	Euglenophyta	Chlorarachniophyta	Prasinophyceae	Chlorophyceae	Green plant plastids
Chlorophyll *a*					AR	AR	AR	AR	AR	AR	AR	AR	AR	AR	AR	AR
[8-Vinyl]-Chlorophyll *a*						AR										
Chlorophyll *b*						A					(A)[c]	A	A	A	A	A
[8-Vinyl]-Chlorophyll *b*						A										
Chlorophylls *c*						(A)		A	A		(A)[c]			A		
Chlorophyll *d*						AR[d]	(A)									
Bacteriochlorophyll *a*	AR	AR		AR												
Bacteriochlorophyll *b*				AR												
Bacteriochlorophylls *c,d*	A	A														
Bacteriochlorophylls *e*		A														
Bacteriochlorophyll *g*			AR													

a) See Green et al. (2003) for taxonomy of algae; b) Cyanophyta I have the classical pigmentation (Chl a plus phycobilins). Cyanophyta II contain Chl *b* in addition to Chl *a*, some abundant marine strains contain large amounts of [8-vinyl]-Chl *a* and *b* (Goericke and Repeta, 1992). c) Pigmentation depends on endosymbiotic photosynthetic organisms, which can be useful as phylogenetic markers. d) Identified only in few species, but here the major pigment. *Acc. marina* (cyanophyta) contains mainly Chl *d*, traces of Chl *a* and Chl *c* and biliproteins (Marquardt et al., 1997)

C. 'Green' Chlorophylls of Anoxygenic Bacteria: Bacteriochlorophylls c, d and e

Both green filamentous bacteria, such as *Chloroflexus aurantiacus,* and green sulfur bacteria like *Chlorobium tepidum,* contain large amounts of a group of closely structurally related, but diverse Chls of the phytochlorin type, namely, BChls *c, d, e*: the anticipated BChl *f*, homologous to BChl e but lacking the C-20 methyl group, is yet to be found in nature (Fig. 2A). In solution, the absorption spectra of BChl *c* and *d* are very similar to that of Chl *a*, and those of BChls *e* and *f* carrying a 7-CHO group are very similar to that of Chl *b*. In situ, the absorption maxima of BChls *c, d* and *e* are strongly red-shifted to 700–750 nm. This red-shift is due to a unique form of aggregation which is related to the presence of the 3^1-OH group and the absence of the sterically demanding 13^2-$COOCH_3$ substituent. It can be mimicked well in vitro by self-organizing aggregates of structurally related porphyrins, chlorins and bacteriochlorins (Balaban et al., 2004; Kunieda et al., 2004; Tamiaki et al., 2004b; Chapter 20, de Boer and de Groot). A similar type of aggregation is probably the key

Table 2. Location, functions and basic spectroscopic properties of photosynthetic pigments. The author is indebted to M. Kobayashi for providing a concise list of extinction coefficients of chlorophylls.

Pigment	Type	Location [a)]	Function	Absorption in solution[b)] λ_{max} (ε) [solvent]	Emission in solution [b,c)] λ_{max} [solvent]	Absorption in situ λ_{max}	Ref [d)]
Chl *a*	Phytochlorin	PA, CA, RC	LH, ET	430, 662(78.8) [A] 430,662(90)[D]	668 [A] 666 [D]	~440, 670-720	1,2[f)]
Phe *a*	Phytochlorin	RC	ET	408,505,534,667(55.2)[D]	673[D]	~680	2,3
Chl *b*	Phytochlorin	PA	LH	457,646(46.6)[A] 454,644(56.3)[D]	652 [A] 646 [D]	~460, 630-680	1,2 [f)]
Chl *c* [g]	Phytoporphyrin	PA	LH	446,578,629(23.9)[AP] 446,579,628[D]	~633 [A][a]	~400, 500-620	1
Chl *d*	Phytochlorin	PA, CA, RC	LH, ET	447, 688 (98.3)[D]	695[D]	~440, ~690	4
BChl *a*	Bacteriochlorin	PA, CA, RC	LH, ET	357,391,573,772(91)[D] 365,608,772(60)[M]	800	<400, ~600, 800–960	2 [f)], 4,5
Bphe *a*	Bacteriochlorin	RC	ET	357,525,749(66.2)[D]	762[D]	770	2,6
BChl *b*	Bacteriochlorin	PA, CA, RC	LH, ET	368,408,578,794(106)[D] 368,407,582,795 [A]	810	<400, ~600, 800–1020	4[f)]
Bphe *b*	Bacteriochlorin	RC	ET	398,776(1:0.42)[D]	785[D]	780-795	7,8
BChl *c*	Phytochlorin	PA	LH	432,622,660 (92.7) [D] 435,620,670 (70,9) [M]	667[D]	~460, 730-760	2 [f)],4[e)]
BChl *d*	Phytochlorin	PA	LH	425,612,650 (87.9) [D] 427,612,659 (64) [M]		~440,720-750	4[e,f)]
BChl *e*	Phytochlorin	PA	LH	338,456,594,649(48.9) [A] 476, 660(41)[M]		~460,~715	9[f)]
BChl *g*	Bacteriochlorin	CA, RC	LH, ET	365,405,566,762(76)[A] 364,767(0.8:1) [D]		<400, 780-850	7,10

a) PA = peripheral antenna, CA = core antenna, RC = reaction center; b) λ_{max} in nm, ε in $cm^{-1}mM^{-1}$, solvent abbreviations: A = acetone, AP = acetone/1% pyridine, D = diethylether, DO = dioxan, M = methanol; c) The fluorescence yield of the pigments varies with their environment; d) 1 = Jeffrey et al., 1997; 2 = Goedheer, 1966; 3 = Germano et al., 2001; 4 = Oelze, 1985; 5 = Permentier et al., 2001; 6 = J. H. C. Smith and Benitez, 1955; 7 = M. Kobayashi, personnel communication; 8 = H. Scheer, unpublished; 9 = Borrego et al., 1999; 10 = Kobayashi et al., 1992; e) extinction coefficients calculated from specific extinction coefficients using the 8-ethyl-11-methyl-17^4-farnesyl structures; f) see Chapter 7 (Porra) for extinction coefficients in other solvents; g) family of pigments, absorptions vary with structure, in Chl $c_{1,2}$ and [8-Vinyl]-Pchlide *a* the band at ≈625 is more intense than that at ≈580 nm, in Chl c_3 and Chl $c_{CS\text{-}170}$ it is less intense.

to the tight packing of these pigments in the unique peripheral antenna of green bacteria, the extra-membranous chlorosomes (Blankenship and Matsuura, 2003), where pigment-protein interactions seem to play little or no role (Niedermeier et al., 1992) in the long-range organization (Chapter 6, Kobayashi et al.; Chapter 20, de Boer and de Groot).

In spite of their names, BChls *c, d* and *e* are not bacteriochlorins, but phytochlorins. Their unifying structural features are the lack of the 13^2-$COOCH_3$ substituent on the isocyclic ring, and the presence of a CHOH-CH_3 substituent at C-3. The biosynthesis of these three BChls is only now beginning to be unravelled (Senge and K. M. Smith, 1995; Chapter 15, Friegaard et al.). The following five additional features of these BChls generate a remarkable structural diversity, the significance of which is only partly understood at present (Oelze and Golecki, 1995; Senge and K. M. Smith, 1995; Kunieda et al., 2004; Tamiaki et al., 2004a,b). Firstly, the *c*-and *e*-type BChls are characterized by a 20-CH_3 substituent, which is lacking in BChls *d* and *f*. In both cases, steric hindrance of the C-20 methyl group induces, in vitro and in vivo, a red-shift (~10 nm) when compared to the respective C-20 unsubstituted pigment. Secondly, BChl *e* type homologues (as well as the putative BChl *f*) carry a 7-CHO substituent like Chl *b*, leading to similar spectral characteristics as for Chl *b*. Thirdly, they show large variations in the esterifying alcohols (Larsen et al., 1995; Caple et al., 1978; Glaeser et al., 2002; Chapter 15, Frigaard et al.; Chapter 37, Keely). Fourthly, the pigments can be methylated once (at $C\text{-}12^1$ or C-20) or up to three times (at $C\text{-}8^2$) (Airs et al., 2001; Chapter 15, Friegaard et al.; Chapter 37, Keely). Fifthly, both epimers of the newly generated asymmetric $C\text{-}3^1$ are found in nature (Fig. 2A) (K. M. Smith and Simpson, 1986; Tamiaki et al., 1994). Not all the theoretically possible combinations of these features have been identified from natural samples, but BChls *c, d* and *e* still provide more than 50% of the currently known chlorophyll structures, even though the green bacteria make a relatively limited contribution to total global photosynthesis. Understanding the role of these variations in the assembly and function of the chlorosome core, which appears to be largely devoid of proteins, is currently a major challenge in chlorophyll research (Chapter 15, Friegaard et al.; Chapter 20, de Boer and de Groot). Unlike most other Chl aggregates, those present in chlorosomes are, in a way not understood, highly fluorescent and avoid concentration quenching (see above).

D. Chlorophylls of the Phytoporphyrin Type: The Chlorophylls c

Various Chl *c*-type pigments are found in heterokonts and the type II cyanobacteria (Stauber, 1988; Jeffrey, Mantoura, and Wright, 1997; Chapter 3, Zapata et al.; Chapter 8, Garrido and Zapata). The *c*-type Chls are phytoporphyrins, and most contain an acrylic acid side chain at C-17 (Fig. 2B). They absorb only moderately (ε ~20,000 $M^{-1}cm^{-1}$) in the region of the 'green gap,' the spectral region where Chls *a* and *b* absorb only weakly (Fig. 3, Table 2). Accordingly, more chromophores are needed to provide the same absorption. They have, however, a relatively intense absorption near 400 nm, which may be advantageous in clear waters (Chapter 18, Larkum). A structural feature of most *c*-type Chls is the unesterified acrylic- or propionic-acid side-chain at C-17; thus, these pigments should be more correctly called chlorophyllides (Chlides), with the ending 'ide' denoting an unesterified acid side chain at C-17. These Chl(ide)s *c* are therefore much more polar than the other Chls. With the development of analytical techniques suitable for pigments with a free C-17 acid side chain (Chapter 8, Garrido and Zapata), the diversity of known *c*-type Chls has dramatically increased in recent times.

The *c*-type Chls may have evolved first among the Chls (Chapter 18, Larkum): [8-vinyl]-protochlorophyllide *a*, also known as 3,8-divinyl-pheoporphyrin *a*-Mg-monomethylester, may be the most ancient Chl still active in photosynthesis: it is also a precursor to most Chls, but has been identified as a genuine antenna pigment in symbiotic prokaryotes (Helfrich et al., 1999). Recently, an increasing number of hitherto only partially characterized Chls *c* have been discovered, which are esterified at $C\text{-}17^3$ by an alcohol including the unique galactolipid shown in Fig. 2A (Chapter 3, Zapata et al.). In view of the immense variety of photosynthetic organisms, especially of marine microalgae, more surprises can be anticipated. The functional significance of these variations still requires clarification. Remarkably, the 'classical' *c*-type Chls, lacking an esterifying alcohol at $C\text{-}17^3$, are bound to proteins of the LHCII type which, in green plants, bind Chls *a* and *b* esterified with phytol.

E: Bacteriochlorin-type Chlorophylls: Bacteriochlorophylls a, b and g

While all pigments of anoxygenic photosynthetic

bacteria are known as BChls, only three of them, BChls *a, b* and *g,* are true bacteriochlorins, that is, 7,8-*trans*,17,18-*trans*-tetrahydrophytoporphyrins or their Δ8,8′-derivatives (see Fig. 2B). The spectroscopic consequence of this hydrogenation of rings B and D is a considerably increased gap among the absorption bands (Fig. 3). The Q_Y-absorption band is red-shifted to 750–800 nm in mono-disperse solution, and even more so (800–1020 nm) in situ (Drews and Giesbrecht, 1966), while the Soret-band is blue-shifted (<400 nm) and split. The organisms containing these Chls thereby extend the useable spectrum in both directions beyond those of all other Chls. BChl *a* is the most widely distributed BChl. It is present in RC and the core-antennas of most anoxygenic bacteria, as well as in the peripheral antennas of the purple bacteria (Tables 1, 2). In some purple bacteria, it is replaced by the structurally related BChl *b*, carrying an 8-ethylidene instead of the 8-ethyl group present in BChl *a* (Scheer et al., 1974; Steiner et al., 1981). BChl *g* is found in the strictly anaerobic Gram-positive heliobacteria, both as a light-harvesting and as an electron transfer pigment in the functionally integrated type I-RC complex (Michalski et al., 1987; Neerken and Amesz, 2001; Chapter 4, Kobayashi et al.).

F. Structural Variants of Chlorophylls

The number of recognized Chls is constantly increasing. Structural variants are found in most photosynthetic organisms, often only in small amounts, and their functions are not always known. Some have been established as biosynthetic precursors or products of (bio)degradation and include pigments esterified with terpenoid alcohols other than phytol including phytadi-, tri- or tetra-ene alcohols (Schoch et al., 1977; Shioi, 1991), and also phytochlorin-pigments bearing a C-8 vinyl rather than an ethyl substituent (Rebeiz et al., 1994). However, many of these unusual Chls are functional in photosynthesis. Pigments with more highly unsaturated terpenoid alcohols can replace phytol in BChl *a* (Katz et al., 1972; Walter et al., 1979) or BChl *b* (Steiner et al., 1981) in certain purple bacteria and, often, these modified pigments are the major Chls present and, therefore, must be functional; the role of the modified alcohols, however, remains unclear (Section III.3). In at least one organism, *Rhodospirillum* (*Rsp.*) *rubrum*, pigments with different alcohols are segregated among different functions: in this organism the BChl *a* present in the RC is esterified with phytol while that in the antennae with geranylgeraniol (Walter et al., 1979). In the elucidated structures of photosynthetic complexes, the esterifying alcohols often interact with other hydrophobic structures including not only the respective alcohols of neighboring Chls, but also lipids and carotenoids. In this context, the presence of non-covalently bound lipid molecules inside the native proteins and in close proximity to Chls is noteworthy. Such lipids have been found in the PS I core (Jordan et al., 2001; Ben-Shem et al., 2003), in PS II (Biesiadka et al., 2004; Ferreira et al., 2004) and even in the water-soluble peridinin-Chl protein (PCP) from *Amphidinium carterae* (Hofmann et al., 1996).

Another variation concerns the central metal which, in almost all cases, is Mg. Several closely related strains of purple bacteria (*Acidiphilium* sp.), however, contain up to 90% [Zn]-BChl (Kobayashi et al., 1999; Stewart et al., 2001; Chapter 4, Kobayashi et al.), which is not only functional but also largely replaces BChl *a* in all pigment proteins, including the primary donor, P870, of the RC (Matsuura and Stewart, 2004). While Mg- and Zn-containing Chls have largely similar properties, a notable chemical difference is the increased stability of the [Zn]-Chls towards acid. Since *Acidiphilium* has been isolated from acidic mine ponds, it is likely that pH constituted the evolutionary pressure responsible for the change of the central metal. As the Zn-concentrations of the ponds were not unusually high, it is probable, therefore, that the Zn was actively incorporated, *either* into the bacteria (where it can then compete by mass action with Mg), *or* by a specialized Zn-chelating enzyme. It is unknown, however, whether the Zn is introduced by a specialized Proto Zn-chelatase, or replaces Mg at a later biosynthetic stage. In vitro, the Mg-containing Chls can be replaced in all accessible sites of antennas and LHC by their Zn-containing analogues without impairing their functions (Kobayashi et al., 1992, 1999; Davis et al., 1996; Noy et al., 1998; Lapouge et al., 2000), and most enzymes accept Chls with either Mg or Zn as central metal as substrates (Schoch et al., 1995). It should be noted that a chlorophyll precursor containing Zn, namely Zn-Proto, has been found in another acidophilic organism, the rhodophyte *Galdieria sulphuraria (Cyanidium caldarium)*, where it was considered as a precursor for biliproteins (Csatorday et al., 1981); however, since biliproteins are formed frome heme, another function is possible. No [Zn]-Chls have been found in this organism.

Transmetallated Chls, with Hg, Cd, Ni, Cu or Pb replacing Mg, have been isolated from lichens, microalgae and, more recently, from water plants grown on media enriched in the respective metals (Küpper et al., 1996, 1998; Chapter 5, Küpper et al.). In these organisms, photosynthesis is strongly impaired (Caspi et al., 1999). It is interesting in this context that prospecting for Cu has been attempted via determination of Chl fluorescence (Lanaras et al., 1993). If judged by experiments with isolated light-harvesting complexes, the afore-mentioned metals (which bind much more strongly than Mg to the tetrapyrrole) can replace the latter spontaneously at concentrations likely to exist within the cells. The rapid internal conversion of metals with unfilled d-shells can well explain the impaired photosynthetic capacity of plants that are stressed with heavy metals (Küpper et al., 1998). [Ni]-BChl *a* shows internal conversion (IC) on a time-scale <100 fs (Musewald et al., 1999; Noy et al., 2000). If it is incorporated in bacterial LH1 complexes, it can compete efficiently with energy transfer at time-scales down to 50 fs. It therefore acts as a 'black hole': any exciton that passes by a [Ni]-complex is degraded to heat. In vitro, this can be used to study unit-sizes and exciton delocalisation (Fiedor et al., 2000; see below).

Unusual or minor Chls with specialized functions have been identified in all RCs. The metal-free pheophytin (Phe) *a* is found in the PS II-RC. Because its redox-potential is ≈200 mV more positive than that of Chl *a* (T. Watanabe and Kobayashi, 1991), it serves as an early electron acceptor from P680 and transfers this electron on to the quinone, Q_A (M. W. C. Evans and Nugent, 1993). In the type II RC of purple (Reed and Peters, 1972) and filamentous green (Vasmel et al., 1983) bacteria, two BChl *a* (or *b*) molecules are structurally and functionally replaced by BPhe *a* (or *b*). One of them, termed H_A, has been shown to be very rapidly (≈1 ps) reduced by the primary acceptor, BChl-B_A (Schenck et al., 1981; S. Schmidt et al., 1995) and to donate its electron subsequently within 200 ps to Q_A (Dimagno and Norris, 1993). The minor Chls of type I-RCs are the 13^2(S)-epimers of the respective major Chls, the so-called 'prime'-Chls. Photosystem I (PS I) of most oxygenic organisms contains Chl *a*′ (Kobayashi et al., 1988), the 13^2(S)-epimer of Chl *a*, while the Chl *d*-containing *Acc. marina* contains Chl *d*′ (Akiyama et al., 2001) and heliobacteria contain BChl *g*′ (Kobayashi et al., 1991). The location of Chl *a*′ as one of the pigments of the special *pair has* been verified by the X-ray structure of a cyanobacterial PS I (Jordan et al., 2001). By contrast, RCs from green sulfur bacteria, which are also likely to be of the type I, do not contain a prime-chlorophyll but rather Chl $a_{\Delta 2,6}$, namely, the 'normal' Chl *a* macrocycle esterified with Δ2,6-phytadienol (Kobayashi et al., 2000). In the RCs of *Heliobacterium chlorum,* Chl *a* bearing a hydroxyethyl substituent at C-8 and esterified with farnesol (8^1-hydroxy-Chl a_F) has been identified: it is believed to function as primary acceptor A_0 (Van de Meent et al., 1991). Finally, the Chl *a*-$\Delta 13^1,13^2$-enol shows some of the spectral features of P700 in PS I-RCs (Wasielewski et al., 1981). The current X-ray structure is still inconclusive in this respect. One Chl *a* of P700 is strongly distorted, but seems incompatible with an enol (Jordan et al., 2001). RC of *Rsp. rubrum* contain BChl a_P (i.e., esterified with phytol) and BPhe a_{GG} esterified with geranygeraniol: the antenna contains only BChl a_{GG} (Walter et al., 1979).

Antenna complexes can also contain modified pigments. Probably the most striking example is the presence of [8-vinyl]-Chls *a* and *b* as the most abundant pigments in marine *Prochlorococcus* species living down to considerable (≈150 m) depths (Goericke and Repeta, 1992), and contributing a large fraction of global photosynthesis. The functional significance of this substituent is currently unclear. In the red region, the [8]-vinyl-Chls absorb only slightly different from the corresponding Chls *a* and *b* bearing the usual 8-ethyl group. However, the Soret bands are shifted by approximately 8 nm to the red, which may be of relevance in the clear oceanic waters where blue light is prevailing.

III. Why Chlorophylls?

Nature has almost exclusively and universally selected Chls for the primary reactions of photosynthesis. In reaction centers, Chls are indispensable as primary electron donors and acceptors, transporting the electron within a few picoseconds across half the thylakoid membrane. They also serve to transport triplet excitation energy to the protective carotenoids (Angerhofer et al., 1998). In most photosynthetic organisms, Chls also provide the majority of light-harvesting pigments which are only supplemented by linear tetrapyrroles and carotenoids. What are the advantages of the Chls over these and other pigments?

The answer is probably a unique combination

of factors: the macrocycle, the central metal, the peripheral substituents and the hydrophobic esterifying alcohol all together provide some unique physical and chemical properties. Among them, the macrocycle and the central Mg, seem to be most important, if judged by their conservation and by their known influence on the chemical and physical parameters of the pigments. Variations in the substituents provide the necessary plasticity for chemical interactions and modulation of certain properties including light absorption and redox potential, while the functional relevance of the hydrophobic esterifying alcohol is less clear.

A. The Macrocycle

The large, aromatic tetrapyrrole macrocycle is the basis for both the absorption and the redox chemistry of Chls. Starting from the last common precursor with hemes, namely protoporphyrin (Proto), the macrocycle has been considerably modified for improved function, by substitution and reduction.

Proto has an intense absorption in the blue spectral range but only a moderate absorption in the visible. The absorption in the visible (VIS) is doubled in porphyrins containing the isocyclic ring which is a characteristic of all Chls, and is slightly red-shifted, which may have been an important factor in the early evolution of Chls. These effects arise from a reduced symmetry of the macrocyclic π-system (Weiss, 1978; Hanson, 1991). They become much more pronounced upon reduction of the 17,18-double bond in ring D, and, even more so, upon further reduction of the 7,8-double bond in the BChls. Thus, the absorbance of an individual chromophore in the Vis and NIR range, respectively, is increased two-three-fold, and the accessible spectral range nearly doubled, without any specific protein interaction required. This contrasts with the second group of photosynthetic tetrapyrrole chromophores, the bilins (Scheer, 2003). Here, the absorbance of the chromophores is similarly high, but due to a conformational change that requires more extensive pigment-protein interactions, which, in turn, require a considerably larger investment of energy in protein biosynthesis (Table 3).

The reduction and oxidation potentials of Chls are closely related to their optical spectra, in particular, their differences should correspond roughly to the energy of the Q_y-band. Accordingly, this gap decreases from porphyrins to chlorins and bacteriochlorins (Fuhrhop, 1975; Felton, 1978). However, the changes of the individual potentials vary considerably with substituents (Watanabe and Kobayashi, 1991), ligation to the central metal (Felton, 1978; Chapter 34, Yerushalmi et al.), H-bonding (Chapter 19, Allen and Williams) and distortions of the macrocycle (Fajer et al., 1990), which are difficult to separate from the influence of ring-reduction per se. In the tetraphenylporphyrin-series, reduction to the chlorin affects mainly the oxidation potential, while further reduction to the bacteriochlorin affects mainly the reduction potential (Felton, 1978). In a series of metallo-octaethylporphyrins, the first oxidation potential is always decreased by ~300 mV if the macrocycle is reduced to the chlorin level (Fuhrhop, 1975), and the same decrease is seen from Mg-octaethylchlorin to Mg-octaethylbacteriochlorin (Felton, 1978). In a series of (B)Chls and (B)Phes, the 1st reduction potential is hardly changed when going from the chlorin to the bacteriochlorin while maintaining the substituents, but the 1st oxidation potential is more affected and lowered by ~0.25 V (Geskes et al., 1995a). When this is compared to the respective changes of ~0.14 and ~0.05 V upon exchanging the 3-acetyl- to a 3-vinyl-

Table 3. Investment into chromophores in different antennas (IP = isoprenoid).

Antenna	Esterifying alcohol investment	Protein investment (kDa)	
	IP units/chromophore	per chromophore	per tetrapyrrole)
Chlorosome (green bacteria)	3	<1	≈ 1
LHCII (green plants)	4	1.7	2.25
LHCII (heterokonts, dinophytes)	4 (Chl *a*) 0 (Chls *c*)	1.7	2.25
LH1 (purple bacteria)	4	4.3	6.5
LH2 (purple bacteria)	4	2.6	4.3
PS I (type I RC with integrated antenna)	4	3,5	4
Allophycocyanin	–	16	16
C-Phycocyanin	–	11	11
C-Phycoerythrin	–	7.5	7.5

substitutent (Geskes et al., 1995a) or the change in oxditation potential of ~100 mV per H-bond (Chapter 19, Allen and Williams), it becomes clear that the redox potentials are only moderately influenced by the reduction of the macrocycle from the porphyrin to the bacteriochlorin.

The aromatic macrocycle is also one reason for the pronounced stacking of Chls. Certain aggregates in organic solvents, but especially in amphiphilic environments, are formed mainly by π-π interactions of the macrocycle (Scheer et al., 1985; Scherz et al., 1991). In contrast to other types of aggregates, they do not require the presence of the central Mg for their formation. These π-π interactions also contribute to pigment-protein interactions in photosynthetic complexes.

Distortions of the macrocycle introduce a red-shift (Gudowska-Nowak et al., 1990). In isolated pigments, this is possible by steric hindrance of peripheral substituents (Woodward et al., 1960): for example, the absorption of BChl *c* is 10 nm red-shifted relative to that of BChl *d*, since the 20-H of the latter is replaced by a CH_3-group in BChl *c* (Senge and K. M. Smith, 1994) (Table 2). Much larger effects have been introduced in porphyrins and chlorins (Medforth et al., 1992; Gentemann et al., 1994; Senge et al., 1998; Senge, 2000; Chapter 2, Senge et al.). Distortions can also be introduced into isolated porphyrins by central metals that do not fit snugly into the central hole of the macrocycle (Buchler, 1975; Sparks et al., 1993). In situ, non-planarity of the macrocycle can also be introduced by interactions with the proteins. This is seen in all highly-resolved structures of chlorophyll-proteins, and is particularly pronounced in one of the BChl-B850 of the purple bacterial LH2 where it probably contributes to the lowering of the site-energy (Robert et al., 2003)

B. The Peripheral Substituents

Considerable variations in the properties of chromophores are possible by changing the substituents. Conjugated carbonyl groups are introduced at several sites. The C-13^1 oxo group, for instance, is present in all Chls. BChls *a* and *b* and Chl *d* also possess C=O groups at C-3 while Chls *b* and c_3 and the BChls *e* (and *f*) have them at C-7. The redox potential is shifted in all cases by about 200 mV. The Soret band system ($B_{x,y}$) is always red-shifted, but the spectral effect on the Q_y band depends on the site to which the C=O group is bound: if they are situated along the y-axis (C-3, C-13^1, see Fig. 1 for definition of the axes), they result in a red-shift of the major visible Q_y-absorption band. On the other hand, if a C=O group is located along the x-axis (C-7 on ring B), it results in a blue-shift of this band. A fine-tuning of these absorption shifts is possible by changing the orbital overlap of the C=O groups with the π-electrons of the macrocycle: this has been studied especially for the 3-acetyl group of BChl *a*, where shifts up to 30 nm are discussed (McLuskey et al., 1999; Robert et al., 2003). The influence of C=O groups on both the spectral and the redox properties can furthermore be modulated by H-bonding. Allen et al. have, for example, shifted the redox potential of the primary donor, P870, of bacterial reaction centers by about 100 mV per H-bond (Chapter 19, Allen and Williams). H-bonding has also been shown for the 3^1-carbonyl group of one of the Chl *d* in the primary donor, P740, of PS I in *Acc. marina* (Sivakumar et al., 2003) or to the 13´-C=O group of BChl in the LH2 antenna (Kwa et al., 2004; Chapter 27, Garcia-Marin et al.).

Another important effect that can be introduced by peripheral substituents is steric hindrance (see above), by which the macrocycle becomes distorted (Barkigia and Fajer, 1993). The red-shifts of BChl *c* vs. BChl *d,* and of BChl *e* vs. BChl *f,* can be rationalized by steric hindrance of the 20-CH_3 group (Section III. A). Considerable distortions of the macrocycle are obvious for several Chls in high-resolution X-ray structures, where they are induced by site-specific interactions with their apo-proteins (Yeates et al., 1988; Deisenhofer and Michel, 1993; Schiffer and Norris, 1993; Tronrud and Matthews, 1993; McDermott et al., 1995; Hofmann et al., 1996; Jordan et al., 2001; Spiedel et al., 2002; Liu et al., 2004; Standfuss et al., 2005): the site-energies of the respective Chls are expected to be modified by such distortions, but their functional significance remains to be explored experimentally.

The functional significance of the most conspicuous and ever-present peripheral carbonyl substituent of the Chls, namely, the C=O group at C-13^1 which is located on the isocyclic ring derived from the oxidized 13-propionic acid side chain of Mg-Proto, is largely unknown. Cyclization renders this C=O group at C-13^1 coplanar with the macrocycle, which may be significant in terms of a pronounced red-shift. It may also increase the stiffness of the macrocycle, and thereby reduce losses in photosynthesis due to internal conversion of excited states. H-bonding to the 13^1-CO group has been recognized as an im-

portant factor for interaction with the protein, e.g. in the LH2 complex of purple bacteria (Chapter 27, Garcia-Martin et al.). Even less is known of the significance of the β-ketoester system, of which the 13^1-CO group is part. This chemically reactive system is present in all Chls except BChls *c, d, e* and *f*, which lack the 13^2-$COOCH_3$ group. The 13^2-$COOCH_3$ group interferes with aggregation (Scheer and Katz, 1975; Oba and Tamiaki, 1999), which is probably a reason for its absence in BChls *c, d* and *e*, which form very large regular aggregates (Blankenship and Matsuura, 2003; Balaban et al., 2004; Chapter 20, de Boer and de Groot). The β-ketoester system is a potential site for chelation, but such chelates have only been observed in vitro (Scheer and Katz, 1978). The β-ketoester group also facilitates enolization, but again there is little hard evidence that enols play a photosynthetic role in vivo (Jordan et al., 2001). It facilitates the formation of the 13^2-epimers and these 'prime' pigments like Chl *a*′ form part of the primary donor of type I RCs (Chapter 4, Kobayashi et al.). Aggregation is influenced by this change in stereochemistry (Oba et al., 1996), as well as the planarity of the macrocycle (Furukawa et al., 2000), which may both be relevant for the formation and symmetry of the *special pair* present as primary donor in these reaction centers (Katz et al., 1978a; Feiler et al., 1995; Plato and Moebius, 1995; Rautter et al., 1995; Bratt et al., 1996; Artz et al., 1997; Bratt et al., 1999; Kaess et al., 2001).

The significance of ring E is further emphasized by site-selective exchanges in a variety of chlorophyll proteins (Scheer and Hartwich, 1995; Davis et al., 1996; Chapter 26, Paulsen) and the substrate specificity of metabolising enzymes (Helfrich et al., 1994; Klement et al., 1999; Chapter 13, Yaronskaya and Grimm; Chapter 14, Rüdiger; Chapter 17, Kräutler and Hörtensteiner). While, in general, considerable variations of substituents are possible on rings A and B without impairing binding or physiological functions, variations on ring D and, in particular, on the isocyclic ring E are critical. Most of these studies have been carried out in vitro; thus, it remains a challenge to complement them with in vivo studies (Vavilin et al., 2003).

C. The Central Metal

The central metal has a decisive influence on the excited state kinetics of tetrapyrroles and, therefore, on their function in photosynthesis. It appears that nature has selected Mg as the central metal which maximizes excited state lifetime, while maintaining low intersystem crossing to the highly toxic triplet (see Chapter 6, Kobayashi et al.). Transition metals with open d shells, as well as all heavy metals, would be deleterious in this respect. Of the remaining metals, K, Na, Li and Ca form very labile complexes, while Be seems too small; the trivalent metals are possibly avoided because they introduce a charge. Thus, only H^+, Mg^{++} and Zn^{++} remain and they are, indeed, the only central metals found in nature as functional chlorophyllous pigments. The preference of Mg over Zn may then relate to its lower mass and concomitantly reduced intersystem crossing (ISC) properties; in other aspects, the [Zn]-Chls seem to be very similar to the respective Mg-complexes. They both have similar redox potentials; indeed, they are the lowest of all sufficiently stable metal complexes, which seems to be another reason for their selection (T. Watanabe and Kobayashi, 1991; Geskes et al., 1995b). [Zn]-Chls can replace the respective Mg-complexes in all complexes where such exchanges have been studied (Scheer and Hartwich, 1995; Davis et al., 1996; Lapouge et al., 2000; Chapter 5, Küpper et al.; Chapter 25, Nango; Chapter 26, Paulsen), and in synthetic chlorophyll-binding proteins (Struck et al., 1998; Rau et al., 2001; Chapter 24, Noy et al.; Chapter 25, Nango). They can also replace the Mg-complexes in all biosynthetic enzymes involved in Chl formation beyond Mg-chelatase, which is the only enzyme specific for Mg (Rüdiger, 2002; Chapter 13, Yaronskaja and Grimm; Chapter 14, Rüdiger).

It has long been recognized that the Mg in Chls binds extra ligands so strongly that it is practically never four coordinate. Removal of the extra ligand in unpolar solvents results in aggregation with another Chl donating a ligand; for example, the highly conserved 13^1-CO group (Katz et al., 1978b). Interactions with the central metal and the 3^1-OH group in BChls *c*, *d* and *e* are likewise important in chlorosomes (Umetsu et al., 2003; Chapter 20, de Boer and de Groot). The central Mg is also important for the interactions of Chls with their apo-proteins. A variety of ligands has been identified in the crystal structures of Chl proteins: in more than 50% of known binding sites the ligand is histidine, but glutamine, asparagine, backbone C=O groups, and even water, are known to be ligated (Yeates et al., 1988; Deisenhofer and Michel, 1993; Schiffer and Norris, 1993; Tronrud and Matthews, 1993; Kühlbrandt et al., 1994; McDermott et al., 1995; Hofmann et al., 1996; Savage

et al., 1996; Jordan et al., 2001; Spiedel et al., 2002; Ben-Shem et al., 2003; Liu et al., 2004; Standfuss et al., 2005). These interactions may be of considerable importance in the organization of Chl proteins, especially in a hydrophobic environment. A Chl ligated to histidine may, for example, be considered a highly modified amino acid. Ligand interactions are known to modulate the electron density of the macrocycle and, thereby, its properties (Alia et al., 2001; Chapter 34, Yerushalmi et al.). They are used as a tool to replace (B)Chls by (B)Phes, and vice versa (Coleman and Youvan, 1990; Shen and Vermaas, 1994; Palaniappan et al., 1995; Czarnecki et al., 1997): when there is no space provided to carry in a ligand, the replacement of, for example, a liganding histidine by a hydrophobic amino acid results in the introduction of a (B)Phe, and the Phe specificity of the PS II-RC is maintained when Phe *a* is replaced by Phe *b* (Vavilin et al., 2003).

Only recently in the study of Chl ligation has the stereochemical aspect been recognized. Due to the dissymmetric arrangement of the substituents, the two 'faces' of the molecule are diasterotopic (see legend Fig. 1 for nomenclature). The two ligation states differ in their energies, with α-ligation (from *below,* α-type) being favored by ~4 kJ/mole over β-ligation (from *above*, β-type) (Oba and Tamiaki, 2002), and they are unevenly distributed in chlorophyll proteins (Balaban et al., 2002; Balaban, 2003). A functional significance is suggested by the preservation of geometries during evolution, but requires further exploration.

D. The Esterifying Alcohol

Of all the structural features of Chls, least is known about the functional significance of the phytol. The influence of the long-chain esterifying alcohol on ground and excited state properties of the tetrapyrrole is negligible. In mono-disperse solution it has, at most, a minor influence on absorption. It is noteworthy, however, that the alcohol moiety has a considerable affect on the aggregation of Chls, especially in micellar systems (Scheer et al., 1985; Agostiano et al., 2000, 2002a). This suggests a function of the long-chain alcohols in interactions with the environment including the apo-protein, other Chls, carotenoids and lipids. The alcohols appear to be important packing factors, to ensure the proper spacing and orientation among the pigments and other cofactors which govern energy and electron transfer. In particular, electron (and the related triplet energy) transfer can be affected by even minor variations of the pigment arrangement, due to changes in orbital overlap. A spacing function for the long-chain alcohol in positioning of the Chls is supported by all available X-ray structures: the esterifying alcohols are generally remarkably well resolved and engaged in interactions, especially among each other and with the carotenoids (Yeates et al., 1988; Deisenhofer and Michel, 1993; Schiffer and Norris, 1993; Tronrud and Matthews, 1993; Kühlbrandt et al., 1994; McDermott et al., 1995; Hofmann et al., 1996; Savage et al., 1996; Jordan et al., 2001; Spiedel et al., 2002; Ben-Shem et al., 2003; Biesiadka et al., 2004; Ferreira et al., 2004; Liu et al., 2004; Standfuss et al., 2005). Certain conformations of the respective alcohols are even conserved in an evolutionary sense over long periods; for example, from bacterial RC to plant PS II-RC (W. Zinth, personal communication).

While terpenoid alcohols function in many proteins as membrane anchors, there is relatively little direct interaction of the Chl esterifying alcohol with the membrane lipids. Thus, the alcohol may be a handle to Chls as is the phosphate group to carbohydrates which, due to their stereochemical complexity, also require precise positioning, for example, in enzymatic reactions. It should be noted in this context that, in *Rsp. rubrum,* the alcohol in the reaction center is different from that of the antenna (Walter et al., 1979), that hydrolysis of the alcohol is an early step in Chl degradation (Chapter 17, Kräutler and Hörtensteiner), and that the long-chain alcohol is retained even in water-soluble Chl proteins (Noguchi et al., 1999; Horigome et al., 2003; K. Schmidt et al., 2003; Reinbothe et al., 2004) including the light-harvesting peridinin-Chl protein (Hofmann et al., 1996) and the FMO complex (Tronrud and Matthews, 1993). It is surprising, therefore, that the alcohol is missing in most Chls *c* which are also membrane located, emphasizing the need for an X-ray structure of a Chl *c*-containing protein.

IV. Functions

A. Light Absorption and Energy Transfer

The first two functions are relevant for light harvesting. Antennas serve to increase the absorption cross-section of reaction centers by orders of magnitude, which is greatly assisted by the intense absorptions ($\varepsilon \approx 10^5 M^{-1}cm^{-1}$) of most Chls. Their individual ab-

sorptions are narrow, but the bands can be shifted by hundreds of cm^{-1} by interactions with protein, and a further spread of the useful absorption is realized by combination with other pigments including other Chls. In combinations, the Chls have strong absorptions over nearly the entire range of the photosynthetically useful spectrum (330 –1050 nm) with, however, the exception of the 'green gap' around 500 nm. Since this spectral range is particularly important in aquatic environments, where blue-green light is often prevalent, algae and photosynthetic bacteria have exploited this 'gap' not only by using *c*-type Chls but also with special carotenoids and biliproteins (Scheer, 2003). There is a cost, however, since excited carotenoids and bile pigments have only very short lifetimes which require considerable 'investments' in the form of binding proteins and biosynthetic enzymes. Plants, however, appear to have evolved a different strategy by investing more heavily in structure in the competition for light, both on a macroscopic (growth towards the light) and on a microscopic scale (leaf structure and internal reflection). For a recent comprehensive treatment of light-harvesting in photosynthetic organisms see Green and Parson (2003).

In the antennas, energy is frequently transported over tens of nm from the site of primary excitation to the reaction center where energy transduction takes place, and this transport is only efficient when conducted by *radiationless* transfer. Among Chls, Förster and exciton mechanisms are considered the dominant modes of transfer (Parson and Nagarajan, 2003), and both require long-lived excited states that are especially important in the vicinity of the reaction center where 'storage rings,' composed of Chls, are believed to hold the excited energy over relatively long (ns) periods.

That energy transfer can also be efficiently conducted by electron exchange (Dexter mechanism) (Parson and Nagarajan, 2003) has been proposed, in particular, for singlet energy transfer between carotenoids and Chls. An extremely fast transfer is necessary in these cases to compete with the very rapid internal conversion of most carotenoids (Section IV.C). The close contact between the donor (carotenoid) and acceptor (Chl) is clearly seen in all sufficiently-resolved structures of light-harvesting Chl-carotenoid-proteins (Freer et al., 1996; Koepke et al., 1996; Hofmann et al., 1996; Cline, 2003; Liu et al., 2004; Standfuss et al., 2005). Since electron exchange, like electron transfer, requires orbital overlap, it is expected to be critically dependent on very small geometrical changes (Section III.D). Electron exchange is also the major mechanism of triplet energy transfer which is especially important in protection against excessive light (Section IV.C).

B. Electron Transfer

Chlorophylls are indispensable for the primary charge separation in photosynthesis (Deisenhofer and Norris, 1993; Chapter 31,Wachtveitl and Zinth). The primary donor is a dimer (*special pair*) of (B)Chl which upon excitation donates within <3 ps an electron to the first acceptor, which also is a (B)Chl in all known RC. The secondary acceptor is also a (B)Chl in type I RCs (present in PSI of oxygenic phototrophs, green sulfur bacteria, heliobacteria), whereas it is replaced by a (B)Phe in type II RCs (present in PS II of oxygenic phototrophs, purple bacteria, green filamentous bacteria). In purple bacteria, the second transfer step is even faster (~1 ps) than the first step (Chapter 31, Wachtveitl and Zinth). The secondary acceptor is, in both types of RC, located halfway across the membrane. Electron transfer across the membrane is completed ~200 ps later when it is passed on to a quinone. All these first steps proceed on only one of the two (nearly) symmetrical branches of the RC. In reaction centers of the purple bacterium, *Rba. sphaeroides,* the other branch serves to protect the RC by transferring, and thereby quenching, triplet excitations to a carotenoid (Angerhofer et al., 1998; Arellano et al., 2004) (see below). For a comprehensive treatment of photosynthetic reaction centers see Deisenhofer and Norris (1993).

C. Protection of the Photosynthetic Apparatus Against Light-induced Damage

The long lifetimes of excited states of Chl are helpful for both energy transfer and efficient photochemistry in the reaction centers: both have to compete with radiationless de-excitation. In the proper structural context, this allows for efficient photosynthesis with minimal energy losses. On the other hand, the relatively long-lived excited states of Chls are potentially hazardous due to the concomitantly increased chance of triplet formation which, in turn, can generate toxic reactive oxygen species (ROS) (Chapters 32, 33, Brandis et al.). Carotenoids are the pigments most intimately involved in photoprotection and protect the photosynthetic apparatus by a variety of direct and indirect mechanisms against damage by excess

light (Frank et al., 1999). Carotenoid-less mutants are highly light-sensitive in all photosynthetic organisms and are unable to survive in the natural environment. Comparatively little is known about the protective role, if any, of Chls: Chl cation radicals, which can be generated in antennas under saturating light conditions, are good quenchers of Chl excited states (Law and Cogdell, 1998). Most chlorophyll aggregates are also excellent quenchers (Katz et al., 1978b; Scherz et al., 1991), with the notable exception of those of BChls *c*, *d* and *e* in the chlorosomes (Blankenship and Matsuura, 2003; Chapter 20, deBoer and deGroot). It has recently been proposed that a light-induced structural change may convert the latter also to a quenching state (Kakitani et al., 2003).

D. Structure Stabilization

As products of a co-evolution, all chromophores are integral components of the light-harvesting and energy transducing systems. As such, they are also integral to the stability of the systems. Chls show a remarkable potential for self-organization in both hydrophobic (Katz et al., 1978b; van Rossum et al., 2001) and hydrophilic media (Gottstein and Scheer, 1983; Katz et al., 1991; Scherz et al., 1991; Agostiano

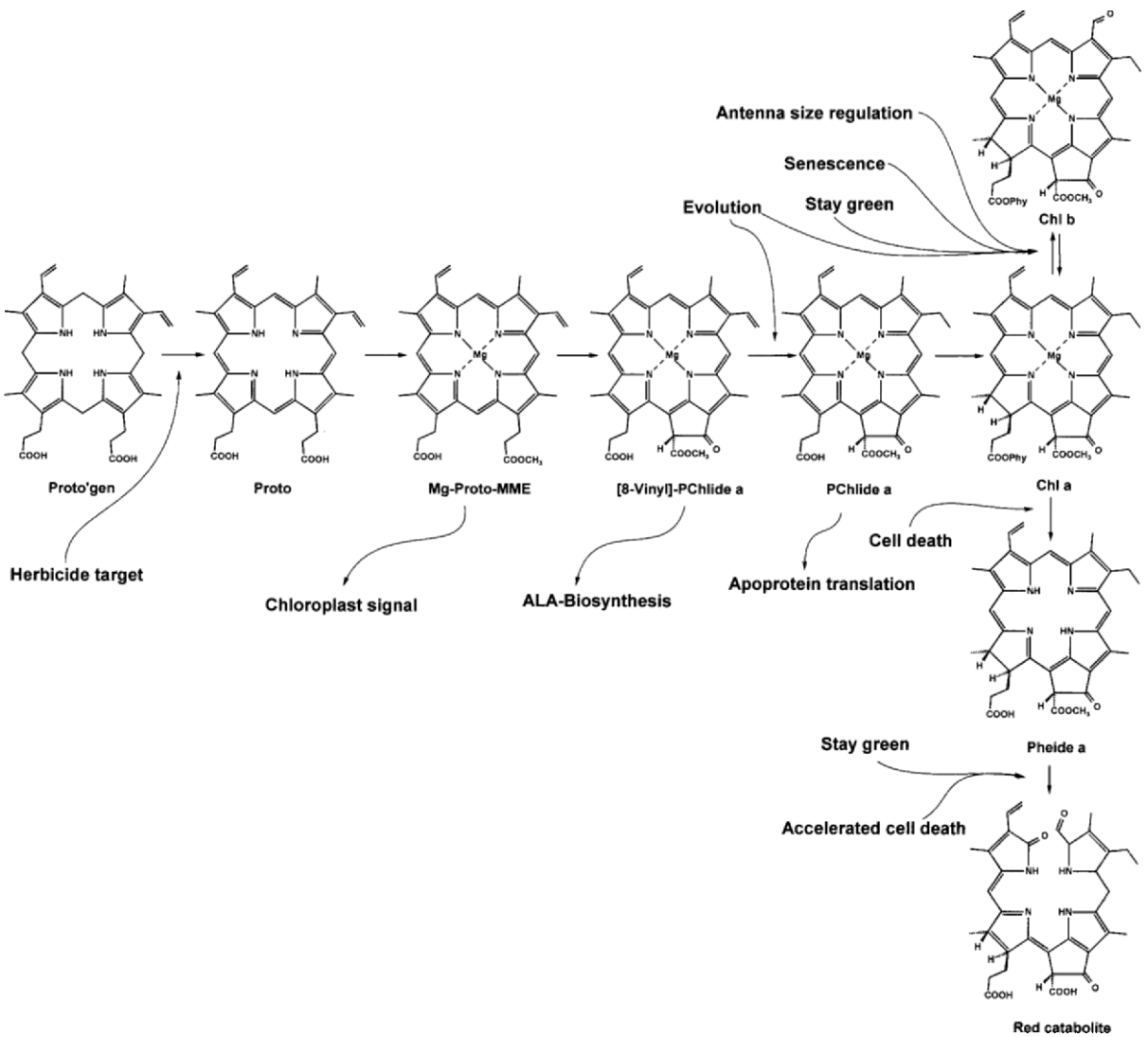

Fig. 4. Involvement of chlorophylls in physiological responses and evolution of photosynthetic organisms. This is a modified version of the scheme presented by A. Tanaka at the International Congress for Photosynthesis, Montréal, 2004).

et al., 2002). Before the identification of Chl proteins, speculation on the organization of light-harvesting complexes had focused on the self-aggregation of Chls as a driving force. This notion has been recently revived in two ways. Firstly, the presence of only very small amounts of protein in the chlorosomes of green bacteria (Chapter 6, Kobayashi et al.) has revived the idea of Chl-only aggregates in these antennas (Hirota et al., 1992; van Rossum et al., 2001; but see Niedermeier et al., 1992). Secondly, X-ray structures of light harvesting systems have shown that Chls are often so close to each other that Chl-Chl interactions can be expected (Tronrud and Matthews, 1993; Freer et al., 1996; Koepke et al., 1996; Jordan et al., 2001; Cline, 2003; Liu et al., 2004; Standfuss et al., 2005), with the pigments in geometric arrangements that are very similar to those found in Chl aggregates in mixed organic-aqueous media (Scherz et al., 1991). Strong interactions among the Chls have been confirmed especially in bacterial antennas (Sundström and Grondelle van, 1995; van Rossum et al., 1998; Leupold et al., 1999; Fiedor et al., 2000; Chapter 21, Köhler and Aartsma; Chapter 29, Leupold et al.). Assembly problems are frequently observed when amino acids binding the central Mg are modified, and, further, apo-protein complexes fail to assemble in the absence of Chls (Eichacker et al., 1996): this strongly suggests that Chls contribute to the formation and stability of light-harvesting pigment-protein complexes. As an example for a quantitative study, the thermodynamics of the influence of the central metal in the association of bacterial LH1 has been evaluated (Lapouge et al., 2000).

E. Other Functions

Chlorophyll metabolism is a central part of metabolism of all photosynthetic organisms and subject to many regulations. Vice versa, chlorophyll precursors are also involved in feedback control of their biosynthesis, in regulating the translation and import of apoproteins of pigment-protein complexes and in the interaction of the plastid with the nucleus in eukaryotic organisms (see Chapter 16, Beck and Grimm, and Fig. 4). Modifications of chlorophylls (Scheer and Hartwich, 1995; Chapter 2, Senge et al.; Chapter 4, Kobayashi et al.; Chapter 24, Noy et al.; Chapter 25, Nango; Chapter 26, Paulsen; Chapter 34, Yerushalmi et al.), Chl interactions with proteins (Chapter 19, Allen and Williams; Chapter 27, Garcia-Martin et al.) and Chl biosynthesis (see Section 'Metabolism' in this volume) have all been key factors in the evolution of photosynthetic organisms (Chapter 18, Larkum). They are primary targets to monitor and control plant health and productivity (Chapter 34, Yerushalmi et al.; Chapter 35, Nedbal and Koblizek; Chapter 36, Morel). Due to the stability of the tetrapyrrole, they also become increasingly important in the interpretation of the fossil record of photosynthesis (Chapter 37, Keely).

Acknowledgments

Work has been supported by the Deutsche Forschungsgemeinschaft (SFB 184 and 533), by the Volkswagen Foundation (I/77 876), by the German Ministry of Research and Technology (BEO 0311152) by the German-Israel Foundation (I-497-140.11/1996), by NEDO (2002 BR048) and by the Hans Fischer Gesellschaft, München.

References

Agostiano A, Catucci L, Colafemmina G, Della Monica M and Scheer H (2000) Relevance of the chlorophyll phytyl chain on lamellar phase formation and organisation. Biophys Chem 84: 189–194

Agostiano A, Catucci L, Colafemmina G and Scheer H (2002a) Role of functional groups and surfactant charge in regulating chlorophyll aggregation in micellar solutions. J Phys Chem B 106: 1446–1454

Agostiano A, Cosma P, Trotta M, Monsu-Scolaro L and Micali N (2002b) Chlorophyll *a* behavior in aqueous solvents: Formation of nanoscale self-assembled complexes. J Phys Chem B 106: 12820–12829

Airs RL, Borrego CM, Garcia-Gill J and Keely BJ (2001) Identification of the bacteriochlorophyll homologues of *Chlorobium phaeobacteroides* strain Ud6053 grown at low light intensity. Photosynth Res 70: 221–230

Akiyama M, Miyashita H, Kise H, Watanabe T, Miyachi S and Kobayashi M (2001) Detection of chlorophyll *d′* and pheophytin *a* in a chlorophyll *d*-dominating oxygenic photosynthetic prokaryote *Acaryochloris marina*. Anal Sci 17: 205–208

Alia, Matysik J, Soede-Huijbregts C, Baldus M, Raap J, Lugtenburg J, Gast P, van Gorkom HJ, Hoff AJ and de Groot HJM (2001) Ultra high field MAS NMR dipolar correlation spectroscopy of the histidine residues in light-harvesting complex II from photosynthetic bacteria reveals partial internal charge transfer in the B850/His complex. J Amer Chem Soc 123: 4803–4809

Allen MB (1966) Distribution of Chlorophylls. In: Vernon LP and Seely GR (eds) The Chlorophylls, pp 511–519. Academic Press, New York

Angerhofer A, Bornhäuser F, Aust V, Hartwich G and Scheer H (1998) Triplet energy transfer in bacterial photosynthetic reac-

tion centres. Biochim Biophys Acta 1365: 404–420
Arellano JB, Melo TB, Fyfe PK, Cogdell RJ and Naqvi KR (2004) Multichannel flash spectroscopy of the reaction centers of wild-type and mutant *Rhodobacter sphaeroides*: Bacteriochlorophyll B-mediated interaction between the carotenoid triplet and the special pair. Photochem Photobiol 79: 68–75
Artz K, Williams JC, Allen JP, Lendzian F, Rautter J and Lubitz W (1997) Relationship between the oxidation potential and electron spin density of the primary electron donor in reaction centers from *Rhodobacter sphaeroides*. Proc Natl Acad Sci USA 94: 13582–13587
Balaban TS (2003) Are syn-ligated (bacterio)chlorophyll dimers energetic traps in light-harvesting systems? FEBS Lett 545: 97–102
Balaban TS, Fromme P, Holzwarth AR, Krauß N and Prokhorenko VI (2002) Relevance of diastereotopic ligation of magnesium atoms of chlorophylls in Photosystem I. Biochim Biophys Acta 1556: 197–207
Balaban TS, Linke-Schaetzel M, Bhise AD and Vanthuyne NaRC (2004) Green self-assembling porphyrins and chlorins as mimics of the natural bacteriochlorophylls *c, d,* and *e*. Eur J Org Chem 3919–3930
Barkigia KM and Fajer J (1993) Models of photosynthetic chromophores: Molecular structures of chlorins and bacteriochlorins. In: Deisenhofer J and Norris JR (eds) The Photosynthetic Reaction Cente, pp 513–540. Academic Press, New York
Ben-Shem A, Frolow F and Nelson N (2003) Crystal structure of plant Photosystem I. Nature 426: 630–635
Bible KC, Buytendorp M, Zierath PD and Rinehart KL (1988) Tunichlorin: A nickel chlorin isolated from the Caribbean tunicate *Trididemnum solidum*. Proc Natl Acad Sci USA 85: 4582–4586
Biesiadka J, Loll B, Kern J, Irrgang K-D and Zouni A (2004) Crystal structure of cyanobacterial Photosystem II at 3.2 Å resolution: A closer look at the Mn cluster. Phys Chem Chem Phys 6: 4733–4736
Blankenship B and Matsuura K (2003) Antenna complexes from green photosynthetic bacteria. In: Green B and Parson W (eds) Light-Harvesting Antennas in Photosynthesis, pp 195–217. Kluwer Academic Publishers, Dordrecht
Borrego CM, Arellano JB, Abella CA, Gillbro T and Garcia-Gil J (1999) The molar extinction coefficient of bacteriochlorophyll *e* and the pigment stoichiometry in *Chlorobium phaeobacteroides*. Photosynth Res 60: 257–264
Bratt PJ, Muhiuddin IP, Evans MCW and Heathcote P (1996) 14N electron spin echo envelope modulation (ESEEM) spectroscopy of the cation radical $P840^+$, the primary electron donor of the *Chlorobium limicola* reaction center. Photochem Photobiol 64: 20–25
Bratt PJ, Ringus E, Hassan A, van Tol H, Maniero A-L, Brunel L-C, Rohrer M, Bubenzer-Hange C, Scheer H and Angerhofer A (1999) EPR on biological samples beyond the limits of superconducting magnets — the primary donor cation of purple bacterial photosynthesis. J Phys Chem B 103: 10973–10977
Buchler JW (1975) Static coordination chemistry of metalloporphyrins. In: Smith KM (ed) Porphyrins and Metalloporphyrins, pp 157–232. Elsevier, Amsterdam
Burrell JWK, Jackman LM and Weedon BCL (1959) Stereochemistry and synthesis of phytol, geraniol, and nerol. Proc Chem Soc 1959: 263–264
Campbell AK and Herring PJ (1987) A novel red fluorescent protein from the deep sea luminous fish *Malacosteus niger*. Comp Biochem Physiol 86b: 411–417
Caple MB, Chow H-C and Strouse CE (1978) Photosynthetic pigments of green sulfur bacteria (The esterifying alcohols of bacteriochlorophylls *c* from *Chlorobium limicola*). J Biol Chem 253: 6730–6737
Caspi V, Droppa M, Horvath G, Malkin S, Marder JB and Raskin VI (1999) The effect of copper on chlorophyll organization during greening of barley leaves. Photosynth Res 62: 165–174
Chen M, Telfer A, Lin S, Pascal A, Larkum AWD and Blankenship RE (2005) The nature of the Photosystem II reaction center of the chlorophyll *d*-containig prokaryote *Acaryochloris marina*. Photochem Photobiol Sce 4: 1060–1064
Cline K (2003) Biogenesis of green plant thylakoid membranes. In: Green B and Parson W (eds) Light-Harvesting Antennas in Photosynthesis, pp 353–372. Kluwer Academic Publishers, Dordrecht
Coleman WJ and Youvan DC (1990) Spectroscopic analysis of genetically modified photosynthetic reaction centers. Annu Rev Biophys Chem 19: 333–367
Crabbe P, Djerassi C, Eisenbraun EJ and Liu S (1959) Optical rotatory dispersion studies. XXIX. Absolute configuration of phytol. Proc Chem Soc 1959: 264–265
Csatorday K, MacColl R and Berns DS (1981) Accumulation of protoporphyrin IX and zinc protoporphyrin IX in *Cyanidium caldarium*. Proc Natl Acad Sci USA 94: 1700–1702
Czarnecki K, Schenck CC and Bocian DF (1997) Resonance Raman characterization of reaction centers in which bacteriochlorophyll replaces the photoactive bacteriopheophytin. Biochemistry 36: 14697–14704
Davis CM, Parkes-Loach PS, Cook CK, Meadows KA, Bandilla M, Scheer H and Loach P.A. (1996) Comparison of the structural requirements for bacteriochlorophyll binding in the core light-harvesting complexes of *Rhodospirillum rubrum* and *Rhodobacter sphaeroides* using reconstitution methodology with bacteriochlorophyll analogs. Biochemistry 35: 3072–3084
Deisenhofer J and Michel H (1993) Three-dimensional structure of the reaction center of *Rhodopseudomonas viridis*. In: Deisenhofer J and Norris JR (eds) The Photosynthetic Reaction Center, pp 541–558. Academic Press, New York
Deisenhofer J and Norris JR (eds) (1993) The Photosynthetic Reaction Center. Academic Press, New York
Dhere C (1932) Some properties of bonellin and remarks on the nature of this pigment. Comp Rend. S Soc Biol 110: 1254–1257
Dimagno TJ and Norris JR (1993) Initial electron transfer events in photosynthetic bacteria. In: Deisenhofer J and Norris JR (eds) The Photosynthetic Reaction Center, pp 105–132. Academic Press, New York
Douglas RH, Mullineaux CW and Partridge JC (2000) Long-wave sensitivity in deep-sea stomiid dragonfish with far-red bioluminescence: Evidence for a dietary origin of the chlorophyll-derived retinal photosensitizer of *Malacosteus niger*. Phil Trans Roy Soc B 355: 1269–1272
Drews G and Giesbrecht P (1966) *Rhodopseudomonas viridis*, nov. spec., ein neu isoliertes obligat phototrophes Bakterium. Arch Microbiol 53: 255–262
Eichacker LA, Helfrich M, Rüdiger W and Müller B (1996) Stabilization of chlorophyll *a*-binding apoproteins P700, CP47, CP43, D2, and D1 by chlorophyll a or Zn-pheophytin a. J Biol Chem 271: 32174–32179

Evans MCW and Nugent HA (1993) Structure and function of the reaction center cofactors in oxygenic organisms. In: Deisenhofer J and Norris JR (eds) The Photosynthetic Reaction Center, pp 391–416. Academic Press, New York

Evans TA and Katz JJ (1975) Evidence for 5-and 6-coordinated Magnesium in bacteriochlorophyll *a* from visible absorption spectroscopy. Biochim Biophys Acta 396: 414–426

Fajer J, Barkigia KM, Smith KM, Zhong E, Gudowska-Nowak E and Newton MD (1990) Micro-environmental effects on photosynthetic chromophores. In: Michel-Beyerle ME (ed) Reaction Centers of Photosynthetic Bacteria, pp 367–376. Springer, Berlin-Heidelberg

Feiler U, Albouy D, Robert B and Mattioli TA (1995) Symmetric structural features and binding site of the primary electron donor in the reaction center of *Chlorobium*. Biochemistry 34: 11099–11105

Felton RH (1978) Primary redox reactions of metalloporphyrins. In: Dolphin D (ed) The Porphyrins, pp 53–126. Academic Press, New York

Ferreira KN, Iverson TM, Maghlaoui K, Barber J and Iwata S (2004) Architecture of the photosynthetic oxygen-evolving center. Science 303: 1831–1838

Fiedor L, Scheer H, Hunter NC, Tschirschwitz F, Voigt B, Ehlert J, Nibbering E, Leupold D and Elsässer T (2000) Introduction of a 60 fs deactivation channel in the photosynthetic antenna LH1 by Ni-bacteriopheophytin *a*. Chem Phys Lett 319: 145–152

Fischer H and Orth H (1940) Die Chemie des Pyrrols, Vol. II, 2nd half. In: Leipzig: Akademische Verlagsgesellschaft, reprinted: New York: Johnson Reprint Corp., 1968

Fischer H and Stangler G (1927) Synthesis of porphyrins. XIII. Synthesis of mesoporphyrin, mesohemin and the constitution of hemin. Ann 459: 53–98

Fischer H and Strell M (1947) Natural pigments. IV. Chlorophyll. Fiat Rev German Sci, Biochemistry Pt 1: 141–186

Fleming I (1967) Chemistry: Absolute configuration and the structure of chlorophyll. Nature 216: 151–152

Frank HA, Young AJ, Britton G and Cogdell RJ (eds) (1999) The Photochemistry of Carotenoids. Kluwer Academic Publishers, Dordrecht

Freer A, Prince S, Sauer K, Papiz M, Hawthornthwaite-Lawless A, McDermott G, Cogdell R and Isaacs NW (1996) Pigment.pigment interactions and energy transfer in the antenna complex of the photosynthetic bacterium *Rhodopseudomonas acidophila*. Structure 4: 449–462

Fremy E (1877) Rechereches chimiques sur la matière verte des feulles. Compt rend 84: 983–989

Fuhrhop J-H (1975) Reversible reactions at the porphyrin periphery. In: Smith KM (ed) pp 593–624. Academic Press, New York

Furukawa H, Oba T, Tamiaki H and Watanabe T (2000) Effect of C13(2)-stereochemistry on the molecular properties of chlorophylls. Bull Chem Soc Jpn 73: 1341–1351

Gentemann S, Medforth CJ, Forsyth TP, Nurco DJ, Smith KM, Fajer J and Holten D (1994) Photophysical properties of conformationally distorted metal-free porphyrins. Investigation into the deactivation mechanisms of the lowest excited singlet state. J Am Chem Soc 116: 7363–7368

Germano M, Shkuropatov AY, Permentier H, de Vijn R, Hoff AJ, Shuvalov VA and van Gorkom HJ (2001) Pigment organization and their interactions in reaction centers of Photosystem II: optical spectroscopy at 6 K of reaction centers with modified pheophytin composition. Biochemistry 40: 11472–11482

Geskes C, Meyer M, Fischer M, Scheer H and Heinze J (1995a) An electrochemical investigation of modified photosynthetic pigments. Chem Phys Lett 99: 17669–17672

Geskes C, Hartwich G, Scheer H, Maentele W and Heinze J (1995b) Electrochemical and spectroelectrochemical investigation of metal-substituted bacteriochlorophyll *a*. J Am Chem Soc 117: 7776–7783

Glaeser J, Baneras L, Rutters H and Overmann J (2002) Novel bacteriochlorophyll *e* structures and species-specific variability of pigment composition in green sulfur bacteria. Arch Microbiol 177: 475–485

Goedheer JC (1966) Visible absorption and fluorescence of Chlorophyll and its aggregates in solution. In: Vernon LP and Seely GR (eds) The Chlorophylls, pp 147–184. Academic Press, New York

Goericke R and Repeta D (1992) The pigments of *Prochlorococcus marinus*: The presence of divinyl-chlorophyll *a* and *b* in a marine procaryote. Limnol Oceanogr 37: 425–433

Gottstein J and Scheer H (1983) Long-wavelength-absorbing forms of bacteriochlorophyll *a* in solutions of Triton X100. Proc Natl Acad Sci USA 80: 2231–2234

Green B and Parson W (eds) (2003) Light-Harvesting Antennas in Photosynthesis. Kluwer Academic Publishers, Dordrecht

Green B, Anderson J and Parson WW (2003) Photosynthetic Membranes and their Light-harvesting Antennas. In: Green B and Parson W (eds) Light-Harvesting Antennas in Photosynthesis, pp 1–28. Kluwer Academic Publishers, Dordrecht

Gudowska-Nowak E, Newton MD and Fajer J (1990) Conformational and environmental effects on bacteriochlorophyll optical spectra: Correlations of calculated spectra with structural results. J Phys Chem 94: 5795–5801

Hanson LK (1991) Molecular orbital theory of monomer pigments. In: Scheer H. (ed) Chlorophylls, pp 993–1014. CRC Press, Boca Raton

Harradine PJ and Maxwell JR (1998) Pyrophaeoporphyrins c_1 and c_2: Grazing products of chlorophyll *c* in aquatic environments. Org Geochem 28: 111–117

Harradine PJ, Harris PG, Head RN, Harris RP and Maxwell JR (1996) Steryl chlorin esters are formed by zooplankton herbivory. Geochim Cosmochim Acta 60: 2265–2270

Helfrich M, Schoch S, Lempert U, Cmiel E and Rüdiger W (1994) Chlorophyll synthetase cannot synthesize chlorophyll *a´*. Eur J Biochem 219: 267–275

Helfrich M, Ross A, King GC, Turner AG and Larkum AWD (1999) Identification of (8-vinyl)-protochlorophyllide *a* in phototrophic prokaryotes and algae: Chemical and spectroscopic properties. Biochim Biophys Acta 1410: 262–272

Hirota M, Moriyama T, Shimada K, Miller M, Olson JM and Matsuura K (1992) High degree of organization of bacteriochlorophyll *c* in chlorosome-like aggregates spontaneously assembled in aqueous solution. Biochim Biophys Acta 1099: 271–274

Hofmann E, Wrench PM, Sharples FP, Hiller RG, Welte W and Diederichs K (1996) Structural basis of light-harvesting by Carotenoids: Peridinin-Chlorophyll-Protein from *Amphidinium carterae*. Science 272: 1788–1791

Hoppe-Seyler F (1881) Über das Chlorophyll der Pflanzen. 2. Z Physiol Chem 4: 193–203

Horigome D, Satoh H and Uchida A (2003) Purification, crystallization and preliminary X-ray analysis of a water-soluble

chlorophyll protein from *Brassica oleracea* L. var. acephala (kale). Acta Cryst D59: 2283–2285

Hu Q, Miyashita H, Iwasaki I I, Kurano N, Miyachi S, Iwaki M and Itoh S (1998) A Photosystem I reaction center driven by chlorophyll *d* in oxygenic photosynthesis. Proc Natl Acad Sci USA 95: 13319–23

Jeffrey SW, Mantoura RFC and Wright SWE (1997) Phytoplankton pigments in oceanography. UNESCO Publications, Paris

Jordan P, Fromme P, Witt HT, Klukas O, Saenger W and Krauss N (2001) Three-dimensional structure of cyanobacterial Photosystem I at 2.5A resolution. Nature 411: 909–917

Kaess H, Fromme P, Witt HT and Lubitz W (2001) Orientation and electronic structure of the primary donor radical cation $P700^{+\bullet}$ in Photosystem I: A single crystals EPR and ENDOR study. J Phys Chem B 105: 1225–1239

Kakitani Y, Rondonuwu FS, Mizoguchi T, Watanabe Y and Koyama Y (2003) Energy dissipations in chlorosomes: Emission from the Qy state following singlet-singlet and triplet-triplet annihilation Reactions in the cylindrical aggregate and its reversible dissociation into the piggy-back dimers. J Phys Chem B 107: 14545–14555

Karuso P, Bergquist PR, Buckleton JS, Cambie RC, Clark GR and Rickard CEF (1986) 13^2,17^3-Cyclopheophorbide enol, the first porphyrin isolated from a sponge. Tetrahedron Lett 27: 2177–2178

Katz JJ, Strain HH, Harkness AC, Studier MH, Svec WA, Janson TR and Cope BT (1972) Esterifying alcohols in the chlorophylls of purple photosynthetic bacteria. A new chlorophyll, bacteriochlorophyll (*gg*), all-*trans* geranylgeranyl bacteriochlorophyllide *a*. J Amer Chem Soc 94: 7938–7939

Katz JJ, Oettmeier W and Norris JR (1976) Organization of antenna and photo-reaction centre. Chlorophylls on the molecular level. Phil Tran. Roy Soc 273: 227–253

Katz JJ, Norris JR, Shipman LL, Thurnauer MC and Wasielewski MR (1978a) Chlorophyll function in the photosynthetic reaction center. Ann Rev Biophys Bioeng 7: 393–434

Katz JJ, Shipman LL, Cotton TM and Janson TR (1978b) Chlorophyll aggregation: Coordination interactions in chlorophyll monomers, dimers and oligomers. In: Dolphin D (ed) The Porphyrins, pp 402–458. Academic Press, New York

Katz JJ, Bowman MK, Michalski TJ and Worcester DL (1991) Chlorophyll aggregation: Chlorophyll-water micelles as models for in vivo long-wavelength Chlorophyll. In: Scheer H (ed) Chlorophylls, pp 211–236. CRC-Press, Boca Raton

Klement H, Helfrich M, Oster U, Schoch S and Rüdiger W (1999) Pigment-free NADPH:protochlorophyllide oxidoreductase from *Avena sativa L*: Purification and substrate specificity. Eur J Biochem 265: 862–874

Kobayashi M, Watanabe T, Nakazato M, Ikegami I, Hiyama T and Matsunaga T (1988) Chlorophyll a´/P700 and Pheophytin a/P680 stoichiometries in higher plants and cyanobacteria determined by HPLC analysis. Biochim Biophys Acta 936: 81–89

Kobayashi M, Vandemeent EJ, Erkelens C, Amesz J, Ikegami I and Watanabe T (1991) Bacteriochlorophyll *g* epimer as a possible reaction center component of Heliobacteria. Biochim Biophys Acta 1057: 89–96

Kobayashi M, Van de Meent EJ, Ohoka H, Inoue K, Itoh S, Amesz J and Watanabe T (1992) Pigment composition of heliobacteria and green sulfur bacteria. In: Research in Photosynthesis 1: 393–396

Kobayashi M, Akiyama M, Watanabe T and Kano H (1999) Exotic chlorophylls as key components of photosynthesis. Curr Top Plant Biol. 1: 17–35

Kobayashi M, Oh-oka H, Akutsu S, Akiyama M, Tominaga K, Kise H, Nishida F, Watanabe T, Amesz J, Koizumi M, Ishida N and Kano H (2000) The primary electron acceptor of green sulfur bacteria, bacteriochlorophyll 663, is chlorophyll *a* esterified with Delta 2,6-phytadienol. Photosynth Res 63: 269–280

Koepke J, Hu X, Muenke C, Schulten K and Michel H (1996) The crystal structure of the light-harvesting complex II (B800-850) from *Rhodospirillum molischianum*. Structure 4: 581–597

Kunieda M, Mizoguchi T and Tamiaki H (2004) Diastereoselective self-aggregation of synthetic 3-(1-hydroxyethyl)-bacteriopyrochlophyll-*a* as a novel photosynthetic antenna model absorbing near the infrared regions. Photochem Photobiol 79: 55–61

Küpper H, Küpper F and Spiller M (1996) Environmental relevance of heavy metal substituted chlorophylls using the example of water plants. J Exp Bot 47: 259–266

Küpper H, Küpper F and Spiller M (1998) In situ detection of heavy metal substituted chlorophylls in water plants. Photosynth Res 58: 123–133

Kurisu G, Zhang H, Smith JL and Cramer WA (2003) Structure of the cytochrome b_6f complex of oxygenic photosynthesis: Tuning the cavity. Science 302: 1009–1014

Kühlbrandt W, Wang DN and Fujiyoshi Y (1994) Atomic model of plant light-harvesting complex by electron crystallography. Nature 367: 614–621

Kwa LG, Garcia-Martin A, Vegh AP, Strohmann B, Robert B and Braun P (2004) Hydrogen bonding in a model bacteriochlorophyll-binding site drives assembly of light harvesting complex. J Biol Chem 279: 15067–15075

Lanaras T, Moustakas M, Simeonides L, Diamantoglou S and Karataglis S (1993) Plant metal content, growth responses and some photosynthetic measurements of field-cultivated wheat growing on ore bodies enriched in Cu. Physiol Planta 88: 307–314

Lapouge K, Näveke A, Robert B, Scheer H and Sturgis JN (2000) Exchanging cofactors in the core antennae from purple bacteria: Structure and properties of Zn-bacteriophaeophytin containing LH1. Biochemistry 39: 1091–1099

Larkum AW and Kühl M (2005) Chlorophyll *d*: The puzzle resolved. Trends Plant Sci 10: 355–357

Larsen KL, Miller M and Cox RP (1995) Incorporation of exogenons long-chain alcohols into bacteriochlorophyll C homologs by *Chloroflexus aurantiacus*. Arch Microbiol 163: 119–123

Law CJ and Cogdell RJ (1998) The effect of chemical oxidation on the fluorescence of the LH1 (B880) complex from the purple bacterium *Rhodobium marinum*. FEBS Lett 432: 1–2

Leupold D, Stiel H, Ehlert J, Nowak F, Teuchner K, Bandilla M, Ücker B and Scheer H (1999) Photophysical characterization of the B800-depleted light harvesting complex B800–>850nm. Chem Phys Lett 301: 537–545

Liu Z, Yan H, Wang K, Kuang T, Zhang J, Gui L, An X and Chang W (2004) Crystal structure of spinach major light-harvesting complex at 2.72 A resolution. Nature 428: 287–292

Ma L and Dolphin D (1998) The metabolites of dietary chlorophylls. Phytochemistry 50: 195–202

Marchlewski L (1909) Die Chemie der Chlorophylle. Vieweg, Braunschweig

Marquardt J, Senger H, Miyashita H, Miyachi S and Morschel E (1997) Isolation and characterization of biliprotein aggregates from *Acaryochloris marina*, a Prochloron-like prokaryote con-

taining mainly chlorophyll *d*. FEBS Lett 410: 428–432
Matsuura Y and Stewart M (2004) Structural basis for the assembly of a nuclear export complex. Nature 432: 872–877
McDermott G, Prince SM, Freer AA, Hawthornthwaite-Lawless AM, Papiz MZ, Cogdell RJ and Isaacs NW (1995) Crystal structure of an integral membrane light-harvesting complex from photosynthetic bacteria. Nature 374: 517–521
McLuskey K, Prince SM, Cogdell RJ and Isaacs NW (1999) Crystallization and preliminary X-ray crystallographic analysis of the B800-820 light-harvesting complex from *Rhodopseudomonas acidophila* strain 7050. Acta-Cryst.-D. Biol Cryst 55: 885–887
Medforth CJ, Senge MO, Smith KM, Sparks LD and Shelnutt JA (1992) Nonplanar distortion modes for highly substituted porphyrins. J Amer Chem Soc 114: 9859–9869
Michalski TJ, Hunt JE, Bowman MK, Smith U, Bardeen K, Gest H, Norris JR and Katz JJ (1987) Bacteriopheophytin *g* — Properties and some speculations on a possible primary role for bacteriochlorophyll *b* and *g* in the biosynthesis of chlorophylls. Proc Natl Acad Sci USA 84: 2570–2574
Mimuro M, Akimoto S, Gotoh T, Yokono M, Akiyama M, Tsuchiya T, Miyashita H, Kobayashi M and Yamazaki I (2004) Identification of the primary electron donor in PS II of the Chl *d*-dominated cyanobacterium *Acaryochloris marina*. FEBS Lett 556: 95–8
Minehan TG and Kishi Y (1999) Totalsynthese des (+)-Tolyporphin-A-O,O-diacetats mit der vorgeschlagenen Struktur. Angew Chem 111: 972–975
Miyashita H, Adachi K, Kurano N, Ikemoto H, Chihara M and Miyachi S (1997) Pigment composition of a novel oxygenic photosynthetic prokaryote containing chlorophyll *d* as the major chlorophyll. Plant Cell Physiol. 38: 274–281.
Montforts FP, Mueller CM and Lincke A (1990) Bonellin: Determination of its absolute configuration. Liebigs Ann Chem 415–418
Moss GP (1988) IUPAC-IUB Joint Commission on Biochemical Nomenclature (JCBN). Nomenclature of tetrapyrroles (Recommendations 1986). Eur J Biochem 178: 277–328; http://www.chem.qmw.ac.uk/iupac/tetrapyrrole
Musewald C, Hartwich G, Lossau H, Gilch P, Pöllinger-Dammer F, Scheer H and Michel-Beyerle ME (1999) Ultrafast photophysics and photochemistry of (Ni)-bacteriochlorophyll *a*. J Phys Chem B 103: 7055–7060
Neerken S and Amesz J (2001) The antenna reaction center complex of heliobacteria: Composition, energy conversion and electron transfer. Biochim Biophys Acta 1507: 278–290
Niedermeier G, Scheer H and Feick R (1992) The functional role of protein in the organization of bacteriochlorophyll *c* in chlorosomes of *Chloroflexus aurantiacus*. Eur J Biochem 204: 685–692
Noguchi T, Kamimura Y, Inoue Y and Itoh S (1999) Photoconversion of a water-soluble chlorophyll protein from *Chenopodium album*: Resonance Raman and Fourier transform infrared study of protein and pigment structures. Plant Cell Physiol. 40: 305–310
Noy D, Fiedor L, Hartwich G, Scheer H and Scherz A (1998) Metal-substituted bacteriochlorophylls. 2. Changes in redox potentials and electronic transition energies are dominated by intramolecular electrostatic interactions. J Amer Chem Soc 120: 3684–3693
Noy D, Yerushalmi R, Brumfeld V, Ashur I, Scheer H, Baldridge KK and Scherz A (2000) Optical absorption and computational studies of [Ni]-bacteriochlorophyll *a*. New insight into charge distribution between metal and ligands. J Am Chem Soc 122: 3937–3944
Oba T and Tamiaki H (1999) Why do chlorosomal chlorophylls lack the C13(2)-methoxycarbonyl moiety? An in vitro model study. Photosynth Res 61: 23–31
Oba T and Tamiaki H (2002) Which side of the p-macrocycle plane of (bacterio)chlorophylls is favored for binding of the fifth ligand? Photosynth Res 74: 1–10
Oba T, Watanabe T, Mimuro M, Kobayashi M and Yoshida S (1996) Aggregation of chlorophyll *a′* in aqueous methanol. Photochem Photobiol 63: 639–648
Oelze J (1985) Analysis in bacteriochlorophylls. Meth Microbiol 18: 257–284
Oelze J and Golecki JR (1995) Membranes and chlorosomes of green bacteria: Structure, composition and development. In: Blankenship R, Madigan MT and Bauer CE (eds) Anoxygenic Photosynthetic Bacteria, pp 259–278. Kluwer Academic Publishers, Dordrecht
Overmann J and Schubert K (2002) Phototrophic consortia: Model systems for symbiotic interrelations between prokaryotes. Arch Microbiol 177: 201–208
Palaniappan V, Schenck CC and Bocian DF (1995) Low-frequency near-infrared-excitation resonance Raman spectra of (M)H202L mutant reaction centers from *Rhodobacter sphaeroides*. Implications for the structural, vibronic, and electronic properties of the bacteriochlorin cofactors. J Phys Chem 99: 17049–58
Parson W and Nagarajan V (2003) Optical spectroscopy in photosynthetic antennas. In: Green B and Parson W (eds) Light-Harvesting Antennas in Photosynthesis, pp 83–127. Kluwer Academic Publishers, Dordrecht
Pelletier PJ and Caventou JB (1818) Sur la matière verte des feuilles. Ann Chim Phys 9: 194–196
Pelter A, Ballantine JA, Murray-Rust P, Ferrito V and Psaila AF (1978) The structures of anhydrobonellin and bonellin, the physiologically active pigment from the marine echiuroid *Bonellia viridis*. Tetrahedron Lett 1881–1884
Permentier HP, Neerken S, Overmann J and Amesz J (2001) A bacteriochlorophyll *a* antenna complex from purple bacteria absorbing at 963 nM. Biochemistry 40: 5573–5578
Peterman EJ, Wenk SO, Pullerits T, Palsson LO, van Grondelle R, Dekker JP, Rögner M and van Amerongen H (1998) Fluorescence and absorption spectroscopy of the weakly fluorescent chlorophyll *a* in cytochrome b_6f of *Synechocystis* PCC6803. Biophys J 75: 389–398
Pierre Y, Breyton C, Lemoine Y, Robert B, Vernotte C and Popot J-L (1997) On the presence and role of a molecule of chlorophyll *a* in the cytochrome b_6f complex. J Biol Chem 272: 21901–21908
Plato M and Moebius K (1995) Structural characterization of the primary donor in photosynthetic bacteria by its electronic g-tensor. Chem Phys 197: 289–295
Prinsep MR, Caplan FR, Moore RE, Patterson GML and Smith CD (1992) Tolyporphin, a novel multidrug resistance reversing agent from the blue-green alga *Tolypothrix nodosa*. J Amer Chem Soc 114: 385–387
Prinsep MR, Patterson GML, Larsen LK and Smith CD (1998) Tolyporphins J and K, two further porphinoid metabolites from the cyanobacterium *Tolypothrix nodosa*. J Nat Prod 61: 1133–1136

Rau HK, Snigula H, Struck A, Scheer H and Haehnel W (2001) Design, synthesis and properties of synthetic chlorophyll proteins. Eur J Biochem 268: 3284–3295

Rautter J, Lendzian F, Schulz C, Fetsch A, Kuhn M, Lin X, Williams JC, Allen JP and Lubitz W (1995) ENDOR Studies of the Primary Donor Cation Radical in Mutant Reaction Centers of *Rhodobacter sphaeroides* with Altered Hydrogen-Bond Interactions. Biochemistry 34: 8130–8143

Rebeiz CA, Reddy KN, Nandihalli UB and Velu J (1990) Tetrapyrrole-dependent photodynamic herbicides. Photochem Photobiol 52: 1099–1118

Rebeiz CA, Parham R, Fasoula DA and Ioannides IM (1994) Chlorophyll *a* biosynthetic heterogeneity. In: Chadwick DJ and Ackrill K (eds) Biosynthesis of the Tetrapyrroles, pp 177–189. Wiley, Chichester

Rebeiz CA, Gut LJ, Lee K, Juvik JA, Rebeiz CC and Bouton CE (1995) Photodynamics of porphyric insecticides. Crit Rev Plant Sci 14: 329–366

Reed DW, Peters GA (1972) Characterization of the pigments in reaction center preparations from *Rhodopseudomonas spheroides*. J Biol Chem 247: 7148–52

Reinbothe C, Satoh H, Alcaraz J-P and Reinbothe S (2004) A novel role of water-soluble chlorophyll proteins in the transitory storage of chlorophyllide. Plant Physiol. 134: 1355–1365

Robert B, Cogdell R and Van Grondelle R (2003) The Light-harvesting system of purple bacteria. In: Green B and Parson W (eds) Light-Harvesting Antennas in Photosynthesis, pp 169–194. Kluwer Academic Publishers, Dordrecht

Rüdiger W (2002) The last steps of chlorophyll synthesis. In: Kadish KM, Smith KM, and Guilard R (eds) The Porphyrin Handbook, pp 71–108. Academic press, Amsterdam

Satoh K (1993) Isolation and properties of the Photosystem II reaction center. In: Deisenhofer J and Norris JR (eds) The Photosynthetic Reaction Center, pp 289–318. Academic Press, New York

Sauer K (1975) Primary events and the trapping of energy. In: Govindjee (ed) Bioenergetics of Photosynthesis., pp 115–181. Academic Press, New York

Savage H, Cyrklaff M, Montoya G, Kühlbrandt W and Sinning I (1996) Two-dimensional structure of light harvesting complex II (LHII) from the purple bacterium *Rhodovulum sulfidophilum* and comparison with LHII from *Rhodopseudomonas acidophila*. Structure 4: 243–252

Savin YV, Goryachev LV, Adamenkov AA, Adamenkov YuA, Bakshin VV, Buzoverya VV, Vyskubenko BA, Yegorov VV, Ilyin SP, Kolobyanin YuV and Kudryashov EA (2003) Luminescence of oxygen-nitrogen mix microwave discharge products in visible and near-IR spectral ranges: The moving microwave discharge as the singlet (a1Dg) oxygen source. Proc SPIE-Intl Soc Opt Eng 5120: 433–436

Scheer H (2003) The pigments. In: Green B and Parson W (eds) Light-Harvesting Antennas in Photosynthesis, pp 29–81. Kluwer Academic Publishers, Dordrecht

Scheer H and Hartwich G (1995) Bacterial reaction centers with modified tetrapyrrole chromophores. In: Blankenship R, Madigan MT and Bauer CE (eds) Anoxygenic Photosynthetic Bacteria, pp 649–663. Kluwer Academic Publishers, Dordrecht

Scheer H and Katz JJ (1975) Nuclear magnetic resonance spectroscopy of porphyrins and metalloporphyrins. In: Smith KM (ed) Porphyrins and Metalloporphyrins., pp 399–524. Elsevier, New York

Scheer H and Katz JJ (1978) Peripheral metal complexes: Chlorophyll isomers with magnesium bound to the ring E β-ketoester system. J Amer Chem Soc 100: 561–571

Scheer H, Svec WA, Cope BT, Studier MH, Scott RG and Katz JJ (1974) Structure of bacteriochlorophyll *b*. J Amer Chem Soc 96: 3714–3716

Scheer H, Paulke B and Gottstein J (1985) Long-wavelength absorbing forms of bacteriochlorophylls. II. Structural requirements for formation in Triton X100 micelles and in aqueous methanol and acetone. In: Blauer G. and Sund H. (eds) Optical Properties and Structure of Tetrapyrrols, pp 507–521. De Gruyter, London

Schenck CC, Parson WW, Holten D and Windsor MW (1981) Transient states in reaction centers containing reduced Bacteriopheophytin. Biochim Biophys Acta 635: 383–392

Scherz A, Rosenbach-Belkin V., Michalski T.J. and Worcester D.L. (1991) Chlorophyll aggregates in aqueous solutions. In: Scheer H (ed) Chlorophylls, pp 237–268. CRC-Press, Boca Raton

Schiffer M and Norris JR (1993) Structure and function of the photosynthetic reaction center of *Rhodobacter sphaeroides*. In: Deisenhofer J and Norris JR (eds) The Photosynthetic Reaction Center, pp 1–12. Academic Press, New York

Schmidt K, Fufezan C, Krieger-Liszkay A, Satoh H and Paulsen H (2003) Recombinant water-soluble chlorophyll protein from *Brassica oleracea* var. Botrys binds various chlorophyll derivatives. Biochemistry 42: 7427–7433

Schmidt S, Arlt T, Hamm P, Huber H, Nägele T, Wachtveitl J, Zinth W, Meyer M and Scheer H (1995) Primary electron-transfer dynamics in modified bacterial reaction centers containing pheophytin *a* instead of bacteriopheophytin *a*. Spectrochim Acta A 51: 1565–1578

Schoch S, Lempert U and Rüdiger W (1977) Über die letzten Stufen der Chlorophyllbiosynthese: Zwischenprodukte zwischen Chlorophyllid und phytolhaltigem Chlorophyll. Z Pflanzenphysiol 83: 427–436

Schoch S, Helfrich M, Wiktorsson B, Sundqvist C, Rüdiger W and Ryberg M (1995) Photoreduction of Zinc-protopheophorbide *b* with NADPH-protochlorophyllide oxidoreductase from etiolated wheat (*Triticum aestivum L.*). Eur J Biochem 229: 291–298

Senge MO (2000) Highly substituted porphyrins. In: Kadish KM, Smit KM, and Guilard R (eds) The Porphyrin Handbook, pp 239–347. Academic Press, San Diego

Senge MO and Smith KM (1994) Structure and conformation of photosynthetic pigments and related compounds.7. On the conformation of the methyl ester of (20-methyl-phytochlorin ato)nickel(II) — A bacteriochlorophyll *c* model compound. Photochem Photobiol 60: 139–142

Senge MO and Smith KM (1995) Biosynthesis and structures of the bacteriochlorophylls. In: Blankenship R, Madigan MT and Bauer CE (eds) Anoxygenic Photosynthetic Bacteria, pp 137–151. Kluwer Academic Publishers, Dordrecht

Senge MO, Kalisch WW and Runge S (1998) Conformationally distorted chlorins via diimide reduction of nonplanar porphyrins. Tetrahedron 54: 3781–3798

Shen GZ and Vermaas WF (1994) Mutation of chlorophyll ligands in the chlorophyll-binding CP47 protein as studied in a *Synechocystis sp*. PCC 6803 Photosystem I-less background. Biochemistry 33: 7379–7388.

Shimomura O (1980) Chlorophyll-derived bile pigment in bioluminescent Euphausiids. FEBS Lett 116: 203–206

Shioi Y (1991) Analytical chromatography of chlorophylls. In: Scheer H (ed) Chlorophylls, pp 59–88. CRC-Press, Boca Raton

Sings HL, Bible KC and Rinehart KL (1996) Acyl tunichlorins: A new class of nickel chlorins isolated from the Caribbean tunicate *Trididemnum solidum*. Proc Natl Acad Sci USA 93: 10560–10565

Sivakumar V, Wang R and Hastings G (2003) Photo-oxidation of P740, the primary electron donor in Photosystem I from *Acaryochloris marina*. Biophys J 85: 3162–72

Smith JHC and Benitez A (1955) Chlorophylls: Analysis in plant materials. In: Paech K and Tracey M (eds) Methods of Plant Analysis, pp 142–196. Springer, Berlin

Smith KM and Simpson DJ (1986) Stereochemistry of the bacteriochlorophyll *e* homologues. J Chem Soc Chem Comm 102: 1682–1684

Sparks LD, Medforth CJ, Park M-S, Chamberlain JR, Ondrias MR, Senge MO, Smith KM and Shelnutt JA (1993) Metal dependence of the nonplanar distortion of Octaalkyltetra-phenylporphyrins. J Amer Chem Soc 115: 581–591

Spiedel D, Roszak AW, McKendrick K, McAuley KE, Fyfe PK, Nabedryk E, Breton J, Robert B, Cogdell RJ, Isaacs NW and Jones MR (2002) Tuning of the optical and electrochemical properties of the primary donor bacteriochlorophylls in the reaction centre from *Rhodobacter sphaeroides*: Spectroscopy and structure. Biochim Biophys Acta 1554: 75–93

Standfuss J, Terwisscha van Scheftinga AC, Lamborghini M and Kühlbrandt W (2005) Mechanisms of photoprotection and nonphotochemical quenching in pea light-harvesting complex at 2.5 Å resolution. EMBO J 24 : 919–928

Stauber JLJSW (1988) Photosynthetic pigments in fifty-one species of marine diatoms. J Phycol 24: 158–172

Steiner R, Schäfer W, Blos I, Wieschhoff H and Scheer H (1981) Δ2,10-Phytodienol as esterifying alcohol of bacteriochlorophyll b from *Ectothiorhodospira halochloris*. Z Naturforsch 36c: 417–420

Stewart M, Baker RP, Bayliss R, Clayton L, Grant RP, Littlewood T and Matsuura Y (2001) Molecular mechanism of translocation through nuclear pore complexes during nuclear protein import. FEBS Lett 498: 145–149

Stokes GG (1864) On the supposed identity of biliverdin with chlorophyll, with remarks on the constitution of chloropohyll. Proc Roy Soc 13: 144–145

Strell M and Kalojanoff A (1962) Reactions in the chlorophyll series. VIII. Synthesis of pheophorbide *a*. Ann 652: 218–224

Stroebel D, Choquet Y, Popot JL and Picot D (2003) An atypical haem in the cytochrome b_6f complex. Nature 426: 413–418

Struck A, Snigula H, Rau H-K, Hörth P, Scheer H and Haehnel W (1998) Synthetic four-helix bundle protein carrying 1 or 2 chlorophyll derivatives. In: Garab. G. (ed) Photosynthesis: Mechanisms and Effects, pp 4213–4216. Kluwer Academic Publishers, Dordrecht

Sundström V and Grondelle van R (1995) Kinetics of excitation transfer and trapping in purple bacteria. In: Blankenship R, Madigan MT and Bauer CE (eds) Anoxygenic Photosynthetic Bacteria., pp 349–372. Kluwer Academic Publishers, Dordrecht

Tamiaki H, Takeuchi S, Tanikaga R, Balaban S, Holzwarth A and Schaffner K (1994) Diastereoselective control of aggregation of 3^1-epimeric Zinc Methyl Bacteriopheophorbides d in apolar solvents. Chem Lett 1994: 401–402

Tamiaki H, Kitamoto H, Nishikawa A, Hibino T and Shibata R (2004a) Determination of 3(1)-stereochemistry in synthetic bacteriochlorophyll-*d* homologues and self-aggregation of their zinc complexes. Bioorg Med Chem 12: 1657–1666

Tamiaki H, Kitamoto H, Watanabe T and Shibata R (2004b) Self-aggregation of synthetic protobacteriochlorophyll-*d* derivatives. Photochem Photobiol 81: 170–176

Tomo T, Hirano E, Nagata J and Nakazato K (2005) Pigment exchange of Photosystem II reaction center by chlorophyll *d*. Photosynth Res 84: 77–83

Topalov G and Kishi Y (2001) Chlorophyll catabolism leading to the skeleton of dinoflagellate and krill luciferins: Hypothesis and model studies. Angew Chemie 113: 4010–4012

Tronrud DE and Matthews BW (1993) Refinement of the structure of a water-soluble antenna complex from green photosynthetic bacteria by incorporation of the chemically determined amino acid sequence. In: Deisenhofer J and Norris JR (eds) The Photosynthetic Reaction Center, pp 13–22. Academic Press, New York

Tswett M (1906) Adsorptionsanalyse und chromatographische Methode. Anwendung auf die Chemie des Chlorophylls. Ber Dt Bot Ges 24: 384–393

Umetsu M, Seki R, Kadota T, Wang Z, Adschiri T and Nozawa T (2003) Dynamic exchange properties of the antiparallel bacteriochlorophyll *c* dimers. J Phys Chem B 107: 9876–9882

Van de Meent EJ, Kobayashi M, Erkelens C, van Veelen PA, Amesz J and Watanabe T (1991) Identification of 8^1-hydroxychlorophyll *a* as a functional reaction center pigment in *heliobacteria*. Biochim Biophys Acta 1058: 356–362

van Rossum B-J, Boender GJ, Mulder FM, Balaban TS, Holzwarth A, Schaffner K, Prytulla S, Oschkinat H and de Groot HJM (1998) Multidimensional CP -MAS ^{13}C NMR of uniformly enriched chlorophyll. Spectrochim Acta 54: 1167–1176

van Rossum BJ, Steensgaard DB, Mulder FM, Boender GJ, Schaffner K, Holzwarth AR and deGroot HJ (2001) A refined model of the chlorosomal antennae of the green bacterium *Chlorobium tepidum* from proton chemical shift constraints obtained with high-field 2-D and 3-D MAS NMR dipolar correlation spectroscopy. Biochemistry 40: 1587–1595

Vasmel H, Meiburg RF, Kramer HJM, Devos LJ and Amesz J (1983) Optical properties of the photosynthetic reaction center of *Chloroflexus aurantiacus* at low-temperature. Biochim Biophys Acta 724: 333–339

Vavilin D, Xu H, Lin S and Vermaas W (2003) Energy and electron transfer in Photosystem II of a chlorophyll *b*-containing *Synechocystis* sp. PCC 6803 mutant. Biochemistry 42: 1731–1746

Verdeil F (1851) Recherche sur la matière colorante verte des plantes et sur la matière rouge du sang. Compt rend 33: 689

Wakao N, Yokoi N, Isoyama N, Hiraishi A, Shimada K, Kobayashi M, Kise H, Iwaki M, Itoh S, Takaichi S and Sakurai Y (1996) Discovery of natural photosynthesis using Zn containing bacteriochlorophyll in an aerobic bacterium *Acidiphilium rubrum*. Plant Cell Physiol 37: 889–893.

Walter E, Schreiber J, Zass E and Eschenmoser A (1979) Bakteriochlorophyll a_{GG} und Bakteriophäophytin a_p in den photosynthetischen Reaktionszentren von *Rhodospirillum rubrum G9*. Helv Chim Acta 62: 899–920

Wasielewski MR, Norris JR, Shipman LL, Lin CP and Svec WA (1981) Monomeric chlorophyll *a* enol — evidence for its possible role as the primary electron donor in Photosystem I of plant

photosynthesis. Proc Natl Acad Sci USA 78: 2957–2961
Watanabe K, Ohta H, Tsuchiya T, Mikami B, Masuda T, Shioi Y and Takamiya K-I (1999) Purification and some properties of pheophorbidase in *Chenopodium album*. Plant Cell Physiol 40: 104–108
Watanabe N, Yamamoto K, Ihshikawa H, Yagi A, Sakata K, Brinen LS and Clardy J (1993) New chlorophyll-*a*-related compounds isolated as antioxidants from marine bivalves. J Nat Prod 56: 305–317
Watanabe T and Kobayashi M (1991) Electrochemistry of chlorophylls. In: Scheer H (ed) Chlorophylls, pp 287–316. CRC Press, Boca Raton
Weiss C (1978) Optical spectra of chlorophylls. In: Dolphin D (ed) The Porphyrins, pp 211–224. Academic Press, New York
Willstätter R and Hocheder F (1907) Über die Einwirkung von Säiuren und Alkalien auf Chlorophyll. Ann Chem 354: 205–258
Willstätter R and Stoll A (1913) Untersuchungen über Chlorophyll. Springer, Berlin**]**
Woodward RB (1961) The total synthesis of chlorophyll. Pure Appl Chem 2: 383–404
Yeates TO, Komiya H, Chirino A, Rees DC, Allen JP and Feher G (1988) Structure of the reaction center from *Rhodobacter sphaeroides R26 and 2.4.1*: Protein-cofactor (bacteriochlorophyll, bacteriopheophytin and carotenoid) interactions. Proc Natl Acad Sci USA 85: 7993–7997

Chapter 2

Synthesis, Reactivity and Structure of Chlorophylls

Mathias O. Senge,*[a] Arno Wiehe[b] and Claudia Ryppa[a]
[a]*Institut für Chemie, Universität Potsdam, Karl-Liebknecht-Str. 24-25, D-14476 Golm, Germany;*
[b] Biolitec AG, Winzerlaer Str. 2a, D-07745 Jena, Germany

Summary

Chlorophylls (Chls) and bacteriochlorophylls (BChls) are complex tetrapyrroles that continue to attract the attention of synthetic chemists. While Chl reactivity is similar to that of porphyrins, the reduced pyrrole rings which lower their stability and the complex substituent pattern which is observed in nature, makes their syntheses challenging. This chapter reviews the literature from 1990 to 2001 and highlights selected new developments in the organic and structural chemistry of Chl and BChl derivatives with the basic five-ring phytochlorin macrocycle. Structural studies have concentrated on elucidating the influence of different metals and peripheral substituents on the conformational flexibility of the underlying macrocycle. In synthetic chemistry, no significant efforts were made with respect to novel total syntheses of Chls; however, significant advances were made with partial syntheses of numerous BChls with phytochlorin structure, the preparation of divinyl-pheophorbides (Pheides), and the modification of the 3-vinyl group and ring E in Pheides.

*Author for correspondence, email: mosenge@chem.uni-potsdam.de

Bernhard Grimm, Robert J. Porra, Wolfhart Rüdiger and Hugo Scheer (eds): Chlorophylls and Bacteriochlorophylls: Biochemistry, Biophysics, Functions and Applications, pp. 27–37.

I. Basic Structure and Reactivity of Chlorophylls

The chemistry of Chls is governed by the aromatic character of the underlying tetrapyrrole moiety and the reactivity of the functional groups in the side chains. As a cyclic tetrapyrrole with a fused five-membered ring, the overall reactivity of Chls is that of a standard heteroaromatic compound. The extended aromatic system, however, which is capable of coordinating almost any known metal with its core nitrogen atoms, together with the variability of its conformation and its side chains, is responsible for its unique role in photosynthesis. The aromatic system of Pheide *a* **1**, as outlined in Fig. 1, is susceptible mainly to electrophilic reactions, e.g., halogenations, with a preference for reaction at C20, the *meso* position closest to the reduced pyrrole ring. Note that the C7-C8 double bond in phytochlorin is not part of the aromatic delocalization pathway and thus offers a convenient point for modification of the Chl macrocycle via addition and oxidation reactions. The side chain substituents undergo standard transformations, e.g., the C3 vinyl group undergoes addition and oxidation reactions, the ester groups at C17[3] and C13[2] can be saponified or transesterified, and the reactivity of ring E is generally governed by enolization and follow-up chemistry of the β-keto ester system. The latter includes the so-called allomerization reactions, i.e. oxidative degradation reactions involving oxidations, hydroxylation, ring-opening or decarboxylations of the *iso*cyclic pentanone ring. The most comprehensive treatise on Chl chemistry remains the article by Hynninen (1991). Only a few developments have been made in the last decade, which will be the focus of this review.

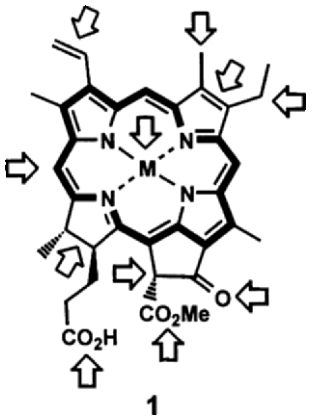

1

Fig. 1. Reactivity profile of pheophorbides also showing ability to incorporate a central metal atom.

II. Conformational Flexibility of Hydroporphyrins

A. The Concept of Macrocycle Flexibility

One aspect of Chls that received more attention in recent years concerned the conformation of the underlying macrocycle. While it is obvious that an extended aromatic system like that of Chl or BChl must be conformationally flexible, the advent of the routine application of X-ray and vibrational spectroscopy to structural studies has enabled more understanding of the importance of this phenomenon for the functional properties of porphyrins. Numerous synthetic, structural and spectroscopic studies have established that macrocycle conformation can control the physicochemical properties of the tetrapyrrole to a significant extent. Increasing nonplanarity with its destabilization of the π-system leads to bathochromically shifted absorption bands, easier oxidation, lower fluorescence yields, larger Stokes shifts, shorter lifetimes of the lowest excited states, faster intersystem crossing and internal conversion. Thus, manipulation of the macrocycle conformation via steric interactions with the surrounding protein side chain in pigment-protein complexes and/or via axial coordination of the central metal can be used to fine-tune the physicochemical properties of the macrocycle. This presents an intriguing rationale for explaining the often diverse (physico)chemical reactivity of the same chromophore in different protein environments. The presence of the reduced pyrrole rings in chlorins and bacteriochlorins leads to even more conformational flexibility than is observed in porphyrins. A complete discussion of this concept and related studies has been presented (Senge, 2000).

B. Structural Studies

Most studies on isolated (B)Chl derivatives have been aimed at providing high-resolution single-crystal X-ray data for theoretical calculations and

Abbreviations: BChl – bacteriochlorophyll; Chl – chlorophyll; DBU– diazabicycloundecene; DMAP– dimethylaminopyridine; PDT– photodynamic therapy; Pheide – pheophorbide; PPTs– pyridinium *p*-toluenesulfonate; TMS– trimethylsilyl

conformational studies (Senge, 1992). As before, no small molecule structure of a Chl or BChl has been reported as the highly amphiphilic character prevents the formation of highly-ordered single crystals. Nevertheless, the more-easily crystallized methyl (B)Pheides and phytochlorins allowed a significant expansion of the structural database.

Studies from my own group included a methyl 12-acetyl-BPheide *d* derivative (Senge et al., 1991), methyl phytochlorin, rhodochlorins, Ni(II) bacteriopetroporphyrins and various methyl metallo-Pheide *a* derivatives (Senge and Runge, 1998). A new crystalline modification of methyl BPheide *a* was described by Barkigia and Gottfried (1994). These studies have also prompted the investigation of atypical metal complexes of Chls; for example, Fe^{II} and Fe^{III} complexes of methyl Pheide *a* derivatives (Kadono et al., 1992; Senge et al., 1995). Several studies on methyl Ni(II) Pheide *a* derivatives, including that of a 20-chloro derivative, allowed comparative analyses of the influence exercised by the central metal, by substituents at $C13^2$, by the degree of reduction (i.e. porphyrin vs. chlorin) and by *meso* substituents (e.g., BChl *c* vs. BChl *d*) on conformation (Senge and Smith, 1994).

III. Chemical Synthesis of Chlorophylls and Bacteriochlorophylls

A. Total Syntheses

Woodward's classic synthesis of Chl *a* and subsequent modifications thereof still remain the only total syntheses of natural (B)Chls (Woodward et al., 1990; Smith, 1991). In the last decade, many strides have been made towards the development of more general chlorin syntheses (Montforts and Glasenapp-Breiling, 1998). However, these were exclusively aimed at the synthesis of hydroporphyrins containing *gem*inally dialkylated saturated pyrrole rings as they are found in compounds like bonellin, factors I-III, heme d_1, siroheme, factor F_{430}, and others. Total syntheses of hydroporphyrins are very laborious and much attention has focused on the development of syntheses using porphyrin-to-hydroporphyrin transformations. These include the typical standard transformations such as S_EAr and S_NAr reactions of the macrocycle and oxidation or reduction reactions. Modern developments include cycloadditions, intramolecular cyclizations, rearrangements and dimerizations (Vicente and Smith, 2000). Nevertheless, the substituent patterns obtained by such transformations are unrelated to naturally-occurring Chls.

B. Partial Syntheses

Two notable synthetic methods were developed in recent years. One involves the synthesis of divinyl derivatives of Chl *a* which are possible intermediates of Chl biosynthesis and important reference compounds. A facile synthesis of an 8-vinyl derivative (see Gerlach et al 1998) involves the reaction of rhodochlorin-15-acetic acid trimethyl ester **2** with OsO_4 to yield the vicinal diol **3** which is dehydrated to the vinyl derivative **4**. Then follows a new type of mild anaerobic recyclization of ring E using triphenylphosphine and sodium bis(trimethylsilyl)amide to form methyl 8-deethyl-8-vinyl Pheide *a* **5** (Scheme 1). Preparation of the 3,8-divinyl derivative (including C13-labeled derivatives) initially involved synthesis of a 3-formyl derivative and then manipulation of the 8-position as shown above. Alternatively, transformation of the 3-vinyl group to an acetal, construction of the 8-vinyl group, followed by reconstruction of the 3-vinyl group gave scaled-up entry to the divinyl chlorin **6**. An even simpler method involves conversion of methyl Pheide *a* to 3-devinyl-3-(1-hexyloxyethyl)-rhodochlorin-15 acetic acid trimethyl ester (Zheng et al., 1999). Reaction with OsO_4/H_2S yielded the respective 7,8-dihydroxy bacteriochlorin derivative and heating in 1,2-dichlorobenzene gave the divinyl compound **6** as the main product.

Similar methods were used by the group of Tamiaki, who developed comprehensive partial syntheses for various derivatives of BChls *d*, *e*, and *f*. Transformation of the 3-vinyl group in methyl $3^1,3^2$-didehydrophytochlorin **7** to an acetyl group followed by synthesis of an 8-vinyl group yielded the central intermediate **8**. The vinyl group can then be cleaved by oxidation with $OsO_4/NaIO_4$ to the 8-formyl derivative **9**, which was alkylated with standard Grignard reagents. Dehydration, hydrogenation and reduction of the 3-acetyl group to a 3-(1-hydroxylethyl) group then resulted in the syntheses of, for example, the methyl 8-propyl-12-methyl BPheide *d* **10** (Tamiaki et al., 1997). The use of 3-acetyl phytochlorins like **11** (or similar BPheides derived from BChl *a*) in asymmetric borane reductions using (*S*)-oxazaborolidines allowed a stereoselective reduction to the (3^1S)-alcohol **12** (Tamiaki et al., 1998).

The use of vicinal diols like **3** also allows an en-

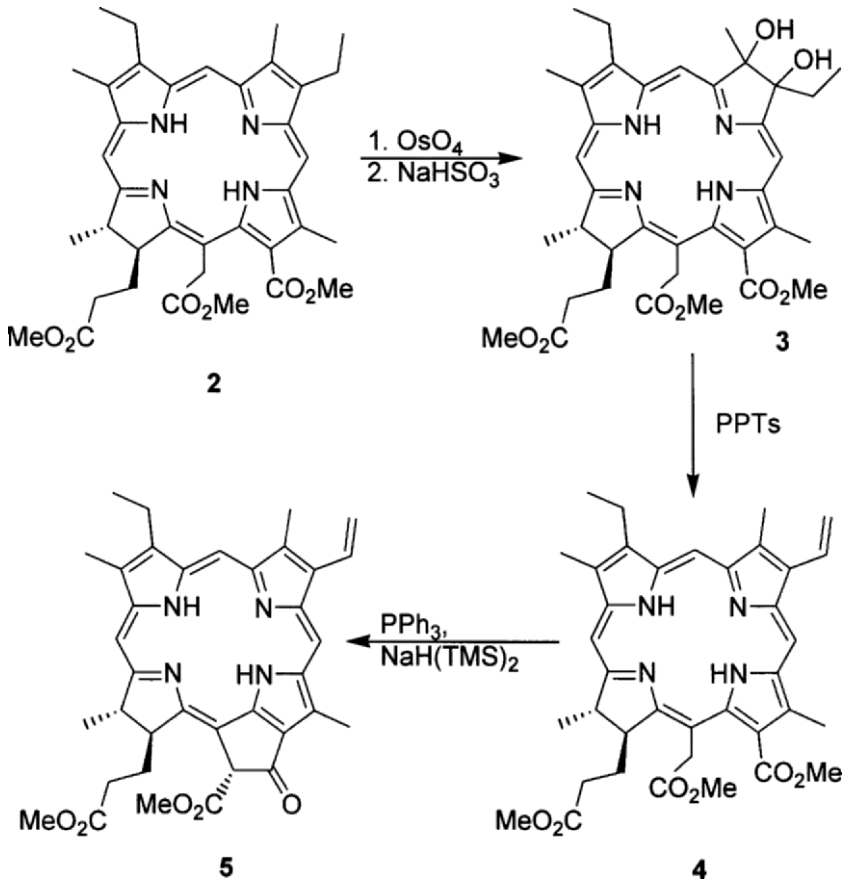

Scheme 1

try into the BChl *e* and *f* series. The 7,8-dihydroxybacteriochlorin derived from **12** with OsO_4 could be dehydrated under mild conditions to a mixture of the primary **13** and secondary alcohols at C7 and C8. The primary alcohol could then be selectively oxidized with pyridinium dichromate to a formyl group yielding a methyl BPheide *f* **14** (Tamiaki et al., 1999). A more facile approach utilized a 3^1,3^2-didehydro-7-demethyl-7-formylphytochlorin **15** (formerly pyropheophytin *b*) synthetically prepared from Pheide *a* (Oba et al., 1997), that was then hydrated with HBr/AcOH to yield a 3^1-epimeric mixture of **14**. Various synthetic derivatives of BChls *e* and *f* suitable for aggregation and spectroscopy studies are accessible via this and related routes (Yagai et al., 1999; Tamiaki et al., 2000). Methyl Pheide *d* **15** (Fischer et al., 1994; Tamiaki et al., 1996a) provided a convenient entry into various Chl *a* homologs **16** with modifications at C3 (Tamiaki and Kouraba, 1997).

IV. Chemical Modifications

A. Manipulation of the Tetrapyrrole Macrocycle

Osmylation of C7-C8 to yield *cis*-diols has become one of the most widely applied methods in Chl chemistry (Pandey et al., 1992a); formally, this constitutes a chlorin to bacteriochlorin conversion. Compared to the old and cumbersome di-imide reduction, this method has the added benefit of yielding β-substituted (dihydro)pyrrole rings that are more stable against oxidation than unsubstituted ones. Using dihydroxylation for initial modification of the Chl macrocycle, further chemistry then allows the various partial syntheses of BChls described above. In addition, this has led to numerous applications in the syntheses of chlorins, bacteriochlorins, and *iso*bacteriochlorins for applications in PDT (Kozyrev et al. 1996a, Pandey, 2000). The *regio*selectivity of this reaction is dependent on the central metal and the

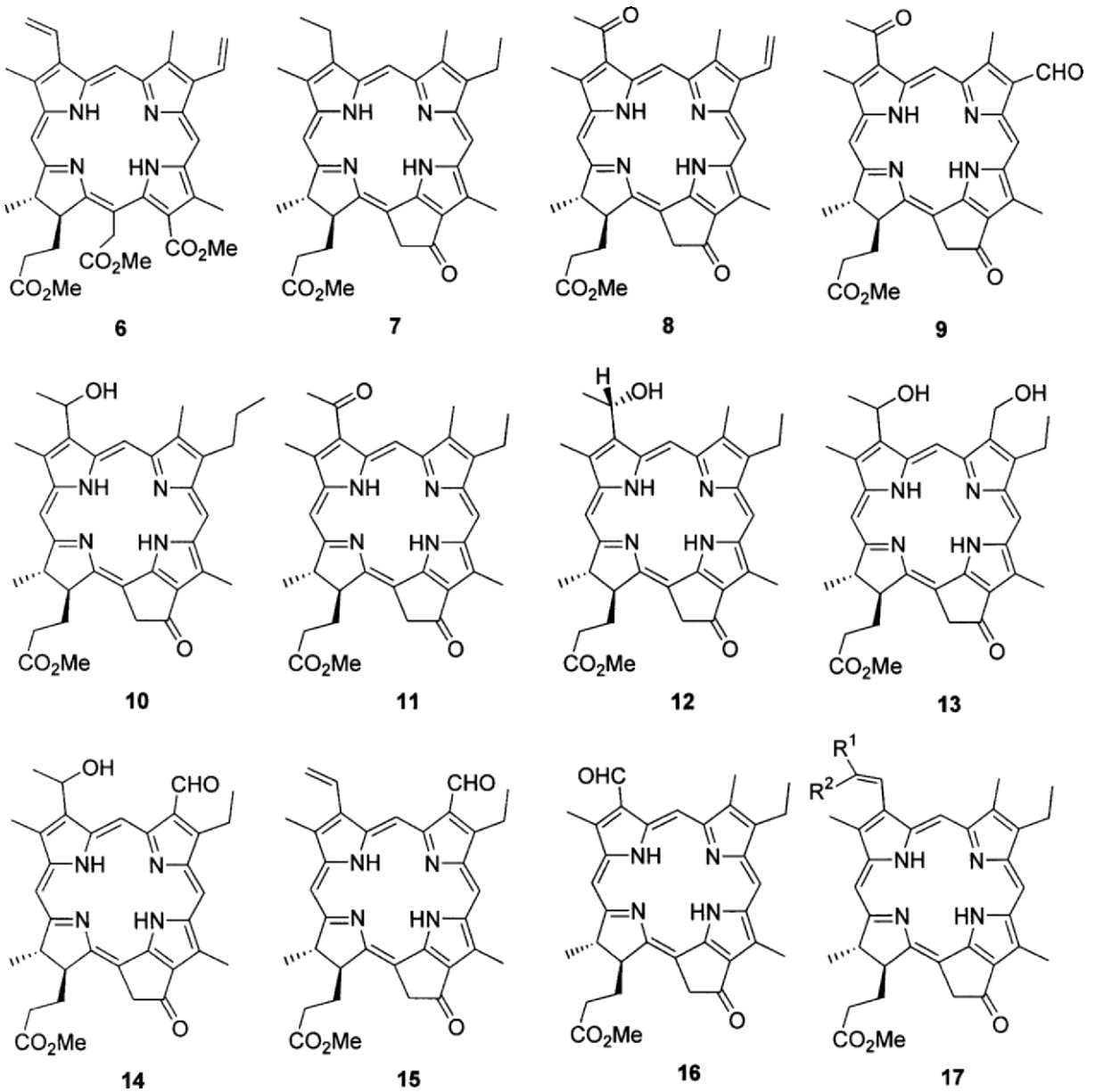

Scheme 2

peripheral substituents. The step following dihydroxylation usually involves *either* dehydratation (to yield 7-methyl-8-vinyl chlorins) *or* pinacol-pinacolone rearrangements (to yield e.g., 7-oxo-8-methyl-8-ethyl bacteriochlorins); however, a thermally induced dimerization yielding C7-C8 linked chlorin dimers that are connected via (–CH=CH–CH_2–)-bridges has also been described (Kozyrev et al., 1999).

Of more specialized interest are methods to prepare 20-halogenated Chl derivatives like **18** as models for BChls *c* and *d*. While some of the compounds have been known for some time, efficient methods for the fluorination (with $CsSO_4F$ or *N*-fluoropyridinium triflate), chlorination (enzymatic with chloroperoxidase or chemically with HCl/H_2O_2 or $NaClO_2$/HCl), and bromination (HBr/H_2O_2) of Pheide and BPheide derivatives have been developed (Senge and Senger, 1989; Kureishi and Tamiaki, 1998; and references cited in both). Several reactions aimed at *regio*selective ring-opening of the macrocycles

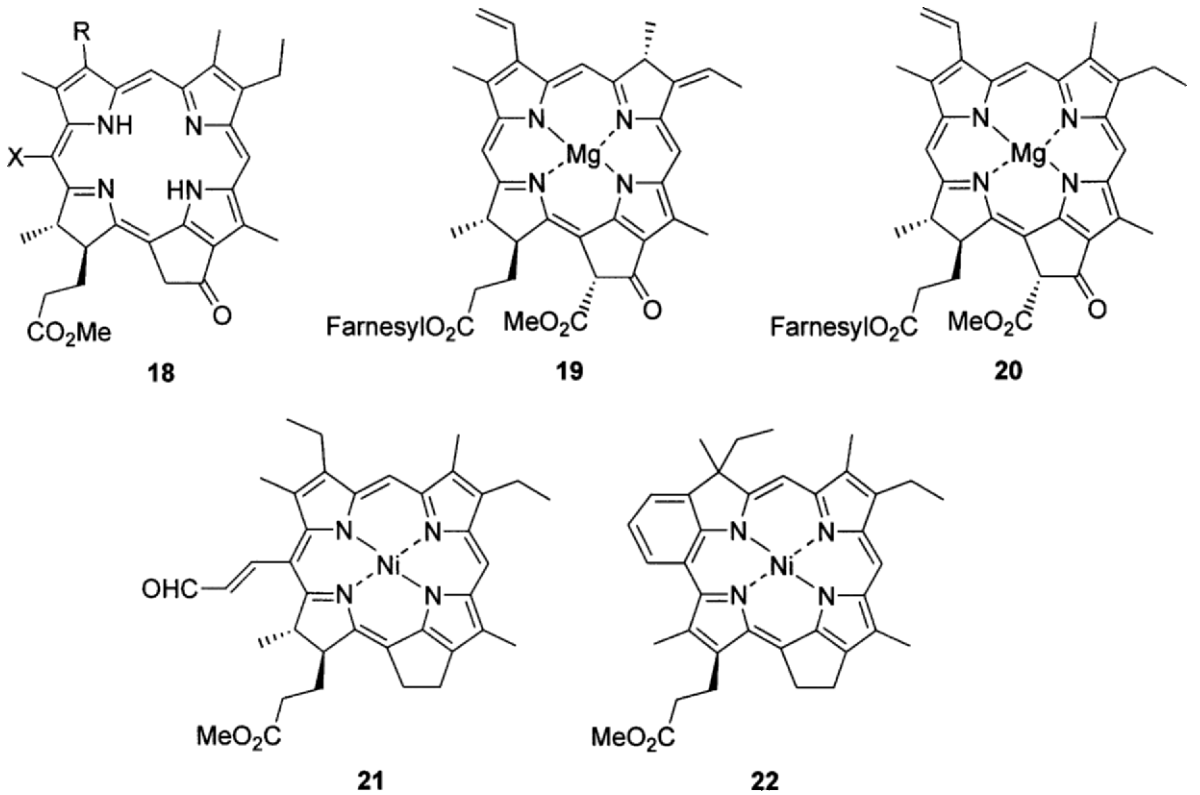

Scheme 3

either at C5 or C20 have been described and will be treated elsewhere (see Kräutler et al., Chapter 17) on Chl degradation.

An interesting BChl to Chl conversion was observed upon treatment of BChl *g* **19** with weak mineral acids in the dark. Within minutes, the more stable Chl *a* derivative **20** is formed via an isomerization reaction (Kobayashi et al., 1998). Unrelated to natural Chls, but interesting from a chemical standpoint, are Chl-derived benzochlorins that carry an annelated benzene ring. These compounds are characterized by significantly red-shifted absorption bands and can be prepared by Vilsmeier reaction of (13^1-deoxo-phytochlorinato methyl ester)nickel(II) with $POCl_3$ and 3-(*N*,*N*-dimethylamino)acrolein to yield **21** followed by acid-catalyzed cyclization to **22** (Mettath et al., 1998).

B. Functional Group Transformations of the Side Chains

Several of the reactions listed in part III.B also serve to yield peripherally altered Chl derivatives (e.g., **17**). A very mild method for the selective reduction of the 7-formyl group in Zn(II) Pheide *b* was developed by Scheumann et al. (1996). In contrast to older methods, the use of $NaBH_3CN$ resulted in sole reduction of the formyl group to the 7^1-hydroxy methyl derivative **23**. Aldehyde functions in Zn(II) Pheide *b* and *d* derivatives have also been used to crosslink Chl derivatives to synthetic proteins carrying an aminooxyacetyl-modified Lys residue via oxime formation (Rau et al., 2001).

Isotopically labeled BPheide *d* models were obtained by Grignard reaction of 3-deethyl-3-formyl-phytochlorins like **16** with $^{13}CH_3MgI$ or CD_3MgI in yields of about 80 % (Tamiaki et al., 1996b). A ^{14}C-labeled Chl derivative, [3^2-^{14}C]Chl *a*, was prepared via ozonolysis of the vinyl group in methyl Pheide *a* and subsequent reduction of the 3^1-formyl group to a -CH_2OH derivative **24**, followed by transformation to the 3-[$CH_2P(Ph)_3$][Br] phosphonium bromide to undergo subsequent Wittig reaction with [^{14}C]para-formaldehyde to yield methyl [3^2-^{14}C]Pheide *a* which was then followed by standard transformation to the Chl *a* derivative (Fischer et al., 1994). The preparation

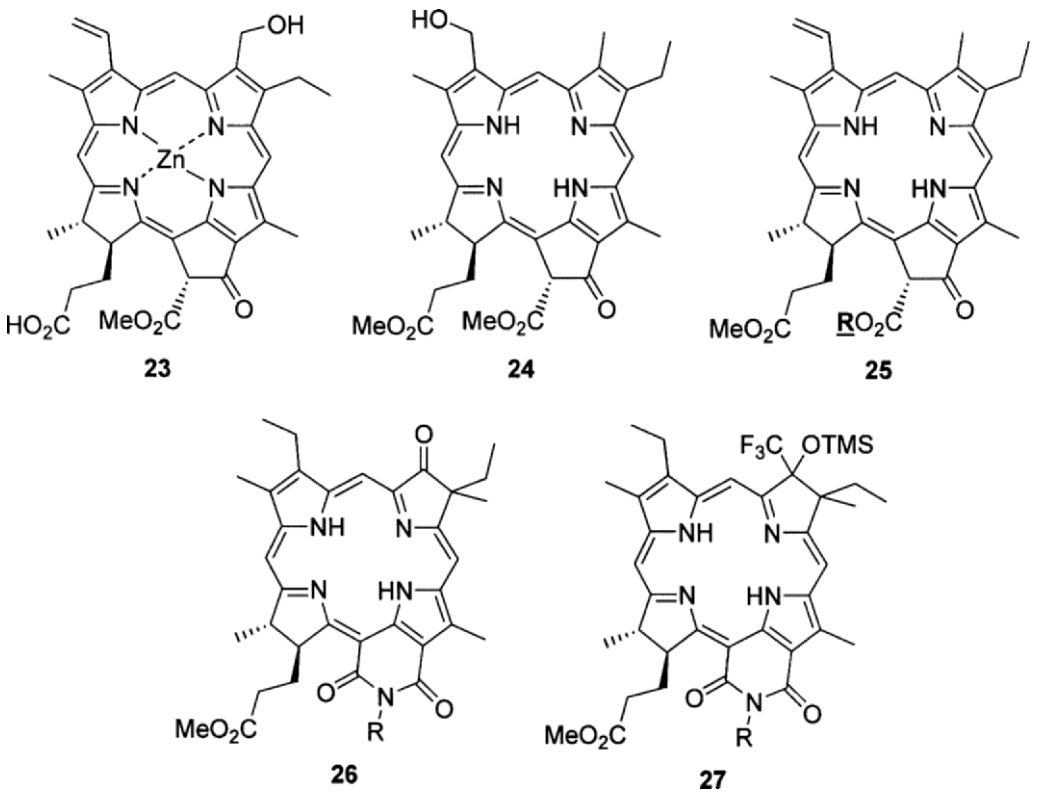

Scheme 4

of 3-deethyl-3-formyl-phytochlorins has also been used to covalently link C_{60} to the Pheide *a* moiety to yield a phytochlorin-fullerene dyad for electron transfer studies (Helaja et al., 1999) while 3-alkoxy-3-deethyl-phytochlorins have been found useful in PDT (Pandey et al., 1996).

Several publications have dealt with new esterification reactions for the carboxylic groups. For example, Pheide-quinone adducts were prepared as esters at C17 in yields of 14 – 25 % using a mixed anhydride method with di-*t*-butyl dicarbonate and a catalytic amount of DMAP (Borovkov et al., 1992). A very convenient method for selective transesterification of the $C13^2$ methyl ester in methyl Pheide *a* was described by Shinoda and Osuka (1996). Treatment of methyl Pheide *a* with various primary and secondary alcohols (including sterols) in the presence of two equiv. of 2-chloro-1-methylpyridinium iodide and 4 equiv. of DMAP exclusively resulted in transesterification of the keto ester to yield compounds of type **25**. Several Zn(II) Chl *a* derivatives esterified with different alcohols in the $C13^4$ position have also been prepared (Furukawa et al., 2000).

A novel approach to perfluorinated hydroporphyrins was reported by Li et al. (1999). $TMSCF_3$ reacted readily with porphyrins containing carbonyl functions and thus could be used for reaction with 7-oxo-8-*gem*inal-dialkyl derivatives **26** (which in turn are derived from vicinal diols like **3** via pinacol-pinacolone rearrangement) to yield trifluoromethylated derivatives **27**.

C. Chemical Manipulations of Ring E

Modification of ring E and the stereochemistry of its substituents plays a major role in controlling the biological function of Chls; e.g., the formation of functional pigment-protein complexes (Storch et al., 1996) or chlorosomal Chl organization (Oba and Tamiaki, 1999). Several analytical studies, mostly employing modern mass spectrometric methods, were aimed at studying the allomerization reaction of Chl (Grese et al., 1990; Rahmani et al., 1993; Brereton et al., 1994; Hyvarinen et al., 1995). A thorough study by Woolley et al. (1998) clearly showed that the 13^2-CO_2Me group is required for allomerization

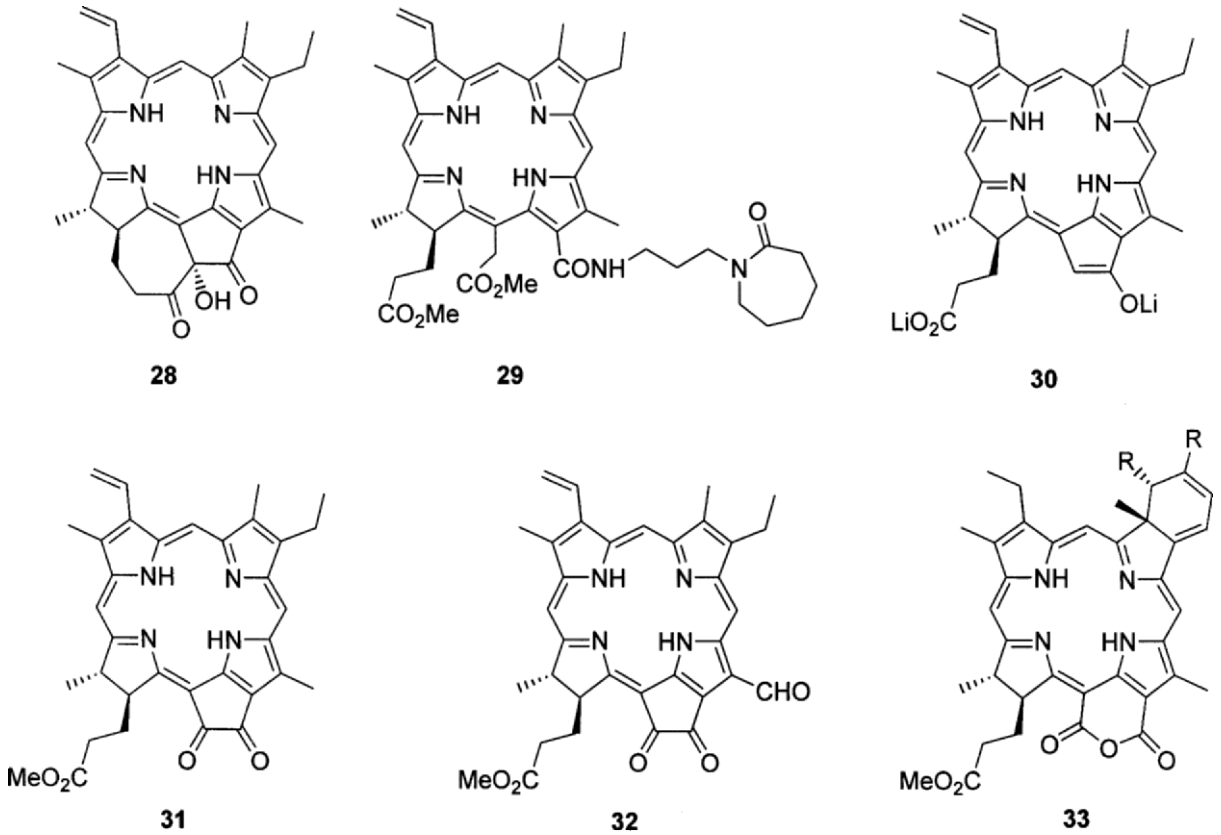

Scheme 5

to occur and that a double rather than single bond between C7 and C8 (e.g., Chl vs. BChl) exerts a significant influence on the reactivity of ring E: ring E in Chl *a* is more susceptible to oxidative ring cleavage and lactone formation than in BChl *a*. Mass spectrometry also played a crucial role in elucidating ring E biosynthesis for (B)Chls from different organisms (Porra and Scheer, 2000).

The isolation of the Ring-E–opened product, 3^1,3^2-didehydrorhodochlorin-15-glyoxylic acid, from a shrub has added another compound to the known list of naturally-occurring allomerization products (Cheng et al., 2001). A rather curious derivative, named chlorophyllone **28**, was isolated from a clam and involves a formerly unknown cyclization of the C17 side chain to ring E at position 13^2 (Sakata et al., 1990).

Another novel reaction was observed upon attempts to prepare stable enol forms of the β-keto ester system (Ma and Dolphin, 1996). Treatment of methyl Pheide *a* with trimethylsilyl triflate to yield an activated electrophilic Pheide species followed by an excess of bases like DBU resulted in a nucleophilic opening of ring E to yield dimethyl 3^1,3^2-didehydro-rhodochlorin-15-acetic acid derivatives like **29** in which the formic acid group is amidated with rearranged products from the base.

A rather intriguing reaction that allows the synthesis of several ring E modified derivatives involves the LiOH promoted allomerization of phytochlorin (Kozyrev et al., 1998). Treatment of 3^1,3^2-didehydrophytochlorin methyl ester with LiOH results in the formation of the stable enolate **30**. This can be autoxidized with O_2/CH_2N_2 to the 13^2-oxophytochlorin **31**. Prolonged oxidation can then yield either 15-carboxyrhodochlorin anhydrides, the 12-demethyl-12-formyl derivative **32** or the related porphyrins. Basic hydrolysis of **31** yields 3^1,3^2-didehydro-15-formyl-rhodochlorin dimethyl ester.

Most synthetic studies in this area were aimed at the preparation of Pheide *a* analogs for applications in PDT (Pandey et al., 1992b; Pandey, 2000). This often concerns the synthesis of either amphiphilic or more soluble derivatives, preferably with either

additional auxochromic groups or an extended aromatic system to yield tetrapyrroles with red-shifted absorption bands. For example, the group of Pandey utilized methyl 3^1,3^2-didehydro-13^2-oxophytochlorin **31** as an entry into Pheides with fused quinoxaline or benzimidazole ring systems (Kozyrev et al., 2000). Purpurins (15-carboxyrhodochlorin anhydrides) or heteroatom derivatives (e.g., **26**) thereof have been used prominently both for the synthesis of chlorins and bacteriochlorins with red-shifted absorption bands. These can then be modified further, e.g., by using the Ring B dihydroxylation method described above (Pandey et al., 1994; Kozyrev et al., 1996b). Alternative methods include the use of either the 3-vinyl or a synthetic 8-vinyl derivative of Pheides as the diene in Diels-Alder reactions. The instability of ring E requires first transformation into e.g., purpurins to then yield benzopurpurins like **33** (R depends on the ene component used) (Zheng et al., 1996).

Acknowledgments

The writing of this article was made possible by support from the Deutsche Forschungsgemeinschaft (Heisenberg Fellowship Se543/3-2) and the Fonds der Chemischen Industrie.

References

Barkigia KM and Gottfried DS (1994) A new crystal form of methyl bacteriopheophorbide *a*. Acta Cryst C50: 2069–2072

Borovkov VV, Gribkov AA, Kozyrev AN, Brandis AS, Ishida A and Sakata Y (1992) Synthesis and properties of pheophorbide-quinone compounds. Bull Chem Soc Japan 65: 1533–1537

Brereton RG, Rahamani A, Liang YZ and Kvalheim OM (1994) Investigation of the allomerization reactions of chlorophyll-*a*. Use of diode-array HPLC, mass spectrometry and chemometric factor. Analysis for the detection of early products. Photochem Photobiol 59: 99–110.

Cheng H-H, Wang, H-K, Ito J, Bastow KF, Tachibana Y, Nakanishi Y, Xu Z, Luo T-Y and Lee K-H (2001) Cytotoxic pheophorbide-related compounds from *Clerodendrum calamitosum* and *C. cyrtophyllum*. J Nat Prod 64: 915–919

Fischer R, Engel N, Henseler A and Gossauer A (1994) Synthesis of chlorophyll *a* labeled at C(3^2) from pheophorbide *a* methyl ester. Helv Chim Acta 77: 1046–1050

Furukawa H, Oba T, Tamiaki H and Watanabe T (2000) Effect of C13^2-stereochemistry on the molecular properties of chlorophylls. Bull Chem Soc Japan 73: 1341–1351

Gerlach B, Brantley SE and Smith KM (1998) Novel synthetic routes to 8-vinyl chlorophyll derivatives. J Org Chem 63: 2314–2320

Grese RP, Cerny RL, Gross ML and Senge M (1990) Determination of structure and properties of modified chlorophylls by using fast atom bombardment combined with tandem mass spectrometry. J Am Soc Mass Spectrom 1: 72–84

Helaja J, Tauber AY, Abel N, Tkachenko NV, Lemmetyinen H, Kilpeläinen I and Hynninen PH (1999) Chlorophylls. IX. The first phytochlorin-fullerene dyads: Synthesis and conformational studies. J Chem Soc, Perkin Trans 1: 2403–2408.

Hynninen, PH (1991) Chemistry of chlorophylls: Modifications. In: Scheer H (ed) Chlorophylls, pp 145–209. CRC Press, Boca Raton

Hyvarinen K, Helaja J, Kuronen P, Kilpelainen and Hynninen PH (1995) H-1 and C-13-NMR spectra of the methanolic allomerization products of 13(2)(R)-chlorophyll-*a*. Magn Res Chem 33: 646–656.

Kadono K, Hori H, Fukuda K, Inoue H, Shirai T and Fluck E (1992) Spectroscopic characterization of iron complexes of methyl pheophorbide with pyridine and its derivatives. Inorg Chim Acta 201: 213–218

Kobayashi M, Hamano T, Akiyama M, Watanabe T, Inoue K, Oh-oka H, Amesz J, Yamamura M and Kise H (1998) Light-independent isomerization of bacteriochlorophyll *g* to chlorophyll *a* catalyzed by weak acid in vitro. Anal Chim Acta 365: 199–203

Kozyrev AN, Dougherty TJ and Pandey RK (1996a) Effect of substituents in OsO_4 reactions of metallochlorins. Regioselective synthesis of isobacteriochlorins and bacteriochlorins. Tetrahedron Lett 37: 3781–3784

Kozyrev AN, Zheng G, Zhu C, Dougherty TJ, Smith KM and Pandey RK (1996b) Syntheses of stable bacteriochlorophyll-*a* derivatives as potential photosensitizers for photodynamic therapy. Tetrahedron Lett 37: 6431–6434

Kozyrev AN, Dougherty TJ and Pandey RK (1998) LiOH promoted allomerization of pyropheophorbide *a*. A convenient synthesis of 13^2-oxopyropheophorbide *a* and its unusual enolization. Chem Commun: 481–482

Kozyrev AN, Zheng G, Shibata M, Alderfer JL, Dougherty TJ, Pandey RK (1999) Thermolysis of *vic*-Dihydroxybacteriochlorins: A new approach for the synthesis of chlorin-chlorin and chlorin-porphyrin dimers. Org Lett 1: 1193–1196

Kozyrev AN, Suresh V, Das D, Senge MO, Shibata M, Dougherty TJ and Pandey RK (2000) Syntheses and spectroscopic studies of novel chlorins with fused quinoxaline or benzimidazole ring systems and the related dimers with extended conjugation. Tetrahedron 56: 3353–3364

Kureishi Y and Tamiaki H (1998) Synthesis and self-aggregation of Zinc 20-halogenochlorins as a model for bacteriochlorophylls *c* / *d*. J Porphyrins Phthalocyanines 2: 159–169

Li G, Chen Y, Missert JR, Rungta A, Dougherty TJ, Grossman ZD and Pandey RK (1999) Application of Ruppert's reagent in preparing novel perfluorinated porphyrins, chlorins and bacteriochlorins. J Chem Soc, Perkin Trans 1: 1785–1787

Ma L and Dolphin D (1996) Nucleophilic reaction of 1,8-diazabicyclo[5.4.0]undec-7-ene and 1,5-diazabicyclo[4.3.0] non-5-ene with methyl pheophorbide *a*. Unexpected products. Tetrahedron 52: 849–860

Mettath S, Shibata M, Alderfer JL, Senge MO, Smith KM, Rein R, Dougherty TJ and Pandey RK (1998) Synthesis and structural properties of novel benzochlorins derived from chlorophyll *a*. J Org Chem 63: 1646–1656

Montforts F-P and Glasenapp-Breiling M (1998) The synthesis

of chlorins, bacteriochlorins, isobacteriochlorins and higher reduced porphyrins. Progr Heterocycl Chem 10: 1–24

Oba T and Tamiaki H (1999) Why do chlorosomal chlorophylls lack the 13^2-methoxy-carbonyl moiety? An in vitro model study. Photosyn Res 61: 23–31

Oba T, Masada Y and Tamiaki H (1997) Convenient preparation of pheophytin *b* from plant extract through the C7-reduced intermediate. Bull Chem Soc Japan 70: 1905–1909

Pandey RK (2000) Recent advances in photodynamic therapy. J Porphyrins Phthalocyanines 4: 368–373

Pandey RK, Shiau F-Y, Isaac M, Ramaprasad S, Dougherty TJ and Smith KM (1992a) Substituent effects in tetrapyrrole subunit reactivity and pinacol-pinacolone rearrangements: *vic*-dihydroxychlorins and *vic*-dihydroxybacteriochlorins. Tetrahedron Lett 33: 7815–7818

Pandey RK, Shiau F-Y, Sumlin AB, Dougherty TJ and Smith KM (1992b) Structure/activity relationships among photosensitizers related to pheophorbides and bacteriopheophorbides. Bioorg Med Chem Lett 2: 491–496

Pandey RK, Shiau F-Y, Sumlin AB, Dougherty TJ and Smith KM (1994) Syntheses of new bacteriochlorins and their antitumor activity. Bioorg Med Chem Lett 4: 1263–1267

Pandey RK, Sumlin AB, Constantine S, Aoudia M, Potter WR, Belinier DA, Henderson BW, Rodgers MA, Smith KM and Dougherty TJ (1996) Alkyl ether analogs of chlorophyll-*a* derivatives. Part 1. Synthesis, photophysical properties and photodynamic efficacy. Photochem Photobiol 64: 194–204

Porra RJ and Scheer H (2000) ^{18}O and mass spectrometry in chlorophyll research: Derivation and loss of oxygen atoms at the periphery of the chlorophyll macrocycle during biosynthesis, degradation and adaptation. Photosynth Res 66: 159–175

Rahmani A, Eckhardt CB, Brereton RG and Maxwell JR (1993) The use of liquid chromatography-mass spectrometry to monitor the allomerization reactions of chlorophyll *a* and pheophytin *a*: Identification of the allomers of pheophytin *a*. Photochem Photobiol 57: 1048–1052

Rau HK, Snigula H, Struck A, Bruno R, Scheer H and Haehnel W (2001) Design, synthesis and properties of synthetic chlorophyll proteins. Eur J Biochem 268: 3284–3295

Sakata K, Yamamoto K-I, Ishikawa H, Yagi A, Etoh H and Ina K (1990) Chlorophyllone-a, a new pheophorbide-a related compound isolated from *Ruditapes philippinarum* as an antioxidative compound. Tetrahedron Lett 31: 1165-1168

Scheumann V, Helfrich M, Schoch S and Rüdiger W (1996) Reduction of the formyl group of zinc pheophorbide *b* in vitro and in vivo: A model for the chlorophyll *b* to *a* transformation. Z Naturforsch 51c: 185–194

Senge MO (1992) The conformational flexibility of tetrapyrroles — current model studies and photobiological relevance. J Photochem Photobiol B: Biol 16: 3–36

Senge MO (2000) Highly substituted porphyrins. In: Kadish KM, Smith KM and Guilard R (hheds) The porphyrin handbook, Vol I, pp 239–347. Academic Press, San Diego

Senge MO and Runge S (1998) Structure and conformation of photosynthetic pigments and related compounds. XI. 5,10,15,20-Tetrabutylbacteriochlorin. Acta Cryst C54: 1917–1919 (and prior articles in this series)

Senge M and Senger H (1989) Enzymic *meso*-chlorination of chlorophylls using chloroperoxidase. Biochim Biophys Acta 977: 177-186

Senge MO and Smith KM (1994) On the conformation of the methyl ester of (20-methyl-phytochlorinato)nickel(II) — A bacteriochlorophyll *c* model compound. Photochem Photobiol 60: 139–142.

Senge MO, Bobe FW and Smith KM (1991) Preparation and crystal structure of methyl [12-acetyl-8-ethyl]-bacteriopheophorbide *d*. — A new bacteriochlorophyll derivative. Liebigs Ann Chem: 871–874.

Senge MO, Ruhlandt-Senge K and Smith KM (1995) Structure and conformation of photosynthetic pigments and related compounds, 8. Molecular structure of an iron(III) chlorophyll derivative — chloro(phytochlorinato methyl ester)iron(III). Z Naturforsch 50b: 139–146

Shinoda S and Osuka A (1996) Transesterification of the *a*-keto ester in methyl pheophorbide-*a*. Tetrahedron Lett 37: 4945–4948.

Smith KM (1991) Chemistry of chlorophylls: Synthesis. In: Scheer H (ed) Chlorophylls, pp 115–143. CRC Press, Boca Raton

Storch K-F, Cmiel E, Schäfer W and Scheer H (1996) Stereoselectivity of pigment exchange with 13^2-hydroxylated tetrapyrroles in reaction centers of *Rhodobacter sphaeroides* R26. Eur J Biochem 238: 280–286

Tamiaki H and Kouraba M (1997) Synthesis of chlorophyll-*a* homologs by Wittig and Knoevenagel reactions with methyl pyropheophorbide-*d*. Tetrahedron 53: 10677–10688

Tamiaki H, Miyata S, Kureishi Y and Tanikaga R (1996a) Aggregation of synthetic zinc chlorins with several esterified alkyl chains as models of bacteriochlorophyll-*c* homologs. Tetrahedron 52: 12421–12432

Tamiaki H, Shimono Y, Rattray AGM and Tanikaga R (1996b) Synthesis of isotopically labeled zinc methyl bacteriopheophorbide-*d* as a model for light harvesting antenna pigments. Bioorg Med Chem Lett 6: 2085–2086

Tamiaki H, Tomida T and Miyatake T (1997) Synthesis of methyl bacteriopheopheophorbide-*d* with 8-propyl group. Bioorg Med Chem Lett 7: 1415–1418

Tamiaki H, Kouraba M, Takeda K, Kondo S-I and Tanikaga R (1998) Asymmetric synthesis of methyl bacteriopheophorbide-*d* and analogues by stereoselective reduction of the 3-acetyl to the 3-(1-hydroxyethyl) group. Tetrahedron: Asymmetry 9: 2101–2112

Tamiaki H, Omoda M and Kubo M (1999) A novel approach toward bacteriochlorophylls-*e* and *f*. Bioorg Med Chem Lett 9: 1631–1632

Tamiaki H, Kubo M and Oba T (2000) Synthesis and self assembly of zinc methyl bacteriopheophorbide-*f* and its homolog. Tetrahedron 56: 6245–6257

Vicente MGH and Smith KM (2000) Porphyrins and derivatives: Synthetic Strategies and reactivity profiles. Curr Org Chem 4: 139–174

Woodward RB, Ayer WA, Breaton JM, Bickelhaupt F, Bonnett R, Buchschacher P, Closs GL, Duffer H, Hannah J, Hauck FP, Ido S, Langemann A, Le Goff E, Leimgruber W, Lwowski W, Sauer J and Valenta Z (1990) The total synthesis of chlorophyll *a*. Tetrahedron 46, 7599–7659

Woolley PS, Moir AJ, Hester RE and Keely BJ (1998) A comparative study of the allomerization reaction of chlorophyll *a* and bacteriochlorophyll *a*. J Chem Soc, Perkin Trans 2: 1833–1839

Yagai S, Miyatake T and Tamiaki H (1999) Self-assembly of

synthetic 8^1-hydroxy-chlorophyll analogues. J Photochem Photobiol B: Biol 52: 74–85

Zheng G, Dougherty TJ and Pandey RK (1999) A simple and short synthesis of divinyl chlorophyll derivatives. J Org Chem 64: 3751–3754

Chapter 3

Chlorophyll *c* Pigments: Current Status

Manuel Zapata
Centro de Investigacións Mariñas, Consellería de Pesca, Xunta de Galicia, Apdo. 13, E36620-Vilanova de Arousa, Spain

José L Garrido
Instituto de Investigacións Mariñas de Vigo (CSIC), Eduardo Cabello 6, E36208-Vigo, Spain

Shirley W. Jeffrey*
CSIRO Division of Marine Research, GPO Box 1538, Hobart, Tasmania 7001, Australia

*Author for correspondence, email: Shirley.Jeffrey@csiro.au

Bernhard Grimm, Robert J. Porra, Wolfhart Rüdiger and Hugo Scheer (eds): Chlorophylls and Bacteriochlorophylls: Biochemistry, Biophysics, Functions and Applications, pp. 39–53.

Summary

Chlorophyll (Chl) *c* pigments are found in nine Divisions of aquatic chromophyte algae, co-occurring with Chl *a* and carotenoids in chloroplast thylakoids, and in two Divisions of photosynthetic prokaryotes. Chls *c* differ from Chls *a*, *b* and *d* in being Mg-phytoporphyrins rather than Mg-chlorins. In addition to Chls c_1, c_2 and c_3, many new Chl *c*-like pigments have recently been isolated and characterized in parallel with advances in separation techniques and spectroscopic methods. Since 1990, the number of known Chls *c* increased from seven (Chls c_1, c_2, c_3, Chl c_{CS-170}, a Chl c_2-like pigment from *Pavlova gyrans*, [DV]-PChlide (i.e. MgDVP) and a nonpolar Chl *c*-like pigment) to eleven compounds. Novel Chls *c* include [MV]-Chl c_3 from the haptophyte *Emiliania huxleyi*, a Chl c_1-like pigment from the dinoflagellate *Kryptoperidinium foliaceum* and two Chl c_2 pigments esterified with monogalactosyl diacylglycerides (MGDG) which have been identified as Chl c_2-MGDG (18:4/14:0) from *E. huxleyi* and Chl c_2-MGDG (14:0/14:0) from *Chrysochromulina polylepis*, respectively. In addition, one nonpolar Chl c_1-like pigment has been isolated from *Prymnesium parvum*. Chl c_2 is the major Chl *c* pigment found in all Divisions of chromophyte algae, either alone or with significant quantities of Chls c_1 and/or c_3. Chl *c* diversity is highest in the Haptophyta.

I. Introduction

The members of the chlorophyll (Chl) *c* family of pigments are widely distributed in the golden-brown eukaryotic algae, the chromophytes, where they function together with Chl *a* and carotenoids as light-harvesting pigments. Chls *c* differ from other Chls in that they are Mg-phytoporphyrins rather than Mg-chlorins (i.e. they have a fully unsaturated tetrapyrrole macrocycle (Budzikiewicz and Taraz, 1971; Jeffrey, 1989; Scheer, 1991). They have a *trans* acrylic (propenoic) acid at C-17 (ring D), instead of the propionic acid side chain of Chls *a* and *b*, which in all polar Chl *c* pigments is not esterified to phytol or other aliphatic long-chain alcohol (i.e. polar Chls *c* are free acid Mg-phytoporphyrins). Structurally, polar Chls *c* are protochlorophyllides (PChlides), but because they are functional light-harvesting pigments, the term 'chlorophyll' will be retained for both polar and nonpolar Chls *c*.

Initially, only Chl c_1 and c_2 were characterized (Jeffrey, 1969, 1972). Subsequently five new Chls *c* were found with advances in separation techniques and spectroscopic methods: Chl c_3 (Jeffrey and Wright, 1987); [DV]-PChlide *a* (also known in phycological literature as MgDVP); Goericke and Repeta, 1993, Helfrich et al., 1999); Chl c_{CS-170} (Jeffrey, 1989); a novel Chl c_2-like pigment from *Pavlova gyrans* (Fawley, 1989a); and a nonpolar Chl *c*-like pigment (presumed 'phytylated') (Nelson and Wakeham, 1989).

Some of these pigments do not have all the characteristics cited above. Both Chl c_{CS-170} (Jeffrey, 1989) and [DV]-PChlide (Helfrich et al., 1999) from green prasinophytes possess a propionic acid side chain at C-17 instead of acrylic acid. In several Chls *c* the C-17 acrylic acid is esterified to a massive lipid side chain (MGDG) (Garrido et al., 2000; Zapata et al., 2001). A modern definition of Chl *c* might therefore be restricted to Mg-containing protochlorophyllide-type compounds, i.e. with fully unsaturated ring D, an *iso*cyclic five carbon atom ring E (Fig. 1 and Table 1), and an oxorhodo-type visible spectrum (Jeffrey, 1989; see Table 2 and Fig. 2).

This chapter reports on the currently known members of the Chl *c* family and their distribution among photosynthetic organisms. We point out the paucity of knowledge of Chls *c* compared to that available for Chls *a* and *b*, and emphasize the need for research on the biosynthesis and function of Chls *c*.

Abbreviations: Chl *c*-MGDG – chlorophyll *c* monogalactosyl-diacylglyceride ester; DV – divinyl; [DV]-PChlide – [3,8-divinyl] protochlorophyllide (or MgDVP); ES-MS – Electrospray mass spectrometry; FAB-MS – fast atom bombardment mass spectrometry; HPLC – high performance liquid chromatography; IUPAC – International Union of Pure and Applied Chemistry; LC-MS – liquid chromatography coupled to mass spectrometry; LHC – light-harvesting complexes; LHCP – light-harvesting chlorophyll proteins; MGDG – monogalactosyl-diacylglycerol; MV – monovinyl; ODS – octadecyl silica; OS – octyl silica; p – phytol; RP-HPTLC – reversed-phase high performance TLC; TLC – thin layer chromatography. Unless otherwise specified, Chls and their derivatives (i.e. Chlides, PChlides, Phes *etc*.) are [3-vinyl-8-ethyl]- (i.e., [MV]-) compounds but some Chls *c* are exceptions: Chls c_2, c_2-MGDG, c_3, $c_{(CS-170)}$ and [DV]-PChlide are all [3,8-divinyl]- (i.e. [DV]-) compounds (see Fig. 1).

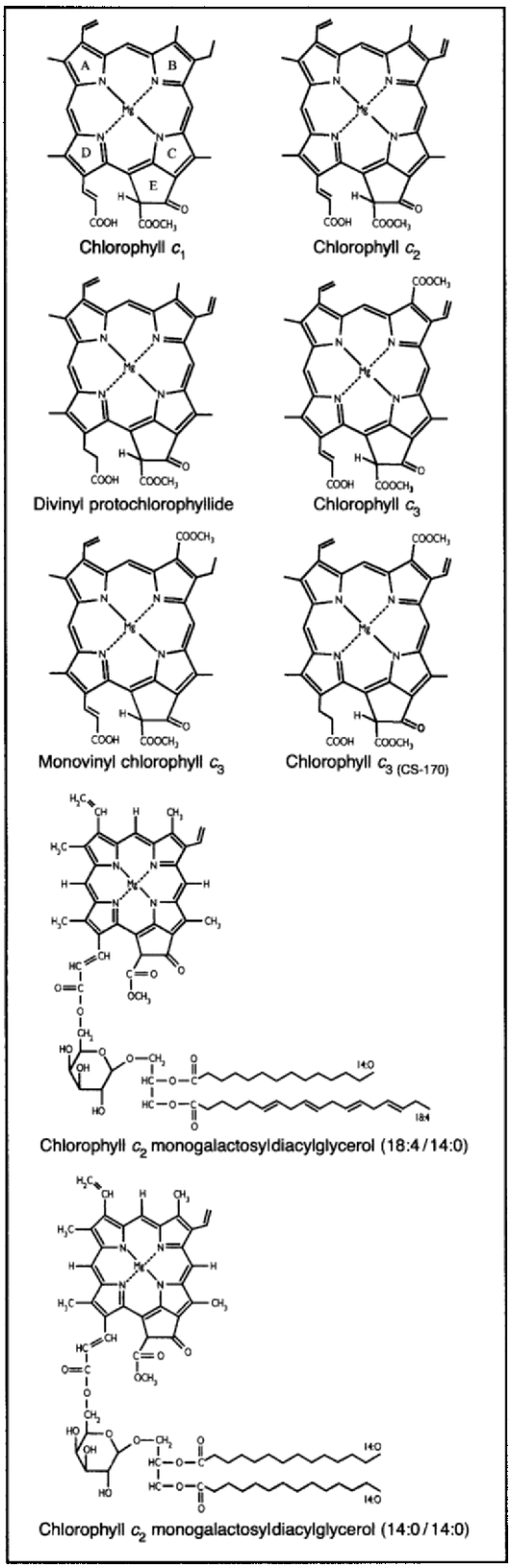

II. Chemistry of Chlorophyll *c* Pigments

A. Polar (Free Acid) Chlorophylls c

1. Chlorphylls c_1 and c_2

The PChlide-like structure of Chl *c* was first deduced by Granick (1949), and the chemical structures were later established by NMR and MS using unresolved mixtures of purified Chl *c* ($c_1 + c_2$) (Dougherty et al., 1966, 1970), and resolved mixtures of Chl *c* methyl esters (Wasley et al., 1970). Both pigments were first separated by TLC, column chromatography and HPLC methods on polyethylene stationary phase (Jeffrey, 1969, 1972, 1989; Shioi and Beale, 1987) and structural confirmation performed on such material (Budzikiewicz and Taraz, 1971; Strain et al., 1971). However, HPLC methods based on monomeric C_{18} columns (Mantoura and Llewellyn, 1983; Zapata et al., 1987; Wright et al., 1991) were unable to separate this [MV]- Chl c_1 and [DV]- Chl c_2 pigment pair (Fig. 1, Table 1) until development of the six sensitive methods lsited in Table 3 of Garrrido and Zapata (Chapter 8).

2. Chlorophyll c_3

A third more polar Chl c_3, was first isolated from the haptophyte alga *E. huxleyi* (Jeffrey and Wright, 1987) and the picoplanktonic chrysophyte *Pelagococcus subviridis* on HPTLC-RP8 plates (Vesk and Jeffrey, 1987). By mass spectrometry (FAB-MS) and ^{1}H-NMR spectroscopy Chl c_3 was identified as [7-methoxycarbonyl]-Chl c_2 (Fookes and Jeffrey, 1989). The presence of a methoxycarbonyl group ($-COOCH_3$) at C-7 (ring B) explained the difference in molecular weight (653 m/z) compared to Chl c_2 (609 m/z), as well as the significant decrease in the absorption band I (Q_y) intensity compared to Chl c_1 and c_2 values (Fig. 2).

Chl c_{CS-170}, isolated on HPTLC-RP8 plates from a tropical strain (CS-170) of the prasinophyte *Micromonas pusilla* (Jeffrey, 1989), was tentatively identified as the propionate derivative of Chl c_3 (Fig. 1) by Fookes and Jeffrey in 1990 (unpublished data) and later reported by Jeffrey et al. (1997).

Analysis of *E. huxleyi* pigment extracts using the polymeric C_{18} HPLC method (Garrido and Zapata,

Fig. 1. Structures of major *c*-type Chls. The IUPAC numbering system (see Chapter 1, Scheer) was used.

Table 1. Comparison of major structural features of chlorophyll *c* pigments. Adapted from Jeffrey (1997a). Substituents assumed at these positions by analogy with: (1) Chl c_3; (2) [DV]-PChlide; (3) Chl c_2; (4) Chl c_1; (5) Chl c_2-MGDG (18:4/14:0).

Chl *c* pigment	Molecular weight	Ring A	Ring B		Acid side chain at C–17	Ester group at C–17[3]	Key references
		C–3	C–7	C–8			
Chl c_1	611	Vinyl	Methyl	Ethyl	Acrylic	_	Budzikiewicz and Taraz (1971), Jeffrey et al. (1997)
Chl c_2	609	Vinyl	Methyl	Vinyl	Acrylic	_	Budzikiewicz and Taraz (1971), Jeffrey et al. (1997)
Chl c_3	653	Vinyl	Methoxycarbonyl	Vinyl	Acrylic	_	Fookes and Jeffrey (1988), Jeffrey et al. (1997)
[MV]-Chl c_3	655	Vinyl	Methoxycarbonyl	Ethyl	Acrylic	_	Garrido and Zapata (1998), Goericke et al. (2000)
Chl $c_{CS\text{-}170}$	655	Vinyl	Methoxycarbonyl (1)	Vinyl (2)	Propionic (2)	_	Jeffrey (1989), C. J. R. Fookes and S. W. Jeffrey (unpublished), Jeffrey et al. (1997)
[DV]-PChlide (MgDVP)	611	Vinyl	Methyl	Vinyl	Propionic	_	Jeffrey (1989), Jeffrey et al. (1997), Helfrich et al. (1999)
Chl c_2-like *Pavlova gyrans*-type	Unknown	Vinyl (3)	Methyl (3)	Vinyl (3)	Acrylic (3)	Unknown	Fawley (1989a)
Chl c_1-like *Kryptoperidinium*-type	Unknown	Vinyl (4)	Methyl (4)	Ethyl (4)	Acrylic (4)	Unknown	M. Zapata, unpublished
Chl c_2-MGDG (18:4/14:0)	1313	Vinyl	Methyl	Vinyl	Acrylic	MGDG (18:4/14:0)	Garrido et al. (2000)
Chl c_2-MGDG (14:0/14:0)	1265	Vinyl	Methyl	Vinyl	Acrylic	MGDG (14:0/14:0)	Zapata et al. (2001)
Nonpolar Chl c_1-like *Prymnesium parvum*-type	1315	Vinyl (5)	Methyl (5)	Ethyl (4)	Acrylic (5)	MGDG (5)	M. Zapata, unpublished

1993) showed the splitting of the Chl c_3 peak into two fractions and both spectral and chromatographic behavior suggested a mixture of the [MV]- and [DV]- forms (Garrido et al., 1995). Later, Garrido and Zapata (1998) obtained evidence by FAB-MS analysis of a molecular ion for the early eluting peak (m/z 655) compatible with [MV]-Chl c_3 and similar results were obtained by Goericke et al. (2000): definitive NMR evidence is still needed.

3. [3,8-Divinyl]-Protochlorophyllide

The occurrence of a Chl *c*-like pigment in green flagellates (class Prasinophyceae) was early recognized (Ricketts, 1966; Jeffrey and Vesk, 1997) but its suggested identification as [DV]-PChlide, frequently abbreviated to MgDVP, was controversial. A Chl *c*-like pigment was identified in *Mantoniella squamata* as Chl c_1, and the simultaneous presence of Chl *a*, *b* and *c* was claimed (Wilhelm, 1987). However, spectral and chromatographic evidence indicated that this pigment was not Chl c_1 but [DV]-PChlide (Jeffrey and Wright, 1987; Jeffrey, 1989; Helfrich et al., 1999).

The coelution of [DV]-PChlide with the above mentioned Chl c_1/Chl c_2 critical pair confused the distribution pattern of [DV]-PChlide in eukaryotic algae. Because only species lacking Chls c_1 and c_2 allowed detection of [DV]-PChlide explains why [DV]-PChlide was considered as a marker pigment for green flagellates of the class Prasinophyceae (see Jeffrey and Vesk, 1997). Once HPLC methods could separate [DV]-PChlide, Chl c_1 and Chl c_2, [DV]-PChlide was found, as a minor compound, in almost all species analyzed (Garrido et al., 1995; Zapata et al., 1998, 2000; Helfrich et al., 1999; Table 3).

Recently, the Chl *c*-like pigment from the green flagellate *Micromonas pusilla* and the cyanobacteria *Prochloron* sp. and *Prochlorococcus marinus* was confirmed as [DV]-PChlide after HPLC isolation and analysis by MS and ^{1}H-NMR spectroscopy (Helfrich et al., 1999).

4. Other Chlorophylls c of Unknown Structure

A novel Chl *c* compound, functioning as a light-harvesting pigment in the haptophyte *Pavlova gyrans* (clone MPPAV), was first reported by Fawley (1989a). Due to the similarity of the absorption spectra, this pigment had previously been misidentified as Chl c_2 (Fawley, 1988). The molecular structure of this polar Chl *c* is unknown.

Another pigment with a chromatographic behavior similar to Chl c_2-like *P. gyrans*-type but spectrally resembling Chl c_1 has recently been isolated from the fucoxanthin-containing dinoflagellate *Kryptoperidinium foliaceum* (M. Zapata and F. Rodriguez, unpublished). Its structure is also unknown.

B. Nonpolar (Esterified) Chlorophylls c

1. Esterified with Phytol?

Gieskes and Kraay (1986) first reported a nonpolar (presumably esterified) Chl *c*-like pigment in seawater samples during a bloom of the haptophyte *Corymbellus aureus*, and characterized its chromatographic retention properties and visible spectrum. Later, Nelson and Wakeham (1989) and Zapata and Garrido (1997) isolated a nonpolar Chl *c* pigment from cultures of the haptophytes *E. huxleyi* and *Isochrysis galbana* respectively. A (partly?) purified fraction analyzed by GC-MS gave positive evidence for phytol (Nelson and Wakeham, 1989), and thus for a phytylated Chl *c*-like pigment both in *E. huxleyi.* and *I. galbana*. Other nonpolar Chl *c* compounds (presumed phytylated derivatives) were reported later by Bidigare et al. (1990) from *Prymnesium parvum*, *Imantonia rotunda* and *Chrysochromulina* sp. and in cultures of many other haptophytes (Jeffrey and Wright, 1994; Garrido et al., 1995; Zapata and Garrido, 1997). Definitive NMR and mass spectra evidence is still needed to confirm the presence of phytol in these nonpolar Chls *c* rather than originating from a possible Chl *a* contaminant.

2. Esterified, but not with Phytol

Garrido et al. (2000) failed to detect phytol by MS in highly purified preparations of a nonpolar Chl *c* from *E. huxleyi*. The high mass molecular ion (m/z 1313) and the fragment ions obtained from it suggested that this nonpolar Chl *c* isolated from *E. huxleyi* had a Chl c_2 chromophore linked to a hydrophobic residue containing the plant membrane lipid, monogalactosyl diacylglyceride (MGDG). Such a chlorophyll, esterified to a massive lipid side chain, is unique in the plant literature (Jeffrey and Anderson, 2000). In the galactolipid moiety, myristic (14:0) and octadecatetraenoic (18:4) fatty acids were identified (Garrido et al., 2000).

Several additional nonpolar Chls *c* were reported in haptophyte algae by Zapata et al. (2001) which shared

common absorption and fluorescence spectra but clearly differed in chromatographic behavior, suggesting that they had the same Chl *c* chromophore linked to MGDG but with different fatty acids attached to the glycerol moiety. This was confirmed when a second very non-polar Chl c_2-MGDG was isolated from the haptophyte C*hrysochromulina polylepis* (Zapata et al., 2001), and found by FAB-MS to have a high mass molecular ion (m/z 1265). The fragmentation pattern was compatible with a Chl c_2-chromophore linked by an ester bond to the sugar moiety of MGDG with two myristic acid (14:0) fatty acid residues.

Another nonpolar Chl *c*-pigment with a Chl c_1-like chromophore was first detected in the haptophyte *Prymnesium parvum* (Garrido et al., 1995). Based on its absorption spectrum and LC-ES (electrospray) MS analysis, the nonpolar Chl *c* pigment was tentatively identified as a Chl c_1-MGDG ester (J. L. Garrido, unpublished).

C. Visible Absorption Spectra

The visible absorption spectra of highly purified and crystalline preparations of Chls c_1 and c_2 from brown seaweeds and chromophyte algae in various solvents were described in the early definitive papers (Jeffrey, 1969, 1972), that of Chl c_3 from *E. huxleyi* (Jeffrey and Wright, 1987), and [DV]-PChlide from the prasinophytes *Micromonas pusilla* and *Mantoniella squamata* (Jeffrey, 1989). These four Chl *c* chromophores are spectrally distinct, particularly in shape, band ratios and position of maxima (Fig. 2). Closely related derivatives of these four chromophores show the spectral characteristics of the parent compounds, e.g. Chl c_3 and Chl $c_{\text{CS 170}}$; Chl c_2 and Chl c_2-MGDG etc (Fig. 2). Table 2 gives spectral characteristics of five recently-described Chl *c* pigments.

D. New High Performance Liquid Chromatography Methods for Analysis of Chlorophyll c Pigments

Many methods have been published since 1991 for separating chlorophyll pigments from microalgal cultures and/or phytoplankton field samples (see review by Jeffrey et al. 1999; also Table 3 in Chapter 8 by Garrido and Zapata). Though similar column chemistry and mobile phase composition are shared by several methods, successful Chl *c* separation by HPLC depends also on elution gradient shape and steepness, flow rate, and column temperature (specially when polymeric columns are employed). The 24 methods listed in Table 3 and its footnote of Garrido and Zapata (Chapter 8) vary widely in their level of Chl *c* resolution.

Basic requirements for the study of Chl *c* pigments in 'new' algal cultures or oceanographic field samples include the clear separation of the key chlorophylls: Chl c_1, c_2, c_3 and [DV]-PChlide and nonpolar esterified pigments. The six methods (listed in Table 3, Chapter 8, Garrido and Zapata) have this basic capability. These six methods use either RP-C_{18} polymeric or RP-C_8 monomeric columns, some with pyridine as solvent modifier, and they separate from six to eleven Chl *c* pigments. However, if all currently recognized Chl *c* pigments need to be assessed for new cultures or field samples, then the RP-C_8 monomeric method with the pyridine modified mobile phase of Zapata et al. (2000) is highly recommended and should be adopted.

One of the methods cited in the footnote of Table 3 of Garrido and Zapata (Chapter 8) is also excellent for carotenoid resolution (Wright et al., 1991), and is recommended for this purpose.

E. Extinction Coefficients and Relative Proportions of Chlorophyll c Pigments

Molar extinction coefficients (ε; $l \cdot mol^{-1} \cdot cm^{-1}$) have only been determined for Chl c_1 and Chl c_2 ($194.3 \cdot 10^3$ at 443.2 nm in 90% aqueous acetone + 1% pyridine and $227.7 \cdot 10^3$ at 443.8 nm in 90% aqueous acetone + 1% pyridine, respectively; Jeffrey, 1972; Jeffrey, 1997b), and [DV]-PChlide ($241 \cdot 10^3$ at 438 nm in 99% acetone + 1% pyridine, Helfrich et al., 1999). To quantify other Chls *c* in chromophyte algae and their isolated LHCs, accurate extinction coefficients must be obtained. In the absence of these data we recommend using the Chl c_1 or Chl c_2 molar extinction coefficients (see Jeffrey et al., 1997) to estimate the *molar* concentration for pigments with the same chromophores (e.g. Chl c_2 coefficient for Chl c_2-MGDG), while an approximate estimation of Chl c_3 and Chl $c_{\text{CS-170}}$ concentrations could be obtained using the mean of the molar extinction coefficients of Chl c_1 and Chl c_2 at the Soret band ($218.4 \cdot 10^3$ at 452.9 nm in acetone + 1% pyridine, see Jeffrey et al., 1997). Note that crystalline polar Chls (c_1, c_2) are not soluble in common solvents (acetone, diethylether, ethanol, etc.) unless first dissolved in a small volume of a highly polar solvent such as pyridine or tetrahydrofuran (Jeffrey, 1972).

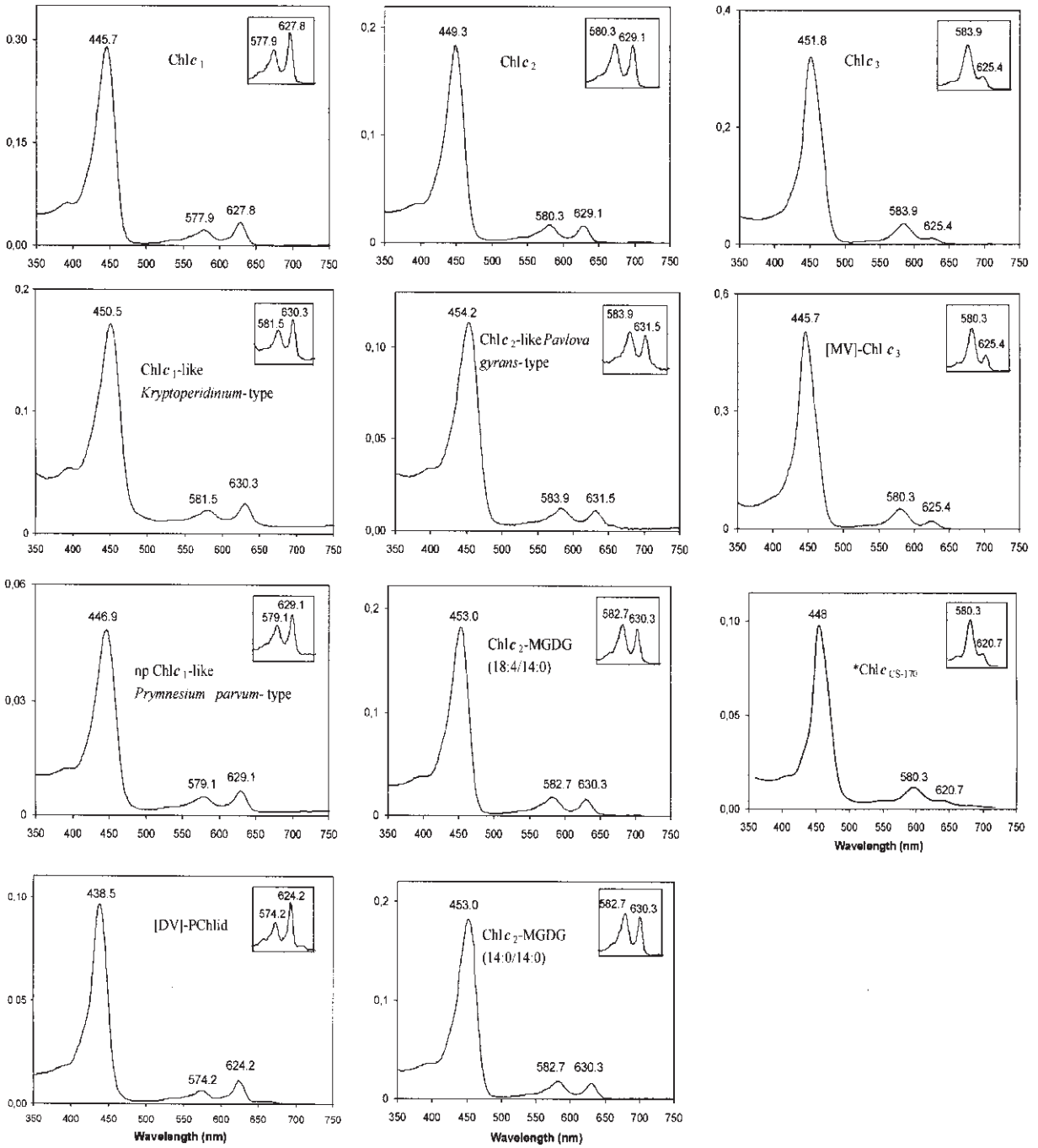

Fig. 2. Visible absorption spectra of major chlorophyll *c* pigments. Spectra of Chl c_1, c_2 and c_3-like pigments are shown in columns beneath the parent compounds (top row) to highlight spectral similarities of chemically-related chromophores; for instance, note that the ratios of band I (at ~630 nm) to band II (at ~580 nm) are >1 (first column; Chl c_1-like chromophores), are ≅1 (second column; Chl c_2-like chromophores) and <1 (third column; Chl c_3-like chromophores). All spectra are in acetone except Chl c_{CS-170}, which is shown in diethyl ether (adapted from Jeffrey et al., 1997). np = non polar.

Table 2. Absorption maxima and band ratios of chlorophyll *c* pigments in various solvents

Chl *c* pigment	Algal source	Solvent	Absorption maxima (nm)			Band ratios		Reference
			III	II	I	III/I	II/I	
Chl c_2-MGDG (18:4/14:0)	*Emiliania huxleyi*	Acetone	452.5	582.0	630.5	10.40	1.10	Garrido et al. (2000)
Chl c_2-MGDG (14:0/14:0)	*Chrysochromulina polylepis*	Diethyl ether	452	581	630	10.32	1.13	Zapata et al. (2001)
Chl c_2-like *Pavlova gyrans*-type	*Pavlova gyrans*	Diethyl ether	454	583	630	13.00	1.07	Fawley (1989a)
Chl c_1-like *Kryptoperidinium*-type	*Kryptoperidinium foliaceum*	Acetone	450.5	581.5	630.3	6.86	0.79	Fig. 2 (this chapter)
Nonpolar Chl c_1-like *Prymnesium*-type	*Prymnesium parvum*	Acetone	450	581	629	8.02	0.64	Fig. 2 (this chapter)

III. Biochemistry of Chlorophyll *c* Pigments

A. Biosynthesis

Based on molecular structure similarities, Bogorad (1976) first suggested that [DV]-PChlide and PChlide could be the biosynthetic precursors to Chl c_2 and c_1, respectively. Beale (1984) also drew attention to these structural similarities postulating that Chl *c* biosynthesis may occur as a closely related branch of the well-studied biosynthetic pathway to Chl *a* (Beale, 1999) diverging from the Chl *a* pathway at either [DV]-PChlide or PChlide. Porra (1997) and Porra et al. (1997) have further developed this scheme for the hypothetical relationships between some newly described Chls *c*.

Porra (1997) suggested that the formation of the 7-methylcarboxylate (i.e. 7-methoxy-carbonyl) group, as in Chl $c_{CS\text{-}170}$ and Chl c_3, may be related to Chl *b* biosynthesis (Porra et al., 1994), but in a hydrophilic environment promoting conversion of Chl *b* to a 7^1-*gem*diol: this is oxidized to a 7-carboxylate and then methylated to a 7-methylcarboxylate by an S-adenosyl-L-methionine-dependent methyltransferase (see scheme 6, Porra, 1997). Since the 7^1-*gem*diol is now known to be an intermediate in Chl *b* synthesis (Oster et al., 2000), the biosynthesis of the 7-methylcarboxylate group would minimally require a 7^1-*gem*-diol oxidase and a methyltransferase. The action of such an enzymatic sequence on [DV]-PChlide and Chl c_2 would result in Chl $c_{CS\text{-}170}$, and Chl c_3, respectively. It is hoped these schemes may soon be tested by direct experimentation.

Accepting the hypothesis that all chloroplasts had a prokaryotic origin, the [DV]- and the [MV]-heterogeneity of Chls observed in chloroplasts of eukaryotic algae and higher plants (Rebeiz et al., 1983) may have resulted from retention of prokaryotic 3,8-DV enzymes (Porra, 1997).

B. Functions

Chl *a*/*c* polypeptides are found in the LHCs of algae in the divisions Heterokonta, Haptophyta, Bacillariophyta, Phaeophyta, Cryptophyta and Dinophyta (Gantt et al., 1998).

It is generally accepted that Chls c_1 and c_2 have a light-harvesting function (Anderson and Barrett, 1986; Grossman et al., 1995; Green and Durnford, 1996; Caron et al., 2001). Evidence is accumulating that other *c*-type Chls may have a similar role: Chl c_3

was found in the LHC of the haptophyte *P. parvum* (Wilhelm and Wiedemann, 1991); a Chl *c* of unknown structure was isolated from the LHC of *Pavlova gyrans* (Fawley, 1989a); and preliminary results suggest a similar LHC location for the Chl *c*-MGDG of *Emiliania huxleyi* (Garrido et al., 2000; Jeffrey and Anderson, 2000). A light-harvesting role for [DV]-PChlide has also been shown in certain prasinophytes (Rhiel et al., 1993) and prochlorophytes (Larkum et al., 1994).

With recently developed chromatographic methods able to resolve the different Chl *c* type compounds (see references in Section II. D), reexamination of LHCs containing Chl *a*/*c* polypeptides by the new HPLC methods (e.g. Zapata et al., 2000) could establish the identity and proportion of Chls *c* present.

An additional role of Chl *c* in the assembly of LHCs has been postulated (Hoober and Eggink, 2001). LHCs usually include an oxidized Chl (i.e., Chl *b,* Chl *c* or Chl *d*) in addition to Chl *a*, which increase the Lewis acid strength of the central Mg atom, strengthening coordination bonds between these oxidized Chls and ligands in LHC apoproteins (LHCPs) and thus promoting assembly of LHCs within the chloroplast envelope. Further, the *trans*-acrylate side chain on ring D transmits electronegativity of the unesterified carboxyl group to the ring π system and reduces basicity of the pyrrole nitrogens in a manner similar to that caused by the formyl group on Chl *b*. LHCPs in chromophytic algae contain the same conserved amino acids as those in chlorophytic organisms (De Martino et al., 1997; Durnford et al., 1999), which suggests that Chl *c* should also form strong coordination bonds with these ligands (Hoober and Eggink, 2001).

Another special role for Chl *c*-MGDG, suggested by Jeffrey and Anderson (2000), may be as a transporter of Chl *c* from the MGDG-rich lipid bilayer of the inner chloroplast envelope membrane (its site of formation and where early stages of pigment biosynthesis occur) to its final location in the thylakoids as an LHCP of the antennae.

IV. Distribution

Chl *c* pigment distribution studies have always been limited by the resolution of available separation methods. The first distribution patterns were determined by a polyethylene TLC procedure which separated Chls c_1 and c_2 (Jeffrey, 1969, 1972, 1976; Jeffrey et al., 1975; Andersen and Mulkey 1983; Jeffrey, 1989). Chl c_2 was considered to be the universal component, since no alga, except a few freshwater chrysophytes, were found with only Chl c_1.

HPTLC-RP8 plates and ODS HPLC systems separated Chl c_3 from Chl [c_1+c_2] (Jeffrey and Wright, 1987, 1994; Vesk and Jeffrey, 1987; Fawley, 1989b; Bidigare et al., 1990; Wright et al., 1991; Stauber and Jeffrey, 1988; Jeffrey, 1989; Johnsen and Sakshaug, 1993). Usually, Chl c_3 replaced Chl c_1, but the three pigments Chls c_1, c_2 and c_3 were found together in the haptophyte *Prymnesium parvum* (Fig. 3D; Fawley, 1989b), one diatom (Stauber and Jeffrey, 1988) and seven species of haptophytes (M. Zapata, S. W. Jeffrey, S. W. Wright, F. Rodriguez, L. L. Garrido and L. Clementson, unpublished).

Other *c*-type Chls show a more restricted distribution, e.g. Chl $c_{CS\text{-}170}$, which has only been detected in *M. pusilla* (CS 170) (Fig. 3A), and [MV]-Chl c_3 in *E. huxleyi* (Fig. 3E); Chl c_2-*P.gyrans*-type in *Pavlova* spp. (Fig. 3B); and, Chl c_1-like-*Kryptoperedinium*-type in *Kryptoperedinium foliaceum* (Fig. 3C). An overview of Chl *c* distribution in microalgae classes, prior to study with the new HPLC methods, is given in Jeffrey and Vesk (1997).

The currently known distribution patterns of Chl *c* pigments in aquatic photosynthetic organisms are shown in Table 3. Most recent data has been obtained by the new HPLC methods based on pyridine-containing mobile phases and monomeric C_8 (Zapata et al., 2000) or polymeric C_{18} columns (Garrido and Zapata, 1997).

The recently described Chls *c*-MGDG may be useful marker pigments of the class Prymnesiophyceae, as well as those small number of dinoflagellates which acquired prymnesiophycean chloroplasts by tertiary endosymbiosis (Tengs et al., 2000). Also, the fatty acid profile of some Chls c_2-MGDG, e.g. those containing 14:0/14:0, seem to be restricted to *Chrysochromulina* species (Fig. 3F) on present evidence (Zapata et al., 2001).

Chromatograms of representative algal species which together contain the full variety of *c*-type pigments are shown in Fig. 3.

V. Applications and Future Directions

Analysis of phytoplankton pigments is widely used in global oceanography to assess phytoplankton biomass, productivity, community structure and eco-

Table 3. Distribution of chlorophyll *c* pigments in major algal classes. Cultures in refs. 1, 3, 4, 6 and 8 were analyzed by using a C_8 HPLC method (Zapata et al., 2000). Cultures in ref. 5 were analyzed using a polymeric C_{18} HPLC method (Garrido and Zapata, 1997); tr: trace.

			Polar Chl *c* pigments									Nonpolar (np) Chl *c* pigments		
Algal Class	Representative species	Ref.	Chl c_2	Chl c_1	[DV]-PChlide	Chl c_3	[MV]-Chl c_3	Chl c_2-like *P. gyrans*-type	Chl c_1-like *Kryptoperidinium*-type	Chl c_{CS+170}	np Chl c_1-like *Prymnesium parvum*-type	Chl c_2-MGDG (18:4/14:0)	Chl c_2-MGDG (14:0/14:0)
Prokaryota													
Oxyphotobacteria	*Prochlorococcus marinus*	1			+								
Oxyphotobacteria	*Acaryochloris marina*	2			+								
Eukaryota													
Cryptophyceae	*Rhodomonas salina*	1	+		tr								
Pavlovophyceae	*Pavlova lutheri*	3	+	+	tr								
Pavlovophyceae	*Pavlova gyrans*	1	+	+	tr			+					
Prymnesiophyceae	*Isochrysis galbana*	3	+	+	tr						+	+	
Prymnesiophyceae	*Prymnesium parvum*	4	+	+	tr	+					+	+	
Prymnesiophyceae	*Emiliania huxleyi*	1	+		tr	+	+					+	
Prymnesiophyceae	*Chrysochromulina polylepis*	4	+		tr	+						+	+
Dinophyceae	*Alexandrium minutum*	1	+		tr								
Dinophyceae	*Prorocentrum lima*	5	+	+	tr								
Dinophyceae	*Kryptoperidinium foliaceum*	6	+	+	tr				+				
Dinophyceae	*Karenia brevis*	6	+		tr	+							tr
Bacillariophyceae	*Skeletonema costatum*	1	+	+	tr								
Bacillariophyceae	*Pseudo-nitzschia multiseries*	5	+	+	tr			+					
Bacillariophyceae	*Navicula jeffreyi*	6	+	+	tr	+							
Bolidophyceae	*Bolidomonas mediterranea*	7	+	+		+							
Raphidophyceae	*Heterosigma akashiwo*	5	+	+	tr								
Pinguiophyceae	*Glossomaxtis chrysoplasta*	6	+	+	tr								
Chrysophyceae	*Phaeoplaca thallosa*	8	+	+				+					
Synurophyceae	*Synura sphagnicola*	8	+	+				+					
Synurophyceae	*Mallomonas papillosa*	8		+					+				
Pelagophyceae	*Pelagococcus subviridis*	1	+		tr	+							
Pelagophyceae	*Pulvinaria* sp.	8	+	+	tr	+							
Dictyophyceae	*Dictyocha speculum*	8	+		tr	+							
Eustigmatophyceae	*Nannochloropsis oculata*	1			tr								
Prasinophyceae	*Micromonas pusilla*	1			+								
Prasinophyceae	*Micromonas pusilla* CS-170	9			+					+			

[1]Zapata et al. (2000), [2]Miyashita et al. (1997), [3]M. Zapata, S. W. Jeffrey, F. Rodriguez, S. W. Wright, L. Clementson and J. L. Garrido (unpublished), [4]Zapata et al. (2001), [5]Zapata et al. (1998), [6]This chapter, [7]Guillou et al. (1999), [8]S.W. Jeffrey and M. Zapata (unpublished), [9]Jeffrey (1989).

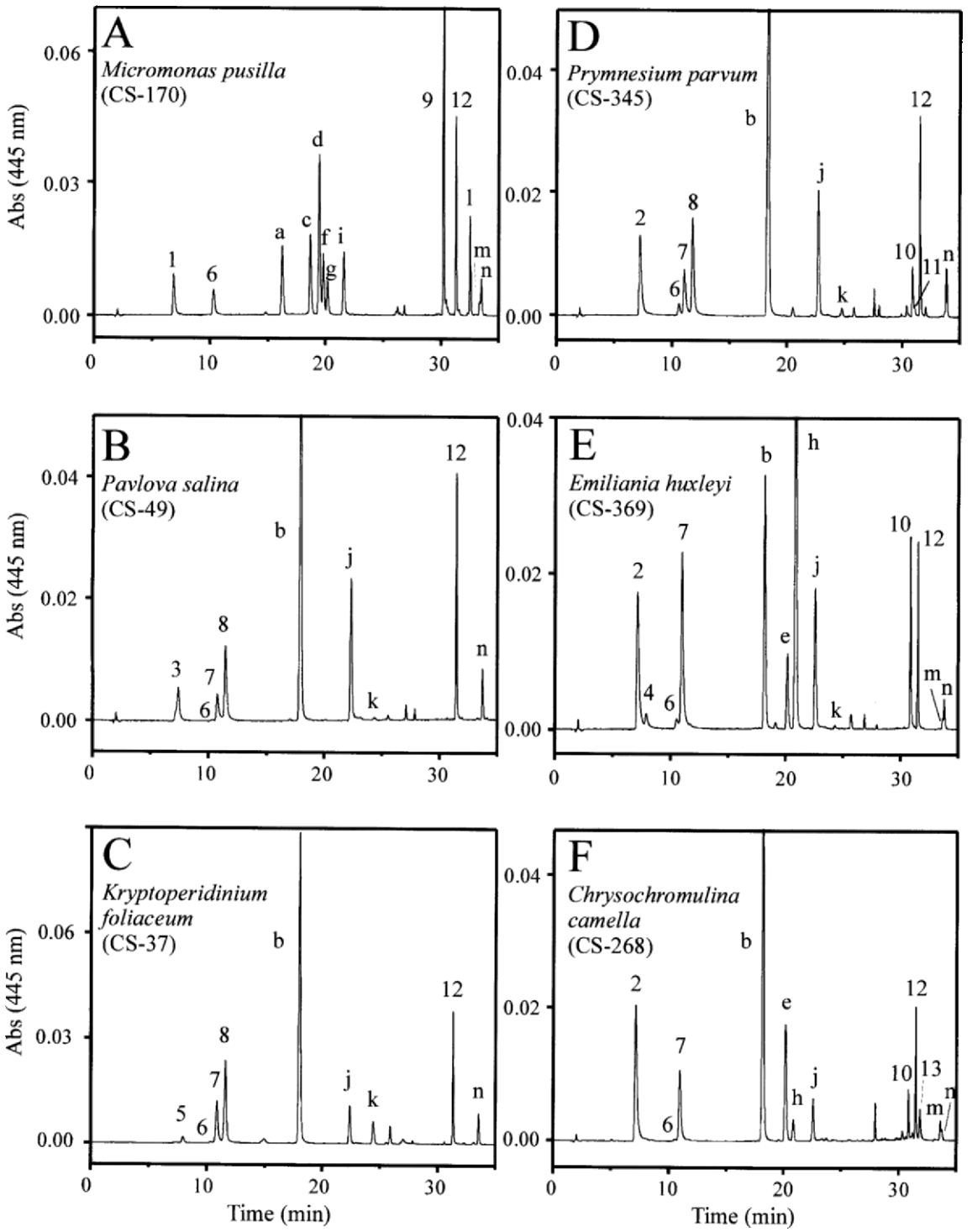

Fig. 3. Chromatograms obtained by high performance liquid chromatography performed on extracts of various algal species (panels A–F) showing separation of 11 chlorophyll *c* pigments. Cultures analyzed by the C_8 HPLC method of Zapata et al. (2000). Pigment code: 1-13 chlorophylls, a-n carotenoids. 1: Chl $c_{CS\text{-}170}$; 2: Chl c_3; 3: Chl c_2-like *Pavlova gyrans*-type; 4: [MV]-Chl c_3; 5: Chl c_1-like *Kryptoperidinium*-type; 6: [DV]-PChlide; 7: Chl c_2; 8: Chl c_1; 9: Chl *b*; 10: Chl c_2-MGDG (18:4/14:0); 11: np Chl c_1-like *Prymnesium parvum*-type; 12: Chl *a*; 13: Chl c_2-MGDG (14:0/14:0); a: uriolide; b: fucoxanthin; c: neoxanthin; d: prasinoxanthin; e: 4-keto-19′-hexanoyloxyfucoxanthin; f: micromonol; g: violaxanthin; h: 19′-hexanoyloxyfucoxanthin; i: micromonal; j: diadinoxanthin; k: diatoxanthin; l: unknown; m: β,ε-carotene; n: β,β-carotene.

logical processes (Wright and van den Enden, 2000; Litaker et al. 2002). Chl *a* is routinely measured by remotely-sensed ocean color in vivo spectra (Chapter 40, Morel), but other pigments, including Chl *c*, require resolution by ship- and laboratory-based HPLC techniques. HPLC pigment data from ships is used to calibrate Chl *a* satellite data at time scales relevant to the satellite observations (Jeffrey and Mantoura, 1997). Sophisticated pigment techniques and remote sensing provide dynamic information of changes in phytoplankton biomass for the global oceans. Improved knowledge of pigment distributions in microalgal taxa can help refine this process.

Much new work is needed to bring understanding of the *c*-type chlorophylls to a level comparable with the well-studied Chls *a* and *b*. In particular, we recommend:

- completing chemical structure elucidation (MS, NMR) of the novel unidentified Chl *c* pigments described above;
- determination of extinction coefficients of Chl *c* pigments for which no data is available;
- exploring biosynthetic pathways of Chls *c* in major chromophyte taxa by identifying the enzymes involved and the specificity of their reactions;
- describing the function of Chl *c* pigments in the LHCs of the photosynthetic apparatus; and,
- understanding the mechanisms and functions of light-induced interconversions of [DV]- and [MV]-Chl *c* pigments (e.g. Chl c_2 ⇆ Chl c_1; Chl c_3 ↔ [MV]-Chl c_3).

Note Added in Proof

Two research papers, published in 2003/04, discussed the phylogenetic distribution of algal pigments (especially the expanding Chl *c* family). They used newly available microalgal cultures and employed the most advanced HPLC pigment methods. Both studied chemotaxonomy of the *Haptophyta* (Van Lenning et al.,2003; Zapata et al., 2004). The latter paper identified nine Chl *c* derivatives by HPLC and distinguished eight new pigment types across 65 cultured strains from seven haptophyte families. This paper demonstrates the value of the most advanced pigment methods for unravelling chemotaxonomic relationships. A review (Jeffrey and Wright, 2005) based pigment distributions on current theories of plastid diversity through serial endosymbiosis (Delwiche, 1999). Sixteen chlorophylls (including 11 Chl *c* derivatives), 37 carotenoids and three phycobiliprotein types across 32 algal pigment groups highlighted new pigment distributions; for example, five new pigment types in the *Chloroxybacteria*, three in the *Prasinophyta*, three in the *Chrysophyta*, eight in the *Haptophyta* and five in the *Dinophyta*. The remaining six microalgal pigment types are well-known from the *Euglenophyta, Cryptophyta, Bolidophyta, Bacillariophyta, Raphidophyta* and *Eustigmatophyta*. Chl *c* distributions were again significant contributors to identifying new chemotaxonomic relationships.

Acknowledgments

We thank Francisco Rodríguez, Lesley Clementson and Simon Wright for helpful comments on the text. Louise Bell of CSIRO Marine Research provided the structures diagram. Santiago Fraga provided *Glossomaxtis chrysoplasta* and *Karenia brevis* cultures.

References

Andersen RA and Mulkey TJ (1983) The occurrence of chlorophylls c_1 and c_2 in the Chrysophyceae. J Phycol 19: 289–294

Anderson JM and Barrett J (1986) Light-harvesting pigment-protein complexes of algae. In: Staehelin LA and Arntzen CAJ (eds) Photosynthesis III. Photosynthetic Membranes and Light Harvesting Systems,. pp 269–285, Springer-Verlag, Berlin

Beale SI (1984) Biosynthesis of photosynthetic pigments. In: Baker NR and Barber J (eds) Chloroplast Biogenesis, pp 135–205. Elsevier, Amsterdam

Beale SI (1999) Enzymes of chlorophyll biosynthesis. Photosynth Res 60: 43–73

Bidigare RR, Kennicutt MC, Ondrusek ME, Keller MD and Guillard RRL (1990) Novel chlorophyll-related compounds in marine phytoplankton: Distributions and geochemical implications. Energy Fuels 4: 653–657

Bogorad L (1976) Chlorophyll biosynthesis. In: Goodwin TW (ed) Chemistry and Biochemistry of Plant Pigments, pp 64–148. Academic Press Inc, London

Budzikiewicz H and Taraz K (1971) Chlorophyll *c*. Tetrahedron 27: 1447–1460

Caron L, Douady D, De Martino A and Quinet M (2001) Light harvesting in brown algae. Cah Biol Mar 42: 109–124

De Martino A, Douady D, Rousseau B, Duval JC and Caron L (1997) Characterization of two light-harvesting subunits

isolated from the brown alga *Pelvetia canaliculata*: Heterogeneity of xanthophyll distribution. Photochem Photobiol 66: 190–197

Delwiche CF (1999) Tracing the thread of plastid diversity through the tapestry of life. Amer Nat 154: S164–S177

Dougherty RC, Strain HH, Svec WA, Uphaus RA and Katz JJ (1966) The structure, properties and distribution of chlorophyll *c*. J Amer Chem Soc 88: 5037–5038

Dougherty RC, Strain HH, Svec WA, Uphaus RA and Katz JJ (1970) The structure, properties and distribution of chlorophyll *c*. J Amer Chem Soc 92: 2826–2833

Durnford DG, Deane JA, Tan S, McFadden GI, Gantt E and Green BR (1999) A phylogenetic assessment of the eukaryotic light-harvesting antenna proteins, with implications for plastid evolution. J Mol Evol 48: 59–68

Fawley MW (1988) Separation of chlorophylls c_1 and c_2 from pigment extracts of *Pavlova gyrans* by reversed-phase high performance liquid chromatography. Plant Physiol 86: 76–78

Fawley MW (1989a) A new form of chlorophyll *c* involved in light-harvesting. Plant Physiol 91: 727–732

Fawley MW (1989b) Detection of chlorophylls c_1, c_2 and c_3 in pigment extracts of *Prymnesium parvum* (Prymnesiophyceae). J Phycol 25: 601–604

Fookes CJR and Jeffrey SW (1989) The structure of chlorophyll c_3, a novel marine photosynthetic pigment. J Chem Soc Chem Commun 23: 1827–1828

Gantt E, Cunningham FX, Grabowski B and Tan S (1998) Relatedness of carotene-chlorophyll antenna complexes in algae and plants. In Garab G (ed) Photosynthesis: Mechanisms and Effects, Vol I, pp 239–247. Kluwer Academic Publishers, Dordrecht

Garrido JL and Zapata M (1993) High performance liquid chromatographic separation of polar and non-polar chlorophyll pigments from algae using a wide pore polymeric octadecylsilica column. J High Resolut Chromatogr 16: 229–233

Garrido JL and Zapata M (1997) Reversed-phase high-performance liquid chromatographic separation of mono- and divinyl chlorophyll forms using pyridine-containing mobile phases and a polymeric octadecylsilica column. Chromatographia 44: 43–49

Garrido JL and Zapata M (1998) Detection of new pigments from *Emiliania huxleyi* (Prymnesiophyceae) by high-performance liquid chromatography, liquid chromatography-mass spectrometry, visible spectroscopy, and fast atom bombardment mass spectrometry. J Phycol 34: 70–78

Garrido JL, Zapata M and Muñiz S (1995) Spectral characterization of new chlorophyll *c* pigments isolated from *Emiliania huxleyi* (Prymnesiophyceae) by high-performance liquid chromatography. J Phycol 31: 761–768

Garrido JL, Otero J, Maestro MA and Zapata M (2000) The main nonpolar chlorophyll *c* from *Emiliania huxleyi* (Prymnesiophyceae) is a chlorophyll c_2-monogalactosyldiacylglyceride ester: a mass spectrometry study. J Phycol 36: 497–505

Gieskes WWC and Kraay GW (1986) Analysis of phytoplankton pigments by HPLC before, during and after mass occurrence of the microflagellate *Corymbellus aureus* during the spring bloom in the open northern North Sea in 1983. Mar Biol 92: 45–52

Goericke R and Repeta DJ (1993) Chlorophylls *a* and *b* and divinyl chlorophylls *a* and *b* in the open subtropical North Atlantic Ocean. Mar Ecol Prog Ser 101: 307–313

Goericke R, Olson RJ and Shalapyonok A (2000) A novel niche for *Prochlorococcus* sp. in suboxic environments in the Arabian Sea and the Eastern Tropical North Pacific. Deep-Sea Res I 47: 1183–1205

Granick S (1949) The pheoporphyrin nature of chlorophyll *c*. J Biol Chem 179: 505

Green BR and Durnford DG (1996) The chlorophyll-carotenoid proteins of oxygenic photosynthesis. Annu Rev Plant Physiol Plant Mol Biol 47: 685–714

Grossman AR, Bhaya D, Apt KE and Kehoe DM (1995) Light-harvesting complexes in oxygenic photosynthesis: Diversity, control and evolution. Annu Rev Genetics 29: 231–288

Guillou L, Chrétiennot-Dinet M-J, Medlin LK, Claustre H, Loiseaux-de Goër S and Vaulot D (1999) *Bolidomonas*: A new genus with two species belonging to a new algal class, the Bolidophyceae (Heterokonta) J Phycol 35: 368–381

Helfrich M, Ross A, King GC, Turner AG and Larkum AWD (1999) Identification of [8-vinyl]-protochlorophyllide *a* in phototrophic prokaryotes and algae: Chemical and spectroscopic properties. Biochim Biophys Acta 1410: 262–272

Hoober JK and Eggink LL (2001) A potential role of chlorophylls *b* and *c* in assembly of light-harvesting complexes. FEBS Lett 489: 1–3

Jeffrey SW (1969) Properties of two spectrally different components in chlorophyll *c* preparations. Biochim Biophys Acta 177: 456–467

Jeffrey SW (1972) Preparation and some properties of crystalline chlorophyll c_1 and c_2 from marine algae. Biochim Biophys Acta 279: 15–33

Jeffrey SW (1976) The occurrence of chlorophyll c_1 and c_2 in algae. J Phycol 12: 349–354

Jeffrey SW (1989) Chlorophyll *c* pigments and their distribution in the chromophyte algae. In: Green JC, Leadbeater BSC and Diver WL (eds) The Chromophyte Algae: Problems and Perspectives, pp 13–36. Clarendon Press, Oxford

Jeffrey SW (1997a) Structural relationships between algal chlorophylls. In: Jeffrey SW, Mantoura RFC and Wright SW (eds) Phytoplankton Pigments in Oceanography: Guidelines to Modern Methods, pp 566–571. UNESCO Publishing, Paris

Jeffrey SW (1997b) Chlorophyll and carotenoid extinction coefficients. In: Jeffrey SW, Mantoura RFC and Wright SW (eds) Phytoplankton Pigments in Oceanography: Guidelines to Modern Methods, pp 595–596. UNESCO Publishing, Paris

Jeffrey SW and Anderson JM (2000) *Emiliania huxleyi* (Haptophyta) holds promising insights for photosynthesis. J Phycol 36: 449–452

Jeffrey SW and Mantoura RFC (1997) Development of pigment methods for oceanography: SCOR-supported Working Groups and objectives. In: Jeffrey SW, Mantoura RFC and Wright SW (eds) Phytoplankton pigments in oceanography: Guidelines to modern methods, pp 19–36. UNESCO Publishing, Paris

Jeffrey SW and Vesk M (1997) Introduction to marine phytoplankton and their pigment signatures. In: Jeffrey SW, Mantoura RFC and Wright SW (eds) Phytoplankton Pigments in Oceanography: Guidelines to Modern Methods, pp 37–84. UNESCO Publishing, Paris

Jeffrey SW and Wright SW (1987) A new spectrally distinct component in preparations of chlorophyll *c* from the microalga *Emiliania huxleyi* (Prymnesiophyceae). Biochim Biophys Acta 894: 180–188

Jeffrey SW and Wright SW (1994) Photosynthetic pigments in the Haptophyta. In: Green JC and Leadbeater BSC (eds) The

Haptophyte Algae, pp 111–132. Clarendon Press, Oxford
Jeffrey SW, Sielicki M and Haxo FT (1975) Chloroplast pigment patterns in dinoflagellates. J Phycol 11: 374–384
Jeffrey SW and Wright SW (2006) Photosynthetic pigments in marine microalgae: Insights from cultures and the sea. In: Subba Rao DV (ed) Algal Cultures, Analogues of Blooms and Applications. Science Publishers, Enfield, in press
Jeffrey SW, Mantoura RFC and Bjørnland T (1997) Data for the identification of 47 key phytoplankton pigments. In: Jeffrey SW, Mantoura RFC and Wright SW (eds) Phytoplankton Pigments in Oceanography: Guidelines to Modern Methods, pp 449–559. UNESCO Publishing, Paris
Jeffrey SW, Wright SW and Zapata M (1999) Recent advances in HPLC pigment analysis of phytoplankton. Mar Freshwater Res 50: 879–896
Johnsen G and Sakshaug E (1993) Bio-optical characteristics and photoadaptive responses in the toxic and bloom-forming dinoflagellates *Gyrodinium aureolum*, *Gymnodinium galatheanum*, and two strains of *Prorocentrum minimum*. J Phycol 29: 627–642
Larkum AWD, Scaramuzzi C, Cox GC, Hiller RG and Turner AG (1994) Light-harvesting chlorophyll *c*-like pigment in *Prochloron*. Proc Natl Acad Sci USA 91: 679–683
Litaker RW, Tester PA, Duke CS, Kenney BE, Pinckney JL and Ramus J (2002). Seasonal niche strategy of the bloom-forming dinoflagellate *Heterocapsa triquetra*. Mar Ecol Prog Ser: 232: 45–62.
Mantoura RFC and Llewellyn CA (1983) The rapid determination of algal chlorophyll and carotenoid pigments and their breakdown products in natural waters by reverse-phase high-performance liquid chromatography. Anal Chim Acta 151: 297–314
Miyashita H, Adachi K, Kurano N, Ikemoto H, Chihara M and Miyachi S (1997) Pigment composition of a novel photosynthetic prokaryote containing chlorophyll *d* as the major chlorophyll. Plant Cell Physiol 38: 274–281
Nelson JR and Wakeham SG (1989) A phytol-substituted chlorophyll *c* from *Emiliania huxleyi* (Prymnesiophyceae). J Phycol 25: 761–766
Oster U, Janaka R, Janake A and Rüdiger W (2000) Cloning and expression of the gene encoding the key enzyme for chlorophyll *b* biosynthesis (CAO) from *Arabidopsis thaliania*. Plant J 21: 306–310
Porra RJ (1997) Recent progress in porphyrin and chlorophyll biosynthesis. Photochem Photobiol. 65: 492–516
Porra RJ, Schäfer W, Cmiel E, Katheder I and Scheer H (1994) The derivation of the formyl group oxygen of chlorophyll *b* in higher plants from molecular oxygen: achievement of high enrichment of the 7-formyl group oxygen from $^{18}O_2$ in greening maize leaves. Eur J Biochem 219: 671–679
Porra RJ, Pfündel EE and Engel N (1997) Metabolism and function of photosynthetic pigments. In: Jeffrey SW, Mantoura RFC and Wright SW (eds) Phytoplankton pigments in oceanography: Guidelines to modern methods, pp 85–126. UNESCO Publishing, Paris
Rebeiz CA, Wu SM, Kuhadja M, Daniell H and Perkins EJ (1983) Chlorophyll *a* biosynthetic routes and chlorophyll *a* chemical heterogeneity in plants. Mol Cell Biochem 57: 97–125
Rhiel E, Lange W and Mörschel E (1993) The unusual light-harvesting complex of *Mantoniella squamata*: Supramolecular composition and assembly Biochim Biophys Acta 1143: 163–172
Ricketts TR (1966) Magnesium 2,4-divinyl pheoporphyrin a_5 monomethyl ester, a protochlorophyll-like pigment present in some unicellular flagellates. Phytochem 5: 223–229
Scheer H (1991) Chemistry of chlorophylls. In: Scheer H (ed) Chlorophylls, pp 3–30. CRC Press, Boca Raton
Shioi Y and Beale SI (1987) Polyethylene-based high-performance liquid chromatography of chloroplast pigments: resolution of mono- and divinyl chlorophyllides and other pigment mixtures. Anal Biochem 162: 493-499
Stauber JL and Jeffrey SW (1988) Photosynthetic pigments in fifty-one species of marine diatoms. J Phycol 24: 158–172
Strain HH, Cope BT, McDonald GN, Svec WA and Katz JJ (1971) Chlorophylls c_1 and c_2. Phytochem 10: 1109-1114
Tengs T, Dahlberg OJ, Shalchian-Tabrizi K, Klaveness D, Rudi K, Delwiche CF and Jakobsen KS (2000) Phylogenetic analyses indicate that the 19′ hexanoyloxy-fucoxanthin-containing dinoflagellates have tertiary plastids of haptophyte origin. Mol Biol Evol 17: 718–729
Van Lenning K, Latasa M, Estrada M, Saez AG, Medlin L, Probert I, Veron B and Young B (2003) Pigment signatures and phylogenetic relationships of the *Pavlovophyceae* (*Haptophyta*). J Phycol 39: 379–389
Vesk M and Jeffrey SW (1987) Ultrastructure and pigments of two strains of the picoplanktonic alga *Pelagococcus subviridis* (Chrysophyceae). J Phycol 23: 322–336
Wasley JWF, Scott WT and Holt AS (1970) Chlorophyllides *c*. Can J Biochem 48: 376-383
Wilhelm C (1987) Purification and identification of chlorophyll c_1 from the green alga *Mantoniella squamata*. Biochim Biophys Acta 892: 23–29
Wilhelm C and Wiedemann I (1991) Evidence of protein bound chlorophyll c_3 in a light-harvesting protein isolated from the flagellate alga *Prymnesium parvum* (*Prymnesiophyceae*). Photosynthetica 25: 249–255
Wright SW and Van den Enden RL (2000) Phytoplankton community structure and stocks in the East Australian marginal ice zone (BROKE survey, January-March 1996) determined by CHEMTAX analysis of HPLC pigment signatures. Deep-Sea Res II 47: 2363–2400
Wright SW, Jeffrey SW, Mantoura RFC, Llewellyn CA, Bjørnland T, Repeta D and Welschmeyer N (1991) Improved HPLC method for the analysis of chlorophylls and carotenoids from marine phytoplankton. Mar Ecol Prog Ser 77: 183–96
Zapata M and Garrido JL (1997) Occurrence of phytylated chlorophyll *c* in *Isochrysis galbana* and *Isochrysis* sp. (clone T-ISO) (Prymnesiophyceae). J Phycol 33: 209–214
Zapata M, Ayala AM, Franco JM and Garrido JL (1987) Separation of chlorophylls and their degradation products in marine phytoplankton by reversed-phase high-performance liquid chromatography. Chromatographia 23: 26–30
Zapata M, Freire J and Garrido JL (1998) Pigment composition of several harmful algae as determined by HPLC using pyridine-containing mobile phases and a polymeric octadecylsilica column. In: Reguera B, Blanco J, Fernández ML and Wyatt T (eds) Harmful Algae, pp 304–307. Xunta de Galicia and Intergovernmental Oceanographic Commission of UNESCO, Santiago de Compostela
Zapata M, Rodríguez F and Garrido JL (2000) Separation of

chlorophylls and carotenoids from marine phytoplankton: a new HPLC method using a reversed phase C_8 column and pyridine-containing mobile phases. Mar Ecol Prog Ser 195: 29–45

Zapata M, Edvardsen B, Rodríguez F, Maestro MA and Garrido JL (2001) Chlorophyll c_2 monogalactosyldiacylglyceride ester (chl c_2-MGDG). A novel marker pigment for C*hrysochromulina* species (Haptophyta). Mar Ecol Prog Ser 219: 85–98

Zapata M, Jeffrey SW, Wright SW, Rodriguez F, Garrido JL and Clementson L (2004) Photosynthetic pigments in 37 species (65 strains) of *Haptophyta*: Implications for oceanography and chemotaxonomy. Mar Ecol Prog Ser 270: 83–10

Chapter 4

Unusual Tetrapyrrole Pigments of Photosynthetic Antennae and Reaction Centers: Specially-tailored Chlorophylls

Masami Kobayashi[1]*, Machiko Akiyama[1], Hideo Kise[1] and Tadashi Watanabe[2]
[1]Institute of Materials Science, University of Tsukuba, Tsukuba, Ibaraki 305-8573, Japan; [2]Institute of Industrial Science, The University of Tokyo, Komaba, Meguro-ku, Tokyo 153-8505, Japan

*Author for correspondence, email: masami@ims.tsukuba.ac.jp

Bernhard Grimm, Robert J. Porra, Wolfhart Rüdiger and Hugo Scheer (eds): Chlorophylls and Bacteriochlorophylls: Biochemistry, Biophysics, Functions and Applications, pp. 55–66.

Summary

Primary charge separation in photosynthesis is initiated by a few specialized chlorophyll (Chl) or bacteriochlorophyll (BChl) molecules in the reaction centers. Excitation of the primary donors leads to reduction of the primary and secondary electron acceptors, which often contain structurally distinct Chl and BChl derivatives: such specially-tailored Chls include 'prime-type,' 'metal-free' and 'Zn-containing' Chls. The functions of many such pigments have long remained unclear, but recently the roles of some have been elucidated. Here, a short overview is given on the minor but specially-tailored Chls that function as key components in photosynthesis.

I. Introduction

Chls *a* and *b* in higher plants, algae and cyanobacteria, BChls in photosynthetic bacteria and Chls *c* in marine microalgae function as antenna or, sometimes, as reaction center (RC) Chls in the primary photophysical and photochemical reactions of photosynthesis. In viewing these Chls as 'normal,' we present in this Chapter a brief review of naturally-occurring 'unusual' or specially-tailored Chls.

II. Specially-tailored Chlorophylls in a Limited Number of Organisms

A. Specially-tailored Chlorophylls in Algae

1. Chlorophyll d in the Cyanobacterium, Acaryochloris marina

Chl *d* is [3-formyl]-Chl *a* (Chapter 1, Scheer) and was first reported as a minor pigment in about 10 species of red macroalgae (Manning and Strain, 1943). A novel cyanobacterium, *Acaryochloris* (*Acc.*) *marina*, was later isolated from colonial ascidians containing Chl *d* as the dominant Chl, with only a small amount (~3% of total Chl) of Chl *a* (Miyashita et al., 1996). In all previously known organisms capable of oxygenic photosynthesis, the major pigment was Chl *a*: one exception was [8-vinyl]-Chl *a*, a 3,8-divinyl compound (i.e., DV-Chl *a*), in some marine phytoplankton. Small amounts of undeveloped phycobiliproteins were found as antennae for PS II (Miyashita et al., 1997), providing an unusual pigment composition for the photosystems of *Acc. marina*. Isolated PS I particles showed a flash-induced absorbance difference maximum at ca. 740 nm, and hence the primary electron donor of PS I was named P740 (Hu et al., 1998), corresponding to P700 in other oxygenic photosynthetic organisms.

Murakami et al. (2001) found Chl *d* in a red seaweed *Ahnfeltiopsis flabelliformis*, where Chl *d* was minor (Chl *d*/*a* = 0.03–0.3) and occasionally undetectable. Small patches on algal thalli surfaces were found to be a cyanobacteria-like prokaryotic epiphyte containing Chl *d* while the thalli lacked Chl *d*. Time-resolved spectroscopy on the epiphyte showed no long-lived fluorescence component corresponding to Chl *d* which, therefore, cannot be the primary electron donor of PS II: the epiphyte may comprise one or more species.

2. Divinyl-Chlorophylls a and b in Prochlococcus sp. Strains

DV-Chl *a* (Chapter 1, Scheer and Chapter 3, Zapata et al.), in which the 8-ethyl substituent of Chl *a* is replaced by a vinyl group, was detected in greening cucumber seedlings (Rebeiz et al., 1980) and, subsequently, DV-Chl *b* was found in *Zea mays* seedlings (Wu and Rebeiz, 1985) as biosynthetic precursors: the divinyl nature of the Chl derivatives was suggested by spectrophotometric and chromatographic considerations (Rebeiz et al., 1980) and unequivocally confirmed, in the case of DV-Chl *a* from a maize mutant, by various mass spectrometric techniques (Bazzaz et al., 1982) and by nuclear magnetic resonance studies (Bazzaz and Brereton, 1982). A number of mature organisms were also shown to contain small amounts of DV-Chl *a* and DV-Chl *b* and their

Abbreviations: CD – circular dichroism; Chl – chlorophyll; HPLC – high performance liquid chromatography; NMR – nuclear magnetic resonance; P680 – the primary donor of Photosystem II; P700 – the primary donor of Photosystem I; P740 – the primary donor of Photosystem I in *Acc. marina;* P798 – the primary donor of heliobacteria; P840 – the primary donor of green sulfur bacteria; P850 – the primary donor of [Zn]-bacteriochlorophyll *a* containing purple bacteria; P865 – the primary donor of green filamentous bacteria; P870 – the primary donor of purple bacteria; P970 – the primary donor of bacteriochlorophyll *b* containing purple bacteria; PS – Photosystem; RC – reaction center

derivatives (Wu et al., 1989). The absorption spectra of DV-Chl *a* in organic solvents revealed slightly red-shifted Soret bands but the Q_Y-bands were almost identical (Goericke and Repeta, 1992).

DV-Chls *a* and *b* were dominant in a mutant of *Zea mays* (Bazzaz, 1981), but were lacking in the stroma. The mutant, however, showed photosynthetic activity, suggesting that Chl *a* can be at least partly replaced by DV-Chl *a* (Bazzaz et al., 1974). Some marine phytoplankton *Prochlococcus* strains possess DV-Chls *a* and *b* as major pigments (Chisholm et al., 1988, Goericke and Repeta, 1992), and are devoid of Chls *a* and *b*.

3. [8-Vinyl]-protochlorophyllide a in Prasinophytes

Ricketts (1966) first detected [8-vinyl]-protochlorophyllide *a* (DV-PChlide *a*; Chapter 1, Scheer) in a unicellular flagellate *Micromonas pusilla*, and it has been found in a variety of algae as minor pigment or as one of the major pigments (see Table 1 in Helfrich et al., 1999). For light-harvesting purposes, DV-PChlide seems to be diverted from Chl biosynthesis before hydrogenation. PChlide (i.e., MV-PChlide), an intermediate in Chl biosynthesis, has not been detected in algae in amounts comparable to DV-PChlide, suggesting the presence of a transport/binding mechanism which carries a portion of the DV-PChlide intermediate from the formation site to the functional site in the antenna (Helfrich et al., 1999).

B. Specially-tailored Chlorophylls in Bacteria

1. Bacteriochlorophyll g in Heliobacteria

Heliobacterium (*Hbt.*) *chlorum*, a phototrophic bacterium, was isolated serendipitously in 1981 from a soil sample collected in front of the Biology Department, Indiana University using an incorrectly prepared culture medium for other anoxygenic bacteria (see a review by Gest, 1994). Later, several other species were isolated from rice fields, hot springs and the banks of soda lakes, etc.

Absorption spectroscopy of both whole cells and isolated membranes showed an unusual absorption maximum near 788 nm, indicating the presence of a new bacteriochlorophyll later designated BChl *g*: the molecular structure was determined by Brockman and Lipinski (1983). BChl *g* like BChl *b* contains an 8-ethylidene group on ring B (Chapter 1, Scheer). Isomerization (intramolecular proton transfer) of BChl *g* on ring B easily takes place to yield Chl *a* esterified with farnesol (Brockmann and Lipinsky, 1983; Michalski et al., 1987; Kobayashi et al., 1998a), suggesting that BChl *g* is a likely candidate for the ancestor of Chl *a* in oxygenic photosynthesis: similar reactions were seen in BChl *b*, but yielded [3-acetyl]-Chl *a* (Steiner et al., 1983; Kobayashi et al., 1998b). Heliobacteria are taxonomically closer to the cyanobacteria than the other groups of anoxygenic photosynthetic bacteria (Xiong et al., 2000), which is also consistent with the notion of Chl *a* arising from BChl *g*.

2. [Zn]-Bacteriochlorophyll a in Acidiphilium Strains

a. Discovery of [Zn]-Bacteriochlorophyll a in Natural Photosynthesis

Natural Chls and BChls were previously assumed, without question, to be magnesium (Mg) complexes of substituted chlorin or bacteriochlorin macrocycles with one obvious and important exception, pheophytins. The reason that Mg is generally the central metal is not thoroughly clear. Therefore, investigations comparing the photoelectrochemical properties of a series of metallo-substituted (B)Chls (e.g., [M]-Chl *a* or [M]-BChl *a*) were performed (see reviews by Watanabe et al., 1985a; Watanabe and Kobayashi, 1991; Scheer and Hartwich, 1995; Kobayashi et al., 1999a): the results indicated that [Zn]-(B)Chl *a* could function as both antenna and primary electron donor in natural photosynthesis.

In 1996 a novel Zn-containing BChl, with a small amount of [Mg]-BChl *a*, was first detected in an aerobic bacterium *Acidiphilium* (*Acp.*) *rubrum* growing in a low pH habitat (Wakao et al., 1996). Its structure was identical to that of BChl *a* esterified with phytol, but the central metal was Zn not Mg (Akiyama et al., 1998b, Kobayashi et al., 1998c). [Zn]-BChl *a* is present in all the *Acidiphilium* species examined (Wakao et al., 1999; Hiraishi et al., 2000; Hiraishi and Shimada, 2001). *Acidiphilium* species contain the *puf* operon coding the L, M and C subunits of RC proteins and the α and β subunits of the light harvesting complex 1 (LH1) analogous to those in the other purple bacteria (Nagashima et al., 1997).

The RC complex isolated from *Acp. rubrum* consisted of four molecules of [Zn]-BChl *a*, two mol-

ecules of BPhe *a* and one molecule of spirilloxanthin, but no [Mg]-BChl *a* was detected (Akiyama et al., 1998a); thus, 4 [Mg]-BChl *a* molecules in the RC of other photosynthetic purple bacteria are entirely replaced by 4 [Zn]-BChl *a* molecules. The minor [Mg]-BChl *a* component found in the cells, therefore, should reside in LH1 where it may channel energy from [Zn]-BChl *a* present in LH1 to the special pair in the RC: this idea is consistent with the longer wavelength of the Q_Y band of [Mg]-BChl *a* compared to [Zn]-BChl *a* in vitro (Chapter 6, Kobayashi et al.). It is not yet clear whether the RC of *Acp. rubrum* grown at higher pH also consists of only [Zn]-BChl *a* or not, because the [Zn]-BChl *a*/[Mg]-BChl *a* ratio in the cells decreases at higher pH.

b. Physicochemical Properties of [Zn]-Bacteriochlorophyll a

Photosynthesis requires pigments with appropriate light absorption characteristics for harvesting sunlight, fluorescence properties for light energy transfer in antenna systems and redox potentials for electron transfer: all are possessed by chlorophyll-protein complexes. Here we briefly consider the effect of the central metal on these physicochemical properties in various [M]-(B)Chls *a*.

No drastic change of light harvesting ability among (B)Chls *a* is induced by transmetalation with Zn: their absorption coefficients and their Q_Y transition energy maxima in organic solvents are quite similar (Chapter 6, Kobayashi et al.). Surprisingly, [Zn]-BChl *a* in several organic solvents was colored 'pink', while dried [Zn]-BChl *a* was seen blue-purple like [Mg]-BChl *a*. Fluorescent pigments retain excitation energy within the molecules and can transfer it to neighboring pigments. In this regard, [Zn]-BChl *a* is suitable as an energy receptor in photosynthesis (Chapter 6, Kobayashi et al.).

First ring redox potentials of (B)Chls are also very important in photosynthesis (Kobayashi et al., 1999b): the oxidation potential of [Zn]-BChl *a* measured in vitro is slightly more positive than that of [Mg]-BChl *a* (Geskes et al., 1995). Comparison of amino acid sequences of the L and M subunits between the *Acidiphilium* species and other purple bacteria shows one characteristic replacement of an amino acid in the region around the special pair; His L168, which is highly conserved in other purple bacteria, is replaced by Glu L168 in the *Acidiphilium* species (Nagashima et al., 1997). This Glu L168 replacement appears to be associated with the regulation of the oxidation potential of the [Zn]-BChl *a*-containing special pair in *Acp. rubrum*. His L168 forms a strong hydrogen bond to the acetyl carbonyl group at ring A of BChl *a* of the special pair in *Rhodobacter* (*Rba.*) *sphaeroides*, which contributes to asymmetrical distribution of the positive charge on the special pair. Removal of the hydrogen bond from the His L168 results in an 80 mV lowering of redox potential of the special pair in the RC of *Rba. sphaeroides* (Mattioli et al., 1994). Thus, inclusion of Glu L168 may be a counter measure of the RC proteins of *Acp. rubrum* to the elevation of the oxidation potential of the [Zn]-BChl *a* special pair.

c. High Acid Resistance of [Zn]-Bacteriochlorophyll a

[Zn]-BChl *a* is highly resistant to acid: at pH3, the optimum pH for growth of *Acp. rubrum*, the half-time ($t_{1/2}$) for pheophytinization (demetallation) of [Zn]-BChl *a* and [Mg]-BChl *a* is 12 years and 9 min, respectively (Kobayashi et al., 1998d). This high resistance of [Zn]-BChl *a* to acid enables *Acp. rubrum* to adapt to its low pH habitat which is consistent with the Pourbaix diagrams for Zn and Mg showing that Mg^{2+} is the dominant form at neutral pH, while the region where Zn^{2+} is the major form is limited to low pH (Yamamura et al., 1998). The low ionization property of Zn is preferable for forming the chelate compounds under low pH conditions, if the external pH exerts any influence in the course of synthesis of [Zn]-BChl *a* molecules and/or their incorporation to structural proteins. [Zn]-BChl *a* is also highly resistant to unwanted transmetallation by Cu and Hg (Chapter 5, Küpper et al.) which produce non-fluorescent pigments (Chapter 6, Kobayashi et al.).

d. Biosynthesis of [Zn]-Bacteriochlorophyll a in Acidiphilium rubrum

Masuda et al. (1999) showed that [Mg]-protoporphyrin IX monomethyl ester ([Mg]-Proto-ME), as an intermediate of [Mg]-BChl *a* biosynthesis, accumulated in *Acp. rubrum* which is consistent with the formation of small amounts of [Mg]-BChl *a* in these cells; however, no [Zn]-Proto-ME was detected. This strongly suggests that Mg may be replaced by Zn at a later step in [Zn]-BChl *a* biosynthesis which is also consistent with the failure to detect a distinct

Zn chelatase. As no 'metal-exchange enzyme' has yet been found, a non-enzymic mechanism for Zn incorporation may occur but, because the growth medium contains only small amounts of Zn (~0.5 $g \cdot l^{-1}$), an incorporation mechanism for Zn into the cells may be required.

III. Specially-tailored Chlorophylls Associated with Reaction Centers

The RCs of photosynthetic organisms are classified into two types according to their electron acceptor chains. 'Type 1 RCs' possess iron-sulfur (FeS) centers in the electron acceptor chain while there are two quinones in series, Q_A and Q_B, in the electron acceptor chains of 'Type 2 RCs' (Fig. 1). In RCs, primary charge separation is driven by a few specialized 'prime-type' and 'metal-free' chlorophylls. Until recently, the functions of these minor pigments has remained unclear.

A. Prime-type Chlorophylls as Primary Electron Donors of Type 1 RCs

1. Chlorophyll a´ in Higher Plants and Cyanobacteria

P700 was first discovered and named by Kok (1956), although the chemical identity was unknown. The idea that P700 was a Chl *a* dimmer was first proposed by Witt et al. (1965), followed by other models including a Chl *a* enol (Wasielewski et al., 1981) and a [13^2-hydroxy-20-chloro]-Chl *a* (Dörnemann and Senger, 1982).

The 13^2-epimer of Chl *a*, Chl *a´* ('*a*-prime') (Chapter 1, Scheer), was first reported by Strain and Manning (1942). In pigment analyses of plant leaves and cyanobacteria by HPLC, Watanabe's group invariably detected a small amounts of Chl *a´* suggesting that it has an in vivo role. Initially, a molar Chl *a´*/P700 ratio of 2 was found, and so it was proposed that P700 was a homodimer of Chl *a´* (Watanabe et al., 1985b). Kobayashi et al. (1988), however,

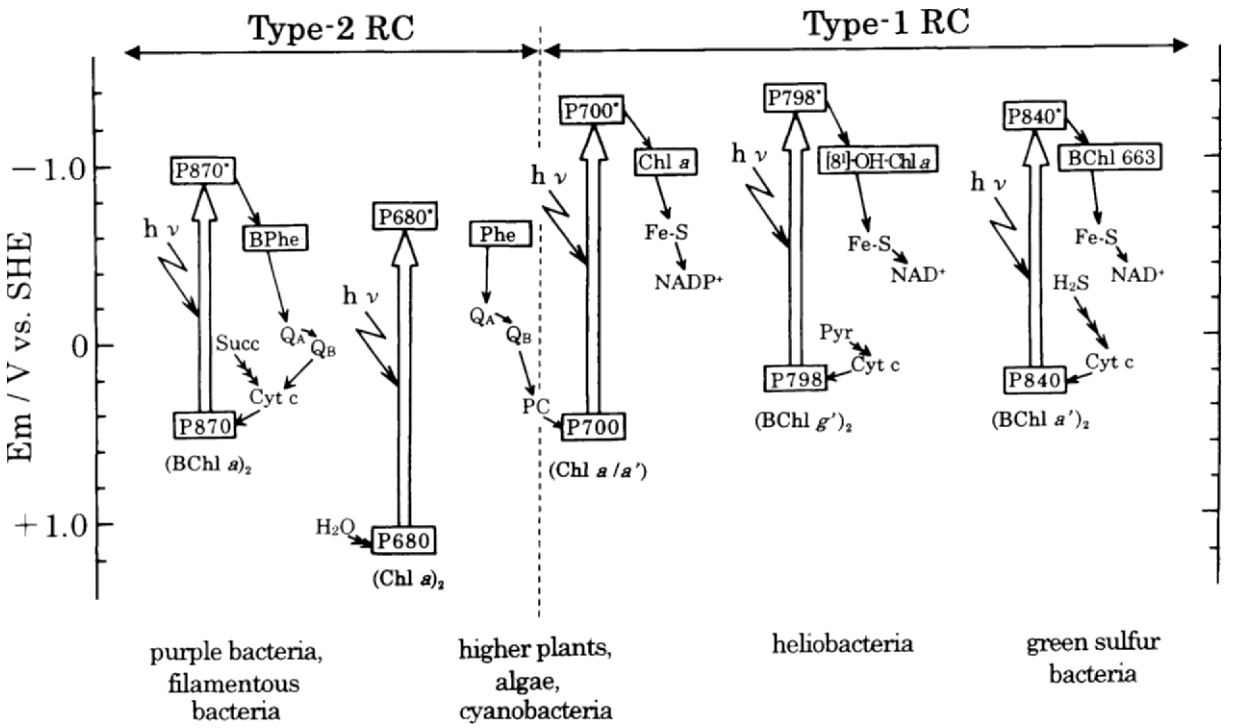

Fig. 1. Schematic comparison of electron transfer components in type-1 RC and type-2 RC. Components are placed according to their estimated or approximate midpoint redox potentials. The arrows indicate the direction of electron flow. To simplify the figure, some primary electron donors, P970, P850, P865 and P740 are omitted here: P970 and P850 are the primary electron donors of BChl *b* and [Zn]-BChl *a* containing purple bacteria, respectively; P865 is the primary electron donor of filamentous bacteria; P740 is the primary electron donor of PS I in *Acc. marina*. See text for more details. Figure adapted from Akiyama et al. (2002)

determined a Chl *a*′/P700 ratio of 1 in chloroform extracts from fresh leaves of 13 higher plants, three cyanobacteria and a series of PS I-enriched particles prepared from spinach, and consequently suggested that P700 was a heterodimer of Chl *a*/*a*′. Later studies determined Chl *a*′/P700 ratios of 2 in acetone or acetone/chloroform extracts (Maeda et al., 1992), of 1 in acetone extracts (Kobayashi et al., 1995), of 2 in acetone/methanol extracts (Nakamura and Watanabe, 1998), and finally of 1 in acetone/methanol extracts (Nakamura and Watanabe, 2001).

The uncertainty about whether Chl *a*′/P700 ratio was 1 or 2 continued for sixteen years. Recent X-ray structural analysis of PS I resolved that P700 was a heterodimer of Chl *a*/*a*′ (Jordan et al., 2001; also see a review by Webber and Lubitz 2001) and the Chl *a*′ component of P700 resided on the PsaA-side of PS I core proteins. In addition, a weaker electronic interaction has been found between the π electron systems in P700 than in the special pair of the RC of purple bacteria.

The asymmetry of P700 appears to arise from differences in the chlorophyll binding pockets, because the P700 binding site of the PsaA protein appears to be designed for Chl *a*′ insertion and so maximizing asymmetry. The steric arrangement of the hydrogen and carboxymethyl group at $C13^2$ may assist incorporation of Chl *a*′ into the PsaA site. There is no obvious reason why Chl *a*′ should be necessary for P700 and we wish to emphasize that no prime-pigments are detected in PS II and in purple bacteria.

The biosynthesis of Chl *a*′ and its assembly into the RC of PS I is interesting because chlorophyll synthetase does not catalyze the prenylation of chlorophyllide (Chlide) *a*′ in vitro (Helfrich et al., 1994). This suggests that Chl *a*′ must be formed after prenylation of Chlide *a* which is consistent with the finding that there is no naturally occurring protochlorophyllide (PChlide) *a*′ and that PChlide *a*′ cannot be photoreduced to Chlide *a*′ (Helfrich et al., 1996). In thylakoid membranes from greening etiolated barely leaves, various $C17^3$ derivatives of Chl *a*′ were detected (Nakamura et al., 2001), suggesting that Chl *a*′ can be derived from Chl $a_{GG,\ DHGG,\ THGG}$ (GG = geranylgeraniol, DHGG = dihydro-GG, THGG = tetrahydro-GG) by epimerization and subsequent hydrogenation or from Chl a_P by epimerization. To date, however, no epimerase has been detected suggesting that Chl *a*′ may be formed during assembly of the P700 complex and perhaps mediated by the RC itself. It is noteworthy that chlorophyllase which hydrolyzes the $C17^3$ phytyl ester linkage is also affected by $C13^2$ stereochemistry of chlorophylls (Fiedor et al., 1992; Nishiyama et al., 1994).

2. Chlorophyll d′ in the Cyanobacterium, Acaryochloris marina

As described in Section II.A.1, Miyashita et al (1996) found Chl *d* in the cyanobacterium, *Acc. marina,* and Hu et al. (1998) isolated PS I particles from this organism which contained a P740 complex corresponding to P700 in other oxygenic photosynthetic organisms. P740 was assumed to be a homodimer of Chl *d*, because its absorbance at 740 nm was 40 nm longer than that of P700 consisting Chl *a*: and this was ascribed to the red-shift of the Q_Y absorption band of Chl *d* as compared to Chl *a*.

Based on analogy with P700, it now seems reasonable to speculate that P740 may also contain Chl *d*′. Akiyama et al. (2001) detected Chl *d*′ as a minor component in the cells of *Acc. marina*, while no Chl *a*′ molecules were detected. The molar ratio of Chl *d*/*d*′ in the cells of *Acc. marina* was about 70, which was roughly half of the Chl *a*/*a*′ ratio of 100–140 observed in other cyanobacterial cells (Kobayashi et al., 1988) which suggested that P740 may be a homodimer of Chl *d*′. According to Miyashita (personal communication), the homology of PsaA and PsaB between *Acc. marina* and other cyanobacteria is low, which may reflect the substitution of Chl *d* for Chl *a* as the pigment associated with these proteins in *Acc. marina*. However, P700 is a Chl *a*/*a*′ heterodimer in agreement with the heterodimeric RC proteins of PS I, and because the RC of PS I in *Acc. marina* also consists of heterodimeric proteins (Miyashita, personal communication), it seems reasonable to speculate that P740 may also be a Chl *d*/*d*′ heterodimer: this is still to be confirmed, but re-examination of *Acc. marina* growing under different light conditions strongly suggests that P740 may be a Chl *d*/*d*′ heterodimer (Akiyama et al., 2002, 2003).

3. Bacteriochlorophyll g′ in Heliobacteria

Fuller et al. (1985) reported reversible photobleaching at 798 nm and ascribed it to the primary electron donor, P798. Prince et al. (1985) showed that P798 may be a BChl *g* dimer on the basis of optical and ESR measurements and also that the positive charge on $P798^{+\cdot}$ was delocalized over the two BChl *g* molecules.

Kobayashi et al. (1991) detected a small amount of BChl *g´* in the cells, membranes and antenna-RC complexes of *Hbt. chlorum* and *Heliobacillus* (*Hba.*) *mobilis*, and the molar ratio of BChl *g*/*g´* was found to be about 18. This ratio, when combined with BChl *g*/P798 ratio of 35–40 (van de Meent et al., 1990), yields a BChl *g´*/P798 ratio of 2. Since the RC consists of two identical subunits (Liebl et al., 1993), P798 was proposed to be a (BChl *g´*)$_2$ homodimer (Kobayashi et al., 1991). The homodimeric RC proteins of heliobacteria may provide a symmetrical environment for P798.

4. Bacteriochlorophyll a´ in Green Sulfur Bacteria

Sybesma and Vredenberg (1963) observed photobleaching at about 840 nm, and the primary donor was hence named P840. The homodimeric nature of P840 was first proposed by Olson et al. (1977), in agreement with the finding that, like heliobacteria, *pscA* is the only gene coding for the RC of green sulfur bacteria (Büttner et al., 1992a,b). This contrasts with the finding of the two genes, *psaA* and *psaB*, coding for the PS I core; therefore, the RC of green sulfur bacteria was expected to be a homodimer formed by two identical proteins.

The homodimeric RC contains 16 BChl *a*-type molecules (Permentier et al., 2000; Hauska et al., 2001), and 2 of them are BChls *a´* (Kobayashi et al., 1992, 2000): these latter 2 are considered to form a homodimeric P840. The estimated midpoint potential of P840 was around +0.24 V (Prince and Olson, 1976), which is about 0.15 V more negative than the special pair of (BChl *a*)$_2$ in the RC of purple bacteria (Fig. 1). The redox potential difference represents the earliest steps in photoreactions (Kobayashi et al., 1999a), and the 13^2-epimers appear to be a general feature of the primary electron donors in the Type 1 RCs (Fig. 1). However, why the primary electron donors in the Type 1 RCs include 13^2-epimer chlorophylls is unclear.

B. Chlorophyll a-type Pigments as Primary Electron Acceptors of Bacterial Type 1 RCs

The primary electron acceptor, A_0, in PS I was regarded to be Chl *a* on the basis of optical, EPR and rapid spectroscopic measurements: this has been confirmed by recent crystal analysis of PS I. Here we briefly discuss the Chl *a*-type pigments as primary electron acceptors, A_0, in the Type 1 RCs of bacteria (Fig. 1).

1. [8^1-OH]-Chlorophyll a Esterified with Farnesol in Heliobacteria

The A_0 in the RC of heliobacteria shows a bleaching around 670 nm (Nuijs et al., 1985a, Fuller et al., 1985), which was thought to be due to a BChl *c* or Chl *a*-like pigment. HPLC analyses of the membranes and antenna-RC complexes of *Hbt. chlorum* and the membranes of *Hba. mobilis*, however, revealed minor amounts of a very polar pigment with an absorption spectrum essentially identical to Chl *a*. NMR spectroscopy revealed its molecular structure as [8^1-OH]-Chl *a* esterified with farnesol which has virtually the same absorption spectrum as Chl *a* (van de Meent et al., 1991). Two molecules of [8^1-OH]-Chl *a* are present in each P798 complex (van de Meent et al., 1991; Neerken et al., 2000). Recent evidence indicated that excitation of [8^1-OH]-Chl *a* gives rise to an alternative primary reaction not involving excited P798 (Neerken and Amesz, 2001), suggesting that [8^1-OH]-Chl *a* in the excited state would function as initiator of the photochemical reaction: P798 $A_0^* \rightarrow P798^+ A_0^-$. Consistent with this idea, excitation of [8^1-OH]-Chl *a* resulted in the generation of a significantly larger amount of P798$^+$ than direct excitation of BChl *g*.

2. Chlorophyll a Esterified with Δ2,6-Phytadienol in Green Sulfur Bacteria

The A_0 in the RC of green sulfur bacteria showed a bleaching around 670 nm and was tentatively suggested to involve BPhe *c* (Nuijs et al., 1985b). Braumann et al. (1986) first isolated the A_0 from a green sulfur bacterium, *Prosthecochloris aestuarii*, using HPLC, and it was designated BChl 663 after its absorption maximum in the HPLC eluent: it was considered to be a lipophilic form of BChl *c*. Later, BChl 663 was thought to be an isomer of Chl *a* (van de Meent et al., 1992), and finally it was identified as Chl *a* esterified at C17^3 with Δ2,6-phytadienol possessing an additional double bond between P6- and P7- carbons of the phytol carbon chain (Chapter 1, Scheer; Kobayashi et al., 2000). Four molecules of BChl 663 were present in the RC (Permentier et al., 2000): two of them function as A_0 molecules and the other two are accessory pigments. Like heliobacteria, evidence was recently obtained for a direct pathway of

charge separation from excited BChl 663 not involving excited antenna BChls (Neerken et al., 1999).

In general, it appears that the A_0 molecules in Type 1 RCs are Chl *a* derivatives (Fig. 1), suggesting that the Type 1 RCs are derived from a common ancestor. Chl *a*-type pigments are thought to be necessary to reduce $NADP^+$ or NAD^+ through an Fe-S center: the reduction potentials of pheophytins are not sufficiently negative to reduce $NAD(P)^+$.

C. Pheophytins as the Primary Electron Acceptors in Type 2 RCs

1. Pheophytin a in Photosystem II

a. Pheophytin a in Higher Plants and Algae

Pheophytin (Phe) *a* is demetallated Chl *a* (Chapter 1, Scheer) and it is found in the RC of PS II. Demetallation of Chl *a* easily occurs during handling of plant pigments, especially under acidic conditions and, until the 1970s, most researchers regarded pheophytins as experimental artifacts. Phe *a* was first postulated to be the primary electron acceptor in PS II by van Gorkom (1974), and this idea was experimentally confirmed using difference absorption, ESR and ENDOR spectroscopies (Klimov et al., 1977b, 1985; Klimov and Krasnowskii, 1981). Klimov et al. (1977c) determined the midpoint potential of Phe *a* in PS II to be approximately –600 mV (Fig. 1) which is close to the reduction potential of Phe *a* in organic solvents (Watanabe and Kobayashi, 1991). Subsequently, the presence of two Phe *a* molecules in the RC of PS II was established (Murata et al., 1986; Nanba and Satoh, 1987) and one of them was shown to function as the primary electron acceptor (Hastings et al., 1992).

b. Pheophytin a in the Cyanobacterium, Acaryochloris marina

Phe *a* was found as a minor pigment in the cyanobacterium, *Acc. marina*, where the dominant pigment is Chl *d* but no Phe *d* could be detected (Akiyama et al., 2001). A Chl *a*/Phe *a* ratio of approximately 4/2 was found in *Acc. marina* cells (Akiyama et al., 2001, 2002, 2003) which is substantially smaller than the reported ratio of about (160–240)/2 in other cyanobacteria (Kobayashi et al., 1988). The very small ratio of Chl *a*/Phe *a*, ca. 4/2, in *Acc. marina* cells is identical to the BChl/BPhe ratio, 4/2, in the RCs of purple bacteria while it is slightly but significantly smaller than the Chl *a*/Phe *a* ratio of 6/2 in D1/D2/Cyt *b*559 RC complexes of PS II in other oxygenic organisms (Kobayashi et al., 1990, Gounaris et al., 1990).

The nature of the primary electron donor of PS II in *Acc. marina* is still debated but, most probably, is identical with that of other oxygenic photosynthetic organisms. If so, the special pair and the accessory pigments in the RC of PS II in *Acc. marina* may be Chl *a* molecules. According to Miyashita (personal communication), the substitution frequencies in the PS I-RC proteins, PsaA and PsaB, as well as in the PS II core antenna proteins, CP47 (PsbB) and CP43 (PsbC), of *Acc. marina* are higher than those in the other cyanobacteria: this indicates a rapid evolution due to Chl *d* incorporation into these proteins. In contrast, the evolutionary rates in D1(PsbA) and D2(PsbD) proteins are comparable with those in other cyanobacteria: this suggests that amino acid substitution in D1/D2 proteins in *Acc. marina* has the same constraint as in other cyanobacteria, and that Chl *a* and Phe *a* may be used for the primary electron donor and acceptor in the PS II core, respectively. Mimuro et al. (1999) observed a long-lived fluorescence at 680 nm and suggested an 'uphill' energy transfer from antenna Chl *d* to P680 (Mimuro et al., 2000); however, Itoh et al. (2001) failed to detect such an absorbance change at 680 nm but detected changes around 720 nm. A clearer picture will emerge when highly purified D1/D2 complexes are obtained.

2. Bacteriopheophytins a and b in Purple and Green Filamentous Bacteria

Bacteriopheophytin (BPhe) *a* (Chapter 1, Scheer) was the first chlorophyll 'alteration' product identified as a native constituent of photosynthetic complexes. BPhe *a* is found in almost all purple bacterial RC and the accepted molar ratio of BChl *a*/BPhe *a* is 4/2: a few species of purple bacteria contain BChl *b* and BPhe *b* rather than BChl *a* and BPhe *a*. In 1975, the notion that BPhe participates in photochemical charge separation was first presented (Parson et al., 1975; Rockley et al., 1975; Fajer et al., 1975). Subsequently, Kaufmann et al. (1975) showed that BPhe *a* is an intermediary electron acceptor in the RC of *Rba. sphaeroides* by picosecond kinetic measurements. Klimov et al. (1977a) estimated the midpoint potential of BPhe *b* in the RC of *Rps. viridis* to be about –600 mV.

Like purple bacteria, BPhe *a* was also found to

function as an intermediary electron acceptor in green filamentous bacteria (Kirmaier et al., 1986; Shuvalov et al., 1986) and one of the accessory pigments on the inactive branch, termed M or B in purple bacteria, was replaced by BPhe *a* (Pierson and Thornber, 1983) resulting in the ratio of BChl *a*/BPhe *a* = 3/3 in the RC.

In conclusion, it is noteworthy that Type 2 RCs need to optimize the quantum yield of the two-electron reduction of Q_B, and hence a unilateral electron transfer should have some advantage, whereas electron transfer in Type 1 RCs involves only a series of one-electron redox reactions and thus unilateral electron transfer seems to have no advantage.

Acknowledgments

We thank Mr. Takanori Gotoh (Univ. Tsukuba) for helpful discussions. This work was supported in part by: a Special Project of Nanoscience, 21st Century COE Program (Univ. Tsukuba); by the Tokyo Ohka Foundation for the promotion of Science and Technology; by a Grant-in-Aid for Scientific Research (No. 12450343) from the Japan Society for the Promotion of Science; and, a Grant-in-Aid for Scientific Research (Nos. 1450029 and 15033212) on Priority Area (417) from the Ministry of Education, Culture, Sports, Science and Technology (MEXT), Japan. One of us, MA, thanks the Japanese Society for the Promotion of Science for Young Scientists for a Research Fellowship.

References

Akiyama M, Kobayashi M, Kise H, Hara M, Wakao N and Shimada K (1998a) Pigment composition of the reaction center complex isolated from an acidophilic bacterium *Acidiphilium rubrum* grown at pH 3.5. Photomed Photobiol 20: 85–87

Akiyama M, Kobayashi M, Kise H, Takaichi S, Watanabe T, Shimada K, Iwaki M, Itoh S, Ishida N, Koizumi M, Kano H, Wakao N and Hiraishi A (1998b) *Acidiphilium rubrum* and zinc-bacteriochlorophyll, part1: Molecular structure of the zinc-containing bacteriochlorophyll. In: Garab G (ed) Photosynthesis: Mechanism and Effects, Vol 2, pp 731–734. Kluwer Academic Publishers, Dordrecht

Akiyama M, Miyashita H, Watanabe T, Kise H, Miyachi S and Kobayashi M (2001) Detection of chlorophyll *d′* and pheophytin *a* in a chlorophyll *d*-dominating oxygenic photosynthetic prokaryote *Acaryochloris marina*. Anal Sci 17: 205–208

Akiyama M, Miyashita H, Kise H, Watanabe T, Mimuro M, Miyachi S and Kobayashi M (2002) Quest for minor but key chlorophyll molecules in photosynthetic reaction centers—Unusual pigment composition in the reaction centers of a chlorophyll *d*-dominated cyanobacterium *Acaryochloris marina*. Photosynth Res 74: 97–107

Akiyama M, Gotoh T, Kise H, Miyashita H, Mimuro M and Kobayashi M (2003) Stoichiometries of chlorophyll *d′*/PS I and chlorophyll *a*/PS II in a chlorophyll *d*-dominated cyanobacterium *Acaryochloris marina*. J Phycol 51, in press

Bazzaz MB (1981) New chlorophyll chromophores isolated from a chlorophyll-deficient mutant of maize. Photobiochem Photobiophys 2: 199–207

Bazzaz MB and Brereton RG (1982) 4-Vinyl-4-desethyl chlorophyll *a*: A new naturally occurring chlorophyll. FEBS Lett 138: 104–108

Bazzaz MB, Govindjee and Paolillo DJ Jr (1974) Biochemical, spectral and structural study of olive necrotic 8147 mutant of *Zea mays* L. Z Pflanzenphysiol Bd 72: 181–192

Bazzaz MB, Bradley CV and Brereton RG (1982) 4-Vinyl-4-desethyl chlorophyll *a*: Characterisation of a new naturally occurring chlorophyll using fast atom bombardment, field desorption and 'in beam' electron impact mass spectroscopy. Tetrahedron Lett 23: 1211–1214

Braumann T, Vasmel H, Grimme LH and Amesz J (1986) Pigment composition of the photosynthetic membrane and reaction center of the green bacterium *Prosthecochloris aestuarii*. Biochim Biophys Acta 848: 83–91

Brockman H Jr and Lipinski A (1983) Bacteriochlorophyll *g*. A new bacteriochlorophyll from *Heliobacterium chlorum*. Arch microbiol 136: 17–19

Büttner M, Xie D-L, Nelson H, Pinther W, Hauska G and Nelson N (1992a) Photosynthetic reaction center genes in green sulfur bacteria and in Photosystem 1 are related. Proc Natl Acad Sci USA 89: 8135–8139

Büttner M, Xie D-L, Nelson H, Pinther W, Hauska G and Nelson N (1992b) The Photosystem I-like P840-reaction center of the green S-bacteria is a homodimer. Biochim Biophys Acta 1101: 154–156

Chisholm SW, Olson RJ, Zettler ER, Goericke R, Waterbury JB and Welschmeyer NA (1988) A novel free-living prochlorophyte abundant in the oceanic euphotic zone. Nature 334: 340–343

Dörnemann D and Senger H (1982) Physical and chemical properties of chlorophyll RCI extracted from Photosystem I of spinach leaves and from algae. Photochem Photobiol 35: 821–826

Fajer J, Brune DC, Davis MS, Forman A and Spaulding LD (1975) Primary charge separation in bacterial photosynthesis: Oxidized chlorophylls and reduced pheophytin. Proc Natl Acad Sci USA 72: 4956–4960

Fiedor L, Rosenbach-Belkin V and Scherz A (1992) The stereospecific interaction between chlorophylls and chlorophyllase. J Biol Chem 26: 22043–22047

Fuller RC, Sprague SG, Gest H and Blankenship RE (1985) A unique photosynthetic reaction center from *Heliobacterium chlorum*. FEBS Lett 182: 345–349

Geskes C, Hartwich G, Scheer H, Mantele W and Heinze J (1995) An electrochemical and spectroelectrochemical investigation of metal-substituted bacteriochlorophyll *a*. J Am Chem Soc 117: 7776–7783

Gest H (1994) Discovery of the heliobacteria. Photosynth Res 41: 17–21

Goericke R and Repeta DJ (1992) The pigments of *Prochlorococcus marinus*: The presence of divinyl chlorophyll *a* and *b* in a marine procaryote. Limnol Oceanogr 37: 425–433

Gounaris K, Chapman DJ, Booth P, Crystall B, Giorgi IB, Klug DR, Porter G and Barber J (1990) Comparison of the D1/D2/cytochrome *b*559 reaction centre complex of photosystem two isolated by two different methods. FEBS Lett 265: 88–92

Hastings G, Durrant JR, Barber J, Porter G and Klug DR (1992) Observation of pheophytin reduction in photosystem two reaction centers using femtosecond transient absorption spectroscopy. Biochemistry 31: 7638–7647

Hauska G, Schoedl T, Remigy H and Tsiotis G (2001) The reaction center of green sulfur bacteria. Biochim Biophys Acta 1507: 260–277

Helfrich M, Schoch S, Lampert U, Cmeil E and Rüdiger W (1994) Chlorophyll synthetase cannot synthesize chlorophyll *a´*. Eur J Biochem 219: 267–275

Helfrich M, Schoch S, Schäfer W, Ryberg M and Rüdiger W (1996) Absolute configuration of protochlorophyllide *a* and substrate specificity of NADPH-Protochlorophyllide oxidoreductase. J Am Chem Soc 118: 2606–2611

Helfrich M, Ross A, King GC, Turner AG and Larkum AWD (1999) Identification of [8-vinyl]-protochlorophyllide *a* in phototrophic prokaryotes and algae: Chemical and spectroscopic properties. Biochim Biophys Acta 1410: 262–272

Hiraishi A and Shimada K (2001) Aerobic anoxygenic photosynthetic bacteria with zinc-bacteriochlorophyll. J Gen Appl Microbiol 47: 161–180

Hiraishi A, Matsuzawa Y, Kanbe T and Wakao N (2000) *Acidisphaera rubrifaciens* gen. nov., sp. nov., an aerobic bacteriochlorophyll-containing bacterium isolated from acidic environments. Int J Syst Evol Microbiol 50: 1539–1546

Hu Q, Miyashita H, Iwasaki I, Kurano N, Miyachi S, Iwaki M and Itoh S (1998) A Photosystem I reaction center driven by chlorophyll *d* in oxygenic photosynthesis. Proc Natl Acad Sci USA 95: 13319–13323

Itoh S, Iwaki M, Noguti T, Kawamori A, Mino H, Hu Q, Iwasaki I, Miyashita H, Kurano KN, Miyachi S and Shen R (2001) Photosystem I and II reaction centers of a new oxygenic organism *Acaryochloris marina* that use chlorophyll. In: PS 2001: Proceedings of the 12th International Congress on Photosynthesis, S6-028. CSIRO Publishing, Melbourne (CD-ROM)

Jordan P, Fromme P, Witt HT, Klukas O, Saenger W, Krauß N (2001) Three-dimensional structure of cyanobacterial Photosystem I at 2.5 Å resolution. Nature 411: 909–917

Kaufmann KJ, Dutton PL, Netzel TL, Leigh JS and Rentzepis PM (1975) Picosecond kinetics of events leading to reaction center bacteriochlorophyll oxidation. Science 188: 1301–1304

Kirmaier C, Blankenship RE and Holten D (1986) Formation and decay of radical-pair P^+I^- in *Chloroflexus aurantiacus* reaction centers. Biochim Biophys Acta 850: 275–285

Klimov VV and Krasnowskii AA (1981) Pheophytin as the primary electron acceptor in Photosystem 2 reaction centres. Photosynthetica 15: 592–609

Klimov VV, Shuvalov VA, Krakhmaleva IN, Klevanik AV and Krasnovskii AA (1977a) Photoreduction of bacteriopheophytin *b* in the primary light reaction of *Rhodopseudomonas viridis* chromatophores. Biokhimiya 42: 519–530

Klimov VV, Klevanik AV, Shuvalov VA and Krasnovsky AA (1977b) Reduction of pheophytin in the primary light reaction of Photosystem II. FEBS Lett 82: 183–186

Klimov VV, Allkhverdiev SI, Demeter S and Krasnovsky AA (1977c) Photoreduction of pheophytin in Photosystem 2 of chloroplasts with respect to the redox potential of the medium. Dokl Akad Nauk SSSR 249: 227–230

Klimov VV, Shuvalov VA and Heber U (1985) Photoreduction of pheophytin as a result of electron donation from the water-splitting system to Photosystem-II reaction centers. Biochim Biophys Acta 809: 345–350

Kobayashi M, Watanabe T, Nakazato M, Ikegami I, Hiyama T, Matsunaga T and Murata N (1988) Chlorophyll *a´*/P700 and pheophytin *a*/P680 stoichiometries in higher plants and cyanobacteria determined by HPLC analysis. Biochim Biophys Acta 936: 81–89

Kobayashi M, Maeda H, Watanabe T, Nakane H and Satoh K (1990) Chlorophyll *a* and β-carotene content in the D1/D2/cytochrome *b*-559 reaction center complex from spinach. FEBS Lett 260: 138–140

Kobayashi M, van de Meent EJ, Amesz J, Ikegami I and Watanabe T (1991) Bacteriochlorophyll *g* epimer as a possible reaction center component of heliobacteria. Biochim Biophys Acta 1057: 89–96

Kobayashi M, van de Meent EJ, Oh-oka H, Inoue K, Itoh S, Amesz J and Watanabe T (1992) Pigment composition of heliobacteria and green sulfur bacteria. In: Murata N (ed) Research in Photosynthesis, Vol 1, pp 393–396. Kluwer Academic Publishers, Dordrecht

Kobayashi M, Iwaki M, Tomo T, Kise H, Satoh K and Itoh S (1995) Heat-induced pigment alteration in the Photosystem I and II reaction center. In: Mathis P (ed) Photosynthesis: From Light to BiosphereVol 2, pp 139–142. Kluwer Academic Publishers, Dordrecht

Kobayashi M, Hamano T, Akiyama M, Watanabe T, Inoue K, Oh-oka H, Amesz J, Yamamura M and Kise H (1998a) Light-independent isomerization of bacteriochlorophyll *g* to chlorophyll *a* catalyzed by weak acid *in vitro*. Anal Chim Acta 365:, 199–203

Kobayashi M, Yamamura M, Akutsu S, Miyake J, Hara M, Akiyama M and Kise H (1998b) Successfully controlled isomerization and pheophytinization of bacteriochlorophyll *b* by weak acid in the dark *in vitro*. Anal Chim Acta 361: 285–290

Kobayashi M, Akiyama M, Kise H, Takaichi S, Watanabe T, Shimada K, Iwaki M, Itoh S, Ishida N, Koizumi M, Kano H, Wakao N and Hiraishi A (1998c) Structural determination of the novel Zn-containing bacteriochlorophyll in *Acidiphilium rubrum*. Photomed Photobiol 20: 75–80

Kobayashi M, Yamamura M, Akiyama M, Kise H, Inoue K, Hara M, Wakao N, Yahara K and Watanabe T (1998d) Acid resistance of [Zn]-Bacteriochlorophyll *a* from an acidophilic bacterium *Acidiphilium rubrum*. Anal Sci 14: 1149–1152

Kobayashi M, Akiyama M, Watanabe T and Kano H (1999a) Exotic chlorophylls as key components of photosynthesis. Current Topics in Plant Biology 1: 17–35

Kobayashi M, Akiyama M, Yamamura M, Kise H, Wakao N, Ishida N, Koizumi M, Kano H and Watanabe T (1999b) Comparison of physicochemical properties of metallobacteriochlorophylls and metallochlorophylls. Z Phys Chem 213: 207–214

Kobayashi M, Oh-oka H, Akutsu S, Akiyama M, Tominaga K, Kise H, Nishida F, Watanabe T, Amesz J, Koizumi M, Ishida N and Kano H (2000) The primary electron acceptor of green sulfur bacteria, bacteriochlorophyll 663, is chlorophyll *a* esterified with Δ2,6-phytadienol. Photosynth Res 63: 269–280

Kok B (1956) Preliminary notes on the reversible absorption change at 705 μm in photosynthetic organisms. Biochim Biophys Acta 22: 399–401

Liebl U, Mockensturm-Wilson M, Trost JT, Brune DC, Blankenship RE and Vermaas W (1993) Single core polypeptide in the reaction center of the photosynthetic bacterium *Heliobacillus mobilis*: Structural implications and relations to other photosystems. Proc Natl Acad Sci USA 90: 7124–7128

Maeda H, Watanabe T, Kobayashi M and Ikegami I (1992) Presence of two chlorophyll *a′* molecules at the core of Photosystem I. Biochim Biophys Acta 1099: 74–80

Manning WM and Strain HH (1943) Chlorophyll *d*, a green pigment of red algae. J Biol Chem 151: 1–19

Masuda T, Inoue K, Masuda M, Nagayama M, Tamaki A, Ohta H, Shimada H and Takamiya K (1999) Magnesium insertion by magnesium chelatase in the biosynthesis of zinc-bacteriochlorophyll *a* in an aerobic acidophilic bacterium *Acidiphilium rubrum*. J Biol Chem 274: 33594–33600

Mattioli TA, Williams JC, Allen JP and Robert B (1994) Changes in primary donor hydrogen-bonding interactions in mutant reaction centers from *Rhodobacter sphaeroides*: Identification of the vibrational frequencies of all the conjugated carbonyl groups. Biochemistry 33: 1636–1643

Michalski TJ, Hunt JE, Bowman MK, Smith U, Bardeen K, Gest H, Norris JR and Katz JJ (1987) Bacteriopheophytin *g*: Properties and some speculations on a possible primary role for bacteriochlorophylls *b* and *g* in the biosynthesis of chlorophylls. Proc Natl Acad Sci USA 84: 2570–2574

Mimuro M, Akimoto S, Yamazaki I, Miyashita H and Miyachi S (1999) Fluorescence properties of chlorophyll *d*-dominating prokaryotic alga, *Acaryochloris marina*: Studies using time-resolved fluorescence spectroscopy on intact cells. Biochim Biophys Acta 1412: 37–46

Mimuro M, Hirayama K, Uezono K, Miyashita H and Miyachi S (2000) Uphill energy transfer in a chlorophyll *d*-dominating oxygenic photosynthetic prokaryote, *Acaryochloris marina*. Biochim Biophys Acta 1456: 27–34

Miyashita H, Ikemoto H, Kurano N, Adachi K, Chihara M and Miyachi S (1996) Chlorophyll *d* as a major pigment. Nature 383: 402

Miyashita H, Adachi K, Kurano N, Ikemoto H, Chihara M and Miyachi S (1997) Pigment composition of a novel oxygenic photosynthetic prokaryote containing chlorophyll *d* as the major chlorophyll. Plant Cell Physiol 38: 274–281

Murakami A, Kawai H, Adachi K, Miyashita H, Sakawa T and Mimuro M (2001) Chlorophyll *d* in Rhodophyceae: Presence and function. In: PS 2001: Proceedings 12th International Congress on Photosynthesis, S31-004. CSIRO Publishing, Melbourne (CD-ROM)

Murata N, Araki S, Fujita Y, Suzuki K, Kuwabara T and Mathis P (1986) Stoichiometric determination of pheophytin in Photosystem II of oxygenic photosynthesis. Photosynth Res 9: 63–70

Nagashima KVP, Matsuura K, Wakao N, Hiraishi A and Shimada K (1997) Nucleotide sequences of genes cording for photosynthetic reaction centers and light-harvesting proteins of *Acidiphilium rubrum* and related aerobic acidophilic bacteria. Plant Cell Physiol 38: 1249–1258

Nakamura A and Watanabe T (1998) HPLC determination of photosynthetic pigments during greening of etiolated barley leaves. Evidence for the biosynthesis of chlorophyll *a′*. FEBS Lett 426: 201–204

Nakamura A and Watanabe T (2001) Separation and determination of minor photosynthetic pigments by reversed-phase HPLC with minimal alteration of chlorophylls. Anal Sci 17: 503–508

Nakamura A, Tanaka S and Watanabe T (2001) Normal-phase HPLC separation of possible biosynthetic intermediates of pheophytin *a* and chlorophyll *a′*. Anal Sci 17: 509–513

Nanba O and Satoh K (1987) Isolation of a Photosystem II reaction center consisting of D-1 and D-2 polypeptides and cytochrome *b*-559. Proc Natl Acad Sci USA 84: 109–112

Neerken S and Amesz J (2001) The antenna reaction center complex of heliobacteria: composition, energy conversion and electron transfer. Biochim Biophys Acta 1507: 278–290

Neerken S, Schmidt KA, Aartsma TJ and Amesz J (1999) Dynamics of energy conversion in reaction center core complexes of the green sulfur bacterium *Prosthecochloris aestuarii* at low temperature. Biochemistry 38: 13216–13222

Neerken S, Aartsma TJ and Amesz J (2000) Pathways of energy transformation in antenna reaction center complexes of *Heliobacillus mobilis*. Biochemistry 39: 3297–3303

Nishiyama Y, Kitamura M, Tamura S and Watanabe T (1994) Purification and substrate specificity of chlorophyllase from *Chlorella regularis*. Chem Lett: 69–72

Nuijs AM, van Dorssen RJ, Duysens LNM and Amesz J (1985a) Excited states and primary photochemical reaction in the photosynthetic bacterium *Heliobacterium chlorum*. Proc Natl Acad Sci USA 82: 6865–6868

Nuijs AM, Vasmel H, Joppe HLP, Duysens LNM and Amesz J (1985b) Excited states and primary charge separation in the pigment system of the green photosynthetic bacterium *Prosthecochloris aestuarii* as studied by picosecond absorbance difference spectroscopy. Biochim Biophys Acta 807: 24–34

Olson JM, Prince RC and Brune DC (1977) Reaction-center complexes from green bacteria. Brookhaven Symp Biol 28: 238–246

Parson WW, Clayton RK and Cogdell RJ (1975) Excited states of photosynthetic reaction centers at low redox potentials. Biochim Biophys Acta 387: 265–278

Permentier HP, Schmidt KA, Kobayashi M, Akiyama M, Hager-Braun C, Neerken S, Miller M and Amesz J (2000) Composition and optical properties of reaction center core complexes from the green sulfur bacteria *Prosthecochloris aestuarii* and *Chlorobium tepidum*. Photosynth Res 64: 27–39

Pierson BK and Thornber JP (1983) Isolation and spectral characterization of photochemical reaction centers from the thermophilic green bacterium *Chloroflexus aurantiacus* strain J-10-f1. Proc Natl Acad Sci USA 80: 80–84

Prince RC and Olson JM (1976) Some thermodynamic and kinetic properties of the primary photochemical reactions in a complex from a green photosynthetic bacterium. Biochim Biophys Acta 423: 357–362

Prince RC, Gest H and Blankenship RE (1985) Thermodynamic properties of the photochemical reaction center of *Heliobacterium chlorum*. Biochim Biophys Acta 810: 377–384

Rebeiz CA, Belanger FC, Freyssinet G and Saab DG (1980) Chloroplast biogenesis. XXIX. The occurrence of several novel chlorophyll *a* and *b* chromophores in higher plants. Biochim Biophys Acta 590: 234–247

Ricketts TR (1966) Magnesium 2,4-divinylphaeoporphyrin a_5 monomethyl ester, a protochlorophyll-like pigment present in some unicellular flagellates. Phytochemistry 5: 223–229

Rockley MG, Windsor MW, Cogdell RJ and Parson WW (1975) Picosecond detection of an intermediate in the photochemical reaction of bacterial photosynthesis. Proc Natl Acad Sci USA 72: 2251–2255

Scheer H and Hartwich G (1995) Bacterial reaction centers with modified tetrapyrrol chromophores. In: Blankenship RE, Madiagan MT and Bauer CE (eds) Anoxygenic Photosynthetic Bacteria, pp 649–663. Kluwer Academic Publishers, Dordrecht

Shuvalov VA, Vasmel H, Amesz J and Duysens LNM (1986) Picosecond spectroscopy of the charge separation in reaction centers of *Chloroflexus aurantiacus* with selective excitation of the primary electron donor. Biochim Biophys Acta 851: 361–368

Steiner R, Cmiel E and Scheer H (1983) Chemistry of bacteriochlorophyll *b* : Identification of some (photo)oxidation products. Z Naturforsch C 38, 748–752

Strain HH and Manning WM (1942) Isomerization of chlorophylls *a* and *b*. J Biol Chem 146: 275–276

Sybesma C and Vredenberg WJ (1963) Evidence for a reaction center P840 in the green photosynthetic bacterium *Chloropseudomonas ethylicum*. Biochim Biophys Acta 75: 439–441

van de Meent EJ, Kleinherenbrink FAM and Amesz J (1990) Purification and properties of an antenna-reaction center complex from heliobacteria. Biochim Biophys Acta 1015: 223–230

van de Meent EJ, Kobayashi M, Erkelens C, Van Veelen PA, Amesz J and Watanabe T (1991) Identification of 8^1-hydroxychlorophyll *a* as a functional reaction center pigment in heliobacteria. Biochim Biophys Acta 1058: 356–362

van de Meent EJ, Kobayashi M, Erkelens C, Van Veelen PA, Otte SCM, Inoue K, Watanabe T and Amesz J (1992) The nature of the primary electron acceptor in green sulfur bacteria. Biochim Biophys Acta 1102: 371–378

van Gorkom HJ (1974) Identification of the reduces primary electron acceptor of Photosystem II as a bound semiquinone anion. Biochim Biophys Acta 347: 439–442

Wakao N, Yokoi N, Isoyama N, Hiraishi A, Shimada K, Kobayashi M, Kise H, Iwaki M, Itoh S, Takaichi S and Sakurai Y (1996) Discovery of natural photosynthesis using Zn-containing bacteriochlorophyllin an aerobic bacterium *Acidiphilium rubrum*. Plant Cell Physiol 37: 889–893

Wakao N, Hiraishi A, Shimada K, Kobayashi M, Takaichi S, Iwaki M and Itoh S (1999) Discovery, characteristics, and distribution of Zinc-BChl in aerobic acidophilic bacteria including *Acidiphilium* species and other related acidophilic bacteria. In: Peschek GA, Loffelhardt W and Schmetterer G (eds) The Phototrophic Prokaryotes, pp 745–750. Plenum Publishing Co., New York,

Wasielewski MR, Norris JR, Shipman LL, Lin C-P and Svec WA (1981) Monomeric chlorophyll *a enol*: Evidence for its possible role as the primary electron donor in Photosystem I of plant photosynthesis. Proc Natl Acad Sci USA 78: 2957–2961

Watanabe T and Kobayashi M (1991) Electrochemistry of chlorophylls. In: Scheer H (ed) Chlorophylls, pp 287–315. CRC Press, Boca Raton

Watanabe T, Machida K, Suzuki H, Kobayashi M and Honda K (1985a) Photoelectrochemistry of chlorophylls. Coord Chem Rev 64: 207–224

Watanabe T, Nakazato M, Mazaki H, Hongu A, Konno M, Saitoh S and Honda K (1985b) Chlorophyll *a* epimer and pheophytin *a* in green leaves. Biochim Biophys Acta 807: 110–117

Webber AN and Lubitz W (2001) P700: The primary electron donor of Photosystem I. Biochim Biophys Acta 1507: 61–79

Witt HT, Rumberg B, Schmidt-Mende P, Siggel U, Skerra B, Vater J and Weikard J (1965) Angew Chem (Intern Ed) 4: 799

Wu SM and Rebeiz CA (1985) Chloroplast biogenesis. Molecular structure of chlorophyll *b* (E489 F666). J Biol Chem 206: 3632–3634

Wu SM, Mayasich, JM and Rebeiz CA (1989) Chloroplast biogenesis: Quantitative determination of monovinyl and divinyl chlorophyll(ide) *a* and *b* by spectrofluorometry. Anal Biochem 178: 294–300

Xiong J, Fischer WM, Inoue K, Nakahara M and Bauer CE (2000) Molecular evidence for the early evolution of photosynthesis. Science 289: 1724–1730

Yamamura M, Kobayashi M, Inoue K, Hara M, Wakao N, Kano H, Watanabe T, Akiyama M and Kise H (1998) *Acidiphilium rubrum* and zinc-bacteriochlorophyll, part 3: High resistance of zinc-bacteriochlorophyll *a* to acid. In: Garab G (ed) Photosynthesis: Mechanism and Effects, Vol 2, pp 739–742. Kluwer Academic Publishers, Dordrecht

Chapter 5

[Heavy metal]-Chlorophylls Formed in Vivo During Heavy Metal Stress and Degradation Products Formed During Digestion, Extraction and Storage of Plant Material

Hendrik Küpper*[1,2], Frithjof C. Küpper[1,3]
[1]Universität Konstanz, Mathematisch-Naturwissenschaftliche Sektion, Fachbereich Biologie Postbox M665, D-78457 Konstanz, Germany; [2]Photosynthesis Research Centre at the Institute of Microbiology and the University of South Bohemia, Opatovický ml´yn, CZ-37981 Trebon, Czech Republic; [3]Department of Chemistry, University of California, Santa Barbara, CA 93106, U.S.A.

Martin Spiller
Institut für Wasserbau und Wasserwirtschaft, Rheinisch-Westfälische Technische Hochschule Aachen, D-52056 Aachen, Germany; and, Institut de Mécanique des Fluides de Toulouse, F-31400 Toulouse, France

Summary

This chapter discusses the occurrence, properties and relevance of chlorophyll (Chl) degradation products that are formed *either* in vivo in heavy metal-stressed plants or by digestion of algae in marine invertebrates, *or* that are formed during extraction or processing of dead plant material. The in vivo substitution of the central Mg^{2+} ion of chlorophyll by heavy metals constitutes an important part of the damage occurring in metal-stressed plants. In *Chlorophyta*, this reaction varies with light intensity. In low irradiance combined with a dark phase, the light-harvesting complex II (LHC II) is the main target, while in high irradiance the LHC II is inaccessible to substitution of Mg^{2+}. Instead, an insertion of heavy metals into the pheophytin (Phe) of the Photosystem II reaction center (PS II RC) has been proposed. In algae with different light harvesting proteins, this light-dependent difference is absent. In brown algae, Chl *a* in the Chl *a*/*c* LHC is always accessible to substitution of Mg^{2+} by heavy metals. While heavy metal chlorophylls are not functional in higher plants and

*Author for correspondence, email: Hendrik.Kuepper@uni-konstanz.de

Bernhard Grimm, Robert J. Porra, Wolfhart Rüdiger and Hugo Scheer (eds): Chlorophylls and Bacteriochlorophylls: Biochemistry, Biophysics, Functions and Applications, pp. 67–77.

algae, [Zn]-bacteriochlorophyll ([Zn]-BChl) was found to function as a photosynthetic pigment in aerobic photosynthetic bacteria of the genus *Acidiphilium*. Since these bacteria live in an acidic environment extremely rich in heavy metals, the advantage of much higher resistance against substitution by metals other than Zn seems to more than compensate for the disadvantages of [Zn]-BChl complex compared to [Mg]-BChl as a photosynthetic pigment. The questionable beneficial in vivo formation of rare-earth chlorophylls ([RE]-Chls) in plants growing on soils rich in rare earths is discussed in this chapter. Further, new knowledge of allomerization and photodegradation of chlorophyll solutions is discussed in relation to the processes of chlorophyll degradation during storage and extraction of plant material for analysis or human consumption. The partial digestion of chlorophyll and subsequent use of the transmetalated product, tunichlorin, in marine invertebrates is also briefly discussed.

I. Introduction

Chlorophylls (Chls) are unstable and prone to diverse modifications that can change not only their photosynthetic function but also their usefulness in heterotrophic organisms including man. In this chapter we focus on those modifications that are unrelated to the enzymatically-controlled processes of plant ontogenesis and senescence, but occur in vivo as a consequence of elevated heavy metal concentrations or occur artifactually during handling and processing of plant material in the laboratory or food industry. The in vivo processes modifying the photosynthetic function of Chls that are discussed here include:

1) the formation of heavy metal substituted chlorophylls ([Hms]-Chls) as a reaction leading to damage in heavy metal-stressed plants;

2) the formation of [Zn]-BChl in acidophilic bacteria as a defense against not only such damage but also pheophytinization; and,

3) the alleged formation of [La]-Chls in La-fertilized plants.

We also discuss the modifications of Chls occurring during handling of plant material which include:

1) the allomerization of Chl in solutions;

2) the photooxidation of Chl in solutions;

3) the degradation of Chls during freezing and storage of plant material; and,

4) artifacts of extraction.

Finally, degradation of Chls during animal digestion of plant material is outside the scope of this chapter: recent reviews of this topic by Ma and Dolphin (1999) and chapter 42 of this book by Goericke et al. are recommended. However, we discuss a Ni-containing pigment, tunichlorin, which is a partial Chl digestion product found in some marine invertebrates, because its formation involves substitution of the central Mg^{2+}, which is the main focus of this chapter.

In each subsection, the conditions leading to the formation of the respective Chl derivatives are described, together with their biological relevance and some of their physical and chemical properties.

II. Substitution of the Central Mg^{2+} Ion Under Elevated Heavy Metal Concentrations in vivo

A. [Heavy metal]-Chlorphyll Formation as a Damage Mechanism in Heavy Metal-Stressed Plants

Many heavy metals (such as Cu^{2+}, Ni^{2+}, Zn^{2+}) are well-known essential trace elements for plants, but at higher concentrations they can also be very toxic. A variety of toxic effects has been observed, but their relative importance depends on the nature of the metal, the plant species involved and on the different environmental conditions encountered, including light intensity. As reviewed by Prasad and Hagemeyer (1999), a number of mechanisms for heavy metal-

Abbreviations: BChl – bacteriochlorophyll; Chl – chlorophyll; F_0 – minimal fluorescence yield of a dark-adapted sample in non-actinic measuring light; F_m – maximum fluorescence yield of a dark-adapted sample; FTIR – Fourier transform infrared spectroscopy; F_v – variable fluorescence; $F_v = F_m - F_0$; [Hms]-Chl – heavy metal substituted Chl (formed by replacement of Mg^{2+} ion by heavy metal ions or via incorporation into Phe); LHC II – light harvesting complex II; MS – mass spectrometry; PS – Photosystem; RC – reaction center; RE – rare earth

induced damage have been proposed including the inhibition of key enzymes, inhibition at various sites of the PS II RC and enhancement of photoinhibition and oxidative stress. However, many of these effects have only been examined in vitro, and some of them could neither be confirmed in vitro nor observed in vivo. Furthermore, the effects of heavy metals were sometimes studied under such extremely high concentrations, as to be environmentally irrelevant.

One mechanism of heavy metal-induced damage that leads to inhibition of photosynthesis, which was studied in higher plants and green algae under environmentally relevant metal concentrations down to the sub-micromolar range (Küpper et al., 1996), involves the in vivo replacement of Mg^{2+} in the Chl molecule by heavy metal ions; that is, [Hms]-Chl formation (Küpper et al., 1996, 1998, 2002b). In metal-sensitive aquatic plants, such as *Elodea canadensis* which absorb metals through the leaf surface and possess only weak defense mechanisms, an almost proportional relationship was found between the ability of a heavy metal ion to form an [Hms]-Chl molecule and its toxicity towards the plants (Küpper et al., 1996), namely, Hg>Cu>Cd>Ni≥Zn>>Pb. Also, earlier studies *either* demonstrated the in vivo formation of [Hms]-Chls in cyanobacteria (Kowalewska and Hoffman, 1989; Kowalewska et al., 1992) and unicellular algae (Gross et al., 1970; De Filippis, 1979), *or* presented data which, in retrospect, indicated in vivo [Hms]-Chl formation in the photosymbionts of lichens (Puckett, 1976). In all these studies, however, the relationship between [Hms]-Chl formation and inhibition of photosynthesis was not investigated. As discussed by Küpper et al. (1996, 1998), [Hms]-Chls are unsuitable for photosynthesis for several reasons.

1) All [Hms]-Chls have much lower in vitro fluorescence quantum yields than [Mg]-Chls (Watanabe and Kobayashi, 1988; see also Chapter 6, Kobayashi et al.) indicating a rather unstable first excitation state that relaxes thermally. For this reason, resonance energy transfer from the antenna pigment complexes to the reaction centers in the thylakoids, which depends on the same excitation states that cause Chl fluorescence (Karukstis, 1991), is either inefficient or impossible. Since many [Hms]-Chls (e.g., [Cu]-Chl or [Ni]-Chl) do not re-emit any absorbed excitons, they are very efficient exciton quenchers; consequently, the conversion of a few percent of the total Chl to [Hms]-Chl dramatically decreases fluorescence (Küpper et al., 1998, 2002b; Prasad et al., 2001). Recently, this heavy metal quenching has been used as an analytical tool (Fiedor et al., 2001).

2) The blue shift of the fluorescence emission maximum of the weakly fluorescent [Zn]-Chl, relative to [Mg]-Chl, reduces the necessary spectral overlap of fluorescence/absorbance bands in the antenna complexes that is required for excitation transfer towards the reaction centers; thus, the efficiency of excitation transfer in the case of [Zn]-Chl is reduced.

3) [Mg]-Chl *a* has a higher capacity to release electrons from the singlet excited state than all [Hms]-Chls (Watanabe et al., 1985), making Mg^{2+} the most favorable ion for the special-pair Chls in the reaction centers.

4) Many [Hms]-Chl complexes (e.g. [Cu]-Chl or [Ni]-Chl) cannot bind axial ligands while others (e.g. [Zn]-Chl or [Cd]-Chl) bind them less readily than [Mg]-Chl (Boucher and Katz, 1967). This binding is required for correct Chl-protein attachment (Rebeiz and Belanger, 1984) and for maintenance of the proper LHC II structure (Paulsen et al., 1993). Therefore, [Hms]-Chl incorporation into LHC II Chls may induce a conformational change resulting in exposure of some Chls to the acidic content of the thylakoid lumen producing Phes, which were indeed detected under heavy metal stress leading to [Hms]-Chl formation (Küpper et al., 2002b).

Hence, the formation of minor proportions of [Hms]-Chl relative to the total Chl may already inhibit photosynthesis completely (Küpper et al., 1996, 1998, 2002b; Prasad et al., 2001). Recently, several studies have confirmed that [Hms]-Chl formation plays an important role in heavy metal-induced damage (Geiken et al., 1998; Prasad and Strzalka, 1999; Patra and Sharma, 2000; Prasad et al., 2001). Resistance in highly metal-resistant plants involves mechanisms that specifically reduce [Hms]-Chl formation (Küpper et al., 2000b, 2001; Psaras et al., 2000; Psaras and Manetas, 2001).

Early in vivo studies of [Hms]-Chl formation in higher plants and green algae (Küpper et al., 1996, 1998) showed that this reaction is strongly dependent on light intensity (Table 1). Under low irradiance conditions associated with a dark phase, *the major-*

Table 1. In vivo occurrence and relevance of heavy metal chlorophylls in photosynthetic organisms

Organism	Metals tested	Light dependence	Relevance	Major references
Higher plants	Cd^{2+}, Cu^{2+}, Hg^{2+}, Ni^{2+}, Pb^{2+}, Zn^{2+}; except Pb^{2+} all found in Chl of stressed plants	low light with dark phase: *shade*, *reaction* high light: *sun reaction*	damage mechanism	Küpper et al., 1996, 1998; Prasad et al., 2001
Green algae	Cu^{2+}, Zn^{2+}; both found in Chl of stressed algae	low light with dark phase: *shade reaction*, high light: *sun reaction*	damage mechanism	Gross et al., 1970; DeFilippis, 1979; Küpper et al., 1998, 2002b
Brown algae	Cu^{2+}, Zn^{2+}; both found in Chl of stressed algae	all irradiances: *shade reaction*	damage mechanism	Küpper et al., 2002b
Red algae	Cu^{2+}; found in Chl of stressed algae	all irradiances: *sun reaction*	damage mechanism	Küpper et al., 2002b
Lichens	Cu^{2+}; found in Chl of stressed lichens	?	damage mechanism	Puckett, 1976
Cyanobacteria	Cu^{2+}; found in Chl of stressed cyanobacteria	?	damage mechanism	Kowalewska and Hoffmann, 1989; Kowalewska et al., 1992
Acidiphilium	Zn^{2+} found in Chl; bacteria resistant against damage by Cd^{2+}, Cu^{2+}, Ni^{2+}, H^{+}, Zn^{2+}	?	acid and metal resistance mechanism	Wakao et al., 1996; Mahapatra and Banerjee, 1996; Masuda et al., 1999; Hiraishi and Shimada, 2001
Higher plants	rare earths (Ce^{3+}, Dy^{3+}, Eu^{3+}, Gd^{3+}, Ho^{3+}, La^{3+}, Nd^{3+}, Pr^{3+}, Sm^{3+}, Tb^{3+}, Y^{3+})	?	enhancement of photosynthetic performance?	Hong et al., 1999; Wei et al., 2000a; Wang et al., 2001

ity of antenna Chls are accessible for [Hms]-Chl formation, leading to a type of damage designated *shade reaction*. The large fraction of total Chl that may become [Hms]-Chl in the *shade reaction* immediately indicated that antenna Chls must be involved (Fig. 1) and a recent study (Küpper et al., 2002b) showed that LHC II is the main target for [Hms]-Chl formation in *Chlorophyta*. In high irradiance conditions, only a small fraction of the total Chl (<2%) is accessible for [Hms]-Chl formation, while bleaching of the bulk of the pigments parallels the destruction of the photosynthetic apparatus (Küpper et al., 1996, 1998, 2002b): this phenomenon has been named *sun reaction* in which direct damage to the PS II core was demonstrated (Küpper et al., 1998, 2002b). Evidence, suggesting that the insertion of heavy metals (especially Cu^{2+}) into the Phe *a* of the PS II RC is the key step in this metal-induced inhibition, was obtained by Küpper et al. (2002b). These *sun* and *shade* reactions also lead to distinct changes of in vivo Chl fluorescence kinetics (Küpper et al., 2002b): the damage during the *sun reaction* to the PS II RC causes a strong decrease of F_v/F_m regardless of the metal applied. In contrast, the *shade reaction* involving non-fluorescent [Hms]-Chl formation (e.g. [Cu]-Chl) in LHC II is characterized by a decrease only of the total fluorescence amplitude without any significant changes of F_v/F_m. In brown and green algae, the relative antenna size does not decrease during the *shade reaction*, indicating that

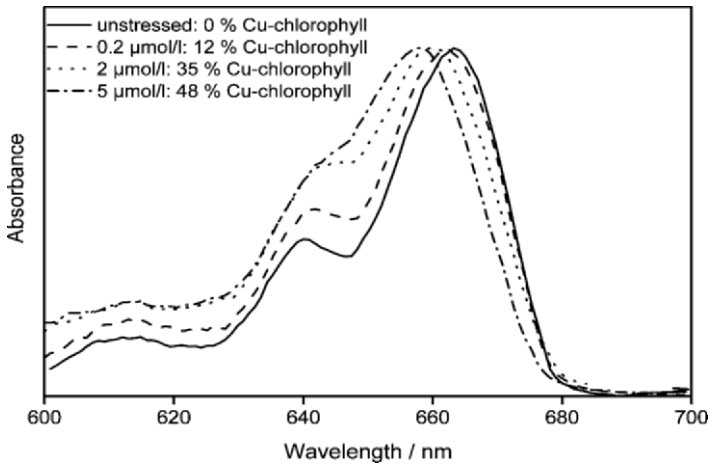

Fig. 1. Change of the UV/VIS absorbance spectrum of extracts from *Elodea canadensis* stressed with varying concentrations of Cu^{2+}. Note that only rather high proportions of [Hms]-Chl formation lead to a visible shift of the absorbance maximum; lower ratios of [Hms]-Chl only yield a small change in the shape of the spectrum (from Küpper et al., 1996, modified).

whole photosynthetic units (antennae plus RCs) are quickly made inoperable by insertion of heavy metal ions into very few Chls of the LHC II (Küpper et al., 2002b). In contrast, in Cu^{2+}-stressed higher plants (*Elodea canadensis*, *Thlaspi caerulescens*, *Thlaspi ochroleucum*), a decrease of the relative antenna size was found (H. Küpper and I. Setlík, unpublished), indicating very effective co-operation between photosynthetic units so that, after destruction of some LHC IIs, the still functional PS II RCs share the remaining functional LHC IIs.

In algae possessing light harvesting proteins different from the LHC II, either the *shade reaction* or the *sun reaction* mechanism, but not both, is found regardless of the ambient irradiance (Küpper et al., 2002b; Table 1). For example, in red algae, where phycobilisomes replace LHC II as the peripheral antenna, the *sun reaction* occurs even at very low irradiance (around the light compensation point). In brown algae, which have Chl *a*/*c*-LHCs rather than LHC II, the *shade reaction* occurs even at irradiance levels saturating photosynthesis. The structural differences between LHC II and Chl *a*/*c*-LHCs that cause the different response to irradiance remain to be identified. [Hms]-Chl formation during the *shade reaction* may occur during the assembly of LHC II trimers. The Chl *a*/*c*-LHCs form large assemblies regardless of irradiance (Katoh and Ehara, 1990; Mimuro et al., 1990), which might reflect their tendency to form [Hms]-Chl in both high and low irradiance. Because the *sun reaction* in *Chlorophyta* takes place when Cu^{2+} is added in the dark to cells previously grown in high light also suggests that the *sun reaction* is dependent on a structural change in the LHC II that occurs during adaptation to high irradiance, and not on a change directly related to the light-dependent energization of thylakoid membranes.

A study of energy transfer between Chl derivatives and singlet oxygen (Küpper et al., 2002a) has shown that [Hms]-Chls are less (i.e. [Cu]-Chls) or equally (i.e. [Zn]-Chls) efficient generators of singlet oxygen as [Mg]-Chls, but both are less efficient quenchers of singlet oxygen. Thus [Hms]-Chl formation does not directly, but may indirectly, lead to an increase of oxidative stress during heavy metal stress.

Studies of [Hms]-Chl formation were greatly facilitated by the development of a novel method for quantifying these pigments, which is based on a mathematical description of the UV/VIS absorption spectra (Küpper et al., 2000a). UV/VIS absorption spectroscopy has been used to detect [Hms]-Chl formation in plant extracts (Jones et al., 1977; White et al., 1977; Küpper et al., 2000a) and in vivo (Küpper et al., 1998); HPLC has been employed with extracts (Kowalewska and Hoffmann, 1989; Kowalewska et al., 1992; Hidenari et al., 1993). [Hms]-Chl formation has also been detected in extracts by spectrofluorimetry (Jones et al., 1977; White et al., 1977) and in vivo using fluorescence microscopy (Küpper et al., 1998). Among [Hms]-Chls, [Cu]-Chl is the easiest to distinguish from [Mg]-Chl by its absorption spectrum and chemical stability, while detection of [Cd]-Chl is very difficult (Küpper et al., 1996, 1998). This, combined with the high irradiance applied,

could explain why Baryla et al. (2001) did not find [Cd]-Chl in Cd-stressed *Brassica napus*.

B. Controlled [Heavy Metal]-Chlorophyll Formation as a Protection Against Uncontrolled [Heavy Metal]-Chlorophyll Formation

Interestingly, photosynthetically active [Zn]-BChl *a* has been reported (Wakao et al., 1996) in acidophilic phototrophic bacteria of the genus *Acidiphilium* (reviewed by Hiraishi and Shimada, 2001). These bacteria replace the Mg^{2+} of BChl with Zn^{2+} (Masuda et al., 1999; Hiraishi and Shimada, 2001). In these highly acidic conditions (~pH 1.5) where [Mg]-BChl is converted to BPhe, the formation and use of [Zn]-BChl as a stable photosynthetic pigment is most opportune. Further, the Zn^{2+} ion in [Zn]-BChl is very resistant to replacement by other metals, which constitutes an adaptive advantage since these organisms live in environments rich in many heavy metals, such as metal mine tailings (Kishimoto and Tano, 1987; Banerjee et al., 1996; Itoh et al., 1998). Mahapatra and Banerjee (1996) studied the extreme tolerance of *Acidiphilium* to cadmium, copper, nickel and zinc. The resistance of [Zn]-BChl against formation of non-functional [Hms]-BChls actually seems to be more important than the acid resistance of this pigment, because the intracellular pH of acidophilic bacteria including *Acidiphilium* was reported to be neutral (Zychlinsky and Matin, 1983; Matin, 1999). The above-mentioned advantages of [Zn]-BChl over [Mg]-BChl appear to more than compensate for the disadvantages of the Zn-complex, including the lower photosynthetic quantum yield, which is ~75% lower than [Mg]-BChl (Watanabe and Kobayashi, 1988; Chapter 6, Kobayashi et al.). However, [Zn]-Chl cannot replace Chls in higher plants or green algae because its blue-shifted absorbance and fluorescence maxima reduce the spectral overlap of fluorescence/absorbance bands required for excitation transfer to plant RCs.

C. In vivo Formation of [Lanthanoid]-Chlorophylls?

Recently, it was reported that diverse lanthanoid (rare earth) derivatives of Chl ([RE]-Chls) occur in the fern *Dicranopteris dichotoma* (Hong et al., 1999) and in *Spinacia oleracea* (Wang et al., 2001) after fertilization with salts of lanthanoids. Furthermore, it was claimed that these [RE]-Chls would have an enhanced function in photosynthesis compared to [Mg]-Chl (Wei et al., 2000a). An X-ray absorption study showed that La^{3+} forms sandwich structures consisting of two parallel Phe rings with a lanthanoid ion in the middle (Wei et al., 2000b), confirming earlier results of Buchler and co-workers with other porphyrins (reviewed by Buchler, 1997).

Although an in vivo function for [RE]-Chls would be highly interesting, the results presented by Hong et al. (1999) and Wang et al. (2001) concerning the occurrence and function of [RE]-Chls in vivo are not convincing for several reasons. Most importantly, in all known Chl-containing proteins the distance between monomeric Chls is too large for formation of a [RE]-Chl sandwich, and the Chl dimers are improperly oriented. Therefore, it is more likely in all the above-mentioned studies that the [RE]-Chls were formed during grinding of the fresh, not lyophilized, plants and their subsequent extraction with ethanol (Hong et al., 1999; Wei et al., 2000b; Section IV.A). In addition, no evidence was presented why [RE]-Chls should enhance photosynthesis; none of the [Hms]-Chls analyzed so far met this criterion. Studies with isolated LHCs and RCs, ideally with selective insertion of [RE]-Chl complexes (analogous to those of Fiedor et al., 2001), should be used to demonstrate the photosynthetic performance of [RE]-Chls.

III. Occurrence of Partially Degraded and Transmetalated Chlorophyll Derivatives in Marine Invertebrates

The first naturally occurring [Ni]-Chl derivative, *Tunichlorin* (Fig. 2), was found in the Caribbean tunicate, *Trididemnum solidum* (Bible et al., 1988; Rinehart et al., 1988), together with much Phe *a* and with didemnins (cytostatic natural products). Tunichlorin, unlike the Ni-porphyrin F430 of methanogenic bacteria (Pfaltz et al., 1982), currently has no proven physiological role (see below). Tunichlorin was also found in the sea hare (mollusc) *Dolabella auricularia* from Papua-New Guinea during the isolation of dolastatin, an anti-cancer agent (Pettit et al., 1993).

Tunichlorin is a labile blue-green pigment resembling pyropheophorbide *a* since it lacks the carboxymethyl group of Chl *a* at C-13[2]: it has absorption maxima in CH_2Cl_2 at 389 nm (ε = 34000), 416 nm (ε = 41600), and 641 nm (ε = 43500). It decomposes rapidly even at low temperatures under N_2 (Bible et al., 1988), but its dimethyl derivative (Fig. 2), used in structural and spectral investigations (Bible et al.,

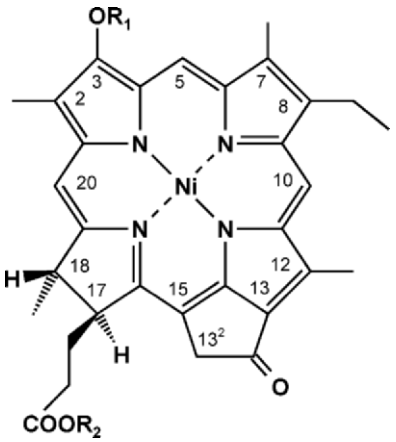

Fig. 2. Structure of tunichlorin and derivatives. (1) tunichlorin. $R_1 = R_2 = H$; (2) acyl-tunichlorins. R_1 = various fatty acid residues (Sings et al., 1996); (3) dimethyltunichlorin. $R_1 = R_2 = CH_3$

1988; Rinehart et al., 1988; Andersson et al., 1990, 1991; Sings et al., 1996), is more stable. The presence of Ni, suggested by mass spectrometry (MS) data, was confirmed by atomic absorption spectroscopy and by demetalation and remetalation experiments (Bible et al., 1988).

Since *Tridemnum* and *Dolabella* both coexist with algal endosymbionts, the biosynthetic origin of tunichlorin (Rinehart et al., 1988) is unclear: the biosynthesis of chlorin-type tetrapyrroles is restricted to photosynthetic organisms, but [Ni]-Chls have not been reported in free-living algae (Bible et al., 1988). Therefore, tunichlorin is probably derived from algal Chl by partial degradation and transmetalation in the animal. This view is supported by the study of Sings et al. (1996) who found that tunichlorin in *Tridemnum* is associated with several dozen structural analogues differing in the acyl side chains (C14:0 to C22:6 fatty acids) esterified to the C-3-hydroxymethyl group (Fig. 2, structure 2): such fatty acyl sidechains are unknown in Chl molecules of photosynthetic organisms. Both the fatty-acyl moieties and the central nickel ion are unusual among known naturally-occurring chlorins.

No physiological function is currently known for tunichlorin but Bible et al. (1988) suggested, by analogy with F430 of methanogenic bacteria, that it might be involved in reductive pathways, while Pettit et al. (1993) similarly proposed an electron transfer role. Sings et al. (1996) alluded to a membrane-located cofactor role involved in formation of the long, hydrophobic fatty-acyl residues. Ma and Dolphin (1999) suggested a function in uptake or storage of nickel: similarly, the copper and zinc chlorins that seem to occur in the marine polychaete *Owenia fusiformis* may also have a role in zinc and copper uptake but supporting evidence is currently lacking (Gibbs et al., 2000).

IV. Chlorophyll Degradation Products Formed During Storage and Extraction of Plant Material

A. Light-independent Allomerization of Chlorphylls

Allomerization is an oxidative degradation of Chl (Willstätter and Stoll, 1911), the exact reaction mechanism of which remained unclear for a long time (Hynninen, 1991). More evidence has been gathered in the last decade using HPLC coupled to MS and diode array detection (Kuronen et al., 1993; Rahmani et al., 1993; Brereton et al., 1994; Woolley et al., 1998; Gauthier-Jaques et al., 2001). The results of Rahmani et al. (1993) suggest that several competing degradation pathways are involved in allomerization. The results of Kuronen et al. (1993) indicate a free radical mechanism. In contrast to Hynninen, however, the study of Woolley et al. (1998) suggests that the hydroxyl and methoxyl radicals may not be the active species in the allomerization reaction.

Recent experiments combining HPLC with Raman spectroscopy, UV/VIS spectroscopy and MS (Woolley et al. 1998) provided comprehensive evidence for a complete reaction mechanism that accounts for all major allomerization products. These results disprove the mechanism of Brereton et al. (1994) and largely confirm that of Hynninen (1991). In contrast to Hynninen, however, the study of Woolley et al. (1998) suggests that the hydroxyl and methoxyl radicals may not be the active species in the allomerization reaction. In summary, Woolley et al. (1998) have shown that:

1) water is the source of the 13^2-hydroxyl group in allomerization.

2) in undried methanol, 15^1-methoxylactone derivative of Chl *a* and [13^2-OH]-Chl *a* are the first and second most-abundant allomerization products and the 15^1-hydroxylactone of Chl *a* and a ring E-opened 7-dimethyl-phytyl ester of 3-vinyl-Mg-

rhodochlorin-15-glyoxylic acid (formerly know in Fischer nomenclature as Mg-purpurin 7) are minor products: in dried methanol no hydroxy derivatives were formed.

3) the major allomerization product of BChl *a* is [13^2-OH]-BChl while the methoxy-lactone-BChl and hydroxy-lactone-BChl occur, but only in minor amounts.

4) allomerization of [3-acetyl]-Chl *a* (bacterioviridin) showed that the reduction state of the C7-C8 bond decides between the different allomerization product patterns of Chl *a* and BChl *a* (see above).

Hyvärinen and Hynninen (1999) showed that allomerization of Chl *b* varies from that of Chl *a* not only by the relative abundance of the three main products (hydroxy-, methoxy- and hydroxylactone-Chls) but, additionally, by the formation of 13^2(S)-hydroxy-10-methoxychlorophyll *b*, which was identified by MS and UV/VIS spectra.

B. Light-dependent Chlorophyll Degradation

Light-dependent Chl degradation, which has been studied for a similarly long time (see Hynninen, 1991), differs from the light-independent allomerization mechanism. Using HPLC in combination with UV/VIS spectroscopy, FTIR spectroscopy and gas chromatography coupled to MS, Llewellyn et al. (1990a, b) revealed that the most abundant end-stage photodegradation product was glycerol, accompanied by lactic, citric, succinic and malonic acids as well as alanine. A comparison of the photodegradation rates of the chlorin ring and the phytyl side chain (Cuny et al., 1999) showed that the latter is more strongly affected by temperature than the former.

C. Chlorophyll Degradation During Storage and Extraction of Dead Plant Material

During storage of dead plant material and its extraction by organic solvents, various types of Chl degradation may occur in addition to the processes described above. Most commonly, the phytyl chain of Chl is lost (mainly due to the action of chlorophyllase) forming chlorophyllides (Chlides), or the central Mg^{2+} ion is lost to form Phes and pheophorbides (Pheides): for more detailed reviews see Scheer (1991). Recent works in this field investigated the influence of different methods of freezing, storage and extraction on Chl degradation. Redden et al. (1993) found that most storage-related degradation occurs during the first week, and that storage at –20 °C causes more degradation than storage in liquid nitrogen or on dry ice. Downes et al. (1993) observed that extraction by solvent mixtures including DMSO and alcohols, as well as high extraction temperatures or long extraction periods, caused more Chl degradation than extraction by cold acetone. This is not surprising considering the earlier knowledge on Chl degradation processes (Hynninen, 1991; Svec, 1991).

Also, the exchange of the central Mg^{2+} ion by other metal ions, mainly Zn^{2+} and Cu^{2+}, not only occurs in vivo (see Section II) but was discovered originally in canned vegetables by Fischbach and Newburger (1943). Recent studies (Mínguez-Mosquera et al., 1995; Canjura et al., 1999) investigated the time course and factors influencing metal incorporation. Conversion of Chl and its derivatives to Zn complexes in canned vegetables has been patented as the 'veri green' procedure (Segner et al., 1984; von Elbe et al., 1986).

Further, [Hms]-Chls (especially [Cu]-Chl and derivatives such as [Cu]-chlorophyllin) are prepared in solutions as dyes for cosmetics and food (Burkhard, 1992; King and Carroll, 1994; Frost and Saleeb, 1999). Metal insertion is very efficient in alcohols (Hidenari et al., 1993; Küpper et al., 1996), in which both the metals and Chls are readily soluble. Tonucci and von Elbe (1992) investigated the kinetics of [Zn]-Chl formation and the effect of temperature as well as the effect of steric hindrance from peripheral groups: Zn^{2+} ions were more readily inserted into pyropheophytin than pheophytin. Hidenari et al. (1993) showed that Zn^{2+} incorporation, like pheophytinization, occurs more slowly with Chl *b* than with Chl *a*: they also described a method for quantification of [Zn]-Chls.

Because, as discussed earlier, formation of [Hms]-Chls can occur in living plants and algae under conditions of heavy metal stress, the question arises how to verify that [Hms]-Chl formation occurs in vivo and not as an artifact of the extraction of plant materials. Küpper et al. (1996, 1998) showed that the formation of such artifacts can be efficiently prevented by freeze-drying (lyophilizing) the plant material before extraction and by choosing an appropriate solvent for extraction. [Hms]-Chl formation is very efficient in alcohols (see above);

consequently, when metal-stressed plants are to be analyzed, alcohol should be replaced by either 100% acetone or a hydrophobic solvent such as diethylether or cyclohexane.

Acknowledgments

Hendrik Küpper was supported by a grant from the Deutsche Forschungsgemeinschaft (DFG) to Peter Kroneck (Universität Konstanz), Frithjof C. Küpper was supported by funds from the National Institutes of Health (N.I.H.) to Alison Butler (University of California, Santa Barbara). Martin Spiller gratefully acknowledges a mobility grant from the Deutsch-Französische Hochschule.

References

Andersson LA, Huff A and Smith KM (1990) Tunichlorin—spectroscopy of the naturally-occurring nickel (II)-pyropheophorbide-A complex and its derivatives. Biophys J 57 (2; part 2): 232a

Andersson LA, Blackburn NJ and Smith KM (1991) Structural and spectral properties of tunichlorin, the novel nickel (II) chlorin of tunicates. Abstracts of Papers of American Chemical Society 202 (part 1, INOR section): Abstract # 139

Banerjee PC, Ray MK, Koch C, Bhattacharyya S, Shivaji S and Stackebrandt E (1996) Molecular characterisation of two acidophilic heterotrophic bacteria isolated from a copper mine of India. Syst Appl Microbiol 19: 78–82

Baryla A, Carrier P, Franck F, Coulomb C, Sahut C and Havaux M (2001) Leaf chlorosis in oilseed rape plants (*Brassica napus*) grown on cadmium-polluted soil: Causes and consequences for photosynthesis and growth. Planta 212: 669–709

Bible KC, Buytendorp M, Zierath PD and Rinehart KL (1988) Tunichlorin—a nickel chlorin isolated from the Caribbean tunicate *Trididemnum solidum*. Proc Natl Acad Sci USA 85: 4582–4586

Boucher LJ and Katz JJ (1967) Aggregation of metallochlorophylls. J Am Chem Soc 89: 4703–4708

Brereton RG, Rahmani A, Liang YiZ and Kvalheim OM (1994) Investigation of the allomerization reaction of chlorophyll *a*: Use of diode array HPLC, mass spectrometry and chemometric factor analysis for the detection of early products. Photochem Photobiol 59: 99–110

Buchler JW (1997) Transition Metal and Rare Earth Porphyrin Aggregates. In: Trautwein A (ed) Bioinorganic Chemistry, Transition Metals in Biology and Their Coordination Chemistry (Research Report, Deutsche Forschungsgemeinschaft), pp 570–584. Wiley-VCH, Weinheim

Burkhard R (1992) Compositions containing chlorophyll derivatives for permanent waving of hair. US patent 6,024,949

Canjura FL, Watkins RH and Schwartz SJ (1999) Color improvement and metallo-chlorophyll complexes in continuous flow aseptically processed peas. J Food Sci 64: 987–990

Cuny P, Romano JC, Beker B and Rontani JF (1999) Comparison of photodegradation rates of chlorophyll chlorin ring and phytol side chain in phytodetritus: Is the phytyldiol versus phytol ratio (CPPI) a new biogeochemical index? J Exp Mar Biol Ecol 237: 271–290

De Filippis LF (1979) The effect of heavy metals on the absorption spectra of *Chlorella* cells and chlorophyll solutions. Z Pflanzenphysiologie 93: 129–137

Downes MT, Hrstich L and Vincent WF (1993) Extraction of chlorophyll and carotenoid pigments from Antarctic benthic mats for analysis by HPLC. J Appl Phycol 5: 623–628

Fiedor L, Leupold D, Teuchner K, Voigt B, Hunter CN, Scherz A and Scheer H (2001) Excitation trap approach to analyze size and pigment-pigment-coupling: Reconstitution of LH1 antenna of *Rhodobacter sphaeroides* with Ni-substituted bacteriochlorophyll. Biochemistry 40: 3737–3747

Fischbach H and Newburger SH (1943) Spectrophotometric study of the green color in okra. J Assoc Off Agric Chem 26: 134–139

Frost JR and Saleeb FZ (1999) Non-staining, acid-stable, cold-water-soluble, edible green color and compositions for preparing acidic foods and beverages. US patent 5,993,880

Gauthier-Jaques A, Bortlik K, Hau J and Fay LB (2001) Improved method to track chlorophyll degradation. J Agric Food Chem 49: 1117–1122

Geiken B, Masojidek M, Rizzuto M, Pompili ML and Giardi MT (1998) Incorporation of [S-35] methionine in higher plants reveals that stimulation of the D1 reaction centre II protein turnover accompanies tolerance to heavy metal stress. Plant Cell Envi 21: 1265–1273

Gibbs PE, Burt GR, Pascoe PL, Llewellyn CA and Ryan KP (2000) Zinc, copper and chlorophyll-derivatives in the polychaete *Owenia fusiformis*. J Mar Biol Ass UK 80: 235–248

Gross RE, Pugno P and Dugger WM (1970) Observations on the mechanism of copper damage in *Chlorella*. Plant Physiol 46: 183–185

Hidenari I, Miki I, Takashi N, Kenji F and Yoshikazu S (1993) Preparation and determination of zinc(II) chlorophylls by reversed-phase liquid chromatography. J Chromatog 645: 259–264

Hiraishi A and Shimada K (2001) Aerobic anoxygenic bacteria with zinc-bacteriochlorophyll. J Gen Appl Microbiol 47: 161–180

Hong F-S, Wei Z-G, Tao Y, Wan S-K, Yang Y-T, Cao X-D and Zhao G-W (1999) Distribution of rare earth elements and structure characterization of chlorophyll-lanthanum in a natural plant fern *Dicranopteris dichotoma*. Acta Botanica Sinica 41: 851–854 (in Chinese, abstract in English)

Hynninen PH (1991) Chemistry of Chlorophylls: Modifications. In: Scheer H (ed),Chlorophylls, pp 145–210. CRC Press, Boca Raton

Hyvärinen K and Hynninen PH (1999) Liquid chromatographic separation and mass spectrometric identification of chlorophyll *b* allomers. J Chromatography A 837: 107–116

Itoh S, Iwaki M, Wakao N, Yoshizu K, Aoki A and Tazaki K (1998) Accumulation of Fe, Cr, Ni metals inside cells of acidophilic bacterium *Acidiphilium rubrum* that produces Zn-containing bacteriochlorophyll *a*. Plant Cell Physiol 39: 740–744

Jones ID, White RC, Gibbs E and Butler LS (1977) Estimation of zinc pheophytins, chlorophylls, and pheophytins in mixtures in

diethyl ether or 80% acetone by spectrophotometry and fluorometry. J Agric Food Chem 73: 146–149
Karukstis KK (1991) Chlorophyll fluorescence as a physiological probe of the photosynthetic apparatus. In: Scheer H (ed) Chlorophylls, pp 770–97. CRC Press, Boca Raton
Katoh T and Ehara T (1990) Supramolecular assembly of fucoxanthin-chlorophyll-protein complexes isolated from a brown alga, *Petalonia fascia*. Electron microscopic studies. Plant Cell Physiol 31: 439–47
King RM and Carroll TF (1994) Aloe vera gel toothpaste. US patent 5,294,434
Kishimoto N and Tano T (1987) Acidophilic heterotrophic bacteria isolated from acidic mine drainage, sewage, and soils. J Gen Appl Microbiol 33: 11–25
Kowalewska G and Hoffmann SK (1989) Identification of the copper porphyrin complex formed in cultures of the blue-green alga *Anabaena variabilis*. Acta Physiol Plant 11: 39–50
Kowalewska G, Lotocka M and Latala A (1992) Formation of the copper-chlorophyll complexes in cells of phytoplankton from the Baltic Sea. Polskie Archiwum Hydrobiologii 39: 41–49
Küpper H, Küpper F and Spiller M (1996) Environmental relevance of heavy metal substituted chlorophylls using the example of water plants. J Exp Bot 47: 259–266
Küpper H, Küpper F and Spiller M (1998) In situ detection of heavy metal substituted chlorophylls in water plants. Photosynth Res 58: 123–133
Küpper H, Spiller M and Küpper F (2000a) Photometric method for the quantification of chlorophylls and their derivatives in complex mixtures: Fitting with gauss-peak-spectra. Anal Biochem 286: 247–256
Küpper H, Lombi E, Zhao FJ and McGrath SP (2000b) Cellular compartmentation of cadmium and zinc in relation to other elements in the hyperaccumulator *Arabidopsis halleri*. Planta 212: 75–84
Küpper H, Lombi E, Zhao FJ, Wieshammer G and McGrath SP (2001) Cellular compartmentation of nickel in the hyperaccumulators *Alyssum lesbiacum, Alyssum bertolonii* and *Thlaspi goesingense*. J Exp Bot 52(365): 2991–2300
Küpper H, Dedic R, Svoboda A, Hála J and Kroneck PMH (2002a) Kinetics and efficiency of excitation energy transfer from chlorophylls, their heavy metal substituted derivatives, and pheophytins to singlet oxygen. Biochim Biophys Acta 1572: 107–113
Küpper H, Setlík I, Spiller M, Küpper FC and Prásil O (2002b) Heavy metal-induced inhibition of photosynthesis: Targets of in vivo heavy metal chlorophyll formation. J Phycol 48: 429–441
Kuronen P, Hyvärinen K and Hynninen PH (1993) High-performance liquid chromatographic separation and isolation of the methanolic allomerization products of chlorophyll *a*. J Chromatography A 654: 93–104
Llewellyn CA, Mantoura RFC and Brereton RG (1990a) Products of chlorophyll photodegradation—1. Detection and separation. Photochem Photobiol 52: 1037–1041
Llewellyn CA, Mantoura RFC and Brereton RG (1990b) Products of chlorophyll photodegradation—2. Structural identification. Photochem Photobiol 52: 1043–1047
Ma LF and Dolphin D (1999) The metabolites of dietary chlorophylls. Phytochemistry 50: 195–202
Mahapatra NR and Banerjee PC (1996) Extreme tolerance to cadmium and high resistance to copper, nickel and zinc in different Acidiphilium strains. Lett Appl Microbiol 23: 393–397
Masuda T, Nagayama M, Inoue K, Ohta H, Shimada H and Takamiya K-I (1999) Magnesium insertion by magnesium chelatase in the biosynthesis of zinc bacteriochlorophyll *a* in an aerobic acidophilic bacterium *Acidiphilium rubrum*. J Biol Chem 274: 33594–33600
Matin A (1999) pH homeostasis in acidophiles. Novartis Found Symp 221: 152–163
Mimuro M, Katoh T and Kawai H (1990) Spatial arrangement of pigments and their interaction in the fucoxanthin-chlorophyll *a/c* protein assembly (FCPA) isolated from the brown alga *Dictyota dichotoma*. Analysis by means of polarized spectroscopy. Biochim Biophys Acta 1015: 450–456
Mínguez-Mosquera MI, Gallardo-Guerrero L, Hornero-Méndez D and Garrido-Fernández J (1995) Involvement of copper and zinc ions in green staining of table olives of the variety *Gordal*. J Food Protect 58: 564–569
Patra M and Sharma A (2000) Mercury toxicity in plants. Bot Review 66: 379–422
Paulsen H, Finkenzeller B and Kühlein N (1993) Pigments induce folding of light-harvesting chlorophyll *a/b*-binding protein. Eur J Biochem 215: 809–816
Pettit GR, Kantoci D, Doubek DL, Tucker BE, Pettit WE and Schroll RM (1993) Isolation of the nickel-chlorin chelate tunichlorin from the south-Pacific Ocean sea hare *Dolabella auricularia*. J Nat Pod 56: 1981–1984
Pfaltz A, Jaun B, Fassler A, Eschenmoser A, Jaenchen R, Gilles HH, Diekert G and Thauer RK (1982) Factor F430 from methanogenic bacteria—structure of the porphinoid ligand system. Helvetica Chimica Acta 65: 828–865
Prasad MNV and Hagemeyer J (eds) (1999) Heavy Metal Stress in Plants: From Molecules to Ecosystems. Springer: Berlin
Prasad MNV and Strzalka K (1999) Impact of heavy metals on photosynthesis. In: Prasad MNV and Hagemeyer J (eds) Heavy Metal Stress in Plants: From Molecules to Ecosystems, pp 117–128. Springer, Berlin
Prasad MNV, Malec P, Waloszek A, Bojko M and Strzalka K (2001) Physiological responses of *Lemna trisulca* L. (duckweed) to cadmium and copper bioaccumulation. Plant Sci 161: 881–889
Psaras GK and Manetas Y (2001) Nickel localization of the metal hyperaccumulator *Thlaspi pindicum* Hausskn. Ann Bot 88: 513–516
Psaras GK, Constantinidis TH, Cotsopoulos B and Manetas Y (2000) Relative abundance of nickel in the leaf epidermis of eight hyperaccumulators: Evidence that the metal is excluded from both guard cells and trichomes. Ann Bot 86: 73–78
Puckett KJ (1976) The effects of heavy metals on some aspects of lichen physiology. Can J Bot 54: 2695–2703
Rahmani A, Eckardt CB, Brereton R and Maxwell JR (1993) The use of liquid chromatography-mass spectroscopy to monitor the allomerisation reactions of chlorophyll *a* and pheophytin *a*: Identification of the allomers of pheophytin *a*. Photochem Photobiol 57: 1048–1052
Rebeiz CA and Belanger FC (1984) Chloroplast biogenesis 46. Calculation of net spectral shifts induced by axial ligand coordination in metalated tetrapyrroles. Spectrochim Acta 40A: 793–806
Redden AM, Thompson RJ and Deibel D (1993) Effects of short- and long-term freezing of chloropigments in cultured diatoms and bivalve digestive gland and faeces as determined by standard

fluorometry and HPLC. Arch Hydrobiol 129: 67–87
Rinehart KL, Kishore V, Bible KC, Sakai R, Sullins DW and Li K-M (1988) Didemnins and tunichlorin—novel natural products from the marine tunicate *Tridemnum solidum*. J Nat Prod 51: 1–21
Scheer H (ed) (1991) Chlorophylls, CRC Press, Boca Raton
Segner WP, Ragusa TJ, Nank WK and Hoyle WC (1984) Process for the preservation of green color in canned vegetables. US patent 4,473,591
Sings HL, Bible KC and Rinehart KL (1996) Acyl tunichlorins: A new class of nickel chlorins isolated from the Caribbean tunicate *Tridemnum solidum*. Proc Nat Acad Sci USA 93(20): 10560–10565
Svec WA (1991) The distribution and extraction of the chlorophylls. In: Scheer H (ed) Chlorophylls, pp 89–102. CRC Press, Boca Raton
Tonucci LH and von Elbe JH (1992) Kinetics of the formation of zinc complexes of chlorophyll derivatives. J Agric Food Chem 40: 2341–2344
Von Elbe JH, Huang AS, Attoe EL and Nank WK (1986) Pigment composition of conventional and veri-green canned beans. J Agric Food Chem 34: 52–54
Wakao N, Yokoi N, Isoyama N, Hiraishi A, Shimada K, Kobayashi M, Kise H, Iwaki M, Itoh S, Takaichi S and Sakurai Y (1996) Discovery of natural photosynthesis using Zn-containing bacteriochlorophyll in an aerobic bacterium *Acidiphilium rubrum*. Plant Cell Physiol 37: 889–893
Wang Q, Lai Y, Yang L and Huang B (2001) Preliminary study of existing species of lanthanum in the spinach leaves after being cultivated with a culture solution containing lanthanum. Anal Sci 17: 789–791
Watanabe T and Kobayashi M (1988) Chlorophylls as functional molecules in photosynthesis. Molecular composition in vivo and physical chemistry in vitro. J Chem Soc Japan (Nipon Kagaku Kaishi) 1988 (issue #4): 383–395 [Note: English title of this issue was Special Articles on Coordination Chemistry of Biologically Important Substances]
Watanabe T, Machida K, Suzuki H, Kobayashi M and Honda K (1985) Photoelectrochemistry of metallochlorophylls. Coordination Chem Rev 64: 207–224
Wei Z-G, Hong F-S and Zhao G-W (2000a) Synthesis and characterization of RE-Chlorophyll-*a* complexes (RE = La, Ce, Eu, Y). J Rare Earths 18: 249–253
Wei Z-G, Hong F-S, Zhao G-W, Tao Y, Hu T-D, Liu T, Xie Y-N, Yin M, Li B and Yang J-H (2000b) Determination of double decker sandwich structured La-substituted chlorophyll a by EXAFS. Acta Chimica Sinica 58: 559–562
White RC, Jones ID, Gibbs E and Butler LS (1977) Estimation of copper pheophytins, chlorophylls, and pheophytins in mixtures in diethyl ether. J Agric Food Chem 25: 143–146
Willstätter R and Stoll A (1911) Untersuchungen über Chlorophyll. XIX. Über die Chlorophyllide. Justus Liebigs Ann Chem 387: 317–386
Woolley PS, Moir AJ, Hester RE and Keely BJ (1998) A comparative study of the allomerization reaction of chlorophyll *a* and bacteriochlorophyll *a*. J Chem Soc, Perkin Trans 2: 1833–1839
Zychlinsky E and Matin A (1983) Cytoplasmic pH homeostasis in an acidophilic bacterium, *Thiobacillus acidophilus*. J Bacteriol 156: 1352–1355

Chapter 6

Spectroscopy and Structure Determination

Masami Kobayashi[1]*, Machiko Akiyama[1], Hiromi Kano[2] and Hideo Kise[1]
[1] *Institute of Materials Science, University of Tsukuba, Tsukuba, Ibaraki 305-8573, Japan;*
[2] *National Institute of Agrobiological Resources, Tsukuba, Ibaraki 305- 8602, Japan*

Summary

Analysis by a combination of absorption-, fluorescence-, circular dichroism-, mass- and nuclear magnetic resonance-spectrometry is often used to investigate the structure of chlorophylls. Here, we show several examples of spectroscopic determination of molecular structure of the recently-discovered chlorophylls and compare them with the well-known chlorophylls, chlorophyll *a* and bacteriochlorophyll *a*.

*Author for correspondence, email: masami@ims.tsukuba.ac.jp

Bernhard Grimm, Robert J. Porra, Wolfhart Rüdiger and Hugo Scheer (eds): Chlorophylls and Bacteriochlorophylls: Biochemistry, Biophysics, Functions and Applications, pp. 79–94.

I. Introduction

A wide variety of analytical methods are used to determine chlorophyll (Chl) structures. Since the review by Treibs (1932), older methods have been improved and new techniques developed. In presenting this review, we are indebted to previous researchers and reviewers. The Chls, known in the 1930s, have been more adequately characterized and new Chls have been discovered; for example, bacteriochlorophyll (BChl) *g*, Chl *d* and [Zn]-BChl *a* (Chapter 4, Kobayashi et al.).

The various naturally-occurring Chls to be treated here are Chls *a*, *a´*, *b*, *d* and *d´* as well as pheophytin (Phe) *a* which is found in oxygenic photosynthesis. Also discussed are BChls *a* and *b,* and bacteriopheophytins (BPhes) *a* and *b* found in purple bacteria, BChls *g*, *g´* and 8^1-OH-Chl *a* occurring in heliobacteria, BChl *a´* and BChl 663 in green sulfur bacteria, and the recently-discovered novel [Zn]-BChl *a* occurring in *Acidiphilium* (*Acp.*) *rubrum*. Some, notably Chl *a* and BChl *a*, have been thoroughly characterized both physically and chemically, but others, such as Chl *a´* and BChl *a´*, have been characterized by little more than name and absorption spectrum. In this chapter, we briefly present some examples of spectroscopic determination of the molecular structures of the more recently-discovered Chls and compare them with well-known Chls.

II. Absorption Spectra

A. Porphyrins, Chlorins and Bacteriochlorins

The absorption spectrum is the simplest, most useful and extensively used analytical property to characterize a Chl and requires only 10 μg or less. Absorption spectroscopy can be used to distinguish the three macrocycle types of Chls as defined by Scheer (Chapter 1), namely, porphyrin (i.e., phytoporphyrin), chlorin (dihydrophytoporphyrin) and bacteriochlorin (tetrahydrophytoporphyrin). To illustrate, we present the absorption spectra of Chl c_1 (a Mg-porphyrin), Chl *a* (a Mg-chlorin) and BChl *a* (a Mg-bacteriochlorin) in Fig. 1. The absorption maxima and the corresponding molar absorption coefficients (ε) are listed in Table 1 (for detailed quantitative data, see Chapter 7, Porra).

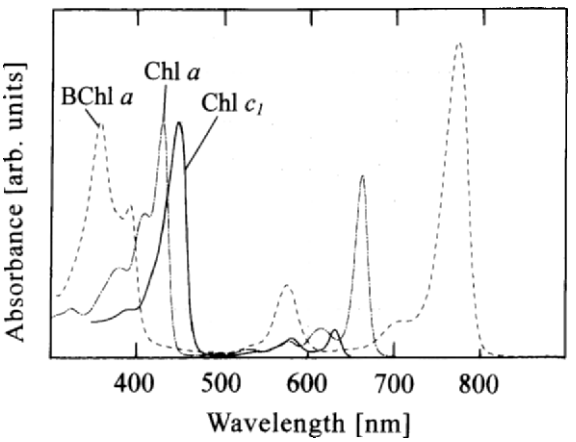

Fig. 1. Absorption spectra of chlorophylls c_1 and *a,* and bacteriochlorophyll *a* in diethyl ether. Soret-band maxima are arbitrarily scaled to a common height. The spectrum of Chl c_1 is reproduced from Jeffrey et al. (1997).

Absorption spectra of Chls show the electronic transitions along the x axis of the Chl running through the two nitrogen (N) atoms of rings B and D, and along the y-axis through the N atoms of rings A and C (Chapter 1, Scheer). The two pairs of absorption bands in the blue and red spectral regions in Chls are called B (or Soret) and Q bands, respectively, and arise from $\pi \rightarrow \pi^*$ transitions of the four frontier orbitals (Weiss, 1978). One band of each pair is polarized along the x-axis (B_x, Q_x), the other along the y-axis (B_X, Q_Y) Chapter 1, Scheer). The polarizations of the transitions along the axes are called x and y (Chapter 1, Scheer). In Chl *a*, for example, the spectrum is characterized by two strong overlapping Soret (B) bands at about 430 nm and a relatively strong Q_Y band near 660 nm with a weak Q_X band near 550 nm (Fig. 1).

The π-electron system of Chl *c* is fully conjugated but, in Chl *a,* ring D is reduced. The difference significantly effects their absorption spectra; for example, the intensities and maximum wavelengths of their Soret bands are similar, but Chl *c* has very much weaker Q bands than Chl *a*. The Soret band is doubly degenerated in Chl *a*, which is clearly seen in the circular dichroism (CD) spectrum; the Soret transition appears as positive and negative CD peaks (Fig. 9B).

Because ring B in BChl *a* is also reduced by two

Abbreviations: Acp. – Acidiphilium; Acc. – Acaryochloris; BChl – bacteriochlorophyll; BPhe – bacteriopheophytin; CD – circular dichroism; Chl – chlorophyll; HPLC – high performance liquid chromatography; MS – mass spectroscopy; NMR – nuclear magnetic resonance; P – phytol; Phe – pheophytin; Δ2,6P – Δ2,6-phytadienol; RC – reaction center

Table 1. Absorption properties of chlorophylls in diethylether at room temperature

Compound	λ max(blue) [nm] (ε [10^3 $M^{-1}cm^{-1}$])	λ max(red) [nm] (ε [10^3 $M^{-1}cm^{-1}$])	Ref.
Chl *a*	428.4	660.3	Watanabe et al. (1984)
	(115)	(89.8)	ibid.
	429.0	660.9	This work
	(1.00)[a]	(0.775)[a]	ibid.
Phe *a*	408.4	667.9	Watanabe et al. (1984)
	(107)	(52.6)	ibid.
	408.4	667.3	This work
	(1.00)[a]	(0.497)[a]	ibid.
Chl *b*	451.9	641.9	Watanabe et al. (1984)
	(159)	(56.7)	ibid.
	452.4	642.5	This work
	(1.00)[a]	(0.355)[a]	ibid.
Phe *b*	432.7	654.6	Watanabe et al. (1984)
	(172)	(34.8)	ibid.
	433.2	654.5	This work
	(1.00)[a]	(0.202)[a]	ibid.
Chl c_1	444.5	628.2	Jeffrey (1969)
	(1.00)[a]	(0.0984)[a]	ibid.
	446.1[b]	629.1[b]	Jeffrey (1972)
	(213)[b]	(23.9)[b]	ibid.
	438	625	Wilhelm (1987)
Chl c_2	448.2	628.2	Jeffrey (1969)
	(1.00)[a]	(0.0668)[a]	ibid.
	444.6[b]	629.6[b]	Jeffrey (1972)
	(195)[b]	(22.7)[b]	ibid.
	445	628	Wilhelm (1987)
Chl *d*	447	688	Smith and Benitez (1955)
	(87.6)	(98.9)	ibid.
	447	688	French (1960)
	(87.6)	(98.5)	ibid.
	445.6	686.2	This work
	(0.853)[a]	(1.00)[a]	ibid .
Phe *d*	421	692	Smith and Benitez (1955)
	(84.9)	(72.2)	ibid.
	421	692	French (1960)
	(84.9)	(72.2)	ibid.
	382.7 421.3	692.0	This work
	(0.881)[a] (1.00)[a]	(0.911)[a]	ibid.
BChl *a*	356	771	Oelze (1985)
	(76)	(96)	ibid.
	357	771	Hartwich et al. (1998)
	(73.3)	(91.0)	ibid.
	357.2	771.1	Permentier et al. (2000)
	(72.9)	(97.0)	ibid.

Continued on next page.

hydrogens, the conjugated system is longer along the y-axis than along the x-axis (Weiss, 1978; see Fig. 5A in Chapter 1, Ke, 2001), but symmetrical along both axes, resulting in the intense and red-shifted (i.e., to longer wavelengths) Q_Y band near 780 nm and blue-shifted (i.e., to shorter wavelengths) Soret bands (Fig. 1). In addition, BChl *a* shows a pronounced and relatively strong Q_X band near 580 nm, and the Soret bands are well separated into B_Y (ca. 360 nm) and B_X (ca. 390 nm) bands, as compared with Chl *a* and

BPhe *a*	354	748	Oelze (1985)
	(106)	(67.6)	ibid.
	356	750	Hartwich et al. (1998)
	(113)	(67.5)	ibid.
	356.5	748.5	Kobayashi et al. (1998a)
	(1.00)[a]	(0.63)[a]	ibid .
	357.0	749.4	This work
	(1.00)[a]	(0.629)[a]	ibid.
BChl *b*	372	791	Oelze (1985)
	(77.3)	(106)	ibid.
	368[c]	795[c]	Jensen et al. (1964)
	(1.00)[a]	(0.96)[a]	ibid.
	371.1	795.5	This work
	(0.702)[a]	(1.00)[a]	ibid .
BPhe *b*	336	776	Oelze (1985)
	(1.00)[a]	(0.678)[a]	ibid.
	368[c]	775[c]	Jensen et al. (1964)
	(1.00)[a]	(0.48)[a]	ibid.
	367.9	778.5	This work
	(1.00)[a]	(0.696)[a]	ibid.
BChl *c*[d]	432	660	Stanier and Smith (1960)
	(139)[e]	(89)[e]	ibid.
BChl *d*[d]	425	650	Stanier and Smith (1960)
	(114)[f]	(88)[f]	ibid.
BChl *e*[d]	456-459[c]	646-648[c]	Gloe et al. (1975)
	(1.00)[a]	(0.24-0.32)[a]	ibid.
BChl *g*	364.0	767.2	Kobayashi et al. (1991)
	(90)	(96)	ibid.
	364.4	767.4	This work
	(0.938)[a]	(1.00)[a]	ibid.
Zn-BChl *a*	353	762	Hartwich et al. (1998)
	(58.9)	(67.7)	ibid.
	353.0	762.5	Kobayashi et al. (1998a)
	(0.801)[a]	(1.00)[a]	ibid.
	353.5	763.2	This work
	(0.788)[a]	(1.00)[a]	Ibid.

a: relative values.
b: in 100 % acetone + 1 % pyridine.
c: in acetone
d: mixture of several homologues.

Chl c_1. Therefore, the fundamental macrocycles of the Chls are readily distinguishable as porphyrins, chlorins and bacteriochlorins by their absorption spectra in organic solvents. We should, however, emphasize that it is often difficult to detect impurities by absorption spectra because they can have very similar spectra to the main Chls. (Kobayashi et al., 1988; Kobayashi, 1989).

B. Chlorophylls a, b and d, and Bacteriochlorophylls a, b and g

Chls *a*, *b* and *d* possess the same chlorin macrocycle and long chain alcohol at C17[3], phytol, but differ in the substituents on rings A and B (Chapter 1, Scheer). In Fig. 2A, the absorption spectra of Chls *a*, *b* and *d* are shown. Compared with Chl *a*, the Soret bands of Chl *b* are red-shifted and its Q_Y band is blue-shifted due to the replacement of an electron-releasing methyl group (-CH_3) at C7 of Chl *a* by an electron-withdraw-

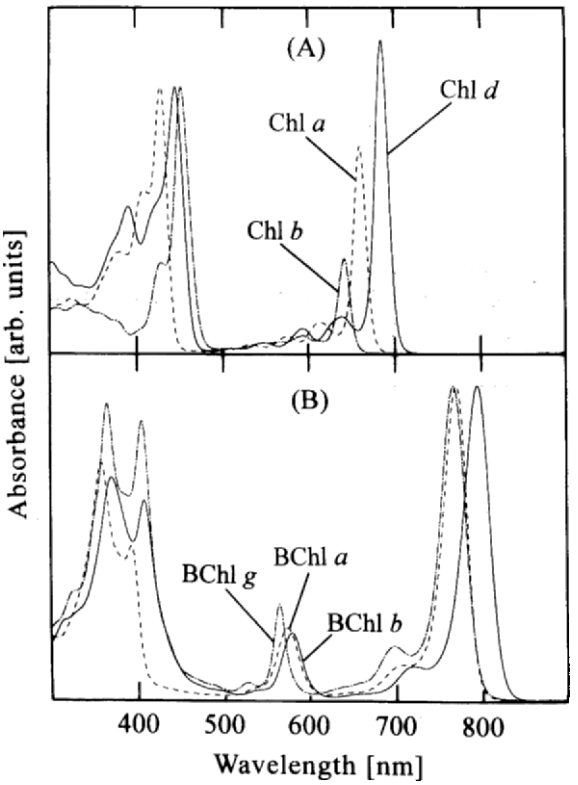

Fig. 2. Absorption spectra of (A) chlorophylls *a*, *b* and *d* and (B) bacteriochlorophylls *a*, *b* and *g* in diethyl ether. Soret-band maxima in (A) and Q_Y-band maxima in (B) are arbitrarily scaled to a common height, respectively.

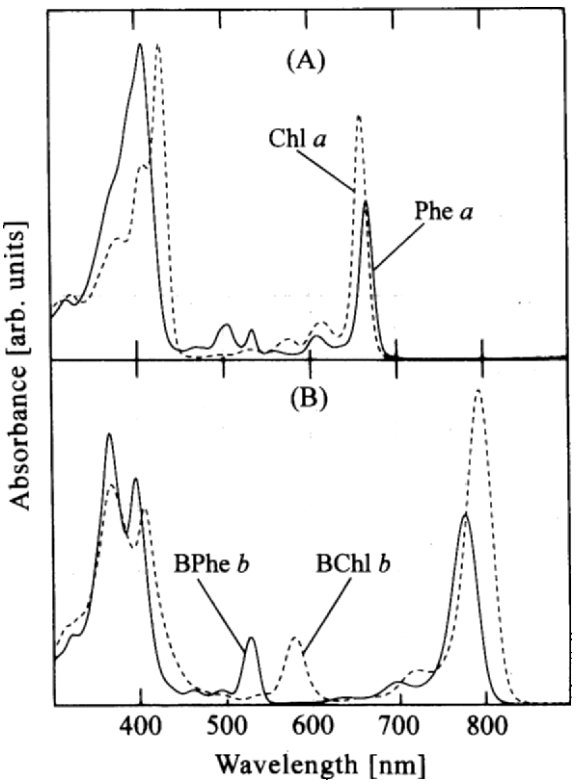

Fig. 3. Absorption spectra of (A) chlorophyll *a* and pheophytin *a*, and (B) bacteriochlorophyll *b* and bacteriopheophytin *b* in diethyl ether. Soret-band maxima in (A) and Q_X-band maxima in (B) are arbitrarily scaled to a common height, respectively.

ing formyl group (–CHO) in Chl *b*. By contrast, both the Soret and Q_Y bands of Chl *d* are red-shifted due to the replacement of the vinyl group ($-CH=CH_2$) at C3 of Chl *a* by a -CHO in Chl *d*. The ratios of Soret/Q_Y band intensities show remarkable differences: ca. 1.3 in Chl *a*, ca. 2.8 in Chl *b*, and ca. 0.85 in Chl *d*. Chl *d* shows a relatively well split Soret band, possibly due to the presence of a –CHO group on ring A in the chlorin macrocycle. The Q_Y transition is most altered by solvent, for example, the Q_Y maxima of Chl *a* is observed between 660 and 675 nm in forty different solvents (Lawlor, 1993).

Absorption spectra of BChls *a*, *b* and *g,* which possess a bacteriochlorin macrocyle, are shown in Fig. 2B: note that bacteriochlorin Q_Y bands are much red shifted relative to the chlorins (see Section II.A). BChls *a* and *g* show very similar absorption spectra and have shorter wavelength for Q_Y maxima than BChl *b* and, hence, BChl *b* is easily distinguished from BChls *a* and *g*. BChl *g* is distinguished from BChl *a* by its better split Soret bands and by its higher Soret/Q_Y band ratio (ca. 0.94 in BChl *g* and ca. 0.75 in BChl *a*).

C. Pheophytin a and Bacteriopheophytins a and b

Figure 3A shows a better split and stronger Q_X band for Phe *a* than for Chl *a*; further, the Soret/Q_Y band ratio in Phe *a* is remarkably higher than in Chl *a*. Removal of the central Mg reduces the symmetry, thus increasing Soret and Q_X. The more structured shape and red shifted Soret band of Chl *a* clearly distinguishes it from Phe *a*. Similar properties are observed in the Chl *b* and Phe *b* pair, and the Chl *d* and Phe *d* pair (Table 1); note that Phes *b* and (probably) *d* are not involved in natural photosynthesis.

As seen in Fig. 5B, BPhe *a* can be easily distinguished from BChl *a* by the shape of its Soret bands, by its higher Soret/Q_Y band ratio (ca.1.6 in BPhe *a*

and ca. 0.75 in BChl *a*) and by its blue shifted Q_X maxima (ca. 520 nm in BPhe *a* and 570 nm in BChl *a*). The Q_X difference is due to ligation and the inductive effect of the central metal (Section II.E).

It is more difficult, however, to distinguish BPhe *b* from BChl *b* by the shape of their absorption spectra (Fig. 3B), but BPhe *b* is distinguished by its higher Soret/Q_Y band ratio (ca. 1.4 in BPhe *b* and 0.7 in BChl *b*) and by its blue shifted Q_X wavelength (ca. 530 nm in BPhe *b* and 580 nm in BChl *b*).

D. Chlorophylls a´ and d´, and Bacteriochlorophylls a´ and g´

In nature, Chl *a* exists as two epimers, Chl *a* and *a´*, involving stereochemistry at the C13^2 position (Chapter 1, Scheer), and a Chl *a*/*a´* heterodimer constitutes P700 (Chapter 4, Kobayashi et al.): these two epimers can be distinguished by their different chromatographic behavior but not by their absorption spectra (see Fig. 9A). Chl *d* exists in *Acaryochloris* (*Acc*.) *marina* as two epimers, Chl *d* and *d´*, which also possess practically identical spectra (Akiyama et al., 2001). Chl *b´*, which is not found in nature, has an identical spectrum to that of Chl *b* (Watanabe et al., 1984). Their metal-free pairs, Phe *a*/*a´*, *b*/*b´* and *d*/*d´*, are also nearly indistinguishable by absorption spectra.

In contrast, the absorption spectra of BChl *g* and *g´* (Chapter 4, Kobayashi et al.) in an HPLC eluent (*n*-hexane:2-propanol:methanol = 100/2/0.3, v/v/v) (Fig. 4C) show marked differences in the Q_X band region and slight differences in the Soret bands (Kobayashi, 1996). Similar differences are seen in benzene (Fig. 10A), but not in diethyl ether or acetone. The BChl *a*/*a´* pair is also distinguishable by absorption spectra in the Q_X region in the same eluent (Fig. 4A) and in benzene (Takahashi et al., 2005). Similar optical differences are seen in the BChl *b*/*b´* pair (Fig. 4B), but BChl *b´* is not involved in natural photosynthesis. There is also an effect of the Q_Y band, but this is much smaller and barely discernible in Fig. 4. Interestingly, the corresponding pheophytins, BPhe *a*/*a´*, *b*/*b´* and *g*/*g´*, are not distinguishable by absorption spectra (data not shown, Takahashi et al., unpublished).

The Q_X-band of BChl *a* (Evans and Katz 1975) and metal-substituted BChl *a* (Hartwich et al 1998, Noy et al., 2000; Chapter 38, Yerushalmi and Scherz) is very sensitive to the coordination state of the central metal, shifting to the red with an increasing number of ligands. Therefore, the differences seen between

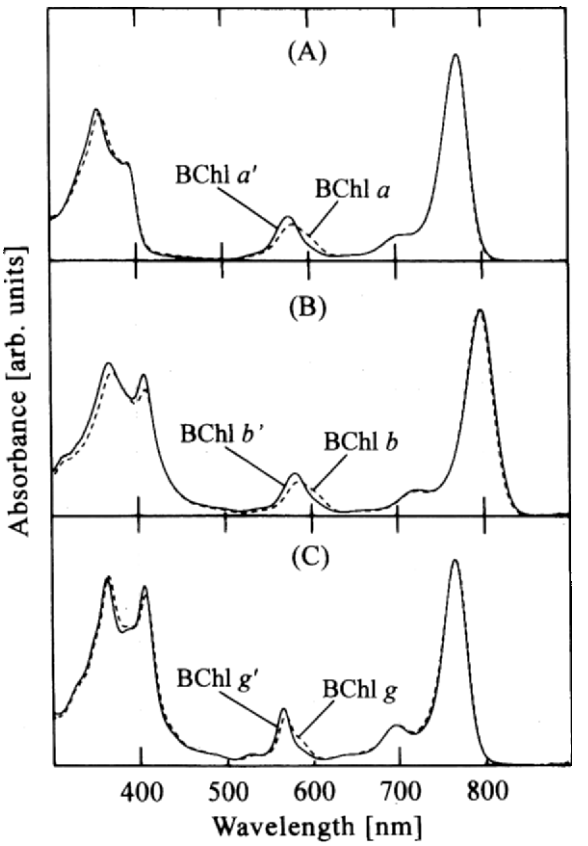

Fig. 4. Absorption spectra of (A) bacteriochlorophylls *a*/*a´*, (B) bacteriochlorophylls *b*/*b´* (C) bacteriochlorophylls *g*/*g´* in *n*-hexane/2-propanol/methanol (100/2/0.3, v/v/v). Q_Y-band maxima are arbitrarily scaled to a common height.

the C13^2-stereoisomers in Fig. 4 are very likely related to a higher proportion of 6-coordinated Mg (two extra ligands) in the 'normal' BChls, while the 'prime' BChls are almost exclusively 5-coordinated. Such considerations explain why the difference appears only in certain solvents (there are few suitable ligands in hexane or benzene, thus emphasizing the differences in ligation strength), and disappears in the pheophytins. The extra ligand for 'normal' BChls is methanol in our HPLC eluent and probably water in benzene.

E. [Zn]-Bacteriochlorophyll a

The shape of the absorption spectrum of [Zn]-BChl *a* is remarkably similar to that of BChl *a* (Fig. 5B); thus, [Zn]-BChl *a* in *Acp*. *rubrum* was first mistaken for 'normal' [Mg]-BChl *a* (Wakao et al., 1993, Kishimoto et al., 1995). When closely compared (see Fig. 5B),

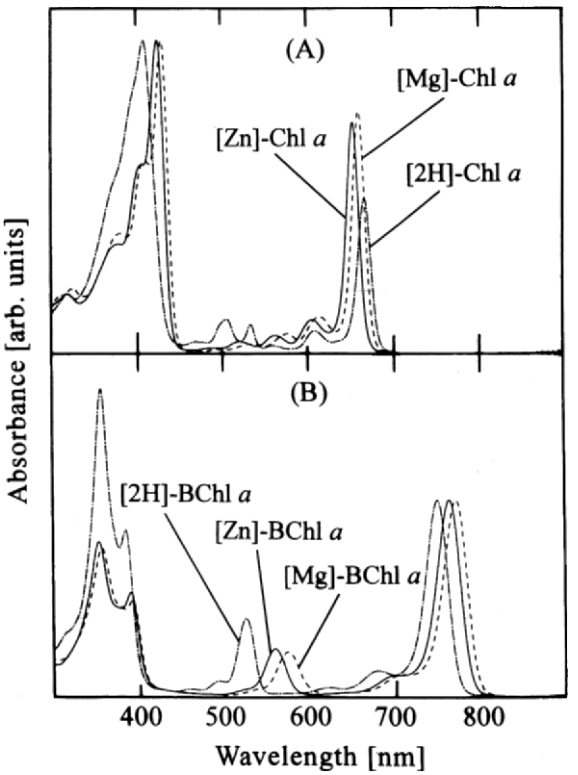

Fig. 5. Absorption spectra of (A) chlorophyll *a* (i.e., [Mg]-Chl *a*), peophytin *a* (i.e., [2H]-Chl *a*), [Zn]-chlorophyll *a* and (B) bacteriochlorophyll *a* (i.e., [Mg]-BChl *a*), bacteriopheophytin *a* (i.e., [2H]-BChl *a*) and [Zn]-bacteriochlorophyll *a* in diethyl ether. Soret-band maxima in (A) and Q_Y-band maxima in (B) are arbitrarily scaled to a common height, respectively.

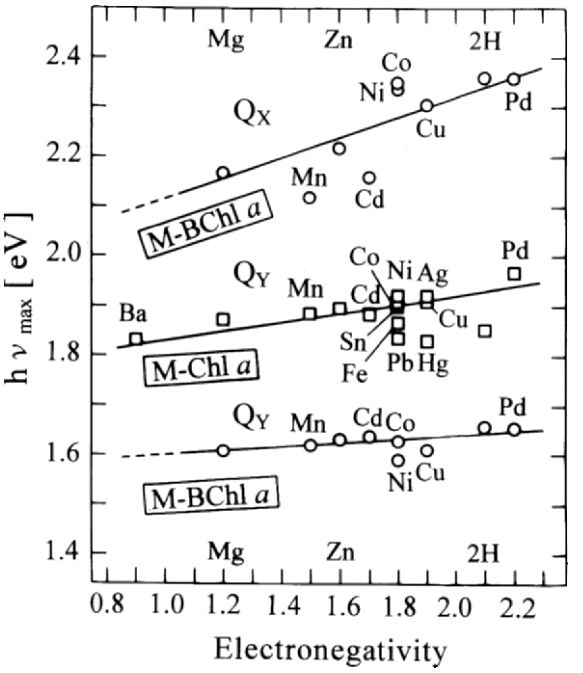

Fig. 6. Correlation of the Q_X and Q_Y transition energy maxima, $h\nu_{max}$, of a series of [M]-bacteriochlorophylls *a* in diethyl ether and the Q_Y transition maxima of [M]-chlorophylls *a* in acetone with the Pauling electronegativity (E_N) of the central metal. M is divalent except for Mn(III), Sn(IV) and Fe(III). Mg, Zn and 2H derivatives are naturally-found pigments and are indicated on the X-axis. Figure adapted from Kobayashi et al. (1999a).

the absorption maxima of [Zn]-BChl *a* are slightly blue-shifted compared to those of BChl *a* in the four solvents examined (see Table 1 in Kobayashi et al., 1998a). The pink-purple color of [Zn]-BChl *a* contrasts with the blue-purple of [Mg]-BChl *a* in organic solvents resulting from the blue-shift of the Q_X-band in [Zn]-BChl *a* relative to [Mg]-BChl *a*; however, the pink-purple color of [Zn]-BChl *a* changes to blue-purple when dried. The close similarity seen in Fig 5B explains the delayed discovery until 1996 of [Zn]-BChl *a* (Chapter 4, Kobayashi et al.).

Except for a blue-shift of 5–8 nm, the absorption spectrum of artificially prepared [Zn]-Chl *a* is deceptively similar to that of [Mg]-Chl *a* (Fig. 5A). Even if [Zn]-Chl *a* participated in natural photosynthesis, it would be very difficult to recognize by its spectrum or coloring, alone.

Figure 6 shows the linear correlation for the absorption maxima, $h\upsilon_{max}$, of synthesized, unnatural [M]-BChls *a* and [M]-Chls *a*, as well as natural BChl *a* ([Mg]-BChl *a*), [Zn]-BChl *a*, BPhe *a* ([2H]-BChl *a*), Chl *a* ([Mg]-Chl *a*) and Phe *a* ([2H]-BChl *a*) against Pauling electronegativity (E_N) values. These values are interpreted as the electron density change in the bacteriochlorin and chlorin π-system, due to the inductive effect of the central metal (Watanabe and Kobayashi, 1991; Geskes et al., 1995; Hartwich et al., 1998; Kobayashi et al., 1998b, 1999a,b; Noy et al., 1998). Figure 6 shows that the change of $h\upsilon_{max}$ between [M]-BChls *a* and [M]-Chls *a* by metal exchange is small, indicating that the difference in light energy harvested would not be a primary reason to select Mg as the central metal of most photosynthetic pigments (Kobayashi et al., 1999a,b).

III. Fluorescence Spectra

A. Fluorescence Wavelength Maxima

Analytical techniques based on fluorescence detection have the advantages of the high selectivity and

Table 2. Fluorescence properties of chlorophylls in diethyl ether at room temperature. A missing fluorescence yield indicates it has not been determined, not that the fluorescence is missing.

Pigments	λ max [nm]	Φ_F	Ref.
Chl *a*	668	–	French et al. (1956)
	666	–	Boardman and Thorne (1971)
	668	–	White et al. (1972)
	–	0.32	Weber and Teale (1957)
	–	0.32	Leupold et al. (1990)
	–	0.33	Latimer et al. (1956)
	670*	0.30*	Kobayashi (1989)
Phe *a*	672.5	–	Smith and Benitez (1955)
	673	–	French et al. (1956)
	672	–	Boardman and Thorne (1971)
	673	–	White et al. (1972)
	674	0.24*	Kobayashi (1989)
	–	0.175*	Weber and Teale (1957)
Chl *b*	648	–	French et al. (1956)
	646	–	Boardman and Thorne (1971)
	649	–	White et al. (1972)
	–	0.17	Weber and Teale (1957)
Phe *b*	657	–	Smith and Benitez (1955)
	661	–	French et al. (1956)
	658	–	Boardman and Thorne (1971)
	661	–	White et al. (1972)
Chl c_1	632	–	Wilhelm (1987)
Chl c_2	632	–	Wilhelm (1987)
Chl *d*	693	–	Manning and Strain (1943)
	696	–	Smith and Benitez (1955)
	699	–	French et al. (1956)
	695	–	Goedheer (1966)
Phe *d*	701	–	French et al. (1956)
BChl *a*	782	0.196	Connolly et al. (1982)
	782	0.19	Teuchner et al. (1997)
BPhe *a*	760	–	Smith and Benitez (1955)
	764.5	0.126	Connolly et al. (1982)
[Zn]-Chl *a*	663*	0.23*	Kobayashi (1989)
[Cd]-Chl *a*	670*	0.043*	ibid.
[Pd]-Chl *a*	638*	0.0025*	ibid.
[Sn(IV)]-Chl *a*	664*	0.110*	ibid.
[Cd]-Chl *a*	670*	0.043*	ibid.
[Ba]-Chl *a*	683*	0.0077*	ibid.
[Zn]-BChl *a*	777	0.14	Teuchner et al. (1997)
[Cd]-BChl *a*	775	0.03	ibid.
[Pd]-BChl *a*	762	0.004	ibid

* in benzene

sensitivity (10 ng or less, i.e., absorbance < 0.001 and, therefore, almost colorless, which is recommended to avoid self-absorption). Due to the high selectivity, fluorescence analyses can often be used to detect impurities (for example, Cl-Chl *a*, OH-Chl *a*) in purified Chl *a*, even when they are difficult to be distinguished by absorption spectra (Kobayashi et al., 1988; Kobayashi, 1989). The corrected fluorescence excitation spectra of Chls is identical to their absorption and that peak fluorescence emission occurs at

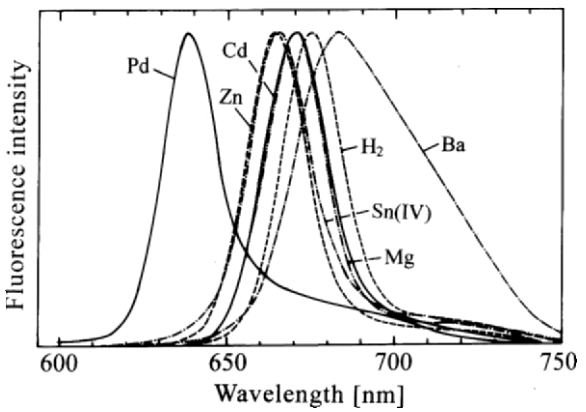

Fig. 7. Emission spectra of [M]-chlorophylls *a* in benzene: M = Mg, 2H, Zn, Sn(IV), Cd, Ba and Pd. Emission maxima are arbitrarily scaled to a common height.

a longer wavelength than the longest red absorption peak (Karukstis, 1991; Hall and Rao, 1995). The wavelengths of the fluorescence maxima of several Chls are listed in Table 2. The fluorescence maximum of Chl *a* in diethylether is ca. 10 nm red-shifted compared to the absorption maximum at 660 nm: the red-shift is called Stoke's shift. Emission spectra of seven kinds of [M]-Chls *a* in benzene are illustrated in Fig. 7. Stoke's shifts observed in [M]-Chls *a* where M = Mg, 2H, Zn, Sn(IV), Cd, Ba and Pd are ca. 7 nm, 6 nm, 8 nm, 11 nm, 10 nm, 5 nm and 7 nm, respectively.

B. Fluorescence Quantum Yields

Chls participating in natural photosynthesis are fluorescent. Only five [M]-BChls *a* among the following seven are fluorescent in organic solvents, and they are marked with an asterisk: M = Mg*, Zn*, Cd*, Pd*, Ni, Cu or 2H* (Connolly et al., 1982; Teuchner et al., 1997). Similarly, only seven [M] Chls a, marked with an asterisk, are fluorescent among the following sixteen: M = Mg*, Zn*, Cd*, Pd*, Ni Cu, 2H*, VO, Mn(III), Fe(III), Co, Ag, Sn(IV)*, Hg, Pb or Ba* (Watanabe et al., 1985; Watanabe and Kobayashi 1988; Leupold et al., 1990; Kobayashi et al., 1998a,b). Figure 8 shows a correlation for the fluorescence quantum yield, ϕ_F, between [M]-Chls *a* in benzene and [M]-BChls *a* in diethyl ether. [Mg]-, [Zn]- and [2H]-(B)Chls *a* are strongly fluorescent, [Sn(IV)]-Chl *a* and [Cd]-(B)Chl *a* show weak fluorescence and [Ba]-Chl *a* and [Pd]-(B)Chl *a* exhibit very weak fluorescence, probably due to the heavy atom effect. The values of ϕ_F of [Sn(IV)]-BChl *a* and

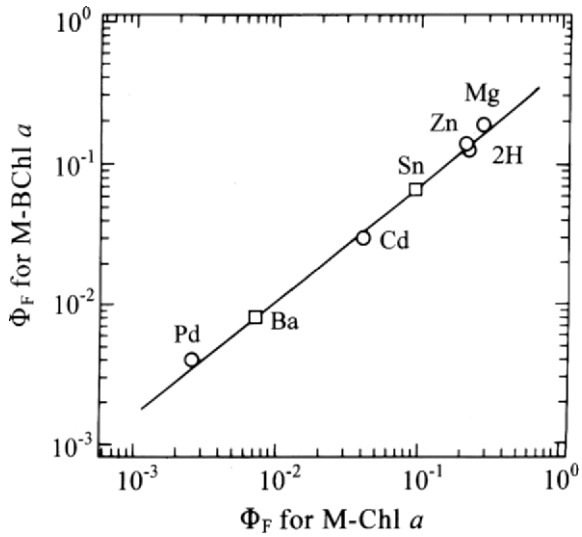

Fig. 8. Correlation for fluorescence quantum yield, Φ_F, between [M]-chlorophylls *a* in benzene and [M]-bacteriochlorophylls *a* in diethyl ether. The values of ϕ_F of [Sn(IV)]-BChl *a* and [Ba]-BChl *a* are predicted values only. Figure adapted from Kobayashi et al. (1999a).

[Ba]-BChl *a* have not been measured yet, but have been predicted using the plot in Fig. 8.

Fluorescence may be dependent on the electronic orbital of the central metals: fluorescent [M]-(B)Chls *a* coordinate non-paramagnetic metals. The metals belonging to the IIa and IIb groups in the periodic table are non-paramagnetic; further, the lighter these metals (e.g., Mg and Zn), the stronger the fluorescence, possibly due to a reduced heavy-atom effect. Fluorescent pigments retain excitation energy within the molecules and are able to transfer it subsequently to neighboring pigments. In this regard, [Zn]- and [Mg]-(B)Chls are suitable as light receptors in the photosystem (see Chapter 1, Scheer).

IV. Circular Dichroism Spectra

A. Chlorophylls a and a´

Circular dichroism (CD) spectroscopy is a useful tool for the examination of the stereochemistry of Chls (see reviews by Wolf and Scheer, 1973, and Weiss, 1978). The standard amount required is 10 µg or less (i.e., absorbance of ca. 1 is recommended). CD is a simple method to distinguish Chl epimers (Chapter 1, Scheer). Figure 9B shows that the CD spectra of Chl *a* and *a´* are considerably different,

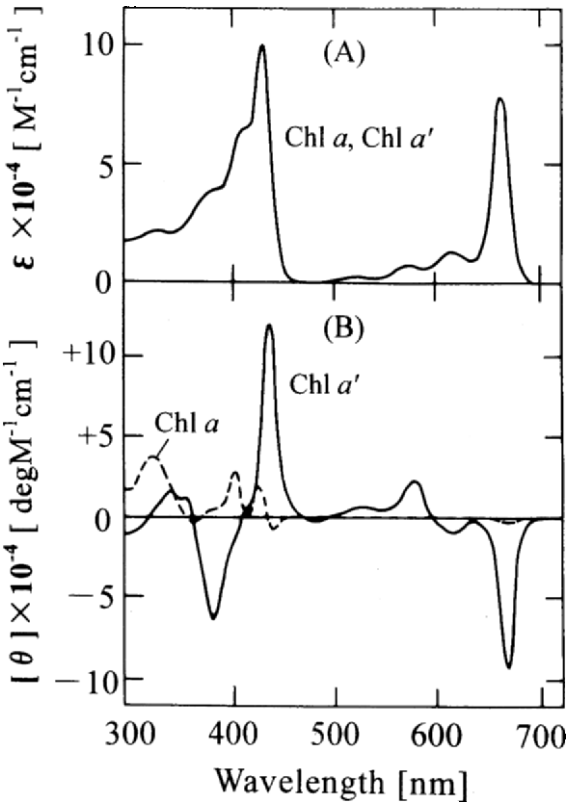

Fig. 9. (A) Absorption spectra and (B) circular dichroism (CD) spectra of chlorophylls *a* and *a´* in benzene. Figure adapted from Watanabe et al. (1984).

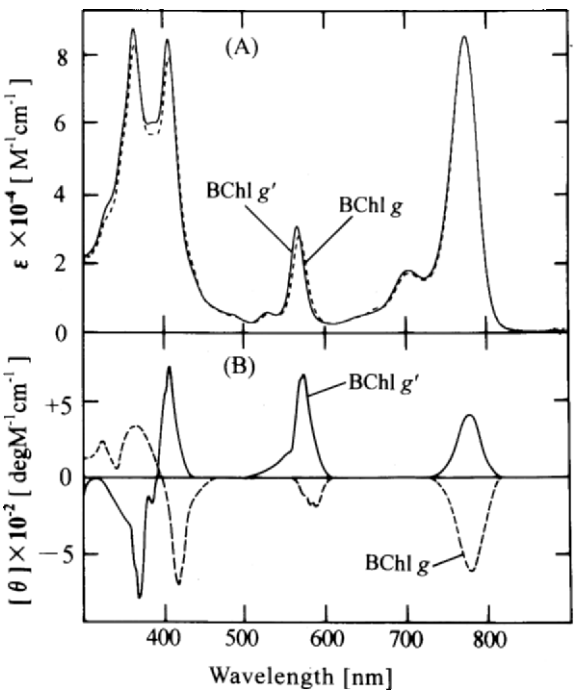

Fig. 10. (A) Absorption spectra and (B) CD spectra of bacteriochlorophylls *g* and *g´* in benzene.

while the absorption spectra are almost identical (Fig. 9A). An intense negative CD band at 668 nm associated with $Q_Y(0,0)$ is observed in Chl *a´* as well as a well-defined negative satellite (615 nm) with $Q_Y(1,0)$. Chl *a´* also shows fairly intense positive CD bands at 530 and 580 nm associated with $Q_X(1,0)$ and $Q_X(0,0)$, respectively; however, Chl *a* exhibits little optical activity in this region. Chl *a´* gives a single, strongly positive CD spectrum associated with the Soret absorption bands (434 nm) due to the $B_X(0,0)$ and $B_Y(0,0)$ transition, suggesting that these two transitions contribute to CD spectra in a similar manner, whereas in Chl *a* the CD spectrum (424 nm and 440 nm) reflects the existence of the two transitions in this region (Watanabe et al., 1984).

B. Bacteriochlorophylls g and g´

Figures. 4C and 10A shows that one can distinguish, only with some difficulty, between BChl *g´* and BChl *g* by absorption spectroscopy in hexane or benzene by the shape of Q_X band. They are hardly distinguishable in other solvents. Like Chl *a*/*a´*, however, the CD spectra of BChl *g* and *g´* (Fig. 10B) are distinctly different, and the two epimers can therefore be readily identified. When compared with the CD spectra of Chl *a*/*a´* (Fig. 9B), the BChl *g*/*g´* pair shows nearly mirror-image CD spectra (Fig. 10B), suggesting the higher planarity of the BChl *g*/*g´* pair due to the presence of C8=C8[1] double bond on ring B (Chapter 1, Scheer). If so, the BChl *b*/*b´* pair, possessing a C8=C8[1] double bond, should also exhibit mirror-image CD spectra.

V. Mass Spectra

Because Chls involved in natural photosynthesis are sometimes present in very small amounts, use of mass spectrometry (MS) can be advantageous since only minute samples (0.1 μg or less) are required. MS can provide accurate and useful information not only on molecular weights and elemental compositions but also on the nature of functional groups attached to the macrocycle (for example, phytol) and of the central metal. Such information is of obvious util-

ity in structural investigations of Chls (see reviews by K. M. Smith,1975; Hunt and Michalski, 1991). MS has also provided useful information about Chl biosynthesis and degradation (see review by Porra and Scheer, 2000).

In mass spectrometric analysis, a molecular ion (usually $M^{+\cdot}$) is produced which may subsequently undergo fragmentation. A variety of ionization techniques are used (see reviews by Hunt and Michalski, 1991; Hoffmann and Stroobant, 2002): electron ionization (EI), electrospray ionization (ESI), fast atom bombardment (FAB), field desorption (FD), laser desorption (LD), matrix-assisted laser desorption ionization (MALDI), plasma desorption (PD) have all been used. Some typical examples of recently discovered Chls which have been identified by FAB-mass spectroscopy are presented below.

A. [Zn]-Bacteriochlorophyll a

The predictable dominance of the molecular fragment is particularly useful for molecular weight (mol wt) determination. In mass spectroscopy (MS), the physical appearance of the molecular fragment enables detection of metals in [M]-Chls because metal ions are generally not lost in fragmentation processes. [Zn]-BChl *a*, found in *Acp. rubrum,* is almost indistinguishable from [Mg]-BChl *a* by absorption spectra (see Fig. 5B), CD spectra (see Fig. 3 in Kobayashi et al., 1998a) or fluorescence spectra (Teuchner et al., 1997); however, they are distinguished by MS.

The FAB-mass spectrum of [Zn]-BChl *a* ($C_{55}H_{74}N_4O_6{}^{64}Zn$; mol wt = 950) purified from *Acp. rubrum* shows a molecular ion $[M]^{+\cdot}$ at *m/z* 950.5 (Fig. 11A), while the $[M]^{+\cdot}$ ion of BChl *a* ($C_{55}H_{74}N_4O_6Mg$) (Fig. 11B) is 39.9 mass units lower at m/z 910.6 which is consistent with the mass difference between ^{64}Zn (63.9) and Mg (24.0) atoms. An intense fragment at *m/z* 672.2 (see Fig. 11A) corresponds to the loss of the phytyl group ($C_{20}H_{39}$; mol wt = 279) from [Zn]-BChl *a* (950.5 - 279 + H)$^+$. The same dephytylated fragment occurs 39.9 mass units lower at *m/z* 632.3 with [Mg]-BChl *a* (Fig. 11B) due to the mass difference between ^{64}Zn and Mg. The FAB-mass spectrum of demetallated [Zn]-BChl *a* (Fig 11C) is identical with that of natural BPhe *a* ([2H]-BChl a) with a $M^{+\cdot}$ ion at *m/z* 888 ($C_{55}H_{74}N_4O_62H$); the fragment at *m/z* 610 arises by loss of the phytyl group (888 – 279 + H)$^{+\cdot}$.

In Fig. 11A, the two satellite peaks at *m/z* 952.5 and 954.5 near $M^{+\cdot}$ of [Zn]-BChl *a* ($C_{55}H_{74}N_4O_6{}^{64}Zn$ at *m/z* 950.5) arise from the isotopic molecular ions, $C_{55}H_{74}N_4O_6{}^{66}Zn$ and $C_{55}H_{74}N_4O_6{}^{68}Zn$, respectively: the natural abundance is ^{64}Zn(48.6%), ^{66}Zn(27.9%), ^{68}Zn(18.8%). Comparing Fig. 11A with Figs. 11B and C and Fig. 12, the above two characteristic satellite peaks observed in Zn-BChl *a* (Fig. 11A) can be clearly distinguished from other satellite peaks around $M^{+\cdot}$ caused by ^2H (natural abundance = 0.012%) and ^{13}C(1.07%). Further, the high-resolution mass spectrum of [Zn]-BChl *a* gives a major peak at *m/z* 950.4935 which can only be explained by one rational formula, $C_{55}H_{74}N_4O_6{}^{64}Zn$ (Calcd. 950.4899); thus, the Zn-containing chlorophyll isolated from *Acp. rubrum* was identified by MS analysis as [Zn]-BChl *a* esterified with phytol (Kobayashi et al., 1998a).

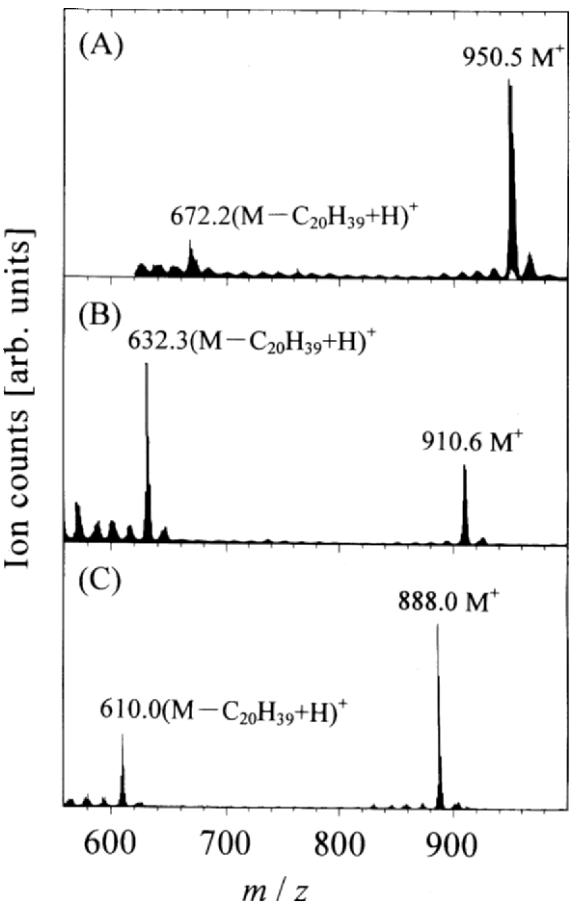

Fig. 11 FAB-mass spectra of (A) [Zn]-bacteriochlorophyll *a*, (B) bacteriochlorophyll *a* (i.e., [Mg]-BChl *a*) and (C) bacteriopheophytin *a* (i.e., [2H]-BChl *a*).

B. Bacteriochlorophyll 663: Chlorophyll a Esterified with Δ2,6-Phytadienol

The characteristic feature of the mass spectra of Chls is the way in which the fragments are split into two separate groups (Figs. 11 and 12): the highest intense mass fragment is due to the molecular ion, M^+, and one of the other strong fragments is due to the subsequent loss of the long alcohol-chain at C17[3], for example, phytol, $(M - phytyl(C_{20}H_{39}) + H)^{+\cdot}$.

The reaction centre (RC) component, A_0, of green sulfur bacteria was designated BChl 663 after its absorption maximum in the HPLC eluent (Chapter 4, Kobayashi et al.). Our first attempt to identify the pigment by ^{252}Cf-plasma desorption mass spectroscopy (^{252}Cf-PDMS) failed due to low resolution: the spectrum of demetallated BChl 663 (BPhe 663) showed two broad intense peaks near *m/z* 592.5 and 871.3, similar to Phe *a* esterified with phytol, Phe a_P. Unfortunately, BChl 663 could not be distinguished from Chl a_P by absorption-, CD- and fluorescence-spectroscopy. However, BChl 663 was clearly separated by HPLC; thus, we tentatively regarded BChl 663 as an isomer of Chl *a* (van de Meent et al., 1992).

BChl 663 has been identified by FAB-mass analyses (Kobayashi et al., 2000). A typical FAB-mass spectrum of BChl 663 (Fig. 12A) has molecular ion peaks $[M]^{+\cdot}$ and $[M + H]^{+\cdot}$ at *m/z* 890.6 and 891.6, respectively, which are 2.0 mass units smaller than the $[M]^{+\cdot}$ and $[M + H]^{+\cdot}$ peaks at *m/z* 892.6 and 893.6 of Chl a_P ($C_{55}H_{72}N_4O_5Mg$, calculated 892.5353; see Fig. 12B). Mass spectra of BPhe 663 (Fig. 12A) and Phe a_P (Fig. 12B) both show an identical intense mass peak at *m/z* 614.3 indicating that the 2.0 mass units difference observed between Chl a_P and BChl 663 is due to a difference in the esterifying alcohol. The high-resolution mass measurement of BChl 663 gives a value of *m/z* 890.5191, consistent with the calculated value of Chl *a* esterified with phytadienol ($C_{55}H_{70}N_4O_5Mg$, Calcd. 890.5197). Thus, MS analysis gave unequivocal evidence for the presence of an additional C=C double bond in the phytyl chain of BChl 663. The position of this double bond, however, could not be determined by MS, and awaited NMR analysis.

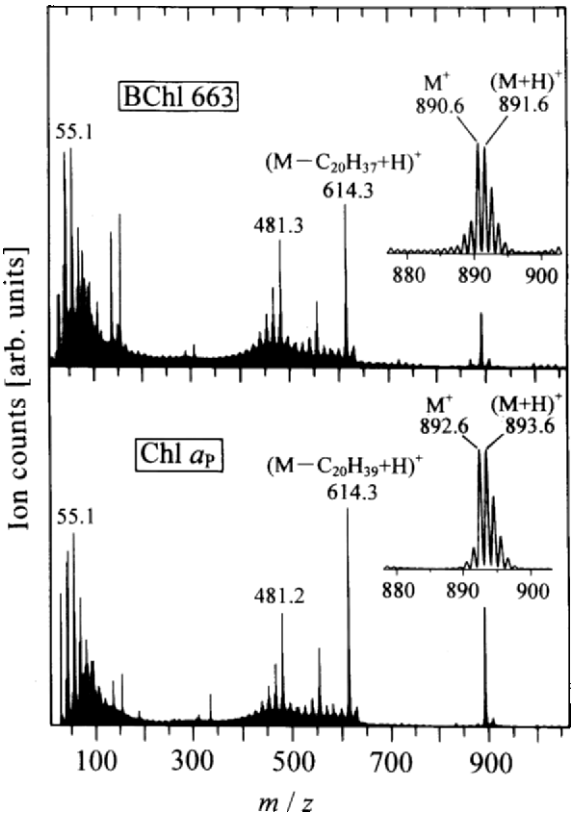

Fig. 12. FAB-mass spectra of (A) bacteriochlorophyll 663 and (B) chlorophyll a_P.

VI. Nuclear Magnetic Resonance Spectra

Nuclear magnetic resonance (NMR) spectroscopy can provide precise information about Chl structure but has the disadvantage that large amounts of purified Chls are required (>0.1 mg is needed for ^{1}H-NMR and >1 mg for ^{13}C-NMR) and colorless impurities cannot be neglected. However, by combining NMR with HPLC, absorption-, CD- and mass-spectrometry, smaller amounts (1 μg or less) can be employed. Such coupled procedures have not only definitively identified the structures of several major naturally-occurring Chls but have also assisted recent studies of minor Chl pigments, present in minute quantities, such as electron donors and acceptors in the RC (Chapter 4, Kobayashi et al.).

A. Chlorophylls a and a´

Because Chls have fingerprint signals in ^{1}H-NMR spectra, this technique was often used in structural determination of Chls (see reviews by Scheer and Katz, 1975; Abraham and Rowan, 1991). For example, the fingerprint region of ^{1}H-NMR spectra for Chl *a* and Chl *a´* in acetone-d_6 is shown in Fig. 13. Signals

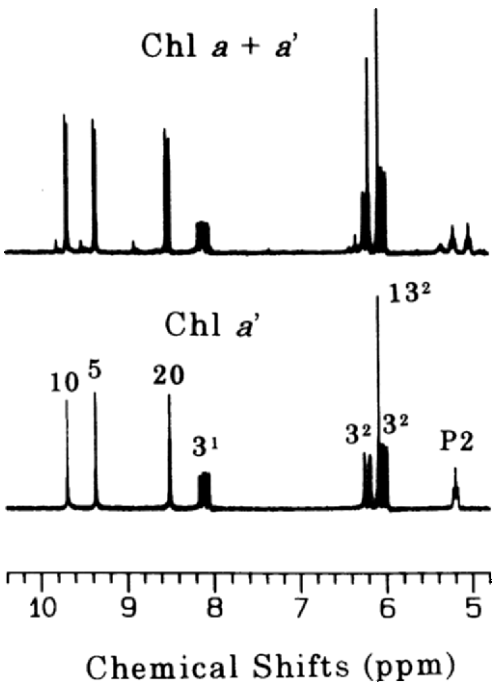

Fig. 13. The fingerprint region of ^{1}H-NMR spectra of (A) a mixture of chlorophylls *a* and *a´*, and (B) pure chlorophyll *a´* in acetone-d_6.

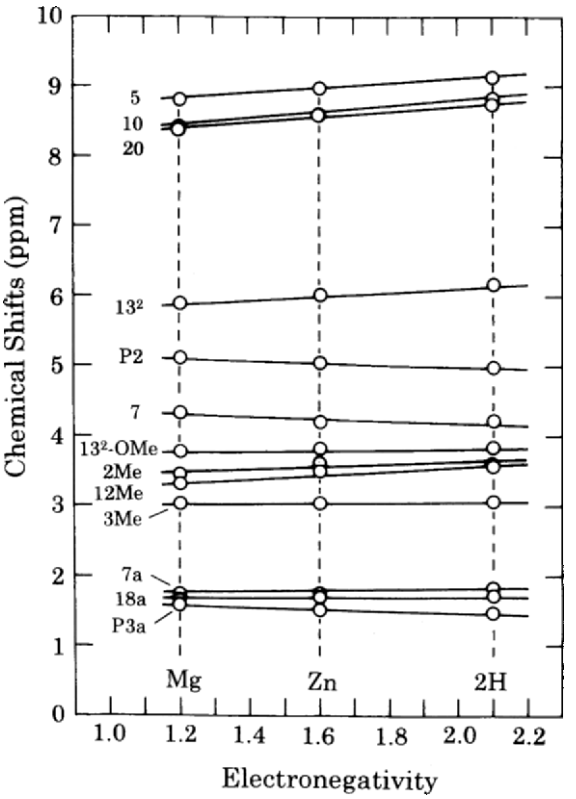

Fig. 14. Correlation of the ^{1}H-NMR chemical shift among bacteriochlorophylls *a* (i.e., [Mg]-, [Zn]-bacteriochlorphyll *a*) and bacteriopheophytin *a* (i.e., [2H]-BChl *a*) in acetone-d_6 with E_N of the central metal. Figure adapted from Kobayashi et al. (1999b).

of *meso*-H (C-5, -10 and -20) on the macrocycle and P2-H on the phytyl chain are clearly downfield shifted in Chl *a´*, as compared to Chl *a*. On the other hand, 13^2-H shows upfield shift in Chl *a´*. Such a difference in stereochemistry is not recognized by most other analytical methods. The ^{13}C chemical shift effects parallel those observed for the ^{1}H-NMR of the epimers (Lötjönen and Hynninen, 1983; Abraham and Rowan, 1991).

B. [Mg]-Bacteriochlorophyll a, [Zn]-Bacteriochlorophyll a and [2H]-Bacteriochlorophyll a (Bacteriopheophytin a)

Changed electron distribution on the [M]-Chl macrocycle, mainly due to the inductive effect of the central metal, can be seen in ^{1}H-NMR spectra. A fair correlation is seen between the electronegativity (E_N) of the central metal and the chemical shifts of ^{1}H-NMR for [Mg]-BChl *a* (BChl *a*), [Zn]-BChl *a* and [2H]-BChl *a* (BPhe *a*) in acetone-d_6 (Fig. 14) as is also observed with blue-shifted absorption maxima (see Fig. 5B). Clear downfield shifts of *meso*-H (at C-5, -10 and -20), 2-Me, 12-Me and 13^2-H on removal of Zn and Mg are observed, although other protons remain almost unchanged or show even slightly upfield shifts. The protons exhibiting large downfield shifts on the removal of metals are located on rings A, C and E. Interestingly, the shifts reported for ^{13}C-NMR for Chls (Boxer et al., 1974) are in the opposite direction to the ^{1}H-NMR signal changes for BChls.

The ^{1}H-NMR chemical shift can be interpreted on the basis of ring current, and in both localized diamagnetic and remote paramagnetic terms. The effect of the ring current in the macrocycle is not related to the observed downfield shift of ^{1}H-NMR signals: the ring current has to shift ^{1}H-NMR signals upfield with regard to the change of the redox potential on introduction of a more electronegative metal (see Fig. 3 in Kobayashi et al., 1999b). The enhanced anti-bonding level with the less electronegative metal coordination, seems to increase electron density not only on the π-system but also on the protons of rings A, C and E. The magnetic field shielding increases, and there is an anisotropic inductive effect from the

metal to rings A and C (Kobayashi et al., 1998b, 1999a,b).

A non-uniform electron distribution on the macrocycle caused by the anisotropic inductive effect may produce forces of different magnitude along an axis through rings A, C and E to those along an axis through rings B and D, and induce bending of the macrocycle. The force is larger in [Mg]-BChl *a* than in [Zn]-BChl *a*, resulting in large instability in the former rather than the latter. In [M]-Chls *a*, increased electron densities by the coordination of less electron negative metals may cause even ring B-related resonances to react (see Steiner and Fowler, Chapter 25). The presence of non-bonding electrons on ring B induces an excessive distortion on the macrocycle, which results in less stability even in [Zn]-Chl *a* compared with [Zn]-BChl *a*, which accounts for the stronger resistance to demetallation of [Zn]-BChl *a* relative to [Mg]-Chl *a* (Chapter 4, Kobayashi et al.).

C. Chlorophyll a_P and Bacteriochlorophyll 663

BChl 663 has been identified as Chl *a* esterified with phytadienol (Section V.B) by absorption-, florescence-, CD- and mass-spectroscopy, but these methods cannot locate where the two C=C double bonds are located in the long chain alcohol at C17[3].

In the one-dimensional ^{1}H-NMR spectra, identical signals corresponding to all ^{1}H atoms of the Chl a_P macrocycle are observed for BChl 663 at identical chemical shifts (see Fig. 5 in Kobayashi et al., 2000), demonstrating that the macrocycles of BChl 663 and Chl a_P are identical. There are, however, marked differences in the signals from the long alcohol chains of each pigment (Fig. 15). A triplet signal (signal A), present in the spectrum of BChl 663 but absent in Chl a_P, appeared at 5.01 ppm on the low-field side of signal P2. This suggests that the environment of the proton is very similar to that of P2. Similarly, a complex signal B appeared at 1.95 ppm on the low-field side of signal P4 at 1.86 ppm. The intensity of signal P4 (denoted as signal C) in the spectrum of BChl 663 is twice that in Chl a_P, suggesting two more protons in Chl a_P in an environment similar to that of P4. Another marked difference is the disappearance of one of the doublet peaks seen in the spectrum of Chl a_P, either at P7^1 or P11^1, at the high-field end of the spectrum, and the concomitant appearance of

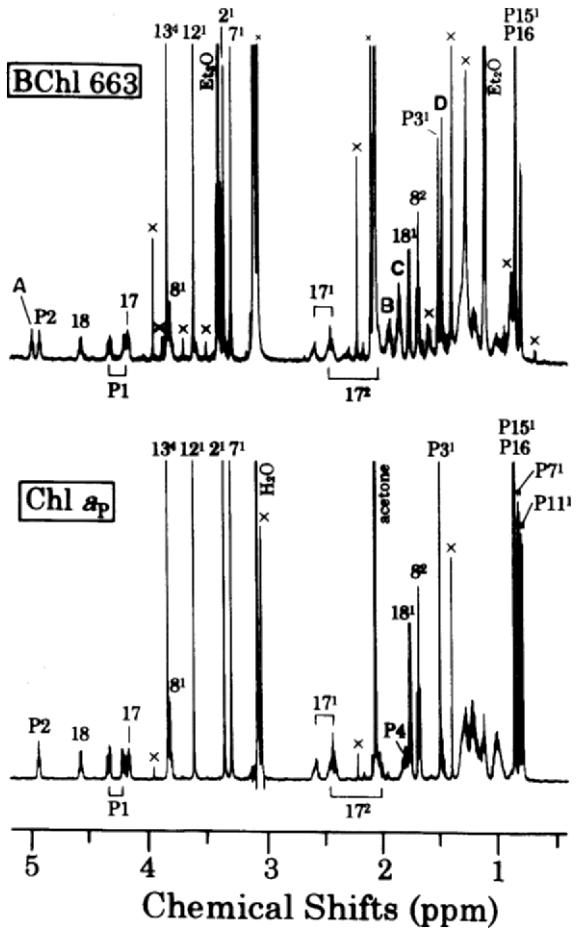

Fig. 15. Expanded ^{1}H-NMR spectra of BChl 663 and Chl a_p in acetone d_6, showing differences in the long alcoholic chain. Characteristic signals observed in the BChl 663 spectrum are indicated by A, B, C and D. Figure adapted from Kobayashi et al. (2000).

a singlet signal (signal D) at 1.49 ppm (near peak P3^1) in the spectrum of BChl 663. These results are consistent with FAB-MS results indicating the presence of an additional double bond in the phytyl chain of BChl 663. The structure of the esterifying alcohol in BChl 663 has been identified as all-*trans*-Δ2,6-phytadienol (Chapter 1, Scheer) from ^{1}H-^{1}H double quantum filtered correlation spectroscopy (DQF-COSY), and from heteronuclear multiple-bond correlation (HMBC)- and heteronuclear multiple-quantum coherence (HMQC)-NMR spectra (see Kobayashi et al., 2000).

Acknowledgments

We thank Kuniyuki Takahashi, Takanori Gotoh, Hajime Koizumi and Miss Yuka Itoh (Univ. Tsukuba) for helpful discussions. This work was supported in part by the Special Projects of Nanoscience and 21st Century COE Program (Univ. Tsukuba), by the Tokyo Ohka Foundation for the promotion of Science and Technology, and by a Grant-in-Aid for Scientific Research on Priority Area (417) from the Ministry of Education, Culture, Sports, Science and Technology (MEXT), Japan. One of us, MA, thanks the Japanese Society for the Promotion of Science for Young Scientists for a Research Fellowship.

References

Abraham RJ and Rowan AE (1991) Nuclear magnetic resonance spectroscopy of chlorophyll. In: Scheer H (ed) Chlorophylls, pp 797–834. CRC Press, Boca Raton

Akiyama M, Miyashita H, Watanabe T, Kise H, Miyachi S and Kobayashi M (2001) Detection of chlorophyll *d′* and pheophytin *a* in a chlorophyll *d*-dominating oxygenic photosynthetic prokaryote *Acaryochloris marina*. Anal Sci 17: 205–208

Boardman NK and Thorne SW (1971) Sensitive fluorescence method for the determination of chlorophyll *a*/chlorophyll *b* rations. Biochim Biophys Acta 253: 222–231

Boxer SG, Closs GL and Katz JJ (1974) The effect of magnesium coordination on the ^{13}C and ^{15}N magnetic resonance spectra of chlorophyll *a*. The relative energies of nitrogen $n\pi^*$ states as deduced from a complete assignment of chemical shifts. J Am Chem Soc 96: 7058–7066

Connolly JS, Samuel EB and Janzen AF (1982) Effects of solvent on the fluorescence properties of bacteriochlorophyll *a*. Photochem Photobiol 36: 565–574

Evans TA and Katz JJ (1975) Evidence for 5- and 6-coordinated magnesium in bacteriochlorophyll *a* from visible absorption spectroscopy. Biochim Biophys Acta 396: 414–426

French CS (1960) The chlorophylls in vivo and in vitro. In: Ruhland W (ed) Handbuch der Pflanzenphysiologie, Bd 5/1, pp 252–297, Springer-Verlag, Berlin

French CS, Smith JHC, Virgin HI and Airth RL (1956) Fluorescence spectrum curves of chlorophylls, pheophytins, phycoerythrins, phycocyanins and hypericin. Plant Physiol 31: 360–374

Geskes C, Hartwich G, Scheer H, Mantele W and Heinze J (1995) An electrochemical and spectroelectrochemical investigation of metal-substituted bacteriochlorophyll *a*. J Am Chem Soc 117: 7776–7783

Gloe A, Pfennig N, Brockmann H Jr and Trowitzsch W (1975) A new bacteriochlorophyll from brown-colored Chlorobiaceae. Arch Microbiol 102: 103–109

Goedheer JC (1966) Visible absorption and fluorescence of chlorophyll and its aggregates in solution. In: Vernon LP and Seely CR (eds) The Chlorophylls, pp 147–185. Academic Press, New York

Hall DO and Rao KK (1995) Photosynthesis, 5th edition, Cambridge University Press

Hartwich G, Fiedor L, Simonin I, Cmiel E, Schäfer W, Noy D, Scherz A and Scheer H (1998) Metal-substituted bacteriochlorophylls. 1. Preparation and influence on metal and coordination on spectra. J Am Chem Soc 120: 3675–3683

Hoffmann E and Stroobant V (2002) Mass Spectrometry: Principles and Applications, Second Edition. John Wiley & Sons, Chichester

Hunt JE and Michalski TJ (1991) Desorption-ionization mass spectrometry of chlorophylls. In: Scheer H (ed) Chlorophylls, pp 835–853. CRC Press, Boca Raton

Jeffrey SW (1969) Properties of two spectrally different components in chlorophyll *c* preparations. Biochim Biophys Acta 177: 456–467

Jeffrey SW (1972) Preparation and some properties of crystalline chlorophyll c_1 and c_2 from marine algae. Biochim Biophys Acta 279: 15–33

Jeffrey SW, Mantoura RFC and Wright SW (1997) Phytoplankton Pigments in Oceanography. UNESCO, Paris

Jensen A, Aasmundrud O and Eimhjellen KE (1964) Chlorophylls of photosynthetic bacteria. Biochim Biophys Acta 88: 466–479

Karukstis KK (1991) Chlorophyll fluorescence as a physiological probe of the photosynthetic apparatus. In: Scheer H (ed) Chlorophylls, pp 769–795. CRC Press, Boca Raton

Ke B (2001) Photosynthesis. Photobiochemistry and Photobiophysics. Kluwer Academic Publishers, Dordrecht

Kishimoto N, Fukaya F, Inagaki K, Sugio T, Tanaka H and Tano T (1995) Distribution of bacteriochlorophyll *a* among aerobic and acidophilic bacteria and light-enhanced CO_2-incorporation in *Acidiphilium rubrum*. FEMS Microbiol Ecol 16: 291–296

Kobayashi M (1989) Study on the molecular mechanism of photosynthetic reaction centers. Thesis, University of Tokyo

Kobayashi M (1996) Study of precise pigment composition of photosystem I-type reaction centers by means of normal-phase HPLC. J Plant Res 109: 223–230

Kobayashi M, Watanabe T, Struck A and Scheer H (1988) Mesochlorination of chlorophyll *a* in the course of pigment extraction FEBS Lett. 235: 293–297

Kobayashi M, Van de Meent EJ, Amesz J, Ikegami I and Watanabe T (1991) Bacteriochlorophyll *g* epimer as a possible reaction center component of heliobacteria. Biochim Biophys Acta 1057: 89–96

Kobayashi M, Akiyama M, Kise H, Takaichi S, Watanabe T, Shimada K, Iwaki M, Itoh S, Ishida N, Koizumi M, Kano H, Wakao N and Hiraishi A (1998a) Structural determination of the novel Zn-containing bacteriochlorophyll in *Acidiphilium rubrum*. Photomed Photobiol 20: 75–80

Kobayashi M, Akiyama M, Yamamura M, Kise H, Ishida N, Koizumi M, Kano H and Watanabe T (1998b) *Acidiphilium rubrum* and zinc-bacteriochlorophyll, part 2: Physicochemical comparison of zinc-type chlorophylls and other metallochlorophylls. In: Garab G (ed) Photosynthesis: Mechanism and Effects, Vol 2, pp 735–738. Kluwer Academic Publishers, Dordrecht

Kobayashi M, Akiyama M, Watanabe T and Kano H (1999a) Exotic chlorophylls as key components of photosynthesis. Curr Topics Plant Biol 1: 17–35

Kobayashi M, Akiyama M, Yamamura M, Kise H, Wakao N, Ishida N, Koizumi M, Kano H and Watanabe T (1999b) Comparison of physicochemical properties of metallobacteriochlorophylls

and metallochlorophylls. Z Phys Chem 213: 207–214
Kobayashi M, Oh-oka H, Akutsu S, Akiyama M, Tominaga K, Kise H, Nishida F, Watanabe T, Amesz J, Koizumi M, Ishida N and Kano H (2000) The primary electron acceptor of green sulfur bacteria, bacteriochlorophyll 663, is chlorophyll *a* esterified with Δ2,6-phytadienol. Photosynth Res 63: 269–280
Latimer P, Bannister TT and Rabinowitch E (1956) Quantum yields of fluorescence of Plant Pigments. Science 124: 585–586
Lawlor DW (1993) Photosynthesis, 2nd edition. Longman Scientific & Technical, Essex
Leupold D, Struck A, Stiel H, Teuchner K, Oberländer S and Scheer H (1990) Excited-state properties of 20-chloro-chlorophyll *a*. Chem Phys Lett 170: 478–484
Lötjönen S and Hynninen PH (1983) Carbon-13 NMR spectra of chlorophyll *a*, chlorophyll *a´*, pyrochlorophyll *a* and the corresponding pheophytins. Org Magn Reson 21: 757–765
Manning WM and Strain HH (1943) Chlorophyll *d*, a green pigment of red algae. J Biol Chem 151: 1–19
Noy D, Fiedor L, Hartwich G, Scheer H and Scherz A (1998) Metal-substituted bacteriochlorophylls. 2. Changes in redox potentials and electronic transition energies are dominated by intramolecular electrostatic interactions. J Am Chem Soc 120: 3684–3693
Noy D, Yerushalmi R, Brumfeld V, Ashur I, Scheer H, Baldridge KK and Scherz A (2000) Optical absorption and computational studies of [Ni]-bacteriochlorophyll-*a*. New insight into charge distribution between metal and ligands. J Am Chem Soc 122: 3937–3944
Oelze J (1985) Analysis of bacteriochlorophylls. Meth Microbiol 18: 257–284
Permentier HP, Schmidt KA, Kobayashi M, Akiyama M, Hager-Braun C, Neerken S, Miller M and Amesz J (2000) Composition and optical properties of reaction center core complexes from the green sulfur bacteria *Prosthecochloris aestuarii* and *Chlorobium tepidum*. Photosynth Res 64: 27–39
Porra RJ and Scheer H (2000) ^{18}O and mass spectrometry in chlorophyll research: Derivation and loss of oxygen atoms at the periphery of the chlorophyll macrocycle during biosynthesis, degradation and adaptation. Photosynth Res 66: 159–175
Scheer H and Katz JJ (1975) Nuclear magnetic resonance spectroscopy of porphyrins and metalloporphyrins. In: Smith KM (ed) Porphyrins and Metalloporphyrins, pp 399–524, Elsevier, Amsterdam
Smith JHC and Benitez A (1955) Chlorophylls: Analysis in plant materials. In: Paech K and Tracey MV (eds) Moderne Methoden der Pflanzenanalyse, Vol IV, pp 142–196. Springer-Verlag, Berlin
Smith KM (1975) Mass spectrometry of porphyrins and metalloporphyrins. In: Smith KM (ed) Porphyrins and Metalloporphyrins, pp 381–398, Elsevier, Amsterdam
Stanier RY and Smith JHC (1960) The chlorophylls of green bacteria. Biochim Biophys Acta 41: 478–484
Takahashi K, Itoh Y, Akiyama M, Watanabe T, Inoue K, Oba T, Umetsu M and Kobayashi M (2005) Delicate distinction between absorption spectra of bacteriochlorophyll epimers. In: van der Est A and Bruce D (eds) Photosynthesis: Fundamental Aspects to Global Perspectives, pp 46–48. Alliance Communications Group, Lawrence
Teuchner K, Stiel H, Leupold D, Scherz A, Noy D, Simonin I, Hartwich, G and Scheer H (1997) Fluorescence and excited state absorption in modified pigments of bacterial photosynthesis: A comparative study of metal-substituted bacteriochlorophylls *a*. J Lumin 72–74: 612–614
Treibs A (1932) Handbuch der Pflanzenanalyse. Bd. III/2, pp 1351. Julius Springer, Wien
Van de Meent EJ, Kobayashi M, Erkelens C, Van Veelen PA, Otte SCM, Inoue K, Watanabe T and Amesz J (1992) The nature of the primary electron acceptor in green sulfur bacteria. Biochim Biophys Acta 1102: 371–378
Wakao N, Shiba T, Hiraishi A, Ito M and Sakurai Y (1993) Distribution of bacteriochlorophyll *a* in species of the genus *Acidiphilium*. Curr Microbiol 27: 277–279
Watanabe T and Kobayashi M (1988) Chlorophylls as functional molecules in photosynthesis: molecular composition in vivo and physical chemistry in vitro. Nippon Kagaku Kaishi 4: 383–395
Watanabe T and Kobayashi M (1991) Electrochemistry of chlorophylls. In: Scheer H (ed) Chlorophylls, pp 287–315. CRC Press, Boca Raton
Watanabe T, Hongu A, Honda K, Nakazato M, Konno M and Saitoh S (1984) Preparation of chlorophylls and pheophytins by isocratic liquid chromatography. Anal Chem 56: 251–256
Watanabe T, Machida K, Suzuki H, Kobayashi M and Honda K (1985) Photoelectrochemistry of chlorophylls. Coord Chem Rev 64: 207–224
Weber G and Teale FWJ (1957) Determination of the absolute quantum yield of fluorescent solutions. Trans Faraday Soc 53: 646–655
Weiss C (1978) Electronic Absorption Spectra of Chlorophylls. In: Dolphin D (ed) The Porphyrins, Vol. III, Physical Chemistry, Part A, pp 211–223. Academic Press, New York
White RC, Jones ID, Gibbs E and Butler LS (1972) Fluorometric estimation of chlorophylls, chlorophyllides, pheophytins and pheophorbides in mixtures. J Agric Food Chem 20: 773–778
Wilhelm C (1987) Purification and identification of chlorophyll c_1 from the green alga *Mantoniella squamata*. Biochim Biophys Acta 892: 23–29
Wolf H and Scheer H (1973) Stereochemistry and chiroptic properties of pheophorbides and related compounds. Ann NY Acad Sci 206: 549–567

Chapter 7

Spectrometric Assays for Plant, Algal and Bacterial Chlorophylls

Robert J. Porra*
Division of Plant Industry, Commonwealth Scientific and Industrial Research Organization, Canberra, ACT 2601, Australia, and Department of Biologie I-Botanik, Universität München, Menzinger Str.67, D-80638 München, Germany

Summary

Chlorophyll (Chl) assays derive their importance from the essential role of Chls in the harvesting of solar energy and its transduction to biologically useful chemical energy (ATP) and reducing power (NADPH or NADH) during photosynthesis in higher plants, marine and aquatic algae, and in photosynthetic bacteria. Accurate determination of Chl *a* and *b* concentrations and of Chl *a*/*b* ratios has been an essential tool in photosynthesis research in higher plants and green algae. Spectrophotometric and spectrofluorimetric assays, relying on the characteristic absorption and fluorescence properties of the chlorophylls, will be described and accurate data presented for spectrophotometric assays in a wide variety of solvents.

*Email: robert.porra@csiro.au

Bernhard Grimm, Robert J. Porra, Wolfhart Rüdiger and Hugo Scheer (eds): Chlorophylls and Bacteriochlorophylls: Biochemistry, Biophysics, Functions and Applications, pp. 95–107.

I. Introduction

The accurate assay of chlorophylls (Chls) *a* and *b* and determination of Chl *a/b* ratios is important in photosynthesis research. Photosynthetic reaction rates are frequently expressed per unit of Chl content. Accurate Chl *a* and *b* determinations also became important in attempts to produce accurate models of the various Chl-protein complexes located in thylakoid membranes of plant and algal chloroplasts. These complexes, light-harvesting complexes (LHCs) and reaction centers (RCs), have very different but characteristic Chl *a/b* ratios and their accurate determination has helped reveal how plants regulate the proportions, size and composition of these complexes to adapt to available light.

As a rapid alternative to quantitative HPLC methods, spectrometric assays have been developed which depend on either the characteristic absorption or the intense fluorescence of Chls. Further, special spectrophotometric and spectrofluorimetric techniques have been developed to determine Chl *b* concentrations in biological situations where Chl *a/b* ratios are so high that the Chl *b* Q_y absorption peak becomes indistinct.

II. Modern Spectrophotometric Assays of Chlorophylls *a* and *b*

Comar and Zscheile (1942) extracted Chls *a* and *b* with pure acetone, transferred them to diethylether and assayed both Chls spectrophotometrically, but without separation, using the simultaneous equation (Eq.) technique (Section IV). A one-step procedure was later devised in which Chls *a* and *b* were extracted with aqueous (aq) 80% acetone and, again, were both assayed without separation using simultaneous equations. (Arnon, 1949). In this solvent, the water-induced red-shift of the Chl Q_y absorption peaks by release of small amounts of cell sap during extraction became insignificant in the presence of 20% water. Arnon's method, therefore, was remarkable for its speed and simplicity. Unfortunately, it later proved to be grossly inaccurate (Vernon, 1960; Ziegler and Egle, 1965, Delaporte and Laval-Martin, 1971a,b; Lichtenthaler, 1987; Porra et al., 1989; Wellburn, 1994) because Arnon's simultaneous equations to determine Chl *a* and *b* concentrations were constructed using the flawed α extinction coefficients of Mackinney (1941). Thus, accurate extinction coefficients for Chls *a* and *b* were urgently required to obtain reliable simultaneous equations.

Abbreviations: aq – aqueous; DMF – N,N′-dimethylformamide; DMSO – dimethylsulfoxide; DV – divinyl; Eq. – equation; LHC I – light-harvesting complex I; MV – monovinyl; PS I and II – Photosystems I and II; RC – reaction center; The numbering and nomenclature systems for tetrapyrroles, approved by the International Union of Pure and Applied Chemistry-International Union of Biochemistry (IUPAC-IUB) Joint Commission on Biochemical Nomenclature, have been used throughout (see Fig. 1).

III. Choice of Extractant and Determination of Accurate Extinction Coefficients for Chlorophylls *a* and *b* in Such Solvents

Accurate millimolar (ε_{mM} = [l·mmol^{-1}·cm^{-1}]) and specific (α = [l·g^{-1}·cm^{-1}]) extinction coefficients for Chls *a* and *b* were obtained in aq 80% acetone, DMF, DMSO, chloroform and 100% methanol or aq 85% methanol containing both 2% KOH and 1.5mM sodium dithionite or 1.5mM dithionite alone (Table 1). The latter two solvents were used to extract Chls *a* and *b* from difficult-to-extract algae (Porra, 1990a,b). Alkali and dithionite presumably hydrolyze and reduce cell-wall proteins, respectively, allowing Chls to be extracted more readily with methanol (Thompson and Preston 1968); with KOH, however, Chls *a* and *b* are converted stoichiometrically to Mg-rhodochlorins (Mg-RChlns) *a* and *b,* and dithionite prevented their further conversion to hydroxylactone derivatives (Fig. 1). A 1:3 (v/v) methanol-chloroform mixture is an exceedingly efficient Chl extractant (Quail et al., 1976). In this method, Chls *a* and *b* are transferred to chloroform by aq. dilution and then determined by the appropriate simultaneous equations (Table 2); this extractant, however, is seldom used. Total extraction of Chls from leaf discs by prolonged immersion in DMF has been claimed (Moran and Porath, 1980) but rapid grinding of finely-cut leaf tissue in the chosen extractant with a pestle and mortar or Potter-Elvejhem homogenizor is the surest method and diminishes photo-oxidation of Chls during the prolonged immersion (Porra et al., 1989).

Of all these solvents, aq 80% acetone is strongly recommended because the Q_y absorption bands of the Chls *a* and *b* in this extractant are as sharply defined as in diethylether, DMF, DMSO and chloroform; however, aqueous acetone is less toxic than DMF, DMSO and chloroform. In methanol, an excellent Chl solvent, the Q_y peaks of Chls *a* and *b* are lower,

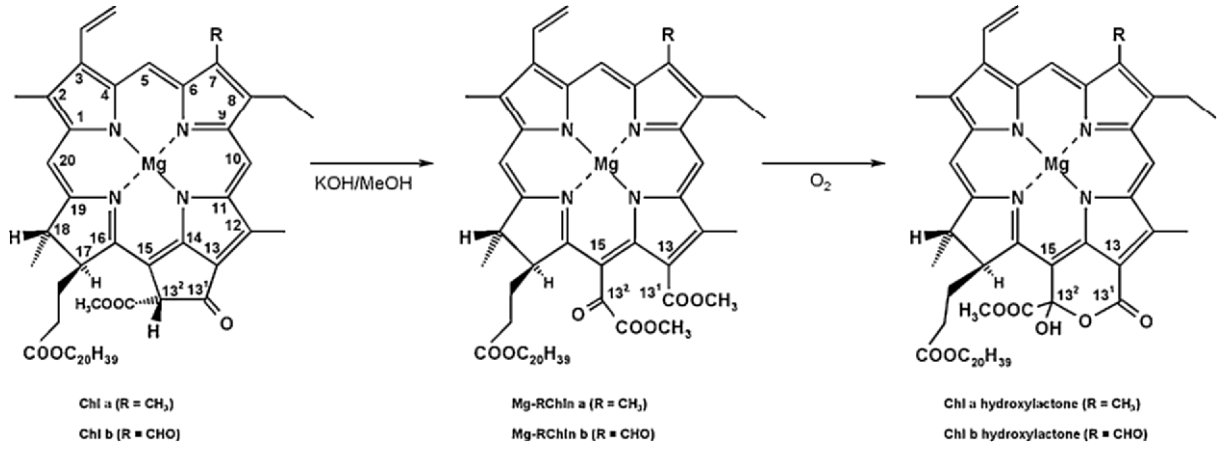

Fig. 1. The conversion of Chls *a* and *b* by alkaline methanolysis to Mg-rhodochlorins (Mg-RChlns) *a* and *b* by opening of isocyclic ring E and the subsequent formation of Mg-hydroxylactones *a* and *b* in the presence of O_2. Inclusion of oxygen into the hydroxylactone macrocycle is inhibited by reductants. The same reactions occur with the Mg-free Phes *a* and *b.*

Table 1. Accurate specific (α) and millimolar (ε_{mM}) extinction coefficients for Chls *a* and *b* in a variety of solvents and determined relative to the extinction coefficients of Smith and Benitez (1955) using the procedure described in Section III

		Difference Extinction Coefficients used in simultaneous equations in Table 2[a]				
		Chl *a*		Chl *b*		
Solvent	Wavelength [nm]	α [l•g^{-1}•cm^{-1}]	ε_{mM} [l•mmol^{-1}•cm^{-1}]	α [l•g^{-1}•cm^{-1}]	ε_{mM} [l•mmol^{-1}•cm^{-1}]	Reference
Buffered aq 80% acetone (pH 7.8)	663.6 646.6	85.95 20.79	76.79 18.58	10.78 51.84	9.79 47.04	Porra et al. (1989)
DMF	663.8 646.8	88.74 20.84	79.29 18.62	13.26 51.23	12.03 46.49	Porra et al. (1989)
DMSO	665.1 649.1	86.73 22.51	77.49[b] 20.11[b]	12.53 43.16	11.37[b] 39.17[b]	Wellburn (1994)
Chloroform	665.6 647.6	90.42 18.74	80.79[b] 16.74[b]	8.26 47.47	7.50[b] 43.08[b]	Wellburn (1994)
Methanol	665.2 652.0	75.95 35.42	71.43 31.65	22.26 42.48	20.20 38.55	Porra et al., (1989)
Aq 85% Methanol with dithionite	664.0 650.0	76.26 31.11	68.18 27.81	20.03 40.62	18.19 36.88	Porra (1990b)
Aq 85% Methanol in 2% KOH with dithionite[c]	640.0[c] 623.0[c]	53.61 19.38	47.93 17.32	7.92 19.49	7.18 17.69	Porra (1990a)

[a] The extinction coefficients are difference coefficients as the extinction at 750 is subtracted to correct for non-specific absorption. [b] These ε_{mM} coefficients in DMSO and chloroform were calculated from the α coefficients of Wellburn (1994) using Eq. (5) (Section IV). [c] The coefficients in alkaline methanol refer to Mg-rhodochlorins (Mg-RChlns) *a* and *b* as alkali opens ring E of the Chls (Fig. 1).

flatter, broader and closer together (Table 1) making the peaks more difficult to accurately measure. Diethylether is too volatile and inflammable to be safely used in routine Chl assays and is, therefore, not included in Table 1.

The updated list of accurate Chl *a* and *b* extinction coefficients in Table 1 were all determined relative to the specific (α) coefficients of Smith and Benitez (1955) in diethylether which are 100.9 for Chl *a* at 662 nm and 62.0 for Chl *b* at 644 nm: these coefficients were shown, by Mg determination using atomic absorption spectrometry, to have an error of less than

Table 2. Recommended simultaneous equations ('post Arnon equations') for assaying Chls *a* and *b* in various solvents using the accurate extinction coefficients presented in Table 1 which were calculated relative to the accurate coefficients of Smith and Benitez (1955) in diethylether.

Solvent	Interval between Chl *a* and *b* Q_y peaks (nm)[a]	Eqns for Chl *a* and *b* concentrations [nmol/ml]	Eqns for Chl *a* and *b* concentrations [µg/ml]	Reference
Buffered aq 80% acetone (pH7.8)	17.0 (i.e. 663.6–646.6)	[Chl *a*] = 13.71 $E^{663.6}$ – 2.85 $E^{646.6}$ [Chl *b*] = 22.39 $E^{646.6}$ – 5.42 $E^{663.6}$ [Chl *a*+*b*] = 19.54 $E^{646.6}$ + 8.29 $E^{663.6}$	[Chl *a*] = 12.25 $E^{663.6}$ – 2.55 $E^{646.6}$ [Chl *b*] = 20.31 $E^{646.6}$ – 4.91 $E^{663.6}$ [Chl *a*+*b*] = 17.76 $E^{646.6}$ + 7.34 $E^{663.6}$	Porra et al. (1989)
DMF	17.0	[Chl *a*] = 13.43 $E^{663.8}$ – 3.47 $E^{646.8}$ [Chl *b*] = 22.90 $E^{646.8}$ – 5.38 $E^{663.8}$ [Chl *a*+*b*] = 19.43 $E^{646.8}$ + 8.05 $E^{663.8}$	[Chl *a*] = 12.00$E^{663.8}$ – 3.11$E^{646.8}$ [Chl *b*] = 20.78$E^{646.8}$ – 4.88$E^{663.8}$ [Chl *a*+*b*] = 17.67$E^{646.8}$ + 7.12$E^{663.8}$	Porra et al. (1989)
DMSO	16.0	[Chl *a*] = 13.95 $E^{665.1}$ – 4.01 $E^{649.1}$ [Chl *b*] = 27.59 $E^{649.1}$ – 7.16 $E^{665.1}$ [Chl *a*+*b*] = 23.58 $E^{649.1}$ + 6.79$E^{665.1}$	[Chl *a*] = 12.47 $E^{665.1}$ – 3.62 $E^{649.1}$ [Chl *b*] = 25.06 $E^{649.1}$ – 6.50 $E^{665.1}$ [Chl *a*+*b*] = 21.44 $E^{649.1}$ + 5.97 $E^{665.1}$	Wellburn (1994)
Chloroform	18.0	[Chl *a*] = 12.84 $E^{665.6}$ – 2.02 $E^{647.6}$ [Chl *b*] = 24.0 $E^{647.6}$ – 4.99 $E^{665.6}$ [Chl *a*+*b*] = 21.98 $E^{647.6}$ + 7.85 $E^{665.6}$	[Chl *a*] = 11.47 $E^{665.6}$ – 2.0 $E^{647.6}$ [Chl *b*] = 21.85 $E^{647.6}$ – 4.53 $E^{665.6}$ [Chl *a*+*b*] = 19.85 $E^{647.6}$ + 6.94 $E^{665.6}$	Wellburn (1994)
Methanol	13.2	[Chl *a*] = 18.22 $E^{665.2}$ – 9.55 $E^{652.0}$ [Chl *b*] = 33.78 $E^{652.0}$ – 14.96 $E^{665.2}$ [Chl *a*+*b*] = 24.23 $E^{652.0}$ + 3.26 $E^{665.2}$	[Chl *a*] = 16.29 $E^{665.2}$ – 8.54 $E^{652.0}$ [Chl *b*] = 30.66 $E^{652.0}$ – 13.58 $E^{665.2}$ [Chl *a*+*b*] = 22.12 $E^{652.0}$ + 2.71 $E^{665.2}$	Porra et al. (1989)
Aq 85% methanol with dithionite	14.0	[Chl *a*] = 18.36 $E^{664.0}$ – 9.06 $E^{650.0}$ [Chl *b*] = 39.94 $E^{650.0}$ – 13.85 $E^{664.0}$ [Chl *a*+*b*] = 30.88 $E^{650.0}$ + 4.51 $E^{664.0}$	[Chl *a*] = 16.41 $E^{664.0}$ – 8.09 $E^{650.0}$ [Chl *b*] = 30.82 $E^{650.0}$ – 12.57 $E^{664.0}$ [Chl *a*+*b*] = 22.73 $E^{650.0}$ + 3.84 $E^{664.0}$	Porra (1990b)
Aq 85% methanol in 2% KOH with dithionite[b]	17.0	[Chl *a*] = 24.45 $E^{640.0}$ – 9.93 $E^{623.0}$ [Chl *b*] = 66.25 $E^{623.0}$ – 23.94 $E^{640.0}$ [Chl *a*+*b*] = 56.32 $E^{623.0}$ + 0.51 $E^{640.0}$	[Chl *a*] = 21.87 $E^{640.0}$ – 8.88 $E^{623.0}$ [Chl *b*] = 60.14 $E^{623.0}$ – 21.74 $E^{640.0}$ [Chl *a*+*b*] = 51.26 $E^{623.0}$ + 0.13 $E^{640.0}$	Porra (1990a)

[a] If an individual spectrophotometer records a different Chl *a* peak, the wavelength of the second reading should maintain the indicated interval. [b] These equations refer to Chls *a* and *b* after stoichiometric conversion to Mg-RChlns *a* and *b* by alkali which opens ring E (Fig. 1)

1% (Porra et al., 1989). Individual stock solutions of Chls *a* and *b* in diethylether were assayed using the Smith and Benitez (1955) coefficients. By removing the diethylether from measured volumes of the stock solutions by evaporation under O_2-free N_2 and replacing with identical volumes of the specified solvents, accurate α and ε_{mM} coefficients were calculated from the recorded absorption spectra (Table 1).

IV. Reliable Simultaneous Equations for the Accurate Assay of Chlorophylls *a* and *b*

A. Equations to Determine Chlorophylls a and b in Solvent Extracts of Plant and Algal Cells

Determining Chl *a* and *b* concentrations with simultaneous equations, correctly assumes that no other pigments in the extracts, such as carotenoids or other Chls and their derivatives, absorb at the Q_y maximum of either Chl *a* or Chl *b*; thus, Eqs. (1) and (2), in which the constants are the α coefficients for Chls *a* and *b* in aq 80% acetone (Table 1), are valid:

$$E^{663.6} = 85.95 \bullet [\text{Chl } a] + 10.78 \bullet [\text{Chl } b] \quad (1)$$

$$E^{646.6} = 51.84 \bullet [\text{Chl } b] + 20.79 \bullet [\text{Chl } a] \quad (2)$$

[Chl *a*] and [Chl *b*] represent Chl *a* and Chl *b* concentrations in g/l, and $E^{663.6}$ and $E^{646.6}$ are the extinctions of the aq 80% acetone extract at 663.6 and 646.6 nm, respectively. By standard mathematical techniques, these equations transform to the simultaneous Eqs. (3) and (4) (Table 2).

$$\text{Chl } a \text{ (}\mu\text{g/ml)} = 12.25 \bullet E^{663.6} - 2.55 \bullet E^{646.6} \quad (3)$$

$$\text{Chl } b \text{ (}\mu\text{g /ml)} = 20.31 \bullet E^{646.6} - 4.91 \bullet E^{663.6} \quad (4)$$

To obtain Chl *a* and *b* concentrations in nmol/ml, simultaneous equations must be generated replacing the specific (α) coefficients with millimolar (ε_{mM}) coefficients which are calculated from α coefficients as follows:

$$\varepsilon_{mM} = \alpha \bullet Mr \bullet 10^{-3} \quad (5)$$

where Mr for Chls *a* and *b* are 893.48 and 907.46, respectively.

Table 2 presents an updated list of reliable simultaneous equations to determine Chl *a* and *b* concentrations in a variety of solvents, either in nmol/ml or µg/ml, which were generated from the accurate extinction coefficients in Table 1: if a spectrophotometer records a wavelength for a Chl *a* peak differing from that in the relevant Eq. (say by 0.5 nm), the wavelength of the second extinction reading must change 0.5 nm to maintain the correct interval (Table 2). Using bandwidths of 2 nm or less, preferably between 0.1–0.5 nm, produce sharper absorption peaks and more accurate extinction coefficients (Wellburn, 1994).

The simultaneous equations in Table 2 can be recommended together with those published by other laboratories that had also detected the inaccuracy of the Arnon equations (Vernon, 1960; Ziegler and Egle, 1965, Delaporte and Laval-Martin, 1971a,b; Lichtenthaler, 1987; Porra et al., 1989; Wellburn, 1994): all such equations, designated here as 'post-Arnon equations', are reliable as they were all constructed with accurate extinction coefficients determined relative to the accurate coefficients of Smith and Benitez (1955) in diethylether. The equations for use with DMF (Moran and Porath, 1980; Moran, 1982; Inskeep and Bloom, 1985) and DMSO (Barnes et al., 1992) were derived from coefficients calculated relative to the faulty coefficients of Mackinney (1941) and should be replaced by the appropriate equations in Table 2.

B. High Chlorophyll a/b Ratios: A Problem for the Simultaneous Equation Method

Because of the very large overlap of the Q_y bands of Chls *a* and *b*, the absorption maximum of the small proportion of Chl *b* present when the Chl *a/b* ratio is high becomes a barely perceptible shoulder at ~647 nm on the rising absorption of the Chl *a* which peaks at ~664 nm. True Chl *a/b* ratios (Chl a/b^T), determined by post-Arnon equations, reach values of 11–14 in PSI-enriched fractions of chloroplast thylakoid membranes (Section V) but can be even higher in Chl *b*-deficient mutant tissues (Chunaev et al., 1991). Chl *a* and *b* determinations at such high Chl *a/b* ratios can be more accurately made spectrophotometrically by converting Chl *b* to its oxime which, like Chl *a,* has a peak at ~664 nm and then recording the increase in extinction at this wavelength: for details see Ogawa and Shibata (1965). Alternatively, Chl *b* can be determined under standard acidification conditions by

spectrophotometrically recording its slow demetallation rate (Laval-Martin, 1985): demetallation of Chl *a* is almost instantaneous. Both these methods have been extensively reviewed (Porra, 1991). Elegant spectrofluorimetric methods are suitable for Chl *a* and *b* determinations in the Chl *a/b* ratio range of 10–220 (Talbot and Sauer, 1997) while the method of Meister (1992) extends this range downwards to ~1.3 (Section IX.D).

V. The Unacceptable Errors and Consequences of Using the Arnon Equations

The errors reported in the extinction coefficients used by Arnon (1949) to construct his simultaneous equations are very large (Porra, 1991, 2002): for Chl *a* the errors are 19.43 and 4.55% at 663 and 645 nm, respectively, and for Chl *b* are 14.01 and 12.03% at the same wavelengths. It is illogical, therefore, that many workers still use Arnon's equations after so many laboratories (Vernon, 1960; Ziegler and Egle, 1965, Delaporte and Laval-Martin, 1971a,b; Lichtenthaler, 1987; Porra et al. 1989; Wellburn, 1994) have not only reported them unreliable but also published reliable post-Arnon equations.

Arnon's equations lead to erroneous Chl *a/b* ratios, designated Chl a/b^A, which are always lower than the true Chl a/b^T ratios determined by post-Arnon equations: the error increases alarmingly as the proportion of Chl *a* increases (see Fig. 2). When constructing Fig. 2, it was found that the true total Chl, $[\text{Chl } a+b]^T$ was always $0.895[\text{Chl } a+b]^A$. Thus, with the true total Chl and the true ratio from Fig. 2 it became a simple matter to correct the results of Arnon's equations and obtain true Chl *a* and *b* concentrations (Porra et al., 1989).

The absurdity of retaining the Arnon equations is apparent when the Chl a/b^A ratio range of 6.0–6.5 reported for PS I-enriched fractions of fragmented chloroplasts (Sane et al., 1970; Andersson et al., 1976) corresponds to a true Chl a/b^T range of 11.4 to 13.4 (Fig. 2) and when the Chl a/b^A ratio for the LHC I protein of 3.6 (Thornber, 1986) corresponds to a true Chl a/b^T value of 5.25.

Chl a/b^A ratios approximating 1.0 incur small errors (Fig. 2) which, however, significantly affect modeling. Using Arnon's assay, Butler and Kühlbrandt (1988) calculated for each LHC II pigment polypeptide a total, $[\text{Chl } a+b]^A$, of 15 Chls and a Chl a/b^A of 1.15 indicating 8 Chl *a* and 7 Chl *b*; however, this equates to $[\text{Chl a+b}]^T$ of 13.4 Chls and Chl a/b^T of 1.42 (Fig. 2) indicating 8 Chl *a* but only 6 Chl *b.* With the aq.80% acetone equations of Porra et al (see Table 2), Kühlbrandt et al (1994) found a $[\text{Chl } a+b]^T$ of 14 Chls and a Chl a/b^T = 1.3 also suggesting 8 Chl *a* and 6 Chl *b* but their electron crystallography results, at 3.4 Å resolution, showed only 12 Chl sites. Both recent high-resolution X-ray crystallography studies, by Liu et al. (2004) and Standfuss et al. (2005), unequivocally show that LHC II contains 8 Chl *a* and 6 Chl *b,* thus unambiguously confirming the

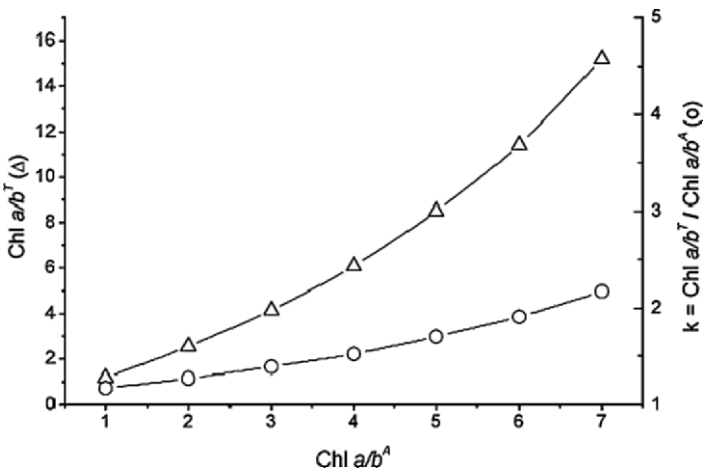

Fig. 2. The plot of true Chl a/b^T ratios against Arnon's Chl a/b^A ratios in aq 80% acetone (open triangles) and of the correction factor (k) against Chl a/b^A ratios (open circles). While $[\text{Chl } a+b]^T$ is simply $0.895[\text{Chl } a+b]^A$, the complex quadratic equation best fitting the first plot of Chl *a/b* ratios is:

$$\text{Chl } a/b^T = 0.593 + 0.4594 \text{ Chl } a/b^A + 0.2294 (\text{Chl } a/b^A)^2$$

accuracy of the 80% aq. acetone equations of Porra et al. (1989) in Table 2

VI. Other Spectrophotometric Assays for Chlorophylls *a* and *b* in Association with Their Derivatives or Other Pigments

Listed below are at least three other spectrophotometric assays employing simultaneous equations which are available for the determination of Chls in the presence of Chl derivatives including protochlorophyll or protochlorophyllide, PChl(id), and pheophytins (Phes). For a full description of these assays, the readers are referred to the original authors (see below) and an earlier review (Porra, 1991).

A. Chlorophylls a and b Together with Total Carotenoids

An assay for this combination of pigments has been developed in aq 80% acetone, DMF and DMSO (Lichtenthaler and Wellburn, 1983; Lichtenthaler, 1987 Wellburn, 1994)

B. Chlorophylls a and b Together with Protochlorophyll(ide)

Brouers and Michel-Wolwertz (1983) have developed an assay for mixtures of these three pigments in aq 80% acetone. PChlid is an intermediate in Chlid *a* biosynthesis (Benz and Rüdiger, 1981) and PChl may arise by oxidation of ring D of Chl *a* but such an oxidase is unknown.

C. Pheophytins a and b

Phe mixtures have been assayed in aq 90% acetone by Laval-Martin (1985) and in diethylether, methanol or aq 80% acetone by Lichtenthaler (1987). Phe(ides) *a* and *b* may arise by enzymic or non-enzymic demetallation of Chl(ides) *a* and *b.* Phe *a* is present in minute amounts in RC II.

VII. Spectrophotometric Assays for Chlorophylls in Chlorophyll *c*-containing Algae

The Chls *c* are an ever-increasing group of Mg-phytoporphyrins functioning as algal antenna Chls in association with Chl *a* or Chls *a* and *b.* The Chl *c* pigments, like other Chls, possess a fifth ring (*iso*-cyclic ring E) but ring D of the Mg-phytoporphyrins is not reduced at C-17 and -18 as in Chls *a* and *b* which are Mg-dihydrophytoporphyrins, also known as Mg-chlorins (see Chapter 1, Scheer; Chapter 2, Senge; Chapter 3, Zapata et al.). As discussed in these chapters, Chls *c* differ markedly in structural complexity having Mr values between 611 (Helfrich et al., 1999) and 1313 (Garrido et al., 2000). The possible biogenetic relationships between members of the Chls *c* group and with the biosynthesis of Chl *a* has been discussed (Porra, 1997; Porra et al., 1997; Chapter 18, Larkum).

HPLC systems interfaced to spectrophotometric or spectrofluorimetric detectors have been extensively used for separation and quantification of carotenoids and Chls of phytoplankton: these methods have been extensively reviewed in a recent book on phytoplankton pigments (Jeffrey et al., 1997). Further, Jeffrey et al. (1999) discuss new HPLC systems permitting the separation of divinyl Chls *a* and *b* and new polar and non-polar Chls *c* (see Chapter 3, Zapata et al. and Chapter 8, Garrido and Zapata).

The most highly recommended simultaneous equations for spectrophotometric determinations of Chls *c,* in association with other Chls, have been extensively reviewed (Porra, 1991; Jeffrey et al., 1997).

VIII. Spectrophotometric Data for the Assay of Bacteriochlorophylls

There are many BChls and they are classified into two categories: Mg-dihydrophytoporphyrins, which include BChls *c, d,* and *e,* and Mg-bacteriochlorins including BChls *a, b* and *g* (Scheer, 1991; Chapter 1, Scheer; Chapter 2, Senge). While Mg-dihydrophytoporphyrins have one reduced ring, ring D (like plant Chls *a* and *b*), the Mg-bacteriochlorins are Mg-tetrahydophytoporphyrins with two reduced rings, rings B and D. For the structures of these pigments and their esterifying alcohols, see Scheer, 1991 and Chapter 1 (Scheer). The spectrophotometric properties and the assay of these pigments has been reviewed by Oelze (1985), Scheer (1988), Porra (1991, 2002) and Richards (1994): an updated list of these properties is presented in Table 3. Currently, no simultaneous equations exist for the determination of these pigments when they occur in combinations with other Chls. Millimolar (ε_{mM}) extinction coefficients from these reviews and other papers are

Table 3. Spectroscopic properties and millimolar extinction coefficients of BChls. The Mg-bacteriochlorins, BChls *a*, *b* and g are grouped together as are the Mg-chlorins, BChls *c*, *d* and *e*

BChl	Solvent	Millimolar Extinction Coefficients Peak wavelengths in nm; [ε_{mM}]						Soret:Q_y	Reference
A:	**Mg-Bacteriochlorin type pigments**								
BChl *a*	Diethylether	358.5 [73.4]	391.5 [48.1]	530 [2.7]	577 [20.9]	697 [9.1]	773 [91.2]	0.80	Smith and Benitez (1955)
		358 [85.4]	391 [52.8]		575 [22.1]	697 [11.5]	772 [96.0]	0.89	Weigl (1953)
		357 [73.4]	392 [47.1]		573 [22.0]		770 [96.0]	0.76	Sauer et al., (1966)
	Acetone	358 [65.7]			576.5 [19.4]		770 [69.2]	0.94	Sauer et al., (1966)
	Methanol						772 [60.0]		Cohen-Bazire et al., (1966)
	Ethanol	365.5 [58.5]			607 [15.2]		773 [62.0]	0.94	Sauer et al., (1966)
BChl *b*	Diethylether	368 [81]	408 [78]		578 [25]	676 [18]	794 [100]	0.81	Steiner (1981)
							794 [106]		Scheer and Steiner (1985)[a]
	Acetone	368 [94]	407 [82]		580 [27]		794 [100]	0.94	Baumgarten (1970)
BChl *g*	Acetone	364.8	404.8		566.4		761.6 [76]		van de Meent et al., (1991)
B.	**Mg-Chlorin type pigments**								
BChl *c*	Diethylether	412 [72.6]	432 [142]			622 [15.9]	660 [91.0]	1.56	Stanier and Smith (1960)
(809)[b]	Acetone	413 [71.8]	433 [115.5]			625 [13.7]	662.5 [74.9]	1.54	Stanier and Smith (1960)
	Methanol	419 [69.7]	435 [79.1]			620 [14.6]	670 [69.6]	1.14	Stanier and Smith (1960)
BChl *d*	Diethylether	406 [69]	425 [115.6]	530 [2.7]	575 [6.8]	612 [12.5]	650 [89.9]	1.28	Stanier and Smith (1960)
(792)[b]	Acetone	406 [69.6]	427 [99.7]	530 [3.1]	575 [7.3]	612.5 [13.0]	654 [77.6]	1.28	Stanier and Smith (1960)
	Methanol	411 [60.6]	427 [66.1]			612.5 [14.3]	659 [65.2]	1.01	Stanier and Smith (1960)
BChl *e*	Acetone		462 [185.0]				649 [48.9]	3.78	Borrego et al., (1999)
(835.1)[c]	Acetone/MeOH (7:2)		466 [155.6]				651 [41.4]	3.76	Borrego et al., (1999)
	Methanol		476 [130.7]				660 [35.5]	3.68	Borrego et al., (1999)
	Ethanol		469 [142.3]				654 [41.0]	3.47	Borrego et al., (1999)

[a] Re-determined by Scheer and Steiner (cf. Oelze 1985). [b] These Mr values were employed to calculate ε_{mM} values from the specific α extinction coefficients of Stanier and Smith (1960). [c] These ε_{mM} values were calculated by Borrego et al., (1999) using an Mr value of 835.1 for the [8-propyl-12-ethyl-17^3-farnesyl]-homologue of BChl *e*.

assembled in Table 3. Many homologues of BChls *c, d* and *e* exist (See Chapter 1, Scheer and Chapter 15, Freegard et al.); for example, Airs et al., (2001) have isolated thirty BChl *e* homologues using HPLC from a *Chlorobium phaeobacteroides* strain with Mr values between 763 and 887. The ε_{mM} value for BChl *e* (see Table 3) was calculated by Borrego et al., (1999) using an Mr value of 835.1 for the [8-propyl-12-ethyl-17^3-farnesyl]-homologue of BChl *e*. Borrego et al. (1999) also calculated the ε_{mM} values for BChls *c* and *d* (see Table 3) from the α coefficients of Stanier and Smith (1960): these original α coefficients can be determined with Eq. (5) using 809 and 792 for the Mr values of BChls *c* and *d*, respectively.

IX. Spectrofluorimetric Assays for Chlorophylls *a* and *b*

A. Advantages and Disadvantages of Spectrofluorimetric Assays

Plant Chls fluoresce strongly when irradiated at their Soret absorption maxima (Chapter 1, Scheer) enabling spectrofluorimetric methods to assay Chls in the pmol/ml range while spectrophotometry is reliable only in the nmol/ml range and only then if the true Chl a/b^T ratio does not exceed ~15 thus obscuring a clear Chl *b* Q_y peak.

Unfortunately, the constants for determining the concentrations of Chl *a* and *b* mixtures by spectrofluorimetry are not as universally applicable as spectrophotometric extinction coefficients (see below): they vary significantly between individual spectrofluorimeters which require frequent calibration. A single Chl can be assayed with a simple fluorimeter from a calibration curve of fluorescence amplitudes (intensities) constructed with Chl solutions of known concentrations but the assay of Chl mixtures requires a sophisticated spectrofluorimeter with automatic correction for photomultiplier responses, for both monochromator characteristics delivering actinic light and receiving emitted fluorescence, and for wavelength-dependent variation in energy output of the actinic light source.

An advantage of spectrofluorimetry for assaying Chl *a* and *b* mixtures is that selective excitation of the minor Chl *b* component by irradiation with 453nm light (the Chl *b* Soret maximum in diethylether) helps negate the disadvantage imposed by the generally lower concentration of Chl *b* because Chl *a* absorption at 453nm relative to Chl *b* is much reduced and thus the fluorescence yield of Chl *a* relative to Chl *b* is lowered. Boardman and Thorne (1971) showed, with 453nm irradiation, that Chl *b* in a diethylether solution (Chl $a/b \equiv 1.3$) produced more intense fluorescence (F_b) at 646nm than Chl *a* (F_a) at 666nm and, because F_a and F_b are related to the molar concentrations of Chls *a* and *b,* respectively, Chl *a* and *b* could thus be accurately determined at room temperature by fluorescence emission even with large excesses of Chl *a* present (Boardman and Thorne, 1971; see also equations in Section IX B).

B. Equations for the Spectrofluorimetric Assay of Chlorophyll a and b Mixtures in Diethylether

For individual solutions of Chl *a* and Chl *b* in diethylether excited with 453nm light at room temperature, Boardman and Thorne (1971) found the following relationships between Chl concentration and fluorescence emission:

$$F_a = k_1[\text{Chl } a] \quad (6)$$

$$F_b = k_2[\text{Chl } b] \quad (7)$$

Because of the overlap in the fluorescence emission spectra of Chls *a* and *b,* Eqs. (6) and (7) do not apply to mixed solutions and must be replaced by Eqs. (8) and (9):

$$F'_a = k_1[\text{Chl } a] + K_b \bullet k_2[\text{Chl } b] \quad (8)$$

$$F'_b = k_2[\text{Chl } b] + K_a \bullet k_1[\text{Chl } a] \quad (9)$$

where K_b is the ratio of the fluorescence emission amplitude of Chl *b* at 666 nm (the Chl *a* emission peak) relative to its amplitude at 646 nm (the Chl *b* emission peak), while K_a is the amplitude of Chl *a* at 646 nm relative to its amplitude at 666 nm. Both K_a (0.185) and K_b (0.142) and also k_1 and k_2 can be calculated directly from the emission spectra of pure solutions of Chls *a* and *b*. Then spectrofluorimetric simultaneous equations can be written to solve for (Chl *a*) and (Chl *b*) as was done for spectrophotometric methods (see Section IV).

C. Determination of Chlorophyll a/b Ratios by Spectrofluorimetry

K_a and K_b were determined in diethylether as 0.185 and 0.142, respectively. Thus Eq. (10), which was calculated from Eqs. (8) and (9) becomes Eq. (11):

$$\text{Chl } a/b = (k_2/k_1)\bullet\{(F'_a/F'_b - K_b) /(1 - K_a F'_a/F'_b)\} \quad (10)$$

$$\text{Chl } a/b = (k_2/k_1)\bullet \{(F'^{666}/F'^{646} - 0.142) /(1 - 0.185\bullet F'^{666}/F'^{646})\}. \quad (11)$$

Equation (10) is sometimes abbreviated as shown in Eq. (12):

$$\text{Chl } a/b = (\mathbf{m})\bullet\{\mathbf{R}\} \quad (12)$$

where **m** equals (k_2/k_1) and **R**, known as the corrected fluorescence ratio, is the term included in **{ }** in Eqs. (10) and (11). The constants k_1, k_2, K_a and K_b, and hence **m** and **R**, are all dependent on the solvent used, the emission wavelengths, and also on instrument parameters such as band widths. Consequently, these constants must be newly determined for each spectrofluorimeter used and for each solvent used.

Boardman and Thorne (1971) plotted Chl *a/b* against **R** for a series of standards with Chl *a/b* ratios of 6–60 and showed that the slope **m** (i.e. k_2/k_1) was 21, so that Eq. (11) becomes Eq. (13) when using their particular instrument and diethylether as solvent.

$$\text{Chl } a/b = 21\bullet\{(F'^{666}/F'^{646} - 0.142) /(1 - 0.185\bullet F'^{666}/F'^{646})\} \quad (13)$$

To obtain the Chl *a/b* ratio, the fluorescence emission values of the Chl mixture at 646 nm (F'^{646}) and at 666 nm (F'^{666}) were entered into Eq. (13).

D. Determination of Chlorophyll a/b Ratios in Water-miscible Solvents

Talbot and Sauer (1997) showed that the spectrofluorimetric method of Boardman and Thorne (1971) is also valid for water-miscible solvents such as aq 80% acetone, DMF and DMSO which are commonly used Chl extractants. Talbot and Sauer (1997) plotted **R** against Chl *a/b* ratio ranges from 10–125 in DMSO and from 10–220 in diethylether, aq 80% acetone, and DMF (see Table 4). The coefficients K_a and K_b and ratio k_2/k_1 results of Boardman and Thorne (1971) in diethylether (shown in brackets) differ from those of Talbot and Sauer (1997) who suggested that instrument differences were involved. This emphasizes the need for constant calibration, for determination of constants for individual spectrofluorimeters and for strict control of entry and exit slit widths for both excitation and emission monochromators.

Talbot and Sauer (1997) showed that sensitivity limits in determining Chl *a/b* ratios in various solvents increased not only with slope **m** and but also, not surprisingly, with increases in the wavelength difference (Δ) between the fluorescence emission peaks of Chls *a* and *b*. Solvents were rated as follows**:** diethylether (**m=39.9**: Δ=19 nm)> aq 80% acetone (**24.3**; 16 nm)> DMF (**18.5**; 16 nm)> DMSO (**11.0**; 12 nm).

Another method (Meister, 1992), using the optimal excitation wavelengths of both pigments, can extend this wide range of ratios to include downwards to normal biological Chl *a/b* ratios (~3.0–4.0), where the single Chl *b* excitation wavelength method is less accurate (Boardman and Thorne 1971; Talbot and Sauer, 1997).

E. Spectrofluorimetric Assays for Chlorophyll Intermediates and Catabolites

Fluorescence spectrometry, by selective excitation of minor Chl components in a mixture, is a very sensitive method for detection of cross-contaminants (e.g. in Chls *a* and *b* isolates); similarly, it can be used to assay Chl intermediates or catabolites using irradiation at their Soret maximum to overcome the disadvantage of their low concentrations relative to those of the major products. Spectrofluorimetric assays have been developed for the following combinations of fluorescent Chl derivatives: PChl(ide) and Chl(ides) *a* and *b* (see Rebeiz et al., 1975); Phe(ides) *a* and *b* and Chl(ides) *a* and *b* (Bazzaz and Rebeiz, 1979); and, Chl(ides) *a* and *b* (which are 3-monovinyl (MV) compounds) and their 3,8 divinyl (DV) forms (Wu et al., 1989). [DV]-Chls *a* and *b* occur only transiently in greening plants (Ioannides et al., 1994) but, in some microalgae of subtropical oceans, they play a major role in global photosynthesis (Chisholm et al., 1992; Goericke and Repeta, 1993). For details of the extraction of the above pigment groups in 90% acetone in 0.01N-NH_4OH, the separation of their phytylated and unphytylated forms, the required excitation and emission wavelengths in ammoniacal acetone, the derivation of the necessary equations, of correction procedures and of the multitude of constants required

Table 4. Calibration parameters for fluorimetric determination of Chls *a* and *b* in various solvents. Data supplied by Talbot and Sauer (1997)

Solvent:	Diethylether		Aq 80% acetone	DMF	DMSO
Excitation maxima	453 nm	(453)[a]	461 nm	462 nm	463 nm
Emission maxima					
Chl *a*	666 nm	(666)[a]	672 nm	672 nm	674 nm
Chl *b*	647 nm	(646)[a]	656 nm	656 nm	662 nm
K_a	0.0573	(0.185)[a]	0.237	0.234	0.433
K_b	0.132	(0.142)[a]	0.423	0.435	0.631
Slope ($m = k_2/k_1$)	39.9	(21.0)[a]	24.3	18.5	11.0

[a] The figures in parentheses are those obtained by Boardman and Thorne (1971)

for their assay, readers are referred to the original papers and their extensive appendices.

New and possibly simpler assays for these intermediates and catabolites are now available using new HPLC methods interfaced with various detection techniques (Chapter 8, Garrido and Zapata).

X. Concluding Remarks

In summary, the light absorption and fluorescence emission properties of Chls provide a vast number of reliable spectrophotometric and spectrofluorimetric assays for Chls and their derivatives after extraction from photosynthetic cells and tissues in a wide variety of solvents.

Acknowledgments

I thank CSIRO-Plant Industry, Canberra, for an Honorary Research Fellowship and the Sonderforschungsbereich (Projekt 533) for financial support while visiting the Department Biologie I-Botanik, Universität München. I am grateful to CSIRO and Universität München for use of their communications and library facilities during the preparation of this chapter. I also thank Professor Hugo Scheer for valuable discussions and Professor Peter Dittrich for generously providing computer facilities, a fine office and his splendid home for living accommodation.

References

Airs RL, Borrego CM, Garcia-Gil and Keely BJ (2001) Identification of the bacteriochlorophyll homologues of *Chlorobium phaeobacteroides* strain UdG6053 grown at low light intensity. Photosynth Res 70: 221–230

Andersson B, Åkerlund H-E and Albertsson, P-Å (1976) Separation of sub-chloroplast membrane particles by counter-current distribution. Biochim Biophys Acta 423: 122–132

Arnon DI (1949) Copper enzymes in isolated chloroplasts. Polyphenoloxidase in *beta vulgaris*. Plant Physiol 24: 1–15

Barnes JD, Balaguer L, Manrique E, Elvira S and Davison AW (1992) A reappraisal of the use of DMSO for the extraction and determination of chlorophylls *a* and *b* in lichens and higher plants. Environm Exp Bot 32: 85–100

Baumgarten D (1970) The structure of bacteriochlorophyll *b*. MS Thesis, University of California, Berkeley

Bazzaz MB and Rebeiz CA (1979) Spectrofluorometric determination of chlorophyll(ide) *a* and *b* and pheophytin (or pheophorbide) *a* and *b* in unsegregated pigment mixtures. Photochem Photobiol 30: 709–721

Benz J and Rüdiger W (1981) Chlorophyll biosynthesis: Various chlorophyllides as exogenous substrates for chlorophyll synthetase Z Naturforsch 36c: 51–57

Boardman NK and Thorne SW (1971) Sensitive fluorescence method for the determination of chlorophyll *a*/chlorophyll *b* ratios. Biochim Biophys Acta 253: 222–231

Borrego CM, Arellano JB, Abella CA, Gillbro T and Garcia-Gil J. (1999) The molar extinction coefficient of bacteriochlorophyll *e* and the pigment stoichiometry in *Chlorobium phaeobacteroides.* Photosynth Res 60: 257–264

Brouers M and Michel-Wolwertz M-R (1983) Estimation of protochlorophyll(ide) contents in plant extracts: Re-evaluation of the molar absorption coefficients of protochlorophyll(ide). Photosynth Res 4: 265–270

Butler PJG and Kühlbrandt W (1988) Determination of the aggregate size in detergent solution of the light-harvesting chlorophyll *a/b*-protein complex from chloroplast membranes. Proc Nat Acad Sci USA 85: 3797–3801

Chisholm SW, Frankel SL, Goericke R, Olson RJ, Palenic B, Waterbury JB, West-Johnsrud L and Zettler ER (1992) *Prochlorococcus marinus* nov. *gen.* nov. *sp.*: An oxyphototropic marine prokaryote containing divinyl chlorophyll *a* and *b.* Arch Microbiol 157: 297–330

Chunaev AS, Mirnaya ON, Maslov VG and Boschetti A (1991) Chlorophyll *b*- and loroxanthin-deficient mutants of *Chlamydomonas reinhardii*. Photosynthetica 25: 291–301

Cohen-Bazire G and Sistrom WR (1966) The procaryotic pho-

tosynthetic apparatus. In: Vernon LP and Seely GR (eds). The Chlorophylls, pp 313–341. Academic Press, New York

Comar CL and Zscheile FP (1942) Analysis of plant extracts for chlorophylls *a* and *b* by a photoelectric spectrophotometric method. Plant Physiol 17: 198–209

Delaporte N and Laval Martin D (1971a) Analyse spectrophotometrique des chlorophylles et des pheophytines *a* et *b* en milieu hydroacetonique: I. Determination extinctions molaires. Anal Chem Acta 55: 415–424

Delaporte N and Laval Martin D (1971b) Analyse spectrophotometrique des chlorophylles et des pheophytines *a* et *b* en milieu hydroacetonique: II. Methode Cinetique de dosage. Anal Chem Acta 55: 425–435

Garrido JL, Otero J, Maestro MA and Zapata M (2000) The main non-polar chlorophyll *c* from *Emiliania huxleyi* (Prymnesiophyceae) is a chlorophyll c_2-monogalactosyldiacyl-glyceride ester: A mass spectrometry study. J Phycol 36: 497–505

Goericke R and Repeta DJ (1993) Chlorophylls *a* and *b* and divinyl chlorophylls *a* and *b* in the open sub-tropical North Atlantic Ocean. Marine Ecol Prog Ser 101: 307–313

Helfrich M Ross A, King GC Turner AG and Larkum AWD (1999) Identification of 8-[vinyl]-protochlorophyllide *a* in phototropic prokaryotes and algae: Chemical and spectroscopic properties. Biochim Biophys Acta 1410: 262–272

Inskeep WP and Bloom PR (1985) Extinction coefficients of chlorophyll *a* and *b* in N,N-dimethylformamide and 80% acetone. Plant Physiol 77: 483–485

Ioannides MI, Fasoula DA, Robertson KR and Rebeiz CA (1994) An evolutionary study of chlorophyll biosynthetic heterogeneity in green plants. Biochem Syst Ecol 22: 211–220

Jeffrey SW, Mantoura RFC and Wright SW (eds) (1997) Phytoplankton Pigments in Oceanography. UNESCO Publishing, Paris

Jeffrey SW, Wright SW and Zapata M (1999) Recent advances in HPLC pigment analysis of phytoplankton. Mar Freshwater Res 50: 879–896

Kühlbrandt W, Wang DN and Fujiyoshi Y (1994) Atomic model of plant light-harvesting complex by electron crystallography. Nature 367: 614–621

Laval-Martin DL (1985) Spectrophotometric method of controlled pheophytinization for the determination of both chlorophylls and pheophytins in plant extracts. Anal Biochem 149: 121–129

Lichtenthaler HK (1987) Chlorophylls and carotenoids: Pigments of photosynthetic membranes. Methods Enzymol 148: 350–382

Lichtenthaler HK and Wellburn AR (1983) Determination of total carotenoids and chlorophylls *a* and *b* of leaf extracts in different solvents. Biochem Soc Trans 11: 591–592

Liu Z, Yan H, Wang K Kuang T, Zang J, Gul L, An X and Chang W (2004) Crystal structure of spinach major light-harvesting complex at 2.72 Å resolution. Nature 428: 287–292

Mackinney G (1941) Absorption of light by chlorophyll solutions. J Biol Chem 140: 315–322.

Meister A (1992) New fluorometric method for determination of chlorophyll *a/b* ratio. Photosynthetica 26: 533–539

Moran R (1982) Formulae for determination of chlorophyllous pigments extracted with N,N-dimethylformamide. Plant Physiol 69: 1376–1381

Moran R and Porath D (1980) Chlorophyll determination in intact tissues using N,N-dimethylformamide. Plant Physiol 65: 478–479

Oelze J (1985) Analysis of bacteriochlorophylls. Methods Microbiol 18: 257–284

Ogawa T and Shibata K (1965) A sensitive method for determining chlorophyll *b* in plant extracts. Photochem Photobiol 4: 193–200

Porra RJ (1990a) The assay of chlorophylls *a* and *b* converted to their respective magnesium-rhodochlorin derivatives by extraction from recalcitrant algal cells with aqueous alkaline methanol: Prevention of allomerization with reductants. Biochim Biophys Acta 1015: 493–502

Porra RJ (1990b) A simple method for extracting chlorophylls from the recalcitrant alga, *Nannochloris atomus*, without formation of spectroscopically-different magnesium-rhodochlorin derivatives. Biochim Biophys Acta 1019: 137–141

Porra RJ (1991) Recent advances and re-assessments in chlorophyll extraction and assay procedures for terrestrial, aquatic, and marine organisms, including recalcitrant algae. In: Scheer H (ed) Chlorophylls, pp 31–57. CRC Press, Boca Raton

Porra RJ (1997) Recent progress in porphyrin and chlorophyll biosynthesis. Photochem Photobiol 65: 492–516

Porra RJ (2002) The chequered history of the development and use of simultaneous equations for the accurate determination of chlorophylls *a* and *b*. Photosynth Res 73: 149–156

Porra RJ, Thompson WA and Kriedemann PE (1989) Determination of accurate extinction coefficients and simultaneous equations for assaying chlorophylls *a* and *b* extracted with four different solvents: Verification of the concentration of chlorophyll standards by atomic absorption spectrometry. Biochim Biophys Acta 975: 384–394

Porra RJ, Pfündel E and Engels N (1997) Metabolism and function of photosynthetic pigments. In: Jeffrey SW, Mantoura RFC and Wright SW (eds) Phytoplankton Pigments in Oceanography, pp 85–126. UNESCO Publishing, Paris

Quail PH, Gallagher A and Wellburn A (1976) Membrane-associated phytochrome: Non-coincidence with plastid membrane marker profiles on sucrose gradients. Photochem Photobiol 24: 495–498

Rebeiz CA, Mattheis JR, Smith BB, Rebeiz CC and Dayton DF (1975) Chloroplast biogenesis: Biosynthesis and accumulation of protochlorophyll by isolated etioplasts and developing cotyledons. Arch Biochem Biophys 171: 549–567

Richards WR (1994) Analysis of Pigments: Bacteriochlorophylls. In: Goodfellow M and O'Donnell AG (eds) Chemical Methods in Prokaryotic Systematics, pp 345–401. John Wiley and Sons Ltd, New York

Sane PV, Goodchild DJ and Park RB (1970) Characterization of chloroplast photosystems 1 and 2 separated by a non-detergent method. Biochim Biophys Acta 216: 162–178

Sauer K, Smith JRL and Schultz AJ (1966) The dimerization of chlorophyll *a*, chlorophyll *b* and bacteriochlorophyll in solution. J Amer Chem Soc 66: 2681–2688

Scheer H (1988) Chromatographic methods for the separation of chlorophylls In: Köst H-P (ed) Handbook of Chromatography: Plant Pigments, pp 235–307. CRC Press, Boca Raton

Scheer H (1991) Structure and occurrence of chlorophylls. In: Scheer H (ed) Chlorophylls, pp 3–30, CRC Press, Boca Raton

Smith JHC and Benitez A (1955) Chlorophylls: Analysis in plant materials. In: Paech K and Tracey MV (eds) Modern Methods of Plant Analysis, Vol IV, pp 142–196. Springer-Verlag, Berlin

Standfuss J, Terwisscha van Scheftinga AC, Lamborghini M and Kühlbrandt W (2005) Mechanisms of photoprotection and nonphotochemical quenching in pea light-harvesting complex at 2.5 Å resolution. EMBO J 24: 919–928

Stanier RY and Smith JHC (1960) The chlorophylls of green bacteria. Biochim Biophys Acta 41: 478–484

Steiner R (1981) Bacteriochlorophyll *b* aus *Ectothiorhodospira halochloris.* Zulassungsarbeit, University of Munich

Talbot MFJ and Sauer K (1997) Spectrofluorimetric method for the determination of large chlorophyll *a/b* ratios. Photosynth Res 53: 73–79

Thompson EW and Preston RD (1968) Evidence for a structural role of protein in algal walls. J Exp Botany 19: 690–697

Thornber JP (1986) Biochemical characterization and structure of pigment-proteins of a photosynthetic organism. In: Staehelin LA and Arntzen CJ (eds) Encyclopedia of Plant Physiology 'Photosynthesis III,' Vol 19, pp 98–142. Springer-Verlag, Berlin

van de Meent EJ, Kobayashi M, Erkelens C, van Veelen PA, Amesz J and Watanabe T (1991) Identification of 8^1-hydroxychlorophyll *a* as a functional reaction centre pigment in heliobacteria. Biochim Biophys Acta 1058: 356–362

Vernon LP (1960) Spectrophotometric determination of chlorophylls and pheophytins in plant extracts. Anal Chem 32: 1144–1150

Weigl JW (1953) The absorption spectrum of bacteriochlorophyll J Amer Chem Soc 75: 999–1000

Wellburn, AR (1994) The spectral determination of chlorophylls *a* and *b*, as well as total carotenoids using various solvents with spectrophotometers of different resolution. J. Plant Physiol 144: 307–313

Wu S-M, Mayasich JM and Rebeiz CA (1989) Chloroplast biogenesis: Quantitative determination of monovinyl and divinyl chlorophyll(ide) *a* and *b* by spectrofluorometry. Anal Biochem 178: 294–300

Ziegler R and Egle K (1965) Zur quantitativen Analyse der Chloroplastenpigmente. I. Kritische Überprüfung der spektralphotometrischen Chlorophyll Bestimmung. Beitr Biol Planzen 41: 11–37

Chapter 8

Chlorophyll Analysis by New High Performance Liquid Chromatography Methods

José L. Garrido*
Instituto de Investigacións Mariñas de Vigo (CSIC), Eduardo Cabello 6, E36208-Vigo, Spain

Manuel Zapata
Centro de Investigacións Mariñas, Consellería de Pesca, Xunta de Galicia, Apdo.13, E36620-Vilanova de Arousa, Spain

Summary

The improvements in high performance liquid chromatography (HPLC) analysis of chlorophylls (Chls) and bacteriochlorophylls (BChls) during the last decade rely mainly on the application of newly developed stationary phases combined with new mobile phases developed with special regard to the nature of the ion-pairing agents employed for achieving the retention of free acid forms, which is especially important for the Chls *c* group. The application of mass spectrometry (MS) as a detection technique coupled on-line with liquid chromatography (LC) has provided important structural information. All these tools have contributed to the discovery of the biosynthetic pathways of higher plant Chls, to the study of the composition and distribution of new Chls in algae, and to the characterization of complex pools of BChls. Faster, more sensitive and more specific HPLC methods are expected in the very near future, with the development of new columns and detection techniques, e.g. monolithic stationary phases and coupled liquid chromatography-nuclear magnetic resonance (LC-NMR) systems.

*Author for correspondence, Email: garrido@iim.csic.es

Bernhard Grimm, Robert J. Porra, Wolfhart Rüdiger and Hugo Scheer (eds): Chlorophylls and Bacteriochlorophylls: Biochemistry, Biophysics, Functions and Applications, pp. 109–121.

I. Introduction

The chromatographic analysis of chlorophylls (Chls) is still an analytical challenge because they constitute a group of compounds that exhibit a wide range of polarities, from the very non polar phytol- and lipid-esterified Chls and Phes to the polar Chl *c* compounds, Chlides and PChlides, all of which contain a free carboxylic acid group (chapters 1, Scheer and 3, Zapata et al.).

Many of these compounds are structurally very similar, and may differ only in the position of a double bond. Recent evidence shows that Chls are formed via two routes containing di- and mono-vinyl ([DV]- and [MV])-tetrapyrrole intermediates (Ioannides et al., 1994; von Wettstein, 1995; Porra, 1997; Rüdiger, 1997; Beale, 1999; chapter 10, Grimm and Rüdiger). This biosynthetic heterogeneity explains the occurrence of various [MV]- and [DV]-derivatives of both porphyrins and/or chlorins during the greening of etiolated tissues in different plants (Shioi and Takamiya, 1992; Rebeiz et al., 1994), the variety of Chl *c* forms described in chromophyte algae (Chapter 3, Zapata et al.) and the prevalence of [DV]-Chl *a* and [DV]-Chl *b* in the euphotic zone of tropical oceans (Chisholm et al., 1992; Goericke and Repeta, 1993). Consequently, much effort in the field of analytical HPLC of Chls has recently focused on the separation of [MV]-pigments from their corresponding [DV]-analogues. The complexity of pigment extracts and the minor differences among Chls often makes separation of individual species difficult. The situation becomes more complicated when accompanying pigments (xanthophylls, carotenes) have also to be analyzed.

Shioi (1991) thoroughly reviewed the instrumental and analytical aspects of chromatographic techniques applied to Chl compounds: most have not changed, so we will concentrate on new methods, their basis and their fields of application.

Abbreviations: C_{18} – octadecylsilica; C_8 – octylsilica; DHgg – dihydrogeranylgeraniol; DV – divinyl; f – farnesol; Gg – geranylgeraniol; HPLC – high performance liquid chromatography; LC – liquid chromatography; MGDG – monogalactosyldiacylglycerol; MgDVP – Mg-[3,8-divinyl]-phytoporphyrin-13^2-methylcarboxylate (i.e. [DV]-PChlide); MS – mass spectrometry; MV – monovinyl; NMR – nuclear magnetic resonance; ODP – octadecyl-polyvinyl-alcohol polymer; ODS – octadecylsilica; OS – octylsilica; p – phytol; RP – reversed phase; THgg – tetrahydrogeranylgeraniol. Unless otherwise specified, Chls and their derivatives (i.e. Chlides, PChlides, Phes *etc.*) are [3-vinyl-8-ethyl]-(i.e. [MV]-) compounds but some Chls *c* are exceptions: Chls c_2, c_2MGDG, c_3, $c_{3(CS\text{-}170)}$ and [DV]-PChlide are all [3,8-divinyl]-(i.e. [DV]-) compounds (see Chapter 3, Figure 1).

II. New Bonded Phase Columns

The development of new HPLC methods comes from the availability of new stationary phases with general characteristics (particle size and shape, base material purity, etc.) which have greatly improved during the past decade. While monomeric octadecyl silica (ODS, C_{18}) columns remain the most frequently used stationary phases for the analysis of Chls, the need to simultaneously separate [MV]- and [DV]-forms of polar and non-polar Chls required different approaches employing polymeric and monomeric silica-based phases and octadecyl-polyvinyl-alcohol polymer (ODP) phases.

A. Silica-Based Columns

1. Polymeric Bonded Phases

Although separation of [MV]-Chl derivatives from their respective [DV]-analogues had been traditionally achieved by employing polyethylene columns (Shioi, 1991), these methods were lengthy and did not allow the simultaneous separation of polar and non polar pigments. By comparison, most of the methods achieving the separation of free and esterified pigments occurring in algae or etiolated tissues from higher plants show several multicomponent peaks corresponding to the coelution of the [MV]- and [DV]-analogues of a particular Chl derivative (Barry et al., 1991; Wright et al., 1991; Van Heukelem et al., 1992; Duke et al., 1993; Schoefs et al., 1995). Silica-based polymeric stationary phases exhibit very high selectivity towards very similar, even isomeric, compounds with rigid molecular structures, the so-called 'shape selectivity' (Sander et al., 1999). This special selectivity has been explained by the rigid nature of the polymeric layer, sometimes represented as a surface with slots into which the solute molecules penetrate during retention. The frequency and depth of this penetration (and, in consequence, the retention) depends on the overall shape of the solute molecule, its size, length and planarity (Sander and Wise, 1990). Several variables (pore size, alkyl chain length, bonding density, temperature and mobile-phase composition) can influence shape selectivity (Sander and Wise, 1990; Sander et al., 1999).

Shape selectivity, applied in the separation of different rigid compounds such as polycyclic aromatic hydrocarbons and carotenoids (Sander et al., 1999), was also used to separate [MV]- and [DV]-pairs of Chls. Although the [DV]-Chls are slightly more polar than the [MV]-Chls, the [DV]-forms elute *after* their [MV]-counterparts on these columns. The separation of 3-vinyl-8-ethyl (i.e. [MV]-) and 3,8-divinyl (i.e. [DV]-) substituted Chls is based on the differences in their molecular shape: in the [DV]-form, the 8-vinyl substituent and the tetrapyrrolic macrocycle are located in the same plane (as conjugated systems are greatly stabilized when the double bonds are coplanar), whereas the [MV]-forms, with an 8-ethyl substituent adopt a non-planar conformation, so that the steric hindrance is the smallest (Fig. 1). In consequence, the more planar [DV]-forms are retained longer than the corresponding [MV]-forms (Garrido and Zapata, 1997).

The difference in molecular shape, induced by an ethyl or a vinyl substituent at C-8, is reduced if a voluminous group is present at C-7 of the macrocycle; i.e. the formyl (–CHO) in Chl *b*, or a methoxycarbonyl ($-COOCH_3$) in Chl c_3. In these cases, the vinyl group appears slightly twisted from the macrocycle plane to relieve steric tension (Fig. 1), which could explain the difficulties in separating Chl *b* from [DV]-Chl *b* in certain methods that successfully resolve Chl *a* and [DV]-Chl *a* (Van Heukelem et al., 1994).

Silica-based polymeric stationary phases were first introduced in the analysis of Chls by Garrido and Zapata (1993a). Since then, several works have been published that explore the role of particle pore size (Garrido and Zapata, 1993b), column temperature (Van Heukelem et al., 1994; Van Lenning et al., 1995), bonded phase length of C_{18} *versus* C_{30} (Schmid and Stich, 1995; Van Heukelem and Thomas, 2001), and mobile phase composition (Garrido and Zapata, 1996, 1997) on the separation of Chls by HPLC.

The influence of ion-pairing agents deserves special attention. For the HPLC analysis of acidic pigments, such as some Chl *c* forms, Chlides and Pheids, either ion-suppression or ion-pairing techniques must be used to achieve sufficient retention and optimal resolution. Many reversed-phase pigment separation methods have used a gradient system where the first eluent contains ammonium acetate as the buffering and ion-pairing reagent (Tables 1, 2 and 3).

The use of pyridine (as pyridinium acetate) as an ion-pairing reagent for the analysis of Chls was introduced by Garrido and Zapata (1996). Pyridine shows several properties which make it a preferred additive in the chromatographic separation of acidic Chls: (i) It is miscible with water and most organic solvents and shows adequate viscosity and boiling point values, (ii) Although it absorbs strongly in the ultraviolet, it does not interfere with the visible pigment spectrum, and (iii) Unlike the ammonium ion, it does not react with acetone (frequently employed as an eluent in RP-HPLC separation of Chls). The planar structure of the pyridinium ion makes it suitable as a counter ion in paired-ion chromatography on polymeric bonded phases that exhibit special selectivity towards molecular shapes.

The use of pyridine-containing mobile phases improves the chromatographic behavior of acidic and esterified Chls both on monomeric and polymeric alkyl silica columns (Garrido and Zapata, 1996,

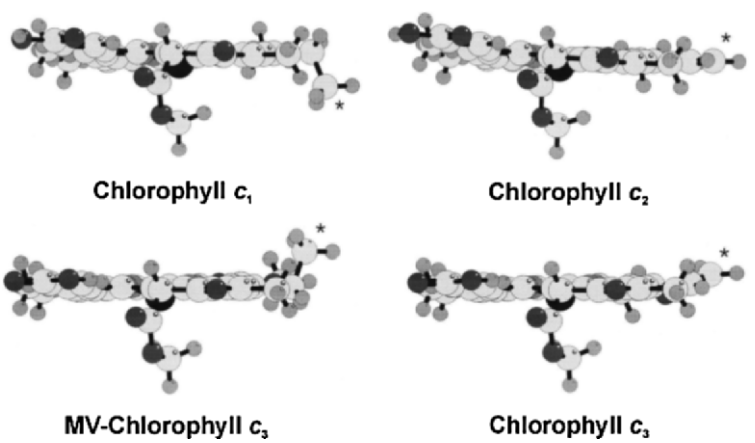

Fig 1. Lateral views (macrocycle perpendicular to the page) of the molecular models of Chl c_1 and [MV]-Chl c_3 ([MV]-forms), and Chls c_2 and c_3 ([DV]-forms). The asterisk indicates the substituent at C-8. MV and DV refer to mono and divinyl, respectively.

1997; Zapata et al., 2000) because the pyridinium ion acts both as a more hydrophobic ion-pairing reagent (increasing the retention of acidic Chls), and as a real mobile phase modifier (co-solvent), affecting the selectivity towards both neutral and charged Chls. A possible explanation for this effect could rely on π-π interactions established between the aromatic ring of pyridine and the aromatic Chl macrocycle.

The combined use of polymeric ODS columns with pyridine-containing eluents has been applied to the separation of algal Chls (Garrido and Zapata, 1997) and of Chlides and PChlide in etiolated plant tissues (Garrido and Zapata, 1997; Schoefs et al., 2000).

The simultaneous separation of polar and non polar [MV]- and [DV]-Chl pairs was achieved (Garrido and Zapata, 1997) by employing polymeric ODS phases operating at low temperature (15 °C) and using pyridine as an ion-pairing and solvent modifying agent (Fig. 2).

2. Monomeric C_8 Bonded Phases

Monomeric OS phases were first used by Goericke and Repeta (1993) to resolve Chl *a* and [DV]-Chl *a*. Their method, and other methods which employed the same stationary phase (Vidussi et al., 1996; Barlow et al., 1997), failed to separate Chl *c* pigments. Since then, Rodríguez et al. (1998) have shown that using adequate gradient profiles and injection conditions, monomeric C_8 columns can separate [MV]- and [DV]-pairs of acidic Chls (e.g. [DV]-Chl c_3 from [MV]-Chl c_3 or Chl c_2 from Chl c_1) simultaneously with other Chls and carotenoids. A more recent method using a C_8 column and pyridine-containing mobile phases was selective enough to resolve [MV]- and [DV]-pairs of polar Chls and [DV]-Chl *a* (a pigment marker for the prokaryote *Prochlorococcus marinus*) from Chl *a* (Zapata et al., 2000) (Fig. 3). On monomeric C_8 columns, the elution order seems to be controlled by subtle differences in the overall polarity of the molecules (Rodríguez et al., 1998), eluting the slightly more polar [DV]-Chl forms before their [MV]-counterparts.

B. Polymer Based Stationary Phases: Octadecyl-polyvinyl-alcohol Polymer (ODP)

Saitoh et al. (1993) showed that an ODP column and an acidic mobile phase can partially resolve the [MV]-/[DV]-pair constituted by Chls c_1 and c_2. To separate acidic and esterified Chls, the same authors developed a column-switching technique that combines two columns, ODP and ODS with the same mobile phase under isocratic conditions (Saitoh et al., 1995).

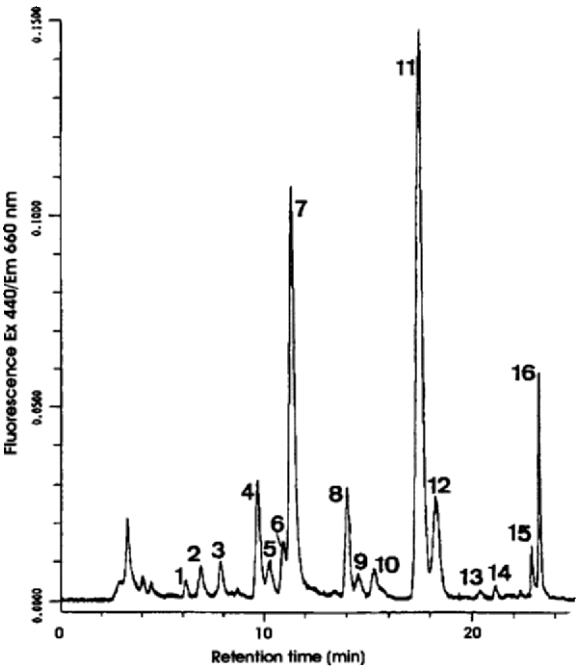

Fig. 2. Chromatogram of chlorophylls extracted from marine phytoplankton obtained with a polymeric octadecyl silica (ODS) column as described by Garrido and Zapata (1997, see Table 3). Peak identification, 1: Chl *c*-like pigment from *Pavlova gyrans*, 2. Chl *c*-like pigment from *P. gyrans*, 3: [DV]-PChlide, 4: Chl c_1, 5: [MV]-Chl c_3, 6: Chl c_3, 7: Chl c_2, 8: Chl *b*, 9: [DV]-Chl *b*, 10: allomerized Chl *a*, 11: Chl *a*, 12: [DV]-Chl *a*, 13 Chl *a*′, 14: [DV]-Chl *a*′, 15: Chl c_2-MGDG, 16: Chl c_2-MGDG. Reproduced from Garrido and Zapata (1997). MV and DV refer to mono and divinyl, respectively.

Considering the acid-labile nature of the Chls, Shioi et al. (1995) applied the neutral ammonium acetate buffered mobile phases, previously developed by Garrido and Zapata (1993b), and an ODP column for the simultaneous gradient elution and separation of BChls, and of acidic and esterified Chls of plant and algal origin: this method also achieved the separation of their [MV]- and [DV]-species.

III. Mass Spectrometry as High Performance Liquid Chromatography Detection Technique Applied to Chlorophylls

Combined LC-MS is one of the most important analytical techniques of the last decade of the twentieth century. In the early period many interfaces were

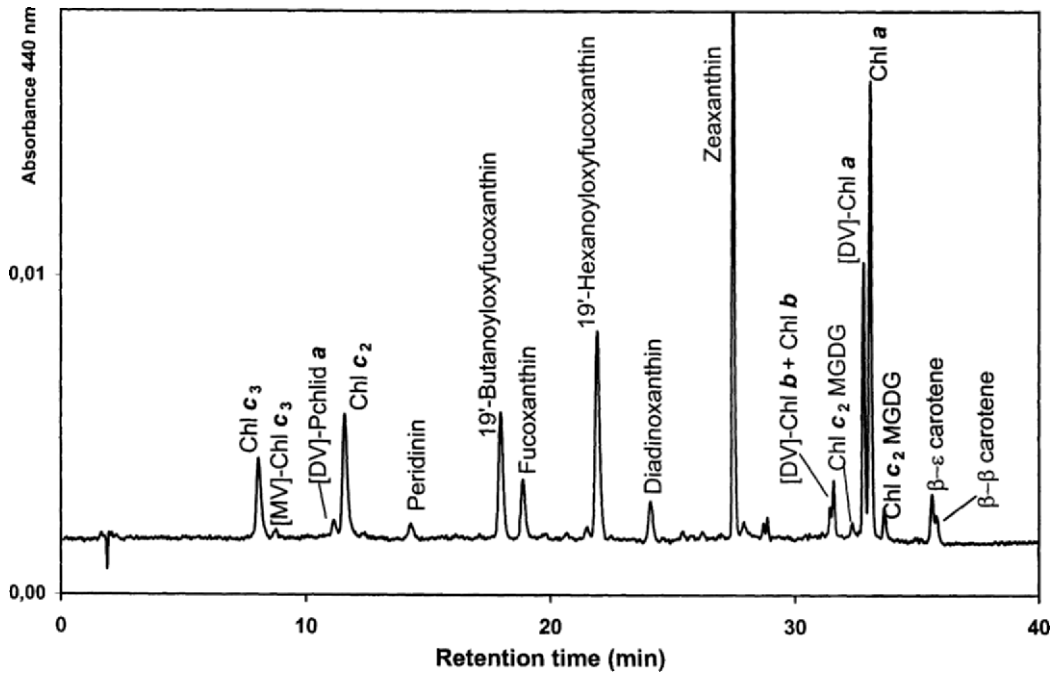

Fig. 3. Chromatogram of a pigment extract from a natural phytoplankton sample from Subtropical North Atlantic waters obtained with the method of Zapata et al. (2000) employing a monomeric octylsilica (OS) column (see Table 3). MV and DV refer to mono and divinyl derivatives.

developed, including moving belt, thermospray and others, which have gradually disappeared. The introduction of interfaces applied in combination with atmospheric pressure ion sources, such as electrospray and atmospheric-pressure chemical ionization, have improved the ease of operation, robustness, detection limits and applicability ranges of LC-MS so that it is routinely used in both industrial and research laboratories. Most LC-MS applications still employ single and triple quadrupole instruments, but other MS instruments (specially ion-trap and time of flight analyzers) are being used successfully (for comprehensive reviews on instruments and applications see Abian, 1999; Niessen and Voyksner, 1998; Niessen, 1999a,b).

Chls presented special analytical challenges to traditional MS methods because of their high mass, low volatility and thermal instability. The introduction of desorption ionization methods offered a new means of molecular ion detection (and thus direct molecular weight determination). The occurrence of additional signals in the lower mass regions enables the building of fragmentation schemes for the target compound, that can be very useful in structure determinations (Schoefs, 2001). Similar information can be obtained from atmospheric ionization methods and their combination with HPLC can provide structural information with very high sensitivity. Consequently, most modern LC-MS methods for Chl analysis employ atmospheric pressure ionization interfaces, always in combination with reversed phase chromatographic methods. The main applications are in the study of Chl alteration products (specially in natural environments like marine or lake sediments) and the characterization of newly discovered algal Chls (Table 1).

IV. Applications

A. Higher Plant Chlorophylls

Generally, a 'standard' method for the separation of higher plant Chls would employ reversed-phase columns, mainly with C_{18} monomeric chemistry, and a gradient system in which a slightly aqueous (5–20%) mobile phase is gradually substituted by an eluent containing an organic solvent of high eluotropic strength (most frequently ethyl acetate or acetone). Different authors have introduced many variations

Table 1. Liquid chromatography-mass spectrometry conditions used in the analysis of chlorophylls

Reference	Liquid chromatography	Interface	Mass spectrometry	Compounds separated
[1] van Breemen et al. (1991)	Column: RP-C_{18} polymeric Mobile phase (composition by volume): A: ethyl acetate: methanol: water: glycerol (15:65:20:0.5) B: ethyl acetate: methanol: water: glycerol (60:30:10:0.5) (binary gradient)	Continuous flow FAB	Positive ions. Double-focusing mass spectrometer	Chl *a*, Chl *b*, Chlide *a*, Chlide *b*, Phe *a*, Phe *b*, Pheide *a*, Pheide *b*, PyroPhe *a*, PyroPhe *b*
[2] Eckardt et al (1991)	RP-C_{18} monomeric Mobile phase: A: acetone; B: methanol; C: water (ternary gradient)	Thermospray	Negative ions Single quadrupole mass spectrometer	Chlorin derivatives from lake sediments
[3] Harris et al. (1995)	RP-C_{18} monomeric Mobile phase: A: acetone; B: methanol; C: water (ternary gradient)	Atmospheric pressure chemical ionization	Positive ions Single quadrupole mass spectrometer	Chlorin derivatives from marine sediments
[4] Garrido and Zapata (1998)	Column: RP-C_{18} polymeric Mobile phase (composition by volume): A: methanol: acetonitrile: 0.25 M pyridinium acetate, pH 5 (45:35:20) B: acetone (binary gradient)	Atmospheric pressure chemical ionization	Positive ions Single quadrupole mass spectrometer	Chl c_2, Chl c_3, Chl *a*, [MV]-Chl c_3
[5] Zissis et al. (1999)	RP-C_{18} monomeric Mobile phase: A: acetone; B: methanol; C: water (ternary gradient)	Electrospray	Positive ions Single quadrupole mass spectrometer	Chl *a*, Chl *a* allomers
[6] Verzegnassi et al. (1999)	RP-C_{18} monomeric Mobile phase: A: acetone; B: methanol; C: water (ternary gradient)	Atmospheric pressure chemical ionization	Positive and negative ions Single quadrupole mass spectrometer	Chlorin derivatives from lake sediments
[7] Airs and Keely (2000)	RP-C_{18} monomeric Mobile phase (composition by volume): A: 1 M ammonium acetate: methanol (25:75) B: methanol: ethyl acetate: acetonitrile: (50:30:20) (binary gradient)	Atmospheric pressure chemical ionisation Post column (pre-interface) addition of formic acid	Positive ions Ion trap mass spectrometer	Chl *a*, Phe *a*
[8] Goericke et al (2000)	RP-C_8 monomeric Mobile phase (composition by volume): A: 0.5 M ammonium acetate: methanol (30:70) B: methanol (binary gradient)	Electrospray	Positive ions Ion trap mass spectrometer	Chl c_1, Chl c_2, Chl c_3, Chl *b*, Chl *a*, [MV]-Chl c_3, [DV]-Chl *a*, [DV]-Chl *b*, [DV]-Phe *b*, [DV]-PyroPhe *a*, *b*.
[9] Verzegnassi et al. (2000)	RP-C_{18} monomeric Mobile phase: A: acetone; B: methanol; C: water (ternary gradient)	Atmospheric pressure chemical ionization	Positive and negative ions Single quadrupole mass spectrometer	Chl *a*, Chl *b*, BChl *a*, BPhe *a*, Chl *a* allomers, Chl *b* allomers
[10] Airs et al. (2001)	RP-C_{18} monomeric Mobile phase (composition by volume): A: 0.1 M ammonium acetate: methanol: acetonitrile (5:80:15) B: methanol: acetonitrile: ethyl acetate (20:15:65) C:methanol: acetonitrile: ethyl acetate (1:1:98) (ternary gradient)	Atmospheric pressure chemical ionization	Positive ions Ion trap mass spectrometer	Chl *a*, Phe *a*, Pheide *a* Pyro-Pheide *a* esters (esterified to different alcohols); BPhe *a*, *c*, *d* and *f* esters(esterified to different alcohols)
[11] Gautier-Jacques et al. (2001)	RP-C_{18} monomeric Mobile phase: A: 0.1 M ammonium acetate; B: methanol; C: acetone (ternary gradient)	Atmospheric pressure chemical ionization	Positive ions Triple quadrupole mass spectrometer	Chl *a*, Chl *b*, Phe *a*, *b*; Phe *a*, Phe *b*, Chl *a* allomers, Chl *b* allomers, PyroPhe *a*, PyroPhe b, Pyro-Pheide *a*, PyroPheide *b*

to this scheme (Table 2) to achieve specifically-tailored methods for the separation of certain Chls. These modifications were made to both mobile and stationary phases: frequently eluents contain different buffering or ion-pairing reagents to achieve adequate retention of acidic Chls, or different organic components to modulate the required selectivity; changes to the stationary phase are mainly to affect the bonding chemistry of the silica-based materials.

Methods developed for algal pigments are versatile and have been used to resolve higher plant compounds: Schoefs et al. (2000) employed a method, originally developed to resolve the [MV]-/[DV]-pair, Chl c_1/c_2 (Garrido and Zapata, 1996), to separate [MV]-PChlide from [DV]-PChlide (also known as MgDVP); and, very recently, McGhie and Ainge (2002) determined the Chl and carotenoid composition of kiwi fruit employing a method originally developed to assess the pigment composition of marine phytoplankton (Wright et al., 1991).

B. Algal and Cyanobacterial Chlorophylls

Aquatic photosynthetic organisms have evolved a great variety of photosynthetic pigments that allowed them to succeed in changing light environments (Jeffrey, 1980). The complexity of their pigment systems has been revealed by development of better HPLC methods over the past decade to better analyze the nature and concentration of the chlorophyll components of algal and cyanobacterial photosystems. The separation of algal and cyanobacterial Chls has been pursued with HPLC (Jeffrey, 1997) using different columns with monomeric or polymeric bonded phases of various carbon chain lengths (C_8, C_{18} or C_{30}), different mobile phases developed with special regard to ion pairing agents such as ammonium, tetrabutylammonium or pyridinium ions, and column temperatures (Table 3). Advances in HPLC have been valuable for the discovery of new forms of Chl *c* in algae (Chapter 3, Zapata et al.), for the detection of Chl *d* as the predominant pigment in the cyanobacterium *Acaryochloris marina* (Miyashita et al., 1997) and for the recognition of the importance of picoplanktonic organisms containing [DV]-forms of Chls *a* and *b* in oceanic ecosystems (Goericke and Repeta, 1993).

HPLC analysis of photosynthetic pigments in phytoplankton and its importance in studies of aquatic ecology has recently been reviewed (Jeffrey et al., 1999).

C. Bacteriochlorophylls

At least six BChl chromophores are known: three are Mg-bacteriochlorins (BChls *a*, *b* and *g*), in which two rings (B and D) are reduced; and three are Mg-chlorins (BChls *c*, *d*, and *e*) in which only ring D is reduced. The esterifying alcohol may be phytol, farnesol or many others and some exist as a series of homologues with different alkyl substituents at C8 and C12 (Chapter 1, Scheer).

The HPLC analysis of BChls has been restricted to the use of monomeric ODS or ODP columns, with good results when separate families of compounds or isolated species are analyzed (Table 4). However, when natural samples have to be examined the chromatograms become extremely complex and very specific detection techniques such as MS are needed for proper identification (Airs et al., 2001).

V. Future Directions in the High Performance Liquid Chromatography Analysis of Chlorophylls

Improvement in HPLC analysis of Chls by introduction of new chromatographic columns, new mobile phases and new detection techniques will achieve shorter analysis times, better sensitivity and higher specificity.

Monomeric OS materials need development for analysis of higher plant Chls: a stationary phase which achieves good separations of [MV]- and [DV]-forms of algal Chls (Rodríguez et al., 1998; Zapata et al., 2000) will probably also separate [MV]- and [DV]-analogues of Chls *a* and *b* and their biosynthetic intermediates.

A major breakthrough can be expected with the introduction of monolithic columns which have one rod of continuous porous silica possessing large through-pores and mesopores, that results in greater permeability, giving rise to columns with high efficiencies and low column back-pressures which can be operated at high flow rates, which increase separation speed, while maintaining a high efficiency comparable with that of particulate materials smaller than 3 μm (Cabrera et al., 2000).

Consequently, separations of Chls that required long analysis periods with traditional packed columns can be achieved in very short analysis times (Garrido et al., 2003). Fig 4 shows the separation of Chls *a* and *b* and their demetallated and dephytylated

Table 2. High performance liquid chromatography methods used for the analysis of higher plant chlorophylls (nr: not reported)

Reference	HPLC method characteristics			Compounds separated
	Stationary phase	Mobile phase		
	Type Brand	Elution type t (run time, min)	Solvent composition (by volume) F (Flow rate, ml min^{-1}), T (Temperature, ºC)	
[1] Canjura and Schwartz (1991)	DP-silica, 4.6 × 250 mm MacMod Analytical	Binary gradient t=28	A: hexane: 2-propanol (98.3:1.7) B: hexane: 2-propanol (75:25) F: 1.6, T= nr	Chl *a*, Chl *b*, Chlide *a*, Chlide *b*, Phe *a*, Phe *b*, Pheide *a*, Pheide *b*
[2] Canjura and Schwartz (1991)	RP-C_{18} monomeric, 5 µm, 4.6 × 250 mm MacMod Analytical	Binary gradient t=22	A: ethyl acetate: methanol: water (15:65:20) B: ethyl acetate: methanol: water (60:30:10) F: 1.3, T= nr	Chl *a*, Chl *b*, Chlide *a*, Chlide *b*, Phe *a*, Phe *b*, Pheide *a*, Pheide *b*
[3] Duke et al. (1993)	RP- C_{18} monomeric 5 µm, 4.6 × 250 mm Spherisorb ODS 1	Binary gradient t=40	A: 0.1 M $(NH_4)_3PO_4$ (pH 5.8) : methanol (20:80) B: methanol F: 1.4, T= nr	PChlide, protoporphyrins
[4] Drexler and Ballschmitter (1994)	DP-diol Serva Polyol Si 100 i)5 µm, 4.0 × 120 mm ii)5 µm, 4.0 × 250 mm	Isocratic t(i)=10 t(ii)=20-30	ethanol: hexane (2:100), column (i) (for chlorophylls) F: 1.5 ethanol: hexane (0.375-0.5:100), column (ii) (for metalloporphyrins) F: 1.0 or 2.0, T= nr	Chl *a*, Chl *a´*, Chl *b*, Phe *a*, Phe *b*, metalloporphyrins
[5] Schoefs et al. (1995)	RP- C_{18} monomeric 4.65 µm, 4.6 × 250 mm Zorbax	Binary gradient t=35	A: acetonitrile: methanol (70:30) B: dichloromethane F: 1.0, T= 20	[MV]-PChlide, Chl *a*, Chl *b*, Chlide *a* and PChlide *a* esterified to gg, DHgg, THgg and p, carotenoids
[6] Shioi et al. (1995)	ODP 5 µm, 4.6 × 250 mm Asahipak ODP 50	Binary gradient t=35	A: 1 M ammonium acetate: methanol (20:80) B: acetonitrile: acetone (70:30) F: 1.0, T= 27	[MV]- and [DV]- forms of Chlides, PChlides, Phes, Ppheids, Chl *a* and Bchl *a* esterified with gg, DHgg, THgg and p
[7] Eijckelhoff and Dekker (1995)	RP-C_8 monomeric 5 µm, 4.6 × 250 mm Spherisorb	Isocratic t=15	Methanol F: 0.7, T= nr	Chl *a*, Chl *a´*, Phe *a*, β,β-carotene
[8] Nakamura and Watanabe (1998)	RP- C_{18} monomeric 5 µm, 4.6 × 250 mm Spherisorb ODS 2	Isocratic t=40	acetone acetonitrile methanol water (43:32:15:10) F: 1.0, T= 20	Chlide *a*, PChlide *a*, Chl a_{gg}, Chl a_{DHgg}, Chl a_{THgg}, Chl *a*, Chl *a´*, Chl *b*
[9] Lebedev and Timko (1999)	RP- C_{18} polymeric 5 µm, 4.6 × 250 mm Vydac	Isocratic t=4	ethyl acetate: methanol: water (36:55:9) F: 1.0, T= nr	Chlide *a*, PChlide *a*
[10] García-Plazaola and Becerril (1999)	RP-C C_{18} monomeric 5 µm, 4.6 × 250 mm Spherisorb ODS 1	Binary gradient t=16	A: acetonitrile: methanol: water (84:9:7) B: ethyl acetate: methanol (32:68) F: 1.2, T= nr	Chl *a*, Chl *b*, Phe *a*, Phe *b*, carotenoids, tocopherols
[11] Darko et al. (2000)	RP- C_{18} monomeric 4.65 µm, 4.6 × 250 mm Zorbax	Ternary gradient t=35	A: acetonitrile B: methanol C: dichloromethane F: 1.0, T= 25	Chl *a*, Chl *b*, Chl *a´*, Chl *b´*, Phe *a* carotenoids
[12] Schoefs et al. (2000)	RP- C_{18} polymeric 5 µm, 4.6 × 250 mm Vydac	Binary gradient t=32	A: methanol: 0.025 M pyridine -pH 5 with acetic acid- (80:20) B: acetonitrile:acetone (70:30) F: 1.2, T= nr	Chlide *a*, PChlide *a*
[13] Nakamura and Watanabe (2001)	RP- C_{18} monomeric 4.6 × 150 mm Nucleosil ODS	Binary (step) gradient t=80	A: acetonitrile: methanol: ethanol: water (85:9:3:3) B: acetonitrile: ethanol (85:15) F: 1.2, T= 20	Chl *a*, Chl *a´*, Phe *a*, phylloquinone
[14] Nakamura et al. (2001)	DP-silica 6 × 150 mm Senshupack	Isocratic t=45	Hexane: toluene: methanol (100:4:0.8) F: 1.0, T= 4	Chl *a*, Chl *a´*, PChl and Phe *a* forms esterified with gg, DHgg, THgg and p
[15] McGhie and Ainge (2002)	RP- C_{18} monomeric 5 µm, 4.6 × 250 mm Spherisorb ODS 2	Ternary gradient t=24	A: methanol : 0.5 M ammonium acetate (80:20) B: acetonitrile: water (90:10) C: ethyl acetate F: 1.0, T= nr	Chl *a*, Chl *b*, carotenoids

Table 3. Selected [(1)] high performance liquid chromatography methods used in the analysis of algal chlorophylls

Reference	HPLC method characteristics			No. of fractions separated for each Chl type			Composition of each Chl fraction (coeluting compounds indicated in brackets)
	Stationary phase		Mobile phase				
	Type Brand	Elution type t (run time, min)	Solvent composition (by volume) F (Flow rate, ml min^{-1}), T (Temperature, ºC)	*c*	*b*	*a*	
[1] Garrido and Zapata (1993b)	RP-C_{18} Polymeric 5µm. 4.6 × 250 mm Vydac 201TP 54	Binary gradient t=35	A: methanol: 1 M ammonium acetate (8:2) B: acetonitrile: acetone (7:3) F=1.0, T=27	7	1	1	[MV]-Chl c_3, Chl c_3, Chl c_1, [DV]-PChlide, Chl c_2, Chl *b*, non polar Chl c_2-like *E. huxleyi*-type (2 fractions), Chl *a*
[2] Van Heukelem et al. (1994)	RP-C_{18} Polymeric 5µm. 4.6 × 250 mm Vydac 201TP 54	Binary gradient t=31	A: methanol: 0.5 M ammonium acetate (8:2) B: methanol: acetone (8:2) F=1.0 (min 0-17), 1.5 (min 22), 2.0 (min 27), T=10	6	1	2	Chlide *a*, Chl c_3, Chl c_1, [DV]- PChlide, Chl c_2, (Chl *b* + [DV]-Chl *b*), Chl *a*, [DV]-Chl *a*, non polar Chl c_2-like *E. huxleyi*-type (2 fractions)
[3] Garrido et al. (1995)	RP-C_{18} Polymeric 5µm. 4.6 × 250 mm Lichrospher PAH	Binary gradient t=40	A: methanol: 1M ammonium acetate 8:2 B: acetone F=0.8, T=27	8	1	1	[MV]-Chl c_3, Chl c_3, Chl c_1, [DV]- PChlide, Chl c_2, Chl *b*, Chl *a*, non polar Chl c_2-like *E. huxleyi*-type, non polar Chl c_1-like *Prymnesium parvum*-type, non polar Chl c_2-like *E. huxleyi*-type
[4] Van Lenning et al. (1995)	RP-C_{18} Polymeric 5µm. 4.6 × 250 mm Lichrospher PAH	Binary gradient t=48	A: methanol: 1 M ammonium acetate (8:2) B: acetone F=0.8, T=Temperature gradient, t_0-t_{15}=31ºC t_{17}=8 ºC	7	2	2	[MV]-Chl c_3, Chl c_3, [DV]- PChlide, Chl c_2, Chl c_1, Chl *b*, [DV]-Chl *b*, Chl *a*, [DV]-Chl a, non polar Chl c_2-like *E. huxleyi*-type (2 fractions)
[5] Garrido and Zapata (1997)	RP-C_{18} Polymeric 5µm. 4.6 × 250 mm Vydac 201TP 54	Binary gradient t=25	A: methanol: acetonitrile: 0.25 M aqueous pyridine pH=5.0 (4.5:3.5:2) B: acetone F= 1.2, T=15	10	2	2	Chl c_2-like *P. gyrans*-type (2 fractions), [DV]-PChlide, Chl c_1, [MV]-Chl c_3, Chl c_3, Chl c_2, Chl *b*, [DV]-Chl *b*, Chl *a*, [DV]-Chl *a*, non polar Chl c_2-like *E. huxleyi*-type, non polar Chl c_1-like *P. parvum*-type, non polar Chl c_2-like *Chrysochromulina*-type
[6] Zapata et al. (2000)	RP-C_8 Monomeric 3.5µm. 4.6 × 150 mm Waters Symmetry	Binary gradient t=40	A: methanol: acetonitrile: 0.25 M aqueous pyridine pH=5.0 (5:2.5:2.5) B: methanol: acetonitrile: acetone (2:6:2) F=1.0, T=25	11	1	2	Chl $c_{CS\text{-}170}$, Chl c_3, Chl c_2-like *P. gyrans*-type, [MV]-Chl c_3, Chl c_1-like *Kryptoperidinium*-type, [DV]- PChlide, Chl c_2, Chl c_1, ([DV]-Chl *b* + Chl *b*), non polar Chl c_2-like *E. huxleyi*-type, non polar Chl c_1-like *P. parvum*-type, [DV]-Chl *a*, Chl *a*, non polar Chl c_2-like *Chrysochromulina*-type

[1] The above six methods separate six or more chlorophyll fractions. Eighteen lesser methods for resolving algal Chls *c* are described in the following papers: Wright et al. (1991), Kraay et al. (1992), Van Heukelem et al. (1992; 1994), Garrido and Zapata (1993a; 1996; 1998), Goericke and Repeta (1993), Saitoh et al. (1993; 1995), Vidussi et al. (1996), Barlow et al. (1997), Miyashita et al. (1997), Rodriguez et al. (1998), Goericke et al. (2000) and Van Heukelem and Thomas (2001).

Table 4. High performance liquid chromatography methods used in the analysis of bacteriochlorophylls

Reference	HPLC method characteristics					Compounds separated
	Stationary phase	Mobile phase				
	Type Brand	Elution	Solvent composition (by volume)	Flow rate (ml min^{-1})	Run time (min)	
[1] Borrego and García-Gil (1994)	RP- C_{18} Monomeric 5 µm. 4.6 × 250 mm Spherisorb S5 ODS2	Binary gradient	A: methanol: 1M ammonium acetate (7:3) B: methanol: ethyl acetate: acetonitrile (5:3:2)	0.5	60	BChl *e*1-*e*3, BChl *c*1, BChl *d*1, BChl *e*4, BChl *c*2, BChl *c*3, BChl *c*4, BChl *d*2, BChl *a*, BChl *d*3*
[2] Shioi et al. (1995)	ODP 5 µm. 4.6 × 250 mm Asahipak ODP-50	Binary gradient	A: methanol: 1M ammonium acetate (8:2) B: acetonitrile: acetone (7:3)	1.0	35	BChlide *a*, BPheide *a*, BChl a_{gg}, BChl a_{gg}, BChl a_{DHgg}, BChl a_{THgg}, BChl a_p, BPhe a_p
[3] Frigaard et al. (1996)	RP- C_{18} Monomeric 4 µm. 3.9 × 300 mm Nova-Pak C18	Binary gradient	A: methanol: acetonitrile: water (42:33:25) B: methanol: acetonitrile: ethyl acetate (39:31:30)	1.0	60	Major BChl *c* homologues, major BChl *d* homologues, major BChl *e* homologues, BChl *b*, BChl *a*
[4] Airs et al. (2001) Method A	RP- C_{18} Monomeric 3 µm. 4.6 × 150 mm Spherisorb ODS2	Ternary gradient	A: 0.1 M ammonium acetate: methanol: acetonitrile (5:80:15) B: methanol: acetonitrile: ethyl acetate (20:15:65) C: methanol: acetonitrile: ethyl acetate (1:1:98)	0.7	110	BPhe c/d_p, BPhe $c_{C\text{-}14}$, BPhe c_{HHf}, BPhe $c_{C\text{-}16}$, BPhe *a*, BPhe $d_{C\text{-}17}$, Chl BPhe $d_{C\text{-}16}$, BPhe $c_{C\text{-}17}$, BPhe $c_{C\text{-}18}$
[5] Airs et al. (2001) Method B	RP- C_{18} Monomeric 3 µm. 4.6 × 150 mm Spherisorb ODS2	Binary gradient	A: 0.1 M ammonium acetate: methanol: acetonitrile (5:80:15) B: 0.1 M ammonium acetate: methanol: Acetonitrile: ethyl acetate (!:32:15:52)	0.7	80	BChls *e*1-*e*4, BChl *e* homologues (I-XII) from *Chlorobium phaeobacteroides**
[6] Airs et al. (2001) Method C	RP- C_V Monomeric 3 µm. 4.6 × 150 mm Spherisorb ODS2	Binary gradient	A: 0.1 M ammonium acetate: methanol: acetonitrile (5:80:15) C: methanol: acetonitrile: ethyl acetate (19:1:80)	0.7	100	BPhe $c_{C\text{-}16}$, BPhe *a*, BPhe $d_{C\text{-}16}$
[7] Goericke (2002)	RP- C_{18} Monomeric 3 µm. 4.6 × 150 mm Supelco Discovery	Binary gradient	A: acetonitrile: water (6:4) B: acetone	1.5	12	BChl *a*

* The numbers for BChls *c*, *d* and *e* are not in subscript text, as in the Chl *c* series, because they refer to an HPLC order of elution rather than a precisely known chemical structure. A nomenclature system for BChls *c*, *d* and *e* of known chemistry has been proposed by Smith (1994).

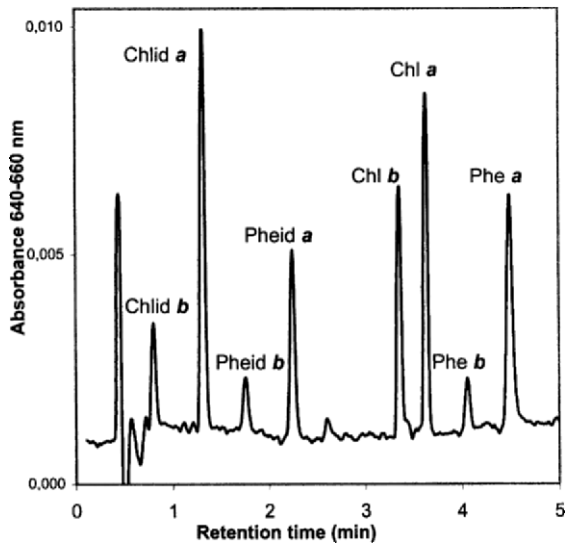

Fig. 4. Chromatogram of chlorophylls, chlorophyllides, pheophytins and pheophorbides *a* and *b* on a monolithic silica column. Chromatographic conditions as described in Garrido et al. (2003).

derivatives in less than five minutes.

The coupling of HPLC with LC-UV-photodiode array detection and LC-MS, has provided powerful tools for the identification of chlorophylls. These techniques, however, do not always allow a full identification. HPLC coupled to NMR represents a potentially interesting complementary technique for detailed on-line structural analysis. Recent progress in NMR technology has given a new impulse to LC/NMR which is now emerging as a powerful analytical tool (Vogler et al., 1998). The development of efficient solvent suppression techniques, both on-flow and stop-flow, allows the measurement of high quality LC/^{1}H-NMR spectra with reversed-phase HPLC conditions. Non-deuterated solvents such as methanol or acetonitrile can be used, while water is replaced by D_20. The concomitant development of robust automated data analysis tools has facilitated interpretation of the vast amount of NMR data generated (Stockman, 2000; Wolfender et al., 2001).

Acknowledgments

We thank S. W. Jeffrey, Lesley Clementson, Simon Wright and Francisco Rodríguez for their critical reading of the manuscript and helpful comments.

References

Abian J (1999) The coupling of gas and liquid chromatography with mass spectrometry. J Mass Spectrom 34: 157–168

Airs RL and Keely BJ (2000) A novel approach for sensitivity enhancement in atmospheric pressure chemical ionisation liquid chromatography/mass spectrometry of chlorophylls. Rapid Commun Mass Spectrom 14: 125–128

Airs RL, Atkinson JE and Keely BJ (2001) Development and application of a high resolution liquid chromatography method for the analysis of complex pigment distributions. J Chromatogr A 917: 167–177

Barlow RG, Cummings DG and Gibb SW (1997) Improved resolution of mono-and divinyl chlorophylls *a* and *b* and zeaxanthin and lutein in phytoplankton extracts using reverse phase C-8 HPLC. Mar Ecol Prog Ser 161: 303–307

Barry P, Young AJ and Britton G (1991) Accumulation of pigments during the greening of etiolated seedlings of *Ordeum vulgare* L. J Exp Bot 42: 229–234

Beale SI (1999) Enzymes of chlorophyll biosynthesis. Photosynth Res 60: 43–73

Borrego C and García-Gil LJ (1994) Separation of bacteriochlorophyll homologues from green photosynthetic sulfur bacteria by reversed-phase HPLC. Photosynth Res 41: 157–163

Cabrera K, Lubda D, Eggenweiler HM, Minakuchi H and Nakashini K (2000) A new monolithic-type HPLC column for fast separations. J High Resol Chromatogr 23: 93–99

Canjura FL and Schwartz SJ (1991) Separation of chlorophyll compounds and their polar derivatives by high-performance liquid chromatography. J Agric Food Chem 39: 1102–1105

Chisholm SW, Frankel SL, Goericke R, Olson RJ, Palenik B, Waterbury JB, West-Johnsrud L and Zettler EK (1992) *Prochlorococcus marinus* nov. gen. Nov. sp.: An oxyphototrophic marine prokaryote containing divinyl chlorophyll *a* and *b*. Arch Microbiol 157: 297–300

Darko E, Schoefs B and Lemoine Y (2000) Improved liquid chromatographic method for the analysis of photosynthetic pigments of higher plants. J Chromatogr A 876: 111–116

Drexler D and Ballschmitter K (1994) Separation of chlorophyll *a* and metalloporphyrins by HPLC in normal-phase mode using a diol-phase. Fresenius J Anal Chem 348: 590–594

Duke SO, Duke MV and Lee HJ (1993) HPLC and in vivo spectrophotometric detection of porphyrins in plant tissues treated with porphyrinogenic herbicides. Z Natursforsch 48c: 317–325

Eckardt CB, Keely BJ and Maxwell JR (1991) Identification of chlorophyll transformation products in a lake sediment by combined liquid chromatography-mass spectrometry. J Chromatogr 557: 271–288

Eijckelhoff C and Dekker JP (1995) Determination of the pigment stoichiometry of the photochemical reaction center of Photosystem II. Biochim Biophys Acta 1231: 21–28

Frigaard NU, Larsen KL and Cox RP (1996) Spectrochromatography of photosynthetic pigments as a fingerprinting technique for microbial phototrophs. FEMS Microbiol Ecol 20: 69–77

García-Plazaola JI and Becerril JM (1999) A rapid high-performance liquid chromatography method to measure lipophilic antioxidants in stressed plants: Simultaneous determination of carotenoids and tocopherols. Phytochem Anal 10: 307–313

Garrido JL and Zapata M (1993a) High performance liquid chro-

matography of chlorophylls c_3, c_1, c_2 and *a* and of carotenoids of chromophyte algae on a polymeric octadecyl silica column. Chromatographia 35: 543–547

Garrido JL and Zapata M (1993b) High performance liquid chromatographic separation of polar and non-polar chlorophyll pigments from algae using a wide pore polymeric octadecyl-silica column. J High Resolut Chromatogr 16: 229–233

Garrido JL and Zapata M (1996) Ion-pair reversed phase high-performance liquid chromatography of algal chlorophylls. J Chromatogr A 738: 285–289

Garrido JL and Zapata M (1997) Reversed phase high performance liquid chromatographic separation of mono- and divinyl chlorophyll forms using pyridine-containing mobile phases and a polymeric octadecyl silica column. Chromatographia 44: 43–49

Garrido JL and Zapata M (1998) Detection of new pigments from *Emiliania huxleyi* (Prymnesiophyceae) by high-performance liquid chromatography, liquid chromatography-mass spectrometry, visible spectroscopy and fast atom bombardment mass spectrometry. J Phycol 34: 70–78

Garrido JL, Zapata M and Muñiz S (1995) Spectral characterization of new chlorophyll *c* pigments isolated from *Emiliania huxleyi* (Prymnesiophyceae) by high-performance liquid chromatography. J Phycol 31: 761–768

Garrido JL, Rodríguez F, Campaña E and Zapata M (2003) Rapid separation of chlorophylls *a* and *b* and their demetallated and dephytylated derivatives using a monolithic silica C18 column and a pyridine-containing mobile phase. J Chromatogr A 994: 85–92

Gauthier-Jaques A, Bortlik K, Hau J and Fay LB (2001) Improved method to track chlorophyll degradation. J Agric Food Chem 49: 1117–1122

Goericke R (2002) Bacteriochlorophyll *a* in the ocean: Is anoxygenic photosynthesis important? Limnol Oceanogr 47: 290–295

Goericke R and Repeta DG (1993) Chlorophylls *a* and *b* and divinyl chlorophylls *a* and *b* in the open Subtropical North Atlantic Ocean. Mar Ecol Prog Ser 101: 307–313

Goericke R, Olson RJ and Shalapyouok A (2000) A novel niche for *Prochlorococcus* sp. in low-light suboxic environments in the Arabian Sea and the Eastern Tropical North Pacific. Deep-Sea Res 47: 1183–1205

Harris PG, Carter JF, Head RN, Harris RP, Eglinton G and Maxwell JR (1995) Identification of chlorophyll transformation products in zooplankton faecal pellets and marine sediment extracts by liquid chromatography/mass spectrometry atmospheric pressure chemical ionization. Rapid Commun Mass Spectrom 9: 1177–1183

Ioannides IM, Fasoula DA, Roberston KR and Rebeiz CA (1994) An evolutionary study of chlorophyll biosynthetic heterogeneity in green plants. Biochem Syst Ecol. 22: 211–220

Jeffrey SW (1980) Algal pigment systems. In: Falkowski PG (ed) Primary productivity of the sea, pp 33-58. Plenum Press, New York

Jeffrey SW (1997) Application of pigment methods in Oceanography. In: Jeffrey SW, Mantoura RFC and Wright SW (eds) Phytoplankton pigments in Oceanography, pp 127-166. UNESCO, Paris

Jeffrey SW, Wright SW and Zapata M (1999) Recent advances in HPLC pigment analysis of phytoplankton. Mar Freshwater Res 50: 879–96

Kraay GW, Zapata M and Veldhuis MJW (1992) Separation of chlorophylls c_1, c_2 and c_3 of marine phytoplankton by reversed-phase C_{18} high-performance liquid chromatography. J Phycol 28: 708–712

Lebedev N and Timko MP (1999) Protochlorophyllide oxidoreductase B-catalyzed protochlorophyllide photoreduction in vitro: Insight into the mechanism of chlorophyll formation in light-adapted plants Proc Natl Acad Sci USA 96: 9954–9959

McGhie TK and Ainge GD (2002) Color in fruit of the Genus *Actinidia*: Carotenoid and chlorophyll composition. J Agric Food Chem 50: 117–121

Miyashita H, Adachi K, Kurano N, Ikemoto H, Chihara M and Miyachi S (1997) Pigment composition of a novel photosynthetic prokaryote containing chlorophyll *d* as the major chlorophyll. Plant Cell Physiol 38: 272–281

Nakamura A and Watanabe T (1998) HPLC determination of photosynthetic pigments during the greening of etiolated barley leaves. Evidence for the synthesis of chlorophyll *a′*. FEBS Lett 426: 201–204

Nakamura A and Watanabe T (2001) Separation and determination of minor photosynthetic pigments by reversed phase HPLC with minimal alteration of chlorophylls. Anal Sci 17: 503–508

Nakamura A, Tanaka S and Watanabe T (2001) Normal phase HPLC separation of possible biosynthetic intermediates of pheophytin *a* and chlorophyll *a′*. Anal Sci 17: 509–513

Niessen WMA (1999a) State-of-the-art in liquid chromatography-mass spectrometry. J Chromatogr A 856: 179–197

Niessen WMA (1999b) Liquid chromatography-mass spectrometry. Marcel Dekker, New York

Niessen WMA and Voyksner RD (eds) (1998) Current Practice of Liquid Chromatography-Mass Spectrometry. Elsevier, Amsterdam

Porra RJ (1997) Recent progress in porphyrin and chlorophyll biosynthesis. Photochem Photobiol 65: 492–516

Rebeiz CA, Parham R, Fasoula DA, and Ioannides IM (1994) Chlorophyll *a* biosynthetic heterogeneity. In: Biosynthesis of tetrapyrrole pigments. Ciba Symposium 180. pp 177–193, John Wiley, New York

Rodríguez F, Zapata M and Garrido JL (1998) High performance liquid chromatographic separation of chlorophyll *c* forms from marine phytoplankton on octylsilica bonded phases. Chromatographia 48: 677–680

Rüdiger W (1997) Chlorophyll metabolism: From outer space down to the molecular level. Phytochemistry 46: 1151–1167

Sander LC and Wise SA (1990) Evaluation of shape selectivity in liquid chromatography. LC GC 8: 378–390

Sander LC, Pursch M and Wise SA (1999) Shape selectivity for constrained solutes in reversed-phase liquid chromatography. Anal Chem 71: 4821–4830

Saitoh K, Awaka I and Suzuki N (1993) Separation of chlorophyll c_1 and c_2 by reversed-phase high-performance liquid chromatography. J Chromatogr A 653: 247–251

Saitoh K, Awaka I and Suzuki N (1995) Determination of chlorophyll by reversed-phase high-performance liquid chromatography with isocratic elution and the column switching technique. J Chromatogr A 693: 176–180

Schmid H and Stich HB (1995) HPLC-analysis of algal pigments: Comparison of columns, column properties and eluents. J Appl Phycol 7: 487–494

Schoefs B (2001) Determination of tetrapyrrole pigments in foodstuffs. Am Lab 33: 34–39

Schoefs B, Bertrand M and Lemoine Y (1995) Separation of photosynthetic pigments and their precursors by reversed phase high-performance liquid chromatography using a photodiode array detector. J Chromatogr A 692: 239–245

Schoefs B, Bertrand M and Funk C (2000) Photoactive protochlorophyllide regeneration in cotyledons and leaves of higher plants. Photochem Photobiol 72: 660–668

Shioi Y (1991) Analytical chromatography of chlorophylls. In: Scheer H (ed) The Chlorophylls, pp 59-88. CRC Press, Boca Raton

Shioi Y and Takamiya K (1992) Monovinyl and divinyl protochlorophyllide pools in etiolated tissues of higher plants. Plant Physiol 100: 1291–1295

Shioi Y, Watanabe K, Takamiya K, Garrido JL and Zapata M (1995) Separation of mono- and divinyl chlorophyll species by high-performance liquid chromatography using an octadecyl polyvinyl alcohol polymer column. Anal Biochem 231: 225–229

Smith KM (1994) Nomenclature of the bacteriochlorophylls *c*, *d*, and *e*. Photosynth Res 41: 23–26

Stockman BJ (2000) Flow NMR spectroscopy in drug discovery. Curr Opin Drug Discovery Dev 3: 269–274

van Breemen RB, Canjura FL and Schwartz SJ (1991) High-performance liquid chromatography-continuous-flow fast atom bombardment mass spectrometry of chlorophyll derivatives. J. Chromatogr 542: 373–383

van Heukelem L and Thomas CS (2001) Computer-assisted high-performance liquid chromatography method development with applications to the isolation and analysis of phytoplankton pigments. J Chromatogr A 910: 31–49

van Heukelem L, Lewitus AJ, Kana TM and Craft NE (1992) High-performance liquid chromatography of phytoplankton pigments using a polymeric reversed phase C_{18} column. J Phycol 29: 867–872

van Heukelem L, Lewitus AJ, Kana TM and Craft NE (1994) Improved separations of phytoplankton pigments using temperature-controlled high-performance liquid chromatography Mar Ecol Prog Ser 114: 303–313

Van Lenning K, Garrido JL, Arístegui J and Zapata M (1995) Temperature-programmed high-performance liquid chromatography separation of mono- and divinyl chlorophyll forms from marine phytoplankton. Chromatographia 41: 539–543

Verzegnassi L, Riffé-Chalard C, Kloeti W and Gülaçar FO (1999) Analysis of tetrapyrrolic pigments and derivatives in sediments by high performance liquid chromatography/atmospheric pressure chemical ionization mass spectrometry. Fresenius J Anal Chem 364: 249–253

Verzegnassi L, Riffé-Chalard C and Gülaçar FO (2000) Rapid identification of Mg-chelated chlorines by on-line high-performance liquid chromatography/atmospheric pressure chemical ionisation mass spectrometry. Rapid Commun Mass Spectrom. 14: 590–594

Vidussi F, Claustre H, Bustillos-Guzmán J, Cailliau C and Marty JC (1996) Determination of chlorophylls and carotenoids of marine phytoplankton: separation of chlorophyll *a* from divinyl chlorophyll *a* and zeaxanthin from lutein. J Plankton Res 18: 2377–2382

Vogler B, Klaiber I, Roos G, Walter CU, Hiller W, Sandor P and Kraus W (1998) Combination of LC-MS and LC-NMR as a tool for the structure determination of natural products. J Nat Products 61: 175–178

von Wettstein D, Gough S and Kannangara CG (1995) Chlorophyll biosynthesis. Plant Cell 7: 1039–1057

Wolfender JL, Ndjoko K and Hostettmann K (2001) The potential of LC-NMR in phytochemical analysis. Phytochem Anal. 12: 2–22

Wright SW, Jeffrey SW, Mantoura RFC, Llewellyn CA, Bjørnland T, Repeta D, Welschmeyer N (1991) Improved HPLC method for the analysis of chlorophylls and carotenoids from marine phytoplankton. Mar Ecol Prog Ser 77: 183–96

Zapata M, Rodríguez F and Garrido JL (2000) Separation of chlorophylls and carotenoids from marine phytoplankton: A new HPLC method using a reversed-phase C_8 column and pyridine-containing mobile phases. Mar Ecol Prog Ser 195: 29–45

Zissis KD, Brereton RG and Dunkerley S (1999) Principal components scores and loading plots for visualisation of the electrospray ionisation liquid chromatography mass spectra of a mixture of chlorophyll degradation products at different cone voltages. Rapid Commun Mass Spectrom 13: 1755–1761

Chapter 9

Large Scale Chlorophyll Preparations Using Simple Open-Column Chromatographic Methods

Yuzo Shioi*
Department of Biology and Geoscience, Faculty of Science, Shizuoka University, Shizuoka 422-8259, Japan

*email: sbysioi@ipc.shizuoka.ac.jp

Bernhard Grimm, Robert J. Porra, Wolfhart Rüdiger and Hugo Scheer (eds): Chlorophylls and Bacteriochlorophylls: Biochemistry, Biophysics, Functions and Applications, pp. 123–131.

Summary

Convenient laboratory techniques for large-scale preparations of chlorophylls (Chls) using dioxane precipitation and column chromatography are described. Partially purified Chls are obtained using a precipitation procedure that involves the selective interaction of Chls with dioxane in the presence of water. This procedure can be used to separate Chls from most of the carotenoids and some lipids present in the initial extract. Simple techniques of open-column chromatography are described using diethylaminoethyl [DEAE]-Toyopearl and Sepharose CL-6B in combination, DEAE-cellulose and powdered sucrose. These chromatographic techniques rely on the use of the partially purified Chls obtained by the dioxane precipitation procedure as a starting material, which makes preparation easier and very effective. An application of these techniques for the isolation of bacteriochlorophyll *a* is also described. Despite the simple procedures, and without elaborate facilities or expensive reagents, contamination of the Chl preparations is low as judged by high-performance liquid chromatography. The methods described are rapid and give good yields of Chls without causing chemical modifications during manipulations.

I. Introduction

Analytical studies of Chls require pure substances isolated from plant materials. The identification and determination of the pigments has long relied largely on the use of paper-, thin-layer- or column- chromatography, followed by spectroscopic examination and determination of the isolated pigments. The technique of high-performance liquid chromatography (HPLC) is now commonly exploited for the separation and determination of plant pigments because of such advantages as speed, high resolution and sensitivity (Shioi, 1991). These useful characteristics of HPLC have been used mainly for analytical purposes and have been largely concerned with quantitative determination and identification of Chls and carotenoids, for checking the purity of isolated pigments (see Chapter 8, Garrido and Zapata) and for chemotaxonomic comparisons as described in detail in Chapter 3 (Zapata et al.). For the isolation of Chls on a preparative scale, HPLC is also an excellent method but its application is limited by the relatively high cost of the packing material.

A variety of chromatographic methods with various adsorbents have been employed to separate plant pigments. In fact, these procedures, although simple and often useful, are not always suitable for preparative isolation of large quantities of pigments. Among the commonly used separation techniques, an open and low-pressure column chromatography remains a very useful technique for the large-scale preparation of the plant pigments from crude and partially purified extracts. Open column chromatography has the advantages of being simple, rapid and easy to scale up without any special facilities or expensive packing materials which makes it very convenient for use in most laboratories.

The chromatographic analysis and preparation of Chls and its historical background have previously been summarized in various reviews (Strain and Svec, 1966; Strain et al., 1971; Holden, 1976; Svec, 1979; Rüdiger and Schoch, 1988; Shioi, 1991). In this chapter, emphasis is placed upon preliminary purification of Chls by dioxane precipitation followed by open column chromatography as a very useful preparatory procedure which is outlined schematically in Fig. 1 for Chls *a* and *b,* and in Fig. 2 for BChl *a*.

Abbreviations: BChl – bacteriochlorophyll; BChlide – bacteriochlorophyllide; BPhe – bacteriopheophytin; BPheide – bacteriopheophorbide; Chl – chlorophyll; Chlide – chlorophyllide; DEAE- – diethylaminoethyl-; HPLC – high-performance liquid chromatography; PChl – protochlorophyll; Phe – pheophytin; Pheide – pheophorbide

II. Extraction of the Pigments

To prevent the chemical alteration and degradation of Chls during extraction, the following precautions are recommended. The extraction of the pigments and processing of the extracts must be carried out as rapidly as possible in subdued light: to prevent oxidation, the materials (homogenate or leaves) should not be extracted with solvents for long periods. Heat treatment of plant materials, to inactivate degrading enzymes, has frequently been used prior to the extraction of pigments but is not recommended because, in the case of tea leaves, chlorophyllase activity still remained even after heating at 120 °C for 30 min (Kohata et al., 1998). Methanol-based extractants

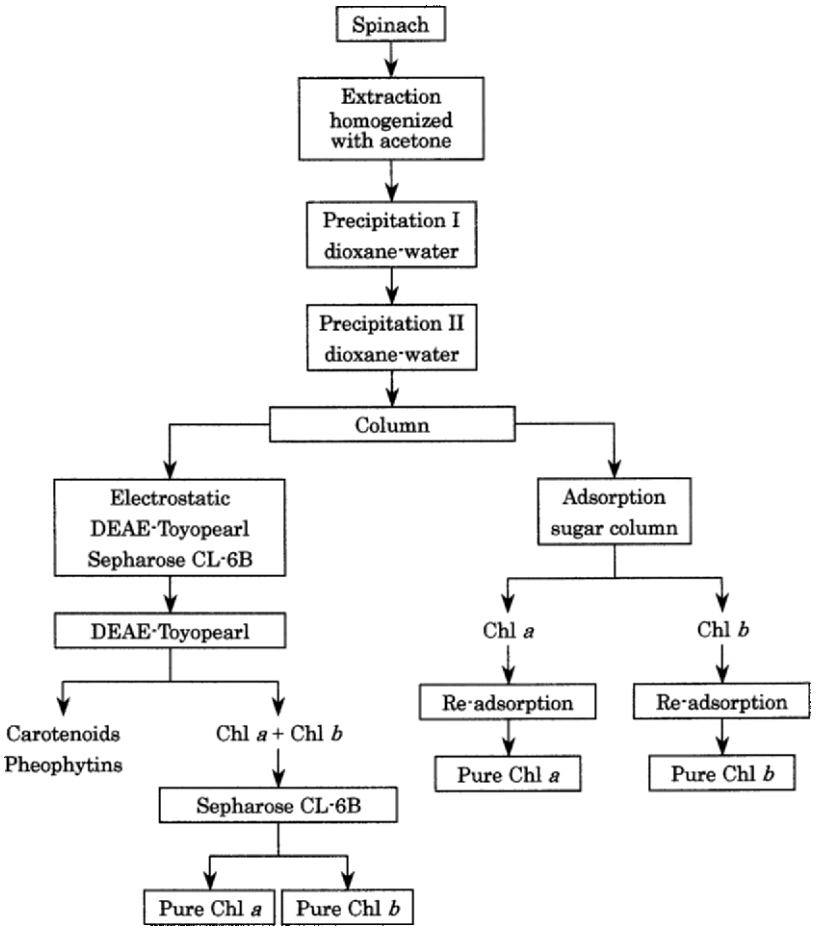

Fig. 1. Preparation of chlorophylls from spinach leaves.

should be avoided to prevent the formation of chemically-modified products of Chls; if chlorophyllase is present, methyl-Chlide will be formed by enzymic transesterification. Additionally, epimers and allomarized Chls are formed much more easily in air and at room temperature in methanol solution.

The following method is an excellent extraction procedure for plant Chls. Fresh, de-ribbed spinach leaves (100 g fresh weight) are homogenized for 3 min in a blender with 500 ml of cold acetone (–20 °C) or buffered aqueous acetone (see Section III.A). The homogenate is immediately filtered through two sheets of Whatman No. 1 paper in a Büchner funnel under reduced pressure to remove tissue debris. The residue is washed with 100 ml of acetone to remove remaining Chls. The combined filtrates are treated with dioxane and water for the preliminary purification of the Chls by their precipitation (see Section III.A).

In the case of BChl *a*, the esterifying alcohol is usually a mixture of geranylgeraniol, phytol and intermediate reduction products (Shioi and Sasa, 1984) but also depends on the bacterial species used; for example, *Rhodospirum rubrum* contains BChl *a* esterified with farnesol. Thus, BChl *a* containing a mixture of esterifying alcohols as a starting material is frequently encountered. *Rhodobacter sulfidophilus* cells (1 g wet weight) are suspended and extracted in 15 ml of aqueous 90% (v/v) acetone by gently mixing with a medical swab or brush which is resistant to solvents. The extract is centrifuged at 10,000 × g for 10 min. The supernatant contained 80–85% of the total BChl *a* and less than 10% of the total carotenoids. This extraction method is fairly selective for BChl *a* and uses no methanol.

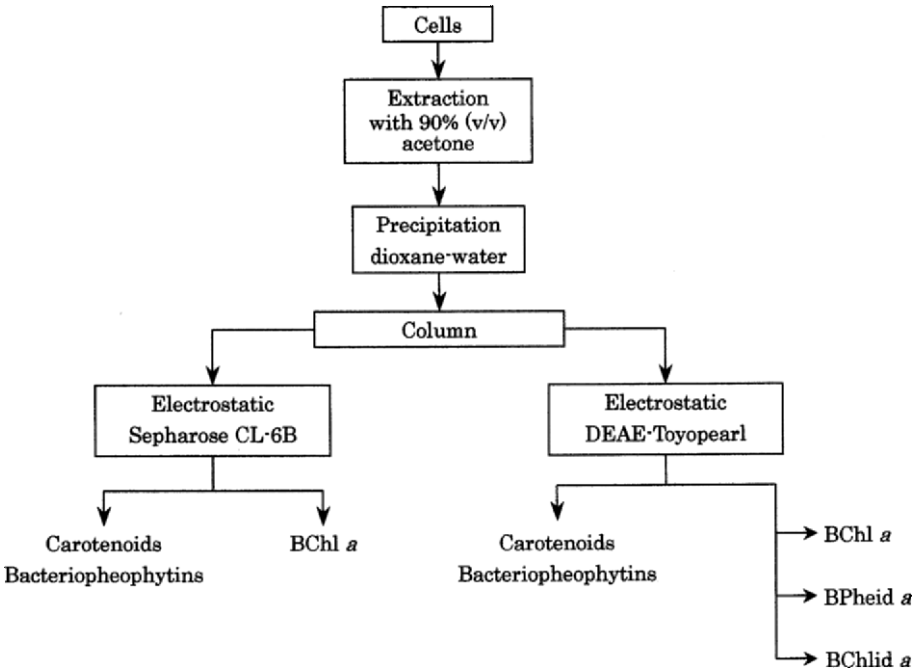

Fig. 2. Preparation of bacteriochlorophylls from photosynthetic bacteria.

III. Precipitation of Chlorophylls

This method relies on the selective interaction of Chl with dioxane in the presence of water (Iriyama et al., 1974a, b). The Chl-dioxane adducts formed are precipitated in microcrystalline form, leaving the bulk of the solvent-extractable constituents in solution. The bulk of carotenoids and lipids present in the crude extract are thus removed by this method without appreciable loss of Chls. This method is not applicable to polar non-esterified Chl derivatives such as Chl *c*, but is applicable to all extracts containing Chl *a*, Chl *b* and BChl *a* as well as their mixtures. This procedure, originally described by Iriyama et al. (1974a), is now commonly used for the preliminary purification of esterified Chls and is recommended for its simplicity and reliability of recovery.

A. Chlorophylls a and b

The acetone pigment extract (see above) is mixed with a one-seventh volume of dioxane. Then about a one-seventh volume of distilled water is added dropwise with stirring until a green precipitate forms. The volume of water required varies depending on the water content of the leaves and hence of the initial acetone extract. The size and shape of the aggregates formed varies widely depending on the conditions of precipitation (Iriyama et al., 1974a). The mixture is placed in a freezer (–20 °C) for 1 h to allow sedimentation. The top clear yellow solution is carefully decanted and the lower dark-green suspension, containing the precipitated Chl-dioxane-hydrate complex, is collected by filtration through two sheets of Whatman No. 1 paper in a Büchner funnel under reduced pressure. The crude Chls are dissolved on the paper in the Büchner funnel with 100 ml of acetone (or less) and collected under reduced pressure until the paper is colorless. This crude Chl solution is again mixed with a one-seventh volume of dioxane and then about a one-fourth volume of distilled water is added dropwise as described above. As this solution contains less water, the proportion to be added is higher in this second precipitation. According to the HPLC analyses of the twice-precipitated Chls obtained from the spinach extracts (Shioi et al., 1983 for Chls; Zapata et al., 2000 for carotenoids), the recovery of Chl in the first and second precipitations was 99% and 94–95%, respectively, and usually these fractions contained less than 2% of Phes and 0.5% of epimers. Extraction of leaves with aqueous 80% acetone containing either 2.5 mM sodium phosphate

(pH 7.8) or 50 mM Hepes-KOH (pH 7.5) buffers (Porra, 1990) minimized formation of Phes but less additional water was then required to precipitate the dioxane adduct. In the second precipitation, most of the polar carotenoids including neoxanthin, violaxanthin and atherxanthin, were almost completely removed and 99.7% of lutein and zeaxanthin were also eliminated. Of the non-polar carotenoids, β-carotene was reduced to 22% and to 17% by the first and second precipitations, respectively. The repeated precipitation of the Chls-dioxane-hydrate is useful and effective prior to column chromatography but never completely eliminates carotenoids.

B. Bacteriochlorophyll a

Precipitation of BChl *a* is basically the same as described for Chls *a* and *b* (see above) but only one treatment with dioxane and water is performed. Because the precipitation of the BChl *a*-dioxane-hydrate complex is slow, the dioxane-extract mixture is left at –20 °C for 6 h or overnight for complete sedimentation. The recovery of BChl *a* and the effectiveness of precipitation is lower than with plant Chls. Judging from HPLC analyses, about 40% of carotenoids were removed by the precipitation and BChl *a,* esterified with different alcohols, were precipitated simultaneously.

IV. Column Chromatographic Methods

Open and low-pressure column chromatographic methods are unsuitable for small-scale analytical purposes but may be employed for the preparation of relatively large quantities of Chls. Various supports have been used for such separations of Chls and those most frequently used include either powdered sucrose, DEAE-cellulose, or a combination of two columns, DEAE-Toyopearl and Sepharose CL-6B. As already mentioned, these procedures are based on the use of the partially purified preparations of Chls *a* and *b* or BChl *a* obtained by the dioxane-water precipitation procedure (Section III).

A. Diethylaminoethyl (DEAE)-Toyopearl, Sepharose CL-6B and DEAE-cellulose Column Chromatography

The column chromatography mentioned in this section is based on the method of Murata and coworkers (Omata and Murata, 1980, 1983; Araki et al., 1984) in which Chls *a* and *b* are separated by electrostatic properties using an ion-exchanger and molecular sieving supports. This method is applicable for the purification of small to large quantities of Chls using various column bed volumes from 1 to 60 ml. There is no difficulty in packing these columns, as is encountered with sucrose columns (Section IV.B.1). Although small amounts of epimers are formed during DEAE-Toyopearl column chromatography (Section IV.A.1), this method allows the rapid separation of Chls *a* and *b* with relatively high resolution, reproducibility and efficiency. Consequently this procedure appears to be a reasonable alternative to chromatography with other types of columns.

1. Diethylaminoethyl-Toyopearl Columns

a. Preparation of Diethylaminoethyl-Toyopearl Columns

An aqueous suspension of DEAE-Toyopearl 650M (100 ml) is washed successively with distilled water, 1 M sodium acetate (pH 7.0), distilled water and finally acetone by filtration and suspension using a sintered-glass filter funnel. The final wash with acetone is repeated several times to accomplish a complete exchange to acetone. This washed material can be stored for several months as a suspension in acetone in a tightly sealed bottle to prevent contamination with water. The used column materials can be re-used if they are regenerated properly by the successive washing procedure described above.

b. Separation of Pheophytins and Chlorophylls a and b

The partially purified Chl preparation is completely dried by evaporation under reduced pressure. The resulting pigments are dissolved in a small amount of acetone and then loaded onto a DEAE-Toyopearl column. The column is washed with acetone and all carotenoids and Phes are completely eluted out while Chls *a* and *b*, Pheides and Chlides remain adsorbed to the top of the column. After removing all carotenoids and Phes from the column, the developing solvent is changed to acetone-methanol (10:3, v/v) to elute Chls *a* and *b* while the Pheides and Chlides remain adsorbed to the column. Subsequent separation of Chls *a* and *b* is performed on a Sepharose CL-6B column as described in Section IV.A.2.

During the DEAE-Toyopearl chromatography, epimerization of Chls occurs but is half that observed with DEAE-Sepharose CL-6B when checked by HPLC using Chl *a*. To minimize the formation of epimers, separation is performed quickly at low temperature (2–4 °C).

c. Separation of a Mixture of Chlorophyll a and its Derivatives

The separation of Chls *a* and *b* and their respective derivatives from a mixture is not easy using a DEAE-Toyopearl column due to their intersecting elution properties; however, the separation of a Chl derivative mixture consisting of the same species of Chl (i.e. Chl *a* or Chl *b*) can be achieved. This method can be extended to include PChl *a* with PChl *a* derivative mixtures, although slight modifications in the proportions of the developing solvents are necessary. Resolution of a Chl *a* solution containing Phe *a*, Pheide *a* and Chlide *a* is shown here as a representative example. The Chl *a* mixture is applied to the DEAE-Toyopearl column prepared as described above. On development with acetone, Phe *a* (pale gray) is eluted first. The developing solvent is changed to 99%(v/v) aqueous acetone and Chl *a* (blue-green) is eluted. Then 98% (v/v) aqueous acetone containing 0.1% (w/v) ammonium acetate is used to elute Pheide *a* (pale gray). Finally Chlide *a* (blue-green) is eluted with 95% (v/v) aqueous acetone containing 0.2% (w/v) ammonium acetate. The separated Chl derivatives are transferred to diethylether and recovered by standard methods. A summary of the separation of Chl *a* and its derivatives is shown in Table 1.

d. Separation of Bacteriochlorophyll a Pigment Mixtures

A mixture of BChl *a*, BPhe *a*, BPheide *a* and BChlide *a* can be separated by DEAE-Toyopearl chromatography in a similar manner to the Chl derivative mixture (Section IV.A.1.c) using identical developing solvents and elution conditions. The finally separated BChl derivatives are transferred to diethylether and recovered by standard procedures.

2. Sepharose CL-6B Columns

a. Preparation of Sepharose CL-6B Columns

An aqueous suspension of Sepharose CL-6B (100 ml) is washed successively with distilled water, acetone, acetone-hexane (2:1, v/v), acetone-hexane (1:2, v/v), hexane-2-propanol (10:1, v/v) and finally hexane-2-propanol (20:1,v/v). The Sepharose CL-6B can be stored as a suspension in the last solvent until required. The column material can be re-used if it is regenerated by successive washing using the procedures described above.

b. Separation of Chlorophylls a and b

The mixture of Chls *a* and *b*, obtained from the DEAE-Toyopearl column (Section IV.A.1.b), is then separated on a Sepharose CL-6B column. The Chls *a* and *b* solution is completely dried by evaporation under reduced pressure and re-dissolved in a small volume of hexane-2-propanol (20:1, v/v) before passing through a syringe filter to remove any undissolved materials. The Chl filtrate is then loaded onto a column of Sepharose CL-6B which is developed with hexane-2-propanol (20:1, v/v) and, after completely eluting the Chl *a*, the developing solvent is changed to a hexane-2-propanol (10:1, v/v) to elute the Chl *b*.

c. Separation of Bacteriochlorophyll a Pigment Mixtures

After evaporating the BChl *a* solution to dryness

Table 1. Separation of chlorophyll *a* and its derivatives by Diethylaminoethyl-Toyopearl column chromatography

Elution order	Solvent	Color	Absroption maximum (nm)	Pigments
1	acetone	pale gray	666	pheophytin *a*
2	99% acetone	blue-green	663	chlorophyll *a*
3	98% acetone + 0.1% ammonium acetate	gray	666	pheophorbide *a*
4	95% aceton + 0.2% ammonium acetate	blue-green	662	chlorophyllide *a*

under reduced pressure, the pigments are dissolved in a small volume (< 2 ml) of hexane/2-propanol (20:1, v/v) and passed through a syringe filter. The filtrate is loaded onto a column of Sepharose CL-6B (6–8 ml bed volume), prepared as described above, and developed with hexane/2-propanol (20:1, v/v). Carotenoids and BPhe *a* are eluted first followed by BChl *a* without any contamination by other pigments and lipids (Omata and Murata, 1983).

3. Diethylaminoethyl-Cellulose Columns

a. Separation of Chlorophylls a and b

A useful open-column method for separating Chls *a* and *b*, and plant carotenoids uses DEAE-cellulose with $CHCl_3$ and $CHCl_3$-methanol mixtures as eluants (Sato and Murata, 1978). The column has considerable resolving power and has been used to separate pigments extracted from leaves with methanol-$NaBH_4$ solutions. Washing with $CHCl_3$ firstly elutes a yellow carotenoid band then a blue Chl *a* band. This is followed by a split blue band of [3-ethyl-7-hydroxymethyl]-Chl *b* and [7-hydroxymethyl]-Chl *b*: after the 3-ethyl derivative was eluted from the column with $CHCl_3$, the [7-hydroxymethyl]-Chl *b* was eluted with $CHCl_3$ containing 2% methanol; finally, a strongly absorbing band of [7-hydroxymethyl-13^1-hydroxy]-Chl *b* was eluted with $CHCl_3$ containing 10% methanol (Porra et al., 1993).

b. Separation of Bacteriochlorophyll a Pigment Mixtures

Carotenoids can be separated from BChl *a* in crude extracts of photosynthetic bacteria on DEAE-cellulose columns with $CHCl_3$ as eluent and the BChl *a* subsequently eluted with $CHCl_3$ containing 0.2% methanol (Sato and Murata, 1978). The column also has sufficient resolution to resolve [3-vinyl]-BChl *a*, BChl *a* and [3-(1-hydroxy)-ethyl]-BChl *a* which can be successively eluted with $CHCl_3$ containing 0.1, 0.2 and 0.4% methanol, respectively (Porra et al., 1995).

B. Sucrose Column Chromatography

Powdered sucrose is a mild and selective adsorbent that is very effective for the preparation of Chls *a* and *b* in large quantities. Therefore, this procedure is used widely, despite its poor reproducibility due to the difficulty of achieving uniform packing density by hand, which leads to a spread of the separating pigment zones during development. Further, care must be taken to prevent the adsorption of atmospheric moisture by the powdered sucrose during column packing and any standing period before its use: moisture affects the spread of the developing pigment zones in the column (Strain and Sherma, 1969). Although it is difficult to obtain purified Chl samples with a single run of this chromatography, highly-purified Chls can be obtained simply by the re-chromatography of the separated Chls in a similar manner. The solvent and elution program described in Section IV.B.2 for the separation of pigments was originally developed by Perkins and Roberts (1962).

1. Powdered Sucrose and Column Packing

The powdered sucrose used for column chromatography is a commercial 'confectioner's sugar' containing 3% corn starch by volume. This sucrose is dried overnight in an oven at 80 °C and, after cooling, is stored in a tightly sealed bottle and kept in a desiccator until use. Prior to column packing, the sucrose is sieved through a household flour sieve. The powdered sucrose columns are prepared by successively packing small portions of dry powder with a neatly-fitting plunger (Strain and Sherma, 1969). Powdered sucrose is poured into the chromatographic glass column fitted with a sintered glass disc and compressed with the plunger to pack the sucrose tightly and uniformly: this procedure is repeated until the required amount is added and the desired column height is achieved. Usually, the loading capacity is about 35–40 mg of Chls per 100 g of powdered sucrose. A wet column-packing method has been described by Iriyama et al. (1979).

The packed column is then fitted to a Büchner flask so that developing solvents can be drawn through the column under reduced pressure generated by an efficient tap pump.

2. Separation of Chlorophylls a and b

The acetone solution of the partially purified Chls from dioxane-water precipitation (Section III.A) is evaporated under reduced pressure and the residue dissolved completely in a minimum volume of diethylether prior to dilution with petroleum ether. Just before loading the sample, the tap pump is turned on to draw petroleum ether through the column and, after

petroleum ether begins to drop from the column, the Chl solution is loaded onto the column and development with petroleum ether is continued. Chls are strongly adsorbed at the top of the column, whereas the non-adsorbed carotenes (first yellow band) are gradually eluted. The column is developed until the carotene band is completely eluted from the column. The developing solvent is then changed to 10% (v/v) diethylether in petroleum ether to separate Chl *a* and xanthophylls. This solvent achieves the separation of the pigments in the following sequence: Phe *a* (grey band), xanthophylls (second yellow band) and Chl *a* (blue-green band). When these bands have almost separated, the developing solvent is again changed to 0.5% (v/v) 2-propanol in petroleum ether to separate Chl *b* as a yellow-green band. Because partially purified Chls (twice dioxane precipitated) are applied to the column, most polar carotenoids have been removed and only a very faint yellow band of lutein and zeaxanthin appeared (Table 2): the examination and effectiveness of the partial purification of Chls by dioxane precipitation prior to sucrose chromatography has been discussed in Section III.A. While contamination of the Chl *a* zone by xanthophylls (second yellow zone) may occur, re-chromatography of the Chl *a* zone effectively eliminates the yellow pigment. The Chls *a* and *b* zones are manually dug out of the glass column with a long-handled spatula, and each zone is transferred to a separate sintered glass filter and the Chls eluted with diethylether. The Chl *a* and Chl *b* are separately recovered by evaporation of the diethylether under reduced pressure. The Chl *a* and the Chl *b* are separately dissolved in diethylether and diluted with petroleum ether, and re-chromatographed on separate columns as described above. Table 2 shows the sequence of development of the zones of Chls *a* and *b*, Chl derivatives and carotenoids by chromatography of the acetone extract of the twice dioxane-precipitated pigments and is useful for the identification of Chls and their derivatives. In these operations, the brief use of a long wavelength (366 nm) UV light source is a convenient tool for checking the resolved zones and the completeness of elution of Chls.

3. Separation of Bacteriochlorophyll a Pigment Mixtures

A complicated method for isolation of BChl *a* uses four successive sucrose columns with four successive solvents including petroleum ether, petroleum ether containing benzene (50%, v/v) and petroleum ether with diethylether (10%, v/v) and then 20% (v/v) to separate BChl *a* from bacterial carotenoids, allomerized BChl *a* and the oxidation product, [3-acetyl]-Chl *a*: for details of this method, see Smith and Benitez (1955). Introducing dioxane-water preparation for initial part-purification of BChl *a* could possibly simplify this procedure; however, the simpler methods with DEAE-Toyopearl or Sepharose CL-6B and especially with DEAE-cellulose are recommended for isolation of BChl *a* (Sections IV. A.1.d, IV.A.2.c and IV.A.3.b).

Acknowledgments

The author thanks Wataru Miyata for his technical assistance in the analysis of chlorophylls and carotenoids.

Table 2. Chromatographic sequence of chlorophylls and carotenoids in a column of powdered sucrose using dioxane-precipitated chlorophylls as a source and developing with petroleum ether containing 0.2–0.5% 1-propanol

Rentention order[a]	Pigments	Color of zones
1	chlorophyll *b*	yellow-green
2	chlorophyll *a*	blue-green
3	lutein and zeaxanthin	yellow[b]
4	pheophytin *a*	gray
5	non-adsorbed carotenes	yellow[c]

[a] Retention order shows the disposition of pigment zones from the top of the column. [b] This is usually a very faint band. [c] These carotenes are completely eluted from column.

References

Araki S, Oohusa T, Omata T and Murata N (1984) Column chromatographic separation of chlorophyllide *a* and pheophorbide *a*. Plant Cell Physiol 25: 841–843

Holden M (1976) Chlorophylls. In: Goodwin, TW (ed) Chemistry and Biochemistry of Plant Pigments, Vol 2, pp 1–37. Academic Press, London

Iriyama K, Ogura N and Takamiya A (1974a) A simple method for extraction and partial purification of chlorophyll from plant material, using dioxane. J Biochem 76: 901–904

Iriyama K, Yoshiura M and Asai H (1974b) Visible absorption spectra of chlorophyll *b* in methanol, dioxane and/or water solutions. Chem Lett 1974: 997–1000

Iriyama K, Shiraki M and Yoshiura M (1979) An improved method for extraction, partial purification, separation and isolation of chlorophyll from spinach leaves. J Liquid Chromatogr 2: 255–276

Kohata K, Hanada K, Yamauchi Y and Horie H (1998) Pheophorbide *a* content and chlorophyllase activity in green tea. Biosci Biotechnol Biochem 62: 1660–1663

Omata T and Murata N (1980) A rapid and efficient method to prepare chlorophyll *a* and *b* from leaves. Photochem Photobiol 31: 183–185

Omata T and Murata N (1983) Preparation of chlorophyll *a*, chlorophyll *b* and bacteriochlorophyll *a* by column chromatography with DEAE-Sepharose CL-6B and Sepharose CL-6B. Plant Cell Physiol 24: 1093–1100

Perkins HJ and Roberts DWA (1962) Purification of chlorophylls, pheophytins and phephorbides for specific activity determinations. Biochim Biophys Acta 58: 486–498

Porra RJ (1990) The assay of chlorophylls *a* and *b* converted to their respective magnesium-rhodochlorin derivatives by extraction from recalcitrant algal cells with aqueous alkaline methanol: Prevention of allomerization with reductants. Biochim Biophys Acta 1015: 493–502

Porra RJ, Schäfer W, Cmiel E, Katheder I and Scheer H (1993) The unexpected reduction of vinyl group of chlorophyll *b* by sodium borohydride in methanolic extracts of maize leaves and its inhibition by 8-hydroxyquinoline. Z Naturforsch 48c: 745–748

Porra RJ, Schäfer W, Katheder I and Scheer H (1995) The derivation of the oxygen atoms of the 13^1-oxo and 3-acetyl groups of bacteriochlorophyll *a* from water in *Rhodobacter sphaeroides* cells adapting from respiratory to photosynthetic conditions: Evidence for an anaerobic pathway for the formation of *iso*cyclic ring E. FEBS Lett 371: 21–24

Rüdiger W and Schoch S (1988) Chlorophylls. In: Goodwin TW (ed) Plant Pigments, pp 1–59. Academic Press, London

Sato N and Murata N (1978) Preparation of chlorophyll *a,* chlorophyll *b,* and bacteriochlorophyll *a* by means of column chromatography with diethylaminoethylcellulose. Biochim Biophys Acta 501: 103–111

Shioi Y (1991) Analytical chromatography of chlorophylls. In: Scheer H (ed) Chlorophylls, pp 59–88. CRC Press, Boca Raton

Shioi Y and Sasa T (1984) Terminal steps of bacteriochlorophyll *a* phytol formation in purple photosynthetic bacteria. J Bacteriol 158: 340–343.

Shioi Y, Fukae R and Sasa T (1983) Chlorophyll analysis by high-performance liquid chromatography. Biochim Biophys Acta 722: 72–79

Smith JHC and Benitez A (1955) Chlorophylls: Analysis in plant materials. In: Paech K and Tracey MV (eds) Modern Methods of Plant Analysis, Vol IV, pp 143–196. Springer-Verlag, Berlin

Strain HH and Sherma J (1969) Modifications of solution chromatography illustrated with chloroplast pigments. J Chem Educ 46: 476–483

Strain HH and Svec WA (1966) Extraction, separation, estimation, and isolation of the chlorophylls. In: Vernon LP and Seely GR (eds) The Chlorophylls, pp 21–66. Academic Press, New York

Strain HH, Cope BT and Svec WA (1971) Analytical procedures for the isolation, identification, estimation, and investigation of the chlorophylls. In: San Pietro A (ed) Methods in Enzymology, Vol 23, Photosynthesis, Part A, pp 452–476. Academic Press, New York

Svec WA (1979) The isolation, preparation, characterization, and estimation of the chlorophylls and the bacteriochlorophylls. In: Dolphin D (ed) The Porphyrins, Vol 5, pp 341–399. Academic Press, New York

Zapata M, Rodriguez F and Garrido, JL (2000) Separation of chlorophylls and carotenoids from marine phytoplankton: A new HPLC method using a reversed phase C_8 column and pyridine-containing mobile phases. Mar Ecol Prog Ser 195: 29–45

Chapter 10

Chlorophyll Metabolism, an Overview

Wolfhart Rüdiger*
Department Biologie I (Botanik), Universität München, Menzinger Str. 67, D-80638 München, Germany

Bernhard Grimm*
Institut für Biologie/Pflanzenphysiologie, Humboldt-Universität zu Berlin, Unter den Linden 6, D-10099 Berlin

Summary

This introductory chapter collates and highlights important issues in the chlorophyll biosynthetic and degradative pathways, which are described and discussed in the following seven chapters. These pathways occur in a large and very diverse range of photosynthetic organisms including photosynthetic bacteria, algae and higher plants. They share some common enzymatic steps; but, many alternative steps have been occasioned by the

*Authors for correspondence, email: ruediger@lrz.uni-muenchen.de; bernhard.grimm@rz.hu-berlin.de

Bernhard Grimm, Robert J. Porra, Wolfhart Rüdiger and Hugo Scheer (eds): Chlorophylls and Bacteriochlorophylls: Biochemistry, Biophysics, Functions and Applications, pp. 133–146.

new environmental conditions encountered, or by the new metabolic arrangements and by special adaptations evolved by the various members of this exceptionally diverse group. A second aim of this introductory chapter is a brief introduction to some aspects on chlorophylls and related tetrapyrroles, which are not treated in the following chapters of this book.

I. Introduction

Metallo-tetrapyrrolic compounds are widespread in nature and have indispensable functions as prosthetic groups in many metabolic and energy transduction pathways. The structural and functional roles in photosynthesis of the magnesium-tetrapyrroles, namely chlorophylls (Chls) and bacteriochlorophylls (BChls), are a thread running through all chapters of this book. Besides the unique and essential role of Chls and BChls in light-harvesting and transduction in photosynthesis, the biosynthesis, accumulation and degradation of Chls and BChls are also conceivably associated with chloroplast development, photomorphogenesis and chloroplast-nuclear genome signaling (Thomas and Howarth, 2000; Papenbrock and Grimm, 2001; Rodermel, 2001; Chapter 16, Beck and Grimm).

The appearance of Chl in terrestrial plants in spring and its disappearance in autumn shows the season-dependent nature of these processes; this is not the case, however, in marine organisms where synthesis and degradation occur all year round. World-wide, more than 10^9 tons of Chl are formed and degraded every year (Hendry et al., 1987; Brown et al., 1991); most of this occurs in the oceans. The biochemical and genetic preconditions for Chl breakdown have been reported, indicating a highly regulated pathway until the degradation intermediates are no longer photochemically active pigments capable of light-initiated cell damage.

Abbreviations: Acp. – Acidiphilium; ALA – 5-aminolevulinic acid; BChl – bacteriochlorophyll; CAO – chlorophyllide oxygenase; Chl – chlorophyll; Chlide – chlorophyllide; DPOR – dark protochlorophyllide oxidoreductase; DV – divinyl; *E. – Escherichia*; GGPP – geranylgeranyl diphosphate; HMB – hydroxymethylbilane; LHC – light harvesting chlorophyll binding complex; LHCB – light harvesting chlorophyll binding protein of Photosystem II; LPOR – light-dependent protochlorophyllide oxidoreductase; MV – monovinyl; PΦB – phytochromobilin; PCB – phycocyanobilin; PChlide – protochlorphyllide; PEB – phycoerythrobilin; PhyPP – phytyl diphosphate; POR – protochlorophyllide oxidoreductase; PPOX – protoporphyrinogen oxidase; Proto – protoprophyrin; Protogen – protoporphyrinogen; *Rba. – Rhodobacter*; RC – reaction center; Urogen – uroporphyrinogen; Zn-Phe – zinc pheophytin

II. The Diversity of Tetrapyrrole Metabolic Pathways

Chl biosynthesis is one biosynthetic pathway occurring in a vast network of branching pathways leading to the formation of various metallo-tetrapyrrole cofactors or prosthetic groups including, amongst others, hemes, cobalamines, and phycobilins (Fig. 1)

In general, Mg-containing Chls or BChls are typical for photosynthetic organisms; an exception, however, is the genus *Acidiphilium (Acp.)* which is a group of obligatory acidophilic chemo-organotrophic bacteria that photosynthesize under aerobic conditions (Hiraishi and Shimada, 2001). This genus contains [Zn]-BChl *a* in both the antennae and in the reaction center (Wakao et al., 1996; Mimuro et al., 2000). Because only Mg-containing BChl precursors were detected in *Acp. rubrum* and, since heterologous expression of the chelatase subunits of *Acp. rubrum* in *Rhodobacter (Rba.) capsulatus* resulted only in Mg-containing BChl (Masuda et al., 1999; Takamiya et al., 2000), one assumes that Zn is introduced in exchange for Mg only at a late biosynthetic step rendering the Zn-BChl *a* secondary product of the Mg branch.

Protoheme, an iron-tetrapyrrole, is present in all subcellular compartments of nearly all organisms where they function as catalases and peroxidases or as either oxygen or electron carriers in respiratory processes. Other important products of the 'iron branch' include modified forms of protoheme (i.e., hemes a_1, a_2, a_3 and *c*) and linear tetrapyrroles formed from protoheme (i.e., phycobilins and phytochromobilin, see Section B.6). In addition to the conversion of uroporphyrinogen (urogen) III to cobalamines (vitamin B_{12}) by the 'cobalt branch,' urogen III may be converted to siroheme by a minor 'iron branch' (see Section B.5), or to coenzyme F_{430} by a 'nickel branch' (Fig. 1). The cobalt and nickel branches are possessed by micro-organisms that synthesize the cobalamine coenzyme, vitamin B_{12} (Battersby, 1994), and coenzyme F-430 (Friedmann et al., 1990), respectively: the latter is a cofactor for methane production. While most enzymatic steps of Chl biosynthesis and the genes encoding the respec-

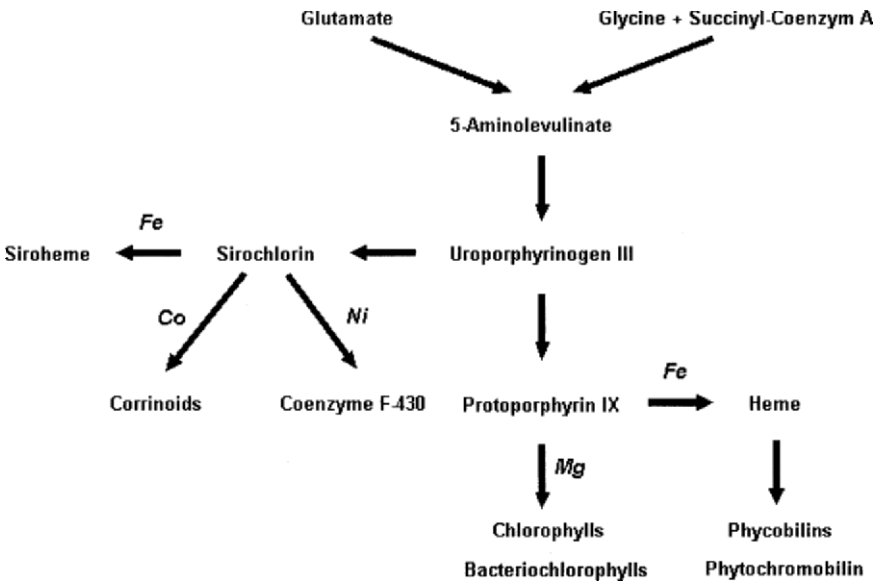

Fig. 1. Scheme of tetrapyrrole biosynthetic pathways. Chlorophyll biosynthesis, the magnesium branch, shares early steps with the iron, cobalt, and nickel branches. Branching points occur at uroporphyrinogen III and protoporphyrin IX.

tive enzymes have been identified, the current view on the regulation is still fragmentary. Nevertheless, a few characteristics and principles of Chl metabolism will be addressed here.

A. The Structure of the Chlorophyll Biosynthetic Pathway

The description of Chl synthesis in this section of the book follows the conventional subdivision into three sections:

1. The formation of 5-aminolevulinic acid (ALA) (Chapter 11, Beale; Chapter 12, Jahn et al.)

2. The transformation of 8 ALA molecules into Mg and Fe–containing porphyrins (Chapter 13, Yaronskaya and Grimm)

3. The pathway from protochlorophyllide (PChlide) to Chl (Chapter 14, Rüdiger) and BChls (Chapter 15, Frigaard et al.)

This subdivision is justified by the enzymatic steps involved, the metabolic intermediates they form, and their organellar localization. Further, the regulatory differences of the multiple enzymatic steps within these three subdivisions also justify this partition into three sections. Although the expression of each enzyme is individually and independently controlled, a few regulatory (rate-limiting) steps of the pathway determine the overall synthesizing activity and the metabolic flow. Consequently, these enzymes are strictly controlled by various endogenous and environmental factors; in contrast, expression of other enzymes of the pathway apparently ensures sufficient formation of their products and that their catalytic capacities do not limit the metabolic flow.

1. Formation of 5-Aminolevulinic Acid

The first specific precursor molecule of tetrapyrrole formation, and common to all branches, is ALA, which can be formed by two alternative pathways. Plants, archaea and most bacteria, including cyanobacteria, synthesize ALA from glutamate in three enzymatic steps via glutamyl-tRNA; this is considered the more ancient and more ubiquitous pathway. The other 'pathway,' catalyzed by a single enzyme, ALA synthase, condenses glycine with succinyl-coenzyme A followed by a spontaneous decarboxylation step to form ALA. This route is found in the α-subgroup of the proteobacteria, which includes several bacteriochlorophyll-producing species, and also in animals and fungi where it is localized in the mitochondria. It has been postulated, on the basis of 16S RNA se-

quences, that the endosymbiontic precursors of mitochondria are closely related to the present α-subgroup of the proteobacteria; further, both mitochondria and α-proteobacteria share the occurrence of ubiquinone. All attempts to find ALA synthase in the mitochondria of higher plants failed. Both ALA-forming pathways are discussed in detail by Beale in Chapter 11, and the structure of the enzymes of the glutamate pathway by Jahn in Chapter 12.

2. Intermediate Steps

There are three enzymatic steps from ALA to urogen III; these are shared by all tetrapyrrole pathways, and the subsequent three steps to protoporphyrin IX (Proto) are common to both heme and Chl formation (see Fig. 1). Details are discussed by Yaronskaya and Grimm in Chapter 13.

It is remarkable that the first tetrapyrrole is a linear series I molecule, hydroxymethylbilane (HMB) I, which is transferred and bound to urogen III synthase which catalyses cyclization to urogen III. In contrast, spontaneous cyclization to urogen I indicates either interruption of this transfer or absence of the urogen III synthase enzyme. Urogen I may also be formed by an overabundance of HMB. It can be caused, for example, by feeding ALA to by-pass the rate-limiting step of ALA formation and, thus, overwhelm the rate-limiting activity of urogen III synthase.

The next enzymatic steps to Proto are shared by both the Fe and the Mg branch. The Mg branch begins with the insertion of Mg into Proto; thus, the enzyme Mg-chelatase is the pacemaker for this branch. The intermediate steps include the formation of Mg-proto-monomethylester ester, the formation of the isocyclic ring E to produce [8-vinyl]PChlide *a*, often named divinyl (DV)-PChlide *a*, and the reduction of the 8-vinyl group leading to PChlide *a*.

3. Formation of Chlorophylls a and b

The late steps include the reduction of PChlide *a* to chlorophyllide (Chlide) *a*, the conversion of Chlide *a* to Chlide *b,* and back into Chlide *a* during Chl *b* degradation (see Chapter 17, Kräutler and Hörtensteiner), and the formation of esterified Chls by prenylation of Chlides. Here some general aspects of these reactions are discussed, but for a detailed treatment see Chapter 14 (Rüdiger).

Two separate enzymes exist for the hydrogenation of PChlide to Chlide: a light-independent (dark) PChlide oxidoreductase, DPOR (D for dark), and a light-dependent enzyme, LPOR (L for light), commonly named POR. The light-independent pathway is the only one present in anoxygenic photosynthetic bacteria, leading to BChl formation. The lack of Chl formation in dark-grown angiosperms indicates that the light-dependent pathway is the only one operating in angiosperms, leading to Chls *a* and *b*; however, a few angiosperms continue to form Chl in darkness after a light period, a process for which a mechanism still needs to be found (Adamson et al., 1997). Both pathways, however, coexist in cyanobacteria, algae, mosses, ferns and gymnosperms, and these organisms have the advantage that after deletion of one pathway, for example by mutation, the other pathway can still maintain Chl synthesis; however, it is not yet known how much each pathway contributes to Chl formation in these organisms under normal physiological conditions.

Mutants of green algae with non-functional DPOR have frequently been isolated and detailed analyses exist for such mutants of *Chlamydomonas reinhardtii* which only form Chl in the light; in addition to a mutation in one of the structural chloroplast genes, *CHLL, CHLN,* or *CHLB* encoding the DPOR subunits, a mutation in one of at least seven nuclear *y*-loci lead to the 'yellow-in-the-dark' phenotype (Fujita and Bauer, 2003). The precise function of the nuclear gene products is not yet known.

The oxygen at C-7 of Chl *b* is introduced into the C7 methyl group of Chlide *a* by oxygenase activity (Schneegurt and Beale, 1992; Porra et al., 1993). Oster et al. (2000) demonstrated that this conversion required two sequential oxygenation steps catalyzed by Chlide *a*-oxygenase (CAO). The preferred substrate for CAO is Chlide *a*, although there is an indication that PChlide *a* may very slowly be oxygenated to PChlide *b* (Xu et al., 2002). That PChlide *b* is the main pigment in prolamellar bodies of etioplasts, and is not photoconverted to Chlide *b* but serves as a light-harvesting pigment (Reinbothe et al., 1999; 2003a,b), has been questioned by others (Scheumann et al., 1999; Armstrong et al., 2000; Kolossov and Rebeiz, 2003). Reduction of the 7-formyl group to a methyl group can take place with Chl *b* and with Chlide *b* (Scheumann et al., 1998). The mutual conversion of Chl *a* into *b* and Chl *b* into *a*, the so-called 'chlorophyll cycle' (Ito et al., 1996), may allow plants to alter their Chl *a/b* ratio to optimize their adaptation to varying light conditions, and may also be important for Chl turnover: degradation of

Chl *b* proceeds in higher plants, in contrast to algae (Gossauer and Engel, 1996), via Chlide *a* (Chapter 17, Kräutler and Hörtensteiner).

The final step of Chl biosynthesis is the introduction of the phytol residue, catalyzed by Chl synthase. Chl synthase accepts either geranylgeranyl diphosphate (GGPP) or phytyl diphosphate (PhyPP) as the first substrate and Chlide *a* or *b* as the second substrate. Hydrogenation of geranylgeraniol to phytol can occur before or after incorporation into the pigment; this allows some flexibility for the pathway. The esterification renders the pigment highly lipophilic and, as expected, most binding sites of Chl-binding proteins are specific for esterified Chls.

B. Other Chlorophylls and Related Tetrapyrroles

1. Chlorophyll c

C-type Chls are Mg-porphyrins. Characteristic for most of them is a 17-acrylate instead of a 17-propionate side chain on ring D. Since spontaneous dehydration of the 13^1-hydroxy intermediate, the putative primary product of the oxidative cyclase responsible for isocyclic ring E formation, would yield a product containing an acrylate side chain on ring C (Leeper, 1991), it seems reasonable to assume an analogous reaction sequence also for the 17-propionate side chain on ring D: oxygenation at $C17^1$ followed by dehydration. So far, no enzyme carrying out these steps has been described. It is noteworthy that Chl c_1 is a competitive inhibitor of the light-dependent POR since it binds to the enzyme but is not reduced to a chlorin (Helfrich et al., 2003): the authors assume that the acrylate double bond between 17^1 and 17^2, which is conjugated to the π system of the macrocycle, changes the electronic structure of the S1 state rendering a photoreduction by POR impossible. Such a change could also be important for energy transfer, the main function of Chls of the c-type.

2. Divinyl and Monovinyl Chlorophylls

In *Prochlorococcus* and several other marine prokaryotes, Chls *a* and *b* are present as 'divinyl' (DV) compounds (see Chapter 4, Kobayashi et al.). The most plausible explanation is the lack of an 8-vinyl reductase in these organisms. This explanation, however, does not hold for chromophytes: in many of them, both the DV compound, Chl c_2, and the 'monovinyl' (MV) compound, Chl c_1, are present (see Chapter 3, Zapata et al.). In higher plants, several Chl precursors have been found as DV and MV forms: this observation is possibly explained by parallel pathways (Tripathy and Rebeiz, 1986); an alternative explanation could be the lack of specificity of the vinyl reductase and/or shortage of NADPH (Griffiths, 1991). In some plants, the reduction of the vinyl group occurs after the reduction of PChlide to Chlide leading to accumulation of DV-PChlide in the dark. The preferential accumulation of either one of the PChlide forms was the basis for a classification as MV and DV plants (Carey and Rebeiz, 1985). Since re-accumulation after a light pulse did not always give the same PChlide species as before the light pulse, Rebeiz et al. (1986) extended the classification to the four classes Dark-DV/Light-DV, Dark-MV/Light-DV, Dark-DV/Light-MV and Dark-MV/Light-MV plants. Among the well-studied plants, cucumber belongs to the first class and barley to the second class. In summary, the genetic disposition of plants (e.g., substrate specificity of vinyl reductase) and environmental conditions (e.g., light pulse leading to a transient depletion of NADPH) can determine when reduction of the 8-vinyl to the 8-ethyl group occurs in the chlorophyll biosynthetic pathway: either early, at the PChlide level, or later, after reduction to the Chlide level. This indicates a certain flexibility of the pathway.

3. Pigments of Reaction Centers

While the bulk of Chl *a* has the $13^2(R)$ configuration, one Chl of the 'special pair' in the reaction center (RC) of cyanobacteria and higher plants is $13^2(S)$ Chl *a*, commonly named Chl *a*′ ('Chl *a* prime'). As outlined by Kobayashi et al. (Chapter 4), other 'prime' pigments probably occur in prokaryotic RCs of type I; for example, Chl *d*′ in the cyanobacterium *Acaryochloris marina*, BChl *g*′ in heliobacteria and BChl *a*′ in green sulfur bacteria. Nothing is known about the biosynthesis of these 'prime' pigments; indirect evidence, however, allows the exclusion of some possibilities. POR does not accept PChlide *a*′ as a substrate, and Chl synthase does not prenylate Chlide *a*′ (Helfrich et al., 1994; 1996); thus, the transition from the $13^2(R)$ to the $13^2(S)$ compound must occur with the esterified Chl unless there are specialized enzymes that have remained undetected. This latter suggestion is unlikely as epimerization of Chl is a spontaneous, acid- or base-catalyzed reac-

tion: formation of some Chl *a*′ is almost unavoidable when a solution of Chl *a* is kept for several hours. Non-enzymatically produced Chl *a*′ can certainly be stabilized by protein binding. Helfrich et al. (1994) discussed the advantage of having an active reversible epimerase at the beginning of greening when Chl is preferentially incorporated into RCs and at the onset of Chl degradation because Chl *a*′ is not hydrolyzed by chlorophyllase (Fiedor et al., 1992).

Another type of pigment found in type II-RCs is the Mg-free pheophytin. Since all enzymes of the Mg-branch, including Chl synthase, do not accept metal-free tetrapyrroles as substrates, it is most likely that pheophytin is formed by demetallation of esterified Chl. Mg-dechelatase activity, however, has been discussed in connection with Chl degradation and is believed to operate on the non-esterified Chlide (Chapter 17, Kräutler and Hörtensteiner); but, for biosynthesis of pheophytin, the dechelatase would be required to react with the esterified Chl. Since Chls readily loose their central Mg^{2+} by an acid-catalyzed reaction, it is difficult to distinguish between an enzymatic and a non-enzymatic reaction.

4. Bacteriochlorophylls

Preliminary ideas about BChl biosynthesis arose from studies of the intermediates accumulated in inhibited cultures of *Rba. sphaeroides* and in cultures of pigment mutants of various photosynthetic bacteria (for a review see Jones, 1978). A more thorough knowledge of this pathway came with the identification and cloning of a gene cluster containing photosynthesis-related genes from *Rba. capsulatus* (Alberti et al., 1995) and the subsequent production and investigation of deletion mutants for the single genes. Thus, the accumulation of BChl intermediates indicated the reaction catalyzed by the respective gene products and the order of the enzymatic reactions.

Formally, the biosynthesis of BChl *a* is the extension of Chl biosynthesis beyond the step of Chlide *a* formation. The steps from simple precursors to Chlide *a* are *not only* formally identical in bacteria and higher plants *but also* are catalyzed by homologous enzymes (with some exceptions regarding oxygenation reactions—see below). Sequence studies with a range of organisms allowed the conclusion that the basic reactions for tetrapyrrole biosynthesis were invented only once during evolution: modifications of and additions to the pathway during evolution are discussed by Larkum (Chapter 18). As a practical consequence, identification of a gene for a certain function in the gene cluster of *Rba. capsulatus* helped to discover the corresponding gene in higher plants. It must be mentioned, however, that some steps are catalyzed by non-homologous enzymes: higher plants use molecular oxygen for coproporphyrinogen III oxidase, protoporphyrinogen (Protogen) IX oxidase (PPOX) and MgProto monomethylester cyclase, while anaerobic bacteria use different mechanisms and different enzymes for the corresponding steps, for example, a hydratase mechanism for introduction of oxygen at C-13^1. Interestingly, experiments with ^{18}O-labelling revealed that the facultative aerobic bacterium *Rhodovulum sulfidophilum* uses a hydratase pathway for isocyclic ring formation anaerobically, but both a hydratase and oxygenase operate in the presence of oxygen (Porra et al., 1998).

Two enzymes, encoded by the gene loci *bchA* and *bchF* of *Rba. capsulatus*, were found to metabolize Chlide *a*; the consequence is a branched pathway at this step, confirmed by the observation that Chlide *a* accumulates only when both loci, *bchA* and *bchF*, are mutated (Bollivar et al., 1994). The *bchA* locus contains the *bchX, bchY,* and *bchZ* genes, which probably encode three subunits of a chlorin reductase. While direct biochemical evidence is still missing, the following evidence, nonetheless, supports this view:

1) the three genes are related to the genes *bchN, bchB* and *bchL* encoding the subunits of DPOR; and,

2) deletion of any of the three genes leads to accumulation of [3^1-hydroxy]-Chlide *a* (Burke et al., 1993a; McGlynn and Hunter, 1993).

The accumulation of [3-vinyl]-BChlide *a* after deletion of the *bchF* gene indicated that its gene product modifies the 3-vinyl group (Burke et al., 1993b); it must be the C-3^1 vinyl hydratase because deletion of *bchC*, which encodes an oxidase, leads to accumulation of [3^1-hydroxy]-BChlide *a* (McGlynn and Hunter, 1993).

The biosynthesis of BChls *c*, *d*, and *e* formally requires different modification reactions of Chlide *a*. Because these pigments are chlorins, there is no chlorin reductase step involved. Since these three BChls lack the 13^2-methoxycarbonyl group, this group must be removed from Chlide *a* or one of its precursors. Further modifications involve multiple methylation reactions; for example, at C-8^2, C-12^1

and C-20. Genetic analysis of the biosynthesis of these three BChls is far advanced and is described in detail by Frigaard et al. (Chapter 15). The last step of biosynthesis of all BChls is the esterification described by Rüdiger (Chapter 14).

5. Siroheme

Siroheme, the cofactor of sulfite and nitrite reductases, is essential for sulfate and nitrate assimilation in eubacteria, archaebacteria, fungi and plants. Its biosynthesis branches off from Chl and heme biosynthesis at urogen III with two successive methylation steps, first at C-2 and then at C-7, producing dihydrosirohydrochlorin also known as precorrin-2: a further methylation at C-20 forms precorrin-3, a committed intermediate in vitamin B_{12} biosynthesis (see Fig.1; for review see Battersby, 1994). A $NAD(P)^+$-dependent dehydrogenation of dihydrosirohydrochlorin generates sirohydrochlorin, which is then chelated with iron to form siroheme.

As in many other cases, knowledge of siroheme formation came from work with bacteria. The c*ysG* gene, first identified by use of cysteine auxotrophs of *Escherichia* (*E.*) *coli*, was shown to encode the multifunctional siroheme synthase, a 50 kDa protein that catalyzes all four reactions converting urogen III to siroheme (Warren et al., 1994). The X-ray structure, with a resolution of 2.2 Å, was recently described for the multifunctional siroheme synthase from another enteric bacterium, *Salmonella enterica* (Stroupe et al., 2003). These same reactions are carried out by three enzymes in *Bacillus megaterium* and by two in *Saccharomyces cerevisiae* (cited by Stroupe et al., 2003). In higher plants, cDNAs encoding urogen III C-methyltransferase have been cloned: a cDNA from maize roots encoding a protein that was induced by nitrate (Sakakibara et al., 1996), and a cDNA from *Arabidopsis thaliana* by functional complementation of an *E. coli cysG* mutant (Leustek et al., 1997). The encoded precursor proteins contained typical pre-sequences and were imported into plastids, confirming the expected plastid location of the methyltransferase. The lack of reductase and chelatase activity, and the comparison of the amino acid sequence with that of the *cysG* gene product, indicated that plants use several enzymes and not one multifunctional enzyme for the complete synthesis of siroheme. The suggestion of covalent binding of the cofactor *S*-adenosyl-L-methionine to siroheme synthase, deduced from biochemical studies, was not supported by the X-ray structure (Stroupe et al., 2003).

6. Phytobilins

Phytobilins, the linear tetrapyrrole bile pigments of plants, include phytochromobilin (PΦB), which is well known as a photoreceptor chromophore in higher plants and some cyanobacteria, phycocyanobilin (PCB) and phycoerythrobilin (PEB) and related bilins, which are major chromophores of light-harvesting complexes in cyanobacteria, red algae and cryptomonads. More recently, phytochrome-related phytobilins have also been found in many other bacteria (Montgomery and Lagarias, 2002). Phytobilins are formed by an extension of heme biosynthesis. The first step is the oxidative cleavage of the heme macrocycle at the C-5 methene bridge with removal of Fe and carbon monoxide: the reaction product is biliverdin IXα. In mammals, this is a step in heme degradation catalyzed by a NADPH-dependent heme oxygenase. Although heme oxygenases in cyanobacteria and higher plants are ferredoxin-dependent, their sequences are related to those of the mammalian enzyme which helped to identify and clone their genes (Cornejo et al., 1998; Davis et al., 1999; Muramoto et al., 1999).

In higher plants, biliverdin IXα is reduced to PΦB by PΦB:ferredoxin oxidoreductase, also known as PΦB synthase (Frankenberg and Lagarias, 2003): this plant enzyme is distinguished from mammalian biliverdin reductase which catalyses an NADPH-dependent formation of bilirubin. The plant enzyme has been isolated from etiolated oat seedlings (McDowell and Lagarias, 2001) and the gene from *Arabidopsis thaliana* has been cloned (Kohchi et al., 2001). The primary product of the reduction is 3*Z*-PΦB, which must be isomerized to 3*E*-PΦB before incorporation into phytochrome. No specific isomerase has been detected and it may not exist since non-enzymatic 3*Z*/3*E*-isomerization of phytobilins occurs easily as a photochemical reaction (Weller and Gossauer, 1980) or as a chemical reaction catalyzed by glutathione (Beale and Cornejo, 1991a) and, is possibly also catalyzed by the apophytochrome protein (Frankenberg and Lagarias, 2003).

Both enzymes are essential for formation of functional phytochromes; defects in heme oxygenase and PΦB synthase of *Arabidopsis* lead to the photomorphogenic mutants *hy1* and *hy2*, respectively (Davis et al., 1999; Muramoto et al., 1999; Kohchi et al., 2001). Interestingly, similar photomorphogenic mutants can be obtained by plastid-directed over-expression of mammalian biliverdin reductase which, due to its high affinity to biliverdin, competes with PΦB synthase

by reducing biliverdin to bilirubin and thus inhibiting formation of functional phytochromes (Lagarias et al., 1997; Montgomery et al., 2001). Since Chl accumulation was also impaired in these transformants, the authors postulated regulatory roles for phytobilins within the plastids.

PΦB is synthesized in the plastids but incorporated into apo-phytochrome proteins in the cytoplasm. In vitro experiments revealed that the covalent linkage between the chromophore and protein is autocatalytically formed in phytochromes. A system for PΦB transport across the plastid membranes to the cytoplasm has not yet been identified. The situation is similar as for other tetrapyrroles that are produced in the plastid compartment: Protogen is further metabolized to heme in the mitochondria, and bilins, originating from Chl degradation in the plastid, are stored in the vacuoles. While the idea of a transporter is attractive, located in the plastid inner membrane and specific for each of these tetrapyrroles, it still awaits verification.

PCB and PEB are formally dihydro-derivatives of PΦB, and it was shown that PΦB is an intermediate of PCB synthesis in the green alga, *Mesotaenium caldariorum* (Wu et al., 1997). A different pathway was originally established in the red alga, *Cyanidium caldarium* (*Galdieria sulphuraria*), whereby biliverdin was first reduced in two steps to PEB, followed by isomerization to PCB (Beale and Cornejo, 1991b). The pathway via PEB was also found in several cyanobacteria (Cornejo and Beale, 1997; Frankenberg et al., 2001); currently, other pathways cannot be excluded since sets of different reductases have been detected (Frankenberg and Lagarias, 2003). In contrast to the phytochromes, the covalent attachment of PCB and PEB in phycobiliproteins additionally requires a lyase; usually, these bilin lyases contain two subunits as was first identified by Fairchild et al. (1992). More recently, it was shown that some bilin lyases can catalyze isomerization of the bilin during the attachment reaction (Zhao et al., 2000, 2002).

III. Subcellular Location of Enzymes

Biosynthesis of Protogen is catalyzed by soluble stroma enzymes in the plastids, whereas subsequent enzymes are membrane-associated or integrated in the membrane (Fig. 2). Localization studies of enzymatic activities revealed that PPOX (Matringe et al, 1992) and ferrochelatase (Watanabe et al., 2001) are not only associated with thylakoids but also linked to the envelope. In barley, ferrochelatase activity was additionally described in the plasma membrane by Jacobs and Jacobs (1995), but this result has never been repeated. The subunits of Mg-chelatase accumulate in the stroma, but later associate with the envelope at higher Mg^{2+} concentrations (Nakayama et al., 1998). Functional MgProto methyltransferase has been demonstrated in both envelope and thylakoid membranes (Block et al., 2002). LPOR protein forms a substantial part of the etioplast prolamellar bodies and its accumulation is confirmed in envelopes and thylakoids (Joyard et al., 1990). Thus, envelope membranes play a role in certain steps of Chl biosynthesis, although they are devoid of Chl. The significance of envelope membranes for tetrapyrrole biosynthesis is possibly explained by their predominance as the major form of proplastid membranes, before thylakoids are formed during the transition to chloroplasts. Although the two metal-chelating enzymes have a different expression pattern, a spatial separation of both chelatases within the chloroplast could be important for controlling the metabolic flow (Matringe et al., 1994; Walker and Weinstein, 1995). While ferrochelatase is located on both the thylakoid and envelope membrane (Roper and Smith, 1997), Mg-chelatase activity was always found in membrane and stroma fractions.

The sub-plastid location of PPOX isoforms suggests that they function in allocation of Proto (Che et al., 2000; Watanabe et al., 2001) for heme and Chl synthesis. Watanabe et. al. (2001) have suggested that PPOX I provides Proto for the Mg-branch and PPOX II for heme synthesis in both plastids and mitochondria: the envelope-located PPOX II could be involved with translocation of Protogen towards the mitochondria. Several results suggest that Chlide synthesis is associated with the envelope; e.g., studies of the fluorescence properties of isolated envelope membranes from spinach chloroplasts demonstrated the presence of small but significant amounts of both PChlide and Chlide (Pineau et al., 1986).

IV. Regulation of Chlorophyll Biosynthesis

A tight regulation of Chl biosynthesis is expected at various levels of expression. Environmental and endogenous factors release signals for controlling the transcriptional activities of genes and metabolic activities of proteins involved in Chl synthesis.

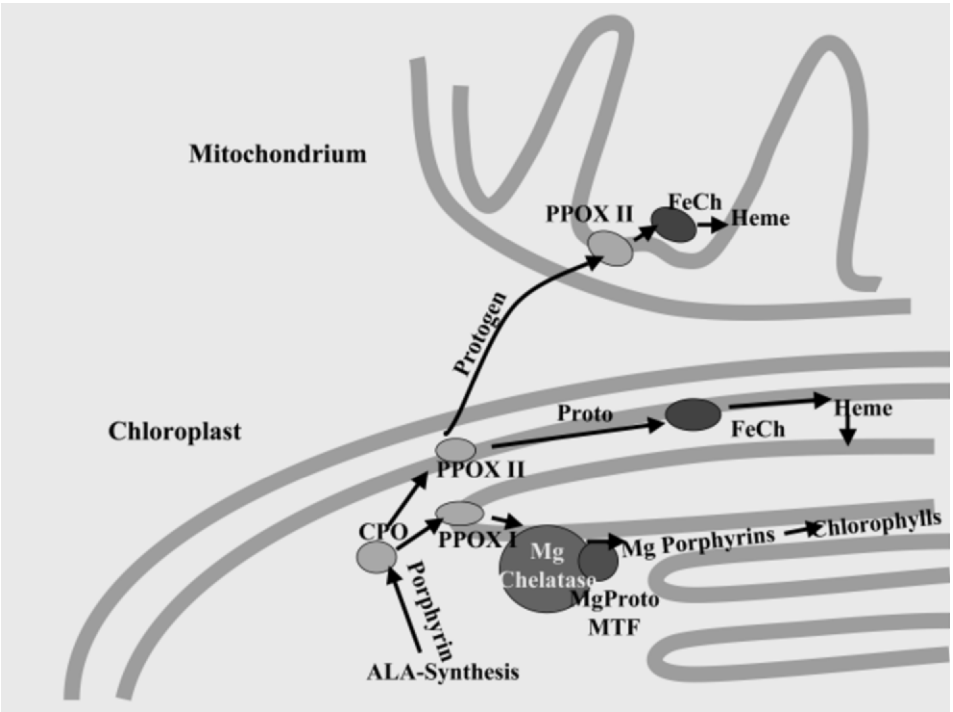

Fig. 2. Scheme for the subcellular location of enzymes at the branch point to chlorophyll and heme synthesis. It is proposed that the two different isoforms of protoporphyrinogen oxidase are located in different subcompartments of plastids and direct protoporphyrin either into the Fe-branch or the Mg branch. CPO – coproporphyrinogen oxidase; FeCh – ferrochelatase; MTF – Mg protoporphyrin methyltransferase; PPOX – protoporphyrinogen oxidase.

A. Light as a Dominant Regulatory Factor

In photosynthetic organisms, light is the most influential factor for controlling the biosynthetic pathways. This factor is not permanently required since most photosynthetic organisms regularly green in darkness; however, the light-dependent PChlide reduction by LPOR restricts Chl synthesis of angiosperms to light periods. Plastids, in particular, are reorganized for photosynthesis and photoprotection on exposure to light. Light is perceived in plants by several photoreceptor systems (e.g., phytochrome, cryptochrome) that control the photomorphogenic changes of the cellular and subcellular structures. Expression of certain genes in tetrapyrrole biosynthesis is controlled by daily variations in the concentrations of active and inactive phytochrome which oscillate under the control of light: the endogenous clock; for example, the genes controlling formation of glutamyl-tRNA reductase and the Mg chelatase subunit CHLH and POR (Armstrong et al., 1995; Papenbrock et al., 1999). Additionally, development- and tissue-dependent control of nuclear transcriptional activity contribute to the regulation of tetrapyrrole biosynthesis. In tissue above ground, almost all genes of the tetrapyrrole pathway investigated, and their encoded proteins, accumulate in light during further development from immature to fully photosynthetically active tissue. Some genes in tetrapyrrole metabolism are encoded in small gene families and individual members can display tissue- and development-dependent expression patterns (e.g., *HemA* for glutamyl-tRNA reductase) while other genes code for proteins which are located in different cellular subcompartments (e.g., genes for PPOX and ferrochelatase). It is probable that the individual enzymatic steps, encoded by small gene families, are so arranged to enable coordinated expression and control within the metabolic pathway in different tissues and for different developmental states.

B. Feedback Regulation in Tetrapyrrole Biosynthesis

Several feedback circuits have been suggested for Chl synthesis in plants to avoid undesirable accumulation of photosensitizing porphyrins which are lethal to living cells. Not only end products but also Mg-porphyrin intermediates are able to control the

rate of synthesis of the first committed tetrapyrrole precursor, ALA.

In dark grown (etiolated) angiosperms, Chl synthesis is blocked by inactivation of the light requiring step of PChlide reduction. ALA synthesis is simultaneously attenuated and prevents the further accumulation of PChlide to potentially hazardous levels lethal to plant cells. It was suggested that ALA synthesis is controlled by a PChlide reduction-dependent feedback mechanism (Beale and Weinstein, 1990), in which the FLU-protein, a negative regulator of tetrapyrrole biosynthesis, is involved (Meskauskiene et al., 2001). Absence of FLU protein prevents suppression of ALA biosynthesis in the dark. The feedback loop via the FLU-protein operates independently of heme and is triggered only by the Mg-porphyrin branch of tetrapyrrole biosynthesis. Reduced Mg-chelatase activity, generated in transgenic tobacco plants, caused a parallel suppression of light-induced ALA synthesis indicating a second regulatory circuit at the beginning of Mg porphyrin biosynthesis (Papenbrock et al., 2000; Chapter 16, Beck and Grimm).

Heme also exerts an inhibitory effect on ALA-synthesizing enzymes from *Chlorella vulgaris* (Weinstein and Beale, 1985), *Chlamydomonas reinhardtii* (Huang and Wang, 1986), higher plants (Chereskin and Castelfranco, 1982) and cyanobacteria (Rieble and Beale, 1991). Heme may act as co-repressor on ALA synthesizing enzymes (Huang and Wang, 1986). The activity of glutamyl-tRNA reductase, the first enzyme committed to ALA synthesis in higher plants, is also a likely target of heme-mediated feedback control (Kannangara et al., 1994) and the activity of barley glutamyl-tRNA reductase was shown to be inhibited by heme (Pontoppidan and Kannangara, 1994).

The extent to which heme contributes to the feedback control of plant tetrapyrrole biosynthesis in photosynthetic tissue is under investigation. Heme-dependent regulatory effects on ALA formation were addressed in mutants with defects in the heme-degrading pathway. These mutants are deficient in heme oxygenase (*yellow-green-2* and *hy 1*) and PΦB synthase (*aurea* and *hy* 2) and cannot synthesize PΦB from heme. *Aurea* and *yg-2* mutations led to reduced PChlide and POR concentrations in etiolated seedlings in comparison to wild type (Terry and Kendrick, 1999), suggesting that an increased plastidic heme pool negatively affected ALA formation.

C. Photosensitization by Porphyrins

Excited porphyrins can transfer energy or electrons to oxygen, lipids and protein resulting in their rapid peroxidation and degradation. Thus, accumulation of photosensitizing porphyrins by chemical or genetic perturbation of tetrapyrrole biosynthesis constitutes a most hazardous threat for plant and animal cells. The photosensitization induces a series of protective responses or hypersensitivity-like responses (Mock et al., 2002; Chapters 32 and 33, Brandis et al.). Thus, the metabolic flow in tetrapyrrole biosynthesis must be tightly controlled to prevent accumulation of photo-reactive intermediates and catabolites.

V. Incorporation into Proteins

It was first discovered that nuclear-encoded Chl-binding proteins are stabilized by Chl. While a light pulse induced expression of *LHCB* genes in angiosperm seedlings, no LHCB proteins accumulated, because insufficient amounts of Chl were synthesized: Chl synthesis required longer exposure of the seedlings to light (Apel and Kloppstech, 1980). If LHCB proteins require esterified Chl for stabilization, such stabilization must occur at the thylakoid or prothylakoid membranes, where Chl synthase activity is confined (Soll et al., 1983; Lindsten et al., 1990). Likewise, stable in vitro insertion of LHCB or precursor LHCB into barley etioplast membranes was only achieved when the membranes were supplemented with Chl *b* or Zn-Phe *b*, either alone or in combination with Chl *a* or Zn-Phe *a*; however, the *a*-type pigments alone were not sufficient (Kuttkat et al., 1997).

The requirement of esterified Chl for protein stabilization was proven with plastid-encoded Chl *a*-binding proteins, P700, D1, D2, CP43, and CP47. It had been known for a long time that these proteins accumulate together with Chl in etiolated leaves, but not in isolated intact plastids, when exposed to light. Eichacker et al. (1990) demonstrated the accumulation of these Chl *a*-binding proteins in plastids by additional synthesis of Chl from added Chlide and PhyPP or GGPP in the dark: the usual procedure for plastid isolation results in the loss of endogenous PhyPP and GGPP. The effect of Chl synthesis was at first assumed to be exercised through translational control (Eichacker et al., 1992); however, a careful analysis showed that polysome-associated translation intermediates were likewise labeled in the presence

and absence of Chl, and the extent of ribosome 'run-off' of the mRNAs did not change in the presence of Chl (Kim et al., 1994). Thus, Chlide or PhyPP did not stabilize the Chl binding protein; however, esterified Chl ensured stabilization of the newly-formed proteins that are otherwise proteolytically degraded (Kim et al., 1994). The artificial [Zn]-Chl, produced via the Chl synthase reaction, stabilizes these proteins at low concentrations, especially CP43, indicating incorporation into specific binding sites. But the proteins are destabilized at higher [Zn]-pigment concentrations, probably due to additional unspecific binding (Eichacker et al., 1996a,b). In chloroplasts, light is required for efficient synthesis of full-length D1 protein and its subsequent incorporation into RCII (van Wijk and Eichacker, 1996; Edhofer et al., 1998). This proved to be a control of translational elongation, mediated by the photosynthesis-dependent proton gradient across the thylakoid membrane (Mühlbauer and Eichacker, 1998).

While RCI and RCII proteins normally bind only Chl *a*, how can the specific assembly of the 'correct' pigment be explained? Which mechanism excludes promiscuous binding of Chl *b* at specific sites of RC proteins? A *Synechocystis* mutant strain that produced large amounts of Chl *b* was shown to incorporate Chl *b* into many of the Chl *a*-binding sites of the proteins of Photosystem II (Xu et al., 2001); since the photosystem remained fully functional, Chl *b* must have been incorporated into 'correct' Chl *a*-binding sites, indicating that an organism that synthesizes only Chl *a* lacks a mechanism for discrimination between different Chls. Examples for incorporation of modified pigments into LHC and RC by in vitro reconstitution and pigment exchange are described by Paulsen (Chapter 26).

VI. Chlorophyll Degradation

In algae, linear tetrapyrroles are produced by degradation of both Chls *a* and *b* and excreted into the surrounding medium (Gossauer and Engel, 1996). By contrast, Chl breakdown in higher plants proceeds through Chl *a*. Chl *b* is first converted to Chl *a*, before the phytyl chain and Mg^{2+} are removed to form pheophorbide a. Ring opening and further reduction produced fluorescent catabolites for transfer to the vacuoles, where degradation to non-fluorescent Chl catabolites and their final storage take place (Chapter 17, Kräutler and Hörtensteiner).

VII. Concluding Remarks

Our understanding of the complex regulatory network controlling both tetrapyrrole biosynthesis and catabolism is being expanded but is far from complete (Eckhardt et al., 2004). It is encouraging, however, to reflect on the progress of investigations in these fields in the past one or two decades as described in the following chapters. Using new genomic tools, precise questions can now be addressed about how temporal and developmental control of tetrapyrrole metabolism is programmed. Further, precise crystallographic data on enzyme-proteins and protein-substrate complexes will soon unravel questions on structure-function relationships in tetrapyrrole metabolism.

References

Adamson HY, Hiller RG and Walmsley J (1997) Protochlorophyllide reduction and greening in angiosperms: An evolutionary perspective. J Photochem Photobiol B 41: 201–221

Alberti M, Burke DH and Hearst JE (1995) Structure and sequence of the photosynthesis gene cluster. In: Blankenship RE, Madigan MT and Bauer CE (eds) Anoxygenic Photosynthetic Bacteria, pp 1083–1106. Kluwer Academic Publishers, Dordrecht

Apel K and Kloppstech K (1980) The effect of light on the biosynthesis of the light-harvesting chlorophyll *a*-*b* protein—Evidence for the requirement of chlorophyll *a* for the stabilisation of the apoprotein. Planta 150: 426–430

Armstrong GA, Runge S, Frick G, Sperling U and Apel K (1995) Identification of NADPH:protochlorophyllide oxidoreductases A and B: A branched pathway for light-dependent chlorophyll biosynthesis in *Arabidopsis thaliana*. Plant Physiol. 108: 1505–1517

Armstrong GA, Apel K and Rüdiger W (2000) Does a light-harvesting protochlorophyllide *a/b*-binding protein complex exist? Trends Plant Sci 5: 40–44

Battersby AR (1994) How nature builds the pigments of life: The conquest of vitamin B_{12}. Science, 264: 1551–1557

Beale SI and Cornejo J (1991a) Biosynthesis of phycobilins. 3(Z)-phycoerythrobilin and 3(Z)-phycocyanobilin are intermediates in the formation of 3(E)-phycocyanobilin from biliverdin IX alpha. J Biol Chem 266: 22333–22340

Beale SI and Cornejo J (1991b) Biosynthesis of phycobilins. 15,16-Dihydrobiliverdin IX alpha is a partially reduced intermediate in the formation of phycobilins from biliverdin IX alpha. J Biol Chem 266: 22341–22345

Beale SI and Weinstein JD (1990) Tetrapyrrole metabolism in photosynthetic organisms. In: Dailey HA (ed) Biosynthesis of Heme and Chlorophylls, pp 287–391. McGraw-Hill, New York

Block MA, Tewari AK, Albrieux C, Marechal E and Joyard J (2002) The plant S-adenosyl-L-methionine:Mg-protoporphyrin IX methyltransferase is located in both envelope and thylakoid chloroplast membranes. Eur J Biochem. 269: 240–248

Bollivar DW, Suzuki JY, Beatty JT, Dobrowolski JM and Bauer CE (1994) Directed mutational analysis of bacteriochlorophyll *a*

biosynthesis in *Rhodobacter capsulatus*. J Mol Biol 237: 622–640

Brown SB, Houghton JD and Hendry GAF (1991) Chlorophyll breakdown. In: Scheer H (ed) Chlorophylls, pp 465–489. CRC Press, Boca Raton

Burke DH, Alberti M and Hearst JE (1993a) The *Rhodobacter capsulatus* chlorin reductase-encoding locus, *bchA*, consists of three genes, *bchX, bchY,* and *bchZ.* J Bacteriol 175: 2407–2413

Burke DH, Alberti M and Hearst JE (1993b) *bchFNBH* bacteriochlorophyll synthesis genes of *Rhodobacter capsulatus* and identification of the third subunit of light-independent protochlorophyllide reductase in bacteria and plants. J Bacteriol 175: 2414–2422

Carey EE and Rebeiz CA (1985) Chloroplast biogenesis 49—Differences among angiosperms in the biosynthesis and accumulation of monovinyl and divinyl protochlorophyllide during photoperiodic greening. Plant Physiol 79: 1–6

Che FS, Watanabe N, Iwano M, Inokuchi H, Takayama S, Yoshida S and Isogai A (2000) Molecular characterization and subcellular localization of protoporphyrinogen oxidase in spinach chloroplasts. Plant Physiol 124: 59–70

Chereskin BM and Castelfranco PA (1982) Effects of iron and oxygen on chlorophyll biosynthesis 2. Observations on the biosynthetic pathway in isolated etiochloroplasts. Plant Physiol 69: 112–116

Cornejo J and Beale SI (1997) Phycobilin biosynthetic reactions in extracts of cyanobacteria. Photosynth Res 51: 223–230

Cornejo J, Willows RD and Beale SI (1998) Phytobilin biosynthesis: Cloning and expression of a gene encoding soluble ferredoxin-dependent heme oxygenase from *Synechocystis* sp. PCC 6803. Plant J 15: 99–107

Davis SJ, Kurepa J and Vierstra R (1999) The *Arabidopsis thaliana HY1* locus, required for phytochrome-chromophore biosynthesis, encodes a protein related to heme oxygenases. Proc Natl Acad Sci USA 96: 6541–6546

Eckhardt U, Grimm B and Hörtensteiner S (2004) Recent advances in chlorophyll biosynthesis and breakdown in higher plants. Plant Mol Biol 56: 1–14

Edhofer I, Mühlbauer SK and Eichacker LA (1998) Light regulates the rate of translation elongation of chloroplast reaction center protein D1. Eur J Biochem 257: 78–84

Eichacker L, Soll J, Lauterbach P, Rüdiger W, Klein RR and Mullet JE (1990) In vitro synthesis of chlorophyll *a* in the dark triggers accumulation of chlorophyll *a* apoproteins in barley etioplasts. J Biol Chem 265: 13566–13571

Eichacker L, Paulsen H and Rüdiger W (1992) Synthesis of chlorophyll *a* regulates translation of chlorophyll *a* apoproteins P700, CP47, CP43 and D2 in barley etioplasts. Eur J Biochem 205: 17–24

Eichacker LA, Mueller B and Helfrich M (1996a) Stabilization of the chlorophyll binding apoproteins, P700, CP47, CP43, D2, and D1, by synthesis of Zn-pheophytin *a* in intact etioplasts from barley. FEBS Lett 395: 251–256

Eichacker LA, Helfrich M, Rüdiger W and Müller B (1996b) Stabilization of chlorophyll *a*-binding apoproteins P700, CP47, CP43, D2, and D1 by chlorophyll a or Zn-pheophytin a. J Biol Chem 271: 32174–32179

Fairchild CD, Zhao JD, Zhou JH, Colson SE, Bryant DA and Glazer AN (1992) Phycocyanin alpha-subunit phycocyanobilin lyase. Proc Natl Acad Sci USA 89: 7017–7021

Fiedor L, Rosenbach-Belin V and Scherz A (1992) The stereospecific interaction between chlorophylls and chlorophyllase. Possible implication for chlorophyll biosynthesis and degradation. J Biol Chem 267: 22043–22047

Frankenberg N and Lagarias JC (2003) Biosynthesis and biological functions of bilins In: Kadish KM, Smith KM and Guilard R (eds) Porphyrin Handbook, Vol 13, pp 211–235. Academic Press, San Diego

Frankenberg N, Mukougawa K, Kohchi T and Lagarias JC (2001) Functional genomic analysis of the HY2 family of ferredoxin-dependent bilin reductases from oxygenic photosynthetic organisms. Plant Cell 13: 965–978

Friedmann HC, Klein A and Thauer RK (1990) Structure and function of the nickel porphinoid, coenzyme F430 and of its enzyme, methyl coenzyme M reductase. FEMS Microbiol Rev 7: 339–348

Fujita Y and Bauer CE (2003) The light-independent protochlorophyllide reductase: A nitrogenase-like enzyme catalyzing a key reaction for greening in the dark. The Porphyrin Handbook, Vol 13, Elsevier, Amsterdam, pp 109–156.

Gossauer A and Engel N (1996) New trends in photobiology: Chlorophyll catabolism—structures, mechanisms, conversions. J Photochem Photobiol B 32: 141–151

Griffiths WT (1991) Protochlorophyllide photoreduction. In: Scheer H (ed) Chlorophylls, pp 433–449. CRC Press, Boca Raton

Helfrich M, Schoch S, Lempert U, Cmiel E and Rüdiger W (1994) Chlorophyll synthetase cannot synthesize chlorophyll *a´*. Eur J Biochem 219: 267–275

Helfrich M, Schoch S, Schäfer W, Ryberg M and Rüdiger W (1996) Absolute configuration of protochlorophyllide *a* and substrate specificity of NADPH-Protochlorophyllide oxidoreductase. J Am Chem Soc 118: 2606–2611

Helfrich M, Bommer B, Oster U, Klement H, Mayer K, Larkum AWD and Rüdiger W (2003) Chlorophylls of the *c* family: Absolute configuration and inhibition of NADPH:protochlorophyllide oxidoreductase. Biochim Biophys Acta 1605: 97–103

Hendry GAF, Houghton JD and Brown SB (1987) Chlorophyll degradation. A biological enigma. New Phytol 107: 255–302

Hiraishi A and Shimada K (2001) Aerobic anoxygenic photosynthetic bacteria with zinc-bacteriochlorophyll. J Gen Appl Microbiol 47: 161–180

Huang DD and Wang WY (1986) Chlorophyll biosynthesis in *Chlamydomonas* starts with the formation of glutamyl-tRNA. J Biol Chem 261: 13451–13555

Ito H, Ohtsuka T and Tanaka A (1996) Conversion of chlorophyll *b* to chlorophyll *a* via 7-hydroxymethyl chlorophyll. J Biol Chem 271: 1475–1479

Jacobs, JM and Jacobs, NJ (1995) Terminal enzymes of heme biosynthesis in the plant plasma membrane. Arch. Biochem. Biophys 323: 274–278

Jones OTG (1978) Biosynthesis of porphyrins, hemes and chlorophylls. In: Clayton RK and Sistrom WR (eds) The Photosynthetic Bacteria, pp 751–777. Plenum, New York

Joyard J, Block M, Pineau B, Albrieux C and Douce R (1990) Envelope membranes from mature spinach chloroplasts contain a NADPH:protochlorophyllide reductase on the cytosolic side of the outer membrane. J Biol Chem. 265(35): 21820–21827

Kannangara CG, Andersen RV, Pontoppidan B, Willows R and von Wettstein D (1994) Enzymic and mechanistic studies on the conversion of glutamate to 5-aminolaevulinate. In: The Biosynthesis of the Tetrapyrrole Pigments (Ciba Foundation

Symposium 180), pp 3–25. Wiley, Chichester
Kim J, Eichacker LA, Rüdiger W and Mullet JE (1994) Chlorophyll regulates accumulation of the plastid-encoded chlorophyll proteins P700 and D1 by increasing apoproteins stability. Plant Physiol 104, 907–916
Kohchi T, Mukougawa K, Frankenberg N, Masuda M, Yokota A and Lagarias JC (2001) The *Arabidopsis HY2* gene encodes phytochromobilin synthase, a ferredoxin-dependent biliverdin reductase. Plant Cell 13: 425–436
Kolossov VL and Rebeiz CA (2003) Chloroplast biogenesis 88. Protochlorophyllide *b* occurs in green but not in etiolated plants. J Biol Chem. 278: 49675–49678
Kuttkat A, Edhofer I, Eichacker LA and Paulsen H (1997) Light-harvesting chlorophyll *a/b*-binding protein stably inserts into etioplast membranes supplemented with Zn-pheophytin *a/b*. J Biol Chem 272: 20451–20455
Lagarias DM, Crepeau MW, Maines MD and Lagarias JC (1997) Regulation of photomorphogenesis by expression of mammalian biliverdin reductase in transgenic *Arabidopsis* plants. Plant Cell 9: 675–688
Leeper FJ (1991) Intermediate steps in the biosynthesis of chlorophylls. In: Scheer H (ed) Chlorophylls, pp 407–431. CRC Press, Boca Raton
Leustek T, Smith M, Murillo M, Singh DP, Smith AG, Woodcock SC, Awan SJ and Warren MJ (1997) Siroheme biosynthesis in higher plants. Analysis of an S-adenosyl-L-methionine-dependent uroporphyrinogen III methyltransferase from *Arabidopsis thaliana*. J Biol Chem 272: 2744–2752
Lindsten A, Welch CJ, Schoch S, Ryberg M, Rüdiger W and Sundqvist C (1990) Chlorophyll synthetase is latent in well preserved prolamellar bodies of etiolated wheat. Physiol Plant 80: 277–285
Masuda T, Inoue K, Masuda M, Nagayama M, Tamaki A, Ohta H, Shimada H and Takamiya K-I (1999) Magnesium insertion by magnesium chelatase in the biosynthesis of zinc bacteriochlorophyll *a* in an aerobic acidophilic bacterium *Acidiphilium rubrum*. J Biol Chem 274: 33594–33600
Matringe M, Camadro JM, Block MA, Joyard J, Scalla R, Labbe P and Douce R (1992) Localization within the chloroplasts of protoporphyrinogen oxidase the target enzyme for diphenylether-like herbicides. J Biol Chem 267: 4646–4651
Matringe M, Camadro JM, Joyard J and Douce R (1994) Localization of ferrochelatase activity within mature pea chloroplasts. J Biol Chem. 269: 15010–15015
McDowell MT and Lagarias JC (2001) Purification and biochemical properties of phytochromobilin synthase from etiolated oat seedlings. Plant Physiol 126: 1546–1554
McGlynn P and Hunter CN (1993) Genetic analysis of the *bchC* and *bchA* genes of *Rhodobacter sphaeroides*. Mol Gen Genet 236: 227–234
Meskauskiene R, Nater M, Goslings D, Kessler F, op den Camp R and Apel K. FLU (2001) A negative regulator of chlorophyll biosynthesis in *Arabidopsis thaliana*. Proc Natl Acad Sci 98: 12826–12831
Mimuro M, Kobayashi M, Shimada K, Uezono K and Nozawa T (2000) Magnetic circular dichroism properties of reaction center complexes isolated from the Zinc-bacteriochlorophyll *a*-containing purple bacterium *Acidiphilium rubrum*. Biochemistry 39: 4020–4027
Mock HP, Keetman U and Grimm B (2002) Photosensitizing tetrapyrroles induce antioxidative and pathogen defence responses in plants. In: Inze D and van Montagu M (eds) Oxidative Stress in Plants, pp 155–170. Taylor & Francis, Inc., London and New York
Montgomery BL and Lagarias JC (2002) Phytochrome ancestry: Sensors of bilins and light. Trends Plant Sci 7: 357–366
Montgomery BL, Franklin KA, Terry MJ, Thomas B, Jackson SD, Crepeau MW and Lagarias JC (2001) Biliverdin reductase-induced phytochrome chromophore deficiency in transgenic tobacco. Plant Physiol 125: 266–277
Mühlbauer S and Eichacker LA (1998) Light-dependent formation of the photosynthetic proton gradient regulates translation elongation in chloroplasts. J Biol Chem 273: 20935–20940
Muramoto T, Kohchi T , Yokota A, Hwang I and Goodman HM (1999) The *Arabidopsis* photomorphogenic mutant *hy1* is deficient in phytochrome chromophore biosynthesis as a result of a mutation in a plastid heme oxygenase. Plant Cell 11: 335–347
Nakayama M, Masuda T, Bando T, Yamagata H, Ohta H and Takamiya K (1998) Cloning and expression of the soybean *chlH* gene encoding a subunit of Mg-chelatase and localization of the Mg^{2+} concentration-dependent ChlH protein within the chloroplast. Plant Cell Physiol. 3: 275–84
Oster U, Tanaka R, Tanaka A and Rüdiger W (2000) Cloning and functional expression of the gene encoding the key enzyme for chlorophyll *b* biosynthesis (CAO) from *Arabidopsis thaliana*. Plant J 21: 305–310
Papenbrock J and Grimm B (2001) Regulatory network of tetrapyrrole biosynthesis –Studies for intracellular signaling involved in metabolic and developmental control of plastids. Planta, 213: 667–681
Papenbrock, J, Mock, H.-P, Kruse, E and Grimm, B (1999) Expression studies in tetrapyrrole biosynthesis—Inverse maxima of magnesium chelatase and ferro chelatase. Planta 208: 264–273
Papenbrock J, Mock H-P, Tanaka R, Kruse E and Grimm B (2000) Role of Mg-chelatase activity for the early steps of the tetrapyrrole biosynthetic pathway. Plant Physiol. 122: 1161–1169
Pineau B, Dubertret G, Joyard J and Douce R (1986) Fluorescence properties of the envelope membranes from spinach chloroplasts. J Biol Chem 261: 9210–9215
Pontoppidan B and Kannangara CG (1994) Purification and partial characterization of barley glutamyl-tRNA(Glu) reductase, the enzyme that directs glutamate to chlorophyll biosynthesis. Eur J Biochem 225: 529–537
Porra RJ, Schäfer W, Cmiel E, Katheder I and Scheer H (1993) Derivation of the formyl-group oxygen of chlorophyll *b* from molecular oxygen in greening leaves of a higher plant (*Zea mays*). FEBS Lett 323: 31–34
Porra RJ, Urzinger M, Winkler J, Bubenzer C and Scheer H (1998) Biosynthesis of the 3-acetyl and 13^1-oxo groups of bacteriochlorophyll a in the facultative aerobic bacterium, *Rhodovulum sulfidophilum*. The presence of both oxygenase and hydratase pathways for isocyclic ring formation. Eur J Biochem 257: 185–191
Rebeiz CA, Tripathy BC, Wu S-W, Montazer-Zouhoor A and Carey EE (1986) Chloroplast biogenesis 52: Demonstration in toto of monovinyl and divinyl monocarboxylic chlorophyll biosynthetic routes in higher plants. In: Akoyunoglou G and Senger H (eds)The Regulation of Chloroplast Differentiation, pp 13–24. A. R. Liss, New York
Reinbothe C, Lebedev N and Reinbothe S (1999) A protochlo-

rophyllide light-harvesting complex involved in detiolation of higher plants. Nature 397: 80–84

Reinbothe S, Pollmann S and Reinbothe C (2003a) In situ conversion of protochlorophyllide *b* to protochlorophyllide *a* in barley. Evidence for a novel role of 7-formyl reductase in the prolamellar body of etioplasts. J Biol Chem 278, 800–806

Reinbothe C, Buhr F, Pollmann S and Reinbothe S (2003b) In vitro reconstitution of light-harvesting POR-protochlorophyllide complex with protochlorophyllides *a* and *b*. J Biol Chem 278: 807–815

Rieble S and Beale SI (1991) Separation and partial characterization of enzymes catalyzing delta-aminolevulinic acid formation in *Synechocystis* sp. PCC 6803. Arch Biochem Biophys 289: 289–97

Rodermel S (2001) Pathways of plastid-to-nucleus signaling. Trends Plant Sci 6: 471–478.

Roper JM and Smith AG (1997) Molecular localization of ferrochelatase in higher plant chloroplasts. Eur J Biochem 246: 32–37

Sakakibara H, Takei K and Sugiyama T (1996) Isolation and characterization of a cDNA that encodes maize uroporphyrinogen III methyltransferase, an enzyme involved in the synthesis of siroheme, which is a prosthetic group of nitrite reductase. Plant J 10: 883–892

Scheumann V, Schoch S and Rüdiger W (1998) Chlorophyll *a* formation in the chlorophyll *b* reductase reaction requires reduced ferredoxin. J Biol Chem 273: 35102–35108

Scheumann V, Klement H, Helfrich M, Oster U, Schoch S and Rüdiger W (1999) Protochlorophyllide *b* does not occur in barley etioplasts. FEBS Lett 445: 445–448

Schneegurt MA and Beale SI (1992) Origin of the chlorophyll *b* formyl oxygen in *Chlorella vulgaris*. Biochem 31: 11677–83.

Soll J, Schultz G, Rüdiger W and Benz J (1983) Hydrogenation of geranylgeraniol: Two pathways exist in spinach chloroplasts. Plant Physiol 71: 849–854

Stroupe ME, Leech HK, Daniels DS, Warren MJ and Getzoff ED (2003) CysG structure reveals tetrapyrrole-binding features and novel regulation of siroheme biosynthesis. Nature Struct Biol 10: 1064–1073

Takamiya K, Masuda T, Inoue K, Masuda M, Nagura A, Nagayama M, Tamaki A, Ohta H and Shimada H (2000) Biosynthesis of zinc-containing bacteriochlorophyll *a*. Porphyrins 9: 227–233

Terry MJ and Kendrick RE (1999) Feedback inhibition of chlorophyll synthesis in the phytochrome chromophore deficient *aurea* and *yellow-green-2* mutants of tomato. Plant Physiol 119: 143–152

Thomas H and Howarth CJ (2000) Five ways to stay green. J Exp Bot 51: 329–337

Tripathy BC, Rebeiz CA (1986) Chloroplast biogenesis. 54. Demonstration of the monovinyl and divinyl monocarboxylic routes of chlorophyll biosynthesis in higher plants. J Biol Chem 261: 3556–3564

van Wijk KJ and Eichacker L (1996) Light is required for efficient translation elongation and subsequent Integration of the D1-protein into Photosystem II. FEBS Lett 388: 89–93

Wakao N, Yokoi N, Isoyama N, Hiraishi A, Shimada K, Kobayashi M, Kise H, Iwaki M, Itoh S, Takaichi S and Sakurai Y (1996) Discovery of natural photosynthesis using Zn-containing bacteriochlorophyll in an aerobic bacterium *Acidiphilium rubrum*. Plant Cell Physiol 37: 889–893

Walker CJ and Weinstein, JD (1995) Re-examination of the localization of Mg-chelatase within the chloroplast. Physiol Plant 94: 419–424

Warren MJ, Bolt EL, Roessner CA, Scott AI, Spencer JB and Woodcock SC (1994) Gene dissection demonstrates that the *Escherichia coli cysG* gene encodes a multifunctional protein. Biochem J 302: 837–844

Watanabe N, Che FS, Iwano M, Takayama S, Yoshida S and Isogai A (2001) Dual targeting of spinach protoporphyrinogen oxidase II to mitochondria and chloroplasts by alternative use of two in-frame initiation codons. J Biol Chem 276: 20474–20481

Weinstein JD and Beale SI (1985) Enzymatic conversion of glutamate to delta-aminolevulinate in soluble extracts of the unicellular green alga, *Chlorella vulgaris*. Arch Biochem Biophys 237: 454–464

Weller JP and Gossauer A (1980) Synthesis of bile pigments. X Synthesis and photoisomerization of racemic phytochromobilin dimethyl ester. Chem Ber 113: 1603–1611

Wu S-H, McDowell MT and Lagarias JC (1997) Phycocyanobilin is the natural precursor of the phytochrome chromophore in the green alga *Mesotaenium caldariorum*. J Biol Chem 272: 25700–25705

Xu H, Vavilin D and Vermass W (2001) Chlorophyll *b* can serve as the major pigment in functional Photosystem II complexes of cyanobacteria. Proc Natl Acad Sci USA 98: 14168–14173

Xu H, Vavilin D and Vermaas W (2002) The presence of chlorophyll *b* in *Synechocystis* sp. PCC 6803 disturbs tetrapyrrole biosynthesis and enhances chlorophyll degradation. J Biol Chem 277: 42726–42732

Zhao KH, Deng MG, Zheng M, Parbel A, Storf M, Meyer M, Strohmann B and Scheer H (2000) Novel activity of a phycobiliprotein lyase: Both the attachment of phycocyanobilin and the isomerization to phycoviolobilin are catalysed by the proteins PecE and PecF encoded in the phycoerythrocyanin operon. FEBS Lett 469: 9–13

Zhao KH, Wu D, Wang L, Zhou M, Storf M, Bubenzer C, Strohmann B and Scheer H (2002) Characterization of phycoviolobilin phycoerythrocyanin-α84-cystein-lyase (isomerising) from *Mastigocladud laminosus*. Eur J Biochem 269: 4542–4550

Chapter 11

Biosynthesis of 5-Aminolevulinic Acid

Samuel I. Beale*
Division of Biology and Medicine, Brown University, Providence, RI 02912, U.S.A.

Summary

The universal tetrapyrrole precursor, 5-aminolevulinic acid (ALA) is formed by one of two alternative routes. Although these pathways are distinctly different with respect to biosynthetic precursors and intermediates, and the nature of the enzymes and the genes that encode them, there are similarities in their regulatory responses to biosynthetic end products and to environmental and metabolic signals in photosynthetic organisms.

I. Alternate Pathways for 5-Aminolevulinic Acid Biosynthesis

All of the carbon and nitrogen atoms in the macrocycles of biological tetrapyrroles are derived from the five-carbon molecule 5-aminolevulinic acid (ALA), and ALA can be considered to be the first universal, committed biosynthetic precursor to all biological tetrapyrroles. ALA is synthesized by two distinctly different biosynthetic routes. In species comprising the α-subgroup of the proteobacteria (which includes facultative aerobes in the phototrophic genera *Rhodopseudomonas* (*Rps.*), *Rhodobacter* (*Rba.*) and *Rhodospirillum* (*Rsp.*), obligately aerobic bacteriochlorophyll (BChl)-containing phototrophs that have been placed in the *Erythrobacter* and *Methylobacterium* groups, and non-chlorophyll (Chl)-containing relatives such as *Agrobacterium*, *Rhizobium*, *Azorhizobium*, and *Bradyrhizobium*) and in eucaryotes that do not contain plastids (e.g., animals, yeasts, fungi), the

*Email: Samuel_Beale@brown.edu

Bernhard Grimm, Robert J. Porra, Wolfhart Rüdiger and Hugo Scheer (eds): Chlorophylls and Bacteriochlorophylls: Biochemistry, Biophysics, Functions and Applications, pp. 147–158.

carbon and nitrogen atoms of ALA are derived from glycine and succinate. In contrast, in plants, algae, archaea, and all or most groups of bacteria except the α-proteobacteria, ALA is formed by a completely different route starting with glutamate.

II. 5-Aminolevulinic Acid Biosynthesis from Glycine and Succinyl-Coenzyme A

ALA formation was first studied in avian erythrocyte preparations, in which heme is the major tetrapyrrole end product (Gibson et al., 1958), and in the photosynthetic α-proteobacteria *Rba. sphaeroides* and *Rsp. rubrum*, which form large quantities of BChl as well as lesser amounts of hemes and corrinoids (Kikuchi et al., 1958).

A. 5-Aminolevulinic Acid Synthase

In the experimental systems described above, ALA is formed by the condensation of succinyl-CoA with glycine, catalyzed by ALA synthase (ALAS; succinyl-CoA:glycine C-succinyltransferase (decarboxylating); EC 2.3.1.37). In the reaction, the glycine carboxyl carbon is lost as CO_2 and the remainder, as well as all of the carbon atoms of succinate, are incorporated into ALA.

ALAS has an apparent native molecular weight of 80,000 to 100,000 and is a homodimer. ALAS from all sources contains pyridoxal-phosphate. Recombinant *Rba. sphaeroides* ALAS had an molecular mass of 46,500 (determined by sodium dodecyl sulfate-polyacrylamide electrophoresis, SDS-PAGE), K_m values of 1.9 mM for glycine and 17 μM for succinyl-CoA, and a turnover number of 430 h^{-1} at 37 °C (Bolt et al., 1999).

The ALAS reaction mechanism has been extensively investigated. Product inhibition studies with *Rba. sphaeroides* ALAS indicate a bi-bi reaction sequence in which glycine binds before succinyl-CoA, and CO_2 is released before ALA (Fanica-Gaignier and Clement-Metral, 1973). During the reaction, the glycine C-2 proton having the *pro-R* configuration is specifically abstracted by the catalytic lysine residue and the *pro-S* C-2 proton of glycine occupies the *pro-S* position at C-5 of ALA (Zaman et al., 1973; Abboud et al., 1974). The retention of only one glycine C-2 proton in the product, and its stereospecific position in the product, indicate that the reaction of pyridoxal-bound glycine with succinyl-CoA precedes decarboxylation, i.e., that enzyme-bound 2-amino-3-ketoadipic acid is an intermediate, and that the decarboxylation step occurs before the final product is released from the enzyme, which means that ALAS is a decarboxylase as well as a condensing enzyme. In the absence of succinyl-CoA, the enzyme catalyzes the exchange of the glycine *pro-R* C-2 proton with the solvent (Laghai and Jordan, 1976), and in the absence of either substrate, the enzyme catalyzes exchange of one of the C-5 protons of ALA with the solvent (Laghai and Jordan, 1977).

The identified ALAS encoding genes are not located within the major oxygen-regulated photosynthetic gene clusters of *Rba. capsulatus* (Biel et al., 1988; Hornberger et al., 1990) and *Rba. sphaeroides* (Tai et al., 1988; Neidle and Kaplan, 1993a). Whereas *Rba. capsulatus* contains a single ALAS-encoding gene, *hemA*, *Rba. sphaeroides* contains two such genes, *hemA* and *hemT*, which, respectively, are located on the large and small chromosomes of these cells (Neidle and Kaplan, 1993b). The *Rba. sphaeroides hemA* and *hemT* genes encode peptides that are 53% identical to each other, and each contains 407 amino acids. The *Rba. capsulatus* and *Rba. sphaeroides* HemA peptides are 76% identical. Interestingly, there is detectable similarity to the peptide sequences of other enzymes in the α-oxoamine synthase sub-family of aminotransferases that catalyze similar condensation reactions, 8-amino-7-oxononanoate synthase (EC 2.3.1.47), 2-amino-3-ketobutyrate coenzyme A ligase (EC 2.3.1.29), and serine palmitoyltransferase (EC 2.3.1.50) (Neidle and Kaplan, 1993a; Ferreira and Cheltsov, 2002).

B. Allosteric Regulation of 5-Aminolevulinic Acid Synthase Activity

Rba. sphaeroides ALAS is reversibly inhibited by protoheme at physiologically relevant concentrations (Burnham and Lascelles, 1963; Yubisui and Yoneyama, 1972). Greater than 50% inhibition was caused

Abbreviations: A. – *Arabidopsis*; ALA – 5-aminolevulinic acid; ALAS – ALA synthase; BChl – bacteriochlorophyll; *C.* – *Chlamydomonas*; Chl – chlorophyll; *Chl.* – *Chlorobium*; Chlide – chlorophyllide; CoA – coenzyme A; *E.* – *Escherichia*; *E.* – *Euglena*; *Erb.* – *Erythrobacter*; GluRS – glutamyl-tRNA synthetase; GluTR – glutamyl-tRNA reductase; GSA – glutamate 1-semialdehyde; GSAT – GSA aminotransferase; *M.* – *Methanopyrus*; Mbc – methylobacterium; PChlide – protochlorophyllide; *Rba.* – *Rhodobacter*; *Rsb.* – *Roseobacter*; *Rsp.* – *Rhodospirillum*; *S.* – *Salmonella*; SDS-PAGE – sodium dodecyl sulfate-polyacrylamide electrophoresis

by 1 μM protoheme, and nearly complete inhibition was achieved at 10 μM protoheme. The enzyme is also inhibited by ATP and inorganic pyrophosphate at physiologically relevant concentrations; purified *Rba. sphaeroides* ALAS was inhibited 60–88% by 1 mM ATP (Fanica-Gaignier and Clement-Metral, 1971, 1973).

Disulfide-containing compounds, such as cystine, oxidized glutathione, and lipoic acid activate ALAS in vitro (Tuboi and Hayasaka, 1972). Later, trisulfides such as cystine trisulfide and the mixed trisulfide of glutathione and cystine, but not disulfides, were shown to activate the enzyme (Sandy et al., 1975). Exposure of whole cells to O_2 reduces the level of extractable ALAS. Cellular levels of trisulfide compounds were found to decrease upon oxygenation, and the decrease was proposed to be responsible for the decrease in extractable active ALAS upon oxygenation of the cells. Finally, proteinaceous activators, such as cystathionase (EC 4.4.1.1) (Inoue et al., 1979) and reduced thioredoxin (Clement-Metral, 1979) were shown to activate ALAS. It remains to be determined whether the influence of the sulfhydryl environment on ALAS activity is of importance in the control of BChl formation by O_2 tension.

C. Transcriptional Regulation of 5-Aminolevulinic Acid Synthase Expression

ALAS is induced upon transfer of dark-grown, aerobic *Rba. sphaeroides* cells to anaerobic, light conditions (Kikuchi et al., 1958), and oxygenation of anaerobically-grown *Rba. sphaeroides* (Lascelles, 1960) and *Rba. palustris* (Viale et al., 1987) cells diminished the level of extractable ALAS by approximately 70%. The degree of influence on the expression of ALAS by oxygen is not as great as the degree of influence on BChl formation, which is completely blocked by oxygen (Cohen-Bazier et al., 1957). This difference is physiologically significant, because the cells need ALA for certain tetrapyrrole end products, such as hemes and corrinoids that are formed even when they are growing nonphotosynthetically. Transcription of the *hemA* genes in *Rba. sphaeroides* and *Rba. capsulatus* is regulated by oxygen tension (Hornberger et al., 1991; Neidle and Kaplan, 1993a). In *Rba. sphaeroides*, disruption of both ALAS-encoding genes, *hemA* and *hemT*, was required to produce ALA auxotrophy (Neidle and Kaplan, 1993b). However, disruption of either *hemA* or *hemT* alone was sufficient to cause decreased cellular contents of BChl, carotenoids, and light-harvesting BChl-proteins, as well as lowered levels of *puc* and *puf* transcripts. Somewhat paradoxically, *hemT* transcripts could not be detected in wild-type cells that had an intact, expressible *hemA* gene, although *hemT* transcripts were present in *hemA* mutant cells (Neidle and Kaplan, 1993a). Transcription of *hemA* is under control of the global oxygen-regulatory system involving the *fnrL* gene, whose product, FnrL, was proposed to interact with a putative FNR consensus sequence within the *hemA* promoter to activate *hemA* transcription (Zeilstra-Ryalls and Kaplan, 1995).

Whereas O_2 prevents BChl synthesis in facultatively aerobic species such as *Rba. sphaeroides*, *Rba. capsulatus*, and *Rsp rubrum*, O_2 is required for BChl synthesis as well as growth in several obligate aerobes. These include the marine species *Erythrobacter* (*Erb.*) *longus* (Harashima et al., 1978) and *Roseobacter* (*Rsb.*) *denitrificans* OCh114 (Harashima et al., 1980), the facultative methylotrophs *Methylobacterium* (*Mbc. Protomonas) ruber* (Sato, 1978) and *Mbc.* (*Pseudomonas) radiora* (Nishimura et al., 1981), and a BChl-containing *Bradyrhizobium*-like organism, strain BTAi1 (Evans et al., 1990). In the facultative methylotrophs, BChl is formed in the dark, but not under continuous illumination. After a shift from light to dark, the ALAS level increased in parallel with the rate of BChl synthesis (Sato et al., 1985). However, detectable ALAS activity was present in light-grown cells, even though BChl was not formed. The cells contain two ALAS isoenzymes, one of which is constitutive and the other is induced in the dark (Sato et al., 1985). Although the marine *Erb.* species, like the facultative methylotrophs, synthesize BChl only in the dark, the ALAS level does not correlate with BChl synthesis, and is actually higher in the light than in the dark (Shioi and Doi, 1988).

III. 5-Aminolevulinic Acid Biosynthesis from Five-Carbon Precursors

The earliest evidence for the operation of a second pathway for ALA formation was obtained when incorporation of radioactivity from ^{14}C-labeled exogenous compounds was measured in the accumulated ALA. Under the experimental conditions in greening plant tissue, glycine and succinate, contrary to expectations, were found to be relatively inefficient contributors of label to ALA, whereas the five-carbon compounds glutamate, α-ketoglutarate,

and glutamine were much better contributors (Beale and Castelfranco, 1974). These finding were subsequently confirmed in a variety of phototrophic cell types, including red (Jurgenson et al., 1976) and green (Meller et al., 1979) algae and cyanobacteria (Meller and Harel, 1978). ^{13}C-NMR analysis was performed on Chl formed from ^{13}C-labeled glycine or glutamate in *Scenedesmus obliquus.* The results indicated that glycine was contributing label only to the 13^2 methoxyl group adjacent to the isocyclic ring, while glutamate contributed label in a manner that was consistent with the exclusive operation of the five-carbon pathway in the formation of ALA leading to Chl (Oh-hama et al., 1982; confirmed in maize by Porra et al. (1983).

A. Intermediates of the Five-Carbon 5-Aminolevulinic Acid Biosynthetic Pathway

Early reports on substrate and cofactor requirements for in vitro conversion of glutamate to ALA (glutamate, ATP, Mg^{2+} and reduced pyridine nucleotide) suggested a likely sequence of three steps for ALA formation as follows: (a) activation of the C_1 of glutamate in a step requiring ATP and Mg^{2+}; (b) reduction of the activated carboxyl group by NADPH to form glutamate 1-semialdehyde (GSA); and (c) transamination of GSA to form ALA. Later, it was shown that the activated form of glutamate is the tRNA adduct, glutamyl-tRNA^{glu}.

An important advance was the discovery that the five-carbon ALA biosynthetic route occurs in the enteric bacteria *Escherichia* (*E.*) *coli* (Li et al., 1989; O'Neill et al., 1989) and *Salmonella* (*S.*) *typhimurium* (Elliott et al., 1990), and in *Bacillus* (*B.*) *subtilis* (O'Neill et al., 1989). It was determined that a *hemA* mutant of *E. coli* lacks glutamyl-tRNA reductase (GluTR) activity (Avissar and Beale, 1989a) and that *hemA* encodes a structural component of GluTR (Avissar and Beale, 1989b). Mutation of a second gene, *hemL*, also confers ALA auxotrophy in *S. typhimurium* (Elliott and Roth, 1989). The *hemL* gene was sequenced and determined to encode GSA aminotransferase (GSAT; EC 5.4.3.8) (Elliott et al., 1990). By complementation of *E. coli* mutant strains with known enzyme deficiencies, it has been possible to clone the genes for GluTR and GSAT from many organisms including plants, algae, cyanobacteria, and anoxygenic phototrophs.

In vitro ALA-forming activity in extracts from plastids and algal cells was blocked by preincubation of the extracts with RNase A (EC 2.7.7.16; Kannangara et al., 1984; Huang et al., 1984). Inhibition caused by RNase is blocked by prior treatment of the extract with ribonuclease inhibitor (RNasin). Purified tRNA could replace the RNase-inactivated factor in the reconstituted assay (Kannangara et al., 1984; Huang and Wang, 1986a).

Charged glutamyl-tRNA^{Glu} was proposed as the C_1 activated form of glutamate which serves a substrate for C_1 reduction (Kannangara et al., 1984). Activity of barley tRNA^{Glu} in ALA formation required the presence of the 3′-terminal CCA, suggesting that the tRNA functions as a glutamate acceptor in the ALA-forming system analogous to its role in protein synthesis (Schön et al., 1986). Glutamyl-tRNA was a substrate for ALA formation in *Chlamydomonas* (*C.*) *reinhardtii* extracts (Huang et al., 1984).

The RNA required for ALA synthesis in barley plastids was purified, sequenced, and characterized as tRNA^{Glu} bearing the UUC glutamate anticodon (Schön et al., 1986). Only one tRNA^{Glu} gene is present in the barley plastid genome and its RNA supports ALA formation (Berry-Lowe, 1987). Affinity to the UUC anticodon enabled purification of the tRNA required for ALA formation (Schneegurt and Beale, 1988). The *C. reinhardtii* plastid genome contains two genes that encode identical tRNA^{Glu} molecules whose anticodon triplets contain a modified first U and an unmodified second U (O'Neill et al., 1990). The two tRNAs were equally effective for both protein synthesis and ALA synthesis (Jahn et al., 1992).

Chemically synthesized GSA was first shown to be used as a substrate for in vitro ALA formation by an extract of barley seedlings (Kannangara and Gough, 1978, 1979). The conversion of GSA to ALA required only GSAT plus GSA, and was inhibited by the transaminase inhibitors, aminooxyacetate and cycloserine. GSA has been found to be a precursor of ALA in all systems that form ALA from glutamate. An efficient synthesis of GSA by reductive ozonolysis of 4-amino-5-hexenoic acid (vinyl-GABA) has been described (Gough et al., 1989).

At high concentrations, GSA is spontaneously transformed to ALA in solution at physiological pH. The transformation rate is highly dependent on GSA concentration and the reaction has been proposed to proceed through a bimolecular aminohemiacetal intermediate (Gough et al., 1989). A bimolecular reaction would result in intermolecular transfer of the amino nitrogen during the conversion of GSA to ALA. The question of whether the enzymatic reaction

involves intramolecular or intermolecular transfer was examined in *C. reinhardtii* (Mau and Wang, 1988) and *Chlorella vulgari*s (Mayer et al., 1993) extracts by the use of ^{13}C- and ^{15}N-labeled glutamate. When the heavy isotope labels were present on separate substrate molecules, a significant proportion of the ALA product molecules contained two heavy atoms, indicating that the conversion occurs by intermolecular nitrogen transfer.

B. Enzymes of the Five-Carbon 5-Aminolevulinic Acid Biosynthetic Pathway

GluRS has been studied in connection with its role in protein synthesis. The single GluRS found in barley chloroplasts has a subunit molecular weight of 54,000 Da (Bruyant and Kannangara, 1987). Similar enzymes from *Chlorella vulgaris* (Weinstein et al., 1987), *C. reinhardtii* (Chang et al., 1990), and *Synechocystis* sp. PCC 6803 (Rieble and Beale, 1991b) have molecular weights of 73,000 Da (native), 32,000 Da (subunit), and 63,000 Da (native), respectively. Two conflicting reports have appeared on the structure of the *C. reinhardtii* chloroplast GluRS: one report describes a monomeric GluRS with a molecular weight of 62,000 Da (Chen et al., 1990a), and the other describes a dimeric GluRS having native and subunit molecular weights of 60,000 Da and 32,500 Da, respectively (Chang et al., 1990).

GluTR has been the most difficult enzyme of the five-carbon ALA biosynthetic pathway to be studied in vitro, owing to its instability, low cellular abundance, and the need to provide a relatively unstable aminoacyl-tRNA substrate. Reported molecular weights of GluTR from plant, algal, and bacterial sources vary over a wide range and are not consistent with peptide molecular weights predicted from gene sequences, which are in the range of 45,000 to 60,000 Da. On gel filtration columns, *B. subtilis* GluTR migrated as an oligomer with an apparent molecular weight of 230,000 Da (Schröder et al., 1992). The *B. subtilis hemA* sequence predicts a subunit molecular weight of 50,800 Da (Petricek et al., 1990). Active barley GluTR was purified to apparent homogeneity with a native molecular weight of 270,000 Da consisting of identical 54,000 Da molecular weight subunits. Barley has three GluTR-encoding genes, all of which encode peptides of approximately 54,000 Da molecular weight (Bougri and Grimm, 1996; Tanaka et al., 1996, 1997). Early reports on the *C. reinhardtii* GluTR indicated that it is a monomer with a molecular weight of 130,000 Da (Chen et al., 1990b; Krishnasamy and Wang, 1990*)*. However, the sequence of the cloned *C. reinhardtii* gene encoding GluTR (designated *Gtr*, generally termed *HemA*), and the properties of the active enzyme expressed from that gene, indicate that *C. reinhardtii* GluTR is a homodimeric 105 kDa protein (A. Srivastava et al., 2005).

GluTR from the hyperthermophilic archaeon *Methanopyrus* (*M.*) *kandlerii* was recently crystallized and its structure was determined to 1.9 Å resolution (Moser et al., 2001; Chapter 12, Jahn et al.).

GluTR from *Chlorella vulgaris* and *Synechocystis* sp. PCC 6803 requires a divalent metal ion for activity (Mayer et al., 1994). Mg^{2+}, Mn^{2+}, and Ca^{2+} supported in vitro activity, but Zn^{2+} was strongly inhibitory. Barley and *M. kandlerii* GluTRs are also inhibited by Zn^{2+} (Pontoppidan and Kannangara, 1994; Moser et al., 1999). Purified recombinant barley GluTR was reported to contain a tightly bound heme molecule that could be reduced by NADPH and oxidized by air (Vothknecht et al., 1996). Expressed recombinant GluTR from *Chlorobium* (*Chl.*) *vibrioforme* and *C. reinhardtii* also contain bound heme (Srivastava and Beale, unpublished; Srivastava et al., 2005).

GluTR from all species contains a conserved active site Cys residue that is required for activity. During the reaction, this residue forms a thioester bond with C_1 of the glutamyl moiety that is transferred from glutamyl-tRNA (Schauer et al., 2002).

GluTR is able to recognize the tRNA portion of the glutamyl-tRNA substrate, and not all glutamyl-tRNA species are able to serve as substrates. GluTRs from different sources accept a different spectrum of the cofactor glutamyl-tRNA. For example, *E. coli* $tRNA^{Glu}$ functions in vitro with GluTRs from *C. reinhardtii* and *Chl. vibrioforme*, but not with those from barley, *Chl. vulgaris*, *Synechocystis* sp. PCC 6803, and *Euglena* (*E.*) *gracilis*. *E. gracilis* plastid $tRNA^{Glu}$, but not cytoplasmic $tRNA^{Glu}$, functions with *E. gracilis* GluTR. The most striking evidence for tRNA recognition is the report that mutation of a single base of *E. gracilis* plastid $tRNA^{Glu}$ renders it inactive as a GluTR substrate in vivo even though it still functions in protein synthesis (Stange-Thomann et al., 1994). Several specific nucleotides of $tRNA^{Glu}$ were identified that are required for activity with barley GluTR (Willows et al., 1995), and an extensive analysis of the tRNA requirements for *E. coli* GluTR has been published (Randau et al., 2004).

GSAT from a range of species has a native mo-

lecular weight of 80–100 kDa. The homodimeric structure of *Synechococcus* sp. PCC 6301 GSAT has been determined by X-ray crystallography (Hennig et al., 1997). GSAT contains a pyridoxamine-phosphate cofactor. GSAT-encoding genes have been cloned and sequenced from many plant and bacterial sources. Predicted peptide sequences have recognizable homology to other enzymes of the aspartate aminotransferase family (Elliott et al., 1990; Mehta and Christen, 1994). A likely GSAT reaction intermediate is 4,5-diaminovaleric acid. Friedmann et al. (1992) synthesized both (*S*)- and (*R*)-4,5-diaminovaleric acid and showed that the (*S*)-isomer is the preferred substrate for *Synechococcus* sp. PCC 6301 GSAT. Recombinant *Synechococcus* sp. PCC 6301 GSAT showed a nearly complete preference for (*S*)-GSA as a substrate, although the (*R*)-isomer was able to bind at the GSAT active site and elicit spectral changes (Smith et al., 1992).

All of the GSATs that have been examined are inhibited by very low concentrations of gabaculine (3-amino-2,3-dihydrobenzoic acid), in vitro and also in vivo, as indicated by inhibition of Chl formation. A gabaculine-resistant mutant GSAT has been reported from *Synechococcus* sp. PCC 6301 (Bull et al., 1989). Other GSA analogs have been found to be powerful inhibitors of GSAT. In contrast to the reversibility of gabaculine inhibition of the *C. vulgaris* GSAT, irreversible inhibition was obtained with 4-amino-5-hexynoic acid (acetylenic-GABA) (Avissar and Beale, 1989b). This result suggests that acetylenic-GABA may become covalently bound to the protein at the active site.

C. Allosteric Regulation of Enzyme Activity

The most commonly observed regulatory effect at the enzyme level is inhibition of GluTR by heme (Gough and Kannangara, 1979; W.-Y. Wang et al., 1984; Weinstein and Beale, 1985; Rieble and Beale, 1988; Rieble et al., 1989). Micromolar or submicromolar heme concentrations inhibit ALA formation from glutamate in most of the unfractionated enzyme systems studied. Other tetrapyrroles, such as protoporphyrin, Mg-protoporphyrin, protochlorophyllide (PChlide), and chlorophyllide (Chlide), are much less effective (Weinstein and Beale, 1985; Huang and Wang, 1986b). There are some exceptions to this general pattern. The sensitivity of the *Chlorella vulgaris* system toward heme was increased several-fold by oxidized and reduced glutathione (GSH) (Weinstein et al., 1993). Other thiol-containing compounds had no effect. Heme is not a very effective inhibitor of GluTR from *M. kandlerii*, which is consistent with the fact that the organism does not synthesize heme (Moser et al., 1999). *S. typhimurium* GluTR is not inhibited by heme, but heme nevertheless regulates the function of the enzyme in vivo by increasing the rate of its proteolytic degradation in vivo (L.-Y. Wang et al., 1999).

Evidence for a second type of feedback regulation of ALA formation that is independent of heme has recently been described in *A. thaliana* (Meskauskiene et al., 2001; Meskauskiene and Apel, 2002). *FLU* is a nuclear gene that encodes a membrane-associated chloroplast protein, FLU. *FLU* mutants have higher levels of ALA formation and PChlide accumulation than wild-type plants, but the cellular concentrations of heme are normal. It was proposed that FLU is a component of a negative regulatory system for ALA synthesis that may inhibit ALA formation when the cells have high levels of PChlide and/or Mg-protoporphyrin. FLU-like proteins which negatively regulate GluTR activity have been found in *C. reinhardtii* (Falciatore et al., 2005) and barley (Lee et al., 2003).

D. Enzyme-Enzyme Interactions

Although each of the three reactions in the conversion of glutamate to ALA can occur independently of the others, there is some evidence to suggest that the enzymes may interact. *C. reinhardtii* GluTR activity was stimulated by the presence of glutamate, ATP, and GluRS (Krishnasamy and Wang, 1990). *C. reinhardtii* GluTR was reported to form a complex with GluRS in the presence of glutamyl-tRNA (Chen et al., 1990a), and that the complex migrated as a single entity on glycerol gradient centrifugation (Jahn, 1992). A complex between GluRS and GluTR may facilitate the channeling of glutamyl-tRNA toward ALA biosynthesis and regulate competition with the protein synthesizing apparatus for glutamyl-tRNA. However, these preliminary reports should be interpreted with caution because GluTR may be an unusually 'sticky' protein: *Synechocystis* sp. PCC 6803 GluTR co-purified to apparent homogeneity with acetohydroxyacid isomeroreductase (EC 1.1.1.86), an enzyme that has no known functional relationship to GluTR (Rieble and Beale, 1991a, 1992). Modeling based on the

structures of *M. kandlerii* GluTR and cyanobacterial GSAT led to the suggestion that GluTR may dock with GSAT and channel the unstable GSA intermediate from one enzyme to the other without releasing it into the solution (Moser et al., 2001; Chapter 12, Jahn et al.). The GluTR and GSAT proteins of *E. coli* were reported to form a complex in vitro (Luer et al., 2005). GluTR and GSAT of *C. reinhardtii* form a 1:1 complex in vitro, and an in vivo complex was also detected (Nogaj and Beale, 2005). The *C. reinhhardtii* GSAT activates *C. reinhardtii* GluTR in vitro, and the two enzymes achieve functional channeling of the intermediate GSA (Nogaj and Beale, 2005).

E. Regulation of Enzyme Abundance

Total ALA-forming activity extractable from greening barley leaves was higher than the dark level (Kannangara and Gough, 1979), and the activity fell after the leaves were placed in the dark (Gough, 1978). GSAT activity was higher in extracts of greening barley leaves than of etiolated or fully green leaves (Kannangara et al., 1978). Cytokinins, which are known to stimulate greening in etiolated plant tissues after light exposure, induced an increase in both chloroplast $tRNA^{Glu}$ and GluTR activity in greening cucumber cotyledons (Masuda et al., 1994, 1995). Dark-grown cells of a mutant *Chlorella vulgaris* strain that requires light for Chl synthesis yielded about one third as much ALA-forming activity as light-grown cells, but the level of $tRNA^{Glu}$ remained constant (Weinstein et al., 1986). $tRNA^{Glu}$ also remained constant in greening etiolated barley leaves (Berry-Lowe, 1987). In *Synechocystis* sp. PCC 6803, $tRNA^{Glu}$ remained constant and was fully charged under various growth conditions leading to differing cellular Chl content (O'Neill and Söll, 1990). Illumination did not change the GSAT level in dark-grown cucumber cotyledons (Masuda et al., 1996). In contrast, different results were obtained in *E. gracilis*, a system in which proplastids develop into mature chloroplasts under the influence of light. Compared to light-grown *E. gracilis* cells, dark-grown cells had reduced levels of all three enzymes as well as of the tRNA involved in ALA synthesis (Mayer and Beale, 1990). GSAT was the most profoundly affected activity, being nearly undetectable in dark-grown cells and least 50-fold higher in light-grown cells. GSAT activity in dark-grown *C. reinhardtii* cells increased about 15-fold during the first few hours of light exposure (Mau et al., 1992). However, in cells that were synchronized to 12-h light/12-h dark cycles, there were only relatively small changes in the cellular levels of GluTR and GSAT throughout the cycle, even though Chl was synthesized only during the light phase (Nogaj et al., 2005). These results indicate that Chl formation in light/dark synchronized *C. reinhardtii* cells is not controlled by the cellular levels of GluTR and GSAT.

F. Regulation of mRNA Levels

Light- and developmentally-regulated expression of *Gtr* genes (generally termed *HemaA*) has been reported in *Arabidopsis thaliana*, barley, and cucumber (Ilag et al., 1994; Bougri and Grimm, 1996; Kumar et al., 1996; Tanaka et al., 1996, 1997; Vothknecht et al., 1996; Kruse et al., 1997; McCormac et al., 2001; Ujwal et al., 2002). In all of these plants, there are multiple *Gtr* genes, some of which are induced by light in greening tissues and others of which are not light induced but are developmentally controlled, with higher mRNA levels being found in non-greening tissues and organs (e.g., roots and flowers) than in greening tissues. For the light-regulated genes, transcript levels parallel the rates of ALA formation in greening tissues.

In higher plants, the *Gsa* transcript levels appear to be less influenced by light and developmental conditions than the *Gtr* transcript levels. The *Gsa* mRNA level in etiolated soybean leaves and *A. thaliana* seedlings was only slightly increased after 24 h of light, and no change in GSAT activity was observed (Sangwan and O'Brian, 1993). In etiolated *A. thaliana* seedlings, modest light induction of GSAT mRNA was observed (Ilag et al., 1994). In barley, the increase of GSAT activity induced by light was not correlated with transcript abundance (Grimm, 1990; Kruse et al., 1997). Barley GSAT mRNA levels were high in etiolated seedlings, remained constant after transfer of seedlings from the dark to the light, and decreased during the later phases of greening. These results suggest that the increase in GSAT activity in greening barley leaves might be regulated by a translational or post-translation event. Further work is required to resolve this question. In contrast to the results from higher plants, *Gsa* mRNA transcribed from the single *C. reinhardtii Gsa* gene increased over 25-fold during the first 2 h after exposure of dark-grown cells to light. (Matters and Beale, 1995).

Experiments with actinomycin D indicated that, in *C. reinhardtii*, *Gsa* mRNA is rapidly turned over both in the light and dark, and that regulation of mRNA abundance is exerted at the level of transcription (Matters and Beale, 1995).

G. Signal Transduction Components in the Regulation of Gene Expression

Aside from the effects of cytokinins on $tRNA^{Glu}$ and GluTR expression, a series of studies has uncovered some of the mechanisms and components of signal transduction pathway linking exposure to light to induction of the *Gsa* gene in *C. reinhardtii* (Matters and Beale, 1994,1995; Im et al., 1996; Herman et al., 1999; Im and Beale, 2000). The results indicate that (a) only light in the blue and green spectral region (below 560 nm) is effective; (b) the photoreceptor is probably a flavoprotein; (c) regulation of transcript abundance is exerted primarily by altering the rate of transcription rather than the rate of mRNA turnover; (d) signal transduction components appear to include phospholipase C (EC 3.1.4.3), an inositol-1,4,5-trisphosphate-dependent increase in the concentration of Ca^{2+} (which can be derived from internal and external sources), calmodulin, a Ca^{2+}/calmodulin-dependent protein kinase, and a phosphoprotein phosphatase. The results suggest that upstream events may involve a receptor tyrosine kinase and direct activation of a phospholipase C by phosphorylation rather than via a G protein.

IV. Phylogenetic Distribution and Evolutionary Implications of the Two 5-Aminolevulinic Acid Biosynthetic Pathways in Photosynthetic Species

Although ALAS activity has been detected in cell-free extracts from many animal and fungal species (including yeast), its occurrence in photosynthetic organisms other than the α-proteobacteria is doubtful. ALAS activity has been found and characterized in extracts of only one oxygenic species, the phytoflagellate *Eug. gracilis* (Beale et al., 1981). However, the physical and kinetic properties of ALAS (Dzelzkalns et al., 1982) and the regulation of its activity (Beale and Foley, 1982; Foley et al., 1982) suggest that in *Eug. gracilis*, ALAS functions exclusively to provide precursors for nonplastid tetrapyrroles. This role was subsequently proven directly by measuring the differential incorporation of labeled precursors into isolated tetrapyrroles specific to plastids and mitochondria (Weinstein and Beale, 1983).

It is unclear why two distinct routes to ALA exist. For example, even though *E. coli* normally uses the five-carbon pathway, strains that are deficient in ALA biosynthesis can be complemented by bacterial and animal genes that encode ALAS (Leong et al., 1982; Schoenhaut and Curtis, 1986). Moreover, yeast ALAS expressed transgenically in tobacco appears to be able to supply ALA for Chl biosynthesis (Zavgorodnyaya et al., 1997). The wide distribution of the five-carbon pathway suggests that it was the earlier one to evolve, perhaps arising before the appearance of the tricarboxylic acid cycle, a component of which, succinyl-CoA, is required for ALA synthesis via ALAS. It is of interest that α-proteobacteria, the only group of bacteria that use the ALAS route, have been proposed to be the progenitor of mitochondria (Yang et al., 1985).

Acknowledgments

I thank A. Srivastava for critically reading the manuscript, and the US National Science Foundation, Department of Energy, and Department of Agriculture for research support.

References

Abboud MM, Jordan PM and Akhtar M (1974) Biosynthesis of 5-aminolevulinic acid: Involvement of a retention-reversion mechanism. J Chem Soc Chem Commun 1974: 643–644

Avissar YJ and Beale SI (1989a) Identification of the enzymatic basis for δ-aminolevulinic acid auxotrophy in a *hemA* mutant of *Escherichia coli*. J Bacteriol 171: 2919–2924

Avissar YJ and Beale SI (1989b) The aminotransferase step in the formation of δ-aminolevulinic acid from glutamate: Isolation of the enzyme from *Chlorella vulgaris*, requirement for pyridoxal phosphate, and inhibition by gabaculine and acetylenic GABA. Plant Physiol 89: S-51

Avissar YJ and Beale SI (1990) Cloning and expression of a structural gene from *Chlorobium vibrioforme* that complements the *hemA* mutation in *Escherichia coli*. J Bacteriol 172: 1656–1659

Beale SI and Castelfranco PA (1974) The biosynthesis of δ-aminolevulinic acid in higher plants. II. Formation of ^{14}C-δ-aminolevulinic acid from labeled precursors in greening plant tissues. Plant Physiol 53: 297–303

Beale SI and Foley T (1982) Induction of δ-aminolevulinic acid synthase and inhibition of heme synthesis in *Euglena gracilis* by N-methyl mesoporphyrin IX. Plant Physiol 69: 1331–1333

Beale SI, Foley T and Dzelzkalns V (1981) δ-Aminolevulinic acid synthase from *Euglena gracilis*. Proc Natl Acad Sci USA 78: 1666–1669

Berry-Lowe S (1987) The chloroplast glutamate tRNA gene required for δ-aminolevulinate synthesis. Carlsberg Res Commun 52 197–210

Biel SW, Wright MS and Biel AJ (1988) Cloning of the *Rhodobacter capsulatus hemA* gene. J Bacteriol 170: 4382–4384

Bolt EL, Kryszak L, Zeilstra-Ryalls J, Schoolingin-Jordan PM and Warren MJ (1999) Characterization of the *Rhodobacter sphaeroides* 5-aminolaevulinic acid synthase isoenzymes, HemA and HemT, isolated from recombinant *Escherichia coli*. Eur J Biochem 265: 290-299

Bougri O and Grimm B (1996) Members of a low-copy number gene family encoding glutamyl-tRNA reductase are differentially expressed in barley. Plant J 9: 867–878

Bruyant P and Kannangara CG (1987) Biosynthesis of δ-aminolevulinate in greening barley leaves, VIII: Purification and characterization of the glutamate-tRNA ligase. Carlsberg Res Commun 52: 99–109

Bull AD, Pakes JF, Hoult RC, Rogers LJ and Smith AJ (1989) Tetrapyrrole biosynthesis in a gabaculin-tolerant mutant of *Synechococcus* 6301. Biochem Soc Trans 17: 911–912

Burnham BF and Lascelles J (1963) Control of porphyrin biosynthesis through a negative-feedback mechanism. Studies with preparations of δ-aminolaevulate synthetase and δ-aminolaevulate dehydratase from *Rhodopseudomonas spheroides*. Biochem J 87: 462–472

Chang T-E, Wegmann B and Wang W-Y (1990) Purification and characterization of glutamyl-tRNA synthetase: An enzyme involved in chlorophyll biosynthesis. Plant Physiol 93: 1641–1649

Chen M-W, Jahn D, Schön A, O'Neill GP and Söll D (1990a) Purification and characterization of *Chlamydomonas reinhardtii* chloroplast glutamyl-tRNA synthetase, a natural misacylating enzyme. J Biol Chem 265: 4054-4057

Chen M-W, Jahn D, O'Neill GP and Söll D (1990b) Purification of the glutamyl-tRNA reductase from *Chlamydomonas reinhardtii* involved in δ-aminolevulinic acid formation during chlorophyll biosynthesis. J Biol Chem 265: 4058–4063

Clement-Metral JD (1979) Activation of ALA synthetase by reduced thioredoxin in *Rhodopseudomonas spheroides* Y. FEBS Lett 101: 116–120

Cohen-Bazire G, Sistrom WR and Stanier RY (1957) Kinetic studies of pigment synthesis by non-sulfur purple bacteria. J Cell Comp Physiol 49: 25–68

Dzelzkalns V, Foley T and Beale SI (1982) δ-Aminolevulinic acid synthase of *Euglena gracilis*: Physical and kinetic properties. Arch Biochem Biophys 216: 196–203

Elliott T and Roth JR (1989) Heme-deficient mutants of *Salmonella typhimurium*. Two genes required for ALA synthesis. Mol Gen Genet 216: 303–314

Elliott T, Avissar YJ, Rhie G and Beale SI (1990) Cloning and sequence of the *Salmonella typhimurium hemL* gene and identification of the missing enzyme in *hemL* mutants as glutamate-1-semialdehyde aminotransferase. J Bacteriol 172: 7071–7084

Evans WR, Fleischman, DE, Calvert HE, Pyati PV, Alter GM and Subba Rao NS (1990) Bacteriochlorophyll and photosynthetic reaction centers in *Rhizobium* strain BTAi 1. Appl Environ Microbiol 56: 3445–3449

Falciatore A, Merendino L, Barneche F, Ceol M, Meskauskiene R, Apel K and Rochaix J-D (2005) The FLP proteins act as regulators of chlorophyll synthesis in response to light and plastid signals in *Chlamydomonas*. Genes Devel 19: 176–187

Fanica-Gaignier M and Clement-Metral JD (1971) ATP inhibition of aminolevulinate (ALA) synthetase activity in *Rhodopseudomonas spheroides* Y. Biochem Biophys Res Commun 44: 192–198

Fanica-Gaignier M and Clement-Metral J (1973) 5-Aminolevulinic-acid synthetase of *Rhodopseudomonas spheroides* Y: kinetic mechanism and inhibition by ATP. Eur J Biochem 40: 19–24

Ferreira GC and Cheltsov AV (2002) Circular permutation of 5-aminolevulinate synthase as a tool to evaluate folding, structure and function. Cell Mol Biol 48: 11-16

Foley T, Dzelzkalns V and Beale SI (1982) δ-Aminolevulinic acid synthase of *Euglena gracilis*: Regulation of activity. Plant Physiol 70: 219–226

Friedmann HC, Duban ME, Valasinas A and Frydman B (1992) The enantioselective participation of (*S*)- and (*R*)-diaminovaleric acids in the formation of δ-aminolevulinic acid in cyanobacteria. Biochem Biophys Res Commun 185: 60–68

Gibson KD, Laver WG and Neuberger A (1958) Formation of δ-aminolaevulic acid in vitro from succinyl-coenzyme a and glycine. Biochem J 70: 71–81

Gough SP (1978) Light stimulated δ-aminolevulinate accumulation in levulinate treated barley seedlings. Carlsberg Res Commun 43: 497–508

Gough SP and Kannangara CG (1979) Biosynthesis of δ-aminolevulinate in greening barley leaves. III. The formation of δ-aminolevulinate in *tigrina* mutants of barley. Carlsberg Res Commun 44: 403–416

Gough SP, Kannangara CG and Bock K (1989) A new method for the synthesis of glutamate 1-semialdehyde: Characterization of its structure in solution by NMR spectroscopy. Carlsberg Res Commun 54: 99–108

Grimm B (1990) Primary structure of a key enzyme in plant tetrapyrrole synthesis: Glutamate 1-semialdehyde aminotransferase. Proc Natl Acad Sci USA 87: 4169–4173

Harashima K, Shiba T, Totsuka T, Simidu U and Taga N (1978) Occurrence of bacteriochlorophyll *a* in a strain of an aerobic heterotrophic bacterium. Agric Biol Chem 42: 1627–1628

Harashima K, Hayasaki J, Ikari T and Shiba T (1980) O_2-stimulated synthesis of bacteriochlorophyll and carotenoids in marine bacteria. Plant Cell Physiol 21: 1283–1294

Hennig M, Grimm B, Contestabile R, John RA and Jansonius JN (1997) Crystal structure of glutamate-1-semialdehyde aminomutase: An a_2-dimeric vitamin-B_6-dependent enzyme with asymmetry in structure and active site reactivity. Proc Natl Acad Sci USA 94: 4866–4871

Herman CA, Im C and Beale SI (1999) Light-regulated expression of the *Gsa* gene encoding the chlorophyll biosynthetic enzyme glutamate 1-semialdehyde aminotransferase in carotenoid-deficient *Chlamydomonas reinhardtii* cells. Plant Mol Biol 39: 289–297

Hornberger U, Liebetanz R, Tichy H-V and Drews G (1990) Cloning and sequencing of the *hemA* gene of *Rhodobacter capsulatus* and isolation of a δ-aminolevulinic acid-dependent mutant strain. Mol Gen Genet 221: 371–378

Hornberger U, Wieseler B and Drews G (1991) Oxygen-tension regulated expression of the *hemA* gene of *Rhodobacter cap-*

sulatus. Arch Microbiol 156: 129-134
Huang D-D and Wang W-Y (1986a) Chlorophyll synthesis in *Chlamydomonas* starts with the formation of glutamyl-tRNA. J Biol Chem 261: 13451–13455
Huang D-D and Wang W-Y (1986b) Genetic control of chlorophyll biosynthesis: Regulation of *delta* aminolevulinate synthesis in *Chlamydomonas*. Mol Gen Genet 205: 217–220
Huang D-D, Wang W-Y, Gough SP and Kannangara CG (1984) δ-Aminolevulinic acid-synthesizing enzymes need an RNA moiety for activity. Science 225: 1482–1484
Ilag LL, Kumar AM and Söll D (1994) Light regulation of chlorophyll biosynthesis at the level of 5-aminolevulinate formation in *Arabidopsis*. Plant Cell 6, 265–275.
Im C and Beale SI (2000) Identification of possible signal transduction components mediating light induction of the *Gsa* gene for an early chlorophyll biosynthetic step in *Chlamydomonas reinhardtii*. Planta 210: 999–1005
Im C, Matters GL and Beale SI (1996) Calcium and calmodulin are involved in blue-light induction of the *gsa* gene for an early chlorophyll biosynthetic step in *Chlamydomonas*. Plant Cell 8: 2245–2253
Inoue I, Oyama H and Tuboi S (1979) On the nature of the activating enzyme of the inactive form of δ-aminolevulinate synthetase in *Rhodopseudomonas spheroides*. J Biochem 86: 477–482
Jahn D (1992) Complex formation between glutamyl-tRNA synthetase and glutamyl-tRNA reductase during tRNA-dependent synthesis of 5-aminolevulinic acid in *Chlamydomonas*. FEBS Lett 314: 77–80
Jahn D, O'Neill GP, Verkamp E and Söll D (1992) Glutamate tRNA: Involvement in protein synthesis and aminolevulinate formation in *Chlamydomonas reinhardtii*. Plant Physiol Biochem 30: 245-253
Jurgenson JE, Beale SI and Troxler RF (1976) Biosynthesis of δ-aminolevulinic acid in a unicellular Rhodophyte, *Cyanidium caldarium*. Biochem Biophys Res Commun 69: 149–157
Kannangara CG and Gough SP (1978) Biosynthesis of δ-aminolevulinate in greening barley leaves: Glutamate 1-semialdehyde aminotransferase. Carlsberg Res Commun 43: 185–194
Kannangara CG and Gough SP (1979) Biosynthesis of δ-aminolevulinate in greening barley leaves. II. Induction of enzyme synthesis by light. Carlsberg Res Commun 44: 11–20
Kannangara CG, Gough SP and von Wettstein D (1978) The biosynthesis of δ-aminolevulinate and chlorophyll and its genetic regulation. In: Akoyunoglou G and Argyroudi-Akoyunoglou HJ (eds) Chloroplast Development, pp 147–160. Elsevier, Amsterdam
Kannangara CG, Gough SP, Oliver RP and Rasmussen SK (1984) Biosynthesis of δ-aminolevulinate in greening barley leaves. VI. Activation of glutamate by ligation to RNA. Carlsberg Res Commun 49: 417–437
Kikuchi G, Kumar A, Talmage P and Shemin D (1958) The enzymatic synthesis of δ-aminolevulinic acid. J Biol Chem 233: 1214–1219
Krishnasamy S and Wang W-Y (1990) Purification of the second enzyme of chlorophyll biosynthesis from *Chlamydomonas reinhardtii*. Plant Physiol 93: S-62
Kruse E, Grimm B, Beator J and Kloppstech K (1997) Developmental and circadian control of the capacity for δ-aminolevulinic acid synthesis in greening barley. Planta 202: 235–241
Kumar AM, Csankovszki G and Söll D (1996) A second and differentially expressed glutamyl-tRNA reductase gene from *Arabidopsis thaliana*. Plant Mol Biol 30: 419–426
Laghai A and Jordan PM (1976) A partial reaction of δ-aminolaevulinate synthetase from *Rhodopseudomonas spheroides*. Biochem Soc Trans 4: 52–53
Laghai A and Jordan PM (1977) An exchange reaction catalysed by δ-aminolaevulinate synthase from *Rhodopseudomonas spheroides*. Biochem Soc Trans 5: 299–300
Lascelles J (1960) The synthesis of enzymes concerned in bacteriochlorophyll formation in growing cultures of *Rhodopseudomonas spheroides*. J Gen Microbiol 23: 487–498
Lee KP, Kim C, Lee DW and Apel K (2003) TIGRINA d, required for regulating the biosynthesis of tetrapyrroles in barley, is an ortholog of the FLU gene of *Arabidopsis thaliana*. FEBS Lett 553: 119-124
Leong SA, Ditta GS and Helinski DR (1982) Heme biosynthesis in *Rhizobium*. Identification of a cloned gene coding for δ-aminolevulinic acid synthetase from *Rhizobium meliloti*. J. Biol. Chem. 257, 8724–8730.
Li J-M, Brathwaite O, Cosloy SD and Russell CS (1989) 5-Aminolevulinic acid synthesis in *Escherichia coli*. J Bacteriol 171: 2547–2552
Luer C, Schauer S, Mobius K, Schulze J, Schubert WD, Heinz DW, Jahn D and Moser J (2005) Complex formation between glutamyl-tRNA reductase and glutamate-1-semialdehyde 2,1-aminomutase in *Escherichia coli* during the initial reactions of porphyrin biosynthesis J Biol Chem 280: 18568–18572
Masuda R, Tanaka R, Shioi Y, Takamiya KI, Kannangara CG and Tsuji H (1994) Mechanism of benzyladenine-induced stimulation of the synthesis of 5-aminolevulinic acid in greening cucumber cotyledons: Benzyladenine increases levels of plastid $tRNA^{Glu}$. Plant Cell Physiol 35: 183–188
Masuda T, Ohta H, Shioi Y, Tsuji H and Takamiya KI (1995) Stimulation of glutamyl-tRNA reductase activity by benzyladenine in greening cucumber cotyledons. Plant Cell Physiol 36: 1237–1243
Masuda T, Ohta H, Shioi Y and Takamiya K (1996) Light regulation of 5-aminolevulinic acid-synthesis system in *Cucumis sativus*: Light stimulates activity of glutamyl-tRNA reductase during greening. Plant Physiol Biochem 34: 11–16
Matters GL and Beale SI (1994) Structure and light-regulated expression of the *gsa* gene encoding the chlorophyll biosynthetic enzyme, glutamate-1-semialdehyde aminotransferase, in *Chlamydomonas reinhardtii*. Plant Mol Biol 24: 617–629
Matters GL and Beale SI (1995) Blue-light-regulated expression of genes for two early steps of chlorophyll biosynthesis in *Chlamydomonas reinhardtii*. Plant Physiol 109: 471–479
Mau Y-HL and Wang W-Y (1988) Biosynthesis of δ-aminolevulinic acid in *Chlamydomonas reinhardtii*. Study of the transamination mechanism using specifically labeled glutamate. Plant Physiol 86: 793–797
Mau Y-H, Zheng P, Krishnasamy S and Wang W-Y (1992) Light regulation of δ-aminolevulinic acid in *Chlamydomonas*. Plant Physiol 98: S-99
Mayer SM and Beale SI (1990) Light regulation of δ-aminolevulinic acid biosynthetic enzymes and tRNA in *Euglena gracilis*. Plant Physiol 94: 1365–1375
Mayer SM, Gawlita E, Avissar YJ, Anderson VE and Beale SI (1993) Intermolecular nitrogen transfer in the enzymatic conversion of glutamate to δ-aminolevulinic acid by extracts of *Chlorella vulgaris*. Plant Physiol 101: 1029–1038

Mayer SM, Rieble S and Beale SI (1994) Metal requirements of the enzymes catalyzing conversion of glutamate to δ-aminolevulinic acid in extracts of *Chlorella vulgaris* and *Synechocystis* sp. PCC 6803. Arch Biochem Biophys 312: 203–209

McCormac AC, Fischer A, Kumar AM, Söll D and Terry MJ (2001) Regulation of *HEMA1* expression by phytochrome and a plastid signal during de-etiolation in *Arabidopsis thaliana*. Plant J 25: 549–561

Mehta PK and Christen P (1994) Homology of 1-aminocyclopropane-1-carboxylate synthase, 8-amino-7-oxononanoate synthase, 2-amino-6-caprolactam racemase, 2,2-dialkylglycine decarboxylase, glutamate-1-semialdehyde 2,1-aminomutase and isopenicillin-*N*-epimerase with aminotransferases. Biochem Biophys Res Commun 198: 138–143

Meller E and Harel E (1978) The pathway of 5-aminolevulinic acid synthesis in *Chlorella vulgaris* and in *Fremyella diplosiphon*. In: Akoyunoglou G and Argyroudi-Akoyunoglou JH (eds) Chloroplast Development, pp 51–57. Elsevier, Amsterdam

Meller E, Harel E and Kannangara CG (1979) Conversion of glutamic-1-semialdehyde and 4,5-dioxovaleric acid to 5-aminolevulinic acid by cell-free preparations from greening maize leaves. Plant Physiol 63: S-98

Meskauskiene R and Apel K (2002) Interaction of FLU, a negative regulator of tetrapyrrole biosynthesis, with the glutamyl-tRNA reductase requires the tetratricopeptide repeat domain of FLU. FEBS Lett 532: 27-30

Meskauskiene R, Nater M, Goslings D, Kessler F, op den Camp R and Apel K (2001) FLU: A negative regulator of chlorophyll biosynthesis in *Arabidopsis thaliana*. Proc Natl Acad Sci USA 98: 12826–12831

Moser J, Lorenz S, Hubschwerlen C, Rompf A and Jahn D (1999) *Methanopyrus kandlerii* glutamyl-tRNA reductase. J Biol Chem 274: 30679–30685

Moser J, Schubert WD, Beier V, Bringemeier I, Jahn D and Heinz DW (2001) V-shaped structure of glutamyl-tRNA reductase, and first enzyme of tRNA-dependent tetrapyrrole biosynthesis. EMBO J 20: 6583–6590

Neidle EL and Kaplan S (1993a) Expression of the *Rhodobacter sphaeroides hemA* and *hemT* genes, encoding two 5-aminolevulinic acid synthase isoenzymes. J Bacteriol 175: 2292–2303

Neidle EL and Kaplan S (1993b) 5-Aminolevulinic acid availability and control of spectral complex formation in HemA and HemT mutants of *Rhodobacter sphaeroides*. J Bacteriol 175: 2304–2313

Nishimura Y, Shimadzu M and Iizuka H (1981) Bacteriochlorophyll formation in radiation-resistant *Pseudomonas radiora*. J Gen Appl Microbiol 27: 427–430

Nogaj LA and Beale SI (2005) Physical and kinetic interactions between glutamyl-tRNA reductase and glutamate-1-semialdehyde aminotransferase of *Chlamydomonas reinhardtii*. J Biol Chem 280: 24301–24307

Nogaj LA, Srivastava A, van Lis R and Beale SI (2005) Cellular levels of glutamyl-tRNA reductase and glutamate-1-semialdehyde aminotransferase do not control chlorophyll synthesis in *Chlamydomonas reinhardtii*. Plant Physiol 139: 389–396

O'Neill GP and Söll D (1990) Expression of the *Synechocystis* sp. PCC 6803 $tRNA^{Glu}$ gene provides tRNA for protein and chlorophyll biosynthesis. J Bacteriol 172: 6363–6371

O'Neill GP, Chen M-W and Söll D (1989) δ-Aminolevulinic acid biosynthesis in *Escherichia coli* and *Bacillus subtilis* involves formation of glutamyl-tRNA. FEMS Microbiol Lett 60: 255–260

O'Neill GP, Schön A, Chow H, Chen MW, Kim Y-C and Söll D (1990) Sequence of $tRNA^{Glu}$ and its genes from the chloroplast genome of *Chlamydomonas reinhardtii*. Nuc Acids Res 18: 5893–5893

Oh-hama T, Seto H, Otake N and Miyachi S (1982) ^{13}C-NMR evidence for the pathway of chlorophyll biosynthesis in green algae. Biochem Biophys Res Commun 105: 647–652

Petricek M, Rutberg L, Schröder I and Hederstedt L (1990) Cloning and characterization of the *hemA* region of the *Bacillus subtilis* chromosome. J Bacteriol 172: 2250–2258

Pontoppidan B and Kannangara CG (1994) Purification and partial characterization of barley glutamyl-$tRNA^{Glu}$ reductase, the enzyme that directs glutamate to chlorophyll biosynthesis. Eur J Biochem 225: 529–537

Porra RJ, Klein O and Wright PE (1983) The proof by ^{13}C-NMR spectroscopy of the predominance of the C_5 pathway over the Shemin pathway in chlorophyll biosynthesis in higher plants and the formation of the methyl ester group of chlorophyll from glycine. Eur J Biochem 130: 509–516

Randau, L, Schauer S, Ambrogelly A, Salazari JC, Moser J, Sekine S, Yokoyama S, Söll D and Jahn D (2004) tRNA recognition by glutamyl-tRNA reductase. J Biol Chem 279: 34931-34937

Rieble S and Beale SI (1988) Transformation of glutamate to δ-aminolevulinic acid by soluble extracts of *Synechocystis* sp. PCC 6803 and other oxygenic prokaryotes. J Biol Chem 263: 8864–8871

Rieble S and Beale SI (1991a) Purification of glutamyl-tRNA reductase from *Synechocystis* sp. PCC 6803. J Biol Chem 266: 9740–9744

Rieble S and Beale SI (1991b) Separation and partial characterization of enzymes catalyzing δ-aminolevulinic acid formation in *Synechocystis* sp. PCC 6803. Arch Biochem Biophys 289: 289–297

Rieble S and Beale SI (1992) Structure and expression of a cyanobacterial *ilvC* gene encoding acetohydroxyacid isomeroreductase. J Bacteriol 174: 7910–7918

Rieble S, Ormerod JG and Beale SI (1989) Transformation of glutamate to δ-aminolevulinic acid by soluble extracts of *Chlorobium vibrioforme*. J Bacteriol 171: 3782–3787

Sandy JD, Davies RC and Neuberger A (1975) Control of 5-aminolaevulinate synthetase activity in *Rhodopseudomonas spheroides*: A role for trisulphides. Biochem J 150: 245–257

Sangwan I and O'Brian MR (1993) Expression of the soybean (*Glycine max*) glutamate 1-semialdehyde aminotransferase gene in symbiotic root nodules. Plant Physiol 102: 829–834

Sato K (1978) Bacteriochlorophyll formation by facultative methylotrophs, *Protaminobacter ruber* and *Pseudomonas* AM1. FEBS Lett 85: 207–210

Sato K, Ishida K, Shirai M and Shimizu S (1985) Occurrence and some properties of two types of δ-aminolevulinic acid synthase in a facultative methylotroph, *Protaminobacter ruber*. Agric Biol Chem 49: 3423–3428

Schauer S, Chaturvedi S, Randau L, Moser J, Kitabatake M, Lorenz S, Verkamp E, Schubert W-D, Nakayashiki T, Murai M, Wall K, Thomann H-U, Heinz DW, Inokuchi H, Söll D and Jahn D (2002) *Escherichia coli* glutamyl-tRNA reductase. Trapping the thioester intermediate. J Biol Chem 277: 48658-48663

Schneegurt MA and Beale SI (1988) Characterization of the RNA required for biosynthesis of δ-aminolevulinic acid from glutamate. Purification by anticodon-based affinity chromatog-

raphy and determination that the UUC glutamate anticodon is a general requirement for function in ALA biosynthesis. Plant Physiol 86: 497–504

Schoenhaut DS and Curtis PJ (1986) Nucleotide sequence of mouse 5-aminolevulinic acid synthase cDNA and expression of its gene in hepatic and erythroid tissues. Gene 48: 55–63

Schön A, Krupp G, Gough S, Berry-Lowe S, Kannangara CG and Söll D (1986) The RNA required in the first step of chlorophyll biosynthesis is a chloroplast glutamate tRNA. Nature 322: 281–284

Schröder I, Hederstedt L, Kannangara CG and Gough SP (1992) Glutamyl-tRNA reductase activity in *Bacillus subtilis* is dependent on the *hemA* gene product. Biochem J 281: 843–850

Shioi Y and Doi M (1988) Control of bacteriochlorophyll accumulation by light in an aerobic photosynthetic bacterium, *Erythrobacter* sp. OCh114. Arch Biochem Biophys 266: 470–477

Smith MA, Kannangara CG and Grimm B (1992) Glutamate 1-semialdehyde aminotransferase: Anomalous enantiomeric reaction and enzyme mechanism. Biochemistry 31: 11249–11254

Srivastava A and Beale SI (2005) Glutamyl-tRNA Reductase of *Chlorobium vibrioforme* is a dissociable homodimer that contains one tightly bound heme per subunit. J Bacteriol 187: 4444–4450

Srivastava A, Lake V, Nogaj LA, Mayer SM, Willows RD and Beale SI (2005) The *Chlamydomonas reinhardtii gtr* gene encoding the tetrapyrrole biosynthetic enzyme glutamyl-tRNA reductase: Structure of the gene and properties of the expressed enzyme. *Plant Mol Biol* 58: 643–658

Stange-Thomann N, Thomann H-U, LLoyd AJ, Lyman H and Söll D (1994) A point mutation in *Euglena gracilis* chloroplast $tRNA^{Glu}$ uncouples protein and chlorophyll biosynthesis. Proc Natl Acad Sci USA 91: 7947–7951

Tai T-N, Moore MD and Kaplan S (1988) Cloning and characterization of the 5-aminolevulinate synthase gene(s) from *Rhodobacter sphaeroides*. Gene 70: 139–151

Tanaka R, Yoshida K, Nakayashiki T, Masuda T, Tsuji H, Inokuchi H and Tanaka A (1996) Differential expression of two *hemA* mRNAs encoding glutamyl-tRNA reductase proteins in greening cucumber seedlings. Plant Physiol 110: 1223–1230

Tanaka R, Yoshida K, Nakayashiki T, Tsuji H, Inokuchi H, Okada K and Tanaka A (1997) The third member of the *hemA* family encoding glutamyl-tRNA reductase is primarily expressed in roots in *Hordeum vulgare*. Photosynth Res 53: 161–171

Tuboi S and Hayasaka S (1972) Control of δ-aminolevulinate synthetase activity in *Rhodopseudomonas spheroides*, II: Requirement of a disulfide compound for the conversion of the inactive form of Fraction I to the active form. Arch Biochem Biophys 150: 690–697

Ujwal ML, McCormac AC, Goulding A, Kumar AM, Söll D and Terry MJ (2002) Divergent regulation of the *HEMA* gene family encoding glutamyl-tRNA reductase in *Arabidopsis thaliana*: Expression of *HEMA2* is regulated by sugars, but is independent of light and plastid signalling. Plant Mol Biol 50: 83-91

Viale AA, Wider EA and Batlle AM del C (1987) Porphyrin biosynthesis in *Rhodopseudomonas palustris*, XII: δ-Aminolevulinate synthetase switch-off/on regulation. Int J Biochem 19: 379–383

Vothknecht UC, Kannangara CG and von Wettstein D (1996) Expression of catalytically active barley glutamyl $tRNA^{Glu}$ reductase in *Escherichia coli* as a fusion protein with glutathione *S*-transferase. Proc Natl Acad Sci USA 93: 9287–9291

Wang L-Y, Elliott M and Elliott T (1999) Conditional stability of the HemA protein (glutamyl-tRNA reductase) regulates heme biosynthesis in *Salmonella typhimurium*. J Bcteriol 181: 1211–1219

Wang W-Y, Huang D-D, Stachon D, Gough SP and Kannangara CG (1984) Purification, characterization, and fractionation of the δ-aminolevulinic acid synthesizing enzymes from light-grown *Chlamydomonas reinhardtii* cells. Plant Physiol 74: 569–575

Weinstein JD and Beale SI (1983) Separate physiological roles and subcellular compartments for two tetrapyrrole biosynthetic pathways in *Euglena gracilis*. J Biol Chem 258: 6799–6807

Weinstein JD and Beale SI (1985) Enzymatic conversion of glutamate to δ-aminolevulinate in soluble extracts of the unicellular green alga, *Chlorella vulgaris*. Arch Biochem Biophys 237: 454–464

Weinstein JD, Mayer SM and Beale SI (1986) RNA is required for enzymatic conversion of glutamate to δ-aminolevulinic acid by algal extracts. In: Akoyunoglou G and Senger H (eds) Regulation of Chloroplast Development, pp 43–48. Liss, New York

Weinstein JD, Mayer SM and Beale SI (1987) Formation of δ-aminolevulinic acid from glutamic acid in algal extracts. Separation into an RNA and three required enzyme components by serial affinity chromatography. Plant Physiol 84: 244–250

Weinstein JD, Howell RW, Leverette RD, Grooms SY, Brignola PS, Mayer SM and Beale SI (1993) Heme inhibition of δ-aminolevulinic acid synthesis is enhanced by glutathione in cell-free extracts of *Chlorella*. Plant Physiol 101: 657–665

Willows RD, Kannangara CG and Pontoppidan B (1995) Nucleotides of tRNA (Glu) involved in recognition by barley chloroplast glutamyl-tRNA synthetase and glutamyl-tRNA reductase. Biochim Biophys Acta 1263: 228–234

Yang D, Oyaizu Y, Olsen H and Woese CR (1985) Mitochondrial origins. Proc Natl Acad Sci USA 82: 4443–4447

Yubisui T and Yoneyama Y (1972) δ-Aminolevulinic acid synthetase of *Rhodopseudomonas spheroides*: purification and properties of the enzyme. Arch Biochem Biophys 150: 77–85

Zaman Z, Jordan PM and Akhtar M (1973) Mechanism and stereochemistry of the 5-aminolaevulinate synthetase reaction. Biochem J 135: 257–263

Zavgorodnyaya A, Papenbrock J and Grimm B (1997) Yeast 5-aminolevulinate synthase provides additional chlorophyll precursor in transgenic tobacco. Plant J 12: 169–178

Zeilstra-Ryalls JH and Kaplan S (1995) Aerobic and anaerobic regulation in *Rhodobacter sphaeroides* 2.4.1: The role of the *fnrL* gene. J Bacteriol 177: 6422-6431

Chapter 12

Transfer RNA-Dependent Aminolevulinic Acid Formation: Structure and Function Of Glutamyl-tRNA Synthetase, Reductase and Glutamate-1-Semialdehyde-2,1-Aminomutase

Dieter Jahn*[2], Jürgen Moser[2], Wolf-Dieter Schubert[1] and Dirk W. Heinz[1]
[1]Department of Structural Biology, German Research Center for Biotechnology, Mascheroder Weg 1, D-38104 Braunschweig, Germany and [2]Institute of Microbiology, Technical University Braunschweig, Spielmannstrasse 7, D-38106 Braunschweig, Germany

Summary

In plants, green algae, archaea and in most bacteria the common precursor of all tetrapyrroles, 5-aminolevulinic acid, is formed by three enzymes. The initial substrate glutamate is converted to glutamyl-tRNA by glutamyl-tRNA synthetase for use in both protein and tetrapyrrole biosynthesis. During the first committed step an NADPH-dependent glutamyl-tRNA reductase reduces glutamyl-tRNA to form glutamate-1-semialdehyde, which is subsequently transaminated by glutamate-1-semialdehyde-2,1-aminomutase to yield 5-aminolevulinic acid. The enzymatic mechanisms deduced from biochemical investigations and recently solved crystal structures are described for all three enzymes. A potential pathway for metabolic channeling of the reactive aldehyde between glutamyl-tRNA reductase and the aminomutase is outlined.

*Author for correspondence, email: d.jahn@tu-bs.de

Bernhard Grimm, Robert J. Porra, Wolfhart Rüdiger and Hugo Scheer (eds): Chlorophylls and Bacteriochlorophylls: Biochemistry, Biophysics, Functions and Applications, pp. 159–171.

I. Two Pathways for 5-Aminolevulinic Acid Biosynthesis

Tetrapyrroles, such as hemes, chlorophylls, vitamin B_{12} and coenzyme F_{430} are widely distributed among all living organisms. The common precursor of all tetrapyrroles, 5-aminolevulinic acid (ALA), may be synthesized by two alternative, unrelated biosynthetic routes: in mammals, fungi and the α-group of the proteobacteria, condensation of succinyl coenzyme A and glycine is catalyzed by 5-aminolevulinic acid synthase to form ALA by the so-called 'Shemin pathway' (Shemin and Russel, 1953; Gibson et al., 1958; Kikuchi et al., 1958). The alternative C_5-pathway found in plants, archaea and most bacteria, incorporates the C_5-skeleton of glutamate (Beale and Castelfranco, 1973; Jahn et al., 1992) and involves the reduction of glutamyl-tRNA to glutamate-1-semialdehyde (GSA) catalyzed by NADPH-dependent glutamyl-tRNA reductase (GluTR) (Jahn et al., 1992; Vothknecht et al., 1996). In a following reaction pyridoxamine 5′-phosphate (PMP)-dependent glutamate-1-semialdehyde-2,1-aminomutase (GSAM) transaminates GSA to form ALA (Grimm et al., 1992; Ilag and Jahn, 1992; Smith et al., 1992; Chapter 11, Beale). This chapter focuses on the structure and function of the enzymes of the C_5-pathway. A detailed description of 5-aminolevulinic acid synthase function has previously been published (Ferreira and Gong, 1995; Chapter 11, Beale).

II. Glutamyl-tRNA Synthetase Forms Glutamyl-tRNA for Protein and Tetrapyrrole Biosynthesis

The precursor of the C_5 pathway for ALA formation is glutamate which is converted by glutamyl-tRNA synthetase (GluRS) to glutamyl-tRNA (Huang et al., 1984; Schön et al., 1986). Glutamyl-tRNA simultaneously participates in protein and tetrapyrrole biosynthesis (O'Neil and Söll, 1990; Jahn et al., 1992). The properties of GluRS and its substrate, $tRNA^{Glu}$, are discussed below only with relevance to ALA biosynthesis.

Abbreviations: ALA – 5-aminolevulinic acid; *C.* – *Chlamydomonas*; DAVA – diaminovalerate; *E.* – *Escherichia*; GluRS – glutamyl-tRNA synthetase; GluTR – glutamyl-tRNA reductase; GSA – glutamate-1-semialdehyde; GSAM – glutamate-1-semialdehyde-2,1-aminomutase; *M.* – *Methanopyrus*; PLP – pyridoxal 5′-phosphate; PMP – pyridoxamine 5′-phosphate; *S.* – *Salmonella*

III. Glutamyl-tRNA

Investigation of barley chloroplast, *Chlamydomonas* (*C.*) *reinhardtii* and *Chlorella* extracts first indicated that a tRNA molecule could be essential for the synthesis of ALA from glutamate (Huang et al., 1984; Kannangara et al., 1984; Weinstein and Beale, 1985). Sequence analysis of the active tRNA species in barley and *C. reinhardtii* confirmed that a $tRNA^{Glu}$ is involved (Schön et al., 1986; O′Neill and Söll, 1990; Chapter 11, Beale). A variety of in vitro and in vivo approaches established the identity elements of *Escherichia* (*E.*) *coli* $tRNA^{Glu}$ for recognition by GluRS (Fig. 1a). The identity set consists of U34, U35, C36 and A37 in the anticodon loop, G1:C72, U2:A71 and C4:G69 in the acceptor stem, U11:A24, U13:G22::A46 and C12:G23::C9 in the augmented D helix formed of the D-stem helix with several neighboring residues and the variable loop (N:N and N::N denote secondary and tertiary nucleotide base pairings). In addition, A46 and the absence of nucleotide 47 (D47) in the short variable loop were found to stabilize U13:G22::A46, a tertiary base pairing which is essential for tRNA-GluRS interaction (Sekine et al., 1996, 1999). The relevance to recognition of the 2-thio groups, in methylaminomethyl-2-thiouridine (mnm5s2U) in the wobble position U34, by *E. coli* GluRS in vitro was challenged by in vivo experiments with hypomodified $tRNA^{Glu}$ (Sylvers et al., 1993; Kruger and Sorensen, 1998; Madore et al., 1999).

In contrast to the detailed analysis of $tRNA^{Glu}$ for GluRS recognition, the identity elements of glutamyl-tRNA for GluTR were mainly subject to theoretical considerations (Jahn et al., 1991; Willows et al., 1995). The isolation of an *Euglena gracilis* plastidic $tRNA^{Glu}$ gene mutant, impaired in chlorophyll biosynthesis but capable of protein biosynthesis, revealed the only verified glutamyl-tRNA identity element in position C56 (Stange-Thomann et al., 1994).

IV. Glutamyl-tRNA Synthetase

GluRS (glutamyl-tRNA synthetase or glutamic acid $tRNA^{Glu}$ ligase, EC 6.1.1.17) esterifies glutamate with the 2′-terminal hydroxy group of tRNA which is specific for this amino acid. A two step mechanism including the activation of the amino acid by ATP and its subsequent transfer to the tRNA is generally accepted (Freist et al., 1997) (Fig. 2a):

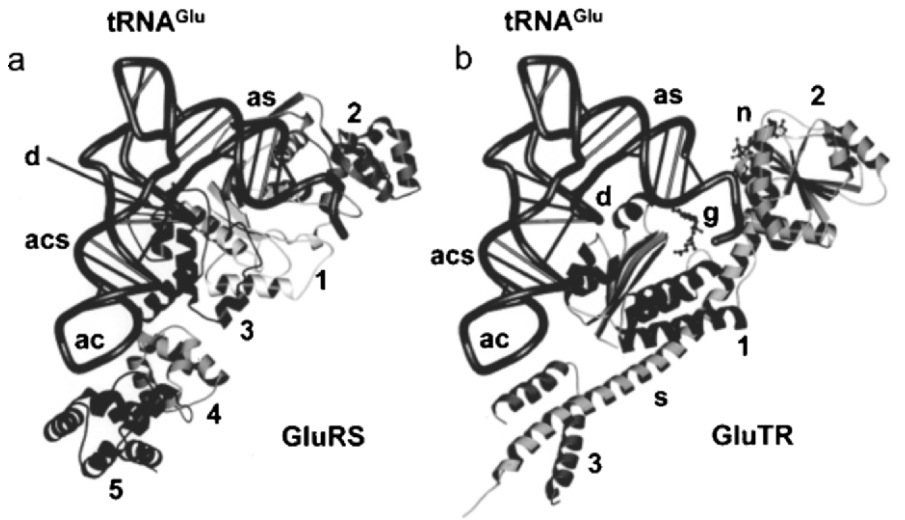

Fig. 1. A ribbon diagram of the complexes of (a) $tRNA^{Glu}$/glutamyl-tRNA synthetase (b) $tRNA^{Glu}$/glutamyl-tRNA reductase monomer (modeled). The complexes have been oriented to provide the equivalent view of the $tRNA^{Glu}$. Individual domains are numbered. as – acceptor stem of $tRNA^{Glu}$, ac – anticodon, acs – anticodon stem, d – D-stem, g - Glutamycin, n – NADPH (modeled), s – spinal helix. Note the similarity in binding modes in both proteins. Generated using *MOLSCRIPT* (Kraulis, 1991) rendered with *POVRAY* (www.povray.org) as implemented in *GL_RENDER* (www.hhmi.swmed.edu/external/Doc/Gl_render).

$$\text{GluRS} + \text{Glu} + \text{ATP} (+ \text{tRNA}^{Glu}) \rightarrow \text{GluRS} + \text{Glu-AMP} + \text{PP}_i (+ \text{tRNA}^{Glu}) \quad (1)$$

$$\text{GluRS} + \text{Glu-AMP} + \text{tRNA}^{Glu} \rightarrow \text{GluRS} + \text{Glu-tRNA}^{Glu} + \text{AMP} \quad (2)$$

GluRS is one of ten class I aminoacyl-tRNA synthetases: its ATP-binding domain bears a variant (HVGG) of the characteristic HIGH motif (Cusack et al., 1990; Eriani et al., 1990). Evolutionarily and sequence-wise, GluRS is closely related to glutaminyl-tRNA synthetase (Breton et al., 1986). Many bacteria, archaea and organelles lack glutaminyl-tRNA synthetase. Here GluRS glutamylates both $tRNA^{Glu}$ and $tRNA^{Gln}$. The misacylated Glu-$tRNA^{Gln}$ is converted to the required Gln-$tRNA^{Gln}$ (glutaminyl-tRNA) by an amidotransferase (Schön et al., 1988; Jahn et al., 1990; Curnow et al., 1997; Tumbula et al., 2000).

A. Biochemical Characterization

The copy number of GluRS molecules per *E. coli* cell is between 300 and 900 depending on the growth medium (Pedersen et al., 1978). The molecular ratio of GluRS to ribosomes and elongation factors is roughly balanced at different growth conditions. Bacterial and green algal enzymes were found to be active as monomers with a M_r of ~50,000 (Freist et al., 1997). In *E. coli* and *Bacillus subtilis,* GluRS forms a complex with adenylosuccinate AMP-lyase (EC 4.3.2.2.). This protects GluRS against heat denaturation, increases its affinity for glutamate and ATP (Lapointe and Söll, 1972; Proulx et al., 1983; Gendron et al., 1992) and coordinates purine metabolism and protein biosynthesis. Chloroplast, mitochondrial and the cytoplasmic wheat GluRS are dimeric (Ratinaud et al., 1983). The K_m of GluRS is in the range of 10^{-4} and 10^{-5} M for ATP, about 10^{-5} M for glutamate and 10^{-7} M for $tRNA^{Glu}$ (Freist et al., 1997). In common with other aminoacyl-tRNA synthetases, GluRS activity is Mg^{2+}-dependent. *E. coli* GluRS enzyme activity is also Zn^{2+}-dependent (Liu et al., 1993). Extended X-ray absorption fine structure (EXAFS) studies identified a non-planar coordination site involving three sulfur atoms and one nitrogen (Cys98, 100, 125, His127). ATP inhibits zinc removal, suggesting that the binding site is near the active site. Analogous studies indicate that ATP-recognition involves the adenine base, two hydroxyl groups of the ribose moiety and the phosphate chain. Only bacterial and plastidic enzymes provide appropriate precursor for tetrapyrrole biosynthesis.

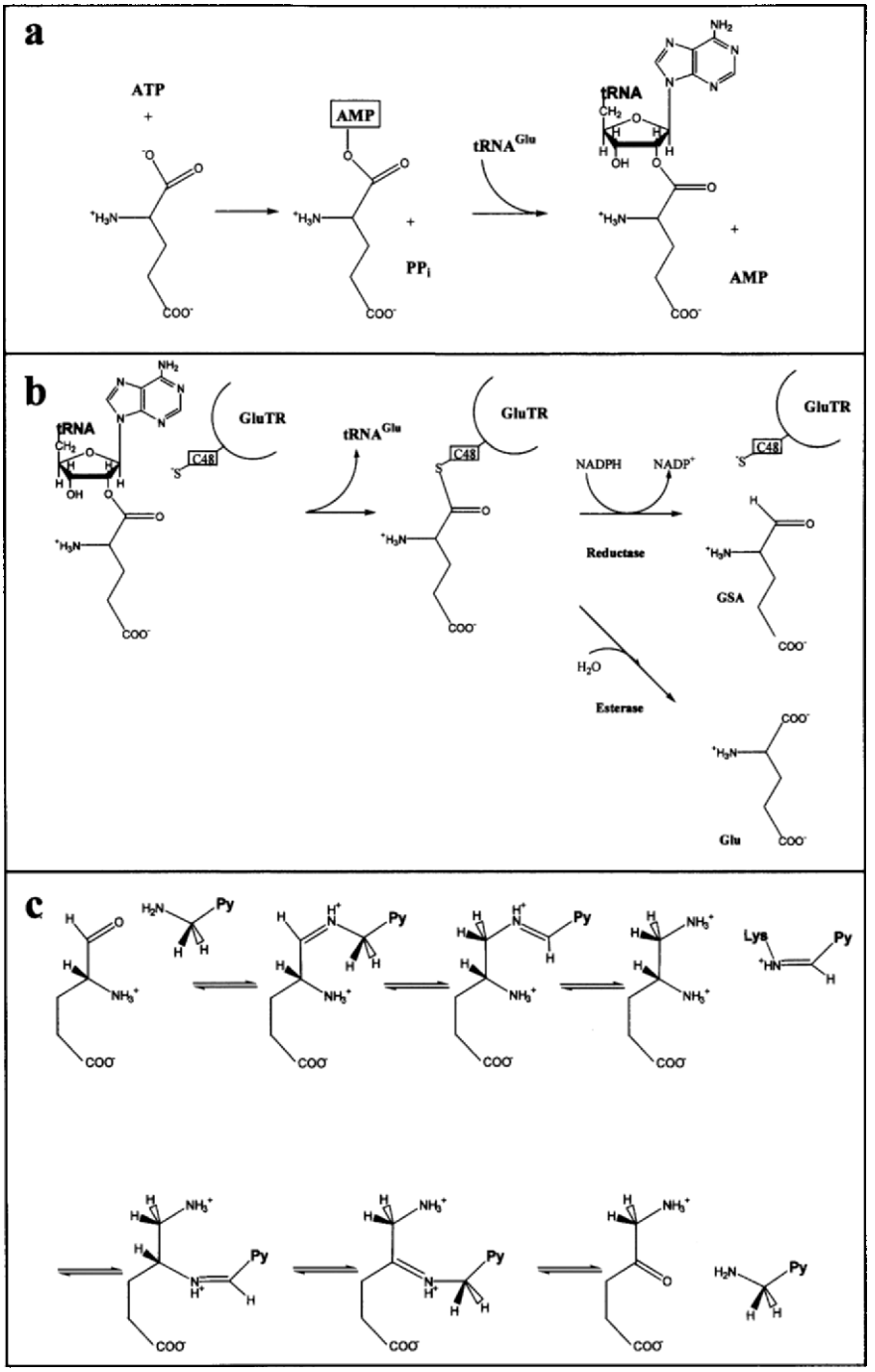

Fig. 2. The chemical reactions catalyzed by a) glutamyl-tRNA synthetase (GluRS), b) glutamyl-tRNA reductase (GluTR) and c) glutamate-1-semialdehyde-2,1-aminomutaseamino (GSAM). a) GluRS specifically binds ATP and glutamate, allowing the amino acid carboxyl oxygen of glutamate to displace pyrophosphate from ATP. In a second step the 2′-OH of glutamyl-tRNA attacks the carbonyl carbon of glutamate-AMP displacing AMP and generating glutamyl-tRNA^{Glu}. b) The thiol group of the catalytic cysteine 48 of GluTR initiates a nucleophilic attack at the tRNA-bound carbonyl carbon of glutamyl-tRNA, covalently binding glutamate to the enzyme and displacing glutamyl-tRNA. In a second step hydride transfer from NADPH releases glutamate-1-semialdehyde (GSA) from GluTR, restoring the latter. In the absence of NADPH, GluTR functions as an esterase, transferring a hydroxyl group from water, producing glutamate. c) GSA from GluTR is transferred to GSAM. Here the pyridoxamine-5-phosphate (PMP) binds the aldehyde of GSA forming an aldimine. Proton transfer and Schiff's base formation producing 5-pyridoxyl phosphate form of GSAM, releases the intermediate 4,5-diaminovalerate (DAVA). Aldimine formation at the former amino group of GSA, proton transfer and release of PMP produces the final 5-aminolevulinic acid (ALA).

B. Crystal Structure

The crystal structure of GluRS from the extreme thermophile *Thermus thermophilus* has been solved for both the uncomplexed protein (Nureki et al., 1995) and in complex with $tRNA^{Glu}$ (Sekine et al., 2001b). The monomeric enzyme (468 residues) consists of five distinct domains arranged to form an elongated, slightly curved molecule (Fig. 1a). Domain 1, a Rossmann ATP-binding fold, is conserved in all class-I tRNA synthetases. It bears the two characteristic ATP-binding motifs, HIGH (HVGG here) and KMSKS. Adjacent regions of domains 2 and 3 are also structurally conserved. Located on either side of the ATP-binding pocket of domain 1, they create a conspicuous groove that accommodates the tRNA acceptor arm. The remaining conserved α-helices of domain 3 interact with both the D-stem region at the concave elbow angle of the tRNA as well as the anticodon stem. The binding mode of the tRNA in class I tRNA synthetase complexes is thus conserved. Regions unique to each synthetase allow for specificity. Such regions of domains 2 and 3 create the glutamate recognition pocket. Domains 4 and 5, structurally unique to GluRS in their entirety, are reserved for $tRNA^{Glu}$-anticodon recognition and discrimination. Arginine residues are crucial for anticodon recognition in GluRS. Arg417 and Arg435, respectively, bind the phosphate and base of C34 while Arg358 hydrogen bonds C36 in a Watson-Crick-like pattern. Only U35 is recognized by a planar main-chain segment (Thr444-O and Pro445-N).

V. Glutamyl-tRNA Reductase

The discovery that $tRNA^{Glu}$ is involved in the biosynthesis of ALA prompted the formulation of the three-step-pathway: In the first step, glutamate is activated by ligation to the cofactor $tRNA^{Glu}$. Then tRNA-bound glutamate is reduced to GSA. Finally in the third step GSA is transaminated to ALA (Huang et al., 1984; Kannangara et al., 1984; Weinstein and Beale, 1985; Schön et al., 1986). The enzyme catalyzing the first committed step of tetrapyrrole formation is glutamyl-tRNA reductase (GluTR), the second enzyme is glutamate-1-semialdehyde-2,1-aminomutase (GSAM).

A. Biochemical Characterization

Early investigations of bacterial and plant GluTRs resulted in controversy regarding cofactor requirements, relative molecular masses and potential catalytic mechanisms (Chapter 11, Beale). In retrospect, the extended structure of GluTR (Moser et al., 1999, 2001), solubility problems due to unspecific disulfide bridge formation and hydrophobic interaction (Schauer et al., 2002) may partly explain these discrepancies.

A combined biochemical and crystallographic approach using recombinant GluTR from the extreme thermophilic archaeon *Methanopyrus* (*M.*) *kandleri* finally established the catalytic mechanism and its structural basis (Moser et al., 1999, 2001). The gene *hemA* encoding GluTR from *M. kandleri* was expressed in *E. coli*. The recombinant enzyme was purified to homogeneity. Using *E. coli* glutamyl-tRNA as substrate, the specific activity was determined to be 0.75 nmol h^{-1} mg^{-1} at 56 °C. Intensive spectroscopic and biochemical analysis of *M. kandleri* GluTR demonstrated that neither heme, flavins nor metal ions are required for catalysis. Reduction and inhibition ability of NADPH analogues were investigated. NADH, lacking the 2′-phosphoryl group, does not substitute for NADPH nor does it inhibit *M. kandleri* GluTR. Reduced β-nicotinamide mononucleotide corresponding to removal of the adenosine phosphate moiety does, by contrast, inhibit NADPH-binding. Removing the adenine amino group (reduced nicotinamide hypoxanthine dinucleotide phosphate) similarly inhibits GluTR. Interestingly, both 2′-NADPH and 3′-NADPH are equally active. Thus, all the major determinants of NADPH are required for efficient recognition and utilization by GluTR. Recently, soluble *E. coli* GluTR was expressed and purified through co-expression with chaperones. Most biochemical characteristics of *M. kandleri* GluTR could be confirmed for the enzyme from *E. coli*. A major difference is a requirement of Mg^{2+} for enzymatic activity in *E. coli* GluTR (Schauer et al., 2002).

The ester bond linking the 2′ end of $tRNA^{Glu}$ and glutamate is by necessity labile. To generate a stable substrate analogue representing the last adenosine residue of the tRNA the bridging O was replaced by N. This analogue was synthesized from the structurally related puromycin aminonucleoside and named glutamycin. *M. kandleri and E. coli* GluTR are competitively inhibited by glutamycin (Moser et al., 1999; Schauer et al., 2002). Other *E. coli* GluTR inhibitors were identified by a cell-based, high-throughput screening method but not further characterized (Loida et al., 1999).

The expression of the gene for GluTR, *hemA,* was intensively studied in *E. coli*, *Salmonella* (*S.*) *typhimurium* and *Pseudomonas aeruginosa*. The level of transcriptional regulation is low and influenced by oxygen tension, cellular heme concentration and the presence of alternative electron acceptors for anaerobic growth like nitrate (Darie and Gunsalus, 1994; Hungerer et al., 1995; Choi et al., 1996; McNicholas et al., 1997; Verderber et al., 1997; Krieger et al., 2002; Schobert and Jahn, 2002). Changes in cellular GluTR concentration were explained by heme-induced proteolytic degradation of the enzyme (Wang et al., 1997; Wang et al., 1999a). The N-terminal region of *S. typhimurium* GluTR was found to bind heme causing structural re-arrangements and leading to proteolytic turnover (Wang et al., 1999b).

B. Enzyme Mechanism

Treatment of GluTR from *M. kandleri* and *E. coli* with iodoacetamide or 5,5´-dithiobis(2-nitrobenzoic acid) abolishes enzyme activity implicating a nucleophilic cysteine in catalysis. All cysteines of both GluTRs were individually replaced by serines. Mutants Cys48Ser (*M. kandleri*) and Cys50Ser (*E. coli*) were completely inactive confirming that these cysteines are the active site nucleophiles. In fact, these residues correspond to the only cysteine conserved in all GluTRs. Surprisingly, both enzymes efficiently turn over glutamyl-tRNA in the absence of NADPH liberating glutamate. The rate of this GluTR-dependent glutamyl-tRNA esterase activity is comparable to GluTR reductase activity in the presence of NADPH. Similar esterase activity is also observed for other enzymes such as glycerinaldehyde-phosphate dehydrogenase, thiol proteinases and aldehyde dehydrogenases that form a covalent acyl-enzyme intermediate involving an active site cysteinyl residue. GluTR mutants Cys48Ser and Cys50Ser, correspondingly, did not possess any esterase activity. A catalytic mechanism for GluTR was proposed whereby the sulfhydryl group of Cys-48 (Cys-50 in *E. coli*) nucleophilically attacks the α-carbonyl group of tRNA-bound glutamate forming an enzyme-bound thioester intermediate with the concomitant release of $tRNA^{Glu}$ (Fig. 2b). This reaction intermediate was isolated and visualized for *E. coli* GluTR. Finally, hydride transfer from NADPH to the thioester-bound glutamate produces GSA. In the absence of NADPH, a water molecule takes its place, hydrolyzing the reactive thioester bond and releasing glutamate (Moser et al., 1999, 2001, Schauer et al., 2002).

C. Crystal Structure

Instead of the anticipated protein tetramer, the crystal structure of *M. kandleri* GluTR revealed an extended V-shaped dimer (Moser et al., 2001) (Fig. 3). Each monomer consists of three distinct domains arranged along an extended curved 'spinal' α-helix. The first, N-terminal domain consists of two subdomains: a small βαββααβ and a larger, three α-helix subdomain. These three helices roughly align with the spinal helix to form a 4-helix bundle. A short loop links domain 1 to domain 2, a classical NAD(P)H-binding fold (Carugo and Argos, 1997). This domain is followed by the 110-Å spinal helix of 18 α-helical turns. N-terminally, the spinal helix reinforces the loop between domain 1 and 2, then passes domain 1, and C-terminally extends into, and forms part of the dimerization domain. This domain 3 is composed of a symmetric six-helix bundle, three helices deriving from each of two interacting monomers.

D. Structural Basis of Catalysis

The crystal structure of GluTR was solved in a complex with glutamycin (Moser et al., 2001). The inhibitor binds within a deep pocket at the interface of the subdomains of domain 1 and is specifically recognized by an array of strictly conserved amino acids (Figs. 1b, 3, 4). A bidentate salt-bridge, between the carboxylate group of glutamycin and Arg50 at the bottom of the pocket, represents the most discriminating interaction. This resembles the carboxylate recognition mode of aspartyl-tRNA synthetase (Eiler et al., 1999) and presumably of glutamyl-tRNA synthetases (Sekine et al., 2001a). Further, the enzyme specifically recognizes the α-amino group and less specifically the ribose moiety of the inhibitor. The structure of the enzyme-inhibitor complex supports the proposed catalytic mechanism for the enzyme (Moser et al., 1999) (Figs. 3, 4). Cys48 is particularly sensitive to oxidation. To obtain crystals of GluTR it had to be replaced by serine resulting in an inactive enzyme (Moser et al., 1999). In the crystal structure, Ser48 (Cys48) is located at the edge of the glutamate-binding pocket and its hydroxyl (sulfhydryl) group is in close proximity to the α-carbonyl carbon atom of glutamycin, ready to nucleophilically attack the activated α-carboxylate of glutamyl-tRNA. This would result in the expected covalent thioacyl intermediate and the release of $tRNA^{Glu}$. In a second step, the thioacyl intermediate would be reduced to the product GSA by hydride transfer form NADPH. Although the

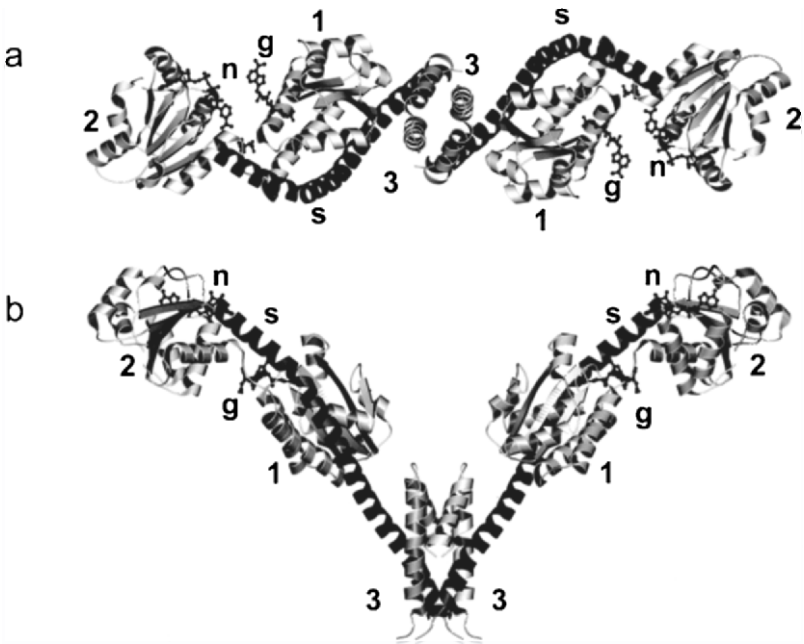

Fig. 3. A schematic diagram of the *Methanopyrus kandleri* GluTR dimer viewed (a) perpendicular to and (b) along the two-fold-axis. GluTR is composed of a catalytic domain (1), an NADPH-binding domain (2) and a dimerization domain (3) linked by a 'spinal' α-helix (s). Glutamycin (black) is recognized by the catalytic domain. Abbreviations and software as in Fig. 1, except rendering by *RASTER3D* (Merritt and Murphy, 1994).

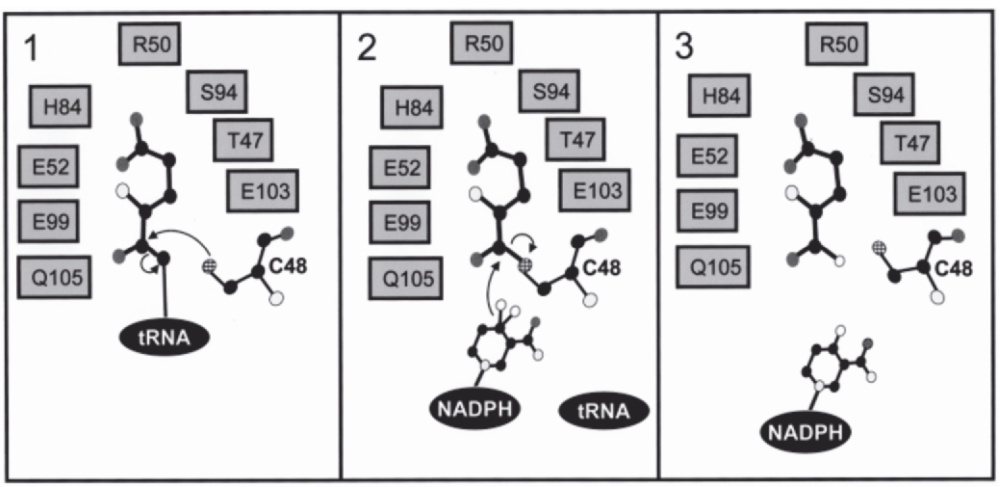

Fig. 4. Catalytic mechanism of GluTR. Conserved residues responsible for specific substrate recognition through an intricate hydrogen-bonding network are indicated. The reactive cysteine residue nucleophilically attacks the aminoacyl bond of glutamyl-tRNA (1). An enzyme-localized thioester intermediate is formed with the release of free $tRNA^{Glu}$ (2). The thioester is reduced by hydride transfer from NADPH leading to GSA (3).

canonical NADPH-binding site in domain 2 is not occupied in the crystal structure, a reliable position for NADPH may be inferred from structurally related NAD(P)H-binding domains. The resulting distance between the nicotinamide moiety and the glutamate-binding pocket of 21 Å indicates that domain 2 must rotate around the end of the spinal helix to close the active site and to place NADPH near the thioacyl-

bound glutamate for hydride transfer to occur. The present open structure of GluTR may, therefore, be described as a 'pre-active' state. To what extent the individual steps (binding of glutamyl-tRNA, tipping of domain 2, opening of the NADPH binding pocket and NADPH-binding) occur in concert or consecutively is presently not clear.

The glutamate-binding pocket of GluTR clearly establishes the location of the 3´-terminal nucleotide of the glutamyl-tRNA. Placing the acceptor arm of the glutamyl-tRNA from the GluRS/glutamyl-tRNA complex from *E. coli* (Sekine et al., 2001b) near the catalytic domain, indicates that the concave elbow region of the tRNA is somewhat complementary to the external surface of the catalytic domain. The glutamyl-tRNA may thus be moved immediately adjacent to the GluTR, placing the acceptor arm into the cleft between the catalytic and the NADPH-binding domains (Fig. 1b). The elbow region of the tRNA and, in particular, the D-stem would interact with the catalytic domain, while the anticodon-region could interact with the α-helical, dimerization domain. Overall, this hypothetical model reveals a large degree of surface complementarity between tRNA and GluTR and, surprisingly, the regions of the tRNA interacting with the reductase are similar to those of the GluRS-tRNA complex: The acceptor arm lies within a large furrow between domains 1 and 2, allowing a multitude of specific interactions. The elbow region and the anticodon stem interact with domain 2 (domain 3 in GluRS). The anticodon itself appears to interact with domain 3, possibly allowing its specific recognition. Interestingly, in both GluRS and GluTR, the (proposed) anticodon-recognition region contains a high number of arginines, though not recognizably conserved. For GluRS, the tRNA complex was required to finally establish which arginines are responsible for anticodon recognition (Sekine et al., 2001b).

VI. Glutamate-1-Semialdehyde-2,1-Aminomutase

The synthesis of ALA from glutamyl-tRNA requires the exchange of amino and aldehyde groups between carbon 1 and 2 of GSA. This reaction is catalyzed by GSAM, EC 5.4.3.8 (Kannangara et al., 1984; Hoober et al., 1988; Jahn et al., 1992). The reaction differs from a classical aminotransferase reaction by its intramolecular nature. Nevertheless, GSAM represents a typical aminotransferase in structure and catalysis (Mehta and Christen, 1994).

A. Biochemical Features

In principle two catalytic routes of GSAM are possible: Starting with the pyridoxal 5´-phosphate (PLP) form of GSAM results in the formation of dioxovalerate, while the PMP form would lead to a diaminovalerate (DAVA) intermediate. Recombinant GSAM from *E. coli*, *Synechococcus* sp. and other sources was found to catalyze both reactions (Smith et al., 1991a; Ilag and Jahn, 1992). However, kinetic investigations of *Synechococcus* sp. and pea GSAM eventually identified diaminovalerate as the true intermediate (Smith et al., 1991b; Friedmann et al., 1992; Pugh et al., 1992). The active site lysine responsible for Schiff´s base formation with PMP was identified for various GSAMs (Grimm et al., 1992; Ilag and Jahn, 1992). The half-reactions of the PMP-dependent amino transfer are outlined in Fig. 2c. Spectroscopic analyses, including stop flow experiments, identified the reaction intermediates (Ilag and Jahn, 1992; Smith and Grimm, 1992; Brody et al., 1995; Smith et al., 1998). GSAM catalyzes an anomalous enantiomeric reaction discriminating between (S)-GSA and (R)-GSA. Interestingly, (R)-GSA is a substrate for the first half-reaction but the resulting (R)-DAVA is either inactive or a poor substrate for the second half-reaction (Friedmann et al., 1992; Smith et al., 1992). GSAMs are inhibited by gabaculine, an inhibitor of γ-aminobutyric acid aminotransferase and other aminotransferases (Hill et al., 1985; Hoober et al., 1988). Other inhibitors, 4-aminohex-5-ynoate, 4-aminohex-5-enoate and enantiomers of diaminopropyl sulfate have been developed (Tyacke et al., 1995; Contestabile et al., 2000).

B. Crystal Structure

GSAM is a member of an extensive family of structurally related, PLP-dependent proteins that include aminotransferases, racemases, decarboxylases, synthetases and mutases. GSAM shares the prototype aspartate aminotransferase fold and is structurally particularly similar to dialkylglycine decarboxylase and 4-aminobutyrate aminotransferase. Mechanistically GSAM differs from aminotransferases in that it exchanges amino and oxo groups in GSA without the need for additional cofactors other than PMP. It

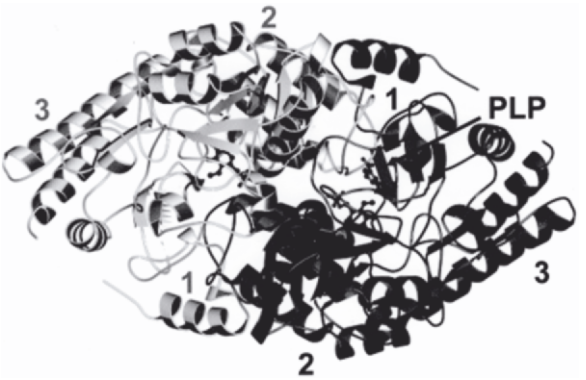

Fig. 5. Ribbon diagram of dimeric glutamate-semialdehyde-2,1-aminomutase (Hennig et al., 1997). One monomer is depicted in white the second in gray. Cofactors (PMP) and inhibitor (gabaculine) are shown as black ball and stick representations.

is a dimeric protein with an overall ellipsoidal shape when viewed along the dimer axis (Fig. 5, Hennig et al., 1997). The monomers interact through a large, convoluted interface. Morphologically distinct domains are not apparent. Instead, three domains may be rationalized based on three β-sheets: A three-stranded, antiparallel β-sheet in domain 1, a seven-stranded, parallel β-sheet (one strand is antiparallel) in domain 2 and a four-stranded, antiparallel β-sheet in domain 3. All domains, as well as interdomain connections, additionally include α-helices and long loops of low secondary structure content. Both cofactor and substrate are bound at the monomer-monomer interface. Domain 2 of one monomer accommodates the PLP/PMP head group, while the phosphate is additionally coordinated by a loop from domain 2 of the second monomer. Loops from all three domains participate in lining the substrate pocket. In the crystal structure, the GSAM dimer is observed to be imperfectly symmetrical. A loop consisting of residues 159–172 and laterally covering the substrate pocket is partly disordered in one monomer, while it is well structured in the second. This loop is essential for proper enzyme function (Contestabile et al., 2000). Presumably, GSAM oscillates between the two conformational states in which one monomer is in the closed, active state (with ordered active-site lid), while the second is in a relaxed state, allowing product and substrate to diffuse out of and in to the active site, respectively.

VII. Metabolic Channeling of Glutamate-1-Semialdehyde

The tRNA-dependent formation of ALA found in plants and most bacteria requires the concerted action of the two enzymes GluTR and GSAM. Metabolically they are linked by the aldehyde GSA. The chemical reactivity of GSA in the cellular medium means that an indirect transfer of the aldehyde from GluTR to GSAM is not probable, as formation of ALA would not be efficient. The three-dimensional shape of both GluTR and GSAM suggests an attractive solution to this metabolic problem. Placing the GSAM dimer from *Synechococcus* sp. (Hennig et al., 1997) alongside the extended and similarly dimeric GluTR, immediately, suggests that the open space delineated by the GluTR monomers could comfortably accommodate GSAM. The resulting model complex (Fig. 6 and Color Plate 1) displays a striking degree of surface complementarity between both enzymes. The most striking result of the proposed GluTR/GSAM complex is that the putative active site entrance of each GSAM monomer (Hennig et al., 1997) is positioned opposite a depression in domain 1 of GluTR. This depression and the glutamate recognition pocket are separated only by Arg50 and guarded by the conserved His84. The proposed complex may thus indicate that the GluTR-product GSA leaves the enzyme via this ‘back door‘ of the glutamate recognition pocket and is directly channeled into the active site of GSAM, a distance of about 26 Å, without exposure to the aqueous environment.

Both $tRNA^{Glu}$ (see above) and GSAM can, thus, be independently docked onto GluTR, each in a single plausible position. Though separately docked, the model of the ternary complex of GluTR, $tRNA^{Glu}$ and GSAM does not lead to steric clashes between GSAM and $tRNA^{Glu}$; instead, GSAM could laterally extend the interaction surface of GluTR for the tRNA.

VIII. Concluding Remarks

Recent decades, and especially the last few years, have witnessed the addition of significant detail to our picture of the tRNA-dependent ALA biosynthesis for tetrapyrrole formation in plants, archaea and most bacteria. The central biological functions of chlorophylls, hemes, vitamin B_{12} and other tetrapyrroles underscore the need for an efficient, robust system to reliably and continuously provide large

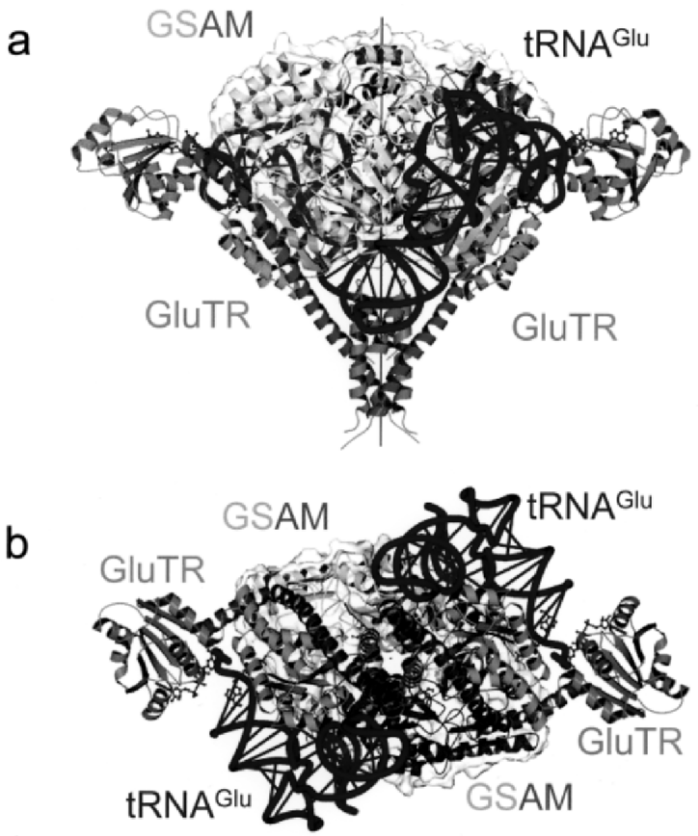

Fig. 6. The proposed ternary complex of GluTR/tRNA^{Glu}/GSAM viewed (a) perpendicular to the common two-fold axis and (b) along this axis from the dimerization domain of GluTR (opposite direction to Fig. 3a). The ribbon depiction of V-shaped GluTR is rendered in shades of gray. tRNA^{Glu} is represented as a backbone model (black), while GSAM is shown by a transparent surface covering a light-gray and white ribbon diagram. (Produced as Fig. 1 with the addition of *GRASP* (Nicholls et al., 1991). See also Color Plate 1.

amounts of this vital intermediate. Understanding the mechanisms involved and their regulation may help us to appreciate the underlying intricacies and adapt this knowledge to our specific needs in such fields as food production, vitamin synthesis, antibiotics and herbicide development.

Acknowledgments

Financial support was granted by the Deutsche Forschungsgemeinschaft and Fonds der Chemischen Industrie.

References

Beale SI and Castelfranco PA (1973) ^{14}C incorporation from exogenous compounds into δ-aminolevulinic acid by greening cucumber cotyledons. Biochem Biophys Res Commun 52: 143–149

Breton R, Sanfacon H, Papayannopoulos I, Biemann K and Lapointe J (1986) Glutamyl-tRNA synthetase of *Escherichia coli*. Isolation and primary structure of the *gltX* gene and homology with other aminoacyl-tRNA synthetases. J Biol Chem 261: 10610–10617

Brody S, Andersen JS, Kannangara CG, Meldgaard M, Roepstorff P and von Wettstein D (1995) Characterization of the different spectral forms of glutamate 1-semialdehyde aminotransferase by mass spectrometry. Biochemistry 34: 15918–15924

Carugo O and Argos P (1997) NADP-dependent enzymes. I: Conserved stereochemistry of cofactor binding. Proteins Struct Genet 28: 10–28

Choi P, Wang L, Archer CD and Elliott T (1996) Transcription of the glutamyl-tRNA reductase (*hemA*) gene in *Salmonella typhimurium* and *Escherichia coli*: Role of the *hemA* P1 promoter and the *arcA* gene product. J Bacteriol 178: 638–646

Contestabile R, Angelaccio S, Maytum R, Bossa F and John RA (2000) The contribution of a conformationally mobile, active site loop to the reaction catalyzed by glutamate semialdehyde

aminomutase. J Biol Chem 275: 3879–3886
Curnow AW, Hong K, Yuan R, Kim S, Martins O, Winkler W, Henkin TM and Söll D (1997) Glu-tRNA^{Gln} amidotransferase: A novel heterotrimeric enzyme required for correct decoding of glutamine codons during translation. Proc Natl Acad Sci USA 94: 11819–11826
Cusack S, Berthet-Colominas C, Hartlein M, Nassar N and Leberman R (1990) A second class of synthetase structure revealed by X-ray analysis of *Escherichia coli* seryl-tRNA synthetase at 2.5 Å. Nature 347: 249–255
Darie S and Gunsalus RP (1994) Effect of heme and oxygen availability on *hemA* gene expression in *Escherichia coli*: Role of the *fnr*, *arcA*, and *hemA* gene products. J Bacteriol 176: 5270–5276
Eiler S, Dock-Bregeon A, Moulinier L, Thierry JC and Moras D (1999) Synthesis of aspartyl-tRNA(Asp) in *Escherichia coli* — a snapshot of the second step. EMBO J 18: 6532–6541
Eriani G, Delarue M, Poch O, Gangloff J and Moras D (1990) Partition of tRNA synthetases into two classes based on mutually exclusive sets of sequence motifs. Nature 347: 203–206
Ferreira GC and Gong J (1995) 5-Aminolevulinate synthase and the first step of heme biosynthesis. J Bioenerg Biomembr 27: 151–159
Freist W, Gauss DH, Söll D and Lapointe J (1997) Glutamyl-tRNA synthetase. Biol Chem 378: 1313–1329
Friedmann HC, Duban ME, Valasinas A and Frydman B (1992) The enantioselective participation of (S)- and (R)-diaminovaleric acids in the formation of delta-aminolevulinic acid in cyanobacteria. Biochem Biophys Res Commun 185: 60–68
Gendron N, Breton R, Champagne N and Lapointe J (1992) Adenylosuccinate lyase of *Bacillus subtilis* regulates the activity of the glutamyl-tRNA synthetase Proc Natl Acad Sci U S A 89: 5389–5392
Gibson KD, Laver WG and Neuberger A (1958) Initial stages in the biosynthesis of porphyrins. The formation of δ-aminolevulinic acid from glycine and succinyl-coenzyme A by particles from chicken erythrocytes. Biochem J 70: 71–81
Grimm B, Smith MA and von Wettstein D (1992) The role of Lys272 in the pyridoxal 5-phosphate active site of *Synechococcus* glutamate-1-semialdehyde aminotransferase. Eur J Biochem 206: 579–585
Hennig M, Grimm B, Contestabile R, John RA and Jansonius JN (1997) Crystal structure of glutamate-1-semialdehyde aminomutase: An α_2-dimeric vitamin B_6-dependent enzyme with asymmetry in structure and active site reactivity. Proc Natl Acad Sci USA 94: 4866-4871
Hill CM, Pearson SA, Smith AJ, and Rogers LJ (1985) Inhibition of chlorophyll synthesis in *Hordeum vulgare* by 3-amino 2,3-dihydrobenzoic acid (gabaculin). Biosci Rep 5: 775–781
Hoober JK, Kahn A, Ash DE, Gough S and Kannangara CG (1988) Biosynthesis of delta-aminolevulinate in greening barley leaves. IX. Structure of the substrate, mode of gabaculine inhibition, and the catalytic mechanism of glutamate 1-semialdehyde aminotransferase. Carlsberg Res Commun 53: 11–25
Huang DD, Wang WY, Gough SP and Kannangara CG (1984) delta-Aminolevulinic acid-synthesizing enzymes need an RNA moiety for activity. Science 225: 1482–1484
Hungerer C, Troup B, Romling U and Jahn D (1995) Regulation of the *hemA* gene during 5-aminolevulinic acid formation in *Pseudomonas aeruginosa*. J Bacteriol 177:1435-1443
Ilag LL and Jahn D (1992) Activity and spectroscopic properties of the *Escherichia coli* glutamate 1-semialdehyde aminotransferase and the putative active site mutant K265R. Biochemistry 31: 7143–7151
Jahn D, Kim YC, Ishino Y, Chen MW and Söll D (1990) Purification and functional characterization of the Glu-tRNA^{Gln} amidotransferase from *Chlamydomonas reinhardtii*. J Biol Chem 265: 8059–8064
Jahn D, Chen MW and Söll D (1991) Two glutamyl-tRNA reductase activities in *Escherichia coli*. J Biol Chem 266: 161–167
Jahn D, Verkamp E and Söll D (1992) Glutamyl-transfer RNA: A precursor of heme and chlorophyll biosynthesis. Trends Biochem Sci 17: 215–218
Kannangara CG, Gough SP, Oliver RP and Rasmussen SK (1984) Biosynthesis of δ-aminolevulinate in greening barley leaves. VI. Activation of glutamate by ligation to RNA. Carlsberg Res Commun 49: 417–437
Kikuchi G, Kumar A, Talmage P and Shemin D (1958) The enzymatic synthesis of δ-aminolevulinic acid. J Biol Chem 233: 1214–1219
Kraulis PJ (1991) MOLSCRIPT: A program to produce both detailed and schematic plots or protein structures. J Appl Crystallogr 24: 964–950
Krieger R, Rompf A, Schobert M and Jahn D (2002) The *Pseudomonas aeruginosa hemA* promoter is regulated by Anr, Dnr, NarL and Integration Host Factor. Mol Gen Genomics 267: 409–417
Kruger MK and Sorensen MA (1998) Aminoacylation of hypomodified tRNAGlu in vivo. J Mol Biol 284: 609–620
Lapointe J and Söll D (1972) Glutamyl transfer ribonucleic acid synthetase of Escherichia coli. 3. Influence of the 46K protein on the affinity of the 56K glutamyl transfer ribonucleic acid synthetase for its substrates. J Biol Chem 247: 4982–4985
Liu J, Lin SX, Blochet JE, Pezolet M and Lapointe J (1993) The glutamyl-tRNA synthetase of *Escherichia coli* contains one atom of zinc essential for its native conformation and its catalytic activity. Biochemistry 32: 11390–11396
Loida PJ, Thompson RL, Walker DM and CaJacob CA (1999) Novel inhibitors of glutamyl-tRNA^{Glu} reductase identified through cell-based screening of the heme/chlorophyll biosynthetic pathway. Arch Biochem Biophys 372: 230–237
Madore E, Florentz C, Giege R, Sekine S, Yokoyama S and Lapointe J (1999) Effect of modified nucleotides on *Escherichia coli* tRNA^{Glu} structure and on its aminoacylation by glutamyl-tRNA synthetase. Predominant and distinct roles of the mnm5 and s2 modifications of U34. Eur J Biochem 266: 1128–1135
McNicholas PM, Javor G, Darie S and Gunsalus RP (1997) Expression of the heme biosynthetic pathway genes *hemCD*, *hemH*, *hemM*, *and hemA* of *Escherichia coli*. FEMS Microbiol Lett 146: 143–148
Mehta PK and Christen P (1994) Homology of 1-aminocyclopropane-1-carboxylate synthase, 8-amino-7-oxononanoate synthase, 2-amino-6-caprolactam racemase, 2,2-dialkylglycine decarboxylase, glutamate-1-semialdehyde 2,1-aminomutase and isopenicillin-N-epimerase with aminotransferases. Biochem Biophys Res Commun 198: 138–143
Merritt EA and Murphy EP (1994) Raster3D: Photorealistic molecular graphics. Methods Enzymol 277: 505–524

Moser J, Lorenz S, Hubschwerlen C, Rompf A and Jahn D (1999) *Methanopyrus kandleri* glutamyl-tRNA reductase. J Biol Chem 274: 30679–30685

Moser J, Schubert W-D, Beier V, Jahn D and Heinz DW (2001) V-shaped structure of glutamyl-tRNA reductase, the first enzyme of tRNA-dependent tetrapyrrole biosynthesis EMBO J 20: 6583–6590

Nicholls A, Sharp K and Honig B (1991) Protein folding and association: Insights from the interfacial and thermodynamic properties of hydrocarbons. Proteins 11: 281-296

Nureki O, Vassylyev DG, Katayanagi K, Shimizu T, Sekine S, Kigawa T, Miyazawa T, Yokoyama S and Morikawa K (1995) Architectures of class-defining and specific domains of glutamyl-tRNA synthetase. Science 267: 1958–1965

O'Neill GP and Söll D (1990) Expression of the *Synechocystis sp*. strain PCC 6803 $tRNA^{Glu}$ gene provides tRNA for protein and chlorophyll biosynthesis. J Bacteriol 172: 6363–6371

Pedersen S, Bloch PL, Reeh S and Neidhardt FC (1978) Patterns of protein synthesis in *E. coli*: A catalog of the amount of 140 individual proteins at different growth rates. Cell 14: 179–190

Proulx M, Duplain L, Lacoste L, Yaguchi M and Lapointe J (1983) The monomeric glutamyl-tRNA synthetase from *Bacillus subtilis* 168 and its regulatory factor. Their purification, characterization, and the study of their interaction J Biol Chem 258: 753–759

Pugh CE, Harwood JL and John RA (1992) Mechanism of glutamate semialdehyde aminotransferase. Roles of diamino- and dioxo-intermediates in the synthesis of aminolevulinate. J Biol Chem 267: 1584–1588

Ratinaud MH, Thomes JC and Julien R (1983) Glutamyl-tRNA synthetases from wheat. Isolation and characterization of three dimeric enzymes. Eur J Biochem 135: 471–477

Schauer S, Chaturvedi S, Randau L, Moser J, Kitabatake M, Lorenz S, Verkamp E, Schubert WD, Nakayashiki T, Murai M, Wall K, Thomann HU, Heinz DW, Inokuchi H, Söll D and Jahn D (2002) *Escherichia coli* glutamyl-tRNA reductase: Trapping of the thioester intermediate J Biol Chem 277: 48657–48663

Schobert M and Jahn D (2002) Regulation of heme biosynthesis in non-phototrophic bacteria. J Mol Microbiol Biotechnol 4: 287–294

Schön A, Krupp G, Gough S, Berry-Lowe S, Kannangara CG and Söll D (1986) The RNA required in the first step of chlorophyll biosynthesis is a chloroplast glutamate tRNA. Nature 322: 281–284

Schön A, Hottinger H and Söll D (1988) Misaminoacylation and transamidation are required for protein biosynthesis in *Lactobacillus bulgaricus*. Biochimie 70: 391–394

Sekine S, Nureki O, Sakamoto K, Niimi T, Tateno M, Go M, Kohno T, Brisson A, Lapointe J and Yokoyama S (1996) Major identity determinants in the 'augmented D helix' of $tRNA^{Glu}$ from *Escherichia coli*. J Mol Biol 256: 685–700

Sekine S, Nureki O, Tateno M and Yokoyama S (1999) The identity determinants required for the discrimination between $tRNA^{Glu}$ and $tRNA^{Asp}$ by glutamyl-tRNA synthetase from *Escherichia coli*. Eur J Biochem 261: 354–360

Sekine S, Nureki O, Shimada A, Vassylyev DG and Yokoyama S (2001a) Major identity determinants in the 'augmented D helix' of $tRNA^{Glu}$ from *Escherichia coli*. Nat Struct Biol 8: 189–191

Sekine S, Nureki O, Shimada A, Vassylyev DG and Yokoyama S (2001b) Structural basis for anticodon recognition by discriminating glutamyl-tRNA synthetase. Nat Struct Biol 8: 203–206

Shemin D and Russell CS (1953) 5-Aminolevulinic acid, its role in the biosynthesis of porphyrins and purines. J Am Chem Soc 75: 4873–4875

Smith MA and Grimm B (1992) Gabaculine resistance of *Synechococcus* glutamate 1-semialdehyde aminotransferase. Biochemistry 31: 4122–4127

Smith MA, Grimm B, Kannangara CG and von Wettstein D (1991a) Spectral kinetics of glutamate-1-semialdehyde aminomutase of *Synechococcus*. Proc Natl Acad Sci USA 88: 9775–9779

Smith MA, Kannangara CG, Grimm B and von Wettstein D (1991b) Characterization of glutamate-1-semialdehyde aminotransferase of *Synechococcus*. Steady-state kinetic analysis. Eur J Biochem 202: 749–757

Smith MA, Kannangara CG and Grimm B (1992) Glutamate 1-semialdehyde aminotransferase: Anomalous enantiomeric reaction and enzyme mechanism. Biochemistry 31: 11249–11254

Smith MA, King PJ and Grimm B (1998) Transient-state kinetic analysis of *Synechococcus* glutamate 1-semialdehyde aminotransferase Biochemistry 37: 319–329

Stange-Thomann N, Thomann HU, Lloyd AJ, Lyman H and Söll D (1994) A point mutation in *Euglena gracilis* chloroplast $tRNA^{Glu}$ uncouples protein and chlorophyll biosynthesis. Proc Natl Acad Sci USA 91: 7947–7951

Sylvers LA, Rogers KC, Shimizu M, Ohtsuka E and Söll D (1993) A 2-thiouridine derivative in $tRNA^{Glu}$ is a positive determinant for aminoacylation by *Escherichia coli* glutamyl-tRNA synthetase. Biochemistry 32: 3836–3841

Tumbula DL, Becker HD, Chang WZ and Söll D (2000) Domain-specific recruitment of amide amino acids for protein synthesis. Nature 407: 106–110

Tyacke RJ, Contestabile R, Grimm B, Harwood JL and John RA (1995) Reactions of glutamate semialdehyde aminotransferase (glutamate-1-semialdehyde 2,1 aminomutase) with vinyl and acetylenic substrate analogues analysed by rapid scanning spectrophotometry. Biochem J 309: 307–313

Verderber E, Lucast LJ, Van Dehy JA, Cozart P, Etter JB and Best EA (1997) Role of the *hemA* gene product and delta-aminolevulinic acid in regulation of *Escherichia coli* heme synthesis. J Bacteriol 179: 4583–4590

Vothknecht UC, Kannangara CG and von Wettstein D (1996) Expression of catalytically active barley glutamyl $tRNA^{Glu}$ reductase in *Escherichia coli* as a fusion protein with glutathione S-transferase. Proc Natl Acad Sci USA 93: 9287–9291

Wang LY, Brown L, Elliott M and Elliott T (1997) Regulation of heme biosynthesis in *Salmonella typhimurium*: activity of glutamyl-tRNA reductase (HemA) is greatly elevated during heme limitation by a mechanism which increases abundance of the protein. J Bacteriol 179: 2907–2914

Wang LY, Elliott M and Elliott T (1999a) Conditional stability of the HemA protein (glutamyl-tRNA reductase) regulates heme biosynthesis in *Salmonella typhimurium*. J Bacteriol 181: 1211–1219

Wang LY, Wilson S and Elliott T (1999b) A mutant HemA protein with positive charge close to the N terminus is stabilized

against heme-regulated proteolysis in *Salmonella typhimurium*. J Bacteriol 181: 6033–6041

Weinstein JD and Beale SI (1985) RNA is required for enzymatic conversion of glutamate to delta-aminolevulinate by extracts of *Chlorella vulgaris*. Arch Biochem Biophys 239: 87–93

Willows RD, Kannangara CG and Pontoppidan B (1995) Nucleotides of $tRNA^{Glu}$ involved in recognition by barley chloroplast glutamyl-tRNA synthetase and glutamyl-tRNA reductase. Biochim Biophys Acta 1263: 228–234

Chapter 13

The Pathway from 5-Aminolevulinic Acid to Protochlorophyllide and Protoheme

Elena Yaronskaya
National Academy of Sciences of Belarus, Institute of Photobiology, Akademicheskaya str. 27, 22072 Minsk, Belarus

Bernhard Grimm*
Institut für Biologie/Pflanzenphysiologie, Humboldt Universität Berlin, Unter den Linden 6, D-10099 Berlin, Germany

Summary

This chapter comprehensively surveys *both* the conversion of 5-aminolevulinic acid to protochlorophyllide in the Mg-porphyrin-synthesizing branch of tetrapyrrole biosynthesis *and also* the formation of protoheme in the iron-chelating branch. This can be considered as the middle and final stages of chlorophyll and heme formation, respectively: the final conversion of protochlorophyllide to chlorophyll is discussed by Rüdiger in Chapter14 (Rüdiger). This chapter reviews the many individual enzymatic steps in these conversions, including enzyme and gene structures and the expression as well as the regulation of these steps.

*Author for correspondence, email: bernhard.grimm@rz.hu-berlin.de

Bernhard Grimm, Robert J. Porra, Wolfhart Rüdiger and Hugo Scheer (eds): Chlorophylls and Bacteriochlorophylls: Biochemistry, Biophysics, Functions and Applications, pp. 173–188.

I. Introduction

This chapter reviews the middle section of the multi-step pathway of tetrapyrrole biosynthesis whereby eight molecules of 5-aminolevulinic acid (ALA) are converted to chlorophyll (Chl) via protochlorophyllide (PChlide), or to protoheme. Eight molecules of ALA are used to generate uroporphyrinogen III (Urogen III) through a linear tetrapyrrolic intermediate, hydroxymethylbilane I (HMB). Urogen III constitutes a first branch point in tetrapyrrole biosynthesis: it can be methylated and subsequently converted to either vitamin B_{12} (cf. Battersby, 1994) or siroheme (Murphy and Siegel, 1973); alternatively it can be decarboxylated and oxidized to form protoporphyrin IX (Proto). Proto constitutes a second branch point: insertion of Fe^{2+} into Proto forms protoheme, while insertion of Mg^{2+} is the first committed step in the biosynthesis of Chl. The individual enzymatic reactions of protoheme and Chl biosynthesis, including enzyme structure, encoding gene structure and expression, as well as their metabolic regulation, are discussed.

II. Enzymes of Porphyrin Synthesis

A. 5-Aminolevulinic Acid Dehydratase (Porphobilinogen Synthase)

ALA dehydratase (porphobilinogen synthase) (ALAD) catalyzes the asymmetric condensation of two molecules of ALA to the monopyrrole, porphobilinogen (PBG) (Fig. 1) (Jordan, 1991). The bacterial, animal and plant enzymes possess structural and catalytic similarities: the exclusive Mg^{2+}-metal ion requirement, pH-optima and thiol sensitivity distinguish the plant-type ALAD from others (Senior et al., 1996). Plant ALAD contains a highly conserved metal-binding domain with Asp residues and can form active homohexameric and octameric complexes (Schaumburg and Schneider-Poetsch, 1992; Cheung et al., 1997). ALAD from other eukaryotic and prokaryotic organisms is octameric, requires both Mg^{2+} and Zn^{2+} and coordinates the latter through Cys and His in the metal-binding domain. X-ray structures of yeast and bacterial ALAD have been presented (Erskine et al., 1999; Frankenberg et al., 1999). Recent structural analysis shows that human allelic ALAD differs from the wild-type protein by an ability to shift between the octameric and hexameric form: this transition appears relevant in a Mg^{2+}-dependent allosteric regulation of ALAD, as only the octameric form makes a Mg^{2+} binding site available (Breinig et al., 2003).

The soluble plant ALAD was located in plastids from pea leaves or arum lily spadices (Smith, 1988). The plant *ALAD* gene encodes a precursor for plastid translocation. Light differently affects *ALAD* gene expression in various plant species. *ALAD* mRNA levels are unchanged during greening of pea leaves, while the enzyme activity increases: a post-transcriptional light-dependent control of this enzymatic step has been proposed (Boese et al., 1991). In soybean, *ALAD* mRNA accumulates during greening without an apparent change in enzyme activity or protein level (Kaczor et al., 1994). An increase in both *ALAD* mRNA and enzyme activity during light exposure corresponds in light-dark synchronized cells of *Chlamydomonas (C.) reinhardtii* with the rate of Chl accumulation (Matters and Beale, 1995a). Although *ALAD* mRNA accumulates under blue light, the *ALAD* gene is also controlled through the cell cycle or the circadian clock (Matters and Beale, 1995b).

B. Porphobilinogen Deaminase (Hydroxymethylbilane Synthase)

Porphobilinogen deaminase (PBGD) catalyzes the condensation of four molecules of PBG into the linear hydoxymethylbilane I (HMB) which is unstable and spontaneously cyclizes to Urogen I (Battersby et al., 1979a) when the succeeding enzyme, uroporphyrinogen III synthase (UROS) is absent, defective or limiting: for example, Uro I, the oxidation product of Urogen I, has been isolated from the urine of the

Abbreviations: ALA – 5-aminolevulinic acid; ALAD – 5-aminolevulinic acid dehydratase; BChl – bacteriochlorophyll; *C.* – *Chlamydomonas*; Chl – chlorophyll; *Chl.* – *Chlorobium*; Chlide – chlorophyllide; Copro – coproporphyrin; Coprogen – coproporphyrinogen; CPO – coproporphyrinogen oxidase; CsCl – cesium chloride; HMB – hydroxymethylbilane I; Mg-chelatase – magnesium protoporphyrin IX chelatase; MgProto – magnesium protoporphyrin IX; MgProtoMe – magnesium protoporphyrin IX monomethylester; MgProtoMeC – magnesium protoporphyrin IX monomethylester cyclase ; MTF – magnesium protoporphyrin IX monomethyl transferase; PBG – porphobilinogen; PBGD – porphobilinogen deaminase; PChlide – protochlorophyllide; POR – protochlorophyllide oxidoreductase; PPOX – protoporphyrinogen oxidase; Proto – protoporphyrin IX; Protogen – protoporphyrinogen IX; *Rba.* – *Rhodobacter*; *Rvi.* – *Rubrivivax*; *Rvu.* – *Rhodovulum*; ROS – reactive oxygen species; Uro – uroporphyrin; UROD – uroporphyrinogen III decarboxylase; Urogen – uroporphyrinogen; UROS – uroporphyrinogen III synthase

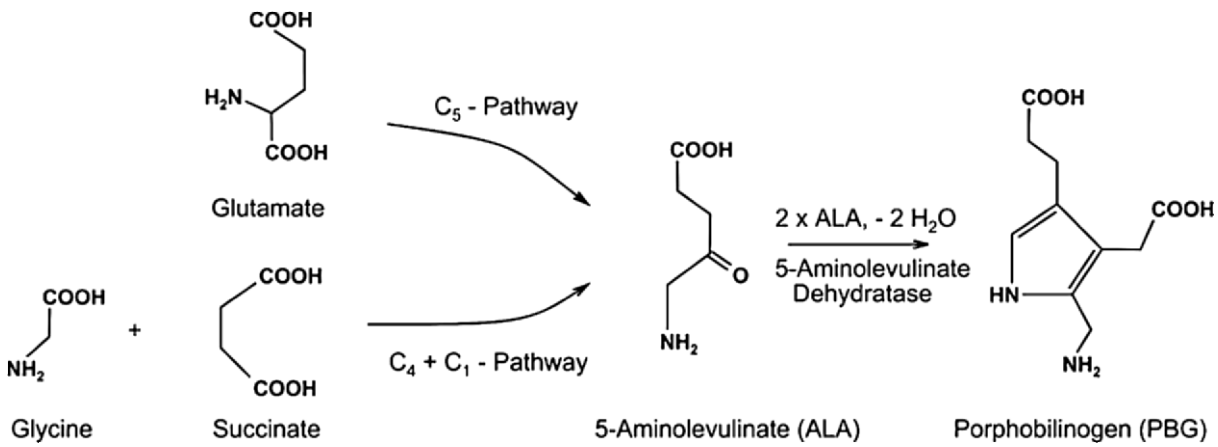

Fig. 1. Two pathways for biosynthesis of ALA, the committed molecule of tetrapyrrole biosynthsis and the subsequent asymmetric condensation of two molecules ALA to porphobilinogen.

congenital porphyria patients (Rimington and Miles, 1951) and coproporphyrin (Copro) I, the oxidation product of coproporphyrinogen (Coprogen) I, which is formed by enzymatic decarboxylation of Urogen I (see Section II.D), has been isolated from anoxic yeast cells (Porra et al., 1973). Coprogen I is not a substrate for Coprogen III oxidase (Section II.E). In the presence of UROS, however, HMB is directly converted to Urogen III (Battersby et al., 1979b; Jordan and Seehra, 1979), an intermediate common to the biosynthesis of protoheme and Chl. The synthesis of HMB involves, as a preparatory step, the synthesis of a unique enzyme-bound dipyrromethane cofactor, which serves as an attachment point for the subsequent assembly of four PBG molecules to form a hexapyrrole (Fig. 2) (Hart et al., 1987; Jordan and Warren, 1987). In *E. coli,* the newly synthesized dipyrromethane cofactor is post-translationally attached to Cys242 of the apoprotein by a thioether linkage. Sequential condensation of four PBG molecules commences at the free α-position of the cofactor. Once the hexapyrrole stage is reached, a linear tetrapyrrole, HMB, is released before the enzyme-dipyrrole complex accepts more PBG molecules (Battersby et al., 1983). X-ray structural studies of the *E. coli* enzyme suggest the stepwise elongation of the polypyrrole chain (Louie et al., 1996). Examination of wild type and mutants revealed essential amino acids for cofactor binding and for enzyme-intermediate complex formation during chain elongation at the catalytic side (Louie et al., 1996). The same amino acids are also conserved in plant and algal PBGD which occurs in the plastid stroma. The pea and *Arabidopsis* precursor proteins have an approximate Mr of 40 kDa: after import into isolated chloroplasts, the Mr of the mature protein was 35 kDa (Witty et al., 1993; Lim et al., 1994). Expression of the pea gene is strongly induced by light: steady-state levels of *PBGD* mRNA increase in parallel with enzyme activity (Witty et al., 1993).

C. Uroporphyrinogen III Synthase (UROS)

UROS simultaneously catalyzes the cyclization and isomerization of HMB by the inversion of ring D to yield the first isomer III cyclic tetrapyrrole, Urogen III, which is the first common tetrapyrrolic intermediate of heme and Chl. Inversion of ring D probably involves formation of a *spiro*-cyclic-intermediate (Fig. 2) (Crockett et al., 1991; Stark et al., 1993). The instability of HMB apparently requires a PBGD-UROS complex in vivo, since an alteration of the sedimentation rate of wheat germ PBGD (Higuchi and Bogorad, 1975) and of the k_m for PBG of the *Euglena* enzyme occurs in the presence of UROS (Battersby et al., 1979a). Purified UROS from *Euglena* is a monomer (Mr = 31 kDa) (Hart and Battersby, 1985). Structural determination by X-ray crystallography of the human enzyme revealed a bilobed structure of a homodimer. Mutation of various residues in the putative active site cleft revealed no essential residue for the catalytic mechanism (Mathews et al., 2001; Schubert et al., 2002).

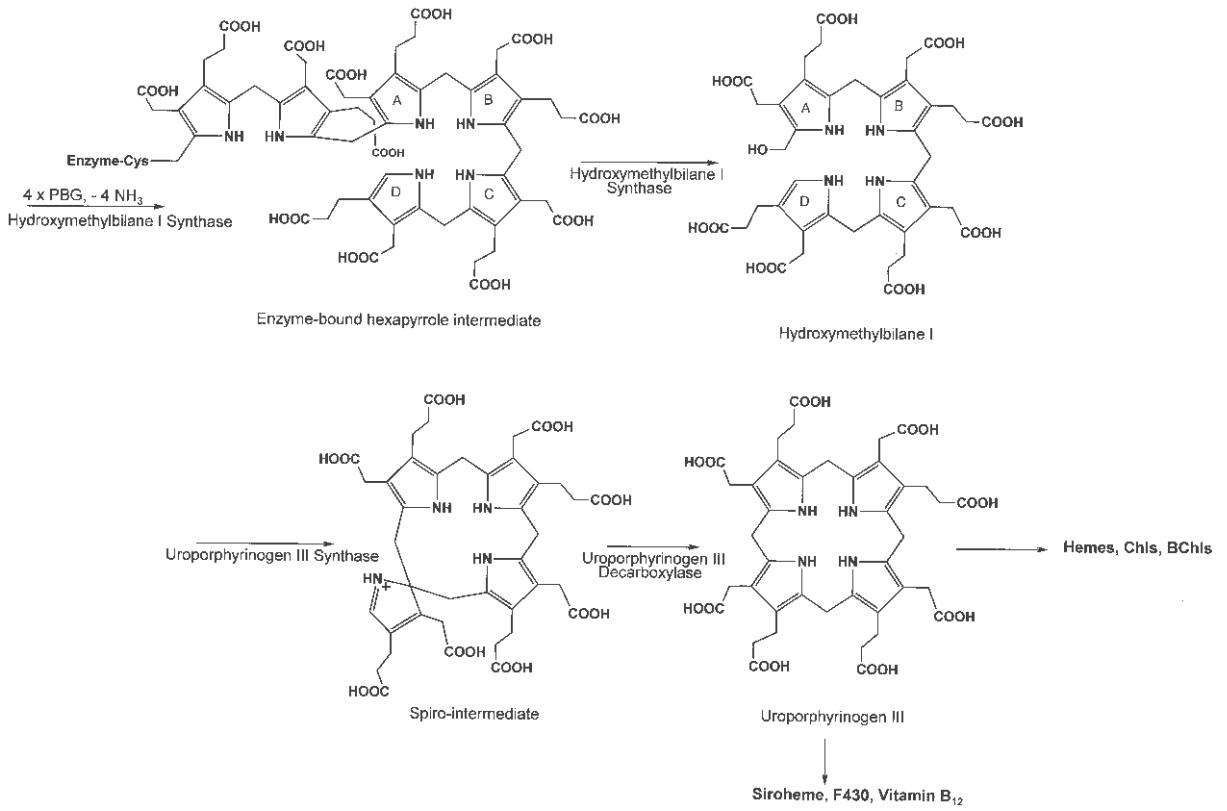

Fig. 2. Enzymatic steps of the tetrapyrrole biosynthetic pathway from porphobilinogen to uroporphyrinogen III.

D. Uroporphyrinogen III Decarboxylase

Uroporphyrinogen III decarboxylase (UROD) is located at the first branch point of the tetrapyrrole biosynthetic pathway: decarboxylation of Urogen III leads to the biosynthesis of protoheme and of Chl or bacteriochlorophyll, whereas its C-methylation initiates synthesis of vitamin B_{12} (Battersby, 1994) and sirohemes (Murphy and Siegel, 1973). UROD catalyzes the decarboxylation of all four acetate side-chains of Urogen III resulting in Coprogen III formation (Fig. 3). Decarboxylation starts from pyrrole ring D followed by a clockwise decarboxylation at rings A, B, and C (Luo and Lim, 1993). Urogen I can also serve as substrate for UROD but the product, Coprogen I, cannot be further metabolized.

All homologous plant UROD sequences, which are derived from cDNA sequences, possess an N-terminal extension for plastid translocation. The recombinant tobacco UROD forms a homodimeric structure under similar ionic strength conditions found in the plastidic stroma fraction. X-ray crystal structure of tobacco UROD (Martins et al., 2001) confirmed the previously published 3D-structure of the homologous human enzyme (Whitby et al., 1998). The analysis reveals one catalytic cleft per monomer with six invariant polar residues. Asp82/86 and Tyr159/164 (tobacco/human enzyme numbering) seem to be the catalytic functional residues, which may serve in substrate recognition and binding. Arg32/37 is proposed to direct the substrate into the hydrophobic catalytic cleft (Whitby et al., 1998; Martins et al., 2001).

URODD mRNA and protein levels increased during greening of etiolated barley leaves (Mock et al., 1995). The expression of *URODD* antisense RNA in tobacco plants leads to the formation of necrotic leaf lesions, which are caused by generating reactive oxygen species (ROS) as a result of accumulating photo-reactive Uro III. The transgenic plants analyzed possessed a minimal wildtype activity of 70% (Mock and Grimm, 1997). The photo-destructive processes in leaves induced an anti-oxidative defense system in several cellular compartments and diminished the total content of reduced low-molecular-mass

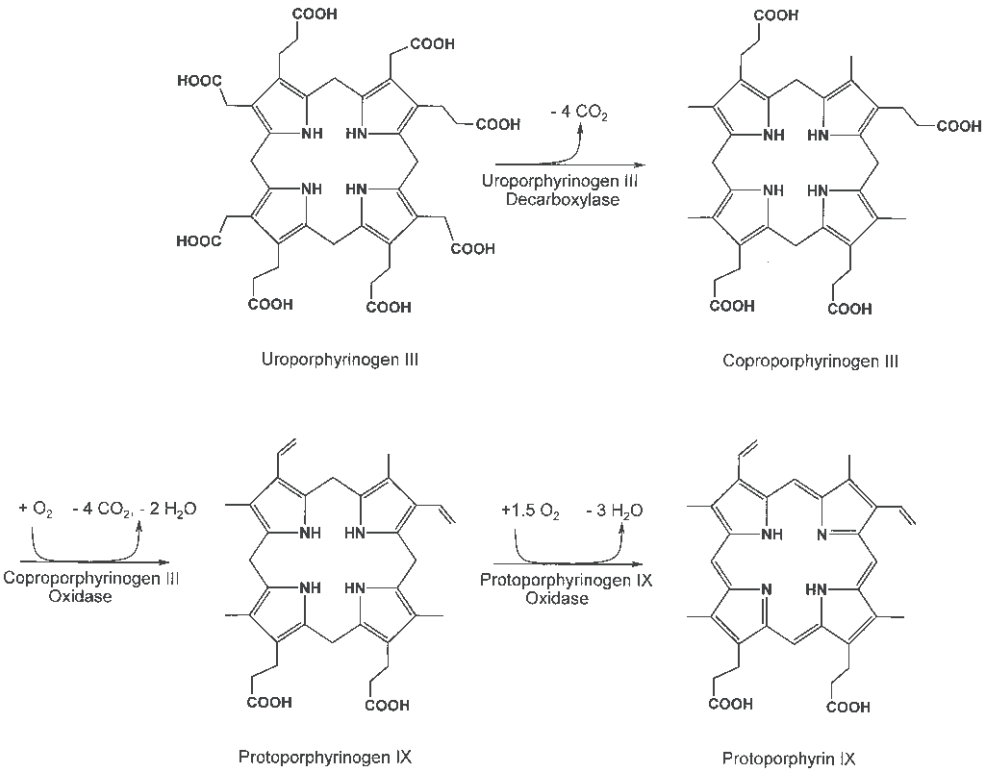

Fig. 3. Enzymatic steps of the tetrapyrrole biosynthetic pathway from uroporphyrinogen III to protoporphyrin IX.

anti-oxidants (Mock et al., 1998). The maize *Les22* mutant carries a mutant *UROD* gene and also shows necrotic lesions (Hu et al., 1998). A similar effect of Uro(gen) III accumulation was observed after cesium chloride (CsCl) treatment of greening barley leaves. However, the excess Urogen III was re-metabolized when the toxic metal cations were removed after less than 8 h of CsCl incubation. Upon longer CsCl exposure, accumulated Uro generated necrotic lesions. It is assumed that photodynamic damage of leaves begins when photoprotective activities were overwhelmed with Urogen, which was infiltrated into the cytoplasm (Shalygo et al., 1997, 1998).

E. Coproporphyrinogen III Oxidase

Coprogen III oxidase (CPO) catalyzes the oxidative decarboxylation of the two propionate side chains of ring A and B to vinyl groups to yield the divinyl compound, protoporphyrinogen IX (Protogen) (Fig. 3). Coprogen I cannot serve as substrate for this enzyme. Analysis of CPO activity in different subcellular compartments of pea and spadices of cuckoo-pint, as well as immuno-detection of CPO in soybean, revealed the exclusive location of this enzyme in plastids (Smith et al., 1993). *CPO* gene expression showed tissue-specific and developmental changes rather than changes upon light exposure or under diurnal and circadian growth conditions (Kruse et al., 1995a; Papenbrock et al., 1999). The content of mRNA reached its maximum in young developing cells and drastically decreased in older differentiated cells. Roots from soybean and pea synthesized elevated levels of CPO during nodulation and displayed also higher activities of ALAD, PBGD, protogen oxidase (PPOX) and ferrochelatase indicating the plant's contribution to plant protoheme biosynthesis for the assembly of cytochrome as well as of nodule leghemoglobin (Santana et al., 1998).

Reduction of CPO activity by antisense RNA expression led, in transgenic tobacco plants, to an accumulation of Copro(gen) and consequently to light-intensity-dependent leaf necrosis (Kruse et al., 1995b). Although the protective system against ROS was generally alerted, the ascorbate and glutathione concentrations were decreased relative to control plants, suggesting that anti-photosensitization processes could not be sufficiently invoked to prevent cell

death (Kruse et al., 1995b; Mock et al., 1998). Likewise, in *UROD* antisense transgenic lines, CPO-deficient plants induced several defense responsive genes resembling the hypersensitive reaction observed in response to pathogen attack (Mock et al., 1999). The recessive *Arabidopsis* lesion initiation (*lin2*) mutant contains a defective gene encoding CPO and forms development- and light-dependent necrotic lesions in leaves and siliques (Ishikawa et al., 2001)

F. Protoporphyrinogen IX Oxidase

Protogen oxidase (PPOX) is the last enzyme common to both Chl and protoheme biosynthesis. This flavin-requiring enzyme catalyzes the six-electron oxidation of Protogen to Proto (Fig. 3) and its activity was detected in plants in both plastids and mitochondria (Jacobs and Jacobs, 1987; Smith et al., 1993). Two different genes, PPOX I and PPOX II, exist in different plant species (e.g., Lermontova et al., 1997; Che et al., 2000; Watanabe et al., 2001). Identical isoforms from different plant species show a high degree of identity (e.g., PPOX II isoforms share approximately 70% identical amino acids), while the sequence identity between isoform I and II of the same species is relatively low (28%). PPOX is the first enzyme of the tetrapyrrole biosynthetic pathway to be located in two different subcellular compartments: the mitochondrion and the chloroplast. The spinach PPOX I enzyme is preferentially associated with the stromal side of the thylakoid membrane, but a small portion is also found on the stromal side of the inner envelope membrane (Che et al., 2000). The spinach *PPOXII* gene encodes two translation products of different size, 59 kDa (PPOX IIL) and 55 kDa (PPOX IIS), by use of two in-frame initiation codons. In situ immunological analysis, by electron microscopy with anti-PPOX II, confirmed the translocation of a 57 kDa PPOX IIL in the inner plastid envelope fraction facing the stromal side while the 55 kDa PPOX IIS was located in the inner mitochondrial membrane fraction (Watanabe et al., 2001).

PPOX is the target enzyme of phthalimide- and diphenylether-type herbicides (Scalla et al., 1990; Duke et al., 1991). The inhibition of PPOX by these photodynamically-acting herbicides causes accumulation of Protogen, which leaks out of plastids and is oxidized to Proto by unspecific herbicide-resistant peroxidases bound to plasma membranes (e.g., Jacobs and Jacobs, 1993). Excessive Proto concentrations are known to cause a potent phytotoxic photosensitization, which results in the generation of lethal amounts of ROS causing membrane peroxidation and cell death (Matringe and Scalla, 1988).

Genetic and biochemical analyses were performed to characterize herbicide-resistant mutants. A single nucleotide substitution (G → A) in the *PPOX* gene of *C. reinhardtii* caused an amino acid alteration (Val291Met) which conferred herbicide tolerance (Randolph-Anderson et al., 1998). An *Arabidopsis* mutant with two substitutions in PPOX I (Tyr426Met and Ser305Leu) was 600-fold more tolerant to PPOX inhibitors (Li et al., 2003). Herbicide tolerance of the photomixotrophic tobacco YZI-1S cell line was explained by amplification of the *PPOX II*-gene leading to increased levels of the corresponding mRNA and a five-fold increase of the mitochondrial enzyme activity (Watanabe et al., 1998, 2002). Transgenic tobacco or rice plants became more resistant to oxyfluorfen by expressing a *B. subtilis PPOX* gene (Choi et al., 1998; Lee et al., 2000). Over-expression of *Arabidopsis PPOX I* gene made transgenic tobacco more resistant to acifluorfen (Lermontova and Grimm, 2000).

The genetic or chemical disruption of the metabolic pathway at the step of Proto synthesis can also induce several defense responses as a result of porphyrin-induced photosensitization. *Arabidopsis* plants expressing *PPOX* antisense genes display the known pattern of necrotic leaf lesions resembling lesions after pathogen-induced hypersensitivity reactions (Molina et al., 1999). Different inhibitors were applied to clarify structural properties of the active site of PPOX (Arnould and Camadro, 1998; Arnould et al., 1998; Birchfield et al., 1998). The crystal structure of a PPOX has recently been published (Koch et al., 2004).

III. The Chlorophyll-synthesizing Branch

A. Mg-Protoporphyrin IX Chelatase

Magnesium protoporphyrin IX chelatase (Mg-chelatase) catalyzes the insertion of Mg^{2+} into Proto and, thus, directs Proto into the Chl biosynthesizing branch (Fig. 4). The complexity of the structural, enzymatic and regulatory properties of Mg-chelatase has been addressed in numerous studies. The protein consists of three different subunits. Transposon mutagenesis studies in *Rba. capsulatus* (Bollivar et al., 1994b) and *Rba. sphaeroides* (Gorchein et al., 1993) have initially demonstrated that the expression of the three gene products *BchI, -D* and *-H,* are required for Mg-chelatase activity. The homologous proteins in plants,

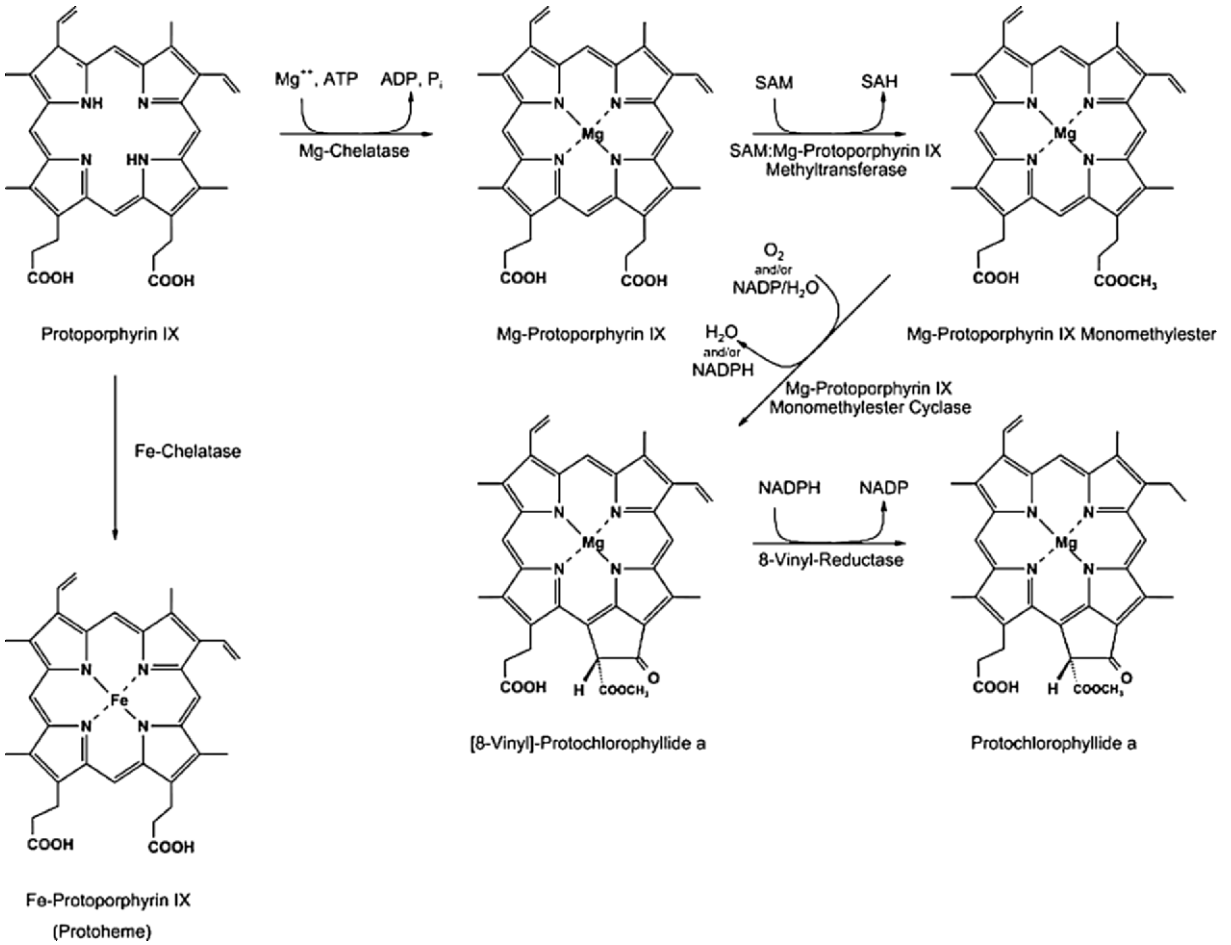

Fig. 4. Enzymatic steps of the tetrapyrrole biosynthetic pathway at the branchpoint to chlorophyll and protoheme biosynthesis. Protoporphyrin IX is either directed into the Mg branch and subsequently converted into protochlorophyllide or into the Fe branch to form protoheme.

algae and cyanobacteria are named CHLI/XAN-H, CHLD/XAN-G, and CHLH/ XAN-F with molecular masses 36–46 kDa, 60–87 kDa and 123-150 kDa, respectively (LCD Gibson et al., 1995, 1996; Jensen et al., 1996a,b; Papenbrock et al., 1997; Petersen et al., 1998). The *ChlI* homologous gene is encoded in the chloroplast genome of most algae and *Euglena gracilis* (Orsat et al., 1992).

By analysis of *Arabidopsis thaliana* (*cs*) and *Antirrhinum majus* (*olive*) mutants, the first plant genes encoding two different subunits of Mg-chelatase were detected (Koncz et al., 1990; Hudson et al., 1993). In barley, the *Xantha-f, Xantha-g* and *Xantha-h* loci were assigned to the structural genes for the three different subunits of Mg-chelatase (Jensen et al., 1996b; Petersen et al., 1999).

Mg-chelatase activities were detected in intact cucumber chloroplasts (Castelfranco et al., 1979), in broken pea chloroplasts (Walker and Weinstein, 1991), in a sub-plastid membrane fraction without a soluble stroma fraction (Lee et al., 1992) and, subsequently, in totally soluble fractions of pea chloroplasts (Guo et al., 1998). Enzyme assays with recombinant *Rba. sphaeroides, Synechocystis* PCC 6803 and *Chlorobium* (*Chl.*) *vibrioforme* subunits revealed that all three proteins were required to reconstitute the Mg-chelatase activity in vitro (LCD Gibson et al., 1995; Jensen et al., 1996a; Willows et al., 1996; Petersen et al., 1998; Willows and Beale, 1998). A stoichiometry of 4 BchI:1 BchD and 2 CHLI:1 CHLD:4 CHLH was found to be optimum in in vitro reconstitution assays with the three recombinant subunits from *Rhodobacter* and *Synechocystis*, respectively (Willows et al., 1996; Hansson et al., 1999; Jensen et al. 1999a).

Analysis of the 3-D structure of the *Rba. capsulatus*

BchI protein revealed that the I-subunit belongs to a chaperone-like family of AAA^+ proteins (possessing ATPase properties associated with various cellular activities) and is proposed to form a hexameric ring structure with a ring diameter of about 110 Å (Fodje et al., 2001). The N-terminal domain of BchI contains Walker A and Walker B motifs, which are generally present in nucleotide triphosphate-hydrolyzing enzymes (Hansson et al., 2002). Due to the structural similarity to BchI, the N-terminus of BchD possibly contains an AAA module and, additionally, an integrin I domain at the C-terminus (Fodje et al., 2001). An integrin I-domain-binding motif was proposed in the C-helical domain of BchI and BchH which could allow interaction of all subunits through BchD and, thus, establishing a linkage between porphyrin metalation by BchH and ATP hydrolysis by BchI (Fodje et al., 2001).

The initial enzymatic studies by several groups permitted an advanced model for the molecular organization and the mechanistic steps of Mg-chelatase. This model proposed that, firstly, an ATP-dependent double-ring structure consisting of BchI and BchD is formed, which hinders the ATPase activity of BchI (Walker and Willows, 1997; Fodje et al., 2001). Secondly, a ternary complex with the substrate-binding BchH is formed upon addition of Mg^{2+} which instigates porphyrin metalation. Then, release of the BchI-ATP-binding site occurs by weakening the protein-protein interaction at the integrin I-domain which triggers ATP hydrolysis (Fodje et al., 2001). These enzymatic analyses of bacterial Mg-chelatase resemble those of recombinant subunits from *Synechocystis* and recombinant tobacco subunits expressed in yeast (Grafe et al., 1999).

Expression of both the *Xan-f/CHLH* and *Xan-h/CHLI* gene in etiolated barley seedlings, in young tobacco plants and in photomixotrophic soybean suspension cultures is light-induced, but *CHLH mRNA* always accumulated more rapidly upon illumination than *CHLI mRNA* (Jensen et al., 1996b; Kruse et al., 1997; Nakayama et al., 1998). The barley Mg-chelatase activity increased three- to four-fold during greening, reaching a maximum after 6 h in light (Petersen et al., 1999). Thus, it is generally accepted that the capacity of Mg-chelatase activity correlates with the expression profile of *XAN-F/CHLH* (Jensen et al., 1996b; Papenbrock et al., 1997; Petersen et al., 1999).

In barley, *Arabidopsis,* tobacco and soybean, the *XAN-F/CHLH* expression was under the control of the circadian clock with a maximum at the beginning of the light period and a minimum at the transition from light to dark (Jensen et al., 1996b; Nakayama et al., 1998; Papenbrock et al., 1999). In contrast, the *CHLI* transcripts remained constant (LCD Gibson et al., 1996; Papenbrock et al., 1999). The tobacco *CHLD m*RNA content inversely oscillated to the *CHLH* level in tobacco over a 24-h light-dark cycle (Papenbrock et al., 1999).

Mg-chelatase subunits can exhibit Mg^{2+}-dependent changes in their distribution between stroma and chloroplast membranes (LCD Gibson et al., 1996; Nakayama et al., 1998; Luo et al., 1999). CHLH is largely soluble at low Mg^{2+} concentrations but attaches to the envelope membrane at Mg^{2+} concentration above 5 mM. The association of CHLD with envelope membranes shows a similar Mg^{2+} dependency. However, while CHLI was detected in the soluble fraction, regardless of the Mg^{2+} concentration, the importance of the sub-compartmental (stroma/membrane) distribution of Mg-chelatase for modulation of its activity remains an open question.

Mutants, lacking one of the subunits, and transgenic plants, with deregulated expression of one of the subunits, illustrate interesting effects on Chl biosynthesis and chloroplast development. Barley *Xantha-h* mutants lack *not only* the XAN-H (CHLI) *but also* the XAN-G (CHLD) subunit (Hansson et al., 1999; Petersen et al., 1999). In contrast, in *Arabidopsis* T-DNA knockout mutants of the *CHLI* locus show wild type *CHLD* mRNA content (Rissler et al., 2002). It was proposed that the *CHLI2* gene product is responsible for a limited CHLD accumulation and, consequently, for Mg-chelatase activity and Chl accumulation in this mutant. Silencing of the tobacco *CHLH* gene by infection with tobacco mosaic virus vectors containing *CHLH* inserts resulted *not only* in strongly decreased levels of *CHLH* mRNA, *but also* of *CHLD* mRNA (Hiriart et al., 2002).

Transgenic tobacco plants expressing antisense *CHLI* and *CHLH* mRNA, respectively, displayed a chlorotic phenotype and reduced plant-growth rate. The loss of Chl correlated with the gradually reduced Mg-chelatase activity in response to antisense inactivation (Papenbrock et al., 2000a,b). In spite of diminished Mg-chelatase activity, the metabolic substrate, Proto, did not accumulate. Lower heme contents exclude the possibility of re-direction of non-metabolized Proto into heme biosynthesis in the transgenic plants. ALA synthesizing capacity was diminished in parallel with reduced Mg-chelatase activ-

ity and was due to lower levels of transcripts encoding glutamyl-tRNA reductase and ALAD (Papenbrock et al. 2000a, Chapter 16, Beck and Grimm).

The barley *chlorina-125, -157,* and *-161* mutants contain point mutations in the *CHLI* gene and display a semi-dominant phenotype due to simultaneous expression of mutant and wild type CHLI. A small proportion of wild-type hexamers rescues the heterozygous plants but cannot provide sufficient Mg-chelatase activity to produce wild-type levels of Chl (Hansson et al., 1999, 2002). Both the *Arabidopsis cs* mutant (Koncz et al., 1990) and the virus-induced silencing of the *sulfur* allele in *Nicotiana benthamiana* (Kjemtrup et al., 1998) display chlorotic phenotypes similar to the *CHLI* antisense plants.

Four out of five *Arabidopsis gun* mutants (genome unregulated) are affected in the expression of genes involved in tetrapyrrole biosynthesis. *Gun5* encodes the CHLH subunit of Mg-chelatase and revealed a point mutation in the *CHLH* gene (Mochizuki et al., 2001; for more details see chapter 16, Beck and Grimm). The allelic Chl-less *C. reinhardtii* mutants, *chl-1* and *brs-1,* could only grow heterotrophically in the dark because of Proto-mediated extreme light sensitivity. The genetic lesions could be assigned to frameshift mutations in the *CHLH* gene, respectively, resulting in a CHLH deficiency, but without alteration in expression of *CHLI* and *CHLD* genes (Chekounova et al., 2001; Chapter 16, Beck and Grimm).

B. S-Adenosyl-L-Methionine:Mg-Protoporphyrin IX Methyltransferase (MTF)

This MTF enzyme catalyzes the transfer of a methyl group from S-adenosyl-methionine to the carboxyl group of the 13-propionate side-chain of MgProto to yield MgProto monomethylester (MgProtoMe) (Fig. 4) (KD Gibson et al., 1963; Ellsworth and Dullaghan, 1972). A ping-pong type mechanism was demonstrated for the plant MTF enzyme (Ellsworth et al., 1974). Expression of the recombinant *BchM/ChlM* from *Rba. sphaeroides, Rba. capsulatus* and *Synechocystis* PCC 6803 revealed a monomeric enzyme of 25–27 kDa (Bollivar et al., 1994a; LCD Gibson and Hunter, 1994; Smith et al., 1996). Consistent with previous suggestions about a Mg-chelatase-MTF complex (Gorchein, 1972), addition of soluble BchH from *Rba. capsulatus* increased seven-fold the activity of recombinant MTF (Hinchigeri et al., 1997), and soluble extracts of cell cultures co-expressing *BchM* and the three Mg-chelatase subunits readily converted Proto to MgProtoMe (Jensen et al., 1999b).

The first plant cDNA sequences encoding MTF with an N-terminal plastid transit sequence were described for *Arabidopsis thaliana* and *Nicotiana tabacum* (Block et al., 2002; Alawady and Grim, 2005; Alawady et al., 2005). It is suggested that a hydrophobic region in the N-terminal half of the mature protein is responsible for anchoring the protein to both the envelope and thylakoid membranes (Block et al., 2002).

C. Mg-Protoporphyrin IX Monomethylester Cyclase (MgProtoMeC)

This oxidative cyclase enzyme catalyzes the complex reaction sequence for formation of the isocyclic ring, which is derived from the C-13-methylpropionate side chain of MgProtoMe (Fig. 4). The reaction sequence consists of three steps: hydroxylation of the methylpropionate side chain at the C-13^1 carbon atom, oxidation of this C-13^1-hydroxyl to a C13^1-oxo group and ligation of the C-13^2 carbon of the newly-formed 13^1-oxo-methylpropionate side chain to the C-15 bridge carbon between pyrrole rings C and D (Wong et al., 1985; Bollivar and Beale, 1996). The oxidative formation of the oxo group is facilitated by methylation of the carboxylate group to prevent its decarboxylation. Two mechanisms of cyclization were found in the tetrapyrrole pathway. In higher plants and green algae, the oxo-group oxygen is derived from molecular oxygen (Chereskin et al., 1982) by an oxygenase mechanism, while a different hydratase-type enzyme in *Rba. sphaeroides* uses oxygen from water under anaerobic conditions (Porra et al., 1995). *Rhodovulum (Rvu.) sulfidophilum,* which forms BChl *a* aerobically in the dark or anaerobically in the light, possesses both the oxygenase and hydratase pathways which can operate simultaneously in aerobic conditions (Porra et al., 1998). Anaerobic isocyclic ring formation for bacteriochlorophyll synthesis in *Rba. capsulatus* was shown to require a cobalamine cofactor (Gough et al., 2000).

Cyclase activity in developing cucumber chloroplasts, wheat etioplasts and *Synechocystis* require a membrane-bound and soluble fraction (Wong and Castelfranco, 1984; Nasrulhaq-Boyce et al., 1987; Walker et al., 1991), while the activity of *C. reinhardtii* was exclusively associated with membranes of lysed chloroplasts (Bollivar and Beale, 1995, 1996). Addition of iron chelators, but not of CO, KCN and NaN_3, inhibited cyclase activity suggesting that nonheme

iron is involved in the reaction (Nasrulhaq-Boyce et al., 1987; Whyte et al., 1992; Bollivar and Beale, 1995, 1996).

Disruption of the *orf358(ascF)* gene in the purple bacterium *Rubrivivax (Rvi.) gelantinosus,* which can form BChl *a* under aerobic growth conditions, causes accumulation of MgProtoMe aerobically indicating that the encoded protein is involved in the subsequent oxidative cyclization step (Pinta et al., 2002). Sequence comparison revealed homology with both the *Crdl* gene of *C. reinhardtii,* which was initially identified by a mutant screen for copper deficiency (Moseley et al., 2002), and also with the *PNZIP* gene in *Pharbitis nil*, which was characterized by phytochrome and endogenous clock induction (Zheng et al., 1998). The encoded protein belongs to the family of di-iron carboxylate proteins, characterized by an iron binding motif consisting of six conserved amino acids (four carboxylate residues and two histidines) (Berthold and Stenmark, 2003). In *Rba. capsulatus,* the *BchE* gene was identified as essential for anaerobic isocyclic ring formation (Bollivar et al., 1994a, b).

It is still not clear whether these homologous proteins (AscF/Crd1/PNZIP) can perform the whole reaction or whether other protein components are required for the entire reconstitution of the enzyme activity. The requirement of at least two plastidal protein fractions for the cyclization reaction was predicted after biochemical analysis of cyclase activity of two different barley mutants, *Xantha l-35* and *viridis K-23* (Walker and Willows, 1997). Thus, it is assumed that the *acsF* gene of *Rvi. gelatinosus* encodes at least a MgProtoMe hydroxylase (Pinta et al., 2002; Berthold and Stenmark, 2003)

D. Vinyl Reductase

8-Vinyl reductase catalyzes the conversion of an 8-vinyl group on ring B to an ethyl group (Fig. 4). Enzyme activity was measured in isolated plastid membranes from cucumber cotyledons, maize and barley (Parham and Rebeiz, 1992). This reaction can be carried out at least at two different steps in the pathway transforming divinyl-PChlide into monovinyl-PChlide or divinyl-Chlide into monovinyl-Chlide (Rebeiz et al., 1983; Tripathy and Rebeiz, 1988). Monovinyl-PChlide and -Chl are mainly found in plants. In the necrotic maize mutant (ON 8147), photosynthetic pigments are represented almost exclusively by divinyl Chl *a* and *b* but, in darkness, divinyl-PChlide is the main Chl precursor. Disruption of the *Rba. capsulatus bchJ* gene leads to increased divinyl-PChlide and lowered bacteriochlorophyll concentrations. Thus, *bchJ* was thought to be a candidate for the structural gene of this enzyme (Bollivar et al., 1994b; Suzuki and Bauer, 1995). But very recently, the first plant gene encoding 8-vinyl reductase was identified by map-based cloning of an *Arabidopsis* mutant that accumulated divinyl-Chl (Nagata et al., 2005). This gene has no similarity to *bchJ* of *Rhodobacter*. Divinyl-Chls *a* and *b* are major pigments in some type II cyanobacteria (Goericke and Repeta, 1993).

IV. The Protoheme-synthesizing Branch

A. Ferrochelatase

The enzyme ferrochelatase (protoheme ferrolyase) is a single membrane-associated- and ATP-independent-protein requiring only Fe^{2+} and Proto as substrates for the final step of heme formation. Ferrochelatase is considered to play an important role in the regulation of metabolite distribution at the branch point of porphyrin biosynthesis. Ferrochelatase activity has been demonstrated in both plant plastids and mitochondria (Porra and Lascelles, 1968). More recently, plastid ferrochelatase was associated *either* with thylakoid membranes in peas (Matringe et al., 1994) *or* with thylakoid and envelope membrane in *Arabidopsis* (Roper and Smith, 1997; Masuda et al., 2003).

The crystal structure of *Bacillus subtilis* and human ferrochelatases indicates that while the major features of the chelation reaction are conserved (Lecerof et al., 2000; Wu et al., 2001) differences were revealed in molecular size, subunit composition, solubility and presence or absence of a [2Fe-2S]-cluster between bacterial, plant and human ferrochelatases (Dailey et al., 2000). Mechanisms of porphyrin distortion and metalation were proposed for the bacterial enzyme, under the assumption that the enzyme attaches to pyrrole rings B, C and D and forces a tilt in ring A, which allows the metal to enter the porphyrin via the distorted pyrrole (Lecerof et al., 2000).

cDNA sequences encoding plant ferrochelatase were obtained from cucumber, barley (*HEMH*; Miyamoto et al. 1994) and *Arabidopsis* (*AtFC-I,* Smith et al., 1994) by complementation of the bacterial or yeast ferrochelatase mutants. Subsequently, a second *Arabidopsis* cDNA sequence (*AtFC-II*) was found that encodes another precursor ferrochelatase

with a 69% identity to AtFCI (Chow et al., 1998). AtFC-I was expressed in all plant tissues and could be imported in vitro both into pea chloroplasts and mitochondria, whereas *AtFC-II* was expressed only in leaves, stems and flowers, where it was solely targeted to chloroplasts (Chow et al., 1998; Singh et al., 2002): *ATFC-II* was not expressed in roots. The importation properties of AtFC1, reported above to be dual-targeted into mitochondria and plastids, have recently been re-evaluated. Both AtFC1 and AtFC2 could not be imported into *Arabidopsis* mitochondria, suggesting that the presence of ferrochelatase in plant mitochondria should be re-investigated (Lister et al., 2001). However, calculations about the contribution of mitochondrial ferrochelatase to the total activity in roots, green and etiolated leaves revealed 30% of total activity in tobacco mitochondria (Papenbrock et al., 2001) and less than 10% in pea mitochondria (Cornah et al., 2002). Only traces of activity, however, were found in cucumber mitochondria (Masuda et al., 2003); indeed, both ferrochelatase isoforms were immunologically detected in plastids but not in mitochondria (Masuda et al., 2003).

Supporting the studies of Chow et al (1998), but not of Lister et al. (2001), the cucumber *CsFeC1* gene, which is homologous with *AtFC1*, showed a light-insensitive expression in non-photosynthetic tissues, such as hypocotyls and roots, but not in cotyledons (Suzuki et al., 2002) and could be imported into mitochondria. The *CsFeC2* mRNA was detected in all tissues and strongly light-induced in cotyledons (Suzuki et al., 2000, 2002). The protein was predominantly translocated to thylakoid membranes and, to a lesser extent, to the envelope membranes. It has been suggested that two routes operate concurrently in plastids for ALA biosynthesis and its conversion to heme by ferrochelatase: one pathway to form heme, which is required for cytochromes, protective roles in non-photosynthetic tissue, and a second for heme and Chl formation in photosynthetic tissue (Singh et al., 2002; Suzuki et al., 2002).

Loss of plastidic ferrochelatase activity by antisense RNA expression in tobacco of the ferrochelatase type II causes accumulation of Proto and, consequently, the formation of necrotic leaf lesions. The activity of a mitochondrial ferrochelatase was not reduced, but could not compensate for lower plastidic ferrochelatase activity. Moreover, excessive Proto attributed for heme synthesis cannot be re-directed to Mg-chelatase suggesting that spatial separation of both ferro- and Mg-chelatase occurs in plastidal sub-compartments as well as tight substrate channeling in multi-enzymatic complexes from the early enzymatic steps through to heme or Chl biosynthesis (Papenbrock et al., 2001).

V. Concluding Remarks

All plant tetrapyrroles are synthesized in plastids with the exception that the last two steps of heme synthesis also occur in mitochondria. All enzymes of the pathway are nuclear-encoded and the genes always encode precursor proteins, which are targeted to their organellar destination. The metabolic flow and the activities of all enzymes are adjusted to developmental, tissue specific, circadian rhythm or environmental conditions. Although each enzymatic step is independently controlled at various steps of gene expression, it is accepted that certain regulatory steps control the general activity of the pathway. Subcellular compartmentation of multi-enzymatic complexes, as well as tight regulation of the expression of each enzyme, is probably essential for appropriate channeling of metabolites between the branched pathways.

In general, tetrapyrrole biosynthesis from ALA to PChlide and protoheme shows some interesting trends: the metabolic intermediates became increasingly hydrophobic and photoreactive. These properties, in turn, affect sub-compartmental location and functions of enzymes involved in photoprotection and substrate channeling. General aspects of enzyme localization, their implication on metabolic flow and the photo-toxic risks of porphyrin accumulation are discussed in Chapter 10, an introductory chapter by Rüdiger and Grimm.

References

Alawady AE and Grimm B (2005) Tobacco Mg protoporphyrin IX methyltransferase is involved in inverse activation of Mg porphyrin and protoheme synthesis. Plant J 41: 282–290

Alawady A, Reski R, Yaronskaya E and Grimm B (2005) Cloning and expression of the tobacco *CHLM* sequence encoding Mg protoporphyrin IX methyltransferase and its interaction with Mg chelatase. Plant Mol Biol 57: 679–691

Arnould S and Camadro JM (1998) The domain structure of protoporphyrinogen oxidase, the molecular target of diphenyl ether-type herbicides. Proc Natl Acad Sci USA 95: 10553–10558

Arnould S, Takahashi M and Camadro JM (1998) Stability of recombinant yeast protoporphyrinogen oxidase: effects of diphenyl ether-type herbicides and diphenyleneiodonium.

Biochemistry 37: 12818–12828
Battersby, AR (1994) How nature builds the pigments of life: the conquest of Vitamin B_{12}. Science 264: 1551–1557
Battersby AR, Fookes CJR, Gustafson-Potter KE, Matcham GWJ and McDonald E (1979a) Proof by synthesis that unrearranged hydroxymethylbilane is the product from deaminase and the substrate for cosynthetase in the biosynthesis of Uro'gen-III. J Chem Soc Chem Commun 1979: 1155–1158
Battersby AR, Fookes CJR, Matcham GWJ and McDonald E (1979b) Order of assembly of the four pyrrole rings during biosynthesis of the natural porphyrins. J Chem Soc Chem Commun 1979: 539–541
Battersby AR, Fookes CJR, Hart G, Matcham GWJ and Pandey PS (1983) Biosynthesis of porphyrins and related macrocycles. Part 21. The interaction of deaminase and its product (hydroxymethylbilane) and the relationship between deaminase and cosynthetase. J Chem Soc Perkin Trans: 3041–3047
Berthold DA and Stenmark P (2003) Membrane-bound diiron carboxylate proteins. Ann Rev Plant Biol 54: 497–517
Birchfield NB, Latli B and Casida JE (1998) Human protoporphyrinogen oxidase: Relation between the herbicide binding site and the flavin cofactor. Biochemistry 37: 6905–6910
Block MA, Tewari AK, Albrieux C, Maréchal E and Joyard J (2002) The plant *S*-adenosyl-*L*-methionine:Mg-protoporphyrin 1X methyltransferase is located in both envelope and thylakoid chloroplast membranes. Eur J Biochem 269: 240–248
Boese QF, Spano AJ, Li J and Timko MP (1991) Aminolevulinic acid dehydratase in pea (*Pisum sarivum* L.). J Biol Chem 266: 17060–17066
Bollivar DW and Beale SI (1995) Formation of the isocyclic ring of chlorophyll by isolated *Chlamydomonas reinhardtii* chloroplasts. Photosynth Res 43: 113–124
Bollivar DW and Beale SI (1996) The chlorophyll biosynthetic enzyme Mg-protoporphyrin IX monomethyl ester (oxidative) cyclase. Plant Physiol 112: 105–114
Bollivar DW, Jiang ZY, Bauer CE and Beale S (1994a) Heterologous expression of the *bchM* gene product from *Rhodobacter capsulatus* and demonstration that it encodes S-adenosyl-*L*-methionine: Mg-protoporphyrin 1X methyltransferase. J Bacteriol 176: 5290–5296
Bollivar DW, Suzuki JY, Beatty JT, Dobrowolski JM and Bauer CE (1994b) Directed mutational analysis of bacteriochlorophyll *a* biosynthesis in *Rhodobacter capsulatus*. J Mol Biol 237: 622–640
Breinig S, Kervinen J, Stith L, Wasson AS, Fairman R, Wlodawer A, Zdanov A and Jaffe EK (2003) Control of tetrapyrrole biosynthesis by alternate quaternary forms of porphobilinogen synthase. Nat Struct Biol 10: 757–763
Castelfranco PA, Weinstein JD, Schwarcz S, Pardo AD and Wezelman BE (1979) The Mg insertion step in chlorophyll biosynthesis. Arch Biochem Biophys 192: 592–598
Che F-S, Watanabe N, Iwano M, Inokuchi H, Takayama S, Yoshida S and Isogai A (2000) Molecular characterization and subcellular localization of protoporphyrinogen oxidase in spinach chloroplasts. Plant Physiol 124: 59–70
Chekounova E, Voronetskaya V, Papenbrock J, Grimm B and Beck CF (2001) Characterization of *Chlamydomonas* mutants defective in the H subunit of Mg-chelatase. Mol Gen Genet 266: 363–373
Chereskin BM, Wong YS and Castelfranco PA (1982) In vitro synthesis of the chlorophyll isocyclic ring. Transformation of Mg-protoporphyrin IX and Mg-protoporphyrin IX monomethyl ester into magnesium-2,4-divinylpheoporphyrin a_5. Plant Physiol 70: 987–993
Cheung KM, Spencer P, Timko MP and Shoolingin-Jordan PM (1997) Characterization of a recombinant pea 5-aminolevulinic acid dehydratase and comparative inhibition studies with the *Escherichia coli* dehydratase. Biochemistry 36: 1148–1156
Choi KW, Han O, Lee HJ, Yun YC, Moon YH, Kim M, Kuk YI, Han SU and Guh JO (1998) Generation of resistance to the diphenyl ether herbicide, oxyfluorfen, via expression of the *Bacillus subtilis* protoporphyrinogen oxidase gene in transgenic tobacco plants. Biosci Biotechnol Biochem 62: 558–560
Chow KS, Singh DP, Walker AR and Smith AG (1998) Two different genes encode ferrochelatase in *Arabidopsis*: Mapping, expression and subcellular targeting of the precursor proteins. Plant J 15: 531–541
Cornah JE, Roper JM, Singh DP and Smith AG (2002) Measurement of ferrochelatase activity using a novel assay suggests that plastids are the major site of haem biosynthesis in both photosynthetic and non-photosynthetic cells of pea (*Pisum sativum* L.). Biochem J 362: 423–432
Crockett N, Alefounder PR, Battersby AR and Abell C (1991) Uroporphyrinogen III synthase: Studies on its mechanism of action molecular biology and biochemistry. Tetrahedron 47: 6003–6014
Dailey HA, Daley TA, Wu CK, Medlock AE, Wang KF, Rose JP and Wang BC (2000) Ferrochelatase at the millennium: Structures, mechanisms and (2Fe-2S) clusters. Cell Mol Life Sci 57: 1909–1926
Duke SO, Becerril JM, Sherman TD, Lehnen LP and Matsumoto H (1991) Protoporphyrinogen oxidase-inhibiting herbicides. Weed Sci 39: 465–473
Ellsworth RK and Dullaghan JP (1972) Activity and properties of *S*-adenosyl-L-methionine: Magnesium-protoporphyrin IX methyltransferase in crude homogenates from wheat seedling. Biochim Biophys Acta 268: 327–333
Ellsworth RK, Dullaghan JP and St. Pierre ME (1974) The reaction mechanism of S-adenosyl-L-methionine: Magnesium protoporphyrin IX methyltransferase of wheat. Photosynth 8: 375–383
Erskine PT, Newbold R, Roper J, Coker A, Warren MJ, Shoolingin-Jordan PM, Wood SP and Cooper JB (1999) The Schiff base complex of yeast 5-aminolaevulinic acid dehydratase with laevulinic acid. Protein Sci 8: 1250–1256
Fodje MN, Hansson A, Hansson M, Olsen JG, Gough S, Willows RD and Al-Karadaghi S (2001) Interplay between an AAA module and an integrin I domain may regulate the function of magnesium chelatase. J Mol Biol 311: 111–122
Frankenberg N, Erskine PT, Cooper JB, Shoolingin-Jordan PM, Jahn D and Heinz DW (1999) High resolution crystal structure of a Mg^{2+}-dependent porphobilinogen synthase. J Mol Biol 289: 591–602
Gibson KD, Neuberger A and Tait GH (1963) Studies on the biosynthesis of porphyrin and bacteriochlorophyll by *Rhodopseudomonas spheriodes*. 4. S-adenosylmethionine-magnesium protoporphyrin methyltransferase. Biochem J 88: 325–334
Gibson LCD and Hunter CN (1994) The bacteriochlorophyll biosynthesis gene, bchM, of *Rhodobacter sphaeroides* encodes *S*-adenosyl-*L*-methionine: Mg protoporphyrin IX methyltransferase. FEBS Lett 352: 127–130
Gibson LCD, Willows RD, Kannangara CG, von Wettstein D

and Hunter CN (1995) Magnesium-protoporphyrin chelatase of *Rhodobacter sphaeroides*: Reconstitution of activity by combining the products of the *bchH, -I*, and *-D* genes expressed in *Escherichia coli*. Biochemistry 92: 1941–1944

Gibson LCD, Marrison JL, Leech RM, Jensen PE, Bassham DC, Gibson M and Hunter CN (1996) A putative Mg chelatase subunit from *Arabidopsis thaliana cv* C24. Plant Physiol 111: 61–71

Goericke R and Repeta DJ (1993) Chlorophylls *a* and *b* and divinyl chlorophylls *a* and *b* in the open subtropical North Atlantic Ocean. Mar Ecol Prog Ser 101: 307–313

Gorchein A (1972) Magnesium protoporphyrin chelatase activity in *Rhodopseudomonas sphaeroides* studies with whole cells. Biochem J 127: 97–106

Gorchein A, Gibson LCD and Hunter CN (1993) Gene expression and control of enzymes for synthesis of magnesium protoporphyrin monomethyl ester in *Rhodobacter sphaeroides*. Biochem Soc Trans 21: 201S

Gough SP, Petersen BO and Duus G (2000) Anaerobic chlorophyll isocyclic ring formation in *Rhodobacter capsulatus* requires a cobalamin cofactor. Proc Natl Acad Sci USA 97: 6908–6913

Grafe S, Saluz HP, Grimm B and Hanel F (1999) Mg-chelatase of tobacco: The role of the subunit CHL D in the chelation step of protoporphyrin IX. Proc Natl Acad Sci USA 96: 1941–1946

Guo R, Luo M and Weinstein JD (1998) Magnesium-chelatase from developing pea leaves. Characterization of a soluble extract from chloroplasts and resolution into three required protein fractions. Plant Physiol 116: 605–615

Hansson A, Kannangara CG, von Wettstein D and Hansson M (1999) Molecular basis for semidominance of missense mutations in the XANTHA-H (42-kDa) subunit of magnesium chelatase. Proc Natl Acad Sci USA 96: 1744–1749

Hansson A, Willows RD, Roberts TH and Hansson M (2002) Three semidominant barley mutants with single amino acid substitutions in the smallest magnesium chelatase subunit form defective AAA^+ hexamers. Proc Natl Acad Sci USA 99: 13944–13949

Hart GJ, and Battersby AR (1985) Purification and properties of uroporphyrinogen III synthase (co-synthase) from *Euglena gracilis*. Biochem J 232: 151–160

Hart GJ, Miller AD and Battersby AR (1987) Evidence that the pyrromethane cofactor of hydroxymethylbilane synthase (porphobilinogen deaminase) is bound through the sulfur atom of a cystein residue. Biochem J 252: 909–912

Higuchi M and Bogorad L (1975) The purification and properties of uroporphyrinogen I synthase and uroporphyrinogen III cosynthase. Interaction between the enzymes. Ann NY Acad Sci 244: 401–418

Hinchigeri SB, Hundle B and Richards WR (1997) Demonstration that the BchH protein of *Rhodobacter capsulatus* activates S-adenosyl-L-methionine:magnesium protoporphyrin IX methyltransferase. FEBS Lett 407: 337–342

Hiriart J-B, Lehto K, Tyystjärvi, Junttila T and Aro E-M (2002) Suppression of a key gene involved in chlorophyll biosynthesis by means of virus-inducing gene silencing. Plant Mol Biol 50: 213–224

Hu G, Yalpani N, Briggs SP and Johal GS (1998) A porphyrin pathway impairment is responsible for the phenotype of a dominant disease lesion mimic mutant of maize. Plant Cell 10: 1095–1105

Hudson A, Carpenter R, Doyle S and Coen ES (1993*) Olive*: A key gene required for chlorophyll biosynthesis in *Antirrhinum majus*. EMBO J 12: 3711–3719

Ishikawa A, Okamoto H, Iwasaki Y and Asahi T (2001) A deficiency of coproporphyrinogen III oxidase causes lesion formation in *Arabidopsis*. Plant J 27: 89–99

Jacobs JM and Jacobs NJ (1987) Oxidation of protoporphyrinogen to protoporphyrin, a step in chlorophyll and haem biosynthesis. Biochem J 244: 219–224

Jacobs JM and Jacobs NJ (1993) Porphyrin accumulation and export by isolated barley (*Hordeum vulgare*) plastids. Plant Physiol 101: 1181–1187

Jensen PE, Gibson LCD, Henningsen KW and Hunter CN (1996a) Expression of the *chlI, chlD,* and *chlH* genes from the cyanobacterium *Synechocystis* PCC6803 in *Escherichia coli* and demonstration that the three cognate proteins are required for magnesium-protoporphyrin chelatase activity. J Biol Chem 271: 16662–16667

Jensen PE, Willows RD, Petersen BL, Vothknecht UC, Stummann BM, Kannangara CG, von Wettstein D and Henningsen KW (1996b) Structural genes for Mg-chelatase subunits in barley: Xantha-*f*, *-g* and *-h*. Mol Gen Genet 250: 383–394

Jensen PE, Gibson LCD and Hunter CN (1999a) ATPase activity associated with the magnesium-protoporphyrin IX chelatase enzyme of *Synechocystis* PCC6803: evidence for ATP hydrolysis during Mg^{2+} insertion, and the MgATP-dependent interaction of the ChlI and ChlD subunits. Biochem J 339: 127–134

Jensen PE, Gibson LCD, Shephard F, Smith V and Hunter CN (1999b) Introduction of a new branchpoint in tetrapyrrole biosynthesis in *Escherichia coli* by co-expression of genes encoding the chlorophyll-specific enzymes magnesium chelatase and magnesium protoporphyrin methyltransferase. FEBS Lett 455: 349–354

Jordan PM (1991) The biosynthesis of 5-aminolevulinic acid and its transformation into uroporphyrinogen III. In: Jordan PM (ed) Biosynthesis of Tetrapyrroles, New Comprehensive Biochemistry, Vol 19, pp 1–86. Elsevier, Amsterdam

Jordan PM and Seehra JS (1979) The biosynthesis of uroporphyrinogen III. Order of assembly of the four porphobilinogen molecules in the formation of the tetrapyrrole ring. FEBS Lett 104: 364–366

Jordan PM and Warren MJ (1987) Evidence for a dipyrromethane cofactor at the catalytic site of *Escherichia coli* porphobilinogen deaminase. FEBS Lett 225: 87–92

Kaczor CM, Smith MW, Sangwan I and O'Brian MR (1994) Plant δ-aminolevulinic acid dehydratase. Plant Physiol 104: 1411–1417

Kjemtrup S, Sampson KS, Peele CG, Hguyen LV, Conkling MA, Thompson WF and Robertson D (1998) Gene silencing from plant DANN carried by a Geminivirus. Plant J 14: 91–100

Koch M, Breithaupt C, Kiefersauer R, Freigang J, Huber R and Messerschmidt A (2004) Crystal structure of protoporphyrinogen IX oxidase: A key enzyme in haem and chlorophyll biosynthesis. EMBO J 23:1720–1728.

Koncz C, Mayerhofer R, Koncz-Kalman Z, Nawrath C, Reiss B, Redei GP and Schell J (1990) Isolation of a gene encoding a novel chloroplast protein by T-DNA tagging in *Arabidopsis thaliana*. EMBO J 9: 1337–1346

Kruse E, Mock HP and Grimm B (1995a) Coproporphyrinogen III oxidase from barley and tobacco — sequence analysis and initial expression studies. Planta 196: 796–803

Kruse E, Mock H-P and Grimm B (1995b) Reduction of copro-

porphyrinogen oxidase level by antisense RNA synthesis leads to deregulated gene expression of plastid proteins and affects the oxidative defense system. EMBO J 14: 3712–3720

Kruse E, Mock HP and Grimm B (1997) Isolation and characterisation of tobacco (*Nicotiana tabacum)* cDNA clones encoding proteins involved in magnesium chelation into protoporphyrin IX. Plant Mol. Biol 35: 1053–1056

Lecerof D, Fodje M, Hansson A, Hansson M and Al-Karadaghi S (2000) Structural and mechanistic basis of porphyrin metallation by ferrochelatase. J Mol Biol 297: 221–232

Lee HJ, Ball MD, Parham R and Rebeiz CA (1992) Chloroplast Biogenesis 65. Enzymic conversion of protoporphyrin IX to Mg-protoporphyrin IX in a subplastidic membrane fraction of cucumber etiochloroplasts. Plant Physiol 99: 1134–1140

Lee HJ, Lee SB, Chung JS, Han SU, Han O, Guh JO, Jeon JS, An G and Back K (2000) Transgenic rice plants expressing a *Bacillus subtilis* protoporphyrinogen oxidase gene are resistant to diphenyl ether herbicide oxyfluorfen. Plant Cell Physiol 41: 743–749

Lermontova I and Grimm B (2000) Overexpression of plastidic protoporphyrinogen IX oxidase leads to resistance to the diphenyl-ether herbicide acifluorfen. Plant Physiol. 122: 75–84

Lermontova I, Kruse E, Mock H-P and Grimm B (1997) Cloning and characterization of a plastidal and a mitochondrial isoform of tobacco protoporphyrinogen 1X oxidase. Proc Natl Acad Sci USA 94: 8895–8900

Li X, Vollrath S, Nicholl DBG, Chilcott CE, Johnson MA, Ward ER and Law MD (2003) Development of protoporphyrinogen oxidase as an efficient selection marker for *Agrobacterium tumefaciens*-mediated transformation of maize. Plant Physiol 133: 736–747

Lim SI, Witty M, Wallace-Cook ADM, Hag LI and Smith AG (1994) Porphobilinogen deaminase is encoded by a single gene in *Arabidopsis thaliana* and is targeted to the chloroplasts. J Mol Biol 26: 863–872

Lister R, Chew O, Rudhe C, Lee M-N and Whelan J (2001) *Arabidopsis thaliana* ferrochelatase-I and -II are not imported into *Arabidopsis* mitochondria. FEBS Lett 506: 291–295

Louie GV, Brownlie PD, Lambert R, Cooper JB, Blundell TL, Wood SP, Malashkevich VN, Hadener A, Warren MJ and Schoolingin-Jordan PM (1996) The three-dimensional structure of *Escherichia coli* porphobilinogen deaminase at 1.76-Å resolution. Proteins 25: 48–78

Luo J and Lim CK (1993) Order of uroporphyrinogen III decarboxylation on incubation of porphobilinogen and uroporphyrinogen III with erythrocyte uroporphyrinogen decarboxylase. Biochem J 289: 529–532.

Luo M, Weinstein JD and Walker CJ (1999) Magnesium chelatase subunit D from pea: Characterization of the cDNA, heterologous expression of an enzymatically active protein and immunoassay of the native protein. Plant Mol Biol 41: 721–731

Martins BM, Grimm B, Mock H-P, Huber R and Messerschmidt A (2001Crystal structure and substrate binding modeling of the uroporphyrinogen-III decarboxylase from *Nicotiana tabacum*. Implications for the catalytic mechanism. J Biol Chem 276: 44108–44116

Masuda T, Suzuki T, Shimada H, Ohta H and Takamiya K (2003) Subcellular localization of two types of ferrochelatase in cucumber. Planta 217: 602–609

Mathews MA, Schubert HL, Whitby FG, Alexander KJ, Schadick K, Bergonia HA, Phillips JD and Hill CP (2001). Crystal structure of human uroporphyrinogen III synthase. EMBO J 20: 5832–5839

Matringe M and Scalla R (1988) Effects of acifluorfen-methyl on cucumber cotyledons: Porphyrin accumulation. Pestic Biochem Physiol 32: 164–172

Matringe M, Camadro JM, Joyard J and Douce R (1994) Localization of ferrochelatase activity within mature pea chloroplasts. J Biol Chem 269: 15010–15015

Matters GL and Beale SI (1995a) Structure and expression of the *Chlamydomonas reinhardtii alad* gene encoding the Chl biosynthetic enzyme, δ-aminolevulinic acid dehydratase (porphobilinogen synthase). Plant Mol Biol 27: 607–617

Matters GL and Beale SI (1995b) Blue-light-regulated expression of genes for two early steps of chlorophyll biosynthesis in *Chlamydomonas reinhardtii*. Plant Physiol 109: 471–479

Miyamoto K, Tanaka R, Teramoto H, Masuda T, Tsuji H and Inokuchi H (1994) Nucleotide sequence of cDNA clones encoding ferrochelatase from barley and cucumber. Plant Physiol 105: 769–770

Mochizuki N, Brusslan JA, Larkin R, Nagatani A and Chory J (2001*) Arabidopsis genomes uncoupled 5 (GUN5)* mutant reveals the involvement of Mg-chelatase H subunit in plastid-to-nucleus signal transduction. Proc Natl Acad. Sci USA 98: 2053–2058

Mock HP and Grimm B (1997) Reduction of uroporphyrinogen decarboxylase by antisense RNA expression affects activities of other enzymes involved in tetrapyrrole biosynthesis and leads to light-dependent necrosis. Plant Physiol 113: 1101–1112

Mock HP, Trainotti L, Kruse E and Grimm B (1995) Isolation, sequencing and expression of cDNA sequences encoding uroporphyrinogen decarboxylase from tobacco and barley. Plant Mol Biol 28: 245–256

Mock HP, Keetman U, Kruse E, Rank B and Grimm B (1998) Defense responses to tetrapyrrole-induced oxidative stress in transgenic plants with reduced uroporphyrinogen decarboxylase or coproporphyrinogen oxidase activity. Plant Physiol 116: 107–116

Mock HP, Heller W, Molina A, Neubohn B, Sandermann H, Jr. and Grimm B (1999) Expression of uroporphyrinogen decarboxylase or coproporphyrinogen oxidase antisense RNA in tobacco induces pathogen defense responses conferring increased resistance to tobacco mosaic virus. J Biol Chem 274: 4231–4238

Molina A, Volrath S, Guyer D, Maleck K, Ryals J and Ward E (1999) Inhibition of protoporphyrinogen oxidase expression in *Arabidopsis* causes a lesion-mimic phenotype that induces systemic acquired resistance. Plant J 17: 667–678

Moseley JL, Allinger T, Herzog S, Hoerth P, Wehinger E, Merchant S and Hippler M (2002) Adaptation to Fe-deficiency requires remodeling of the photosynthetic apparatus. EMBO J 21: 6709–6720

Murphy MJ and Siegel LM (1973) Sirohaem and sirohydrochlorin. The basis for a new type of porphyrin-relatedf prosthetic group common to both assimilatory and dissimilatory sulfite reductases. J Biol Chem 248: 6911–6919

Nagata N, Tanaka R, Satoh S and Tanaka A (2005) Identification of a vinyl reductase gene for chlorophyll synthesis in *Arabidopsis thaliana* and implications for the evolution of *Prochlorococcus* species. Plant Cell 17: 233–240

Nakayama M, Masuda T, Bando T, Yamagata H, Ohta H and Takamiya K-i (1998) Cloning and expression of the soybean

chlH gene encoding a subunit of Mg-chelatase and localization of the Mg^{2+} concentration-dependent ChlH protein within the chloroplast. Plant Cell Physiol 39: 275–284

Nasrulhaq-Boyce A, Griffiths WT and Jones OTG (1987) The use of continuous assays to characterize the oxidative cyclase that synthesizes the chlorophyll isocyclic ring. Biochem J 243: 23–29

Orsat B, Monfort A, Chatellard P and Stutz E (1992) Mapping and sequencing of an actively transcribed *Euglena gracilis* chloroplast gene (*ccsA*) homologous to the *Arabidopsis thaliana* nuclear gene *cs* (*ch42*). FEBS Lett 303: 181–184

Papenbrock J, Gräfe S, Kruse E, Hänel F and Grimm B (1997) Mg-chelatase of tobacco: Identification of a *Chl D* cDNA sequence encoding a third subunit, analysis of the interaction of the three subunits with the yeast two-hybrid system, and reconstitution of the enzyme activity by co-expression of recombinant CHL D, CHL H and CHL I. Plant J 12: 981–990

Papenbrock J, Mock H-P, Kruse E and Grimm B (1999) Expression studies in tetrapyrrole biosynthesis: Inverse maxima of magnesium chelatase and ferrochelatase activity during cyclic photoperiods. Planta 208: 264–273

Papenbrock J, Mock H-P, Tanaka R, Kruse E and Grimm B (2000a) Role of magnesium chelatase activity in the early steps of the tetrapyrrole biosynthetic pathway. Plant Physiol 122: 1161–1169

Papenbrock J, Pfündel E, Mock H-P and Grimm B (2000b) Decreased and increased expression of the subunit CHL I diminishes Mg chelatase activity and reduces chlorophyll synthesis in transgenic tobacco plants. Plant J 22: 155–164

Papenbrock J, Mishra S, Mock H-P, Kruse E, Schmidt E-K, Petersmann A, Braun H-P and Grimm B (2001) Impaired expression of the plastidic ferrochelatase by antisense RNA synthesis leads to a necrotic phenotype of transformed tobacco plants. Plant J 28: 41–50

Parham R and Rebeiz CA (1992) Chloroplast biogenesis: [4-Vinyl] chlorophyllide *a* reductase is a divinyl chlorophyllide *a*-specific, NADPH-dependent enzyme. Biochemistry 31: 8460–8464

Petersen BL, Jensen PE, Gibson LCD, Stummann BM, Hunter CN and Henningsen KW (1998) Reconstitution of an active magnesium chelatase enzyme complex from the *bchl, -D,* and *-H* gene products of the green sulfur bacterium *Chlorobium vibrioforme* expressed in *Escherichia coli*. J Bacteriol 180: 699–704

Petersen BL, Møller MG, Jensen PE and Henningsen KW (1999) Identification of the *Xan-g* gene and expression of the Mg-chelatase encoding genes *Xan-f*, *-g* and *-h* in mutant and wild type barley *(Hordeum vulgare* L*)*. Hereditas 131: 165–170

Pinta V, Picaud M, Reiss-Husson F and Astier C (2002) *Rubrivivax gelantinosus acsF* (previously *orf358*) codes for a conserved, putative binuclear-iron-cluster-containing protein involved in aerobic oxidative cyclization of Mg-protoporphyrin IX monomethylester. J Bacteriol 184: 746–753

Porra RJ and Lascelles J (1968) Studies on ferrochelatase: the enzymic formation of haem in proplastids, chloroplasts and plant mitochondria. Biochem J 108: 343–348

Porra RJ, Barnes R and Jones OTG (1973) The over-production of poprphyrins by semi-anaerobic yeast. Enzyme 16: 1–8

Porra RJ, Schäfer W, Katheder I and Scheer H (1995) The derivation of the oxygen atoms of the 13´-oxo and 3-acetyl groups of bacteriochlorophyll *a* from water in *Rhodobacter sphaeroides* cells adapting from respiratory to photosynthetic conditions: evidence for an anaerobic pathway for the formation of isocyclic ring E. FEBS Lett 371: 21–24

Porra RJ, Urzinger M, Winkler J, Bubenzer C, and Scheer H (1998) Biosynthesis of the 3-acetyl and 13^1-oxo groups of bacteriochlorophyll *a* in the facultative aerobic bacterium, *Rhodovulum sulfidophilum:* The presence of both oxygenase and hydratase pathways for isocyclic ring formation. Eur J Biochem 252: 185–191

Randolph-Anderson BL, Sato R, Johnson AM, Harris EH, Hauser CR, Oeda K, Ishige F, Nishio S, Gillham NW and Boynton JE (1998) Isolation and characterization of a mutant protoporphyrinogen oxidase gene from *Chlamydomonas reinhardtii* conferring resistance to porphyric herbicides. Plant Mol Biol 38: 839–859

Rebeiz CA, Wu SM, Kuhagja M, Daniell H and Perkins EJ (1983) Chlorophyll *a* biosynthetic routes and chlorophyll *a* chemical heterogeneity in plants. Mol Cell Biochem 57: 97–125

Rimington C and Miles PA (1951) A study of porphyrins excreted in the urine by a case of congenital porphyria . Biochem J 50: 202–206

Rissler HM, Collakova E, DellaPenna D, Whelan J and Pogson BJ (2002) Chlorophyll biosynthesis. Expression of a second *Chl I* gene of magnesium chelatase in *Arabidopsis* supports only limited chlorophyll synthesis. Plant Physiol 128: 770–779

Roper JM and Smith AG (1997) Molecular localization of ferrochelatase in higher plant chloroplasts. Eur J Biochem 246: 32–37

Santana MA, Pihakaski-Maunsbach K, Sandal N, Marcker KA and Smith AG (1998) Evidence that the plant host synthesizes the heme moiety of leghemoglobin in root nodules. Plant Physiol 116: 1259–1269

Scalla R, Matringe M, Camadro JM and Labbe P (1990) Recent advances in the mode of action of diphenyl ether and related herbicides. Z Naturforsch 45c: 503–511

Schaumburg A and Schneider-Poetsch HAW (1992) Characterization of plastid 5-aminolevulinate dehydratase (ALAD; EC 4.2.1.24) from spinach (*Spinacia oleracea*) by sequencing and comparison with non-plant ALAD enzymes. Z Naturforsch 47c: 77–84

Schubert HL, Raux E, Matthews MA, Phillips JD, Wilson KS, Hill CP and Warren MJ (2002) Structural diversity in metal ion chelation and the structure of uroporphyrinogen III synthase. Biochem Soc Trans 30: 595–600

Senior NM, Brocklehurst K, Cooper JB, Wood SP, Erskine P, Shoolingin-Jordan PM, Thomas PG and Warren MJ (1996) Comparative studies on the 5-aminolaevulinic acid dehydratases from *Pisum sativum*, *Escherichia coli* and *Saccharomyces cerevisiae*. Biochem J 320: 401–412

Shalygo NV, Averina NG, Grimm B and Mock H-P (1997) Influence of cesium on tetrapyrrole biosynthesis in etiolated and greening barley leaves. Physiol Plant 99: 160–168

Shalygo NV, Mock H-P, Averina NG and Grimm B (1998) Photodynamic action of uroporphyrin and protochlorophyllide in greening barley leaves treated with cesium chloride. J Photochem Photobiol 42: 151–158

Singh DP, Cornah JE, Hadingham S and Smith AG (2002) Expression analysis of the two ferrochelatase genes in *Arabidopsis* in different tissues and under stress conditions reveals their different roles in haem biosynthesis. Plant Mol Biol 50: 773–788

Smith AG (1988) Subcellular localization of two porphyrin-synthesis enzymes in *Pisum sativum* (pea) and *Arum* (cuckoo-pint)

species. Biochem J 249: 423–428

Smith AG, Marsh O and Elder GH (1993) Investigation of the subcellular location of the tetrapyrrole-biosynthesis enzyme coproporphyrinogen oxidase in higher plants. Biochem J 292: 503–508

Smith AG, Santana MA, Wallace-Cook AD, Roper JM and Labbe-Bois R (1994) Isolation of cDNA encoding chloroplast ferrochelatase from *Arabidopsis thaliana* by functional complementation of a yeast mutant. J Biol Chem 259: 13405–13413

Smith CA, Suzuki JY and Bauer CE (1996) Cloning and characterization of the chlorophyll biosynthesis gene *chlM* from *Synechocystis* PCC 6803 by complemention of a bacteriochlorophyll biosynthesis mutant of *Rhodobacter capsulatus.* Plant Mol Biol 30: 1307–1314

Stark WM, Hawker CJ, Hart GJ, Philippides A, Petersen PM, Lewis JD, Leeper FJ and Battersby AR (1993) Biosynthesis of porphyrins and related macrocycles. Part 40. Synthesis of a spiro-lactam related to the proposed spiro-intermediate for porphyrin biosynthesis: Inhibition of cosynthetase. J Chem Soc Perkin Trans I 1993: 2875–2891

Suzuki JY and Bauer CE (1995) Altered monovinyl and divinyl protochlorophyllide pools in *bchJ* mutants of *Rhodobacter capsulatus.* Possible monovinyl substrate discrimination of light-independent protochlorophyllide reductase. J Biol Chem 270: 3732–3740

Suzuki T, Masuda T, Inokuchi H, Shimada H, Ohta H and Takamiya K-i (2000) Overexpression, enzymatic properties and tissue localization of a ferrochelatase of cucumber. Plant Cell Physiol 41: 192–199

Suzuki T, Masuda T, Singh DP, Tan F-C, Tohru T, Shimada H, Ohta H, Smith AG and Takamiya K-i (2002) Two types of ferrochelatase in photosynthetic and non- photosynthetic tissues of cucumber; their difference in phylogeny, gene expression and localization. J Biol Chem 277: 4731–4737

Tripathy BC and Rebeiz CA (1988) Chloroplast biogenesis 60: Conversion of divinyl protochlorophyllide to monovinyl protochlorophyllide in green(ing) barley, a dark monovinyl/light divinyl plant species. Plant Physiol 87: 89–94

Walker CJ and Weinstein JD (1991) In vitro assay of the chlorophyll biosynthetic enzyme Mg-chelatase: Resolution of the activity into soluble and membrane-bound fractions. Biochemistry 88: 5789–5793

Walker CJ and Willows RD (1997) Mechanism and regulation of Mg-chelatase. Biochem J 327: 321–333

Walker CJ, Castelfranco PA and Whyte BJ (1991) Synthesis of divinyl protochlorophyllide. Enzymological properties of the Mg-protoporphyrin 1X monomethyl ester oxidative cyclase system. Biochem J 276: 691–697

Watanabe N, Che F-S, Iwano M, Takayama S, Nakano T, Yoshida S and Isogai A (1998) Molecular characterization of photomixotrophic tobacco cells resistant to protoporphyrinogen oxidase-inhibiting herbicides. Plant Physiol 118: 751–758

Watanabe N, Che F-S, Iwano M, Takayama S, Yoshida S and Isogai A (2001) Dual targeting of spinach protoporphyrinogen oxidase II to mitochondria and chloroplasts by alternative use of two in-frame initiation codons. J Biol Chem 276: 20474–20481

Watanabe N, Takayama S, Yoshida S, Isogal A and Fang-Sik C (2002) Resistance to protoporphyrinogen oxidase-inhibiting compound S23142 from overproduction of mitochondrial protoporphyrinogen oxidase by gene amplification in photomixotrophic tobacco cells. Biosci Biotechnol Biochem 66: 1799–1805

Whitby FG, Phillips JD, Kushner JP and Hill CP (1998) Crystal structure of human uroprophyrinogen decarboxylase. EMBO J 17: 2463–2471

Whyte BJ, Vijayan P and Castelfranco PA (1992) In vitro synthesis of protochlorophyllide: effects of Mg^{2+} and other cations on the reconstituted (oxidative) cyclase. Plant Physiol Biochem 30: 279–284

Willows RD and Beale SI (1998) Heterologous expression of the *Rhodobacter capsulatus bchI, -D*, and *-H* genes that encode magnesium chelatase subunits and characterization of the reconstituted enzyme. J Biol Chem 273: 34206–34213

Willows RD, Gibson LCD, Kanangara CG, Hunter CN and von Wettstein D (1996) Three separate proteins constitute the magnesium chelatase of *Rhodobacter sphaeroides.* Eur J Biochem 235: 438–445

Witty M, Wallace-Cook ADM, Albrecht H, Spano AJ, Michel H, Shabanowitz J, Hunt DF, Timko MP and Smith AG (1993) Structure and expression of chloroplast-localized porphobilinogen deaminase from pea (*Pisum sativum* L.) isolated by redundant polymerase chain reaction. Plant Physiol 103: 139–147

Wong Y-S and Castelfranco PA (1984) Properties of the Mg-protoporphyrin IX monomethyl ester (oxidative) cyclase system. Plant Physiol 79: 730–733

Wong Y-S, Castelfranco PA, Goff DA and Smith KM (1985) Intermediates in the formation of the chlorophyll isocyclic ring. Plant Physiol 79: 725–729

Wu CK, Dailey HA, Rose JP, Burden A, Sellers VM and Wang BC (2001) The 2.0 A structure of human ferrochelatase, the terminal enzyme of heme biosynthesis. Nat Struct Biol 8: 156–160

Zheng CC, Porat R, Lu P and O'Neill SD (1998) PNZIP is a novel mesophyll-specific cDNA that is regulated by phytochrome and the circadian rhythm and encodes a protein with a leucine zipper motif. Plant Physiol 116: 27–35

Chapter 14

Biosynthesis of Chlorophylls *a* and *b*: The Last Steps

Wolfhart Rüdiger*
Botanisches Institut, Universität München, D-86038 München, Germany

Summary

The last steps of chlorophylls (Chls) *a* and *b* biosynthesis comprise the formation of chlorophyllide (Chlide) *a* from protochlorophyllide (PChlide) *a*, the oxygenation of Chlide *a* to Chlide *b*, the esterification of Chlides to the corresponding Chls, and the reduction of *b*-type pigments to *a*-type pigments. Two separate pathways exist for the biosynthesis of Chls, a light-dependent and a light-independent (dark) pathway. The decisive step is the hydrogenation of PChlide *a* to Chlide *a*, catalyzed either by a light-dependent PChlide oxidoreductase (POR) or by a light-independent PChlide oxidoreductase (DPOR, D for dark). The conversion of *a*- to *b*-type pigments and conversely of *b*- to *a*-type pigments, the 'chlorophyll cycle,' presumably allows the plants to adjust the Chl *a/b* ratio to the environment: the reduction of Chl *b* to Chl *a* precedes the degradation of the *b*-type pigment. This chapter describes the last steps of Chl biosynthesis with emphasis on the enzymes that catalyze the individual steps: included are discussions of the corresponding genes and recombinant enzymes.

Supplementary material to this chapter is available at: http://epub.ub.uni-muenchen.de/archive/00000776/

*Email: ruediger@botanik.biologie.uni-muenchen.de

Bernhard Grimm, Robert J. Porra, Wolfhart Rüdiger and Hugo Scheer (eds): Chlorophylls and Bacteriochlorophylls: Biochemistry, Biophysics, Functions and Applications, pp. 189–200.

I. Introduction

Angiosperms synthesize chlorophylls (Chls) *a* and *b* only in the light. The enzymatic steps leading to the formation of protochlorophyllide (PChlide) *a* take place in darkness in all higher plants including angiosperms: the light-dependent step and all subsequent steps are the 'last steps' of Chl biosynthesis. The light-dependent step is the photoconversion of PChlide *a* to chlorophyllide (Chlide) *a* catalyzed by NADPH:protochlorophyllide oxidoreductase (POR). Phototrophic bacteria, cyanobacteria, algae, mosses, ferns and most gymnosperms synthesize Chl also in the absence of light. These organisms contain an alternative, light-independent enzyme (DPOR) for the conversion of PChlide *a* to Chlide *a*. The light-independent pathway is the sole pathway in anoxygenic photosynthetic bacteria, leading to the formation of bacteriochlorophylls (BChls), and the light-dependent pathway is the only pathway in angiosperms, leading to Chls *a* and *b*. Both pathways coexist in cyanobacteria, algae, mosses, ferns, and gymnosperms; these organisms have the advantage that after deletion of one pathway (e.g,. by mutation) the other can still maintain Chl synthesis. It is not yet known how much each pathway contributes to Chl formation under normal physiological conditions.

This chapter deals with the formation of Chls *a* and *b* from PChlide *a* with emphasis on the enzymes for the single steps. Fig. 1 gives an overview over these steps, cross-correlations to other biosynthetic routes, not discussed in this chapter, are indicated in brackets.

II. Protochlorophyllide Reduction

A. The Light-independent Reaction

Only some recent results are discussed here; for more details see the review by Armstrong (1998). The first indication that the DPOR consists of three subunits came from genetic studies which demonstrated that three genes, *bchL, bchN* and *bchB* in photosynthetic bacteria and *chlL, chlN* and *chlB* in cyanobacteria and algae, are involved in PChlide reduction. Surprisingly, the deduced amino acid sequences were found to possess a high degree of similarity to the sequences of NifH, NifD and NifK, the subunits of nitrogenase, leading to the speculation that DPOR, like nitrogenase, receives reduction equivalents from ferredoxin in an ATP-dependent reaction. Convincing proof of the composition of DPOR came from the reconstitution of the active enzyme from the isolated BchL, BchN and BchB subunits, purified after overexpression of their genes in *Rhodobacter* (*Rba.*) *capsulatus* (Fujita and Bauer, 2000). The in vitro reduction of PChlide *a* to Chlide *a* required all three subunits, ATP and an ATP-regenerating system but, instead of ferredoxin, dithionite was used as electron donor. Fujita and Bauer (2000) discuss the relationship of the BchB/BchN complex of DPOR to the NifE/NifN complex: the latter is presumed to provide a framework on which the MoFe-containing cofactor of nitrogenase is constructed prior to its transfer to the NifD/NifK nitrogen reductase protein. The number and position of cysteine residues indicate 4Fe-4S clusters in the DPOR-BchB/BchN complex as in the NifE/NifN complex while NifD/NifK contains 8Fe:7S P-clusters.

B. The Light-dependent Reaction

The observation that angiosperms fail to synthesize Chl when kept in complete darkness but become green when exposed to light prompted, over the years, many investigations of the light-dependent step of Chl biosynthesis catalyzed by POR. Recently, a resurgence of interest in this reaction occurred because it is a rare example where substrate binding can be separated from the commencement of the reaction: substrate and cosubstrate bind to the enzyme in darkness and subsequently the reaction is started by a suitable flash of light permitting even the fast initial phase of the reaction, in the ps or sub-ps range, to be investigated, which is not possible in most enzyme reactions.

While chloroplasts are formed from proplastids in the light, etioplasts develop in darkness. Etioplasts

Abbreviations: A. – Arabidopsis; BChl – bacteriochlorophyll; *C. – Chlamydomonas;* CAO – chlorophyllide *a* oxygenase; *Cfl. – Chloroflexus;* Chl – chlorophyll, the esterifying alcohol is indicated by subscripts, e.g. Chl_{GG} for Chl esterified with geranyl-geraniol; Chlide – chlorophyllide; DPOR – light-independent (= dark) protochlorophyllide reductase; *E. – Escherichia;* GG – geranyl-geraniol; GGPP – geranyl-geranyl-pyrophosphate; LHCB – light-harvesting chlorophyll protein of photosystem II, often also termed LHCII; PChlide – protochlorophyllide; Phe – pheophytin; Pheide – pheophorbide; PhyPP – phytyl-pyrophosphate; PLB – prolamellar body; POR – NADPH:protochlorophyllide oxidoreductase, light-dependent; PPheide – protopheophorbide; PS I – photosystem I; PT – prothylakoid; *Rba. – Rhodobacter*

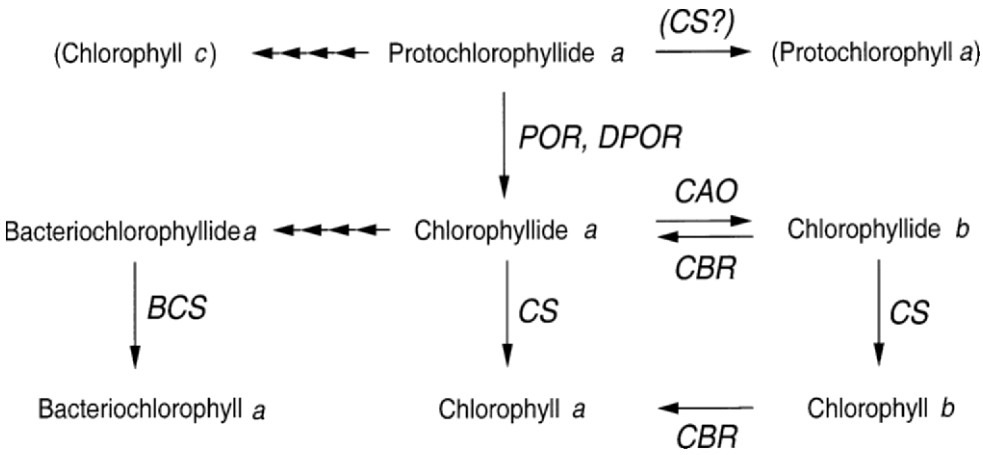

Fig. 1. Overview of the last steps of Chl biosynthesis. Two alternative pathways lead from protochlorophyllide *a* to chlorophyllide *a*: a light-dependent (catalyzed by LPOR) and a light-independent pathway (catalyzed by DPOR). The enzymes discussed in this chapter and indicated in the figure are: *POR*, NADPH:protochlorophyllide oxidoreductase; *CAO*, chlorophyllide *a* oxygenase, *CBR*, chlorophyll(ide) *b* reductase and 7^1-hydroxy-chlorophyll(ide) *a* reductase; *CS*, chlorophyll synthase; *BCS*, bacteriochlorophyll synthase. In brackets are the pathways to chlorophyll *c* and protochlorophyll *a*, which are not treated in this chapter.

contain typical inner membranes known as prolamellar bodies (PLBs) and prothylakoids (PTs). There is a close connection between the PLB structure and the accumulation of POR. The regular structure of PLBs depends on the presence of the pigment-POR complex and 98% of the protein of PLBs is POR (Ryberg and Sundqvist, 1991): in the *cop 1* photomorphogenic mutant which has nearly no POR and lacks PLBs, the formation of PLBs can be restored by overexpressing POR (Sperling et al., 1998).

When etiolated plants are transferred from darkness to light, etioplasts develop into chloroplasts. In the first step, PTs protrude out of the PLBs which can be observed only 2–5 min after a single flash of light (Domanskii et al., 2003). Interestingly, POR is translocated by illumination from PLBs into the growing PTs (Ryberg and Dehesh, 1986). The transformation of PLBs, a lipid tubular system with a bicontinuous cubic phase organization, into the lamellar lipid phase of PTs is generally believed to be triggered by the phototransformation of PChlide into Chlide indicating that the NADPH:PChlide-POR complex acts as photoreceptor for this process; however, the participation of other photoreceptors cannot be excluded at present.

C. POR Genes and Proteins

The first POR gene to be isolated, now called *PORA*, was obtained from barley (reviewed by Schulz and Senger, 1993). Its down-regulation by light, leading to nearly complete disappearance of the POR protein at the onset of maximum Chl synthesis, was considered a paradox until a second constitutively-expressed gene, *PORB*, was detected in barley (Holtorf et al., 1995) and in *Arabidopsis* (*A.*) *thaliana* (Armstrong et al., 1995). Even a third gene, *PORC*, which is up-regulated by light is present in *A. thaliana* (Oosawa et al., 2000). The different expression patterns indicate specific roles for the different POR enzymes during development in the dark and in the light, an assumption, which was verified by investigation of *Arabidopsis* mutants deficient in either one or other of the *POR* genes (Masuda et al., 2003). Attempts to demonstrate completely different functions for different POR proteins failed: PORA and PORB are redundant for PLB formation and for photoprotection of plants (Sperling et al., 1998), different mechanisms for the import of the precursor proteins pPORA and pPORB into the plastids (Reinbothe et al., 2000) were questioned (Aronsson et al., 2000; 2003a; 2003b), and the proposal of a light-harvesting role, specific for PORA (Reinbothe et al., 1999; 2003b) was rejected by others (Armstrong et al., 2000; Franck et al., 2000). The notion of such different functions can also be questioned because only one *POR* gene was detectable in pea (Sundqvist and Dahlin, 1997), cucumber (Fusada et al., 2000), *Chlamydomonas* (*C.*) *reinhardtii* (Li and Timko, 1996) and cyanobacteria (Rowe and Griffiths, 1995; Suzuki and Bauer, 1995).

Early in vitro investigations on the activity of POR were performed with etioplasts or etioplast membrane fractions (reviewed by Griffiths, 1991). POR occurs as a photoactive ternary complex together with NADPH and PChlide *a* in these preparations, and the availability of only the preformed enzyme-substrate complex sets certain limitations for the investigation of the enzyme reaction. The isolation of pigment-free POR from oat etioplasts was more-recently described (Klement et al., 1999). Alternatively, pigment-free POR has been obtained by heterologous expression of *POR* genes in *Escherichia* (*E.*) *coli*; for example, the *POR* gene from pea (Martin et al., 1997), *PORB* from barley (Lebedev and Timko, 1999) and *POR* from *Synechoystis* (Heyes et al., 2000, 2003a,b). Using the latter enzyme, Heyes et al. (2002, 2003a,b) identified intermediates of the reaction by time-resolved and low-temperature spectroscopy.

Several modified PChlide derivatives were tested in a substrate specificity study of POR (Griffiths, 1991; Klement et al., 1999; see also supplement). Various modifications of the side chains on rings A and B, even the introduction of bulky substituents, were tolerated without essential loss of activity; however, modification of ring E is not tolerated (for details see supplement). Of particular interest is the replacement of the C-7 methyl group of PChlide *a* by a formyl group to form PChlide *b*. The observation that PChlide *b* and its Zn analogue can be photoreduced (Schoch et al., 1995) prompted the proposal that PLBs contained mainly PChlide *b* (Reinbothe et al., 1999, 2003a); the authors postulated that PChlide *b*, bound to PORA, was not immediately photoreduced at the onset of illumination but served rather as a light-harvesting pigment. Scheumann et al. (1999a), however, found that exogenous PChlide *b* was readily photoreduced to Chlide *b* in the presence of etioplast membranes and extraction of etioplasts with 80% acetone yielded only PChlide *a* and no PChlide *b* was detected. Later, Reinbothe et al. (2003a) reported detection of PChlide *b* as the major tetrapyrrole of etioplasts after extraction with 99% acetone containing 0.1% diethyl pyrocarbonate and suggested that PChlide *b* was rapidly metabolized to PChlide *a* in the presence of 80% acetone (see also Section IIIB).

D Phototransformation of Protochlorophyllide in Vivo

The in vivo transformation of PChlide to Chlide is accompanied by characteristic spectral shifts of PChlide *a* and Chlide *a* (Fig. 2; reviewed by: Griffiths, 1991; Ryberg and Sundqvist, 1991). The situation is complex since there exist 4 or more spectral forms of PChlide *a* in dark-grown plants of which at least 2 are phototransformable (Böddi et al., 1992). One explanation for the different spectral forms is the assumption that POR aggregates are red-shifted with increasing aggregate size, the largest being present in PLBs and the smaller in PTs. Immediately after the phototransformation, Chlide *a*, still bound to POR, is translocated from PLBs to PTs, and the prominent shift from 684 nm to 672 nm (Shibata shift) has been

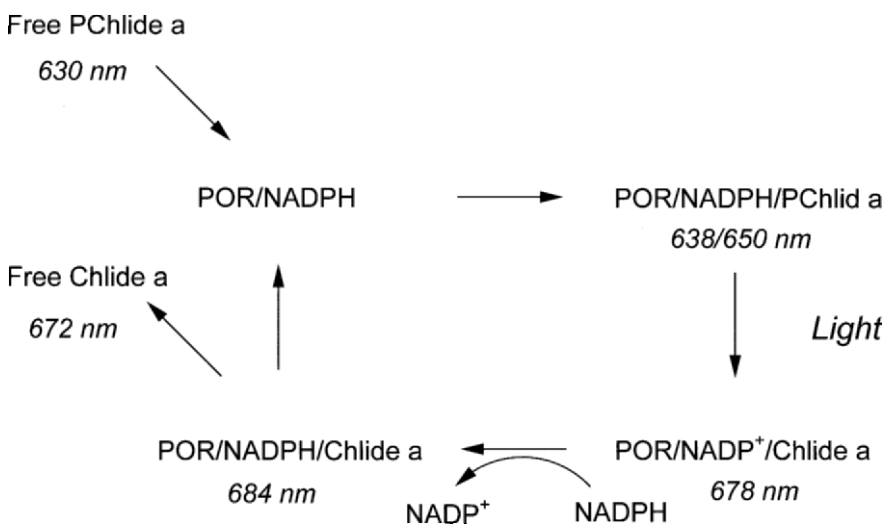

Fig. 2. Schematic representation of pigment-POR complex formation. Also shown are associated shifts of absorption maxima, observed when etioplast membranes are supplied with exogenous Pchlide *a* and NADPH (after Griffiths, 1991).

tentatively attributed to disaggregation of POR complexes during this translocation (Böddi et al., 1990); however, conformational changes of the Chlide-POR complex may also contribute to these shifts (Zhong et al., 1996). The Shibata shift is inhibited by fluoride, indicating the involvement of a phosphatase (Wiktorsson et al., 1996).

An alternative explanation for different spectral forms was based on in vitro experiments with etioplast membranes, consisting of PLBs and PTs in which the PLBs were probably disaggregated (Griffiths, 1991). The binding of PChlide *a* to POR in the membrane caused a red shift, and the addition of NADPH increased this red shift. After phototransformation, the exchange of $NADP^+$ by NADPH resulted in a red shift of Chlide *a*. The Shibata shift was then assumed to be connected with the release of Chlide *a* from POR. The in vitro shifts were reproduced with isolated, pigment-free POR supplied with PChlide *a* or Zn-PPheide *a* and NADPH; the typical red shift required monogalactosyldiacylglycerol and a reduction of the water potential, achieved by dialysis against 80% glycerol (Klement et al., 2000). Unfortunately, it is not yet known whether reduction of the water potential leads to increased aggregation, conformational changes of POR or altered interaction of PChlide with NADPH. Because these processes seem to be intimately interconnected, it will be difficult to recognize causal relationships from in vivo experiments.

III. Metabolism of Chlorophyll *b* and Chlorophyllide *b*

A. Synthesis of Chlorophyllide b

Indirect evidence led to the hypothesis of Chl *b* formation from Chl *a* or 'newly-synthesized Chl *a*' (Shlyk, 1971). The successful incorporation of $^{18}O_2$ into Chl *b* in *Chlorella vulgaris* (Schneegurt and Beale, 1992) and greening seedlings of *Zea mays* (Porra et al., 1994) indicated a dioxygenase or monooxygenase mechanism. The authors proposed a hydroxylation of Chl *a* at C-7^1 followed by dehydrogenation of the putative hydroxy intermediate to form the C-7 formyl group of Chl *b*. We now know that the reaction consists of two hydroxylation steps and takes place with Chlide *a* and not the (esterified) Chl *a* (see below).

A milestone for our understanding of Chl *b* formation was the detection of the Chlide *a* oxygenase (*CAO*) gene (Tanaka et al., 1998). The authors mutagenized *C. reinhardtii* and found deletions in the same region of the genomic DNA in all Chl *b*-less mutants; further, they were able to reinstate Chl *b* formation in the mutants by transformation with a genomic DNA fragment of this region containing a gene which they later named *CAO*. The encoded protein was thought to be an oxygenase because it contained consensus sequences for both a Rieske-type [2Fe-2S] cluster and for a mononuclear non-heme Fe-binding site. Using the *Chlamydomonas CAO* sequence, Espineda et al. (1999) cloned the homologous gene (*AtCAO*) from *A. thaliana* and showed that a Chl *b*-less *Arabidopsis* mutant (*ch1-3*) contained a lesion in the *CAO* sequence. The studies with both organisms indicated that this gene is essential for Chl *b* biosynthesis and that no alternative pathway for Chl *b* formation exists.

Oster et al. (2000) isolated the full-length cDNA from *A. thaliana* and showed its intactness and functionality by rescue of Chl *b*-free mutants. After expression of the *CAO* gene in *E. coli*, the cell extract was able to catalyze the formation of Chlide *b* from Chlide *a*; traces of 7^1-OH-Chlide *a* were likewise produced. Oster et al. then demonstrated that the incubation of the cell extract with Zn-7^1-OH-Pheide *a* (Pheide = pheophorbide) gave a high yield of Zn-Pheide *b*. This second reaction step was also catalyzed by CAO, no reaction of the hydroxy-compound was found in the extract of control cells which did not contain the *CAO* gene. On the other hand, CAO did not catalyze the oxygenation of esterified Chl *a* or of PChlide *a* in the in vitro test indicating that Chlide *a* is the sole substrate for formation of the formyl group of Chl *b*. This does not exclude side reactions with these substrates under special conditions (see the work of Xu et al., 2002, discussed below).

Interesting aspects of chloroplast evolution came from further investigations of the *CAO* gene. Chl *b* has been detected in a wide range of organisms extending from cyanobacteria ('prochlorophyta') to higher plants. The Chl *a/b*-binding proteins of the prokaryotes are unrelated to those of the eukaryotes indicating at least two independent evolutionary origins for these proteins (La Roche et al., 1996). The hypothesis that the synthesis of Chl *b* was also invented at least twice during evolution has been questioned. Tomitani et al. (1999) compared the *CAO* genes from cyanobacteria to higher plants and found at least 50% identity for any of two of the deduced amino acid sequences. This high degree of homology

excluded the possibility that Chl *b* biosynthesis has been re-invented several times, provided that the CAO reaction is the obligatory step for Chl *b* formation in all organisms. Tomitani et al. (1999) have proposed that the common ancestor of chloroplasts and recent cyanobacteria contained both antenna pigments, namely, biliproteins and Chl *b*, and that the loss of one of these pigments occurred several times, either before or after endosymbiosis: loss of biliproteins resulted in prochlorophyta and chlorophyta while loss of Chl *b* resulted in biliprotein-containing cyanobacteria and rhodophyta. Support for the existence of such a common ancestor came from the earlier detection of a *Prochlorococcus marinus* strain which contained both Chl *b* and biliprotein (Hess et al., 1996).

Very few investigations on the molecular basis of the regulation of Chl *b* biosynthesis have been reported. Espineda et al. (1999) found up- and down-regulation of the *AtCAO* mRNA level with the light intensity, possibly related to the well-known changes in the Chl *a/b* ratio during acclimation of plants to different light conditions. Overexpression of the *AtCAO* gene in *A. thaliana* resulted in an increase of about 20% of the light-harvesting chlorophyll protein of Photosystem II (LHCB) content together with an increase in Chl *b* content (Tanaka et al., 2001). When *Synechocystis* sp., a biliprotein-containing cyanobacterium, was transformed with the same gene, about 10% of the total Chl was Chl *b*, incorporated mainly into the P700 complex (Satoh et al., 2001). The same cyanobacterium strain, transformed with both the *CAO* and the *LHCB* genes, produced as much as 80% of its Chl as Chl *b* but did not accumulate any LHCB protein: Chl *b* had replaced Chl *a* in most of the Chl *a*-binding proteins under these conditions (Xu et al., 2001). When this strain, which was unable to synthesize Chl in darkness due to a deficiency in the *chlL* gene, was kept in darkness for several days, it first produced PChlide *a* and, after a delay of several more days, produced PChlide *b* (Xu et al., 2002). These surprising results have still to be explained.

B. Reduction of Chlorophyll b and the Chlorophyll Cycle

The chemical reduction of a formyl group to a hydroxy group under mild conditions is well-known. This reaction, performed with aqueous cyanoborohydride and pheophorbide *b* (Pheide *b*), readily yields 7^1-hydroxy-Pheide *a* but, in methanol, the 7^1-methoxy-derivative is formed. The 13^1-oxo group is only reduced by prolonged incubation with a large excess of the reductant. Surprisingly, the same incubation with Zn-Pheide *b* proceeded further to Zn-Pheide *a*: the 7^1-hydroxy- and 7^1-methoxy-compounds proved to be intermediates in this reaction (Scheumann et al., 1996). The electron-withdrawing effect of the central metal is apparently so strong at C-7 that the formyl group can be reduced to a methyl group while, again, the 13^1-oxo group is essentially unaffected under the same conditions.

The biochemical reduction of *b*-type to *a*-type pigments was demonstrated in vitro with etioplast membranes (Ito et al., 1996; Scheumann et al., 1998). The reduction was successful with Chlide *b*, Zn-Pheide *b* and the esterified Chl *b*; the 7^1-hydroxy-compounds were also intermediates in this biochemical reaction. Reductant for the first step was NADPH while the second step, the reduction of the hydroxymethyl to the methyl group, required reduced ferredoxin. The existence of two enzymes, provisionally named Chl *b* reductase and OH-Chl reductase, was supported by more observations on their substrate specificity: Chl *b* reductase also reduced PChlide *b* (but not the metal-free Pheide *b*), Zn-Pheide *b* and Zn-Pheide *d* to their respective hydroxy compounds while no further reduction of these hydroxy compounds was observed in etioplast membranes (Scheumann, 1999). Reinbothe et al. (2003a), however, described indirect evidence for the reduction of endogenous PChlide *b* to PChlide *a* in etioplast preparations while exogenous PChlide *b* was not reduced at all. The occurrence of endogenous PChlide *b* in etioplasts has not yet been confirmed in other laboratories (see also Section IIC).

The physiological significance of the Chl *b* to Chl *a* reduction is not entirely clear. The discussion concentrates on two situations where the reduction could play a role. (i) Many plants can acclimate to changing light condition by a change in the Chl *a*/*b* ratio (Tanaka et al., 1991). It is difficult to distinguish between a direct reduction of Chl *b* to Chl *a* and the alternative, which is Chl *b* degradation with new synthesis of Chl *a*; however, the formation of Chl *a* and Zn-pheophytin (Zn-Phe *a*) after infiltrating etiolated plants with Chlide *b* and Zn-Pheide *b*, respectively, proved that direct reduction occurred in the tissue (Scheumann et al., 1996; Vezitskii, 2000). (ii) Both Chls *a* and *b* disappear in senescing plants. While degradation products derived from both Chls *a* and *b* were found in algae (Gossauer and Engel, 1996), all the degradation products of angiosperms exclusively

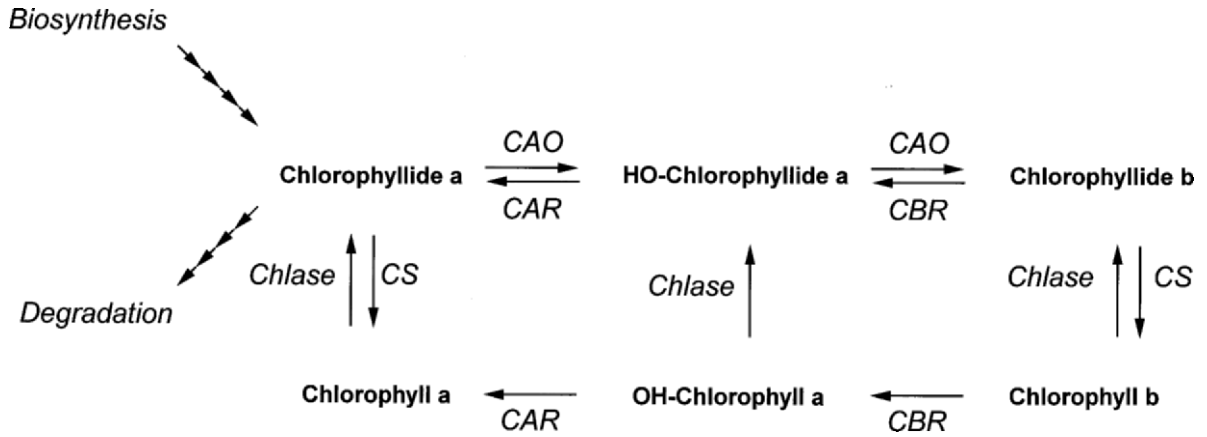

Fig. 3. The Chl cycle. The reversible transformation of Chl *a* into Chl *b* proceeds via Chlide *a* which is the key intermediate for biosynthesis and degradation of Chls. *CS* = chlorophyll synthase; *Chlase* = Chlorophyllase; *CAO* = chlorophyllide *a* oxygenase; *CBR* = chlorophyll(ide) *b* reductase; *CAR* = 7^1-hydroxy-chlorophyll(ide) *a* reductase.

contain the 7-methyl group characteristic for Chl *a* (Kräutler and Matile, 1999). Senescence of barley in the presence of D_2O resulted in a labeled methyl group, indicating reduction of the formyl group of Chl *b* before degradation (Folly and Engel, 1999). Consistent with this interpretation, the higher-plant degrading enzyme, Pheide oxygenase, accepts only Pheide *a* while Pheide *b* is an inhibitor (Hörtensteiner et al., 1995). Scheumann et al. (1999b) found a transient increase in the Chl *b* reductase activity corresponding to the onset of Chl degradation. Since the activity could be localized in the thylakoid membrane of gerontoplasts, in contrast to all other degrading enzymes which are located in the envelope (Matile and Schellenberg, 1996), the reductase can be assumed to be the first enzyme of Chl *b* degradation. It is tempting to assume a key role for Chl *b* reductase in LHCII degradation: the reaction product, 7^1-OH-Chl *a*, does not bind to LHCB (Ohtsuka et al., 1997), and Chl-binding proteins are generally degraded if not bound to Chl.

Ito et al. (1996) coined the name 'chlorophyll cycle' for the mutual conversion of Chl *a* into Chl *b* in angiosperms but they assumed a direct inter-conversion of the esterified pigments. In view of the properties of the enzymes involved which are discussed in this chapter, a more detailed description of the individual steps of the cycle is now possible (Fig. 3). The Chl cycle is not an obligatory metabolic cycle running always in one direction; rather, it consists of a number of enzymatic steps enabling the plants, when necessary, to adapt to ambient conditions by altering Chl *a/b* ratios. The key intermediate Chlide *a,* which is synthesized from PChlide *a,* can be considered as entry point into the cycle for the biosynthesis of Chls *a* and *b.* It is likewise an obligatory intermediate in the degradation of Chls and, therefore, can also be considered as the exit point from the cycle. Completion of Chl *a* biosynthesis is achieved by esterification of Chlide *a*, catalyzed by Chl synthase (Section IV), and Chl *b* biosynthesis requires the CAO reaction of Chlide *a* followed by esterification of Chlide *b*. In higher-plants, degradation of Chl *b* starts by reduction to the hydroxy intermediate which is a good candidate for the transport from the thylakoids to the envelope where chlorophyllase can hydrolyze the phytyl ester to be followed by reduction to Chlide *a*. Currently, it cannot be excluded, however, that Chl *b* and Chl *a* are also transported to the envelope to react with chlorophyllase.

IV. Esterification

A. Chlorophyll and Bacteriochlorophyll Synthases

Esterification of Chlides *a* and *b* is the last step of Chl *a* and *b* biosynthesis, and the substrate specificity of the respective enzymes, discussed below, indicates that esterification is also the last step of BChl synthesis. The reaction type is a prenylation, and the Chl and BChl synthases are prenyl transferases. The activity of Chl synthase was detected in etio-

plast membranes and most early investigations were performed with membrane fractions of etioplasts or chloroplasts (reviewed by Rüdiger and Schoch, 1991). A general disadvantage of this material was the uncertainty concerning the number of synthases present. More recent investigations were carried out with single recombinant enzymes that became available after isolation of the genes encoding Chl and BChl synthases.

B. Synthase Genes and Recombinant Enzymes

Disruption of the *bchG* gene of *Rhodobacter* (*Rba.*) *capsulatus* resulted in lack of BChl synthesis and accumulation of non-esterified BChlide indicating that this gene coded for BChl synthase (reviewed by Suzuki et al., 1997). Homologous *bchG* genes were isolated from different photosynthetic bacteria (*Chloroflexus* (*Cfl.*) *aurantiacus*: Niedermeier et al., 1994; Lopez et al., 1996; *Heliobacillus mobilis*: Xiong et al., 1998; *Rba. sphaeroides*: Naylor et al., 1999), and *chlG* genes encoding Chl synthases were described for *A. thaliana* (Gaubier et al., 1995), *Synechocystis* sp. (Oster et al., 1997), and *Avena sativa* (Schmid et al., 2001). Except for *Cfl. aurantiacus*, only a single Chl synthase gene was detected in these organisms. Nine membrane-spanning helices were predicted for the deduced amino acid sequences (Schmid et al., 2001): this prediction agreed with the membrane localization of Chl and BChl synthases and explained why all attempts to obtain a soluble, active enzyme failed.

Expression of the recombinant *ChlG* genes from *A. thaliana and Avena sativa* in *E. coli* resulted in active enzymes in the bacterial membrane fraction. The substrate specificity of the recombinant Chl synthase, derived from *Avena sativa,* was identical with that in the *Avena sativa* etioplast membranes (Schmid et al., 2002). Modification of the Chlide structure gave results with Chl synthase comparable to those with POR after modification of the PChlide structure: exchange of the substituents at rings A and B are tolerated including even the introduction of bulky side chains while steric hindrance exists around ring E: Chlide *a´*, the 13^2-epimer of Chlide *a,* was not accepted as a substrate (Helfrich et al., 1994; for details see supplement). If Chlide *a´* is also unacceptable to Chl synthase in vivo, then the esterified Chl *a´* that occurs naturally in PS I (Watanabe et al., 1985; Jordan et al., 2001; Chapter 4, Kobayashi et al.) must be produced by epimerization of Chl *a* after esterification.

Expression of *bchG* genes in *E. coli* yielded active BChl synthases. The gene product from *Rba. capsulatus* accepted BChlide *a* but not Chlide *a* which is a precursor in the biosynthesis of BChlide *a* (Oster et al., 1997). The two *bchG* genes from *Cfl. aurantiacus* yielded two BChl synthases with different substrate specificities (Schoch et al., 1999). The best substrate for bchG was BChlide *a* while BChlides *c, e* and *d* were not accepted: the bchG2 enzyme esterified BChlides *c, e* and *d* but not BChlide *a* (for details see supplement).

C. Biosynthesis of Phytol and Esterification of Chlorophyllide in Vivo

With only relatively few exceptions, natural Chls and BChls contain the isoprenoid alcohol phytol. The last step of phytol biosynthesis is the hydrogenation of geranylgeranyl diphosphate (GGPP): the earlier steps of isoprenoid synthesis in plants are discussed by Lichtenthaler (1999). The reductase, encoded by the *bchP* gene of BChl-producing organisms (Bollivar et al., 1994) and the *chlP* gene of Chl-forming organisms (Addlesee et al., 1996), can reduce geranylgeraniol both as the diphosphate and as the ester group of Chl (Keller et al., 1998). The main pathway for Chl biosynthesis is probably the reduction of Chl_{GG}, as outlined below, however, the reduction of GGPP also plays a role in vivo since tobacco plants that expressed antisense RNA for *ChlP* showed not only reduced levels of Chls *a* and *b*, some Chl_{GG}, but also reduced levels of tocopherol (Tanaka et al., 1999): it is known that tocopherol synthesis in tobacco depends on phytyl diphosphate.

The sequence Chlide $\rightarrow Chl_{GG} \rightarrow Chl_P$ (Chl containing phytol), at first described for the initiation of Chl synthesis in etioplasts, was also more recently reported to be true in tissues containing proplastids; since the hydrogenation of Chl_{GG} was more rapid in proplastids than in etioplasts, Chl_{GG} could only be detected as an intermediate at 0 °C (Schoefs and Bertrand, 2000). It is not unlikely that the same reaction sequence is true also for green tissue; the finding of Chl_P after 20 min (Rüdiger, 1987), when Chl_{GG} predominated in etioplast-containing tissue, may indicate a rapid hydrogenation of Chl_{GG} in green tissue.

A rapid phase of esterification was detected in flash-illuminated etiolated seedlings (Adra and Rebeiz, 1998; Domanskii and Rüdiger, 2001; Domanskii et

al., 2003) that was completed within about 15s and involved only 10–15% of the Chlide formed by full photoconversion. After a lag phase of 2–5 min, the residual 85–90% of the Chlide was esterified in the main phase within 30–40 min. The lag phase coincides with the beginning of PLB dispersal (Domanskii et al., 2003) and translocation of Chl synthase from PLBs, where it is inactive, to PTs (Lindsten et al., 1990; 1993). Since preloading of recombinant Chl synthase with phytyldiphosphate resulted in a similar rapid esterification (Schmid et al., 2002), preloading was also assumed in vivo. The reaction sequence via Chl_{GG} indicates that Chl synthase is preloaded with GGPP in vivo. Kinetics of the rapid phase are identical at 20 °C and 0 °C while esterification of the main phase is completely blocked at 0 °C. Domanskii et al. (2003) assumed a close connection of POR and Chl synthase in vivo, possibly as a complex of defined composition, to explain the rapid and direct transfer of Chlide, formed by phototransformation while bound to POR, to Chl synthase for esterification. Direct proof of the existence of such a complex is still missing.

Supplement

The supplement contains data on the substrate specificity of POR, Chl synthase and BChl synthase, determined with chemically modified substrates. PChlide *a*, the substrate of POR, was modified at rings A and B (Table S1) and at rings D and E (Table S2). Chlide *a*, the substrate of Chl synthase, was modified at C-7 and C-20 (Table S3) and at ring E (Table S4). The specificity of two BChl synthases, BChG and BChG2, was tested with Bchlid *a* modified at C-3, C-7, C-13^2 and C-20 (Table S5). This material is available at http://epub.ub.uni-muenchen.de/archive/00000776/.

Note Added in Proof

The nitrogenase model for DPOR was supported by more recent results using overexpression of BchL and BchN-BchB in photosynthetically competent strains of *Rhodobacter casulatus* (Nomata et al., 2005). Reduced ferredoxin served as electron donor in the assay system, which was stable for at least six months under anaerobic conditions. In analogy to nitrogenase subunits $(NifH)_2$ and $[(NifE)_2(NifN)_2]$, DPOR subunits form a homodimer $(BchL)_2$ and a heterotetramer $[(BchN)_2(BchB)_2]$, respectively. The presence of PChlide *b* in etiolated seedlings, reported by Reinbothe et al. (2003a) was later questioned: Kolossov and Rebeiz, repeating the extraction with 99% acetone containing 0.1% diethyl pyrocarbonate, were not able to detect any Pchlide *b* (Kolossov and Rebeiz, 2003).

Acknowledgments

The work of the author's laboratory was supported by the Deutsche Forschungsgemeinschaft, Bonn, and the Fonds der Chemischen Industrie, Frankfurt.

References

Addlesee HA, Gibson LCD, Jensen PE and Hunter CN (1996) Cloning sequencing and functional assignment of the Chl biosynthesis gene *chlP* of *Synechocystis* sp PCC 6803. FEBS Lett 389: 126–130

Adra AN and Rebeiz CA (1998) Chloroplast biogenesis 81: Transient formation of divinyl chlorophyll *a* following a 2.5 ms light flash treatment of etiolated cucumber cotyledons. Photochem Photobiol 68: 852–856

Armstrong GA (1998) Greening in the dark: Light-independent chlorophyll biosynthesis from anoxygenic photosynthetic bacteria to gymnosperms. J Photochem Photobiol B Biol 43: 87–100

Armstrong GA, Runge S, Frick G, Sperling U and Apel, K. (1995) Identification of NADPH:protochlorophyllide oxidoreductases A and B: A branched pathway for light-dependent chlorophyll biosynthesis in *Arabidopsis thaliana*, Plant Physiol 108: 1505–1517

Armstrong GA, Apel K and Rüdiger W (2000) Does a light-harvesting protochlorophyllide *a/b*-binding protein complex exist? Trends Plant Sci 5: 40–44

Aronsson H, Sohrt K and Soll J (2000) NADPH:Protochlorophyllide oxidoreductase uses the general import route into chloroplasts. Biol Chem 381: 1263–1267

Aronsson H, Sundqvist C and Dahlin C (2003a) POR-import and membrane association of a key element in chloroplast development Physiol Plant 118: 1–9

Aronsson H, Sundqvist C and Dahlin C (2003b) POR hits the road: Import and assembly of a plastid protein. Plant Mol Biol51: 1–7

Böddi B, Lindsten A, Ryberg M and Sundqvist C (1990) Phototransformation of aggregated forms of protochlorophyllide in isolated etioplast inner membranes. Photochem Photobiol 52: 83–87

Böddi B, Ryberg M and Sundqvist C (1992) Identification of four universal protochlorophyllide forms in dark-grown leaves by analysis of the 77 K fluorescence spectra. J Photochem Photobiol B Biol 12: 389–401

Bollivar DW, Wang SJ, Allen JP and Bauer CE (1994) Molecular

genetic analysis of terminal steps in bacterioChl *a* biosynthesis: Characterization of a *Rhodobacter capsulatus* strain that synthesizes geranylgeraniol-esterified bacterioChl *a*. Biochemistry 33: 12763–12768

Domanskii V and Rüdiger W (2001). On the nature of the two pathways in chlorophyll formation from protochlorophyllide. Photosynth Res 68: 131–139

Domanskii V, Rassadina V, Gus-Mayer S, Wanner G, Schoch S and Rüdiger W (2003) Characterization of two phases of chlorophyll formation during greening of etiolated barley leaves. Planta, 216: 475–483

Espineda CE, Linford AS, Devine D and Brusslan JA (1999) The *AtCAO* gene, encoding chlorophyll *a* oxygenase, is required for chlorophyll *b* synthesis in *Arabidopsis thaliana*. Proc Natl Acad Sci USA 96: 10507–10511

Folly P and Engel N (1999) Chlorophyll *b* to chlorophyll *a* conversion precedes chlorophyll degradation in *Hordeum vulgare* L. J Biol Chem 274: 211811–21816

Franck F, Sperling U, Frick G, Pochert B, Cleve vB, Apel K and Armstrong GA (2000) Regulation of etioplast pigment-protein complexes, inner membrane architecture, and protochlorophyllide a chemical heterogeneity by light-dependent NADPH: protochlorophyllide oxidoreductases A and B. Plant Physiol 124: 1678–1696

Fujita Y and Bauer CA (2000) Reconstitution of light-independent protochlorophyllide reductase from purified Bchl and BchN-BchB subunits. In vitro confirmation of nitrogenase-like features of a bacteriochlorophyll biosynthesis enzyme. J Biol Chem 275: 23583–23588

Fusada N, Masuda T, Kuroda H, Shiraishi T, Shimada H, Ohta H and Takamiya K, (2000) NADPH:protochlorophyllide oxidoreductase in cucumber is encoded by a single gene and its expression is transcriptionally enhanced by illumination. Photosynth Res 64: 147–154

Gaubier P, Wu H-J, Laudie M, Delseny M and Grellet F (1995) A chlorophyll synthetase gene from *Arabidopsis thaliana*. Mol Gen Genet 249: 58–64

Gossauer A and Engel N (1996) New trends in photobiology: Chlorophyll catabolism— structures, mechanisms, conversions. J Photochem Photobiol B 32: 141–151

Griffiths WT (1991) Protochlorophyllide photoreduction. In: Scheer H (ed) Chlorophylls, pp 433–449. CRC Press, Boca Raton

Helfrich M, Schoch S, Lempert U, Cmiel E and Rüdiger W (1994) Chlorophyll synthetase cannot synthesize chlorophyll a´. Eur J Biochem 219: 267–275

Hess WR, Partensky F, van der Staay GWM, Garcia-Fernandez JMG, Börner T and Vaulot D (1996) Coexistence of phycoerythrin and a chlorophyll *a/b* antenna in a marine prokaryote. Proc Natl Acad Sci USA 93: 11126–11130

Heyes DJ, Martin GE, Reid RJ, Hunter CN and Wilks HM (2000) NADPH:protochlorophyllide oxidoreductase from *Synechocystis*: Overexpression, purification and preliminary characterization. FEBS Lett 483: 47–51.

Heyes DJ, Ruban AV, Wilks HM and Hunter NC (2002) Enzymology below 200 K: The kinetics and thermodynamics of the photochemistry catalyzed by protochlorophyllide oxidoreductase. Proc Natl Acad Sci USA 99: 11145–11150

Heyes DJ, Ruban AV and Hunter CN (2003a) Protochlorophyllide oxidoreductase: 'Dark' reactions of a light-driven enzyme. Biochemistry 42:523–528

Heyes DJ, Hunter CN, van Stokkum IH, van Grondelle R and Groot ML (2003b) Ultrafast enzymatic reaction dynamics in protochlorophyllide oxidoreductase. Nat Struct Biol. 10: 491–492

Holtorf H, Reinbothe S, Reinbothe C, Bereza B and Apel, K (1995) Two routes of chlorophyll synthesis that are differentially regulated by light in barley (Hordeum vulgare L.). Proc Nat Acad Sci USA 92: 3254–3258

Hörtensteiner S, Vicentini F and Matile P (1995) Chlorophyll breakdown in senescent cotyledons of rape, *Brassica napus* L.: Enzymatic cleavage of phaeophorbide *a* in vitro. New Phytol 129: 237–246

Ito H, Ohtsuka T and Tanaka A (1996) Conversion of chlorophyll *b* to chlorophyll *a* via 7-hydroxymethyl chlorophyll. J Biol Chem 271: 1475–1479

Jordan P, Fromme P, Witt HAT, Klukas O, Saenger W and Krauß N (2001) Three-dimensional structure of cyanobacterial Photosystem I at 2.5 Å resolution. Nature 411: 909–917

Keller Y, Bouvier FD and Harlingue A (1998) Metabolic compartmentation of plastid prenyllipid biosynthesis — Evidence for the involvement of a multifunctional geranylgeranyl reductase. Eur J Biochem 251: 413–417

Klement H, Helfrich M, Oster U, Schoch S and Rüdiger W (1999) Pigment-free protochlorophyllide oxidoreductase from *Avena sativa* L. Purification and substrate specificity. Eur J Biochem 265: 862–874

Klement H, Oster U and Rüdiger W (2000) The influence of glycerol and chloroplast lipids on the spectral shifts of pigments associated with NADPH:protochlorophyllide oxidoreductase from *Avena sativa* L. FEBS Lett 480: 306–310

Kolossov VL and Rebeiz CA (2003) Chloroplast biogenesis 88. Protochlorophyllide b occurs in green but not in etiolated plants. J Biol Chem 278: 49675–49678)

Kräutler B and Matile P (1999) Solving the riddle of chlorophyll breakdown. Acc Chem Res 32: 35–43

LaRoche J, van der Staay GWM, Partensky F, Ducret A, Aebersold R, Li R, Golden SS, Hiller RG, Wrench PM, Larkum AWD and Green BR (1996) Independent evolution of the prochlorophyte and green plant chlorophyll *a/b* light-harvesting proteins. Proc Natl Acad Sci USA 93: 15244–15248

Lebedev N and Timko MP (1999) Protochlorophyllide oxidoreductase B-catalyzed protochlorophyllide photoreduction in vitro: Insight into the mechanism of chlorophyll formation in light-adapted plants. Proc Natl Acad Sci USA 96: 9954–9959

Li J and Timko MP (1996) The pc-1 phenotype of *Chlamydomonas reinhardtii* results from a deletion mutation in the nuclear gene for NADPH:protochlorophyllide oxidoreductase. Plant Mol Biol 30: 15–37

Lichtenthaler HK (1999) The 1-deoxy-D-xylulose-5-phosphate pathway of isoprenoid biosynthesis in plants. Annu Rev Plant Physiol Plant Mol Biol 50: 47–65

Lindsten A, Welch CJ, Schoch S, Ryberg M, Rüdiger W and Sundqvist C (1990) Chlorophyll synthetase is latent in well preserved prolamellar bodies of etiolated wheat. Physiol Plant 80: 277–285

Lindsten A, Wiktorsson B, Ryberg M and Sundqvist C (1993) Chlorophyll synthase activity is relocated from transforming prolamellar bodies to developing thylakoids during irradiation of dark-grown wheat. Physiol Plant 88: 29–36

Lopez JC, Ryan S and Blankenship RE (1996) Sequence of the bchG Gene from *Chloroflexus aurantiacus*: Relationship be-

tween chlorophyll synthase and other polyprenyltransferases. J Bacteriol 178: 3369–3373

Martin GEM, Timko MP and Wilks HM (1997) Purification and kinetic analysis of pea (*Pisum sativum* L.) NADPH: protochlorophyllide oxidoreductase expressed as a fusion with maltose-binding protein in *Escherichia coli*. Biochem J 325: 139–145

Masuda T, Fusada N, Oosawa N, Takamatsu K, Yamamoto YY, Ohto M, Nakamura K, Goto K, Shibata D, Shirano Y, Hayashi H, Kato T, Tabata S, Shimada H, Ohta H and Takamiya KI (2003) Functional analysis of isoforms of NADPH:protochlorophyllide oxidoreductase (POR), PORB and PORC, in *Arabidopsis thaliana*. Plant Cell Physiol 44:963–974

Matile P and Schellenberg M (1996) The cleavage of pheophorbide *a* is located in the envelope of barley gerontoplasts. Plant Physiol Biochem 34: 55–59

Naylor GW, Addlesee HA, Gibson LCD and Hunter CN (1999) The photosynthesis gene cluster of *Rhodobacter sphaeroides*. Photosynth Res 62: 121–139

Niedermeier G, Shiozawa JA, Lottspeich F and Feick RG (1994) The primary structure of two chlorosome proteins from *Chloroflexus aurantiacus*. FEBS Lett 342: 61–65

Nomata J, Swem LR, Bauer CE and Fujita Y (2005) Overexpression and characterization of dark-operative protochlorophyllide reductase from *Rhodobacter capsulatus.* Biochim Biophys Acta 1708: 229–237

Ohtsuka T, Ito H and Tanaka A (1997) Conversion of chlorophyll *b* to chlorophyll *a* and the assembly of chlorophyll with apoproteins by isolated chloroplasts. Plant Physiol 113: 137–147

Oosawa N, Masuda T, Awai K, Fusada N, Shimada H, Ohta H and Takamiya K (2000) Identification and light-induced expression of a novel gene of NADPH:protochlorophyllide oxidoreductase isoform in *Arabidopsis thaliana*. FEBS Lett 474: 133–136

Oster U, Bauer CE and Rüdiger W (1997) Characterization of chlorophyll *a* and bacteriochlorophyll *a* synthases by heterologous expression in *Escherichia coli*. J Biol Chem 272:, 9671–9676

Oster U, Tanaka R, Tanaka A and Rüdiger W (2000) Cloning and functional expression of the gene encoding the key enzyme for chlorophyll *b* biosynthesis (CAO) from *Arabidopsis thaliana*. Plant J 21: 305–310

Porra RJ, Schäfer W, Cmiel E, Katheder I and Scheer H (1994) The derivation of the formyl-group oxygen of chlorophyll *b* in higher plants from molecular oxygen. Achievement of high enrichment of the 7-formyl-group oxygen from $^{18}O_2$ in greening maize leaves. Eur J Biochem 219: 671–679

Reinbothe C, Lebedev N and Reinbothe S (1999) A protochlorophyllide light-harvesting complex involved in deetiolation of higher plants. Nature 397: 80–84

Reinbothe S, Mache R and Reinbothe C (2000) A second, substrate-dependent site of protein import into chloroplasts. Proc Natl Acad Sci USA 97: 9795–9800

Reinbothe S, Pollmann S and Reinbothe C (2003a) In situ conversion of protochlorophyllide *b* to protochlorophyllide *a* in barley. Evidence for a novel role of 7-formyl reductase in the prolamellar body of etioplasts. J Biol Chem 278: 800–806

Reinbothe C, Buhr F, Pollmann S and Reinbothe S (2003b) In vitro reconstitution of light-harvesting POR-protochlorophyllide complex with protochlorophyllides *a* and *b*. J Biol Chem 278:807–815

Rowe JD and Griffiths WT (1995) Protochlorophyllide reductase in photosynthetic prokaryotes and its role in chlorophyll synthesis. Biochem J 311: 417–424

Rüdiger W (1987) Chlorophyll synthetase and its implication for regulation of chlorophyll biosynthesis. In: Biggins J (ed) Progress in Photosynthesis Research, pp 461–467. Martinus Nijhoff Publishers, Dordrecht

Rüdiger W and Schoch S (1991) The last Steps of chlorophyll biosynthesis. In: Scheer H (ed) Chlorophylls, pp 451–464. CRC Press, Boca Raton

Ryberg M and Dehesh K (1986) Localization of NADPH-protochlorophyllide oxidoreductase in dark-grown wheat (*Triticum aestivum*) by immuno-electron microscopy before and after transformation of the prolamellar bodies. Physiol Plant 66: 616–624

Ryberg M and Sundqvist C (1991) Structural and functional significance of pigment-protein complexes of chlorophyll precursors. In: Scheer H (ed) Chlorophylls, pp 587–612. CRC Press, Boca Raton

Satoh S, Ikeuchi M, Mimuro M and Tanaka A (2001) Chlorophyll *b* expressed in cyanobacteria functions as a light-harvesting antenna in Photosystem I through flexibility of the proteins. J Biol Chem 276: 4293–4297

Scheumann V (1999) Reduktion von Chlorophyll *b* zu Chlorophyll *a* in vitro und in vivo. PhD thesis, University of Munich

Scheumann V, Helfrich M, Schoch S and Rüdiger W (1996) Reduction of the formyl group of zinc pheophorbide *b* in vitro and in vivo: A model for the chlorophyll *b* to *a* transformation. Z Naturforsch 51c: 185–194

Scheumann V, Schoch S and Rüdiger W (1998) Chlorophyll *a* formation in the chlorophyll *b* reductase reaction requires reduced ferredoxin. J Biol Chem 273: 35102–35108

Scheumann V, Klement H, Helfrich M, Oster U, Schoch S and Rüdiger W (1999a) Protochlorophyllide *b* does not occur in barley etioplasts. FEBS Lett 445: 445–448

Scheumann V, Schoch S and Rüdiger W (1999b) Chlorophyll *b* reduction during senescence of barley seedlings. Planta 209: 364–370

Schmid HC, Oster U, Kögel J, Lenz S and Rüdiger W (2001) Cloning and characterisation of chlorophyll synthase from *Avena sativa*. Biol Chem 382: 903–911

Schmid HC, Rassadina V, Oster U, Schoch S and Rüdiger W (2002) Pre-loading of chlorophyll synthase with tetraprenyl diphosphate is an obligatory step in chlorophyll biosynthesis. Biol Chem 383: 1769–1776

Schneegurt MA and Beale SI (1992) Origin of the chlorophyll *b* formyl from oxygen in *Chlorella vulgaris*. Biochemistry 31: 11677–11683

Schoch S, Helfrich M, Wiktorsson B, Sundqvist C, Rüdiger W and Ryberg M (1995) Photoreduction of zinc protopheophorbide *b* with NADPH-protochlorophyllide oxidoreductase from etiolated wheat (*Triticum aestivum* L.). Eur J Biochem 229: 291-298

Schoch S, Oster U, Mayer K, Feick R and Rüdiger W (1999). Substrate specificity of overexpressed bacteriochlorophyll synthase from *Chloroflexus aurantiacus*. In: Argyroudi-Akoyunoglou J, Senger H (eds) The Chloroplast: From Molecular Biology to Biotechnology, pp 213–216. Kluwer Academic Publishers, Dordrecht, Netherlands

Schoefs B and Bertrand M (2000) The formation of chlorophyll from chlorophyllide in leaves containing proplastids is a four-

step process. FEBS Lett 486 : 243–246
Schulz R and Senger H (1993 Protochlorophyllide reductase: A key enzyme in the greening process. In: Sundqvist C, Ryberg M (eds) Pigment-Protein Complexes in Plastids, Synthesis and Assembly, pp 179–218. Academic Press, San Diego
Shlyk AA (1971) Biosynthesis of chlorophyll *b*. Ann Rev Plant Physiol 22: 169–184
Sperling U, Franck F, van Cleve B, Frick G, Apel K and Armstrong GA (1998) Etioplast differentiation in *Arabidopsis*: Both PORA and PORB restore the prolamellar body and photoactive protochlorophyllide-F655 to the cop1 photomorphogenic mutant. Plant Cell 10: 283–296
Sundqvist C and Dahlin C (1997) With chlorophyll pigments from prolamellar bodies to light-harvesting complexes. Physiol Plant 100: 748–759
Suzuki JY and Bauer CE (1995) A prokaryotic origin for light-dependent chlorophyll biosynthesis of plants. Proc Natl Acad Sci USA 92: 3749–3753
Suzuki JY, Bollivar DW and Bauer CE (1997) Genetic analysis of chlorophyll biosynthesis. Annu Rev Genet 31: 87–100
Tanaka A, Yamamoto Y and Tsuji H (1991) Formation of chlorophyll-protein complexes during greening. 2. Redistribution of chlorophyll among apoproteins. Plant Cell Physiol 32: 195–204
Tanaka A, Ito H, Tanaka R, Tanaka NK, Yoshida K and Okada K (1998) Chlorophyll *a* oxygenase (*CAO*) is involved on chlorophyll *b* formation from chlorophyll *a*. Proc Natl Acad Sci USA 95: 12719–12723
Tanaka R, Oster U, Kruse E, Rüdiger W and Grimm B (1999) Reduced activity of geranylgeranyl reductase leads to loss of chlorophyll and tocopherol and to partially geranylgeranylated chlorophyll in transgenic tobacco plants expressing antisense RNA for geranylgeranyl reductase Plant Physiol 120: 695–704
Tanaka R, Koshino Y, Sawa S, Ishiguro S, Okada K and Tanaka A (2001) Overexpression of chlorophyllide *a* oxygenase (CAO) enlarges the antenna size of Photosystem II in *Arabidopsis thaliana*. Plant J 26: 365–373
Tomitani A, Okada K, Miyashita H, Matthijs HCP, Ohno T and Tanaka A (1999) Chlorophyll *b* and phycobilins in the common ancestor of cyanobacteria and chloroplasts. Nature 400: 159–162
Vezitskii AY (2000) Chlorophyll *a* formation in etiolated rye seedlings as dependent on the concentration of infiltrated chlorophyllide *b*. Russ J Plant Physiol 47: 499–503
Watanabe T, Kobayashi M, Hongu A, Nakazako M, Hiyama T and Murata N (1985) Evidence that a chlorophyll a′ dimer constitutes the photochemical reaction centre 1 (P700) in photosynthetic apparatus. FEBS Lett 191: 252–256
Wiktorsson B, Ryberg M and Sundqvist C (1996) Aggregation of NADPH:protochlorophyllide oxidoreductase-pigment complexes is favored by protein phosphorylation. Plant Physiol Biochem 34: 23–34
Xiong J, Inoue K and Bauer CE (1998) Tracking molecular evolution of photosynthesis by characterization of a major photosynthesis gene cluster from *Heliobacillus mobilis*. Proc Natl Acad Sci USA 95: 14851–14856
Xu H, Vavilin D and Vermaas W (2001) Chlorophyll *b* can serve as the major pigment in functional Photosystem II complexes of cyanobacteria. Proc Natl Acad Sci USA 98: 14168–14173
Xu H, Vavilin D and Vermaas W (2002) The presence of chlorophyll *b* in *Synechocystis* sp. PCC 6803 disturbs tetrapyrrole biosynthesis and enhances chlorophyll degradation. J Biol Chem 277: 42726–42732
Zhong LB, Wiktorsson B, Ryberg M and Sundqvist C (1996) The Shibata shift: Effects of in vitro conditions on the spectral blue shift of chlorophyllide in irradiated isolated prolamellar bodies. J Photochem Photobiol B Biology 36: 263–270

Chapter 15

Bacteriochlorophyll Biosynthesis in Green Bacteria

Niels-Ulrik Frigaard, Aline Gomez Maqueo Chew,
Julia A. Maresca and Donald A. Bryant*
Department of Biochemistry and Molecular Biology, The Pennsylvania State University, University Park, PA 16802, U.S.A.

Summary

The photosynthetic green sulfur bacteria synthesize a complex mixture of bacteriochlorophylls and chlorophylls. Depending on the strain, the dominant species is bacteriochlorophyll (BChl) *c*, *d*, or *e*, which serves as the major light-harvesting pigment in the chlorosome antenna. Each of these BChl species occurs as a mixture of homologs differing in stereochemistry, methylation, and esterifying alcohol. In addition, BChl *a* is present in various protein-based antenna complexes and in the reaction centers. A third chlorophyll (Chl) species, Chl *a* esterified with Δ2,6-phytadienol, functions as the primary electron acceptor in the reaction center. Until recently, relatively little was known about the biosynthesis of the so-called 'chlorosome Chl' (formerly '*Chlorobium*

*Author for correspondence, email: dab14@psu.edu

Bernhard Grimm, Robert J. Porra, Wolfhart Rüdiger and Hugo Scheer (eds): Chlorophylls and Bacteriochlorophylls: Biochemistry, Biophysics, Functions and Applications, pp. 201–221.

Chl'; Smith, 1994), BChl *c*, *d*, and *e*. However, it is now clear that these species are not derived from BChl *a* but that their biosynthesis involves some enzymes shared with BChl *a* biosynthesis as well as several novel enzymes. This chapter summarizes the current knowledge of BChl *c* biosynthesis in the green sulfur bacterium *Chlorobium* (*Chl.*) *tepidum*, for which the complete genome has been sequenced and analyzed. Because BChl *c* is not required for the viability of *Chl. tepidum*, it has been possible to inactivate genes postulated to play roles in BChl *c* biosynthesis by interposon mutagenesis. This genomics-enabled, biochemical genetics approach has led to the identification of several BChl *c*-specific gene products and has allowed the general features of BChl *c* biosynthesis to be established. Comparative genomics has also allowed some general conclusions concerning BChl synthesis in *Chloroflexus aurantiacus* to be drawn.

I. Introduction

The green sulfur bacteria and the green filamentous bacteria (collectively called green bacteria) are unique among photosynthetic organisms in synthesizing BChl *c*, *d*, and *e* (Fig. 1). These pigments differ from other BChls and Chls by having a chiral C-3[1] hydroxyl group and by lacking a C-13[2] methylcarboxylate group (Holt et al., 1966; Smith et al., 1982, 1983a; Smith, 2003). Moreover, BChl *c* and *e* have a C-20 methyl group, and in green sulfur bacteria BChl *c*, *d*, and *e* may have additional methyl groups at the C-8[2] and C-12[1] positions. BChl *c*, *d*, and *e* exclusively occur in light-harvesting antennas called chlorosomes, which are large, light-harvesting antenna structures appressed to the cytoplasmic surface of the cytoplasmic membrane (Blankenship et al., 1995; Oelze and Golecki, 1995; Frigaard et al., 2001, 2003; Blankenship and Matsuura, 2003). The characteristic structural features of the BChl *c*, *d* and *e* molecules are undoubtedly related to their organization within the chlorosome, in which they form rod-like aggregates stabilized by pigment-pigment interactions and not by pigment-protein interactions as is commonly found in other antenna systems (Holzwarth et al., 1992; van Rossum et al., 2001). The chlorosome antenna and the organization of the BChls within it have been extensively investigated (for reviews, see Holzwarth et al., 1992; Blankenship et al., 1995; Blankenship and Matsuura, 2003; Chapter 20, DeBoer and DeGroot).

The second most abundant (B)Chl species in green bacteria is BChl a_P (BChl *a* esterified with phytol), which occurs in the reaction center, in the CsmA antenna protein of the chlorosome envelope (Sakuragi et al., 1999; Bryant et al., 2002; Montaño et al., 2003), in the FMO antenna protein in green sulfur bacteria, and in the LH1-like, B808-B866 antenna protein in green filamentous bacteria (Feick and Fuller, 1984; Wechsler et al., 1987, 1991). The least abundant (B)Chl species in green sulfur bacteria is Chl $a_{\Delta 2,6}$ (Chl *a* esterified with Δ2,6-phytadienol), which is found in the Type 1 reaction centers where it acts as the primary electron acceptor (Kobayashi et al., 2000).

The biosynthesis of Chl *a* and BChl *a* is reasonably well understood from genetic and biochemical analyses (for reviews, see Senge and Smith, 1995; Porra, 1997; Suzuki et al., 1997; Willows, 2003; also Chapters 10–14). However, in spite of numerous speculations (Senge and Smith, 1995; Porra, 1997; Smith, 2003), this was not the case for BChl *c* biosynthesis until very recently. Present knowledge of BChl *c* biosynthesis derives from comparative analyses of the genome sequence of *Chlorobium* (*Chl.*) *tepidum* (Eisen et al., 2002; Frigaard et al., 2003) with data derived from the genomes of other photosynthetic organisms. Using information derived from gene duplications in *Chl. tepidum* and sequence similarity comparisons, predictions were made concerning the genes likely to be involved in BChl *c* biosynthesis, and a general scheme was proposed (Eisen et al., 2002). Because BChl *c* is not required for the viability of *Chl. tepidum* (Frigaard et al., 2002) and because *Chl. tepidum* is naturally transformable (Frigaard and Bryant, 2001), it has been possible to inactivate many of these genes (Frigaard

Abbreviations: ALA – 5-aminolevulinic acid; (B)Chl – bacteriochlorophyll or chlorophyll, prefixes in square brackets indicate the specific substituents at sites with variable substituents; BChl – bacteriochlorophyll; BChlide – bacteriochlorophyllide; BPhe – bacteriopheophytin; *Cfx*. – *Chloroflexus*; Chl – chlorophyll; *Chl*. – *Chlorobium*; Chlide – chlorophyllide; DV – divinyl; E – ethyl; *E.* – *Escherichia*; F – farnesyl, this and other esterifying alcohols are indicated as subscripts to the respective (B)Chls; FMO protein – Fenna-Matthews-Olson protein; GG – geranylgeranyl; *Hba.* – *heliobacillus*; HE – 1-hydroxyethyl; I – *iso*-butyl; M – methyl; P – phytyl; PChlide – protochlorophyllide; Pr – *n*-propyl; Proto – protoporphyrin IX; *Rba*. – *Rhodobacter*; *Rsp.* – *Rhodospirillum*; S – stearyl; V – vinyl; SAM – s-adenosylmethionine; Δ2,6 – Δ2,6-phytadienyl

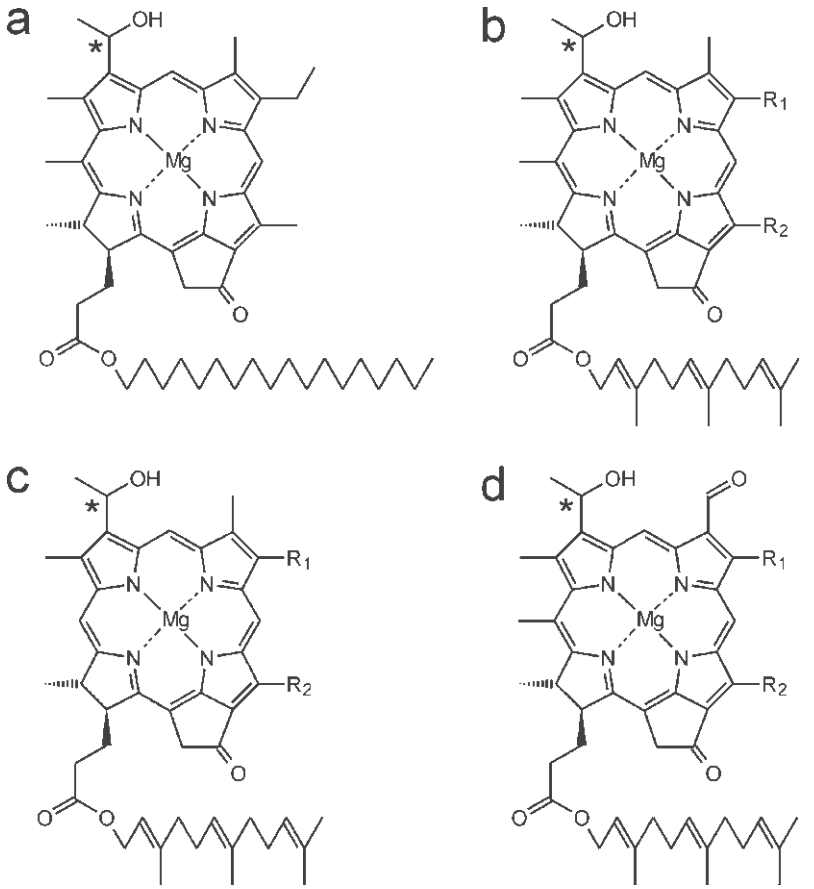

Fig. 1. (a) Structure of [8-E,12-M]-BChl *c* esterified with stearol, which is the predominant BChl *c* homolog in the green filamentous bacterium *Cfx. aurantiacus*. (b, c, d) Structures of the [8-R_1,12-R_2] homologs of BChl *c*, BChl *d*, and BChl *e*, respectively, esterified with farnesol as they typically occur in green sulfur bacteria. (R_1 = ethyl, *n*-propyl, *iso*-butyl, or *neo*-pentyl; R_2 = methyl or ethyl; a star denotes the chiral carbon C-3[1], which can be either R or S configured).

et al., 2002, 2003). The resulting mutants that have been generated by this approach have been characterized and their pigment contents analyzed by HPLC and mass spectroscopic analyses. Although BChl *a* is required for the viability of *Chl. tepidum*, it has nevertheless been possible to generate mutations in some genes thought to be involved in the synthesis of this BChl. These findings can be used to probe those portions of BChl *a* that are most critically involved in its functions in vivo.

II. Approach to Elucidating Bacteriochlorophyll Biosynthesis in Green Bacteria

When the photosynthesis gene cluster, a region of approximately 46 kb that includes all genes necessary for photosynthesis, was identified and completely sequenced in the purple bacterium *Rhodobacter* (*Rba.*) *capsulatus*, new approaches became possible for the elucidation of the biosynthetic pathway for BChl *a* (Alberti et al., 1995; Naylor et al., 1999). A similar organization has been found in other proteobacteria (Béjà et al., 2002) and *Heliobacillus* (*Hba.*) *mobilis* (Xiong et al., 1998). The facile identification of the genes for BChl *a* biosynthesis in purple bacteria facilitated extensive studies by genetic complementation of mutants deficient in BChl *a* biosynthesis, by the inactivation of genes in *Rhodobacter* species (Coomber et al., 1990; Bollivar et al., 1994b; Naylor et al., 1999), and by the characterization of heterologously expressed enzymes (Bollivar et al., 1994a; Porra, 1997; Suzuki et al., 1997; Willows, 2003; Chapters 10–14). Unfortunately, no extensive clustering of photosynthesis genes is observed in the green bacteria. This drawback and the lack of suit-

able genetic methods meant that the study of BChl biosynthesis in green bacteria lagged significantly behind that in purple bacteria. An approach to the elucidation of the BChl *c* biosynthetic pathway in the green bacteria has been to identify genes encoding potential BChl biosynthetic enzymes in the genome sequences of *Chl. tepidum* and *Chloroflexus* (*Cfx.*) *aurantiacus* by sequence similarity to genes encoding known enzymes involved in the synthesis of Chl *a* and BChl *a* in other organisms. As candidates for novel activities, ancillary genes, which are found in putative operons and other gene clusters that contain genes encoding BChl biosynthesis or other photosynthesis genes in both *Chl. tepidum* and *Cfx. aurantiacus*, have additionally been targeted for mutagenesis.

A. Bacteriochlorophyll Biosynthesis Genes in Chlorobium tepidum

Orthologs of all genes known to be involved in the oxygen-independent, anaerobic synthesis of BChl *a* are found in the genome of *Chl. tepidum* (Eisen et al. 2002; see Fig. 2 and Table 1). Additionally, the *Chl. tepidum* genome contains numerous duplications of related genes: two paralogs (*CT0372/hemN* and *CT2010/hemN-II*) of the oxygen-independent coproporphyrinogen oxidase (HemN); two paralogs (*CT1421/bchF* and *CT1776/bchV*) of the 3-vinyl hydratase (BchF); two paralogs (*CT2256/bchP* and *CT1232/bchO*) of a BchP-like geranylgeranyl reductase; three paralogs (*CT1992/bchK*, *CT1610/bchG*, and *CT1270/chlG*) of (B)Chl synthases; three paralogs (*CT1957/bchH*, *CT1955/bchS*, and *CT1295/bchT*) of the large subunit of magnesium chelatase (BchH); and seven paralogs (*CT1959/bchE*, *CT1777/bchQ*, *CT1320/bchR*, *CT0072*, *CT1502*, *CT1697*, and *CT1903*) of enzymes related to the oxidative cyclase (BchE) and C- and P-methyltransferases. Fig. 2a shows the organization of operons encoding some of these genes. Only a few (B)Chl biosynthesis genes in *Chl. tepidum* are encoded in operons, e.g., *bchNBL*, *bchFCX*, and *bchID* (Fig. 2a), and these are

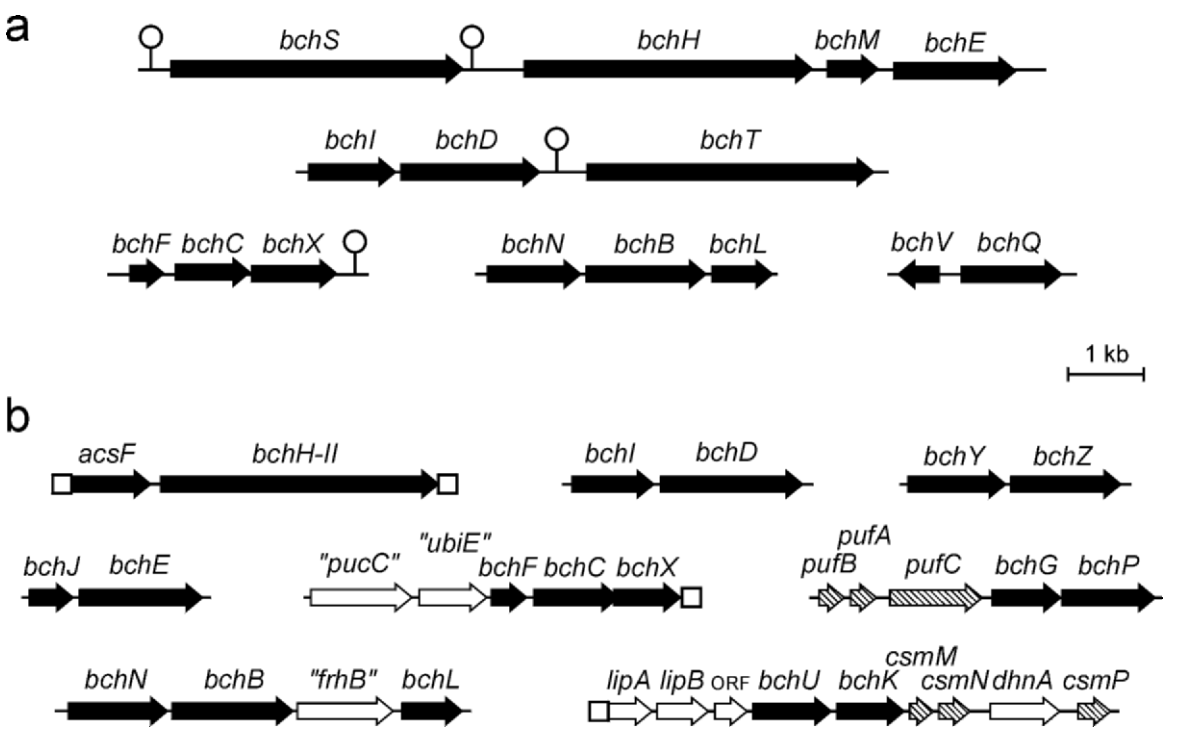

Fig. 2. Organization of genes involved in BChl biosynthesis in (a) *Chl. tepidum* (Eisen et al., 2002) and (*b*) *Cfx. aurantiacus* (DOE Joint Genome Institute, http://www.jgi.doe.gov). BChl biosynthesis-related genes are shown in black, other known photosynthesis-related genes in stripes, and other genes in white. Circles indicate potential Rho-independent transcription termination sequences (no analysis of such sequences was carried out on the *Cfx. aurantiacus* data) and squares indicate end of available DNA sequence. Only genes that cluster with other photosynthesis-related genes are shown. The following genes do not cluster with other known photosynthesis-related genes in *Chl. tepidum*: *bchG, bchJ, bchK, bchP, bchU, bchY, bchZ*, and *chlG* and in *Cfx. aurantiacus*: *bchH-I, bchM* and *bchS*.

Table 1. Confirmed and predicted genes functioning in BChl and Chl biosynthesis in *Chl. tepidum*

Gene	Locus	Gene product	Comments
bchB	*CT2151*	Protochlorophyllide reductase subunit B	
bchC	*CT1422*	[3-Hydroxyethyl]-bacteriochlorophyllide *a* dehydrogenase	BChl *a*-specific
bchD	*CT1296*	Mg chelatase subunit D	
bchE	*CT1959*	Mg-protoporphyrin IX methyl ester cyclase	Possibly also [13-vinyl] Mg-protoporphyrin IX cyclase
bchF	*CT1421*	3-Vinyl hydratase	Probably produces C-3^1 R-stereochemistry
bchG	*CT1610*	BChl *a* synthase	BChl *a*-specific
bchH	*CT1957*	Mg-chelatase subunit H	Possibly BChl *a* and Chl *a* specific; gene inactivated
bchI	*CT1297*	Mg-chelatase subunit I	
bchJ	*CT2014*	8-Vinyl reductase	
bchK	*CT1992*	BChl *c* synthase	BChl *c*-specific; gene inactivated (mutant lacks BChl *c*)
bchL	*CT2150*	Protochlorophyllide reductase subunit L	
bchM	*CT1958*	SAM:Mg-protoporphyrin IX methyl transferase	Possibly BChl *a* and Chl *a* specific
bchN	*CT2152*	Protochlorophyllide reductase subunit N	
bchO	*CT1232*	Geranylgeranyl reductase II	Gene inactivated (altered tailing for BChl *a* and Chl *a*); BchP paralog
bchP	*CT2256*	Geranylgeranyl reductase I	Gene inactivated (altered tailing for BChl *a* and Chl *a*)
bchQ	*CT1777*	C-8^2 methyltransferase	BChl *c*-specific; gene inactivated
bchR	*CT1320*	C-12^1 methyltransferase	BChl *c*-specific; gene inactivated
bchS	*CT1955*	Mg-chelatase subunit S	BChl *c*-specific; gene inactivated; BchH paralog
bchT	*CT1295*	Mg-chelatase subunit T	Probably BChl *a*-specific; gene inactivated; BchH paralog
bchU	*CT0028*	C-20 methyltransferase	BChl *c*-specific; gene inactivated; CrtF homolog
bchV	*CT1776*	3-Vinyl hydratase	BChl *c*-specific; gene inactivated; probably produces C-3^1 S-stereochemistry; BchF paralog
bchX	*CT1423*	Chlorophyllide *a* reductase subunit X	BChl *a*-specific
bchY	*CT1826*	Chlorophyllide *a* reductase subunit Y	BChl *a*-specific
bchZ	*CT2125*	Chlorophyllide *a* reductase subunit Z	BChl *a*-specific
chlG	*CT1270*	Chl *a* synthase	Chl *a*-specific

similar to operons found in *Cfx. aurantiacus* (Fig. 2b; see below). Interestingly, analysis of potential Rho-independent transcription terminator sequences suggests that, although the *bchS* and *bchT* genes are clustered with other genes encoding proteins with functions related to BChl biosynthesis, these genes are probably transcribed independently of the other genes in their respective clusters (Fig. 2a).

B. Bacteriochlorophyll Biosynthesis Genes in Chloroflexus aurantiacus

Orthologs of all known genes involved in BChl *a* biosynthesis can also be found in the genome of *Cfx. aurantiacus* (DOE Joint Genome Institute, http://www.jgi.doe.gov). In contrast to *Chl. tepidum*, obvious paralogs of genes involved in BChl biosynthesis are more limited in number. They include two paralogs of the oxygen-independent coproporphyrinogen oxidase (HemN); two paralogs (BchG and BchK) of BChl synthases; three paralogs of the gene encoding the large subunit of magnesium chelatase (BchH); and two paralogs of the oxidative cyclase (BchE). The *bchU* gene, encoding the BChl C-20 methyltransferase (Section VII.D), is found upstream of *bchK* encoding BChl *c* synthase and genes encoding chlorosome proteins CsmM, CsmN, and CsmP. Homologs of the BchQ and BchR C-methyltransferases are not found, since unlike green sulfur bacteria, *Cfx. aurantiacus* does not synthesize BChl *c* with additional methylations at the C-8^2 and C-12^1 positions (Section VII.C).

III. Overview of Proposed Pathways

Several BChl *c*-specific genes have been identified by interposon mutagenesis. This group includes genes that encode a Mg-chelatase subunit (*bchS*), a C-20 methyltransferase (*bchU*), a C-8^2 methyltransferase (*bchQ*), a C-12^1 methyltransferase (*bchR*), a C-3^1 hydratase (*bchV*), and a BChl *c* synthase (*bchK*) (see Section VII and Table 1). All of these genes, except *bchU*, encode proteins that are paralogous to enzymes that function in BChl *a* biosynthesis. Some genes encoding enzymes with activities required in both BChl *a* and BChl *c* biosynthesis are obviously not duplicated in the *Chl. tepidum* genome, and the enzymes encoded by these genes probably function in both pathways. This category includes genes encoding two Mg-chelatase subunits (*bchD* and *bchI*), Mg-Proto monomethyl ester oxidative cyclase (*bchE*), C-8 vinyl reductase (*bchJ*), and PChlide reductase (*bchN*, *bchB*, and *bchL*) (Section V.A).

It is not yet clear at which step the BChl *c* and BChl *a* pathways bifurcate, but the bifurcation is most likely related to removal of the C-13^2 carboxylate moiety. The removal of this C-13^2 carboxylate or methylcarboxylate group could conceivably involve any intermediate from Proto up to Chlide *a*, and it is not clear whether decarboxylation occurs before or after formation of the isocyclic ring. In any case, it appears likely that *Chl. tepidum* uses different subunits of the Mg-chelatase to regulate the relative yields of BChl *c* and BChl *a* (and possibly Chl $a_{\Delta 2,6}$). Since green sulfur bacteria typically synthesize about 30 times more BChl *c* than BChl *a* and about 10 times more BChl *a* than Chl $a_{\Delta 2,6}$, such regulation is essential (Frigaard et al., 2002, 2003). If all three Mg-chelatases accept Proto as substrate, substrate destiny could be controlled if the BchH, BchS, and BchT subunits bind the substrate until several enzymes have acted upon it (a phenomenon known as 'substrate channeling'). If removal of the C-13^2 carboxylate moiety occurs after chelation, then Chlide *a* would seem to be the most logical substrate and would lead to the production of [3-vinyl]-BChlide *d*. An attractive aspect of this postulated pathway is that only BChl *c*-specific enzymes are required to produce BChlide *c* from Chlide *a* (except C-3^1 hydration which most likely involves BchF). Pathway A in Figs. 3 and 4 illustrates this possibility. If removal of the C-13^2 carboxylate group occurs prior to chelation, the substrate for chelation would likely be [13-vinyl]-Proto and this could explain the need for a BChl *c*-specific chelatase (BchSDI). Pathway C in Figs. 3 and 4 illustrates this possibility. The proposed Pathways A and C require unidentified enzyme(s) to remove the C-13^2 group. If the BchSID enzyme prevents methylation by BchM, the subsequent oxidative cyclization by BchE could lead to spontaneous decarboxylation. This possibility, which does not require enzymes other than those currently known, is illustrated in Pathway B in Figs. 3 and 4.

Anesthetic gases, such as ethylene, acetylene or N_2O, have been found to inhibit BChl *d* synthesis but not BChl *a* formation in *Chl. vibrioforme,* and they cause the accumulation of Mg-Proto monomethyl ester (Ormerod et al., 1990; Frigaard and Ormerod, 1995). One interpretation of this observation is that the anesthetic gases inhibit an enzyme that is specific for BChl *d* biosynthesis, most likely the one involved

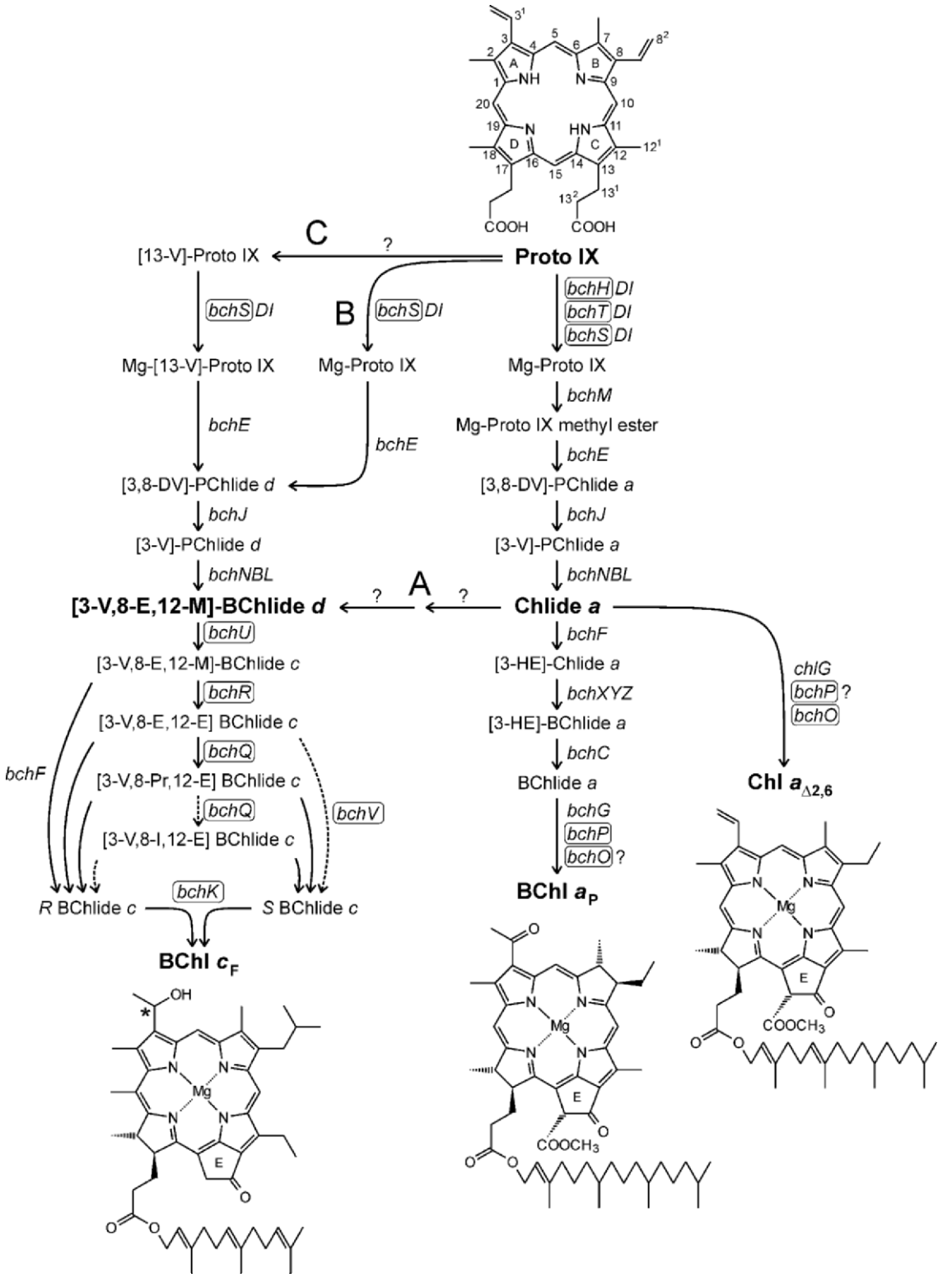

Fig. 3. Proposed biosynthetic pathways of BChl c_P, BChl a_P, and Chl $a_{\Delta 2,6}$ in *Chl. tepidum*. Genes that have been inactivated are boxed. The three alternative pathways A, B, and C leading to [3-vinyl]-BChlide *d* are indicated. See text for details. Only the maximally methylated BChl *c* is shown as the final product.

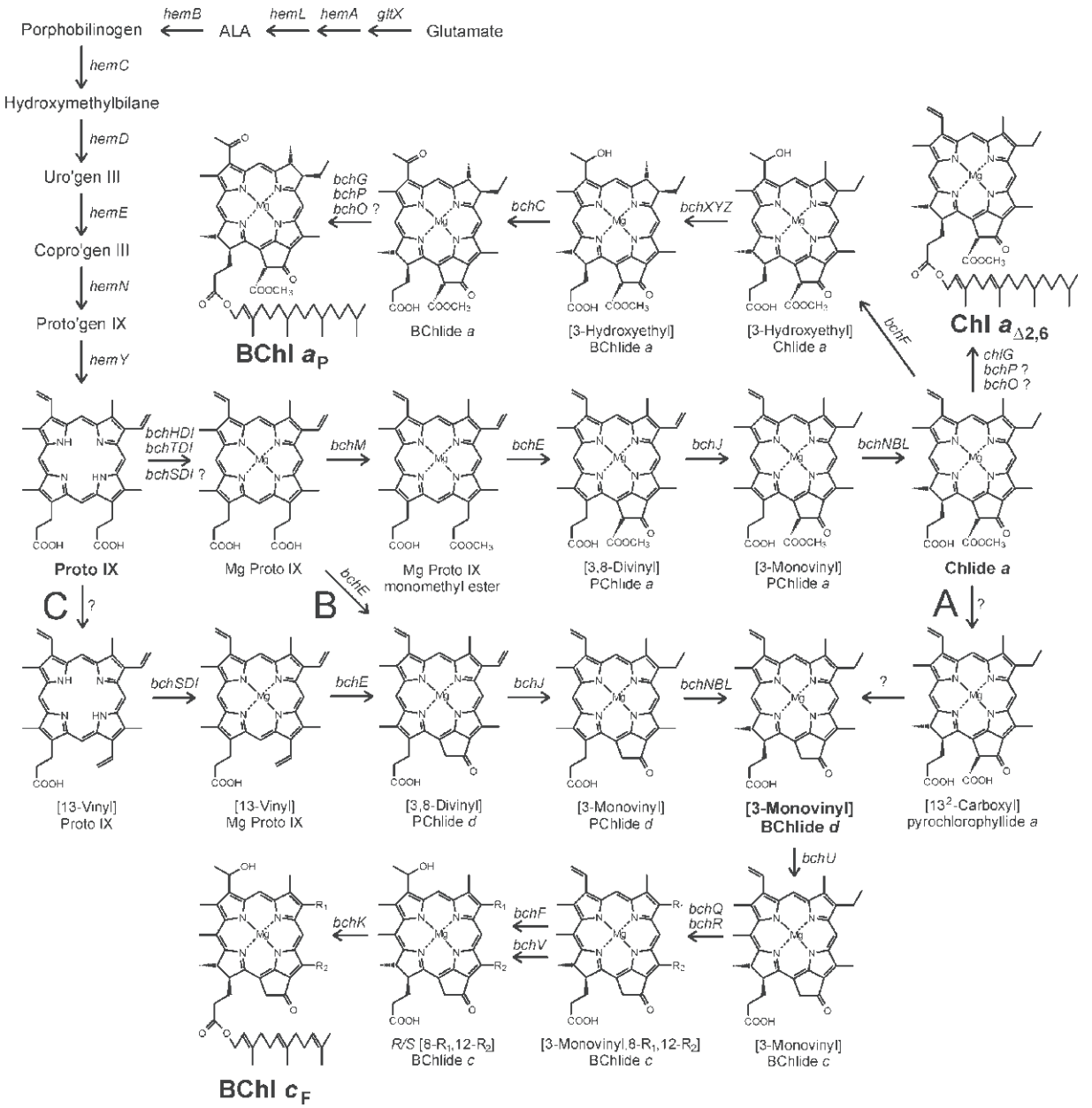

Fig. 4. Proposed biosynthetic pathways of BChl c_F, BChl a_P, and Chl $a_{\Delta 2,6}$ in *Chl. tepidum* showing structures of the intermediates. The three alternative pathways A, B, and C leading to [3-monovinyl]-BChlide *d* are indicated. See text for details

in removal of the C-13^2 carboxylate or methylcarboxylate group. Pathway A proposed above for BChl *c* biosynthesis seems to be most consistent with this observation, since a block in this pathway could potentially cause the accumulation and excretion of Mg-Proto monomethyl ester.

Although the relationship may not be immediately apparent, the synthesis of BChl *c*, which is a pyrochlorophyll (i.e., a Chl that has no carbon substituents at C-13^2), could be related evolutionarily, or at least mechanistically, to Chl degradation in eukaryotic algae and higher plants. Pyropheophytins and pyropheophorbides have been detected in various organisms, including photosynthetic bacteria (Haidl et al., 1985), eukaryotic algae (Schoch et al., 1981; Ziegler et al., 1988), and plants (Shimokawa et al.,

1990). Similar to the proposed reactions in Figs. 3 and 4, specific enzymatic reactions eliminate the C-13[2] methylcarboxylate group as early steps in the Chl *a* degradation pathways of some organisms (Matile et al., 1996, 1999; Hörstensteiner, 1999; Matile, 2000; Takamiya et al., 2000; Suzuki et al., 2002). Three possible mechanisms have been proposed: 1) a methyl esterase and a decarboxylase may act in succession; 2) a methyl esterase acts alone and is followed by spontaneous decarboxylation; and 3) a single unidentified enzyme removes the methylcarboxylate group in a concerted fashion. Kräutler and Hörtensteiner (Chapter 17) provide a detailed description of Chl biodegradation.

IV. Early Steps in Porphyrin Biosynthesis

The first universal, committed precursor in tetrapyrrole biosynthesis is 5-aminolevulinate (ALA) (Beale, 1995; Chapter 11, Beale). Plants and most bacteria synthesize ALA from glutamate, whereas purple bacteria, other α-proteobacteria, and eukaryotes other than plants synthesize ALA from glycine and succinyl-CoA. In both *Chlorobium* and *Chloroflexus* species, ALA is synthesized via the C_5 glutamate pathway as shown by isotope labeling studies (Anderson et al., 1983; Smith and Huster, 1987; Avissar et al., 1989; Rieble et al., 1989; Swanson and Smith, 1990; Smith, 1991; Beale, 1995). Beale and coworkers (Majumdar et al., 1991) showed that *Chl. vibrioforme hemA* could complement an *Escherichia* (*E.*) *coli hemA* mutant, thereby establishing that *hemA* encodes the glutamyl-tRNA reductase. In agreement with these studies, the *gltX*, *hemA*, and *hemL* genes, encoding glutamyl-tRNA synthetase, glutamyl-tRNA reductase, and glutamate-1-semialdehyde 2,1-aminomutase, respectively, of the glutamate C_5 pathway are found in the genome sequence of *Chl. tepidum* and *Cfx. aurantiacus* (Fig. 4). No gene encoding 5-aminolevulinate synthase, the enzyme responsible for the synthesis of 5-aminolevulinate in the alternative succinyl-CoA pathway (Beale, 1995), has been found in the genomes of these green bacteria (Eisen et al., 2002; DOE Joint Genome Institute, http://www.jgi.doe.gov).

The genes encoding the remaining enzymes leading to the key tetrapyrrole intermediate, Proto, have also been identified in the *Chl. tepidum* genome sequence by their sequence similarity to the known enzymes of *Chl. vibrioforme* (Rhie et al., 1996) and other bacteria such as *E. coli* (Eisen et al., 2002). These include *hemB* (5-aminolevulinate dehydratase), *hemC* (porphobilinogen deaminase), *hemD* (uroporphyrinogen III synthase), *hemE* (uroporphyrinogen III decarboxylase), *hemN* (oxygen-independent coproporphyrinogen III oxidase), and *hemY* (protoporphyrinogen oxidase) (Fig. 4). A single *hemH* gene, encoding ferrochelatase, which converts Proto into protoheme used in cytochrome biogenesis, is also found in *Chl. tepidum*. The *hemA*, *hemC* and *hemD* genes appear to form an operon in *Chl. tepidum*, and are additionally located near the *hemB* gene, as is the case in *Chl. vibrioforme* (Majumdar et al., 1991; Rhie et al., 1996). The *hemE*, *hemH*, *hemN*, and *hemY* genes of *Chl. tepidum* are not clustered with other genes that encode enzymes for tetrapyrrole biosynthesis.

In *Cfx. aurantiacus*, the genes encoding *hemC*, *hemD*, and *hemH* have not yet been sequenced or are too dissimilar to be identified by sequence similarity search methods (DOE Joint Genome Institute, http://www.jgi.doe.gov). However, most of the remaining genes are found in two apparent operons: *hemN-hemY* and *hemB-hemE-hemL-hemF*. Interestingly, the *Cfx. aurantiacus* genome has genes encoding enzymes for both oxygen-independent and oxygen-dependent enzymes coproporphyrinogen III oxidase (HemN and HemF, respectively) and protoporphyrinogen IX oxidase (HemY and HemK, respectively). These observations are consistent with the ability of *Cfx. aurantiacus* to grow heterotrophically under oxic conditions or photoautotrophically or photoheterotrophically under anoxic conditions.

V. Bacteriochlorophyll *a* Biosynthesis

A. Bacteriochlorophyllide *a* Biosynthesis

Three genes, *bchF*, *bchG*, and *bchM*, involved in BChl *a* biosynthesis in *Chl. tepidum* have been identified by complementation of *Rba. capsulatus* mutants (Xiong et al., 2000). Orthologs of all other genes that are known to be involved in oxygen-independent BChl *a* biosynthesis in purple bacteria have been identified in the *Chl. tepidum* genome by sequence similarity (Eisen et al., 2002). Thus, the biosynthetic pathway for BChlide *a* in *Chl. tepidum* is likely to be identical to that in *Rhodobacter* spp. (Suzuki et al., 1997; Porra, 1997; Willows, 2003; Chapters 10–14) and can briefly be described as follows (see also

Figs. 3 and 4): A heterotrimeric Proto Mg-chelatase (BchHDI) converts Proto to Mg-Proto (Gibson et al., 1995; Willows et al., 1996; Willows and Beale, 1998; Fodje et al., 2001). The C-13^2 carboxylate group of Mg-Proto is then methylated by BchM (Bollivar et al., 1994a; Gibson and Hunter, 1994), possibly while the substrate is still bound to the BchHDI Mg-chelatase (Hinchigeri et al., 1997; Karger et al., 2001). This methylation reaction is followed by the oxidative cyclization reaction, catalyzed by BchE, that forms ring E of [3,8-divinyl]-PChlide *a* (Bollivar et al., 1994b; Gough et al., 2000). The C-8 vinyl group is reduced by BchJ to form [3-monovinyl]-PChlide *a* (Suzuki and Bauer, 1995), and the double bond between C-17 and C-18 of ring D is reduced by PChlide reductase (BchNBL) to form Chlide *a* (Burke et al., 1993b; Fujita and Bauer, 2000). Reduction of the double bond between C-7 and C-8 by BchXYZ produces [3-vinyl]-BChlide *a* (Burke et al., 1993a; McGlynn and Hunter, 1993). The C-3 vinyl group is hydrated by BchF (Burke et al., 1993b), and the resulting hydroxyl is oxidized by BchC to form the C-3^1 oxo group of BChlide *a* (Wellington and Beatty, 1989; McGlynn and Hunter, 1993).

B. Esterification and Reduction

The esterifying isoprenoid tail is added to BChlide *a* and reduced by the combined action of BChl *a* synthase (BchG) and geranylgeranyl reductase (BchP) (Bollivar et al., 1994b,c; Oster et al., 1997; Addlesee and Hunter, 1999, 2002; Addlesee et al., 2000). It is still uncertain whether the reduction of the geranylgeranyl moiety to a phytyl moiety takes place before or after the esterification with BChlide *a* (Oster et al., 1997; Addlesee and Hunter, 1999; Addlesee et al., 2000). In vitro studies with recombinant BChl synthase from *Rba. capsulatus* suggest that the preferred substrate for the esterification reaction is phytyl (P) diphosphate rather than geranylgeranyl (GG) diphosphate, although both substrates are utilized by the BchG enzyme (Oster et al., 1997). This could imply that reduction by BchP takes place prior to esterification. However, Addlesee and coworkers (Addlesee and Hunter, 1999, 2002; Addlesee et al., 2000) have reached the opposite conclusion based on studies with enzymes from *Rba. sphaeroides* and *Rhodospirillum* (*Rsp.*) *rubrum*. They find that BchP can act after esterification of BChlide *a*, and have additionally identified a homolog of BchP that can reduce the double bonds of BPhe a_{GG} to produce BPhe a_P in *Rsp. rubrum* (Addlesee and Hunter, 2002).

The esterifying alcohol in Chl $a_{\Delta 2,6}$, Δ2,6-phytadienol, is also most likely derived from geranylgeranyl diphosphate by reduction of two double bonds, but again it is unclear whether this reduction takes place before or after esterification and whether the reductase is the same that reduces three double bonds in the geranylgeranyl moiety in BChl *a* to phytyl. Biochemical characterization of the BChl *a* synthase (BchG) and Chl *a* synthase (ChlG) will be required to resolve this issue, although even this may not adequately account for possible substrate channeling effects and the relative in vivo concentrations of phytyl diphosphate and geranylgeranyl diphosphate.

Two paralogous *bchP* genes, *CT2256* and *CT1232*, are present in the *Chl. tepidum* genome. The product of *CT2256* is more similar to the BchP proteins of purple bacteria, while the product of *CT1232*, denoted BchO (Table 1), is more distantly related to the BchP proteins of purple bacteria. Because the esterifying alcohols of BChl *a* and Chl $a_{\Delta 2,6}$ are different, it was initially hypothesized (Eisen et al., 2002) that these different gene products would catalyze the reduction of these two different esterifying alcohols in a fashion similar to that suggested by Addlesee and Hunter (2002) recently for BChl *a* and bacteriopheophytin (BPhe) *a*. However, the HPLC profiles of pigments extracted from *Chl. tepidum* mutants lacking either BchP or BchO were virtually identical, although clearly different from wild type (A. Gomez Maqueo Chew, N.-U. Frigaard, and D. A. Bryant, unpublished). Both mutants contain BChl *a* and Chl *a* species with esterifying alcohols that appear to be less reduced than in the wild-type strain. Further studies will be required to establish the roles of these two enzymes.

VI. Chlorophyll *a* Biosynthesis

It is possible that Chl $a_{\Delta 2,6}$ is derived from the same pool of Chlide *a* that is used for BChl *a* biosynthesis (Section III; Figs. 3 and 4). However, since the *Chl. tepidum* genome encodes three homologs of the large subunit of Mg-chelatase, and since one of these homologs clearly is nearly specific for BChl *c* biosynthesis, it is also possibly that Chl $a_{\Delta 2,6}$ is synthesized from Proto via intermediates sequestered from those of BChl *a* biosynthesis by a substrate channeling mechanism (Sections III and VII).

The *Chl. tepidum* genome encodes a polyprenyl transferase (CT1270) that is apparently orthologous to

cyanobacterial and plant-like Chl *a* synthases (Eisen et al., 2002; Frigaard et al., 2002), and Chl $a_{\Delta 2,6}$ is probably synthesized from Chlide *a* by this synthase. Attempts to inactivate this gene have not yet been successful (Frigaard et al., 2002). These results suggest that Chl $a_{\Delta 2,6}$ is essential in *Chl. tepidum* and cannot easily be substituted by another (B)Chl species.

VII. Bacteriochlorophyll *c* Biosynthesis

A. Magnesium Chelation

The first committed step in Chl *a* and BChl *a* biosynthesis is the Mg insertion into Proto by magnesium chelatase (Bollivar et al., 1994b; Gibson et al., 1995; Jensen et al., 1996; Willows et al., 1996; Porra, 1997; Suzuki et al., 1997; Willows and Beale, 1998; Willows, 2003). This enzyme consists of a large, Proto-binding subunit of about 140 kDa (BchH) and two smaller subunits with masses of approximately 70 kDa (BchD) and 40 kDa (BchI) (Bollivar et al., 1994; Gibson et al., 1995; Petersen et al., 1998a,*b*). The structure of the BchI ATPase was recently determined by X-ray crystallography (Fodje et al., 2001). The *Chl. tepidum* genome has only single genes encoding each of the smaller subunits, *bchD* and *bchI* (Table 1) but has three paralogous genes, *CT1295*, *CT1955*, and *CT1957,* that encode the largest subunit (Eisen et al., 2002). These have been designated *bchT*, *bchS*, and *bchH*, respectively (Table 1), and the phylogenetic relationship of these proteins to one another and to related proteins in *Cfx. aurantiacus* and other organisms is shown in Fig. 5. One simple hypothesis for the presence of multiple BchH-like proteins in *Chl. tepidum* is that each performs a specialized function. Inactivation of the *bchS* gene (*CT1955*) caused the nearly complete elimination of BChl *c* biosynthesis (A. Gomez Maqueo Chew, N.-U. Frigaard, D. A. Bryant, unpublished), although small amounts of BChl *c* are still synthesized in this mutant. This result suggests that BChl *c* cannot readily be synthesized from the tetrapyrrole intermediates produced by the BchHID and BchTID enzymes that presumably participate in BChl *a* and Chl $a_{\Delta 2,6}$ biosynthesis. Inactivation of the *bchH* gene had little effect on the (B)Chl content of the cells, but a *bchT* mutant produced somewhat less BChl *c* than the wild type.

One hypothesis to explain these observations is that the BchH, BchS, and BchT proteins do not release their Mg-chelated products but instead channel these

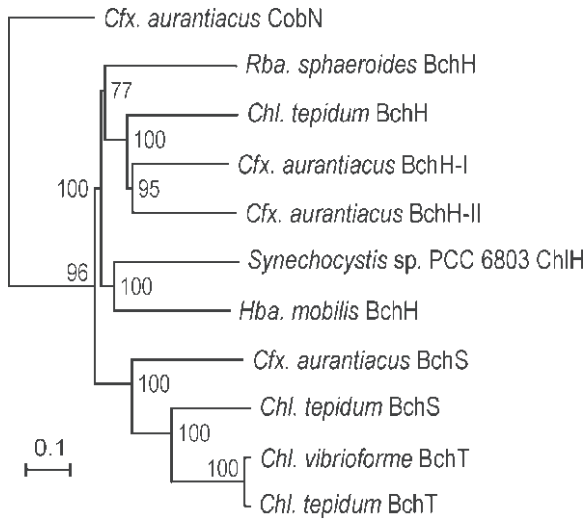

Fig. 5. Phylogenetic neighbor-joining distance tree showing the relationships among the largest subunit of Proto Mg-chelatase (BchH, BchS, BchT, and ChlH) from various photosynthetic organisms. CobN, a subunit of cobalt chelatase for cobalamin biosynthesis, was used as an outgroup. The scale bar relates the branch lengths to the relative number of amino acid substitutions. Bootstrap values (in percentage) based on 1000 replications are also shown. Abbreviations: *Rba*., *Rhodobacter*; *Chl*., *Chlorobium*; *Cfx*., *Chloroflexus*; *Hba*., *Heliobacillus*.

products, possibly through several enzymatic steps, to specific product endpoints ('substrate channeling,' Pathway A in Fig. 3). Several lines of evidence suggest that this could be the case. Hinchigeri et al. (1997) found that exogenously added BchH stimulated the conversion of Mg-Proto to Mg-Proto monomethyl ester by BchM. Jensen et al. (1996) showed that, when ChlH, ChlI, and ChlD were expressed in *E. coli*, Mg-Proto accumulated, but when ChlM was coexpressed in the same cells, only Mg-Proto monomethyl ester was detected. In these in vitro experiments, the ratio of ChlH to ChlM determined whether Mg-Proto or only its monomethyl ester accumulated. At substoichiometric ratios of these proteins, Mg-Proto was detected, but only the monomethyl ester was detected when the ratio of these proteins was 1:1. Since *Chl. tepidum* produces three classes of (B)Chls (BChl *a*, Chl *a*, and BChl *c*), each BchH homolog might channel Mg-Proto towards a specific (B)Chl end product. Finally, Karger et al. (2001) recently reported that the K_d for Mg-Proto of BchH is actually lower than the K_d for the substrate, Proto (i.e., the product is more tightly bound by BchH than the substrate). This observation is consistent with the idea that a BchH-Mg-Proto complex is the substrate for

BchM, the next enzyme in the biosynthetic pathway for BChl *a* and Chl *a*.

Yet unidentified enzymes, possibly an esterase and a decarboxylase, would be required to remove the C-13^2 methylcarboxylate moiety (Pathway A in Figs. 3 and 4). Another possibility is that the BchSID Mg-chelatase prevents subsequent methylation by the BchM methyltransferase. During the subsequent oxidative cyclization reaction catalyzed by BchE, decarboxylation of the C-13^2 carboxyl group might occur (Pathway B in Figs. 3 and 4). Finally, it is possible that the substrate for the BchSID Mg-chelatase is different from those for the BchHID and BchTID enzymes. Since the major structural feature that distinguishes BChl *c*, *d*, and *e* from BChl *a* and Chl *a* is the absence of the C-13^2 methylcarboxylate moiety, it is possible that an intervening enzymatic reaction leads to decarboxylation of the C-13 propionate of Proto prior to Mg-chelation by BchSID (Pathway C in Figs. 3 and 4).

B. Isocyclic Ring Formation

In BChl *a* biosynthesis, the C-13 propionate group of Mg-Proto is converted into ring E of PChlide by a complex oxidation that is catalyzed by BchE (Bollivar et al., 1994b; Gough et al., 2000). This oxidation occurs after the carboxylate group is protected by methylation by BchM (Bollivar et al., 1994a; Gibson and Hunter, 1994). The exact substrate for the formation of ring E in BChl *c* biosynthesis is not yet known; it would be determined by when decarboxylation or demethylcarboxylation at C-13^2 occurs (see Figs. 3 and 4, pathways A, B, and C).

The *Chl. tepidum* genome contains seven *bchE* paralogs and all except *CT1959* have been insertionally inactivated (A. Gomez Maqueo Chew, N.-U. Frigaard, D. A. Bryant, unpublished). Since CT1959 is most similar in sequence to the BchE product of *Rba. capsulatus*, and since the *CT1959* gene lies downstream from *bchM*, it is likely that this gene encodes the oxidative cyclase in *Chl. tepidum* and would thus be required for viability. Consistent with this interpretation, none of the six mutants, each lacking a single *bchE* paralog, is devoid of BChl *c*, BChl *a*, or Chl *a*. These results provide further evidence that the product of *CT1959* probably participates in the biosynthesis of BChl *a*, Chl $a_{\Delta 2,6}$ and BChl *c*.

In contrast to BChl *a* and Chl $a_{\Delta 2,6}$ (see Figs. 1 and 3), BChl *c* has no C-13^2 methylcarboxylate group. BchE could play a role in the removal of this group in BChl *c* biosynthesis. If the BchSID chelatase prevents methylation of the Mg-proto IX by BchM, then BchE could cause oxidative decarboxylation during the cyclization reaction (Pathway B in Figs. 3 and 4). Alternatively, if decarboxylation occurs prior to Mg chelation in BChl *c* biosynthesis, then BchE would have to convert [13-vinyl]-Mg-proto IX to [3,8-divinyl]-PChlide *d* (Pathway C in Figs. 3 and 4). Resolution of this issue will probably require in-depth biochemical studies with BchE and the predicted substrates described above, although it is possible that mass spectroscopic analyses of intermediates that accumulate in various mutants will also help to resolve this issue.

C. C-8^2 and C-12^1 Methylation

The typical distribution of BChl *c* homologs in *Chl. tepidum* obtained under laboratory growth conditions is about 5% [8-E,12-M]-BChl *c*, 60% [8-E,12-E]-BChl *c*, 30% [8-Pr,12-E]-BChl *c*, and 5% [8-I,12-E]-BChl *c* but the exact composition varies with growth conditions (Borrego et al., 1999). The 8-*neo*-pentyl homolog is not routinely detected in *Chl. tepidum*, although this molecule is found in small amounts in some other green sulfur bacteria containing BChl *c*, *d*, or *e* (Smith et al., 1983a; Bobe et al., 1990). In general, at least 90% of the BChl *c*, *d*, or *e* in green sulfur bacteria is methylated to the ethyl species in the C-12^1 position, and between 30 and 60% is methylated in the C-8^2 position (Borrego et al., 1999; Airs et al., 2001; Glaeser et al., 2002). It is not known how this methylation is regulated, but the observation that the degree of methylation increases slightly at low light intensity indicates that light intensity or growth rate may influence the regulation (Bobe et al., 1990; Huster and Smith, 1990; Borrego and Garcia-Gil, 1995; Borrego et al., 1998, 1999; Bañeras et al., 1999; Airs et al., 2001; Guyoneaud et al., 2001). The major esterifying alcohol is farnesol, although subsets of homologous BChl *c* molecules with other long-chain, esterifying alcohols are usually detected (Section VII.F). However, the methylation pattern on C-8^2 and C-12^1 is similar in all subsets regardless of the esterifying alcohol (Steensgaard et al., 1996; Airs et al., 2001; Glaeser et al., 2002), which indicates that the methylation reactions occur before the esterifying alcohol is added. Methylation on the C-8^2 and C-12^1 carbons does not occur in *Cfx. aurantiacus*.

As noted above, the *Chl. tepidum* genome contains seven paralogs of *bchE*, the gene that encodes

the oxidative cyclase that forms ring E in PChlide (Section VII.B). This group of enzymes belongs to the P-methyltransferase/oxidative cyclase superfamily, and since BchE acts on a porphyrin substrate, it was suggested that some of the BchE homologs probably function as C-methyltransferases in BChl *c* biosynthesis (Eisen et al., 2002). Indeed, two of the *bchE* homologs in *Chl. tepidum* have been shown to encode C-methyltransferases: inactivation of *CT1777*, now designated *bchQ*, causes the accumulation of [8-E,12-M]-BChl *c* and [8-E,12-E]-BChl *c* and inactivation of *CT1320*, now designated *bchR*, causes the accumulation of three BChl *c* homologs, tentatively identified as [8-E,12-M]-BChl *c*, [8-Pr,12-M]-BChl *c*, and [8-I,12-M]-BChl *c* (A. Gomez Maqueo Chew, N.-U. Frigaard, D.A. Bryant, unpublished). Thus, BchQ is the C-8^2 methyltransferase and BchR is the C-12^1 methyltransferase. A double mutant in both *bchQ* and *bchR* accumulates only [8-E,12-M] BChl *c*. Inactivation of other *bchE* homologs did not cause any detectable changes in BChl *c* biosynthesis, and thus BchQ is able to catalyze the introduction of multiple methyl groups on the C-8^2 carbon. Since the *bchR* mutant still produces homologs that differ in the degree of methylation at C-8^2, it is clear that the introduction of these additional methyl groups at C-8^2 does not depend upon prior methylation at C-12^1.

All BchE homologs in *Chl. tepidum* are proteins with masses of 50 to 60 kDa, and they share sequence similarity to biotin synthase, lipoic acid synthase and other enzymes that contain a Cys-X_3-Cys-X_2-Cys-X_n-Cys [4Fe-4S] cluster and a sequence signature for binding cobalamin (Gough et al., 2000). The methyl groups on the C-8^2 and C-12^1 carbons have been shown to originate from *S*-adenosylmethionine (SAM) (Huster and Smith, 1990). The methylation reactions catalyzed by BchQ and BchR probably involve hydrogen abstraction from the C-8^2 or C-12^1 position followed by transfer of a methyl group from methylcobalamin to the carbon radical at C-8^2 or C-12^1. By analogy to other enzymes of this family, it is presumed that SAM binds to the $[4Fe\text{-}4S]^{2+}$ cluster of BchQ or BchR, which is reduced to the +1 state; this is accompanied by the reductive cleavage of SAM into methionine and a 5′-deoxyadenosyl radical. This radical would then abstract a hydrogen atom from the C-8^2 or C-12^1 position of the substrate to yield 5′-deoxyadenosine and a substrate radical. This substrate radical is proposed to abstract a methyl radical from methylcobalamin to yield the methylated substrate and cob(II)alamin. Reduction of cob(II)alamin and a subsequent reaction with a second molecule of SAM would regenerate the methylcobalamin moiety with adenosylhomocysteine as the byproduct. Thus, two SAM molecules would be consumed during the addition of one methyl group to the substrate: one would act to generate a hydrogen-abstracting radical and one would serve as the methyl donor.

The C-8^2 and C-12^1 methylations most likely occur on intermediates lacking a long-chain esterifying alcohol, since the tetrapyrroles that accumulate in a *bchK* mutant of *Chl. tepidum* (Section VII.F) appear to be a complex mixture of species carrying from none to three methyl groups (N.-U. Frigaard, D. A. Bryant, unpublished data). The C-8^2 and C-12^1 methylations probably take place on 3-vinyl BChlide precursors because a C-3^1 hydratase *bchV* mutant of *Chl. tepidum* accumulates 3-vinyl BChl *c* species that are methylated in both C-8^2 and C-12^1 (Section VII.E).

D. C-20 Methylation

A single enzyme is apparently responsible for the methylation of the C-20 methine carbon in the BChl *c* and BChl *e* biosynthetic pathways. This methyltransferase enzyme is expected to be of a different class than the C-8^2 and C-12^1 methyltransferases discussed above, since it acts on an activated carbon atom that is part of an aromatic system. As for the C-8^2 and C-12^1 methylations, the methyl group at C-20 is derived from SAM (Huster and Smith, 1990).

In an effort to identify the C-20 methyltransferase, the *Chl. tepidum* genome was initially surveyed for paralogs of *cbiL* (*CT0388*), which encodes a C-20 methyltransferase involved in cobalamin biosynthesis. Only one gene (*CT1763*) was found that predicted a product with some sequence similarity to CbiL. However, a mutant of *Chl. tepidum* in which *CT1763* was insertionally inactivated retained the ability to synthesize BChl *c*, and thus it was concluded that *CT1763* could not encode a BChl C-20 methyltransferase (Maresca et al., 2004).

In a different approach, it was noticed that, in *Cfx. aurantiacus*, a *crtF* paralog occurs immediately upstream of *bchK*, encoding BChl *c* synthase, and genes encoding chlorosome envelope proteins CsmM, CsmN, and CsmP (Fig. 2b). This operon structure suggested that the *crtF* paralogous gene might also play some role in BChl *c* synthesis and/or in chlorosome formation or function. Although this *Cfx. aurantiacus* gene was originally annotated *crtF* by Niedermeyer et al. (1994), the protein product is in fact not very

similar to the CrtF proteins of purple bacteria; however, the predicted protein is unusually similar in sequence to a homolog in *Chl. tepidum* (CT0028). Since neither *Chl. tepidum* nor *Cfx. aurantiacus* are known to synthesize O-methylated carotenoids (Takaichi et al., 1995, 1997; Takaichi, 1999), it seemed unlikely that these proteins could be true orthologs of the CrtF enzymes of purple bacteria. Subsequent insertional inactivation of *CT0028* in *Chl. tepidum* produced a BChl *d*-producing mutant; this confirms that CT0028 is a C-20 methyltransferase, and this gene has been named *bchU* (Table 1; Maresca et al., 2004).

Other experimental observations are consistent with CT0028 being the C-20 methyltransferase. *Chl. vibrioforme* strain 8327d synthesizes BChl *d* and therefore lacks the C-20 methyltransferase activity (Broch-Due and Ormerod, 1978; Bobe et al., 1990). However, when cultured under very low light intensities, this strain has been reported to produce revertants that have regained the ability to synthesize BChl *c* (Broch-Due and Ormerod, 1978). This observation indicates that *Chl. vibrioforme* strain 8327d is a mutant that produces a defective C-20 methyltransferase, but that this mutant can regain its C-20 methyltransferase activity through reversion or a second-site suppressor mutation. The open reading frame corresponding to *bchU* has been amplified by PCR from three *Chlorobium* strains: *Chl. tepidum*, *Chl. vibrioforme* strain 8327d, and *Chl. phaeobacteroides* strain 1549 (Maresca et al., 2004). When compared to the same sequence from *Chl. tepidum* and *Chl. phaeobacteroides* 1549, the DNA fragment amplified from *Chl. vibrioforme* 8327d contained a single nucleotide insertion that causes a frameshift mutation in this gene. The protein produced from this mutated gene would be about half the normal predicted size due to premature termination at a stop codon. The *bchU* gene amplified from a BChl *c*-producing revertant of *Chl. vibrioforme* 8327d, denoted strain 8327c, showed a second mutation that restored the reading frame necessary to produce a full-length BchU product.

The actual substrate(s) for the C-20 methyltransferase is not clear. Concentrated cell suspensions of BChl *c*-producing *Chlorobium* sp. fed with various tetrapyrrole precursors have been found to excrete uroporphyrins, coproporphyrin III, Mg-Proto monomethyl ester, and other compounds, none of which are methylated in the C-20 position (Richards and Rapoport, 1966; 1967). A similar examination of the non-esterified tetrapyrroles excreted by the *bchK* mutant of *Chl. tepidum* may reveal those substrates on which C-20 methylation can take place (Frigaard et al., 2002). The observation that BChl *d* apparently is produced in a similar amount in the *bchU* mutant as BChl *c* in the wild type either suggests that C-20 methylation occurs late in the pathway or suggests that, if the methylation occurs early in the pathway, the subsequent enzymes do not strongly discriminate against the presence or absence of a methyl group in the C-20 position.

E. C-3^1 Hydration

BChl *c* has a chiral carbon at the C-3^1 position, which is produced by hydration of the C-3 vinyl group (Figs. 3 and 4). Both the R and S epimers at C-3^1 have been identified in BChl *c*, *d*, and *e* from *Chlorobium* species as well as in BChl *c* from *Cfx. aurantiacus* (Smith et al., 1983b; Smith and Simpson, 1986; Fages et al., 1990; Senge and Smith, 1995). In *Chlorobium* species the ratio of the R and S epimers is highly correlated with the degree of methylation at the C-8^2 and C-12^1 positions, such that highly methylated BChl species are more likely to have S-stereochemistry at C-3^1 and a similar distribution is found in BChl *c*, *d*, and *e* from all *Chlorobium* species investigated (Senge and Smith, 1995). All [8-E,12-M] homologs have R stereochemistry at C-3^1, and most of the [8-E,12-E] homologs also have R stereochemistry. The [8-Pr,12-E] homologs are roughly equally divided into R and S stereochemistry; however, nearly all [8-I,12-E] homologs have S stereochemistry.

The *Chl. tepidum* genome contains two paralogs of the *Rhodobacter* sp. *bchF* gene, which encodes the C-3^1 vinyl hydratase of the BChl *a* pathway (Burke et al., 1993b). One of these paralogs in *Chl. tepidum*, *CT1421*, encodes a protein which is most closely related to the BchF proteins found in purple bacteria, while the second, *CT1776*, has been denoted *bchV* (Table 1) and encodes a more distantly related paralog. BchF presumably functions as the C-3^1-vinyl hydratase in the BChl *a* biosynthetic pathway (Figs. 3 and 4), and the presence of the paralogous *bchV* gene initially suggested that this gene product might be specific for BChl *c* biosynthesis (Eisen et al., 2002). Insertional inactivation of *bchV* in *Chl. tepidum* causes the accumulation of abnormal BChl *c* species which have tentatively been identified through a combination of absorption and mass spectrometry as [3-vinyl]-BChl c_F (A. Gomez Maqueo Chew, N.-U. Frigaard, D. A. Bryant, unpublished). However, only

about 15% of the BChl *c* is affected, which suggests that *bchV* indeed is specific, but not essential, for BChl *c* biosynthesis. The dominant BChl *c* species in the *bchV* mutant is [8-E,12-E]-BChl c_F, and smaller amounts of the [8-E,12-M] and [8-Pr,12-E] homologs are present, but no detectable [8-I,12-E] homolog is found. In the *bchV* mutant the most abundant homolog of [3-vinyl]-BChl c_F is [8-Pr,12-E]; smaller amounts of [8-E,12-E] and [8-I,12-E] were also found, but no [8-E,12-M] homolog was detected. These data suggest that BchF inefficiently hydrates the more highly methylated species and that BchV thus functions to hydrate the more highly methylated BChl homologs. Since the more highly methylated species of BChl *c* are predominantly S epimers, it seems reasonable to suggest that BchV is a hydratase that specifically produces S stereochemistry at C-3[1] and that BchF is a hydratase that produces R stereochemistry at C-3[1]. Assuming these conclusions are correct, a corollary would be that the [3-hydroxyethyl]-BChlide *a* intermediate in BChl *a* biosynthesis should have predominantly if not exclusively R stereochemistry at C-3[1].

F. Esterification

When green sulfur bacteria are grown under optimal laboratory conditions, the predominant esterifying alcohol for BChl *c*, *d*, and *e* is farnesol (Steensgaard et al., 1996; Borrego et al., 1999). However, in contrast to other classes of (B)Chls, other long-chain alcohols are also found in varying amounts including phytol, Δ2,6-phytadienol, geranylgeraniol, hexadecanol, hexadecenol, and tetradecanol (Caple et al., 1978; Airs et al., 2001; Glaeser et al., 2002). *Chl. tepidum* can also readily incorporate alcohols such as phytol, geranylgeraniol, and dodecanol into BChl *c* if these alcohols are supplied in the growth medium (Steensgaard et al., 1996). The synthase incorporating alcohols into BChl *c* seems to be quite promiscuous in its choice of the esterifying alcohol, and thus appears to have less stringently defined specificity for the esterifying alcohol than other (B)Chl synthases.

Insertional inactivation of open reading frame *CT1992* in *Chl. tepidum*, which has strong sequence similarity to Chl *a* and BChl *a* synthases from other organisms, resulted in a BChl *c*-less mutant (Frigaard et al., 2002). Thus, this gene encodes BChl *c* synthase and was subsequently designated *bchK*. Although the *bchK* mutant does not form chlorosomes, it does synthesize vestigial chlorosomes that contain carotenoids and BChl *a* (Frigaard et al., 2002, 2003). These structures, denoted carotenosomes, have a simplified protein composition relative to mature chlorosomes, and they may provide clues to how chlorosomes are formed in vivo. These structures are easily isolated because of their very low density, and they provide an ideal starting material for characterizing the organization of the chlorosome-associated BChl *a*. Finally, a surprising finding is that the *bchK* mutant grows nearly as fast as the wild-type at light intensities above 300 μE m^{-2} s^{-1}; this is mostly due to photoinhibition of the wild type at high light intensities (Frigaard et al., 2002).

VIII. Bacteriochlorophyll *d* Biosynthesis

BChl *d* differs from BChl *c* only by the absence of the C-20 methyl group. BChl *d* biosynthesis is thus expected to be identical to BChl *c* biosynthesis except that C-20 methyl transferase activity would be lacking. *Chl. vibrioforme* strain 8327d, which naturally produces BChl *d* but readily mutates under low-light growth conditions to produce BChl *c* (Broch-Due and Ormerod, 1978; Bobe et al., 1990), is a natural frameshift mutant that encodes a *bchU* gene carrying a single nucleotide insertion (Maresca et al., 2004). Although some reports suggest that some strains exhibit a regulation of the relative amounts of BChl *c* and BChl *d* (Bañeras et al., 1999), BChl *c* and BChl *d* rarely coexist in a green sulfur bacterium in comparable amounts. Since the C-20 methyltransferase in *Chl. tepidum* has now been identified by insertional inactivation (Section VII.D), it will now be possible to use this information to examine the structure and regulation of the C-20 methyltransferase in such species.

IX. Bacteriochlorophyll *e* Biosynthesis

BChl *e* differs from BChl *c* by the presence of a formyl group rather than a methyl group at position C-7. Thus, BChl *e* biosynthesis probably differs from BChl *c* biosynthesis only by the addition of an enzyme to oxidize the C-7 methyl group to a formyl moiety. This enzyme may also belong to the BchE/P-methyltransferase/C-methyltransferase superfamily, since BchE can introduce an oxo group anaerobically (Section VII.B). Alternatively, an enzyme similar to ethylbenzene dehydrogenase of *Azoarcus* sp. could

introduce an oxo group into this position (Johnson et al., 2001). Chl *b* of prochlorophytes, green algae and higher plants also has a C-7 formyl group, but its formation occurs by a different mechanism, since the activity of Chl *a* oxygenase is dependent upon the availability of oxygen (Tanaka et al., 1998).

BChl *e* biosynthesis also requires a C-20 methyltransferase activity similar to BChl *c* biosynthesis (Section VII.D). Polymerase chain reaction has been employed to amplify most of the coding sequence for a *bchU* ortholog from the BChl *e*-containing strain *Chl. phaeobacteroides* 1549, and sequence analysis confirms that this strain has a C-20 methyltransferase with strong sequence similarity to BchU of *Chl. tepidum* (Maresca et al., 2004; Section VII.D). Inactivation of the *bchU* paralog in a strain that synthesizes BChl *e* would presumably cause production of BChl *f*, the structure of which has been proposed (Smith, 2003) but has not been identified from natural sources.

X. Bacteriochlorophyll *c* Biosynthesis in Green Filamentous Bacteria

The photosynthetic green filamentous bacteria are the only organisms other than green sulfur bacteria that contain BChl *c* and chlorosomes, but these eubacteria are otherwise not closely related either phylogenetically or physiologically to the green sulfur bacteria (Pierson and Castenholz, 1995). *Cfx. aurantiacus* contains both BChl *a* and BChl *c* and while the BChl *a* is esterified with phytol as in green sulfur bacteria, the BChl *c* occurs exclusively as the [8-E,12-M] homolog and is predominantly esterified with stearol (Gloe and Risch, 1978; Bobe et al., 1990). Similar to green sulfur bacteria, *Cfx. aurantiacus* can vary its homolog composition through changes in the esterifying alcohol (Larsen et al., 1994) and can incorporate exogenously added long-chain alcohols into BChl *c* (Larsen et al., 1995). Both BChl *a* synthase (BchG) and BChl *c* synthase (BchK) from *Cfx. aurantiacus* have been overexpressed in *E. coli* and tested for substrate specificity (Schoch et al., 1999). It can be anticipated that BChl *c* biosynthesis in *Cfx. aurantiacus* will occur by the same pathway that is employed in *Chl. tepidum*.

Homologs of all genes discussed above as playing a role in BChl *c* biosynthesis in *Chl. tepidum* are found in the currently available genome sequence data of *Cfx. aurantiacus*, with the exception of *bchQ*, *bchR*, and *bchV* (DOE Joint Genome Institute, http://www.jgi.doe.gov). The absence of *bchQ* and *bchR* is expected, since *Cfx. aurantiacus* synthesizes only [8-E,12-M]-BChl *c* (Gloe and Risch, 1978; Bobe et al., 1990; Section VII.C). The absence of *bchV* may also be explained if the product of this gene alone is specifically involved in hydration of BChl *c* precursors that have increased methylation in the C-8 and C-12 positions (Section VII.E). The chirality of the C-3[1] carbon in BChl *c* in *Cfx. aurantiacus* is about 67% R and 33% S isomers (Fages et al., 1990). Although one BchF hydratase might produce this mixture of R and S stereoisomers, it is also possible that a *bchV* ortholog, which would encode an S-specific hydratase as suggested in Section VII.E, can not yet be identified since the genome data is incomplete. Alternatively, if BchF produces only one BChl *c* epimer, an unidentified epimerase could account for the observed mixture of epimers.

Cfx. aurantiacus can grow under both oxic and anoxic conditions. Consistent with this ability, the genome of this bacterium encodes some enzymes of tetrapyrrole biosynthesis as both the oxygen-independent and oxygen-dependent forms. Examples include the Mg-Proto monomethylester oxidative cyclase (anoxic, BchE; oxic, AcsF), coproporphyrinogen III oxidase (anoxic, HemN; oxic, HemF), and protoporphyrinogen IX oxidase (anoxic, HemY; oxic, HemK). *Cfx. aurantiacus* also contains three BchH paralogs: two BChl *a*-type (BchH-I and BchH-II) and one BChl *c*-type (BchS) (see Figs. 2b and 5). The latter is most closely related in sequence to the BchS and BchT proteins of *Chl. tepidum*, of which BchS appears to be specifically involved in BChl *c* biosynthesis under anoxic growth conditions (Section VII.A). BchH-I is probably used for BChl *a* biosynthesis under anoxic conditions and BchH-II for BChl *a* biosynthesis under micro-oxic conditions, since *bchH-II* clusters with *acsF*, which encodes a binuclear iron protein that catalyzes the oxygen-dependent, oxidative cyclization of Mg-Proto monomethylester in *Rubrivivax gelatinosus* (Pinta et al., 2002). Transcription in *Cfx. aurantiacus* is modulated by oxygen tension (Gruber and Bryant, 1998), and this gene arrangement could compensate for the oxygen-mediated repression of *bchH-I*.

Recent research suggests that the distinction between BChl *c* biosynthesis in green sulfur bacteria and green filamentous bacteria may not be so clearly delineated as described above. A recently characterized strain of green filamentous bacterium, a *Chloronema* sp., has chlorosomes that have characteristics

of both green filamentous bacteria (BChl *c* esterified with stearol and little redox-dependent fluorescence quenching) and green sulfur bacteria (C-8^2 and C-12^1 methylation, chlorobactene) (C. M. Borrego, personal communication).

XI. Future Directions

Although many new details of BChl *c* biosynthesis have been identified in the past two years, the precise order of all reaction steps is still not certain. Of critical importance will be a demonstration of when and how the removal of the C-13^2 carboxylate or methylcarboxylate moiety occurs. Clues to resolve this and other issues may be obtained from more careful analyses of the intermediates that accumulate in the various mutant strains that have been constructed. Now that most of the genes encoding enzymes of BChl *c* biosynthesis have been identified, heterologously expressed enzymes functioning in BChl *c* biosynthesis can be prepared and characterized with respect to substrate specificity and reaction mechanism. Interesting proteins include the three BchH homologs of magnesium chelatase from *Chl. tepidum*, the C-8^2 and C-12^1 methyltransferases BchQ and BchR, the C-20 methyltransferase BchU, the C-3^1 hydratases BchF and BchV, and the BChl *c* synthase BchK (the latter from both *Chl. tepidum* and *Cfx. aurantiacus*). Important questions to answer are whether Mg-Proto, when it is bound to Mg-chelatase, can be methylated by BchM, and if this methylation is specifically affected by binding to a different chelatase subunit (BchH, BchS, or BchT). It should also be possible to verify the biosynthetic pathway in *Cfx. aurantiacus* by complementing *Chl. tepidum* BChl *c* biosynthesis mutants with the appropriate genes. An interesting question here is whether the BchK of *Cfx. aurantiacus* would exhibit relaxed substrate specificity when expressed in the *Chl. tepidum bchK* mutant background. It should be possible to purify various substrates for in vitro characterization of specific enzymatic reactions from the appropriate mutant strains of *Chl. tepidum*.

Note added in Proof

Nagata et al. (2005) recently identified the [3,8-divinyl]-protochlorophyllide 8-vinyl reductase of higher plants and *Synechococcus* sp. WH8102, and surprisingly they identified a close homolog (*CT1063*) of these genes in the genome of *Chl. tepidum*. Inactivation of *CT1063* in *Chl. tepidum* leads to the accumulation of the 8-vinyl derivatives of BChl c_F (with methyl or predominantly ethyl substituents at the C-12 position), Chl $a_{\Delta 2,6}$, and BChl a_P (A. Gomez Maqueo Chew and D. A. Bryant, unpublished). A small amount of BChl a_P with an ethyl substituent at the C-8 position (i. e., normal BChl a_P) was also detected. These results indicate that the predominant 8-vinyl reductase activity in *Chl. tepidum* is the product of *CT1063* and that the *bchJ* gene (*CT2014*) in the genome is at most responsible for a weak, residual activity in the synthesis of BChl a_P. Efforts to inactivate the *bchJ* gene and to produce a *CT1063 bchJ* double mutant of *Chl. tepidum* are in progress. No homologs of *CT1063* have yet been identified in the incompletely sequenced genomes of *Chl. limicola* DSMZ 245, *Chl. phaeobacteroides* DSMZ 266, *Chl. phaeobacteroides* BS-1 (Black Sea Strain 1), and *Cfx. aurantiacus*. In contrast, proteins with strong sequence similarity to BchJ have been found in all eight green sulfur bacterial genomes that have been sequenced as well as in the incomplete genome of *Cfx. aurantiacus*. These results suggest that some green sulfur bacteria may use a BchJ-like reductase while others may use a plant-type (CT1063-like) 8-vinyl reductase. Recent progress in the understanding of (B)Chl biosynthesis in green bacteria has been reviewed in Frigaard and Bryant (2004).

Acknowledgments

This work was supported by U. S. Department of Energy grant DE-FG02-94ER20137 to D. A. B. The authors thank Dr. Carsten Krebs (The Pennsylvania State University) for helpful discussions concerning the mechanism of the C-8^2 and C-12^1 methyltransferase reactions.

References

Addlesee HA and Hunter (1999) Physical mapping and functional assignment of the geranylgeranyl-bacteriochlorophyll reductase gene, *bchP*, of *Rhodobacter sphaeroides*. J Bacteriol 181: 7248–7255

Addlesee HA and Hunter CN (2002) *Rhodospirillum rubrum* possesses a variant of the *bchP* gene, encoding geranylgeranyl-bacteriopheophytin reductase. J Bacteriol 184: 1578–1586

Addlesee HA, Fiedor L and Hunter CN (2000) Physical map-

ping of *bchG*, *orf427*, and *orf177* in the photosynthesis gene cluster of *Rhodobacter sphaeroides*: Functional assignment of the bacteriochlorophyll synthetase gene. J Bacteriol 182: 3175–3182

Airs RL, Borrego CM, Garcia-Gil, J and Keeley BJ (2001) Identification of the bacteriochlorophyll homologues of *Chlorobium phaeobacteroides* strain UdG6053 grown at low light intensity. Photosynth Res 70: 221–230

Alberti M, Burke DH and Hearst JE (1995) Structure and sequence of the photosynthesis gene cluster. In: Blankenship RE, Madigan MT and Bauer CE (eds) Anoxygenic Photosynthetic Bacteria, pp 1083–1106. Kluwer Academic Publishers, Dordrecht

Andersen T, Briseid T, Nesbakken T, Ormerod JG, Sirevåg R and Thorud M (1983) Mechanisms of synthesis of 5-aminolevulinate in purple, green and blue-green bacteria. FEMS Microbiol Lett 19: 303–306

Avissar YJ, Ormerod JG and Beale SI (1989) Distribution of δ-aminolevulinic acid biosynthetic pathways among phototrophic bacterial groups. Arch Microbiol 151: 513–519

Bañeras L, Borrego CM and Garcia-Gil LJ (1999) Growth rate-dependent bacteriochlorophyll *c*/*d* ratio in the antenna of *Chlorobium limicola* strain UdG6040. Arch Microbiol 171: 350–354

Beale SI (1995) Porphyrins and hemes. In: Blankenship RE, Madigan MT and Bauer CE (eds) Anoxygenic Photosynthetic Bacteria, pp 153–177. Kluwer Academic Publishers, Dordrecht

Béjà O, Suzuki MT, Heidelberg JF, Nelson WC, Preston CM, Hamada T, Eisen JA, Fraser CM and DeLong EF (2002) Unsuspected diversity among marine aerobic anoxygenic phototrophs. Nature 415: 630–633

Blankenship RE and Matsuura K (2003) Antenna complexes from green photosynthetic bacteria. In: Green BR and Parson WW (eds) Light-Harvesting Antennas, pp 195–217. Kluwer Academic Publishers, Dordrecht

Blankenship RE, Olson JM and Miller M (1995) Antenna complexes from green photosynthetic bacteria. In: Blankenship RE, Madigan MT and Bauer CE (eds) Anoxygenic Photosynthetic Bacteria, pp 399–435. Kluwer Academic Publishers, Dordrecht

Bobe FW, Pfennig N, Swanson KL and Smith KM (1990) Red shift of absorption maxima in *Chlorobiineae* through enzymatic methylation of their antenna bacteriochlorophylls. Biochemistry 29: 4340–4348

Bollivar DW, Jiang Z-Y, Bauer CE and Beale SI (1994a) Heterologous overexpression of the *bchM* gene product from *Rhodobacter capsulatus* and demonstration that it encodes for *S*-adenosyl-L-methionine:Mg-protoporphyrin methyltransferase. J Bacteriol 176: 5290–5296

Bollivar DW, Suzuki JY, Beatty JT, Dobrowolski JM and Bauer CE (1994b) Directed mutational analysis of bacteriochlorophyll *a* biosynthesis in *Rhodobacter capsulatus*. J Mol Biol 237: 622–640

Bollivar DW, Wang S, Allen JP and Bauer CE (1994c) Molecular genetic analysis of terminal steps in bacteriochlorphyll *a* biosynthesis: characterization of a *Rhodobacter capsulatus* strain that synthesizes geranylgeranyl esterified bacteriochlorophyll *a*. Biochemistry 33: 12763–12768

Borrego CM and Garcia-Gil LJ (1995) Rearrangement of light-harvesting bacteriochlorophyll homologs as a response of green sulfur bacteria to low-light intensities. Photosynth Res 45: 21–30

Borrego CM, Garcia-Gil J, Cristina XP, Vila X and Abella CA (1998) Occurrence of new bacteriochlorophyll *d* forms in natural populations of green photosynthetic sulfur bacteria. FEMS Microbiol Ecol 26: 257–267

Borrego CM, Gerola PD, Miller M and Cox RP (1999) Light intensity effects on pigment composition and organisation in the green sulfur bacterium *Chlorobium tepidum*. Photosynth Res 59: 159–166

Broch-Due M and Ormerod JG (1978) Isolation of a-*c* mutant from *Chlorobium* with BChl-*d* by cultivation at low-light intensity. FEMS Microbiol Lett 3: 305–308

Bryant DA, Vassilieva EV, Frigaard N-U, and Li H (2002) Selective protein extraction from *Chlorobium tepidum* chlorosomes using detergents. Evidence that CsmA forms multimers and binds bacteriochlorophyll *a*. Biochemistry 41: 14403–14411

Burke DH, Alberti M and Hearst JE (1993a) The *Rhodobacter capsulatus* chlorin reductase-encoding locus, *bchA*, consists of three genes, *bchX*, *bchY*, and *bchZ*. J. Bacteriol 175: 2407–2413

Burke DH, Alberti M and Hearst JE (1993b) *bchFNBH* bacteriochlorophyll synthesis genes of *Rhodobacter capsulatus* and identification of the third subunit of light-independent protochlorophyllide reductase in bacteria and plants. J Bacteriol 175: 2414–2422

Caple MB, Chow H-C and Strouse CE (1978) Photosynthetic pigments of green sulfur bacteria. The esterifying alcohols of bacteriochlorophylls *c* from *Chlorobium limicola*. J Biol Chem 253: 6730–6737

Coomber SA, Chaudri AM, Connor A, Britton G and Hunter CN (1990) Localized transposon Tn5 mutagenesis of the photosynthetic gene cluster of *Rhodobacter sphaeroides*. Mol Microbiol 4: 977–989

Eisen JA, Nelson KE, Paulsen IT, Heidelberg JF, Wu M, Dodson RJ, Deboy R, Gwinn ML, Nelson WC, Haft DH, Hickey EK, Peterson JD, Durkin AS, Kolonay JL, Yang F, Holt I, Umayam LA, Mason T, Brenner M, Shea TP, Parksey D, Nierman WC, Feldblyum TV, Hansen CL, Craven MB, Radune D, Vamathevan J, Khouri H, White O, Venter JC, Gruber TM, Ketchum KA, Tettelin H, Bryant DA and Fraser CM (2002) The complete genome sequence of *Chlorobium tepidum* TLS, a photosynthetic, anaerobic, green-sulfur bacterium. Proc Natl Acad Sci USA 99: 9509–9514

Fages F, Griebenow N, Griebenow K, Holzwarth AR and Schaffner K (1990) Characterization of light-harvesting pigments of *Chloroflexus aurantiacus*—2 new chlorophylls—oleyl (octadec-9-enyl) and cetyl (hexadecanyl) bacteriochlorophyllides-*c*. J Chem Soc Perkin Trans 1, 10: 2791–2797

Feick RG and Fuller RC (1984) Topography of the photosynthetic apparatus of *Chloroflexus aurantiacus*. Biochemistry 23: 3693–3700

Fodje MN, Hansson A, Hansson M, Olsen JG, Gough S, Willows RD and Al-Karadaghi S (2001) Interplay between an AAA module and an integrin I domain may regulate the function of magnesium chelatase. J Mol Biol 311: 111–122

Frigaard N-U and Bryant DA (2001) Chromosomal gene inactivation in the green sulfur bacterium *Chlorobium tepidum* by natural transformation. Appl Environ Microbiol 67: 2538–2544

Frigaard N-U and Bryant DA (2004) Seeing green bacteria in a new light: Genomics-enabled studies of the photosynthetic apparatus in green sulfur bacteria and filamentous anoxygenic phototrophic bacteria. Arch Microbiol 182: 265–276

Frigaard N-U and Ormerod J (1995) Hydrophobic modification of antenna chlorophyll in *Chlorobium* during growth with

acetylene. In: Mathis P (ed) Photosynthesis: From Light to Biosphere, Vol I, pp 163–166. Kluwer Academic Publishers, Dordrecht

Frigaard N-U, Vassilieva EV, Li H, Milks KJ, Zhao J and Bryant DA (2001) The remarkable chlorosome. PS2001: Proceedings 12th International Congress on Photosynthesis, S1-003. CSIRO Publishing, Melbourne (CD-ROM)

Frigaard N-U, Voigt GD and Bryant DA (2002) *Chlorobium tepidum* mutant lacking bacteriochlorophyll *c* made by inactivation of the *bchK* gene, encoding bacteriochlorophyll *c* synthase. J Bacteriol 184: 3368–3376

Frigaard N-U, Gomez Maqueo Chew A, Li H, Maresca JA, and Bryant DA (2003) *Chlorobium tepidum*: Insights into the structure, physiology, and metabolism of a green sulfur bacterium derived from the complete genome sequence. Photosynth Res 78: 93–117

Fujita Y and Bauer CE (2000) Reconstitution of light-independent protochlorophyllide reductase from purified BchL and BchN-BchB subunits. In vitro confirmation of nitrogenase-like features of a bacteriochlorophyll biosynthesis enzyme. J Biol Chem 275: 23583–23588

Gibson LCD and Hunter CN (1994) The bacteriochlorophyll biosynthesis gene, *bchM*, of *Rhodobacter sphaeroides*, encodes *S*-adenosyl-methionine:Mg-protoporphyrin IX methytransferase. FEBS Lett 352: 127–130

Gibson LC, Willows RD, Kannangara CG, von Wettstein D and Hunter CN (1995) Magnesium-protoporphyrin chelatase of *Rhodobacter sphaeroides*: Reconstitution of activity by combining the products of the *bchH*, *-I*, and *-D* genes expressed in *Escherichia coli*. Proc Natl Acad Sci USA 92: 1941–1944

Glaeser J, Bañeras L, Rutters H and Overmann J (2002) Novel bacteriochlorophyll *e* structures and species-specific variability of pigment composition in green sulfur bacteria. Arch Microbiol 177: 475–485

Gloe A and Risch N (1978) Bacteriochlorophyll c_S, a new bacteriochlorophyll from *Chloroflexus aurantiacus*. Arch Microbiol 118: 153–156

Gough SP, Petersen BO and Duus JØ (2000) Anaerobic chlorophyll isocyclic ring formation in *Rhodobacter capsulatus* requires a cobalamin cofactor. Proc Natl Acad Sci USA 97: 6908–6913

Gruber TM and Bryant DA (1998) Characterization of the group 1 and group 2 sigma factors of the green sulfur bacterium *Chlorobium tepidum* and the green non-sulfur bacterium *Chloroflexus aurantiacus*. Arch Microbiol 170: 285–296

Guyoneaud R, Borrego CM, Martinez-Planells A, Buitenhuis ET and Garcia-Gil LJ (2001) Light responses in the green sulfur bacterium *Prosthecochloris aestuarii*: Changes in prosthecae length, ultrastructure, and antenna pigment composition. Arch Microbiol 176: 278–284

Haidl H, Knödlmayr K, Rüdiger W, Scheer H, Schoch S and Ullrich J (1985) Degradation of bacteriochlorophyll *a* in *Rhodopseudomonas sphaeroides* R26. Z Naturforsch 40C: 685–692

Hinchigeri SB, Hundle B and Richards WR (1997) Characterization of the binding of deuteroporphyrin IX to the magnesium chelatase H subunit and spectroscopic properties of the complex. FEBS Lett 407: 337–342

Holt AS, Purdie WS and Wasley JWF (1966) Structures of *Chlorobium* chlorophylls. Can J Chem 44: 88–93

Holzwarth AR, Griebenow K and Schaffner K (1992) Chlorosomes, photosynthetic antennae with novel self-organized pigment structures. J Photochem Photobiol A: Chem 65: 61–71

Hörtensteiner S (1999) Chlorophyll breakdown in higher plants and algae. Cell Mol Life Sci 56: 330-347

Huster MS and Smith KM (1990) Biosynthetic-studies of substituent homologation in bacteriochlorophylls *c* and *d*. Biochemistry 29: 4348–4355

Jensen PE, Gibson LCD, Henninsen KW and Hunter CN (1996) Expression of the ChlI, ChlD, and ChlH genes from the cyanobacterium *Synechocystis* PCC6803 in *Escherichia coli* and demonstration that the three cognate proteins are required for magnesium-protoporphyrin chelatase activity. J Biol Chem 271: 16662–16667

Johnson HA, Pelletier DA, and Spormann AM (2001) Isolation and characterization of anaerobic ethylbenzene dehydrogenase, a novel Mo-Fe-S enzyme. J Bacteriol 183: 4536-4542

Karger GA, Reid JD and Hunter CN (2001) Characterization of the binding of deuteroporphyrin IX to the magnesium chelatase H subunit and spectroscopic properties of the complex. Biochemistry 40: 9291–9299

Kobayashi M, Oh-oka H, Akutsu S, Akiyama M, Tominaga K, Kise H, Nishida F, Watanabe T, Amesz J, Koizumi M, Ishida N and Kano H (2000) The primary electron acceptor of green sulfur bacteria, bacteriochlorophyll 663, is chlorophyll *a* esterified with Δ2,6-phytadienol. Photosynth Res 63: 269–280

Larsen KL, Cox RP and Miller M (1994) Effects of illumination intensity on bacteriochlorophyll *c* homolog distribution in *Chloroflexus aurantiacus* grown under controlled conditions. Photosynth Res 41: 151–156

Larsen KL, Cox RP and Miller M (1995) Incorporation of exogenous long-chain alcohols into bacteriochlorophyll *c* homologs by *Chloroflexus aurantiacus*. Arch Microbiol 163: 119–123

Majumdar D, Avissar YJ, Wyche JH and Beale SI (1991) Structure and expression of the *Chlorobium vibrioforme hemA* gene. Arch Microbiol 156: 281–189

Maresca JA, Gomez Maqueo Chew A, Ros Ponsatí M, Frigaard N-U, Ormerod JG, and Bryant DA (2004) The *bchU* gene of *Chlorobium tepidum* encodes the C-20 methyltransferase in bacteriochlorophyll *c* biosynthesis. J Bacteriol 186: 2558–2566

Matile P (2000) Biochemistry of Indian summer: Physiology of autumnal leaf coloration. Exper Gerontol 35: 145-158

Matile P, Hörtensteiner S, Thomas H and Kräutler B (1996) Chlorophyll breakdown in senescent leaves. Plant Physiol 112: 1403-1409

Matile P, Hörtensteiner S and Thomas H (1999) Chlorophyll degradation. Annu Rev Plant Physiol Plant Mol Biol 50: 67-95

McGlynn P and Hunter CN (1993) Genetic analysis of the *bchC* and *bchA* genes of *Rhodobacter sphaeroides*. Mol Gen Genet 236: 227–234

Montaño GA, Wu H-M, Lin S, Brune DC and Blankenship RE (2003) Isolation and characterization of the B798 light-harvesting baseplate from the chlorosomes of *Chloroflexus aurantiacus*. Biochemistry42: 10246–10251

Nagata N, Tanaka R, Satoh S and Tanaka A (2005) Identification of a vinyl reductase gene for chlorophyll synthesis in *Arabidopsis thaliana* and implications for the evolution of *Prochlorococcus* species. Plant Cell 17: 233–240

Naylor, GW, Addlesee HA, Gibson LCD and Hunter CN (1999) The photosynthesis gene cluster of *Rhodobacter sphaeroides*. Photosynth Res 62:121–139

Niedermeier G, Shiozawa JA, Lottspeich F and Feick RG (1994) Primary structure of two chlorosome proteins from *Chloroflexus*

aurantiacus. FEBS Lett 342: 61–65

Oelze J and Golecki JR (1995) Membranes and chlorosomes of green bacteria: Structure, composition and development. In: Blankenship RE, Madigan MT and Bauer CE (eds) Anoxygenic Photosynthetic Bacteria, pp 259–278. Kluwer Academic Publishers, Dordrecht

Ormerod JG, Nesbakken T and Beale SI (1990) Specific inhibition of antenna bacteriochlorophyll synthesis in *Chlorobium vibrioforme* by anesthetic gases. J Bacteriol 172: 1352–1360

Oster U, Bauer CE and Rüdiger W (1997) Characterization of chlorophyll *a* and bacteriochlorophyll *a* synthases by heterologous expression in *Escherichia coli*. J Biol Chem 272: 9671–9676

Petersen BL, Jensen PE, Gibson LCD, Stummann BM, Hunter CN and Henningsen KW (1998a) Reconstitution of an active magnesium chelatase enzyme complex from the *bchI*, *-D*, and *-H* gene products of the green sulfur bacterium *Chlorobium vibrioforme* expressed in *Escherichia coli*. J Bacteriol 180: 699–704

Petersen BL, Møller MG, Stummann BM and Henningsen KW (1998b) Structure and organization of a 25 kbp region of the genome of the photosynthetic green sulfur bacterium *Chlorobium vibrioforme* containing Mg-chelatase encoding genes. Hereditas 129: 131–142

Pierson BK and Castenholz RW (1995) Taxonomy and physiology of filamentous anoxygenic phototrophs. In: Blankenship RE, Madigan MT and Bauer CE (eds) Anoxygenic Photosynthetic Bacteria, pp 31–47. Kluwer Academic Publishers, Dordrecht

Pinta V, Picaud M, Reiss-Husson F, and Astier C (2002) Rubrivivax gelatinosus *acsF* (previously *orf358*) codes for a conserved, putative binuclear-iron-cluster-containing protein involved in aerobic oxidative cyclization of Mg-protoporphyrin IX monomethylester. J Bacteriol 184: 746–753

Porra RJ (1997) Recent progress in porphyrin and chlorophyll biosynthesis. Photochem Photobiol 65: 492–516

Rhie G, Avissar YJ and Beale SI (1996) Structure and expression of the *Chlorobium vibrioforme hemB* gene and characterization of its encoded enzyme porphobilinogen synthase. J Biol Chem 271: 8176–8182

Richards WR and Rapoport H (1966) The biosynthesis of *Chlorobium* chlorophylls-660. The isolation and purification of porphyrins from *Chlorobium thiosulfatophilum*-660. Biochemistry 5: 1079–1089

Richards WR and Rapoport H (1967) The biosynthesis of *Chlorobium* chlorophylls-660. The production of magnesium protoporphyrin monomethyl ester, bacteriochlorophyll, and *Chlorobium* pheoporphyrins by *Chlorobium thiosulfatophilum*-660. Biochemistry 6: 3830–3840

Rieble S, Ormerod JG and Beale SI (1989) Transformation of glutamate to delta-aminolevulinic acid by soluble extracts of *Chlorobium vibrioforme*. J Bacteriol 171: 3782–3787

Sakuragi Y, Frigaard N-U, Shimada K and Matsuura K (1999) Association of bacteriochlorophyll *a* with the CsmA protein in chlorosomes of the photosynthetic green filamentous bacterium *Chloroflexus aurantiacus*. Biochim Biophys Acta 1413: 172–180

Schoch S, Scheer H, Schiff JA, Rüdiger W and Siegelman HW (1981) Pyropheophytin *a* accompanies pheophytin *a* in darkened light grown cells of *Euglena*. Z Naturforsch 36C: 827-833

Schoch S, Oster U, Mayer K, Feick R and Rüdiger W (1999) Substrate specificity of overexpressed bacteriochlorophyll synthases from *Chloroflexus aurantiacus*. In: Argyroudi-Akoyunoglou JH and Senger H (eds) The Chloroplast: From Molecular Biology to Biotechnology, pp 213–216. Kluwer Academic Publishers, Dordrecht

Senge MO and Smith KM (1995) Biosynthesis and structures of the bacteriochlorophylls. In: Blankenship RE, Madigan MT and Bauer CE (eds) Anoxygenic Photosynthetic Bacteria, pp 137–151. Kluwer Academic Publishers, Dordrecht

Shimokawa K, Hashizume A and Shioi Y (1990) Pyropheophorbide *a*, a catabolite of ethylene-induced chlorophyll *a* degradation. Phytochemistry 29: 2105-2106

Smith KM (1991) The structure and biosynthesis of bacteriochlorophylls. In Jordan PM (ed) Biosynthesis of Tetrapyrroles, pp 237–255. Elsevier Science Publ, Amsterdam

Smith KM (1994) Nomenclature of the bacteriochlorophylls *c*, *d*, and *e*. Photosynth Res 41: 23-26

Smith KM (2003) Chlorosome chlorophylls (Bacteriochlorophylls *c*, *d*, and *e*): structures, partial syntheses, and biosynthetic proposals. In: Kadish KM, Smith KM, and Guilard R (eds) The Porphyrin Handbook, Vol 13, pp 157-182. Elsevier Science, New York.

Smith KM and Huster MS (1987) Bacteriochlorophyll-*c* formation via the glutamate C-5 pathway in *Chlorobium* bacteria. J Chem Soc Chem Commun: 14–16

Smith KM and Simpson DJ (1986) Stereochemistry of the bacteriochlorophyll-*e* homologues. J Chem Soc Chem Commun: 1682–1684

Smith KM, Goff DA, Fajer J and Barkigia JM (1982) Chirality and structures of bacteriochlorophylls *d*. J Am Chem Soc 104: 3747–3749

Smith KM, Goff DA, Fajer J and Barkigia KM (1983a) Isolation and characterization of two new bacteriochlorophyll *d* bearing neopentyl substituents. J Am Chem Soc 105: 1674–1676

Smith KM, Craig, GW, Kehres LA and Pfennig N (1983b) Reversed phase HPLC and structural assignments of the bacteriochlorophylls *c*. J Chromatogr 281: 209–223

Steensgaard DB, Cox RP, and Miller M (1996) Manipulation of the bacteriochlorophyll *c* homolog distribution in the green sulfur bacterium *Chlorobium tepidum*. Photosynth Res 48: 385–393

Suzuki JY and Bauer CE (1995) Altered monovinyl and divinyl protochlorophyllide pools in *bchJ* mutants of *Rhodobacter capsulatus*. Possible monovinyl substrate discrimination of light-independent protochlorophyllide reductase. J Biol Chem 270: 3732–3740

Suzuki JY, Bollivar DW and Bauer CE (1997) Genetic analysis of chlorophyll biosynthesis. Annu Rev Genet 31: 61–89

Suzuki Y, Doi M, and Shioi Y (2002) Two enzymatic reaction pathways in the formation of pyropheophorbide *a*. Photosynth Res 74: 225–233

Swanson KL and Smith KM (1990) Biosynthesis of bacteriochlorophyll-*c* via the glutamate C-5 pathway in *Chloroflexus aurantiacus*. J Chem Soc Chem Commun 1990: 1696–1697

Takaichi S (1999) Carotenoids and carotenogenesis in anoxygenic photosynthetic bacteria. In: Frank HA, Young AJ, Britton G, and Cogdell, RJ (eds), The Photochemistry of Carotenoids, pp 39–69. Kluwer Academic Publishers, Dordrecht

Takaichi S, Tsuji K, Matsuura K and Shimada K (1995) A monocyclic carotenoid glucoside ester is a major carotenoid in the green filamentous bacterium *Chloroflexus auranatiacus*. Plant Cell Physiol 36: 773–778

Takaichi S, Wang Z-Y, Umetsu M, Nozawa T, Shimada K and Madigan MT (1997) New carotenoids from the thermophilic green sulfur bacterium *Chlorobium tepidum*: 1′,2′-dihydro-β-carotene, 1′, 2′-dihydrochlorobactene, and OH-chlorobactene glucoside ester, and the carotenoid composition of different strains. Arch Microbiol 168: 270–276

Takamiya K-I, Tsuchiya T, and Ohta H (2000) Degradation pathway(s) of chlorophyll: What has gene cloning revealed? Trends Plant Sci 5: 426–431

Tanaka A, Ito H, Tanaka R, Tanaka NK, Yoshida K and Okada K (1998) Chlorophyll *a* oxygenase (CAO) is involved in chlorophyll *b* formation from chlorophyll *a*. Proc Natl Acad Sci USA 95: 12719–12723

van Rossum BJ, Steensgaard DB, Mulder FM, Boender GJ, Schaffner K, Holzwarth AR and de Groot HJ (2001) A refined model of the chlorosomal antenna of the green bacterium *Chlorobium tepidum* from proton chemical shift constraints obtained with high-field 2-D and 3-D MAS NMR dipolar correlation spectroscopy. Biochemistry 40: 1587–1595

Wechsler TD, Brunisholz RA, Frank G, Suter F and Zuber H (1987) The complete amino acid sequence of the antenna polypeptide B806-B866-β from the cytoplasmic membrane of the green bacterium *Chloroflexus aurantiacus*. FEBS Lett 210: 189–194

Wechsler TD, Brunisholz RA, Frank G and Zuber H (1991) Isolation and protein chemical characterization of the B806-B866 antenna complex of the green thermophilic bacterium *Chloroflexus aurantiacus*. J Photochem Photobiol B: Biol 8: 189–197

Wellington CL and Beatty JT (1989) Promoter mapping and nucleotide sequence of the *bchC* bacteriochlorophyll biosynthesis gene from *Rhodobacter capsulatus*. Gene 83: 251–161.

Willows RD (2003) Biosynthesis of chlorophylls from protoporphyrin IX. Nat Prod Rep 20: 327–341

Willows RD and Beale SI (1998) Heterologous expression of the *Rhodobacter capsulatus* BchI, -D, and -H genes that encode magnesium chelatase subunits and characterization of the reconstituted enzyme. J Biol Chem 273: 34206–34213

Willows RD, Gibson LC, Kanangara CG, Hunter CN and von Wettstein D (1996) Three separate proteins constitute the magnesium chelatase of *Rhodobacter sphaeroides*. Eur J Biochem 1996 235: 438–443

Xiong J, Inoue, K and Bauer CE (1998) Tracking molecular evolution of photosynthesis by characterization of a major photosynthesis gene cluster from Heliobacillus mobilis. Proc Natl Acad Sci USA 95:14851–14856

Xiong J, Fischer WM, Inoue K, Nakahara M and Bauer CE (2000) Molecular evidence for the early evolution of photosynthesis. Science 289: 1724–1730

Ziegler R, Blaheta A, Guha N and Schönegge B (1988) Enzymatic formation of pheophorbide and pyropheophorbide during chlorophyll degradation in a mutant of *Chlorella fusca* Shihira et Kraus. J Plant Physiol 132: 327–332

Chapter 16

Involvement of Tetrapyrroles in Cellular Regulation

Christoph F. Beck*
Institut für Biologie III, Albert-Ludwigs-Universität Freiburg,
Schaenzlestrasse 1, D-79104 Freiburg, Germany

Bernhard Grimm*
Institut für Biologie/Pflanzenphysiologie, Humboldt Universität Berlin,
Unter den Linden 6, D-10099 Berlin, Germany

Summary

In eukaryotic cells, tetrapyrrole intermediates and end-products play a crucial role as intra-organellar regulators within the chloroplast or mitochondrion, which are sites of heme and chlorophyll biosynthesis, by exerting a feedback control on the enzyme activities of their own biosynthetic pathway. It is proposed that some tetrapyrrole metabolites also act as inter-organellar signals communicating with the nucleus to coordinate nuclear and organellar activities by regulating nuclear gene expression in response to the physiological and developmental state of the mitochondrion or plastid.

*Authors for correspondence, email: beck@uni-freiburg.de, bernhard.grimm@rz.hu-brlin.de

Bernhard Grimm, Robert J. Porra, Wolfhart Rüdiger and Hugo Scheer (eds): Chlorophylls and Bacteriochlorophylls: Biochemistry, Biophysics, Functions and Applications, pp. 223–235.

I. Introduction

It is well known that heme-proteins are important respiratory pigments (Section II.A), while chlorophyll-proteins are photoactive pigments in photosynthesis (Section III.B), and that cobalamines (not discussed in this Chapter) function as cofactors in mutase and methylation reactions. The multiplicity and ubiquity of these tetrapyrrole pigments correlate with their many biochemical and biophysical properties. This chapter reviews another aspect of tetrapyrrole involvement in metabolism: in subcellular communication resulting in *either* an adjustment of nuclear transcriptional activities, *or* in modulation of stromal (plastid) or matrix (mitochondrial) enzymatic activities in response to the metabolic and developmental requirements of plastids and mitochondria.

In plants, plastids possess the entire tetrapyrrole biosynthetic pathway to heme and to chlorophylls, but all of the enzymes involved are encoded by the nucleus. The synthesis of protoporphyrinogen IX (Protogen) from eight molecules of 5-aminolevulinate (ALA) in plants occurs exclusively in plastids (Chapter 13, Yaronskaya and Grimm). Oxidation of Protogen to protoporphyrin IX (Proto) and the subsequent insertion of Fe^{2+} ions by ferrochelatase into the tetrapyrrole ring structure can occur in either the plastid or the mitochondrion. Thus, Protogen is translocated from plastid to mitochondrion for the formation of heme for mitochondrial respiratory-pigment formation. Protoheme formed in the plastid, however, is the substrate for formation of *both* the different types of plastid hemes, *and* of phytochromobiline, the linear tetrapyrrolic chromophore of the phytochromes, which are a family of sensory photoreceptors. In addition, and very significantly, the plastids possess a Proto magnesium chelatase (Mg-chelatase) so that plastidal Proto serves also as a precursor for Chl. Details on the biochemistry of tetrapyrrole biosynthesis are discussed in this book (Chapter 11, Beale; Chapter 13, Yaronskaya and Grimm; Chapter 14, Rüdiger) and have also been outlined in recent reviews (Beale, 1999; Grimm, 2003); these chapters also contain the relevant reaction schemes.

Since Mg-porphyrins and porphyrins (including Proto) can absorb photons, transfer excitation energy and perform photochemical reactions, they are hazardous molecules for the cell (Spikes and Bommer, 1991; Chapters 32 and 33, Brandis et al.). Because of these photochemical and photophysical properties of porphyrins and Mg-porphyrins, the pathway of tetrapyrrole biosynthesis require tight regulation. Furthermore, tetrapyrrole intermediates and end-products contribute to metabolic control via feedback mechanisms within mitochondria and chloroplasts, implying that their pool levels are modulated in response to developmental, metabolic and extrinsic cues.

Recent studies, using mutants and transgenic plants, indicate a contribution by tetrapyrrolic intermediates in inter-organellar communication. While at least two DNA-containing organelles, nuclei and mitochondria, exist in all eukaryotic cells, eukaryotic algae and higher plants possess a third genome-containing organelle, the chloroplast. Coordinating gene expression between these organelles poses a challenge to cellular control mechanisms. It is generally accepted that nuclear genes play a dominant role in controlling all cellular processes; thus, nuclear encoded proteins imported into plastids and mitochondria exert major controls over biogenesis and other functions in these organelles (Goldschmidt-Clermont, 1998; Leon et al., 1998). On the other hand, intact and functional plastids are a pre-requisite for the expression of a subset of genes within the plant nucleus (Bradbeer et al., 1979; Harpster et al., 1984; Mayfield and Taylor, 1984; Batschauer et al., 1986; Oelmüller and Mohr, 1986; Ernst and Schefbeck, 1988; Oelmüller and Briggs, 1990; Hess et al., 1994). These observations support the concept of a bi-directional exchange of information between the DNA-containing organelles. It was proposed that signals originating from plastids (and mitochondria) affect transcriptional control of specific nuclear genes (Oelmüller, 1989; Taylor, 1989, Poyton and McEwen, 1996) and now much evidence has accumulated which supports the operation of multiple signaling pathways that may coordinate the expression of nuclear genes with the requirements of plastids and mitochondria (Escoubas et al., 1995; Maxwell et al., 1995; Durnford and Falkowski, 1997; Karpinski et al., 1997; Beck, 2001; Papenbrock and Grimm, 2001; Pfannschmidt et al., 2001; Rodermel, 2001; Surpin et al., 2002; Gray et al., 2003). In some

Abbreviations: A. – Arabidopsis; ALA – 5-aminolevulinic acid; ALAS – 5-aminolevulinic acid synthase; *C. – Chlamydomonas*; Chl – chlorophyll; Chlide – chlorophyllide; *E. – Escherichia*; LHCB – light harvesting chlorophyll *a/b* binding protein of Photosystem II; Mg-chelatase – magnesium protoporphyrin IX chelatase; MgProto – Mg-protoporphyrin IX; MgProtoMe – Mg-protoporphyrin IX monomethylester; PChlide – protochlorophyllide; Proto – protoporphyrin IX; Protogen – protoporphyrinogen IX; *S. – Saccharomyces*

of the pathways discussed in this chapter, tetrapyrroles appear to play an important role.

II. Intra-organellar Regulation by Tetrapyrroles

A. Feedback Inhibition by Heme in Animals and Yeast

Heme is indispensable for metabolic and regulatory processes. Its functions comprise oxygen binding (in hemo- and myo-globins), activation of H_2O_2 (catalases and peroxidases), the sensing of oxygen, carbon monoxide and NO, and as redox reactive centers (cytochromes) in electron transport chains. These functions are linked to the properties of the central iron in the porphyrin ring that coordinates two further ligands at the axial position which could be amino acids or small molecules, such as O_2, CO or NO.

Heme, as part of a regulatory system, may be effective by its direct binding to other proteins. Regulatory functions of heme have mainly been investigated in yeast and mammals. Early experiments demonstrated heme-dependent inhibition of ALA synthase (ALAS) activity in liver cells and showed that ALA synthesis under feedback control by heme is the rate-limiting step in porphyrin biosynthesis (Granick, 1966). Subsequently, heme was also shown to influence the expression of the ALA synthase gene (*ALAS)* at various levels, e.g., transcription, mitochondrial import (Andrew et al., 1990; Labbe-Bois and Labbe, 1990). A free heme pool was proposed that exerts control on ALAS expression and activity: depletion of this pool reduced inhibition and accelerated heme biosynthesis. At least in non-erythroid tissue, heme-mediated control renders ALAS the rate-limiting step in heme biosynthesis (Kikuchi and Hayashi, 1981). In *Saccharomyces*, intracellular heme content decreased with diminishing ambient oxygen concentration indicating that the oxygen concentration is sensed to control the activity of metabolic enzymes, e.g., those involved in the synthesis of heme (Labbe-Bois and Bois; 1990; Zhang and Hach, 1999).

A massive amount of coproporphrin I was excreted by *Sacharomyces* (*S.*) *cerevisiae* cells grown for 20 h under continuous flushing with O_2-free N_2, but these cells contained no detectable heme. This suggests that coproporphyrinogen III oxidase and protoporphyrinogen IX oxidase, as expected, were inhibited without O_2 while, in the absence of heme, ALAS activity was unregulated so that uroporphyrinogen III synthase became limiting, thus forming uroporphyrinogen I non-enzymically from hydroxymethylbilane I, which was then enzymically decarboxylated to form coproporphyrinogen I (Porra et al., 1973).

B. Feedback Inhibition by Heme in Plants

The repression of ALA synthesis in the dark and its reactivation during light exposure is an appropriate example of control of the metabolic flow in angiosperms (Chapter 11, Beale) and it indicates that a direct feedback control on ALA biosynthesis also occurs in plants to regulate the concentration of the endproducts of tetrapyrrole biosynthesis. By analogy with the regulatory role of heme in both its own biosynthesis and other regulatory processes of erythroid and hepatic cells, heme may similarly be involved in plant cells. Initial experiments with exogenous heme supported the view that heme functions in the feedback control of plant ALA synthesis (Gough and Kannangara, 1977; Wang et al., 1984, Weinstein and Beale, 1985; Rieble and Beale, 1988). Heme involvement in controlling metabolic activities in the tetrapyrrole pathway of plants and algae was substantiated when heme was shown to be an allosteric inhibitor of glutamyl-tRNA reductase (Pontoppidan and Kannangara, 1994; Vothknecht et al., 1996).

Studies with the pale green *Arabidopsis* (*A.*) *hy1* and *hy2* mutants (Koorneef et al., 1980) or the *Solanum lycopersicum* and pea mutants *aurea and yellow-green2* (*yg2*) have supported the regulatory role of heme. Both *Arabidopsis* mutants were initially identified because their photomorphogenic development is perturbed and it was then shown that the mutant genes encoded heme oxygenase (*yg2* and *hy1*) and phytochromobiline synthase (*aurea, hy2*), respectively. Two allelic mutants, *gun2* and *gun3* (see Section III.B.2), were detected by additional screening for modified *LHCB* expression that is uncoupled from the plastidic development or metabolic activity (Susek et al., 1993). The dark-grown tomato *aurea* mutant had reduced levels of PChlide but exogenous ALA caused similar PChlide accumulation in both mutant and control seedlings (Terry and Kendrick, 1999). It was proposed that impaired heme degradation caused increased heme concentrations in the regulating pool which, in turn, led to feedback inhibition of ALA synthesis (Terry and Kendrick, 1999). Conversely, a reduction of the heme level by adding an iron chelator to wild-type plants to reduce

free ferrous and ferric ion, caused an increase in the level of PChlide (Duggan and Gassman, 1974). These experiments suggested that feedback control by heme content is the main regulator in controlling metabolic flux through the tetrapyrrole pathway (Cornah et al., 2003). However, this hypothesis was derived from experiments with dark-grown or etiolated tissue where heme may indeed play a general regulatory role. In green photosynthetically-active cells, additional regulatory tools are likely to be required to adjust the activities of ALA synthesis to the requirements of the Mg-porphyrin branch of tetrapyrrole biosynthesis.

The demonstration 40 years ago by Granick (1959) that PChlide accumulated in barley seedlings fed with ALA, indicated that inhibition of ALA biosynthesis is an excellent target for feedback control to prevent excess formation of damaging photosensitising tetrapyrrole intermediates and endproducts. Mutant *tigrina* barley seedlings accumulated PChlide in the dark due to non-suppressed ALA synthesis (Nielsen, 1974; von Wettstein et al., 1974). As angiosperms do not convert PChlide to Chlide in the dark, it was proposed that, apart from heme-mediated inhibition of ALA synthesis, a further feedback control by suppression of ALA biosynthesis, is exerted by PChlide accumulation (Beale and Weinstein, 1990); however, experimental evidence showing that PChlide or its enzymatic conversion to Chlide are involved in this regulatory circuit is still missing.

Recently, following an *Arabidopsis* mutant screen, a regulatory mechanism was proposed which enabled the Mg-branch of tetrapyrrole biosynthesis to contribute to feedback control of the pathway. Mutants were selected that accumulate fluorescent Chl intermediates in the dark. Genetic analyses showed that multiple mutants exhibiting this phenotype were defective in a single gene (*Flu*), which encodes FLU, a negative regulator protein of tetrapyrrole biosynthesis. Compared to wildtype seedlings, FLU-defective mutants exhibited an up-regulation of ALA synthesis and an over-accumulation of PChlide, but not of heme (Meskauskiene et al., 2001); thus, FLU is a heme-independent feedback control system mediated by the Mg-porphyrin synthesizing branch. This nuclear-encoded regulator is tightly bound to plastid membranes and physically interacts with glutamyl-tRNA reductase, the first enzyme committed to ALA and tetrapyrrole biosynthesis in plants. It has been suggested that predicted coiled coil and TPR domains are involved in this protein-protein interaction (Meskauskiene and Apel, 2002). The nature of a factor that modulates FLU activity has not yet been defined. However, it became very likely that glutamyl-tRNA reductase is not only a possible target for feedback control by heme as previously suggested (Beale, 1999), but can also be independently controlled through the Mg-protoporphyrin synthesizing branch of the pathway.

III. Role for Tetrapyrroles in Inter-organellar Signaling

A. Heme as an Extra-mitochondrial Regulatory Factor in Mammals and Yeast

Heme, the endproduct of porphyrin biosynthesis in mammalian and yeast mitochondria, where it is used for mitochondrial-cytochrome formation, is transported to other cellular compartments to function in many other cellular processes. In yeast, heme is an internal sensor of oxygen tension since its synthesis is directly correlated with oxygen levels in the extracellular environment (Labbe-Rois and Labbe, 1990). In non-erythroid cells heme controls the *ALAS-1* gene expression in the cytoplasm (see Section II.A) by decreasing the half-life of its mRNA (Hamilton et al., 1991) and by blocking translocation of the ALAS-1 precursor from the cytoplasm of liver cells into the mitochondria (Hayashi et al. 1980).

In nuclei, heme modulates gene expression through a transcription activator, HAP1 (Zhang and Hach, 1999). Heme disrupts a protein complex containing HAP1 which results in HAP1 activation and the promoting of the transcription of genes, which encode functions required for respiration and control for oxidative damage (Zhang et al., 1998). Thus, these genes are activated by high and repressed by low concentrations of heme. Some heme interacting proteins, including HAP1, contain a short consensus sequence of ten amino acids, the heme regulatory motif (Forsburg and Guarente, 1989) which binds heme as a prosthetic group. This motif has been observed in eukaryotic and prokaryotic proteins that are located in different subcellular compartments, such as yeast ALAS, human erythroid heme oxygenase II, *S. cerevisiae* heme lyase, *Escherichia* (*E.*) *coli* catalase, rabbit heme-regulated initiator factor kinase, bacterial iron response regulator and *S. cerevisiae* HAP1 (Lathrop and Timko, 1993, Zhang and Guarente, 1995; Qi et al., 1999; Huang et al., 2001).

Thus, this regulatory motif contributes to a variety of heme-dependent functions, such as transcriptional activity, organelle targeting and other cellular activities. For example, the conserved motif in the transit sequence of the ALAS precursor is involved in heme inhibition of transport of this enzyme into mouse mitochondria (Lathrop and Timko, 1993); and, for the bacterial iron response regulator, it was suggested that iron-dependent protein degradation requires the binding of heme to its regulatory motif (Qi et al., 1999). Although a heme-mediated inhibition of glutamyl-tRNA reductase has been demonstrated, this conserved heme regulatory motif was not found in this enzyme.

B. Contribution of Mg-Porphyrins to Inter-organellar Regulation in Plants

1. Regulatory Role of Mg-Porphyrins in Inter-organellar Communication in Green Algae

Plants possess, within the chloroplasts, all biosynthetic enzymes required for the synthesis of Chl *a* and *b*. A role of Mg-porphyrin intermediates, and possibly their biosynthetic enzymes, in the communication between plastids and the nucleus has been demonstrated in recent years. The unicellular alga, *Chlamydomonas* (*C.*) *reinhardtii*, is well suited for studies on the role of tetrapyrroles as inter-organellar regulators. In light-dark synchronized cultures of this alga, the *LHCB* mRNA accumulates two hours after the transition from dark to light (Johanningmeier and Howell, 1984), a process that appears to be mediated by blue light (Kindle, 1987). Treatment of *Chlamydomonas* cultures at the beginning of the light phase with α, α′-dipyridyl, an iron chelator that inhibits the formation of PChlide and protoheme, prevented the light-induced accumulation of *LHCB* mRNA. It was suggested that inhibition of PChlide synthesis results in the accumulation of Mg-protoporphyrin IX monomethyl ester (MgProtoMe) and other precursors, which subsequently prevent *LHCB* transcripts to accumulate. Partial blocking of the entire porphyrin biosynthetic pathway by feeding inhibitors of ALA biosynthesis (levulinate or hemin) did not affect *LHCB* mRNA accumulation induced by light. However, when the inhibitors of both early and late steps were applied simultaneously, a light-induced increase in *LHCB* mRNA was observed, though at a reduced rate. This, presumably, was a consequence of a lowered accumulation of Chl precursors; however, these data may also arise from the α, α′-dipyridyl-induced accumulation of tetrapyrroles and, on exposure to light, the ensuing photodynamic damage prevented accumulation of *LHCB* transcripts.

While these results showed that direct or indirect interference with tetrapyrrole biosynthesis might affect the expression of a nuclear *LHCB* gene (Johanningmeier and Howell, 1984; Johanningmeier, 1988; Jasper et al., 1991), they provided only indirect evidence for a role of individual tetrapyrroles in this regulation since no analysis of Chl precursors was performed. Furthermore, other factors that control *LHCB* gene expression in light-dark synchronized *C. reinhardtii* cultures, such as the endogenous clock (Jacobshagen et al., 1996), were not considered.

More direct evidence for tetrapyrroles regulating nuclear genes came from studies on the light induction of nuclear genes of the *HSP70* family (von Gromoff et al., 1989) which were shown to affect the chloroplast by enhancing protection of photosystem II and accelerating recovery from damage inflicted by high light intensities (Schroda et al., 1999, 2001). The *Chlamydomonas* mutant *brs-1* has a defective *CHLH* gene encoding the H-subunit of Mg-chelatase (Chekunova et al., 2001) and is, therefore, impaired in Mg-porphyrin synthesis and accumulates Proto but no detectable amounts of subsequent products. When a dark-grown culture of this mutant was exposed to dim light for 1–3 hours, no light induction of *HSP70* expression was observed, although the *HSP70* genes could still be induced by heat shock (Kropat et al., 1997). A mutant of the *yellow-in-the-dark* type, blocked in the conversion of PChlide to Chlide in the dark, has no defect in the light regulation of these chaperone genes, indicating that either Mg-chelatase or Mg-porphyrins are involved in signaling from chloroplast to the nuclear *HSP70* genes.

That intermediates of Chl biosynthesis play a role in this induction was determined by adding various precursors to *Chlamydomonas* cells in the dark. Adding MgProto, or its methylester, resulted in induction of the *HSP70* genes: this suggests that these intermediates could replace the light signal. Since Proto, PChlide and Chlide were unable to induce these nuclear genes, the inducing specificity of these two tetrapyrroles was verified (Kropat et al., 1997).

These data established that tetrapyrroles are intermediates in the signaling pathway whereby light induces the *HSP70* genes. While there is still no direct evidence for transport of MgProto/MgProtoMe out of the chloroplast, there is evidence that light plays a dual role in this signaling pathway:

1) A shift of dark-adapted cultures into light caused a rapid and transient increase in the pool levels of Proto, MgProto and MgProtoMe (Kropat et al., 1999, 2000) which preceded the accumulation of *HSP70* mRNA. Conditions that abolished the light-induced increase in porphyrin-pool levels (e.g., inhibitors of cytoplasmic protein synthesis or the use of gametic cells) also abolished the light induction of the *HSP70* genes, but on adding MgProto to such cell cultures induction of the *HSP70* genes was restored. Thus, a causal relationship between the light-induced increase in Chl precursor levels and the induction of nuclear genes was deduced (Kropat et al., 2000).

2) Evidence for the involvement of additional light-requiring steps in the tetrapyrrole-mediated light induction of the *HSP70* genes came from analyses of porphyrin pool levels in *Chlamydomonas* after adding Proto in the dark which is taken up by the cells and converted to MgProto and MgProtoMe to increase their intracellular pool sizes, which are located, presumably, within the plastids. These plastid tetrapyrroles apparently do not access the cytosol and/or nucleus as they do not contribute to *HSP70* gene induction; thus, these Mg-porphyrins appear to be retained by the chloroplasts in dark-grown cells. Since adding MgProto directly to cells in the dark resulted in *HSP70* induction, it is proposed that Mg-porphyrins are exported out of the chloroplast, actively or passively, only in response to light.

2. Role of Mg-Porphyrins in Chloroplast-to-Nucleus Signaling in Higher Plants

Evidence of tetrapyrroles involvement in plastid-to-nucleus signaling also came from the analysis of *gun* mutants of *A. thaliana* in which expression of an *LHCB* gene is uncoupled from plastidal development (Susek and Chory, 1992; Susek et al., 1993, Surpin et al., 2002). In these mutants, *LHCB* gene expression is less diminished when chloroplasts are rendered by norflurazon inhibition of carotenoid biosynthesis; thus, the expression of a subset of nuclear genes became uncoupled from the physiological state of the plastid. The identified genes of four out of five of these *gun* (*g*enome *un*coupled) mutants encode proteins involved in tetrapyrrole synthesis.

While mutants *gun2* and *gun3*, like mutants *hy1* and *hy2,* are blocked in the breakdown of heme (see also Section II.B), mutant *gun5* has a leaky point mutation in the *CHLH* gene (Mochizuki et al., 2001) which only weakly impaired Chl synthesis, suggesting an involvement of the Mg-chelatase H subunit (CHLH) in regulating plastid-to-nucleus-signaling (Mochizuki et al., 2001). A special regulatory role for CHLH is further supported by the observation that *Arabidopsis* mutants with defects in the CHLI-subunit of Mg-chelatase were unaffected in *LHCB* regulation (Mochizuki et al., 2001).

Subsequently, *LHCB* expression observed during norflurazon treatment was shown to be inversely correlated with steady state levels of MgProto in the *gun5* strain: during norflurazon treatment, this mutant exhibits reduced MgProto accumulation relative to the wild type (Strand et al., 2003). The finding that incubation of leaf protoplasts with MgProto, but not with porphobilinogen, Proto or heme, repressed *LHCB* expression was also consistent with experiments where the *gun*5 mutant was treated with the iron chelator, α, α′-dipyridyl, which presumably increased MgProto accumulation resulting in repressed *LHCB* expression. Moreover, other mutants defective in MgProto formation, comprising those encoding defective genes for coproporphyrinogen oxidase, porphobilinogen deaminase, as well as the D and H subunits of Mg-chelatase, were also non-repressed for *LHCB* formation when grown with norflurazon. Consequently, mutants with reduced MgProto synthesizing capacity should exhibit the *gun* phenotype, namely, non-repressed expression of *LHCB* in the presence of norflurazon.

The *gun4* mutant also appears to fall into this category. A defect in the *gun4* gene results in reduced Chl accumulation and elevated levels of *LHCB* mRNA in the presence of norflurazon. While Mg-porphyrin levels in this mutant have not been reported, the plastid-localized GUN4 protein binds Proto/MgProto and activates Mg-chelatase (Larkin et al., 2003).

Further insight in the regulatory mechanisms that involve the Mg-porphyrin branch of tetrapyrrole biosynthesis came from the analysis of transgenic tobacco plants expressing antisense genes for the CHLI and CHLH subunits of Mg-chelatase. Selected tobacco plants were pale green and exhibited reduced Mg-chelatase activity, leading to lower steady state levels of the Chl precursors MgProto and MgProtoMe. Reduced levels of Proto, the Mg-chelatase substrate, were found in these transformants (Papenbrock et al., 2000a,b) which was assigned to reduced activities of

ALA synthesis in both types of modified plants. In the *CHLH* antisense lines, the reduced ALA synthesizing activity was partially attributed to lowered transcript levels of the nuclear genes *HEMA* and *ALAD* encoding glutamyl-tRNA reductase and 5-aminolevulinic acid dehydratase, respectively (Papenbrock et al., 2000a). Tobacco lines with *CHLI* antisense constructs exhibited the same phenotype and lower contents of mRNA coding for glutamyl-tRNA reductase, ALA dehydratase and MgProto methyltransferase (CHLM) (Papenbrock et al., 2000b). In addition, both these transgenic lines had lower steady-state contents of MgProto(ME) and, in contrast to the *Arabidopsis gun*-phenotype upon norflurazon treatment, exhibited reduced levels of *LHCB* mRNA.

Using antisense and sense genes under the control of the 35S CaMV-promoter, transgenic tobacco plants were generated that exhibited either reduced or increased expression and activity of CHLM (MgProto methyltransferase), resulting in either yellow-pale green or green leaf phenotypes, respectively. Lower CHLM activity in transgenic plants led to increased MgProto levels while plants over-expressing *CHLM* did not affect the MgProto levels. Similar to Mg-chelatase deficient plants, *CHLM* antisense plants showed a lower rate of ALA synthesis. Plants over-expressing *CHLM,* on the other hand, exhibited a higher ALA synthesis rate than wild-type plants. Interestingly, *CHLM* antisense expression resulted in lower transcript levels *not only* of the *HEMA* (glutamyl-tRNA reductase) and the *LHCB* genes, *but also* of the *CHLH* gene. Conversely, *CHLM* over-expression enhanced expression of *HEMA, CHLH* and *LHCB.* Besides the mutually-dependent expression of *CHLM* and *CHLH* genes*,* Mg-chelatase and methyltransferase show coordinated changes in activities (Alawady and Grimm, 2005; Alawady et al., 2005), suggesting a physical interaction between them (Gorchein, 1972; Hinchigeri et al., 1997). We suggest that the control exerted by the initial steps of Mg-porphyrin synthesis on the metabolic flux through the entire tetrapyrrole biosynthetic pathway is coordinated with the metabolic and physiological state of the chloroplast and, further, these initial Mg-porphyrin intermediates are also employed for signaling to the nucleus.

Other experimental approaches using higher plants also support a correlation between the accumulation of Mg-porphyrins and lower levels of *LHCB* and *RBCS* transcripts. Treating etiolated cress seedlings with thujaplicin inhibited PChlide formation and resulted in the accumulation of MgProto and MgProtoME and the inhibition (by at least 50%) of light-induced accumulation of several *LHCB* transcripts (Oster et al., 1996). Moreover, inhibition of etiolated barley seedlings with amitrole, an inhibitor of carotenoid biosynthesis, also caused increased levels of ALA, MgProto and MgProtoME, but lower steady state levels of *LHCB* and *RBCS* transcripts. The authors proposed that the elevated Mg-porphyrin levels reduced the transcriptional activities of these two nuclear gene families (La Rocca et al., 2001).

Several groups have determined pool levels of various tetrapyrroles in green algae and higher plants and correlated them with nuclear gene expression. The physiological significance of these correlations between MgProto levels and metabolic activities of the Chl synthesizing branch or between *LHCB* expression and photosynthetic activities appear cogently significant. However, these measurements of heme or Mg-porphyrins disregard the partitioning of these metabolites between different intracellular compartments and do not necessarily reflect the pool size involved in regulation. Such problems have not yet been addressed due to experimental difficulties. These limitations must be considered when Mg-porphyrin pool levels and nuclear gene expression are correlated. Such considerations could possibly solve some vexing riddles. For instance, tobacco lines with reduced expression of individual genes encoding enzymes of Mg-porphyrin biosynthesis showed lower contents of Mg-porphyrins and reduced *LHCB* mRNA levels (Papenbrock et al., 2000a; Alawady and Grimm, 2005) while norflurazon-treated *Arabidopsis gun* mutants and thujaplicin-treated cress seedlings, inhibited at specific steps of carotenoid or tetrapyrrole biosynthesis, exhibited opposite properties: a decrease in MgProto and/or MgProtoMe, but increased *LHCB* mRNA levels and vice versa (Larkin et al., 2003.).

Thus, the physiological consequences of modified *LHCB* expression as a result of lower or higher steady state levels of MgProto remains to be fully elucidated. It is generally accepted that *LHCB* gene expression depends on the developmental and functional state of chloroplasts and that synthesis of both Chl and the Chl binding protein of the light harvesting complex are synchronized (Nagy et al., 1988; Plumley and Schmidt, 1995). The pale green leaves of some *gun* mutants under normal growth conditions (without norflurazon treatment) argues for impaired Chl synthesis and accumulation of intermediates in response to the mutation. Further, reduced Chl content is also

associated with reduced *LHCB* expression in the pale green transgenic tobacco lines with decreased Mg-chelatase activity (see above).

IV. Transport of Tetrapyrroles

While there is yet no evidence for release of porphyrins, especially Mg-porphyrins, from chloroplasts or mitochondria, clearly some porphyrins must leave the synthesizing organelles: heme must enter the cytoplasm to function as cofactor in heme-requiring proteins. Protogen is routed from plastids to mitochondria in plant cells for the final steps in mitochondrial heme synthesis. Phytochromobilin must also be released from plastids into the cytoplasm for the assembly of holophytochrome.

How tetrapyrrole intermediates are transported out of the chloroplast is presently unknown: no plastidal transporter for porphyrins or heme has yet been described and identified in plants. The multispecific ABC transporters, AtMRP1 and AtMRP2, can transport both glutathione-conjugates and the non-fluorescent chlorophyll catabolite NCC-1 of *Brassica napus* (Lu et., 1998; Tommasini et al., 1998). These transporters, located in the tonoplast, may dispose chlorophyll breakdown products into the vacuole.

A gene, encoding a plastid-localized protein that belongs to the protein family of ABC-like transporters, has been detected by mutant analysis in *Arabidopsis* (Møller et al., 2001). This mutant lacks phytochrome responses under far-red light. Loss of this protein results in a two-fold Proto accumulation, suggesting that it is involved in the inner-plastidic transport and distribution of Proto. Possibly, this protein contributes to the coordination of intercompartmental activities in response to a phytochrome-released signal (Møller et al., 2001): that the ABC-like protein assists either Protogen transport from plastids to mitochondria, or (Mg)-porphyrin export out of the plastids, is currently only a speculation.

A putative candidate for intercompartmental porphyrin transport is the peripheral-type benzodiazepine receptor-like protein, which has been identified in different organisms. This receptor, originally found in the outer membrane of mammalian mitochondria, apparently facilitates both mitochondrial uptake of coproporphyrinogen III and the export of Protogen and heme (Verma et al., 1987; Taketani et al., 1994, Ponka, 1999). A *Rhodobacter sphaeroides* homologue (tryptophan rich sensory transducer) may assist porphyrin efflux from the cells (Yeliseev and Kaplan, 1995, 2000). A peripheral-type benzodiazepine receptor-homologue of *Arabidopsis*, sharing 20% identical residues with both the *Rhodobacteriaceae* and mammalian protein, has recently been identified in the mitochondrial membrane (Lindemann et al., 2004). Since the recombinant receptor protein caused a benzodiazepine-stimulated Proto uptake, it may participate in the distribution of Proto(gen) between plastids and mitochondria.

V. Concluding Remarks

Clearly, different types of tetrapyrroles play different regulatory and metabolic roles in various subcellular compartments. Tetrapyrrole contribution to intra-organellar control mechanisms appears confined to the feedback control of certain enzyme activities in the tetrapyrrole biosynthetic pathway. The obvious enzymatic targets in both chloroplasts and mitochondria are the first enzymes of tetrapyrrole biosynthesis: either glutamyl-tRNA reductase in plants and most bacteria or ALAS in animals, yeast and α-proteobacteria. Both, in vitro and in vivo evidence supports a key role for heme as feedback inhibitor in this regulation. Moreover, control of the biosynthesis of all tetrapyrrole endproducts correlates with the formation of the tetrapyrrole-binding apoproteins; however, the regulatory interplay between the pathway of tetrapyrrole and apoprotein biosynthesis as well as the control of the assembly of the physiologically-functioning holoproteins is still to be clarified.

Strong support for the involvement of the Mg-porphyrin synthesizing branch in intra-plastidal metabolic regulation comes from studies of *Flu* mutants that specifically accumulate PChlide (Meskauskiene et al., 2001). Furthermore, an interaction of FLU with glutamyl-tRNA reductase has been documented in yeast two-hybrid studies; nonetheless, molecule(s) that may act as effector(s) have not yet been identified. However, since levels of 'free' heme in the mutants did not cause significant metabolic alterations relative to control plants, models assigning an exclusive role to heme in intra-organellar regulation of porphyrin biosynthesis (Cornah et al., 2003) are not supported. Although feedback control of tetrapyrrole synthesis and repression of ALA synthesis by excessive heme has also been demonstrated in photosynthetic organisms in many experiments, further discussions are needed about postulated heme pools, their function and their location.

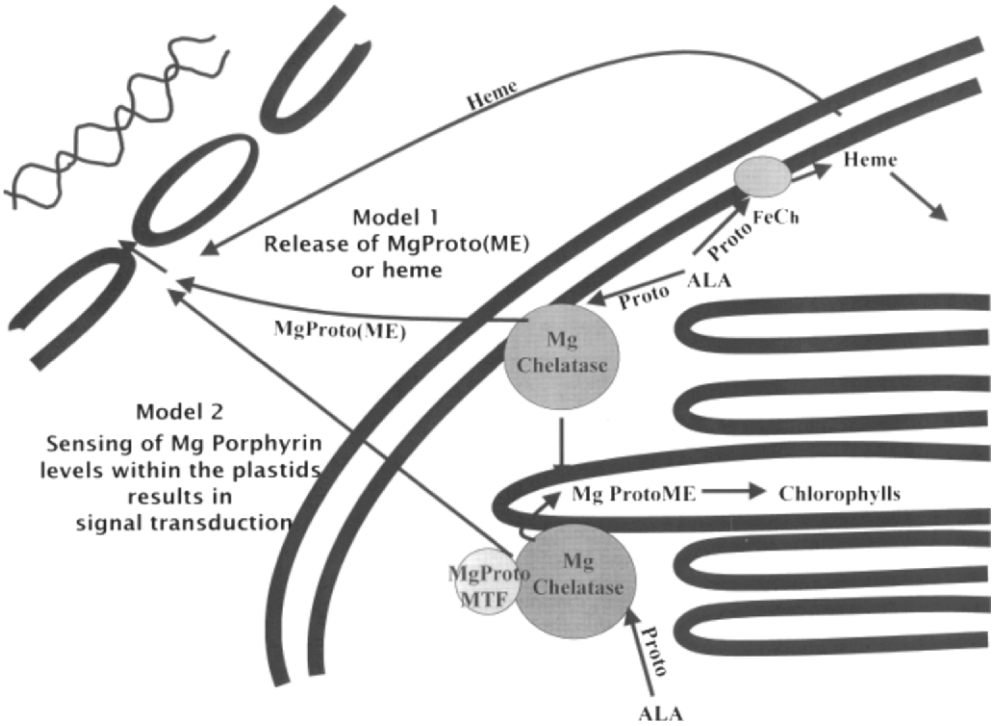

Fig. 1. Two alternative signaling models illustrating the regulatory impact of Mg-porphyrins and heme on tetrapyrrole biosynthesis are shown. *Either* Mg-porphyrins are released into the cytoplasm and transferred to the nucleus to modulate nuclear gene expression *or* the Mg-porphyrin levels are sensed in plastids to release a signal cascade to the cytoplasm. Further details are described in the text. FeCh = ferrochelatase

Independent studies using yeast, mammals, eukaryotic algae and various species of higher plants clarify the role of Mg- and Fe-tetrapyrroles in inter-organellar communication. The targets of these metallo-tetrapyrroles so far defined in subcellular regulatory networks include: 1) the control of genes involved in tetrapyrrole biosynthesis, and 2) genes that respond to environmental changes like light and oxygen.

Correlation of Mg-porphyrin levels with changes in nuclear gene expression implies an inter-organellar regulatory role for these chlorophyll precursors. This raises two intriguing questions: 1) do the signals mediated by Mg-porphyrins require that they be in the cytosol and/or nucleus? If so, they must be translocated from either the chloroplasts or mitochondria. 2) Alternatively, do these Mg-porphyrins trigger signals from the chloroplast site of their synthesis? If so, the signaling pathways must traverse both chloroplast and nuclear membranes.

An up-to-date model of the regulatory impact of Mg-porphyrins and heme on tetrapyrrole biosynthesis is presented in Fig. 1, which illustrates two alternative signaling models and integrates the present knowledge on their roles in inter-organellar regulatory pathways.

Signaling model 1 is based on observations of regulatory responses in the nucleus upon adding Mg-porphyrins: the induction of *HSP70* genes in *Chlamydomonas* and the repression of *LHCB* genes in higher plants. These findings can be explained by a direct interaction of MgProto and/or MgProtoMe with regulatory factors present in cytoplasm/nucleus. The communication from the plastids is ensured by the transferring the Mg-porphyrins through the plastid membrane. This concept is supported by an experiment in which the accumulation of Mg-porphyrins, presumably held within the chloroplast, was uncoupled from the induction of the *HSP70* genes (Kropat et al. 2000).

Also, heme, synthesized in either yeast or mammalian mitochondria, is transferred to the cytoplasm and other compartments to serve as a prosthetic group for regulatory factors and as a cofactor for various pro-

teins. Porphyrin transporters present in mitochondrial membranes may allow controlled transport of heme. The mode of action of heme in cytoplasmic metabolic and regulatory processes is well documented. Plants also require heme to be transported from the site of its synthesis to cytoplasmic destinations; however, the transfer routes of heme from plastids and mitochondria are still unresolved.

In signaling model 2, the Mg-porphyrin levels are sensed at the sites of Mg-porphyrin synthesis by an enzyme complex consisting of Mg-chelatase, Mg-Proto methyltransferase and other putative MgProto-binding proteins. This complex possibly mediates transmembrane signaling from the stroma side of the inner envelope to the cytoplasm. A crucial role may be assigned to alterations in MgProto steady state levels that, via the plastidic protein complex, are communicated to the nucleus.

Some data are consistent with a role of CHLH and/or GUN4 in the signal transfer according to model 1 and 2. CHLH has been found in the inner envelope of chloroplasts in the presence of 5 μM Mg^{2+}, which is in the range of plastidal Mg^{2+} concentration, although the enzyme is also localized in the stroma at lower Mg^{2+} concentrations (Gibson et al., 1996; Leegood et al., 1985). The interaction with the inner envelope may activate signaling on the cytoplasmic side by yet unknown mechanisms.

In summary, while a role for tetrapyrroles in inter-organellar signaling is clearly emerging, the data also suggest that the signaling networks triggered by these compounds are highly complex.

References

Alawady AE and Grimm B (2005) Tobacco Mg protoporphyrin IX methyltransferase is involved in inverse activation of Mg porphyrin and protoheme synthesis. Plant J 41: 282–290

Alawady A, Reski R, Yaronskaya E and Grimm B (2005) Cloning and expression of the tobacco *CHLM* sequence encoding Mg protoporphyrin IX methyltransferase and its interaction with Mg chelatase. Plant Mol Biol 57: 679–691

Andrew TL, Riley PG and Dailey HA (1990) Regulation of heme biosynthesis in higher animals. In: Dailey HA (ed) Biosynthesis of Heme and Chlorophylls, p 163. McGraw-Hill, New York

Batschauer A, Mösinger E, Kreuz K, Dörr I and Apel K (1986) The implication of a plastid-derived factor in the transcriptional control of nuclear genes encoding the light-harvesting chlorophyll *a/b* protein. Eur J Biochem. 154: 625–634

Beale SI (1999) Enzymes of chlorophyll biosynthesis. Photosynth Res 60: 43–73

Beale SI and Weinstein JD (1990) Tetrapyrrole metabolism in photosynthetic organisms. In: Dailey HA (ed) Biosynthesis of Heme and Chlorophylls, pp 287–391. McGraw-Hill, New York

Beck CF (2001) Signalling pathways in chloroplast-to-nucleus communication. Protist 152: 175–182

Bradbeer JW, Atkinson, YE, Börner T and Hagemann R (1979) Cytoplasmic synthesis of plastid polypeptides may be controlled by plastid-synthesised RNA. Nature 279: 816–817

Chekounova E, Voronetskaja V, Papenbrock J, Grimm B and Beck CF (2001) Characterization of *Chlamydomonas* mutants defective in the H-subunit of Mg-chelatase. Mol Gen Genom 266: 363–373

Cornah JE, Terry MJ and Smith AG (2003) Green or red: What stops the traffic in the tetrapyrrole pathway? Trends Plant Sci 8: 224–230

Duggan J, Gassman M (1974) Induction of porphyrin synthesis in etiolated bean leaves by chelators of iron. Plant Physiol 53: 206–215

Durnford DG and Falkowski PG (1997) Chloroplast redox regulation of nuclear gene transcription during photoacclimation. Photosynth Res 53: 229–241

Ernst D and Schefbeck K (1988) Photooxidation of plastids inhibits transcription of nuclear encoded genes in rye (*Secale cereale*). Plant Physiol 88: 255–258

Escoubas JM, Lomas M, La Roche J and Falkowski PG (1995) Light intensity regulation of *cab* gene transcription is signaled by the redox state of the plastoquinone pool. Proc Natl Acad Sci USA 92: 10237–10241

Forsburg SL and Guarente L (1989) Communication between mitochondria and the nucleus in regulation of cytochrome genes in the yeast *Saccharomyces cerevisiae*. Annu Rev Cell Biol 5: 153–180

Gibson LCD, Marrison JL, Leech RM, Jensen PE, Bassham DC, Gibson M and Hunter CN (1996) A putative Mg chelatase subunit from Arabidopsis thaliana cv C24. Plant Physiol 111: 61–71

Goldschmidt-Clermont M (1998) Coordination of nuclear and chloroplast gene expression in plant cells. Int Rev Cytol 177: 115–180

Gorchein A. (1972) Magnesium protoporphyrin chelatase activity *in Rhodopseudomonas spheroides*. Studies with whole cells. Biochem J 127: 97–106

Gough SP and Kannangara CG (1977) Synthesis of δ-aminolevulinate by a chloroplast stroma preparation from greening barley leaves. Carlsberg Res Commun 42: 459–464

Granick S (1959) Magnesium porphyrins formed by barley seedlings treated with δ-aminolevulinic acid. Plant Physiol 34 (Suppl.): XVIII

Granick S (1966) The induction in vitro of the synthesis of delta-aminolevulinic acid Synthetase in chemical porphyria: A response to certain drugs, sex hormones, and foreign chemicals. J Biol Chem 241: 1359–1375

Gray JC, Sullivan JA, Wang JH, Jerome CA and MacLean D (2003) Coordination of plastid and nuclear gene expression. Philos Trans R Soc Lond B Biol Sci 358: 135–144

Grimm B (2003) Regulatory mechanisms of eucaryotic tetrapyrrole biosynthesis. In: Kadish, KM, Smith KM and Guilard R (eds) The Porphyrin Handbook, Volume 12, pp 1–32. Academic Press, San Diego

Hamilton JW, Bement WJ, Sinclair PR, Sinclair JF, Alcedo JA and Wetterhahn KE (1991) Heme regulates hepatic 5-aminolevulinate synthase mRNA expression by decreasing mRNA half-

life and not by altering its rate of transcription. Arch Biochem Biophys 289: 387–392

Harpster MH, Mayfield SP and Taylor WC (1984) Effects of pigment-deficient mutants on the accumulation of photosynthetic protein in maize. Plant Mol Biol 3: 59–71

Hayashi N, Terasawa M and Kikuchi G (1980) Immunochemical studies of the turnover of δ-aminolevulinate synthase in rat liver mitochondria and the effect of hemin on it. J Biochem 88: 921–926

Hess WR, Müller A, Nagy F and Börner T (1994) Ribosome-deficient plastids affect transcription of light-induced nuclear genes: Genetic evidence for a plastid-derived signal. Mol Gen Genet 242: 305–312

Hinchigeri SB, Hundle B and Richards WR (1997) Demonstration that the BchH protein of *Rhodobacter capsulatus* activates S-adenosyl-L-methionine:magnesium protoporphyrin IX methyltransferase. FEBS Lett 407: 337–342

Huang TJ, McCoubrey WK Jr and Maines MD (2001) Heme oxygenase-2 interaction with metalloporphyrins: Function of heme regulatory motifs. Antioxid Redox Signal 3: 685–696

Jacobshagen S, Kindle KL and Johnson CH (1996) Transcription of CABII is regulated by the biological clock in *Chlamydomonas reinhardtii*. Plant Mol Biol 31: 1173–1184

Jasper F, Quednau B, Kortenjann M and Johanningmeier U (1991) Control of *cab* gene expression in synchronized *Chlamydomonas reinhardtii* cells. J Photochem Photobiol B 11: 139–150

Johanningmeier U (1988) Possible control of transcript levels by chlorophyll precursors in *Chlamydomonas*. Eur J Biochem 177: 417–424

Johanningmeier U and Howell SH (1984) Regulation of light-harvesting chlorophyll-binding protein mRNA accumulation in *Chlamydomonas reinhardtii*. J Biol Chem 259: 13541–13549

Karpinski S, Escobar C, Karpinska B, Creissen G and Mullineaux PM (1997) Photosynthetic electron transport regulates the expression of cytosolic ascorbate peroxidase genes in *Arabidopsis* during excess light stress. Plant Cell 9: 627–640

Kikuchi G and Hayashi N (1981) Regulation by heme of synthesis and intracellular translocation of delta-aminolevulinate synthase in the liver. Mol Cell Biochem 37: 27–41

Kindle KL (1987) Expression of a gene for light-harvesting chlorophyll *a/b*-binding protein in *Chlamydomonas reinhardtii*. Plant Mol Biol 9: 547–563

Koorneef M, Rolff E and Spruitt CJP (1980) Genetic control of light inhibited hypocotyl elongation in *Arabidopsis thaliana* (L.) Heynh. Z Pflanzenphysiol 100: 147–160

Kropat J, Oster U, Rüdiger W and Beck CF (1997) Chlorophyll precursors are signals of chloroplast origin involved in light induction of nuclear heat-shock genes. Proc Natl Acad Sci USA 94: 14168–14172

Kropat J, Pöpperl G, Rüdiger W and Beck CF (1999) Identification of Mg-protoporphyrin IX as a chloroplast signal that mediates the expression of nuclear genes. In: Wagner E, Normann J, Greppin H, Hackstein JHP, Hermann RG, Kowallik KV, Schenk HEA and Seckbach J (eds) From Symbiosis to Eukaryotism. Endocytobiol, Vol VII, pp 341–348. University of Geneva

Kropat J, Oster U, Rüdiger W and Beck CF (2000) Chloroplast signalling in the light induction of nuclear HSP70 genes requires the accumulation of chlorophyll precursors and their accessibility to cytoplasm/nucleus. Plant J 24: 523–531

Labbe-Bois R and Labbe P (1990) Tetrapyrrole and heme biosynthesis in the yeast Saccharomyces cerevisiae. In: Dailey HA (ed) Biosynthesis of Heme and Chlorophylls, pp 235–285. Green Publishing Associates and Wiley-Interscience, New York

Larkin RM, Alonso JM, Ecker JR and Chory J (2003) GUN4, a regulator of chlorophyll synthesis and intracellular signaling. Science 299: 902–906

La Rocca N, Rascio N, Oster U and Rüdiger W (2001) Amitrole treatment of etiolated barley seedlings leads to deregulation of tetrapyrrole synthesis and to reduced expression of *Lhc* and *RbcS* genes. Planta 213: 101–108

Lathrop JT and Timko MP (1993) Regulation by heme of mitochondrial protein transport through a conserved amino acid motif. Science 259: 522–525

Leegood RC, Walker DA and Foyer CH (1985) Regulation of the Benson-Calvin cycle. In: Barber J and Baker NR (eds) Photosynthetic Mechanisms and the Environment, pp 199–258. Elsevier Science Publishers Amsterdam

Leon P, Arroyo A and Mackenzie S (1998) Nuclear control of plastid and mitochondrial development in higher plants. Annu Rev Plant Physiol Plant Mol Biol 49: 453–480

Lindemann P, Koch A, Degenhardt B, Hause G, Grimm B and Papadopoulos V (2004) A novel *Arabidopsis thaliana* protein is a functional peripheral-type benzodiazepine receptor. Plant Cell Physiol 45: 723–733

Lu YP, Li ZS, Drozdowicz YM, Hörtensteiner S, Martinoia E and Rea PA (1998) AtMRP2, an Arabidopsis ATP binding cassette transporter able to transport glutathione S-conjugates and chlorophyll catabolites: Functional comparisons with Atmrp1. Plant Cell 10: 267–282

Maxwell DP, Laudenbach, DE and Huner NPA (1995) Redox regulation of light-harvesting complex II and cab mRNA abundance in *Dunaliella salina*. Plant Physiol 109: 787–795

Mayfield SP and Taylor WC (1984) Carotenoid-deficient maize seedlings fail to accumulate light-harvesting chlorophyll *a/b* binding protein (LHCP) mRNA. Eur J Biochem 144: 79–84

Meskauskiene R and Apel K (2002) Interaction of FLU, a negative regulator of tetrapyrrole biosynthesis, with the glutamyl-tRNA reductase requires the tetratricopeptide repeat domain of FLU. FEBS Lett 532: 27–30

Meskauskiene R, Nater M, Goslings D, Kessler F, op den Camp R and Apel K (2001) FLU: A negative regulator of chlorophyll biosynthesis in *Arabidopsis thaliana*. Proc Natl Acad Sci USA 98: 12826–12831

Mochizuki N, Brusslan JA, Larkin R, Nagatani A and Chory J (2001) *Arabidopsis* genomes uncoupled 5 (GUN 5) mutant reveals the involvement of Mg-chelatase H subunit in plastid-to-nucleus signal transduction. Proc Natl Acad Sci USA 98: 2053–2058

Møller SG, Kunkel T and Chua N-H (2001) A plastidic ABC protein involved in intercompartmental communication of light signalling. Genes Dev 15: 90–103

Nagy F, Kay SA and Chua NH (1988) A circadian clock regulates transcription of the wheat *Cab-1* gene. Genes Dev 2: 376–382

Nielsen OF (1974) Macromolecular physiology of plastids. XII. Tigrina mutants in barley: Genetic, spectroscopic and structural characterization. Hereditas 76: 269–304

Oelmüller R (1989) Photooxidative destruction of chloroplasts and its effect on nuclear gene expression and extraplastidic enzyme levels. Photochem Photobiol 49: 229–239

Oelmüller R and Mohr H (1986) Photooxidative destruction or

chloroplasts and its consequences for expression of nuclear genes. Planta 167: 106–113

Oelmüller R and Briggs WR (1990) Intact plastids are required for nitrate- and light-induced accumulation of nitrate reductase activity and mRNA in squash cotyledons. Plant Physiol 92: 434–439

Oster U., Brunner H and Rüdiger W (1996) The greening process in cress seedlings. V. Possible interference of chlorophyll precursors, accumulated after thujaplicin treatment, with light-regulated expression of *Lhc* genes. J Photochem Photobiol B 36: 255–261

Papenbrock J and Grimm B (2001) Regulatory network of tetrapyrrole biosynthesis — Studies for intracellular signalling involved in metabolic and developmental control of plastids. Planta 213: 667–681

Papenbrock J, Mock H-P, Tanaka R, Kruse E and Grimm B (2000a) Role of magnesium chelatase activity in the early steps of the tetrapyrrole biosynthetic pathway. Plant Physiol 122: 1161–1169

Papenbrock J, Pfündel E, Mock H-P and Grimm B (2000b) Decreased and increased expression of the subunit CHLI diminishes Mg-chelatase activity and reduces chlorophyll synthesis in transgenic tobacco plants. Plant J 22: 155–164

Pfannschmidt T, Allen JF and Oelmüller R (2001) Principles of redox control in photosynthesis gene expression. Physiol Plant 112: 1–9

Plumley FG and Schmidt GW (1995) Light-harvesting chlorophyll *a/b* complexes: Interdependent pigment synthesis and protein assembly. Plant Cell 7: 689–704

Ponka P (1999) Cell biology of heme. Am J Med Sci 318: 241–256

Pontoppidan B and Kannangara CG (1994) Purification and partial characterisation of barley glutamyl-tRNA(Glu) reductase, the enzyme that directs glutamate to chlorophyll biosynthesis. Eur J Biochem 225: 529–537

Porra RJ, Barnes R and Jones OT (1973) The over-production of porphyrins by semi-anaerobic yeast. Enzyme 16: 1–8

Poyton, RO, and McEwen, JE (1996). Crosstalk between nuclear and mitochondrial genomes. Annu Rev Biochem 65: 563–607

Qi Z, Hamza I and O'Brian MR (1999) Heme is an effector molecule for iron-dependent degradation of the bacterial iron response regulator (Irr) protein. Proc Natl Acad Sci USA 96: 13056–13061

Rieble S and Beale SI (1988) Transformation of glutamate to delta-aminolevulinic acid by soluble extracts of *Synechocystis* sp. PCC 6803 and other oxygenic prokaryotes. J Biol Chem 263: 8864–8871

Rodermel S (2001) Pathway of plastid-to-nucleus signalling. Trends Plant Sci 6: 471–478

Schroda M, Vallon O, Wollman F-A and Beck CF (1999) A chloroplast-targeted heat shock protein 70 (HSP70) contributes to the photoprotection and repair of photosystem II during and after photoinhibition. Plant Cell 11: 1165–1178

Schroda M, Kropat J, Oster U, Rüdiger W, Vallon O, Wollman F-A and Beck CF (2001) A role for molecular chaperones in assembly and repair of photosystem II? Biochem Soc Transact 29: 413–418

Spikes JD and Bommer JC (1991) Chlorophyll and related pigments as photosensitizers in biology and medicine. In: Scheer H (ed) Chlorophylls, pp 1181–1204. CRC Press, Boca Raton

Strand A, Asami T, Alonso J, Ecker JR and Chory J (2003) Chloroplast to nucleus communication triggered by accumulation of Mg-protoporphyrinIX. Nature 421: 79–83

Surpin M, Larkin RM and Chory J (2002) Signal transduction between the chloroplast and the nucleus. Plant Cell 14 (Suppl): S327–338

Susek R and Chory J (1992) A tale of two genomes: Role of a chloroplast signal in coordinating nuclear and plastid genome expression. Austr J Plant Physiol 19: 387–399

Susek RE, Ausubel FM and Chory J (1993) Signal transduction mutants of *Arabidopsis* uncouple nuclear CAB and RBCS gene expression from chloroplast development. Cell 74: 787–799

Taketani S, Kohno H, Okuda M, Furukawa T and Tokunaga R (1994) Induction of peripheral-type benzodiazepine receptors during differentiation of mouse erythroleukemia cells. A possible involvement of these receptors in heme biosynthesis. J Biol Chem 269: 7527–7531

Taylor WC (1989) Regulatory interactions between nuclear and plastid genomes. Annu Rev Plant Physiol Plant Mol Biol 40: 211–233

Terry MJ and Kendrick RE (1999) Feedback inhibition of chlorophyll synthesis in the phytochrome chromophore-deficient aurea and yellow-green 2 mutants of tomato. Plant Physiol 119: 143–152

Tommasini R, Vogt E, Fromenteau M, Hortensteiner S, Matile P, Amrhein N and Martinoia E (1998) An ABC-transporter of *Arabidopsis thaliana* has both glutathione-conjugate and chlorophyll catabolite transport activity. Plant J 13: 773–780.

Verma A, Nye JS and Snyder SH (1987) Porphyrins are endogenous ligands for the mitochondrial (peripheral-type) benzodiazepine receptor. Proc Natl Acad Sci USA 84: 2256–2260

von Gromoff ED, Treier U and Beck CF (1989) Three light-inducible heat shock genes of *Chlamydomonas reinhardtii*. Mol Cell Biol 9: 3911–3918

von Wettstein D, Kahn A, Nielsen S and Gough S (1974) Genetic regulation of chlorophyll synthesis analyzed with mutants in barley. Science 184: 800–802

Vothknecht UC, Kannangara CG and von Wettstein D (1996) Expression of catalytically active barley glutamyl $tRNA^{Glu}$ reductase in *Escherichia coli* as a fusion protein with glutathione *S*-transferase. Proc Natl Acad Sci USA 93: 9287–9291

Wang WY, Huang DD, Stachon D, Gough SP, Kannangara CG (1984) Delta-aminolevulinic acid-synthesizing enzymes need an RNA moiety for activity. Science 225: 1482–1484

Weinstein JD and Beale SI (1985) Enzymatic conversion of glutamate to delta-aminolevulinate in soluble extracts of the unicellular green alga, *Chlorella vulgaris*. Arch Biochem Biophys 237: 454–464

Yeliseev AA and Kaplan S (1995) A sensory transducer homologous to the mammalian peripheral-type benzodiazepine receptor regulates photosynthetic membrane complex formation in *Rhodobacter sphaeroides* 2.4.1. J Biol Chem 270: 21167–21175

Yeliseev AA and Kaplan S (2000) TspO of *Rhodobacter sphaeroides*. A structural and functional model for the mammalian peripheral benzodiazepine receptor. J Biol Chem 275: 5657–5667

Zhang L and Guarente L (1995) Heme binds to a short sequence that serves a regulatory function in diverse proteins. EMBO J 14: 313–320

Zhang L and Hach A (1999) Molecular mechanism of heme

signalling in yeast: The transcriptional activator Hap1 serves as the key mediator. Cell Mol Life Sci 56: 415–426

Zhang L, Hach A and Wang C (1998) Molecular mechanism governing heme signalling in yeast: A higher-order complex mediates heme regulation of the transcriptional activator HAP1. Mol Cell Biol 18: 3819–3828

Chapter 17

Chlorophyll Catabolites and the Biochemistry of Chlorophyll Breakdown

Bernhard Kräutler
Institute of Organic Chemistry, University of Innsbruck, Innrain 52a, A-6020 Innsbruck, Austria

Stefan Hörtensteiner
Institute of Plant Sciences, University of Bern, Altenbergrain 21, CH-3013 Bern, Switzerland

Summary

Although chlorophyll synthesis in Spring and its degradation in Autumn are undoubtedly the most colorful manifestations of life on Earth, chlorophyll catabolism remained an enigma until about fifteen years ago. Contrary to expectation, chlorophyll breakdown in vascular plants rapidly leads to colorless degradation products and only fleetingly involves colored intermediates, which result from enzymatic oxidative opening of the chlorophyll macrocycle. This key oxygenolytic step in higher plants is rapidly followed by an enzymatic reduction to form short-lived fluorescent catabolites. These latter tetrapyrroles isomerize rapidly in an acid-catalyzed chemical step to colorless tetrapyrrolic catabolites. The colorless and non-fluorescent bilanones finally accumulate in the vacuoles of the degreened plant tissues. This chapter outlines the structural features of chlorophyll catabolites from natural sources and the biochemistry of chlorophyll breakdown.

*Author for correspondence, email: bernhard.kraeutler@uibk.ac.at

Bernhard Grimm, Robert J. Porra, Wolfhart Rüdiger and Hugo Scheer (eds): Chlorophylls and Bacteriochlorophylls: Biochemistry, Biophysics, Functions and Applications, pp. 237–260.

I. Introduction

Only in the last fifteen years has chlorophyll (Chl) catabolism in plants begun to yield some of its mysteries (Kräutler et al., 1991; Matile et al., 1996). The earlier lack of knowledge (Brown et al., 1991) is surprising, considering man's fascination with the seasonal appearance and disappearance of the green plant pigments and the emergence of autumnal colors which are probably the most visual signs of life on Earth, observable even from outer space. Chl metabolism is also of obvious ecological and economic importance. More than 10^9 tons of Chl are biosynthesized and degraded every year on earth (Hendry et al., 1987).

This lack of information on the fate of the green plant pigments (Hendry et al., 1987) contrasts with the extensive literature on Chl biosynthesis (Beale and Weinstein, 1991; Chapters 10–15). In this chapter, we review our present knowledge on the structures and reactivity of known Chl catabolites in higher plants, microorganisms and from synthetic sources, as well as the catabolic pathway leading to their formation from the plant Chls. Some of this work has been described in recent reviews (Hörtensteiner, 1999; Kräutler and Matile, 1999; Hörtensteiner and Kräutler, 2000; Kräutler, 2003).

Earlier research failed to detect Chl breakdown products which would permit an informed glimpse at the biological degradative pathway. This earlier search for Chl catabolites was generally directed at finding colored compounds (Matile, 1987), but the major Chl catabolites from vascular plants are now known to be colorless (Kräutler et al., 1991; Matile et al., 1996; Kräutler and Matile, 1999). By analogy to heme breakdown in plants and animals, an oxygenolytic opening of the porphinoid macrocycle was commonly considered as the key step in Chl breakdown (Brown et al., 1991). However, based on the reactivity of chlorins towards electrophilic agents (Woodward and Skaric, 1961), it was assumed that the Chl macrocycle would open at the 'western' C20 meso position (next to the peripherally reduced ring D of the macrocycle, see Scheme 1), where photooxygenolysis of chlorins was also found to occur (Brown et al., 1991); further, Kishi and coworkers (Nakamura et al., 1988, 1989) found that luciferin from the dinoflagellate *Pyrocystis lunula* and a luminescent compound from krill (see Scheme 14, Section IV) were linear tetrapyrroles derived from Chls by cleavage of the macrocycle at C20. Nonetheless, as shown later, macrocycle opening in the major Chl degradative pathway in plants occurs at the 'northern' C5 bridge carbon. For the numbering of the macrocycle, see Scheme 2 and Chapter 1 (Scheer).

Matile et al. (1987) and Thomas et al. (1989) provided the first evidence of non-green Chl catabolites in extracts of senescent leaves of a non-yellowing genotype of the grass *Festuca* (*F.*) *pratensis.* When such extracts were analyzed by chromatography on silica-gel plates and compared with extracts from the naturally degreening wild-type, 'pink' and 'rusty' pigments were formed on the plates but only from extracts of the senescent (degreened) wild-type leaves. These pigments were thought to be artifactual chemical degradation products of the natural colorless catabolites. Similar pigments were formed in yellowing primary leaves of barley (Matile et al., 1988; Bortlik et al., 1990) when forced to degreen in permanent darkness; surprisingly, they were found in the vacuoles rather than in the de-greened chloroplasts

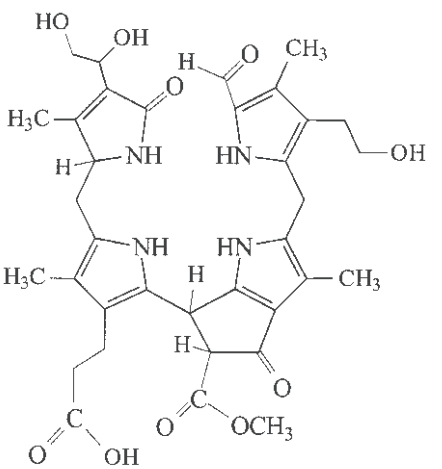

1: *Hv*-NCC-1

Scheme 1

Abbreviations: A. – Arabidopsis; *acd* – accelerated cell death; ALA – aminolevulinic acid; *B. – Brassica*; *C. – Chlorella*; Chl – chlorophyll; Chlide – chlorophyllide; *E. – Escherichia*; *F. – Festuca*; FCC – fluorescent chlorophyll catabolite; LHCP – light harvesting chlorophyll protein; *lls* – lethal leaf spot; MRP – multidrug resistance-associated protein; MS – mass spectrometry; NCC – non-fluorescent chlorophyll catabolite; NMR – nuclear magnetic resonance; PaO – pheophorbide *a* oxygenase; pFCC – primary fluorescent chlorophyll catabolite; Pheide – pheophorbide; RCC – red chlorophyll catabolite

(Matile et al., 1988). Incorporation of ^{14}C isotopic label from [4-^{14}C]-5-aminolevulinic acid (ALA) into these 'rusty pigments' suggested that Chl was their precursor (Peisker et al., 1990). One of these so-called 'rusty pigments', earlier known as RP-14 but now designated as *Hv*-NCC-1 (**1**) (Kräutler et al., 1991), was identified by mass spectrometry (MS) and nuclear magnetic resonance (NMR) spectroscopy as 3^1,3^2,8^2-trihydroxy-1,4,5,10,15,20-(*22H*,*24H*)-octahydro-13^2-[methoxycarbonyl]-4,5-dioxo-4,5-seco-phytoporphyrinate, a colorless catabolite of Chl *a* (**2a**) (see Scheme 1 and section II.C: also Kräutler et al., 1991; 1992); the numbering system used for the linear tetrapyrroles follows that of the Chls (Moss, 1987)). This work on the first structure of a non-green Chl catabolite from plants provided the first clues about Chl catabolism during plant senescence (Matile et al., 1996, 1999; Hörtensteiner, 1999; Kräutler and Matile, 1999; Kräutler, 2003).

II. Chlorophyll Breakdown and Chlorophyll Catabolites in Higher Plants

A. Early Events in Chlorophyll Breakdown

The structure of *Hv*-NCC-1 (**1**) was consistent with dephytylation of Chl *a* (**2a**) as one of the first events of Chl breakdown. In the early 20th century, Arthur Stoll (1912) contributed to this subject by discovering chlorophyllase which catalyses the enzymatic hydrolysis of Chl *a* (**2a**) yielding chlorophyllide (Chlide) *a* (**3a**) and phytol (see Scheme 2). Chlorophyllase thus removes the lipophilic phytol anchor of the Chl molecules, which is necessary for binding the green pigment to the Chl-binding proteins and for insertion of the Chl-protein complexes into the thylakoid membranes of chloroplasts (Paulsen et al., 1993).

Until recently, chlorophyllase was the only known enzyme of the Chl degradative pathway: the subsequent steps remained enigmatic, as further Chl catabolites were unknown. We now know (Bachmann et al., 1994; Matile et al., 1996), that the hydrolytic loss of phytol sets the stage for further enzymatic degradation of both the Chlide and the proteins (Thomas and Hilditch, 1987).

Chlorophyllase is localized in the chloroplast envelope (Matile et al., 1997) and exhibits a remarkable latency. Although it is constitutively present, chlorophyllase activity can only be measured in vivo in the presence of high concentrations of detergents or solvents (Trebitsh et al., 1993); further, the in vivo expression of chlorophyllase in orange fruit requires induction by ethylene and methyl jasmonate

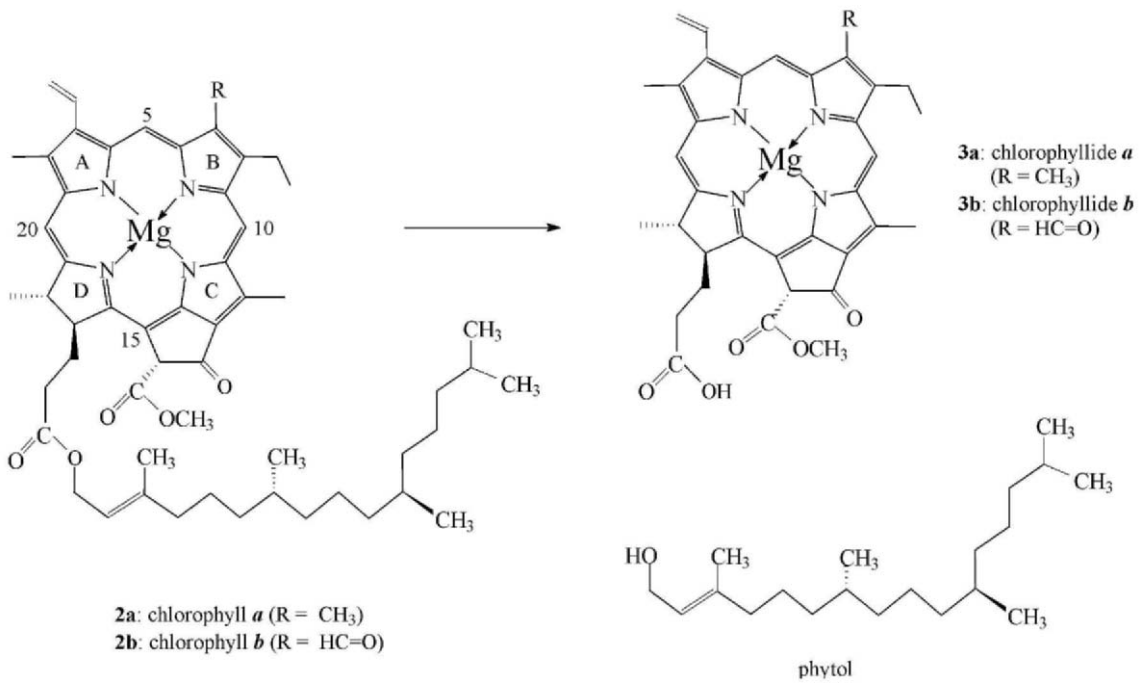

Scheme 2

(Jacob-Wilk et al., 1999). Chlorophyllase has been purified from different plant sources (Trebitsh et al., 1993; Tsuchiya et al., 1997) and has been cloned and functionally over-expressed in *Escherichia* (*E.*) *coli* (Jacob-Wilk et al., 1999; Tsuchiya et al., 1999). The cloned chlorophyllase proteins all contained a highly conserved serine lipase motif, but otherwise the overall homology was rather low (30–40%). Chlorophyllase hydrolyses or transesterifies Chl *a* (**2a**), Chl *b* (**2b**) and the demetallated pheophytin *a* (**4a**), but not the phytyl ester of magnesium protochlorophyllide (**5**) (see Scheme 3) (McFeeters, 1975; Hynninen, 1991).

Remarkably, the Chl catabolites detected in extracts from vascular plants were all derived from Chl *a* (**2a**) and none from Chl *b* (**2b**), the 7-formyl analogue of **2a** (Kräutler and Matile, 1999; Hörtensteiner, 1999; Kräutler, 2003). The fate of Chl *b* (**2b**) during Chl breakdown was, therefore, of particular concern (Matile et al., 1996; Kräutler and Matile, 1999) but the recent discovery of a biochemical pathway from the *b*-type to the *a*-type chlorophyll(ide)s (Chapter 14, Rüdiger) now provides a clue for the absence of Chl *b*-type catabolites (Ito et al., 1993; Ito and Tanaka, 1996; Scheumann et al., 1996; 1999). The well-known oxidative biochemical link between the *a*-type and the *b*-type Chls (Porra et al., 1994; Tanaka et al., 1998) has thus obtained an unexpected reductive counterpart which, together, establish a 'Chl *a*/Chl *b* cycle' (Rüdiger, 1997; Chapter 14, Rüdiger). The reductive step to Chl *a* may function as a very early and obligatory step in Chl *b* breakdown (Ohtsuka et al., 1997; Rüdiger, 1997) in higher plants; indeed, Chl *b* reductase activity is enhanced during senescence (Scheumann et al., 1999). The Chl b reductase and the 'Chl cycle' may also participate in regulating Chl *a/b* ratios in plants during acclimation of the photosynthetic apparatus to changing light intensities (Rüdiger, 1997). These discoveries were consistent with other findings that pheophorbide *a* oxygenase (PaO), the crucial oxygenase which is specifically expressed during senescence, cleaves the chlorin macrocycle of pheophorbide (Pheide) *a* (**6a**), but is inhibited by Pheide *b* (**6b**) (see Section II.B. below) (Hörtensteiner et al., 1995). Thus, the reductive transformation of Chlide *b* (**3b**) to Chlide *a* ensures the availability of all plant Chls for the 'Pheide *a*' degradative pathway (Hörtensteiner, 1999; Matile et al., 1999; Hörtensteiner and Kräutler, 2000). Analysis of the deuterium content of the non-fluorescent Chl

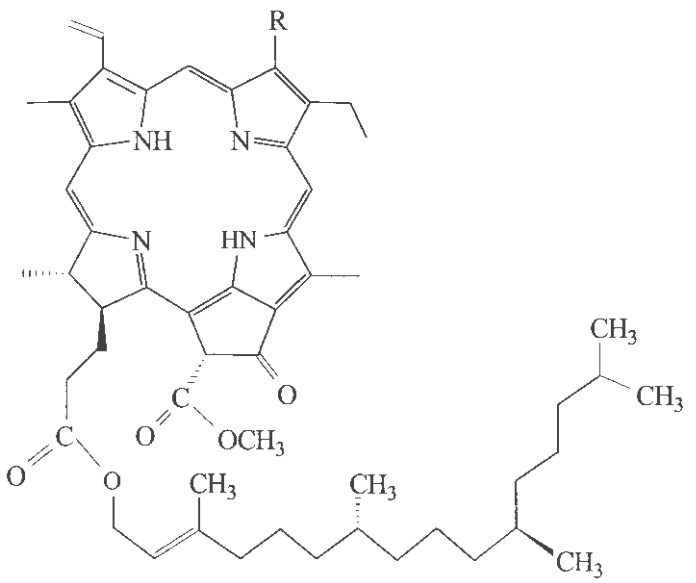

4a: pheophytin ***a*** (R = CH_3)
4b: pheophytin ***b*** (R = HC=O)

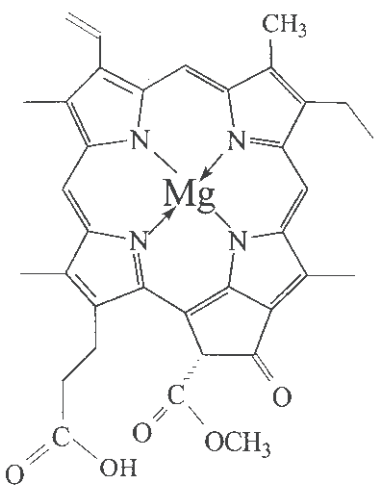

5: Mg-protochlorophyllide

Scheme 3

catabolite *Hv*-NCC-1 (**1**), obtained from artificially degreened primary leaves of barley, provided further independent evidence for the operation of a Chl(ide) *b* (to *a*) reduction in Chl catabolism during senescence (Folly and Engel, 1999).

Most available information suggests that dephytylation and reductive conversion of *b*-Chl(ide)s to *a*-type analogues precedes the loss of the magnesium ion (Langmeier et al., 1993; Shioi et al., 1996a). While the magnesium ion is easily removed from Chlide *a* (**3a**) with dilute acid to generate Pheide *a* (**6a**) (see Scheme 4), a magnesium dechelatase activity has been detected in senescent leaves of *Chenopodium album* (Shioi et al., 1996a) as well as in oilseed rape, *Brassica* (*B.*) *napus* (Langmeier et al., 1993). In the former, it is reported that the magnesium ion is removed and sequestered by a low molecular weight and heat stable 'magnesium dechelating substance' (Shioi et al., 1996a). Much of the magnesium, liberated by Chl degradation during senescence, is transported out of the senescent leaves and stored in the remaining parts of the plant (Matile, 1987).

Pyropheophorbide *a* (**7**), observed in *C. fusca*, *Euglena gracilis* and *Chenopodium album,* has been considered an 'early' Chl catabolite in these green organisms (Schoch et al., 1981; Ziegler et al., 1988; Shioi et al., 1991) and an enzyme, referred to as a 'decarbomethoxylase,' was isolated from *Chenopodium album* (Shioi et al., 1991). Consistent with this, the green alga *Chlamydomonas reinhardtii* showed accumulation of Pheide *a* (**6a**) and of pyropheophorbide *a* (**7**) (Doi et al., 2001) when senescence was artificially induced by lack of light but Chl degradation, beyond the stage of green pigments, was blocked by strictly anaerobic conditions. While these observations suggest enzymatic loss of the 13^2-methoxycarbonyl group in senescing plant leaves and algae during an early phase of Chl breakdown, all presently known colorless, non-fluorescent Chl catabolites from higher plants still possess a methoxycarbonyl function or a carboxylic acid function at C13^2 (Kräutler,` 2003). Indeed, a non-green tetrapyrrolic Chl catabolite having a 13^2-methylene group (as in the pyropheophorbides) has not been isolated from senescent higher plants (Kräutler, 2003; Berghold et al., 2004).

More recent investigations with *Chenopodium album*, however, suggested that only hydrolysis of the methyl ester function of Pheide *a* (**6a**) was enzyme-catalyzed, as significant amounts of 13^2-carboxy-pyropheophorbide *a* (**8**) could be identified by chromatography (Shioi et al., 1996b). The active enzyme, now tentatively named 'pheophorbidase', was specific for chlorins with the highest affinity for Pheide *a* (K_m 12.5 μM). In addition, the reaction was inhibited by methanol, a presumed product of the demethylation (Shioi et al., 1996b). The β-keto-carboxylic acid function of the dicarboxylic acid **8** was found to readily undergo non-enzymatic

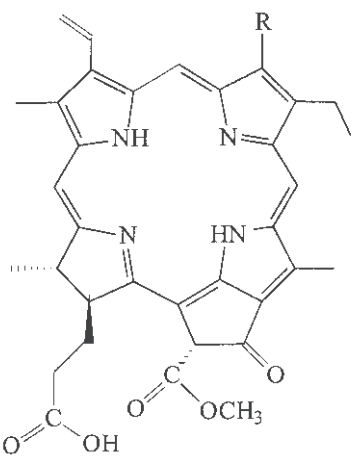

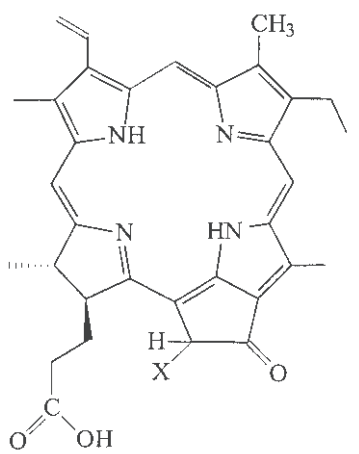

6a: pheophorbide ***a*** (R = CH_3)
6b: pheophorbide ***b*** (R = CH=O)

7: pyropheophorbide ***a*** (X = H)
8:13^2-carboxy-pyropheophorbide ***a*** (X = CO_2H)

Scheme 4

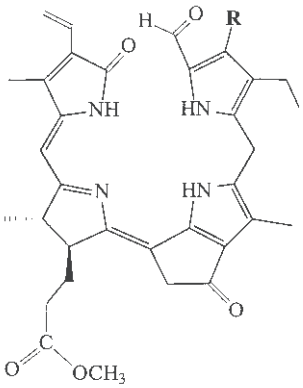

9a: methyl-4,5-dioxo-4,5-seco-pyropheophorbidate *a* (R = CH_3)
9b: methyl-4,5-dioxo-4,5-seco-pyropheophorbidate *b* (R = HC=O)

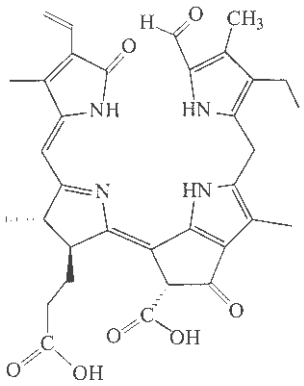

10: 13^2-carboxy-4,5-dioxo-4,5-seco-pyropheophorbide *a*

Scheme 5

decarboxylation at ambient temperature to give the pyropheophorbide *a* (**7**) (Shioi et al., 1996b; Doi et al., 2001). Mühlecker and Kräutler (1996) had suggested the feasibility of the non-enzymatic origin of the latter (see Scheme 4). Likewise, the original characterization of the red, ring-opened derivative (**9a**) of pyropheophorbide from Chl breakdown in the green alga *C. prototheco*ides (Engel et al., 1991) was found more recently to be due to a non-enzymatic decarboxylation during work-up of the corresponding dicarboxylic acid **10** (see section III and Scheme 5; also Engel et al., 1996; Gossauer and Engel, 1996). Currently, therefore, no direct link exists between the observation of pyropheophorbide *a* (**7**) and the later stages of Chl catabolism in higher plants (and green algae).

B. Central Steps of Chlorophyll Breakdown

Colorless, non-fluorescent Chl catabolites have been observed in several senescent vascular plants (Kräutler and Matile, 1999; Kräutler, 2003). When high rates of Chl breakdown were observed in senescent cotyledons of oilseed rape, tiny amounts of nearly colorless but fluorescent compounds were fleetingly observed (Bachmann et al., 1994). These compounds were named 'fluorescent Chl catabolites' (FCCs), because ^{14}C-labeling by [4-^{14}C]-ALA identified them as porphyrin derivatives (Matile et al., 1992; Ginsburg et al., 1994). The FCCs did not accumulate in vivo and were thus deemed to be early, possibly 'primary', products of cleavage of the porphinoid macrocycle of **6a**. This assumption was supported by their location in intact chloroplasts of senescent barley leaves, from which (under appropriate conditions) they were released (Matile et al., 1992).

Another clue about the early steps in Chl breakdown was the discovery that Pheide *a* (**6a**), but not Pheide *b* (**6b**), accumulated in a *F. pratensis* mutant which stays green during senescence (Vicentini et al., 1995a). Also, the accumulation of polar green pigments occurred only in the absence of O_2 (Thomas et al., 1989) suggesting, therefore, that O_2 and **6a** were common substrates in an enzymatic oxidation during Chl breakdown. Similarly, as mentioned above, senescent cells of *Chlamydomonas reinhardtii,* accumulated Pheide *a* (**6a**) or pyropheophorbide *a* (**7**) in the absence of O_2 (Doi et al., 2001).

1. Enzymatic Experiments with Synthetically-derived Red Chlorophyll Catabolite

Determination of the structure of the 'primary' fluorescent Chl catabolite (pFCC; **11**) as (3^1,3^2-didehydro-1,4,5,10,17,18,20,(*22H*)-octahydro-13^2-(methoxycarbonyl)-4,5-dioxo-4,5-seco-phytoporphyrin, see Scheme 6) (Mühlecker et al., 1997) suggested that the key step in Chl breakdown was an oxygenolytic

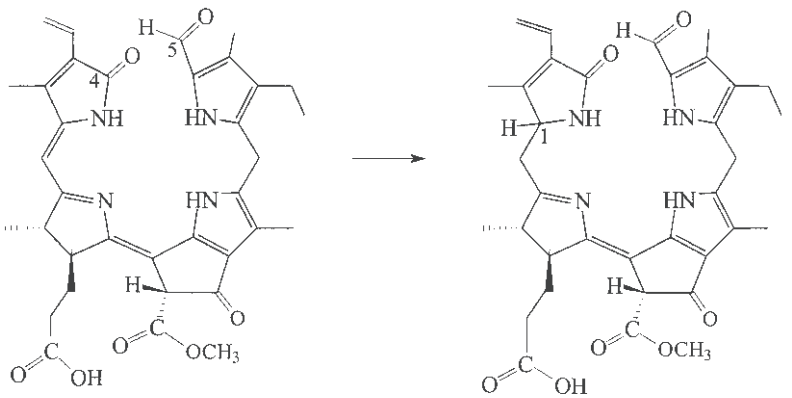

12: "red" chlorophyll catabolite (RCC)

11: "primary" fluorescent chlorophyll catabolite (pFCC)

11-*epi*: 1-*epi*-pFCC (C(1)-epimer of pFCC)

Scheme 6

cleavage at the 'northern' C5 position of the porphinoid macrocycle of Pheide *a* (**6a**) by an elusive oxygenase (Ginsburg and Matile, 1993; Hörtensteiner et al., 1995), followed by hydrogenation of the 'western' C20 meso position, thus generating the pFCC (**11**). Consequently, the 'red chlorophyll catabolite' (RCC) **12** (3^1,3^2-didehydro-4,5,10,17,18,(*22H*)-hexahydro-13^2-(methoxycarbonyl)-4,5-dioxo-4,5-seco-phytoporphyrin) was proposed as a precursor of pFCC (**11**), since it differed only by addition of two hydrogen atoms at C1 and C20. This suggested that RCC (**12**), which shared the same chromophore structure as some red bilinones excreted as final Chl degradation products by *C. protothecoides* (Engel et al., 1996; Gossauer and Engel, 1996), was an intermediate in Chl breakdown in higher plants (Mühlecker et al., 1997).

By analogy to the earlier chemical preparation of red tetrapyrrolic isolate **9a** from *C. protothecoides* by Iturraspe and Gossauer (1992), RCC **12** could be prepared in a sequence of five chemical steps by partial degradation of methyl pheophorbidate *a* (**13**) via methyl-4,5-dioxo-4,5-seco-pheophorbidate **14** (RCC methyl ester; see Scheme 7; also Kräutler et al., 1997; and reviewed in Kräutler, 2003). The UV/Vis-spectrum of the weakly fluorescing red diester **14** has prominent absorbance maxima near 500 and 316 nm (Fig. 1). The diester **14** was spectroscopically identical with the methylation product of the di-acid **10** from the green alga *C. protothecoides* (Gossauer and Engel, 1996; Kräutler et al., 1997).

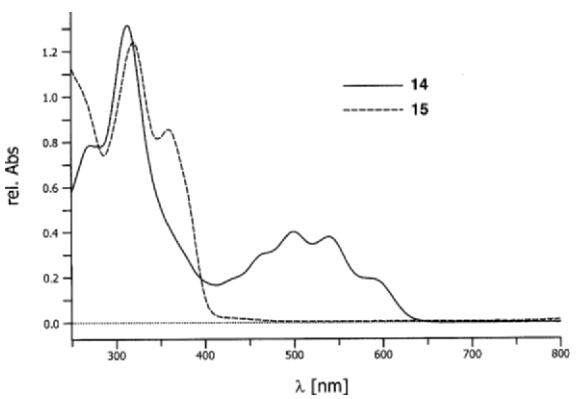

Fig. 1. UV/Vis-spectra of RCC methyl ester (**14**, in chloroform) (Kräutler et al., 1997) and of the methyl ester of pFCC (**15**, in methanol) (Oberhuber and Kräutler, 2002).

With the authentic RCC (**12**) now available (Kräutler et al., 1997), the identical red compound was found in senescent plants as the elusive RCC in the experiments of Rodoni et al. (1997a,b): small amounts of the red compound **12** were obtained from Pheide *a* (**6a**) by enzyme-catalyzed oxygenolysis during aerobic incubation with extracts of washed senescent canola chloroplast membranes supplied with reduced ferredoxin. The identity of the elusive RCC, thus produced, was confirmed by co-chromatography with synthetic **12** using HPLC. The enzymatic activity in the washed senescent chloroplast membranes was achieved by a single enzyme, an oxygenase meanwhile termed PaO. The putative oxygenase possessed a non-heme

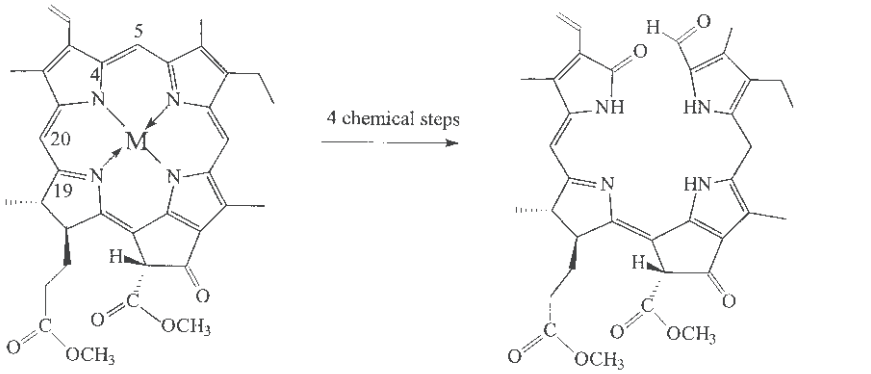

13: methyl-pheophorbidate *a* (M = 2H)

14: methyl-4,5-dioxo-4,5-seco-pheophorbidate *a* (RCC methyl ester)

Scheme 7

iron-containing reactive center as shown by the in vitro and *in organello* inhibition of fluorescent catabolite formation by chelators, such as 2,2′-dipyridyl (Schellenberg et al., 1990; Hörtensteiner et al., 1995). Thus, the enzyme was probably related to other non-heme iron-dependent (mono)oxygenases (Lippard and Berg, 1994).

Anaerobic incubation of chemically-prepared RCC (**12**) with stroma proteins, isolated from barley chloroplasts, and reduced ferredoxin produced three fluorescing compounds which had the same UV/Vis-spectrum as the pFCC **11**: one of these compounds shared identical HPLC characteristics with pFCC (**11**) (Rodoni et al., 1997a,b).

2. Pheophorbide a Oxygenase Cleaves the Porphyrin Macrocycle

PaO catalyzes the crucial and (effectively) irreversible cleavage of the porphinoid macrocycle and may be considered to represent a key enzyme of Chl breakdown. Since the oxygenolytic transformation of Pheide *a* to enzyme-bound **12** involves O_2 (Rodoni et al., 1997a), this transformation could be achieved either by a mono-oxygenase or by the joint action of a dioxygenase and a reductase. An in vitro assay of PaO was developed using an oilseed-rape preparation containing partially purified oxygenase and the reductase (see below; see also Hörtensteiner et al., 1998). As the oxygenase was known to be inhibited by its product (Hörtensteiner et al., 1995), the presence of the reductase was essential to achieve useful turn-over and the reduction product, pFCC (**11**), was analyzed. In the presence of $^{18}O_2$, this active enzyme mixture converted Pheide *a* (**6a**) into ^{18}O-labeled pFCC (**11**-^{18}O) containing one ^{18}O-atom per molecule of catabolite, as determined by MS analysis of the molecular ion (see Scheme 8). From MS analysis of fragmentation ions of **11**-^{18}O, the isotopic label was localized to the formyl group attached to 'ring B' thus indicating the incorporation of one oxygen atom from O_2 at the C5 position of **6a**. As only one of the two oxygen atoms introduced in the oxidation of **6a** to **12** is derived from O_2, PaO is a mono-oxygenase and the other oxygen atom is, most likely, derived (directly or indirectly) from water (Hörtensteiner et al., 1998).

As attempts to purify PaO were not overly successful (Hörtensteiner et al., 1998) a functional genomic approach was used to clone PaO. Exploiting known biochemical properties of PaO, the *A. thaliana* protein database (Arabidopsis Genome Initiative, 2000) was screened for candidate proteins that may encode PaO. From 21 proteins identified this way, one protein (At3g44880) was subsequently shown to encode *A. thaliana* PaO (AtPaO) (Pružinská et al., 2003). Thus, the biochemical properties of the recombinant protein were identical to PaO isolated from natural sources. AtPaO is a Rieske-type iron-sulfur protein that is identical to the previously identified *A. thaliana* accelerated cell death 1 (ACD1) and homologous to lethal leaf spot 1 (LLS1) from maize (Gray et al., 2002). Using a *lls1* mutant, the function of PaO could be confirmed: *lls1* leaves showed a stay-green phenotype in the dark and accumulated Pheide *a* upon senescence induction (Pružinská et al., 2003).

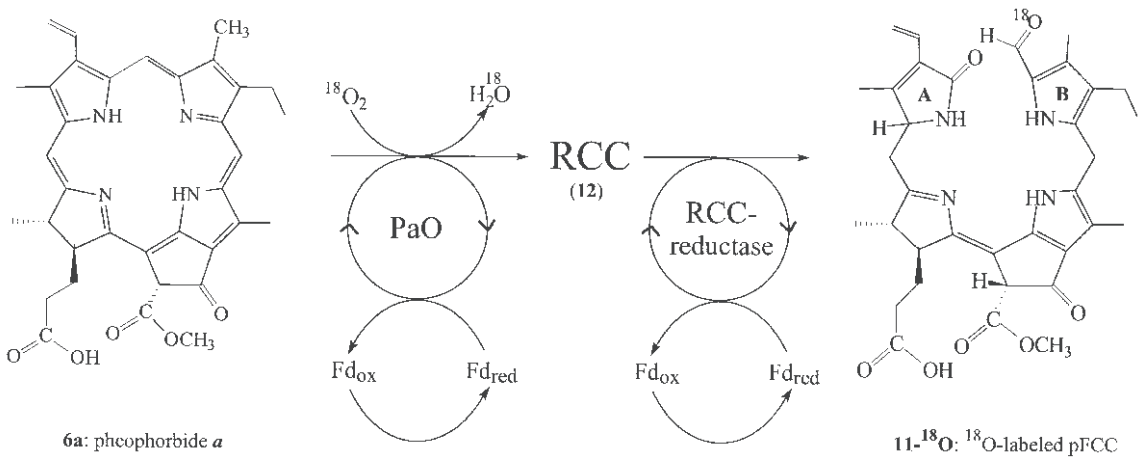

Scheme 8

The enzymatic oxidation of Pheide *a* (**6a**) into the RCC, **12,** by PaO is a remarkable structural transformation. The oxygenase is intriguingly specific for Pheide *a* (**6a**) (Hörtensteiner et al. 1995), and ferredoxin drives its redox cycle (Schellenberg et al., 1993). Besides the incorporation of two oxygen atoms, the ring opening at the newly oxygenated sites includes also formation of two carbonyl functions and the saturation of the 'eastern' C10 meso position. Formally, **12** arises from Pheide *a* (**6a**) by addition of one equivalent each of dioxygen and dihydrogen, but the mechanism of the hypothetical isomerization of the primary enzymatic oxygenation product to the ring-opened (enzyme-bound) form of **12** is not clear. Section III describes the related problem of the formation of red catabolites (such as **9a** and **10**) in the green alga *C. protothecoides* (Curty et al., 1995; Gossauer and Engel, 1996; Curty and Engel, 1997).

Chl breakdown and the process catalyzed by PaO had a crucial impact on the development of the laws of genetics that Mendel established in the 19th century (Mendel, 1865). The puzzling observation of the phenotype of a recessive allele in Mendel's 'green peas' is now known to be connected to a deficiency of the activity of this oxygenase (Thomas et al., 1996). In addition, a stay-green mutant of *F. pratensis*, Bf 993, which is unable to degreen during senescence, has been demonstrated to be biochemically deficient in PaO (Vicentini et al., 1995a). The mutation of Bf 993 is inherited as a single recessive gene, *sid* (Thomas, 1987) suggesting that the *Sid* locus encodes or regulates the gene for PaO.

3. Red Chlorophyll Catabolite Reductase Produces Colorless, Fluorescent Chlorophyll Catabolites

As described above, RCC (**12**) is bound strongly to the membrane-attached oxygenase, PaO, and inhibits further oxygenase activity; however, a stromal reductase, employed in an in vitro assay (see above), reduces authentic **12** to pFCC (**11**) which is no longer enzyme bound (Mühlecker et al., 1997; Rodoni et al., 1997a). This reductase, named RCC reductase (Rodoni et al., 1997a; Wüthrich et al., 2000), is dependent on reduced ferredoxin as electron donor (Wüthrich et al., 2000). As the cleavage of the Chl macrocycle in higher plants requires the intimate cooperation of the membrane-bound PaO and the stromal RCC reductase, it may represent an example of 'metabolic channeling' (Rodoni et al., 1997a,b; Matile et al., 1999). Evidence for this is the lack of accumulation of RCC in coupled in vitro assays of PaO activity. RCC reductase produces pFCC by stereospecifically reducing C1 of PaO-produced (and enzyme-bound) **12**. However, authentic chemically-derived **12** was transformed to three FCCs by tissue extracts containing RCC-reductase (Rodoni et al., 1997a; Wüthrich et al., 2000), suggesting that the interaction with PaO confers stereospecificity to RCC reductase (Wüthrich et al., 2000). Further, the finding that RCC reductase activity is inhibited by O_2 (Rodoni et al., 1997a,b), while PaO requires O_2 for activity (Hörtensteiner et al., 1998), supports the idea of a PaO-RCC reductase interaction, whereby O_2 consumption by PaO could

generate an O_2-depleted micro-environment at the site of RCC-reductase activity.

The molecular formula of **11** ($C_{35}H_{40}N_4O_7$) determined from high-resolution MS, indicated **11** to be derived from **6a** by formal addition of one equivalent of O_2 and two equivalents of H_2. By NMR spectroscopy, **11** was identified as $3^1,3^2$-didehydro-1,4,5,10,17,18,20(*22H*)-octahydro-13^2(methoxycarbonyl)-4,5-dioxo-4,5-seco-phytoporphyrin, a linear tetrapyrrole derived from Pheide *a* by an oxygenolytic cleavage at the 'northern' C5 meso position and by reductive saturation of the 'western' C20 and C1 positions (Mühlecker et al., 1997). This structure clearly showed **11** to be an intermediate in Chl catabolism preceding the stage of the 'non-fluorescent' Chl catabolites (NCCs, see below). Meanwhile, a second fluorescent Chl catabolite (**1**-*epi*-pFCC, **11**-*epi*) was isolated from sweet pepper (*Capsicum annuum*) and its structure was determined (Mühlecker et al., 2000): **11**-*epi* was shown to be a stereoisomer of **11** differing only in its configuration at C1, the asymmetric carbon center newly-introduced by the two highly stereo-selective RCC reductases present in sweet pepper and oilseed rape (Hörtensteiner et al., 2000; Mühlecker et al., 2000). Thus, these two FCCs (**11** and **11**-*epi*) are direct reduction products of two different RCC reductases and both should, therefore, be considered as pFCCs (Mühlecker et al., 1997, 2000). The UV/Vis-spectrum of 11 and of 11-*epi* shows two prominent absorption bands, near 361 and 320 nm (see Fig. 1), and solutions of the pFCCs possess a luminescence maximum near 436 nm. The remarkable stereo-dichotomy of the respective RCC reductases of the two plant species indicates an apparent functional irrelevance of the absolute configuration at the C1 chiral center generated by these reductases (Mühlecker et al., 2000). Meanwhile, screening a variety of plant species by HPLC for their pFCC epimer type revealed a species-dependent distribution of the two classes of RCC reductases (Hörtensteiner et al., 2000): within a plant family, all genera and species produce the same epimeric pFCC. The RCC reductase activity found in the ancient terrestrial species, *Selaginella* (Hörtensteiner et al., 2000) and the livermoss *Marchantia polymorpha* (Wüthrich et al., 2000), but not in the green alga *C. prototheco ides* (S. Hörtensteiner, unpublished), indicates that the 'invention' of RCC reductase might have been an important evolutionary step from the unicellular aquatic stage to multicellular land plants; indeed, in *C. prototheco ides*, Chl catabolism ends with the excretion of RCC-like linear tetrapyrroles into the medium (Section III).

RCC reductase has been purified from senescent barley primary leaves (Rodoni et al., 1997b; Wüthrich et al., 2000) and a cDNA fragment was subsequently isolated. Database searches identified homologous sequences from different species, and RCC-reductase from *A. thaliana* (AtRCCR) was cloned and functionally expressed in *E. coli* (Wüthrich et al., 2000). Recombinant AtRCCR converted chemically-prepared RCC (**12**) (Kräutler et al., 1997) to the epimeric pFCCs, **11** and **11**-*epi*. As observed with native RCC reductase (Hörtensteiner et al., 2000), when heterologously-expressed AtRCCR was assayed in the presence of PaO (Wüthrich et al., 2000), the reaction was stereo-selective for the production of **11**. In barley and *A. thaliana*, RCC reductase is encoded by a single copy gene which seems to be constitutively expressed. Independently, an *accelerated cell death 2* (*acd2*) mutant of *A. thaliana* was identified (Greenberg et al., 1994) which is defective in the RCC reductase gene (Mach et al., 2001). This mutant spontaneously forms spreading lesions and activates a constitutive pathogen defense even in the absence of pathogen infection. This hypersensitive reaction only occurred in the light, suggesting that the Chl catabolic pathway has an important role in disease resistance by removing photoactive Chl catabolites.

That RCC reductase required no cofactors, other than reduced ferredoxin, for reduction of RCC (**12**) to form **11** appeared puzzling and suggested that the enzyme-bound RCC (**12**) was a sufficiently redox-active substrate to undergo a ferredoxin-driven reduction to form 11 without requiring further reducing cofactors. To test this assumption, the electrochemical reduction of the methyl ester (**14**) of RCC, available from partial synthesis (Kräutler et al., 1997), was studied in both analytical and preparative electrochemical experiments (Oberhuber and Kräutler, 2002); indeed, electrochemical reduction of **14** in methanol at room temperature proceeded stereo-unselectively and gave two major compounds with UV/Vis-absorbance properties of pFCC, **11** (see Fig. 1). It resulted in about 12% each of the strongly luminescent tetrapyrroles, **15** and **15**-*epi*, the methyl esters of the two epimeric pFCCs, **11** and **11**-*epi*, (see Scheme 9). In addition, about 30% of a new type of reduction products was formed which possessed a different chromophore structure with a UV/Vis-spectrum showing peaks near 310 and 420 nm. MS studies showed the four main

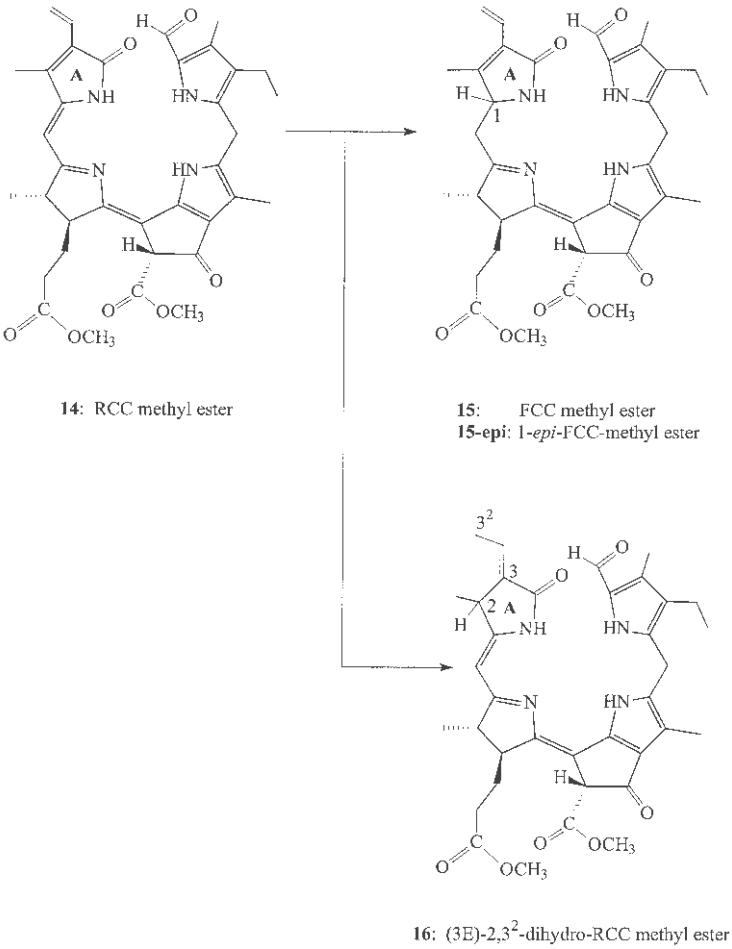

Scheme 9

fractions to have the same molecular formula as **15**. The almost non-fluorescent linear tetrapyrrole **16** and its three stereoisomers were further characterized by NMR-spectroscopy (Oberhuber and Kräutler, 2002). They were found to differ in their stereochemistry at C2- and C13^2 and to be linear tetrapyrrolic reduction products with an ethylidene group on ring A; that is, to be regio-isomers of **15**. The structures of the methyl-3^1,3^2-didehydro-1,4,5,10,17,18,20*(22H)*-octahydro-13^2-(methoxycarbonyl)-4,5-dioxo-4,5-seco-(22H)-phyto-porphyrin (**15**) and of the methyl-3^1-dehydro-2,4,5,10,17,18,22-heptahydro-13^2-(methoxycarbonyl)-4,5-dioxo-4,5-seco-(22H)-phytoporphyrin (**16**), as well as of their stereo-isomers, were spectroscopically determined. These two electrochemical reduction paths to **15** and **16** are reminiscent of the known pair of isomeric enzymatic reductions of biliverdin (**17**) to phytochromobilin (**18**) and 15,16-dihydrobiliverdin (**19**) (Beale and Weinstein, 1991; Beale and Cornejo, 1991).

These electrochemical model experiments suggest, therefore, that RCC (**12**) is sufficiently redox-active to undergo ferredoxin-driven and enzyme mediated reduction to **11** or **11**-*epi* (Oberhuber and Kräutler, 2002); thus, reduction of RCC by RCC reductase may occur in single electron reduction and protonation steps. The following functions can therefore be assigned to RCC reductase:

(i) binding PaO with bound **12** and reduced ferredoxin,

(ii) mediating the electron transfer reactions from ferredoxin to the bound substrate, and

(iii) controlling properly the regio- and stereo-selective protonation at C20 and C1 of the protein-bound tetrapyrrolic reduction intermediates.

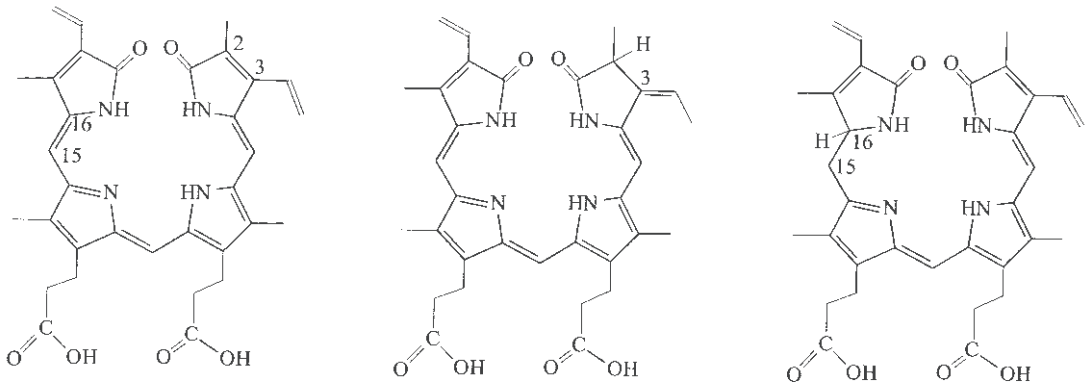

17: biliverdin

18: (3Z)-phytochromobilin

19: 15,16-dihydrobiliverdin

Scheme 10

In this model, RCC reductase would not carry out the reduction steps, but would direct them in an optimal way in the manner of a 'chaperone.'

RCC reductases show remarkable homology with some ferredoxin-dependent biliverdin reductases (Frankenberg et al., 2001). Not only the sequence homologies but also the requirement for ferredoxin as a reductant (Wüthrich et al., 2000), as well as the similar chemical transformations catalyzed by these reductases indicate unexpected similarities between the biodegradation of heme (Beale and Cornejo, 1991; Falk, 1989) and Chl in higher plants (Hörtensteiner et al., 2000; Oberhuber and Kräutler, 2002).

C. Late Stages of Chlorophyll Breakdown

The chemically labile, fluorescent Chl catabolites, such as pFCC (**11**), do not accumulate during Chl breakdown in vascular plants, but are readily transformed further to the colorless NCCs, such as *Hv*-NCC-1, (**1**, 3^1,3^2,8^2-trihydroxy-1,4,5,10,15,20-(*22H*,*24H*)-octahydro-13^2-(methoxycarbonyl)-4,5-dioxo-4,5-seco-phyto-porphyrinate, (see Fig. 1 for structure of **1** and Fig. 2 for UV- and CD-spectra; also Kräutler et al., 1991, 1992; Kräutler, 2003). The colorless NCCs are the first linear tetrapyrrolic intermediates during chlorophyll breakdown, in which the four pyrrolic units are completely de-conjugated. A direct isomerization of FCCs to the corresponding NCCs may achieve this result (Mühlecker et al., 1997; Kräutler and Matile, 1999; Hörtensteiner and Kräutler, 2000). Such a reaction is likely to be thermodynamically favorable, by analogy with studies of the tautomerization of various hydro-porphinoids (Eschenmoser, 1988). Indeed, recent non-enzymatic experiments showed the stereo-selective isomerization of the authentic *p*FCC **11**-*epi* to the NCC **21** (see Scheme 11) to occur very readily at ambient temperatures and in weakly acidic aqueous medium (Oberhuber et al., 2003). Therefore, this 'final stage' in the natural breakdown of the intensely-colored Chl into colorless NCCs possibly occurs under rather mild, non-enzymatic, conditions.

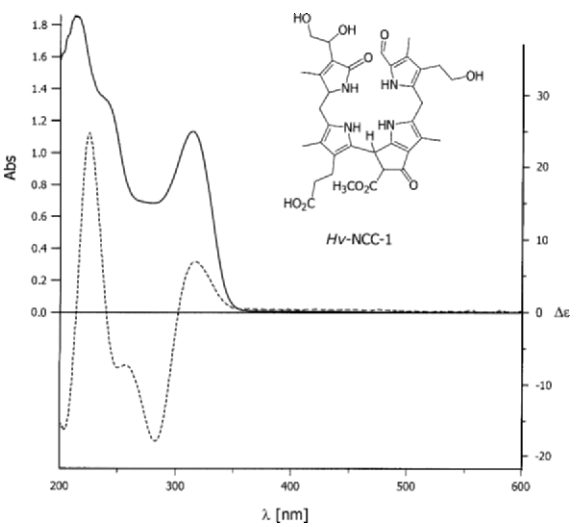

Fig. 2. UV-/Vis- (—) and CD-spectra (- - -) of the nonfluorescent chlorophyll catabolite *Hv*-NCC-1 (**1**, in water) (Kräutler et al., 1992).

Careful re-analysis of extracts of senescent leaves of the tree, *Cercidiphyllum japonicum,* confirmed not only the dominant presence of the non-fluorescent Chl catabolite (*Cj*-NCC-1, **20**) (Curty and Engel, 1996), but also revealed the less polar *Cj*-NCC-2. NMR-spectroscopic analysis showed *Cj*-NCC-2 to be a $3^1,3^2$-didehydro-1,4,5,10,15,20-(*22H,24H*)-octahydro-13^2-(methoxycarbonyl)-4,5-dioxo-4,5-seco-phytoporphyrinate and to be identical with *Cj*-NCC-2, **21**. the latter is is an isomer of a 'primary' FCC (**11** or **11**-*epi*) and is the first of the known NCCs lacking the characteristic hydroxyl function at ring B (see Scheme 11; also Kräutler, 2002; Oberhuber et al., 2003). *Cj*-NCC-2 (**21**) is thus suggested to be formed directly by (nonenzymatic) isomerization of pFCC **11**-*epi* and to be a 'primary' NCC (pNCC) of *Cercidiphyllum japonicum* (Kräutler and Matile, 1999; Hörtensteiner and Kräutler, 2000; Oberhuber et al., 2003).

The timing and the organellar location within the senescent leaf cell (see Fig. 3) of the isomerization of FCCs into the corresponding NCCs during Chl breakdown, have been a matter of special interest (Matile et al., 1996; Hörtensteiner, 1999; Kräutler and Matile, 1999). This (hypothetical) isomerization may occur before, in parallel with or after the side chain modification (refunctionalization) reactions, which are indicated by the structures of the known NCCs (see below). As low pH values are typical of vacuoles, the isomerization of FCCs to NCCs is now suggested to occur as a non-enzymatic process in the vacuoles during the natural course of Chl breakdown. The vacuoles thus appear to be the sites for this final isomerization, as well as the final storage compartment for the NCCs.

As a prerequisite for the isomerization of FCCs to NCCs, the controlled transport of the FCCs to the vacuoles becomes an important event in Chl breakdown. Consideration of the observed side chain functions of the NCCs suggests the availability of polar peripheral groups to be relevant for a carrier-mediated transport (of the FCCs) into the vacuoles. This further suggests that side chain modifications would occur at the level of the pFCCs and in the senescent chloroplasts (Kräutler and Matile, 1999; Hörtensteiner and Kräutler, 2000). Treatment of the pFCC **11** by an active extract of soluble enzymes from degreened cotyledons of oilseed rape produced an FCC with significantly higher polarity which was tentatively assigned the structure of the $3^1,3^2$-didehydro-1,4,5,10,17,18,20-(22H)-octahydro-13^2-(carboxy)-4,5-dioxo-4,5-seco-phytoporphyrin (**22**) (see Scheme 11; Hörtensteiner and Kräutler, 2000). The same extract from senescent cotyledons of oilseed rape did not hydrolyze the methyl ester function in several NCCs, indicating that hydrolysis of the 13^2-methoxycarbonyl function in these senescent leaves occurs at the stage of the FCCs (Hörtensteiner, unpublished). This view is consistent with the observation in senescent leaf extracts of small amounts of unknown

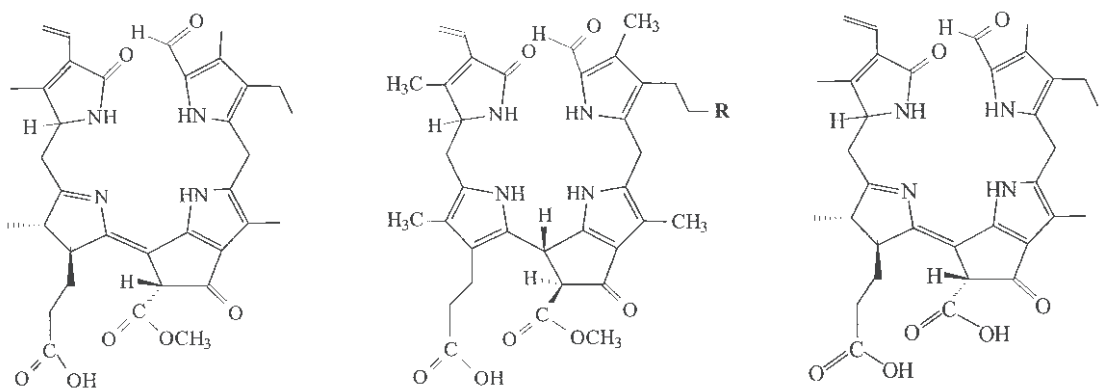

Scheme 11

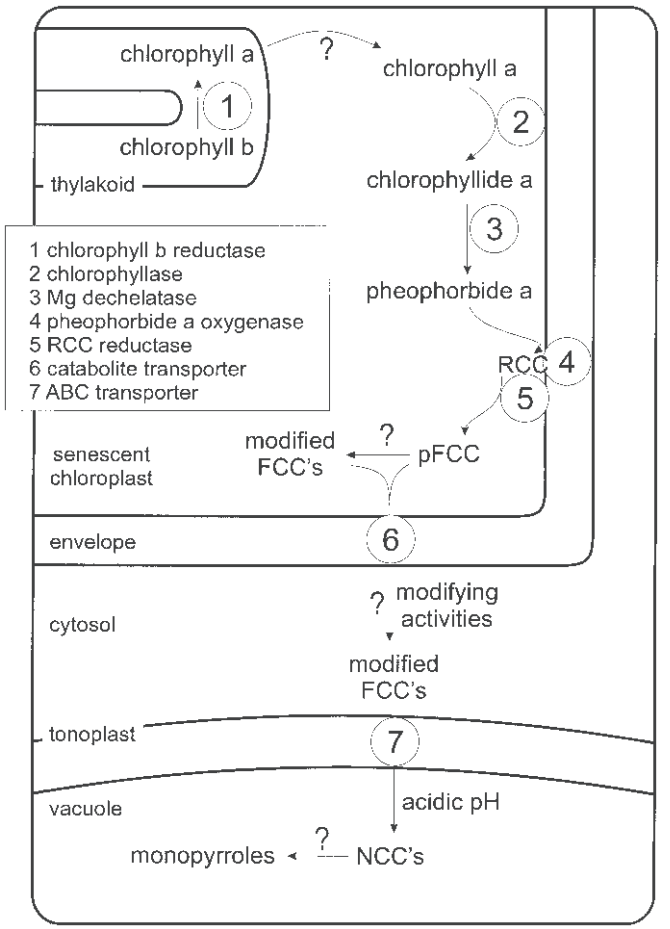

Fig. 3. Topographical overview of the biochemistry of chlorophyll catabolism in higher plants. Numbers refer to enzymes or transporters that are thought to be involved. Putative (enzymatic) steps are indicated with a question mark.

compounds displaying fluorescence properties similar to those of the pFCCs (Hörtensteiner, 1999; Hörtensteiner and Kräutler, 2000).

The discovery in naturally degreened cotyledons of the dicot, *B. napus,* of three NCCs, namely, *Bn*-NCC-1 (**23**), *Bn*-NCC-2 (**24**) and *Bn*-NCC-3 (**25**), which have the same basic structure as **1** (see Scheme 12; Mühlecker and Kräutler, 1996), strengthened the general significance of the original structure of *Hv*-NCC-1 (**1**) as a natural Chl breakdown in higher plants (Ginsburg and Matile, 1993; Mühlecker et al., 1993). Most notably, the *Bn*-NCCs proved to be linear tetrapyrroles which were again derived from Chl *a* (**2a**) by an oxygenolytic ring opening at the 'northern' C5 meso position, while differing from catabolite **1** of barley merely by some of the peripheral side chains (see Scheme 12). More recently, compounds with spectral characteristics of NCCs were also found in autumn leaves of sweet gum, *Liquidambar styraciflua* (Iturraspe et al., 1995), and of *Cercidiphyllum japonicum* (the *Cj*-NCCs, see Curty and Engel, 1996), in naturally degreened leaves of spinach (the *So*-NCCs, see Oberhuber et al., 2001; Berghold et al., 2002) and of tobacco leaves (the *Nr*-NCCs, see Berghold et al., 2004). All NCCs isolated so far from a variety of degreened plants represent linear tetrapyrroles of uniform basic structure (see Schemes 1 and 12) and relate to Chl *a* (**2a**) rather than to Chl *b* (**2b**) (Kräutler and Matile, 1999; Kräutler, 2003). It is noteworthy that *So*-NCC-2 (**26**), the most abundant of the four NCCs detected in spinach, has the same constitution as the catabolite from barley, *Hv*-NCC-1 (**1**), but differs from **1** by the configuration at C1 (**26** and **1** are epimers). With osmium tetroxide, the catabolite *Cj*-NCC-1 (**20**) from *Cercidiphyllum japonicum* (or its methyl ester **27**) could be regio-selectively dihydroxylated at its

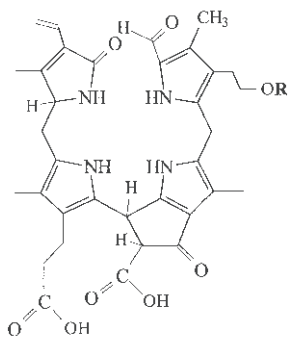

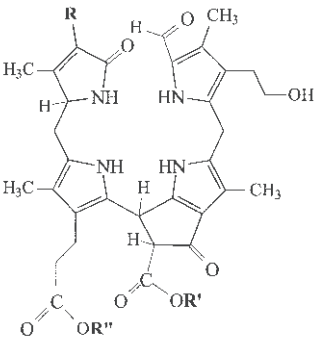

23: *Bn*-NCC-1 R = 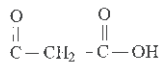

24: *Bn*-NCC-2 R = 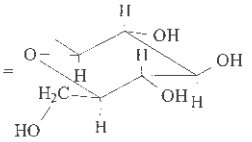

25: *Bn*-NCC-3 R = H

26: *So*-NCC-2 (R = $CH(OH)–CH_2–OH$; R' = CH_3, R" = H)

28: *So*-NCC-3 (R = $CH=CH_2$; R' = R" = H)

29: *So*-NCC-4 (R = $CH=CH_2$; R' = CH_3, R" = H)

27: *Cj*-NCC-1 methyl ester (R = $CH=CH_2$, R' = R" = CH_3)

Scheme 12

vinyl group and one of the two stereo-unselectively prepared dihydroxylation products of **20** proved to be identical with *So*-NCC-2 (**26**) (see Scheme 12; also Oberhuber et al., 2001).

The most remarkable of the peripheral side chain modifications found in the NCCs is the hydroxylation of the terminal position of the ethyl group on ring B which would be difficult to achieve in a non-enzymatic reaction (Kräutler et al., 1991; Kräutler, 2003). The primary alcohol function appears to represent an anchor point for further conjugations with hydrophilic moieties, such as the malonyl group in *Bn*-NCC-1 (**23**) and the β-glucopyranosyl group in *Bn*-NCC-2 (24) (see Scheme 12; also Mühlecker and Kräutler, 1996). Several NCCs with a free 8^2-hydroxyl function could be esterified with a malonyl moiety using a protein preparation from canola cotyledons and malonyl-CoA as co-substrate, while 1-aminocyclopropane-1-carboxylic acid (ACC), the substrate for ACC malonyltransferase, was not accepted as a substrate (Hörtensteiner, 1998). The two tobacco *Nr*-NCCs are also conjugated to glucosyl moieties (Berghold et al., 2004). Esterification and glucosylation, as in **23** and in **24**, are reminiscent of many secondary plant metabolites which are deposited in the vacuoles (Hinder et al., 1996; Matile, 1997).

While all *Bn*-NCCs possess a β-keto carboxylic acid group at $C13^2$ of the characteristic cylopentanone moiety (Hörtensteiner and Kräutler, 2000), the 13^2-methyl ester function of the Chls is retained in *Hv*-NCC-1 (**1**) and in many other NCCs (Kräutler, 2003). Interestingly, in naturally degreened leaves of spinach, *So*-NCC-2 (**26**) and *So*-NCC-3 (**28**) retain the $C13^2$ methyl ester but *So*-NCC-4 (**29**) carries a free β-keto carboxylic acid group at $C13^2$. The occurrence of both the methyl ester and of free acid groups at $C13^2$ in some So-NCCs raises the question of the possible timing of the methyl ester hydrolysis (Berghold et al., 2002).

Currently, the further endogenous breakdown of Chl in senescent plant tissue, beyond the stage of the NCCs, has not been well established and may not follow a specific pathway. Indeed, the NCCs are accumulated in the vacuoles of senescent leaves of higher plants (Hinder et al., 1996; Matile, 1997) and, in samples of degreened cotyledons from oilseed rape, the amount of *Bn*-NCCs present corresponded to the calculated amount of Chls *a* and *b* initially present in the green leaf (Mühlecker and Kräutler, 1996). Further, the total content of NCCs in degreened leaves of barley, oilseed rape and French beans did not markedly decrease over a period of several days (Bortlik et al., 1990; Matile, 1992; Ginsburg and Matile, 1993); thus, the NCCs may be the final products of controlled Chl breakdown in senescent vascular plants (Kräutler and Matile, 1999; Hörtensteiner and Kräutler, 2000).

First evidence of tetrapyrrolic products of further

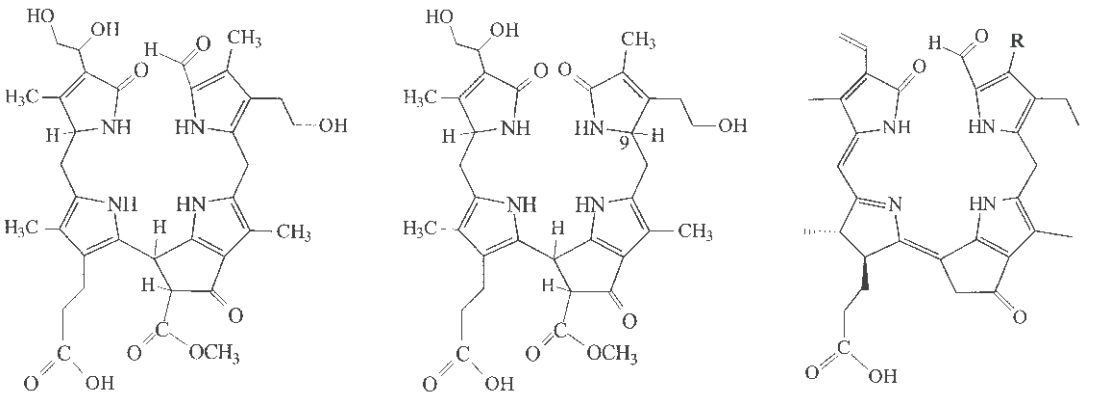

1: *Hv*-NCC-1

30
30-*epi*: C(9)-epimer of **30**

31a: R = CH_3
31b: R = CH=O

Scheme 13

degradation of NCCs was the recent identification of colorless urobilinogen-like linear tetrapyrroles in extracts of degreened primary leaves of barley, described as the two stereoisomers **30** and **30**-*epi* (see Scheme 13). Since both **30** and **30**-*epi* were associated with further degradation of *Hv*-NCC-1 (**1**) by loss of the C5-derived formyl group on ring B, it was suggested they represent a new type of Chl catabolite in barley (Losey and Engel, 2001).

Possibly **30** and **30**-*epi* arise in senescent barley leaves by non-enzymatic oxidative loss of the C5 formyl group of the NCCs as has been noted in related linear tetrapyrroles (Losey and Engel, 2001). Indeed, the original characterization of *Hv*-NCC-1 (**1**) as a 'rusty' pigment indicates the readiness of these colorless reduced linear tetrapyrroles to undergo spontaneous reactions to develop the rust color (Bortlik et al., 1990; Kräutler and Matile, 1999). Clearly, such transformations, as well as the suggested oxidative loss of the formyl group of *Hv*-NCC-1 (**1**), and any further reactions of the NCCs, may be dependent on factors modifying the environment within the senescent plant tissue; for example, further degradation of NCCs in degreened leaves or other plant tissues will depend on their eventual fate, including their further use or their consumption by heterotrophic organisms. Fungal pathogens are also known to exploit and, in some instances, to exert local control over senescence processes in the plants (Hammond-Kosack and Jones, 2001). Earlier considerations of further degradation to monopyrrolic oxygenation products (Llewellyn et al., 1990; Brown et al., 1991) received renewed support from Suzuki and Shioi (1999) who detected hematinic acid, ethyl-methyl-maleimide and a putative degradation product of the C-E-ring moiety of Pheide *a*.

D. Subcellular Organization and Regulation of Chlorophyll Breakdown in Higher Plants

The NCCs, formed during rape- and barley-leaf senescence, accumulate in the central vacuoles of mesophyll cells (Matile et al., 1988; Hinder et al., 1996), whereas Chl resides in the thylakoid membranes of the chloroplast. The different subcellular location of the enzymes of Chl catabolism and the requirement for catabolites to cross intra-cellular membranes raises interesting questions about the subcellular organization of the pathway.

The 'early' Chl breakdown reactions to FCCs occur within the plastids as demonstrated in barley and oilseed rape (Schellenberg et al., 1990; Ginsburg et al., 1994) (see Fig. 3). Chl *b* reductase, which reduces Chl *b* to Chl *a,* is located in the thylakoid membrane (Scheumann et al., 1999).

The second catabolic enzyme, chlorophyllase (see Fig. 3), is located in the plastid membrane system and, in *Citrus* and barley (Brandis et al., 1996; Matile et al., 1997), it was demonstrated on the inner envelope membrane; however, the cloning of chlorophyllases from different plants raises doubts about its plastid membrane location, since no potential trans-membrane domains are present in the amino acid sequences. Further, different subcel-

lular locations were predicted for chlorophyllase by Jacob-Wilk et al. (1999) and Tsuchiya et al. (1999). These latter findings were interpreted in terms of an alternative degradation pathway located outside the plastid (Takamiya et al., 2000). Although chlorophyllase is present during all stages of development, its activity is modulated by hormones that also affect leaf senescence and fruit ripening, such as kinetin and ethylene (Trebitsh et al., 1993; Jacob-Wilk et al., 1999).

The subcellular location of the third enzyme of Chl breakdown, Mg dechelatase (see Fig. 3), is not well established but preliminary information indicates that this constitutive enzyme is also located in the plastid envelope (Schellenberg and Matile, 1995; Vicentini et al., 1995b).

The key macrocycle cleavage enzymes, PaO, together with RCC reductase, both reside outside the thylakoid membrane. PaO has been attributed to the plastid envelope (Matile and Schellenberg, 1996), whereas RCC reductase is a soluble stroma protein (Rodoni et al., 1997a,b; Wüthrich et al., 2000). As for chlorophyllase, the expression of PaO and RCC reductase genes is not restricted to senescence (Wüthrich et al., 2000; Pružinská et al., 2003). Whereas RCC reductase is a constitutive enzyme, PaO activity is regulated in a senescence-specific way. Therefore, it has been proposed that PaO may be regulated post-transcriptionally, probably by protein modification (Pružinská et al., 2003).

In summary, most early reactions of Chl catabolism occur outside the thylakoid membrane and are, therefore, spatially separated from the primary substrate, Chl. This suggests that a carrier protein is necessary to establish contact between Chl and the early catabolic enzymes (Matile et al., 1996). While Pheide *a* (**6a**) and the Chlides (**3a** and **3b**) accumulate in the stay-green mutant Bf 993 of *F. pratensis* due to the absence of PaO, these dephytylated pigments do not occur when senescent leaves are treated with a protein biosynthesis inhibitor (Thomas et al., 1989). This suggests that a nuclear-encoded protein may be necessary for chlorophyllase to interact with Chl.

Chl catabolism includes catabolite export through the chloroplast membrane and import across the tonoplast into the vacuole (see Fig. 3). Both transport processes have been only partially characterized in isolated gerontoplasts of oilseed rape or barley leaves which not only synthesize FCCs but also excrete different FCCs, of currently unknown structures, across the plastid membrane in the presence of ATP (Matile et al., 1992). ATP is also required for import of Chl catabolites into the vacuole where the carrier on the tonoplast is a primary active ATPase (Hinder et al., 1996) of the multi-drug resistance-associated protein (MRP) type (Lu et al., 1998; Tommasini et al., 1998). These proteins , classified as ATP-binding cassette transporters, are implicated in the vacuolar import of a broad range of secondary compounds and xenobiotics (Martinoia et al., 2000). Thus, for example, AtMRP2 and AtMRP3 of *A. thaliana* can transport not only *Bn*-NCC-1 (**23**) but also glutathione S-conjugates into the vacuole (Lu et al., 1998; Tommasini et al., 1998). Unfortunately, the nature of the genuine tetrapyrrole substrate for vacuolar uptake has not been firmly established. Due to the low substrate specificity of such transport proteins (see above), both NCCs and FCCs might serve as substrates. It is noteworthy, however, that the catabolite carrier(s) of barley vacuoles had a particularly high affinity for a structurally unidentified FCC (Hinder et al., 1996) and contained small amounts of FCCs when isolated from senescent primary leaves (Matile et al., 1988). Consideration of the above-mentioned acid-catalyzed, non-enzymatic tautomerization of the pFCC (**11**-*epi*) to the corresponding NCC (**21**) (Oberhuber et al., 2003), suggests that transport of Chl catabolites across the tonoplast in vivo occurs at the level of FCCs which are then converted non-enzymatically to NCCs in the acidic milieu of the vacuole (see Fig. 3).

E. Chlorophyll Breakdown and the Nutrient Economy of Plants

Breakdown of Chl during plant senescence occurs within a major developmental program ultimately leading to the death of the respective tissues, such as leaves or fruits. Chl, together with lipids, proteins and nucleic acids, is degraded in large quantities during this process (Matile, 1992). Leaf senescence can be regarded as programmed cell death, but also serves in plants to re-mobilize nutrients to surviving organs (Smart, 1994). Major structural changes first occur within the chloroplasts: the contact between the grana stacks of the thylakoid membranes is loosened and, finally, the membranes disappear with concomitant loss of Chl and of soluble and membrane-bound proteins. Later in senescence, mitochondria and the nucleus are also affected before the cells finally die through the rupture of the tonoplast by autolysis (Thomas and Hilditch, 1987; Matile, 1992; Hörtensteiner and Feller, 2002).

The chloroplasts during senescence contribute substantially to nitrogen re-mobilization: about 75% of total cellular nitrogen is located within the chloroplasts (Makino and Osmond, 1991). The most abundant soluble chloroplast protein, Rubisco, and the Chl-binding apo-proteins of the thylakoid membranes are the main proteins lost during senescence (Matile, 1992). In contrast, the Chl molecule accounts for only about 2% of total cellular nitrogen (Peoples and Dalling, 1988). Polypeptide degradation of the light harvesting complex (LHC) II requires the simultaneous degradation of Chl: stay-green mutants of *F. pratensis* and *Phaseolus vulgaris,* which retain most of their Chl during senescence, cannot degrade LHCP II, whereas Rubisco is degraded as rapidly as in their respective wild types (Thomas and Hilditch, 1987); thus, Chl-binding in such pigment-proteins as LHCP II confers stability against proteolysis (White and Green, 1987).

While Chl catabolism is a prerequisite for the re-mobilization of the apo-proteins during plant senescence, the fact that Chl nitrogen is not released at the same time, but deposited as NCCs in the vacuole, raises the question: why do plants degrade Chl at all? There is striking evidence suggesting that Chl is transformed into colorless pigments to abolish its lethal photodynamic properties when it is released from the pigment-protein complexes (Kräutler et al., 1991; Hörtensteiner, 1999; Pružinská et al., 2003). Indeed, Chl catabolism in higher plants resembles, in many aspects, the stepwise detoxification of xenobiotics and herbicides (Kreuz et al., 1996).

III. Chlorophyll Breakdown and Chlorophyll Catabolites in Green Algae

It has been known since the 1960s that the green alga, *C. protothecoides,* when grown in nitrogen-deficient and glucose-rich medium, excretes red pigments (Oshio and Hase, 1969) which were structurally examined in the laboratory of Gossauer (Engel et al., 1991, 1996; Iturraspe et al., 1994; Curty et al., 1995; Gossauer and Engel, 1996; Curty and Engel, 1997). These red pigments were linear tetrapyrroles, similar to the colorless Chl catabolite, *Hv*-NCC-1 (**1**), resulting from oxygenolytic cleavage of the macrocycle at the 'northern' C5 bridge carbon. In contrast to the plant systems, the red catabolites were found to be derived from both Chls *a* (**2a**) and *b* (**2b**) (see Scheme 5; Iturraspe et al., 1994). Subsequent results indicated that the diacid **10** was the authentic product of enzymatic catabolism in *C. protothecoides* (Engel et al., 1996; Gossauer and Engel, 1996) rather than the monoacids, **31a** and **31b**, which were originally isolated and identified by Engel et al. (1991) as their respective monomethyl esters, **9a** and **9b** (see Schemes 5 and 13).

Labeling studies with $^{18}O_2$ followed by MS analysis of the excreted pigment as its ^{18}O-labeled methyl ester **9a**, clearly indicated incorporation of only one ^{18}O-atom into **9** (Curty et al., 1995). Analysis of a fragment confirmed that the ^{18}O-label was in the formyl group at the C5 carbon of Chl indicating that a monooxygenase cleaved the macrocycle in green alga (Curty et al., 1995): the direct substrate(s) and product(s) are not yet known. Deuterium labeling during degradation of the Chls in this green alga, showed highly stereo-selective attachment of one hydrogen atom (from water) at the 'eastern' C10 bridge carbon of the red isolate **9a**, indicating that this was an enzymatic step in the formation of the red catabolites (Curty and Engel, 1997). Based on the available chemical evidence, it was suggested that the formation of the RCCs in *C. protothecoides* arose from hydration of an epoxide intermediate and subsequent rearrangement (Engel et al., 1991, 1996; Curty and Engel, 1997). These, and related mechanistic considerations concerning Chl degradation in algae and higher plants, require further critical experiments. However, the structural resemblance of the algal catabolites and the plant RCC (**12**) and the similar oxygenolytic macrocycle cleavage mechanisms in higher plants (Hörtensteiner et al. 1998) and in *C. protothecoides* (Curty et al., 1995) indicate a clear biochemical relationship. Hence, the respective oxygenase of *C. protothecoides* and PaO of higher plants may display comparable catalytic properties. Notable differences concern the restriction of substrate specificity of the higher-plant enzyme to Chl *a* and its absolute requirement for a second enzyme, namely, RCC reductase (Hörtensteiner, 1999; Kräutler and Matile, 1999; Hörtensteiner and Kräutler, 2000): for this latter reason, the simple excretion of RCCs by the green alga is clearly not possible in vascular plants.

The excretion of another group of red bile pigments from senescent forms of a Chl *b*-less mutant of the green alga, *Chlamydomonas. reinhardtii,* has been reported (Doi et al., 1997). The UV/Vis-spectrum of the major pigment, tentatively named P535, displays absorbance maxima near 535, 385 and 275 nm, but these newly-found pigments have not yet

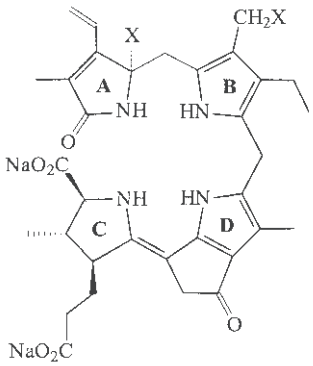

32: X = H
36: X = OH

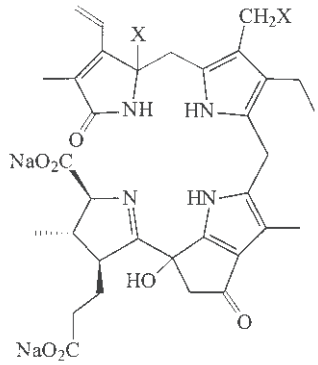

33: X = H
37: X = OH

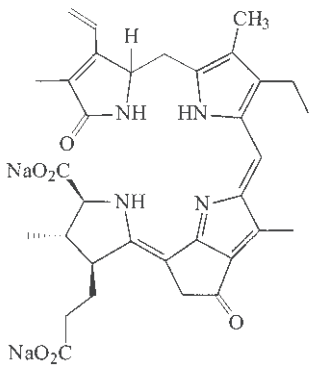

34

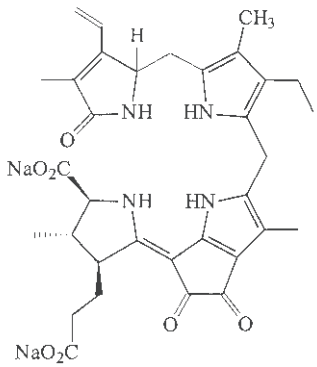

35

Scheme 14

been structurally identified. Accumulation of P535 required aerobic growth conditions and was prevented by inhibitors of cytoplasmic protein biosynthesis (Doi et al., 2001).

IV. Chlorophyll Catabolites from Marine Organisms

Photosynthetic organisms are widely distributed in the oceans. Relative to the information available on Chl catabolism in two green algae and in several higher plants, little is known about the fate of the Chls or bacteriochlorophylls from marine environments. One exception concerns a luciferin, isolated from the dinoflagellate, *Pyrocystis lunula,* which appeared structurally related to Chl (Dunlap et al., 1981). This colorless, luminescent compound, **32**, and two air oxidation products, **33** and **34**, were identified by spectroscopic and chemical degradation methods in the laboratory of Y. Kishi (see Scheme 14; Nakamura et al., 1989). Similar methods showed that the bioluminescent transformation of luciferin, **32**, by the dinoflagellate luciferase produced the oxidation product **35**. A related study of the light emitter from krill (*Euphasia pacifica*), assigned the structure of the related linear tetrapyrrole **36** which is also readily air oxidized to **37** (Nakamura et al., 1988). Both luminescent compounds (**32**, **36**) were identified as Chl derivatives, namely, 1,20-dioxo-1,20-seco-pyropheophorbides arising by an oxygenolytic cleavage at the 'western' C20 bridge carbons of their Chl precursor(s).

Further studies by Kishi and coworkers on the photooxygenolysis of the 20-methoxy-pyropheophorbide 38 have confirmed the tendency of some similarly

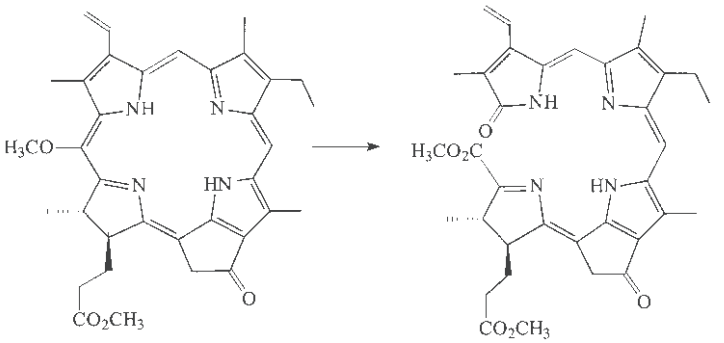

38 39

Scheme 15

substituted Pheides to undergo oxygenolytic cleavage of the chlorin macrocycle at the 'western' meso-position, between C20 and C1. This provides synthetic access to the 1,20-seco-pyropheophorbidate **39** (see Scheme 15; Topalov and Kishi, 2001).

Considering the absence of O_2 in deep sea water, an oxygenolytic mechanism may not be the dominant form of degradation of Chls from marine photosynthetic organisms.

V. Conclusions and Outlook

In the last fifteen years, the structures of many relevant Chl catabolites in higher plants were established thus gradually revealing the nature of plant Chl catabolism. The key step in the known degradation paths in green algae and in plants is an oxygenolytic cleavage of the porphinoid macrocycle. In higher plants this primary ring cleavage reaction specifically involves only Pheide *a*. In a series of (coupled) step(s) Chl breakdown rapidly reduces the chromophore of a photoactive and intensely colored chlorin to that of a colorless tetrapyrrole with de-conjugated hetero-cyclic rings. Nonfluorescent tetrapyrrolic Chl catabolites are considered to constitute the 'final' products of controlled Chl breakdown in senescent higher plants while in green algae the red pigments, which are excreted, are the final products of Chl catabolism. The degradation of the Chls in senescent leaves is reminiscent of the operation of detoxification processes.

The knowledge of the structure of key Chl catabolites and of some of the relevant higher plant enzymes involved in their formation now sets the stage for a series of further investigations in areas such as: (i) molecular regulation and cellular control of Chl breakdown, (ii) modes of action (and interaction) of the catabolic enzymes, (iii) possible physiological roles of tetrapyrrolic Chl breakdown products in senescent leaves, and (iv) the further general fate of the tetrapyrrolic remnants of the Chls in the senescent plant.

Note Added in Proof

Since preparation of this chapter, major progress has been achieved by the detailed analysis of Chl breakdown in the model plant *A. thaliana* (Pružinskà et al., 2005). It was shown that in contrast to the previous assumption of a posttranslational regulation of PAO, regulation mainly occurs at the level of *Pao* gene expression. Analysis of a *pao1* knockout mutant corroborates earlier work on maize (Pružinskà et al., 2003) and substantiates a key role for PAO in Chl breakdown.

Furthermore, this work includes the isolation and structural identification of colorless Chl catabolites. Thus, five different NCCs (*At*-NCC-1 to *At*-NCC-5) and three FCCs (*At*-FCC-1 to *At*-FCC-3) were identified during leaf senescence in *A. thaliana*; thereby *At*-NCC-1 and *At*-NCC-2, respectively, were identical to *Bn*-NCC-2 (**24**) and *Bn*-NCC-3 (**25**) of canola, and *At*-FCC-3 was identified with pFCC-1 (**11**). An NCC of intermediate polarity, named *At*-NCC-3, was discovered to be a constitutional isomer of *At*-NCC-2. In *At*-NCC-3, the substituents at C-8 and at C-7 were an ethyl group and a (functionalized) hydroxyl-methyl group, respectively. So far, the substituent at C-7 has always

been found to be a methyl group in all other NCCs, including *At*-NCC-2. The structure of *At*-NCC-3 thus indicated a deviation from the known path of Chl breakdown in *A. thaliana* (Müller, 2005). Rather large quantities of FCCs accumulated in *A. thaliana* during leaf senescence as compared to other systems analyzed so far. The identification of modified FCCs and structure elucidation of one of these corroborated an earlier suggestion that modifications as seen in the structures of NCCs occur at the FCC level.

Acknowledgments

We are indebted to Philippe Matile and his earlier coworkers, for their experimentally and intellectually fruitful collaboration, to Howard Thomas and his group for their important contributions to the problem of Chl breakdown. We thank specifically the members of the Chl group in Innsbruck: Michael Oberhuber, Joachim Berghold, Walter Mühlecker, Thomas Müller, Kathrin Breuker and Benjamin Gerlach, and in Bern: Adiana Pružinská and Iwona Anders for their enthusiastic work. We gratefully acknowledge financial support for this work from the Austrian National Science Foundation (FWF, projects No. P13503 and P16097) and from the Swiss National Science Foundation (project No. 31.63628).

References

Arabidopsis Genome Initiative (2000) Analysis of the genome sequence of the flowering plant *Arabidopsis thaliana*. Nature 408: 796–813

Bachmann A, Fernández-López J, Ginsburg S, Thomas H, Bouwcamp JC, Solomos T and Matile P (1994) *Stay-green* genotypes of *Phaseolus vulgaris* L.: Chloroplast proteins and chlorophyll catabolites during foliar senescence. New Phytol 126: 593–600

Beale SI and Cornejo J (1991) Biosynthesis of phycobilins. 15,16-Dihydrobiliverdin IXα is a partially reduced intermediate in the formation of phycobilins from biliverdin IXα. J Biol Chem 266: 22341–22345

Beale SI and Weinstein JD (1991) Biochemistry and regulation of photosynthetic pigment formation in plants and algae. In: Jordan, P M (ed) Biosynthesis of Tetrapyrroles, pp 155–235. Elsevier, Amsterdam

Berghold J, Breuker K, Oberhuber M, Hörtensteiner S and Kräutler B (2002) Chlorophyll breakdown in spinach: On the structure of five nonfluorescent chlorophyll catabolites. Photosynth Research 74: 109–119

Berghold J, Eichmüller C, Hörtensteiner S, Kräutler B (2004) Chlorophyll breadkown in tobacco: On the structure of two non-fluorescent chlorophyll catabolites. Chem Biodiv 1: 657–668

Bortlik K-H, Peisker C and Matile P (1990) A novel type of chlorophyll catabolite in senescent barley leaves. J Plant Physiol 136: 161–165

Brandis A, Vainstein A and Goldschmidt EE (1996) Distribution of chlorophyllase among components of chloroplast membranes in *Citrus sinensis* organs. Plant Physiol Biochem 34: 49–54

Brown SB, Houghton JD and Hendry GAF (1991) Chlorophyll breakdown. In: Scheer H (ed) Chlorophylls, pp 465–489. CRC Press, Boca Raton

Curty C and Engel N (1996) Detection, isolation and structure elucidation of a chlorophyll *a* catabolite from autumnal senescent leaves of *Cercidiphyllum japonicum*. Phytochemistry 42: 1531–1536

Curty C and Engel N (1997) Chlorophyll catabolism: High stereoselectivity in the last step of the primary ring cleaving process. Plant Physiol Biochem 35: 707–711

Curty C, Engel N and Gossauer A (1995) Evidence for a monooxygenase-catalyzed primary process in the catabolism of chlorophyll. FEBS Lett 364: 41–44

Doi M, Shima S, Egashira T, Nakamura K and Okayama S (1997) New bile pigment excreted by a *Chlamydomonas reinhardtii* mutant: A possible breakdown catabolite of chlorophyll *a*. J Plant Physiol 150: 504–508

Doi M, Inage T and Shioi Y (2001) Chlorophyll degradation in a *Chlamydomonas reinhardtii* mutant: An accumulation of pyropheophorbide *a* by anaerobiosis. Plant Cell Physiol 42: 469–474

Dunlap JC, Hastings JW and Shimomura O (1981) Dinoflagellate luciferin is structurally related to chlorophyll. FEBS Letters 135: 273–276

Engel N, Jenny TA, Mooser V and Gossauer A (1991) Chlorophyll catabolism in *Chlorella protothecoides.* Isolation and structure elucidation of a red bilin derivative. FEBS Lett 293: 131–133

Engel N, Curty C and Gossauer A (1996) Chlorophyll catabolism in *Chlorella protothecoides*. 8. Facts and artifacts. Plant Physiol Biochem 34: 77–83

Eschenmoser A (1988) Vitamin B_{12}: Experiments concerning the origin of its molecular structure. Angew Chem 100: 5–40; Angew Chem Int Ed Engl 27: 5–40

Falk H (1989) The Chemistry of Linear Oligopyrroles and Bile Pigments. Springer Verlag, Wien

Folley P and Engel N (1999) Chlorophyll *b* to chlorophyll *a* conversion precedes chlorophyll degradation in *Hordeum vulgare* L. J Biol Chem 274: 21811–21816

Frankenberg N, Mukougawa K, Kohchi T and Lagarias JC (2001) Functional genomic analysis of the HY2 family of ferredoxin-dependent bilin reductases from oxygenic photosynthetic organisms. Plant Cell 13: 965–978

Ginsburg S and Matile P (1993) Identification of catabolites of chlorophyll porphyrin in senescent rape cotyledons. Plant Physiol 102: 521–527

Ginsburg S, Schellenberg M and Matile P (1994) Cleavage of chlorophyll-porphyrin. Requirement for reduced ferredoxin and oxygen. Plant Physiol 105: 545–554

Gossauer A and Engel N (1996) Chlorophyll catabolism. Structures, mechanisms, conversions. J Photochem Photobiol B: Biol 32: 141–151

Gray J, Janick-Bruckner D, Bruckner B, Close PS and Johal GS (2002) Light-dependent death of maize *lls1* cells is mediated

by mature chloroplasts. Plant Physiol 130: 1894-1907
Greenberg JT, Guo A, Klessig DF and Ausubel FM (1994) Programmed cell death in plants: A pathogen-triggered response activated coordinately with multiple defense functions. Cell 77: 551–563
Hammond-Kosack K and Jones JDG (2001) Responses to plant pathogens. In: Buchanan BB, Gruissem W and Jones RL (eds) Biochemistry and Molecular Biology of Plants, pp 1102–1156. American Society of Plant Physiologists, Rockville
Hendry GAF, Houghton JD and Brown SB (1987) Chlorophyll degradation. A biological enigma. New Phytol 107: 255–302
Hinder B, Schellenberg M, Rodoni S, Ginsburg S, Vogt E, Martinoia E, Matile P and Hörtensteiner S (1996) How plants dispose of chlorophyll catabolites. Directly energized uptake of tetrapyrrolic breakdown products into isolated vacuoles. J Biol Chem 271: 27233–27236
Hörtensteiner S (1998) NCC malonyltransferase catalyses the final step of chlorophyll breakdown in rape (*Brassica napus*). Phytochemistry 49: 953–956
Hörtensteiner S (1999) Chlorophyll breakdown in higher plants and algae. Cell Mol Life Sci 56: 330–347
Hörtensteiner S and Feller U (2002) Nitrogen metabolism and remobilization during senescence. J Exp Bot 53: 927–937
Hörtensteiner S and Kräutler B (2000) Chlorophyll breakdown in oilseed rape. Photosynth Res 64: 137–146
Hörtensteiner S, Vicentini F and Matile P (1995) Chlorophyll breakdown in senescent cotyledons of rape, *Brassica napus L.*: Enzymatic cleavage of pheophorbide *a* in vitro. New Phytol 129: 237–246
Hörtensteiner S, Wüthrich KL, Matile P, Ongania K-H and Kräutler B (1998) The key step in chlorophyll breakdown in higher plants. Cleavage of pheophorbide *a* macrocycle by a monooxygenase. J Biol Chem 273: 15335–15339
Hörtensteiner S, Rodoni S, Schellenberg M, Vicentini F, Nandi OI, Qiu Y-L and Matile P (2000) Evolution of chlorophyll degradation: The significance of RCC reductase. Plant Biol 2: 63–67
Hynninen PH (1991) Chemistry of chlorophylls: Modifications. In: Scheer H (ed) Chlorophylls, pp 145–209. CRC Press, Boca Raton
Ito H and Tanaka A (1996) Determination of the activity of chlorophyll *b* to chlorophyll *a* conversion during greening of etiolated cucumber cotyledons by using pyrochlorophyllide *b*. Plant Physiol Biochem 34: 35–40
Ito H, Tanaka Y, Tsuji H and Tanaka A (1993) Conversion of chlorophyll *b* to chlorophyll *a* by isolated cucumber etioplasts. Arch Biochem Biophys 306: 148–151
Iturraspe J and Gossauer A (1992) A biomimetic partial synthesis of the red chlorophyll-*a* catabolite from *Chlorella protothecoides*. Tetrahedron 48: 6807–6812
Iturraspe J, Engel N and Gossauer A (1994) Chlorophyll catabolism. Isolation and structure elucidation of chlorophyll *b* catabolites in *Chlorella protothecoides*. Phytochemistry 35: 1387–1390
Iturraspe J, Moyano N and Frydman B (1995) A new 5-formylbilinone as the major chlorophyll *a* catabolite in tree senescent leaves. J Org Chem 60: 6664–6665
Jakob-Wilk D, Holland D, Goldschmidt EE, Riov J and Eyal Y (1999) Chlorophyll breakdown by chlorophyllase: Isolation and functional expression of the *Chlase1* gene from ethylene-treated *Citrus* fruit and its regulation during development. Plant J 20: 653–661
Kräutler B (2002) Unravelling chlorophyll catabolism in higher plants. Biochem Soc Trans 30: 625–630
Kräutler B (2003) Chlorophyll breakdown and chlorophyll catabolites. In: Kadish K M, Smith K M and Guilard R (eds) The Porphyrin Handbook, Vol. 11, pp. 183–209. Elsevier Science
Kräutler B and Matile P (1999) Solving the riddle of chlorophyll breakdown. Acc Chem Res 32: 35–43
Kräutler B, Jaun B, Bortlik K-H, Schellenberg M and Matile P (1991) On the enigma of chlorophyll degradation: The constitution of a secoporphinoid catabolite. Angew Chem Int Ed Engl 30: 1315–1318
Kräutler B, Jaun B, Amrein W, Bortlik K-H, Schellenberg M and Matile P (1992) Breakdown of chlorophyll: Constitution of a secoporphinoid chlorophyll catabolite isolated from senescent barley leaves. Plant Physiol Biochem 30: 333–346
Kräutler B, Mühlecker W, Anderl M and Gerlach B (1997) Breakdown of chlorophyll: Partial synthesis of a putative intermediary catabolite. Helv Chim Acta 80: 1355–1362
Kreuz K, Tommasini R and Martinoia E (1996) Old enzymes for a new job. Herbicide detoxification in plants. Plant Physiol 111: 349–353
Langmeier M, Ginsburg S and Matile P (1993) Chlorophyll breakdown in senescent leaves: Demonstration of Mg-dechelatase activity. Physiol Plant 89: 347–353
Lippard SJ and Berg JM (1994) Oxygen-atom transfer reactions: Fe. In: Lippard SJ and Berg JM, Principles of Bioinorganic Chemistry, pp 302–318. University Science Books, Mill Valley
Llewellyn CA, Mantoura RFC and Brereton G (1990) Products of chlorophyll photodegradation. 2. Structural identification. Photochem Photobiol 52: 1043–1047
Losey FG and Engel N (2001) Isolation and characterization of a urobilinogenoidic chlorophyll catabolite from *Hordeum vulgare* L. J Biol Chem 276: 27233–27236
Lu Y-P, Li Z-S, Drozdowicz Y-M, Hörtensteiner S, Martinoia E and Rea PA (1998) AtMRP2, an *Arabidopsis* ATP binding cassette transporter able to transport glutathione *S*-conjugates and chlorophyll catabolites: Functional comparisons with AtMRP1. Plant Cell 10: 267–282
Mach JM, Castillo AR, Hoogstraten R and Greenberg JT (2001) The *Arabidopsis*-accelerated cell death gene ACD2 encodes red chlorophyll catabolite reductase and suppresses the spread of disease symptoms. Proc Natl Acad Sci USA 98: 771–776
Makino A and Osmond B (1991) Effect of nitrogen nutrition on nitrogen partitioning between chloroplasts and mitochondria in pea and wheat. Plant Physiol 96: 355–362
Martinoia E, Klein M, Geisler M, Sánchez-Fernández R and Rea PA (2000) Vacuolar transport of secondary metabolites and xenobiotics. In: Robinson DG and Rogers JC (eds) Vacuolar Compartments. Annual Plant Reviews, Vol 5, pp 221–253. Sheffield Academic Press, Sheffield
Matile P (1987) Seneszenz bei Pflanzen und ihre Bedeutung für den Stickstoffhaushalt. Chimia 41: 376–381
Matile P (1992) Chloroplast senescence. In: Baker NR and Thomas H (eds) Crop Photosynthesis: Spatial and Temporal Determinants, pp 413–440. Elsevier Science Publishers, Amsterdam
Matile P (1997) The vacuole and cell senescence. In: Callow JA (ed) Advances in Botanical Research, Vol 25, pp 87–112. Academic Press, New York

Matile P and Schellenberg M (1996) The cleavage of pheophorbide *a* is located in the envelope of barley gerontoplasts. Plant Physiol Biochem 34: 55–59

Matile P, Ginsburg S, Schellenberg M and Thomas H (1987) Catabolites of chlorophyll in senescent leaves. J Plant Physiol 129: 219–228

Matile P, Ginsburg S, Schellenberg M and Thomas H (1988) Catabolites of chlorophyll in senescing barley leaves are localized in the vacuoles of mesophyll cells. Proc Natl Acad Sci USA 85: 9529–9532

Matile P, Schellenberg M and Peisker C (1992) Production and release of a chlorophyll catabolite in isolated senescent chloroplasts. Planta 187: 230–235

Matile P, Hörtensteiner S, Thomas H and Kräutler B (1996) Chlorophyll breakdown in senescent leaves. Plant Physiol 112: 1403–1409

Matile P, Schellenberg M and Vicentini F (1997) Localization of chlorophyllase in the chloroplast envelope. Planta 201: 96–99

Matile P, Hörtensteiner S, Thomas H (1999) Chlorophyll degradation. Annu Rev Plant Physiol Plant Mol Biol 50: 67–95

McFeeters RF (1975) Substrate specificity of chlorophyllase. Plant Physiol 55: 377–381

Mendel G (1865) Versuche über Pflanzenhybriden. Verh Naturf Ver 4: 3–47

Moss GP (1987) Nomenclature of Tetrapyrroles. Pure Appl Chem 59: 779–832

Mühlecker W and Kräutler B (1996) Breakdown of chlorophyll: Constitution of nonfluorescing chlorophyll-catabolites from senescent cotyledons of the dicot rape. Plant Physiol Biochem 34: 61–75

Mühlecker W, Kräutler B, Ginsburg S and Matile P (1993) Breakdown of chlorophyll: The constitution of a secoporphinoid chlorophyll catabolite from senescent rape leaves. Helv Chim Acta 76: 2976–2980

Mühlecker W, Ongania K-H, Kräutler B, Matile P and Hörtensteiner S (1997) Tracking down chlorophyll breakdown in plants: Elucidation of the constitution of a 'fluorescent' chlorophyll catabolite. Angew Chem Int Ed Engl 36: 401–404

Mühlecker W, Kräutler B, Moser D, Matile P and Hörtensteiner S (2000) Breakdown of chlorophyll: A fluorescent chlorophyll catabolite from sweet pepper (*Capsicum annuum*). Helv Chim Acta 83: 278–286

Müller T, Moser S, Ongania K-H, Hörtensteiner S and Kräutler B (2005) A divergent path of chlorophyll breakdown in the model plant *Arabidopsis thaliana*. ChemBioChem 7: 40–42

Nakamura H, Musicki B, Kishi Y and Shimomura O (1988) Structure of the light emitter in krill (*Euphausia pacifica*) bioluminescence. J Am Chem Soc 110: 2683–2685

Nakamura H, Kishi Y, Shimomura O, Morse D and Hastings JW (1989) Structure of dinoflagellate luciferin and its enzymatic and nonenzymatic air-oxidation products. J Am Chem Soc 111: 7607–7611

Oberhuber M and Kräutler B (2002) Breakdown of chlorophyll: Electrochemical bilin reduction provides synthetic access to fluorescent chlorophyll catabolites. Chem Bio Chem 3: 104–107

Oberhuber M, Berghold J, Mühlecker W, Hörtensteiner S and Kräutler B (2001) Chlorophyll breakdown — on a nonfluorescent chlorophyll catabolite from spinach. Helv Chim Acta 84: 2615–2627

Oberhuber M, Berghold J, Breuker K, Hörtensteiner S and Kräutler B (2003) Breakdown of chlorophyll: A nonenzymatic reaction accounts for the formation of the colorless 'nonfluorescent' chlorophyll catabolites. Proc. Natl Acad Sci USA 74: 6910–6915

Ohtsuka T, Ito H and Tanaka A (1997) Conversion of chlorophyll *b* to chlorophyll *a* and the assembly of chlorophyll with apoproteins by isolated chloroplasts. Plant Physiol 113: 137–147

Oshio Y and Hase E (1969) Studies on red pigments excreted by cells of *Chlorella protothecoides* during the process of bleaching induced by glucose or acetate. I. Chemical properties of the red pigments. Plant Cell Physiol 10: 41–49

Paulsen H, Finkenzeller B and Kühnlein N (1993) Pigments induce folding of light-harvesting chlorophyll *a*/*b*-binding protein. Eur J Biochem 215: 809–816

Peisker C, Thomas H, Keller F and Matile P (1990) Radiolabelling of chlorophyll for studies on catabolism. J Plant Physiol 136: 544–549

Peoples MB and Dalling MJ (1988) The interplay between proteolysis and amino acid metabolism during senescence and nitrogen allocation. In: Noodén LD and Leopold AC (eds) Senescence and Aging in Plants, pp 181–217. Academic Press, San Diego

Porra RJ, Schäfer W, Cmiel E, Katheder I and Scheer H (1994) The derivation of the formyl-group oxygen of chlorophyll *b* in higher plants from molecular oxygen. Achievement of high enrichment of the 7-formyl-group oxygen from $^{18}O_2$ in greening maize leaves. Eur J Biochem 219: 671–679

Pružinská A, Tanner G, Anders I, Roca M and Hörtensteiner S (2003) Chlorophyll breakdown: Pheophorbide *a* oxygenase is a Rieske-type iron-sulfur protein, encoded by the *accelerated cell death 1* gene. Proc Natl Acad Sci USA 100: 15259–15264

Pružinskà A, Tanner G, Aubry S, Anders I, Moser S, Müller T, Ongania K-H, Kräutler B, Youn J-Y, Liljegren SJ and Hörtensteiner S (2005) Chlorophyll breakdown in senescent *Arabidopsis* leaves. Characterization of chlorophyll catabolites and of chlorophyll catabolic enzymes involved in the degreening reaction. Plant Physiol 139: 52–63

Rodoni S, Mühlecker W, Anderl M, Kräutler B, Moser D, Thomas H, Matile P and Hörtensteiner S (1997a) Chlorophyll breakdown in senescent chloroplasts. Cleavage of pheophorbide *a* in two enzymic steps. Plant Physiol 115: 669–676

Rodoni S, Vicentini F, Schellenberg M, Matile P and Hörtensteiner S (1997b) Partial purification and characterization of red chlorophyll catabolite reductase, a stroma protein involved in chlorophyll breakdown. Plant Physiol 115: 677–682

Rüdiger W (1997) Chlorophyll metabolism: From outer space down to the molecular level. Phytochemistry 46: 1151–1167

Schellenberg M and Matile P (1995) Association of components of the chlorophyll catabolic system with pigment-protein complexes from solubilized chloroplast membranes. J Plant Physiol 146: 604–608

Schellenberg M, Matile P and Thomas H (1990) Breakdown of chlorophyll in chloroplasts of senescent barley leaves depends on ATP. J Plant Physiol 136: 564–568

Schellenberg M, Matile P and Thomas H (1993) Production of a presumptive chlorophyll catabolite in vitro: Requirement for reduced ferredoxin. Planta 191: 417–420

Scheumann V, Ito H, Tanaka A, Schoch S and Rüdiger W (1996) Substrate specificity of chlorophyll(ide) *b* reductase in etioplasts of barley (*Hordeum vulgare*). Eur J Biochem 242: 163–170

Scheumann V, Schoch S and Rüdiger W (1999) Chlorophyll *b* reduction during senescence of barley seedlings. Planta 209: 364–370

Schoch S, Scheer H, Schiff JA, Rüdiger W and Siegelman HW (1981) Pyropheophytin *a* accompanies pheophytin *a* in darkened light grown cells of *Euglena*. Z Naturforsch 36c: 827–833

Shioi Y, Tatsumi Y and Shimokawa K (1991) Enzymatic degradation of chlorophyll in *Chenopodium album*. Plant Cell Physiol 32: 87–93

Shioi Y, Tomita N, Tsuchiya T and Takamiya K (1996a) Conversion of chlorophyllide to pheophorbide by Mg-dechelating substance in extracts of *Chenopodium album*. Plant Physiol Biochem 34: 41–47

Shioi Y, Watanabe K and Takamiya K (1996b) Enzymatic conversion of pheophorbide *a* to a precursor of pyropheophorbide *a* in leaves of *Chenopodium album*. Plant Cell Physiol 37: 1143–1149

Smart CM (1994) Gene expression during leaf senescence. New Phytol 126: 419–448

Stoll A (1912) Über Chlorophyllase und die Chlorophyllide. Thesis, ETH Zürich

Suzuki Y and Shioi Y (1999) Detection of chlorophyll breakdown products in the senescent leaves of higher plants. Plant Cell Physiol 40: 909–915

Takamiya K, Tsuchiya T and Ohta H (2000) Degradation pathway of chlorophyll in higher plants. What gene cloning has brought about. Trends Plant Sci 5: 426–431

Tanaka A, Ito H, Tanaka R, Tanaka NK, Yoshida K and Okada K (1998) Chlorophyll *a* oxygenase (*CAO*) is involved in chlorophyll *b* formation from chlorophyll *a*. Proc Natl Acad Sci USA 95: 12719–12723

Thomas H (1987) Foliar senescence mutants and other genetic variants. In: Thomas H and Grierson D (eds) Developmental Mutants in Higher Plants, pp 245–265. Cambridge University Press, Cambridge

Thomas H and Hilditch P (1987) Metabolism of thylakoid membrane proteins during foliar senescence. In: Thomson WW, Nothnagel EA and Huffaker RC (eds) Plant Senescence: Its Biochemistry and Physiology, pp 114–122. The American Society of Plant Physiologists, Rockville

Thomas H, Bortlik K-H, Rentsch D, Schellenberg M and Matile P (1989) Catabolism of chlorophyll in vivo: Significance of polar chlorophyll catabolites in a non-yellowing senescence mutant of *Festuca pratensis* Huds. New Phytol 111: 3–8

Thomas H, Schellenberg M, Vicentini F and Matile P (1996) Gregor Mendel's green and yellow pea seeds. Bot Acta 109: 3–4

Tommasini R, Vogt E, Fromenteau M, Hörtensteiner S, Matile P, Amrhein N and Martinoia E (1998) An ABC transporter of *Arabidopsis thaliana* has both glutathione-conjugate and chlorophyll catabolite transport activity. Plant J 13: 773–780

Topalov G and Kishi Y (2001) Chlorophyll catabolism leading to the skeleton of dinoflagellate and krill luciferins: Hypothesis and model studies. Angew Chem Int Ed Engl 40: 3892–3894

Trebitsh T, Goldschmidt EE and Riov J (1993) Ethylene induces *de novo* synthesis of chlorophyllase, a chlorophyll degrading enzyme, in *Citrus* fruit peel. Proc Natl Acad Sci USA 90: 9441–9445

Tsuchiya T, Ohta H, Masuda T, Mikami B, Kita N, Shioi Y and Takamiya K (1997) Purification and characterization of two isozymes of chlorophyllase from mature leaves of *Chenopodium album*. Plant Cell Physiol 38: 1026–1031

Tsuchiya T, Ohta H, Okawa K, Iwamatsu A, Shimada H, Masuda T and Takamiya K (1999) Cloning of chlorophyllase, key enzyme in chlorophyll degradation: Finding of a lipase motif and induction by methyl jasmonate. Proc Natl Acad Sci USA 96: 15362–15367

Vicentini F, Hörtensteiner S, Schellenberg M, Thomas H and Matile P (1995a) Chlorophyll breakdown in senescent leaves: Identification of the biochemical lesion in a *stay-green* genotype of *Festuca pratensis* Huds. New Phytol 129: 247–252

Vicentini F, Iten F and Matile P (1995b) Development of an assay for Mg-dechelatase of oilseed rape cotyledons, using chlorophyllin as the substrate. Physiol Plant 94: 57–63

White MJ and Green BR (1987) Polypeptides belonging to each of the three major chlorophyll *a*+*b* protein complexes are present in a chlorophyll-*b*-less barley mutant. Eur J Biochem 165: 531–535

Woodward RB and Skaric VJ (1961) A new aspect of the chemistry of chlorins. J Am Chem Soc 83: 4676–4678

Wüthrich KL, Bovet L, Hunziker PE, Donnison IS and Hörtensteiner S (2000) Molecular cloning, functional expression and characterization of RCC reductase involved in chlorophyll catabolism. Plant J 21: 189–198

Ziegler R, Blaheta A, Guha N and Schönegge B (1988) Enzymatic formation of pheophorbide and pyropheophorbide during chlorophyll degradation in a mutant of *Chlorella fusca* Shiria et Kraus. J Plant Physiol 132: 327–332

Chapter 18

The Evolution of Chlorophylls and Photosynthesis

Anthony W. D. Larkum*
School of Biological Sciences, Building AO8, University of Sydney, NSW 2006, Australia

Summary

Photosynthesis evolved very early on the Earth, but after respiration, and probably after the metabolic processes for methanogenesis and sulfur oxidation. This occurred in ancestors of anoxygenic photosynthetic bacteria. An ancestral reaction center of Photosystem I and II (RCI/II) type of photosynthesis arose in which a five membrane-spanning helix (MSH) protein bound two molecules of chlorophyll (Chl)/bacteriochlorophyll (BChl) in a special pair and had a Chl/quinone primary acceptor, and this protein fused, early on, with a six MSH antenna protein. Logic suggests that the earliest photopigments were protoporphyrin IX, followed by Mg protochlorophyllide *a*, followed by Chl/BChl. It is not clear whether Chl or BChl came first. The evolution of the modern RCI type occurred later but it is not clear under what selection pressure it arose, possibly when ferric salts and sulfur compounds became more available in the Proterozoic Eon.

*Email: Alark@mail.usyd.edu.au

Bernhard Grimm, Robert J. Porra, Wolfhart Rüdiger and Hugo Scheer (eds): Chlorophylls and Bacteriochlorophylls: Biochemistry, Biophysics, Functions and Applications, pp. 261–282.

The revolutionary water-splitting mechanism that liberated molecular oxygen into the environment evolved later than earlier supposed, around 2.8–3.0 gigayears ago (Ga). This occurred in chloroxybacteria, precursors of Cyanobacteria, and defined as organisms possessing Chl *a* and a water splitting apparatus. It is probable that chloroxybacteria arose with the fusion of an RCI and RCII type RCs: RC Fusion Hypothesis. During the Proterozoic Eon, chloroxybacteria diversified with the development of light-harvesting based on Chl *a, b, c* and *d* and on phycobiliproteins. The Cyanobacteria with phycobiliproteins and phycobilisomes are seen as a late development, as is the evolution of Chl *d.* Because of many sinks, molecular oxygen remained negligible in the oceans and the atmosphere until about 2.3 Ga. During the period from 2.3 Ga to 1.0–0.5 Ga, oxygen levels remained low (1% present atmospheric level). Oxygen was at first toxic to most organisms but detoxification mechanisms that evolved must have been quickly gained by the first eukaryotic cells and this opened the way for the evolution of the first mitochondriate protists. Eukaryotic algae arose by about 1.5 Ga, by endosymbiosis of chloroxybacteria in mitochondriate protists.

I. Introduction

Not withstanding the theory of punctuated equilibria (Eldredge and Gould, 1972) and the recent evidence for widespread lateral gene transfer in Bacteria and Archaebacteria (Gogarten et al., 2002; Woese, 2002; Rivera and Lake, 2004) the modern synthesis on evolutionary theory still suggests that evolution occurs by small steps. This is even more true for the evolution of enzymatic pathways. In a previous review of Chl evolution (Larkum, 1991) it was noted: 'It is perhaps surprising to note how little Darwinian evolutionary theory has entered into the thinking on Chl evolution. Thus in considering the evolution of Chl it is reasonable to suggest that in broad terms its evolution is recapitulated in the biosynthetic pathway of Chl *a* and BChl *a.*' However it was also noted that a contrary view has been taken (Horowitz, 1945) — that evolutionary pathways could be built from the top down—and this alternative has been augmented recently by a patchwork theory (Copley, 2000). The recapitulation hypothesis for Chl evolution was proposed by Granick (1957), but has gained little acceptance, with the notable exceptions of Olson (1970, 2000) and Mauzerall (1973,1978); perhaps, because of the difficulty of gaining evidence on events that occurred more than 3 gigayears ago (Ga), but also because of the emphasis, hitherto, on photosynthetic bacteria, possessing BChl, as the first photosynthetic organisms. However, if one considers the implications of the recapitulation theory, it becomes apparent that the earliest photosynthetic pigments were probably closely related to porphyrins and that Chl *a* may have preceded BChl. Even more surprisingly, it is an easy step to suggest, as Granick (1957) did (in a throwaway line), that Chl *c* or a close relative may have preceded Chl *a*. This is a hypothesis supported below.

Abbreviations: Acc. –Acaryochloris; BChl – bacteriochlorophyll; BPhe – bacteriopheophytin; CAB – chlorophyll *a/b* binding protein; CAC – chlorophyll *a/c* binding protein; CAO – chlorophyll *a* oxygenase; *Cfx. – Chloroflexus*; Chl – chlorophyll; *Chl. – Chlorobium*; D1 – D1 polypeptide of RCII coded by *psbA*; D2 – D2 polypeptide of RCII coded by *psbB*; Ga – giga years (10^9 yr) ago; *Hbt. – Heliobacterium*; IR – infrared; LHC – light-harvesting complex; MgDVP – Mg-divinyl-3,8-divinyl pheoporphyrin A_5 monomethyl ester; MSH – membrane-spanning helix; PAL – present atmospheric level; PCB– prochlorophyte Chl *a/b* binding protein; Phe – pheophytin; POR – protochlorophyllide oxido-reductase; RC – reaction center; PS I – Photosystem II; PS II – Photosystem II; RCI – reaction center of PS I; RCII – reaction center of PS II; SSU rRNA – single subunit ribosomal ribonucleic acid; UV-B – ultraviolet B radiation; UVR – ultraviolet radiation

II. The Early Earth and the Origins of Photosynthesis

The Earth formed ~4.5 Ga and very soon after this the moon formed, possibly by a collision of a smaller early planet (Kuhn, 1998). For the next 0.5 giga years the Earth was bombarded by meteors (Owen and Bar-Nun, 2001), which meant not only that the surface was too hot for life to take hold, but which also changed the planet by, i) doubling the water content so that the oceans eventually covered 70% of the Earth's surface, ii) introducing significant amounts of organic material into the Earth's mantle, which were very significant for the start of life on the early Earth, and iii) probably introducing much of the diatomic (gaseous) nitrogen into the Earth's atmosphere. By about 4.0 Ga conditions were becoming more favorable to the evolution of life and by 3.8 Ga, most experts now agree, life had started.

Conditions on this early Earth were as follows: a highly reducing atmosphere, with oxygen levels

at ~0.01% of present atmospheric levels (PAL), a relatively high level of CO_2 of 9 kPa (vs. 0.03 today), relatively high residual hydrogen remaining from Earth formation plus additional amounts from chemical processes in the mantle. Previous predictions of high methane levels seem to have been in error, as it is now thought that early organisms formed methane at a slightly later date. The Sun was, at this stage, in the early phase of its development with a solar radiation of about 80% of today's radiant flux.

It is likely, though difficult to prove, that photosynthetic organisms evolved between the period 3.7–3.5 Ga (Blankenship, 2002). However, the proposal that oxygenic photosynthetic organisms (i.e., organisms that produced oxygen) were present from ~3.5 Ga (Schopf, 1993) is now widely discounted (e.g., Brassier et al., 2002). The oldest substantial evidence for such organisms (here called 'chloroxybacteria', but elsewhere in the literature called 'Cyanobacteria') now comes from chemical 'fossils' in rocks, which are considerably younger, viz. 2.8 Ga, than those of the earlier microfossils (Brocks et al., 1999; Summons et al., 1999). In these circumstances, it seems reasonable to assert that photosynthetic bacteria began to evolve ~ 3.6 Ga, but that chloroxybacteria did not begin to evolve, with a mechanism for splitting water and releasing molecular oxygen, until ~3.0 Ga.

Thus, significant input of molecular oxygen on the Earth would not have occurred until after 3.0 Ga and the rise of oxygen in the atmosphere would have been slow because of: i) the large reservoirs of reducing sediments and gases on the early Earth; and, ii) the slow evolution of an efficient photosynthetic water splitting mechanism, and the spread of the chloroxybacterial organisms in which it evolved (see Section VI). Current evidence suggests that atmospheric and upper ocean levels of oxygen would have risen to only 1% PAL at ~ 2.3 Ga (Kasting, 2001; Bjerrum and Canfield, 2002; Shen et al., 2003) and would have remained at this level until ~1.0–0.6 Ga (Canfield and Raiswell, 1999; Anbar and Knoll, 2002; Kasting and Siefert, 2002).

This establishes a timescale for the further development of organisms on the Earth: the period from 3.0–2.0 Ga would have seen the development of aerobic bacteria and the first primitive eukaryotes, leading to the first mitochondrial eukaryotes by ~1.8 Ga (Knoll, 1999), and then to the first photosynthetic eukaryotes (algae), a short time thereafter.

III Evolution of the Pathway to the Earliest Photosynthetic Pigments

A. The Pathway to Mg-Protoporphyrin IX

An early role of porphyrinogens and porphyrins in the evolution of organisms on the primitive Earth, between 3.8–3.0 Ga, is implicated by the central role of these compounds in the formation of cytochromes, hemes, biliproteins, Chls, phytochrome, F430 and vitamin B_{12} (Hodgson and Ponnamperuma, 1968; Georgopapadakou. and Scott, 1977)(Fig. 1). Porphyrins have been produced by Urey-Miller experiments, using both electrical discharges (Hodgson and Pannamperuma, 1968) and ultraviolet radiation (Szutka, 1965; Hodgson and Baker, 1967; Simionescu et al., 1978) and they have been found in early rocks and in meteorites (Hodgson and Baker, 1964). A surface-catalysed synthesis of porphyrins with high yield, starting from pyrrole and aldehydes, on an aqueous clay suspension, has also been reported (Cady and Pinnavaia, 1978). Such abiotic syntheses are stimulated by cations and by a range of metals that coordinate with the porphyrins. Thus, it is likely that porphyrinogens accumulated on the early Earth by abiotic reactions, which were later augmented by enzyme-catalysed reactions, which could have followed the Shemin or glutamate pathway (Larkum, 1991).

Porphyrinogens are colorless, since they are hexahydroporphyrins, i.e., the closed system of conjugated double bonds that exists around the macrocycle of porphyrins, chlorins and bacteriochlorins is not present. In the modern biosynthetic pathway, the route from the porphyrinogens to the porphyrins is from uroporphyrinogen III via coproporphyrinogen III to protoporphyrinogen IX and then to protoporphyrin IX: the first natural porphyrin pigment (Fig. 1; Table 1; Chapter 1, Scheer; Chapter 13, Yaronskaja and Grimm). Alternatively uroporphyrinogen could be converted to uroporphyrin III, which is also colored (Table 1) and then on to protoporphyrin IX. In contrast to the porphyrinogens, all the relevant porphyrins, from uroporphyrin to protoporphyrin, are colored (Table 1), with intense absorption maxima between 400 and 410 nm and four minor, but characteristic, bands in the green region (Mauzerall, 1973,1978; Treibs, 1973). Since porphyrins are produced in Urey-Miller experiments, it seems very plausible that the first-formed macrocycle, uroporphyrinogen III was oxidized abiotically to a dihydro- or fully oxidized

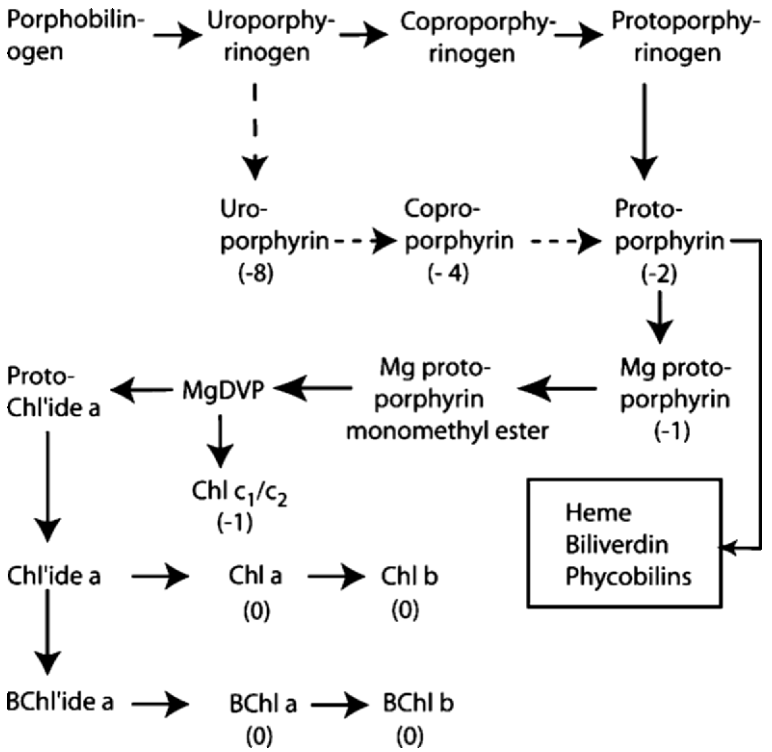

Fig. 1. Outline of the major steps in the biosynthetic pathway of chlorophyll and bacteriochlorophyll synthesis (solid lines) and another possible route for chlorophyll evolution (hatched followed by solid). Numbers in parentheses indicate molecular charge.

uroporphyrin III (Mauzerall, 1960; Mercer-Smith and Mauzerall, 1984). It is possible, therefore, that uroporphyrin took part in an early light-driven reaction (Treibs, 1973; Mercer-Smith and Mauzerall, 1984), as set out below: a reaction that presumably was abandoned long ago by these early organisms. From experimental results of several groups (Krasnovsky, 1971; Runquist and Loach, 1981; Ilani et al., 1989), it can be suggested that an early type of light-driven redox pump could have used porphyrins or porphyrinogens (Fig. 2). Such a mechanism could have been employed, for example, to oxidize organic compounds, to reduce ferric ions and to create a proton gradient (Fig. 2A). This could have been a forerunner of the reaction center (RC).

These ideas have been extended with the suggestion that the photoreaction itself could also have been involved in the oxidation of uroporphyrinogen to uroporphyrin, driven by UV radiation with a wavelength shorter than 230 nm (Mercer-Smith et al., 1985). The self-catalysed photooxidation, it is proposed, was accompanied by the formation of molecular hydrogen, with organic compounds acting as electron donors. With the absence of oxygen in the atmosphere (see above), the amount of UV radiation (UVR, 200–240 nm), penetrating to the Earth's surface would have been relatively high. However, if the recent proposal for high methane levels in the late Archean and early Proterozoic Eons is correct, then a methane haze would have reduced the UVR considerably about the time 3.5–2.7 Ga (Pavlov et al., 2003). Nonetheless, this is well after the period of evolution of porphyrins, and the proposal for UV-driven formation of uroporphyrin in the early Archean is plausible. Other mechanisms such as catalytic action of clays or serendipitous enzymic sites on other proteins or nucleic acids remain a possibility. Furthermore, the early pigments may well have evolved as a mechanism for UV protection (Larkum, 1991; Mulkidjanian and Junge, 1997) and there would have been a strong selection pressure to use this radiation for useful purposes, that is, in an early photoreaction (Fig. 2).

The role of metals in the early light absorption processes is of great interest. A number of metals, abundant in the primitive earth (Fe, Zn), may have

Table 1. Absorption characteristics of chlorophyll, bacteriochlorophyll and their colored biosynthetic precursors (adapted from Larkum, 1991)

Pigment	λ [nm] (ε [mM^{-1} cm^{-1}]) *							Reference
Uroporphyrin III	406 (215)	502 (16)	536 (9)	572 (7)		627 (4)		KM Smith, 1975
Protoporphyrin IX	404 (158)	503 (15)	536 (12)	576 (7)	605 (2)	633 (7)		KM Smith, 1975
Mg-protoporphyrin monomethyl ester	419 (100)	510 (1)	553 (6)	591 (6)				Jones, 1963
Mg-3,8-divinyl pheoporphyrin a_5 monomethyl ester	437 (10)		574 (0.5)		624 (1)			Jones, 1963
Protochlorophyll *a*	432 (102)	438 (137)	533 (4)	570 (8)	602 (7)	622 (22)		Houssier and Sauer, 1970
Chlorophyll *a*	410 (85)	430 (118)	530 (3)	578 (8)	615 (13)	662 (90)		Houssier and Sauer, 1970
Chlorophyll *b*	430 (63)	455 (175)	549 (7)		595 (13)	644 (62)		JHC Smith and Benitez, 1966
Chlorophyll *c* (combined)		447 (227)		580 (21)		628 (51)		JHC Smith and Benitez, 1966
Chlorophyll *d*	399 (81)	455 (80)	550 (7)	595 (9)		698 (88)		JHC Smith and Benitez, 1966
Bacteriochlorophyll *g**	408 (100)	418 (95)	470 (27)	575 (21)			763 (51)	Brockman and Lipinski, 1883
Bacteriochlorophyll *a*	357 (73)	392 (47)		573 (22)			770 (96)	Houssier and Sauer, 1970
Bacteriochlorophyll *b*	368 (86)	408 (77)		578 (26)			794 (106)	JHCSmith and Benitez, 1966

Absorptivity (ε) values are listed beneath the appropriate wavelengths (λ) for the pigments. Solvents, in general, diethylether; dioxane for BChl *g* and chloroform for uroporphyrin.
*For BChl g the values in parenthesis are $\varepsilon/\varepsilon_{max}$ (%)

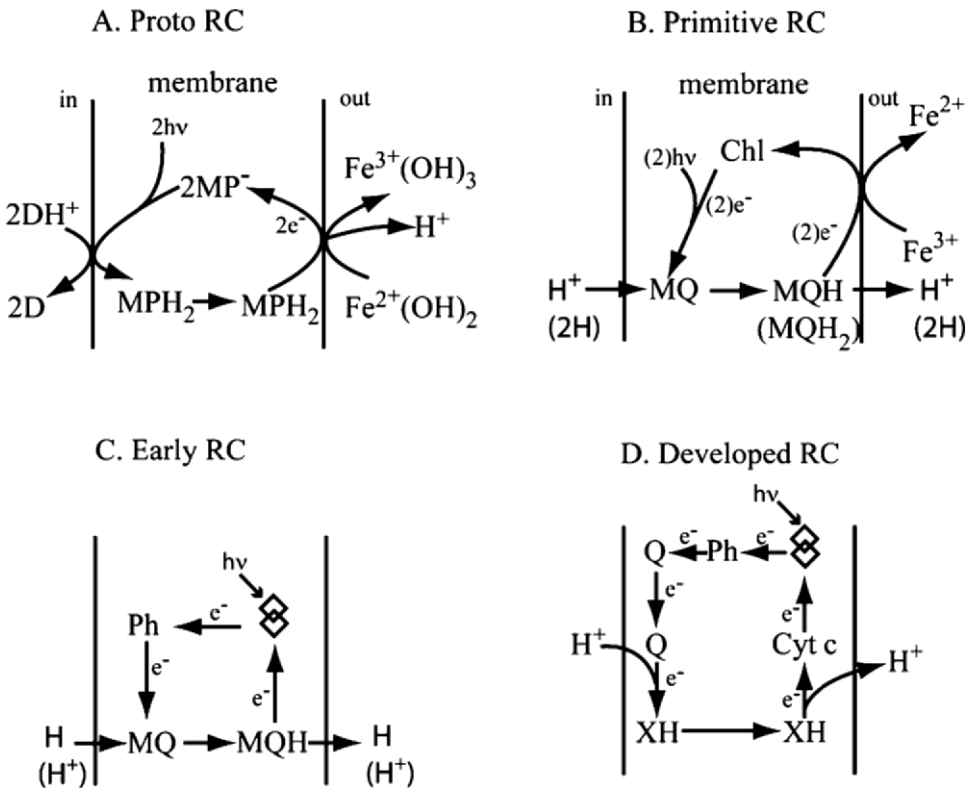

Fig. 2. Possible developments in the evolution of primitive RCs of photosynthesis linked to electron transport across a membrane (adapted from Larkum, 1991; see also Olson, 1999). Cyt *c*, cytochrome *c*: D, hydrogen donor; MP, metalloporphyrin; MQ, menaquinone; Ph, pheophytin *a*; Q, bound quinone; overlapping diamonds, special pair of Chls; XH, membrane-bound hydrogen carrier.

interacted with porphyrins and related compounds to form pigments and complexes that no longer exist. Zinc porphyrins were less successful photoxidizing agents for organic compounds than free-base porphyrins (Mauzerall, 1978; but see Zn BChl, below). However studies with porphyrin-platinum complexes, where the porphyrin and the metal catalyst are held in close association by the molecular complex, but the metal is not complexed within the tetrapyrrole ring, indicate that, with certain porphyrins, rates were higher than with the free-base (Mercer-Smith and Mauzerall, 1984). The nature of the redox reaction changes, however, with the free base: in general, the porphyrin becomes reduced in photoreactions, but this is strongly dependent on the reaction conditions. In the metal complex, as with RC Chl, the porphyrin undergoes photooxidation (Mercer-Smith and Mauzerall, 1984). Thus, evolutionary experimentation with metal complexes having long excited-state lifetimes may have led to the modern type of photooxidation of the photoactive pigment.

The next steps must have led to the formation of copro- and protoporphyrin (Fig. 1), yielding pigments with useful and similar absorption properties in the near-ultraviolet and violet (Table 1), but with greater stability, better redox properties (Mercer-Smith and Mauzerall, 1984) and much less charge [–8 for uroporphyrinogen to –2 for protoporphyrin (Mauzerall, 1978)]. The trend to lower charge is an important consideration for membrane-located systems. For the formation of coproporphyrin a non-enzymatic step could have occurred (Mauzerall, 1978) but light and near UV may also have played a part (Jacobs and Jacobs, 1984). Next, the formation of protoporphyrin IX is problematic since the reaction is thermodynamically unfavorable under non-oxidizing conditions. It has been suggested that an enzyme was needed to carry out specific oxidation of two of the four propionic residues on rings A and B (Mauzerall, 1978) but a non-enzymatic step is not impossible (Jacobs and Jacobs, 1984). Today, all organisms have a single pathway from ALA to protoporphyrin IX, the branch point to protoheme or Chl synthesis (Chapter 13, Yaronskaya and Grimm).

The final step, which differentiates heme synthesis from Chl synthesis, and produces arguably the first

'modern' pigment in photosynthesis (Table 1), is the formation of Mg-protoporphyrin IX, with a spectrum similar to Mg-protoporphyrin monomethyl ester. This step is catalyzed by Mg-protoporphyrin IX chelatase, which is made up of 3 subunits in cyanobacteria, algae and plants, encoded by *chlD*, *chlI* and *chlH*: one product (ChlD) mediates an ATP hydrolysis. This reaction could have occurred in the absence of enzymic catalysts, especially with locally high magnesium concentrations, for example, in clays, but it would have been hard to control the formation of heme vs. that of (B)Chl. Nevertheless, it was a pivotal reaction, which, however slow, would have been selected for because of the favorable spectral properties of the product. Once this was formed the next five steps on the route to (B)Chl formation would have evolved inexorably in the selection of pigments better for absorbing visible light. In this evolution the addition of the fifth isocyclic ring played a key role as discussed by many previous workers (Mauzerall, 1973,1978; Chapter 1, Scheer)

B. Strong Conclusions on the Early Evolution of Photopigments

1. The earliest light-driven reactions must be distinguished from the evolution of modern photopigments and photosynthetic systems (discussed in Section V). This evolutionary phase took place as far back as 3.7 Ga and little hard evidence remains about the evolutionary events involved.

2. Respiration preceded photosynthesis (Castresana and Sarastre, 1995; Castresana, 2001). This provided a firm base for the evolution of heme compounds and ferroprotoporphyrins. Thus some form of early cytochromes would have been in existence before the evolution of the first light-driven reactions

3. The present view is that ultraviolet radiation (UVR) was the driving force in the development of the first organisms to use light-driven reactions. This is contrary to the previous view that UVR was harmful, largely due to damage to DNA, to the development of early organisms (Olson and Pierson, 1987). According to the new view, a primitive type of photoreaction preceded, not only photosynthesis, but might have preceded heme-related respiratory systems, as well.

4. A fourth conclusion, implicit in 2., is that evolution of primitive photoactive pigments (i.e., primitive photosynthesis) occurred after the evolution of the redox-active hemes taking advantage of pigments which evolved initially to protect from UVR.

IV. Evolution of Extant Photosynthetic Pigments and Early Photosynthetic Organisms

A. Evolution of Chlorophylls and Bacteriochlorophylls

1. Evolution of the First Modern Photosynthetic Pigments

There is little doubt that the first effective photosynthetic pigments were Mg-porphyrins, such as Mg-protoporphyrin monomethyl ester. Indeed, it is the chelation of Mg^{2+} at this stage in the biosynthetic pathway that distinguishes this line of development from that of heme formation where $Fe^{2+/3+}$ is involved, the hemes have only very short excited state lifetimes. Alternatively, these Mg-compounds may have been intermediates, naturally formed without the intervention of specific enzymes, on the pathway to what may be viewed as the first true Chl, Mg-3,8-pheoporphyrin a_5 monomethyl ester (Mg-DVP, or Mg protochlorophyllide *a* and is now confirmed as a *c* type chlorophyll). The structure of this pigment has been elucidated (Helfrich et al., 1999) and its presence shown in anoxygenic photosynthetic bacteria, in two prochlorophytes and in primitive green algae such as *Micromonas* spp (Helfrich et al., 1999). It is an easy extension from there to suggest that other Chls *c*, such as Chl c_1 and Chl c_2 arose by small chemical modifications and were used in photosynthesis (Larkum, 1991, 1999). However, the early involvement of any other Chls *c* is made less likely by the absence, so far, of any pigments, other than Mg-DVP, in any prokaryotic photosynthetic organisms. It may be that replacement of Chl *c*, by (B)Chls, i.e., through reduction of a porphyrin to a chlorin or bacteriochlorin, was likely as soon as these evolved, since they are much better pigments (Larkum, 1991, 1992, 1999).

2. Evolution of the Pigments After Mg-Divinyl Pheoporphyrin

The evolutionary pathway from Mg-DVP to Chl/BChl is unclear. The evidence based on Chl/BChl biosynthesis and other photosynthesis genes is discussed in the Section IV.B. It is certain, however, that oxygenic photosynthetic bacteria, viz. chloroxybacteria, evolved from an ancient group of anoxygenic photosynthetic bacteria. However it is not proven that these earliest anoxygenic forms possessed BChl. Lockhart et al. (1996a) and Larkum (1999) suggested that the earliest enzymes were multifunctional to the extent that they produced both Chl- and BChl-type pigments from protochlorophyllide *a* and only later evolved into their present forms, which make exclusively Chl- or BChl-type pigments. There is enough experimental work to show that either of these pigments would bind to several of today's Chl- or BChl-binding proteins (Larkum, 2003; Chapter 1, Scheer; Chapter 26, Paulsen) and therefore one would expect even greater adaptability in the distant past.

The alternative hypothesis to Chl first is BChl first. While many scientists have adopted this view (Blankenship, 2002), it involves invoking arguments for i) why Chl *a* was not among the first pigments formed (above), and ii) how a BChl system was later converted into a Chl system (Blankenship, 2002).

3. Evidence from Light-Harvesting Characteristics

Larkum (1992) argued as follows: i) that (B)Chl would have been a very prevalent pigment in early photosynthetic bacteria of whatever type; ii) as these (B)Chl-based forms multiplied and were able to compete for most of the light in the violet and red regions of the spectrum, a situation would arise whereby selection pressure would induce the formation of other (B)Chls.)

With hindsight we can say that chloroxybacteria, with Chl, prevailed because: a) with the extended redox spans of Chl vs. BChl, they could use water as a source of electrons and protons; and b) because, of the Chl and BChl pigments, they were most suited to harvest that part of the Sun's spectrum with the highest flux. According to this argument, anoxygenic photosynthetic bacteria were relegated to refugia where: a) oxygen was often restricted; b) where hydrogen sources (H_2, H_2S, organic compounds) were available; and, 3) where the light climate was likely to be stripped of visible light by chloroxybacteria and/or water-quality effects. These were the sites where single-photosystem-photosynthesis, based on BChl, would be selected for and these are still the sites where anoxygenic photosynthetic bacteria are most often found, although some can now survive in aerobic environments, such as the open ocean (Kolber et al., 2001; Rappé and Giovannoni, 2003). Furthermore, we should remember that chloroxybacteria, and their descendants, Cyanobacteria, have competed for the last 1.5 Ga with algal protists and, later, with higher plants, as these came to dominate the terrestrial photosynthetic systems on Earth. As a result it is likely that many former types of chloroxybacteria/Cyanobacteria were pushed to extinction, just as many early anoxygenic photosynthetic bacteria were, and we are now left with a relict population.

4. Evolution of Chlorophylls

The diversity of Chls is discussed by Kobayashi et al. (Chapter 4), Rüdiger and Grimm (Chapter 10) and by Frigaard et al. (Chapter 15). The path of evolution of Chls proposed here is that the original MgDVP (see above) is followed and replaced by Chl *a*. Later Chl *b* and Chls *c* evolved in the light-harvesting antennae (Larkum, 1991) in deeper water or more shaded sites where light capture, especially of blue and green light, was at a premium.

Until recently, there would have been no argument over the primary role of Chl *a* among the Chls, but the discovery of *Acaryochloris (Acc.) marina* (Miyashita et al., 1996) has challenged that view. Chl *d* in *Acc. marina* is present in proportions of ~95 % of the total Chl, with Chl *a* as the only other Chl (MgDVP has not been detected). Chl *d* is the pigment of the special pair of PS I (Hu et al., 1998) and it is possible that it plays an important role in PS II and may form the special pair (Chen et al., 2005b), notwithstanding previous evidence for Chl *a* (Mimuro et al., 1999). Chl *a* and Chl *d* also act in a light-harvesting capacity (Larkum, 2003). Until the biosynthetic pathway of Chl *d* and Chl *b* in Cyanobacteria is clarified (see discussion below) no firm evolutionary conclusions can be made. However it seems more likely that Chl *d* evolved 'late,' in chloroxybacteria, under selection pressure for a particular niche that developed, as algae, Cyanobacteria and anoxygenic photosynthetic bacteria harvested most of the light penetrating algal mats or symbiotic associations such as didemnid ascidians (Kühl and Larkum, 2001), leaving only a window of

light in the 700–740 nm region (Kühl et al., 2005). This is consistent with the view that prochlorophyte Chl *a/b*-binding proteins (PCB), which bind Chl *a* and *b* or Chl *d* are a fairly late development in chloroxybacteria (Zhang et al., 2004). Another possibility, put forward by Blankenship and Hartmann (1998), is that it was one of the intermediates on their proposed evolutionary pathway from BChl-based organisms to Chl-based organisms.

Chl *b* occurs in prochlorophytes (Cyanobacteria), green algae, euglenoids, chlorarachniophytes, charophytes and land plants (Larkum, 2003) and is bound to either a PCB protein, in prochlorophytes, or a Chl *a/b*-binding (CAB) light-harvesting protein in all the others. Chl *c* (c_1, c_2 c_3, etc) is found in a variety of chromophytic algae (Larkum, 2003) and is bound to a Chl *a/c*-binding (CAC) light-harvesting protein. MgDVP is bound either to PCB in prochlorophytes or to CAB proteins in prasinophytes [primitive green algae (Larkum, 2003)]. Divinyl Chl *a* and divinyl Chl *b* are found in deep water strains of the prochlorophyte *Prochlorococcoccus marinus* (Partensky and Garczarek, 2003) and this seems to be an adaptation to match the spectra of these forms to the prevailing blue light at depth in the ocean (Ting et al., 2002). It is accomplished by deletion of the gene for reduction of the divinyl group at position 5.

Chl *b* almost certainly arose in chloroxybacteria and was passed on to Cyanobacteria. Larkum (1992) proposed that Chl *b* arose as one of the earliest forms of accessory Chls, well before phycobiliproteins evolved, in response to selection pressure to increase light harvesting in the visible light spectrum.

Since Raven (1996) showed that the addition of MgDVP would make a significant difference to the light harvesting capacity of a unicellular organism with Chl *a* plus Chl *b*, it is clear that the addition of Chl *b* would have made a much greater contribution, since the red peak is so much larger in Chl *b* vs. MgDVP (Table 1). Furthermore, a special role of Chl *b* in binding and stabilizing antenna Chl proteins has been suggested by Hoober and Eggink (2001) and a similar argument was also made for Chls *c* (Hoober and Eggink, 2001). However, Larkum (2003) has pointed out that the contribution of Chls *c* is less obvious than that of Chl *b*; Chl *c* may play some other role, such as facilitating the transfer of resonant energy from carotenoids to Chl *a*. It is important to note that Chl *c* (MgDVP, Chl c_1, Chl c_2, Chl c_3, etc.) is a violet/blue absorbing pigment. Against this is the evidence that in the peridinin Chl complex, no Chl *c* is present, yet the transfer efficiency is very high (Larkum and Barrett, 1983) and the binding is very tight (two Chl *a* and eight peridinin; Hofmann et al., 1996), but this may have more to do with the special chemistry of peridinin, which has a very long excited life time of 150 ps in solution.

Both Chl *b* and Chl *d* have (oxygenated) formyl groups not present in Chl *a*. This oxygenation step might be taken to imply the need for molecular oxygen in the environment (Larkum and Barrett, 1983; but see Raymond and Blankenship, 2004). In the case of Chl *b* it is now known that the methyl group of Chl *a* is oxygenated to a formyl group by a Chl *a* oxygenase (CAO)(Tomitani et al., 1999), which is found in prochlorophytes, green algae and higher plants. However, a gene for CAO is absent in *Prochlorococcus* (Rocap et al., 2003). The biosynthetic pathway for Chl *d* is not known.

From the phylogenetic point of view the big question is why chromophytes adopted the same light-harvesting chlorophyll-binding complex (LHC) as those algae that utilize Chl *b*, but chose a different light harvesting Chl? In the prochlorophytes Chl *a*, Chl *b* and MgDVP are all bound onto a single PCB antenna protein and in eukaryotic micromonads the same pigments are bound onto a CAB antenna protein (see above). Perhaps, the answer is explained most easily by a stochastic event that produced an organism at the prokaryotic level viz. a chloroxybacterium, that possessed only Chl *c* and which gained a gene for CAC by lateral transfer. Larkum (1991,1992) suggested that Chl *c* (viz. MgDVP) was the first modern Chl to evolve in a photosynthetic system, to be rapidly replaced by Chl *a*, but that Chls *c* then took on an early light-harvesting role. However no Chls *c,* apart from MgDVP, have yet been found in Cyanobacteria.

5. Evolution of Bacteriochlorophylls

The diversity of BChls is discussed by Frigaard et al. (Chapter 15). All 'true' BChls have a bacteriochlorin ring structure (i.e., the porphyrin ring is reduced in rings B and D; Chapter 1, Scheer). Based on its widespread occurrence and its proximity to protochlorophyllide *a* on the biosynthetic pathway, it is logical to see BChl *a* as the earliest BChl. The bacteriochlorin macrocycle of BChls is brought about today by the reduction of ring B by three enzymes, coded by the genes, *bchX*, *bchY* and *bchZ*. These genes are clearly homologous to the genes that code for the

light-independent reductase that reduces the D ring to form the chlorin macrocycle from the porphyrin macrocycle; inferences based on these gene sequence similarities are discussed in the next section (Section IV B). However, BChl *a* is not produced simply by the reduction of the B ring: the vinyl group on ring A (of Chl) is replaced by an acetyl group in BChl *a* (Fig. 3). Consequently, it is possible to imagine a number of other schemes (Fig. 2, Larkum, 1991). It has been suggested that BChl *g* and Chl *a* are isomers, which could be more than a coincidence (Margulis and Obar, 1985; Olson and Pierson, 1987; Xiong et al., 2000; Dismukes et al., 2001). Blankenship and Hartman (1998) proposed that Chl *d* (Section IV.A.4) was an evolutionary intermediate between BChl *a* and Chl *a*. While the spectral properties of BChl *b, c, d,* and *e* might make them attractive in terms of evolutionary pathways, their detailed structural properties are not so easy to incorporate into schemes of BChl/Chl evolution (Larkum, 1991). BChl *c, d* and *e* (chlorins) have their Q_y absorption band in the red or near infrared (IR) (Table 1, Chapter 1, Scheer): BChl *a, b* and *g* (bacteriochlorins) absorb in the IR (~773, 794 and 764 nm, respectively), and also have a relatively intense Q_X-band near 580 nm. For BChls *c, d* and *e,* which are Mg-chlorins (Chapter 1, Scheer; Chapter 15, Friegaard et al.) this band is minor (λ_{max} ~ 600 nm). In all cases the Soret band is in the UV-A to violet region of the visible spectrum, so anoxygenic photosynthetic bacteria can use visible light if necessary. However, in the niches in which these bacteria exist (algal mats, muds, sediments of hot springs, etc.), UV and violet light is generally filtered out, so that near IR radiation forms the major energy source, as it does also for *Acc. marina* (see Section IV.A.4). BChls are generally esterified by either farnesol or phytol alcohols, but in the case of BChl *c*, *d* and *e*, many other alcohols can be used (Chapter 1, Scheer).

Further progress in discussing the evolutionary pathways involved should be possible when we have more detail about biosynthetic pathways. This will come when we have more whole genome sequences for the anoxygenic photosynthetic bacteria and for the Chl *d*-containing organism, *Acc. marina*.

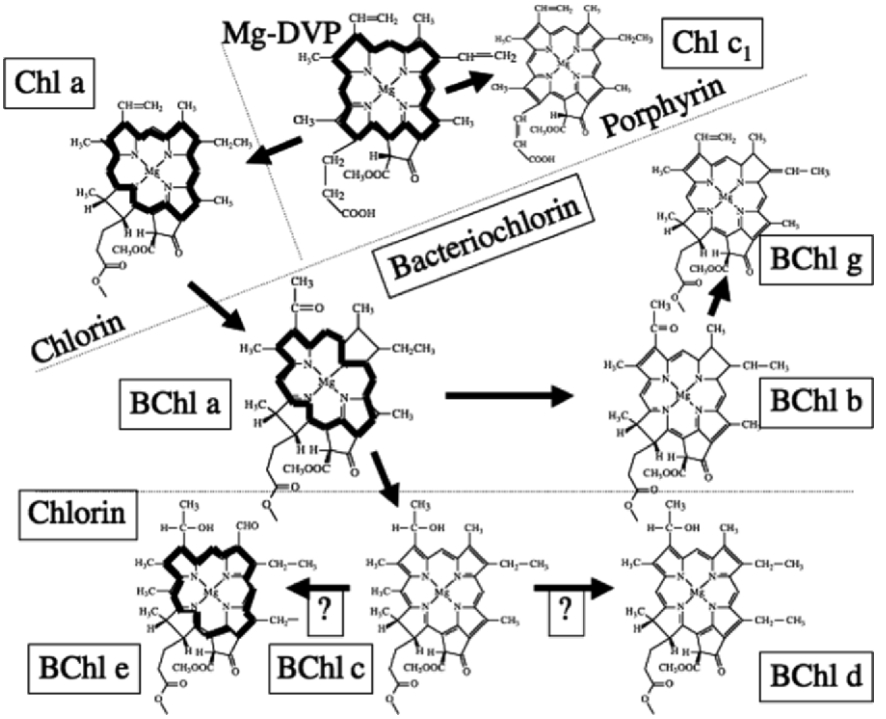

Fig. 3. Chemical structures of chlorophylls and bacteriochlorophylls with indications of possible routes on the evolution of their biosynthesis. Heavy lines indicate the π-bond resonance pathway (these are not shown, for convenience, for all the bacteriochlorophylls, see Chapter 23, Steiner and Fowler). The esterified hydrocarbon tail of various chlorophylls and bacteriochlorophylls is not shown.

B. Molecular Phylogenetic Analyses

The use of gene sequences to reconstruct evolutionary history is a potentially powerful tool, with perhaps its greatest success so far being the theoretical division of life into three domains, Archaebacteria, Bacteria and Eukarya (Woese, 1987). This was done on the basis of the aligned sequence of small subunit ribosomal RNA (SSU rRNA). Despite this success, there is still some doubt about the general applicability of this approach, especially in terms of prokaryote evolution (Rivera and Lake, 2004). Photosynthesis is a particularly good example of the difficulties encountered at the prokaryotic level since, when applied to photosynthetic bacteria, the results are not easily understood (Woese, 1987; Blankenship, 1992): there is no clear evolutionary development, in terms of photosynthesis, of RCI (PS I) or RCII (PS II) anoxygenic photosynthetic bacteria, and the origin of Cyanobacteria is apparently not a development of any of these earlier lines. The conclusion is that there has either been massive lateral transfer of genes and suites of genes across widely separated taxa or the SSU rRNA trees are not reliable, or both. Certainly there is now far-reaching evidence for lateral transfer both from whole genome studies, in a variety of organisms (Gogarten et al., 2002; Woese, 2002; Xiong and Bauer, 2002) and particularly in photosynthetic organisms (Raymond et al., 2002).

Molecular phylogenetic analysis was used to test the question of whether Chl or BChl evolved first. Burke et al. (1993) made tree reconstructions based on the genes coding for the enzymes that reduce porphyrin ring to the chlorin ring and the chlorin ring to the bacteriochlorin ring: this is the light-independent protochlorophyllide oxido-reductase (POR) dark mechanism, not the light-activated POR mechanism that replaces it in higher plants. Photosynthetic bacteria have two sets of genes: *bchL/bchN/bchB* reduce the porphyrin ring D to a chlorin and *bchlX/bchY/bchlZ* reduce the chlorin ring B to a bacteriochlorin. Cyanobacteria, and all descendants of this oxygenic photosynthetic line, algae and higher plants, have just one set of enzymes, differing in detail but homologous to those found in anoxygenic photosynthetic bacteria: *chlL/chlN/chlB* enzymes. All the subunits of these reductases are homologous and show distant homology with *nif* (nitrogen fixation) genes, which Burke et al. (1993) used as the out-group. The latter, using well-founded phylogenetic reconstruction based on maximum likelihood, found that the *bchX* gene was the earliest branch within the Chl/BChl reductases. The authors argued that this meant that the earliest reductases were BChl reductases, suggesting that BChl preceded Chl in evolution.

This view was contested by Lockhard et al. (1996a), who showed that the results of Burke et al. (1993) were not supported when only sites-free-to-vary were analyzed. Lockhart et al. (1996a) argued that there is not enough information in the sequence data to reach a significant conclusion. They also argued that even if the result of Burke et al. (1993) was the correct one, this would not be a definitive indication that BChl preceded Chl: Burke et al. (1993) put forward the hypothesis that an early version of the reductase could carry out both steps (reduction of ring B and ring D). Lockhart et al. (1996a) further suggested that this would mean that both Chl *a* and BChl *a* would have been formed. The final Chl/BChl molecules are formed by esterifying with a phytyl tail, and in the case of BChl after modification of the vinyl group on ring A to a acetyl group (Fig. 3). Only by further evolution, Lockhart el al. (1996a) proposed, were the specific enzymes (*chlL*, *bchX*, *bchN*) evolved. Therefore, it was impossible to decide whether Chl or BChl came first; probably the answer was that both arose together. Thus, it can be argued that Chl may have operated in the earliest photosynthetic mechanism(s) alongside BChl. Perhaps this condition persisted until the rise of chloroxybacteria (Section II). The rise of chloroxybacteria would have placed such strong selective pressure on anoxygenic photosynthetic bacteria that in the latter organisms only BChl was selected (see Section IV.A.3).

More recently it has been possible to assemble all the genes for Chl/BChl reductases (Xiong et al., 2000) and to produce phylogenetic trees of all the major anoxygenic/oxygenic taxa (Xiong et al., 2000; Xiong and Bauer, 2002). The first analyses, based on *bchL*/*chlL* indicated that the purple sulfur bacteria were the oldest photosynthetic group, while the heliobacteria (often proposed as an early evolutionary group) were placed closest to the Cyanobacteria (often placed as a late group). This general arrangement was supported by other genes (*bchH*/*chlH*, *petB*, *bchI*/*chlI*/*bchD*/*chlD* and RCII-type genes). However it should be remembered that the actual taxon and the photosynthetic mechanism that each taxon possesses, cannot be easily connoted, since, as shown by Raymond et al. (2002), it is highly probable that there has been a great deal of lateral gene transfer within the Eubacteria involving large parts

of the photosynthetic apparatus. Therefore, the possession of a particular photosynthetic apparatus does not indicate the taxonomic position of a particular anoxygenic bacterial group. To further complicate the issue, Jermiin et al. (2001) have shown that the analyses of Xiong et al. (2000) are not powerful enough to make a full discrimination of the true tree. Based on an analysis of informative sites, Jermiin et al. (2001) showed that the position of heliobacteria, close to Cyanobacteria, was not firm and, overall, the information in the data available is not sufficient to accurately predict the true tree (also see Gupta et al., 1999; Gupta, 2003).

The recent proliferation of whole genomes has ushered in a new era of phylogenetic analysis, which gives a new impetus to evolutionary studies. Methods for assessing the information in phylogenetic terms are still at an early stage. While, at present, it is possible to see in qualitative terms how genes or suites of genes have been inherited, assessment in reliable quantitative terms, afforded by gene order and gene sequence analysis, is in its infancy (House et al., 2003). For Eubacteria there are many whole genomes at present and the list is increasing rapidly (see http://www.genomesonline.com) although some outstanding omissions from anoxygenic bacteria also exist. To date 14 whole genomes have been sequenced from cyanobacteria, including the recent deep-water *Synechococcus* WH8102 (Palenik et al., 2003), and at least another two for *Prochlorococcus* (Dufresne et al., 2003; Rocap et al., 2003). There are three whole nuclear genomes available for algae (a red (*Cyanidioschyzon*), a diatom (*Thalassiosira*) and a green (*Chlamydomonas*) and others are being done, and as well as a number of plastid genomes (Douglas et al., 2003). In higher plants, the whole genomes of *Arabidopsis thaliana* and rice were sequenced and several others will be completed shortly. This patchy record gives a tantalizing glimpse of the evolution of photosynthetic systems, which is most clear for the anoxygenic photosynthetic bacteria, but as more whole genomes are added the situation should yield many new insights into evolutionary pathways (Rivera and Lake, 2004).

In summary the emerging picture indicates that there has been much lateral gene transfer involving the photosynthetic apparatus (Raymond et al., 2002; Xiong and Bauer, 2002) and, in future, the combined use of sets of genes will also be required. However, if there has been lateral transfer of photosynthesis genes there may well have been lateral transfer of whole suites of genes, thus making a 'natural' classification and phylogeny of bacteria an impossible task, as discussed by Woese (2002) and Gogarten et al. (2002).

C. Some Strong Conclusions on Anoxygenic Photosynthetic Bacterial Evolution

a) The evolution of bacterial photosynthesis was a very early event but was preceded by the evolution of respiratory enzymes.

b) Anoxygenic photosynthetic bacteria preceded oxygenic photosynthetic organisms, but these may not resemble modern photosynthetic bacteria.

c) A homodimeric structure of the RC preceded a heterodimeric structure, but this does not necessarily mean that *Chloroflexus* (*Cfx.* and allies) and *Heliobacter* (*Hbt.* and allies) have the oldest photosynthetic apparatus (even if lateral gene transfer has not occurred).

d) Oxygenic photosynthesis emerged at a later time, that is not accurately known, either by a fusion or fission hypothesis of a reaction center of PS I-type (RCI) and a reaction center of PS II-type (RCII).

e) Chloroxybacteria, an ancient lineage, gave rise to the extant Cyanobacteria (including prochlorophytes and *Acaryochloris* and allies) relatively recently and after much evolution and lateral transfer of genes and suites of genes.

V. Reaction Centers

A. Earliest Reaction Centers

In the strict sense, photosynthesis is a vectorial charge transfer across a membrane causing oxidation on one side and reduction on the other, powered by a Chl-, or, more loosely, a porphyrin-based light reaction. Lake and coworkers (Lake et al., 1985) proposed a group within the bacteria called the photocytes (including the Eubacteria and Halobacteria) on the basis of carotenoid content and light-driven systems. This proposal would mean that a common ancestor gave rise to both light-driven systems. However, this

has not received wide support (Gouy and Li, 1989). Bacteriorhodopsin is a light-driven proton pump (Oesterhelt and Tittor, 1989) that does not involve Chl, and occurs in archaebacteria and an increasing number of eubacteria (Rappé and Giovannnoni, 2003). It has been suggested, for example by Lake et al. (1985), that bacteriorhodopsin may represent a precursor of early photosynthetic mechanisms, but one with less evolutionary potential than the light-driven redox mechanism.

Speculations on the functioning of primitive mechanisms are summarized in Fig. 2. Mauzerall and colleagues (Mauzerall, 1978; Ilani and Mauzerall, 1981; Mercer-Smith and Mauzerall, 1984; Ilani et al., 1989) have explored, over many years, the possible involvement of Chl precursors in such charge transfer reactions. They have also shown that a number of porphyrinogens and porphyrins can carry out rapid vectorial reductions across artificial membranes (Woodle et al., 1987; Ilani et al., 1989). Iron salts might well have been involved as electron acceptors and donors in such systems (Borowska and Mauzerall, 1987) (see Fig. 2A). It has even been suggested that the geologically ancient and abundant Banded Iron Formations may have resulted from abiotic reactions (Cairns-Smith, 1978) as occurs, for instance, when UV radiation acts on ferrous salts to cause reduction of water and the release of hydrogen gas (Borowska and Mauzerall, 1987, 1988). It is also possible that early RCs were harnessed to oxidize ferrous salts and cause the reduction of organic compounds (Borowska and Mauzerall, 1988)(see Fig. 2B) or as a proton pump. Iron may have been the coordinated metal in some of these early RCs, but the poor photoactivity and the strong redox properties of Fe-porphyrins make it much more likely that Mg- or Zn-porphyrins were favored for light (and UV) reactions, and that Fe-porphyrins acted as the intermediary electron carriers from earliest times.

There is now strong evidence for respiration preceding photosynthesis (Castresana and Sarastre, 1995; Castresana, 2001); it is likely that this involved use of nitrates, ferrous salts and a number of other electron sinks, rather than the early use of oxygen on the Earth: since oxygen would have been scarce until photosynthetic oxygen evolution evolved. Nevertheless an important outcome, if this assumption is correct, is that the first photosynthetic organisms could form ATP by a proton motive force mechanism and thus could fix CO_2 by a Rubisco-based or another mechanism (linked to a reductive NAD mechanism as in extant anoxygenic photosynthetic bacteria).

B. Evolution of Modern Reaction Centers

Evolution of the RCs must have led eventually to modern photosynthetic RCs. The crystal structures of the RCI and RCII (Jordan et al., 2001; Zouni et al., 2001; Ferreira et al., 2004) now give abundant evidence for homology between these two RCs. In anoxygenic photosynthetic bacteria no organism has been found with both a RCI and a RCII type of RC, and these organisms are divided into those with a RCI-type and those with a RCII-type mechanism (Baymann et al., 2001; Fyfe et al., 2002). Heterodimers (pairs of similar, but not identical, polypeptides) are a feature of many RCs, including the filamentous photosynthetic bacterium *Cfx. aurantiacus* (Shiozawa et al., 1989). Of the RCI-types, however, two RCIs are homodimeric: *Hbt. chlorum* and *Chlorobium* (*Chl.*) (see Fig. 4). There is strong homology, on the one hand, between the L and M polypeptides of purple bacteria and, on the other, the D1 and D2 polypeptides of PS II (Michel and Deisenhofer, 1988; Baymann et al., 2002). There is also strong homology between the L and M polypeptides of green filamentous photosynthetic bacteria and those of purple bacteria (Ovchinnikof et al., 1988a,b). This suggests that from an early stage, perhaps even before the evolution of BChl *a*/Chl *a*, all RCs are phylogenetically related. It seems reasonable to suggest that the original RC was homodimeric like the RCI-types of *Hbt.* and *Chl.* However, they were probably not at all similar and possibly resembled the RCII-type.

The existence of the special pair may have been an inevitable consequence of the structure of Chl and indeed may have been the reason why the Chls developed their present chemical structure. However, the recent X-ray crystal structures mentioned above illustrate that this may be an over-simplification, since in RCI the special pair turns out to be formed from one molecule of Chl *a* and one molecule of Chl *a´*, whereas in RCII the two Chl molecules involved may not overlap sufficiently to form a special pair (Zouni et al., 2001; Ferreira et al., 2004).

It would be useful if gene sequence analysis could be applied effectively to RCs to ascertain their relationship. However, the long periods of time involved and the degree of divergence (<30% similarity of peptide residues) means that any such inferences would be very weak (Baymann et al., 2001; Xiong et al., 2000). However, the structural information

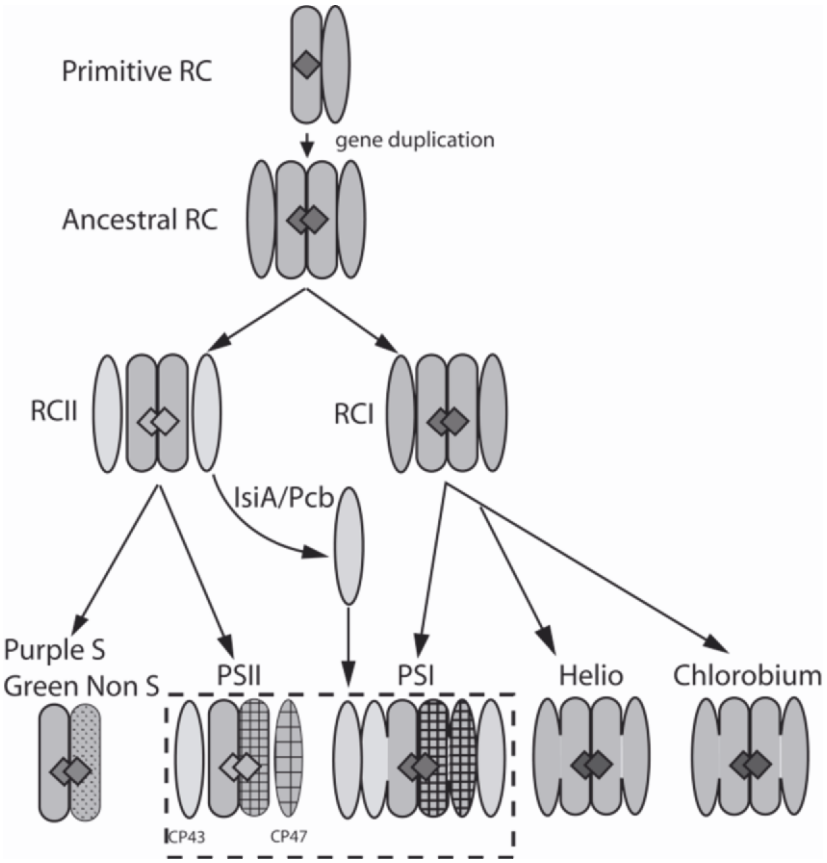

Fig. 4. Outline of the evolution of the ancestral RC and its transition into modern RCs, assuming an early, independent evolution of the six membrane spanning helix antenna protein. Helio, Heliobacteria; isiA, iron stress-induced chlorophyll protein A (CP43´); PCB, prochlorophyte chlorophyll *a/b* binding protein.

concerning homologous polypeptide sequences is very strong (Fyfe et al., 2002). Zhang et al. (2004) have presented evidence that the scheme of Fig. 4 is not correct. In the future it should be possible to incorporate sequence data with specific 3D information of active- or coenzyme-sites and so construct a much more reliable phylogeny. Another untested method is to use the presence or absence of accessory polypeptides; however, none of these avenues of evidence currently add to the debate.

Clearly, gene duplication and differentiation is an important aspect of photosynthetic systems. Most RCs are the result of a gene duplication (see above). It is probable that, initially, each polypeptide acted independently and that the two Chls/BChls of each polypeptide acted as a special pair (van Gorkom, 1987). Gene duplication of the original polypeptide may have been favored because it facilitated the formation of the special pair.

The similar arrangement of the two core RCII polypeptides in both purple photosynthetic bacteria (L and M) and oxygenic phototrophs (D1 and D2) suggests that gene duplication occurred at an early stage. However, the order of these events in the two organisms is undecided (Beanland, 1990; Lockhart et al., 1996b). It might be logical to think that the differentiation of the RC occurred before the separation of these two lines of evolution, but it is possible that the opposite occurred. A more important selection pressure, however, in later stages, but not in the early stage, may have been the need, in the case of RCII, to transfer two electrons, in quick succession, to the tightly-bound primary quinones on each polypeptide, to prevent the decay of the semiquinones (Dutton, 1986). It is tempting to see the two-electron gating mechanism of PS II and the RC of purple bacteria as occurring at this stage but it may have been a later development for protecting the semiquinones from reacting with molecular oxygen generated by the water-splitting system (Ort, 1986). In this case the

situation may be one of convergent evolution, but the gating mechanisms are very similar suggesting that these two gating systems are homologous (Zouni et al., 2001).

It is also interesting to note that there is a quinone (phylloquinone), acting at the electron acceptor site, A_1 of RCI (Jordan et al., 2001). This may suggest that the RCII-type is closer to the ancestral form, in this respect, and gave rise to the RCI-type by the evolution of the secondary FeS acceptors (F_X, F_A and F_B). Such acceptors occur today to varying degrees in extant anoxygenic photosynthetic bacteria with an RCI-type RC (Golbeck, 2003) (Fig. 4). It is possible that only when iron became available in estuarine and oceanic waters in the Proterozoic Eon, due to molecular oxygen liberated by chloroxybacteria (Section III.C), that the FeS acceptor systems became possible. Earlier the RC of *Hbt. chlorum,* called an RC-1q type (Olson and Pierson, 1987) was considered to be a likely early ancestor to RCI and RCII (Vermaas, 1994), and there are proponents of this view today (Gupta et al., 1999; Gupta, 2003). However, the phylogenetic position of *Hbt.* is equivocal (see Section IV.B).

The existence of pheophytin (Phe) and bacteriopheophytin (BPhe) in type II RCs (Michel and Deisenhofer, 1988; Zouni et al., 2001; Chapter 4, Kobayashi et al.) has been a puzzle and could be taken as an indication of an earlier biosynthetic route to Chl via Phe. However, the role of Phe/BPhe as the primary acceptor of the 'special pair' suggests that this role emerged later than that of Chl (in the 'special pair'). It also suggests that a specific mechanism evolved quite early to remove the Mg^{2+} from only the Chl in that specific position and that this mechanism has been conserved. It has to be noted that in PS II, unlike purple sulfur bacteria RC, the Chls of the 'special pair' are relatively far apart and excitonic coupling is weak (Zouni et al., 2001; Fereira et al., 2004). This may be a special adaptation to the need for a more oxidizing redox potential in the RCII (see Section VI.B). It should also be noted that in RCI, the special pair has one Chl *a* and one Chl *a′* (Jordan et al., 2001; Chapter 4, Kobayashi et al.), which requires a special mechanism for the formation of Chl *a′* and its insertion into the special pair.

A summary of the likely events in the evolution of modern RCs is given in the scheme of Fig. 4. It proposes that the ancestral RC of five membrane spanning helices (5 MSHs) was joined by an ancestral light harvesting protein (6 MSHs) which belongs to the family which gave rise to CP43, CP47, IsiA and PCB proteins in Cyanobacteria (La Roche et al., 1996). However, this RC-antenna fusion hypothesis is by no means the universal favorite. Xiong et al. (2000) have proposed that the ancestral protein was an 11 MSH unit (Mulkijanian and Junge, 1997; Baymann et al., 2001), which split later in some organisms to a 5 MSH RC and a 6 MSH antenna (RC antenna fission hypothesis). The latter hypothesis is supported by fewer facts, in that it has to account for the emergence of the 11 MSH protein and the evolutionary developments that led from there to the RCs of extant anoxygenic photosynthetic bacteria and PS I and PS II. Proof of which alternative is most likely should be possible by careful analysis of conserved sequences and conserved geometry among the various RCs.

VI. Evolution of Oxygenic Photosynthesis

A. Evolution of the First Organisms to Evolve Oxygen

As discussed in Section II, the existence of organisms, which split water in photosynthesis is not known from fossilized remains, but can be inferred from chemical 'fossils.' These organisms certainly came from anoxygenic photosynthetic bacteria. However, the relationship of these organisms, which are here called chloroxybacteria (Section II.B), to extant anoxygenic photosynthetic bacteria is not clear (Section V). A clearer picture may emerge from whole genome studies of anoxygenic photosynthetic bacteria, but, as already apparent, much lateral transfer has occurred (Raymond et al., 2002; Rivera and Lake, 2004) and a definitive scheme may be elusive.

The evolution of the ability to split water and evolve oxygen in photosynthesis, driven by the need to provide reducing equivalents for the reduction of CO_2, was the second great innovation in photosynthesis after the invention of the RC. As discussed in Section II, this occurred in chloroxybacteria as early as 3.0 Ga. There are two important considerations: i) how the water splitting apparatus evolved, and ii) how the arrangement of two different photosystems in series came about.

B. Evolution of the Water-Oxidizing Complex

The best working hypothesis for the evolutionary developments that gave rise to water-splitting is still that of Olson (1970): that selective pressure, for the evolution of two populations of photoreactions with

overlapping, but non-identical redox spans, came into play as suitable electron donors (including H_2, H_2S and simple organic compounds) were used up on the early Earth. A crucial point is that there developed a pool of quinone in the photosynthetic membrane of an evolving chloroxybacterium, which could either be reduced or oxidized by adjacent photosystems: the use of quinones, which is quite different in Cyanobacteria from anoxygenic photosynthetic bacteria, still needs explanation (Baymann et al., 2001). It is proposed that consumption of available oxidants in the environment forced the oxidizing end of the proto-PS II (Olson, 1970, 2000; Dismukes et al., 2001) to change to more oxidizing E_h values, oxidizing thereby a range of intermediate compounds and finally able to oxidize water.

Only on the very early Earth, where H_2 and other reducing sources were more readily available, would the opportunity for a great abundance of anoxygenic photosynthetic organisms have occurred, which is in contrast to the relative scarcity of these organisms on the Earth today. This might have been in the period up to 3.5 Ga, after which out-gassing and microbial activity would have considerably reduced earlier levels of H_2, CH_4, H_2S, etc., (Kasting and Siefert, 2002). With the exhaustion of these sources and the oxygenation of environments following the 'invention' of oxygen evolution, these organisms would have been driven to restricted niches in the environment, with later accommodation in a small number of instances to aerobic metabolism. This had implications for a number of associated reactions because of the increased exposure to singlet oxygen and the damage due to reactive oxygen species (Larkum, 2003).

Three proposals have been put forward for compounds that were precursors to water in supplying electrons to RCII: 1) Formate and similar weak oxidants (Olson, 1970); 2) hydrogen peroxide (Blankenship and Hartman, 1998); and 3) bicarbonate (HCO_3^-) (Dismukes et al., 2001).

Almost certainly a number of compounds preceded bicarbonate, although there is no evidence that hydrogen peroxide was ever very abundant. Bicarbonate has merit because it is abundant in seawater (currently ~2 mM) and would have been more concentrated in the past when CO_2 levels were higher (Walker et al., 1983; Rye et al., 1995)]. There is also a well-known bicarbonate effect on PS II (Dismukes et al., 2001) and a putative site for bicarbonate has recently been indicated at the site of oxygen evolution (Ferreira et al., 2004). Furthermore, carbonic anhydrase activity is found associated with PS II (Dismukes et al., 2001; Stemler, 2002) which may well enhance the rate of photosynthesis by speeding up the movement of CO_2 to the stroma (or cytoplasm of chloroxybacteria/Cyanobacteria) (Raven and Beardall, 2003).

The evolution of the Mn-complex, the S-state cycle and the extrinsic polypeptides which modulate the Mn site are all still speculative and will advance rapidly with knowledge of the exact mechanism by which water is split. The current proposal for the water-splitting tetra-manganese complex, which has been the 'holy grail' for photosynthesis workers, is an asymmetric manganese-oxo cubane structure ($CaMn_4O_4$) with three Mn and one Ca in the cubane assemblage, and one Mn displaced to one side (Ferreira et al., 2004). Ideas on how this structure catalyses the splitting of water are still speculative (Dismukes and van Willigen, 2005) and therefore it is difficult to speculate on how this complex evolved. Suggestions in the past have involved a Mn-dependent catalase enzyme (Dismukes, 1996). However, the Ferreira et al. (2004) structure indicates the Mn-Ca complex to be ligated to D1, CP43 and CP47 polypeptides, so a further evolutionary link to another polypeptide is difficult to imagine.

Dismukes et al. (2001) give a scheme for the evolution of water-splitting starting from a conventional green non-sulfur photosynthetic bacterium; Fig. 5 is based on that scheme, with the exception that Chl *a* is considered a possibility in the RC from the beginning, a possible replacement for Chl *d* in the RC.

C. Fusion or Fission Hypotheses for Water Splitting Photosynthesis

As pointed out above, it is attractive to propose that RCI and RCII arose from an ancestral RC, within a single chloroxybacterium (RC Fission Hypothesis)(Olson, 1970, 2000). This hypothesis has the disadvantage that it implies the secondary evolution, from this primitive chloroxybacterium, of anoxygenic photosynthetic bacteria with either RCI or RCII. This hypothesis, although logically compelling, conflicts with our preconceived idea that anoxygenic bacteria preceded chloroxybacteria. For those who hold to the precedence of anoxygenic bacteria, the alternative hypothesis is that two lines evolved, giving rise to the RCI- and RCII-types of modern anoxygenic photosynthetic bacteria; later, fusion of these two into one organism gave rise to chloroxybacteria/Cyanobacteria, which over time

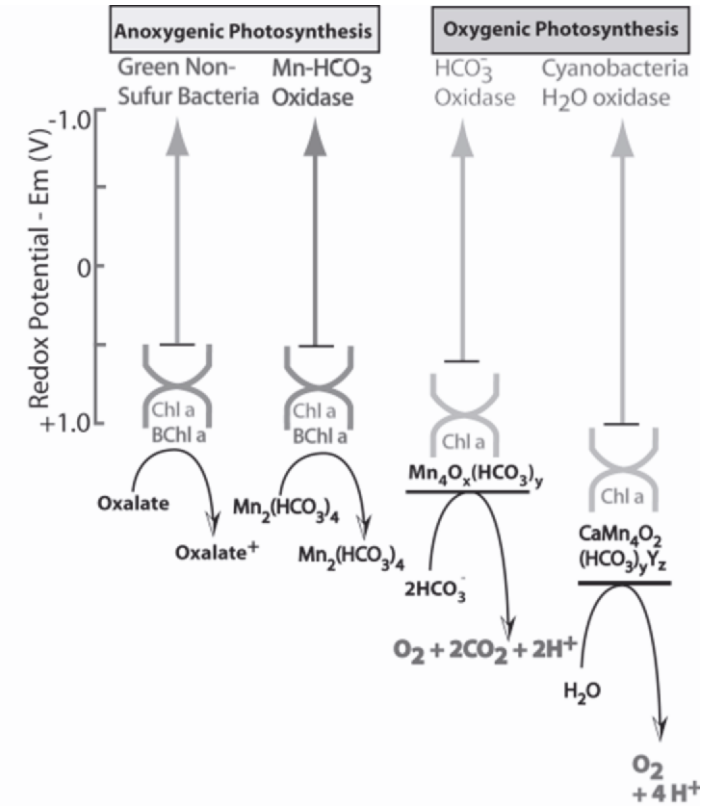

Fig. 5. Possible stages in the evolution of photosynthetic water splitting and oxygen formation. Adapted from Dismukes et al., 2001.

evolved into the modern PS I and PS II (RC Fusion Hypothesis). Olson (1970, 2000) preferred the RC Fission Hypothesis while others have preferred the RC Fusion Hypothesis (Blankenship, 1992; Baymann et al., 2001). Vermaas (1994) suggested that the ancestral RC was close to the *Hbt* RC. It will be seen from Fig. 4 that basically both hypotheses incorporate an ancestral RC, although not necessarily in the form of a *Hbt.*-like RC. With a fission hypothesis at least one fairly difficult lateral transfer is involved (Baymann et al., 2001).

VII. Light-Harvesting Chlorophyll Proteins

In all photosynthetic organisms there is a clear requirement to have a light harvesting mechanism to supply absorbed light energy to the RCs so that the latter can operate at reasonable efficiency. The antenna proteins, which bind the Chl, BChl and other light-harvesting proteins, clearly evolved almost as soon as photosynthesis itself and may be seen as one of the major advances of Chl-based photosynthesis compared to retinal (bacteriorhodopsin)-based photosynthesis. It is perhaps for this reason that the origin of the various light-harvesting Chl/BChl proteins is so obscure.

Chls/BChls are bound to specific proteins in their functional light-harvesting states, but surprisingly these proteins are quite different between the anoxygenic photosynthetic bacteria and the oxygenic photosynthetic organisms (Green, 2003; Green and Parson, 2003). Thus the anoxygenic photosynthetic bacteria have as their principle light harvesting proteins, LH1 and LH2, which bear little similarity to each other (Green and Parson, 2003). The crystal structure of LH2 has been determined at the 2.3 Å resolution (Cogdell et al., 1999). In chloroxybacteria and modern Cyanobacteria an ancient light harvesting antenna has given rise recently to a group of antenna proteins that, under certain circumstances, form a ring around PS I (Bibby et al., 2001, 2003; Boekema et al. 2001; Chen et al., 2005b). In PS II similar proteins form a supramolecular complex attached to dimeric

or quadrimeric PS II units. These antenna proteins bind Chl *a*, and additionally, in prochlorophytes, Chl *b,* and sometimes MgDVP (Larkum et al., 1994), and in *Acc. marina*, Chl *d*. They are recently derived from CP43 (Zhang et al., 2004) but are related to the ancient antenna 6 MSH protein that fused with the 5 MSH RC protein early in the evolution of all extent photosynthetic organisms (Zhang et al., 2004; Section V.B).

In algae and higher plants, another light-harvesting antenna protein occurs: a light-harvesting Chl-binding protein. In green algae, euglenoids and *Chlorarachnion* there is a family of LHC proteins (CAB proteins) that bind Chl *a* and Chl *b* (Durnford, 2003). In Chl *c*-containing algae, a homologous family of proteins bind Chl *a* and Chl *c* (CAC proteins)(Durnford, 2003). In red algae, a small group of homologous LHC proteins bind only Chl *a*, and are only found attached to PS I (Grabowski et al., 2001).

The evolutionary origin of these LHC antenna proteins, which are 3 MSH proteins, appears to be from a single high light-induced protein (HLIP) MSH protein found in cyanobacteria. This HLIP protein, with a homologous single MSH, functions as a Chl carrier protein (Dolganov et al., 1995), but does not function in light-harvesting. In higher plants an early light-inducible protein (ELIP), with two homologous MSHs has been found (Heddad and Adamska, 2000). Thus the 3 MSH LHC antenna may have arisen by two serial gene duplications, via possibly a PsbS-type protein (with 4 MSH)(Larkum, 2003).

Nothing is known of how the IsiA, PCB antenna proteins of some chloroxybacteria/cyanobacteria were replaced by the entirely distinct family of light-harvesting antenna proteins (Green, 2003; Larkum, 2003). It appears to have taken place during the early stages of the symbioses that gave rise to plastids. This is one of the great challenges for understanding evolution of the photosynthetic mechanisms in eukaryotic algae.

VIII. Outlook

The basis on which the evolution of photosynthesis can be assessed will change dramatically in the near future as whole genome studies reveal the genes and gene structure of many of the photosynthetic organisms that lie at the heart of the questions now being asked. Such studies will require new techniques for comparing complex data sets. However, they promise answers to many of the questions posed here. Side by side with these studies will come detailed crystallographic and functional studies of RCs and their ancillary apparatus. And on the broader scale, there will be a growing consensus of the physical and chemical environment of the early Earth, its atmosphere and its oceans: this should prove a crucial tool in deciding the course of past photosynthetic events.

References

Anbar AD and Knoll AH (2002) Proterozoic ocean chemistry and evolution: A bioinorganic bridge? Science 297: 1137–1142

Baymann F, Brugna M, Mühlenhoff U and Nitschke W (2001) Daddy, where did (PS)I come from? Biochim Biophys Acta 1507: 291–310

Beanland TJ (1990) Evolutionary relationship between 'Q–type' photosynthetic reaction centers: Hypothesis testing using parsimony. J Theoret Biol 145: 535–545

Bibby T, Mary I, Nield J and Barber J (2003) Lowlight-adapted *Prochlorococcus* species possess specific antennae for each photosystem. Nature 424: 1051–1054

Bibby TS, Nield J, Partensky F and Barber J (2001) Oxyphotobacteria. Antenna ring around photosystem I. Nature 413: 590

Bjerrum CJ and Canfield DE (2002) Ocean productivity before about 1.9 Gyr ago limited by phosphorus adsorption onto iron oxides. Nature 417: 159–162

Blankenship RE (1992) Origin and early evolution of photosynthesis. Photosynthesis Res 33, 91–111

Blankenship RE (2002) Molecular Mechanisms of Photosynthesis. Blackwell Science Ltd, Oxford

Blankenship RE and Hartman H (1998) The origin and evolution of oxygenic photosynthesis. Trends Biochem Sci 23: 94–97

Borowska Z and Mauzerall D (1987) Efficient near ultraviolet light-induced formation of hydrogen by ferrous hydroxide. Origin Life Evol Biosphere 17: 251–259

Borowska Z and Mauzerall D (1988) Photoreduction of carbon dioxide by aqueous ferrous ions: An alternative to the strongly reducing atmosphere for the chemical origin of life. Proc Natl Acad Sci USA 85: 6577–6580

Brassier MD, Green OR, Jephcoat AP, Kleppe AK, van Kranendonk MJ, Lindsay JF, Steele A and Grassineau NV (2002) Questioning the evidence for Earth's oldest fossils. Nature 416: 76–81

Brockman H Jr and Lipinski A (1983) Bacteriochlorophyll *g*. A new bacteriochlorophyll from *Heliobacterium chlorum*. Arch Mikrobiol 136: 17–25

Brocks JJ, Logan GA, Buick R and Summons RE (1999) Archean molecular fossils and the early rise of eukaryotes. Science 285: 1033–1036

Burke DH, Hearst JE and Sidow A (1993) Early evolution of photosynthesis: Clues from nitrogenase and chlorophyll iron proteins. Proc Natl Acad Sci USA 90: 7134–7138

Cady SS and Pinnavaia TJ (1978) Porphyrin intercalation in mica-type silicates. Inorg Chem 17: 1501–1507

Cairns-Smith AG (1978) Precambrian solution photochemistry,

inverse segregation, and banded iron formations. Nature 276: 807,

Canfield DE and Raiswell, R (1999) The evolution of the sulfur cycle. Amer J Sci 299: 697–723

Castresana J (2001) Comparative genomics and bioenergetics. Biochim. Biophys Acta 1505: 147–162

Castresana J and Sarastre N (1995) Evolution of energetic metabolism: The respiration-early hypothesis. Trends Biochem Sci 20: 443–448

Chen M, Bibby TS, Nield J, Larkum AWD and Barber J (2005a) Iron effect on formation and localization of antenna system binding with chlorophyll *d*. Biochim Biophys Acta 1708: 367–374

Chen M, Telfer A, Lin S, Pascal A, Larkum AWD and Blankenship RE (2005b) The nature of the Photosystem II reaction centre in the chlorophyll *d* containing prokaryote, *Acaryochloris marina*. Photochem Photobiol Sci 4: 1060–1064

Cogdell RJ, Isaacs NW, Howard TD, Mcluskey K, Fraser NJ and Prince SM (1999) How photosynthetic bacteria harvest solar energy. J Bacteriol 181: 3869–3879

Copley SD (2000) Evolution of a metabolic pathway for degradation of a toxic xenobiotic: The patchwork approach. Trends Biochem Sci 25: 261–266

Dismukes GC (1996) Manganese enzymes with binuclear active sites. Chem Rev 96: 2909–2926

Dismukes GC and van Willigen RT (2005) Manganese: The oxygen-evolving complex and models. In: King R (ed) Encyclopedia of Inorganic Chemistry II. Wiley Interscience, in press

Dismukes GC, Klimov VV, Varanov, SV, DasGupta J and Tyryshkin A (2001) The origin of atmospheric oxygen on Earth: The innovation of oxygenic photosynthesis. Proc Natl Acad Sci USA 98: 2170–2175

Dolganov NA, Bhaya D and Grossman AR (1995) Cyanobacterial protein with similarity to the chlorophyll *a/b* binding-protein of higher plants — evolution and regulation. Proc Natl Acad Sci USA 92: 636–640

Douglas SE, Raven JA and Larkum AWD (2003) The algae and their general characteristics. In: Larkum AWD, Douglas SE and Raven JA (eds) Photosynthesis in Algae, pp 1–10. Kluwer Academic Publishers, Dordrecht

Dufresne A, Salanoubat M, Partensky F, Artiguenave F, Axmann I M, Barbe V, Duprat S, Galperin MY, Koonin EV, Le Gall F, Makarova KS, Ostrowski M, Oztas S, Robert C, Rogozin IB, Scanlan DJ, Tandeaau de Marsac N. Weissenbach J, Wincker P, Wolf Y and Hess WR (2003) Genome sequence of cyanobacterium *Prochlorococcus marinus* SS120, a nearly minimal oxyphototrophic genome. Proc Natl Acad Sci USA 100: 10020–10025

Durnford, D (2003) Genes for Chl *a/b* and Chl *a/c* light harvesting proteins. In: Larkum AWD, Douglas Sand Raven JA (eds) Photosynthesis in Algae, pp 63–82, Kluwer Academic Publishers, Dordrecht

Dutton PL (1986) Energy transduction in anoxygenic photosynthesis. In: Staehelin LA and Arntzen CJ (eds) Encyclopedia of Plant Physiology, Photosynthesis III, pp 197–232. Springer-Verlag, Berlin

Eldredge N and Gould SJ (1972) Punctuated equilibria: An alternative to phyletic gradualism. In: Schopf TJM (ed) Models in Paleobiology, pp 82–115. Freeman, Cooper and Co., San Francisco

Ferreira KN, Iverson TM, Maghlaoui K, Barber J and Iwata S (2004) Architecture of the photosynthetic oxygen-evolving center. Science 303: 1831–1838

Fyfe PK, Jones MR and Heathcote P (2002) Insights into the evolution of the antenna domains of Type-I and Type-II photosynthetic reaction centers through homology modeling. FEBS Lett 530: 117–123

Georgopapadakou NH and Scott AI (1977) On B_{12} biosynthesis and evolution. J Theor Biol 69: 381–384

Golbeck JH (2003) The binding of cofactors to Photosystem I analyzed by spectroscopic and mutagenesis methods. Ann Rev Biophys Biomolec Struct 32: 237–256

Gogarten JP, Doolittle WF and Lawrence JC (2002) Prokaryotic evolution in the light of gene transfer. Mol Biol Evol 19: 2226–2238

Gouy M and Li W-P (1989) Phylogenetic analysis based on rRNA sequence supports the archaebacterial rather than eocyte tree. Nature 339: 145–147

Grabowski B, Cunningham FX, and Gantt E (2001) Chlorophyll and carotenoid binding in a simple red algal light-harvesting complex crosses phylogenetic lines. Proc Natl Acad Sci USA 98: 2911–2916

Granick S (1957) Speculations on the origins and evolution of photosynthesis. Ann NY Acad Sci 69: 292– 301

Green BR (2003) The evolution of light-harvesting antennas. In: Green BR and Parson WF (eds) Light Harvesting Antennas in Photosynthesis, pp 129–168. Kluwer Academic Publishers, Dordrecht

Green BR and Parson WF (eds) (2003) Light Harvesting Antennas in Photosynthesis. Kluwer Academic Publishers, Dordrecht

Gupta RS (2003) Evolutionary relationships among photosynthetic bacteria. Photosynth Res 76: 173–183

Gupta RS, Mukhtar T and Singh B (1999) Evolutionary relationships among photosynthetic prokaryote (*Heliobacterium chlorum, Chloroflexus aurantiacus*, cyanobacteria, *Chlorobium tepidum* and proteobacteria): Implication regarding the origin of photosynthesis. Mol Microbiol 32: 893–906

Heddad M and Adamska I (2000) Light stress-regulated two-helix proteins in *Arabidopsis thaliana* related to the chlorophyll *a/b*-binding gene family. Proc Natl Acad Sci USA 97: 3741–3746

Helfrich M, Ross A, King GC, Turner AG and Larkum AWD (1999) Identification of [8-vinyl]-protochlorophyllide *a* in phototrophic prokaryotes and algae: Chemical and spectroscopic properties. Biochim Biophys Acta 1410: 262–272

Hodgson GW and Baker GL (1964) Evidence for porphyrin in the Orgueil meteorite. Nature 202: 125–127

Hodgson GW and Baker GL (1967) Porphyrin abiogenesis from pyrrole and formaldehyde under simulated geochemical conditions. Nature 216: 29–32

Hodgson GW and Ponnamperuma C (1968) Prebiotic porphyrin genesis: Porphyrins from electric discharge in methane, ammonia and water vapour. Proc Natl Acad Sci USA 31: 153–158

Hofmann E, Wrench PM, Sharples FP, Hiller RG, Welte W and Diederichs K (1996) Structural basis of light-harvesting by Carotenoids: Peridinin-Chlorophyll-Protein from *Amphidinium carterae*. Science 272: 1788–1791

Hoober JK and Eggink LL (2001) A potential role of chlorophylls *b* and *c* in assembly of light-harvesting complexes. FEBS Lett 489: 1–3

House CH, Runnegar B and Fitz-Gibbon ST (2003) Geobiological analysis using whole genome-based tree building applied to the

bacteria, Archaea, and Eukarya. Geobiology 1: 15–26
Houssier C and Sauer K (1970) Circular dichroism and magnetic circular dichroism of chlorophyll and protochlorophyllide pigments. J Am Chem Soc 92: 779–790
Hu Q, Miyashita H, Iwasaki I Kurano N, Miyachi S, Iwaki M and Itoh S (1998) A Photosystem I reaction center driven by chlorophyll *d* in oxygenic photosynthesis. Proc Natl Acad Sci USA 95: 13319–13323
Ilani A and Mauzerall D (1981) The potential span of photoredox reactions of porphyrins and chlorophyll at the lipid bilayer-water interface. Biophys J 35: 79–92
Ilani A, Woodle M and Mauzerall D (1989) Photoinduced electron transfer across lipid bilayers containing magnesium octaethylporphyrin. Photochem Photobiol 29: 673–679
Jacobs JM and Jacobs NJ (1984) Protoporphyrinogen oxidation, an enzymatic step in heme and chlorophyll synthesis: Partial characterization of the reaction in plant organelles, and comparison with mammalian and bacterial systems. Arch Biochem Biophys: 229: 312–319
Jermiin LJ, Blankenship RE, Lockhart PJ and Larkum AWD (2001) Phylogenetic reconstruction of ancient photosynthetic lineages using chlorophyll and bacteriochlorophyll biosynthetic genes. In: PS2001: Proceedings 12th International Congress on Photosynthesis, S09–12. CSIRO Publishing, Melbourne (CD-ROM)
Jones OTG (1963) The production of magnesium protoporphyrin monomethyl ester by *Rhodopseudomonas spheroides*. Biochem J 86: 429–435
Jordan P, Fromme P, Witt HT, Klukas O Saenger W and Krauss N. (2001) Three-dimensional structure of cyanobacterial Photosystem I at 2.5 Ångstrom resolution. Nature 411: 909–917
Kasting JF (2001) The rise of atmospheric oxygen. Science 293: 819–820
Kasting JF and Siefert JL (2002) Life and the evolution of Earth's atmosphere. Science 296: 1066–1068
Knoll AH (1999) Paleontology — A new molecular window on early life. Science 285: 1025–1026
Kolber Z.S, Plumley FG, Lang AS, Beatty JT, Blankenship RE, Vandover CL, Vetriani C, Koblizek, M, Cathgeber C and Falkowski P (2001) Contribution of aerobic photoheterotrophic bacteria to the carbon cycle in the ocean. Science 292: 2492–2495
Krasnovsky AA (1971) The evolution of photochemical electron transfer systems. In: Krimball AP and Oro J (eds) Prebiotic and Biochemical Evolution, pp 207–216. North Holland, Amsterdam
Kühl M and Larkum AWD (2001) The microenvironment and photosynthetic performance of *Prochloron* sp. in symbiosis with didemnid ascidians. In: Seckbach J (ed) Symbiosis, pp 273–290. Kluwer Academic Publishers, Dordrecht
Kühl M, Chen M, Ralph P, Schreiber U and Larkum AWD (2005) Niche and photosynthesis of chlorophyll *d*-containing cyanobacteria. Nature 433: 820
Kuhn KF (1998) In Quest of the Universe. Jones and Barlett, Boston
La Roche J, van der Staay GWM, Ducret A, Aebersold R, Li R, Golden SS, Hiller RG, Wrench PM, Larkum AWD and Green BR. (1996) Independent evolution of the prochlorophyte and green plant chlorophyll *a/b* light-harvesting proteins. Proc Natl Acad Sci USA 93: 15244–15248
Lake JA., Clarke MW, Henderson E, Fay SP, Oaks M, Scheinman A, Thornber JP and Mah RA (1985) Eubacteria, Halobacteria, and the origin of photosynthesis: The photocytes. Proc Natl Acad Sci USA 82: 3716–3720
Larkum AWD (1991) The evolution of chlorophylls. In: Scheer H (ed) Chlorophylls, pp 367–383. CRC Press, Boca Raton
Larkum AWD (1992). Evolution of photosynthetic systems. In: Murata (ed) Research in Photosynthesis, Vol III, pp 475–482, Kluwer Academic Publishers, Dordrecht
Larkum AWD (1999) The evolution of algae. In: Seckbach J (ed) Enigmatic Microorganisms and Life in Extreme Environments, pp 31–48. Kluwer Academic Publishers, Dordrecht
Larkum AWD (2003) Light-harvesting systems in algae In: Larkum AWD, Douglas S and Raven JA (eds) Photosynthesis in Algae, pp 277–304. Kluwer Academic Publishers, Dordrecht
Larkum AWD and Barrett J (1983) Light-harvesting systems in algae. Adv Bot Res 10: 1–221
Larkum AWD and Vesk M (2003) Algal plastids: Their fine structure and properties. In: Larkum AWD, Douglas S and Raven JA (eds) Photosynthesis in Algae, pp 11–28. Kluwer Academic Publishers, Dordrecht
Larkum AWD, Scaramuzzi C, Cox GC, Hiller RG and Turner AG (1994) Light-harvesting chlorophyll *c*-like pigment in *Prochloron*. Proc Natl Acad Sci USA 91: 679–683
Lockhart P, Howe CJ, Bryant DA, Beanland TJ and Larkum AWD (1992) Substitutional bias may preclude phylogenetic inference of chloroplast origins. J Mol Evol 34: 153–162
Lockhart PJ, Larkum AWD, Steel MA, Wardell P and Penny D (1996a) Evolution of chlorophyll and bacteriochlorophyll: The problem of invariant sites in sequence analysis. Proc Natl Acad Sci USA 93: 1930–1934
Lockhart PJ, Steel MA and Larkum AWD (1996b) Gene Duplication and the evolution of photosynthetic reaction centers. FEBS Lett 385: 193–196
Margulis LM and Obar R (1985) Heliobacterium and the origin of chrysoplasts. BioSystems, 17: 317–325
Mauzerall D (1960) The condensation of porphobilinogen to uroporphyrinogen. J Am Chem Soc 82: 2605–2609
Mauzerall D (1973) Why chlorophyll? Ann NY Acad Sci 206: 483–494
Mauzerall D (1978) Porphyrins, chlorophyll and photosynthesis. In: Trebst AA and Avron M (eds) Encyclopedia of Plant Physiology, Vol V, pp 117–124. Springer, New York
Mercer-Smith JA and Mauzerall DC (1984) Photochemistry of porphyrins: A model for the origin of photosynthesis. Photochem Photobiol 39: 397–405
Mercer-Smith, JA, Raudino A and Mauzerall DC (1985) A model for the origin of photosynthesis. III The ultraviolet photochemistry of uroporphyrinogen. Photochem Photobiol 42: 239–244
Michel H and Deisenhofer J (1988) Relevance of the photosynthetic reaction center from purple bacteria to the structure of Photosystem II. Biochemistry 27: 1–7
Mimuro M., Akimoto S, Yamazaki I, Miyashita H and Miyachi S (1999) Fluorescence properties of chlorophyll *d*-dominating alga, *Acaryochloris marina*: Studies using time-resolved fluorescence microscopy on whole cells. Biochim Biophys Acta 1412: 37–46
Miyashita H, Ikemoto H, Kurano N, Adachi K, Chilara M and Miyachi S (1996) Chlorophyll *d* as a major pigment. Nature 383: 402
Mulkidjanian AY and Junge W (1997) On the origin of photo-

synthesis as inferred from sequence analysis — a primordial UV-protector as common ancestor of reaction centers and antenna proteins. Photosynth Res 51: 27–42
Olson JM (1970) The evolution of photosynthesis. Science 168: 438–446
Olson JM (1999) Early evolution of chlorophyll-based photosynthesis. Chemtracts 12: 468–482
Olson JM (2000) 'Evolution of photosynthesis' (1970). Re-examined thirty years later. Photosynth Res 68: 95–117
Olson JM and Pierson BK (1987) Evolution of reaction centers in photosynthetic prokaryotes. Int Rev Cytol 108: 209–248
Ort DR (1986) Energy transduction in oxygenic photosynthesis: An overview of structure and mechanism. In: Staehelin LA and Arntzen CJ (eds) Encyclopedia of Plant Physiology, Photosynthesis III, pp 143–196. Springer, Berlin
Oesterhelt D, Tittor J (1989) Two pumps, one principle: Light-driven ion transport in halobacteria. Trends Biochem Sci 14: 57–61
Ovchinnikof YA, Abdulaev NG, Zolotarev AS, Shmukler BE, Zargarov AA, Kutuzov MA, Telezhinskaya TN and Levina NB (1988a) Photosynthetic reaction centre of *Chloroflexus aurantiacus*. 1. Primary structure of the L-subunit. FEBS Lett 231: 237–242
Ovchinnikof YA, Abdulaev NG, Shmukler BE, Zargarov AA, Kutuzov MA, Telezhinskaya TN, Levina NB and Zolotarev AS (1988b) Photosynthetic reaction centre of *Chloroflexus aurantiacus*. Primary structure of the M-subunit. FEBS Lett 232: 364–368
Owen TC and Bar-Nun A (2001) Contributions of icy planetisimals to the Earth's early atmosphere. Origins Life Evol Biosphere 31: 435–458
Palenik B, Brahamsha B, Larimer FW, Land M, Hauser L, Chain P, Lamerdin J, Regala W, Allen EE, McCarren J, Paulsen I, Dufresne A, Partensky F, Webb EA and Waterbury J (2003) The genome of a motile marine *Synechococcus*. Nature 424: 1037–1042
Partensky F and Garczarek L (2003) The photosynthetic apparatus of chlorophyll *b*- and *d*-containing oxyphotobacteria. In: Larkum AWD, Douglas S and Raven JA (eds) Photosynthesis in Algae, pp 29–62. Kluwer Academic Publishers, Dordrecht
Pavlov AA, Hurtgen MT, Kasting JF and Arthur MA (2003) Methane-rich Proterozoic atmosphere? Geology 31: 87–90
Rappé MS and Giovannoni SJ (2003) The unknown microbial majority. Ann Rev Microbiol 57: 369–394
Raven JA (1996) The bigger the fewer: Size, taxonomic diversity and the range of chlorophyll(ide) pigments in oxygen-evolving marine photolithotrophs. J Mar Biol Ass UK 76: 211–217
Raven JA and Beardall J (2003) Carbon acquisition mechanisms of algae: Carbon dioxide diffusion and carbon dioxide concentrating mechanisms. In: Larkum AWD, Douglas S and Raven JA (eds) Photosynthesis in Algae, pp 225–244. Kluwer Academic Publishers, Dordrecht
Raymond J and Blankenship RE (2004) Biosynthetic pathways, gene replacement and the antiquity of life. Geobiology 2: 199–203
Raymond J, Zhaxybayeva O, Gogarten JP, Gerdes SV and Blankenship RE (2002) Whole-genome analysis of photosynthetic prokaryotes. Science 298: 1616–1620
Rivera MC and Lake J (2004) The ring of life provides evidence for a genome fusion origin of eukaryotes. Nature 431: 152–155
Rocap G, Larimer FW, Lamerdin J, Mafattl S, Chain P, Ahigren NA, Areliano A, Coleman M, Hauser L, Hess WR, Johnson ZI, Land M, Lindell D, Post AF, Regala W, Shah M, Shaw SL, Steglich C, Sullivan MB, Ting CS, Tolonen A, Webb EA, Zinser ER and Chisholm SW (2003) Genome divergence in two *Prochlorococcus* ecotypes reflects oceanic niche differentiation. Nature 424: 1042–1047
Runquist JA and Loach PA (1981) Catalysis of electron transfer across phospholipid bilayers by iron-porphyrin complexes. Biochim Biophys Acta 637: 231–244
Rye R, Kuo PH and Holland HD (1995) Atmospheric carbon dioxide concentration before 2.2 billion years ago. Nature 378: 603–605
Schopf JW (1993) Microfossils of the early archean apex chert: New evidence on the antiquity of life. Science 260: 640–646
Shen Y, Knoll AH and Walter MR 2003 Evidence for low sulphate and anoxia in a mid-Proterozoic marine basins. Nature 423: 632–635
Shiozawa JA, Lottspeich F, Osterhelt D and Feick R (1989) The primary structure of *Chloroflexus aurantiacus* reaction center polypeptides. Eur J Biochem 180: 75–84
Simionescu CI, Simionescu BC, Mora R and Leanca M (1978) Porphyrin-like compounds genesis under simulated geochemical conditions. Origins Life Evol Biosphere 9: 103–114
Smith KM (1975) Appendix: Atomic absorption spectra. In: Smith KM (ed) Porphyrins and Metalloporphyrins, p 871. Elsevier, Amsterdam
Smith JHC and Benitez A (1955) Chlorophyll analysis in plant materials. In: Paech K and Travey MV (eds) Modern Methods of Plant Analysis, Vol 4, pp 142–165. Springer, Berlin
Stemler AJ (2002) The bicarbonate effect, oxygen evolution, and the shadow of Otto Warburg. Photosynth Res 73: 177–183
Summons RE, Jahnke LL, Hope JM and Logan GA (1999) 2-Methylhopanoids as biomarkers for cyanobacterial oxygenic photosynthesis. Nature 400: 554–557
Szutka A (1965) Probable synthesis of porphine-like substances during chemical evolution. In: Fox SW (ed) Origin of Prebiological Systems and Their Molecular Matrices, p 245. Academic Press, New York
Ting CS, Rocap G, King J and Chisholm SW (2002) Cyanobacterial photosynthesis in the oceans: The origin and significance of divergent light-harvesting strategies. Trends Microbiol 10: 134–142
Tomitani A, Okada K, Miyashita H, Matthijs HCP, Ohno T and Tanaka A (1999) Chlorophyll *b* and phycobilins in the common ancestor of cyanobacteria and chloroplasts. Nature 400: 159–162
Treibs A (1973) On the chromophores of porphyrin systems. Ann NY Acad Sci 206: 97–115
Van Gorkom HJ (1987) Evolution of photosynthesis. In: Amesz J (ed) Photosynthesis, pp 343–350. Elsevier, Amsterdam
Vermaas WFJ (1994) Evolution of heliobacteria: Implications for photosynthetic reaction center complexes. Photosynth Res 41: 285–294
Walker JGC, Klein C., Schidlowski M, Schopf JW, Stevenson DJ and Walker MR (1983) Environmental evolution of the Archean-early Proterozoic Earth. In: Schopf JW (ed) Earth's Earliest Biosphere, pp 260–290. Princeton University Press, Princeton
Woese CR (1987) Bacterial Evolution. Microbiol Rev 51: 221–271
Woese CR (2002) On the evolution of cells. Proc Natl Acad Sci

USA 99: 8742–8747

Wolfe GR, Cunningham FX, Durnford D, Green BR and Gantt E (1994) Evidence for a common origin of chloroplasts with light-harvesting complexes of different pigmentation. Nature 367: 566–568

Woodle M, Zhang JW and Mauzerall D (1987) Kinetics of charge transfer at the lipid bilayer-water interface on the nanosecond time scale. Biophys J 52: 577– 586

Xiong J and Bauer CE (2002) Complex evolution of photosynthesis. Annu Rev Plant Biol 53: 503–521

Xiong J, Fischer M, Inoue K, Nakahara M and Bauer CE (2000) Molecular evidence for the early evolution of photosynthesis. Science 289: 1724–1729

Zhang Y, Jermiin L and Larkum AWD (2004) Phylogenetic analysis of light-harvesting antenna peptides from plants and bacteria. In: van der Est A and Bruce D (eds) Photosynthesis: Fundamental Aspects and Global Perspectives. Proc. 13th International Congress on Photosynthesis, Montréal, p. 745. International Society of Photosynthesis Research

Zouni A, Witt HT, Kern J, Fromme P, Krauss N, Saenger W and Orth P (2001) Crystal structure of Photosystem II from *Synechococcus elongatus* at 3.8 Ångstrom resolution. Nature 409: 739–743

Chapter 19

The Influence of Protein Interactions on the Properties of the Bacteriochlorophyll Dimer in Reaction Centers

James P. Allen* and JoAnn C. Williams
Department of Chemistry and Biochemistry and Center for the Study of Early Events in Photosynthesis, Arizona State University, Tempe, AZ 85287-1604, U.S.A.

Summary

In anoxygenic photosynthetic bacteria, the primary photochemical process in the conversion of light energy involves the transfer of an electron from a primary electron donor, a bacteriochlorophyll dimer, to a series of electron acceptors in the reaction center. The effects of the surrounding protein on the properties of the bacteriochlorophyll dimer are discussed for three types of interactions: magnesium coordination to histidines, electrostatic interactions with charged amino acid residues, and hydrogen-bonding to the side chains of amino acid residues. Alterations of these interactions through mutagenesis are found to be correlated to changes in the oxidation/reduction midpoint potential, electron spin density, and optical spectra. The correlation is explained using models of the electronic structure of the dimer. The use of mutants in which the energies of different electron transfer states have been manipulated has provided the opportunity to explore the relationship between driving force and rate, the factors controlling the asymmetry of electron transfer, and new electron transfer reactions involving tyrosine residues.

*Author for correspondence, email: jallen@asu.edu

Bernhard Grimm, Robert J. Porra, Wolfhart Rüdiger and Hugo Scheer (eds): Chlorophylls and Bacteriochlorophylls: Biochemistry, Biophysics, Functions and Applications, pp. 283–295.

I. Introduction

In photosynthetic bacteria, light is absorbed in antenna complexes and the energy is transferred to the reaction center, where the primary photochemistry, the creation of a charge-separated state, occurs (Blankenship et al., 1995). The reaction center is an integral membrane protein that was first isolated over thirty years ago from the purple bacterium *Rhodobacter (Rba.) sphaeroides* (reviewed in Feher, 1998). This pigment-protein complex consists of three protein subunits, termed the L, M, and H subunits, and 10 cofactors: 4 bacteriochlorophyll (BChl) *a* molecules, 2 bacteriopheophytin (BPhe) *a* molecules, 2 quinones, a non-heme iron, and a carotenoid (Fig. 1; carotenoid not present). The crystallization and X-ray diffraction analysis of reaction centers from *Blastochloris* (*Blc.*) *viridis* and *Rba. sphaeroides* described in Allen (2004), led to the determination of the three-dimensional structures (Deisenhofer et al., 1985, 1995; Allen et al., 1987; Chang et al., 1991; Ermler et all 1994; McAuley et al., 1999; Camara-Artigas et al., 2002b). The core protein subunits, the L and M subunits, each have 5 transmembrane helices that are related to each other by an approximate two-fold symmetry axis (Feher et al., 1989). The H subunit has one transmembrane helix and a large cytoplasmic domain. The cofactors are divided into two branches that are also related by the two-fold symmetry axis; however, only one branch is active. After excitation of the primary electron donor (P), a BChl dimer, an electron is transferred along the active branch to the secondary quinone. After reduction of $P^{\bullet+}$ by an exogeneous cytochrome c_2 or a tetraheme cytochrome subunit, P can be excited again, leading to the transfer of a second electron to the secondary quinone in a process that is coupled to the uptake of two protons. The quinone carries the electrons and protons to the cytochrome bc_1 complex in a cycle that generates the proton gradients needed for the creation of energy-rich compounds.

The two BChls forming P overlap at the ring A position, and the close distance of 3.5 Å results in them being electronically coupled together, as was shown in some of the earliest spectroscopic measurements of the reaction center (Norris et al., 1971, 1975; Feher et al., 1975). Due to this coupling, the spectral properties of P are distinctive from those of the other tetrapyrroles, allowing experimental characterization of P using both optical and magnetic resonance spectroscopy. In this chapter we review how the combination of these spectroscopic techniques with the alteration of amino acid residues provides a detailed understanding of how the interactions of P with the surrounding protein play a critical role in determining the functional properties of the reaction center. The residue numbering used in this chapter is for the subunits from *Rba. sphaeroides*, although mutations have also been made in *Blc. viridis* and *Rba. capsulatus*.

The protein environment interacts with P in a number of different ways. For example, in wild-type reaction centers, each magnesium of the BChls of P is coordinated to a histidine residue. Another type of direct interaction is hydrogen-bonding between amino acid residues and carbonyl groups on the BChls. The protein surrounding these tetrapyrroles also contributes both electrostatic interactions with polar and charged amino acid residues and largely non-specific hydrophobic interactions with aromatic and aliphatic amino acid residues. This review will focus on the influence of three types of interactions: magnesium coordination, electrostatic interactions involving charged amino acid residues, and hydrogen bonding. Each of these interactions has been altered using mutagenesis and found to result in specific changes in the spectroscopic properties of P (Section II). Some mutations, notably those at Tyr M210 (Jia et al., 1993; Nagarajan et al., 1993), have not been included, as their effects are more complex, involving polar and steric interactions with P as well as other cofactors. The availability of many different mutations that alter specific interactions with P has led to the development of a detailed molecular model of the electronic structure (Section III). Changes in the rates of electron transfer that depend upon the changes in the energy of P and $P^{\bullet+}$ due to these mutations can be modeled using Marcus theory. In addition, the second pathway of cofactors can be activated and new electron transfer reactions can be created by manipulating the energy of the BChls (Section IV).

Abbreviations: BChl – bacteriochlorophyll; *Blc.* – *Blastochloris*; BPhe – bacteriopheophytin; ENDOR – Electron nuclear double resonance spectroscopy; FTIR – Fourier transform infrared spectroscopy; P – bacteriochlorophyll dimer; P_A, P_B – A and B halves, respectively, of the bacteriochlorophyll dimer; *Rba.* – *Rhodobacter*; Y_Z,Y_D – redox active tyrosines of Photosystem II

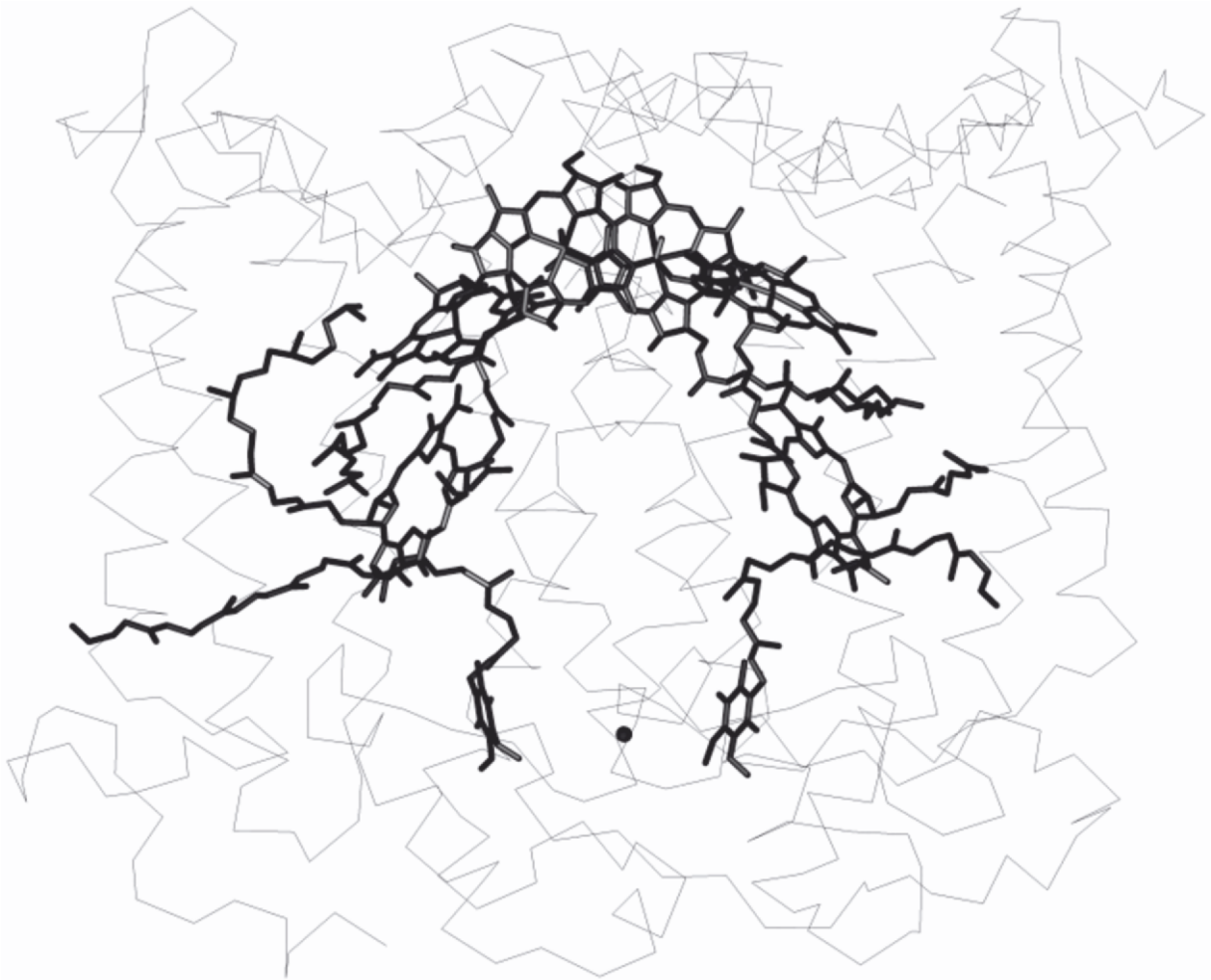

Fig. 1. Three-dimensional structure of the reaction center from the carotenoidless mutant R-26 of *Rba. sphaeroides* showing the backbone of the L and M subunits with 9 cofactors. The active branch of cofactors is on the right. The two-fold symmetry axis of the protein passes approximately in the plane of the paper from P, near the periplamic surface (top of figure), to the non-heme iron (black sphere). Not shown is the H subunit. A carotenoid is present in wild-type strains near the inactive BChl monomer.

II. Protein Interactions that Influence the Properties of the Dimer

A. Coordination to Magnesium and the Heterodimer Mutant

In reaction centers, each central magnesium of the BChls is coordinated with a His residue. Residues His L173 and His M202 ligate to the BChls, P_A and P_B, respectively, that constitute each half of the dimer (Fig. 2). Mutation of His to Leu at either position results in significant changes of the properties of the donor due to incorporation of a BChl-BPhe 'heterodimer' (Bylina and Youvan, 1988; Kirmaier et al., 1988; McDowell et al., 1991; Allen et al., 1996; van Brederode et al., 1999; King et al., 2001). Many spectral changes in these heterodimer mutants are apparent, including a greatly broadened absorption spectrum of P. The initial electron transfer rate slows from approximately 3 ps to 14–18 ps, and the quantum yield drops by approximately a factor of two. However, electrons are still preferentially transferred along the active branch. Many of the observed differences between the heterodimer mutant and wild type arise because the two halves in the heterodimer have much different energies, since BPhe *a* molecules

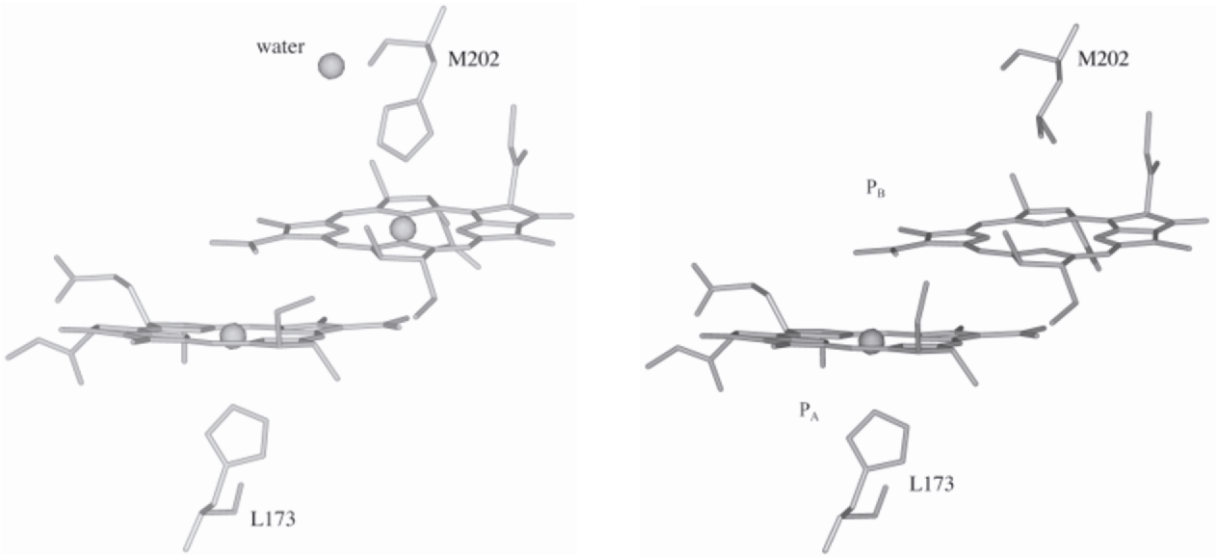

Fig. 2. (Left) Structure of wild-type reaction centers from *Rba. sphaeroides* showing the BChl dimer, coordinating residues His L173 and His M202, and the water molecule that forms a hydrogen bond to the imidazole ring of His M202. (Right) Structure of the heterodimer mutant showing the BChl-BPhe dimer, coordinating residue His L173, and mutated residue Leu M202. The water molecule is lost in this mutant. The two views are approximately down the two-fold symmetry axis of the protein.

are more difficult to oxidize than BChl *a* molecules by approximately 100 mV (Chapters 1, Scheer; 4, Kobayashi et al.; and 23, Steiner and Fowler). Limited changes are observed due to adding a hydrogen bond to the BPhe side of the dimer, in contrast to the alteration of the midpoint potential and spectrum when the BChl side has a hydrogen bond (Allen et al., 1996; Laporte et al., 1996). When glycine replaces His M202, the amino acid ligand to the magnesium is lost, but the properties of the mutant are found to be essentially the same as the wild type. Thus the functional changes of the heterodimer arise from the change in cofactor composition rather than the loss of the His that is presumably replaced by a water molecule (Goldsmith et al., 1996).

The structure of the heterodimer mutant was determined initially to a resolution limit of 3.0 Å and then improved to a resolution of 2.55 Å (Fig. 2) (Chirino et al., 1994; Camara-Artigas et al., 2002a). The electron density maps show that the mutant does indeed contain a BChl-BPhe heterodimer, consistent with the interpretation of the spectroscopic data. The heterodimer is in approximately the same position as the BChl dimer of the wild type. Other structural changes are small except for the loss of a bound water molecule that in the wild type is hydrogen-bonded to both His M202 and the monomer BChl in the active branch of cofactors. The loss of this hydrogen bond may alter the energetics of this monomer BChl and contribute to the observed change in electron transfer rates.

B. Electrostatic Interactions with Charged Amino Acid Residues

The energy of $P^{\bullet+}$ should be sensitive to electrostatic interactions with charged amino acid residues with a dependence that is inversely related to the product of the distance and effective dielectric constant. Electrostatic interactions between P and the protein were investigated by alterations that either insert or remove ionizable residues at several different locations approximately 10–15 Å from P (Fig. 3) (Williams et al., 2001; Johnson and Parson 2002; Johnson et al., 2002). For several of these mutants, the presence of the introduced electrostatic interactions was confirmed by the pH dependence of the $P/P^{\bullet+}$ midpoint potential (Williams et al., 2001; Haffa et al., 2002). The $P/P^{\bullet+}$ midpoint potential was generally found to decrease up to 60 mV due to a negative charge located approximately 10 Å from the donor or increase up to 50 mV due to a positive charge for all of these mutants. These changes in the potential show that the introduced charges are screened with a bulk dielectric constant of approximately 20 that, at a molecular scale, can be more explicitly modeled using an exponential dependence for the dielectric constant. The changes of the midpoint potential of

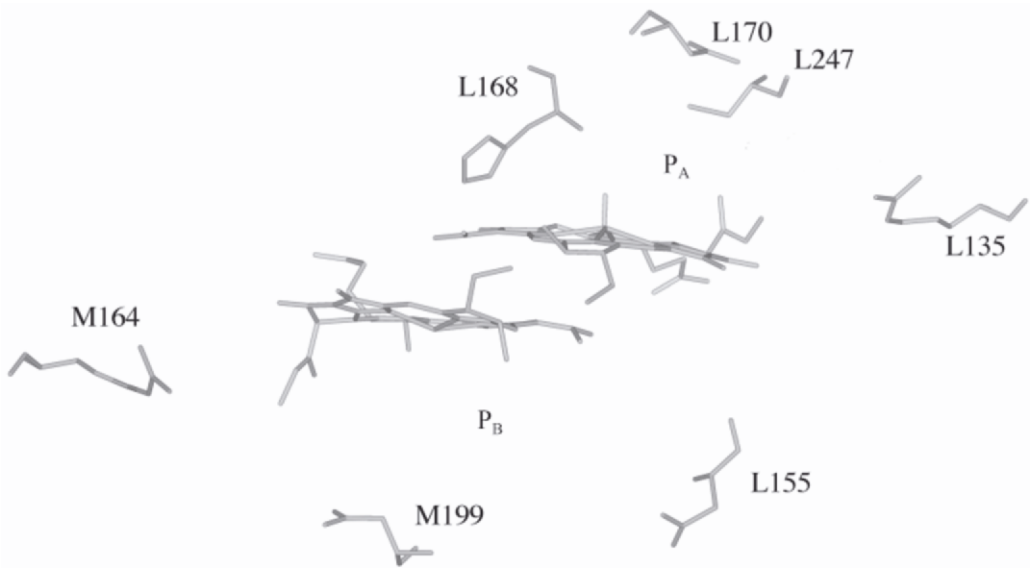

Fig. 3. Structure of reaction centers from *Rba. sphaeroides* showing P with amino acid residues that have been altered to introduce or remove ionizable residues to study the effects of electrostatic interactions with the dimer. Shown are residues Arg L135, Asp L155, His L168, Asn L170, Cys L247, Arg M164, and Asn M199. The view is approximately down the two-fold symmetry axis of the protein.

these mutants are in agreement with electrostatic models, provided that the charges due to the altered amino acid residues are largely screened (Johnson and Parson, 2002).

C. Hydrogen Bonding to the Conjugated Macrocycle

BChl *a* has two positions, the acetyl group of ring A and the oxo carbonyl of ring E, that are part of the conjugated macrocycle and can serve as proton acceptors. To investigate how hydrogen bonds influence the electronic structure of the dimer, mutants were constructed in which the number of hydrogen bonds to these positions was altered (Fig. 4). Wild-type reaction centers have one hydrogen bond between His L168 and the acetyl group of P_A, and this hydrogen bond can be removed by a His to Phe mutation, while the complementary mutation, Phe to His at M197 at the symmetry related residue, introduces a hydrogen bond to the acetyl group of P_B (Stocker et al., 1992; Murchison et al., 1993; Arlt et al., 1996; Spiedel et al., 2002). Histidines introduced at Leu L131 and Leu M160 form hydrogen bonds with the oxo carbonyl groups of P_A and P_B, respectively (Williams et al., 1992). By combinations of these mutations, the number of bonds can be decreased to zero or increased to four (Lin et al., 1994). The gain or loss of a hydrogen bond at each position was measured by use of Fourier transform infrared (FTIR) spectroscopy. For the mutants that were designed to introduce new hydrogen bonds to the oxo carbonyls of P by the substitutions Leu to His at L131 and Leu to His at M160, large frequency downshifts of the vibrational bands assigned to the oxo carbonyl groups were observed (Nabedryk et al., 1993). The gain of a hydrogen bond to the acetyl substitutent of P_B in the phenylalanine to His at M197 mutant and the loss of the hydrogen bond to the acetyl substitutent of P_A in the His to phenylalanine at L168 mutant are clearly evident in the infrared spectra of the primary donor obtained by using Fourier transform Raman spectroscopy (Mattioli et al., 1994). Furthermore, these experiments show that the mutants containing different combinations of these individual mutations also have the designed changes of the hydrogen-bonding pattern.

The most striking effect of the alteration of the hydrogen bonds is the pronounced change in the midpoint potential of P. Oxidation-reduction titrations show that for each mutant that has an additional hydrogen bond, the $P/P^{\bullet+}$ midpoint potential is increased compared to the wild-type value of approximately 500 mV. Removal of the hydrogen bond with the His to Phe mutation at L168 results in a 90 mV decrease in the midpoint potential. These changes in midpoint potential due to hydrogen bonds are additive, as the midpoint potential increases by 60 to 125 mV for each addition of a hydrogen bond from a His residue in every mutant. Due to this additive effect, the midpoint

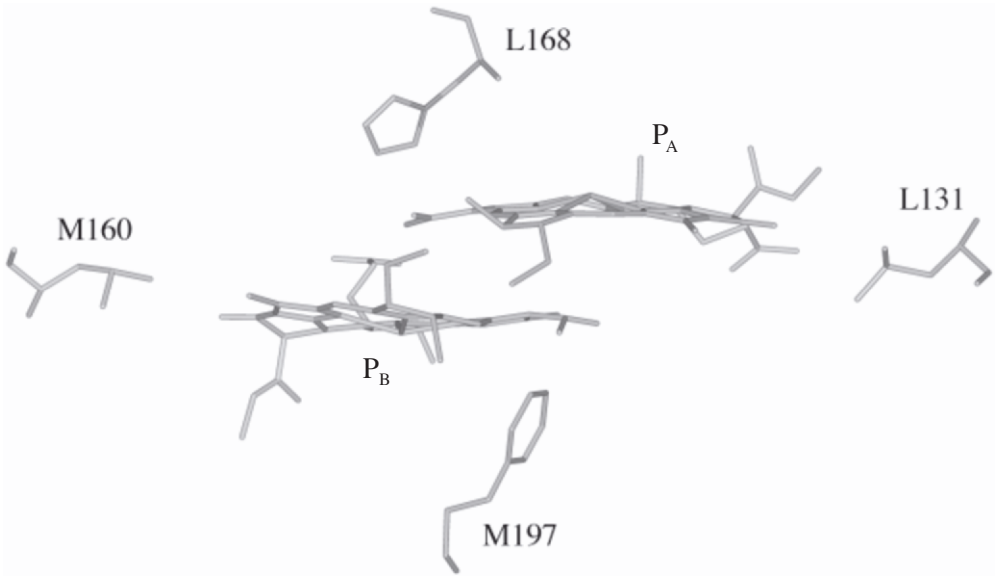

Fig. 4. Structure of wild-type reaction centers from *Rba. sphaeroides* showing the P and residues His L168, Leu L131, Leu M160, and Phe M197. His L168 is hydrogen-bonded to the acetyl group of P_A in wild type, while histidine substitutions at Leu L131, Leu M160, and Phe M197 form hydrogen bonds to P in mutants. The view is approximately down the two-fold symmetry axis of the protein.

potentials systematically ranged from 410 mV for a mutant with no hydrogen bonds up to 765 mV for a mutant that had a total of four hydrogen bonds.

When the single hydrogen bond between His L168 and the acetyl group of P_A in the wild type is removed by replacement of His with Phe, the optical absorption band due to P has a small blueshift in addition to the decrease in the midpoint potential of P (Murchison et al., 1993; Arlt et al., 1996; Spiedel et al., 2002). Structural studies show that the substitution of His L168 with Phe does not alter the overall structure of the protein, and the only significant changes other than the mutation are a 20–27° rotation of the acetyl group and a small displacement of P_A (Fig. 5) (Lancaster et al., 2000; Spiedel et al., 2002). When several amino acid residues were substituted at L168, systematic shifts were observed in the decrease in the $P/P^{\bullet+}$ midpoint potential and blueshift of the P band, with His forming the strongest bond (Spiedel et al., 2002). The structure of a mutant with His residues substituted at L131, M160 and M197 is consistent with these residues serving as hydrogen bond donors with no other significant structural changes near P (Thielges et al., 2005).

III. Modeling the Effect of Protein Interactions on the Electronic Structure of the Dimer

A. Hückel Model

The impact of changes in interactions with the protein on the electronic structure of P can be described with the use of molecular models. For the BChl dimer, the simplest approach to describe the two interacting BChls is in terms of a Hückel molecular orbital model (Fig. 6). In a Hückel model, P is represented as two molecules coupled together to an extent described by the parameter β. The energies of the molecular orbitals that describe the distribution of electrons in the conjugated rings of a dimer are split by 2β. In reaction centers, another term, $\Delta\alpha$, is included because the two BChls in the dimer are energetically inequivalent due to different interactions with the surrounding protein. These different interactions are modeled by poising the two molecules at energies ε_A and ε_B that differ by $\Delta\alpha$. The energy difference between the two molecular orbitals, ΔE, is then given by:

$$\Delta E = \sqrt{\Delta\alpha^2 + 4\beta^2} \tag{1}$$

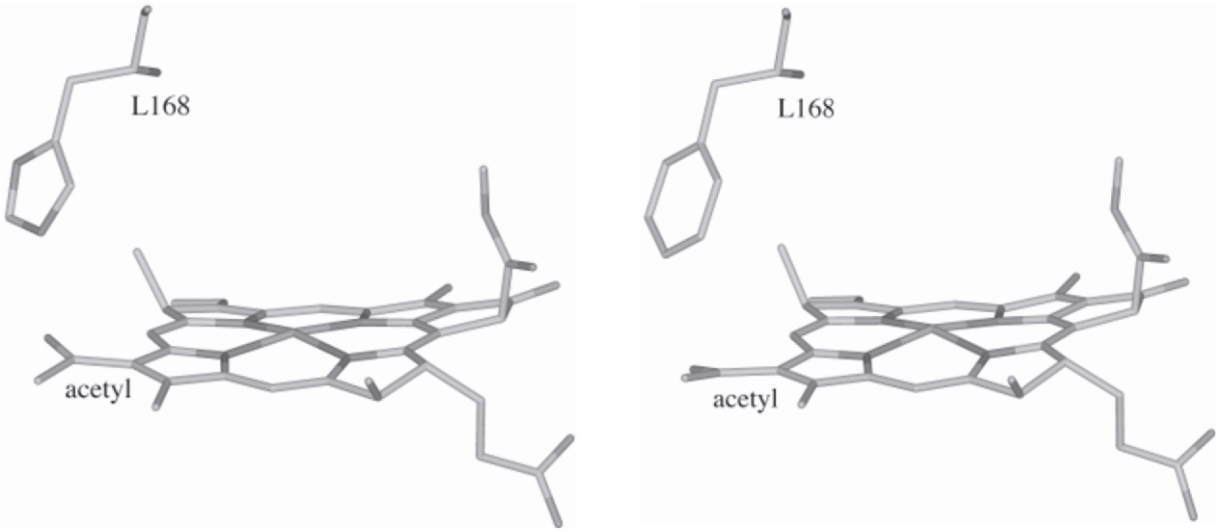

Fig. 5. Structure of reaction centers from *Blc. viridis* showing residue L168 and P_A. Left: In the wild type, His L168 is hydrogen-bonded to the acetyl group of P_A, leading to a slight out-of-plane angle for that group. Right: In the mutant with histidine to phenylalanine at L168, the acetyl group is rotated by 27° compared to the wild type in response to the lack of a hydrogen bond to L168. No other significant differences are evident for the mutant compared to the wild type.

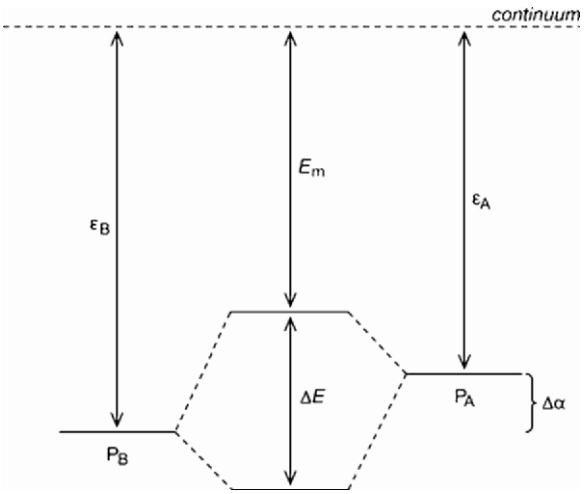

Fig. 6. Hückel model of P. The two halves, P_A and P_B, interact differently with the surrounding protein and have two different energies, ε_A and ε_B, respectively. The difference between these two energies is $\Delta\alpha$. The two halves are coupled together, resulting in two molecular orbitals separated in energy by ΔE. The midpoint potential E_m is the energy required to move an electron from the highest occupied molecular orbital to the continuum.

This approach was utilized to provide a qualitative explanation for a number of features of the electronic structure of P (Breton et al., 1992; Plato et al., 1992; Huber, 1997). The model predicts that on the two molecules, P_A and P_B, the electron spin densities, ρ_A and ρ_B, respectively, will be inequivalent by the ratio:

$$\frac{\rho_A}{\rho_B} = \left[\frac{\Delta\alpha + \Delta E}{2\beta}\right]^2 \tag{2}$$

The $P/P^{\bullet+}$ midpoint potential is determined by the energy of the highest occupied molecular orbital, and so the model makes a specific prediction for the relationship between the midpoint potential E_m and the spin density ratio ρ_A/ρ_B:

$$E_m = -\varepsilon_B - \beta\sqrt{\frac{\rho_A}{\rho_B}} \tag{3}$$

B. Testing the Hückel Model

Several measurements of wild-type reaction centers can be interpreted in terms of the Hückel model, although the parameters β and $\Delta\alpha$ cannot be calculated uniquely from these data. For example, in the FTIR spectrum of wild-type reaction centers, a broad band centered at 2500 cm^{-1}, or equivalently representing a transition with an energy of 320 meV, is assigned as an intervalence charge-transfer band providing a value for ΔE (Breton et al., 1992). Similarly, the spin density ratio ρ_A/ρ_B was determined by electron

nuclear double resonance (ENDOR) spectroscopy to be approximately 0.66 for wild type, yielding an estimate for $\Delta\alpha/\beta$ (Plato et al., 1992).

A test of this molecular model was provided by the substitution of different amino acids at the hydrogen-bonding positions for the BChl dimer. These substitutions were made initially at residue M160 and were then extended to include substitutions at L131 in combination with the M160 mutants (for a total of 25 mutants) (Artz et al, 1997; Müh et al., 2002). This series of mutants all involve changes near the 13^1 oxo group of the BChl, and so the mutations should only alter the energy of P and not lead to any structural rearrangements. Measurements were made of the spin density ratio ρ_A/ρ_B using ENDOR spectroscopy and on the energy difference ΔE using FTIR spectroscopy. In addition, the $P/P^{\bullet+}$ midpoint potential, E_m, was measured for each mutant.

The simple Hückel model qualitatively explains many of the features of the series of hydrogen bond mutants at L131 and M160. Hydrogen bonds to M160 stabilize P_A, making the two halves more asymmetric, whereas changes at L131 stabilize P_B, making the dimer more symmetric (Fig. 6). Because the spin density reflects the asymmetry, the M160 mutants increase the ρ_A/ρ_B spin density ratio while the L131 mutations decrease this ratio. In both cases stabilization results in a higher midpoint potential; that is, a larger amount of energy is required to remove an electron. Changes on the A side have a larger effect on the midpoint potential than changes on the B side because the highest molecular orbital in wild type has a larger contribution from P_A compared to P_B. This model also provides estimates of energies that are consistent with the observed changes for the heterodimer mutant (Artz et al., 1997), although the broadness of the optical spectrum of the heterodimer requires the contribution of charge transfer states (Zhou and Boxer, 1997).

C. Models with Vibrational States and Additional Electronic States

The molecular model provides a simple qualitative description of the effects of different mutations on the properties of the BChl dimer. However, more complete descriptions of the electronic states are required to accurately describe the effects. For example, the reorganization energy associated with charge transfer, λ, is the energy change needed to move a charge from one side of the dimer to the other (Reimers et al., 2000). Large values of this term compared to ΔE would drive the localization of charge and asymmetry of P. Incorporating this term results in modifications of the expressions for ΔE and E_m such that:

$$\Delta E = \sqrt{\left(\Delta\alpha + \lambda\left(\rho_A - \rho_B\right)\right)^2 - 4\beta^2} \tag{4}$$

$$E_m = -\varepsilon_B + \lambda\rho_A^2 - \beta\sqrt{\frac{\rho_A}{\rho_B}} \tag{5}$$

Using this model, analysis of the data for the relationship between the midpoint potential and spin density in the L131 and M160 hydrogen bond mutants provides estimates that the energy associated with the introduction of a hydrogen bond to stabilize a BChl is approximately 100 meV, the coupling β is 120–160 meV, and the reorganization energy λ is 100–200 meV (Müh et al., 2002).

To model the broadness of the optical bands in the near infrared region, it is necessary to include the contribution of vibrational states (Johnson and Parson, 2002). Also contributing to the IR band at 2500 cm^{-1} is a second electronic transition between the second highest occupied molecular orbital and the highest occupied molecular orbital, which is only partially filled in the state $P^{\bullet+}$ (Reimers et al., 2000). Combining the contributions of the two transitions with the use of several vibrational modes results in a greatly improved correspondence between the calculated and experimental optical spectra (Reimers and Hush, 2003) including the Stark spectrum of $P^{\bullet+}$(Treynor et al., 2003). The resulting values of the coupling and reorganization energy are $\beta = 126$ meV and $\lambda = 139$ meV, respectively, with a value of 69 meV for $\Delta\alpha$ in wild type.

IV. The Effect of Protein Interactions on Electron Transfer

A. Free Energy Dependence of Electron Transfer

When the hydrogen-bond mutants are coupled with the electrostatic mutations that lower the midpoint potential of P, mutants with a very wide range of energies are available for spectroscopic study. Associated with each change in $P/P^{\bullet+}$ midpoint potential is a change in various electron transfer rates (Allen and Williams,

1995). Assuming that the change in midpoint potential causes a corresponding change in the free energy difference for these reactions, the correlation between electron transfer rates and midpoint potential can be modeled using Marcus theory (Marcus and Sutin, 1985). Increasing the midpoint potential results in a decrease for the free energy difference between the excited state and the initial charge-separated state. The initial electron transfer rates in these mutants are slower than in the wild type, as expected for the 'normal' region of the Marcus curve. The rates in mutants with lower midpoint potentials than in the wild type are similar to the wild type, indicating that the wild type is not at the top of the Marcus curve (Haffa et al., 2002).

In contrast to the initial electron transfer, the free energy difference for charge recombination increases as the midpoint potential increases. The charge recombination rates from the primary and secondary quinones both increase as the $P/P^{\bullet+}$ midpoint potential increases, which is consistent behavior for the normal region of the Marcus curve even though the charge recombination rate from the primary quinone differs by two orders of magnitude from that of the secondary quinone. Since the primary and secondary quinones are approximately equidistant from P, comparable couplings should be associated with charge recombination, and the rates might be expected to be similar (Moser et al., 1992). The difference in the charge recombination rates from the quinones has been modeled as arising from significantly different reorganization energies (Allen et al., 1998). The charge recombination from the active BPhe is independent of the $P/P^{\bullet+}$ midpoint potential, accounted for by unusual features of the 'inverted' region of the Marcus curve, where the free energy difference is larger than the reorganization energy (Tang et al., 1999).

B. Altering the Pathway of Electron Transfer

In wild-type reaction centers, only one branch of cofactors participates in the primary electron transfer processes (Woodbury and Allen, 1995). Since the heterodimer mutants, which radically alter the energy of each side of the dimer, do not alter the directionality of transfer, the lack of transfer through the other branch cannot be due to specific properties of P. Instead the directionality arises from differences in the energies of the BChl monomers and BPhes, as shown by the use of two mutations that significantly change the energies of these cofactors (Heller et al., 1995; deBoer et al., 2002). The introduction of a His near the active BPhe results in the incorporation of a BChl in this position, and BChl is a much poorer electron acceptor than BPhe (Chapter 2, Senge et al.). The second mutation was the introduction of an aspartic acid near the active BChl monomer. Together the mutations lead to the normally active branch being less unfavorable for electron transfer and a 15% yield for transfer along the other branch. The energies of the different cofactors have been subsequently manipulated by the introduction of arginine and lysine residues near the BChls (Heller et al., 1996; Kirmaier et al., 1999). A mutant with two ionizable amino acid residues introduced asymmetrically into the reaction center results in a pH dependent switch for electron transfer with electron transfer being preferential along the normally active branch at low pH but along the other branch at high pH (Haffa et al., 2003). The directionality has also been investigated by spectroscopic studies of reaction centers whose cofactor composition was modified by biochemical pigment exchange (Scheer and Hartwich, 1995). Reaction centers with different pigments substituting for the BChl monomers and BPhes exhibit changes in the electron transfer rates that probably arise from the changes in the energetics due to the new pigments (Finkele et al., 1992; Arlt et al., 1993; Shkurupatov and Shuvalov 1993).

C. New Electron Transfer Processes in Highly Oxidizing Reaction Centers

For both reaction centers and Photosystem II, light excitation drives the transfer of an electron from an excited donor to quinone acceptors. In the bacterial reaction center, the donor is subsequently reduced by a cytochrome in a cyclic process that forms an electrochemical proton gradient across the membrane. In contrast, Photosystem II oxidizes water using a tyrosine residue as a secondary donor in a four-electron process involving a manganese cluster (Ort and Yocum, 1996). The water-oxidizing ability arises from three critical differences between reaction centers and Photosystem II (Diner and Babcock, 1996). First, the chlorophyll donor absorbs light at 680 nm, and so the light contributes 1.8 V of energy compared to only 1.4 V for bacterial reaction centers that absorb at 865 nm. Second, the chlorophyll donor is an excellent oxidant with a midpoint potential of about 1.1 V compared to only 0.5 V for P. Third, Photosystem II

has an electron transfer pathway involving a tyrosine residue and a manganese cluster that can perform the sequential steps required for conversion of water to molecular oxygen.

The addition of three hydrogen bonds to the BChl dimer results in a midpoint potential of 0.76 V. The addition of the mutation of Tyr to Trp at M210 with these hydrogen-bond mutations results in a midpoint potential of at least 0.8 V (Kálmán et al., 1999). With a midpoint potential of at least 0.8 V, the oxidation of a tyrosine residue will be energetically favorable provided the highly oxidizing reaction centers have an engineered tyrosine that has a potential at the lower end of the estimated 0.7 to 1.0 V range for tyrosyl radicals (Stubbe and van der Donk, 1998). In Photosystem II, two tyrosine radicals that are generated by photochemically-initiated electron transfer reactions, Y_Z and Y_D, have been identified as Tyr 161 of the D1 polypeptide and Tyr 160 of the D2 polypeptide. The residues in bacterial reaction centers that correspond to the positions of the Y_Z and Y_D tyrosine residues of Photosystem II are Arg L135 and Arg M164. Two mutants, designed to examine potential tyrosine oxidation in reaction centers, have tyrosine residues substituted at L135 and M164 along with the three hydrogen-bond mutations and the M210 mutation that result in a very high $P/P^{\bullet+}$ midpoint potential (Kálmán et al., 1999). Residues L135 and M164 are approximately 10 Å from the dimer (Fig. 3), indicating a favorable coupling factor for the electron transfer reaction.

The introduction of the engineered tyrosine residues as secondary donors in the highly oxidizing reaction center results in specific changes in the light-induced absorption and EPR spectra that are consistent with Tyr M164 and Tyr L135 serving as secondary electron donors. In models of Photosystem II, the oxidized tyrosyl Y_Z abstracts both an electron and a proton from the manganese cluster during the S state transitions by which water is oxidized (Tommos and Babcock, 2000). The proton-electron coupling is postulated to provide the necessary driving force required for the oxidization of the manganese cluster in its higher S states. The availability of proton acceptors is a critical factor to generate tyrosyl radicals, as oxidation of tyrosine is energetically unfavorable unless the phenolic proton is released to a proximal base. The influence of the local environment is demonstrated by the pH dependence of tyrosine oxidation in reaction centers (Kálmán et al., 1999; Narváez et al., 2002). The distinctive pH dependence for the formation of the tyrosyl radical can be manipulated by changing the identity of the proton acceptor for the phenolic proton of Tyr M164.

Coupled to Y_Z in Photosystem II is the manganese cluster, which stores the four electron equivalents needed for water oxidation. Wild-type reaction centers are not capable of oxidizing manganese, but the highly oxidizing reaction center can oxidize Mn^{2+} in solution (Kálmán et al., 2003). By introducing a Mn^{2+} binding site into highly oxidizing reaction centers, Mn^{2+} can be bound and serve as an efficient electron donor to P^+ (Thielges et al., 2005).

V. Conclusions

This chapter has presented our current understanding of the influence of protein interactions on the properties of the BChl dimer in reaction centers. Based upon extensive investigations using spectroscopy and mutagenesis, the electronic structure of BChl dimer has been successfully modeled, and the effect of amino acid residues can be predicted. Our knowledge of other photosystems, such as the reaction center from green bacteria, Photosystem I, and Photosystem II, is more limited. Although many detailed differences exist between these complexes, the general features of the bacterial reaction center should serve as a useful framework for understanding the properties of these complexes. For example, the asymmetry of hydrogen bonding of the primary chlorophyll donor in Photosystem I has been modeled using ideas from the simple Hückel model to describe asymmetry in the electronic structure (Jordan et al., 2001). As the arrangement of the primary donor and its interactions with the surrounding protein is obtained for Photosystem II, a molecular understanding of that complex should also emerge. Of particular interest for Photosystem II will be how the structural features of the region forming the primary donor, Y_Z, and the manganese cluster give rise to the ability of this complex to oxidize water, a multi-electron reaction that has been partially mimicked in the bacterial reaction center.

Acknowledgments

The work described from our laboratory is supported by a grant from the National Science Foundation, MCB 0131764.

References

Allen JP (2004) My daily constitutional in Martinsreid. Photosynth Res 80: 157–163

Allen JP and Williams JC (1995) Relationship between the oxidation potential of the bacteriochlorophyll dimer and electron transfer in photosynthetic reaction centers. J Bioenerget-Biomemb 27: 275–283

Allen JP, Feher G, Yeates TO, Komiya H and Rees DC (1987) Structure of the reaction center from *Rhodobacter sphaeroides* R-26: the cofactors. Proc Natl Acad Sci USA 84: 5730–5734

Allen JP, Artz K, Lin X, Williams JC, Ivancich A, Albouy D, Mattioli TA, Fetsch A, Kuhn M and Lubitz W (1996) Effects of hydrogen bonding to a bacteriochlorophyll-bacteriopheophytin dimer in reaction centers from *Rhodobacter sphaeroides*. Biochemistry 35: 6612–6619

Allen JP, Williams JC, Graige MS, Paddock ML, Labahn A, Feher G and Okamura MY (1998) Free energy dependence of the direct charge recombination from the primary and secondary quinones in reaction centers from *Rhodobacter sphaeroides*. Photosynth Res 55: 227–233

Arlt T, Schmidt S, Kaiser W, Lauterwasser C, Meyer M, Scheer H and Zinth W (1993) The accessory bacteriochlorophyll ; a real electron carrier in primary photosynthesis. Proc Natl Acad Sci USA 90: 11757–11761

Arlt T, Bibikova M, Penzkofer H, Oesterhelt D and Zinth W (1996) Strong acceleration of primary photosynthetic electron transfer in a mutated reaction center of *Rhodopseudomonas viridis*. J Phys Chem 100: 12060–12065

Artz K, Williams JC, Allen JP, Lendzian F, Rautter J and Lubitz W (1997) Relationship between the oxidation potential and electron spin density of the primary electron donor in reaction centers from *Rhodobacter sphaeroides*. Proc Natl Acad Sci USA 94: 13582–13587

Blankenship RE, Madigan MT, and Bauer CE (eds) (1995) Anoxygenic Photosynthetic Bacteria. Kluwer Academic Publishers, Dordrecht

Breton J, Nabedryk E and Parson WW (1992) A new infrared electronic transition of the oxidized primary donor in bacterial reaction centers: A way to access resonance interactions between the bacteriochlorophylls. Biochemistry 31: 7503–7510

Bylina EJ and Youvan DC (1988) Directed mutations affecting spectroscopic and electron transfer properties of the primary donor in photosynthetic reaction center. Proc Natl Acad Sci USA 85: 7226–7230

Camara-Artigas A, Magee C, Goetsch A and Allen JP (2002a) The structure of the heterodimer reaction center from *Rhodobacter sphaeroides* at 2.55 Å resolution. Photosynth Res 74: 87–93

Camara-Artigas A, Brune D and Allen JP (2002b) Interactions between lipids and bacterial reaction centers determined by protein crystallography. Proc Natl Acad Sci USA 99: 11055–11060

Chang CH, El-Kabbani O, Tiede D, Norris J and Schiffer M (1991) Structure of the membrane-bound protein photosynthetic reaction center from *Rhodobacter sphaeroides*. Biochemistry 30: 5352–5360

Chirino AJ, Lous EJ, Huber M, Allen JP, Schenck CC, Paddock ML, Feher G and Rees DC (1994) Crystallographic analyses of site-directed mutants of the photosynthetic reaction center from *Rhodobacter sphaeroides*. Biochemistry 33: 4584–4593

DeBoer AL, Neerken S, de Wijn R, Permentier HP, Gast P, Vijgenboom E and Hoff AJ (2002) B-branch electron transfer in reaction centers of *Rhodobacter sphaeroides* assessed with site-directed mutagenesis. Photosynth Res 71: 221–239

Deisenhofer J, Epp O, Miki K, Huber R and Michel H (1985) Structure of the protein subunits in the photosynthetic reaction centre of *Rhodopseudomonas viridis* at 3 Å resolution. Nature 318: 618–624

Deisenhofer J, Epp O, Sinning I and Michel H (1995) Crystallographic refinement at 2.3 Å resolution and refined model of the photosynthetic reaction centre from *Rhodopseudomonas viridis*. J Mol Biol 246: 429–457

Diner BA and Babcock GT (1996) Structure, dynamics, and energy conversion efficiency in Photosystem II. In: Ort DR and Yocum CF (eds) Oxygenic Photosynthesis: The Light Reaction, pp 213–247. Kluwer Academic Publishers, Dordrecht

Ermler U, Fritzsch G, Buchanan SK and Michel H (1994) Structure of the photosynthetic reaction centre from *Rhodobacter sphaeroides* at 2.65 Å resolution: Cofactors and protein-cofactor interactions. Structure 2: 925–936

Feher G (1998) Three decades of research in bacterial photosynthesis and the road leading to it: A personal account. Photosynth Res 55: 1–40

Feher G, Hoff AJ, Isaacson RA and Ackerson LC (1975) ENDOR experiments of chlorophyll and bacteriochlorophyll in vitro and in the photosynthetic unit. Ann NY Acad Sci 244: 239–259

Feher G, Allen JP, Okamura MY and Rees DC (1989) Structure and function of bacterial photosynthetic reaction centres. Nature 339: 111–116

Finkele U, Lauterwasser C, Struck A, Scheer H and Zinth W (1992) Primary electron transfer kinetics in bacterial reaction centers with modified bacteriochlorophylls at the monomeric sites B_{AB}. Proc Natl Acad Sci USA 89: 9514–9518

Goldsmith JO, King B and Boxer SG (1996) Mg coordination by amino acid side chains is not required for assembly and function of the special pair in bacterial photosynthetic reaction centers. Biochemistry 35: 2421–2428

Haffa ALM, Lin S, Katilius E, Williams JC, Taguchi AKW, Allen JP and Woodbury MW (2002) The dependence of the initial electron-transfer rate on driving force in *Rhodobacter sphaeroides* reaction centers. J Phys Chem B 106: 7376–7384

Haffa ALM, Lin S, Williams JC, Taguchi AKW, Allen JP and Woodbury NW (2003) High yield of long-lived B-side charge separation at room temperature in mutant bacterial reaction centers. J Phys Chem B 107: 12503–12510

Heller BA, Holten D and Kirmaier C (1995) Control of electron transfer between the L- and M-sides of photosynthetic reaction centers. Science 269: 940–945

Heller BA, Holten D and Kirmaier C (1996) Effects of Asp residues near the L-side pigments in bacterial reaction centers. Biochemistry 35: 15418–15427

Huber M (1997) On the electronic structure of the primary electron donor in bacterial photosynthesis — the bacteriochlorophyll dimer as viewed by EPR/ENDOR methods. Photosynth Res 52: 1–26

Kálmán L, LoBrutto R, Williams JC and Allen JP (2003) Manganese oxidation by modified reaction centers from *Rhodobacter sphaeroides*. Biochemistry 42: 11016–11022

Jia Y, DiMagno TJ, Chan C-K, Wang Z, Du M, Hanson DK, Schiffer M, Norris JR, Fleming GR and Popov MS (1993) Primary charge separation in mutant reaction centers of *Rhodobacter capsulatus.* J Phys Chem 97: 13180–13191

Johnson ET and Parson WW (2002) Electrostatic interactions in an integral membrane protein. Biochemistry 41: 6483–6494

Johnson ET, Müh F, Nabedryk E, Williams JC, Allen JP, Lubitz W, Breton J and Parson WW (2002) Electronic and vibronic coupling of the special pair of bacteriochlorophylls in photosynthetic reaction centers from wild-type and mutant strains of *Rhodobacter sphaeroides.* J Phys Chem B 106: 11859–11869

Jordan P, Fromme P, Witt HT, Klukas O, Saenger W and Krauss N (2001) Three-dimensional structure of cyanobacterial Photosystem I at 2.5 Å resolution. Nature 411: 909–917

Kálmán L, LoBrutto R, Allen JP and Williams JC (1999) Modified reaction centres oxidize tyrosine in reactions that mirror Photosystem II. Nature 402: 696–699

King BA, de Winter A, McAnaney TB and Boxer SG (2001) Excited state energy transfer pathways in photosynthetic reaction centers. 4. Asymmetric energy transfer in the heterodimer mutant. J Phys Chem B 105: 1856–1862

Kirmaier C, Holten, D, Bylina EJ and Youvan DC (1988) Electron transfer in a genetically modified bacterial reaction center containing a heterodimer. Proc Natl Acad Sci USA 85: 7562–7566

Kirmaier C, Weems D and Holten D (1999) M-side electron transfer in reaction center mutants with a lysine near the nonphotoactive bacteriochlorophyll. Biochemistry 38: 11516–11530

Lancaster CRD, Bibikova MV, Sabatino P, Oesterhelt D and Michel H (2000) Structural basis of the drastically increased initial electron transfer rate in the reaction center from a *Rhodopseudomonas viridis* mutant described at 2.00-Å resolution. J Biol Chem 275: 39364–39368

Laporte LL, Palanliappan V, Davis DG, Kirmaier C, Schenck CC, Holten D and Bocian DF (1996) Influence of electronic asymmetry on the spectroscopic and photodynamic properties of the primary electron donor in the photosynthetic reaction center. J Phys Chem 100: 17696–17707

Lin X, Murchison HA, Nagarajan V, Parson WW, Allen JP and Williams JC (1994) Specific alteration of the oxidation potential of the electron donor in reaction centers from *Rhodobacter sphaeroides*. Proc Natl Acad Sci USA 91: 10265–10269

Marcus RA and Sutin N (1985) Electron transfers in chemistry and biology. Biochim Biophys Acta 811: 265–322

Mattioli TA, Williams JC, Allen JP and Robert B (1994) Changes in primary donor hydrogen-bonding interactions in mutant reaction centers from *Rhodobacter sphaeroides*: Identification of the vibrational frequencies of all conjugated carbonyl groups. Biochemistry 33: 1636–1643

McAuley KE, Fyfe PK, Ridge JP, Isaacs NW, Cogdell RJ and Jones MR (1999) Structural details of an interaction between cardiolipin and an integral membrane protein. Proc Natl Acad Sci USA 96: 14706–14711

McDowell LM, Gaul D, Kirmaier C, Holten D and Schenck CC (1991) Investigation into the source of electron transfer asymmetry in bacterial reaction centers. Biochemistry 30: 8315–8322

Moser CC, Keske JM, Warncke K, Farid RS and Dutton PL (1992) Nature of biological electron transfer. Nature 355: 796–799

Müh F, Lendzian F, Roy M, Williams JC, Allen JP and Lubitz W (2002) Pigment-protein interactions in bacterial reaction centers and their influence on oxidation potential and spin density distribution of the primary donor. J Phys Chem B 106: 3226–3236

Murchison HA, Alden RG, Allen JP, Peloquin JM, Taguchi AKW, Woodbury NW and Williams JC (1993) Mutations designed to modify the environment of the primary electron donor of the reaction center from *Rhodobacter sphaeroides*: Phenylalanine to leucine at L167 and histidine to phenylalanine at L168. Biochemistry 32: 3498–3505

Nabedryk E, Allen JP, Taguchi AKW, Williams JC, Woodbury NW and Breton J (1993) Fourier transform infrared study of the primary electron donor in chromatophores of *Rhodobacter sphaeroides* with reaction centers genetically modified at residues M160 and L131. Biochemistry 32: 13879–13885

Nagarajan V, Parson WW, Davis D and Schenck CC (1993) Kinetics and free energy gaps of electron-transfer reactions in *Rhodobacter sphaeroides* reaction centers. Biochemistry 32: 12324–12336

Narváez AJ, Kálmán L, LoBrutto R, Allen JP and Williams JC (2002) Influence of the protein environment on the properties of a tyrosyl radical in reaction centers from *Rhodobacter sphaeroides*. Biochemistry 41: 15253–15258

Norris JR, Uphaus RA, Crespi HL and Katz JJ (1971) Electron spin resonance of chlorophyll and the origin of signal I in photosynthesis. Proc Natl Acad Sci USA 68: 625–628

Norris JR, Scheer H and Katz JJ (1975) Models for antenna and reaction center chlorophylls. Ann NY Acad Sci 244: 625–628

Ort DR and Yocum CF (eds) (1996) Oxygenic Photosynthesis: The Light Reactions, Kluwer Academic Publishers, Dordrecht

Plato M, Lendzian F, Lubitz W and Möbius K (1992) Molecular orbital study of electronic asymmetry in primary donors of bacterial reaction centers. In: Breton J and Vermeglio A (eds) The Photosynthetic Bacterial Reaction Center II: Structure, Spectroscopy, and Dynamics, pp 109–118. Plenum, New York

Reimers JR and Hush NS (2003) Modelling the bacterial photosynthetic reaction centre: VII. Full simulation of the intervalence hole-transfer absorption spectrum of the special-pair radical cation. J Chem Phys 119: 3262–3277

Reimers JR, Hughes JM and Hush NS (2000) Modeling the bacterial photosynthetic reaction center 3: Interpretation of effects of site-directed mutagenesis on the special-pair midpoint potential. Biochemistry 39: 16185–16189

Scheer H and Hartwich G (1995) Bacterial reaction centers with modified tetrapyrrole chromophores. In: Blankenship RE, Madigan MT and Bauer CE (eds) Anoxygenic Photosynthetic Bacteria, pp 649–663. Kluwer Academic Publishers, Dordrecht

Shkurupatov AY and Shuvalov VA (1993) Electron transfer in pheophytin *a*-modified reaction centers from *Rhodobacter sphaeroides* R-26. FEBS Lett 322: 168–172

Spiedel D, Roszak AW, McKendrick K, McAuley KE, Fyfe PK, Nabedryk E, Breton J, Robert B, Cogdell RJ, Isaacs NW and Jones MR (2002) Tuning the optical and electrochemical properties of the primary donor bacteriochlorophylls in the reaction centre from *Rhodobacter sphaeroides*: Spectroscopy and structure. Biochim Biophys Acta 1554: 75–93

Stocker JW, Taguchi AKW, Murchison HA, Woodbury NW and Boxer SG (1992) Spectroscopic and redox properties of sym1 and (M)F195H: *Rhodobacter capsulatus* reaction center symmetry mutants which affect the initial electron donor. Biochemistry 31, 10356–10362

Stubbe J and van der Donk WA (1998) Protein radicals in enzyme catalysis. Chem Rev 98: 705–762

Tang CK, Williams JC, Taguchi AKW, Allen JP and Woodbury NW (1999) $P^{+}H_{A}^{-}$ charge recombination reaction rate constant

in *Rhodobacter sphaeroides* reaction centers is independent of the P/P^+ midpoint potential. Biochemistry 38: 8794–8799

Thielges MT, Uyeda GH, Cámara-Artigas A, Kálmán L, Williams JC and Allen JP (2005) Design of a redox-linked active metal site: Manganese bound to bacterial reaction centers at a site resembling that of Photosystem II. Biochemistry 44: 7389–7394

Tommos C and Babcock GT (2000) Proton and hydrogen currents in photosynthetic water oxidation. Biochim Biophys Acta 1458: 199–219

Treynor TP, Andrews SS and Boxer SG (2003) Intervalence band Stark effect of the special pair radical cation in bacterial photosynthetic reaction centers. J Phys Chem B 107: 11230–11239.

van Brederode ME, van Stokkum IHM, Katilius E, van Mourik F, Jones MR and van Grondelle R (1999) Primary charge separation routes in the BChl:Bphe heterodimer reaction centers of *Rhodobacter sphaeroides*. Biochemistry 38: 7545–7555

Williams JC, Alden RG, Murchison HA, Peloquin JM, Woodbury NW and Allen JP (1992) Effects of mutations near the bacteriochlorophylls in reaction centers from *Rhodobacter sphaeroides*. Biochemistry 31: 11029–11037

Williams JC, Haffa ALM, McCulley JL, Woodbury NW and Allen JP (2001) Electrostatic interactions between charged amino acid residues and the bacteriochlorophyll dimer in reaction centers from *Rhodobacter sphaeroides*. Biochemistry 40: 15403–15407

Woodbury NW and Allen JP (1995) The pathway, kinetics and thermodynamics of electron transfer in wild type and mutant reaction centers of purple nonsulfur bacteria. In: Blankenship RE, Madigan MT and Bauer CE (eds) Anoxygenic Photosynthetic Bacteria, pp 527–557. Kluwer Academic Publishers, Dordrecht

Zhou H and Boxer SG (1997) Charge resonance effects on electronic absorption line shapes: Application to the heterodimer absorption of bacterial photosynthetic reaction centers. J Phys Chem B 101: 5759–5766

Chapter 20

Magic Angle Spinning Nuclear Magnetic Resonance of the Chlorosomes

Ido de Boer and Huub J. M. de Groot*
Leiden Institute of Chemistry, Einsteinweg 55, P.O. Box 9502, 2300 RA Leiden, The Netherlands

Summary

Chlorosomes, the oblong light-harvesting bodies of green photosynthetic bacteria, are attached to the inner side of the cytoplasmic membrane. Magic Angle Spinning Nuclear Magnetic Resonance (MAS NMR) was used to study isotopically labeled chlorosomes and in vitro model compounds. Using uniform isotope labeling of chlorophyll molecules, 2D and 3D MAS NMR dipolar correlation spectroscopy was performed in high magnetic field. The chemical shifts provided invaluable information about the structure via ring current effects, while long range correlations were generated that lead to intermolecular distance constraints. Novel methodology was developed and implemented using a Chl *a*/H_2O aggregate, and a structural arrangement of bilayers of Chl sheets with interdigitating tails was resolved. Application of this technology to chlorosomes and BChl *c* aggregates provided unambiguous evidence that self-organization of BChl *c* is the principal structural factor in establishing the rod elements in chlorosomes. This confirms that proteins do not play an essential role in the light harvesting function, which is of fundamental biological interest. Finally, MAS NMR leads to a bilayer model for the tubular supra-structure of sheets of BChl *c* in the chlorosomes of *Chlorobium tepidum*.

Note: Readers are encouraged to visit the website (http://epub.ub.uni-muenchen.de/archive/00000776/) for 'supplementary material,' where Figs. S1–S2 referred to in the text are posted.

I. Introduction

Chlorosomes are found in photosynthetic green bacteria as ellipsoid vesicles of about 100–300 nm in length attached to the inner surface of the cytoplasmic membrane, where they provide a large cross-section for the absorption of sunlight (Blankenship et al., 1995; Olson, 1998). The chlorosomes contain rod-shaped elements of 5 nm in diameter for *Chloroflexus* (*Cfl.*) and 10 nm for *Chlorobium* (*Chl.*)

*Author for correspondence, email: groot_h@chem.leidenuniv.nl

Bernhard Grimm, Robert J. Porra, Wolfhart Rüdiger and Hugo Scheer (eds): Chlorophylls and Bacteriochlorophylls: Biochemistry, Biophysics, Functions and Applications, pp. 297–307.

as visualized by electron microscopy (Staehelin et al., 1978, 1980). The assumption that the rods are formed by protein-pigment complexes, as found in other photosynthetic elements, has been challenged by increasing evidence that self-organized bacteriochlorophyll (BChl) *c* is responsible for the shape and function of the antennae. The crucial evidence is that the in vitro aggregation of BChl *c* leads to similar structures and spectroscopic properties as occur in the natural system (for review, see Tamiaki et al., 2002). Small-angle neutron scattering studies have indicated cylindrical shaped micelles for aggregates prepared in organic media (Worcester et al., 1986). In addition, various spectroscopic methods suggest a highly ordered structure of both aggregated BChl *c* and the chlorosomes (Griebenow et al., 1991; Matsuura et al., 1993; Hildebrandt et al., 1994). Molecular modeling has also been used to explain the structural features of the cylindrical micelles (Holzwarth and Schaffner, 1994). For the chlorosomes, an intermolecular bonding network has been proposed, where the 3^1-hydroxy group of BChl *c* coordinates to the central metal of a neighboring BChl *c* molecule and also hydrogen bonds with the 13^1 carbonyl-oxygen of yet another BChl molecule (Holzwarth and Schaffner, 1994; Chiefari et al., 1995).

In the past, NMR has contributed significantly to the study of chlorophyll chemistry, which was reviewed extensively (Abraham and Rowan, 1991). Two different routes have been worked out to use NMR data for structure determination in uniformly ^{13}C-labeled chlorophylls. Firstly, the chemical shift assignment obtained from correlation experiments can provide information about the spatial structure. This is consistent with the early analyses of the stacking in small chlorophyll aggregates from ring current shifts (Abraham and Rowan, 1991). In particular, ^{1}H aggregation shifts are important for the purpose of structure determination. The chemical shift of ^{1}H is relatively insensitive to electronic perturbations, while shifts induced by ring currents are large on the ^{1}H shift scale of 10–15 ppm. In a similar way, the ring current shifts are indispensable for structure elucidation in the solid state. Secondly, structural information in the solid state may be obtained from the measurement of distance restraints revealing close contacts between molecular moieties.

In this Chapter, recent progress in resolving the nature of the chlorosomal antennae that has been acquired by magic angle spinning (MAS) NMR studies is discussed. The structure elucidation strategy using a chlorophyll (Chl) *a*/H_2O model system is summarized and the MAS NMR investigations of the chlorosomes are reviewed. It has been found that the chlorosomes consist mainly of aggregated BChl that is indistinguishable from BChl *c* precipitated from hexane. Based on MAS NMR experiments, a bilayer tube model for the chlorosomes has been proposed.

II. Aggregated Hydrated Chlorophyll (Chl *a*/H_2O) as a Model for Magic Angle Spinning Nuclear Magnetic Resonance Technology Development

Much of the MAS NMR methodology was first tested using a Chl *a*/H_2O aggregate and then applied in a second step to study the structure of the chlorosomes. The Chl *a*/H_2O aggregate is very suitable to develop and evaluate novel pulse sequences. As a moderately-sized molecular system, it represents an intermediate between small model compounds, such as the tyrosine HCl salt, that are frequently used for a demonstration of principles of pulse techniques, and larger systems of genuine biological interest. The chemical structure of Chl *a* is depicted in Fig. 1. The aggregation of Chl *a* and the Chl-water interaction in Chl *a*/H_2O micelles has been extensively studied in the past (Katz et al., 1991). Chl *a* can only form solid aggregates by incorporation of H_2O, which is believed to coordinate the central magnesium atom and form hydrogen bonds with the carbonyl functions of surrounding molecules. Recent MAS NMR results suggest a close homology between the structure of Chl *a*/H_2O and crystalline ethyl-chlorophyllide *a*, with two water molecules forming the bridging network (Boender et al., 1995; de Boer et al., 2002; van Rossum et al., 2002).

Complete ^{1}H and ^{13}C assignments were obtained in a field of 14.1 T using the ^{13}C-^{13}C radio frequency-driven dipolar recoupling (RFDR) and ^{1}H-^{13}C Lee Goldburg/cross polarization (LG-CP) methods (van Rossum et al., 2002) (see Table S1 in Supplementary Material). The line widths are small (120–200 Hz) revealing a rigid and well-ordered structure. The ^{1}H and ^{13}C shifts of the monomer in solution were used

Abbreviations: BChl – bacteriochlorophyll; *Cfl.* – *Chloroflexus*; Chl – chlorophyll; *Chl.* – *Chlorobium*; CP – cross polarization; CS – chemical shift; LG – Lee Goldburg; MAS – magic angle spinning; NMR – nuclear magnetic resonance; RFDR – radio frequency-driven dipolar recoupling; WISE – wideline separation

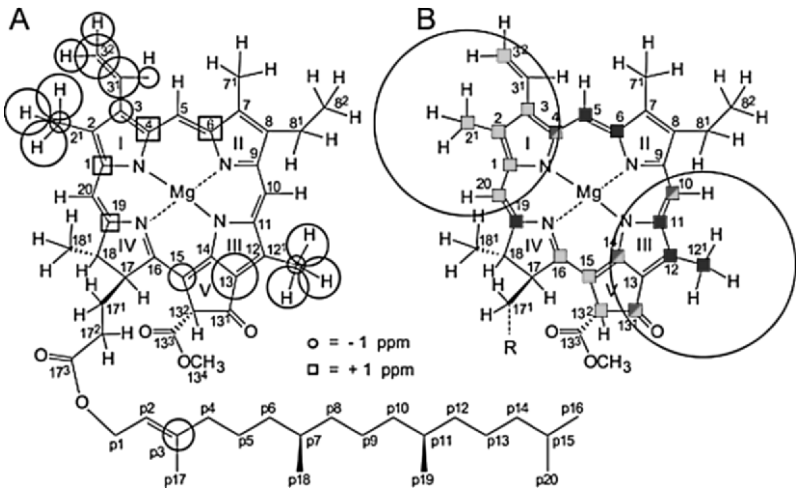

Fig. 1. (A) Visual representation of the carbon and proton aggregation shifts ($\Delta\sigma$) for aggregated Chl *a*. The circles around the carbon and hydrogen atoms represent upfield aggregation shifts, squares represent downfield shifts. The sizes of the circles and squares reflect the magnitude of the aggregation shifts. (B) Schematic representation of the assignment of heteronuclear correlations involving the 2^1-H_3, which are shown in shaded grey or the 12^1-H_3, which are solid black. For the 4-C, 10-C, 13^1-C and 14-C the correlations with proton signals are assigned to transfer from both methyl groups. The ranges for intramolecular transfer for the two methyl groups are indicated with the circles. Intramolecular correlations involving the 3^1-C and 13-C could not be assigned. Reprinted from Van Rossum et al. (2002). Copyright (2002), with permission from Elsevier.

to estimate the aggregation shifts. The ^{1}H aggregation shifts are consistent with the pattern for ^{13}C (Fig. 1). Upfield aggregation shifts up to ~5 ppm are observed, mostly induced by ring currents. The shift pattern is in agreement with models for the Chl *a*/water aggregates that assume strong overlap between the rings A and the rings C and E of adjacent molecules forming stacks (Worcester et al., 1986). In addition, in a 2D ^{13}C-^{13}C RFDR spectrum recorded with a long mixing time of τ_m = 10 ms, several cross-peaks are observed that can be attributed to intermolecular transfer (Boender et al., 1995).

Heteronuclear ^{1}H-^{13}C spectra were recorded with long LG-CP times to generate intermolecular correlations (van Rossum et al., 2002). For a LG-CP time of 2 ms, a maximum transfer distance (d_{max}) of ~4.2 Å was estimated from an analysis of the correlations involving the 2^1-H_3 and 12^1-H_3 protons. Weak transfer was observed from the 2^1-H_3 protons to the 10, 13^1, 13^2, 14, 15 and 16 carbons at the opposite side of the molecule (Fig. 1B), which was assigned to intermolecular contact over distances ~4 Å. Similarly, weak correlations between the 12^1-H_3 protons and the 4, 5, 6 and 19 carbons indicate intermolecular transfer. They confirm the 2D arrangement of the Chl *a* in sheets (Fig. 3A).

In addition, a CP^3 experiment can provide intermolecular ^{13}C-^{13}C correlations employing mixing by ^{1}H spin diffusion. An example of a CP^3 experiment, using a short mixing time of 0.1 ms, is shown in

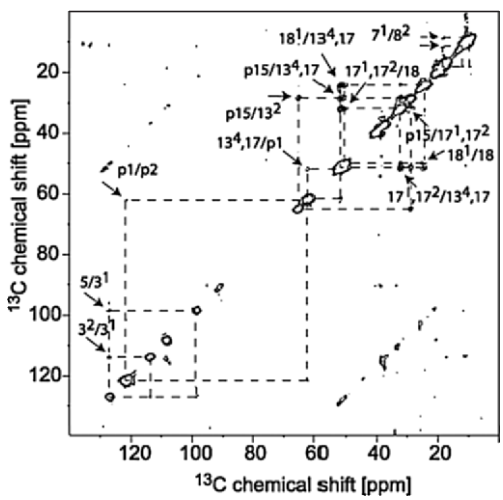

Fig. 2. Contour plot of an absorption mode 2D ^{13}C-^{13}C CP^3 MAS NMR correlation spectrum of aggregated Chl *a*/H_2O recorded with a spinning speed of 14.5 kHz in a field of 17.6 T. Arrows and labels are used to indicate cross-peaks, which are connected to the corresponding diagonal peaks and mirror peaks by dashed lines. Data were acquired with τ_m = 100 µs. A prescan delay of 1 s was used for a total of 192 scans for each of 200 t_1 points.

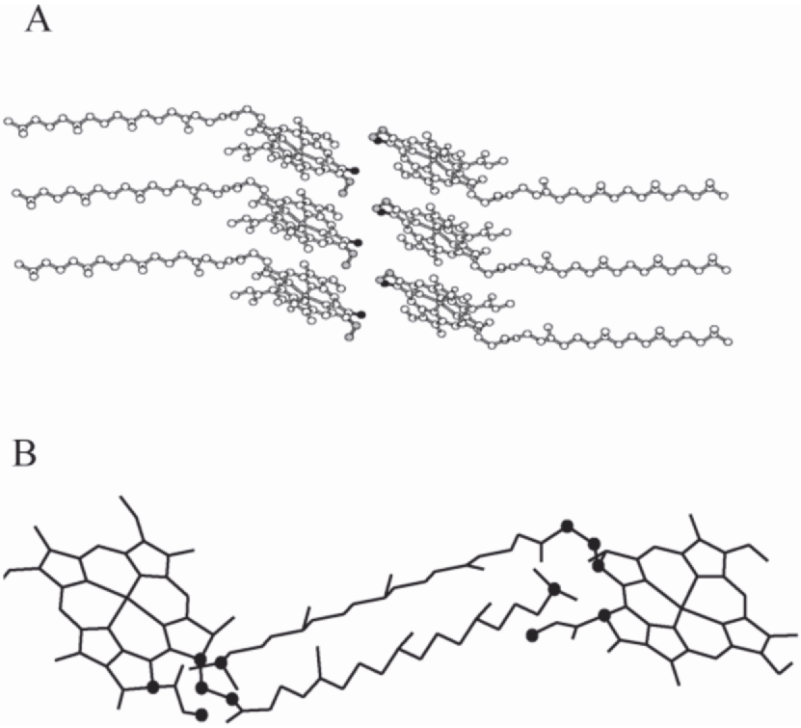

Fig. 3. (A) Schematic representation of a bilayer formed from two sheets of microcrystalline aggregated Chl *a*/H_2O. The orientation of the 2-D sheets is perpendicular to the plane of the paper and the view is parallel to the stack. The 7-Me and 8-Et moieties are shown in black and grey, respectively. (B) The proposed structural arrangement of the two Chl *a* molecules in the unit cell. Solid circles indicate the carbons involved in the intermolecular correlations.

Fig. 2 (de Boer et al., 2002). Correlations between the P15 carbon at the end of the phytyl chain and the 17^1, 17^2, 13^2 and 13^4 carbons near the base of the tail are observed. From a series of experiments using increasing mixing times, it is estimated that d_{max} is about ~4 Å for a mixing time of 0.1 ms. The length of the phytyl tail is ~20 Å, much longer than d_{max} and hence the correlations involving P15 are attributed to intermolecular transfer, over distances no larger than ~4 Å. This leads to the bilayer model with stretched and inter-digitating tails (Fig 3B). This model is supported by the very modest inhomogeneous line broadening for the phytyl tails and the absence of aggregation shifts for the tails, which provides strong evidence that the tails have essentially the same conformation as in solution.

Finally, ^{1}H signals, correlating with similar bridging moieties in the heteronuclear MAS NMR spectra, could be assigned to structural water similar to ethylchlorophyllide *a*. In addition, a small doubling of the 7-C, 7^1-CH_3 and $8^{1,2}$-C was resolved. This provides evidence for two marginally different well-defined molecular environments at the interface between two bilayers (Fig. 3A).

III. Self-organization of Bacteriochlorophyll is the Main Structural Feature of the Chlorosomal Antennae

A complete ^{13}C assignment was made for the NMR response of the chlorosomes and various BChl *c* homologues from the uniformly ^{13}C labeled chlorosomes of *Chl. tepidum* (Balaban et al., 1995) (see Table S2 in Supplementary Material). Figure 4 shows the chemical structure of the most abundant [8-Et, 12-Et]BChl *c* homologue. 2D ^{13}C-^{13}C RFDR dipolar correlation spectra of solid BChl *c* aggregated in hexane and the chlorosomal antennae are depicted in Fig. 5 (Balaban et al., 1995; Boender, 1996). Many peaks are resolved in the spectra, and the two spectra are almost identical. The predominant component of the MAS NMR signals in the chlorosomes is from BChl *c*. Only a minor fraction is observed in the chlorosomes that is not present in the aggregate. These peaks are attributed to lipids and proteins in the chlorosomes. Correlations between the carbonyl and α carbons of a small protein component are indicated in Fig 5.

The 2D response of the BChl *c* in intact chlorosomes is virtually indistinguishable from the data

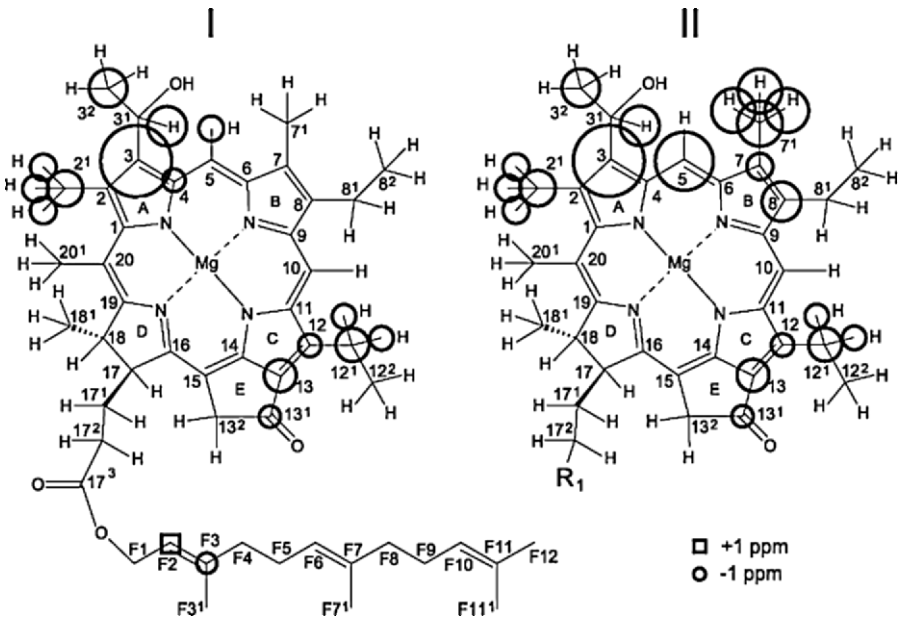

Fig. 4. Carbon and proton aggregation shifts $|\Delta\sigma_i| \geq 1.5$ ppm of BChl *c* with $\Delta\sigma_i = \sigma_i - \sigma_{liq}$. The NMR response comprises two components, denoted **I** and **II**. The circles around the carbon and hydrogen atoms represent upfield aggregation shifts, the squares downfield aggregation shifts. The size of a circle or square is proportional to the magnitude of the aggregation shift. Reprinted with permission from Van Rossum et al. (2001). Copyright (2001) Am. Chem. Soc.

collected from the in vitro aggregate with respect to chemical shifts, line widths and relative intensities of the cross-peaks. This demonstrates that the minor fractions of proteins and lipids are not an integral part of the BChl *c* assembly (Balaban et al., 1995; Boender, 1996). In this way, the NMR data provide conclusive evidence that self-assembly of BChl *c* is the structural basis for the BChl *c* organization in vivo, without the intervention of proteins.

In earlier 1D MAS NMR experiments, solid BChl *c* was also compared with the chlorosomes, providing the first evidence for the same aggregated forms (Nozawa et al., 1990, 1991, 1994). The T_{CH} and $T_{1\rho}{}^{H}$ values were also comparable for both samples, which corroborates the structural correspondence between the aggregate and the natural system.

The observation that a biological function can be realized without active participation of protein can be considered anomalous, since the central dogma of molecular biology states that all function originates from the DNA code via protein: DNA → RNA → protein → function. In a chlorosome, the biological function of the antennae is based on self-assembly steered by the physico-chemical properties of the constituting molecules and top-down control from higher levels in the biological hierarchy. Other examples of this principle have been encountered in the past, such as biomineralization of inorganic matter into a morphology controlled by the organism (Bäuerlein, 2003). For instance, the magnetite crystals in the magnetosomes of magnetobacteria correspond to single magnetic domains of 40–120 nm, and allow the bacteria to orient themselves using the earth magnetic field.

The self-organization of BChl *c* may be of interest for artificial photosynthesis. The elucidation of the functional concepts behind photosynthesis in nature is expected to be of assistance in improving artificial devices like photovoltaic cells. Although the actual application of artificial molecular solar energy converters may still be years away, elucidation of the concepts behind nature's efficient energy converting system will be of use to photovoltaics and molecular electronics research. In particular, the discovery of natural light-harvesting systems without proteins may be of help to indicate novel routes in photovoltaics research.

To produce aggregates resembling the chlorosomes, the solvent used in the process is essential. In particular, the effect of different solvents to form

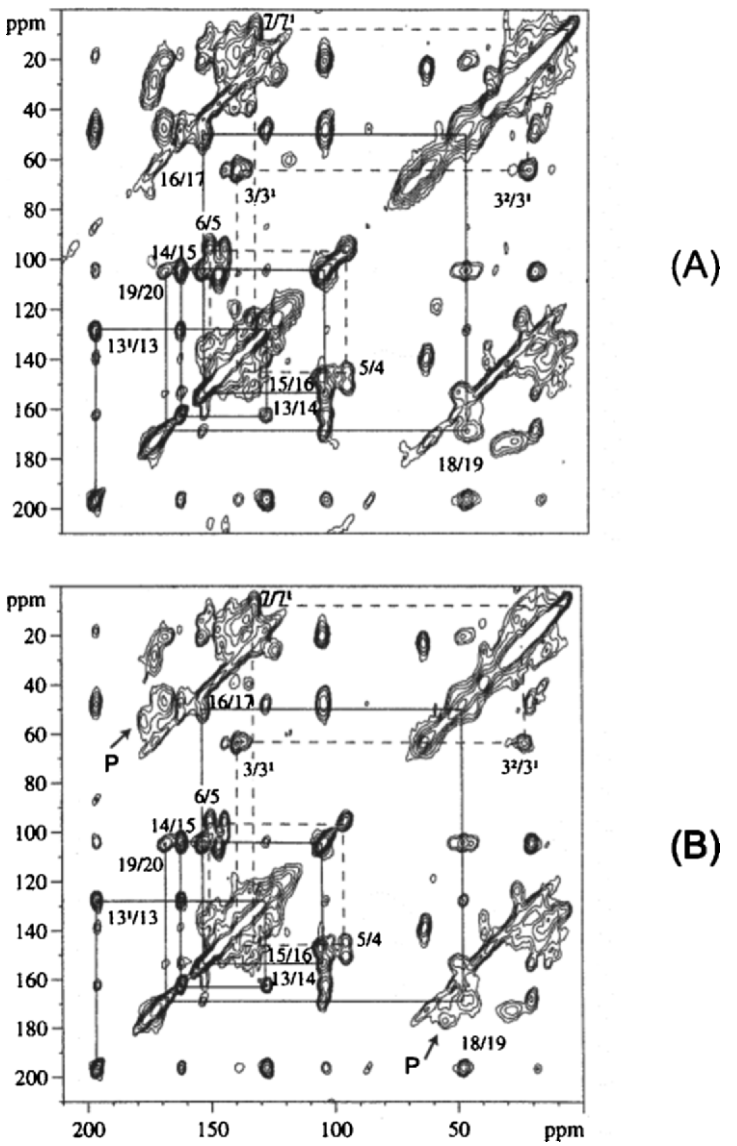

Fig. 5. Contour plots of 2D MAS NMR dipolar correlation NMR spectra of uniformly ^{13}C labeled BChl *c* aggregates (A) and ^{13}C labeled chlorosomes (B), recorded in a magnetic field of 9.4 T. The MAS rate was 11 kHz and a CP time of 1 ms was used. The lines indicate sequences of nearest neighbor correlations. A small protein fraction in (B) is indicated with P. Reprinted from Boender (1996).

solid aggregates of (3^1 *R*) BChl *c* was recently studied (Umetsu et al., 1999). Various techniques including ^{13}C CP/MAS were applied to investigate the size and order of the aggregates formed after drying in diethyl ether, CH_2Cl_2, CCl_4 or CH_2Cl_2 in an excess of hexane. From the magnetic circular dichroism spectra, the aggregates treated with CCl_4 and hexane were estimated to be larger than those with diethyl ether and CH_2Cl_2. The circular dichroism spectra show differences between the CH_2Cl_2-treated aggregates and the diethyl ether and CCl_4-treated samples, indicating a different molecular arrangement. In addition, the BChl *c* treated with CH_2Cl_2 is weakly diffracting by X-ray similar to methyl-BChlide *c* formed in hexane. This shows that the tails leave the stacking of the BChl *c* intact. In addition, recent MAS NMR experiments revealed two distinct sets of resonances for a CH_2Cl_2-treated uniformly ^{13}C and ^{15}N labeled (3^1 *R*) BChl *c* aggregate, indicating the formation of a transient species between the dimer and the stacked form (Umetsu et al., 2004).

IV. A 3-Dimensional Model for the Structure of the Chlorosomal Antennae

The structure of the chlorosomal antennae was recently investigated with 2D and 3D MAS NMR. The ^{13}C shifts assigned from the 2D RFDR experiments provided the first step to a structural model (Balaban et al., 1995). The relatively large ^{13}C line widths contrast with the microcrystalline Chl *a*/H_2O aggregates and reveal significant disorder down to the microscopic level. Large ring current shifts are detected in the regions of rings A, -C and E (Fig. 4). ^{13}C-^{13}C RFDR experiments were performed, using long mixing times of 5–10 ms (Boender, 1996; van Rossum et al., 1998a). Correlations between the 13^1-carbon and the 19-, 20-, 1-, 2- and 3-carbons were attributed to intermolecular transfer and appear to confirm the layer structure. In addition, rotational resonance experiments show that the $C3^1$-$C13^1$ distance is similar to the C20-$C3^1$ distance in accordance with hydrogen bonding between the 3^1 and 13^1 groups (Nozawa et al., 1994).

The ^1H shifts were determined in a 3D experiment using rapid MAS in combination with a high magnetic field. Under these conditions, it was shown that proton shifts can be determined and intermolecular heteronuclear correlations as well as hydrogen–bonding characteristics can already be determined with simple pulse schemes such as the wideline separation (WISE) technique (van Rossum et al., 1996). Since the chlorosome response is considerably inhomogeneously broadened, a 2D ^{13}C-^{13}C RFDR experiment was extended in a straightforward fashion by a third ^1H WISE dimension to construct a 3D ^1H-^{13}C-^{13}C MAS NMR experiment (van Rossum et al., 2001). As a result, all ^1H resonances of the chlorosomes could be assigned (see Table S2 in Supplementary Material). The aggregation shifts (Fig. 4) are consistent with the ^{13}C pattern. Two fractions **I** and **II** are observed in the NMR dataset. In both fractions, two regions with pronounced upfield shifts are visible around ring A and C/E. In addition, in fraction **II**, large upfield shifts for the 5-C and the 7-Me are detected. This suggests the existence of two distinct structural arrangements, related to the rod-like suprastructure in the chlorosomes.

The chemical shift data were used to refine the structural model for the chlorosomes. Firstly, the molecular structure was optimized by quantum chemical calculations for the (3^1 *R*) or (3^1 *S*) stereoisomers using methanol as a fifth ligand. The Mg ion can be positioned at the same side of the porphyrin plane as the 17^1-C (*syn*) or at the opposite side (*anti*). The two energetically most favorable forms are the (3^1 *R*)-*anti* and the (3^1 *S*)-*syn* combinations. Stacks of molecules of the *syn* or *anti* type can be formed by successive coordination of the 3^1-OH to the Mg of the next molecule (Fig. 6). From model studies, it was concluded that the ratio between the two stereoisomers can vary considerably. Provided a minor fraction of either form is present, the rods can be formed (Steensgaard et al., 2000). This suggests that both species can be accommodated in a stack by rotating the 3-side chain.

The stacks can be combined to form layers by hydrogen bonding between the 3^1-OH groups of one stack with the 13^1-C=O of a neighboring stack. Evidence for this has also been found by ^{13}C CP/MAS experiments. From the CP build-up of the 13^1-carbon signal in the chlorosomes of *Cfl. aurantiacus* and in the hexane treated aggregate, it was concluded that the 13^1 carbonyl is hydrogen bonded, probably to the 3-hydroxyethyl group (Nozawa et al., 1990).

Based on the NMR results, a bilayer tube model was proposed for the chlorosome rods in *Chl. tepidum*, where a predominantly *syn* layer forms the inner tube with the tails filling the center, while a layer of *anti* character constitutes the outer tube with the tails pointing away from the surface (Fig. 6) (van Rossum et al., 2001). In the *anti* conformation, the layer of BChls corresponds to the model of Holzwarth et al., where the tails are directed outward (Holzwarth and Schaffner, 1994). The layer formed from *syn* stacks has an opposite curvature with the tails directed inward. The existence of two different parallel chain stacks with *syn* and *anti* configurations has also been detected by NMR in solution (Mizoguchi et al., 1998). The two different layers (Fig. 6) have virtually identical aggregation shifts. Evidently, the overlap in both cases is similar and induces the same ring current shifts. The bilayer model is supported by electron microscopy, since the rod-shaped structures with an outer diameter of 10 nm and an internal hole of 3 nm (Cruden and Stanier, 1970; Staehelin et al., 1980) can be formed easily from the bilayer tube inferred from the MAS NMR data. Calculations of optical spectra based on a single outer layer at least explain the measured spectra satisfactorily, and refinements including the bilayer are expected (Prokhorenko et al., 2000; Psencik et al., 2003).

For the bilayer tubes, an intensity ratio between components **I** and **II** of approx. 3:2 is observed (van

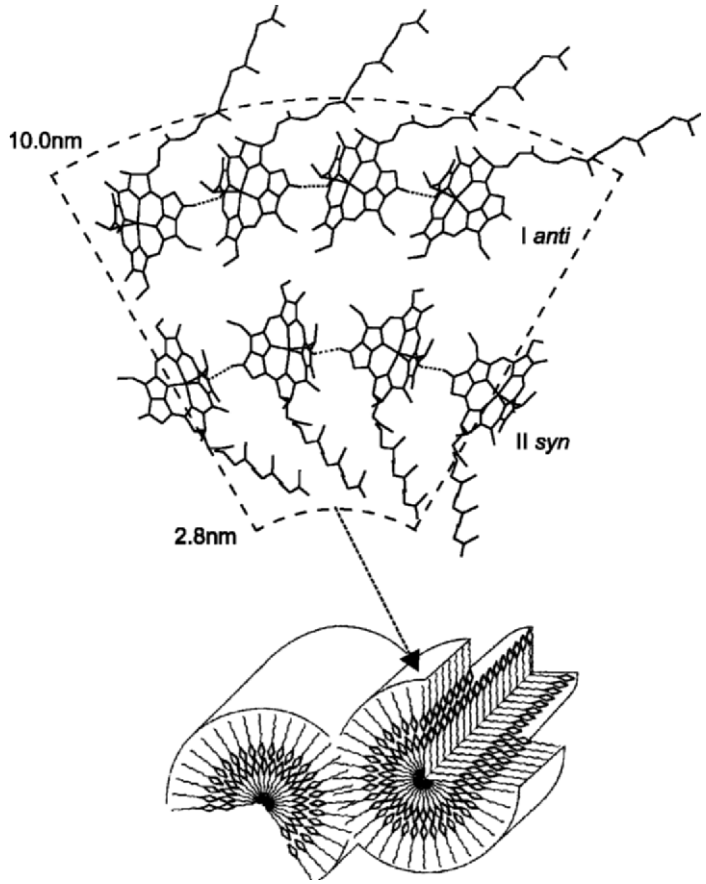

Fig. 6. Schematic representation of a radial wall section of a bilayer tube formed from curved 2-D sheets of *anti* (**I**) and *syn* (**II**) stacks. The chlorin rings are completed with the farnesyl tails, which were not included in the *ab initio* calculations. The curvature leads in a natural way to the dimensions determined with electron microscopy. The direction of the stacks is perpendicular to the plane of the paper. The dotted lines indicate hydrogen bonds between 13^1-C=O and 3^1-OH of adjacent stacks. In reality, the interface between the outer and inner tube is expected to be more dense than in this schematic representation, to account for the aggregation shifts of the 7^1 methyls.

Rossum et al., 2001). The splitting of the chemical shift pattern was explained by an interaction between *syn* and *anti* layers yielding a different electronic environment. The component **I** in the NMR spectra was attributed to a (3^1 *R*) *anti* structure and the component **II** to a (3^1 *S*) *syn* structure. The upfield shifts around the 7^1-CH_3 in component **II** may reflect a different structural arrangement for the 7-Me groups at the interface of the layers leading to an extended overlap for this component only. Finally, comparison of the proton responses of the farnesyl chain of BChl *c* with the phytyl chain of self-aggregated Chl *a*/H_2O reveals a significant excess line broadening of the BChl *c* proton signals, suggesting that the farnesyl chain may exhibit some random folding. On the other hand, it was demonstrated that the NMR relaxation parameters of the farnesyl chain are highly similar to those of the rigid ring system, from which it was concluded that at least a substantial fraction of the farnesyl chains should be relatively immobile (van Rossum et al., 1998b). This is consistent with the bilayer tube model of Fig. 6, since it can be expected that at least the fatty tails on the inside will be rigidly held in place.

V. Conclusions and Future Prospects

With a combination of chemical shift data and intermolecular constraints, detailed information about the structure of chlorosomes and solid chlorophyll aggregates can be obtained. Access to the proton chemical shifts in the solid state yields aggregation shifts that can be related to the stacking of the mac-

rocycles. The intermolecular correlations provide direct structural information in terms of close contacts between molecules. A few contacts strongly reduce the number of possible space filling arrangements for the chlorophyll aggregates.

For the study of the chlorosomes, MAS NMR has proved to be a valuable tool, and the model structure of Fig. 6 is increasingly accepted (Brown and Spiess, 2001; Glaeser et al., 2002; Vassilieva et al., 2002). MAS NMR in conjunction with other spectroscopic methods and microscopy provide converging evidence for the bilayer tube model of Fig. 6. The aggregation shift pattern in the 7-C region of component II in Fig. 4 was not yet explained quantitatively from the model structure. In addition, the large shift for the 5-C is not yet fully clear.

One key issue to be addressed in the near future is to prove that specific side chains can steer the supramolecular structure through the aggregation process. In particular, the role of the (3^1 *R*) and (3^1 *S*) stereoisomers, the long ester tails and their interplay appears to be important. It is expected that MAS NMR will contribute in the near future by resolving the structures of model compounds and other chlorosomes such as those found in *Chloroflexus*.

More material is available on the web, see [WEBSITE]. This includes a section describing the MAS NMR methods for structure determination. In addition, the web section includes tables with the ^{1}H and ^{13}C chemical shifts for solid Chl *a*/H_2O and BChl *c* as well as the aggregation shifts relative to the shifts in solution.

Note Added in Proof

To investigate the molecular control over the supramolecular structure, two model cadmium chlorins were studied that were uniformly ^{13}C and ^{15}N enriched in the ring moieties (de Boer et al., 2003, 2004). The chlorin models differ from the natural BChl *c* in the central metal and the 3-, 12-, 17-, and 20-side chains. One model system has the farnesyl tail replaced by a methyl, whereas the other has a stearyl tail. The ^{113}Cd MAS NMR signals reveal a five-coordination of the Cd metal, very similar to the HO•••Mg coordination in the natural system. Large ^{1}H ring-current shifts of up to 10 ppm reveal a dense orderly stacking of the molecules in planar layers, for which a correlation length of at least 24 Å was defined from long-range ring-current shift calculations (de Boer et al., 2004). The ring current shift calculations are a critical assay in discriminating between tubular and planar structures, since they can be applied to confront models deduced from e.g., electron microscopy with the NMR spectroscopy data from intact chlorosomes. The model structures confirm and validate the essential role of the [3^1R] and [3^1S] stereoisomers in the formation of the chlorosomal antennae. The 3D arrangement of the layers is revealed by intermolecular ^{13}C-^{13}C correlations obtained from CHHC experiments. With the tail truncated to methyl, a microcrystalline solid is formed with favorable interactions between the planar sheets in a head-to-tail orientation. The stearyl tails lead to a considerably disordered aggregate consisting of both *syn* and *anti* layers similar to the chlorosomes, as indicated by a doubling of the ^{15}N-D NMR signal. The MAS results provide converging evidence for a balance between strong local interactions and contributions to the free energy of the system associated with a longer length scale. The metal coordination and hydrogen bonding between stacks lead to a robust layer structure on a mesoscopic length scale, stable against thermodynamic noise. This allows for fine-tuning of the structure by various microscopic functionalities. The chirality of 3^1 side chain provides a bias for the two opposite plane curvatures, while bulky side chains like the 20 methyl provide fine tuning of the π-π overlap between individual macrocycles (de Boer et al., 2004). Finally the long tails promote an organization into bilayers with a 180° screw axis between the layers (de Boer et al., 2003).

Note: Readers are encouraged to visit the website (http://epub.ub.uni-muenchen.de/archive/00000776/) for 'supplementary material,' where Figs. S1–S2 referred to in the text are posted.

References

Abraham RJ and Rowan AE (1991) Nuclear magnetic resonance spectroscopy of chlorophyll. In: Scheer H (ed) Chlorophylls, pp 797–834. CRC Press, Boca Raton

Balaban TS, Holzwarth AR, Schaffner K, Boender GJ and de Groot HJM (1995) CP-MAS C-13-NMR Dipolar correlation spectroscopy of C-13-enriched chlorosomes and isolated bacteriochlorophyll *c* aggregates of *Chlorobium tepidum*: The self-organization of pigments is the main structural feature of chlorosomes. Biochemistry 34: 15259–15266

Bäuerlein E (2003) Biomineralization of unicellular organisms: An unusual membrane biochemistry for the production of

inorganic nano- and microstructures. Angew Chem Intl Ed 42: 614–641

Blankenship RE, Olson JM and Miller B (eds) (1995) Anoxygenic Photosynthetic Bacteria. Kluwer Academic Publishers, Dordrecht

Boender GJ (1996) The stacking of chlorophylls in the chlorosomal antennae of green bacteria. PhD Thesis. Leiden University. Leiden

Boender GJ, Raap J, Prytulla S, Oschkinat H and de Groot HJM (1995) MAS NMR structure refinement of uniformly C-13 enriched chlorophyll-*a* water aggregates with 2D dipolar correlation spectroscopy. Chem Phys Lett 237: 502–508

Brown SP and Spiess HW (2001) Advanced solid-state NMR methods for the elucidation of structure and dynamics of molecular, macromolecular, and supramolecular systems. Chem Rev 101: 4125–4155

Chiefari J, Griebenow K, Griebenow N, Balaban TS, Holzwarth AR and Schaffner K (1995) Models for the pigment organization in the chlorosomes of photosynthetic bacteria — diastereoselective control of in-vitro bacteriochlorophyll c_s aggregation. J Phys Chem 99: 1357–1365

Cruden DL and Stanier RY (1970) The characterization of *Chlorobium* vesicles and membranes isolated from green bacteria. Arch Microbiol 72: 115–134

de Boer I, Bosman L, Raap J, Oschkinat H and de Groot HJM (2002) 2D C-13-C-13 MAS NMR correlation spectroscopy with mixing by true 1H spin diffusion reveals long-range intermolecular distance restraints in ultra high magnetic field. J Magn Reson 157: 286–291

de Boer I, Matysik J, Amakawa M, Yagai S, Tamiaki H, Holzwarth AR and de Groot HJM (2003) MAS NMR structure of a microcrystalline Cd-bacteriochlorophyll *d* analoge. J Am Chem Soc 125: 13374–13375

de Boer I, Matysik J, Erkelens K, Sasaki S, Miyatake T, Yagai S, Tamiaki H, Holzwarth AR and de Groot HJM (2004) MAS NMR structures of aggregated cadmium chlorins reveal molecular control of self-assembly of chlorosomal bacteriochlorophylls. J Phys Chem B 108: 16556–16566

Glaeser J, Baneras L, Rutters H and Overmann J (2002) Novel bacteriochlorophyll *e* structures and species-specific variability of pigment composition in green sulfur bacteria. Arch Microbiol 177: 475–485

Griebenow K, Holzwarth AR, van Mourik F and van Grondelle R (1991) Pigment organization and energy-transfer in green bacteria. 2. Circular and linear dichroism spectra of protein-containing and protein-free chlorosomes isolated from *Chloroflexus aurantiacus* strain Ok-70-Fl. Biochim Biophys Acta 1058: 194–202

Hildebrandt P, Tamiaki H, Holzwarth AR and Schaffner K (1994) Resonance Raman-spectroscopic study of metallochlorin aggregates — implications for the supramolecular structure in chlorosomal BChl *c* antennae of green bacteria. J Phys Chem 98: 2192–2197

Holzwarth AR and Schaffner K (1994) On the structure of bacteriochlorophyll molecular aggregates in the chlorosomes of green bacteria — a molecular modeling study. Photosynth Res 41: 225–233

Katz JJ, Bowman MK, Michalski TJ and Worcester DL (1991) Chlorophyll aggregation: Chlorophyll/water micelles as models for in vivo long-wavelength chlorophyll. In: Scheer H (ed) Chlorophylls, pp 211–235. CRC Press, Boca Raton

Matsuura K, Hirota M, Shimada K and Mimuro M (1993) Spectral forms and orientation of bacteriochlorophyll-*c* and bacteriochlorophyll-*a* in chlorosomes of the green photosynthetic bacterium *Chloroflexus aurantiacus*. Photochem Photobiol 57: 92–97

Mizoguchi T, Sakamoto S, Koyama Y, Ogura K and Inagaki F (1998) The structure of the aggregate form of bacteriochlorophyll *c* showing the Q(y) absorption above 740 nm as determined by the ring-current effects on H-1 and C-13 nuclei and by H-1-H-1 intermolecular NOE correlations. Photochem Photobiol 67: 239–248

Nozawa T, Manabu S, Kanno S and Shirai S (1990) CP/MAS C-13-NMR Studies on the structure of bacteriochlorophyll *c* in chlorosomes from *Chloroflexus aurantiacus*. Chem Lett 1990: 1805–1808

Nozawa T, Suzuki M, Ohtomo K, Morishita Y, Konami H and Madigan MT (1991) Aggregation structure of bacteriochlorophyll *c* in chlorosomes from *Chlorobium tepidum*. Chem Lett 1991: 1641–1644

Nozawa T, Ohtomo K, Suzuki M, Nakagawa H, Shikama Y, Konami H and Wang ZY (1994) Structures of chlorosomes and aggregated BChl *c* in *Chlorobium tepidum* from solid state high resolution CP/MAS C-13 NMR. Photosynth Res 41: 211–223

Olson JM (1998) Chlorophyll organization and function in green photosynthetic bacteria. Photochem Photobiol 67: 61–75

Prokhorenko VI, Steensgaard DB and Holzwarth AR (2000) Exciton dynamics in the chlorosomal antennae of the green bacteria *Chloroflexus aurantiacus* and *Chlorobium tepidum*. Biophys J 79: 2105–2120

Psencik J, Ma YZ, Arellano JB, Hala J and Gillbro T (2003) Excitation energy transfer dynamics and excited-state structure in chlorosomes of *Chlorobium phaeobacteroides*. Biophys J 84: 1161–1179

Staehelin LA, Golecki JR, Fuller RC and Drews G (1978) Visualisation of the supramolecular architecture of chlorosomes (*Chlorobium* type vesicles) in freeze-fractured cells of *Chloroflexus aurantiacus*. Arch Mikrobiol 119: 269–277

Staehelin LA, Golecki JR and Drews G (1980) Supramolecular organization of chlorosomes (*Chlorobium* vesicles) and of their membrane attachment sites in *Chlorobium limicola*. Biochim Biophys Acta 589: 30–45

Steensgaard DB, Wackerbarth H, Hildebrandt P and Holzwarth AR (2000) Diastereoselective control of bacteriochlorophyll *e* aggregation. 3(1)-S-BChl e is essential for the formation of chlorosome-like aggregates. J Phys Chem B 104: 10379–10386

Tamiaki H, Amakawa M, Holzwarth AR and Schaffner K (2002) Aggregation of synthetic metallochlorins in hexane. A model of chlorosomal bacteriochlorophyll self-assemblies in green bacteria. Photosynth Res 71: 59–67

Umetsu M, Wang ZY, Zhang J, Ishii T, Uehara K, Inoko Y, Kobayashi M and Nozawa T (1999) How the formation process influences the structure of BChl *c* aggregates. Photosynth Res 60: 229–239

Umetsu M, Hollander JG, Matysik J, Wang ZY, Adschiri T, Nozawa T and de Groot HJM (2004) Magic-angle spinning NMR under ultra-high field reveals two forms of intermolecular interaction within CH_2Cl_2-treated 3(1)-R-type bacteriochlorophyll *c* solid aggregate. J Phys Chem B 108: 2726–2734

van Rossum BJ, Boender GJ and deGroot HJM (1996) High magnetic field for enhanced proton resolution in high- speed CP/MAS heteronuclear H-1-C-13 dipolar-correlation spectros-

copy. J Magn Reson Ser A 120: 274–277

van Rossum BJ, Boender GJ, Mulder FM, Raap J, Balaban TS, Holzwarth A, Schaffner K, Prytulla S, Oschkinat H and de Groot HJM (1998a) Multidimensional CP-MAS C-13 NMR of uniformly enriched chlorophyll. Spectrochim Acta A54: 1167–1176

van Rossum BJ, Van Duyl BY, Steensgaard DB, Balaban ST, Holzwarth AR, Schaffner K and De Groot HJM (1998b) Evidence from solid state NMR dipolar correlation spectroscopy for dual interstack arrangements in the chlorosome antenna system. In: Garab G (ed) Photosynthesis: Mechanisms and Effects, pp 117–120. Kluwer Academic Publishers, Dordrecht

van Rossum BJ, Steensgaard DB, Mulder FM, Boender GJ, Schaffner K, Holzwarth AR and de Groot HJM (2001) A refined model of the chlorosomal antennae of the green bacterium *Chlorobium tepidum* from proton chemical shift constraints obtained with high-field 2-D and 3-D MAS NMR dipolar correlation spectroscopy. Biochemistry 40: 1587–1595

van Rossum BJ, Schulten EAM, Raap J, Oschkinat H and de Groot HJM (2002) A 3-D structural model of solid self-assembled chlorophyll *a*/H_2O from multispin labeling and MAS NMR 2-D dipolar correlation spectroscopy in high magnetic field. J Magn Reson 155: 1–14

Vassilieva EV, Stirewalt VL, Jakobs CU, Frigaard NU, Inoue-Sakamoto K, Baker MA, Sotak A and Bryant DA (2002) Subcellular localization of chlorosome proteins in *Chlorobium tepidum* and characterization of three new chlorosome proteins: CsmF, CsrnH, and CsmX. Biochemistry 41: 4358–4370

Worcester DL, Michalski TJ and Katz JJ (1986) Small-angle neutron scattering studies of chlorophyll micelles: Models for bacterial antenna chlorophyll. Proc Natl Acad Sci USA 83: 3791–3795

Chapter 21

Single Molecule Spectroscopy of Pigment Protein Complexes from Purple Bacteria

Jürgen Köhler*
Experimental Physics IV and BZMB, University of Bayreuth, 95440, Bayreuth, Germany

Thijs J. Aartsma
Department of Biophysics, Huygens Laboratory, Leiden University, P.O. Box 9504, 2300 RA Leiden, The Netherlands

Summary

In bacterial photosynthesis, light energy is absorbed by a network of antenna pigment proteins and efficiently transferred to the photochemical reaction center where a charge separation takes place providing the free energy for subsequent chemical reactions. Most photosynthetic purple bacteria contain two types of antenna complexes: light-harvesting complex 1 (LH1) and light-harvesting complex 2 (LH2). It is known that the photochemical reaction center is closely associated with the LH1 complex while the LH2 complexes are arranged around the perimeter of LH1 in a two-dimensional structure. The transfer of energy from LH2 to LH1 and subsequently to the reaction center occurs in vivo on a time scale of 30–40 ps, i.e., very fast compared to the decay of an isolated LH2 which has a fluorescence lifetime of about 1 ns. As yet, there is no consensus about the details of the mechanisms of the energy-transfer process, and the full three-dimensional structure of the whole photosynthetic unit is still unknown. The great difficulty encountered when determining the various parameters that play a role in the description of the electronic structure of light-harvesting complexes and the process of energy transfer, is the fact that the optical absorption lines are inhomogeneously broadened as a result of heterogeneity in the ensemble of absorbing pigments. To circumvent this problem we have applied single-molecule detection schemes to study the pigment-protein complexes individually thereby avoiding ensemble averaging. Here we present an overview of our work on LH1 and LH2 from *Rhodopseudomonas acidophila*.

*Author for correspondence, email: juergen.koehler@uni-bayreuth.de

Bernhard Grimm, Robert J. Porra, Wolfhart Rüdiger and Hugo Scheer (eds): Chlorophylls and Bacteriochlorophylls: Biochemistry, Biophysics, Functions and Applications, pp. 309–321.

I. Introduction

A prominent challenge of current biological research is to understand how basic principles of physics govern life processes. An important example of such a process is photosynthesis which sustains all life on earth. Photosynthesis is carried out by many different organisms, i.e., plants, algae and photosynthetic bacteria which all have developed highly efficient and optimized systems to collect the light of the sun, and to use the light energy as the driving force for their metabolic reactions. Basically, the photosynthetic light reactions occur in four primary steps: 1) absorption of (sun)light by a pigment, 2) ultra-fast transfer of the excitation energy to a 'photoactive' pigment, 3) oxidation of this excited photoactive pigment, and 4) stabilization of the charge-separated state by secondary electron-transfer reactions. These reactions take place in specialized proteins, which bind the pigment and/or electron transfer cofactors at optimized binding sites ensuring high efficiency in various organisms. The protein-pigment complexes involved in the first two processes are often called antenna or light-harvesting complexes. These complexes permit the organism to significantly increase its absorption cross-section for sunlight. The primary electron transfer steps (processes 3 and 4) usually occur in a special protein-pigment complex which is referred to as the reaction center (RC).

In most purple bacteria, the photosynthetic unit (PSU) present in the membrane contains, besides the RC, two types of antenna complexes, the core complex which is usually termed light-harvesting complex 1 (LH1) and the peripheral complex called light-harvesting complex 2 (LH2). Depending on the growth conditions of the bacterium, some species show another peripheral complex, LH3, which is a spectroscopic variant of LH2. It is known that LH1 is closely associated with the RC, whereas LH2 is not in direct contact with the RC, but transfers the energy to the RC via the LH1 complex (Hu et al., 2002). The progress made in high-resolution structural studies of light-harvesting complexes of purple bacteria (McDermott et al., 1995; Koepke et al., 1996; Mcluskey et al., 2001) has strongly stimulated experimental and theoretical investigations to understand the efficient energy transfer in these antenna systems. The X-ray structure of the LH2 complex (McDermott et al., 1995), along with the lower resolution structural information for LH1 (Karrasch et al., 1995; Jungas et al., 1999), shows a remarkable symmetry in the arrangement of the light-absorbing pigments in their protein matrix. The basic building block of LH2 is a protein heterodimer (αβ), which binds three BChl *a* pigments and one carotenoid molecule. The LH2 complex consists either of nine (*Rps. acidophila, Rba. sphaeroides*) or eight (*Rsp. molischianum*) such αβ-polypeptide heterodimers.

In contrast, it has not yet been possible to obtain high-quality crystals of LH1 and therefore the three-dimensional arrangement of its subunits remains to be ascertained. The LH1 subunit is believed to contain only two coupled pigments, contributing to its absorption band around 870 nm. Figure 1 shows a model of the PSU of the purple bacterium *Rba. sphaeroides* where the organization of the different protein-pigment complexes are depicted (Hu et al., 2002). However, the full three-dimensional structure of the whole photosynthetic unit is as yet unknown.

By now, it has been established that the spatial structure of photosynthetic complexes, especially the mutual orientation of the pigments, determine to a large extent their spectroscopic features and excited-state dynamics (van Amerongen et al., 2000). For LH2 the intermolecular interactions of the pigments are relatively strong, they contain few inequivalent binding sites, and their symmetry is very high. All these factors contribute to the consensus that in these systems, but particularly in LH2, collective excitations, Frenkel excitons, play an important role in the excited-state properties and in the process of energy transfer. Generally, information about the parameters that determine the description of the electronic structure of light harvesting complexes can be obtained by optical spectroscopy. Figure 2 shows the low-temperature absorption spectrum of membrane fragments of the purple bacterium *Rps. acidophila*. In the near infrared, it shows broad bands at 800 and 870 nm and a small band at 910 nm. The first two bands are assigned to the LH2 antenna, whereas the third band is assigned to the LH1 antenna.

But even isolated protein-pigment complexes of photosynthetic systems are rather complex, and it has been proven difficult to analyze the excited state properties of these systems in all details. This is mainly caused by the pronounced disorder in these types of systems, which masks details in the steady-state opti-

Abbreviations: BChl – bacteriochlorophyll; FWHM – full width half maximum; LH – light harvesting; P – primary donor; PSU – photosynthetic unit; PVA – polyvinyl alcohol; *Rba.* – *Rhodobacter*; RC – reaction center; *Rps.* – *Rhodopseudomonas; Rsp.* – *Rhodospirillum*

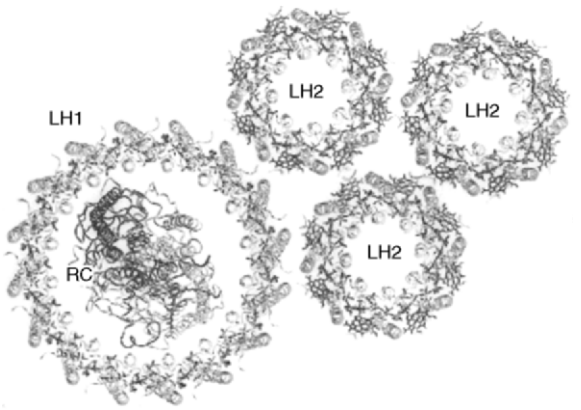

Fig. 1. Model for the PSU of the purple bacterium *Rba. sphaeroides.* The PSU consists of the photosynthetic reaction center and the light-harvesting complexes. Figure taken from Schulten (1999).

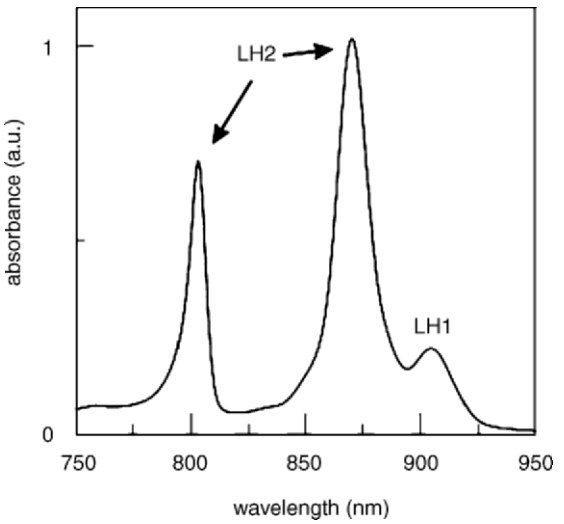

Fig. 2. Absorption spectrum of a solution of membrane fragments of *Rps. acidophila.* The membrane fragments were diluted in a standard LH2 buffer in the presence of 67% glycerol. The spectrum was taken at 10 K.

cal spectra, even at low temperature. Consequently, the parameters obtained from different experimental and theoretical approaches show a large spread and no consensus has yet been achieved about the details of the mechanism of energy transfer (Kennis et al., 1996, 1997a; Pullerits et al., 1996; Kühn and Sundström, 1997; Monshouwer et al., 1997).

Important parameters that determine the character of the electronically excited states of a molecular aggregate are the transition-dipole-dipole interaction, V, between neighboring molecules and the variation in site energies of these molecules. These factors can be combined into the following Hamiltonian:

$$H = \sum_{n=1}^{N} \left(E_0 + \Delta E_n\right) |n\rangle\langle n| + \sum_{n=1}^{N} \sum_{m \neq n} \left(V_{nm} + \Delta V_{nm}\right) |n\rangle\langle m|, \quad (1)$$

where $|n\rangle$ and $|m\rangle$ correspond to excitations localized on molecule 'n' and 'm', respectively, E_0 denotes the site-energy of each pigment, and V_{nm} denotes the interaction between molecules 'n' and 'm' in a perfect circular system. Local variations in the protein environment of the binding sites give rise to static disorder in the site-energies of the pigments, represented by a random shift of ΔE_n. This disorder is referred to as diagonal disorder and is usually modeled by a Gaussian distribution of site-energies (Sundström et al., 1999). Any structural disorder or deformation of the ring will cause deviations from perfect symmetry and results in a variation of the interactions, represented by ΔV_n. This disorder is referred to as off-diagonal disorder. The resulting energy levels of the total system are determined by the strength of the coupling and the site-energies of the system. Commonly, one distinguishes two limiting cases: the regime of weak coupling, i.e. $|V/\Delta E| \ll 1$, where the excitation energy is mainly localized on the individual pigments, and the regime of strong coupling, i.e. $|V/\Delta E| \gg 1$, where the excitation energy is completely delocalized over the whole assembly. If the electronic coupling and the site-energy difference are similar in magnitude, the character of the excited states is expected to be intermediate between the extremes of weak and strong coupling.

Accordingly, the optical properties of such systems are determined not only by the intrinsic properties of the individual molecular building blocks but also by the intermolecular interactions between those units. These interactions depend strongly on the relative orientations and distances of the molecules and, consequently, the geometrical arrangement of the molecules has a crucial influence on the electronic excitations of the aggregate. Numerous approaches to calculate the resulting energies of the lowest electronically excited states of pigment-protein complexes have been reported in the literature (Schulten, 1999; Mostovoy and Knoester, 2000; Jang et al., 2001).

In the last decade, the development of techniques to optically study single molecules in the condensed phase opened the way for the investigation of molecular interactions on a truly microscopic scale (Rigler et al., 2001) and it became immediately obvious

that single-molecule spectroscopy can reveal spectroscopic details that are normally obscured by the ensemble average in bulk experiments. In this chapter, we present an overview of the results of a series of experiments on individual LH2 and LH1 complexes (van Oijen et al., 1998, 1999a; Ketelaars et al., 2001, 2002; Matsushita et al., 2001).

II. Spectroscopy of Individual Light-harvesting Complexes

A. Light-harvesting Complex 2 of Rps. acidophila

The three-dimensional structure of LH2 of *Rps. acidophila* is depicted in Fig. 3, where parts a and b of the figure show the pigment-protein complex as a whole, while parts c and d show only the BChl *a* pigments for clarity. Two BChl *a* pigment pools can be distinguished and are labeled B800 and B850, according to their room-temperature absorption maxima in the near infrared. The B800 ring consists of nine pigments, which have their molecular plane perpendicular to the symmetry axis. The B850 ring consists of nine repeating pairs of α- and β-bound pigments which are tightly organized like blades of a turbine with their molecular planes parallel to the symmetry axis. Both types of molecules are depicted on an enlarged scale in part e of Fig. 3 in light-gray (B800) and black (B850), respectively.

A very pronounced feature of the complex is the fact that, at least in crystalline form, this complex has a nine-fold rotational symmetry (C_9; McDermott et al., 1995). Upon excitation, energy is transferred from the B800 to B850 molecules in 1 to 2 ps, while energy transfer among the B850 molecules is an order of magnitude faster. The transfer of energy from LH2 to LH1 and subsequently to the RC occurs in vivo on a time scale of 30 – 40 ps, i.e., very fast compared to the fluorescence decay of B850 in isolated LH2, which has a time constant of about 1 ns (Blankenship, 2002).

Despite the fact that the LH2 complex has been intensively investigated during recent years using a wide variety of spectroscopic tools, no clear picture describing the electronic structure of its excited

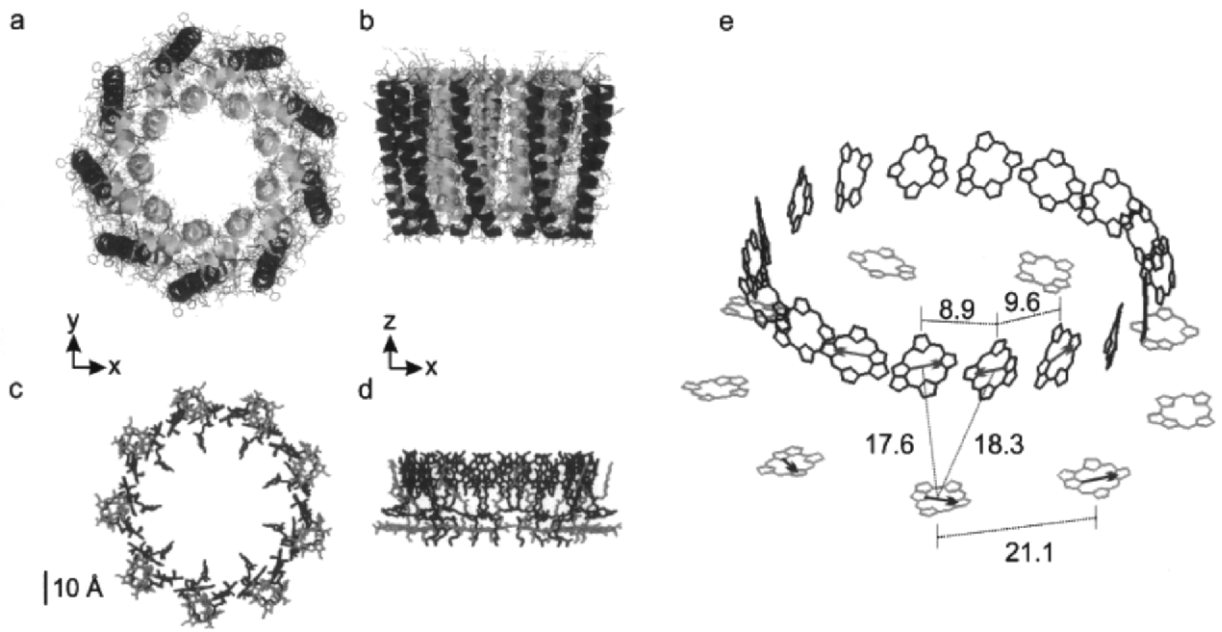

Fig. 3. Structure of the LH2 complex from *Rps. acidophila* as determined by X-ray diffraction (McDermott et al., 1995). Parts a) and b) show the whole pigment-protein complex; parts c) and d) the BChl *a* chromophores only. Parts a) and c) display a top view; parts b) and d) a side view, respectively. e) The spatial arrangement of the BChl *a* pigments in LH2 of *Rps. acidophila,* in a tilted side-view. The numbers indicate the center to center distances of the pigments in Å. The bars indicate the direction of the Q_y transition moments. The phytol chains of the pigments are removed for clarity.

states exists. The great difficulty encountered when determining the various parameters that play a role in the description of the electronic structure of light-harvesting complexes and the process of energy transfer, is the fact that the optical absorption lines are inhomogeneously broadened as a result of heterogeneity in the ensemble of absorbing pigments. To avoid the difficulties arising from the heterogeneity of these types of systems we applied the technique of single-molecule spectroscopy to study LH2. The fluorescence-excitation spectra of several individual LH2 complexes are shown in Fig. 4. The upper trace shows, for comparison, the fluorescence-excitation spectrum taken from a bulk sample (dashed line) together with the spectrum that results from the summation of the spectra of nineteen individual LH2 complexes (solid line). The two spectra are in excellent agreement and both feature two broad structureless bands around 800 and 860 nm corresponding to the absorptions of the B800 and B850 pigments of the complex. By measuring the fluorescence-excitation spectra of the individual complexes, remarkable features become visible which are obscured in the ensemble average. In particular, a striking difference between the B800 and B850 bands becomes evident: the spectra around 800 nm show a distribution of narrow absorption bands, whereas in the B850 spectral region 2–3 broad bands are present.

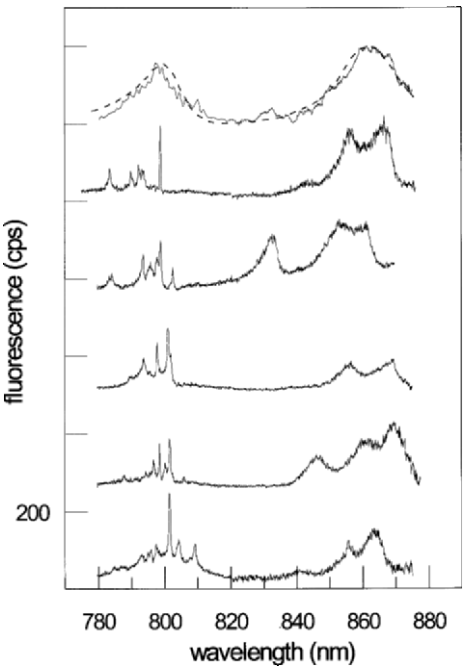

Fig. 4. Fluorescence-excitation spectra of individual LH2 complexes of *Rps. acidophila.* The top traces show the comparison between an ensemble spectrum (dashed line) and the sum of spectra recorded from nineteen individual complexes (solid line). The lower five traces display spectra from single LH2 complexes. Each individual spectrum has been averaged over all possible excitation polarizations. All spectra were measured at 1.2 K at 20 W/cm^2 with LH2 dissolved in a PVA-buffer solution. The individual spectra were taken from Ketelaars et al. (2001).

1. B800 Band

The fluorescence-excitation spectra of single LH2 complexes show a wide distribution of narrow absorption bands in the B800 region of the spectrum. These bands are spread over the whole inhomogeneously broadened ensemble spectrum.

To understand the origin of these bands we should compare the dipolar coupling between the pigments with the spread in site-energies (diagonal disorder). From the crystal structure, the dipolar coupling between neighboring pigments is estimated to be about –24 cm^{-1} (Fig. 5a; Sauer et al., 1996). The variation in site-energies, as estimated from the inhomogeneously broadened ensemble spectrum, is around 180 cm^{-1}. This yields a V/ΔE ratio of about 0.l which is clearly in the weak coupling regime and a strong localization of excitation on the individual BChl *a* is expected (Alden et al., 1997; Kennis et al., 1997b). We therefore attribute the pattern of spectral bands to absorptions of more or less individual pigments in the B800 band that are separated in their spectral positions due to differences in their local environment (inhomogeneous broadening). The interpretation of localized excitations in the B800 band is corroborated by the strong dependence of the relative intensities of these lines on the polarization of the incident radiation. Seven fluorescence-excitation spectra of the B800 band of an individual LH2 complex are shown in Fig. 5b, each taken with a different orientation of the polarization vector of the exciting laser light. It is seen that the intensities of the absorption lines vary appreciably upon changing the polarization. This would be expected if the excitations are largely localized on the individual BChl *a* pigments, because their transition-dipole moments are arranged in a circular manner and, as a result of this, all have different orientations. When analyzing the polarization-dependent spectra of a single LH2 complex, one would expect to observe 9 absorption lines, corresponding to local-

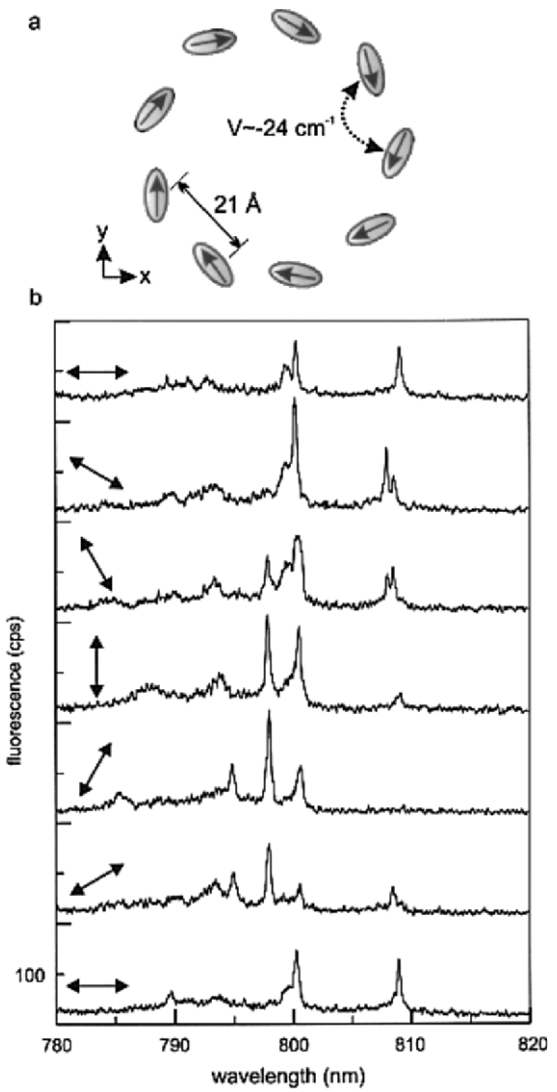

Fig. 5. a) Schematic representation of the transition-dipole moments of the B800 pigments of LH2. b) Dependence of the B800 fluorescence-excitation spectrum of a single LH2 complex from *Rps. acidophila* on the polarization of the incident radiation. The polarization vector has been changed in steps of 30° from one spectrum to the next. The vertical scale is valid for the lowest trace, all other are displaced for clarity. Figure taken from van Oijen et al. (1999b).

ized excitations of the 9 individual BChl *a* pigments; however, in these combined spectra typically only 6–7 absorption lines were found, which supports the conjecture that a slight delocalization of the excited state occurs over 2 or 3 neighboring BChl *a* pigments in the B800 manifold with a concomitant redistribution of oscillator strength. This arises from occasional (near)-degeneracy of the site-energies of adjacent B800 pigments. Meanwhile we have been able to confirm this conjecture in a detailed study on the B800 band of LH2 from *Rsp. molischianum* (Hofmann et al., 2003).

2. B850 band

For the B850 band, we have to consider the intermolecular interactions to understand the optical spectra. As a starting point, we calculate the excited-state manifold of the B850 assembly using Eq. (1) with N = 18 and $\Delta E_n = \Delta V_n = 0$. The proper eigenstates are exciton states and are characterized by a new quantum number, k, which can take the values $0, \pm1, \pm2, ..., \pm8, 9$. The lower part of this exciton manifold is shown in the inset of Fig. 6a. Owing to the circular symmetry, only the states $k = \pm 1$ carry an appreciable transition-dipole moment which makes them accessible for optical spectroscopy. Moreover, their transition moments are mutually orthogonal as indicated by the two arrows in the inset. The respective fluorescence-excitation spectra of the B850 spectral region are shown in Fig. 6a. They have been obtained for excitation with mutual orthogonal polarization. Apparently, the transition-dipole moments of these two transitions are perpendicular with respect to each other. We have observed this feature for all the complexes that have been studied. Based on this observation and the fact that these bands are by far the most intense ones in absorption, we attribute these transitions to the $k = \pm 1$ exciton states. The observed line widths of the bands reflect the ultra-fast relaxation (~ 100 fs) to the $k = 0$ exciton state, consistent with time-resolved data (Sundström et al., 1999).

A crucial check for this assignment would be the observation of the $k = 0$ exciton state. For this transition, which gains oscillator strength by any deviation from the perfectly symmetric situation, a relatively narrow absorption line is expected according to the lifetime of about 1 ns for the $k = 0$ state. To monitor this transition, we had to modify our data acquisition scheme slightly to suppress dynamical processes that occur on a timescale slower than 100 ms. Indeed, after doing so, we observed a narrow line on the low-energy side of the B850 band, (see Fig. 6b): this provides strong evidence that the description of the lowest electronically excited states of the B850 assembly in terms of the exciton model is justified. The spectral properties of these observed narrow transitions are summarized in Table 1. They feature an oscillator strength of 2–10% of the total

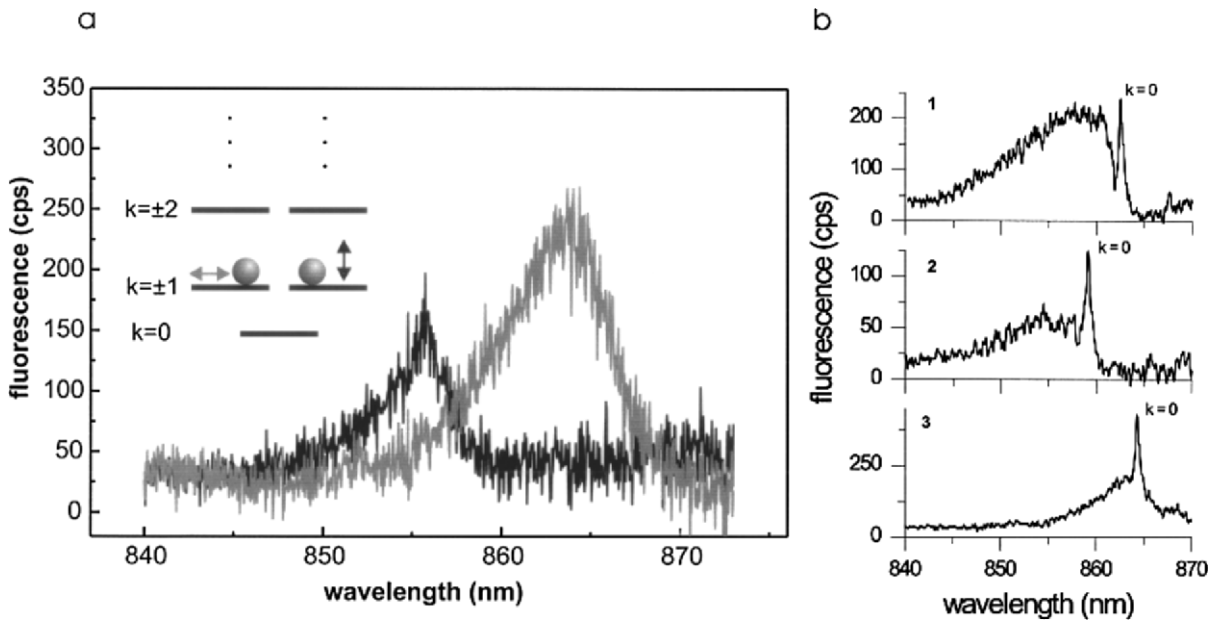

Fig. 6. a) Fluorescence-excitation spectrum of the long-wavelength region of an individual LH2 complex for mutually orthogonal polarized excitation. The inset shows a schematic representation of the energy-level scheme of the lowest states in the excited-state manifold of the B850 ring in LH2 of *Rps. acidophila* for nine-fold rotational symmetry of the pigment arrangement. The grey circles indicate the initial population of a given excited state and the arrows the relative orientation of the transition-dipole moments in the plane of the ring. b) Fluorescence-excitation spectra of the long wavelength part of the B850 band of three different complexes (1–3), featuring a very narrow transition at the red wing of the k = ±1 absorptions. The spectra are obtained by a summation of repetitively scanned spectra at a high scan rate, where the k = 0 transitions are aligned before summation to correct for spectral diffusion. Details are given in Table 1 and Ketelaars et al. (2001).

Table 1. Properties of the narrow features in the spectra of the individual LH2 complexes shown in Fig. 6b. The relative oscillator strength of the transition has been obtained by dividing its intensity by the total intensity observed in the B850 spectral region. δE_{01} denotes the spectral separation between the narrow line and the average spectral position of the two broad k = ± 1 absorptions. (FWHM, full width half maximum).

complex (see Fig. 6)	spectral position (nm) (wavenumber)	FWHM (cm^{-1})	relative oscillator strength (%)	δE_{01} (cm^{-1})
1	862.5 (11594 cm^{-1})	10	2	58
2	859.3 (11637 cm^{-1})	13	9	93
3	864.2 (11571 cm^{-1})	12	10	102

oscillator strength in the B850 band, in good agreement with theoretical calculations (Mostovoy and Knoester, 2000). Although the statistics are poor, the k = 0 transition in the three complexes suggests that the transition-dipole moment of the k = 0 state becomes stronger when the energy separation between the k = 0 and k = ±1 states increases. This is in qualitative agreement with model calculations on this system (Alden et al., 1997; Monshouwer et al., 1997; Freiberg et al., 1999).

However, for the circular arrangement of the pigments, the exciton model predicts that the k = ± 1 states are degenerate, i.e. feature the same transition energy and have the same intensity. Instead, we observe a splitting for the energies of these states as well as an intensity ratio for these bands which clearly deviates from 1. The energy separation varies from complex to complex and shows a distribution centered at about 110 cm^{-1} whereas the distribution for the intensity ratio is centered at 0.7. After analyzing our data, we

had to conclude that this results from a deviation of the B850 pigment ring from the perfect circular symmetry and that an elliptical distortion is most probable (Ketelaars et al., 2001; Matsushita et al., 2001). Based on fluorescence-polarization experiments, other groups came to similar conclusions (Bopp et al., 1999; Tietz et al., 2000). The experiments of Bopp et al. (1999) indicate, moreover, that the structural deformation undergoes fluctuations on a timescale of seconds under ambient conditions.

B. Light-harvesting Complex 1 of Rps. acidophila

In contrast to the structures of two LH2 complexes and one LH3 complex (Mcluskey et al., 2001), which have been determined with X-ray crystallography, the three dimensional arrangement of LH1 is not yet known with atomic resolution. Based on homology arguments, the LH1 ring is frequently modeled as a closed ring which encloses the reaction center. Some experimental data, e.g. from electron microscopy experiments (Karrasch et al., 1995; Walz et al., 1998), seem to support such a model. Nevertheless, the general validity of a closed-ring model may be questioned for various reasons. Firstly, the pigment analyses (Francke and Amesz, 1995; Qians et al. 2000) indicate that in many strains the number of pigments in LH1 per RC may be significantly lower than 32, i.e., too small to incorporate a RC in its core. Non-circular structures of LH1 have also been reported (Stahlberg et al., 1998; Jungas et al., 1999). It has been argued (Cogdell et al., 1996) that the LH1 complex actually cannot be a closed ring, because it would prohibit secondary electron transport which occurs by diffusion of the reduced quinone; in fact, by a shuttle of electrons, from the RC towards the cytochrome. This requires at least a passage for the quinone through the LH1 enclosure, either through a gap in the ring or by a special protein which might function as a gateway. Indeed, a small trans-membrane protein, called PufX has been found in the case of some species of purple bacteria (Farchaus et al., 1992; Lilburn et al., 1992), which is required for photosynthetic growth (Farchaus et al., 1992; Lilburn et al., 1992; Barz et al., 1995). PufX is assumed to function as a gateway in the LH1 enclosure for exchange of quinones. In species with no PufX, other proteins, like the Ω-peptide in the case of *Rsp. rubrum*, might have a similar function (Ghosh et al., 1994). However, there is no direct structural evidence that PufX, the Ω-peptide or other membrane proteins form an integral part of the LH1-RC core complex. Moreover, both PufX and the Ω-peptide have not been found in *Rps. acidophila*, but it is not known if there is another protein with a similar function as part of the LH1 ring in this species. Alternatively, it is possible in this case that LH1 is not a closed but an open ring, because photosynthetic growth is not then impaired as concluded from experiments on *Rba. sphaeroides*. The motivation for optical spectroscopy measurements on individual LH1 and LH1-RC complexes is that such experiments can elucidate structural heterogeneity and variations by correlating the electronic structure derived from the optical spectra with the spatial arrangement of pigments in the LH1 complex.

To investigate the implications of the different structural arrangements proposed for LH1 on the optical properties of individual LH1 complexes, we simulated the optical spectrum of an individual LH1 complex as a function of its oligomeric structure in the absence of site heterogeneity. We assumed a similar structure for LH1 and essentially the same parameters as for the B850 system of LH2, except that the number of pigments in a complete ring was assumed to be 32 (with a corresponding increase of the diameter of the ring). The results of these calculations are depicted in Fig. 7 for three different oligomeric structures.

Breaking the circular symmetry by removing an αβ-subunit, Fig. 7b, lifts the pairwise degeneracy of the exciton states. The lowest state is no longer labeled $k^{circ} = 0$, but k = 1, similar to that of a linear aggregate. The second state becomes k = 2 etc. This lowest state (k = 1) is no longer optically forbidden and strongly gains oscillator strength (10%), while its energy is slightly blue shifted. The third state (k = 3) loses oscillator strength due to the curvilinear shape of the array of subunits, and is blue shifted (1.4 nm) compared to the degenerate states of the circular structure. When reducing the ring structure even further into a half-ring consisting of eight subunits (Fig. 7c) the k = 1 state gains even more oscillator strength. The k = 2 state still has oscillator strength, but less than in the case with one subunit missing, and is blue shifted. Due to the half-circular shape of the array, the third k = 3 state has almost no oscillator strength left. Higher exciton states (k = 4 and k = 6), however, gain some oscillator strength. The two states with most of the oscillator strength (k = 1 and k = 2) are mutually orthogonal.

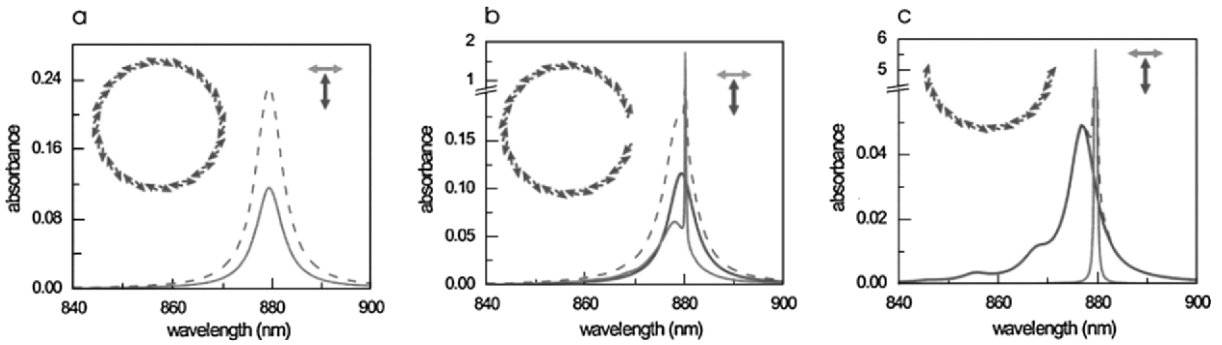

Fig. 7. a) Simulation of the absorption spectrum of an individual LH1 complex which forms a complete ring, b) a LH1 ring with 1 subunit missing c) and a LH1 complex with a partial ring consisting of eight αβ -subunits. The overall absorption spectrum in the xy-plane of the complex is plotted (dashed gray line) together with the absorption spectra along the x axis (full black line) and y axis (full gray line). The x-axis is chosen along the transition-dipole moment of one of the $k^{circ} = \pm 1$ states in the case of (a) and along the k = 2 state in the cases (b) and (c). The insets sketch the arrangement of the subunits in the xy-plane, showing the Q_y transition-dipole moments (arrows).

In summary, the removal of subunits from the closed circular arrangement has important implications for the optical spectrum of an individual LH1 complex. In particular, the increase in the oscillator strength of the lowest energetic state is remarkable. Degenerate states in the manifold are no longer present. However, the spectrum of an open ring consisting of 15 subunits will still be dominated by two, broad orthogonal bands. For a half circular arrangement two orthogonal bands will also dominate the spectrum. Since one of them represents the lowest energetic state, it is likely to appear as a narrow line in the spectrum. Partial rings with a variable number of subunits, together with site heterogeneity, would strongly exacerbate the variation in the spectra from one individual complex to the other.

Figure 8 summarizes the experimental data that were obtained by optical spectroscopy measurements on 24 individual LH1-RC complexes. In general, the observed bands are rather broad, but most spectra (80%) show also narrow absorption lines. The intensities of these lines vary from complex to complex. For most of these lines the signal-to-noise ratio is good enough to determine their width within one scan, reducing the influence of spectral diffusion. The widths of these narrow features are approximately 1–3 cm^{-1} and are mainly determined by the spectral width of the laser excitation source (1 cm^{-1}). The spectral positions of the narrow lines are always on the red wing of a broad absorption band.

In total, based on the polarization behavior and additional spectral features, the different individual LH1-RC complexes can be roughly divided into four

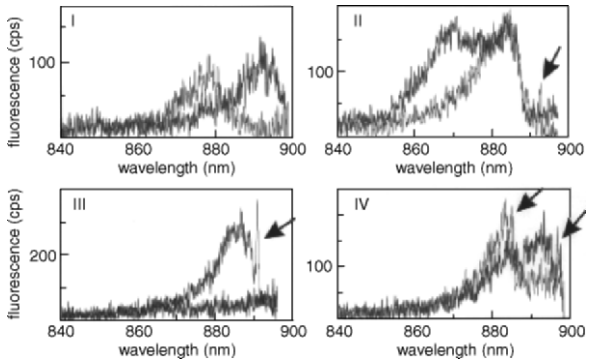

Fig. 8. Four different types of polarization behavior of the fluorescence-excitation spectra of individual LH1-RC complexes from *Rps. acidophila* according to the four groups, I – IV, discussed in the text. Each panel shows two fluorescence excitation spectra recorded for different mutual polarization of the excitation light. I) 90°, II) 64°, III) 90°, IV) 50°. The arrows point towards the narrow absorption lines present in some of the spectra.

different types labeled I to IV. An example of each type is depicted in Fig. 8. The spectra belonging to type I (30% of the complexes so far studied) are dominated by two broad bands around 870 – 880 nm. The polarization of these bands is mutually orthogonal within a few degrees. Such a polarization pattern is very similar to that observed for the LH2 complex (van Oijen et al., 1999a; Ketelaars et al., 2001) and we tentatively assign the two bands to the lowest degenerate states of a circular exciton denoted by their quantum number $k^{circ} = \pm 1$. The degeneracy of these two states is lifted, with an average energy separation of 116 ±77 cm^{-1}, similar to that in LH2. Most of the spectra show a narrow absorption line on the low-energy site of the $k^{circ} = \pm 1$ states which

represents the long-lived emitting state, $k^{circ} = 0$.

The spectra of type II show two broad bands with a mutual angle of polarization significantly less than 90 degrees. The angles vary between 30–64 degrees. Two spectra show a narrow absorption line on the low-energy side of the spectrum. Despite the fact that the mutual orthogonality of the two broad bands is not maintained, we believe that these states might still represent the lowest degenerate states of a circular exciton. We therefore label them 'k^{circ}' and 17% of the complexes (4 in total) exhibit this behavior.

A third type (III) of complex shows a behavior characterized by an angle for the polarization of the excitation light where no emission can be detected. This becomes even more obvious by comparing the optical spectra recorded for polarizations of 45 and 135 degrees, as shown in Fig. 8. It is noteworthy that the narrow line at the red edge of the spectra has the same polarization as the broad band and 17% of the total number of complexes belong to this group.

The spectra of type IV show two narrow absorption lines that are both located on the red edge of a broad absorption band. They are visible in the two spectra which have been taken at different polarizations. The relative angle of polarization of the two broad bands for this particular complex is approximately 50 degrees. Other complexes in this group show angles that are significantly different. Complexes with a narrow line in the middle of their spectrum and a broad band on the red side extending in the detection window, also belong to this group, since the detection window could be masking a second narrow line. In total, 36% of the studied complexes exhibit a type IV behavior.

The two most pronounced features of the fluorescence-excitation spectra of the individual LH1-RC complexes of *Rps. acidophila* are the observation of a limited number of bands with a characteristic polarization behavior, and a large variation in their appearance. In general, 3 – 4 bands (broad and narrow) are observed in one spectrum. This suggests that the spectroscopic features have to be described in terms of a collective excitation of the ring-like structure of pigment-molecules. The variation in the fluorescence-excitation spectra manifests itself in the number of bands, their polarization behavior, bandwidths and spectral positions (see Fig. 8). A large part of the complexes (80%) shows a narrow absorption line. In addition, 20% of the spectra show multiple narrow absorption lines. All spectra show broad bands which indicate dephasing times of tens of femtoseconds with a clear dependence on the polarization of the excitation light. Since most of the observed bands are broad (150–200 cm^{-1}), it is not always possible to resolve all the bands in the spectrum.

To understand these observations, it should be realized that the excitation spectra of the individual complexes are strongly influenced by site heterogeneity, structural heterogeneity and the orientation of the complexes in the polymer film. These three effects are not mutually exclusive and it is likely that the properties of each group of spectra is determined by a combination of all three. The presence of the RC is not expected to significantly influence the electronic structure of LH1, because the primary donor (P) and the pigments of the LH1 ring are separated by about 4.3 nm (Papiz et al., 1996); thus, coupling between P and LH1 is reduced (Novoderezhkin and Razjivin, 1995). The mismatch between the energy of P and the lowest state of LH1 will further reduce the effect of this coupling.

Of the four different types of spectral behavior of the LH1-RC complex, type I and type II resemble the behavior of a circular exciton. In particular, the type I spectra show the typical orthogonal polarization of the two strongest bands in the spectra. The type II spectra reveal an angle of 30–64 degrees between the polarization of the two major bands. This may be explained by considering the spatial model of the LH1-RC complex proposed by the Cogdell group (Cogdell et al., 1996; Papiz et al., 1996) which shows that the RC sticks out about 20 Å on the N-terminus site of the LH1 ring. This additional protein part might tilt the plane of the LH1 ring in the polymer film. As a result, the orthogonality of the $k^{circ} = \pm 1$ transitions is lost since only a projection of these states on the plane perpendicular to the excitation beam is observed. A tilt of the ring relative to this plane will lead to a smaller mutual polarization angle of the $k^{circ} = \pm 1$ states in the recorded spectra. In the limiting case, where the plane of the LH1 ring is oriented parallel to the propagation vector of the excitation light, the mutual angle of the $k^{circ} = \pm 1$ states as detected in the experiment is zero. This would imply that the LH1-RC ring structure is oriented sideways, i.e., with the plane of the ring (12 nm diameter) perpendicular to the substrate, while the short side of the structure (~5.5 nm) is parallel to the substrate, but such an orientation seems highly unlikely. If the LH1-RC complexes are no longer complete rings, the overall protein structure could become asymmetric. The orientation of such a structure is expected to be completely different

and may vary strongly between complexes. Thus we conclude that the variation of the polarization of the transitions may very well be caused by a variation in the alignment of the complexes.

The type III complexes show a polarization behavior that is difficult to interpret in terms of a closed circular structure. Only an extreme sideways orientation of the ring structure could account for the lack of absorption at certain polarizations. Further, a half-ring structure of LH1 oriented perpendicular to the excitation beam cannot explain the polarization behavior as observed in Fig. 8 (type III). In such a case two orthogonal bands will dominate the optical spectrum. A possible explanation is that the type III spectra correspond to a half-ring structure that is tilted with respect to the direction of the excitation beam.

In the type IV spectra, two narrow absorption lines are observed. This indicates the presence of at least two aggregates weakly coupled to each other. There are two possibilities for this kind of behavior. First the spectra might originate from two LH1-RC complexes. Dimerization of the LH1-RC structure has been reported (Francia et al., 1999). They proposed a dimeric structure of the LH1-RC complex under native conditions which could be converted into a monomeric structure by increasing the detergent concentration during biochemical isolation. Since our preparation procedure was performed at a high detergent concentration, a dimeric aggregation of the LH1-RC complexes is improbable. A second possibility might be the presence of more or less isolated domains of pigment arrays within one LH1 ring. These domains are isolated from each other either by defects in the ring or by additional proteins that form part of the LH1 structure but do not participate in energy transfer.

The experiments presented show that the optical spectra of individual pigment-protein complexes carry valuable information about their spatial structure. The limited number of bands with linewidths of 150–200 cm^{-1} and the presence of one or two preferred polarization directions that were observed for most of the complexes, indicate that the excited states of LH1 at low temperature should be described as collective excitations or Frenkel excitons. The spectra show a large variation in spectral features like the number of bands, bandwidths and their polarization behavior. We suggest that the variation in the optical spectra of individual LH1-RC complexes reflects the heterogeneity in the spatial structure of the LH1 assembly of pigments in combination with various orientations of the complexes in the polymer film, which may be enhanced or even induced by structural heterogeneity. It is not clear to what extent these structural variations are representative of LH1-RC complexes in the native system, as they could also be induced by isolation, purification and deposition of the sample. Future advances may be expected by studying these complexes in a more native-like environment, e.g., through incorporation in lipid bilayers and by controlling their orientation.

Acknowledgments

We thank C. Hofmann, M. Ketelaars and A. M. van Oijen who performed most of the described experiments. The LH1 samples have been provided by R. Cogdell which is gratefully acknowledged. Our work is financially supported by the VolkswagenStiftung and the 'Stichting voor Fundamenteel Onderzoek der Materie (FOM)' with financial aid also from the 'Nederlandse Organisatie voor Wetenschappelijk Onderzoek (NWO).'

References

Alden RG, Johnson E, Nagarajan V, Parson WW, Law CJ and Cogdell RJ (1997) Calculations of spectroscopic properties of the LH2 bacteriochlorophyll-protein antenna complex from *Rhodopseudomonas acidophila.* J Phys Chem B 101: 4667–4680

Barz WP, Francia SF, Venturoli G, Melandri BA, Vermeglio A and Oesterhelt D (1995) Role of PufX protein in photosynthetic growth of *Rhodobacter sphaeroides*. Photophosphorylation under anaerobic conditions' 1. PufX is required for efficient light-driven electron transfer and photophosphorylation under anaerobic conditions. Biochemistry 34: 15235–15247

Blankenship RE (2002) Molecular mechanisms of photosynthesis. Blackwell Sciences, Oxford

Bopp MA, Sytnik A, Howard TD, Cogdell RJ and Hochstrasser RM (1999) The dynamics of structural deformations of immobilized single light-harvesting complexes. Proc Natl Acad Sci 96: 11271–11276

Cogdell RJ, Fyfe PK, Barrett SJ, Prince SM, Freer AA, Isaacs NW, McGlynn P and Hunter CN (1996) The purple bacterial photosynthetic unit. Photosynth Res 48: 55–63

Farchaus JW, Barz WP, Grunberg H and Oesterhelt, D (1992) Studies on the expression of the PufX polypeptide and its requirement for photoheterotrophic growth in *Rhodobacter sphaeroides.* EMBO J 11: 2779–2788

Francia F, Wang J, Venturoli G, Melandri BA, Barz WP and Oesterhelt D (1999) The reaction center-LH1 antenna complex of *Rhodobacter sphaeroides* contains one PufX molecule which

is involved in dimerization of this complex. Biochemistry 38: 6834–6845

Francke C and Amesz J (1995) The size of the photosynthetic unit in purple bacteria. Photosynth Res 46: 347–352

Freiberg A, Timpmann K, Ruus R and Woodbury NW (1999) Disordered exciton analysis of linear and nonlinear absorption spectra of antenna bacteriochlorophyll aggregates: LH2-only mutant chromatophores of *Rhodobacter sphaeroides* at 8 K under spectrally selective excitation, J Phys Chem B 103: 10032–10041

Ghosh R, Ghosh-Eicher S, DiBeradino M and Bachofen R (1994) Protein phosphorylation in *rubrum*: Purification and characterization of a water-soluble *Rhodospirillum* B873 protein kinase and a new component of the B873 complex, Ω, which can be phosphorylated. Biochim Biophys Acta 1184: 28–36

Hofmann C, Ketelaars M, Matsushita M, Michel H, Aartsma TJ and Köhler J (2003) Single molecule study of the electronic couplings in a circular array of molecules: Light harvesting 2 complex from *Rhodospirillum molischianum*. Phys Rev Lett 90: 013004-1–013004-4

Hu X, Ritz T, Damjanovic A, Autenrieth F and Schulten K (2002) Photosynthetic apparatus of purple bacteria. Quart Rev Biophys 35: 1–62

Jang S, Dempster SE and Silbey RJ. (2001) Characterization of the static disorder in the B850 band of LH2. J Phys Chem B 105: 6655–6665

Jungas C, Ranck J-L, Rigaud J-L, Joliot P and Vermeglio A (1999) Supramolecular organization of the photosynthetic apparatus of *Rhodobacter sphaeroides.* EMBO J 18: 534–542

Karrasch S, Bullough PA and Ghosh R (1995) The 8.5 Å projection map of the light harvesting complex I from *Rhodospirillum rubrum* reveals a ring composed of 16 subunits. EMBO J 14: 631–638

Kennis JTM, Streltsov AM, Aartsma TJ, Nozawa T and Amesz J (1996) Energy transfer and excition coupling in isolated B800-850 complexes of the photosynthetic purple sulfur bacterium chromatium tepidum. The effect of structural symmetry on bacteriochlorophyll excited states. J Phys Chem C 100: 2438–2442

Kennis JTM, Streltsov AM, Permentier H, Aartsma TJ and Amesz J (1997a) Exciton coherence and energy transfer in the LH2 antenna complex of *Rhodopseudomonas acidophila* at low temperature. J Phys Chem B 101: 8369–8374

Kennis JTM, Streltsov AM, Vulto SIE, Aartsma TJ, Nozawa T and Amesz J (1997b) Femtosecond dynamics in isolated LH2 complexes of various species of purple bacteria. J Phys Chem B 101: 7827–7834

Ketelaars M., van Oijen AM, Matsushita M, Köhler J, Schmidt J and Aartsma TJ (2001) Spectroscopy on the B850 band of individual light-harvesting 2 complexes of *Rhodopseudomonas acidophila*; I. Experiments and Monte-Carlo simulations. Biophys J 80: 1591–1603

Ketelaars M, Hofmann C, Köhler J, Howard TD, Cogdell RJ, Schmidt J and Aartsma TJ (2002) Spectroscopy on individual light-harvesting 1 complexes of *Rhodopseudomonas acidophila*. Biophys J 83: 1701–1715

Koepke J, Hu X, Muenke C, Schulten K and Michel H (1996) The crystal structure of the light harvesting complex II (B800-B850) from *Rhodospirillum molischianum.* Structure 4: 581–597

Kühn O and Sundström V (1997) Pump probe spectroscopy of dissipative energy transfer dynamics in photosynthetic antenna complexes: A density matrix approach. J Chem Phys 107: 4154–4164

Lilburn TG, Haith CE, Prince RC and Beatty TJ (1992) Pleiotropic effects of pufX gene deletion on the structure and function of the photosynthetic apparatus of Rhodobacter capsulatus. Biochim Biophys Acta 1100: 160–170

Matsushita M, Ketelaars M, van Oijen AM, Köhler J, Aartsma TJ and Schmidt J (2001) Spectroscopy on the B850 band of individual light-harvesting 2 complexes of *Rhodopseudomonas acidophila*; II. Exciton states of an elliptically deformed ring aggregate. Biophys J 80: 1604–1614

McDermott G, Prince SM, Freer AA, Hawthornthwaite-Lawless AM, Papiz MZ, Cogdell RJ and Isaacs NW (1995) Crystal structure of an integral membrane light-harvesting complex from photosynthetic bacteria. Nature 374: 517–521

Mcluskey K, Prince SM, Cogdell RJ and Isaacs NW (2001) The crystallographic structure of the B800-820 LH3 light-harvesting complex from the purple bacteria *Rhodopseudomonas acidophila* strain 7050. Biochemistry 40: 8783–8789

Monshouwer R, Abrahamson M, van Mourik F and van Grondelle R (1997) Superradiance and exciton delocalization in bacterial photosynthetic light-harvesting systems. J Phys Chem B 101: 7241–7248

Mostovoy, MV and Knoester J (2000) Statistics of optical spectra from single ring aggregates and its application to LH2. J Phys Chem B 104: 12355–12364

Novoderezhkin, VI and Razjivin AP (1995) Exciton dynamics in circular aggregates: Application to antenna of photosynthetic purple bacteria- Biophys J 68: 1089–1100

Papiz MZ, Prince AM, Hawthornthwaite-Lawless AM, McDermott G, Freer AA, Isaacs NW and Cogdell RJ (1996) A model for the photosynthetic apparatus of purple bacteria. Trends Plant Sci 1: 198–206

Pullerits T, Chachisvillis M and Sundström V (1996) Exciton delocalization length in the B850 antenna of *Rhodobacter sphaeroides*. J Phys Chem 100: 10787–10792

Qians P, Agura T, Oyama Y and Cogdell RJ (2000) Isolation and purification of the reaction center (RC) and the core (RC-LH1) complex from *Rhodobium marinum*: The LH1 ring of the detergent-solubilized core complex contains 32 bacteriochlorophylls. Plant Cell Physiol 41: 1347–1353

Rigler R, Orrit M and Baschè T (eds) (2001) Single Molecule Spectroscopy, Nobel Conference Lectures, Springer-Series in Chemical Physics. Springer-Verlag, Berlin

Sauer K, Cogdell RJ, Prince SM, Freer AA, Isaacs NW and Scheer H (1996) Structure based calculations of the optical spectra of the LH2 bacteriochlorophyll-protein complex from *Rhodopseudomonas acidophila.* Photochem Photobiol 64: 564–576

Schulten K (1999) From simplicity to complexity and back: Function, architecture and mechanism of light harvesting systems in photosynthetic bacteria. In: Frauenfelder H, Deisenhofer J and Wolynes PG (eds) Simplicity and Complexity in Proteins and Nucleic Acids, pp 227–253. Dahlem University Press, Berlin

Stahlberg H, Dubochet J, Vogel H and Ghosh R (1998) The reaction centre of the photounit of *Rhodospirillum rubrum* is anchored to the light-harvesting complex with four-fold rotational disorder. Photosynth Res 55: 363–368

Sundström V, Pullerits T and van Grondelle R (1999) Photosynthetic light-harvesting: Reconciling dynamics and structure of purple bacterial LH2 reveals function of photosynthetic unit. J Phys Chem B 103: 2327–2346

Tietz C, Gerken U, Jelezko F and Wrachtrup J (2000) Polarization measurements on single pigment protein complexes. Single Molecules 1: 67–72

van Amerongen H, Valkunas L and van Grondelle R (2000) Photosynthetic Excitons. World Scientific Publishing Co., Singapore

van Oijen AM, Ketelaars M, Köhler J, Aartsma TJ and Schmidt J (1998) Spectroscopy of single light-harvesting complexes from purple photosynthetic bacteria at 1.2 K. J Phys Chem B 102: 9363–9366

van Oijen AM, Ketelaars M, Köhler J, Aartsma TJ and Schmidt J (1999a) Unraveling the electronic structure of individual photosynthetic pigment-protein complexes. Science 285: 400–402

van Oijen AM, Ketelaars M, Köhler J, Aartsma TJ and Schmidt J (1999b) Spectroscopy of individual LH2 complexes of *Rhodopseudomonas acidophila*: Localized excitations in the B800 band. Chem Phys 247: 53–60

Walz T, Jamieson SJ, Bowers CM, Bullough PA and Hunter CN (1998) Projection structures of three photosynthetic complexes from *Rhodobacter Sphaeroides*: LH2 at 6 Angstrom LH1 and RC-LH1 at 25 Angstrom. J Mol Biol 282: 833–845

Chapter 22

Effects of Axial Coordination, Electronic Excitation and Oxidation on Bond Orders in the Bacteriochlorin Macrocycle, and Generation of Radical Cation on Photo-Excitation of in vitro and in vivo Bacteriochlorophyll *a* Aggregates: Resonance Raman Studies

Yasushi Koyama*[1], Yoshinori Kakitani[1], Leenawaty Limantara[2] and Ritsuko Fujii[1]
[1] Faculty of Science and Technology, Kwansei Gakuin University, 2-1 Gakuen, Sanda, Hyogo 669-1337, Japan; [2] Faculty of Science and Mathematics, Satya Wacana Christian University, Jl. Diponegoro 52-60, Salatiga 50711, Indonesia

Note: Readers are encouraged to visit the website http://epub.ub.uni-muenchen.de/archive/00000776/ for 'supplementary material,' where Figs. S1–S7 referred to in the text are posted.

*Author for correspondence, email: ykoyama@kwansei.ac.jp

Bernhard Grimm, Robert J. Porra, Wolfhart Rüdiger and Hugo Scheer (eds): Chlorophylls and Bacteriochlorophylls: Biochemistry, Biophysics, Functions and Applications, pp. 323–335.

Summary

Solutions of bacteriochlorophyll (BChl) *a* in both monomeric and aggregated forms, and also in solutions of pigment-protein complexes, were examined by resonance-Raman spectroscopy. The results permit us to report and discuss:

(1) The effects of axial coordination forming the 5- and 6-coordinated states as well as those of triplet excitation and one-electron oxidation forming the T_1 (lowest triplet) and the D_0 (radical-cation) states on bond orders in the macrocycle of BChl *a*, as probed by the ring-breathing frequency. A core-expansion mechanism is proposed by which the ring-breathing frequency reflects the coordination states in the S_0, T_1 and D_0 electronic states. Solvent parameters determining the relative stabilities of the 5- and 6-coordinated states are also discussed.

(2) Changes in bond order in the macrocycles of BChl *a* and bacteriopheophytin *a* upon photo-excitation to the T_1 and S_1 (the first-excited singlet) states as determined by changes in stretching force constants that were obtained by normal-coordinate analysis of the Raman spectra of the unlabeled and totally ^{15}N-, ^{13}C- and ^{2}H-labeled species. Based on the results, the implications of the pigment arrangement in the reaction center, facilitating electron transfer and triplet energy-transfer reactions, are discussed in terms of the partial localization of the HOMO and LUMO (the highest occupied and the lowest unoccupied molecular orbitals) that were identified as large changes in bond order.

(3) The generation of the T_1 state and subsequent transformation into the D_0 state on photo-excitation of BChl *a* aggregates, both in solution and in the carotenoid-less light harvesting complexes, LH1 and LH2. These have been identified by the use of the key ring-breathing Raman lines in the T_1 and D_0 states, and then, confirmed by electronic-absorption and EPR spectroscopy.

I. The 5- and 6-Coordinated States of Bacteriochlorophyll *a* in the S_0, T_1 and D_0 Electronic States as Probed by the Ring-Breathing Frequency

A. The Ring-Breathing Frequencies in the S_0, T_1 and D_0 States

1. The S_0 State

The strongest Raman line of bacteriochlorophyll (BChl) *a* was associated with the C_a–C_m and $C_{a'}$–C_m stretchings (Lutz, 1984; Donohoe et al., 1988; Hu et al., 1993); see Fig. 1 for the designation of carbon atoms in the conjugated part of the macrocycle. The assignment has been established to be the C_a–C_m and $C_{a'}$–C_m asymmetric stretchings coupled with C_a–C_b stretchings (simplified as 'the C_a–C_m asymmetric stretching') based on the normal-coordinate analysis of unlabeled and isotope-labeled BChl *a* (Sashima et al., 2000) as will be described in Sec. II A. Since this normal mode causes the shrinkage and expansion of the inner 16-membered ring of the BChl *a* macrocycle, we name it 'the ring-breathing mode.' In particular, we will call the ring-breathing mode in the S_0 state as 'ν_r'. By the use of the ν_r frequency, Callahan and Cotton (1987) classified the axial coordination of BChl *a* into the 5- and 6-coordinated states after measuring the ν_r Raman line in 15 different solvents and concluded that it appears at 1609 cm^{-1} and at 1595 cm^{-1} in the 5- and 6-coordinated states, respectively. Table 1 lists the ν_r frequencies in 20 different solvents; those solvents giving rise to a mixture of the 5- and 6-coordinated states are excluded (Y. Umemoto, K. Furukawa and Y. Koyama, unpublished; Nishizawa et al., 1994a; Misono et al., 1996; Koyama and Limantara, 1998). Actually, the ν_r frequency is in the region of 1605–1611 cm^{-1} in the 5-coordinated state and between 1594–1599 cm^{-1} in the 6-coordinated state.

The basis for the classification into the 5- and 6-coordinated states is as follows: When BChl *a* was dissolved in highly electron-donating (i.e., strongly-ligating) solvents such as methanol, pyridine

Abbreviations: BChl – bacteriochlorophyll; BPhe – bacteriopheophytin; Car – carotenoid; DN – donor number; D_0 – the radical-cation state; HOMO – highest occupied molecular orbital; LH1, LH2 – light harvesting complexes 1 and 2; LUMO – lowest unoccupied molecular orbital; MO – molecular orbital; *Rba. – Rhodobacter*; RC – reaction center; S_0 – the ground state; S_1 – the first singlet-excited state; T_1 – the lowest triplet-excited state; ν_r – the ring-breathing frequency in the S_0 state; ν_r' – the ring-breathing frequency in the S_1 state; ν_r'' – the ring-breathing frequency in the T_1 state; ν_r^+ – the ring-breathing frequency in the D_0 state

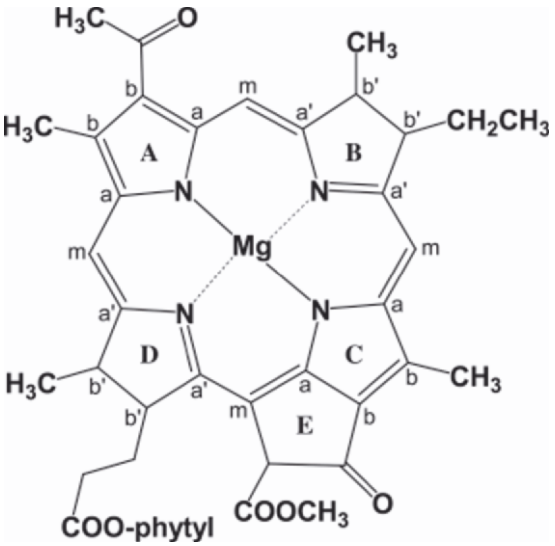

Fig. 1. Chemical structure of BChl *a* and designation of the rings and the carbon atoms in the macrocycles.

and tetrahydrofuran, the ν_r Raman line appeared at 1596, 1594 and 1595 cm^{-1}, respectively. When those solvents were diluted with methylene chloride, the ν_r Raman line shifted to 1609 cm^{-1}. The above changes in the ν_r frequency were ascribed to transformation from the 6- to the 5-coordinated state, respectively (Callahan and Cotton, 1987). In general, those solvents having high and low electron-donating power tend to form the 6- and 5-coordinated states, respectively (see Sec. B for the detailed mechanism).

2. The T_1 State

Nishizawa et al. (1994a) recorded the T_1 Raman spectra of BChl *a* in 16 different solvents (the raw Raman data are presented in Fig. S1; hereafter, figures appearing in supplementary material will be numbered as S2, S3, ...). Table 1 also lists the frequencies of the ring-breathing mode in the T_1 state (hereafter called 'ν_r'''). The ν_r'' frequencies are in the 1585–1591 cm^{-1} or in the 1578–1581 cm^{-1} regions in solvents having low and high electron-donating power, respectively. Therefore, it is reasonable to conclude that T_1 BChl *a* is in the 5- (6-) coordinated state in the former (the latter) solvents. Table 1 lists the resultant classification into the pair of coordinating states in the T_1 state, which is in complete agreement with that in the S_0 state. The ν_r'' frequencies in general are much lower than the ν_r frequencies, but both of them are definitely lower in the 6-coordinated state than in the 5-coordinated state.

3. The D_0 State

Misono et al. (1996) measured the Raman spectra of BChl *a* in the radical-cation (D_0) state that was generated electrochemically by one-electron oxidation in 13 different solvents (the raw Raman data are presented in Fig. S2). Hereafter, we *mainly* use the term 'the D_0 state' as an electronic state of BChl *a* and the term 'radical cation' in reference to the chemical species. Table 1 also lists the frequencies of the ring-breathing mode in the D_0 state (hereafter called 'ν_r^+'). The ν_r^+ frequencies are in the 1595–1599 cm^{-1} or in the 1584–1588 cm^{-1} regions in solvents having low and high electron-donating power, respectively; therefore, the former and latter regions can be ascribed to the 5- and 6-coordinated states, respectively. In general, the ν_r^+ frequencies are between the ν_r and ν_r'' frequencies, and the ν_r^+ frequencies in the 6-coordinated state are lower than those in the 5-coordinated state. Here again, the two coordination states exhibit two distinct frequency regions. (The ν_r, ν_r'' and ν_r^+ frequency regions in general and in the 5- and 6-coordinated states are summarized in Table S1.)

B. Mechanisms by Which the Ring-Breathing Frequency Reflects the 5- and 6-Coordinated States

Two possible mechanisms by which the ring-breathing frequency reflects the 5- and 6-coordinated states have been proposed, i.e., the core-expansion mechanism and the axial-polarization mechanism (Nishizawa et al., 1994a). The mechanisms were originally proposed for the T_1 state of BChl *a*; however, they should apply to the S_0 and the D_0 states as well.

1. The Core-Expansion Mechanism

When the central Mg atom of BChl *a* has only one axial ligand (in addition to the four nitrogen atoms in the macrocycle; see Fig. 1), it can sit out of the macrocycle plane. When the Mg atom has two equivalent axial ligands, however, it needs to sit in the macrocycle plane, and then, the 16-membered ring is to be expanded. Therefore, the lower ring-breathing frequency in the 6-coordinated state is supposed to reflect decrease in bond order in the expanded 16-membered ring (alternatively called 'the core').

2. The Axial-Polarization Mechanism

When the oxygen or nitrogen atom of the solvent

Table 1. The ring-breathing frequencies in the S_0 (ν_r), T_1 (ν_r'') and D_0 (ν_r^+) states of BChl *a* for classification into the 5-coordinated (V) and the 6-coordinated (VI) states, and those in the S_1 (ν_r') state. Solvent parameters to determine the relative stability of the two coordination states, in solution and bound to pigment-protein complexes (see foot notes), are also listed.

solvents / complexes	the ring-breathing frequencies										solvent parameters		
	ν_r		ν_r''		ν_r^+		ν_r'		$\nu_r^{+\,a}$		DN [b]	β [c]	π^* [d]
acetonitrile	1606	V	1590	V							14.1	0.31	0.75
propionitrile	1611	V			1597	V					16.1	0.37	0.71
1-butyronitrile	1609	V			1596	V					16.6		0.71
acetone	1608	V	1588	V	1598	V	1568				17.0	0.48	0.71
2-butanone	1610	V	1586	V	1595	V						0.48	0.67
3-pentanone	1610	V	1590	V	1596	V						0.45	0.72
2-octanone	1608	V	1589	V	1599	V							
diethyl ether	1607	V	1591	V							19.2	0.47	0.27
propyl ether	1608	V	1591	V									
methylene chloride	1609	V			1599	V			1597	V		0.00	0.82
carbon tetrachloride	1605	V							1599	V		0.00	0.28
2-propanol	1608	V	1585	V	1588	VI						0.95	0.48
methanol	1596	VI			1584	VI					19.0	0.62	0.60
ethanol	1599	VI			1585	VI					20.0	0.77	0.54
1-propanol	1598	VI			1584	VI							0.52
1-butanol	1597	VI	1580	VI	1588	VI						0.88	0.47
1-hexanol	1594	VI	1578	VI									
1-decanol	1596	VI	1579	VI									
pyridine	1594	VI	1581	VI			1568				33.1	0.64	0.87
tetrahydrofuran	1595	VI	1580	VI	1586	VI	1567				20.0	0.55	0.58
LH1	1610	V	1590	V					1596	V			
LH2	1608	V	1589	V					1596	V			
RC	1609	V							1598, 1599	V			

[a] Radical cation generated by photo-excitation. [b] Donor number which scale the electron-donating power of the solvent (Gutmann, 1978). [c] Taft parameter scaling the electron-donating power of the solvent (Kamlet et al., 1983). [d] Taft parameter scaling dielectric stabilization of a dipole by the solvent system (Kamlet et al., 1977, 1983; Kamlet and Taft, 1979)

molecule axially ligates the magnesium atom in the bacteriochlorin macrocycle, some electronic charge is to be transferred from the ligand to the metal. A Pariser-Parr-Pople calculation (Nishizawa et al., 1994a) including configurational interactions predicts that this axial polarization, (i.e., an effective positive charge on the oxygen or nitrogen atom and a negative charge on the magnesium atom) which should cause decrease in the bond orders of the $C_{a'}$–C_m, C_a–C_m and C_a–C_b bonds leading to decreased ring-breathing frequency and increased bond orders of the C_a–N, C_b–C_b and $C_{a'}$–N bonds (see Fig. 1 for the designation of the carbon atoms). Such changes upon ligation can take place in both coordination states; the calculated effects should be doubled in the 6-coordinated state with two axial ligands.

The core-expansion mechanism neatly explains the large and discrete change in the ring-breathing frequency upon transformation from the 5- to the 6-coordinated state in each electronic state. Comparison of the ring-breathing frequencies between BChl *a* and bacteriopheophytin (BPhe) *a* in the S_0, T_1 and S_1 states (see Table S1) rationalizes the core-expansion mechanism: in both the S_0 and the T_1 states, the ring-breathing frequencies of BChl *a* in the 5-coordinated state (ν_r 1605–1611 cm^{-1} and ν_r'' 1585–1591 cm^{-1}) roughly agree with those of BPhe *a* (ν_r 1606–1610 cm^{-1} and ν_r'' 1586–1589 cm^{-1}). In both electronic states, those frequencies may reflect that the intrinsic bond order in the 16-membered ring are common to both BChl *a* and BPhe *a*. (In other words, because the magnesium atom is located out of the macrocycle plane in the 5-coordinated BChl *a*, the ring-breathing frequencies would not be affected by its presence.) In the 6-coordinated state of BChl *a*, however, the expansion of the 16-membered ring by the magnesium atom should cause the down-shift of the ring-breathing frequency as described in the previous section.

The frequencies of the ring-breathing mode in the S_1 state (called 'ν_r'') are much lower in BChl *a* (1567–1568 cm^{-1}) than in BPhe *a* (1582–1587 cm^{-1}) thus indicating that the electronic structure of BChl *a* differs from BPhe *a*, and that the bond orders in the 16-membered ring are substantially lower in BChl *a* than in BPhe *a*. Therefore, the ring may be so expanded in the S_1 state of BChl *a* that the presence of the magnesium atom in or out of the macrocycle plane may make no difference at all. (The ν_r, ν_r'' and ν_r' frequency regions of BPhe *a* are summarized and compared with those of BChl *a* in Table S1.)

C. Solvent Parameters Determining the Relative Stability of the 5- and 6-Coordinated States

The core-expansion mechanism predicts that the selection of one of the coordination states is due to a balance between the steric hindrance and the power of ligation: the steric hindrance between the magnesium atom and the core (the 16-membered ring) of the macrocycle must push the equilibrium toward the 5-coordinated state, whereas the stabilization on ligation of the solvent molecule must push it toward the 6-coordinated state. Therefore, solvent molecules having high or low electron-donating power are expected to form the 6- or 5-coordinated states, respectively. On the other hand, a strong axial dipole can be generated by ligation of a single solvent molecule in the 5-coordinated state, whereas a pair of dipoles formed by ligation of two equivalent solvent molecules should be canceled out in the 6-coordinated state. Therefore, the dielectric stabilization of the axial dipole can be an additional factor to determine the relative stability of the coordination states; strong (weak) dielectric stabilization is expected to shift the equilibrium toward the 5- (6-) coordinated state.

Table 1 shows that the classification into the two coordination states is consistent among all the S_0, T_1 and D_0 electronic states except for the case of 2-propanol, which will be discussed later. Table 1 also lists the relevant solvent parameters, such as DN (Gutmann, 1978), and Taft's β and π^* parameters (Kamlet et al., 1977, 1983; Kamlet and Taft, 1979), which supposedly determine the relative stability of the 5- and 6-coordinated states. The DN value indicates the electron-donating power of the solvent and, in general, those solvents having small (large) DN values tend to form the 5- (6-) coordinated state; an exception is diethyl ether that may cause strong ligating power but more serious steric hindrance. One of the Taft parameters, β, also measures the electron-donating power of the solvent. Figures 2a, b and c show the ν_r, ν_r'' and ν_r^+ frequencies as a function of β. Interestingly, the 5- (6-) coordinated state is formed whenever $\beta < 0.5$ ($\beta > 0.5$) in all the S_0, T_1 and D_0 electronic states. The other Taft parameter, π^*, indicates the dielectric stabilization of a dipole by the solvent system. Figure 2d shows that the 5- (6-) coordinated state is stabilized in those solvents having large (small) π^* values.

In the case of 2-propanol (see Table 1 and the shadowed plot in Fig. 2), the very high value of β

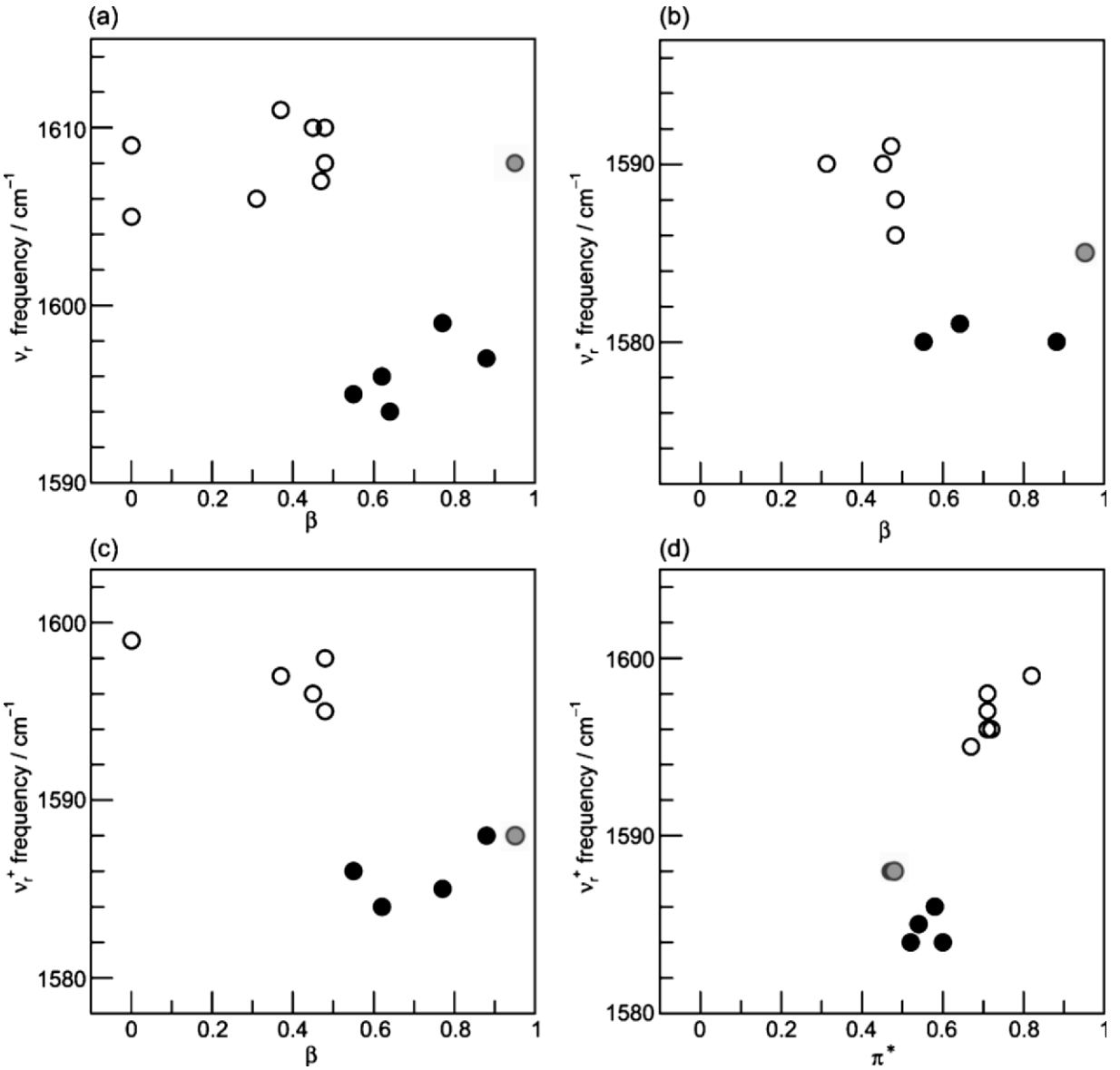

Fig. 2. Correlation between the ring-breathing frequencies reflecting the coordination states and the Taft parameters, β and π^* (Kamlet et al., 1977, 1983; Kamlet and Taft, 1979); β measures the electron-donating power of the solvent, whereas π^* indicates the dielectric stabilization of the dipole that is generated by ligation of the solvent. The (a) ν_r – β, (b) ν_r'' – β and (c) ν_r^+ – β correlations, and (d) the ν_r^+ – π^* correlation all in the 5- (○) and 6- (●) coordinated states. An exceptional case of the solvent, 2-propanol, is also indicated (gray circle).

and the very low value of π^* predict that the 6-coordinated state should be favorable. Presumably, strong steric interaction due to the structure of this particular solvent is expected to prevent the formation of the 6-coordinated state in the neutral S_0 and T_1 states. However, in the case of positively-charged radical cation (the D_0 state), stabilization on ligation becomes a predominant factor to form the 6-coordinated state. Thus, transformation from the 5- to the 6-coordinated state should take place upon one-electron oxidation.

II. Changes in Bond Orders as Scaled by Stretching Force Constants in the Conjugated Systems of Bacteriochlorophyll *a*, Bacteriopheophytin *a* and Carotenoid: Implication of the Arrangement of Those Pigments in the Reaction Center

A. Determination of the Normal Modes and the Stretching Force Constants in the Macrocycles of BChl a and BPhe a

Sashima et al. (2000) measured the Raman spectra of unlabeled and ^{15}N, ^{13}C and ^{2}H totally-labeled BChl *a* and BPhe *a* in the S_0, T_1 and S_1 states, and performed normal-coordinate analyses to establish the assignment of the Raman lines and to determine the stretching force constants of the carbon-carbon and the carbon-nitrogen bonds in the macrocycles. (The detailed results of the normal-coordinate analyses are shown in Figs. S3, S4 and S5.)

Figure 3 depicts the normal modes of the ring-breathing vibrations of BChl *a* and BPhe *a* in the S_0, T_1 and S_1 states, which justify the usage of these particular modes in probing the effects of coordination and electronic excitation in the bacteriochlorin macrocycle as described in Sec. I. Those normal modes are very similar to one another among the three different electronic states, and even between BChl *a* and BPhe *a*. The normal modes can be referred to as the C_a–C_m and $C_{a'}$–C_m stretchings coupled with the C_a–C_b stretchings (simplified as 'the C_a–C_m asymmetric stretching'), as defined at the beginning of the previous section.

Figure 4 depicts changes in the stretching force constants in the macrocycles of (a) BChl *a* and (b) BPhe *a* after singlet and triplet excitation (Sashima et al., 2000). The figure also includes changes in the stretching force constants on triplet excitation of the conjugated chain of a carotenoid (Car),15-*cis*-spheroidene, bound to the reaction center (RC) (Mukai-Kuroda et al., 2002). The changes in stretching force constants can be characterized as follows: *(a) BChl a.* On excitation to the S_1 state, the largest changes in the stretching force constants take place in the C_b–C_b bonds of ring A and ring C (+1.32), and the second largest changes take place in the $C_{a'}$–$C_{b'}$ bonds of ring B and ring D (+0.93). On excitation to the T_1 state, the largest changes take place in the $C_{a'}$–$C_{b'}$ bonds of rings B and D (+0.93), and the second largest changes in the C_a–N bonds (+0.40). *(b) BPhe a.* On excitation to the S_1 state, the largest changes in the stretching force constants take place in the C_b–C_b bonds of ring A and ring C (+1.36), and the second largest changes in the C_a–C_m and $C_{a'}$–C_m bonds of the 16-membered ring (–0.23). (Here, no changes take place at all in the $C_{a'}$–$C_{b'}$ bonds of rings B and D in contrast to the case of BChl *a*.) On excitation to the T_1 state, the largest changes take place in the $C_{a'}$–$C_{b'}$ bonds of rings B and D (+0.53), but the second largest changes take place in the C_a–N bonds (+0.28) and the C_b–C_b and C_a–C_b bonds of rings A and C (–0.28). *(c) Car.* On triplet excitation, the largest three changes in the stretching force constants take place in the C13=C14 (–0.73), C11=C12 (–0.59) and C12–C13 (+0.43) bonds.

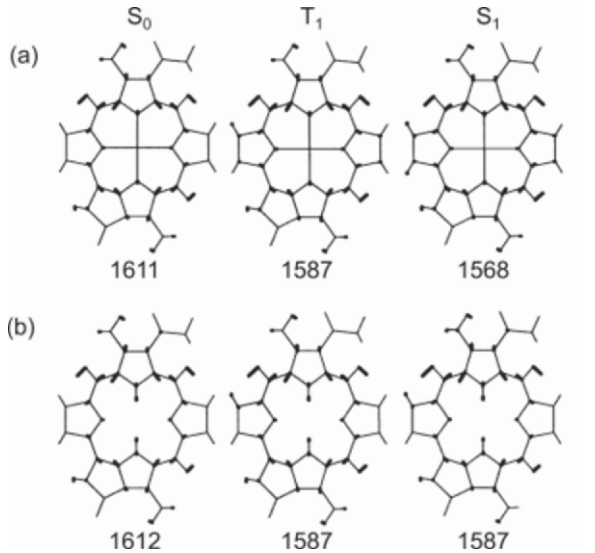

Fig. 3. Atomic displacements in the ring-breathing modes, i.e., 'the C_a–C_m asymmetric stretchings' in (a) BChl *a* and (b) BPhe *a* in the S_0, T_1 and S_1 states. The observed frequencies are also shown.

B. Localization of the Molecular Orbitals as Identified by Changes in Bond Orders upon Excitation, and the Arrangement of Pigment Molecules in the Reaction Center to Facilitate Charge Separation and Triplet Energy Transfer

In a Hückel-type molecular orbital (MO) description, where the MOs are expressed as a linear combination of the 2p atomic orbitals (χ_i) using coefficients (c_i) for atom *i*, the net change in bond order upon electronic excitation for an *a*–*b* bond is approximately given by $\Delta P_{ab} = -c_a^{\mathrm{HOMO}} \cdot c_b^{\mathrm{HOMO}} + c_a^{\mathrm{LUMO}} \cdot c_b^{\mathrm{LUMO}}$, where one of the coefficients, c_a or c_b, changes in its sign upon

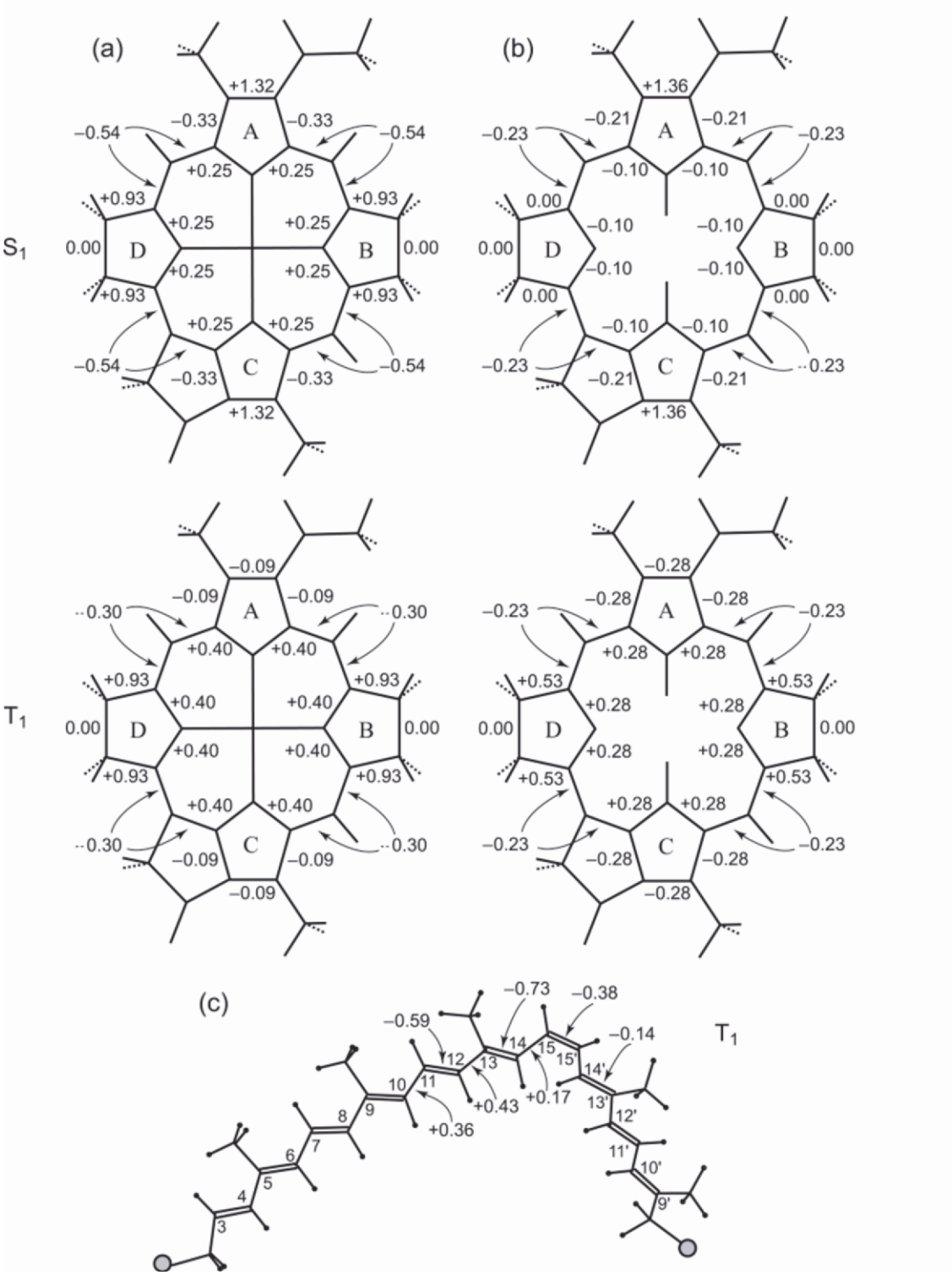

Fig. 4. Changes in the carbon-carbon and the carbon-nitrogen stretching force constants, upon singlet and triplet excitation, in the macrocycles of (a) BChl *a* and (b) BPhe *a* in solution, and (c) changes in the carbon-carbon stretching force constants, upon triplet excitation, in the conjugated chain of 15-*cis*-spheroidene bound to the RC.

the HOMO → LUMO transition. Here, partial localization of the HOMO and the LUMO in the macrocycle of BChl *a* (or BPhe *a*) is assumed. Then, a relation of $|\Delta P_{ab}| = |c_a^{\mathrm{HOMO}}| \cdot |c_b^{\mathrm{HOMO}}| + |c_a^{\mathrm{LUMO}}| \cdot |c_b^{\mathrm{LUMO}}|$ holds; ΔP_{ab} can be either positive or negative. When there is a large increase or decrease in bond order for the *a*–*b* bond, the absolute values of those coefficients will be large. Then, the HOMO (LUMO) of a molecule must be expanded spatially to facilitate their overlap with that of the neighboring molecule. Therefore, we can postulate that the charge-separation and the electron-transfer reactions, both using the overlap of the LUMOs of a pair of neighboring molecules, should be facilitated in a particular region where large changes in bond order upon singlet excitation take place in both the donor and the acceptor molecules. We can also postulate that the triplet energy-transfer reaction, using the overlap of both the HOMOs and LUMOs of the neighboring molecules, should be facilitated in a particular region where large changes in bond order take place upon triplet excitation in the donor and the acceptor molecules.

Figure 5 (and Color Plate 2) shows the arrangement of the BChl *a*, BPhe *a* and Car molecules in the RC from *Rhodobacter* (*Rba.*) *sphaeroides* strain AM260W that was determined by X-ray crystallography (R. J. Cogdell, personal communication). Now, changes in the stretching force constant, mentioned in the previous section, will be used as a scale for changes in bond order. In Fig. 5, in which the phytyl sidechains are truncated, bonds in the macrocycle giving rise to the largest and the second-largest changes in bond order (Fig. 4) are indicated by wavy and dotted lines, respectively. Based on the above postulates, we will explain the implications of the arrangement of those pigments from the viewpoint of the efficient charge-separation, electron-transfer and triplet energy-transfer reactions.

Charge Separation in the Special-Pair BChls. Figure 5a shows that a pair of C_b–C_b bonds in rings A (where the largest changes in bond order take place) of the special-pair BChls (P, temporarily named 'P_L' and 'P_M') overlap. In the overlap region, indicated by a black circle, separation is as little as 3.43 Å (i.e., van der Waals contact) thus facilitating charge separation.

Electron Transfer from one of the Special-Pair BChls (P_M) to the Accessory BChl (B_L) and then to the BPhe (H_L). Figure 5b shows that the C_b–C_b bond in ring A of P_M is close to that in ring C of B_L (the smallest distance, 5.63 Å), whereas Fig. 5c shows that the C_b–C_b bond in ring A of B_L is close to that in ring A of H_L (the smallest distance, 5.16 Å). The pigment arrangements described above must enhance the series of electron-transfer reactions in the order, $P_M \rightarrow B_L \rightarrow H_L$, where the regions of the largest changes in bond order of both the donor and the acceptor are used.

Triplet-energy Transfer from one of the Special-pair BChls (P_M) to the Accessory BChl on the M Branch (B_M), and then to the Car. Figure 5d shows that a C_a–N bond in ring C of P_M is close to a $C_{a'}$–$C_{b'}$ bond in ring B of B_M (the smallest distance, 5.42 Å), whereas Fig. 5e shows that a C_a–N bond of B_M is in close contact with the C13=C14 bond of Car (the smallest distance, 4.49 Å). The arrangements must facilitate the triplet energy-transfer reactions in the order $P_M \rightarrow B_M \rightarrow$ Car; here, the region of the second-largest change in bond order of the donor and that of the largest change in bond order of the acceptor are used. No efficient triplet-energy transfer is expected between the B_M and H_M molecules (Fig. 5f).

It is to be noted that each pair of pigments on the L and M branches exhibit approximate C_2 symmetry. In general, the arrangement of the BChl and BPhe molecules on the L branch enabling the extremely fast charge-separation and electron-transfer reactions seems to be of first priority. The arrangement of BChl molecules on the M branch to facilitate the much slower triplet energy-transfer reaction may be less important. It cannot be over-emphasized that the P_L, P_M, B_L and H_L molecules are perfectly arranged to achieve the overlap of C_b–C_b bonds thereby promoting the most important charge-separation and electron-transfer reactions in the RC.

III. Generation of the T_1 State and Subsequent Transformation into the D_0 State upon Photo-Excitation of in vitro and in vivo Bacteriochlorophyll *a* Aggregates

A. Bachteriochlorophyll a Aggregates in Solution

The generation of the D_0 state by photo-excitation of BChl *a* aggregates was first identified in methylene chloride and carbon tetrachloride solutions and the ring-breathing Raman lines appeared at 1597 and 1599 cm^{-1}, respectively (Nishizawa et al., 1994a), which is in the region of the 5-coordinated radical cation (1595–1599 cm^{-1}); see Table 1 or Table S1.

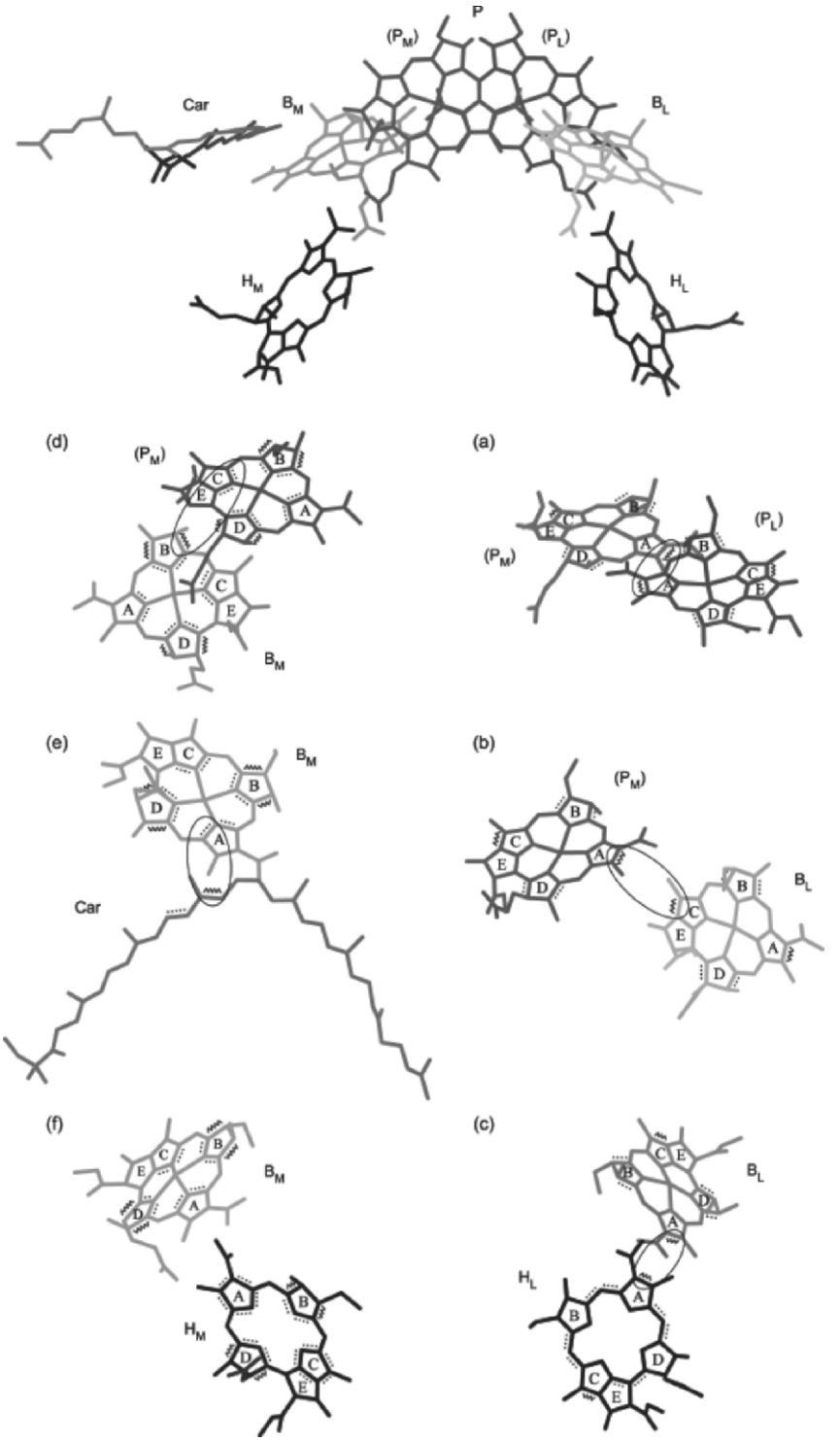

Fig. 5. Spatial arrangement of the special pair BChls (P, tentatively named 'P_L' and 'P_M'), the accessory BChls (B_L and B_M), the BPhes (H_L and H_M) and the Car molecules in the RC from *Rba. sphaeroides* strain AM260W (R. J. Cogdell, personal communication). The regions where the largest and the second-largest changes in bond order take place (where the HOMO and/or the LUMO are/is expected to be most or second-most localized) are indicated by wavy and dotted lines, in each pigment molecule (see Fig. 4); further, overlap of those regions is indicated by a black circle for each pigment pair. See also Color Plate 2.

Actually, the Raman spectrum of the transient species in methylene chloride agrees, within the limit of experimental error, with the stationary-state Raman spectrum of the radical cation (Fig. S2-g). Since both methylene chloride and carbon tetrachloride are chlorine-containing solvents forming BChl *a* aggregates, the electron ejected from BChl *a* to form BChl $a^{+\bullet}$ (the radical cation) is most probably transferred to the entire aggregate to form $BChl_n^{-\bullet}$ and, subsequently, to the chlorine atom in the solvent to form $Cl^{-\bullet}$.

Definitive evidence for the generation of the radical-cation (D_0) state by photo-excitation was obtained by time-resolved absorption spectroscopy of BChl *a* aggregates in carbon tetrachloride solution (Nishizawa et al., 1994b): Figure 6a shows the transient absorption spectrum of BChl *a* in pyridine (a 6-coordinating solvent): The absorption spectrum is typical of the T_1 state (Connolly et al., 1973; Nishizawa et al., 1994b). On the other hand, Fig. 6b shows the transient absorption spectrum of BChl *a* in carbon tetrachloride, which is consistent with the stationary-state absorption spectrum of BChl *a* radical cation that was electrochemically generated by one-electron oxidation (Misono et al., 1996). Thus, the radical cation (D_0 state) can be generated within 200 ns after excitation in carbon tetrachloride forming a higher aggregate.

Transformation from the T_1 state to the D_0 state was traced by time-resolved absorption spectroscopy of BChl *a* in methylene chloride solution (Nishizawa et al., 1994b); Figs. 6c, d and e show time-resolved absorption spectra recorded at 200 ns, 1 μs and 100 μs after excitation, respectively. Spectrum (c) exhibits the contribution of the T_1 state (401 nm) as the major component and that of the D_0 state as a minor component (a shoulder ~420 nm); spectrum (d) exhibits comparable intensity contributions by both states; and spectrum (e) exhibits only the contribution of the D_0 state. Spectrum (e) is almost identical to the stationary-state absorption spectrum of the D_0 state electrochemically generated in this particular solvent (see Fig. 5a of Misono et al., 1996). When spectrum (e) is subtracted from spectrum (c), spectrum (f) emerges as a pure T_1-state spectrum thus identifying

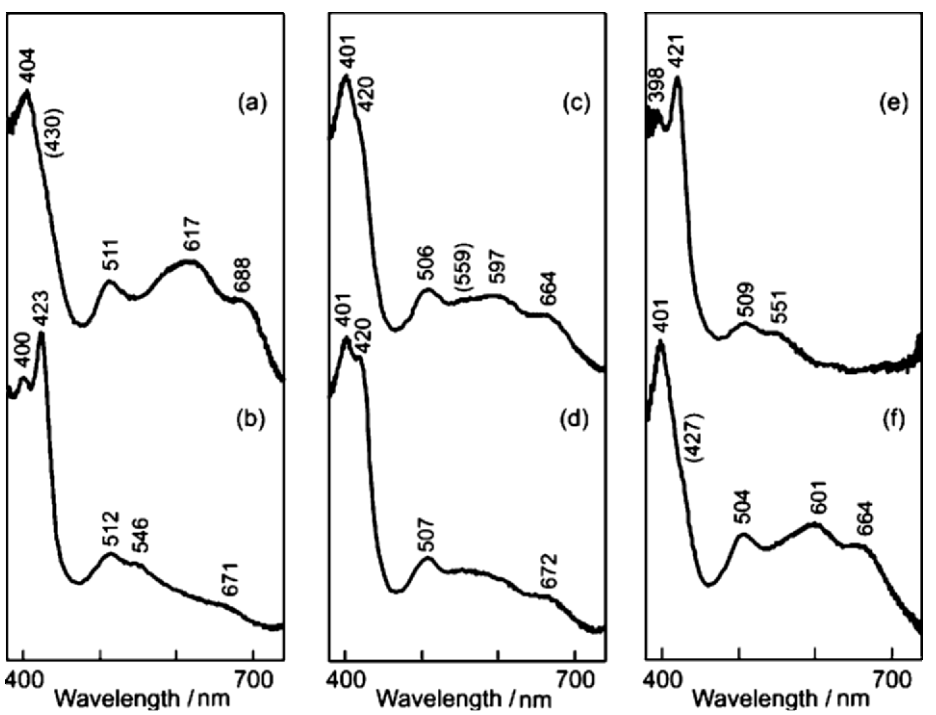

Fig. 6. (a) The transient T_1-state spectrum of BChl *a* monomer in pyridine, and (b) the transient D_0-state spectrum of BChl *a* aggregates in carbon tetrachloride, both at 200 ns after excitation. Time-resolved absorption spectra showing transformation from the T_1 to the D_0 state for BChl *a* aggregates in methylene chloride at (c) 200 ns, (d) 1 μs and (e) 100 μs after excitation. The difference spectrum (f) of (c) minus (e) exhibits the T_1-state spectrum, whereas spectrum (e) shows a pure D_0-state spectrum. Each sample solution was excited by the use of the 355nm, 12 ns pulses.

Table 2. The g-values, the linewidths and the lifetimes of the EPR signals from radical cation generated by photo-excitation of BChl *a* aggregates in carbon tetrachloride and in the carotenoid-less LH1, LH2 and RC complexes (at 110 K)

BChl *a* aggregates in	g-value	ΔH_{pp} [a] (gauss)	line shape	lifetime (ms)
CCl_4 solution	2.0026 ± 0.0002	12.3 ± 0.5	G [b]	5 ± 1
LH1	2.0026 ± 0.0002	9.3 ± 0.2	G	27 ± 3
LH2	2.0026 ± 0.0002	9.3 ± 0.2	G	27 ± 3
RC	2.0026 ± 0.0002	10.3 ± 0.2	G	25 ± 3

[a] ΔH_{pp} indicates peak-to-peak first-derivative linewidth. [b] G indicates the Gaussian line shape.

the T_1 state as the precursor of the D_0 state in methylene chloride forming a lower aggregate.

The generation of radical cation (the D_0 state) by photo-excitation of the BChl *a* aggregate in carbon tetrachloride was established by EPR spectroscopy (Limantara et al., 1998). Table 2 shows the g-value, the linewidth, the line shape and the lifetime of this radical-cation signal. (Figure S6 shows a raw EPR spectrum of the D_0 state generated by photo-excitation of BChl *a* aggregates in carbon tetrachloride.)

B. Carotenoid-less Antenna Complexes

Limantara et al. (1998) discovered, by picosecond and nanosecond transient Raman spectroscopy, the generation of the T_1 state and its subsequent transformation into the D_0 state in the carotenoid-less LH1 and LH2 antenna complexes from *Rba. sphaeroides* R26 and R26.1. Here, the frequencies of the ν_r'' and ν_r^+ modes described in Sec. I played a key role. In transient Raman spectroscopy using ~50 ps pulses, the LH1 and LH2 complexes exhibited the ring-breathing Raman lines at 1590 and 1589 cm^{-1}, indicating that T_1 BChl *a* in the 5-coordinated state (the ν_r'' frequency region, 1585–1591 cm^{-1}) was generated during the pulse duration of ~50 ps (Table 1). On the other hand, the RC complex exhibited the ring-breathing Raman line at 1598 cm^{-1}, indicating, instead, that D_0 BChl *a* in the 5-coordinated state (the ν_r^+ frequency region, 1595–1599 cm^{-1}) is generated within 2.8 ps (Martin et al., 1986). (Figure S7 compares the S_0 Raman spectra (1) and transient Raman spectra obtained by the use of the ~50 ps pulses and ~12 ns (2 and 3, respectively) among the (a) LH1, (b) LH2 and (c) RC complexes from *Rba. sphaeroides* R26 and R26.1.)

In transient Raman spectroscopy using 12 ns pulses, both the LH1 and LH2 complexes exhibited transient ring-breathing Raman lines at 1596 cm^{-1} indicating that the T_1 state had already transformed into the D_0, 5-coordinated state within that particular pulse duration; see the ν_r'' and ν_r^+ frequency regions shown above. Again, the RC complex exhibited the ring-breathing Raman line at 1599 cm^{-1}, indicating that the D_0 state still remains. Thus, the generation of the D_0 state via the T_1 state by photo-excitation of the ring-shaped BChl *a* aggregates in the carotenoid-less antenna complexes was identified by transient Raman spectroscopy using the picosecond and the nanosecond pulses. In all the S_0, T_1 and D_0 states, the ring-breathing frequencies show that the BChl *a* molecules in the LH1, LH2 and RC complexes are in the 5-coordinated state.

The generation of the radical cation (D_0 state) by photo-excitation of the carotenoid-less LH1 and LH2 complexes was confirmed by EPR spectroscopy. Table 2 shows the g-values, the linewidths, the line shapes and the lifetimes of the radical cation signals generated in the LH1, LH2 and RC complexes. (Figure S6 shows the raw EPR signals of the carotenoid-less LH1, LH2 and RC complexes.) Comparison of the linewidths shows that the extent of electron delocalization is in the following order: LH1 and LH2 antenna complexes < RC < in vitro aggregates in carbon tetrachloride solution.

Most importantly, the precursor of the radical cation, i.e., T_1 BChl *a*, is quenched by Car, all-*trans*-spheroidene, in the LH1 and LH2 complexes from the wild type *Rba. sphaeroides*, preventing the oxidative degradation of the BChl *a* molecules (Limantara et al., 1998).

Acknowledgments

The authors thank Prof. Hugo Scheer, Prof. Hiroyoshi Nagae and Dr. Leszek Fiedor for reading the manuscript. This work has been supported by a grant from NEDO (New Energy and Industrial Technol-

ogy Development Organization, 'International Joint Research Grant'), and a grant from the Ministry and Education, Culture, Sports, Science and Technology for an Open Research Center Project, 'The Research Center of Photo-Energy Conversion.'

References

Callahan PM and Cotton TM (1987) Assignment of bacteriochlorophyll *a* ligation state from absorption and resonance Raman spectra. J Am Chem Soc 109: 7001–7007

Connolly JS, Gorman DS and Seely GR (1973) Laser flash photolysis studies of chlorin and porphyrin systems. I. Energetics of the triplet state of bacteriochlorophyll. Ann NY Acad Sci 206: 649–669

Donohoe RJ, Frank HA and Bocian DF (1988) Resonance Raman spectra and normal mode descriptions of a bacteriochlorophyll *a* model complex. Photochem Photobiol 48: 531–537

Gutmann V (1978) The Donor-Acceptor Approach to Molecular Interactions. Plenum Press, New York

Hu S, Mukherjee A and Spiro TG (1993) Synthesis, vibrational spectra, and normal mode analysis of nickel(II) 1,5-dihydroxy-1,5-dimethyloctaethylbacteriochlorin: A model for bacteriochlorophylls. J Am Chem Soc 115: 12366–12377

Kamlet MJ and Taft RW (1979) Linear solvation energy relationships. Part 1. Solvent polarity-polarizability effects on infrared spectra. J Chem Soc Perkin Trans 2: 337–341

Kamlet MJ, Abboud JL and Taft RW (1977) The solvatochromic comparison method. 6. The π* scale of solvent polarities. J Am Chem Soc 99: 6027–6038

Kamlet MJ, Abboud J-L M, Abraham MH and Taft RW (1983) Linear solvation energy relationships. 23. A comprehensive collection of the solvatochromic parameters, π*, α, and β, and some methods for simplifying the generalized solvatochromic equation. J Org Chem 48: 2877–2887

Koyama Y and Limantara L (1998) Effects of singlet and triplet excitation, oxidation and axial coordination on the bond orders in the macrocycle of bacteriochlorophyll *a* as revealed by resonance Raman spectroscopy. Spectrochim Acta Part A 54: 1127–1139

Limantara L, Fujii R, Zhang J-P, Kakuno T, Hara H, Kawamori A, Yagura T, Cogdell RJ and Koyama Y (1998) Generation of triplet and cation-radical bacteriochlorophyll *a* in carotenoidless LH1 and LH2 antenna complexes from *Rhodobacter sphaeroides*. Biochemistry 37: 17469–17486

Lutz M (1984) Resonance Raman studies in photosynthesis. In: Clark RJH and Hester RE (eds) Advances in Infrared and Raman Spectroscopy, Vol 11, pp 211–300. John Wiley & Sons, Chichester

Martin J-L, Breton J, Hoff AJ, Migus A and Antonetti A (1986) Femtosecond spectroscopy of electron transfer in the reaction center of the photosynthetic bacterium *Rhodopseudomonas sphaeroides* R-26: Direct electron transfer from the dimeric bacteriochlorophyll primary donor to the bacteriopheophytin acceptor with a time constant of 2.8 ± 0.2 psec. Proc Natl Acad Sci USA 83: 957–961

Misono Y, Limantara L, Koyama Y and Itoh K (1996) Solvent effects on the resonance Raman and electronic absorption spectra of bacteriochlorophyll *a* cation radical. J Phys Chem 100: 2422–2429

Mukai-Kuroda Y, Fujii R, Ko-chi N, Sashima T, Koyama Y, Abe M, Gebhard R, van der Hoef I and Lugtenburg J (2002) Changes in molecular structure upon triplet excitation of all-*trans*-spheroidene in *n*-hexane solution and 15-*cis*-spheroidene bound to the photo-reaction center from *Rhodobacter sphaeroides* as revealed by resonance-Raman spectroscopy and normal-coordinate analysis. J Phys Chem A 106: 3566–3579

Nishizawa E, Limantara L, Nanjou N, Nagae H, Kakuno T and Koyama Y (1994a) Solvent effects on triplet-state bacteriochlorophyll *a* as detected by transient Raman spectroscopy and the environment of bacteriochlorophyll *a* in the light-harvesting complex of *Rhodobacter sphaeroides* R26. Photochem Photobiol 59: 229–236

Nishizawa E, Nagae H and Koyama Y (1994b) Transient absorption spectroscopy of bacteriochlorophyll *a*: Cation radical generated in solvents forming aggregates and T_1 species generated in solvents forming penta- and hexacoordinated monomers with and without hydrogen bonding. J Phys Chem 98: 12086–12090

Sashima T, Limantara L and Koyama Y (2000) Changes in the carbon-carbon and carbon-nitrogen stretching force constants in the macrocycles of bacteriochlorophyll *a* and bacteriopheophytin *a* upon triplet and singlet excitation: Resonance-Raman spectroscopy and normal-coordinate analysis of the unlabeled and totally ^{15}N-, ^{13}C-, and ^{2}H-labeled species. J Phys Chem B 104: 8308–8320

Chapter 23

Mapping the Global Ring Currents in Porphyrins and Chlorins

Erich Steiner and Patrick W. Fowler*†
Department of Chemistry, Stocker Road, University of Exeter, Exeter EX4 4QD, U.K.

Summary

Visualization and mapping of induced current density using the *ab initio* ipsocentric distributed-origin method reveals the global ring currents in anionic, free-base and metallo- forms of porphin, chlorin and bacteriochlorin. All exhibit an essentially monocyclic circulation, but with characteristic additional bifurcations through unsaturated pyrrole units. The orbital model specific to the ipsocentric approach rationalizes the diatropic ring currents in all these systems in terms of magnetic activity of just a few electrons. The greater part of the magnetic response is ascribed to virtual transitions involving the two highest occupied π and two lowest unoccupied π* orbitals, the same set invoked in the longstanding four-orbital model of the electronic spectra of these systems. A model, based on charge screening, accounts for the different degrees of bifurcation observed in the delocalisation pathways.

I. Introduction

The nature of the electronic structure of the porphin macrocycle in porphyrins and chlorins, and its stability in a wide range of biologically important systems, has been a challenge to theoretical chemists for over half a century. The parent molecule is free-base porphin (Fig. 1) in which four pyrrole-like motifs are linked by four methine bridges to form a macrocycle (Smith, 1975). Porphyrins are formally derived from porphin by substitution at some or all the peripheral positions (2,3), (7,8), (12,13) and (17,18), by various side-chains (Fig. 1). Chlorins are 17,18-dihydroporphyrins, and a subset of their magnesium complexes are chlorophylls. Bacteriochlorins are 7,8,17,18-tetrahydroporphyrins in which rings

*Author for correspondence, email: P.W.Fowler@sheffield.ac.uk. †Address from 1 August 2005: Dept. of Chemistry, University of Sheffield, Sheffield S3 7HF, U.K.

Bernhard Grimm, Robert J. Porra, Wolfhart Rüdiger and Hugo Scheer (eds): Chlorophylls and Bacteriochlorophylls: Biochemistry, Biophysics, Functions and Applications, pp. 337–347.

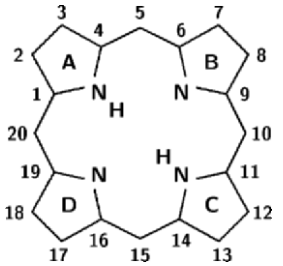

Fig. 1. Free-base porphin (heavy-atom skeleton, omitting detailed bonding)

B and D have been reduced in peripheral positions (Fig. 1), and a subset of their magnesium complexes are bacteriochlorophylls (Chapter 1, Scheer).

II. Electronic Structure and Spectra

The porphin macrocycle is highly conjugated, with 26 electrons in a π-electron system that is delocalized over 20 carbon and 4 nitrogen sites in the porphyrins. In the chlorins, there are two fewer π electrons and conjugated sites, and two fewer again in the bacteriochlorins. Several delocalization pathways can be devised for the flow of π electrons around the macrocycle, all conforming to the Hückel (4n+2) rule for aromaticity of a *mono*cycle. The evidence for classical aromaticity is manifold (Smith, 1975). It includes: heat of combustion; planarity; ^{1}H NMR, with NH protons at very high field, and bridge CH protons at very low; stability of the molecular ion; color, with main absorption bands having very high extinction coefficients; the intense Soret band which is characteristic of macrocyclic conjugation and disappears when the macrocycle is ruptured.

An early proposal for the π delocalization is the [18/18] (18 electrons on 18 sites) pathway shown in Fig. 2b (Rabinowitch, 1944), with local C=C double bonds in the pyrrole units B and D. Hydrogenation of one or both bonds, to give chlorin or bacteriochlorin, leaves the delocalization pathway unchanged. This approach formed the basis of free-electron descriptions of the π-structure and the electronic spectrum arising from π–π* transitions. Simpson (1949) simulated the pathway as an 18-membered cyclic

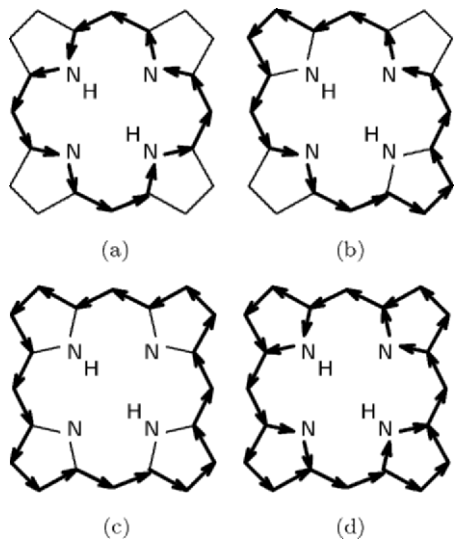

Fig. 2. Some delocalisation pathways in the porphin macrocycle. Diamagnetic (diatropic) circulation of electrons is shown as anticlockwise.

polyene and used free-electron theory to rationalize the presence of two double absorption bands, one strong and one weak (forbidden in free-electron theory) at longer wavelength. The strong band was taken to represent the near-UV Soret band and the weaker band in the visible. Similar results are obtained from Hückel theory of the 18-sided monocycle, the spectrum arising from the four possible one-electron transitions from doubly degenerate HOMO to doubly degenerate LUMO. This pattern of transitions is shown by every monocycle with the magic number of (4n+2) electrons. The first explicit molecular-orbital treatments were the Hückel-type calculations with nearest-neighbor overlap by Longuet-Higgins et al. (1950), in which electronic transitions in free-base and tetrahydro-porphin were again interpreted as simple one-electron orbital transitions.

The possible patterns of frontier π-orbital levels of the macrocycle are illustrated in Fig. 3, along with the transitions allowed by electric-dipole selection rules. In all cases, there are two low-lying unoccupied orbitals (degenerate in molecules with D_{4h} symmetry), which we will call the LUMO (strictly LUMO and LUMO+1), and two high-lying occupied molecular orbitals, the HOMO (strictly HOMO and HOMO–1). In addition, a group of four or five occupied orbitals (not shown) lie 150–250 kJ mol^{-1} below the HOMO. Free-base porphin has D_{2h} symmetry, with the pattern shown in Fig. 3a, as have bacteriochlorin (7,8,17,18-

Abbreviations: HOMO – highest occupied molecular orbital; LUMO – lowest unoccupied molecular orbital; NMR – nuclear magnetic resonance. Point-group symbols and symmetry labels for orbitals are explained in Altmann and Herzig (1994).

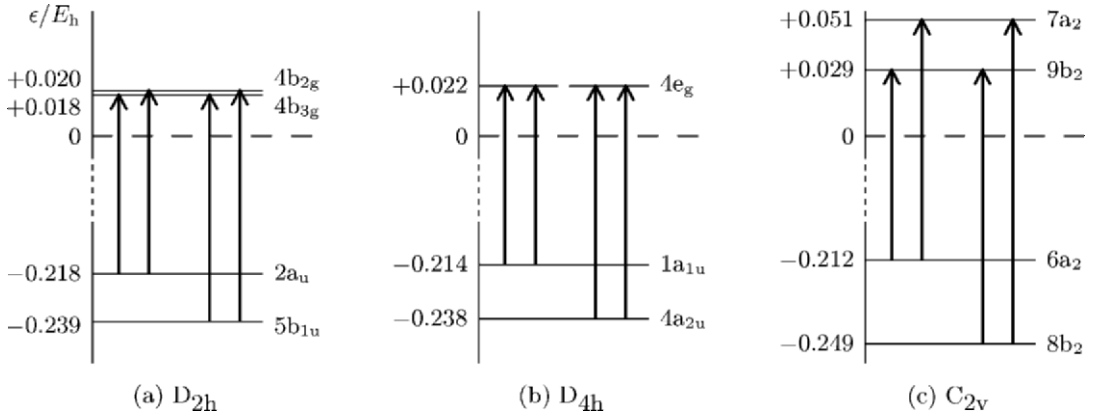

Fig. 3. Patterns of HOMO and LUMO π-orbital energy levels of the planar porphin macrocycle in D_{2h}, D_{4h} and C_{2v} symmetries. The energies are computed values for (a) free-base porphin, (b) magnesium porphin and (c) free-base chlorin (see Appendix for computational details). Also shown are the HOMO-LUMO transitions allowed by electric dipole-moment selection rules.

tetrahydroporphin is considered here), its dianion and metal complexes. The porphin dianion and metal complexes have the highest symmetry, D_{4h} with the pattern shown in Fig 3b, and chlorin and its metal complexes have the lowest, C_{2v} with pattern shown in Fig. 3c. In cases (a) and (b) the (near) degeneracy of HOMO and LUMO pairs suggests that the structure of the porphin macrocycle can be regarded as that of a perturbed monocycle. Closest to this ideal is the porphin dianion, type (b), with computed $a_{1u} - a_{2u}$ separation of 16 kJ mol^{-1}, and we will see that the π ring current in the dianion follows an almost perfect monocycle pathway dominated by the [18,16] 'internal-cross' illustrated in Fig. 2a. In free-base and metallo-porphyrins, perturbation by positive charges within the ring leads to more complex pathways. As indicated by the larger orbital-energy splittings in Fig. 3c, the perturbation is stronger in chlorins and bacteriochlorins.

In molecular orbital theory, the electronic spectrum is interpreted in terms of single-electron transitions from occupied to unoccupied orbitals. As shown in Fig. 3, all transitions between the two highest occupied and two lowest unoccupied orbitals are allowed by electric-dipole selection rules. In the case of D_{4h} symmetry, as exemplified by magnesium porphin, the lowest-lying excited electronic states of the system are doubly degenerate, with symmetry E_u, and are assigned to configurations (a_{1u}, e_g) and (a_{2u}, e_g).

In 1959, Gouterman observed that a more accurate description of the two lowest-lying E_u excited states is obtained by configuration interaction, whereby each state is a mixture of the two orbital configurations (a_{1u}, e_g) and (a_{2u}, e_g). This 'four-orbital model' provides a more realistic interpretation of the relative intensities of the transitions, with weak absorption (Q bands) in the visible spectrum and intense Soret absorption (B bands) in the near UV. This has formed the basis for much subsequent theoretical work over 40 years on the electronic structure and spectra of the porphyrin family (see Baraldi et al., 1995 for a concise review; also: Hasegawa et al., 1996; Nakatsuji et al., 1996; Gwaltney and Bartlett, 1998; Serrano-Andrés et al., 1998; Rubio et al., 1999). Gouterman's four-orbital model survives as an essentially correct first approximation for the Q bands. For example (Serrano-Andrés et al., 1998), the porphin $^1B_{3u}$ band is dominated by approximately equal contributions of the transitions ($2a_u \rightarrow 4b_{3g}$) and ($5b_{1u} \rightarrow 4b_{2g}$), and the $^1B_{2u}$ band by contributions of ($2a_u \rightarrow 4b_{2g}$) and ($5b_{1u} \rightarrow 4b_{3g}$). Similarly (Rubio et al., 1999), both Q (^1E_u) bands of magnesium porphin are determined largely by approximately equal contributions of ($4a_{2u} \rightarrow 4e_g$) and ($1a_{1u} \rightarrow 4e_g$). The four-orbital model is less successful for the higher-energy Soret bands, with an important contribution from a lower occupied orbital ($4b_{1u}$) in porphin, but only a small contribution from $3a_{2u}$ in magnesium porphin, where the system remains closer to the ideal monocycle.

III. Ring Currents

The concept of ring current in cyclic conjugated systems has its origins in interpretations by Pauling (1936) and Lonsdale (1937) of the large anisotropy of

the magnetizability of benzene, and by Pople in 1956 of the low-field chemical shift of external protons in the ^{1}H NMR spectrum (Lazzeretti, 2000; Gomes and Mallion, 2001). Together with the related concept of π-electron delocalization, ring currents have become essential ingredients in the interpretation of physical and chemical properties of conjugated systems. In particular, they are intimately linked with the widely used concept of aromaticity in organic chemistry (Garratt, 1986; Minkin et al., 1994). The ability to sustain a diatropic (or paratropic) current has become a criterion of aromaticity (or antiaromaticity) (Schleyer and Jiao, 1996; Schleyer et al., 1996).

Benzene and porphin are compared in Table 1 in terms of the historical indices: magnetizability, exaltation and ^{1}H chemical shifts. The perpendicular component of magnetizability, ξ_{zz}, and magnetic anisotropy, $\Delta\xi$, measure the extent of electron circulation parallel to the molecular plane. In the classical theory of diamagnetism, the magnitude of magnetizability in the direction of an applied magnetic field is proportional to the number of circulating electrons and the area of circulation. In benzene, the distance of the carbon atoms from the center is 1.39 Å, and the average distance of carbons and nitrogens in porphin is 3.52 Å. The ratio $[r(porphin)/r(benzene)]^2$ is 6.4, whilst the ratio of ξ_{zz} is 8.2 and of $\Delta\xi$ is 9.5. If the classical interpretation of ring current is valid, the inference is that the number of electrons contributing in 26 π-electron porphin is not much greater than in 6 π-electron benzene. The magnetizability anisotropy is closely related to the empirical diamagnetic susceptibility exaltation, Λ, used by Dauben et al. (1971) as a direct measure of the extent of electron delocalization in a molecule.

^{1}H NMR shifts are widely used and sensitive measures of π-electron delocalization. Computed values shown in Table 1 demonstrate the overall reliability of the level of *ab initio* theory used here (see Appendix). The shifts for porphin reproduce the observed down-field shifts for peripheral protons and are broadly consistent with the large up-field shift of the internal protons.

From the early days, discussions of the electronic structure of the porphin macrocycle used the Hückel (4n+2) rule as a unifying principle of stability and aromaticity. Benzene is the archetypal example, although variations on the basic hexagonal structure which retain planarity and the magic Hückel count of six π electrons can lead to molecules with widely differing magnetic response. At one extreme are systems supporting fully delocalized ring currents (e.g. $C_5H_5^-$, $C_7H_7^+$, *sym*-triazine, pyridine and pyrrole); at the other are those with only islands of localized current (e.g. borazine and boroxine) (Fowler and Steiner, 1997).

Table 1. Computed magnetic properties (see Appendix for computational details)

		benzene	porphin
magnetizability (i)	ξ_{zz}	−21.3 (−19.9)	−174.3
	$\bar{\xi}$	−10.3 (−11.5)	−70.3
	$\Delta\xi$	−16.5 (−12.6)	−156.0
exaltation (ii)	Λ	13.7	156*
^{1}H NMR shift (iii)	δ	7.3 (7.3)	H2 9.9 (9.7)
			H7 9.5 (9.7)
			H5 10.0 (10.6)
			NH −10.1 (−3.8)

(i) Magnetizability component perpendicular to the molecular plane, ξ_{zz}, mean value, $\bar{\xi}$, and anisotropy, $\Delta\xi=\xi_{zz}-\xi_{xx}$, (in units of a.u. $= e^2a_0^2/m_e = 7.89104 \times 10^{-29}$ J T^{-1} $= 4.75209 \times 10^{-6}$ cgs emu; to convert to conventional magnetic susceptibility in ppm cgs, multiply values by 4.75209), (ii) diamagnetic susceptibility exaltation and (iii) ^{1}H NMR δ values Experimental values shown in brackets are taken from (Smith, 1975, chapter 1). *Extrapolated from $\Delta\xi$ (Steiner et al., 2001).

No simple (4n+2) rule exists for fused-ring systems. The practice for multi-ring systems is either to treat the perimeter as a Hückel pathway with, for example, 10 electrons in naphthalene (n=2) and 14 in pyrene (n=3) or as a collection of linked Hückel systems as in fluoranthene, where benzene and naphthalene perimeters are joined by formal single bonds.

The porphin macrocycle is not a simple monocycle, and multiple Hückel delocalization pathways can be postulated. Some are summarized in Fig. 2. Figure 2b shows the original [18/18] pathway (Rabinowitch, 1944) while Fig. 2a represents the [18/16] 'internal-cross' (Cyrañski et al., 1998). The 2c pathway runs round the carbon perimeter, whilst 2d extends over all 24 contributing atoms and is bifurcated through the pyrrole rings. Recently, Jusélius and Sundhom (2000) have discussed the roles of pathways 2a and 2b, and some superposition pathways invoking local circulations within the pyrrole units.

The difficulties inherent in such discussions are avoided by the direct visualization which has been made possible by advances in the theory of electron current density by Keith and Bader (1993a,b), the Modena group of Lazzeretti and Zanasi (Coriani et al., 1994; Lazzeretti et al., 1994; Zanasi et al., 1995; Za-

nasi, 1996) and the Exeter group (Steiner and Fowler, 2001a,b; Steiner et al., 2002a). Although ring currents are not directly observable, they can nevertheless be obtained from theory by computing the response of a molecular system to an applied magnetic field. For example, mapping shows a simple π ring current around the perimeter in naphthalene, but in the longer linear homologues the picture is complicated by the presence of more than one Hückel pathway, with delocalization failing to keep up with increasing length (Steiner and Fowler, 1996). In the highly fused multi-ring systems coronene and corannulene, current density maps show diamagnetic (diatropic) circulation on the rim, and paramagnetic counter-circulation on the hub (Steiner et al., 2001).

IV. Orbital Model of Ring Currents

It is now known that a detailed analysis of current density provides a theoretical and practical tool for the interpretation of ring currents in terms of frontier-orbital transitions between high-lying occupied and low-lying unoccupied π molecular orbitals (Steiner and Fowler, 2001a,b).

When a molecule is placed in a constant uniform magnetic field, all points in the molecular space experience the same external force. In the *ipsocentric* formulation, the current density at each point is computed with respect to that point as effective center of rotation and, *in this formulation only* (Steiner and Fowler, 2001a), the current density is determined *wholly* by the change in the molecular wave function. For a molecule in its ground electronic state, the change in the wave function can be expressed as a sum of contributions from one-electron excitations to the accessible excited states, as can the concomitant current density. In the orbital approximation, for a closed-shell ground state, these excitations correspond to one-electron transitions from doubly occupied to unoccupied orbitals, and the total current density is the sum of contributions, one for each doubly occupied orbital.

Two types of transition are possible: translational and rotational. For a planar system perturbed by a perpendicular magnetic field, in-plane *translational transitions* generally lead to *diamagnetic circulation* of charge. The same transitions are allowed under the electric dipole selection rules that determine the π–π* electronic spectrum. In consequence, as will be seen, the description of ring currents in porphyrins in the ipsocentric formulation parallels the interpretation of the dominant features of the electronic spectrum of these molecules. *Rotational transitions* induced by the field generally lead to *paramagnetic circulation* of charge, and are allowed under magnetic dipole selection rules.

The analysis of current density in terms of orbital transitions gives rise to Hückel-like rules for both types of circulation (Steiner and Fowler, 2001b). In the Hückel theory of monocycles: (i) the diamagnetic ring current in *aromatic* (4n+2)-electron systems can be attributed to the *four* electrons in the doubly-degenerate HOMO; (ii) the paramagnetic ring current in *anti-aromatic* (4n)-electron systems can be attributed to the *two* electrons in the non-degenerate HOMO.

In both cases, currents are interpreted in terms of HOMO-LUMO transitions. The rules of 4-electron diamagnetism and 2-electron paramagnetism, like the classical Hückel rules, are strictly valid only for monocycles, but can be used to rationalize the circulations of electrons in more complex systems.

V. The Four-Orbital Model of the Ring Current in Porphyrins

Figure 4 shows the computed π-orbital energy level diagram of a model porphin macrocycle in which the internal protons of free-base porphin have been replaced by a single +2 charge at the center: all por-

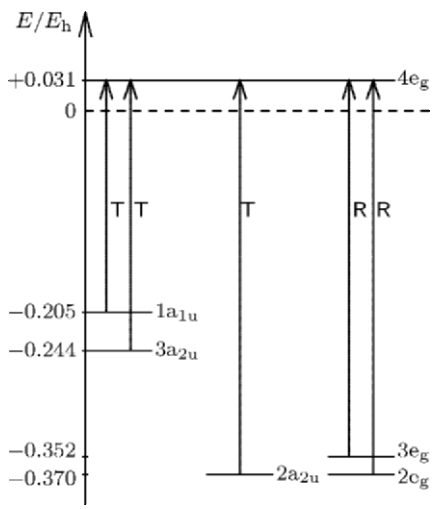

Fig. 4. π-orbital energy level diagram of the model porphin system. T indicates a translational transition to the LUMO, R a rotational transition.

phyrins and chlorins can be treated as perturbations of this model. The system is of type (b) shown in Fig. 3, with a near-degenerate HOMO pair (a_{1u},a_{2u}), and low-lying doubly-degenerate LUMO e_g. Also shown are some lower orbital levels from which the LUMO are accessible. Transitions to higher unoccupied levels have much higher energies.

In Fig. 5, the current density maps for this model system demonstrate that, as in benzene and other (4n+2) systems, the π ring current is a global diamagnetic circulation extending over all 24 centers and is dominated by the HOMO-LUMO translational transitions. The individual $1a_{1u}$ and $3a_{2u}$ orbital contributions of the HOMO pair are shown in Figs 5a and 5b. Their sum is shown in Fig. 5c and the contribution of the remaining 22 π electrons in lower-lying orbitals is shown in Fig. 5d. Comparison of Figs. 5c and 5d confirms the dominance of the four HOMO electrons. A semi-quantitative measure of the relative importance of the contributions is given by the maximum magnitude of current density (in a.u.) in the plotting plane: 0.081 for $1a_{1u}$ (Fig. 5a), 0.093 for $3a_{2u}$ (Fig. 5b), 0.174 for their sum (Fig. 5c) and 0.033 for the remainder (Fig. 5d). The value, 0.166, for the total π current (Fig. 5e) is about twice that in benzene (0.079). The σ electrons make only a small contribution in the plotting plane (the maximum σ density is in the molecular plane), and they increase the maximum density to 0.181 (Fig. 5f). The dominance of just a few π electrons explains the scaling behavior of the magnetic properties noted in section III.

A notable feature of the current density maps is the *bifurcation* of the global current across the pyrrole units in the separate HOMO contributions (see Figs. 5a and 5b), as well as in the total. This shows that the delocalization pathway illustrated in Fig. 2d should be considered as a distinct *single* pathway and not as a superposition of simpler pathways. Indeed (Steiner and Fowler, 2002), the computed orbital current densities of several porphyrins suggest that actual pathways are modifications of the case shown in 2d, with the cases shown in 2a to 2c as particular limiting cases.

VI. Pathways

Insight into the origin of bifurcation is obtained by varying the magnitude of the charge Z at the center of the porphin ring. Fig. 5e is the total π current density map for Z=2. The corresponding maps for (a) Z=0, the porphin dianion P^{2-}, and (b) Z=6 are shown in Fig. 6. For the dianion, the ring current closely follows the internal-cross pathway (Fig. 2a), leaving little current density on the peripheral carbons. On the other hand, a large positive central charge pushes the ring current out onto the periphery, following the outer pathway (Fig. 2c) with little current density on the nitrogens. The currents in Fig. 6 are therefore close to the limiting cases of bifurcation, whereas the neutral model (Z=2) is a more typical intermediate example.

This apparently counter-intuitive dependence on central charge can be explained in terms of *screening*. The electrons in low-lying π orbitals, symmetry by symmetry, are attracted to the positive charge at the center, thereby excluding the electrons in the higher-lying orbitals and effectively screening them from the center, in a two-dimensional analogue of the screening of valence-shell electrons in atoms by inner-shell electrons of the same kind. This explanation is supported by orbital densities: in the neutral model system, with Z=2, HOMO and LUMO span the molecular space of both inner and outer pathways, resulting in a bifurcated ring current. For larger Z, the lower-lying orbitals of each symmetry are increasingly contracted towards the center, localizing on the inner pathway, whilst higher-lying orbitals are polarized towards the outer ring. The $4e_g$ LUMO pair also concentrates on the periphery, resulting in the simple perimeter current of type Fig. 6b. Confirmation of the analysis is provided by the HOMO pair for Z=6: whereas orbital $3a_{2u}$ is localized on the periphery, orbital $1a_{1u}$, the only representative of this symmetry, retains its inner-outer delocalization; nevertheless it contributes current density on the perimeter alone, because only there does it have access to the LUMO. Reduction of the central charge leads to the opposite effect, as demonstrated for the dianion (Z=0) in Fig.6a.

The influence of charge flow within the σ- and π-systems of metalloporphyrins on the optical spectra is discussed in Chapter 34 (Yerushalmi et al.).

VII. Porphin and Magnesium Porphin

The current density maps in Fig. 7 for free-base porphin are similar to those in Fig. 5 for the model system in which the internal protons have been replaced by central +2e charge. They demonstrate the same 4-electron diamagnetism, but with modified patterns of bifurcation across the two types of pyrrole units. The bifurcation is strong across rings A and C (Fig. 1) but

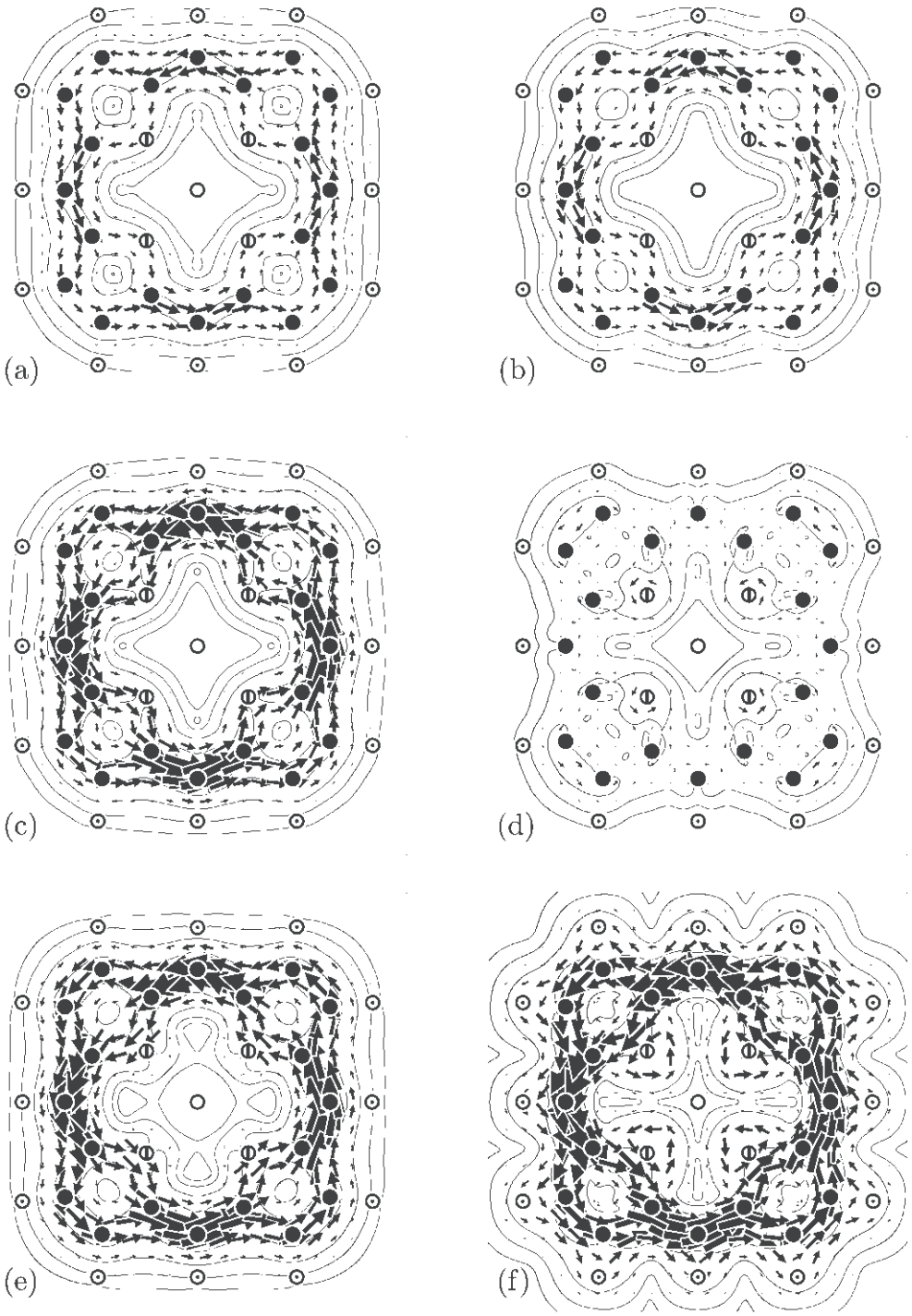

Fig. 5. π current density maps for the model porphin system. (a) orbital $1a_{1u}$, (b) orbital $3a_{2u}$, (c) $1a_{1u}+3a_{2u}$, (d) total π except $1a_{1u}$ and $3a_{2u}$, (e) total π, (f) total σ+π contributions, respectively. Plotting conventions: the mapping plane lies at 1 bohr (~0.529 Å) above the macrocycle. Contours show the modulus of current density in the plotting plane, and arrows indicate the in-plane projection of the vector current density. Diamagnetic circulation is anticlockwise, paramagnetic circulation clockwise. Projected positions of carbon, nitrogen and hydrogen centers are denoted by filled, barred and dotted circles, respectively. See Appendix for computational details for all maps.

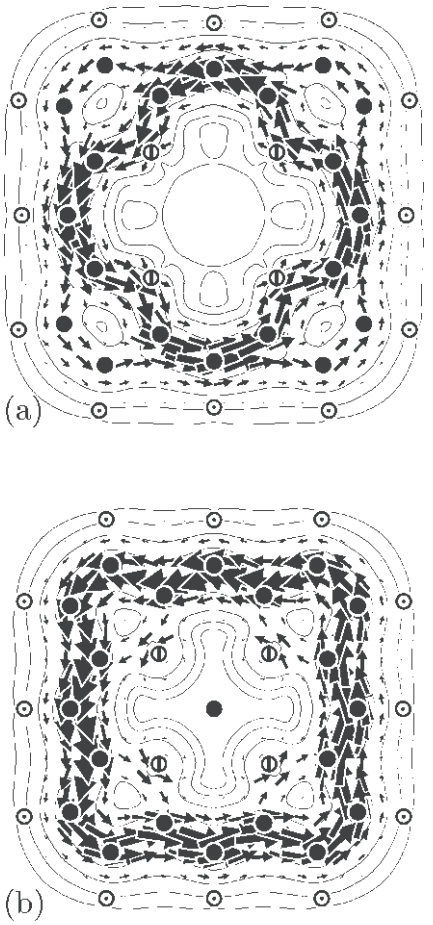

Fig. 6. Total π current density in (a) porphin dianion P^{2-}, (b) as (a) with central charge +6e. Plotting conventions as in the legend to Fig. 5. See also Color Plate 1.

weaker across the unprotonated rings B and D. This effect is seen most strongly in 7b for orbital $5b_{1u}$, and is readily explained in terms of the two-dimensional screening model. The resulting global pattern of circulation, in fact, resembles the original 18-center pathway (Fig 2b and Color Plate 1).

Full bifurcation is retrieved in the dication obtained by protonation of the internal nitrogens, and is also shown by magnesium porphin, whose patterns of orbital levels and current density are almost identical to those shown in Figs 4 and 5, with hardly any π circulation on the central atom.

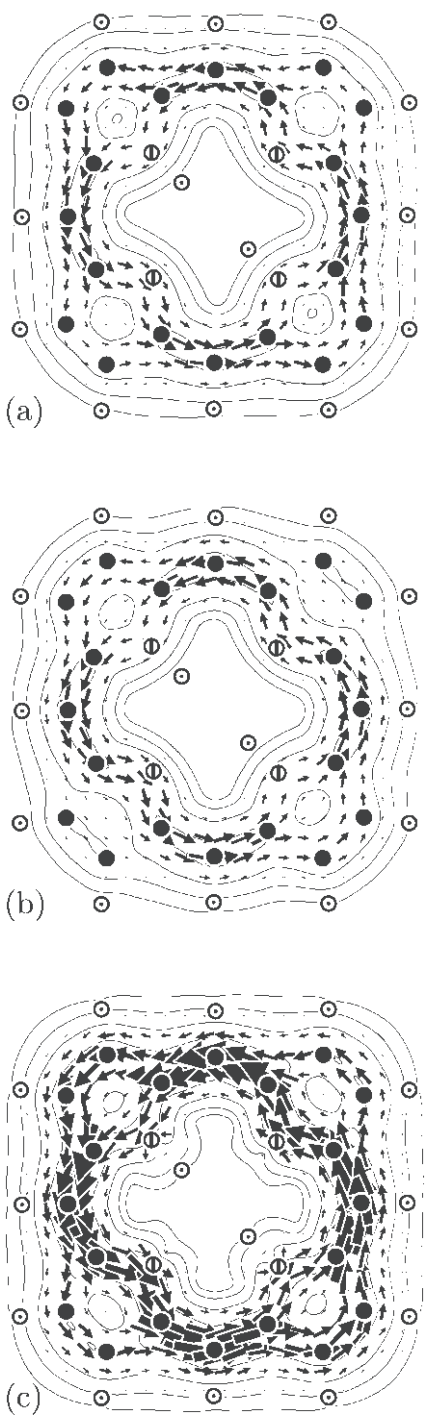

Fig. 7. π current density maps for free-base porphin. (a) orbital $2a_u$, (b) $5b_{1u}$, (c) total π contributions, respectively. Plotting conventions as in the legend to Fig. 5.

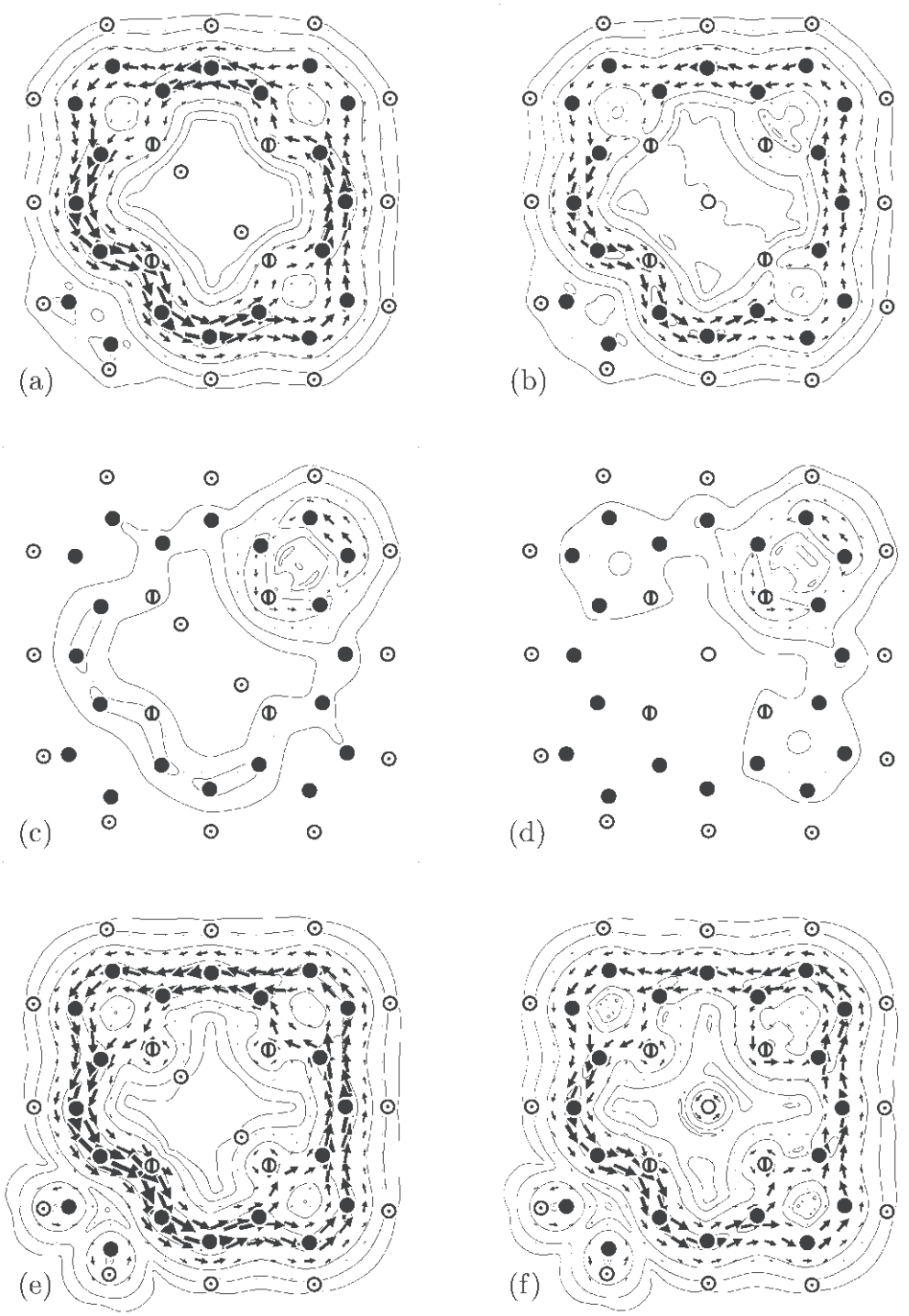

Fig. 8. π current density maps for chlorin (left column) and magnesium chlorin (right column). (a) $6a_2$+$8b_2$ and (b) $6a_2$+$9b_2$ are HOMO + HOMO-1; (c) $7b_2$ and (d) $8b_2$ are HOMO-2; (e) and (f) are total π contributions, respectively. Plotting conventions are as in the legend to Fig. 5.

VIII. Chlorins

The possibility of flow through the pyrrole rings along both inner and outer pathways means that the global ring current can survive when some pathways are blocked. Figure 8 shows that the current bypasses the saturated 17,18 positions in chlorins. The circulation remains dominated by 4-electron diamagnetism but is weaker than in porphyrins. In units of the benzene π value (0.079 a.u.), the maximum current density of the frontier orbitals is 1.4 in chlorin (Fig. 8a) and 0.9 in magnesium chlorin (Fig. 8b), compared with 2.2 in porphin. The contribution of the lower-lying orbitals is now more significant and arises mainly from the electrons in the HOMO-2. This orbital is localized on pyrrole ring B, opposite saturated ring D and, as shown in Figs 8c and 8d, gives rise to local diamagnetism (strength 0.5 benzene units), which in magnesium chlorin determines the direction of flow along the inner pathway of pyrrole unit B.

In contrast, the bacteriochlorins, obtained by hydrogenation of the 7,8 positions in ring B, have a much simpler pattern of circulation, as shown in the color plate for magnesium bacteriochlorin (the pattern in free-base bacteriochlorin is almost identical). There is a return to the strength of current found in the porphyrins (2.3 benzene units), with 90% coming from the four HOMO electrons. Both pairs of saturated carbons are bypassed along the inner pathway and there is strong bifurcation across rings A and C.

Appendix

The maps calculated for the present work were obtained with the methodology previously used to visualize ring currents in coronene and corannulene (Steiner et al, 2001), pyrene and its cyclopenta-fused congeners (Steiner et al., 2002b), and many other π systems. Geometries were optimized at the RHF/6-31G** level, current densities were calculated using the ipsocentric (CTOCD-DZ) coupled Hartree-Fock method and integrated properties using the PZ2 variant. The figures show computed current density distributions induced by a magnetic field perpendicular to the plane of the macrocycle. The mapping plane lies at 1 bohr radius above the macrocycle, close to maximum π charge and current densities. Contours show the modulus of current density in the plotting plane (in atomic units, a.u.) and arrows the in-plane projection of the vector current density. In the maps, diamagnetic circulation is anticlockwise and paramagnetic circulation clockwise.

Note Added in Proof

In a more complete description of the π shielding effect discussed in Section VI on pathways (Steiner et al., 2005), we have shown that the dependence of the current density distribution on the central charge can be explained in detail by adopting the principle (i) that changes in current densities follow changes in charge densities, or more precisely, transition densities, and the hypothesis (ii) that, whereas all the electrons are attracted to the central charge, there exists a specific π shielding effect whereby electrons in high-lying π orbitals of each symmetry type are shielded from the centre by the lower-lying orbitals of the same symmetry, resulting in a partial separation of charge within the π system. This arises in two ways: (a) electrostatic shielding, whereby an electron at a given radius is shielded from the center by the electron density within that radius and (b) radial orthogonality, whereby higher-lying orbitals are progressively excluded from the space occupied by lower-lying orbitals of the same symmetry, leading to a relative shift of orbital density away from the center. The π shielding effect is closely analogous to the familiar nuclear shielding in atoms, with screening constant increasing up the orbital ladder.

Radial orthogonality, which applies to all orbitals, occupied and unoccupied, is already seen in the hydrogen atom, and for each symmetry results in an increasing number of radial nodes, as in the series 1s, 2s, 3s, …, with maximum orbital density at larger distances from the center. In the porphyrin macrocycle, the significant consequence of radial orthogonality is the shift of density from inner to outer pathway.

References

Altmann SL and Herzig P (1994) Point-group Theory Tables. Oxford University Press, Oxford

Baraldi I, Carnevali A, Ponterini G and Vanossi D (1995) Electronic spectrum of porphyrins. CS INDO CI study. J Mol Struct (Theochem) 333: 121–133

Coriani S, Lazzeretti P, Malagoli M and Zanasi R. (1994) On CHF calculations of second-order magnetic properties using the method of continuous transformation of origin of current density. Theoret Chim Acta 89: 181–192

Cyrañski MK, Krygowski TM, Wisiorowski M, Hommes NJR van E, and Schleyer P von R (1998) Global and local aromaticity in porphyrins: An analysis based on molecular geometries and nucleus-independent chemical shifts.. Angew Chem Int Ed 37: 177–180

Dauben HJ, Wilson JD and Laity JL (1971) Diamagnetic susceptibility exaltation as a criterion of aromaticity. In: Snyder JP (ed) Nonbenzenoid aromatics II, pp 167–206. Academic Press, New York

Fowler PW and Steiner E (1997) Ring currents and aromaticity of monocyclic π-electron systems. J Phys Chem A 101: 1409–1413

Garratt PJ (1986) Aromaticity. Wiley, New York

Gomes JANF and Mallion RB (2001) Aromaticity and ring currents. Chem Rev 101: 1349–1383

Gouterman M (1959) Study of the effects of substitution on the absorption spectra of porphin. J Chem Phys 30: 1139-1161

Gwaltney SR and Bartlett RJ (1998) Coupled-cluster calculations of the electronic excitation spectrum of free base porphin in a polarized basis. J Chem Phys 108: 6790–6798

Hasegawa J, Hada M, Nonoguchi M and Nakatsuji H (1996) Ground and excited states of Mg porphin studied by the SAC/SAC-CI method. Chem Phys Lett 250: 159–164

Jusélius J and Sundholm D (2000) The aromatic pathways of porphyrins, chlorins and bacteriochlorins. Phys Chem Chem Phys 2: 2145–2151

Keith TA and Bader RFW (1993a) Calculation of magnetic response properties using a continuous set of gauge transformations. Chem Phys Lett 210: 223–231

Keith TA and Bader RFW (1993b) Topological analysis of magnetically induced molecular current distributions. J Chem Phys 99: 3669–3682

Lazzeretti P (2000) Ring currents. Prog NMR Spect 36: 1–88

Lazzeretti P, Malagoli M, and Zanasi R (1994) Computational approach to molecular magnetic properties by continuous transformation of the origin of the current density. Chem Phys Lett 220: 299–304

Longuet-Higgins HC, Rector CW and Platt JR (1950) Molecular orbital calculation on porphine and tetrahydroporphine. J Chem Phys 18: 1174–1181

Lonsdale K (1937) Magnetic anisotropy and electronic structure of aromatic molecules. Proc Roy Soc London A159: 149–161

Minkin VI, Glukhovtsev MNY and Simkin BY (1994) Aromaticity and Antiaromaticity. Electronic and Structural Aspects. Wiley, New York

Nakatsuji H, Hasegawa J and Hada M (1996) Excited and ionized states of free base porphin studied by symmetry adapted cluster-configuration interaction (SAC-CI) method. J Chem Phys 104: 2321–2329

Pauling L (1936) The diamagnetic anisotropy of aromatic molecules. J Chem Phys 4: 673–677

Pople JA (1956) Proton magnetic resonance of hydrocarbons. J Chem Phys 24: 1111

Rabinowitch E (1944) Spectra of porphyrins and chlorophyll. Rev Mod Phys 16: 226–235

Rubio M, Roos BO, Serrano-Andrés L and Merchán M (1999) Theoretical study of the electronic spectrum of magnesium porphyrin. J Chem Phys 110: 7202–7209

Schleyer P von R and Jiao H (1996) What is aromaticity? Pure Appl Chem 68: 209-218

Schleyer P von R, Maerker C, Dransfeld A, Jiao H and Hommes NJR van E (1996) Nucleus-independent chemical shifts: A simple and efficient aromaticity probe. J Amer Chem Soc 118: 6317–6318

Serrano-Andrés L, Merchán M, Rubio M and Roos BO (1998) Interpretation of the electronic absorption spectrum of free base porphin by using multiconfigurations second-order perturbation theory. Chem Phys Lett 295: 195-203

Simpson WT (1949) On the theory of the π-electron system in porphines. J Chem Phys 17: 1218–1221

Smith KM (1975) General features of the structure and chemistry of porphyrin compounds. In: Smith K M (ed) Porphyrins and Metalloporphyrins, pp 3–28. Elsevier, Amsterdam

Steiner E and Fowler PW (1996) Ring currents in aromatic hydrocarbons. Int J Quantum Chem 60: 609–616

Steiner E and Fowler PW (2001a) Patterns of ring currents in conjugated molecules: A few-electron model based on orbital contributions. J Phys Chem A 105: 9553–9562

Steiner E and Fowler PW (2001b) Four- and two-electron rules for diatropic and paratropic ring currents in monocyclic π systems. Chem Commun: 2220–2221

Steiner E and Fowler PW (2002) Ring currents in the porphyrins. A four-orbital model. Chem Phys Chem 3: 114–116

Steiner E, Fowler PW and Jenneskens LW (2001) Counter-rotating ring currents in coronene and corannulene. Ang Chem Int Ed 40: 362–366

Steiner E, Fowler PW and Havenith RWA (2002a) Current densities of localized and delocalized electrons in molecules. J Phys Chem A 106: 7048–7056

Steiner E, Fowler PW, Jenneskens LW and Havenith EWA (2002b) Local and global paratropic and diatropic ring currents in pyrene and its cyclopenta-fused congeners. Eur J Org Chem :163–169

Steiner E, Soncini A and Fowler PW (2005) Ring currents in the porphyrins: π shielding, delocalisation pathways and the central cation. Org Biomol Chem **3**: 4053–4059

Zanasi R (1996) Coupled Hartree-Fock calculations of molecular magnetic properties annihilating the transverse paramagnetic current density. J Chem Phys 105: 1460–1469

Zanasi R, Lazzeretti P, Malagoli M and Piccinini F (1995) Molecular magnetic properties within continuous transformation of origin of the current density. J Chem Phys 102: 7150–7157

Chapter 24

Bacteriochlorophyll Protein Maquettes

Dror Noy*, Christopher C. Moser and P. Leslie Dutton
Biochemistry and Biophysics Department and Johnson Research Foundation, University of Pennsylvania, Philadelphia PA, U.S.A.

Summary

The photosystems of plants and photosynthetic bacteria are robust, adaptable and highly efficient light-harvesting/charge-separating systems that use chlorophylls (Chls) or bacteriochlorophylls (BChls) as photoreceptors. These solar energy collectors are built for increased light absorbance by providing environmental control over large pigment arrays with as little protein mass as possible. We wish to resolve the features of protein architecture necessary for effective light harvesting and electron transfer per se from other features of the natural protein some of which may be simply historical accidents.

To overcome the complexity of biological systems and test the basic principles that appear to underlie natural design we use protein maquettes: synthetic proteins that are minimal yet functional versions of the natural proteins of interest. Our success with heme-binding protein maquettes and the close homology between hemes, Chls, and BChls has encouraged us to design Chl- or BChl-protein maquettes according to the guidelines set by heme-binding maquette design. By choosing to design proteins that a) consist of only natural amino acids, b) bind cofactors non-covalently, and c) fold and assemble spontaneously, we expect to readily exploit successful designs by overproducing them in bacterial expression systems.

Using natural bacterial light-harvesting proteins (LHs) as templates for new protein maquettes, we were able to design and identify a minimal unit as short as 24 amino acids that is capable of binding BChls non-covalently, and self-assembling to form analogs of the LH protomeric subunit with the same absorbance and circular dichroism (CD) properties. However, these minimal LH proteins are susceptible to BChl-driven aggregation that result in very large particles. The balance between BChl self-aggregation and protein complex

*Author for correspondence. Current address: Dept. of Structural Biology, The Weizmann Institute of Science, Rehovot, Israel; email: dror.noy@weizmann.ac.il

Bernhard Grimm, Robert J. Porra, Wolfhart Rüdiger and Hugo Scheer (eds): Chlorophylls and Bacteriochlorophylls: Biochemistry, Biophysics, Functions and Applications, pp. 349–363.

formation appears to be an important design element for LH engineering, suggesting that the protein's most important role is in imposing steric restrictions through the overall shape and surface complementarity of the protomeric subunits. New designs of protein maquettes based on our basic 24 amino acid subunit are expected to reveal some of the principles behind the self assembly of LHs as well as other oligomeric constructs of membrane proteins.

I. Protein Maquette Tools for Exploring Natural Design of Chlorophyll- and Bacteriochlorophyll-Proteins

Photosynthetic organisms utilize chlorophylls (Chls) or bacteriochlorophylls (BChls) as photoreceptors for collecting light energy and converting it into electrochemical potential. Their photosystems are highly efficient multi-component pigment-protein complexes comprised of a reacton center (RC) protein unit coupled to a set of at least one type of light-harvesting (LH) proteins in which large arrays of Chls or BChls trap and transfer light energy to photoexcite a special Chl- or BChl pair in the RC initiating a charge separation reaction (see Chapters 28–31). The protein environment sets the spatial organization and electronic properties of the Chl or BChl cofactors so that they have the appropriate energetic and electronic coupling parameters to function as both light harvesting and charge separating centers. These light-harvesting/charge-separating systems, like many natural proteins, are robust and adaptable to variable environmental conditions while keeping close to 100% quantum conversion yield, but unlike most proteins, solar energy collectors also favor increasing light absorbance and therefore high pigment density (Markvart, 2000; Sundström, 2000). Optimal photosystem architecture must therefore provide environmental control over large pigment arrays with as little protein mass as possible.

The unique properties of the photosystems have inspired many attempts to create artificial systems that seek to uncover the basic rules of natural design and the general guidelines for engineering efficient, molecular-level, solar energy conversion devices (Cogdell and Lindsay, 2000; Mongin et al., 2000; Bahr et al., 2001; Gust et al., 2001; Benites et al., 2002; Holten et al., 2002; Kodis et al., 2002). However, since the features of protein architecture necessary for effective light harvesting and electron transfer per se have evolved through repeated mutation and natural selection over billions of years (see Chapter 18, Larkum,) they are difficult to separate from a multitude of different structural features some of which may be simply historical accidents. Figure 1 (and Color Plate 3) demonstrates the variety of size, fold, complexity, pigment organization, and pigment/protein ratio in natural Chl- and BChl-protein complexes. Clearly, vastly different natural designs are consistent with the basic engineering principles that lead to high energy conversion efficiency with maximal absorption, ranging from the rod-like 'mostly pigment' chlorosomes of green bacteria (0.5 (w/w) proteins/pigment ratio) (Olson, 1998; van Rossum et al., 2001) shown in Fig. 1a, to the large and elaborate protein scaffold of higher plant photosystems that maintains a non-symmetric, well defined array of Chls around the RCs (Fig. 1d). Nevertheless, the variety of protein-pigment architectures no doubt reflects a number of biological requirements such as protein stability, transport and insertion into the membrane, and photoprotection that are not necessarily directly related to high-energy conversion yield.

One way to overcome the complexity of enzymatic systems and test the basic principles that appear to underlie natural design is to create new synthetic proteins that are minimal yet functional versions of the natural proteins of interest. Recent advances in protein engineering have made it possible to design such peptides de novo, employing structural and functional motifs from natural enzymes (Robertson et al., 1994). We call these peptides protein maquettes by analogy to the scaled-down models used by sculptors and architects for gauging the properties of their real designs. Heme-binding protein maquettes have already provided adaptable, well-characterized, simple functional models of native heme-containing enzymes and have been applied successfully to mimic cytochromes and flavocytochromes (Dutton, 1995; Gibney et al., 1996, 1997a,b,c, 1998; Kalsbeck et al., 1996; Sharp et al., 1998a, b; Shifman et al., 1998; Skalicky et al., 1998). The technological adaptability

Abbreviations: BChl – bacteriochlorophyll; CD – circular dichroism; Chl – chlorophyll; LH – light-harvesting (protein), a subsequent Arabic numeral (1,2,3) indicates the subtypes of bacterial LH; OG – β-octylglucoside; *Rba. – Rhodobacter*; RC – reaction center; *Rsp. – Rhodospirillum*

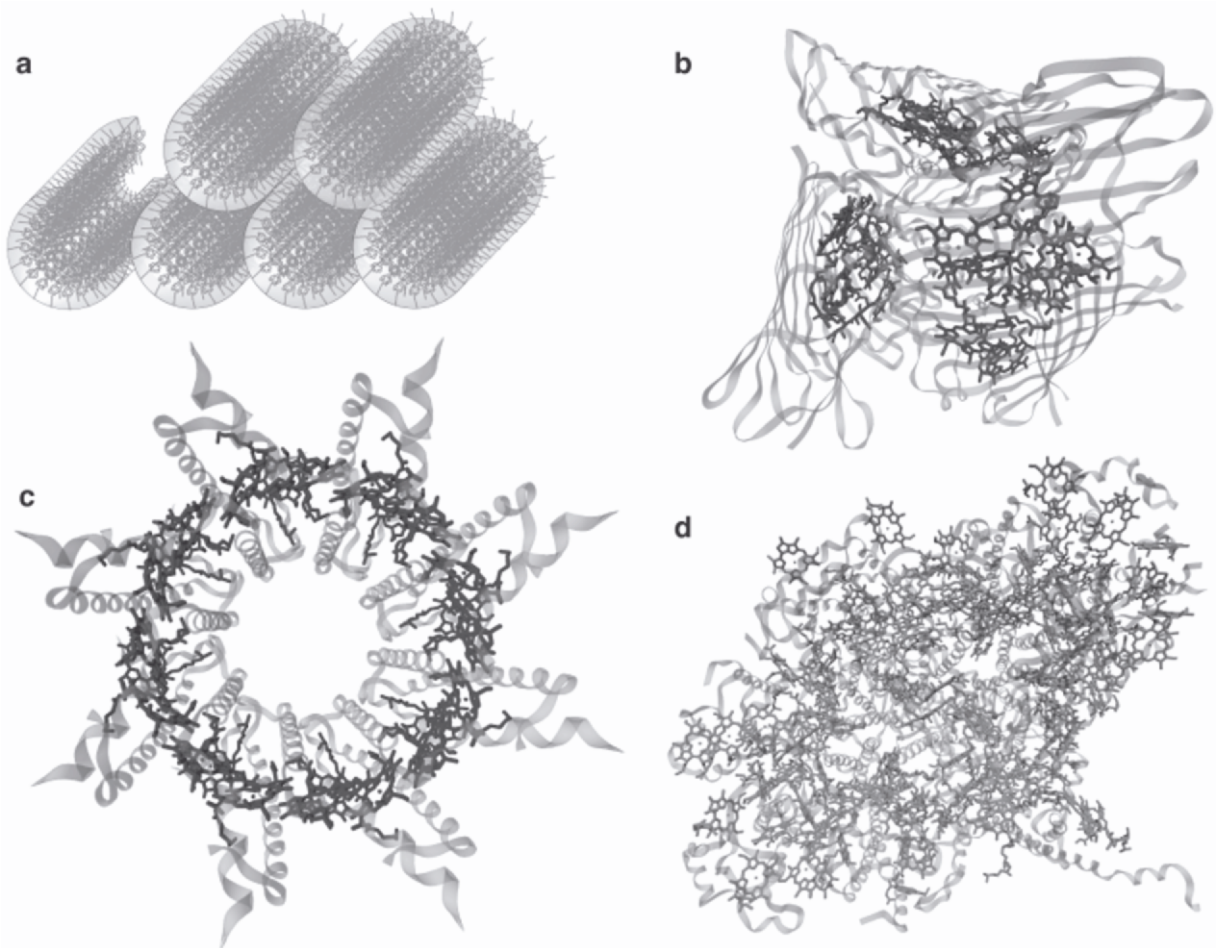

Fig. 1: (Bacterio)chlorophyll arrangement in different types of photosynthetic complexes. a) Chlorosome of green bacteria containing BChls *c, d* or *e*, this complex is largely devoid of protein (*Chlorobium tepidum,* van Rossum et al., 2001, model based on nuclear magnetic resonance, see Chapter 20, de Boer and de Groot); b) trimeric unit of Fenna-Matthews-Olson (FMO) protein of green sulfur bacteria containing BChl *a* (*Prostecochloris aestuarii*, Tronrud et al., 1993, pdb acc. no. 4BCL; c) peripheral antenna LH2 of purple bacteria (*Rhodospirillum molischianum,* Koepke et al., 1996, pdb acc. no. 1LGH), only the densely packed BChl-B850 are shown, the monomeric BChl-B800 are omitted; d) Photosystem I core (*Synechococcus elongatus,* Jordan et al., 2001, pdb acc. no. 1JB0). In b,c and d, the protein backbone is shown as a light grey ribbon). See also Color Plate 3.

of such systems has also prompted many studies aimed at creating macroscopic arrays of vectorially assembled maquettes such as monolayers adsorbed on electrodes, or Langmuir-Blodget films (Chen et al., 1998; Pilloud et al., 1998).

Our success with heme-binding protein maquettes and the close homology between hemes, Chls, and BChls has encouraged us to design Chl- or BChl-protein maquettes according to the guidelines set by heme-binding maquette design. Some strategies that have been used to create mimics of LH and RC complexes include molecular designs based on covalently linked porphyrin derivatives (Bahr et al., 2001; Gust et al., 2001; Rucareanu et al., 2001; Benites et al., 2002; Kodis et al., 2002) and on template-assisted synthetic peptides with covalently linked Chl cofactors (Rau et al., 2001). However, we choose to design proteins that a) consist of only natural amino acids, b) bind cofactors non-covalently, and c) fold and assemble spontaneously. This strategy allows us to readily exploit successful designs by overproducing them in bacterial expression systems.

Here, we present the progress made in designing BChl-protein maquettes that exploit this strategy and use bacterial LHs as structural templates. Recently, we have prepared new peptides based on hybrids between

heme binding maquette and a natural hydrophobic heme-binding motif. These amphiphylic maquettes are soluble in detergent solutions and were shown to bind heme B and heme A, as well as Zn and Ni substituted BChl derivatives. The close similarity of our designs to the native system makes them useful models for studying the engineering principles of LH proteins with the benefits of high yield and flexibility through standard solid-phase peptide synthesis, the use of commonly available cofactors, and the possibility of mass-production by molecular biology.

II. Essentials of De Novo Designing Protein Maquettes

The construction of protein maquettes 'from scratch' immediately faces the fundamental questions of protein sequence-structure-function relationships, the most important of which are a) what amino-acid sequence will fold into a prescribed structure with unique, native-like conformation?, b) what structural features are required for binding a given cofactor specifically at well-defined conformation? and c) what features enable the cofactor to perform a prescribed biochemical function? Despite rapid progress in the field of protein de novo design, these questions still await their full and general answers (DeGrado et al., 1999; Hill et al., 2000; Voigt et al., 2000; Baltzer et al., 2001; Kraemer-Pecore et al., 2001; Pokala and Handel, 2001). Nevertheless, by adding insight based on our current knowledge of specific natural systems, significant and useful advances have been made in each of these basic design questions.

A. Protein Structure Design

The problem of protein de novo design is generally formulated as: 'what amino acid sequence will have a prescribed three dimensional structure as its lowest energy state?' which is the inverse problem of protein structure prediction formulated as: 'what will be the three dimensional structure of a given amino acid sequence upon spontaneously folding into its lowest energy state?' The major challenge of protein de novo design is reaching a unique native-like lowest energy conformation with the desired structure that is energetically well separated from undesired conformations (DeGrado et al., 1999). This could be broken down to the rather straightforward task of stabilizing the desired conformation (positive design) and a more complicated task of predicting and destabilizing all undesired conformations (negative design). Several computational algorithms have been suggested (Dahiyat and Mayo, 1997; Voigt et al., 2000; Wernisch et al., 2000; Bolon and Mayo, 2001; Kraemer-Pecore et al., 2001; Woolfson, 2001) and successfully applied for designing α-helical bundles (Bryson et al., 1998; Johansson et al., 1998; Hill et al., 2000), β-sheets (Kortemme et al., 1998), and α/β mixed motifs (Struthers et al., 1996). However, in most cases the computer generated amino acid sequence must be refined manually to yield the desired native-like structure. Such refinement could be achieved either randomly by combinatorial methods or rationally by judicious mutations of the amino acid sequence based on specific features of analogous native structure.

B. Cofactor Binding and Functionality

Cofactors such as metal ions and small organic molecules are essential structural and functional elements in many natural proteins, but the interplay between the cofactor role in imposing structural constraints on the protein fold and its being forced by the protein into an atypical conformation that serves a catalytic function can not be easily resolved. De novo design of cofactor binding proteins must address this problem quantitatively by finding the free energy balance between two driving forces: a) the cofactor's tendency to reorganize the protein around it in a typical solution-like coordination/solvation environment, and b) the protein's folding tendency that may impose an unusual conformation and/or coordination sphere on the cofactors, potentially adjusting their electronic structure according to the protein's functional requirements.

A computational approach to this design balance is problematic. Calculating specific, atomic level interactions between the cofactors, their surrounding amino acid residues and, in some cases, other substrates, requires highly evolved quantum mechanical calculations in order to achieve a sufficiently accurate solution (Siegbahn and Blomberg, 2000; Field, 2002; Segall, 2002). Such a task is resource intensive and time consuming even for a single given cofactor/protein structure. Adapting computational methods for treating cofactor binding and functionality through the iterative process of protein design is therefore only feasible at the cost of losing accuracy and generality. The problem is even more acute in the case of LH

complexes because of the relatively large pigment-to-protein ratio.

An alternative way to design functional active sites in synthetic proteins is to adapt known structural elements of natural active sites into a new synthetic structure; thereby building new sequences around natural motifs while identifying what structural elements are needed for efficient cofactor binding and chemical reactivity. This approach has proven valuable for testing structure-function relationships in heme-protein maquettes that adapted the B and D helices of cytochrome bc_1 into a symmetric, water-soluble, four-helix bundle (Robertson et al., 1994). Further optimization through a combinatorial survey of a series of parallel and anti-parallel four-helix bundle prototypes, secured a uniquely structured apo-protein design (Gibney et al., 1997b, 1999b; Skalicky et al., 1999). However, the unique apoprotein-conformation was not preserved upon heme binding, and the maquette required redesign for a unique holo-structure (Huang, 2001). Intriguingly, a unique conformation is not strictly required for functionality and in most cases the heme spectra and mid-point potentials are not only well defined and typical of protein bound heme (Robertson et al., 1994; Gibney et al., 1998, 1999a, 2001), but can also couple electron transfer to protonation of specific nearby glutamate residues (Shifman et al., 1998).

Designing functional proteins is a separate task from designing uniquely structured proteins. Indeed, conformational rigidity can interfere with functionality when, for example, the reactants and products of a bound substrate have significantly different geometry. Until we understand more about the balance between structural uniqueness and functionality in natural proteins, synthetic protein designs with some multiplicity of microstructural states can be tolerated, provided the desired functions are clearly achieved.

C. Membrane Proteins

Since native Chls and BChls are hydrophobic cofactors suited for the membrane environment of the photosynthetic apparatus, a hydrophobic, membrane soluble protein would be the most appropriate design for a synthetic Chl-/BChl-protein. Unfortunately, our understanding of the principles that underlie structure and folding design of membrane proteins lag significantly behind our understanding of water-soluble proteins, partly because of the difficulties in obtaining high-resolution structural information about native membrane proteins (Bechinger, 2000; Bowie, 2000). Consequently, only a few attempts have been made toward membrane protein de novo design, none of which have addressed cofactor binding (Lear et al., 1997; Choma et al., 2001; Gratkowski et al., 2001; Chapter 27, Garcia-Martin et al.). Until progress in this area clarifies the similarities and differences between water soluble and hydrophobic protein de novo design, it is probably best not to attempt to predict from first principles which amino acid sequence will be the most likely to have the right fold required for arranging and securing the LH cofactors. Instead, especially in view of the substantial amount of structural and functional information currently available for native proteins such as plant and bacterial photosynthetic RCs and LHs, a strategy that simplifies and adjusts natural sequences to discriminate the essential from incidental in sequence and structural features appears more suitable to Chl-/BChl-protein maquette design.

III. Adapting Natural LHs to Maquettes

The key to photosystem functionality is controlling pigment organization while maintaining high pigment density, therefore, a useful protein maquette should allow exploring the means of gaining such control by design. An ideal Chl-/BChl-protein maquette should have a unique structure and well-defined pigment organization controllable by changes to specific amino-acid residues. Given the state of the art in the field of protein de novo design as described above, we opted for designing a Chl-/BChl-protein maquette by using a natural protein template. LHs appeared to be the most promising template because a) substantial structural information for these systems is available including the high-resolution crystal structures of three native bacterial LH (McDermott et al., 1995; Koepke et al., 1996; McLuskey et al., 2001) and lower resolution electron cryomicroscopy images of several others (Savage et al., 1996; Stahlberg et al., 1998; Walz et al., 1998; Ikeda-Yamasaki et al., 1998; Jungas et al., 1999; Ranck et al., 2001), b) it consists of short, mostly α-helical subunits that are suitable for solid phase peptide synthesis, and c) the factors affecting their BChl binding properties have been extensively studied and characterized by genetic and biochemical methods (Fowler et al., 1994, 1997; Hunter, 1995; Meadows et al., 1995, 1998; Davis et al., 1996; Gall et al., 1997; Olsen et al., 1997; Hu et

al., 1998a; Kehoe et al., 1998; Todd et al., 1999).

A. LHs as a Template for Bacteriochlorophyll-Protein Maquette Design

The bacterial LH protein family consists mostly of two types of homologous BChl-proteins: LH1, a core antenna complex built around the bacterial RC, and LH2, a peripheral antenna complex (Hu et al., 1998b; Cogdell et al., 1999). Additionally, some species synthesize LH3, a LH2 variant, under low light and/or low temperature conditions. Since the natural habitat of photosynthetic bacteria lies underneath Chl containing species, their absorption spectra are complementary to the Chl spectrum, thus, LH3 absorbs light at 800 and 820 nm, LH2 absorbs at 800 and 850 nm and LH1 absorbs at 870 nm. All three LH types are oligomers of two short, hydrophobic, mostly α-helical apo-proteins, labeled α and β, that bind BChls at α:β:BChl molar ratio of 1:1:2 in LH1, or 1:1:3 in LH2 and LH3. Information from 2D crystals of LH1 (Karrasch et al., 1995; Oling et al., 1996; Savage et al., 1996; Ikeda-Yamasaki et al., 1998; Jungas et al., 1999; Ranck et al., 2001), and 3D crystals of LH2 (McDermott et al., 1995; Koepke et al., 1996) and LH3 (McLuskey et al., 2001) indicate that a) the protomeric subunit is a complex of α:β-apo-protein, a BChl dimer, a carotenoid molecule, and an additional BChl molecule in LH2 and LH3, b) the subunits are arranged in circular geometry whereby the α- and β-apo-proteins form inner and outer concentric cylinders, respectively, with the pigments arranged as concentric rings in between, c) the number of subunits per complex varies from 8 or 9 (24 or 27 BChls, respectively) in LH2 and LH3 to 16 (32 BChls) in LH1, d) the BChl dimers interact with each other through partial overlap of their large conjugated π-systems, and with specific protein residues through their central Mg atom and other peripheral side groups, and e) the BChl monomers of LH2 and LH3 interact electronically only with the protein environment and not with each other.

The role of the protein environment in controlling the spectral properties of BChls in LHs is twofold (Alden et al., 1997; Prince et al., 1997; Scholes and Fleming, 2000): a) it determines the aggregation size and relative orientation of BChls within the complex, thereby tuning the excitonic interactions between the closely spaced BChls, that is, the predominant effect on the LHs spectral features; b) it tunes the electronic properties of the individual BChls by interactions with specific protein residues. These effects lead to significant changes in the LH spectra compared to isolated BChl, hence the distinctive absorption and CD spectra of LHs are useful reporters of a complex's structure and aggregation state. The intense Q_y transition band of monomeric BChl is red shifted from 780 nm to 820 nm upon forming a LH subunit heterodimeric complex labeled B820; further aggregation of the LH subunits red shifts the Q_y band of the BChl dimers to 850–890 nm. Depending on bacterial species and LH type, they are labeled accordingly B850-B890 (Beekman et al., 1997). The same interactions lead to intense negative and positive CD bands centered near the absorption maximum.

Bacterial LHs have been extensively studied by site directed mutagenesis (Hunter, 1995; Olsen et al., 1997; Sturgis et al., 1997; Braun et al., 2002; Chapter 27, Garcia-Martin et al.) and pigment exchange methods (Davis et al., 1996; Fiedor et al., 2001) in order to identify the specific protein-pigment interactions determining BChl binding and complex formation. The studies of Loach and colleagues (Loach and Parkes-Loach, 1995; Meadows et al., 1995, 1998; Kehoe et al., 1998; Todd et al., 1998, 1999), who established a protocol for reconstituting native and modified LH1 complexes from their isolated pigment and apo-protein components in micelles of β-octylglucoside (OG), have provided a wealth of valuable structural information and the inspiration for choosing LHs as templates for BChl-protein maquettes. Table 1 summarizes some of the peptides tested for in vitro reconstitution in OG. Loach's work has shown that isolated LH1 apo-proteins and BChls can self-assemble to form complexes with the same absorption and CD spectra as native LH1. Moreover, it was shown that native and modified apo-proteins and their fragments, obtained either by enzymatic cleavage (Meadows et al., 1995) or solid-phase peptide synthesis (Kehoe et al., 1998; Meadows et al., 1998), can self-assemble with BChls reproducing some or all of the spectral features of LH1. As shown in Table 1, B820, the common intermediate in the assembly and dissociation processes of all bacterial LHs (Loach and Parkes-Loach, 1995), is a rather robust construct that can form even with truncated and modified versions of the native β-apo-protein alone, pointing to a general BChl binding motif common to all bacterial LHs.

Table 1. Q_y absorption maxima of in vitro reconstituted LH1 beta apo-proteins and BChls in OG

Apo-Protein[3]	Length[4]	β:β[1] subunit	oligomer	α:β[2] subunit	oligomer	Reference
sphβ48[5]	48	823	–	822	874	(Todd et al.,1999)
sphβ48(W-10→R)	48	822	–	823	873	(Todd et al.,1999)
sphβ48(H-18→V)	48	824	–	824	–	(Todd et al.,1999)
sphβ48(S-7→I)	48	823	–	823	874	(Sturgis et al., 1997)
sphβ48(Y+4→M)	48	822	–	822	879	(Sturgis et al., 1997)
sphβ48(H0→N)	48	–	–	–	–	(Sturgis et al., 1997)
sphβ48(F-)	47	821	–	822	871	(Meadows et al.,1995)
sphβ48(WF-)	46	812	–	812	860	(Kehoe et al.,1998)
sphβ41	41	820	–	823	870	(Kehoe et al.,1998)
sphβ37	37	820	847	820	847	(Kehoe et al.,1998)
sphβ31	31	820	849	820	849	(Meadows et al.,1998)
sphβ31(W+9→F)	31	812	–	812	–	(Kehoe et al.,1998)
sphβ31(R+7→F)	31	820	–	820	–	(Kehoe et al.,1998)
sphβ31(W+6→F)	31	820	849	820	849	(Kehoe et al.,1998)
sphβ16-KSIK	20	–	–	–	–	(Meadows et al.,1998)
sphβ16	16	–	–	–	–	(Meadows et al.,1998)
rrβ54[5]	54	819	–	820	872	(Meadows et al.,1995)
rrβ38	38	819	–	818	870	(Meadows et al.,1995)
rrβ37	37	817		816	862	(Meadows et al.,1995)
rrβ35	35	818	–	820	–	(Kehoe et al.,1998)
rrβ33	33	816	–	–	–	(Meadows et al.,1995)
rrβ31	31	820	–	820	–	(Meadows et al.,1998)
virβ38	38	–	872	810	865	(Meadows et al.,1995)

[1] Reconstitution with β-apo-protein and BChl only. [2] Reconstitution with β-apo-protein, BChl and the corresponding native α-apo-protein. [3] Abbreviation: sph – *Rhodobacter sphaeroides*, rr – *Rhodospirilum rubrum*, vir – *Blastochloris viridis*. [4] Number of amino-acid residues. [5] Native protein.

B. Designing a Minimal Bacteriochlorophyll Binding Protein

Our first goal was to design a minimal B820 maquette that can serve as a fundamental building block for constructing more elaborate LH type maquette designs. In order to identify the most crucial structural motifs for B820 assembly, we have combined the experimental data from Loach and colleagues (Table 1) with comparing LH1 protein sequences from different organisms as shown in Fig. 2, and analyzing the BChl binding site structure of LH2 from *Rhodospirillum* (*Rsp.*) *molischianum* (PDB reference: 1LGH; Koepke et al., 1996), illustrated in Fig. 3, that shares a high sequence homology with LH1 from *Rhodobacter* (*Rba.*) *sphaeroides*. The following structural features appear to be the most generally conserved for both α- and β-LH1 apo-proteins and are therefore key for a successful design: a) a histidine ligand to the BChl central Mg atom; for clarity, we adapt the residue numbering of Loach and colleagues whereby residues are numbered relative to this histidine ligand, numbered 0, with positive numbers toward the carboxy terminal and negative numbers toward the amino terminal; b) a tryptophan-rich carboxy terminal loop with the last tryptophan residue, W+9, forming a hydrogen bond to the BChl C3 keto carbonyl group; c) an aromatic residue at position –8 interacting with the BChl phytyl chain; the BChl molecule is actually flanked by this residue and the carboxy terminal's W+9, as shown in Fig. 3; d) hydrophobic residues at positions +1 to +3 and –1 to –6, including a strictly conserved alanine residue at position –1. Residues from position –9 further away from the BChl toward the amino terminal are less conserved and probably less important for binding (Chapter 27, Garcia-Martin et al.).

Our smallest design was therefore a 19 residues

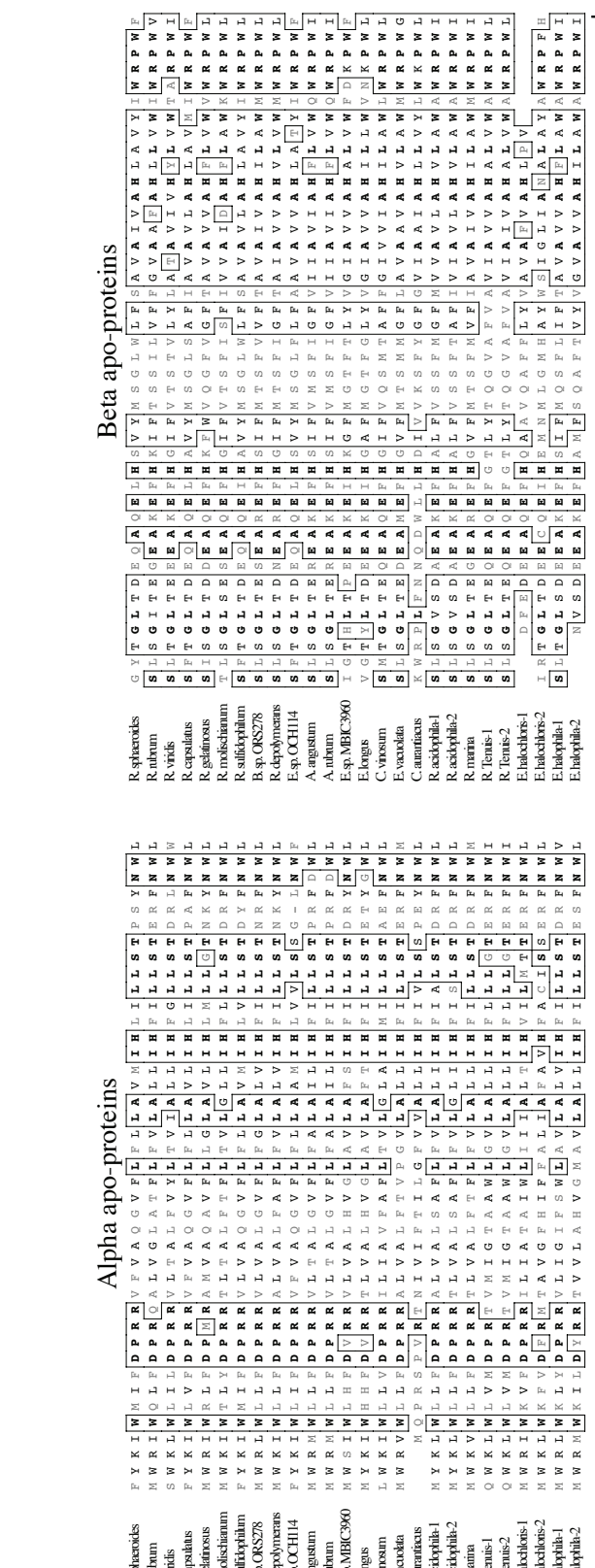

Fig. 2. Sequence alignment of the α- and β-apo-proteins of bacterial LH1. o-hydroxyl residues (S, T), Δ-Acidic residues (D, E), ρ-Basic residues (K, H, R), ϕ-Aromatic residues (F, W, Y), :- hydrophobic residues (I, L, V, A)

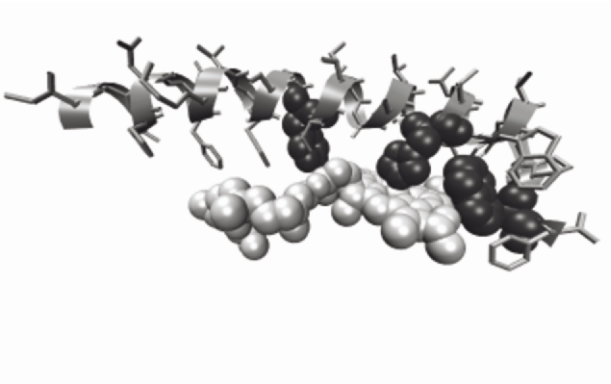

Fig. 3. Binding Site of BChl in natural LH2 β-apo-protein of *Rhodospirilum molischianum* (PDB reference 1LGH; Koepke et al., 1996). This protein shares a high sequence homology with LH1 β-apo-proteins. 31 amino acid residues are shown in medium grey with residues in contact shown space filled in dark grey. The BChl (space filled light grey) is ligated to histidine and flanked by a tryptophane hydrogen bonding to its C3 keto carbonyl side chain, and a phenylalanine interacting with its phytyl chain. Image was created with the software VMD (Humphrey et al., 1996)

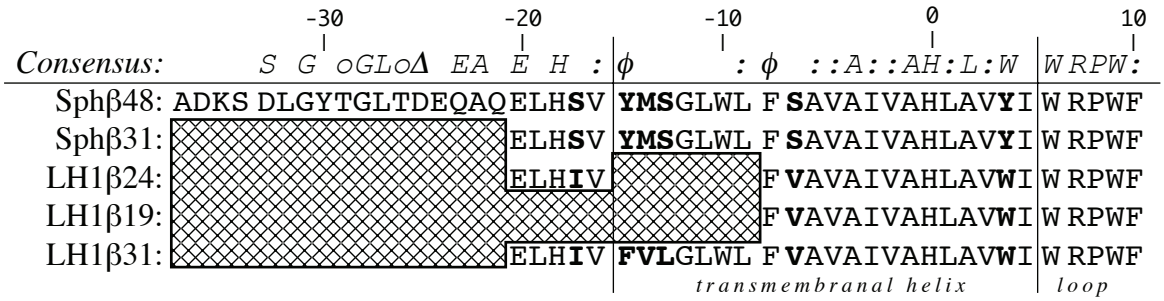

Fig. 4. Protein maquette designs based on native beta apo-protein of *Rhodobacter sphaeroides* (sphβ48), and the 75% consensus sequence of LH1 β-apo-proteins. o-hydroxyl residues (S, T), Δ-acidic residues (D, E), ϕ-aromatic residues (F, W, Y), :- hydrophobic residues (I, L, V, A).

peptide, labeled LH1β19 (Fig. 4) based mostly on the LH1 β-apo-protein of *Rba. sphaeroides* because sphβ31, a 31 residue truncated version of the native protein, was shown to have the largest equilibrium constant for B820 formation. This design was highly insoluble in OG and could not assemble BChls into a B820 complex. To improve the design, an ELHIV motif was added at the amino terminal of LH1β19, which includes the strictly conserved E-20 and H-18 residues of LH1 beta chains. The addition of another helix turn with polar residues was expected to improve the helix stability and solubility within the detergent micelles. Indeed, this design, labeled LH1β24, was more successful and readily assembled BChls into a B820 complex. Figure 5 shows the CD and absorbance spectra of LH1β24 compared to the spectra of sphβ31 at similar conditions. The spectral features of LH1β24 are typical of a B820 complex whereas the sphβ31 spectra indicate the formation of a higher oligomer with a Q_y absorption maximum at 850 nm.

Figure 6 compares a model of LH1β24, based on the *Rsp. molischianum* crystal structure, with the respective sphβ31 model and the native subunit structure. Clearly, the LH1β24 apo-protein is just long enough to span the length of a BChl molecule and is about half the size of typical native LH1 beta apo-protein. Thus, it is most probably the smallest peptide capable of assembling BChls into a B820 subunit complex and can serve as a fundamental building block in constructing functional LH maquettes.

C. Controlling Bacteriochlorophyll Binding and Aggregation

The successful design of LH1β24 as a minimal BChl-binding subunit demonstrates that as little as

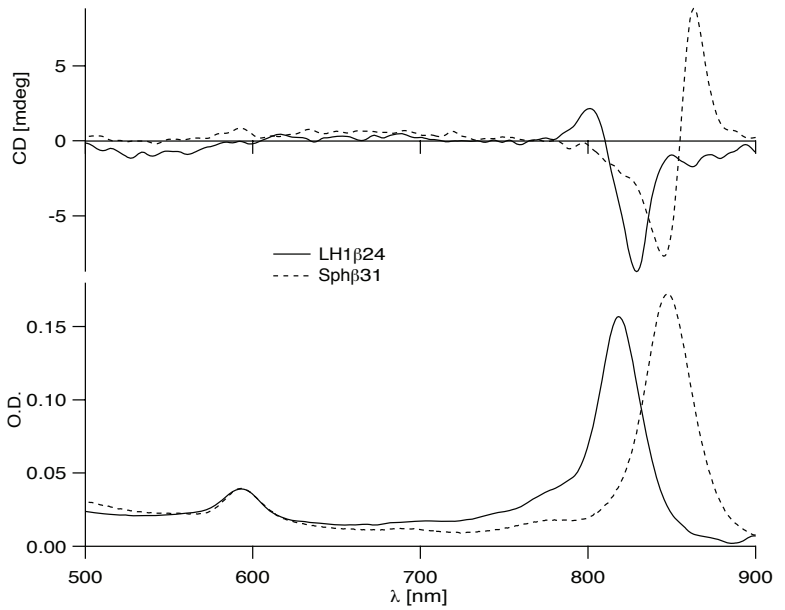

Fig. 5. Absorbance (bottom) and CD (top) spectra of sphβ31 and LH1β24 in 0.64% OG, 50 mM phosphate buffer pH 7.5 at 4 ºC.

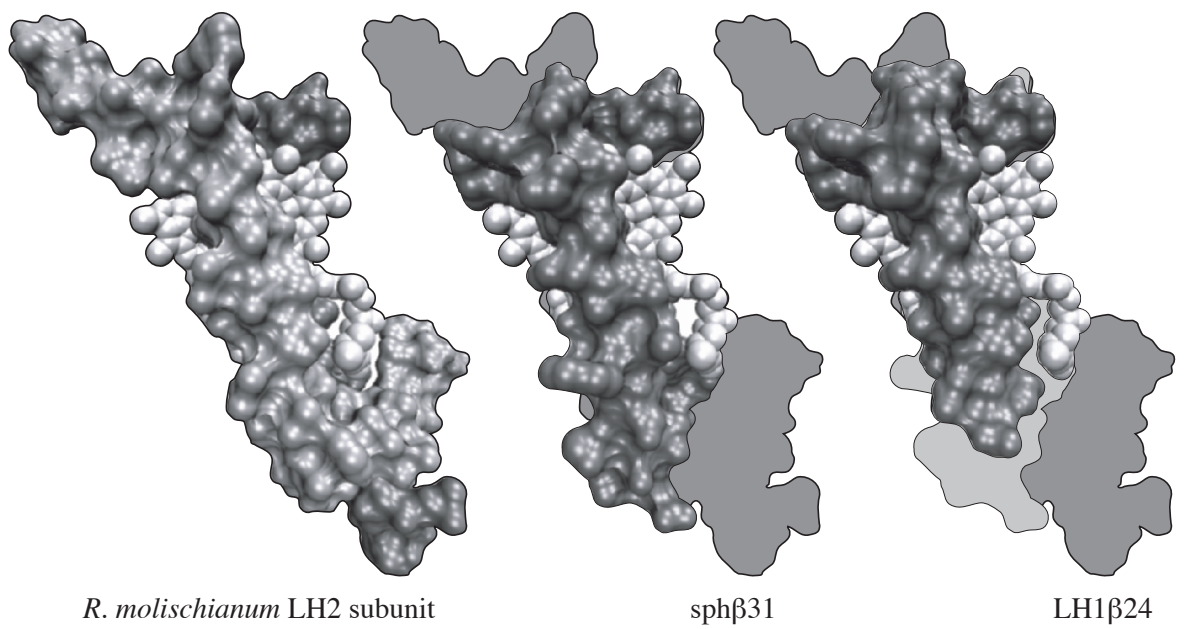

Fig. 6. 3D models of sphβ31 and LH1β24 subunit complexes compared to the crystal structure of native LH2 subunit complex (BChls are lightest grey, α-apo-protein medium grey, and β chains dark grey). Image was created with the software VMD (Humphrey et al., 1996)

a 24 amino acids peptide is sufficient to bind BChl and control its spectral properties while maximizing pigment per protein ratio. However, as shown in Fig. 5, LH1β24 does not form the longer wavelength species typical of the larger oligomers formed by native apo-proteins; in contrast the 31 residues peptide

sphβ31 forms a B850 species (absorbance maximum at 850 nm), similar to the 870 nm maximum of native LH1 complex (Meadows et al., 1995, 1998). This suggests that longer peptides are required in order to control self-organizations of pigments and peptides into aggregates of well-defined stoichiometry, size, and shape.

To further explore the factors that control BChl binding and subunit aggregation we designed another maquette, labeled LH1β31 (Fig. 4), in which the 12 amino terminal residues of sphβ31 were added to LH1β19, but serines and methionine suggested to be involved in hydrogen bonding between subunits (Loach and Parkes-Loach, 1995; Kehoe et al., 1998) were replaced by aliphatic residues, and tyrosine with phenylalanine.

The temperature dependence of B820 and B850 assembly by LH1β24, LH1β31, and sphβ31 was monitored spectroscopically at 0.9% OG using the same pigment and peptide concentrations. Figure 7 compares the results from the three peptides indicating a transition from the monomeric B780 species to B820 with an isosbestic point at 800 nm. Clearly, length alone is not sufficient for multimeric associa-

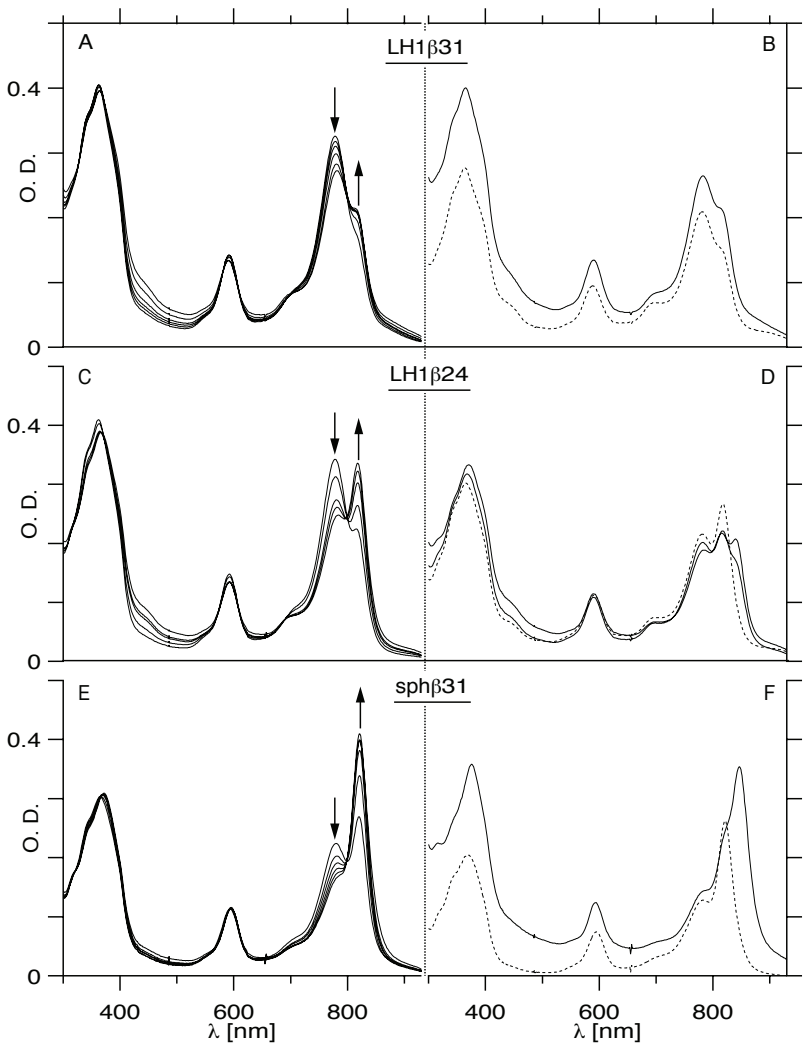

Fig. 7. Effect of temperature (left) and centrifugation (right) on the association and aggregation of LH1β31 (A,B), LH1β24 (C,D) and sphβ31 (E, F) at 0.9% OG, 50 mM phosphate buffer solution and pH 7.5. Peptide and BChl concentrations were ~8 μM. Panels A, C, and E show cooling from 20 ºC to 6 ºC, Panels B, D and F show spectra at 4 ºC before and after 20 min centrifugation at 14000 rpm (solid and dotted line respectively). LH1β24 required cooling to 0 ºC before a significant amount of B850 could be detected (panel D, additional solid line).

tion; although sphβ31 forms the multimeric B820 the most readily, the short LH1β24 peptide forms B820 more readily than the longer LH1β31. At lower temperatures (0 to 4 °C), all three peptides form larger B850 aggregates, especially sphβ31. However, these aggregates appear to have uncomfortably large molecular weights. Besides the increased scattering upon forming the B850, in each case B850 sediments easily after 20 min at 14000 rpm on a bench top centrifuge (Fig. 7 B, D, F). Additional results from sedimentation equilibrium and confocal microscopy (not shown) support our observation that these B850 are very large, non-specific aggregates probably dominated by BChl self-association.

The balance between BChl self-aggregation and subunit oligomerization appears to be a central design concern for LH complex formation. Model studies of BChl aggregation, in a 3:1 formamide/water solution (Fisher et al., 1990; Scherz et al., 1990), have determined that the free energies for BChl dimerization and oligomerization are –18.7 and –38.5 kJ, respectively, compared to –100 kJ for native LH1 subunit carotenoid free complex formation and at least –58 kJ for B870 complex formation in 0.75% OG in water (Loach and Parkes-Loach, 1995). BChl self-aggregation is certainly a competitive process for LH assembly on one hand, but may be used to drive the LH oligomerization and contribute significant stabilization energy to the LH complex on the other hand. The protein's most important role in such case is not in driving the assembly but in imposing steric restrictions to limit and manage the BChl aggregation process.

IV. Concluding Remarks

The design of protein maquettes as a way of exploring the overall engineering guideline of native proteins is complementary to site directed mutagenesis methods focused primarily on the role of specific amino acid residues within a protein. Here, we have demonstrated the use of protein maquettes for identifying a minimal unit for the B820 protomeric subunit of bacterial LHs and demonstrated that a peptide as short as 24 amino acids is capable of binding BChls non-covalently, and self-assembling to form B820 analogs.

Subsequent aggregation of B820 into larger native like complexes is harder to control by short peptides. Unlike the native LH complexes the B850 species, formed by truncated and modified LH1 and LH2 β-apo-proteins, are very large particles, probably dominated by BChl aggregates. The balance between BChl self-aggregation and protein complex formation appears to be crucial for LH engineering. Given the spontaneous self-aggregation of BChls, the protein's most important role in LH assembly may not be driving the aggregation but rather restricting BChl aggregates to a unique desired conformation. The steric restrictions imposed by the overall shape and surface complementarity of the protomeric subunits are at least as important to the protein role as specific interactions between protein residues (Bailey et al., 1998). The guidelines for controlling LH subunits aggregation into their native oligomeric structure are yet to be determined. New designs of protein maquettes based on our basic 24 amino acid subunit are expected to reveal some of the principles behind the self assembly LH complexes as well as other oligomeric constructs of membrane proteins.

Acknowledgments

Dror Noy is supported by a long-term fellowship from the Human Frontiers Science Program.

References

Alden RG, Johnson E, Nagarajan V, Parson WW, Law CJ and Cogdell RG (1997) Calculations of spectroscopic properties of the LH2 bacteriochlorophyll—Protein antenna complex from *Rhodopseudomonas acidophila*. J Phys Chem B 101: 4667–4680

Bahr JL, Kodis G, de la Garza L, Lin S, Moore AL, Moore TA and Gust D (2001) Photoswitched singlet energy transfer in a porphyrin-spiropyran dyad. J Am Chem Soc 123: 7124–7133

Bailey MJ, Schulten K and Johnson JE (1998) The use of solid physical models for the study of macromolecular assembly. Curr Opin Struct Biol 8: 202–208

Baltzer L, Nilsson H and Nilsson J (2001) De novo design of proteins—What are the rules? Chem Rev 101: 3153–3163

Bechinger B (2000) Understanding peptide interactions with the lipid bilayer: A guide to membrane protein engineering. Curr Opin Chem Biol 4: 639–644

Beekman LMP, Steffen M, van Stokkum IHM, Olsen JD, Hunter CN, Boxer SG and van Grondelle R (1997) Characterization of the light-harvesting antennas of photosynthetic purple bacteria by stark spectroscopy. 1. LH1 antenna complex and the B820 subunit from Rhodospirillum rubrum. J Phys Chem B 101: 7284–7292

Benites MD, Johnson TE, Weghorn S, Yu LH, Rao PD, Diers JR, Yang SI, Kirmaier C, Bocian DF, Holten D and Lindsey JS (2002) Synthesis and properties of weakly coupled dendrimeric multiporphyrin light-harvesting arrays and hole-storage

reservoirs. J Mater Chem 12: 65–80
Bolon DN and Mayo SL (2001) Enzyme-like proteins by computational design. Proc Natl Acad Sci USA 98: 14274–14279
Bowie JU (2000) Understanding membrane protein structure by design. Nat Struct Biol 7: 91–94
Braun P, Olsen JD, Strohmann B, Hunter CN and Scheer H (2002) Assembly of light-harvesting bacteriochlorophyll in a model transmembrane helix in its natural environment. J Mol Biol 318: 1085–1095
Bryson JW, Desjarlais JR, Handel TM and DeGrado WF (1998) From coiled coils to small globular proteins: Design of a native-like three-helix bundle. Protein Sci 7: 1404–1414
Chen XX, Moser CC, Pilloud DL and Dutton PL (1998) Molecular orientation of Langmuir-Blodgett films of designed heme protein and lipoprotein maquettes. J Phys Chem B 102: 6425–6432
Choma CT, Tieleman DP, Cregut D, Serrano L and Berendsen HJC (2001) Towards the design and computational characterization of a membrane protein. J Mol Graphics Modell, 20: 219–234
Cogdell RJ and Lindsay JG (2000) Tansley Review No. 109—The structure of photosynthetic complexes in bacteria and plants: an illustration of the importance of protein structure to the future development of plant science. New Phytol 145: 167–196
Cogdell RJ, Isaacs NW, Howard TD, McLuskey K, Fraser NJ and Prince SM (1999) How photosynthetic bacteria harvest solar energy. J Bacteriol, 181: 3869–3879
Dahiyat BI and Mayo SL (1997) De novo protein design: Fully automated sequence selection. Science 278: 82–87
Davis CM, Parkes-Loach PS, Cook CK, Meadows KA, Bandilla M, Scheer H and Loach PA (1996) Comparison of the structural requirements for bacteriochlorophyll binding in the core light-harvesting complexes of *Rhodospirillum rubrum* and *Rhodobacter sphaeroides* using reconstitution methodology with bacteriochlorophyll analogs. Biochemistry 35: 3072–3084
DeGrado WF, Summa CM, Pavone V, Nastri F and Lombardi A (1999) De novo design and structural characterization of proteins and metalloproteins. Annu Rev Biochem, 68: 779–819
Dutton PL (1995) Design and synthesis of redox proteins. Protein Eng 8: 83–83
Fiedor L, Leupold D, Teuchner K, Voigt B, Hunter CN, Scherz A and Scheer H (2001) Excitation trap approach to analyze size and pigment-pigment coupling: Reconstitution of LH1 antenna of *Rhodobacter sphaeroides* with Ni-substituted bacteriochlorophyll. Biochemistry 40: 3737–3747
Field MJ (2002) Simulating enzyme reactions: Challenges and perspectives. J Comput Chem 23: 48–58
Fisher JRE, Rosenbach-Belkin V and Scherz A (1990) Cooperative polymerization of photosynthetic pigments in formamide-water solution. Biophys J 58: 461–470
Fowler GJS, Sockalingum GD, Robert B and Hunter CN (1994) Blue shifts in bacteriochlorophyll absorbency correlate with changed hydrogen-bonding patterns in light-harvesting 2 mutants of *Rhodobacter sphaeroides* with alterations at Alpha-Tyr-44 and Alpha-Tyr-45. Biochem J 299: 695–700
Fowler GJS, Hess S, Pullerits T, Sundström V and Hunter CN (1997) The role of beta Arg(–10) in the B800 bacteriochlorophyll and carotenoid pigment environment within the light-harvesting LH2 complex of *Rhodobacter sphaeroides*. Biochemistry 36: 11282–11291
Gall A, Fowler GJS, Hunter CN and Robert B (1997) Influence of the protein binding site on the absorption properties of the monomeric bacteriochlorophyll in *Rhodobacter sphaeroides* LH2 complex. Biochemistry 36: 16282–16287
Gibney BR, Mulholland SE, Rabanal F and Dutton PL (1996) Ferredoxin and ferredoxin-heme maquettes. Proc Natl Acad Sci USA 93: 15041–15046
Gibney BR, Rabanal F and Dutton PL (1997a) Synthesis of novel proteins. Curr Opin Chem Biol 1: 537–542
Gibney BR, Rabanal F, Skalicky JJ, Wand AJ and Dutton PL (1997b) Design of a unique protein scaffold for maquettes. J Am Chem Soc 119: 2323–2324
Gibney BR, Johansson JS, Rabanal F, Skalicky JJ, Wand AJ and Dutton PL (1997c) Global topology and stability and local structure and dynamics in a synthetic spin-labeled four-helix bundle protein. Biochemistry 36: 2798–2806
Gibney BR, Rabanal F, Reddy KS and Dutton PL (1998) Effect of four helix bundle topology on heme binding and redox properties. Biochemistry 37: 4635–4643
Gibney BR, Huang SS, Skalicky JJ, Wand AJ and Dutton PL (1999a) Controlling synthetic heme protein redox potentials. J Inorg Biochem 74: 142–142
Gibney BR, Rabanal F, Skalicky JJ, Wand AJ and Dutton PL (1999b) Iterative protein redesign. J Am Chem Soc 121: 4952–4960
Gibney BR, Huang SS, Skalicky JJ, Fuentes EJ, Wand AJ and Dutton PL (2001) Hydrophobic modulation of heme properties in heme protein maquettes. Biochemistry 40: 10550–10561
Gratkowski H, Lear JD and DeGrado WF (2001) Polar side chains drive the association of model transmembrane peptides. Proc Natl Acad Sci USA 98: 880–885
Gust D, Moore TA and Moore AL (2001) Mimicking photosynthetic solar energy transduction. Acc Chem Res 34: 40–48
Hill RB, Raleigh DP, Lombardi A and Degrado NF (2000) De novo design of helical bundles as models for understanding protein folding and function. Acc Chem Res 33: 745–754
Holten D, Bocian DF and Lindsey JS (2002) Probing electronic communication in covalently linked multiporphyrin arrays. A guide to the rational design of molecular photonic devices. Acc Chem Res 35: 57–69
Hu QH, Sturgis JN, Robert B, Delagrave S, Youvan DC and Niederman RA (1998a) Hydrogen bonding and circular dichroism of bacteriochlorophylls in the *Rhodobacter capsulatus* light-harvesting 2 complex altered by combinatorial mutagenesis. Biochemistry 37: 10006–10015
Hu XC, Damjanovic A, Ritz T and Schulten K (1998b) Architecture and mechanism of the light-harvesting apparatus of purple bacteria. Proc Natl Acad Sci USA 95: 5935–5941
Huang S (2001) Structure of a Molecular Maquette Scaffold. Ph.D. thesis, University of Pennsylvania, Philadelphia
Humphrey W. Dalke A. and Schulten K. (1996) VMD—Visual molecular dynamics. J Molec Graphics. 14: 33–38
Hunter CN (1995) Genetic manipulation of the antenna complexes of purple bacteria. In: Blankenship RE, Madigan MT and Bauer CE (eds), Anoxygenic Photosynthetic Bacteria, pp 473–501. Kluwer Academic Publishers, Dordrecht
Ikeda-Yamasaki I, Odahara T, Mitsuoka K, Fujiyoshi Y and Murata K (1998) Projection map of the reaction center-light harvesting 1 complex from *Rhodopseudomonas viridis* at 10 Ångstrom resolution. FEBS Lett 425: 505–508
Johansson JS, Gibney BR, Skalicky JJ, Wand AJ and Dutton PL (1998) A native-like three-alpha-helix bundle protein from structure-based redesign: A novel maquette scaffold. J Am

Chem Soc 120: 3881–3886
Jordan P, Fromme P, Witt HT, Klukas O, Saenger W and Krauss N (2001) Three-dimensional structure of cyanobacterial photosystem I at 2.5A resolution. Nature 411: 909–917
Jungas C, Ranck JL, Rigaud JL, Joliot P and Vermeglio A (1999) Supramolecular organization of the photosynthetic apparatus of *Rhodobacter sphaeroides*. EMBO J 18: 534–542
Kalsbeck WA, Robertson DE, Pandey RK, Smith KM, Dutton PL and Bocian DF (1996) Structural and electronic properties of the heme cofactors in a multi-heme synthetic cytochrome. Biochemistry 35: 3429–3438
Karrasch S, Bullough PA and Ghosh R (1995) The 8.5-Ångstrom projection map of the light-harvesting complex-I from *Rhodospirillum rubrum* reveals a ring composed of 16 subunits. EMBO J 14: 631–638
Kehoe JW, Meadows KA, Parkes-Loach PS and Loach PA (1998) Reconstitution of core light-harvesting complexes of photosynthetic bacteria using chemically synthesized polypeptides. 2. Determination of structural features that stabilize complex formation and their implications for the structure of the subunit complex. Biochemistry 37: 3418–3428
Kodis G, Liddell PA, de la Garza L, Clausen PC, Lindsey JS, Moore AL, Moore TA and Gust D (2002) Efficient energy transfer and electron transfer in an artificial photosynthetic antenna-reaction center complex. J Phys Chem A 106: 2036–2048
Koepke J, Hu XC, Muenke C, Schulten K and Michel H (1996) The crystal structure of the light-harvesting complex II (B800- 850) from *Rhodospirillum molischianum*. Structure 4: 581–597
Kortemme T, Ramirez-Alvarado M and Serrano L (1998) Design of a 20-amino acid, three-stranded beta-sheet protein. Science 281: 253–256
Kraemer-Pecore CM, Wollacott AM and Desjarlais JR (2001) Computational protein design. Curr Opin Chem Biol 5: 690–695
Lear JD, Schneider JP, Kienker PK and DeGrado WF (1997) Electrostatic effects on ion selectivity and rectification in designed ion channel peptides. J Am Chem Soc 119: 3212–3217
Loach PA and Parkes-Loach PS (1995) Structure-function relationships in core light-harvesting complexes (LHI) as determined by characterization of the structural subunit and by reconstitution experiments. In: Blankenship RE, Madigan MT and Bauer CE (eds) Anoxygenic Photosynthetic Bacteria, pp 437–471. Kluwer Academic Publishers, Dordrecht
Markvart T (2000) Light harvesting for quantum solar energy conversion. Prog Quantum Electron 24: 107–186
McDermott G, Prince SM, Freer AA, Hawthornthwaite-Lawless AM, Papiz MZ, Cogdell RJ and Isaacs NW (1995) Crystal-structure of an integral membrane light-harvesting complex from photosynthetic bacteria. Nature 374: 517–521
McLuskey K, Prince SM, Cogdell RJ and Isaacs NW (2001) The crystallographic structure of the B800-820 LH3 light-harvesting complex from the purple bacteria *Rhodopseudomonas acidophila* strain 7050. Biochemistry 40: 8783–8789
Meadows KA, Iida K, Tsuda K, Recchia PA, Heller BA, Antonio B, Nango M and Loach PA (1995) Enzymatic and chemical cleavage of the core light-harvesting polypeptides of photosynthetic bacteria — determination of the minimal polypeptide size and structure required for subunit and light-harvesting complex-formation. Biochemistry 34: 1559–1574
Meadows KA, Parkes-Loach PS, Kehoe JW and Loach PA (1998) Reconstitution of core light-harvesting complexes of photosynthetic bacteria using chemically synthesized polypeptides. 1. Minimal requirements for subunit formation. Biochemistry 37: 3411–3417
Mongin O, Hoyler N and Gossauer A (2000) Synthesis and light-harvesting properties of niphaphyrins. Eur J Org Chem 7: 1193–1197
Oling F, Boekema EJ, deZarate IO, Visschers R, van Grondelle R, Keegstra W, Brisson A and Picorel R (1996) Two-dimensional crystals of LH2 light-harvesting complexes from *Ectothiorhodospira* sp. and *Rhodobacter capsulatus* investigated by electron microscopy. Biochim Biophys Acta Bioenergetics 1273: 44–50
Olsen JD, Sturgis JN, Westerhuis WHJ, Fowler GJS, Hunter CN and Robert B (1997) Site-directed modification of the ligands to the bacteriochlorophylls of the light-harvesting LH1 and LH2 complexes of *Rhodobacter sphaeroides*. Biochemistry 36: 12625–12632
Olson JM (1998) Chlorophyll organization and function in green photosynthetic bacteria. Photochem Photobiol 67: 61–75
Pilloud DL, Rabanal F, Gibney BR, Farid RS, Dutton PL and Moser CC (1998) Self-assembled monolayers of synthetic hemoproteins on silanized quartz. J Phys Chem B 102: 1926–1937
Pokala N and Handel TM (2001) Review: Protein design — Where we were, where we are, where we're going. J Struct Biol 134: 269–281
Prince SM, Papiz MZ, Freer AA, McDermott G, Hawthornthwaite-Lawless AM, Cogdell RJ and Isaacs NW (1997) Apoprotein structure in the LH2 complex from *Rhodopseudomonas acidophila* strain 10050: Modular assembly and protein pigment interactions. J Mol Biol 268: 412–423
Ranck JL, Ruiz T, Pehau-Arnaudet G, Arnoux B and Reiss-Husson F (2001) Two-dimensional structure of the native light-harvesting complex LH2 from *Rubrivivax gelatinosus* and of a truncated form. Biochim Biophys Acta Bioenergetics 1506: 67–78
Rau HK, Snigula H, Struck A, Scheer H and Haehnel W (2001) Design, synthesis and properties of synthetic chlorophyll proteins. Eur J Biochem 268: 3284–3295
Robertson DE, Farid RS, Moser CC, Urbauer JL, Mulholland SE, Pidikiti R, Lear JD, Wand AJ, DeGrado WF and Dutton PL (1994) Design and synthesis of multi-haem proteins. Nature 368: 425–432
Rucareanu S, Mongin O, Schuwey A, Hoyler N, Gossauer A, Amrein W and Hediger HU (2001) Supramolecular assemblies between macrocyclic porphyrin hexamers and star-shaped porphyrin arrays. J Org Chem 66: 4973–4988
Savage H, Cyrklaff M, Montoya G, Kühlbrandt W and Sinning I (1996) Two-dimensional structure of light harvesting complex II (LHII) from the purple bacterium *Rhodovulum sulfidophilum* and comparison with LHII from *Rhodopseudomonas acidophila*. Structure 4: 243–252
Scherz A, Rosenbach-Belkin V and Fisher JRE (1990) Distribution and self-organization of photosynthetic pigments in micelles — implication for the assembly of light-harvesting complexes and reaction centers in the photosynthetic membrane. Proc Natl Acad Sci USA 87: 5430–5434
Scholes GD and Fleming GR (2000) On the mechanism of light harvesting in photosynthetic purple bacteria: B800 to B850 energy transfer. J Phys Chem B 104: 1854–1868
Segall MD (2002) Applications of ab initio atomistic simulations to biology. J Phys Condens Matter 14: 2957–2973

Sharp RE, Diers JR, Bocian DF and Dutton PL (1998a) Differential binding of iron(III) and zinc(II) protoporphyrin IX to synthetic four-helix bundles. J Am Chem Soc 120: 7103–7104

Sharp RE, Moser CC, Rabanal F and Dutton PL (1998b) Design, synthesis, and characterization of a photoactivatable flavocytochrome molecular maquette. Proc Natl Acad Sci USA 95: 10465–10470

Shifman JM, Moser CC, Kalsbeck WA, Bocian DF and Dutton PL (1998) Functionalized de novo designed proteins: Mechanism of proton coupling to oxidation/reduction in heme protein maquettes. Biochemistry 37: 16815–16827

Siegbahn PEM and Blomberg MRA (2000) Transition-metal systems in biochemistry studied by high- accuracy quantum chemical methods. Chem Rev 100: 421–437

Skalicky JJ, Bieber RJ, Gibney BR, Rabanal F, Dutton PL and Wand AJ (1998) Sequence-specific resonance assignments for a designed four-alpha-helix bundle protein. J Biomol NMR 11: 227–228

Skalicky JJ, Gibney BR, Rabanal F, Urbauer RJB, Dutton PL and Wand AJ (1999) Solution structure of a designed four-alpha-helix bundle maquette scaffold. J Am Chem Soc 121: 4941–4951

Stahlberg H, Dubochet J, Vogel H and Ghosh R (1998) Are the light-harvesting I complexes from *Rhodospirillum rubrum* arranged around the reaction centre in a square geometry? J Mol Biol 282: 819–831

Struthers MD, Cheng RP and Imperiali B (1996) Design of a monomeric 23-residue polypeptide with defined tertiary structure. Science 271: 342–345

Sturgis JN, Olsen JD, Robert B and Hunter CN (1997) Functions of conserved tryptophan residues of the core light-harvesting complex of *Rhodobacter sphaeroides*. Biochemistry 36: 2772–2778

Sundström V (2000) Light in elementary biological reactions. Prog Quantum Electron 24: 187–238

Todd JB, Parkes-Loach PS, Leykam JF and Loach PA (1998) In vitro reconstitution of the core and peripheral light-harvesting complexes of *Rhodospirillum molischianum* from separately isolated components. Biochemistry 37: 17458–17468

Todd JB, Recchia PA, Parkes-Loach PS, Olsen JD, Fowler GJS, McGlynn P, Hunter CN and Loach PA (1999) Minimal requirements for in vitro reconstitution of the structural subunit of light-harvesting complexes of photosynthetic bacteria. Photosynth Res 62: 85–98

Tronrud DE and Matthews BW (1993) Refinement of the structure of a water-soluble antenna complex from green photosynthetic bacteria by incorporation of the chemically determined amino acid sequence. In: Deisenhofer J and Norris JR (eds) The Photosynthetic Reaction Center, pp 13–22. Academic Press, New York

van Rossum BJ, Steensgaard DB, Mulder FM, Boender GJ, Schaffner K, Holzwarth AR and de Groot HJM (2001) A refined model of the chlorosomal antennae of the green bacterium *Chlorobium tepidum* from proton chemical shift constraints obtained with high-field 2-D and 3-D MAS NMR dipolar correlation spectroscopy. Biochemistry 40: 1587–1595

Voigt CA, Gordon DB and Mayo SL (2000) Trading accuracy for speed: A quantitative comparison of search algorithms in protein sequence design. J Mol Biol 299: 789–803

Walz T, Jamieson SJ, Bowers CM, Bullough PA and Hunter CN (1998) Projection structures of three photosynthetic complexes from *Rhodobacter sphaeroides*: LH2 at 6 angstrom LH1 and RC-LH1 at 25 angstrom. J Mol Biol 282: 833–845

Wernisch L, Hery S and Wodak SJ (2000) Automatic protein design with all atom force-fields by exact and heuristic optimization. J Mol Biol 301: 713–736

Woolfson DN (2001) Core-directed protein design. Curr Opin Struct Biol 11: 464–471

Chapter 25

Molecular Assembly of Bacteriochlorophyll Complexes Using Synthetic Light-Harvesting Model Polypeptides

Mamoru Nango*
Department of Applied Chemistry, Nagoya Institute of Technology, Showa-ku, Nagoya 466-8555, Japan

Summary

Molecular assembly of bacteriochlorophyll *a* (BChl *a*) or zinc-substituted bacteriochlorophyll *a* ([Zn]-BChl *a*) into an artificial antenna complex using synthetic light-harvesting (LH) model polypeptides has been achieved.

Synthetic 1α-helix hydrophobic polypeptides, which have similar amino acid sequences to the hydrophobic core in the native LH-β polypeptide from *Rba. sphaeroides,* formed a BChl *a* complex in n-octyl-β-D-glucopyranoside (OG) micelles, analogous to the light-harvesting polypeptide complex of photosynthetic bacteria: this process is dependent on temperature and the polar amino acid sequences in the C-terminal segment. The minimum amino acid sequence in the N-terminal segment of the light-harvesting polypeptides of photosynthetic bacteria necessary for LH1-type complex-formation was that of type 2 of our synthetic hydrophobic polypeptides. A stable BChl *a* complex with a 2α-helix polypeptide, possessing disulfide linkage, was obtained in lipid bilayers and in OG micelles, analogous to the subunit complex, B820, of the LH 1 complex of photosynthetic bacteria.

Further, the water-soluble synthetic 4α-helix polypeptide, HAHA formed a complex with BChl *a* and its analogues, similar to the LH1-type complex. Appropriate analogues of HAHA are also useful in providing an insight into the effect of polypeptide structure on LH complex formation and also for construction of an artificial LH complex.

I. Introduction

It is interesting that light-harvesting (LH) polypeptides organize bacteriochlorophyll *a* (BChl *a*) complexes so that an efficient energy transfer between BChls may occur in the LH complex of photosynthetic bacteria (Olsen et al., 1994; Karrasch et al., 1995; Loach and Parkes-Loach, 1995; Mcdermott et al., 1995; Pullerits and Sundstrome, 1996; Sturgis et al., 1997; Cogdell and Lindsay, 1998). The structure of

* email: nango@ach.nitech.ac.jp

Bernhard Grimm, Robert J. Porra, Wolfhart Rüdiger and Hugo Scheer (eds): Chlorophylls and Bacteriochlorophylls: Biochemistry, Biophysics, Functions and Applications, pp. 365–373.

the LH 2 complex of *Rsp. acidophila* strain 10050 has been resolved to atomic resolution (Mcdermorr et al., 1995), showing that the LH 2 complex consists of a ring of nine heterodimeric subunits. However, no atomic resolution structure has yet been determined for a LH 1 complex although low-resolution projection structures have been determined from two-dimensional crystals of the LH1 complex (Karrasch et al., 1995, Stuart et al., 2002). It is probable that the LH1 complex forms a larger ring, but that BChl *a* binding-sites in the LH1 complex are very similar to those associated with the LH2 complex.

The LH 1 complex includes LH-α and LH-β polypeptides with molecular weights of about 6000 Da and contains approximately 65% α-helical character based on far-UV CD data. Each polypeptide has a central hydrophobic core to allow the LH polypeptides to assume transmembrane topology. The topographical analysis of the arrangement has revealed that C- and N-terminals of both polypeptides are found on the periplasmic and cytoplasmic sides of the membrane, respectively. By analogy with X-ray analysis of the LH2 complex (Mcdermott et al., 1995) and of the reconstitution studies of Loach and Parkes-Loach (1995), the transmembrane helices of LH-α polypeptides are packed side by side to form a hollow cylinder, while the LH-β polypeptides are also arranged radially with the LH-α polypeptides forming an outer cylinder. BChl *a* binds at the histidine sites of LH-α or LH-β polypeptides, which face outwards and inwards, respectively, and the faces are perpendicular to the membrane. Thus, it is considered that the LH polypeptides organize the BChl *a* antenna complex through some non-covalent bonds, and the helices of the LH polypeptides can form inter-subunits between radial and adjacent LH-α and -β polypeptides through several hydrophobic interactions and hydrogen bonds at the C-terminal hydrophilic residues. Olsen et al., (1994) proposed a protein structure for the LH 1 minimal unit of *Rba. sphaeroides*. Further, site-directed mutagenesis was examined on the basis of modeling data (Sturgis et al., 1997). These results indicate that the hydrogen bond between tryptophan on the C-terminus of LH polypeptides and BChl *a* probably plays an important role in the orientation and aggregation of BChl *a* in complex-formation. Loach and coworkers reported that the LH 1 complex of purple photosynthetic bacteria can be reconstituted from separately isolated LH-α and -β polypeptides or from chemically synthesized polypeptides with BChl *a* in lipid bilayers as well as in OG micelles (Bustamante and Loach, 1994; Loach and Parkes-Loach, 1995; Meadows et al., 1995, 1998; Kehoe et al., 1998). In the formation of the reconstituted LH1 complex in OG micelles, the Q_Y band of BChl *a* is shifted from 777 nm (monomeric form) to near 820 nm in the subunit form of the B820 complex of the photosynthetic bacteria and fully shifted to near 870 nm in the B870 complex of the photosynthetic bacteria, indicating that the purified LH polypeptides or chemically-synthesized polypeptides have a key role in the binding and orientation of BChl *a* during complex-formation.

Zinc-containing bacteriochlorophyll *a* ([Zn]-BChl *a*) was discovered in the LH complex and the RC of *Acp. rubrum* (Wakao et al., 1996; Mimuro et al., 2000). The UV-vis absorption spectrum of the LH 1 complex of *Acp. rubrum* resembles that of *Rsp. rubrum*, indicating that *Acp. rubrum* has a similar molecular arrangement of binding sites for [Zn]-BChl *a* as for BChl *a* in the LH 1 complex. [Zn]-BChl *a,* which has been obtained synthetically by the transmetalation of BChl *a* (Hartwich et al., 1998), is more stable than BChl *a*, and Zn-porphyrin derivatives, therefore, have been widely used in model studies of photosynthesis. Interestingly, metallo-substituted BChls have also been used in reconstitution studies with separately isolated LH-α and LH-β polypeptides from *Rsp. rubrum* and *Rba. sphaeroides* (Davis et al., 1996) but there is little information on the interaction of [Zn]-BChl *a* with LH polypeptides (Davis et al., 1996; Hartwich et al., 1998; Kashiwada et al., 1999, 2000a,b,c, 2002; Nango et al., 2001, 2002).

Further, work from several laboratories has demonstrated assembly of porphyrins with synthetic polypeptides to organize formation of artificial hemoprotein or LH complex models (Pasternack et al., 1991; Chome et al., 1994; Benson et al., 1995; Rabanal et al., 1996; Arnold et al., 1997). There has been little work, however, using native light-harvesting polypeptides or their synthetic model polypeptides to study organization and assembly of native or artificial LH complexes in lipid bilayers as well as in OG micelles (Bustamante and Loach, 1994; Iida

Abbreviations: Acp. – Acidiphilium; cmc – critical micelle concentration; DSL – dynamic light scattering; Fmoc – 9-fluor enylmethyloxycarbonyl; LH 1 – core light-harvesting complex; LH 2 – peripheral light-harvesting complex; OG – n-octyl-β-D-glucopyranoside; *Rba. – Rhodobacter; Rsp. – Rhodospirillum ;* SAXS – small-angle X-ray scattering

et al., 1998, 2000; Kehoe et al., 1998; Meadows et al., 1998; Kashiwada et al., 2000a,b,c; Nango et al., 2001, 2002; Ogawa et al., 2002).

In this chapter, we report the molecular assembly of BChl *a* or [Zn]-BChl *a* complexes using light-harvesting (LH) polypeptides separately isolated from the purple photosynthetic bacterium, *Rba. sphaeroides,* and their analogous synthetic model polypeptides (see Figs. 1 and 6) (Kashiwada et al., 1999, 2000 a, Nango et al., 2002).

We reasoned that LH polypeptides from *Rba. sphaeroides* should be used because the native polypeptide forms a stable subunit-complex, B820, of the LH complex in OG micelles (Loach and Parkes-Loach, 1995). Further, we selected synthetic model polypeptides (Fig. 1), which have similar amino acid sequences to the hydrophobic core of the native LH-β polypeptide from *Rba. sphaeroides*. We selected the synthetic 4α-helix polypeptides (the 57-peptide; Fig. 6), which have histidine residues buried in the hydrophobic domain and also have a hydrophilic domain to form a 4α-helix bundle structure in an aqueous solution.

The molecular assembly of BChl *a* or [Zn]-BChl *a* antenna complexes was examined by near-IR and CD spectra, small-angle X-ray scattering (SAXS) and dynamic light scattering (DLS) measurements, as well as by resonance Raman spectroscopy. To gain an insight into the structural requirements for assembly of the LH1 complex, the construction of an artificial LH complex from synthetic model polypeptides and of a native LH complex from native polypeptides, separately isolated from photosynthetic bacteria, was examined.

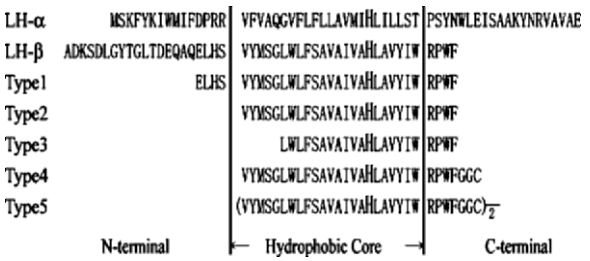

Fig. 1. Amino acid sequences of LH polypeptides from *Rba. sphaeroides* and its synthetic model polypeptides.

II. Molecular Assembly of Bacteriochlorophylls with Isolated Light-Harvesting Subunits from *Rhodobacter sphaeroides* and Synthetic Models

The molecular assembly of BChl *a* or [Zn]-BChl *a* with synthetic hydrophobic polypeptides (Fig. 1) in OG micelles was examined (Kashiwada et al., 2000a; Nango et al., 2002). We selected these α-helical polypeptides, types 1–5, which have similar amino acid sequences to the hydrophobic core in the native LH-β polypeptide from *Rba. sphaeroides*, because the LH-β polypeptide forms a stable BChl *a* complex analogous to the LH 1 subunit-type complex (Loach and Parkes-Loach, 1995; Meadows et al., 1995, 1998; Kehoe et al., 1998). Polypeptides, types 1–3, were synthesized to determine the smallest amino acid sequence in the N-terminal segment required to form the LH complex, while types 4–5 were synthesized to investigate the effect of the disulfide-linkage in the C-terminal segment on the formation of the LH complex. These polypeptides were synthesized by the solid-phase peptide synthesis method on Rink amide resin, using Fmoc protected amino acids (Kashiwada et al., 2000d). The native LH-α and -β polypeptides were separately isolated from the LH 1 complex of *Rba. sphaeroides* and BChl *a* or [Zn]-BChl *a* were obtained as previously described (Loach and Parkes-Loach, 1995; Meadows et al., 1995). The molecular assembly of BChl *a* or [Zn]-BChl *a* using the synthetic polypeptides was carried out by the previously reported reconstitution method (Meadows et al., 1995). 10 nmol of each of the polypeptides was dissolved in 4.5% OG in 50 mM phosphate buffer, pH 7.5, diluted to 0.90% OG with buffer, and then 7 nmol of BChl *a* or [Zn]-BChl *a,* dissolved in acetone, were added. The solution was further diluted to 0.78% OG (the condition for subunit-type complex formation) and chilled at 4 °C overnight (for LH1-type complex formation), in which the concentration of OG (26.7 mM) is approximately at its cmc (Ito et al., 2000).

Table 1 shows the Q_Y absorption band and the CD signal of BChl *a* or [Zn]-BChl *a* in the presence of the synthetic hydrophobic polypeptides. It is clear from Table 1 that the Qy band of the BChl *a*-monomer in acetone (777 nm) is red-shifted to 818 nm in the presence of type 1 or 2 polypeptides in 0.78% OG at 25 ˚C. This is consistent with the subunit-type complex formation as formed previously with both LH-α /-β polypeptides or with LH-β alone at 25 ˚C

Table 1. Near IR and CD spectral data of BChl *a* or [Zn]-BChl *a* in the presence of LH polypeptides from *Rba. sphaeroides* and its synthetic model polypeptides[a]

Polypeptides	BChl *a*				[Zn]-BChl *a*			
	The Q_Y absorption band/λ_{max}[nm]		CD spectra 4 °C		The Q_Y absorption band/λ_{max}[nm]		CD spectra 4 °C	
	25 °C	4 °C	λ[nm](θ [10^{-4} deg cm^2 dmol^{-1}])		25 °C	4 °C	λ[nm](θ [10^{-4} deg cm^2 dmol^{-1}])	
Type 1	818	848	849 (41)	828 (–34)	810	834	838(33)	817(–36)
Type 2	818	843	841 (51)	822 (–30)	809	834	833(49)	812(–34)
Type 3	777[d] 850	777[d] 850	—[e]		810	810	—[e]	
Type 4	777 818	843	854 (6.0)	813 (–7.0)	809	809 830	836(6.0)	792(–20)
Type 5	814	814	823 (10)	802 (–20)	807	807	822(5.6)	792(–23)
LH-β [b]	821	823	828 (–4.5)		814	817	822(–6.2)	
LH-α and LH -β [b]	821	873	888 (8.2)	855 (–6.1)	812	859	867(7.7)	832(–5.6)
none[c]	777	777	no signal		770	770	no signal	

[a] Measured in 0.78% n-octyl-β -D-glucopyranoside (OG) solution (phosphate buffer pH 7.5), [BChl *a*] = 2.4×10^{-6} M, [polypeptides] = 3.4×10^{-6} M. [b] LH polypeptides separately isolated from *Rba. sphaeroides*. [c] In acetone. [d] Broad peaks were observed. [e] No clear signal was observed.

(Loach and Parkes-Loach, 1995; Meadows et al., 1995). On cooling the sample to 4 ˚C, the Q_Y band is further red-shifted to 847 or 843 nm for type 1 or 2 polypeptides, respectively, consistent with the LH 1-type complex formation using native LH-α /-β polypeptides. Similar red-shifted Qy bands were observed for type 1 and type 2 polypeptides using [Zn]-BChl *a* (Table 1). These results indicate that type 1 polypeptide organizes [Zn]-BChl *a* and BChl *a* complex formation analogous to the LH1-type complex where the N-terminal segment of the native LH-β is not crucial in forming the LH1-type complex (Meadows et al., 1995; Meadows et al., 1998; Kehoe et al., 1998). Resonance Raman spectra indicated that the absorption of the $C3^1$ and $C13^1$ carbonyl groups of [Zn]-BChl *a* were shifted down-field by hydrogen-bonding due to the presence of type 1 or LH-β polypeptide in the OG micelles, respectively. These data show that the [Zn]-BChl *a* complex can be organized by these synthetic hydrophobic 1α-helix polypeptides, such as type 1, in OG micelles where two of the amino acid residues, W (+9) and W (+6) in the C-terminal segment of type 1, are essential to the formation of LH1-type complex as previously described (Kehoe et al., 1998; Kashiwada et al., 2000a; Fig. 2); further, it is clear that the [Zn]-BChl *a* complex is more stable than the BChl *a* complex. However, no clear red-shift of the Q_Y band of BChl *a,* due to the presence of type 3 polypeptide, is observed at 25 and 4 ˚C; rather, broad absorption bands are observed at about 777 and 850 nm (Table 1) which are analogous to those of the aggregated BChl *a* complex in OG micelles. In contrast, sharp absorption bands of the Q_Y band of [Zn]-BChl *a* are observed around 810 nm at 25 and 4˚C, analogous to subunit type complex formation (Table 1). Further, a large split CD signal of [Zn]-BChl *a* and of BChl *a* in the presence of type 2 or type 1 polypeptides is observed around the Q_Y band at 4˚C. This split signal is again seen in the LH 1-type complex using the LH-α /-β polypeptides (Table 1). These UV-vis absorption and CD spectral data indicate that the minimum amino acid sequence at the N-terminal segment of the LH polypeptides necessary for LH 1-type complex formation is that possessed by type 2 of our synthetic hydrophobic polypeptides (Kehoe et al., 1998; Meadows et al., 1998; Nango et al., 2002).

To see the effect of the amino acid sequence at the C-terminal segment of the LH polypeptides on the formation of the LH complex, we examined the molecular assembly of BChl *a* or [Zn]-BChl *a* with type 4 and 5 polypeptides and found that the Q_Y absorption band of BChl *a* in 0.78% OG micelles at 4 ˚C was red-shifted to 843 nm (Fig. 3) in the presence of type 4 polypeptide which is similar to that seen in the presence of type 1 or 2 polypeptides (Table 1). It is interesting that a similar red shift of the Q_Y band is *not* observed in the presence of type 5 polypeptide; instead, the Qy band was blue-shifted to 814 nm and dramatically sharpened, especially in comparison to that seen in the presence of type 4 polypeptide in 0.90% OG at 25 or 4 ˚C: the Qy band at 814 nm is similar to that observed when the subunit-type complex is disorganized by high OG concentrations.

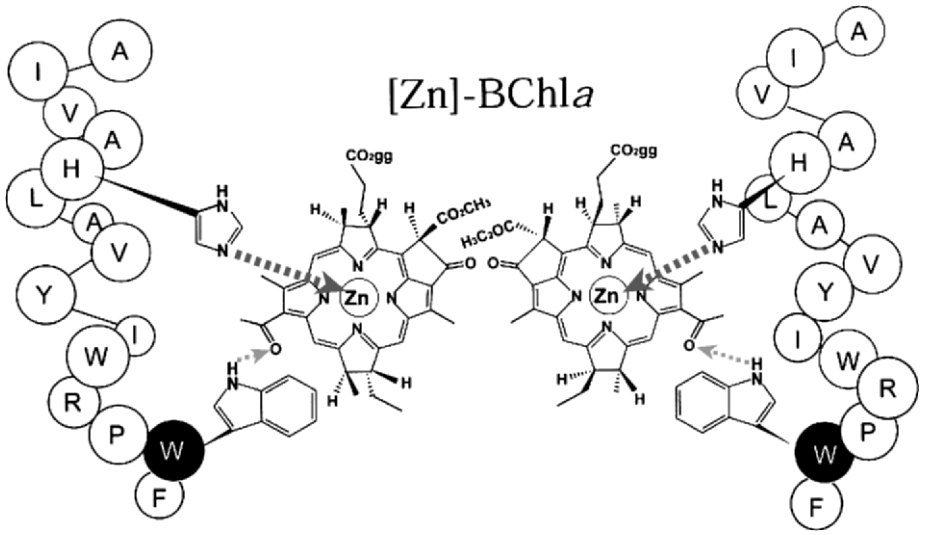

Fig. 2. Schematic model of a [Zn]-BChl *a* complex with synthetic 1α-helix polypeptides. Synthetic 1α-helix polypeptides (type 1) organize the [Zn]-BChl *a* complex analogous to the LH-type complex of photosynthetic bacteria. Tryptophan residues of the C-terminal hydrophilic segment of LH polypeptide play an important role on the molecular assembly of the [Zn]-BChl *a* complex.

This result reveals that the disulfide-linkage in the C-terminal segment obstructs formation of a LH 1-type complex. Interestingly, the CD signal-intensity of the type 5 polypeptide at 208 nm decreases due to the presence of BChl *a* in the OG micelle at 4 ˚C, while the intensity at 222 nm increases which implies that cooperative packing interactions between the α-helical polypeptides occur due to the presence of BChl *a* (Graddis et al., 1993; Arnold et al., 1997; Kashiwada et al., 2000d). Further, a large split-CD signal in the Q_Y band of BChl *a* in the presence of type 5 relative to those in the presence of type 4 polypeptide, also supports the idea of cooperative packing interactions between type 5 and BChl *a* (Table 1). These near-IR and CD data reveal that the disulfide-linkage at the C-terminal segment of type 5 polypeptide strongly influences the stabilization of the subunit-type complex formation and similar results were observed for [Zn]-BChl *a* complex formation with type 4 and type 5 polypeptides (Table 1).

To further examine the effect of the disulfide-linkage at the C-terminal segment of type 5 polypeptide on LH-type complex formation, the molecular assembly of BChl *a* or [Zn]-BChl *a* with type 4 or 5 polypeptides was carried out in lipid bilayers (Bustamante and Loach, 1994): 0.78% OG solution, containing type 5 or 4 polypeptides complexed with BChl *a* or [Zn]-BChl *a* was mixed with a solution of liposomal membranes containing egg yolk phosphatidylethanolamine, dipalmitoylphosphatidylglycerol, phosphatidylglycerol and cholesterol (2:1:1:4). The Q_Y band of BChl *a* or [Zn]-BChl *a* was red-shifted due to the presence of type 5 polypeptide in the lipid bilayers, analogous to the subunit-type complex in OG micelles. However, no shift of the Q_Y band of BChl *a,* which would indicate complex formation, was observed in the presence of type 4 polypeptide: the complex was destroyed during incorporation into the lipid bilayers while the [Zn]-BChl *a* complex was not destroyed. These data show that a stable BChl *a* complex due to the presence of type 5 polypeptide can be obtained in lipid bilayers as shown in Fig. 4; indeed, a stable [Zn]-BChl *a* complex was observed in the lipid bilayer in the presence of both type 4 and type 5 polypeptides.

III. Molecular Assembly of Bacteriochlorophyll *a* Complex and Its Analogues by Synthetic 4α-Helix Polypeptides

Again, molecular assembly of BChl *a* and its analogues with 4α-helix polypeptides, HAHA and HHHH (see Fig. 6), was examined in OG micelles (Kashiwada et al., 1999). We selected synthetic 4α-helix polypeptides, the 57-peptides, which have histidine residues on the hydrophobic core buried in the hydrophobic domain and also have hydrophilic domains to form 4α-helix bundle structure in aqueous solution. Synthetic 4α-helix polypeptides

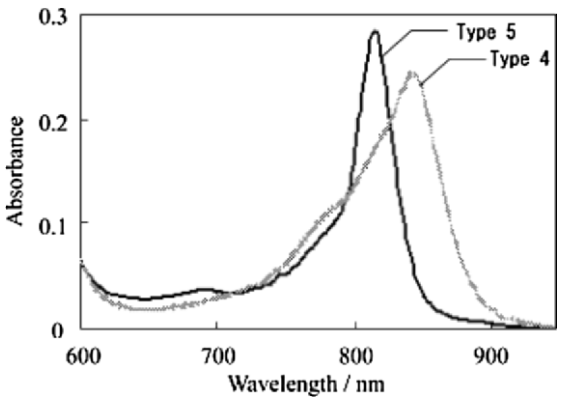

Fig. 3. Vis and near IR absorption spectra of BChl *a* in the presence of type 4 and type 5 polypeptides in 0.78 % n-octyl-β-D-glucopyranoside (OG) solution at 4 °C. Concentrations: [BChl *a*] = 2.4×10^{-6} M, [polypeptides] = 3.4×10^{-6} M.

were prepared and purified by Sephadex LH-60 gel chromatography and then by HPLC as previously described (Kashiwada et al., 2000*d*). The molecular assemblies of BChl *a* and its Zn analogue with synthetic 4α-helix polypeptides were performed as described above (Meadows et al., 1995).

Figure 5 shows near-IR absorption spectra of BChl *a* in the presence and absence of the 4α-helix polypeptide, HAHA, in 0.78% OG solution. The Q_Y absorption band of monomeric BChl *a* at 777 nm decreased while, in the presence of HAHA, the absorbance at 863 nm increased and became sharper, especially when cooling from 25 to 4 °C: this large-red shift and sharpening of the Q_Y absorption band is of interest because it is consistent with the shift of the Q_Y band in the LH complex of photosynthetic bacteria. Thus, this red shift of the Q_Y band to 863 nm in the presence of HAHA may be caused by exciton coupling interactions between BChl *a* molecules. Interestingly, this red shift was not clearly observed in the presence of HHHH (Table 2) possibly because the α-helicity of HHHH is too poor to form a tightly packed complex: the α-helix content in the BChl *a* complex with HAHA is 25%, but only 15%, with HHHH. A similar red shift of the Q_Y band was observed for [Zn]-BChl *a* in the presence of HAHA (Table 2) and the [Zn]-BChl *a* complex was more stable than the BChl *a* complex. No red-shift of the Q_Y band was observed for Chl *a* or BPhe *a* suggesting that coordination of the Mg and Zn atoms of the pigments with histidine and other polar amino acid residues of HAHA together with the presence of the $C3^1$ carbonyl group of the Chl derivatives play a crucial role in the red-shift of the Q_Y band.

A largely-split CD signal at the corresponding Q_Y band in the presence of HAHA supported strong exciton-coupling between BChl *a*'s (Table 2); however, magnetic circular dichroism data indicated that BChl *a* may partially aggregate in the presence of HAHA in OG micelles (data not shown). Further, near-IR FT Raman spectra of [Zn]-BChl *a* when excited at 1064 nm were recorded in the presence of HAHA polypeptides in 0.78% OG at 4 °C and the results indicated that bands due to the stretching modes of the $C13^1$ and $C3^1$ carbonyl groups in [Zn]-BChl *a* were shifted from 1700 to 1665 cm^{-1} and from 1687 to 1637 cm^{-1}, respectively, in the presence of HAHA. However, the band at 1603 cm^{-1} remained indicating that the 5-coordinated Zn complex was not shifted. These results implied that the stretching modes of $C13^1$ and $C3^1$ carbonyl groups in [Zn]-BChl *a* were shifted by hydrogen bonding between BChls and polar amino acid residues of HAHA. Thus, these near-IR

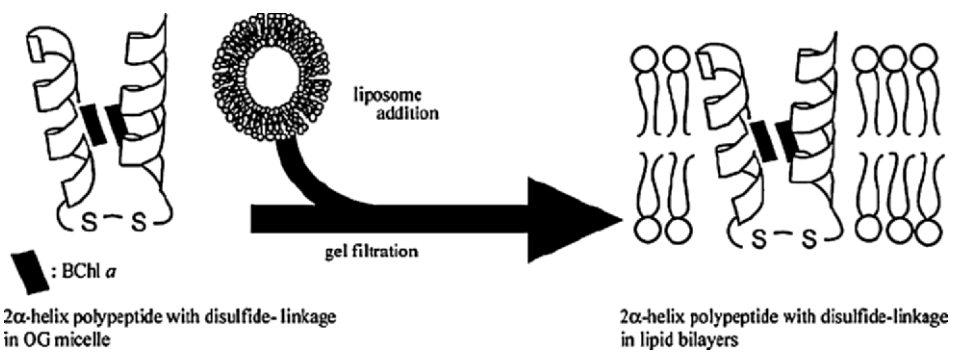

Fig. 4. Schematic diagram of incorporation of the BChl *a* complex using 2α-helix polypeptides with disulfide-linkage, type 5, into lipid bilayers.

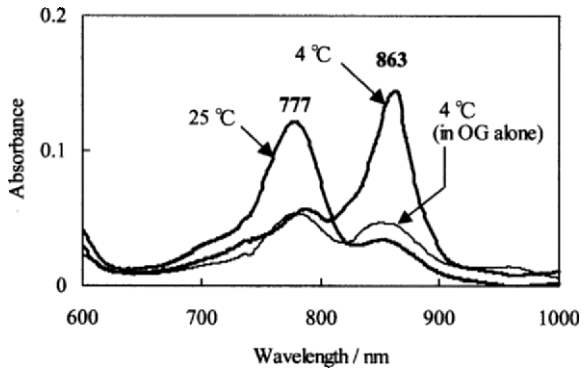

Fig. 5. Vis and near IR absorption spectra of BChl *a* in the absence and presence of the 4α-helix polypeptide HAHA. Concentrations: [BChl *a*] = 3.45×10^{-6} M, [HAHA] = 1.73×10^{-6} M.

CD, and near-IR-FT Raman spectra suggested that BChl *a* might coordinate with histidine residues as well as polar amino acid residues of HAHA.

To analyze the molecular size of the BChl *a*-HAHA complex in OG micelle, SAXS was employed (Wang et al., 1997). The data indicated that the diameter of the BChl *a*-HAHA complex in 0.78% OG at 4 °C was 9.1 nm, while that of the subunit complex, BChl *a*-LH polypeptide, in 0.78% OG at 25 °C was 5.5 nm. Thus, the diameter of the former complex is comparable to that of the subunit B820 complex, which may correspond to two BChl *a* and a pair of LH-α and -β polypeptides (Loach and Parkes-Loach, 1995).

These data show that the molecular assembly of BChl *a* or [Zn]-BChl *a* occurs at low temperature in the presence of synthetic 4α-helix polypeptides, especially HAHA.

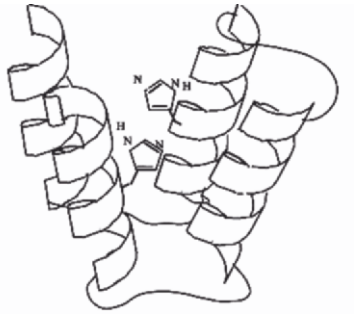

4α-helix polypeptide (HAHA)

	X	Y
DAPGELLKAXAELLK-		
DAPGELLKAYAELLK-	HAHA	His	Ala
DAPGELLKAXAELLK-		
DAPGELLKAYAELLK-Naf	HAHA	His	His

Fig. 6. Schematic model of the synthetic 4α -helix polypeptide HAHA and amino acid sequences of synthetic 4α-helix polypeptides HHHH and HAHA. Naf = 1-naphthyl alanine.

IV. Concluding Remarks

Synthetic LH model polypeptides such as 1α-helix hydrophobic polypeptides, types 1 and 2 (Fig. 1), and a water-soluble 4α-helix polypeptide, HAHA (Fig. 6), were used with BChl *a* and [Zn]-BChl *a* to attempt the construction of an artificial antenna complex. The [Zn]-BChl *a* complex was more stable than the BChl *a* complex. Interestingly, stable BChl *a* and [Zn]-BChl *a* complexes were obtained in the presence of a 2α-helix polypeptide with disulfide linkage (type 5; Fig. 1), in lipid bilayers in an analogous manner to the subunit complex, B820, of the LH 1 complex of photosynthetic bacteria. Complexes of BChl *a* and

Table 2. Near IR and CD spectral data of BChl *a* or [Zn]-BChl *a* in the presence of 4α helix polypeptide, HAHA

Bacteriochlorophyll derivatives[a]	Polypeptides[b]	UV-vis. The Qy absorption band/λ_{max}[nm]	CD spectra(4°C) λ[nm](θ [10^{-4} deg cm^2 dmol^{-1}])	
BChl *a*	HAHA	863	868(34)	835(–7.6)
BChl *a*	HHHH	850, 780	866(30)	831(–15)
BChl *a*	LH-α [c]+LH-β [c]	873	888(8.2)	855(–6.1)
BChl *a*	none	848, 777	868(29)	832(–13)
[Zn]-BChl *a*	HAHA	858	875(45)	841(–29)
[Zn]-BChl *a*	none	850, 774	872(28)	840(–9.2)

[a][BChl derivatives] = 3.45×10^{-6} M in 0.78% at OG solution (phosphate buffer pH 7.5) at 4°C. [b][polypeptides] = 3.45×10^{-6} M in 0.78% at OG solution (phosphate buffer pH 7.5) at 4 °C. [c]separately isolated from *Rba. sphaeroides*.

[Zn]-BChl *a* with types 1, 2 and HAHA polypeptides also provided an insight into the effect of polypeptide structure on LH complex formation while also constructing an artificial LH complex.

Acknowledgments

M.N. thanks Professors P. A. Loach and P. Parks-Loach, Northwestern University, U.S.A. for a kind gift of the photosynthetic bacterium, *Rba. sphaeroides* (*puc* 705-BA) and for helpful discussions on molecular assembly. M.N. also thanks Professor Toshiki Tanaka, Nagoya Institute of Technology and Professor Norikazu Nishino, Institute of Technology for synthesis of polypeptides. The present work was partially supported by a Grant-in-Aid from the Ministry of Education, Science and Culture, Japan and NEDO International Joint Grant, Japan.

References

Arnold PA, Shelton WR and Benson DR (1997) Peptide helix induction in a self-assembling hemoprotein model. J Am Chem Soc 119: 3181–3182

Benson DR, Hart BR, Zhu X and Doughty MB (1995) Design, synthesis, and circular dichroism investigation of a peptide-sandwiched mesoheme. J Am Chem Soc 117: 8502–8510

Bustamante PL and Loach PA (1994) Reconstitution of a functional photosynthetic receptor complex with isolated subunits of core light-harvesting complex and reaction centers. Biochemistry 33: 13329–13339

Chome CT, Lear JD, Nelson MK, Dutton PL, Robertoson DE and DeGrado WF (1994) Design of a heme-binding four-helix bundle. J Am Chem Soc 116: 856–865

Cogdell RJ and Lindsay JG (1998) Can photosynthesis provide a 'biological blueprint' for the design of novel solar cells. Biotech 16:521–527

Davis CM, Parkes-Loach PS, Cook CK, Meadows KA, Bandilla M, Scheer H and Loach PA (1996) Comparison of the structural requirements for bacteriochlorophyll binding in the core light-harvesting complexes of *Rhodospirillum rubrum* and *Rhodobacter sphaeroides* using reconstitution methodology with bacteriochlorophyll analogs. Biochemistry 35: 3072–3084

Graddis TJ, Myszka DG and Chaiken IM (1993) Controlled formation of model homo- and heterodimer coiled coil polypeptides. Biochemistry 32: 12664–12672

Hartwich G, Fiedor L, Simonin I, Cmiel E, Schafer W, Noy D, Fiedor L, Scheer H and Schera A (1998) Metal-substituted bacteriochlorophylls. 2. changes in redox potentials and electronic transition energies are dominated by intramolecular electrostatic interactions. J Am Chem Soc 120: 3684–3693

Iida K, Nango M, Yasue H, Okuda K, Okita M, Kashiwada A, Takada N, Maekawa M and Kurono Y (1998) The effect of denaturants on the stability of light-harvesting complex. Colloid Polym Sci 276: 152–159

Iida K, Ohya N, Kashiwada A, Mimuro M and Nango M (2000) Characterization of the light-harvesting polypeptide/bacteriochlorophyll *a* complex isolated from photosynthetic bacteria by the linear dichroism spectra. Bull Chem Soc Jpn 73: 221–229

Iida K, Kiriyama H, Fukai A, Konings WN and Nango M (2001) Two-dimensional self-organization of the light-harvesting polypeptides/BChl *a* complex into a thermostable liposomal membrane. Langmuir 17: 2821–2827

Ito H, Ishido S, Nomura M, Hayakawa T and Mitaku S (2000) Estimation of the hydrophobicity in microenvironments by pyrene fluorescence measurements: n-octyl-β-D-octylglucoside micelles. J Am Chem Soc 122: 212–215

Karrasch S, Bullough P and Ghosh R (1995) The 8.5 A projection map of the light-harvesting complex I from *Rhodospirillum rubrum* reveals a ring composed of 16 subunits. EMBO J 14: 631–638

Kashiwada A, Nishino N, Wang ZY, Nozawa T, Kobayashi M and Nango M (1999) Molecular assembly of bacteriochlorophyll *a* and its analogues by synthetic 4α -helix polypeptides. Chem Lett 1999: 1301-–1302

Kashiwada A, Watanabe H, Tanaka T and Nango M (2000a) Molecular assembly of zinc bacteriochlorophyll a by synthetic hydrophobic 1α-helix polypeptides. Chem Lett 2000: 24–25

Kashiwada A, Watanabe T, Mizuno T, Iida K, Miytake T, Tamiaki H, Kobayashi M and Nango M (2000b) Structural requirements of zinc porphyrin derivatives on the complex-forming with light-harvesting polypeptides. Chem Lett 2000: 158–159

Kashiwada A, Takeuchi Y, Watanabe H, Mizuno T, Yasue H, Kitagawa K, Iida K, Wang ZY, Nozawa T, Kawai H, Nagamura T, Kurono Y and Nango M (2000c) Molecular assembly of covalently-linked mesoporphyrin dimers with light-harvesting polypeptides. Tetrahedron Lett 41: 2115–2119

Kashiwada A, Hiroaki H, Kohda D, Nango M and Tanaka T (2000d) Design of heterotrimetric α -helical bundle by hydrophobic core engineering. J Am Chem Soc 122: 212–215

Kehoe JW, Meadows KA, Parkes-Loach PS and Loach PA (1998) Reconstitution of core light-harvesting complexes of photosynthetic bacteria using chemically synthesized polypeptides. 2. determination of structural features that stabilize complex formation and their implications for the structure of the subunit complex. Biochemistry 37: 3418–3428

Loach PA and Parkes-Loach PS (1995) Structure-function relationships in core light-harvesting complexes (LH1) as determined by characterization of the structural subunit and by reconstitution experiments. In: Blankenship RE, Madigan MT, and Bauer CE (eds) Anoxygenic Photosynthetic Bacteria, pp 438–458. Kluwer Academic Publishers, Dordrecht

Mcdermott G, Prince SM, Freer AA, Hawthornthwaite-Lawless AM, Papiz MZ, Cogdell RJ and Issacs NW (1995) Crystal structure of an integral membrane light-harvesting complex from photosynthetic bacteria. Nature 374: 517–521

Meadows KA, Iida K, Tsuda K, Recchia PA, Heller BA, Antonio B, Nango M and Loach PA (1995) Enzymic and chemical cleavage of the core light-harvesting polypeptides of photosynthetic bacteria: Determination of the minimal polypeptide size and structure required for subunit and light-harvesting complex formation. Biochemistry 34: 1559–1574

Meadows KA, Parkes-Loach PS, Kehoe JW and Loach PA (1998) Reconstitution of core light-harvesting complexes of photosynthetic bacteria using chemically synthesized polypeptides.

1. Minimal requirements for subunit formation. Biochemistry 37: 3411–3417

Mimuro M, Kobayashi M, Shimada K, Uezono K and Nozawa T (2000) Magnetic circular dichroism properties of reaction center complexes isolated from the zinc-bacteriochlorophyll *a*-containing purple bacterium *Acidiphilium rubrum*. Biochemistry 39: 4020–4027

Nango M, Kashiwada A, Yamada S, It S, Sawa N, Iida K (2001) Construction of artificial light-harvesting complex using light-harvesting polypeptide or its model synthetic polypeptides with zinc substituted bacteriochlorophyll *a*. In: PS 2001: Proceedings of the 12th International Conference on Photosynthesis, S1-021. CSIRO, Melbourne (CD-ROM)

Nango M, Kashiwada A, Watanabe H, Yamada S, Yamada T, Ogawa M, Tanaka T and Iida K (2002) Molecular assembly of bacteriochlorophyll a using light-harvesting model 1α -helix polypeptides and 2α-helix polypeptides with disulfide-linkage. Chem Lett 2002: 312–313

Ogawa M, Kanda R, Dewa T, Iida K, Nango M (2002) Molecular assembly of light-harvesting antenna complex on ITO electrode. Chem Lett 2002: 466–467

Olsen JD, Sockalingum GD, Robert B, and Hunter CN (1994) Modification of a hydrogen bond to a bacteriochlorophyll *a* molecule in the light-harvesting 1 antenna of *Rhodobacter sphaeroides*. Proc Natl Acad Sci USA 91: 7124–7128

Pasternack RF, Giannetto A, Pagano P and Gibbs EJ (1991) Self-assembly of porphyrins on nucleic acids and polypeptides. J Am Chem Soc 113: 7799–7800

Pullerits T and Sundstrome V (1996) Photosynthetic light-harvesting pigment-protein complexes: Toward understanding how and why. Acc Chem Res 29: 381–389

Rabanal F, DeGrado WF and Dutton PL (1996) Toward the synthesis of a photosynthetic reaction center maquette: A cofacial porphyrin pair assembled between two subunits of a synthetic four-helix bundle multiheme protein. J Am Chem Soc 118: 473–474

Stuart J, Wang P, Qian P, Kirkland Y, Conroy MJ, Hunter CN and Bullough PA (2002) Projection structure of the photosynthetic reaction centre-antenna complex of *Rhodospirillum rubrum* at 8.5 Å resolution. EMBO J. 21: 3927–3935

Sturgis JM, Olsen JO, Robert B and Hunter CN (1997) Functions of conserved tryptophan residues of the core light-harvesting complex of *Rhodobacter sphaeroides.* Biochemistry 36: 2772–2778

Wakao N, Yokoi N, Isoyama N, Hiraishi A, Shimada K, Kobayashi M, Kise H, Iwaki M, Itoh S, Takaichi S and Sakurai Y (1996) Discovery of natural photosynthesis using Zn-containing bacteriochlorophyll in an aerobic bacterium *Acidiphilium rubrum*. Plant Cell Physiol 37: 889–893

Wang ZY, Umetsu M, Yoza K, Kobayashi M, Imai M, Matsushita Y, Niimura N and Nozawa T (1997) A small-angle neutron scattering study on the small aggregates of bacteriochlorophylls in solutions. Biochim Biophys Acta 1320:73–82

Chapter 26

Reconstitution and Pigment Exchange

Harald Paulsen*
Institut für Allgemeine Botanik, Universität Mainz, Müllerweg 6, D-55099 Mainz, Germany

Summary

Reconstitution and pigment exchange are two experimental techniques that have proven extremely useful to elucidate structure-function relationships in chlorophyll (Chl)-protein complexes. In reconstitution experiments the Chl-binding apoproteins, usually in their recombinant form, are folded in the presence of pigments to form pigment-protein complexes that are often virtually indistinguishable from their native counterparts. Since both the protein and the pigment building blocks in such an assembly kit can easily be modified, this approach serves to elucidate the functional significance of the structural elements modified. Pigment exchange can be viewed as a partial reconstitution: rather than completely taking a Chl-protein complex apart and then reconstituting it, only a limited number of pigments is dissociated and then restored. This, too, allows alteration of the pigments bound to specific positions and, thus, to learn more about the functional contribution of these particular pigment binding sites. Reconstitution and pigment exchange are complementary techniques in that some complexes are accessible to pigment exchange that cannot (yet) be reconstituted in vitro.

This chapter lists a selection of recent examples where the reconstitution in vitro of light-harvesting complexes from purple bacteria and light-harvesting Chl-*a/b* complexes from higher plants has been instrumental in assessing their function and where the reconstitution of other Chl-protein complexes has opened up new possibilities for their analysis. Very different kinds of light-harvesting complexes all exhibit an astonishing capability of self-organization during in vitro reconstitution. It is proposed that, if this also reflects any significant in vivo feature, then this ability to self-organize may help to regulate the light-harvesting capacity by rapid dis- and re-assembly of the light-harvesting complexes.

An exciting new possibility, opened up by the pigment-exchange approach, is to place the Ni derivative of (B)Chl in well-defined binding sites. This pigment dissipates excitation energy extremely rapidly and, therefore, will help to elucidate pathways of excitation energy migration in photosynthetic complexes.

*Email: paulsen@mail.uni-mainz.de

Bernhard Grimm, Robert J. Porra, Wolfhart Rüdiger and Hugo Scheer (eds): Chlorophylls and Bacteriochlorophylls: Biochemistry, Biophysics, Functions and Applications, pp. 375–385.

I. Introduction

A number of chlorophyll- (Chl-) protein complexes can be reconstituted in vitro from their apoprotein and pigment components. The term reconstitution potentially leads to confusion because it often describes the integration of proteins into native or synthetic liposomes. In the context of this chapter it denotes the formation of Chl-protein complexes that are similar to or virtually identical with their native counterparts in the same environment. These complexes are not necessarily reconstituted in lipid vesicles during this process and several Chl-protein complexes can be reconstituted, i.e. formed, in the complete absence of lipids. Typically, the components to be reconstituted are mixed in detergent solution and brought under conditions promoting self-assembly, resulting in the formation of pigment-protein complexes. The Chl-protein complexes amenable to this technique include all Chl *a/b* complexes of higher plants and some of their relatives as well as the inner and outer light-harvesting complexes, LH1 and LH2, respectively, of purple bacteria. The advantage of assembling these complexes in vitro is the possibility of introducing modifications into the components. Thus, recombinant apoproteins or, in the case of the shorter LH1 and LH2 proteins, even synthetic peptides have been employed. Studies of the minor Chl *a/b* complexes CP29, CP26, and CP24 (Jansson et al., 1992) that are difficult to isolate in substantial amounts, have been greatly facilitated by their reconstitution with apoprotein overexpressed by bacteria whereby large amounts of the protein became easily accessible. More importantly, the use of recombinant or synthetic apoprotein makes it easy to introduce alterations into the amino acid sequence to perform mutational analyses of protein function. Likewise, in Chl complexes assembled outside the organism, or with its biosynthetic capacity altered, the pigment composition of the complex can easily be varied to yield information about the specificity of pigment binding by these apoproteins.

Pigment exchange can be viewed as a partial reconstitution of Chl-protein complexes. The complexes are not completely dissociated into pigments and proteins; instead one or more pigments are removed and then re-assembled. Pigment exchange has been established in several pigment-protein complexes that cannot be reconstituted in vitro such as the RCs in some purple bacteria, or allows for site-selective replacements. The pigment binding sites that are susceptible to pigment exchange reactions can be analyzed to determine the structural requirements and functional properties of the pigments bound.

In this chapter, the reconstitution and pigment-exchange studies reviewed will be grouped by the Chl proteins studied. No experimental procedures will be presented. For these, the reader is referred to the original literature cited or, in the case of Chl-*a/b* complexes, to a review focusing on various reconstitution techniques for these complexes (Paulsen and Schmid, 2001).

II. Reconstitution

The Chl-protein complexes whose reconstitution has been described so far are listed in Table 1. In the following, a few selected examples are given of the kinds of questions that have been addressed and answered by reconstituting these complexes.

A. Light-harvesting Complexes of Purple Bacteria

Based on the dissociation experiments of R. Ghosh and, in particular of P. A. Loach, the latter group devised a simple procedure to reconstitute the core light-harvesting complex LH1 of purple bacteria: The α and β subunits plus BChl are mixed in detergent and then assembled by diluting the detergent below the critical micellar concentration (Parkes-Loach et al., 1988). Not only does this establish pigment binding to the protein but also the oligomeric complex absorbing at 873 nm is formed. Reconstitution studies of LH1 allowed a detailed analysis of protein segments involved in assembly (Meadows et al., 1995, 1998; Davis et al., 1997; Kehoe et al., 1998) as well as a description of the structural features in BChl that are essential for binding (Parkes-Loach et al., 1990; Davis et al., 1996).

The core light-harvesting complex LH1 from several strains of purple bacteria has been successfully reconstituted, whereas among the peripheral

Abbreviations: CP24, CP26, CP29 – minor subunits of LHCII with apoproteins Lhcb6, Lhcb5, and Lhcb4, respectively; LH1, LH2 – Core and peripheral light-harvesting complexes of purple bacteria, respectively; LHCI, LHCII – light-harvesting Chl *a/b* complex of PS I and PS II, respectively; LHCI-730, -680 – subunits of LHCI with apoproteins Lhca1,4 and Lhca2,3, respectively; LHCIIb – major subunit of LHCII with apoproteins Lhcb1-3; PS I, PS II – photosystems I and II, respectively

Table 1. Reconstituted Chl-protein complexes

Complex	Reconstituted protein[a]	References[b]
LH1	n.p. from purple bacteria	(Parkes-Loach et al., 1988, 2001)
	r.p. from purple bacteria	(Davis et al., 1997)
	s.p. from purple bacteria	(Kehoe et al., 1998)
LH2	n.p. and r.p. from purple bacteria	(Todd et al., 1998)
LHCI-730	r.p. from tomato	(Schmid et al., 1997; Rupprecht et al., 2000)
LHCI-680	r.p. from tomato	(V. H. R. Schmid, personal communication)
LHCIIb	n.p. from pea	(Plumley and Schmidt, 1987)
	r.p. from pea	(Paulsen et al., 1990; Reinsberg et al., 2001; Rogl et al., 2002)
	r.p. from maize	(Remelli et al., 1999)
CP29	r.p. from maize	(Giuffra et al., 1996; Pascal et al., 2001)
CP26	r.p. from maize	(Ros et al., 1998; Frank et al., 2001)
CP24	r.p. from maize	(Pagano et al., 1998)
Chl-*a/b* LHC	n.p. from *Chlorella fusca*	(Meyer and Wilhelm, 1993)
Chl-*a/b/c* LHC	n.p. from *Mantoniella squamata*	(Meyer and Wilhelm, 1993)
LhaR1	r.p. from red algae	(Grabowski et al., 2000)

[a] n.p., native protein; r.p., recombinant protein; s.p., synthetic polypeptide; [b] The list of references is far from being complete and meant to provide a starting point for surveys of the literature.

complexes LH2, only that of *Rhodospirillum molischianum* has been assembled in vitro (Todd et al., 1998). When mutations are introduced into the LH2 β subunit of *Rhodobacter sphaeroides*, including the exchange of 4 C-terminal amino acids with those of the LH1 β subunit, this protein also forms monomeric pigment-protein complexes but, even in the presence of LH1 or LH2 α subunits, forms no LH1- or LH2-type oligomeric complexes (Todd et al., 1999). Consistently, the 4 C-terminal amino acids in the β subunit of *Rs. molischianum* LH2 are identical with those of the β subunit in *Rb. sphaeroides* LH1, confirming the significance of these C-terminal amino acids for the proteins' ability to bind pigments under reconstitution conditions. It is unclear why LH1 appears to reconstitute more readily than LH2 although the overall structure is thought to be similar, except for the different number of subunits in the circular arrangements. Either this is a technical problem and the optimum conditions for LH2 reconstitution have not yet been identified. Or this different behavior is based on structural differences. In an NMR structural analysis of an LH1 β subunit it was recently discovered that the trans-membrane domain of this protein contains two α-helical segments forming a kink (Conroy et al., 2000) whereas LH2 β subunits contain one consecutive trans-membrane α helix (McDermott et al., 1995; Koepke et al., 1996). Possibly the bent structure in LH1 adds some flexibility to the structure that is advantageous for assembly in vitro.

B. Chlorophyll a/b Proteins

In 1987 the group of G. W. Schmidt found that the major light-harvesting Chl *a/b* protein, LHCIIb, reconstitutes with pigments when the denatured apoprotein is mixed with pigments in sodium dodecylsulfate solution and refolded by freeze-thaw cycles (Plumley and Schmidt, 1987). This was then extended to the recombinant LHCIIb apoprotein (Cammarata et al., 1990; Paulsen et al., 1990) and later it eventuates that all known Chl *a/b* proteins of higher plants can be reconstituted following this or a similar procedure (see Table 1).

Deletion mutations in LHCI (Rupprecht et al., 2000) and LHCIIb (Cammarata and Schmidt, 1992; Paulsen and Hobe, 1992) defined the minimum protein requirements for complex formation. A major question addressed by reconstitution studies has been the assignments of Chl *a* and *b* to binding sites in LHCIIb and other Chl *a/b* complexes. The resolution of the electron-crystallographic structure analysis of LHCIIb was not sufficient to distinguish between these two pigments; however, a tentative assignment was made (Fig. 1) on the basis of theoretical considerations (Kühlbrandt et al., 1994). These assignments have been tested by mutating single Chl-binding amino acids and testing, biochemically or spectroscopically, whether Chl *a* or Chl *b* had disappeared from the complex. In these studies, most of the original assignments have been confirmed whereas for some binding sites contradic-

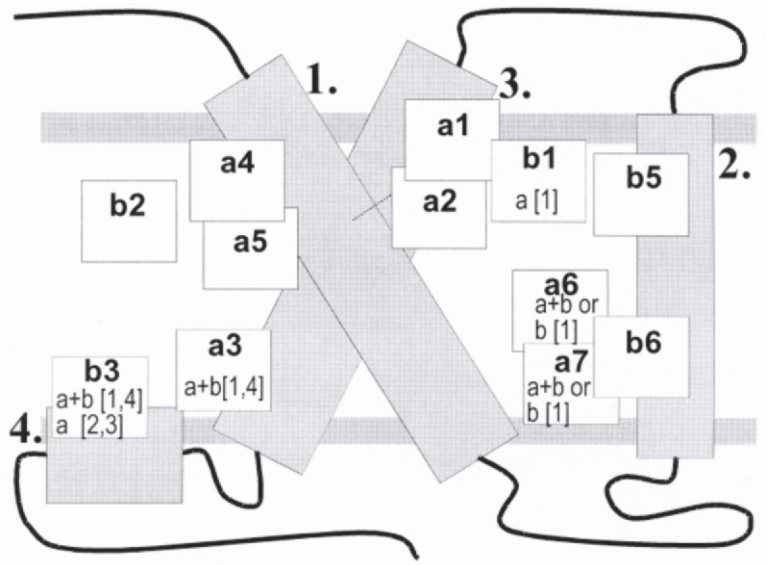

Fig. 1. Sketch of LHCIIb structure as derived from Kühlbrandt et al. (1994). The hatched boxes indicate the trans-membrane α helices numbered as counting from the N terminus, the horizontal gray bars indicate the stromal (upper) and lumenal (lower) surface of the thylakoid membrane. The squares denote Chl molecules with the assignments given by Kühlbrandt et al. (1994) in bold text. Given in plain text are the alternative assignments made on the basis of mutational analyses of reconstituted LHCIIb. [1], (Remelli et al., 1999); [2], (Rogl and Kühlbrandt, 1999); [3], (Yang et al., 1999); [4], (Rogl et al., 2002).

tory data have been obtained (Fig. 1). One surprising observation was that some binding sites in LHCIIb appear to bind Chl *a* or Chl *b* rather non-specifically. Mutational analyses of recombinant CP29 led to the same conclusion (Giuffra et al., 1997; Bassi et al., 1999; Simonetto et al., 1999). This raises the question whether in vivo some binding sites also hold a mixed population of Chl *a* and Chl *b* or whether some selection mechanism ensures a higher specificity of these binding sites towards the two Chl species than is seen in vitro. Single-molecule studies may help to solve this question. Spectroscopic studies on individual (B)Chl-protein complexes have already been performed with LH2 (Bopp et al., 1999; Tietz et al., 1999; van Oijen et al., 1999; Köhler et al., 2001, see also Chapter 21, Köhler and Aartsma), LHCIIb (Tietz et al., 2001), and PS I (Jelezko et al., 2000).

Spectroscopy of reconstituted Chl-*a/b* complexes with a modulated Chl *a/b* population, or with individual binding sites staying empty, permitted the deduction of the spectroscopic properties of individual Chl molecules in CP29 (Giuffra et al., 1997; Bassi et al., 1999; Simonetto et al., 1999; Cinque et al., 2000; Pascal et al., 2001) and LHCIIb (Remelli et al., 1999; Rogl and Kühlbrandt, 1999; Cinque et al., 2000; Rogl et al., 2002; Zucchelli et al., 2002). The same extends to the carotenoid binding sites in Chl *a/b* complexes (Croce et al., 1999a,b, 2001; Hobe et al., 2000; Caffarri et al., 2001; Formaggio et al., 2001). Such studies led Croce et al. (1999a) to calculate even the orientation of neoxanthin, the carotenoid presumably invisible in the electron-crystallographic structure analysis of LHCIIb (Kühlbrandt et al., 1994), with regard to the rest of the complex. It will be interesting to see whether this prediction will be verified by a more refined structure determination.

Time-resolved measurements of LHCIIb reconstitution (Booth and Paulsen, 1996) revealed some molecular details of the assembly process. The concentrations of all components, protein, Chl and carotenoids, are rate-limiting, indicating that at least some of each molecule species is bound into the complex during the rate-limiting step(s) (Reinsberg et al., 2000, 2001). Moreover, the formation of the protein α helix in the reconstitution process occurs during the same kinetic step(s) as does the assembly of pigments; so, protein folding and pigment binding are apparently closely coupled processes (Horn and Paulsen, 2002).

Reconstituted LHCIIb forms trimers in the presence of phosphatidyl glycerol (Hobe et al., 1994). Mutational analyses revealed a 'trimerization motif'

near the N-terminus of the protein (Hobe et al., 1995), and a C-proximal tryptophan residue (Kuttkat et al., 1996) which when deleted or involved in a non-conservative amino acid exchange abolishes trimer formation. Similarly, mutant versions of recombinant LHCI-730 apoproteins were used to identify the protein segments essential for formation of heterodimeric LHCI-730 (Schmid et al., 2002)

C. Other Light-harvesting Proteins

Some light-harvesting proteins from marine algae, showing sequence homology to the Chl *a/b* proteins of higher plants and green algae, have also been reconstituted in vitro. These are the Chl *a/b/c* protein of the unicellular prasinophyte *Mantoniella squamata* (Meyer and Wilhelm, 1993; Meyer et al., 1996) and the LHCI protein, LhcaRI, from the red alga *Porphyridium cruentum* (Grabowski et al., 2000). Interestingly, both of these recombinant algal proteins exhibit astonishing flexibility in their pigment binding. The Chl *a/b/c* protein, from *M. squamat* can be reconstituted with pigment extracts from the green alga *Chlorella vulgaris* (Meyer and Wilhelm, 1993; Meyer et al., 1996), and the Chl *a*-zeaxanthin protein from *P. cruentum* forms complexes with pigments extracted from a higher plant (Chl *a/b*, lutein, neoxanthin, violaxanthin, β-carotene), a diatom (Chl *a/c*, fucoxanthin, diadinoxanthin) and a dinoflagellate (Chl *a/c*, peridinin) (Grabowski et al., 2001). This finding confirms the relationship between Chl *a/b*-like proteins and suggest that the flexibility of apoproteins in binding various Chls and carotenoids has helped in the evolution of different types of light-harvesting units in various branches of plant evolution.

Surprisingly, another member of the extended Chl *a/b* protein family, the PS II protein PsbS, has resisted attempts to reconstitute it with pigments in vitro (Dominici et al., 2002). Sequence analysis of this protein suggests 4 trans-membrane domains of which the first and third show extensive similarity with Chl *a/b* light-harvesting proteins (Kim et al., 1992; Wedel et al., 1992). PsbS has been isolated in a pigmented form (Funk et al., 1995b) but, in contrast to Chl *a/b* proteins, is also stable without bound pigments (Funk et al., 1995a). Of course, a negative result in reconstitution experiments does not prove that PsbS in fact is unable to bind pigments in vitro; possibly the correct conditions for this protein simply have not yet been found. Thus, it remains to be seen whether or not PsbS can be reconstituted with pigments.

A recombinant water-soluble light-harvesting peridinin-Chl protein (PCP) from a diatom can be reconstituted with pigments in vitro (R. G. Hiller, personal communication). PCP bears no resemblance with Chl-*a/b* proteins since it contains a 30-kDa protein wrapped around eight peridinin and two Chl *a* molecules (Hofmann et al., 1996).

D. Water-soluble Chlorophyll Protein

A recombinant fusion of a water-soluble Chl protein (WSCP) from cauliflower with maltose-binding protein was reconstituted by simply adding it to a thylakoid suspension; the protein apparently extracts Chl molecules from the membrane and binds them tightly (Nishio and Satoh, 1997). A number of water soluble Chl proteins have been isolated from higher plants: WSCP from *Chenopodium album* (Yakushiji et al., 1963) changes its absorption spectrum upon illumination whereas WSCPs from *Brassicaceae* such as cauliflower (Murata et al., 1971), cress (Murata and Ishikawa, 1981) and Japanese radish (Shinashi et al., 2000) do not. The physiological function of WSCPs is unknown: those from *Brassicaceae* share extensive sequence homology with a drought-induced protein, Bnd22, from rapeseed and, therefore, are thought to be involved in scavenging Chls during (stress-induced) senescence. Nothing is known yet about how the Chls are bound. WSCP fused to maltose-binding protein appeared to oligomerize upon Chl binding (Nishio and Satoh, 1997). It is to be expected that a closer examination of this reconstitution in vitro will yield information about Chl organization and possible functions of this Chl-protein complex.

III. Pigment Exchange

A. LH1 and LH2

Instead of fully reconstituting *Rs. rubrum* LH1 from its apoprotein and pigments (see above), the complex can also be partially dissociated by detergents at an elevated temperature and then be re-associated, by detergent removal, to contain various amounts of exogenously added pigment derivatives such as the Zn analogue of BChl *a*. This approach allowed the titration of different BChl *a* derivatives competing for their binding into the B873 sites. An interesting observation in these experiments was that there are at least two biochemically distinguishable B873 binding sites in LH1, possibly due to their localization either

Table 2. Chl exchange in Chl-protein complexes

Complex	Pigment(s) exchanged	References[a]
LH1	B873 → [Zn]-BChl *a* etc.	(Lapouge et al., 2000)
	B873 → [Ni]-BChl *a*	(Fiedor et al., 2000; Fiedor et al., 2001)[b]
LH2	B800 → [3^1-OH]-BChl etc.	(Bandilla et al., 1998)
	B800 → BChl *a*	(Fraser et al., 1999)
	B800 → [3-acetyl]-Chl *a*	(Herek et al., 2000)
RC[c]	B_A, B_B → [3-vinyl] BChl *a*	(Hartwich et al., 1995)
	B_A, B_B → [13^2-OH]-BChl *a*	(Storch et al., 1996)
	H_A, H_B → Phe *a*	(Meyer and Scheer, 1995; Franken et al., 1997)
PS II RC	Chl *a* → [3-acetyl]-Chl *a*	(Scheer und Hartwich, 1995; Gall et al., 1998)

[a] Not a complete list of references; [b] This work actually describes complex reconstitution but is listed here because its main point is partial pigment exchange; [c] RC of purple bacteria

on the α or the β subunits (Lapouge et al., 2000).

A similar approach can be extended to LH2 and RCs from purple bacteria and to PS II from higher plants (Table 2).

LH2 of *Rhodopseudomonas acidophila* was completely stripped of its B800 pigments by low pH/detergent treatment; subsequently, up to 80% of B800 binding sites could be re-filled with BChl *a* or derivatives such as [13^2-OH]-, [3-vinyl] BChl *a* or [3-acetyl-Chl] *a*. The energy transfer of these pigments to B850 was significantly higher than predicted by the Förster theory, indicating that B800 and B850 interact more closely than merely by resonance of their transition dipoles (Herek et al., 2000)

B. Reaction Centers

Pigment exchange experiments with bacterial reaction centers have been reviewed by Scheer and Hartwich (1995). The BChl *a* molecules in the monomer binding sites(B_A, B_B) of both the A and B branches in *Rb. sphaeroides* RCs were selectively exchanged with a BChl derivative, e.g. with [3-vinyl]-BChl. The experimental procedure took advantage of the fact that the carotenoid spheroiden(on)e present in these complexes selectively protects the B_B site. Thus, B_A was selectively exchanged in these complexes. In RCs from a carotenoid-deficient mutant, both monomeric BChl molecules were exchanged at the same time. If subsequently the carotenoids were reconstituted into the complex, the [3-vinyl]-BChl in the B_A site could then be re-exchanged with non-modified BChl, yielding a RC specifically modified in the B_B binding site. This allowed the individual analysis B_A and B_B with regard to their spectroscopic properties and BChl-carotenoid interaction. (Hartwich et al., 1995). The binding of BChls into B_A and B_B is selective for the configuration of $C13^2$ in the isocyclic ring. If BChls are hydroxylated at $C13^2$, which blocks epimerization and fixes BChls in either the natural or the unnatural configuration, only the natural epimer binds into B_A and B_B (Storch et al., 1996).

The pigment exchange reaction established for RCs of purple bacteria can be extended to PS II RCs of higher plants. Several Chl molecules can be exchanged with derivatives such as the Zn-containing analogue or the [3-acetyl] derivative (Gall et al., 1998). First steps towards assigning the sites of pigment exchange have been taken (Zehetner et al., 2002). Also the Phe molecules in PS II RC have been successfully exchanged (Germano et al., 2000).

C. [Ni]-BChl a, a 'Black-hole Pigment'

A particularly interesting (B)Chl *a* derivative to be exchanged or reconstituted into pigment-protein complexes is the Ni analogue as it dissipates excitation energy very efficiently and thus acts as an excitation trap. [Ni]-BChl *a* has a much shorter excited state lifetime than BChl *a*, due to extremely rapid internal conversion from the electronically excited to the ground state (Musewald et al., 1999; Noy et al., 2000). When [Ni]-BChl *a* is introduced into LH1 from *Rb. sphaeroides*, it dissipates BChl excitation energy within 60 fs, even when only one Ni-derivative is bound per LH1 holocomplex. This is much faster than the time required for Förster resonance energy transfer between pigments. Therefore, all the pigments in the LH1 ring must be excitonically coupled to each other (and the Ni-derivative). This excludes alternative models of LH1 being composed of excitonically isolated clusters of BChl *a* that exchange energy only by the Förster transfer mechanism (Fiedor et al., 2000, 2001). Such an ap-

proach, in combination with the reconstitution or pigment exchange technique, clearly offers a great advantage in elucidating excitation energy pathways in photosynthetic complexes by placing excitation energy traps in defined positions.

IV. Concluding Remarks

The number of self-organizing membrane proteins that can be refolded in vitro is still rather small. It is actually quite astonishing that light-harvesting Chl-binding proteins of both plants and bacteria belong into this group. All of these proteins are capable of binding quite a number of different pigments more or less specifically. The contribution of these pigments to the total mass of the complexes is significant (roughly one third in LHCIIb and somewhat less in LH1 and LH2). In terms of pigment-protein ratios, the chlorosome of green sulfur bacteria goes to the extreme: the arrays of BChl *c* in these complexes can self-organize in the absence of any protein (Chapter 20, DeBoer and DeGroot). This raises the possibility that also in the other pigment-protein complexes, the self-organizing capacity is partly, or even mostly, due to pigment-pigment interactions. However, the observation that very limited alterations in the LHCIIb protein structure, such as single amino-acid exchanges in a loop domain, can totally destroy the stability of the complex (Heinemann and Paulsen, 1999) proves that proteins, even protein domains not directly involved in pigment binding, make important contributions to the cooperative stabilization of Chl-protein complexes. Moreover, the experimental procedure of re-folding Chl *a/b* proteins is very similar to the procedure used for re-folding bacterioopsin (London and Khorana, 1982; Booth, 2000) This membrane protein binds one chromophore, retinal, to form bacteriorhodopsin but virtually completely folds in vitro even in the absence of retinal (Riley et al., 1997). Although Chl *a/b* proteins, by contrast, need pigment binding as a trigger for re-folding (see below), the example of bacteriorhodopsin demonstrates that a membrane protein can principally re-fold in vitro without the help of any pigments or other co-factors.

No successful reconstitution of any Chl-binding RC protein nor of the Chl-*a* binding inner antennae CP43 and CP47 has yet been reported. Why is it that among the pigment-protein complexes of the photosynthetic apparatus only the more peripheral ones, involved in light harvesting (Chl *a/b* complexes and their relatives, LH1 and LH2, and PCP), seem to be able to spontaneously organize? Although the possibility to reconstitute these complexes is relevant only in vitro, it is tempting to speculate that it reflects a property that plays some role also in vivo; possibly during the biogenesis and degradation of the various photosynthetic units. Light harvesting is a process regulated, depending on light intensity, in all photosynthesizing organisms. A minimum light-harvesting capacity is necessary to render photosynthesis efficient enough to meet and compete for the energy needs of the organism, whereas over-energizing of the photosynthetic apparatus must be avoided as it is potentially very harmful. Possibly the self-organizing power of light-harvesting units helps to accelerate the assembly and disassembly of light-harvesting units in vivo, thus facilitating the regulation of the light-harvesting capacity.

A somewhat different prerequisite applies to Chl complexes for individual pigments to be exchanged. These complexes must stay sufficiently stable with the corresponding Chl binding sites at least transiently empty. In fact, for LH2 from purple bacteria it has been shown that the B800 binding sites can be completely stripped and then re-filled (Fraser et al., 1999). An NMR study of LH1 from *Rb. sphaeroides* showed that this protein folds into its apparently native structure even in the absence of pigments or lipids (Kikuchi et al., 1999). By contrast, the apoprotein of LHCIIb needs pigment binding to refold in vitro (Reinsberg et al., 2000, 2001; Horn and Paulsen, 2002). On the other hand, mutation analyses of Chl binding sites in LHCIIb and CP29 show that stable complexes can be formed lacking one or few Chl molecule(s). Therefore, it seems likely that the pigment exchange technique should also be amenable for the Chl molecules in Chl *a/b* complexes.

Note Added in Proof

This chapter has been written in mid-2002 and reflects the knowledge available at that point. It is not possible here to give a full update—my apologies to all colleagues whose new and important contributions have not been included.

It should be noted, however, that Fig. 1 is thoroughly outdated. Two X-ray crystallographic structures have been published of LHCIIb from spinach (Liu et al., 2004) and pea (Standfuss et al., 2005) at 2.72 Å and 2.5 Å resolution, respectively. Both groups find eight

Chl-*a* and six Chl-*b* molecules in LHCIIb, residing in non-mixed binding sites. Thus, the binding sites accommodating both Chl *a* and Chl *b* (described in Section II.B of this review) appear to be a reconstitution artifact.

References

Bandilla M, Ücker B, Ram M, Simonin I, Gelhaye E, McDermott G, Cogdell RJ and Scheer H (1998) Reconstitution of the B800 bacteriochlorophylls in the peripheral light harvesting complex B800-850 of *Rhodobacter sphaeroides* 2.4.1 with BChl *a* and modified (bacterio-)chlorophylls. Biochim Biophys Acta 1364: 390–402

Bassi R, Croce R, Cugini D and Sandonà D (1999) Mutational analysis of a higher plant antenna protein provides identification of chromophores bound into multiple sites. Proc Natl Acad Sci USA 96: 10056–10061

Booth PJ (2000) Unravelling the folding of bacteriorhodopsin. Biochim Biophys Acta 1460: 4–14

Booth PJ and Paulsen H (1996) Assembly of light-harvesting *a/b* complex in vitro. Time-resolved fluorescence measurements. Biochemistry 35: 5103–5108

Bopp MA, Sytnik A, Howard TD, Cogdell RJ and Hochstrasser RM (1999) The dynamics of structural deformations of immobilized single light-harvesting complexes. Proc Natl Acad Sci USA 96: 11271–11276

Caffarri S, Croce R, Breton J and Bassi R (2001) The major antenna complex of Photosystem II has a xanthophyll binding site not involved in light harvesting. J Biol Chem 276: 35924–35933

Cammarata KV and Schmidt GW (1992) In-vitro reconstitution of a light-harvesting gene product—deletion mutagenesis and analyses of pigment binding. Biochemistry 31: 2779–2789

Cammarata KV, Plumley F and Schmidt GW (1990) Reconstitution of light-harvesting complexes: A single apoprotein binds Chla, Chlb and xanthophylls. In: Baltscheffsky M (ed) Current Research in Photosynthesis, Vol 2, pp 341–344. Kluwer Academic Publishers Dordrecht.

Cinque G, Croce R, Holzwarth A and Bassi R (2000) Energy transfer among CP29 chlorophylls: Calculated Förster rates and experimental transient absorption at room temperature. Biophys J 79: 1706–1717

Conroy MJ, Westerhuis WHJ, Parkes Loach PS, Loach PA, Hunter CN and Williamson MP (2000) The solution structure of *Rhodobacter sphaeroides* LH1 beta reveals two helical domains separated by a more flexible region: Structural consequences for the LH1 complex. J Mol Biol 298: 83–94

Croce R, Remelli R, Varotto C, Breton J and Bassi R (1999a) The neoxanthin binding site of the major light harvesting complex (LHCII) from higher plants. FEBS Lett 456: 1–6

Croce R, Weiss S and Bassi R (1999b) Carotenoid-binding sites of the major light-harvesting complex II of higher plants. J Biol Chem 274: 29613–29623

Croce R, Müller MG, Bassi R and Holzwarth AR (2001) Carotenoid-to-chlorophyll energy transfer in recombinant major light-harvesting complex (LHCII) of higher plants. I. Femtosecond transient absorption measurements. Biophys J 80: 901–915

Davis CM, Parkes-Loach PS, Cook CK, Meadows KA, Bandilla M, Scheer H and Loach PA (1996) Comparison of the structural requirements for bacteriochlorophyll binding in the core light-harvesting complexes of *Rhodospirillum rubrum* and *Rhodobacter sphaeroides* using reconstitution methodology with bacteriochlorophyll analogs. Biochemistry 35: 3072–3084

Davis CM, Bustamante PL, Todd JB, Parkes-Loach PS, McGlynn P, Olsen JD, McMaster L, Hunter CN and Loach PA (1997) Evaluation of structure function relationships in the core light harvesting complex of photosynthetic bacteria by reconstitution with mutant polypeptides. Biochemistry 36: 3671–3679

Dominici P, Caffari S, Armenante F, Ceoldo S, Crimi M and Bassi R (2002) Biochemical properties of the PsbS subunit of Photosystem II either purified from chloroplasts or recombinant. J Biol Chem 277: 22750-22758

Fiedor L, Scheer H, Hunter CN, Tschirschwitz F, Voigt B, Ehlert J, Nibbering E, Leupold D and Elsaesser T (2000) Introduction of a 60 fs deactivation channel in the photosynthetic antenna LH1 by Ni-bacteriopheophytin *a*. Chem Phys Lett 319: 145–152

Fiedor L, Leupold D, Teuchner K, Voigt B, Hunter CN, Scherz A and Scheer A (2001) Excitation trap approach to analyze size and pigment-pigment coupling: Reconstitution of LHI antenna of Rhodobacter sphaeroides with Ni-substituted bacteriochlorophyll. Biochemistry 40: 3737–3747

Formaggio E, Cinque G and Bassi R (2001) Functional architecture of the major light-harvesting complex from higher plants. J Mol Biol 314: 1157–1166

Frank HA, Das SK, Bautista JA, Bruce D, Vasil'ev S, Crimi M, Croce R and Bassi R (2001) Photochemical behavior of xanthophylls in the recombinant Photosystem II antenna complex, CP26. Biochemistry 40: 1220–1225

Franken EM, Shkuropatov AJ, Francke C, Neerken S, Gast P, Shuvalov VA, Hoff AJ and Aartsma TJ (1997) Reaction centers of *Rhodobacter sphaeroides* R-26 with selective replacement of bacteriopheophytin by pheophytin *a*. I. Characterisation of steady-state absorbance and circular dichroism and of the $P^+Q_A^-$ state. Biochim Biophys Acta 1319: 242–250

Fraser NJ, Dominy PJ, Ücker B, Simonin I, Scheer H and Cogdell RJ (1999) Selective release, removal, and reconstitution of bacteriochlorophyll a molecules into the B800 sites of LH2 complexes from *Rhodopseudomonas acidophila* 10050. Biochemistry 38: 9684–9692

Funk C, Adamska I, Green BR, Andersson B and Renger G (1995a) The nuclear-encoded chlorophyll-binding Photosystem II-S protein is stable in the absence of pigments. J Biol Chem 270: 30141–30147

Funk C, Schröder WP, Napiwotzki A, Tjus SE, Renger G and Andersson B (1995b) The PS II-S protein of higher plants: A new type of pigment-binding protein. Biochemistry 34: 11133–11141

Gall B, Zehetner A, Scherz A and Scheer H (1998) Modification of pigment composition in the isolated reaction center of Photosystem II. FEBS Lett 434: 88–92

Germano M, Shkuropatov AYa, Permentier H, Khatypov RA, Shuvalov VA, Hoff AJ and Van Gorkom HJ (2000) Selective replacement of the active and inactive pheophytin in reaction centres of Photosystem II by 13^1-deoxo-13^1-hydroxy-pheophytin *a* and comparison of their 6 K absorption spectra. Photosynth Res 64: 189–198

Giuffra E, Cugini D, Croce R and Bassi R (1996) Reconstitution and pigment-binding properties of recombinant CP29. Eur J

Biochem 238: 112–120
Giuffra E, Zucchelli G, Sandoná D, Croce R, Cugini D, Garlaschi FM, Bassi R and Jennings RC (1997) Analysis of some optical properties of a native and reconstituted Photosystem II antenna complex, CP29: Pigment binding sites can be occupied by chlorophyll *a* or chlorophyll *b* and determine spectral forms. Biochemistry 36: 12984–12993
Grabowski B, Tan S, Cunningham FX and Gantt E (2000) Characterization of the Porphyridium cruentum Chl *a*-binding LHC by in vitro reconstitution: LHCaR1 binds 8 Chl *a* molecules and proportionately more carotenoids than CAB proteins. Photosynth Res 63: 85–96
Grabowski B, Cunningham Jr. FX and Gantt E (2001) Chlorophyll and carotenoid binding in a simple red algal light-harvesting complex crosses phylogenetic lines. Proc Natl Acad Sci USA 98: 2911–2916
Hartwich G, Scheer H, Aust V and Angerhofer A (1995) Absorption and ADMR studies on bacterial photosynthetic reaction centres with modified pigments. Biochim Biophys Acta 1230: 97–113
Heinemann B and Paulsen H (1999) Random mutations directed to trans-membrane and loop domains of light-harvesting chlorophyll *a/b* protein: Impact on pigment binding. Biochemistry 38: 14088–14093
Herek JL, Fraser NJ, Pullerits T, Martinsson P, Polivka T, Scheer H, Cogdell RJ and Sundström V (2000) B800-B850 Energy transfer mechanism in bacterial LH2 complexes investigated by B800 pigment exchange. Biophys J 78: 2590–2596
Hobe S, Prytulla S, Kühlbrandt W and Paulsen H (1994) Trimerization and crystallization of reconstituted light-harvesting chlorophyll *a/b* complex. EMBO J. 13: 3423–3429
Hobe S, Förster R, Klingler J and Paulsen H (1995) N-proximal sequence motif in light-harvesting chlorophyll *a/b*-binding protein is essential for the trimerization of light-harvesting chlorophyll *a/b* complex. Biochemistry 34: 10224–10228
Hobe S, Niemeier H, Bender A and Paulsen H (2000) Carotenoid binding sites in LHCIIb—Relative affinities towards major xanthophylls of higher plants. Eur J Biochem. 267: 616–624
Hofmann E, Wrench PM, Sharples FP, Hiller RG, Welte W and Diederichs K (1996) Structural basis of light harvesting by carotenoids: Peridinin-chlorophyll-protein from *Amphidinium carterae*. Science 272: 1788–1791
Horn R and Paulsen H (2002) Folding in vitro of light-harvesting chlorophyll *a/b* protein is coupled with pigment binding. J Mol Biol 318: 547–556
Jansson S, Pichersky E, Bassi R, Green BR, Ikeuchi M, Melis A, Simpson DJ, Spangfort M, Staehelin LA and Thornber JP (1992) A nomenclature for the genes encoding the chlorophyll *a/b*-binding proteins of higher plants. Plant Mol Biol Rep 10: 242–253
Jelezko F, Tietz C, Gerken U, Wrachtrup J and Bittl R (2000) Single-molecule spectroscopy on Photosystem I pigment-protein complexes. J Phys Chem B. 104: 8093–8096
Kehoe JW, Meadows KA, Parkes-Loach PS and Loach PA (1998) Reconstitution of core light-harvesting complexes of photosynthetic bacteria using chemically synthesized polypeptides. 2. Determination of structural features that stabilize complex formation and their implications for the structure of the subunit complex. Biochemistry 37: 3418–3428
Kikuchi J, Asakura T, Loach PA, Parkes-Loach PS, Shimada K, Hunter CN, Conroy MJ and Williamson MP (1999) A light-harvesting antenna protein retains its folded conformation in the absence of protein-lipid and protein-pigment interactions. Biopolymers 49: 361–372
Kim S, Sandusky P, Bowlby NR, Aebersold R, Green BR, Vlahakis S, Yocum CF and Pichersky E (1992) Characterization of a spinach psbS cDNA encoding the 22 kDa protein of Photosystem II. FEBS Lett 314: 67–71
Koepke J, Hu XC, Muenke C, Schulten K and Michel H (1996) The crystal structure of the light-harvesting complex II (B800-850) from *Rhodospirillum molischianum*. Structure 4: 581–597
Köhler J, van Oijen AM, Ketelaars M, Hoffmann C, Matsushita M, Aartsma TJ and Schmidt J (2001) Optical spectroscopy of individual photosynthetic pigment-protein complexes. Int J Modern Phys B 15: 3633–3636
Kühlbrandt W, Wang DN and Fujiyoshi Y (1994) Atomic model of plant light-harvesting complex by electron crystallography. Nature 367: 614–621
Kuttkat A, Hartmann A, Hobe S and Paulsen H (1996) The C-terminal domain of light-harvesting chlorophyll-*a/b*-binding protein is involved in the stabilisation of trimeric light-harvesting complex. Eur. J. Biochem. 242: 288–292
Lapouge K, Näveke A, Robert B, Scheer H and Sturgis JN (2000) Exchanging cofactors in the core antennae from purple bacteria: Structure and properties of Zn-bacteriopheophytin-containing LH1. Biochemistry 39: 1091–1099
Liu Z, Yan H, Wang K, Kuang T, Zhang J, Gul L, An X and Chang W (2004) Crystal structure of spinach major light-harvesting complex at 2.72 Å resolution. Nature 428: 287–292
London E and Khorana HG (1982) Denaturation and renaturation of bacteriorhodopsin in detergents and lipid-detergent mixtures. J Biol Chem 257: 7003–7011
McDermott G, Prince SM, Freer AA, Hawthornthwaite-Lawless AM, Papiz MZ, Cogdell RJ and Isaacs NW (1995) Crystal structure of an integral membrane light-harvesting complex from photosynthetic bacteria. Nature 374: 517–521
Meadows KA, Iida K, Tsuda K, Recchia PA, Heller BA, Antonio B, Nango M and Loach PA (1995) Enzymatic and chemical cleavage of the core light-harvesting polypeptides of photosynthetic bacteria: Determination of the minimal polypeptide size and structure required for subunit and light-harvesting complex formation. Biochemistry 34: 1559–1574
Meadows KA, Parkes-Loach PS, Kehoe JW and Loach PA (1998) Reconstitution of core light-harvesting complexes of photosynthetic bacteria using chemically synthesized polypeptides. 1. Minimal requirements for subunit formation. Biochemistry 37: 3411–3417
Meyer M and Wilhelm C (1993) Reconstitution of light-harvesting complexes from *Chlorella fusca* (Chlorophyceae) and *Mantoniella squamata* (Prasinophyceae). Z Naturforsch C 48: 461–473
Meyer M and Scheer H (1995) Reaction centers of *Rhodobacter sphaeroides* R26 containing C-3 acetyl and vinyl (bacterio) pheophytins at sites $H_{A,B}$. Photosynth. Res. 44: 55-65
Meyer M, Wilhelm C and Garab G (1996) Pigment-pigment interactions and secondary structure of reconstituted algal chlorophyll *a/b*-binding light-harvesting complexes of *Chlorella fusca* with different pigment compositions and pigment-protein stoichiometries. Photosynth Res 49: 71–81
Murata T and Ishikawa C (1981) Chemical, physicochemical and spectrophotometric properties of crystalline chlorophyll-protein complexes from *Lepidium virginicum* L. Biochim Biophys

Acta 635: 341–347
Murata T, Toda F, Uchino K and Yakushihi E (1971) Water-soluble chlorophyll protein of *Brassica oleracea* var. Botrys (cauliflower). Biochim Biophys Acta 245: 208–215
Musewald C, Hartwich G, Lossau H, Gilch P, Pöllinger-Dammer F, Scheer H and Michel-Beyerle ME (1999) Ultrafast photophysics and photochemistry of [Ni]-bacteriochlorophyll *a*. J Phys Chem 103: 7055–7060
Nishio N and Satoh H (1997) A water-soluble chlorophyll protein in cauliflower may be identical to Bnd22, a drought-induced, 22-kilodalton protein in rapeseed. Plant Physiol 115: 841–846
Noy D, Yerushalmi R, Brumfeld V, Ashur I, Scheer H, Baldridge KK and Scherz A (2000) Optical absorption and computational studies of [Ni]-bacteriochlorophyll-*a*. New insight into charge distribution between metal and ligands. J Amer Chem Soc 122: 3937–3944
Pagano A, Cinque G and Bassi R (1998) In vitro reconstitution of the recombinant Photosystem II light-harvesting complex CP24 and its spectroscopic characterization. J Biol Chem 273: 17154–17165
Parkes-Loach PS, Sprinkle JR and Loach PA (1988) Reconstitution of the B873 light-harvesting complex of *Rhodospirillum rubrum* from the separately isolated alpha and beta-polypeptides and bacteriochlorophyll *a*. Biochemistry 27: 2718–2727
Parkes-Loach PS, Michalski TJ, Bass WJ, Smith U and Loach PA (1990) Probing the bacteriochlorophyll binding site by reconstitution of the light-harvesting complex of *Rhodospirillum rubrum* with bacteriochlorophyll-*a* analogues. Biochemistry 29: 2951–2960
Parkes-Loach PS, Law CJ, Recchia PA, Kehoe J, Nehrlich S, Chen J and Loach PA (2001) Role of the core region of the PufX Protein in inhibition of reconstitution of the core light-harvesting complexes of *Rhodobacter sphaeroides* and *Rhodobacter capsulatus*. Biochemistry 40: 5593–5601
Pascal A, Gastaldelli M, Ceoldo S, Bassi R and Robert B (2001) Pigment conformation and pigment-protein interactions in the reconstituted Lhcb4 antenna protein. FEBS Lett 492: 54–57
Paulsen H and Hobe S (1992) Pigment-binding properties of mutant light-harvesting chlorophyll *a/b*-binding protein. Eur J Biochem 205: 71–76
Paulsen H and Schmid VHR (2001) Analysis and reconstitution of chlorophyll proteins. In: Witty M and Smith AG (eds) Analytical Methods in Heme, Chlorophyll, and Related Molecules, pp 235–254. Eaton Publishing, Natick, MA
Paulsen H, Rümler U and Rüdiger W (1990) Reconstitution of pigment-containing complexes from light-harvesting chlorophyll *a/b*-binding protein overexpressed in *E. coli*. Planta 181: 204–211
Plumley FG and Schmidt GW (1987) Reconstitution of chlorophyll *a/b* light-harvesting complexes: Xanthophyll-dependent assembly and energy transfer. Proc Natl Acad Sci USA 84: 146–150
Reinsberg D, Booth PJ, Jegerschöld C, Khoo BJ and Paulsen H (2000) Folding, assembly, and stability of the major light-harvesting complex of higher plants, LHCII, in the presence of native lipids. Biochemistry 39: 14305–14313
Reinsberg D, Ottmann K, Booth PJ and Paulsen H (2001) Effects of chlorophyll *a*, chlorophyll *b*, and xanthophylls on the in vitro assembly kinetics of the major light-harvesting chlorophyll *a/b* complex, LHCIIb. J Mol Biol 308: 59–67
Remelli R, Varotto C, Sandonà D, Croce R and Bassi R (1999) Chlorophyll binding to monomeric light-harvesting complex—A mutation analysis of chromophore-binding residues. J Biol Chem 274: 33510–33521
Riley ML, Wallace BA, Flitsch SL and Booth PJ (1997) Slow α helix formation during folding of a membrane protein. Biochemistry 36: 192–196
Rogl H and Kühlbrandt W (1999) Mutant trimers of light-harvesting complex II exhibit altered pigment content and spectroscopic features. Biochemistry 38: 16214–16222
Rogl H, Schödel R, Lokstein H, Kühlbrandt W and Schubert A (2002) Assignment of spectral substructures to pigment-binding sites in higher plant light-harvesting complex LHC-II. Biochemistry 41: 2281–2287
Ros F, Bassi R and Paulsen H (1998) Pigment-binding properties of the recombinant Photosystem II subunit CP26 reconstituted in vitro. Eur J Biochem 253: 653–658
Rupprecht J, Paulsen H and Schmid VHR (2000) Protein domains required for formation of stable monomeric Lhca1-and Lhca4-complexes. Photosynth Res 63: 217–224
Scheer H and Hartwich G (1995) Bacterial reaction centers with modified tetrapyrrole chromophores. In: Blankenship R, Madigan MT and Bauer CE (eds) Anoxygenic Photosynthetic Bacteria, pp 649-663. Kluwer Academic Publishers, Dordrecht
Schmid VHR, Cammarata KV, Bruns BU and Schmidt GW (1997) In vitro reconstitution of the Photosystem I light-harvesting complex LHCI-730: Heterodimerization is required for antenna pigment organization. Proc Natl Acad Sci USA 94: 7667–7672
Schmid VHR, Paulsen H and Rupprecht J (2002) Identification of N- and C-terminal amino acids of Lhca2 and Lhca4 required for formation of the heterodimeric peripheral Photosystem I antenna LHCI-730. Biochemistry 41: 9126–9131
Shinashi K, Satoh H, Uchida A, Nakayama K, Okada M and Oonishi I (2000) Molecular characterization of a water-soluble chlorophyll protein from main veins of Japanese radish. J Plant Physiol 157: 255–262
Simonetto R, Crimi M, Sandonà D, Croce R, Cinque G, Breton J and Bassi R (1999) Orientation of chlorophyll transition moments in the higher-plant light-harvesting complex CP29. Biochemistry 38: 12974–12983
Standfuss R, van Scheltinga ACT, Lamborghini M and Kühlbrandt W (2005) Mechanisms of photoprotection and nonphotochemical quenching in pea light-harvesting complex at 2.5 Å resolution. EMBO J 24: 919–928
Storch KF, Cmiel E, Schäfer W and Scheer H (1996) Stereoselectivity of pigment exchange with 13(2)-hydroxylated tetrapyrroles in reaction centers of Rhodobacter sphaeroides R26. Eur J Biochem 238: 280–286
Tietz C, Chechklov O, Drabenstedt A, Schuster J and Wrachtrup J (1999) Spectroscopy on single light-harvesting complexes at low temperature. J Phys Chem B 103: 6328–6333
Tietz C, Jelezko F, Gerken U, Schuler S, Schubert A, Rogl H and Wrachtrup J (2001) Single molecule spectroscopy on the light-harvesting complex II of higher plants. Biophys J 81: 556–562
Todd JB, Parkes-Loach PS, Leykam JF and Loach PA (1998) In vitro reconstitution of the core and peripheral light-harvesting complexes of *Rhodospirillum molischianum* from separately isolated components. Biochemistry 37: 17458–17468
Todd JB, Recchia PA, Parkes Loach PS, Olsen JD, Fowler GJS, McGlynn P, Hunter CN and Loach PA (1999) Minimal re-

quirements for in vitro reconstitution of the structural subunit of light-harvesting complexes of photosynthetic bacteria. Photosynth Res 62: 85–98

van Oijen AM, Ketelaars M, Kohler J, Aartsma TJ and Schmidt J (1999) Unraveling the electronic structure of individual photosynthetic pigment-protein complexes. Science 285: 400–402

Wedel N, Klein R, Ljungberg U, Andersson B and Herrmann RG (1992) The single-copy gene psbS codes for a phylogenetically intriguing 22 kDa polypeptide of Photosystem II. FEBS Lett 314: 61–66

Yakushiji EUK, Sugimura Y, Shiratori I and Takamiya F (1963) Isolation of water-soluble chlorophyll protein from the leaves of *Chenopodium album*. Biochim Biophys Acta 75: 293–298

Yang CH, Kosemund K, Cornet C and Paulsen H (1999) Exchange of pigment-binding amino acids in light-harvesting chlorophyll *a/b* protein. Biochemistry 38: 16205—16213

Zehetner A, Scheer H, Siffel P and Vacha F (2002) Photosystem II reaction center with altered pigment-composition: Reconstitution of a complex containing five chlorophyll *a* per two pheophytin *a* with modified chlorophylls. Biochim Biophys Acta 1556: 21–28

Zucchelli G, Jennings RC, Garlaschi FM, Cinque G, Bassi R and Cremonesi O (2002) The calculated in vitro and in vivo chlorophyll *a* absorption bandshape. Biophys J 82: 378–390

Chapter 27

Assembly of Model Bacteriochlorophyll Proteins in the Native Lipid Environment

Adela Garcia-Martin, Lee Gyan Kwa, Mathias von Jan,
C. Neil Hunter and Paula Braun*
Department Biologie 1 – Botanik, Universität München, Menzinger Str. 67, D-80638 München, Germany

Summary

Protein design is used as an approach to further the understanding of membrane protein assembly, in particular, the assembly of transmembrane (bacterio)chlorophyll-binding pockets. Pigment-protein interaction motifs have been explored by (i) use of model proteins in which the native amino acid sequence in the pigment binding pockets are substantially altered and (ii) theoretical analyses of binding pockets of natural photosynthetic proteins. The bacteriochlorophyll binding sites of light harvesting complex 2, LH2, are replaced by model sites and expressed in vivo by the use of a modified *Rhodobacter sphaeroides* strain. The artificial helices are shown to bind bacteriochlorophyll and support the assembly of light-harvesting active complexes in the native membrane. A H-bond, which has been introduced at the membrane embedded bacteriochlorophyll/helix model site, is shown to drive the assembly of the model LH2 complex. Statistical analyses of natural (bacterio)chlorophyll binding pockets reveal the presence of distinct interaction motifs at the pigment/helix interface. One example is intra-membrane H-bonding between the pigments and the surrounding polypeptides, particularly between the chlorophylls' $C13^1$ keto carbonyl groups and the residues of the binding helices. With this system at hand, specific interaction motifs, such as the H-bonding motif, and their contribution to the folding and assembly can now be directly addressed within a highly simplified sequence context and in the polypeptides' native membrane environement.

*Author for correspondence, email: paula.braun@lrz.uni-muenchen.de

Bernhard Grimm, Robert J. Porra, Wolfhart Rüdiger and Hugo Scheer (eds): Chlorophylls and Bacteriochlorophylls: Biochemistry, Biophysics, Functions and Applications, pp. 387–396.

I. Introduction

Photosynthetic pigment protein complexes chiefly belong to the family of integral membrane proteins. The transmembrane α-helix (TMH), the central structural element of most membrane proteins, traverses the lipid bilayer and usually binds, together with adjoining TMHs, the photosynthetic cofactors, primarily (bacterio)chlorophyll ((B)Chl) and carotenoids. In nature, such membrane-embedded pigment-helix-structures are formed either by oligomerization of monotopic polypeptides (as in light-harvesting (LH) systems of photosynthetic bacteria) or by association of helices from polytopic helix-bundle polypeptides (as in most other LH proteins and reaction center complexes). Recently, the understanding of membrane protein folding, in particular interactions at helix-helix interfaces, has been greatly advanced by the increasing numbers of high resolution structures, by the availability of genomic sequencing data (Arkin et al., 1997; Wallin and von Heijne, 1998; Senes et al., 2000) and by a number of model studies (Choma et al., 2000; Zhou et al., 2000, 2001; Gratkowski et al., 2001; Lear et al., 2001). In the case of BChl- and Chl-proteins, however, additional factors have to be accounted for as these molecules may contribute significantly to the pigment protein assembly in the bilayer (Kim et al., 1994; Davis et al., 1995; Plumley and Schmidt, 1995; Remelli et al., 1999; Horn and Paulsen, 2002; Schmid et al., 2002).

The factors which drive the assembly of (B)Chl and polypeptide into unique arrangements have been addressed in numerous studies. Four principal experimental approaches have previously been used to investigate the interplay between the proteins and pigments in Chl- and BChl-proteins. These are: firstly, exchange of pigment with chemically modified pigment in natural pigment-protein complexes in vitro (Scheer and Hartwig, 1995; Lapouge et al., 2000; Chapter 26, Paulsen); secondly, chemical synthesis of *de novo* proteins or of truncated versions of natural proteins followed by reconstitution of the complex in vitro (Davis et al., 1997; Meadows et al., 1998; Kehoe et al., 1998; Todd et al., 1998, 1999; Kashiwada et al., 1999; Rau et al., 2001; Chapter 24, Noy et al.; Chapter 25, Nango); thirdly, mutagenesis and over-expression of the gene, followed by reconstitution of the pigments in vitro (Bassi et al., 1999; Heinemann and Paulsen, 1999; Remelli et al., 1999; Lapouge et al., 2000; Chapter 26, Paulsen); and, fourthly, site-directed or combinatorial mutagenesis combined with assembly of the complex in vivo (Fowler et al., 1992; Olsen et al., 1994; Hu et al., 1998).

In the model synthesis approach, synthetic α-helical peptides have been made which are comprised of bundles of amphipathic helices; although they are water-soluble, they bind cofactors in the hydrophobic interior and mimic important features of membrane-inserted redox-proteins. The first examples of this approach were the heme-binding maquettes from the groups of de Grado and Dutton (Robertson et al., 1994; Gibney et al., 1997). Lately, the *de novo* design of a BChl-binding site has been accomplished by synthesis of an orthogonal, four-helix protein. It mimics the coordination of (B)Chl-derivatives through one or two His residues located in the hydrophobic interior of the helix bundle, which is similar to the situation in natural (B)Chl-proteins. In a first attempt, the Chls were bound covalently to the helices to enable efficient Chl incorporation (Rau et al., 2001), but more recently, non-covalent binding has been achieved (Kashiwada et al., 1999; Snigula et al., 2001).

These first two approaches each depend on reconstitution with the pigments in a non-native system and they require the use of aqueous systems either by use of detergents or by rendering the helices water-soluble. A new approach has recently been introduced, namely, the in vivo use of artificial model TMHs to explore both BChl-binding and the assembly of light-harvesting systems in their native lipid-environment.

II. Bacteriochlorophyll Proteins with Model Transmembrane Helices

A. Design and Expression

The design of the model BChl-proteins is based on the peripheral light-harvesting complex 2 (LH2) from purple bacterium, *Rhodobacter (Rba.) sphaeroides*. LH2 is made of two short α-helical membrane proteins: the α- (LH2-α) and β- (LH2-β) subunits together with three BChl and one or two caroteinoid molecules. In essence, the membrane-embedded BChl-binding pocket of LH2 subunits has been re-designed by replacing the large portions of the

Abbreviations: (B)Chl – (bacterio)chlorophyll; CD – circular dichroism; ET – energy transfer; LH – light harvesting; *Rba.* – *Rhodobacter*; *Rps.* – *Rhodopseudomonas*; TMH – transmembrane helix; wt – wild type

helix regions, which make up the scaffold for the BChls, with simplified alternating alanine-leucine stretches (AL) (Fig. 1). In vivo expression of these model LH proteins has been accomplished by use of an engineered strain of the purple bacterium, *Rba. sphaeroides* (Jones et al., 1992); it lacks the operons encoding the apoproteins of the photosynthetic apparatus, but provides the assembly factors, pigments and membranes which are required to test the fitness of the model proteins as light harvesting units within a near-native system. Difficulties, likely to arise during expression of heterologous or artificial proteins in situ (Steiner and Scheer, 1985; McDermott et al., 1995; Drews, 1996; McGlynn et al., 1996; Braun and von Heijne, unpublished), have been initially avoided by retaining polypeptide domains which do not directly participate in pigment binding, namely, the domains that protrude out of the membrane. These, however, appear to be critical for the targetting and insertion of the helices into the membrane and for the overall assembly of the complex.

A contiguous stretch of 16 residues is replaced from α–Val–7[1] to α-Thr+6 in the LH2-α TMH, and another of 12 residues is replaced from β-Gly–7 to β-Ala+4 in the LH2-β TMH (Fig. 1). In wild type (wt) LH2, these stretches include all the residues that are proposed to interact with the BChl-B850 of both of the α- and β-subunits at distances of <4.5Å, except for residues α-Trp+9, α-Tyr+13 and α-Tyr+14 as well as β-Thr+7 and β-Trp+9, which lie outside of the TMH (McDermott et al., 1995; Prince et al., 1997). To retain the ligation with the central metal of the BChl, His0[1] was not replaced, nor was the neighboring α-Ile-1 residue replaced because of its proximity to the Mg-coordination site on the BChl-helix interface (McDermott et al., 1995). Alanine residues already occur in the wt sequence at positions –4, +1, +2 (for LH-α) and at positions –4, –1, +3, +4 (for LH2-β), while leucine residues already occur at position +4 (for LH2-α) and –3, +2 (for LH2-β). This results in a total of eight 'new' residues in the 16-residue-long stretch and five 'new' residues in the 12-residue-long stretch, enclosing all TMH residues of the BChl-B850 site. Obviously, when screening LH2 sequences for

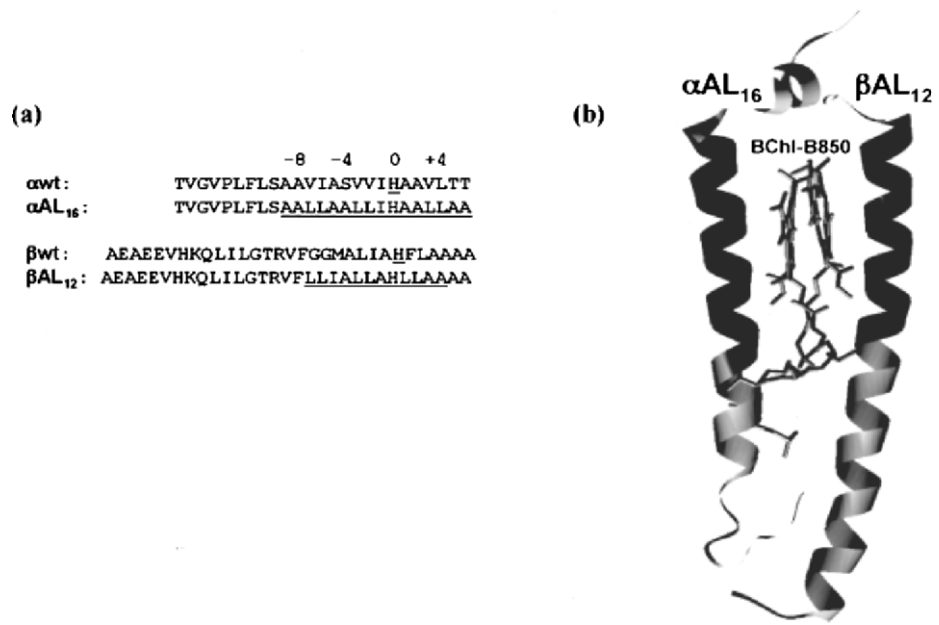

Fig. 1. LH2 complex with model helices as BChl binding sites. (a) Amino acid sequences of the model helices α-AL_{16} and β-AL_{12}. The model sequences which replace the native sequences in α-AL_{16} and β-AL_{12} as well as His0[1], which binds the central Mg are underlined. Wt sequences are shown above the model sequences. (b) Schematic view of model LH2 complexes with α-AL_{16} and β-AL_{12}. The helix stretches which are replaced by the model sequences are shown in dark grey, the native sequences and the BChl-B850 dimer are shown in light grey. For clarity, only the polypeptide's backbone and the BChl-B850 are shown.

[1] The numbering specifies the aa position relative to the histidine, designated His (0), which binds the central Mg of the α- or β-BChl-850. Positive numbers indicate the C-terminal, negative the N-terminal direction.

lower overall Ala-Leu content from other purple non-sulfur bacteria, we found that the Ala and Leu content is usually relatively high in this stretch of the TMH. The novel LH2 complexes consist of assemblies either of chimeric α-subunits and wt β-subunits and vice versa, or of both chimeric α-subunits and chimeric β-subunits (Fig. 1b, see also 3.1).

B. Spectral Properties

The novel LH2 complexes with α-AL_{16} or β-AL_{12} support not only binding of BChl but also its association into structures with a geometry producing the red-shift characteristic of B850 pigments and of a natural B800 binding site. The absorption bands of the novel LH2 with model TMH have the 'red shifted' transition maxima, namely, at ~852 nm for α-AL_{16} (see Fig. 2a) and at ~848 nm for β-$AL_{12,}$ which is typical for the B850 pigments of LH2 in membranes. The absorption at 800 nm of the monomeric, weakly coupled BChl, proposed to be bound to the terminal N-formylated α-Met (McDermott et al., 1995), is well preserved in the model LH2, and is indicative of an intact B800 binding site in this complex (Fig. 2a). There are minor, but noticeable, red-shifts from 849 to 853 nm in the Q_y-transition of α-AL_{16} which may indicate certain minor alterations in the BChl-850 geometry. The structural information responsible for the shift in the absorption of the Q_y band from 770 nm ('free' BChl) to 850 nm is, however, clearly retained if the stretches α-Val–7 to Thr+6 or β-Gly–7 to Ala+4 (Fig. 1a) are replaced by the much simplified Ala-Leu sequence. It should be noted, that the spectral properties of the BChl-B850 may be further tuned by altering the surrounding sequence in the TMH. For example, a mutagenesis study in *Rba. capsulatus* showed that combinatorial changes of 3, 4, 5 and 6 residues in the TMH of the β-subunit caused spectral shifts of the B800-850 absorption (Hu et al., 1998). In the light of these findings, it is remarkable that the simplified Ala-Leu sequence in the vicinity of BChl-B850 did not produce significantly altered spectral properties.

The BChl arrangement in LH2 with α- or β-AL seems to be largely preserved judged by the circular dichroism (CD) spectra, which serve as fingerprints for the BChl geometries (Cogdell and Scheer, 1985; van Grondelle, 1985; Braun et al., 1990; Braun and Scherz, 1991; Koolhaus et al., 1998). Typically, there is a conservative, S-shaped CD signal in the 'near IR' with a positive peak near 848 nm and a negative trough near 872 nm (see Fig. 2b), very similar to those observed in wt LH2 (Bandilla et al., 1998; Georgakopoulou et al., 2002). In addition, the optical activity of BChl-B800, seen as a negative trough near 800nm is retained in the α-AL_{16} complex (Fig. 2b).

The fitness of the model TMH to support proper light harvesting function of the complex is demon-

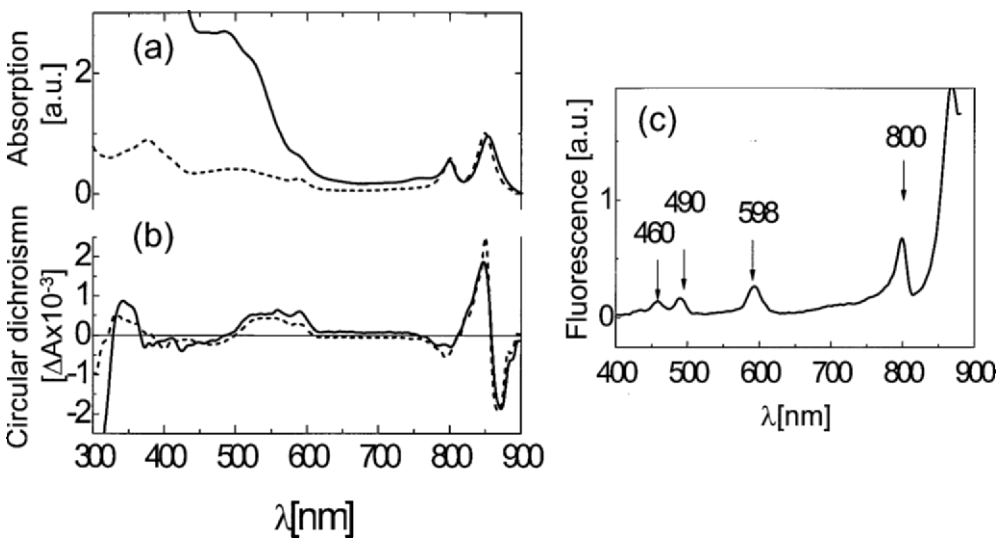

Fig. 2. Absorption (a), circular dichroism (b) and fluorescence excitation (c) spectra of model LH2 complexes with α-AL_{16} model LH2 (———) and wt LH2(- - - - -).

strated by energy transfer within the pigment assembly. The similarity of the excitation spectra (Fig. 2c) with the absorption spectra shows that efficient energy transfer takes place from BChl-B800 to BChl-B850. In particular, there is a pronounced 800 nm excitation band when detecting at 900 nm (Fig. 2c). Energy transfer (ET) occurs not only from B800 to B850 but also from carotenoids to BChl-B850, as indicated by the excitation bands in the spectra range of the caroteinoids of the complex (455–550nm). ET from carotenoid to BChl has only been observed in pigment-protein complexes or covalent constructs (Gust et al., 1993) and never in BChl-Car mixtures.

Thus, the model BChl-B850 site supports both pigment-protein assembly and the function of this complex as a light harvesting unit. Further, the residues in this region of the TMH, notably also at the BChl-protein interface, do not seem to be critical for specifying either the BChl-B850 array or the light-harvesting function in LH2. Possibly, the minimal requirements for this site in LH2 are fulfilled already by His, which binds the central Mg of BChl, together with a few key residues, such as the aromatic residues anchored in the bilayer interface which have been shown to form H-bonds with BChl-B850 (Fowler et al., 1992, 1994). Indeed, the sequence variability around the BChl-B850-binding region is high and most residues in the BChl-binding site with the exception α-His0 and β-Ala–4 are not strictly conserved (Braun et al., 2002). In view of that, it may not be surprising that additional extension of the AALL model sequence three residues towards the N-terminus of the TMH in LH2-α, does not impair BChl-B850 assembly. There is, however, significant loss of BChl-B800, indicating the importance of residues in this region for the binding of BChl-B800. Furthermore, the extension of the AALL sequence by only one residue towards the N-terminus of β-AL_{12} results in the total loss of LH2 complex assembly.

III. Assembly Motifs of (Bacterio)chlorophyll Proteins

Simultaneous replacement of the native TMH with the model AL (see Fig. 1) in both, the LH2 α- and β-subunits, abolishes assembled LH2 from the membrane. In order to rescue assembly of the novel LH2 complex, we aimed at designing stabilizing interaction motifs at the model protein/BChl interface. To that end, theoretical analyses of (B)Chl-proteins, particularly the BChl-binding pockets, have been undertaken.

A. Statistical Analyses of (Bacterio)chlorophyll Binding Proteins

Several strategies have been employed for the prediction of potential assembly motifs: Firstly, statistical analysis of existing high resolution structures, in particular, Photosystem I (PSI) with nearly 100 Chl binding pockets; secondly, alignment of aa sequences of LH2 subunits; and, thirdly, computational analysis of the aa distribution in putative (B)Chl-binding pockets of 'non-homologous' (B)Chl-proteins retrieved from protein databases.

In Photosystem I, remarkably consistent patterns of interactions were found (Fig. 3) at the Chl/TMH interface, i.e., between the binding helix and its attached Chl (Garcia-Martin et al., 2005). The macrocycle substituents chiefly interact with residues at the positions –4, +3, –1 and ±7 (relative to the liganding His0), most noticeably the $C13^2$ oxo groups interact almost exclusively with residues at –4 of the binding helix while the $C3^2$ of the vinyl group primarily interacts with residues at +3 and, to a lesser extent, with residues at –1, –4 and –7 (see Fig. 3). Sequence alignment and mutation 'hot spot' studies indicate two conserved residues besides the His0 in the TMH of the LH2 α-subunit: one of these two residues is located at position –4 (Braun et al., 2002). The sequence analysis showed that specific residues are found with significantly higher or lower probability than expected from random distribution at the positions which are critical for Chl binding (Table 1; Garcia-Martin et al., 2005). These findings point towards distinct amino acid motifs, which bind (B)Chl to its apoproteins.

Interestingly, the structural analysis of the Chl binding pockets indicate that H-bonding at the Chl/TMH interface is wide-spread: nearly half of the 100 Chl in PS I are likely to be H-bonded to the surrounding polypeptide, frequently through the $C13^1$ carbonyl group oxygen, but the oxygen atoms of other Chl substituents may also participate in H-bonding (Liebl et al., 1996; Braun et al., 2003). The residues participating in these bonds vary: for the H-bonds to the $C13^1$ oxo group, it included backbone NH (10×), heteroatoms of aromatic residues (13× Trp and Tyr, 7× His), side chain amino (2× Lys), guanidinium (5× Arg), amide (5× Asn or Gln) and hydroxl groups (4× Ser or Thr).

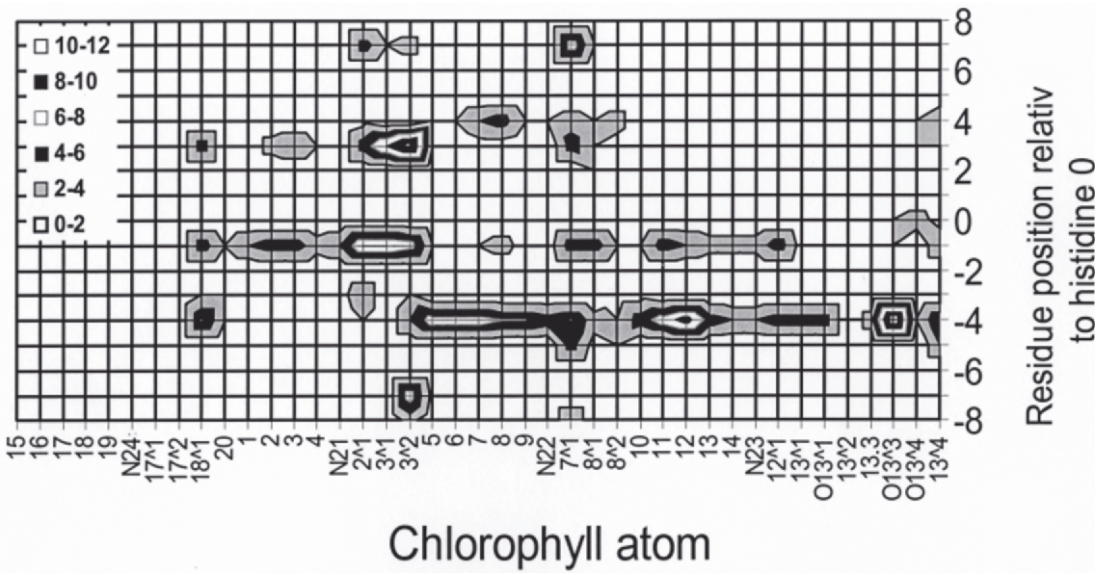

Fig. 3. Statistical analysis of Chl-binding pockets in Photosystem I from the structure of PS I (Fromme et al., 2001). Position dependent interactions between the atoms of the Chl macrocycle and the residues at positions ±8 relative to the His0 a distance ≤ 3.5Å. The shading code (top) corresponds to the interaction frequencies (see inset).

H-bonds have previously been identified in antenna and reaction center complexes (Fowler et al., 1994; Gall et al., 1997; Olsen et al., 1997; Sturgis and Robert, 1997). The currently identified H-bonds seem to participate primarily by modulating of the spectral properties of the BChls and, in reaction centers, in modulation of the redox potential (Chapter 19, Allen and Williams). It is not yet understood if polar interactions, in particular H-bonds, also contribute to the stability of the (B)Chl-polypeptide association in the membrane. The contribution of such intra-membrane H-bonding at BChl/TMHs interfaces has been studied in LH2 with the model helices (Kwa et al., 2004; Garcia-Martin et al., 2005).

B. Identification of Assembly Motifs by 'Rescue Mutagenesis'

With the intention to construct a H-bonding motif at the BChl/helix interface in the model proteins, residues with potential H-bonding properties have, therefore, been placed at position –4 in close vicinity of the C13 oxo groups of BChl-B850. The restoration of the model LH2 with α-AL_{16} and β-AL_{12} is achieved by the insertion of a single serine residue at –4 in α-AL_{16} (Fig. 4). This approach enables us to identify and analyze in depth local BChl-protein interactions

Table 1. Occurrences of aa residues in (B)Chl-binding sites. A set of BChl-binding proteins (2104 TM residues) has been investigated by computer based sequence analysis. The position of the residue in the helix relative to the histidine ligand are listed according their interaction frequencies with Chl (see Fig. 3). Bold type letters indicate deviation from random with a confidence interval of 95%, the regular type letters of 90% and the small letters of 85%.

Position	More frequent	Less frequent
-4	**D** A F	H L
-1	**H**	**L**
3	**L W K** H	M
7	**W C** P	A M
4	**A** G	H W
-8	**L N Q R** P Y K	A M V
-3	G	
-5	**S D E L**	
-7	**C** G Q	A F I
2	**D** W G	
5	**G** I	L W

in the model sequence context. The implementation of a strong H-bond at the BChl/TMH interface, most likely between the re-introduced serine at position –4 in α-AL_{16} (α-$AL_{16/S-4}$) and the $C13^1$ oxo group of β-BChl-B850, has been confirmed by resonance

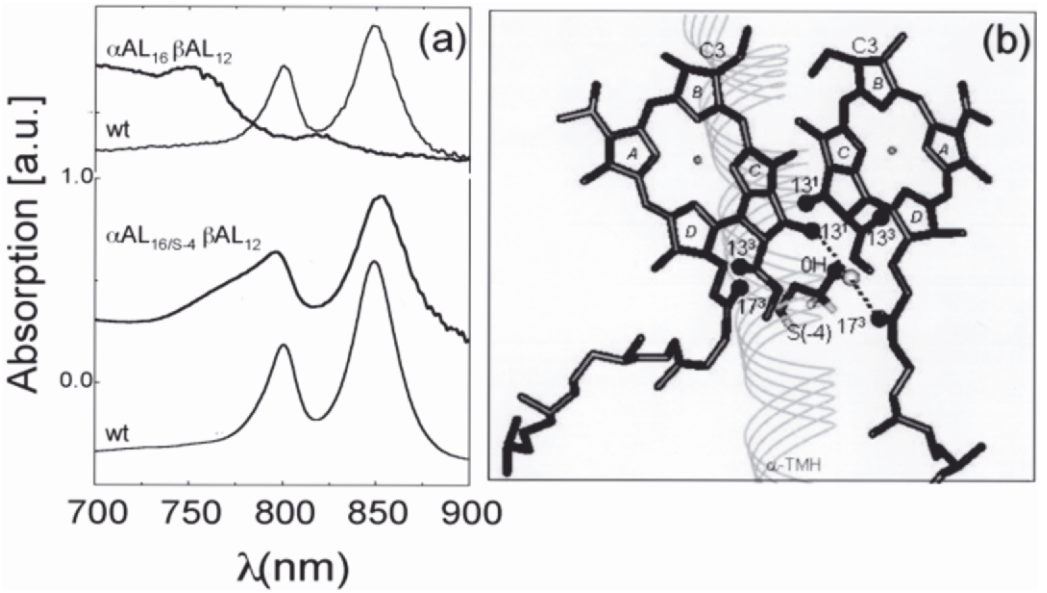

Fig. 4. H-bonding drives assembly of LH2 complex with model BChl binding site. (a) 'In situ' 'near IR' absorption spectra of LH2 wt and of model LH2 with $\alpha AL_{16}/\beta AL_{12}$ and with $\alpha AL_{16/S-4}/\beta AL_{12}$. (b) Model of H-bonds at the BChl-B850/TMH interface in LH2 from *Rba. sphaeroides*. In the high resolution structure of LH2 from *Rps. acidophila* (McDermott et al., 1995), residues 18–37 of the α-subunit have been replaced with residues 18–37 of the α-subunit of *Rba. sphaeroides*. Energy minimisation has been carried out on the replaced stretch and the BChl-B850 carbomethoxy groups (software WebLab ViewerPro™ 3.7). BChl-B850 and α-serine –4 are depicted in detail. The OH of serine and the O atoms of the C-13^1, C13^3 and C17^3 carbonyl groups are shown as spheres. Putative H-bonds to the C-13^1 carbonyl group of β-BChl-B850 and to the C-17^3 carbonyl group of the α-BChl-B850, are indicated by dotted lines.

Raman spectroscopy (Kwa et al., 2004) and by protein modeling (Braun et al., 2003; Fig. 4.) based on the high resolution structure of *Rhodopseudomonas* (*Rps.*) *acidophila* (McDermott et al., 1995). The BChl arrangment in α-$AL_{16/S-4}$ is very similar to wt LH2 as confirmed by absorption, CD, fluorescence excitation and resonance Raman spectroscopy. By use of this 'rescue-mutagenesis' approach we have thus identified H-bonding as a key assembly motif in the model BChl-proteins.

C. H-Bonding at the Bacteriochlorophyll/Protein Interface

In the model LH2 with α-AL_{16}, quantification of the complex content in membranes as well as thermal denturation experiments indicate that replacement of the native TMH in the BChl-B850 region by the Ala-Leu repeat sequence leads to (i) reduction of the model antenna complexes in the membrane and (ii) destabilized assembly of the complex. Remarkably, with serine at position –4, both expression levels and the thermal stability of the complex significantly improved and came close to the thermal stability of wt LH2 (Kwa et al., 2004; Garcia-Martin et al., 2005).

However, exchange by most other residues tested, for example, tryptophane, tyrosine, phenylalanine, cysteine, lysine, aspartate, asparagine, glutamate and glutamine, resulted in total loss of LH2; and, exchange of serine –4 by a threonine or alanine, resulted in more or less pronounced reduction of assembled complexes relative to α-AL_{16}. Thus, the residue at position –4 has a key function in the assembly of the model BChl-protein, although disturbances may be amplified by the inherent instability of LH2 with α-AL_{16}: this could be compensated in the native complex by other effects.

Curiously, removal of the H-bond between serine –4 and the $C13^1$ oxo group only slightly affected the thermal stability in wt LH2 (Braun et al., 2003). Furthermore, most LH2-α in related purple bacteria species possess an alanine residue at –4. Thus, contrary to the situation in the model proteins, the strong H-bond at the $BChl/TMH_{wt}$ interface of *Rba. sphaeroides* LH2 apparently does not contribute critically to either the spectral properties or the stability of the native wt complex. One possible explanation for this apparent discrepancy maybe that alanine –4 favorably interacts

with the 13^1 group either by H-bonding interactions with Cβ-H of the methyl side chain (Jiang and Lai, 2002) or by close packing interactions within the native sequence context. These interactions may be prevented in the model sequence context due to the slight reorganization of the pigments as reflected in minor red shifts of the red-most transition (Fig. 2). Nevertheless, in the context of the model sequences, a single intra-membrane H-bond at the BChl/TMH interface converts the highly unstable model BChl protein complex into a complex with almost native-like thermal stability and expression levels in the membrane. To what extent the H-bond increases the inherent stability of the complex or its assembly in the membrane has not yet been determined. Using this system, however, the contribution of distinct interaction motifs such as H-bonding between a (B)Chl and its binding polypeptide can now be directly assessed within the native membrane environement.

Acknowledgments

We thank Brigitte Strohmann for assistance with production of model LH2 and John D. Olsen for his advice and help in handling the modified *Rba. sphaeroides* expression system.

References

Arkin IT, Brunger AT and Engelman DM (1997) Are there dominant membrane protein families with a given number of helices? Proteins 28: 465–466

Bandilla M, Ucker B, Ram M, Simonin I I, Gelhaye E, McDermott G, Cogdell RJ and Scheer H (1998) Reconstitution of the B800 bacteriochlorophylls in the peripheral light harvesting complex B800-850 of *Rhodobacter sphaeroides* 2.4.1 with BChl a and modified (bacterio-)chlorophylls. Biochim Biophys Acta 1364: 390–402

Bassi R, Croce R, Cugini D and Sandona D (1999) Mutational analysis of a higher plant antenna protein provides identification of chromophores bound into multiple sites. Proc Natl Acad Sci USA 96: 10056–10061

Braun P and Scherz A (1991) Polypeptides and bacteriochlorophyll organization in the light-harvesting complex B850 of *Rhodobacter sphaeroides* R-26.1. Biochemistry 30: 5177–5184

Braun P, Greenberg BM and Scherz A (1990) D1-D2-cytochrome b_{559} complex from the aquatic plant *Spirodela oligorrhiza*: Correlation between complex integrity, spectroscopic properties, photochemical activity, and pigment composition. Biochemistry 29: 10376–10387

Braun P, Olsen J, Strohmann B, Hunter CN and Scheer H (2002) Assembly of light-harvesting bacteriochlorophyll in a model transmembrane helix in its natural environment. J Mol Biol 318: 1085–1095

Braun P, Vegh A, Strohmann B, Hunter N, Robert B and Scheer H (2003) Hydrogen bonding between the $C13^1$ keto group of bacteriochlorophyll and intramembrane serine residue α27 stabilizes LH2 antenna complex. Biochim Biophys Acta 1607, 19–26.

Choma C, Gratkowski H, Lear JD and DeGrado WF (2000) Asparagine-mediated self-association of a model transmembrane helix. Nat Struct Biol 7: 161–166

Cogdell RJ and Scheer H (1985) Circular dichroism of light-harvesting complexes from purple photosynthetic bacteria. Photochem Photobiol 42: 669–678

Davis CM, Bustamante PL and Loach PA (1995) Reconstitution of the bacterial core light-harvesting complexes of *Rhodobacter sphaeroides* and *Rhodospirillum rubrum* with isolated alpha- and beta-polypeptides, bacteriochlorophyll alpha, and carotenoid. J Biol Chem 270: 5793–804

Davis CM, Bustamante PL, Todd JB, Parkes-Loach PS, McGlynn P, Olsen JD, McMaster L, Hunter CN and Loach PA (1997) Evaluation of structure-function relationships in the core light-harvesting complex of photosynthetic bacteria by reconstitution with mutant polypeptides. Biochemistry 36: 3671–3679

Drews G (1996) Formation of the light-harvesting complex I (B870) of anoxygenic phototrophic purple bacteria. Arch Microbiol 166: 151–159

Fowler GJ, Visschers RW, Grief GG, van Grondelle R and Hunter CN (1992) Genetically modified photosynthetic antenna complexes with blueshifted absorbance bands. Nature 355: 848–850

Fowler GJ, Sockalingum GD, Robert B and Hunter CN (1994) Blue shifts in bacteriochlorophyll absorbance correlate with changed hydrogen bonding patterns in light-harvesting 2 mutants of *Rhodobacter sphaeroides* with alterations at alpha-Tyr-44 and alpha-Tyr-45. Biochem J 299 : 695–700

Fromme P, Jordan P and Krauss N (2001) Structure of Photosystem I. Biochim Biophys Acta 1507: 5–31

Gall A, Fowler GJ, Hunter CN and Robert B (1997) Influence of the protein binding site on the absorption properties of the monomeric bacteriochlorophyll in *Rhodobacter sphaeroides* LH2 complex. Biochemistry 36: 16282–16287

Garcia-Martin A, Kwa LG, von Jan M, Vegh A, Robert B, Scheer H and Braun P (2005) H-bonding drives assembly of model bacteriochlorophyll protein in the native membrane. In: van der Est A and Bruce D (eds) Photosynthesis: Fundamental Aspects to Global Perspectives, pp 138–140. Allen Press, Montréal

Georgakopoulou S, Frese RN, Johnson E, Koolhaas C, Cogdell RJ, van Grondelle R and van der Zwan G (2002) Absorption and CD spectroscopy and modeling of various LH2 complexes from purple bacteria. Biophys J 82: 2184–2197

Gibney BR, Rabanal F and Dutton PL (1997) Synthesis of novel proteins. Curr Opin Chem Biol 1: 537–542

Gratkowski H, Lear JD and DeGrado WF (2001) Polar side chains drive the association of model transmembrane peptides. Proc Natl Acad Sci USA 98: 880–885

Gust D, Moore TA and Moore AL (1993) Molecular mimicry of photosynthetic energy and electron transfer. Acc Chem Res 26: 198–205

Heinemann B, Paulsen H (1999) Random mutations directed to transmembrane and loop domains of the light-harvesting chlorophyll *a/b* protein: Impact on pigment binding. Biochemistry

38: 14088–14093
Horn R, Paulsen H (2002) Folding in vitro of light-harvesting chlorophyll *a/b* protein is coupled with pigment binding. J Mol Biol 318: 547–556
Hu Q, Sturgis JN, Robert B, Delagrave S, Youvan DC and Niederman RA (1998) Hydrogen bonding and circular dichroism of bacteriochlorophylls in the *Rhodobacter capsulatus* light-harvesting 2 complex altered by combinatorial mutagenesis. Biochemistry 37: 10006–10015
Jiang L, and Lai L (2002) CH...O hydrogen bonds at protein-protein interfaces. J Biol Chem 277: 37732–37740
Jones MR, Fowler GJ, Gibson LC, Grief GG, Olsen JD, Crielaard W and Hunter CN (1992) Mutants of *Rhodobacter sphaeroides* lacking one or more pigment-protein complexes and complementation with reaction-centre, LH1, and LH2 genes. Mol Microbiol 6: 1173–1184
Kashiwada A, Nishino N, Wang Z-H, Nozawa T, Kobayashi M and Nango M (1999) Molecular Assembly of Bacteriochlorophyll *a* and its Analogues by Synthetic 4α-Helix Polypeptides. Chem Lett 1301–1302
Kehoe JW, Meadows KA, Parkes-Loach PS and Loach PA (1998) Reconstitution of core light-harvesting complexes of photosynthetic bacteria using chemically synthesized polypeptides. 2. Determination of structural features that stabilize complex formation and their implications for the structure of the subunit complex. Biochemistry 37: 3418–3428
Kim J, Eichacker LA, Rüdiger W and Mullet JE (1994) Chlorophyll regulates accumulation of the plastid-encoded chlorophyll proteins P700 and D1 by increasing apoprotein stability. Plant Physiol 104: 907–916
Koolhaus MH, Frese RN, Fowler GJ, Bibby TS, Georgakopoulou S, van der Zwan G, Hunter CN and van Grondelle R (1998) Identification of the upper exciton component of the B850 bacteriochlorophylls of the LH2 antenna complex, using a B800-free mutant of *Rhodobacter sphaeroides*. Biochemistry 37: 4693–4698
Lapouge K, Naveke A, Robert B, Scheer H and Sturgis JN (2000) Exchanging cofactors in the core antennae from purple bacteria: Structure and properties of Zn-bacteriopheophytin-containing LH1. Biochemistry 39: 1091–1099
Lear JD, Gratkowski H and Degrado WF (2001) *De novo* design, synthesis and characterization of membrane-active peptides. Biochem Soc Trans 29: 559–564
Liebl U, Nitschke Wa, and Mattioli TA. (1996) Pigment-protein interactions in the antenna-reaction center complex of *Heliobacillus mobilis*. Photochem Photobiol 64, 38–45.
McDermott G, Prince SM, Freer AA, Hawthornthwaite-Lawless AM, Papiz MZ, Cogdell RJ and Isaacs NW (1995) Crystal structure of an integral membrane light-harvesting complex from photosynthetic bacteria. Nature 374: 517–521
McGlynn P, Westerhuis WH, Jones MR and Hunter CN (1996) Consequences for the organization of reaction center-light harvesting antenna 1 (LH1) core complexes of *Rhodobacter sphaeroides* arising from deletion of amino acid residues from the C terminus of the LH1 alpha polypeptide. J Biol Chem 271: 3285–3292
Meadows KA, Parkes-Loach PS, Kehoe JW and Loach PA (1998) Reconstitution of core light-harvesting complexes of photosynthetic bacteria using chemically synthesized polypeptides. 1. Minimal requirements for subunit formation. Biochemistry 37: 3411–3417
Olsen JD, Sockalingum GD, Robert B and Hunter CN (1994) Modification of a hydrogen bond to a bacteriochlorophyll a molecule in the light-harvesting 1 antenna of *Rhodobacter sphaeroides*. Proc Natl Acad Sci USA 91: 7124–7128
Olsen JD, Sturgis JN, Westerhuis WH, Fowler GJ, Hunter CN and Robert B (1997) Site-directed modification of the ligands to the bacteriochlorophylls of the light-harvesting LH1 and LH2 complexes of *Rhodobacter sphaeroides*. Biochemistry 36: 12625–12632
Plumley GF, and Schmidt GW (1995) Light-Harvesting Chlorophyll *a/b* Complexes: Interdependent Pigment Synthesis and Protein Assembly. Plant Cell 7: 689–704
Prince SM, Papiz MZ, Freer AA, McDermott G, Hawthornthwaite-Lawless AM, Cogdell RJ and Isaacs NW (1997) Apoprotein structure in the LH2 complex from *Rhodopseudomonas acidophila* strain 10050: Modular assembly and protein pigment interactions. J Mol Biol 268: 412–423
Rau HK, Snigula H, Struck A, Robert B, Scheer H and Haehnel W (2001) Design, synthesis and properties of synthetic chlorophyll proteins. Eur J Biochem 268: 3284–3295
Remelli R, Varotto C, Sandona D, Croce R and Bassi R (1999) Chlorophyll binding to monomeric light-harvesting complex. A mutation analysis of chromophore-binding residues. J Biol Chem 274: 33510–21
Robertson DE, Farid RS, Moser CC, Urbauer JL, Mulholland SE, Pidikiti R, Lear JD, Wand AJ, DeGrado WF and Dutton PL (1994) Design and synthesis of multi-haem proteins. Nature 368: 425–432
Scheer H and Hartwig G (1995) Bacterial reaction centers with modified tetrapyrrole chromophors. In: Blankenship R, Madigan MT and Bauer CE (eds) Anoxygenic Photosynthetic Bacteria, pp 649–663. Kluwer Academic Publishers, Dordrecht
Schmid VH, Potthast S, Wiener M, Bergauer V, Paulsen H and Storf S (2002) Pigment binding of Photosystem I light-harvesting proteins. J Biol Chem 277: 37307–37314
Senes A, Gerstein M and Engelman DM (2000) Statistical analysis of amino acid patterns in transmembrane helices: The GxxxG motif occurs frequently and in association with beta-branched residues at neighboring positions. J Mol Biol 296: 921–936
Snigula H, Monien B, Drepper F, de Jonge N, Haehnel W and Scheer H (2001) Non-covalent binding of a transmetalated Ni-bacteriochlorophyllide *a* to a four-helix bundle proteins obtained by orthogonal combinatorial synthesis. In: PS2001 Proceedings: 12th International Congress on Photosynthesis. CSIRO Publishing, Melbourne, S38-014. (CD-ROM)
Steiner R and Scheer H (1985) Characterization of a B800/1020 antenna from the photosynthetic bacteria *Ectothiorhodospira halochloris* and *Ectothiorhodospira abdelmalekii*. Biochim Biophys Acta 807: 278–284
Sturgis JN and Robert B. (1997) Pigment binding site and electronic properties in light-harvesting proteins of purple bacteria. J Phys Chem 101, 7227–7231
Todd JB, Parkes-Loach PS, Leykam JF and Loach PA (1998) In vitro reconstitution of the core and peripheral light-harvesting complexes of *Rhodospirillum molischianum* from separately isolated components. Biochemistry 37: 17458–17468
Todd JB, Recchia PA, Parkes-Loach PS, Olsen JO, Fowler GJS, McGlynn P, Hunter CN, and Loach PA (1999) Minimal requirements for in vitro reconstitution of the structural subunit of light harvesting complexes of photosynthetic bacteria. Photosynth Res 62, 85–98

van Grondelle R (1985) Excitation energy transfer, trapping and annihilation in photosynthetic systems. Biochim. Biophys. Acta 811: 147–195

Wallin E and von Heijne G (1998) Genome-wide analysis of integral membrane proteins from eubacterial, archaean, and eukaryotic organisms. Protein Sci 7: 1029–1038

Zhou FX, Cocco MJ, Russ WP, Brunger AT and Engelman DM (2000) Interhelical hydrogen bonding drives strong interactions in membrane proteins. Nat Struct Biol 7: 154–160

Zhou FX, Merianos HJ, Brunger AT and Engelman DM (2001) Polar residues drive association of polyleucine transmembrane helices. Proc Natl Acad Sci USA 98: 2250–2255

Chapter 28

Photosynthetic Functions of Chlorophylls

Alexander N. Melkozernov and Robert E. Blankenship*
Department of Chemistry and Biochemistry, Center for the Study of Early Events in Photosynthesis, Arizona State University, Tempe, AZ 85287–1604 U.S.A.

Summary

Chlorophylls (Chls) are the signature pigments of photosynthetic organisms and have several distinct functions, including photochemical activity and antenna function. Chls carry out reversible photochemical oxidations and reductions, which determine the basic mechanism of functioning of the photosynthetic reaction center (RC). The light-harvesting function of chlorophylls is based on their ability to absorb light over a wide spectral region. The variety of Chls (and bacteriochlorophylls) that are found in photosynthetic systems is formed by peripheral substitutions and reductions of the molecule's macrocycle. Chls undergo specific adjustments of their absorption properties due to pigment-pigment and pigment-protein interactions. Complexes of RC supplemented with light-harvesting antennas and additional electron transfer proteins are known as photosynthetic units (PSU). Despite the structural variety of the chlorophyll-based photosynthetic antennas known to date, the principles of the antenna design conform to fulfilling its biological function, capturing the energy of sun and conveying it via excitation energy transfer to the reaction center. A number of very different strategies for energy collection, delivery to the RC and regulation can be found in different photosynthetic systems. Chls are also involved in photoprotective processes of excess excitation deactivation in carotenoid-Chl complexes and Chl clusters, accumulation of stress-related Chl binding polypeptides and specific photoprotective electron transfer pathways.

*Author for correspondence, email: Blankenship@asu.edu

Bernhard Grimm, Robert J. Porra, Wolfhart Rüdiger and Hugo Scheer (eds): Chlorophylls and Bacteriochlorophylls: Biochemistry, Biophysics, Functions and Applications, pp. 397–412.

I. Introduction

Photosynthesis is one of the most important biological processes in the Biosphere. The yearly global net primary production of the biomass in photosynthesis is estimated to be ca. $10.5 \cdot 10^{10}$ tons of carbon, with roughly equal contributions from ocean and terrestrial ecosystems (Field et al., 1998). Since the advent of oxygenic photosynthesis, oxygen, a by-product of the process, has fundamentally changed the biosphere (Blankenship, 2002). This impressive impact of photosynthesis on the Earth highlights a significant role of the molecule of chlorophyll, which sensitizes the whole process of conversion of solar energy into the chemical energy of ATP, a major fuel used by organisms for living, as well as the generation of reductants that reduce CO_2 to sugars. This chapter reviews the major photosynthetic functions of chlorophylls.

II. Structure of Chlorophylls and Their Relevance to Photosynthetic Functions

Chlorophylls (Chls) were naturally selected as photosensitizers that are not consumed in photosynthetic reactions because they have a unique electronic structure. Chlorophylls are tetrapyrroles with a system of coplanar conjugated double bonds that form an aromatic structure with delocalization of electron density in π-orbitals. Structures for all the various chlorophylls can be found in Chapter 1 and are not repeated here. In the tetrapyrrole macrocycle π-orbitals form a ring with shared electron density of 18 electrons around the tetrapyrrole structure (Chapter 23, Steiner and Fowler; Chapter 34, Yerushalmi et al.). This mobile electronic structure leads to a high probability of electronic transitions from the highest occupied molecular orbitals to the lowest unoccupied molecular orbitals and ensures absorption of light in the blue (Soret) region and the green-to-red or near infrared part of the spectrum (Q_x and Q_y absorption bands) (van Amerongen et al., 2000).

In the majority of photosynthetic systems a Mg-ion in the center of the Chl macrocycle is bound via coordinative bonds to four nitrogen atoms of the tetrapyrrole, and to a fifth ligand donated generally by a protein. In derivatives of Chl with Ni or Fe in the center of the macrocycle the energy of the excited singlet state in the molecule dissipates radiationlessly within picoseconds. In proto-photosynthetic organisms biosynthetic pathways adaptively acquired Mg chelatase, an enzyme that inserts Mg into the tetrapyrrole molecule. The only exception is the occurrence of [Zn]-BChl discovered in the aerobic bacterium *Acidiphilium rubrum* (Wakao et al., 1996). This organism lives in an acidic environment in which Mg-BChl is not stable due to loss of metal, with replacement by hydrogen ions to form the bacteriopheophytin (BPhe). While photochemically very similar to BChl, [Zn]-BChl is more resistant to loss of metal and is therefore more suited to this environment.

The presence of the closed shell ions Mg^{2+} or Zn^{2+} in the center of the macrocycle lengthens the lifetime of the excited singlet state in Chl (BChl) to nanoseconds. This time is enough for photosynthetic energy transfer in light-harvesting antennas and storage in reaction centers (see below).

Chlorophylls are planar molecules, however, planarity of the macrocycle might be distorted by alkyl substituents or protein interactions. While suitable to produce red-shifted absorptions, significant distortions by massive side groups would result in a shortening of the excited state lifetime (Fajer, 2000). The variety of (B)Chls that can be found in photosynthetic systems is formed by peripheral substitutions and reductions of the macrocycle that are imposed in a series of biosynthetic modifications of Chls from Mg-protoporphyrin IX (Chl precursor) to Chls (Chapters 13, Yaronskaya and Grimm; 14, Rüdiger; 15, Frigaard et al.). Asymmetry in the π-electron distribution in substituted chlorins correlates with the extent of the low energy shift and the intensity of the Q_y absorption bands (van Amerongen et al., 2000).

A. Overview of Chlorophyll Functions

Chlorophyll-type pigments serve two primary functions in photosynthetic systems. These functions are as light-harvesting antenna pigments and as electron transfer cofactors. It is perhaps surprising that in many cases the same molecules can do both

Abbreviations: A – acceptor of electrons in photosynthetic reaction centers; BChl – bacteriochlorophyll; BPhe – bacteriopheophytin; Chl – chlorophyll; D –secondary donor of electrons in the reaction centers; FMO – Fenna-Matthew-Olson protein; LH – bacterial light-harvesting complex; LHC – light-harvesting complex of oxygenic photosynthesis; P680 (P700, P840, P870) – primary donor of electron in the reaction center (number indicates absorption maximum in nanometers); Phe – pheophytin; PS – Photosystem; PSU – photosynthetic unit; Q – quinone as an electron acceptor in the reaction center; RC – reaction center

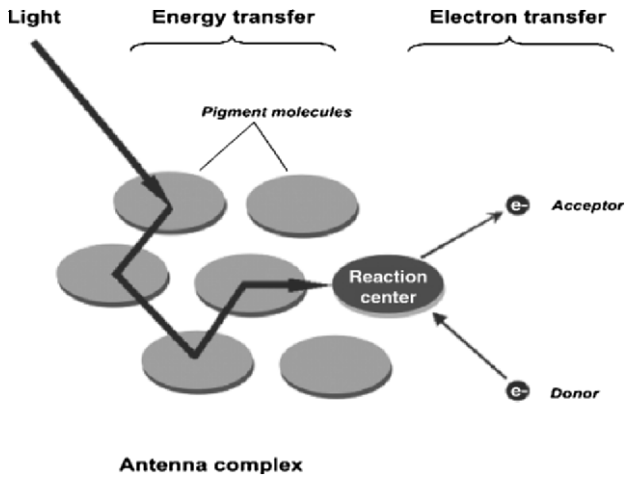

Fig. 1. Schematic depiction of the overall concept of the light harvesting antenna and reaction center. The antenna pigments absorb light and transfer excitation energy to the reaction center where photochemistry takes place. Generally, antennas may serve more than one reaction center.

of these rather different jobs in the process of photosynthesis, as some of the properties that make them suited for one function make them less suited for the other. Some types of chlorophylls are only found as antenna pigments, including Chl *b* and *c*, and BChl *c,d,e*. Other Chls can function as both antenna and electron transfer cofactors, including Chl *a* and *d* and BChl *a, b* and *g*. Some specialized Chls and the demetallated pheophytins, Phe *a*, BPhe *a* and *b* also perform essential functions as electron transfer cofactors (Chapter 4, Kobayashi). Figure 1 shows the overall concept of the light-gathering antenna that feeds energy to the electron transfer complex known as the reaction center (RC).

Functions of chlorophylls that are not related in any way to photosynthesis are extremely rare. The most dramatic is the use of a pigment derived from BChl *d* as a visual pigment in the eye of deep-sea dragon fish (Douglas et al., 1998, 2000). This pigment enables these fish to see in the red region where none of their prey is able to see and therefore gives them an advantage. It is not certain how the dragon fish obtains this pigment, although it is probably derived via the diet and then incorporated into the eye.

III. Chlorophyll-Sensitized Electron Transfer

The primary function of the Chls in reaction centers is photo-induced electron transfer. The ability of (B)Chl to carry out reversible photochemical oxidations and reductions (Krasnovsky reactions) determines the basic mechanism of the photosynthetic RC as an oxido-reductase sensitized by reversible photodisproportionation of Chls. Chls (BChls) possess the redox properties and control of reactivity that are required for reaction centers to extract electrons from a variety of substrates in the environment only when they are bound to protein.

The primary electron donor pigment forms a highly reactive photoexcited singlet state upon photoexcitation, which ejects an electron into the active electron transfer chain. Excited states can act either as strong reductants or strong oxidants (Blankenship and Prince, 1985). In solution, both oxidative and reductive behavior of excited pigments is well documented (Seely, 1978). However, in all known RCs the excited state acts as a strong reductant and the oxidative activity is not observed. The redox potential of the excited state can be estimated using the following simple equation, which relates the redox potential of the ground state of the photoactive pigment and its excitation energy:

$$E_m(P^{\bullet+}/P^*) = E_m(P^{\bullet+}/P) - E(P/P^*) \quad (1)$$

where $E_m(P^{\bullet+}/P^*)$ is the midpoint redox potential of the excited state reaction:

$$P^{\bullet+} + e^- \Leftrightarrow P^* \quad (2)$$

$E_m(P^{\bullet+}/P)$ is the midpoint potential of the ground state reaction:

$$P^{\bullet+} + e^- \Leftrightarrow P \quad (3)$$

and $E(P/P^*)$ is the 0-0 spectroscopic energy of the excited state above the ground state (in units of electron volts):

$$P + h\nu \Leftrightarrow P^* \quad (4)$$

P stands for the photoactive pigment. All the reactions shown are written as reductions, according to custom. The 1.4 to 1.8 eV photon energy and the typical ground state redox potential of 0.5 to 1 V (vs. the normal hydrogen electrode), depending on the type of RC, gives excited state redox potentials of –0.9 to –1.3 V, which makes the excited pigments extremely strong reductants. This is schematically illustrated in Fig. 2.

In order to permit multiple turnovers of the pigments and not have them be sacrificial electron donors, reversible electron transfer reactions are necessary. The neutral ground state of the primary donor regenerates from donation by immediate secondary electron donors. Back transfer of electrons from the primary acceptors to the primary donor is prevented by a chain of ultrafast electron transfer reactions via a system of secondary and tertiary electron acceptors, where in each step the back reaction is order(s) of magnitude slower than forward reaction (Chapter 31, Wachtveitl and Zinth). These rapid reactions serve to spatially separate the oxidized and reduced species and therefore reduce their reactivity. This 'kinetic steering' of the fate of the primary photoproducts is an essential aspect of efficient energy conversion in photosynthetic systems.

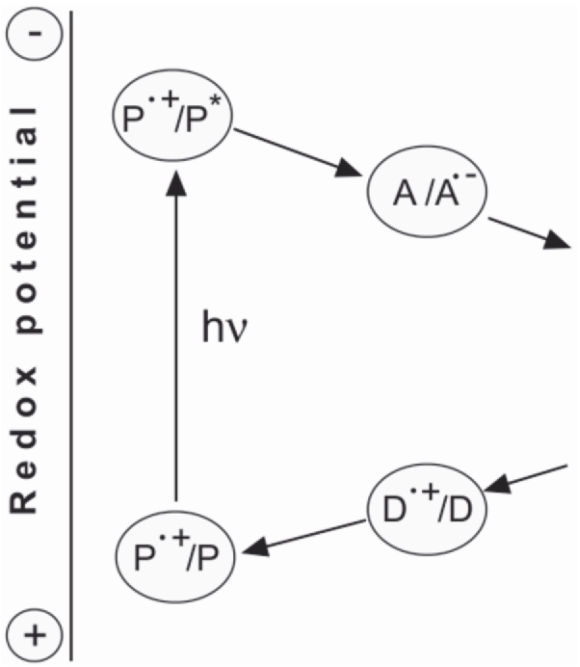

Fig. 2. Energy diagram of basic photochemical reactions in the reaction centers. The ground state and excited state redox reactions are written in the ox/red form according to equations 1–4.

A. Reaction Centers

The reaction center is a pigment-protein complex that is the site of the early electron transfer reactions of photosynthesis. The overall organization of the pigments in the RC is similar in all known photosynthetic organisms. The electron transfer chain starts with the primary donor, in most cases a dimer, and continues in two potential branches of redox cofactors, the closest to the primary donor being another tetrapyrrole pigment.

Depending on the sets of electron donors and acceptors there are two types of the RCs, iron-sulfur type (type I) and pheophytin-quinone type (type II), each adapted to specific secondary electron donors/substrates (sources of electrons). While the two classes of reaction centers have significant differences in the types of redox cofactors that serve as electron acceptors, structural studies strongly suggest that both are descended from a common ancestor (Schubert et al., 1998). Figure 3 shows the arrangement of the electron transfer cofactors in Photosystem I and the purple bacterial reaction center.

Iron-sulfur or type I RCs operate at low redox potentials. A major structural feature of the all known type I RCs is a fusion of the protein that binds core antenna Chls (BChls), with the protein that binds the redox cofactors of the electron transfer (Jordan et al., 2001). This type of RC is found in the anoxygenic green sulfur bacteria (BChl *a*) and heliobacteria (BChl *g*) and in the oxygenic cyanobacteria and chloroplasts (Chl *a*).

Of type I RC's, the structure of the cyanobacterial PS I is known in detail (2.5 Å resolution, Jordan et al., 2001), and recently the structure of the PS I/light-harvesting complex I assembly (PS I-LHCI) from pea has been solved with resolution of 4.4 Å (Ben-Shem et al., 2003). In the PS I RC a primary electron donor,

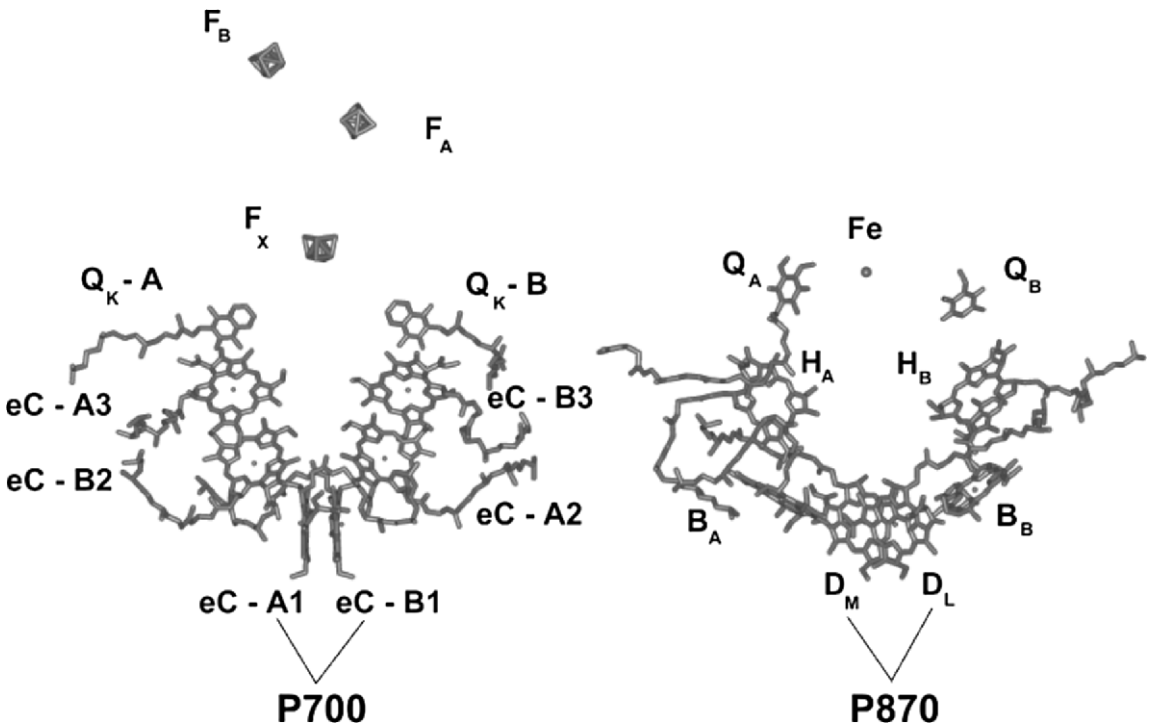

Fig. 3. Redox cofactors of electron transfer in two types of the photosynthetic reaction centers. *Left*: The iron-sulfur (type I) RC. Two branches of potential electron carriers in the PS I include eC-A1-eC-B1, primary donor P700; eC-A2 (eC-B2), accessory Chls; eC-A3 (eC-B3), primary acceptor A_0 and its symmetric counterpart; Q_K-A (Q_K-B), phylloquinones (secondary acceptors); F_X, F_A, F_B, iron-sulfur clusters. Figure produced from Protein Data Bank file 1JB0 with atomic coordinates of the PS I from the cyanobacterium *Synechococcus elongatus* (Jordan et al., 2001). Antenna Chls are not shown. *Right*: Pheophytin-quinone (type II) RC from purple bacteria. Active (A) branch of electron carriers: D_L-D_M, primary donor P870; B_A, 'accessory' BChl; H_A, 'primary' acceptor, bacteriopheophytin; Q_A, secondary acceptor, ubiquinone; Q_B, tertiary acceptor, ubiquinone. Inactive (B) branch of electron carriers: B_B, accessory BChl; H_B, bacteriopheophytin. Figure produced from Protein Data Bank file 1M3X (Camara-Artigas et al., 2002) with atomic coordinates of the RC from the purple bacterium *Rhodobacter sphaeroides.* Both models are shown at the same scale. Note the relative positions of the quinones in two types of the RC. Molecular graphics rendered using Web Lab Viewer from Accelrys, Inc.

P700, is a modified dimer consisting of Chl *a* and its C13[2] epimer, Chl *a*′. The relative positions of interacting Chls in the dimer are fixed by binding to the protein. Pigment-pigment interactions in the dimer and an asymmetric distribution of the H-bonds in the vicinity of P700 is thought to result in red spectral shift of P700 and a highly asymmetric distribution of the spin density over two parts of $P700^{\bullet+}$, respectively (Golbeck, 2003). The photooxidized primary donor $P700^{\bullet+}$ is a strong oxidant, which ensures extraction of the electrons from the substrates via a system of secondary electron donors (cytochromes/plastocyanins). In green sulfur bacteria the oxidized primary donor, $P840^{\bullet+}$, accepts electrons via secondary donors from reduced sulfur compounds.

Upon excitation of the primary donor the redox potential of P700 dramatically decreases to –1.1 V, which guarantees a rapid (picosecond) photoreduction of the primary electron acceptor, a monomeric Chl *a* molecule designated A_0. This molecule also possesses a highly negative redox potential (–1.05 V), and transfers electrons via a chain of consecutive cofactors (phylloquinones and iron-sulfur clusters) with descending redox potentials to ferredoxins on the stromal side of the thylakoid membrane (Chitnis, 2001; Golbeck, 2003). The unique redox properties of monomeric Chl *a* in the PS I type RC may be indispensable in type I RCs because this molecule is thought to function as the primary acceptor in RC from green sulfur bacteria (van de Meent et al., 1992) and a similar molecule is found in heliobacteria (van de Meent et al., 1991). The structural model visualizes the bridging Chls located between P700 and A_0, however, their functional significance

is unknown although their position in the structure undoubtedly indicates their involvement in electron transfer. Earlier, the intermediate function of the accessory BChl has been demonstrated in bacterial RC (Chekalin et al., 1987; Arlt et al., 1993; Chapter 31, Wachtveitl and Zinth).

Acquisition of the sets of the electron donors and acceptors in the type II RC was driven by selective pressure towards efficient extraction of electrons from a broader variety of terminal electron donors including water in PS II from cyanobacteria and chloroplasts. The RC from purple bacteria reveals the elements of common design, which include a BChl *a/b* special pair of the primary donor and two branches of electron transfer cofactors (Allen and Williams, 1998). In contrast to the PS I type RC, a complex of immediate electron acceptors in the type II RC includes BPhe *a/b* with intermediate BChls *a/b* located between the primary donor and the BPhe molecule. Rates of the charge separation between the primary electron donor and the spectroscopically detectable primary acceptor seem to be similar in both types of the RC. Although the secondary electron acceptor in type II RCs is also a quinone (ubiquinone or menaquinone), its redox potential is significantly less negative. Photoreduction of the primary quinone in purple bacterial RCs occurs within 200 ps. Differences in the tertiary electron acceptors (loosely bound Q_B in the type II purple bacterial RCs and PS II versus iron-sulfur clusters in the type I RC) indicate differences in the stabilization of the separated charges in the two types of RCs, as well as the ultimate destination of the electrons. These are soluble ferredoxins (Fd) for type I RCs versus the integral membrane quinone-oxidizing cytochrome bc_1 or b_6f complexes for type II RCs.

Mutagenesis studies of purple bacterial RCs showed that the redox potential of the primary donor could be significantly altered by changes in the protein environment, in particular the hydrogen-bonding pattern (Lin et al., 1994) (Chapter 19, Allen and Williams). This demonstrates an ability of the purple bacterial RCs to withstand active protein modifications without loss in function. In cyanobacteria and chloroplasts this evolutionary potential manifests itself in the form of PS II with a redox potential of the primary electron donor (+1 V in P680) being sufficient to oxidize water (+0.82 V). As confirmed by recent X-ray structure analysis of the PS II from Chl *a* containing cyanobacteria (Zouni et al., 2001; Kamiya and Shen, 2003; Ferreira et al., 2004), the D1 and D2 proteins that form the core of the PS II RC retain the pigment design of the type II RC, however, with some spatial reorganization in the structure of the primary donor and the accessory Chls. This reorganization is likely influenced by changes in the system of secondary electron donors in PS II. The highly reactive photoexcited singlet state of P680* launches an electron transfer to Phe. The resulting cation-radical of P680, an extremely strong oxidant, is capable to oxidize the protein as well as water, so its reactivity must be highly controlled and channeled. The nearby tyrosine residue (Tyr_Z) transfers an electron to $P680^{\bullet+}$ thus mediating water oxidation in the manganese cluster.

IV. Light-harvesting and Energy Transfer

Sunlight is a relatively dilute energy source, such that even in full sun each chlorophyll pigment will absorb only approximately ten photons per second (Blankenship, 2002). To avoid the reaction center idling while it waits for another photon, all photosynthetic organisms contain light-harvesting antennas. Reaction centers supplemented with antennas and additional electron transfer proteins are known as photosynthetic units (PSU). Despite the structural variety of the antennas known to date, the principles of the PSU design conform to fulfilling its biological function, capturing the energy of sun and conveying it safely and efficiently via excitation energy transfer to the reaction center where it is transformed into interchangeable forms used by the cell. Selective pressure during the evolution of the antenna complexes was directed towards fast utilization of the excitation energy before its dissipation or conversion into the long-lived triplet states capable of generating the reactive singlet oxygen species.

The major classes of photosynthetic antennas are peripheral membrane complexes, which are attached to the membrane but largely protrude into the cytoplasm, and integral membrane complexes, which are largely made up of transmembrane pigment-proteins and have most of their mass associated with the membrane. In many cases these integral membrane complexes are directly associated with the reaction center or are even part of the minimal complex, such as in the Type I RCs described above. The light-harvesting complexes closest to the reaction center are often called ‘core’ antennas, while those that are more distant spatially are known as peripheral

antennas. The term peripheral is therefore used in two somewhat different ways to describe antennas. Examples of the peripheral membrane complexes are the phycobilisome found in cyanobacteria and red algae and the chlorosome found in anoxygenic green bacteria (Green and Parson, 2003). Examples of the peripheral antennas that are integral membrane complexes are the light-harvesting complexes 2 (LH2) complexes from purple bacteria and the LHC class of antennas associated with both PS I and II of oxygenic organisms. Figure 4 illustrates the various classes of antenna complexes.

The remarkably different structural forms of the various antenna complexes, including distinct pigment types and organizational principles, strongly suggest that they have evolved independently multiple times in response to both the general need to increase absorption cross section and the specific aspects of the environment of organisms such as light quality or intensity.

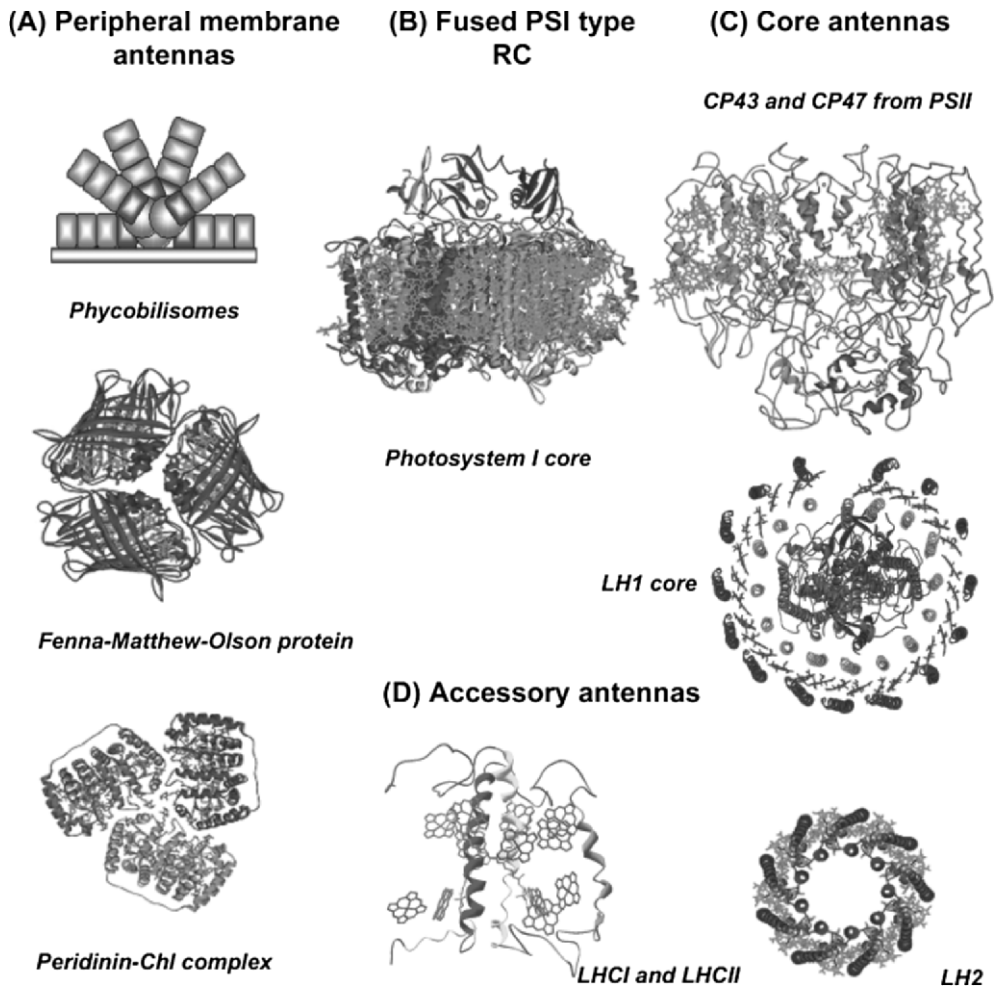

Fig. 4. Classes of light-harvesting antenna complexes. (A) Peripheral antennas: phycobilisomes from cyanobacteria and red algae (schematic); Fenna-Matthew-Olson protein from a green sulfur bacterium *Prosthecochloris aestuarii* (pdb code 4BCL, Tronrud et al., 1986) and peridinin-Chl complex from a dinoflagellate *Amphidinium carterae* (pdb code 1PPR, Hofmann et al., 1996); (B) fused PS I type RC from a cyanobacterium *Synechococcus elongatus* (pdb code 1JB0, Jordan et al., 2001); (C) Core antennas: CP43 and CP47 from the PS II of cyanobacterium *Synechococcus elongatus* (pdb code 1FE1, Zouni et al., 2001) and LH1 core from purple bacterium *Rhodopseudomonas palustris* (1PYH, Roszak et al., 2003); (D) Peripheral antennas: LHCI and LHCII from algae and higher plants (pdb file of LHCII provided by Werner Kühlbrandt, Kühlbrandt et al., 1994) and LH2 from *Rhodopseudomonas acidophila* (pdb code 1KZU, Prince et al., 1997). Molecular graphics rendered using Web Lab Viewer from Molecular Simulations, Inc. See also Color Plates 4 and 5.

A. Spectral Forms and Energy Gradient of Pigments

The protein environment modifies the energies of the excited singlet state transitions of the Chls (BChls) resulting in a heterogeneous absorption spectrum of the PSU. The spectral forms of the pigments within the PSU are distributed so that absorption maxima form a more or less distinct energy gradient directed towards the reaction center. Movement of the excitation from one pigment to another within the peripheral and the core light-harvesting antennas occurs typically on the sub-or low-picosecond time scale. In all known cases of peripheral light-harvesting antennas, the pigments absorb maximally at shorter wavelengths than the primary electron donor in the reaction centers, so that transfer of energy from shorter wavelength pigments to the longer wavelength pigments is accompanied by a loss of energy. This 'funneling' provides a degree of irreversibility to the energy transfer, thereby rapidly transferring the excitations from the distal parts of the peripheral antenna to the membrane and the core antenna and reaction center pigments. In core antennas, this energetic funneling is not always observed to be the case, and sometimes some or even most of the pigments are at a lower energy than the electronic trap, a molecule of the primary donor in the reaction center. In these cases, thermal energy combined with a charge separation that is fast in comparison to the back transfer of excitation energy, is sufficient to ensure efficient excitation trapping. Functional connectivity of pigments in the peripheral antenna and the core antenna in the PSU is determined both by the degree of overlap of spectral forms and the structural coupling of the components of the PSU, including distance and orientation.

Pigment-pigment and pigment-protein interactions are primarily responsible for the distribution of the spectral forms and filling of the energy gradient in the PSU. The primary donors in the RCs absorb at lower energies than the majority of (B)Chl in the PSU. The red spectral shift is caused by the excitonic interactions in a dimer of pigments with all oscillator strength distributed towards the low energy exciton band. Similar interactions occur in the rings of strongly coupled BChls in LH2/LH1 from purple bacteria (Chapter 21, Köhler and Aartsma) or in aggregates of BChl *c/d/e* in chlorosomes (Blankenship and Matsuura, 2003; Chapter 20, deBoer and deGroot). Pigment-pigment interactions in clusters of the Chl *a* antenna network in the PS I core result in appearing of the long-wavelength absorbing Chls that expand the absorption cross section of the complex (Gobets and van Grondelle, 2001). Earlier Trissl (1993) proposed that concentration of the excitation around the PS I reaction center is one of the possible functions of the red pigments.

The protein scaffold fixes the relative orientations of the pigments, thus preventing the excitation on the pigments from quenching, which is observed in concentrated solutions of pigments (Beddard and Porter, 1976). This is one of the most important and yet poorly understood aspects of pigment-protein structure and function. Pigment-protein interactions also affect the site energy of the Q_y absorption bands in Chl (BChl) in light-harvesting antennas. The spectral shifts may be induced by distortions of the macrocycle system by large amino acid side chains or by hydrogen bonding from the protein to the side groups of the porphyrin macrocycle (Fajer, 2000). Structural studies of the LH2 revealed that a loss of the hydrogen bond from an aromatic amino acid to an acetyl group in BChl B850 due to a site-directed mutation correlates with a spectral shift of the 850 nm absorption band to 820 nm and an out-of-plane displacement of the BChl acetyl group, which resulted in a loss of one conjugated double bond in the electronic structure of the BChl (Cogdell et al., 2002).

B. Adaptive Increase of Light-Harvesting Capacity

Photosystems undergo adaptive changes in light-harvesting capacity as a response to variable environmental conditions, including changes in both quality (spectral distribution) and quantity (photon flux) of illumination or other factors such as availability of essential nutrients. Structurally, this can manifest itself as oligomerization of pigment-protein complexes, for example, an increase in number of LH2 rings relative to LH1 in purple bacteria under low light, trimerization of cyanobacterial PS I, formation of rings of the iron-stress-induced proteins around the PS I trimer in aquatic cyanobacteria and oxyphotobacteria, dimerization of PS II in higher plants, LHCII trimerization in the peripheral antennas of green algae and higher plants, etc (see below).

C. Energy Transfer Strategies

A number of very different strategies for energy collection, delivery to the RC and regulation are found in different systems (Chapter 29, Lokstein et al.).

1. Light-Harvesting Capacity Based on Pigment Aggregation in Chlorosomes

A funnel concept fully applies to the PSU in green sulfur bacteria and filamentous anoxygenic phototrophs (Olson, 1998; Blankenship and Matsuura, 2003). Direct aggregation of BChl *c/d/e* in chlorosomes is a simple and metabolically cheap solution for significant increase of light-harvesting capacity and fast energy delivery to the RCs. Despite the dense pigment packing, which can be at a bulk concentration of greater that 1 M, chlorosomes show no signs of concentration quenching. The aggregation results in strong excitonic interactions with the subpicosecond excitation energy delocalization over the aggregate unit. As a result, the absorption spectrum of chlorosomes is significantly red shifted (750 nm relative to absorption of monomers of BChl *c/d/e* at ~ 670 nm), which optimizes the overlap of their fluorescence spectrum with the BChl *a*-carotenoid binding baseplate absorbing at about 800 nm (Montaño et al., 2003). In green sulfur bacteria and green filamentous bacteria the coupling of the chlorosome baseplate with the RC is carried out by different antennas. In green sulfur bacteria with the BChl *a* containing type I RC, this function is provided by a peripheral BChl *a*-binding protein, also known as the Fenna-Matthew-Olson (FMO) protein. Green filamentous bacteria (e.g., *Chloroflexus aurantiacus*) lack the FMO antenna, however, spectral overlap and energy connectivity of the chlorosomes with the type II RC in these organisms are provided by the core light-harvesting antennas, which are analogous to the LH1 in purple bacteria. The strategy of utilizing less protein and more pigments helped these primitive phototrophs to settle in habitats with variable and sometimes extreme conditions, especially low light environments. A schematic structural model of the photosynthetic unit from green sulfur bacteria is shown in Fig. 5. Some of these organism inhabit environments where the light intensity is so low that each pigment absorbs a photon on average once every several hours, making them the champions of photosynthesis at extremely low light intensities.

2. Fast Energy Delocalization and Storage in Light-harvesting Complex 2/Light-harvesting Complex 1/Reaction Center Complex of Purple Bacteria

The LH2-LH1-RC supercomplex in purple bacteria is an example of the light-harvesting strategy based on

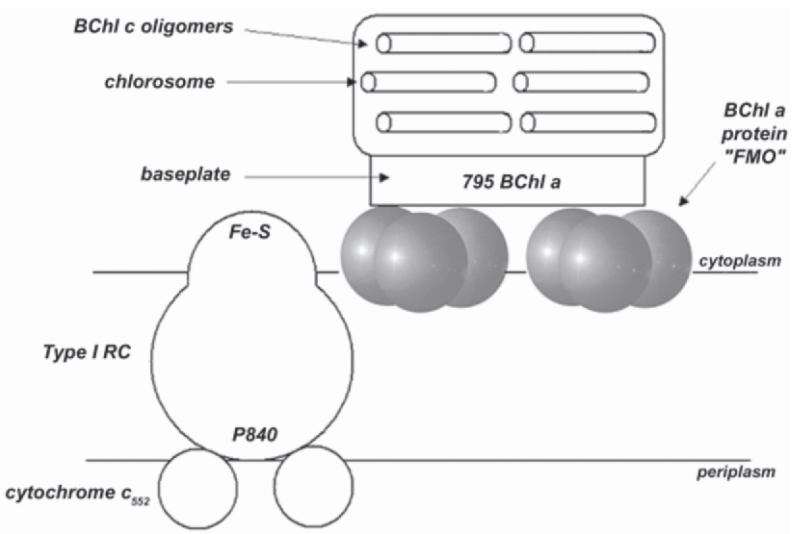

Fig. 5. Schematic model of the photosynthetic unit from the green sulfur bacteria. The peripheral light-harvesting antenna complex of the PSU includes the BChl *c* containing chlorosomes, BChl *a*-carotenoid binding baseplate absorbing at 795–800 nm and BChl *a* containing trimers of the FMO protein. The integral core antenna and the cofactors of the transmembrane electron transfer are fused in the iron-sulfur (Fe-S) type I RC. The primary donor in the RC, a special pair P840, accepts electrons from the cytochromes c_{552} on the periplasmic side of the membrane. Figure modified with permission from Blankenship and Matsuura, 2003. The components of the PSU are not drawn to scale.

the ring structure of the BChl-carrying polypeptides. In photosynthetic membranes of BChl *a/b* containing purple bacteria the geometrical features of the PSU components translate into the physical properties that support biological function (Hu et al., 2002). In the rings (both the peripheral LH2 and the core LH1) the specific structure of the proteins and the arrangement of the chromophores determine the ultrafast delocalization of the excitation energy throughout the ring (Sundström et al., 1999; Cogdell et al., 1999). Two major spectral forms of BChl *a* in LH2, B800 and B850, correspond to absorption of 8–9 BChls in the 'lower' monomeric ring of pigments and 16–18 BChls in the 'upper' ring of strongly coupled pigments, respectively. The architecture of the primary light-harvesting LH1 is similar in structure to LH2, although it is larger to accommodate the RC inside the LH1 ring and lacks the monomeric BChls. The major spectral form of the LH1 is B875 in BChl *a* containing organisms, and B1020 in BChl *b* containing organisms. A ladder of spectral forms such as B800–B850–B875 provides funneling of the energy to the RC (P870). Distances between LH2 and LH1 rings enable a picosecond energy transfer ensured by a good spectral overlap of the fluorescence of B800-B850 complexes (LH2) and B875 in LH1. In turn, the core LH1 complex spectrally overlaps with the RC, which provides efficient energy transfer from the low energy absorbing BChls to the RC. This process takes approximately 35–50 ps and is largely irreversible, so once the excitation has reached the electronic trap in the RC (P870) the probability of escaping back to the antenna is relatively low (10–20%). This transfer-to-trap behavior is determined by the long distance (35–40 Å) between the B875 pigments in LH1 and the pigments in the RC, in combination with the rapid charge separation (~3 ps). The antenna size in the PSU is subject to regulation depending on the light conditions. The final step in the energy transfer into the RC is sometimes slightly uphill, such that the excited state of the LHI antenna is lower in energy than the special pair in the RC. At the temperatures that the organisms live in nature, thermal energy is sufficient to ensure that the excitations are delivered to the RC with little or no loss of efficiency. At cryogenic temperatures, this efficiency is often much reduced due to the fact that the low energy spectral forms of the antennas become irreversible traps. A structural model of the purple bacterial LH2-LH1-RC complex is shown in Fig. 6.

3. Optimized Energy Transfer in the Photosystem II Core Antenna Networks: Speed and 100% Delivery to the Reaction Center

The PS I core in cyanobacteria and chloroplasts of green algae and higher plants is an example of the fused core antenna-reaction center complexes where the Chl *a* antenna network is bound to the same protein as the redox cofactors of the RC (Fromme et al., 2001; Ben-Shem et al., 2003). In this kind of photosynthetic system the relative positions of Chls are optimized for efficient delivery of the excitations to the reaction center. A dense packing of the pigments in the PS I core (Chl *a*/protein ratio of ~1.2) reduces the metabolic cost of the antenna and increases the connectivity of the antenna via random subpicosecond hopping of the excitations in the network (Cogdell and Lindsay, 2000; Byrdin et al., 2002). Optimal connectivity within the network as well as the spectral overlap of antenna pigments with the redox active Chls (primary donor P700) allows equilibration of the excitation energy in the depth of the whole membrane within picoseconds and delivery of the excitation to the primary donor P700 within 20–30 ps (Melkozernov, 2001; Gobets and van Grondelle, 2001). Structural coupling of the Chl antenna network and the redox active Chls in the RC allows for excitations to make multiple visits to the trap before the photochemical quenching due to the primary charge separation in the RC. The PS I excitation dynamics are known as trap-limited when the rate constant for escape of the excitation back to the core antenna is much larger than the intrinsic rate constant for photochemistry, so that multiple visits of the excitation to the trap are the norm. A special feature of the PS I core is clustering of (some of) the pigments. Excitonic interactions in clusters favor further broadening of the absorption spectra, their red shift and better overlap with the absorption spectrum of the primary donor in the reaction center, which leads to efficient energy trapping. Pigments with the strongest pigment-pigment interactions (red pigments) in such an effective network increase the absorption cross-section of the PS I complex and localize the excitation near the RC (Trissl, 1993). (See however the problem of concentration quenching mentioned above).

Some aquatic cyanobacteria have a remarkable adaptation to low light and iron deficiency in the form of a ring of 18 Chl *a* binding CP43-like proteins around the PS I trimers (Bibby et al., 2001a;

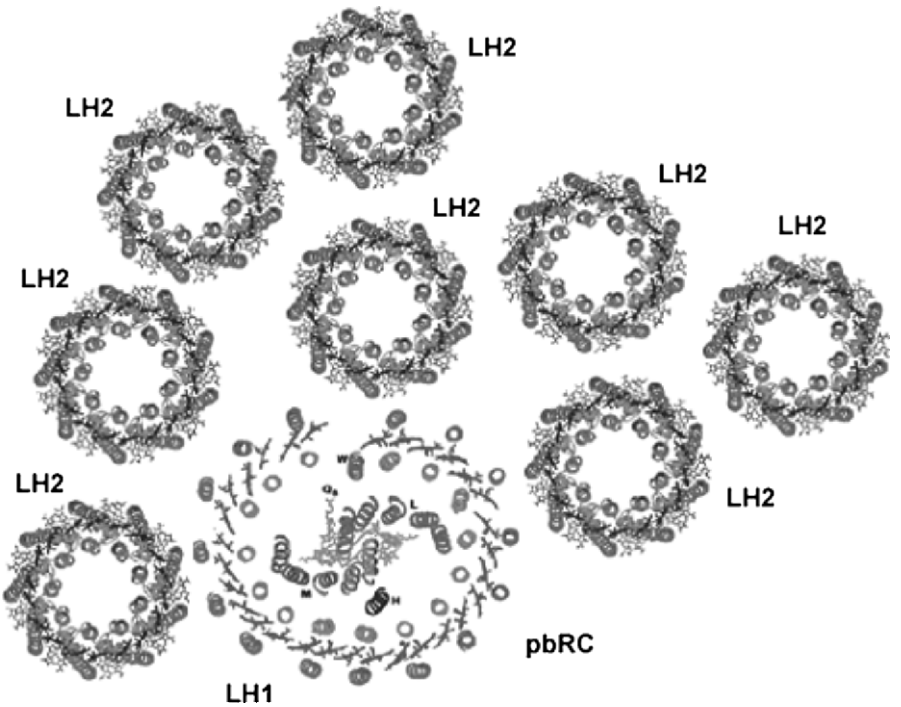

Fig. 6. Structural model of the photosynthetic unit from the purple photosynthetic bacterium *Rhodopseudomonas palustris* (pdb file 1PYH, Roszak et al., 2003*).* See also Color Plate 6.

Boekema et al., 2001). It is likely that the principle of optimal connectivity of pigments and fast delivery of the excitation to the RC holds even for such a large complex based on recent reports of an efficient energy coupling of the iron-stress induced antenna and the PS I trimer (Melkozernov et al., 2003). A model of the cyanobacterial supercomplexes is shown in Fig. 7.

4. Light-harvesting Complex I/Photosystem I and Light-harvesting Complex II/Photosystem II Supercomplexes: Balance of Efficient Energy Delivery and Regulation

In chloroplasts of algae and green plants both PS I and PS II are associated with accessory light-harvesting antennas. Light-harvesting complex I (LHCI) and LHCII are very similar in structure (Kühlbrandt et al., 1994; Ben-Shem et al., 2003) although LHCI complexes form dimers in vitro and possess long wavelength absorbing pigments (red pigments) and the majority of the LHCII complexes form trimers. PS I holocomplex assembles as the PS I monomer associated with four LHCI proteins (Scheller et al., 2001; Ben-Shem et al., 2003). The PS II supercomplex consists of the dimer of the PS II core complexes,

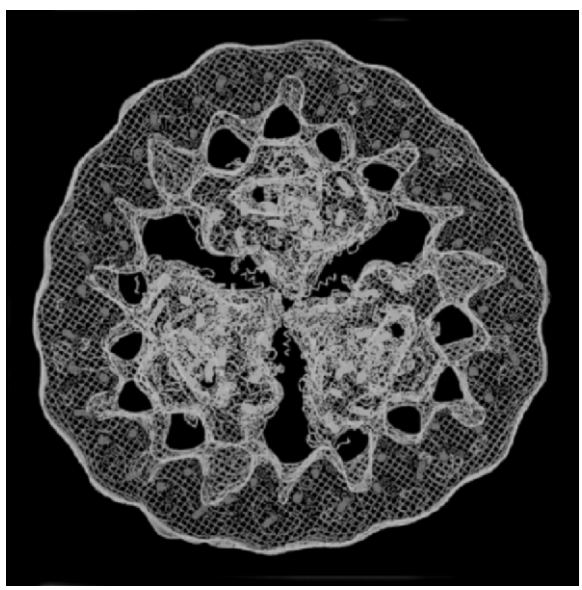

Fig. 7. Structural model of the PS I supercomplex from iron-depleted cyanobacteria. The complex consists of the Photosystem I trimer surrounded by 18 copies of the iron-stress induced CP43-like antenna pigment protein. Figure used with permission from Bibby et al., 2001b. See also Color Plate 6.

several LHCII trimers and monomeric Lhcb antennas associated with both PS II core and LHCII trimers (Boekema et al., 1999; Yakushevska et al., 2001; Barber, 2003). Elementary energy transfer processes in the Chl *a/b* binding LHCI and LHCII are as effective as in the Chl *a*-binding core complexes of PS I and PS II and occur on subpicosecond and picosecond time scales (Melkozernov, 2001; van Amerongen and van Grondelle, 2001). The PS I core belongs to a fast type of the RCs with a photochemical energy trapping occurring within 20–30 ps (see above). Coupling of the PS I core to LHCI significantly slows the time of the excitation delivery to the RC from the periphery of the supercomplex (Melkozernov, 2001). In the PS II core complex (D1/D2-CP43-CP47) the electronic trap in the RC seems to be shallow (Jennings et al., 1996). As a result trapping times are comparable with the excitation delivery times from the peripheral antennas to the PS II core.

In both PS I and PS II supercomplexes the LHC content is flexible and varies with the intensity and spectral properties of the light. Furthermore, the antenna size in both supercomplexes is regulated via physiological State 1 – State 2 transition mechanisms (Wollman, 2001; Haldrup et al., 2001). The time scale of physiological responses in both supercomplexes is seconds, minutes and hours. Striking a balance between the efficient delivery of the excitation to the RC and the regulation of the antenna size appears to be an adaptive strategy for PS I and PS II supercomplexes from green algae and higher plants.

V. Structural Function

In light-harvesting antennas with minimal protein content such as chlorosomes in green sulfur bacteria, the self-assembly of BChl *c/d/e* is determined by the planar structure of the BChl macrocycle, hydrogen bonding between the carbonyl groups and central Mg atoms of neighbors as well as by π-π stacking. Topologically, two-dimensional pigment layers assemble as rod elements. Bundles of rods, which are covered by the lipid envelope, constitute a chlorosome incorporating hundreds of thousands of pigments (Blankenship and Matsuura, 2003; Chapter 20, de Boer and de Groot).

Reaction center complexes only tolerate selective replacements and limited modifications of the pigments (Scheer and Hartwich, 1995). On the contrary, in many light-harvesting antennas the structural role of the protein is balanced with the structural role of the pigments. This is illustrated by successful in vitro reconstitution of the (B)Chl-protein complexes from their components. Oligomers of LH1 antennas from purple bacteria easily dissociate into the monomeric BChl-protein complexes and reassemble with reconstitution of the red-shifted BChl spectral forms resulting from pigment-pigment interactions (Loach and Parkes-Loach, 1995). Successful reconstitution of LH1 from individual components (isolated proteins and purified pigments) demonstrated a stabilizing effect of BChls on the structure of the complexes, which is mediated by affinity of the pigment to the protein ligand, by specific interactions of the BChl's side groups with the protein environment and BChl/BChl interactions (Loach and Parkes-Loach, 1995; Lapouge et al., 2000).

Similar results were obtained for in vitro reconstitution of the Chl *a/b* binding polypeptides from LHCII and LHCI (Paulsen and Schmid, 200; Chapter 26, Paulsen). LHCII apoproteins can be reconstituted with pigments starting from a fully denatured protein (Yang et al., 2003). Chl *b* as well as carotenoids were found to be essential for reconstitution of stable LHCII in vitro because of their exclusive binding to certain binding sites (Chapter 26, Paulsen).

Results of experiments performed in vivo also point to specific structural roles of Chl *a* and Chl *b* in an insertion and assembly of LHCs in thylakoid membranes (Hoober and Eggink, 1999). In higher plants a block in Chl *b* biosynthesis correlates with a decreased LHC antenna. Regulation of the LHC antenna size is suggested to be realized either via gene expression or via reversible enzymatic conversion of Chl *a* and Chl *b* (Rüdiger, 2002; Tanaka and Tanaka, 2000; Chapter 16, Beck and Grimm).

V. Photoprotective Function of Chlorophylls

Free monomeric Chl in solution is dangerous for living photosynthetic (and any other) cells (Chapters 33 and 34, Brandis et al.) cells because the excited singlet state of the Chl molecule easily converts into the relatively stable excited triplet state with a lifetime of 10^{-5}–10^{-3} sec. The triplet state of Chl can induce formation of harmful free radicals and singlet oxygen via photosensitized electron and proton transfer. In photosynthetic systems, production of these deleterious compounds is minimized by mechanisms, which

are still partly unknown. One is the organization in a protein scaffold, which enables excitation energy transfer between neighboring Chls towards the RC. If the excitation is localized on a Chl molecule, its excited triplet state tends to be efficiently quenched by carotenoid molecules, which are commonly located close to Chls in the majority of pigment-protein complexes. The carotenoid triplet state is usually energetically unable to induce formation of reactive oxygen species. Instead, the excitation energy dissipates through the vibrations of the isoprenoid chain of the carotenoid molecule due to overlap of the low-lying excited triplet state and the ground state (see Frank et al., 1999).

A more sophisticated enzymatic xanthophyll cycle in the peripheral antenna of PS II from higher plants and some algae (Niyogi, 2000) involves light-intensity dependent de-epoxidation of carotenoids like violaxanthin, resulting in formation in high light of zeaxanthin, a carotenoid molecule with the energy of its excited S_1 state believed to be sufficiently low to accept energy from the Q_y state of the Chls. This favors a direct protective quenching of the excitation on the Chl molecule (Ma et al., 2003)

In contrast to PS II, PS I quenches excitations at the same rate regardless of whether P700 is oxidized or reduced. Structure of the PS I core with its significant connectivity of pigments predicts that the photoprotective Chl-to-carotenoid channel might be redundant in the PS I core antenna because the ultrafast energy transfer in a well connected antenna leaves little time for formation of Chl triplet states. In the peripheral antenna of the PS I in green algae and higher plants such a channel could work. So far, the xanthophyll cycle has been reported only for the peripheral antenna of the PS II. It is not yet clear whether there is a similar regulatory mechanism that operates in PS I. Although in the PS I core the red pigments are thought to extend the absorption cross-section and concentrate the excitation towards the reaction center, in the peripheral antenna the red pigments might be involved in a photoprotection through localization of the excess excitation energy followed by a nonphotochemical quenching (Melkozernov, 2001). Competition of nonphotochemical trapping in the LHCI and photochemical trapping in the PS I-LHCI complex might be a possible regulatory process, however, the mechanism of this process is unknown. A photoprotective function of the peripherally located red pigments was suggested also for the PS I trimers from the cyanobacterium *Spirulina platensis*, which are characterized by a unique red shifted emission at 760 nm (Karapetyan et al., 1999).

Photoprotective functions of Chls are not limited to deactivation of excess excitation in carotenoid-Chl and Chl clusters. Stress-related Chl binding polypeptides that accumulate in the photosynthetic cells under stress conditions have recently been discovered in many groups of photosynthetic organisms. These polypeptides comprising one, two or three helices show a similarity in sequences with Chl *a/b* binding proteins (Heddad and Adamska, 2002), which suggests their common origin. In addition to Chls, some stress proteins bind carotenoids (luteins, zeaxanthins), which led to a suggestion that the function of an ancient antenna was not associated primarily with light-harvesting but with non-photochemical quenching of the excess energy (Montané and Kloppstech, 2000). The small cab-like polypeptide may function for transient storage of pigments with a regulated release in the sites of the assembly of pigment-protein complexes in membranes.

Chls exhibit their photoprotective functions not only in the antenna complexes but also in the electron transfer pathways. A low quantum yield cyclic electron transfer around P680 discovered in PS II was suggested to function as a photoprotective valve preventing PS II from accumulation of photooxidized P680 and doubly reduced Q_A under high light intensities (photoinhibition) (Hanley et al., 1999). This electron transfer pathway includes plastoquinone Q_B, Cyt *b*559, β-carotene and Chl Z in the core antenna. All the components of this pathway are identified in the structural model of the PS II (Zouni et al., 2001). Additionally, the oxidized Chl Z is an efficient quencher of the excess excitation energy in the vicinity of P680.

In the pheophytin-quinone-type reaction centers from purple bacteria molecular arrangements of the cofactors of electron transfer (BChls and BPhes) and their immediate protein environment favor electron transfer via only the A-branch of electron carriers (P870-B_A-H_A-Q_A, see Fig. 3, right panel). Under specific conditions of excitation with higher energy (blue light) the electron might be transferred from the primary donor via cofactors of the B-side, $BChl_B$ and $BPhe_B$. This pathway is thought to protect the RC from deleterious overexcitation (Lin et al., 2001). Recombination of the charges in the RC may result in formation of the excited triplet state of the primary donor. A carotenoid molecule, which is located in close proximity to the accessory BChl of

the B-branch, is a possible site for the quenching of the BChl triplet state in the reaction center, which is mediated by the 'accessory' BChl-B_B in the 'inactive' branch (Frank, 1999).

Acknowledgments

The authors would like to acknowledge financial support from the grants funded by NSF, DOE and USDA.

References

Allen JP and Williams JC (1998) Photosynthetic reaction centers. FEBS Lett 438: 5–9

Arlt T, Schmidt S, Kaiser W, Lauterwasser, C, Meyer M, Scheer H and Zinth W (1993) The accessory bacteriochlorophyll: A real electron carrier in primary photosynthesis. Proc Natl Acad Sci USA 90: 11757–11761

Barber J (2003) Photosystem II: The engine of life. Biophys Quart Revs 36: 71–89

Beddard GS and Porter G (1976) Concentration quenching in chlorophyll. Nature 260: 366–367

Ben-Shem A, Frolow F and Nelson N (2003) Crystal structure of plant Photosystem I. Nature 426: 630–635

Bibby TS, Nield J and Barber J (2001a) Iron deficiency induces the formation of an antenna ring around trimeric Photosystem I in cyanobacteria. Nature 412: 743–745

Bibby TS, Nield J and Barber J (2001b) Three-dimensional model and characterization of the iron stress-induced CP43`-Photosystem I supercomplex isolated from the cyanobacterium *Synechocystis* PCC 6803. J Biol Chem 276: 43246–43252

Blankenship RE (2002) Molecular mechanisms of photosynthesis. Blackwell Science, Malden

Blankenship RE and Prince RC (1985) Excited state redox potentials and the Z scheme of photosynthesis. Trends Biochem Sci 10: 382–383

Blankenship RE and Matsuura K (2003) Antenna Complexes from green photosynthetic bacteria. In: BR Green and WW Parson (eds) Light-Harvesting Antennas, pp 195–217. Kluwer Academic Publishers, Dordrecht

Boekema EJ, van Roon H, van Breemen JFL and Dekker JP (1999) Supramolecular organization of Photosystem II and its associated light-harvesting antenna in partially solubilized photosystem II membranes. Eur J Biochem 266: 444–452

Boekema EJ, Hifney A, Yakushevska AE, Piotrowski M, Keegstra W, Berry S, Michel K-P, Pistorius EK and Kruip J (2001) A giant chlorophyll-protein complex induced by iron deficiency in cyanobacteria. Nature 412: 745–748

Byrdin M, Jordan P, Krauss N, Fromme P, Stehlik D and Schlodder E (2002) Light Harvesting in Photosystem I: Modeling Based on the 2.5-Å Structure of Photosystem I from *Synechococcus elongatus.* Biophys J 83: 433–457

Camara-Artigas A, Brune D and Allen JP (2002) Interactions between lipids and bacterial reaction centers determined by protein crystallography. Proc Natl Acad Sci USA 99: 11055–11060

Chekalin SV, Matveetz YuA, Shkuropatov AYa, Shuvalov VA and Yartzev AP (1987) Femtosecond spectroscopy of primary charge separation in modified reaction centers of *Rhodobacter sphaeroides* (R-26). FEBS Lett 216: 245–248

Chitnis PR (2001) Photosystem I: Function and Physiology. Annu Rev Plant Physiol Plant Mol Biol 52: 593–626

Cogdell RJ and Lindsay JG (2000) The structure of photosynthetic complexes in bacteria and plants: An illustration of the importance of protein structure to the future development of plant science. TANSLEY New Phytol 145: 167–196

Cogdell RJ, Isaaks HW, Howard TD, McLaskey K, Fraser, NJ and Prince SM (1999) How photosynthetic bacteria harvest solar energy. J Bacteriol 181: 3869–3879

Cogdell RJ, Howard TD, Isaaks HW, McLaskey K and Gardiner AT (2002) Structural factors which control the position of the Q_y absorption band of bacteriochlorophyll *a* in purple bacteria antenna complexes. Photosynth Res 74: 135–141

Douglas RH, Partridge JC, Dulai K, Hunt D, Mullineaux CW, Tauber AY and Hynninen PH (1998) Dragon fish see using chlorophyll. Nature 393: 423–424

Douglas RH, Mullineaux CW and Partridge JC (2000) Long-wave sensitivity in deep-sea stomiid dragonfish with far-red bioluminescence: Evidence for a dietary origin of the chlorophyll-derived retinal photosensitizer of *Malacosteus niger*. Philos Trans R Soc Lond B Biol Sci 355: 1269–1272

Fajer J (2000) Structural effects in chemistry and biology. J Porphyrins Phtalocyanins 4: 382–385

Ferreira KN, Iverson TM, Maghlaoui K, Barber J and Iwata (2004) Architecture of the photosynthetic oxygen-evolving center. Science 303: 1831–1838

Field CB, Behrenfeld MJ, Randerson JT and Falkowski P (1998) Primary production of the Biosphere: Integrating terrestrial and Oceanic components. Science 281: 237–240

Frank HA (1999) Incorporation of carotenoids into reaction center and light-harvesting pigment-protein complexes. In: Frank HA, Young AJ, Britton B, and Cogdell RJ (eds) The Photochemistry of Carotenoids, pp 235–244. Kluwer Academic Publishing, Dordrecht

Frank HA, Young AJ, Britton and Cogdell RJ (eds) (1999) The Photochemistry of Carotenoids. Kluwer Academic Publishers, Dordrecht

Fromme P, Jordan P and Krauss N (2001) Structure of Photosystem I. Biochim Biophys Acta 1507: 5–31

Gobets B and van Grondelle R (2001) Energy transfer and trapping in Photosystem I. Biochim Biophys Acta 1507: 80–99

Golbeck JH (2003) The binding of cofactors to Photosystem I analyzed by spectroscopic and mutagenic methods. Annu Rev Biophys Biomol Struct 32: 237–256

Green BR and Parson WW (eds) (2003) Light-Harvesting Antennas in Photosynthesis. Kluwer Academic Publishers, Dordrecht

Haldrup A, Jensen PE, Lunde C and Scheller HV (2001) Balance of power: A view of the mechanism of photosynthetic state transitions. Trends Plant Sci 6: 301–305

Hanley J, Deligiannakis Y, Pascal A, Faller P and Rutherford AW (1999) Carotenoid oxidation in Photosystem II. Biochemistry 38: 8189–8195

Heddad M and Adamska I (2002) The evolution of light stress proteins in photosynthetic organisms. Comp Funct Genom 3: 504–510

Hofmann E, Wrench PM, Sharples FP, Hiller RG, Welte W and

Diederichs K (1996) Structural basis of light harvesting by carotenoids: Peridinin-chlorophyll-protein from *Amphidinium carterae*. Science 272: 1788 - 1791

Hoober JK and Eggink LL (1999) Assembly of light-harvesting complex II and biogenesis of thylakoid membranes in chloroplasts. Photosynth Res 61: 197–215

Hu X, Ritz T, Damjanovic A, Autenrieth F and Schulten K (2002) Photosynthetic apparatus of purple bacteria. Quart Rev Biophys 35: 1–62

Jennings RC, Garlaschi FM, Finzi L and Zucchelli G (1996) Slow exciton trapping in Photosystem II: A possible physiological role. Photosynth Res 47: 167–173

Jordan P, Fromme P, Witt HT, Klukas O, Saenger W and Krauss N (2001) Three-dimensional structure of cyanobacterial Photosystem I at 2.5 Å resolution. Nature 411: 909–917

Kamiya N and Shen J-R (2003) Crystal structure of oxygen-evolving Photosystem II from *Thermosynechococcus vulcanus* at 3.7 Å resolution. Proc Natl Acad Sci USA 100: 98–103

Karapetyan NV, Holzwarth AR and Rögner M (1999) The Photosystem I trimer of cyanobacteria: Molecular organization, excitation dynamics and physiological significance. FEBS Lett 460: 395–400.

Kühlbrandt W, Wang DN and Fujiyoshi Y (1994) Atomic model of plant light-harvesting complex by electron crystallography. Nature 367: 614–621

Lapouge K, Näveke A, Robert B, Scheer H and Sturgis JN (2000) Exchanging cofactors in the core antenna from purple bacteria: Structure and properties of Zn-bacteriopheophytin-containing LH1. Biochemistry 39: 1091–1099

Lin S, Katilius E, Haffa ALM, Taguchi AKW and Woodbury NW (2001) Blue light drives B-side electron transfer in bacterial photosynthetic reaction centers. Biochemistry 40: 13767–13773

Lin X, Murchison HA, Nagarajan V, Parson WW, Allen JP and Williams JC (1994) Specific alteration of the oxidation potential of the electron-donor in reaction centers from *Rhodobacter sphaeroides*. Proc Natl Acad Sci USA 91: 10265–10269

Loach PA and Parkes-Loach PS (1995) Structure-function relationships in Core Light-harvesting complexes (LH1) as determined by characterization of the structural subunits and by reconstitution experiments. In: Blankenship RE, Madigan MT and Bauer SE (eds) Anoxygenic Photosynthetic Bacteria, pp 437–471. Kluwer Academic Publishing, Dordrecht

Ma YZ, Holt NE, Li XP, Niyogi KK and Fleming GR (2003) Evidence for direct carotenoid involvement in the regulation of photosynthetic light harvesting. Proc Natl Acad Sci USA 100: 4377–4382

Melkozernov AN (2001) Excitation energy transfer in Photosystem I from oxygenic organisms. Photosynth Res 70: 129–153

Melkozernov AN, Bibby TS, Lin S, Barber J and Blankenship RE (2003) Time-resolved absorption and emission show that the CP43´ antenna ring of iron-stressed *Synechocystis sp*. PCC6803 is efficiently coupled to the Photosystem I reaction center core. Biochemistry 42: 3893–3903

Montané M-H and Kloppstech K (2000) The family of light-harvesting-related proteins (LHCs, ELIPs, HLIPs): Was the harvesting of light their primary function? Gene 258: 1–8

Montaño GA, Wu H-M, Lin S, Brune DC and Blankenship RE (2003) Isolation and Characterization of the B798 Baseplate Light-Harvesting Complex from the Chlorosomes of *Chloroflexus aurantiacus*. Biochemistry 42: 10246–10251

Niyogi KK (2000) Safety valves for photosynthesis. Curr Op Plant Biol 3: 455–460

Olson JM (1998) Chlorophyll organization and function in green photosynthetic bacteria. Photochem Photobiol 67: 61–75

Paulsen H and Schmid V (2002) Analysis and reconstitution of Chl-proteins. In: Smith AG and Witty M (eds) Heme, Chlorophylls and Bilins: Methods and Protocols, pp 235–253. Humana Press, Totowa

Prince SM, Papiz MZ, Freer AA, McDermott G, Hawthornthwaite-Lawless AM, Cogdell RJ and Isaacs NW (1997) Apoprotein structure in the LH2 complex from *Rhodopseudomonas acidophila* strain 10050: Modular assembly and protein pigment interactions. J Mol Biol 268: 412–423

Roszak AW, Howard TD, Southall J, Gardiner AT, Law CJ, Isaacs NW and Cogdell RJ (2003) Crystal structure of the RC-LH1 core complex from *Rhodopseudomonas palustris*. Science 302: 1969 - 1972

Rüdiger W (2002) Biosynthesis of chlorophyll *b* and the chlorophyll cycle. Photosynth Res 74: 187–193

Scheer H and Hartwich G (1995) Bacterial reaction centers with modified tetrapyrrole chromophores. In: Blankenship RE, Madigan MT and Bauer CE (eds) Anoxygenic Photosynthetic Bacteria, pp 649–663. Kluwer Academic Publishers, Dordrecht

Scheller HV, Jensen PE, Haldrup A, Lunde C and Knoetzel J (2001) Role of subunits in eukaryotic Photosystem I. Biochim Biophys Acta 1507: 41–60

Schubert W-D, Klukas O, Saenger W, Witt HT, Fromme P and Krauss N (1998) A common ancestor for oxygenic and anoxygenic photosynthetic systems: A comparison based on the structural model of Photosystem I. J Mol Biol 280: 297–314

Seely GR (1978) Energetics of electron-transfer reactions of chlorophyll and other compounds. Photochem Photobiol 27: 639–654

Sundström V, Pullerits T and van Grondelle R (1999) Photosynthetic light-harvesting: Reconciling dynamics and structure of purple bacterial LH2 reveals function of photosynthetic unit. J Phys Chem B 103: 2327–2346

Tanaka R and Tanaka A (2000) Chlorophyll *b* is not just an accessory pigment but a regulator of the photosynthetic antenna. Porphyrins 9: 240–245

Trissl H-W (1993) Long-wavelength absorbing antenna pigments and heterogeneous absorption bands concentrate excitons and increase absorption cross section. Photosynth Res 35: 247–263

Tronrud DE, Schmid MF and Matthews BW (1986) Structure and X-ray amino acid sequence of a bacteriochlorophyll *a* protein from *Prosthecochloris aestuarii* refined at 1.9 Å resolution. J Mol Biol 188: 443–454

van Amerongen H, Valkunas L and van Grondelle R (2000) Photosynthetic Excitons. World Scientific, Singapore.

van de Meent EJ, Kobayashi M, Erkelens C, Vanveelen PA, Amesz J and Watanabe T (1991) Identification of 8(1)-hydroxychlorophyll-*a* as a functional reaction center pigment in heliobacteria. Biochim Biophys Acta 1058: 356–362

van de Meent EJ, Kobayashi M, Erkelens C, Vanveelen PA, Otte SCM, Inoue K, Watanabe T and Amesz J (1992) The nature of the primary electron-acceptor in green sulfur bacteria. Biochim Biophys Acta 1102: 371–378

Wakao N, Yokoi N, Isoyama N, Hiraishi A, Shimada K, Kobayashi

M, Kise H, Takaichi M, Iwaki M, Itoh S and Sakurai Y (1996) Discovery of natural photosynthesis using Zn-containing bacteriochlorophyll in an aerobic bacterium *Acidiphilium rubrum*. Plant Cell Physiol 37: 889–893

Wollman F-A (2001) State transitions reveal dynamics and flexibility of the photosynthetic apparatus. EMBO J 20: 3623–3630

Yakushevska AE, Jensen PE, Keegstra W, van Roon H, Scheller HV, Boekema EJ and Dekker JP (2001) Supermolecular organization of Photosystem II and its associated light-harvesting antenna in *Arabidopsis thaliana*. Eur J Biochem 268: 6020–6028

Yang CH, Horn R and Paulsen H (2003) The light-harvesting chlorophyll a/*b* complex can be reconstituted in vitro from its completely unfolded apoprotein. Biochemistry 42: 4527–4533

Zouni A, Witt H-T, Kern J, Fromme P, Krauss N, Saenger W and Orth P (2001) Crystal structure of Photosystem II from *Synechococcus elongatus* at 3.8 Å resolution. Nature 409: 739–743

Chapter 29

Excitation Energy Transfer Between (Bacterio)Chlorophylls—the Role of Excitonic Coupling

Dieter Leupold*
Institut für Physik/Photonik, Universität Potsdam, Postfach 601553, D-14415 Potsdam, Germany

Heiko Lokstein*
Institut für Biochemie und Biologie/Pflanzenphysiologie, Universität Potsdam, Karl-Liebknecht-Str. 24-25, D-14476 Golm, Germany

Hugo Scheer
Department Biologie I – Botanik, Universität München, Menzinger Strasse 67, D-80683 München, Germany

Summary

The function of photosynthetic light harvesting complexes (LHCs) comprises absorption and regulated excitation energy transfer (EET) to the photochemical reaction centers (RCs). Photosynthesizing organisms have developed a variety of LHCs but, apart from phycobilins in cyanobacteria and certain algae, use only two types of pigments, (bacterio)chlorophylls ((B)Chl) and carotenoids. Adaptation of their electronic excited state properties to the requirements of efficient, yet safe light harvesting is realized by pigment-protein as well as pigment-pigment interactions, thereby varying: i) the mutual orientations and distances of the pigments; and,

*Authors for correspondence, email: dieter.e.leupold@web.de, lokstein@rz.uni-potsdam.de

Bernhard Grimm, Robert J. Porra, Wolfhart Rüdiger and Hugo Scheer (eds): Chlorophylls and Bacteriochlorophylls: Biochemistry, Biophysics, Functions and Applications, pp. 413–430.

ii) the pigments' local environments. This will be exemplified for the seemingly irregular (B)Chl networks of the main light-harvesting complex (LHC II) of higher plants and the so-called Fenna-Matthews-Olsen-Protein (FMO) of green photosynthetic bacteria, and the highly-ordered BChl arrangements in the LH2 antenna of purple bacteria and in chlorosomes of green bacteria. The occurrence and extent of excitons will be discussed.

I. Introduction

The two essential functions of (bacterio)chlorophylls ((B)Chls) in photosynthetic light harvesting complexes (LHCs) are absorption of light and subsequent electronic excitation energy transfer (EET) to a photosynthetic reaction center (RC). The latter can also absorb light, but such events occur at rates <10 Hz whereas the RC can turn over excitations at rates around 1000 Hz (Mauzerall and Greenbaum, 1989). LHCs deliver excitation energy to the RCs to assure optimal performance according to the external and internal conditions. Isolated (B)Chls, however, do not harvest light efficiently: they absorb light only in narrow regions of the spectrum, the electronic excitation energy is partly lost as heat (especially in aggregates), and potentially dangerous triplet states are formed by intersystem crossing (ISC). LHCs have evolved to minimize and control these losses in efficient EET arrays. While using relatively small amounts of protein, they broaden or extend the (B)Chl absorption regions and reduce wasteful and dangerous ISC to (B)Chl triplets, thereby increasing safely the effective cross section for absorption of the RC by orders of magnitude.

Remarkable progress has been achieved in understanding photosynthetic EET processes. In particular, LH2 of purple bacteria of which detailed structural, spectroscopic and biochemical information is available, has triggered various theoretical investigations which, in turn, inspired further experiments. A nearly complete picture of EET through the bacterial photosynthetic unit (PSU) has been proposed (Hu et al., 2002). Such a model is still lacking for the main light-harvesting complex II (LHC II) of higher plants and, also for EET through Photosystem (PS) II and PS I.

In LHC, there are two extreme cases of EET between donor (D) and acceptor (A), depending on their transition-dipole coupling: there can be 'hopping' of a completely localized excitation (weak coupling, Förster transfer), or coherent exciton motion with delocalization of excitation (strong coupling). In the case of intermediate coupling, EET may start with coherent motion, which is quickly perturbed by vibrations (called partial exciton) or coherence may be lost early, so that EET and vibrational relaxation coincide (hot transfer; Kimura et al., 2000).

In LHCs all these modes of EET have been observed. The known LHC structures show two types of pigment arrangements: highly ordered arrays in purple bacterial LHC (Karrasch et al., 1995; McDermott et al., 1995; Koepke et al., 1996; Robert et al., 2003), or in chlorosomes of green bacteria (Chapter 20, de Boer and de Groot,), as well as arrangements of much lower symmetry in LHCs of higher plants or the Fenna-Matthews-Olsen-protein (FMO) (see Chapter 28, Melkozernov and Blankenship; and Fig. 1 and Color Plate 3 from Chapter 24, Noy et al.) .

In the monomeric subunits of LHC II, 12–15 Chls are located in distinct protein environments. Here, broadening of the absorption regions, compared to monomeric Chl in solution, is assumed to occur mainly as result of heterogeneities caused by site-specific Chl-protein interaction. A similar assumption is made for the FMO complex of green sulfur bacteria.

By contrast, the 24–27 BChl *a* of LH2 are arranged in two distinct, ring-like structures of high symmetry. In one of the compartments, B850, it is not the diversity of BChl-protein interactions which extends the absorption regions, but band broadening and splitting caused by strong pigment-pigment excitonic interactions. Strong pigment-pigment interactions also cause the broad near infrared (NIR) absorptions of chlorosomes, which are nearly devoid of protein

Abbreviations: A – acceptor in EET; BChl – bacteriochlorophyll; BChl-Bxxx – BChl in a complex absorbing at xxx nm; BPhe – bacteriopheophytin; CD – circular dichroism; Chl – chlorophyll; *Chl. – Chlorobium;* CIEM – configuration interaction exciton method; CP29 – minor Photosystem II antenna complex (Lhcb4); D – donor in EET; EET – excitation energy transfer; FMO – Fenna-Matthew-Olsen complex; ISC – intersystem crossing; LH1, LH2 – core and peripheral light-harvesting complexes of purple bacteria, respectively; LHC – light-harvesting complex; LHC II – main light-harvesting complex of higher plants and algae, alternatively also termed LHCB; NIR – near infrared; NLPF – non-linear polarization in the frequency domain; PCP – peridinin chlorophyll *a*-protein; PS – Photosystem; PSU – photosynthetic unit; *Ptc. – Prostecochloris*; *Rba. – Rhodobacter*; *Rps. – Rhodopseudomonas*; *Rsp. – Rhodospirillum*

(Blankenship et al., 1995; Chapter 15, Frigaard et al.; Chapter 20, de Boer and de Groot).

The aforementioned strategies, alone or in combination, are useful not only to broaden the absorption regions, but they may also speed up EET within and between sub-complexes of the respective PS. Light absorption by any of these components with populations of an excited state is generally followed by deactivation to the vibrationally relaxed lowest excited state(s). Then, EET to a spatially and spectrally suitable acceptor (A) in the EET chain takes place with high quantum yield. Hence, EET overcomes the competing deactivation routes by radiative and radiationless processes in the lowest excited singlet state of D. The EET rate, k_{DA}, in case of weak D-A interaction is described:

$$k_{DA} = \frac{2\pi}{\eta}\left|V_{DA}\right|^2 J_{DA} \quad (1)$$

where V_{DA} is the electronic coupling factor. All nuclear factors are contained in the Förster spectral overlap integral J_{DA}. If the distance between D and A is much larger than the size of D and A themselves (long-range transfer), the Coulomb coupling can be expanded into a multipole series and restricted to the dipole-dipole term, which gives the Förster formula:

$$k_{DA} = \frac{9000(\ln 10)\kappa^2\phi_D}{128\pi^5 n^4 N r^6 \tau_D}\int_o^\infty \frac{f_D(\tilde{\nu})\varepsilon_{DA}(\tilde{\nu})}{\tilde{\nu}^4}\, d\tilde{\nu} \quad (2)$$

where κ^2 and r describe the orientation and distance, respectively, of the D and A transition dipoles; ϕ_D and τ_D are fluorescence quantum yield and excited state lifetime, respectively, of D in the absence of A, N is the Avogadro number; $f_D(\tilde{\nu})$ is the normalized fluorescence intensity of D; $\varepsilon_A(\tilde{\nu})$ the extinction coefficient of A at wavenumber $\tilde{\nu}$; and n is the refractive index of the medium in the optical range of the local environment of the D-A pair. Since k_{DA} depends inversely on n^4, determination of n of the respective pigments local environment is of considerable importance for assessment of absolute rates. A broad variety of values and their meaning is found in the literature (Knox and van Amerongen, 2002). Below, we refer to a recently-determined value for n for the local environment responsible for EET 800 → 850 nm in LH2 (n = 1.59; I. Eichwurzel, unpublished), which is similar to that for Chl *a* in the peridinin chlorophyll *a*-protein (PCP) (n = 1.6; Kleima et al., 1997). The weak coupling limit is applicable, at least in good approximation, for most EET processes *between* LHC. It is also applicable for EET to the RC, where relatively long distances prevail in order to prevent electron transfer to the antenna.

II. Excitation Energy Transfer in Purple Bacteria

A. General

A prototypical purple bacterial PS consists of several peripheral light-harvesting complexes, LH2, comprised of 8–9 identical units, each carrying 3 BChl *a* and 1–2 carotenoids. They surround a core antenna (LH1) complex with approximately 16 identical units each carrying 2 BChl *a* and 1 (or more) carotenoid which, in turn, encases the RC (data for the *Rhodopseudomonas* (*Rps.*) *acidophila*-type of purple bacteria; Papiz et al., 1996). Whereas the ratio of RC/LH1 complexes is fixed, the amount of LH2, if present, depends on growth conditions (Georgakopoulou et al., 2002). An important modification of this model is a clustering of LH1-RC complexes in a 'lake' of LH2 (Nagarajan and Parson, 1997). An interrupted ring is found in crystals of LH1-RC-complexes of *Rhodoseudomonas* (*Rps.*) *palustris* (Roszak et al., 2003), and two LH1 complexes, forming an elongated S-shaped super-complex with two RCs, have been seen in bacteria containing the PufX protein (Jungas et al., 1999; Westerhuis et al., 2002; for more details and examples see Hu et al., 2002).

The NIR absorptions differ for LH1 (875 nm) and LH2 (800 and 850 nm) complexes. NIR photons can start the EET chain in either LH1 or LH2, and within the latter at either BChl-B850 or a BChl-B800, resulting in different numbers and types of EET steps before reaching the RC.

B. Light Harvesting Complex 2: Strong and Weak Coupling, Excitation Energy Transfer from Higher Excited States, Deactivation

In LH2, a photon is absorbed by one of the circular aggregates, either BChl-B800 or BChl-B850, or by a carotenoid. It is assumed that Q_y of BChl-B850 is the terminal state for all light-harvesting processes in LH2 and, hence, the donor in EET to LH1.

The following discussion will focus on the Q_y absorptions in the red to NIR region. Investigations

involving higher excited states are scarce, they include EET from higher excited (Soret-region) BChl to carotenoids (Limantara et al., 1998), radiative transitions (low-yield) from B_x and Q_x states of BChl to the ground state (Leupold et al., 2002; D. Leupold et al., unpublished) and processes from higher excited states, which bypass the Q_y excitonic manifold (Limantara et al., 1998). Energy transfer from carotenoids is discussed in Chapter 30 (Koyama and Kakitani).

1. The Q_y-Band Region

Experiments and theoretical description of EET following excitation in the 800 nm-centered absorption band of LH2 (belonging mainly to the monomeric BChl-B800, but see Leupold et al., 1999b) and detection in the 850 nm band have concentrated on LH2 from *Rps. acidophila*, *Rhodobacter* (*Rba.*) *sphaeroides*, and *Rhodospirillum* (*Rsp.*) *molischianum*. LH2s have been classified as either '*acidophila*-like' or '*molischianum*-like', with the main difference in the orientation of the BChl-B800 molecules. LH2 of *Rba. sphaeroides* is disputably grouped to '*molischianum*-like' (Georgakopoulou et al., 2002).

The experimentally determined k_{DA}^{-1} values for EET from BChl-B800 → BChl-B850 at room temperature are 600–900 fs (Table 1). It has been a general problem of Förster-formalism based simulations that, neglecting among other issues (see below) the excitonic level structure, the calculated EET rates were too low by a factor of about 5 (Pullerits et al., 1997). This has been corroborated by a study of B800 → B850 EET with complexes in which BChl-B800 was completely exchanged (Herek et al., 2000), thereby blue-shifting the NIR absorption maximum (originally located at 800 nm) stepswise down to 670 nm, while maintaining the BChl-B850 (see Table 1). The simulated data nicely parallel the experimental increase of transfer times, but are systematically lower by a factor of 5 (Herek et al., 2000). For LH2, precise structural data are available, as well as a wealth of data from linear as well as nonlinear optical spectroscopy. Improved calculations, using the configuration interaction exciton method (CIEM), on LH2 from *Rsp. molischianum* and *Rps. acidophila* by the group of Korppi-Tommola (Linnanto et al., 1999; Linnanto and Korppi-Tomola, 2000; Ihalainen et al., 2001) satisfactorily described many of the experimental data. Important contributions to the recent improvement of the theoretical understanding of light harvesting in LH2 were also provided by Krueger et al. (1998), Cory et al. (1998), Scholes and Fleming (2000), Hu et al. (1997, 2002), Damjanovic et al. (2002), and data derived from single-moleucle spectroscopy (Chapter 21, Köhler and Aartsma). Remaining discrepancies regarding a few experimental results are stimulating for both, theory and experiment.

a. Excitonic Model for B800-B850

Excitonic models for the Q_y transition range of LH2 of *Rps. acidophila* and *Rsp. molischianum* (Cory et al., 1998; Krueger et al. 1998, Linnanato et al., 1999;

Table 1. Experimentally observed and calculated EET time constants for BChl-B800 → BChl-B850 in LH2 of purple bacteria

Antenna complex (modification)	λ_{pump} [nm]	λ_{probe} [nm]	k_{DA}^{-1} [ps], exp. RT	77 K	4.2 K	k_{DA}^{-1} [ps], calc.
Rba. sphaeroides 2.4.1	795/800	800/840	0.7 [1]	1.2 [1]	1.5/1.3 ± 0.2 [1]	
Rba. sphaeroides (M(Y)210)	810	860	0.7 [2]			
Rps. acidophila 10050	810	870	0.9 [2]			
	801		0.8 [3]	1.3 [3]		
	785	870	0.9 ± 0.1 [4]			0.7–1.3 ps [a,5]; 0.91 [6]
Rps. acidophila modif. (ZnBPhe *a*) [8]	785	870	0.8 ± 0.1 [4]			0.8–1.1 ps [a,5]; 0.75 [6]
Rps. acidophila (3-vinyl-BChl *a*) [8]	754	870	1.4 ± 0.2 [4]			1.1–1.5 ps [a,5]; 0.75 [6]
Rps. acidophila (3^1-OH-BChl *a*) [8]	742	870	1.8 ± 0.2 [4]			1.2–1.6 ps [a,5]; 1.34 [6]
Rps. acidophila (3-acetyl-Chl *a*) [8]	685	870	4.4 ± 0.5 [4]			29.1–38.1 ps [a,5]; 13.8 [6]
Rps. acidophila (Chl *a*) [8]	660	870	8.3 ± 0.5 [4]			548–702.8 ps [a,5]; 43.7 [6]
Rsp. molischianum	790	(790–870)	1.2 [7]			1.3 [7]
	800	(790–870)	0.9 [7]			0.8 [7]
	810	(790–870)	1.0 [7]			0.9 [7]
	830	(790–870)	0.5 [7]			0.4 [7]

[a] Stokes shift 80 cm^{-1}–0 cm^{-1}; [1] Pullerits et al., 1997; [2] Kennis et al., 1997; [3] Ma et al., 1997; [4] Herek et al., 2000; [5] Linnanto and Korppi-Tommola, 2002; [6] Scholes and Fleming, 2000; [7] Ihalainen et al., 2001; [8] modified pigment at site B800 (see text)

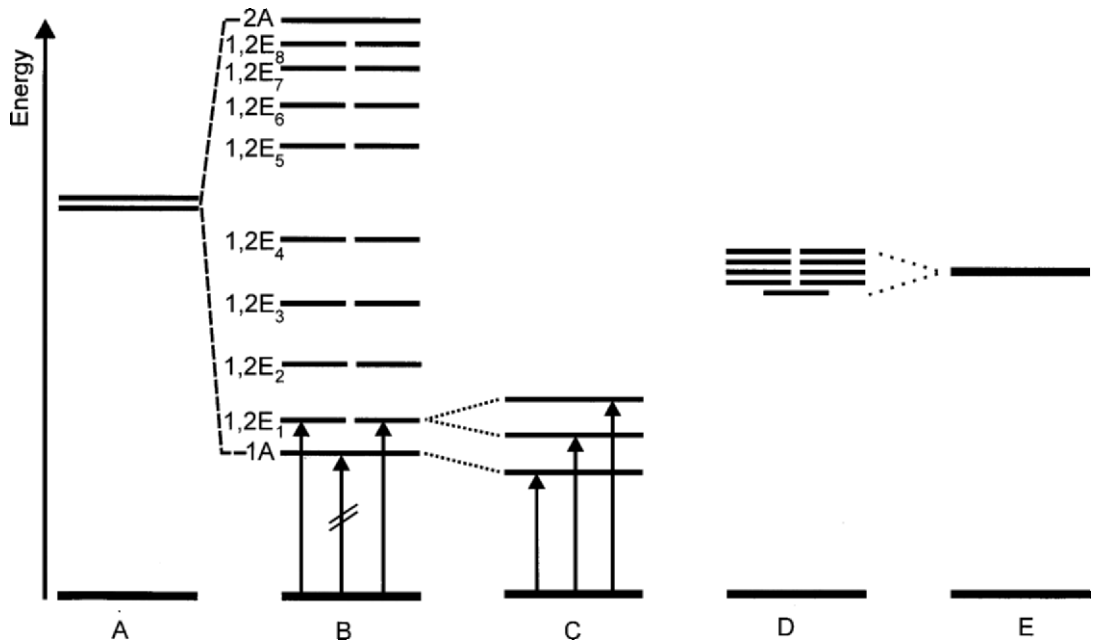

Fig. 1. Schematic representation (not to scale) of the energy level structures of the circular aggregates BChl-B800 (D) and BChl-B850 (B) consisting of 9 weakly and 18 strongly coupled BChls *a,* and of their building blocks, monomeric BChl-'B800' (E) and dimeric BChl-'B850'$_{\alpha,\beta}$ (A). Whereas (B, D) represent the perfect C_9 symmetry, the influence of disorder on the lowest three transitions in BChl-B850 is shown in (C).

Ihalainen et al., 2001) take into account interactions between all BChl in the highly symmetric (C_8, C_9) circular structures (McDermott et al., 1995, Hu et al., 1997). The B800 compartment of *Rps. acidophila* is a ring of 9 BChl *a* molecules with Mg-Mg distances of 21.2 Å and the B850 waterwheel-like compartment is a ring of 18 BChl *a* molecules with alternating distances of 8.9 and 9.6 Å. The closest BChl-BChl distances between the two rings are approximately 18 Å. There are analogous results for *Rsp. molischianum* (Ihalainen et al., 2001), where the 8 BChls *a* and 16 BChls *a* in the respective compartments are separated by somewhat smaller distances, with distinct differences in the orientation of the BChl-B800 transition dipole moments (Koepke et al., 1996).

The B850 Circular Aggregate without Disorder. In LH2 from *Rps. acidophila*, the site energies of BChl-B850$_\alpha$ and BChl-B850$_\beta$ (diagonal elements of the B850-part of the Hamiltonian) were calculated (with explicit inclusion of the binding histidine residues) to 784 nm and 779 nm, respectively (Linnanto et al., 1999). The interaction energies (off-diagonal elements) between neighboring BChl-B850 (calculated by treating them as a supermolecule) amount to 622 cm^{-1} (intra-) and 562 cm^{-1} (inter-subunit). They are larger than those obtained by calculations using point monopole-approximations (Sauer et al., 1996) or the transition density cube approximation (Krueger et al., 1998). The exciton level manifold including also dipole-dipole interactions of non-neighboring BChl-B850 in a perfect circular arrangement, is given in Fig. 1, with each energy level representing a coherent superposition of individual BChl excitations. The optically-allowed transitions terminate in the degenerate 1,2E$_1$ state (main transition at 862 nm) and the 2A-state (weak transition at 719 nm). The dipole moment of the former is enhanced by a factor of about $\sqrt{9}$, compared to monomeric BChl *a,* but the excitation density is identical at all 18 BChl *a*-sites, predicting an (initial) exciton delocalization over the entire ring. The results are remarkable with respect to EET: i) the lowest excited state is 'optically dark' and therefore very long-lived, which strongly reduces competition of radiative processes with EET; ii) excitation into the dominating transition(s) to 1,2E$_1$ renders the energy immediately available at each site of the entire B850 ring; iii) there is a large overall splitting of the energy levels ('exciton splitting') of more than 2000 cm^{-1}, which should accelerate B800-B850 as well as the carotenoid-to-B850 EET (see below and Chapter 30,

Koyama and Kokitani); and, iv) interactions between BChl-B800 and BChl-B850 are very weak.

Considering these predictions that are based on the C_9 symmetry and assuming no disorder, it is interesting to look at some experimental data. B800-depleted LH2 have been studied from *Rba. sphaeroides* (Bandilla, 1995; Bandilla et al., 1998; Koolhaas et al., 1998; Leupold et al., 1999b) and *Rps. acidophila* (Herek et al., 2000). The properties of their 850 nm-bands are almost identical to wild type (WT) complexes; that is, the influence of BChl-B800 is negligible (Bandilla, 1995; Koolhaas et al., 1998; Nowak, 1999; Leupold et al., 1999b; Herek et al., 2000). The B850 bands of both samples show clear indications of disorder (Nowak, 1999; Leupold et al., 2000). Steady state and ultrafast kinetic absorption data indicate an even larger exciton splitting (and/or exciton-vibronic manifold) than calculated, and suggest non-negligible higher-energy transitions of BChl-B850 around 800 nm (Koolhaas et al., 1998; Leupold et al., 1999b; Herek et al., 2000).

The B800 Circular Aggregate without Disorder. Linnanto et al. (1999) calculated a Q_y transition at 797 nm for monomeric BChl-B800 of *Rps. acidophila,* including 9 neighboring amino acid residues, part of the carotenoid and the phytyl chain of the closest BChl-B850. Using a similar approach, Ihalainen et al. (2001) obtained a value of 798 nm for LH2 from *Rsp. molischianum*. These values are considerably red-shifted compared to BChl in any polar solvent (e.g., 786 nm in quinoline; Limantara et al., 1997), suggesting the presence of special pigment-protein interactions like H-bonding to the 3-acetyl-group (Sturgis and Robert, 1996; Hu et al., 2002), steric distortions or axial ligation (Hu et al., 2002); therefore, explicit inclusion of the protein environment in the calculation of the BChl-B800 site energy is essential (Scholes et al., 1999). When applied to LH2 with exchanged B800-pigments (Table 1; Herek et al., 2000), environment-induced red-shifts are observed for all but one substitute pigment (Chl *a*). Assuming that the latter lacks specific protein interactions, its Q_y absorption maximum can be used to determine a refractive index of n = 1.59 at the B800 binding site (Eichwurzel et al., 2000; I. Eichwurzel, unpublished).

Using these Q_y energies as diagonal elements of the B800-part of the Hamiltonian and off-diagonal interaction energies of 30–40 cm^{-1}, as calculated according to the point-dipole model, a (disorder-free) C_9-symmetric B800 energy-level is obtained with only half of the level numbers as for B850, and a much closer spacing (excitonic splitting <100 cm^{-1}) (see Fig. 1). Again, the most intense radiative transition from the ground state is that to the lowest pair of degenerate E levels (λ_{max}=799 nm) (Linnanto et al., 1999).

B800-B850 Interactions. Including BChl *a* interring interactions (≤30 cm^{-1}) reduces excitonic splitting of the Q_y manifold of BChl-B800, while slightly increasing that of neighboring BChl-B850 levels (Linnanto et al., 1999), predicting a small red-shift of B850 in LH2, compared to the BChl-B800 depleted pB850. Experimental results for the disordered systems of native complexes are in agreement with this prediction: namely a red-shift of 2 nm for *Rba. sphaeroides* (Leupold et al., 1999b).

Consequences of Deviations from Highly Symmetric Circular Structures. For a simulation of the optical properties of single LH2 complexes (van Oijen et al., 1999; Chapter 21, Köhler and Aartsma), homogeneous broadening and intra-aggregate disorder have to be considered. Corresponding simulations for LH2 ensembles must additionally include inter-aggregate disorder:

i) Variations of the BChl environment in the circular aggregate may result in a Gaussian distribution of Q_y energies (diagonal disorder) while symmetry is conserved, resulting in non-negligible oscillator strengths in higher — originally forbidden — transitions (among them 1A). The respective absorption bands become increasingly inhomogeneously broadened (Hu et al., 1997).

ii) Variations of BChl *a* positions and orientations along the circular aggregate result in changes of interactions (off-diagonal disorder) and give rise to similar changes, but should be of minor importance (Wu and Small 1997, 1998).

iii) Elliptical deviations from perfect circular arrangements were invoked from low-temperature fluorescence excitation spectra of single LH2 complexes (van Oijen et al., 1999; Chapter 21, Köhler and Aartsma), causing a split of the B850 Q_y-band into two sub-bands (Matsushita et al., 2001; Hu et al., 2002; for an analysis of intra- and inter-aggregate disorder, see Mostovoy and Knoester, 2000).

iv) For 'broken' rings a lift of level degeneracy

would also be expected. In this case, the oscillator strength would not be symmetrically distributed to the two sub-bands (van Oijen et al., 1999).

Experimentally, intra-aggregate disorder is evident for B800: several narrow bands around 800 nm are seen in single-complex spectra of LH2 from *Rps. acidophila* at 1.2 K, while the B850 Q_y band consists (in most cases) of two broad sub-bands of unequal intensities (interpreted as an elliptical deformation, van Oijen et al. 1999; Matsushita et al., 2001; Chapter 21, Köhler and Aartsma). Remarkably, such double-band substructure has also been resolved for ensemble-averaged B850 in LH2 from *Rba. sphaeroides* at room temperature using nonlinear polarization spectroscopy in the frequency domain (NLPF), indicating that intra-aggregate disorder is small (Leupold et al., 2000). This would argue for a relatively uniform degree of ellipticity in the B850 ensemble. There is no such substructure in the C_8-symmetric LH2 of *Rsp. molischianum* (Leupold et al., 2000).

Optical Properties Derived from the LH2 Q_y Exciton Model. To simulate the Q_y absorption and the CD spectrum of LH2, homogeneous broadening has to be considered (Linnanto et al., 1999; Ihalainen et al., 2001). The results obtained for *Rps. acidophila* (Linnanto et al., 1999; Linnanto and Korppi-Tommola, 2000) and for *Rsp. molischianum* (Ihalainen et al., 2001) appear to be promising. In particular, the maxima and shapes of the two Q_y absorption bands as well as the main features of the circular dichroism (CD) spectra are relatively well reproduced. Also well reproduced is the red-shift of the CD zero-crossing with respect to the absorption maximum, and the CD fine structure in the 800 nm region resulting from overlap of B800 and higher excitonic B850 contributions (Bandilla, 1995; Koolhaas et al., 1997; Bandilla et al., 1998).

b. Excitation Energy Transfer B800 → B850

The excitonic energy level systems of BChl-B800 (Donor) and BChl-B850 (Acceptor) have been used to calculate EET rates according to Fermi's Golden Rule (Linnanto and Korppi-Tommola, 2000; Ihalainen et al., 2001). Spectral overlap of D and A exciton states with pump and probe pulses has been considered. For comparison with the experimental rates, the resulting distribution of EET rates is fitted by triple exponentials (Table 1). Remarkably, the calculated EET rates are not lower, but actually somewhat higher than the experimental values. In LH2 from *Rps. acidophila*, the 'dark states' $1,2E_2$, $1,2E_3$ of B850 located in the gap between $3,4E_1$ of B800 and $1,2E_1$ of B850 (Fig. 1), play an essential role. For LH2 of *Rsp. molischianum*, only $1,2E_2$ are in that gap, which is in agreement with the somewhat slower EET (Ihalainen et al., 2001).

Using the same method (CIEM), the effect of exchanging the BChl *a* of the B800 ring by modified pigments (Bandilla, 1995; Bandilla et al. 1998; Fraser et al., 1999) has also been investigated (Linnanto and Korppi-Tommola, 2002). The energetic positions of the shifted 800 nm-absorption bands (Herek et al., 2000) are well reproduced by the calculations, but the calculated EET rates from the modified pigments to BChl-B850 are still too slow (Table 1). The same discrepancy in EET rates was obtained using the transition density cube approach (Scholes and Fleming, 2000), and has been discussed by these authors and also by Linnanto and Korppi-Tommola (2002).

In their Förster-type calculation of EET rates for modified B'800' → BChl-B850, Herek et al. (2000) obtained a perfect qualitative reproduction of the diminished rates after introducing different pigments, but with a constant deviation by a factor of five. These calculations were based on a monomeric Q_y-transition dipole for the acceptor, BChl-B850. From nonlinear absorption measurements, however, the Q_y-transition dipole moment of BChl-B850 has been determined to be ≈ 25 D (Leupold et al., 1996; Stiel et al., 1997), reflecting the high degree of initial exciton delocalization in B850: the transition dipole moment scales with the square root of the pigment number (N_{del}) over which the exciton is delocalized, resulting in $N_{del} = 14 \pm 6$ for LH2 from *Rps. acidophila* (Stiel et al., 1997) and 16 ± 4 for the *Rba. sphaeroides* complex (Leupold et al., 1996). Recently, Book et al. (2000) determined a comparably high initial coherence length for LH2 from *Rba. sphaeroides* ($N_{del} \approx 13$) and asserted that *it is this delocalization length which is relevant to the energy transfer process* (Kimura and Kakitani, 2003). These enhanced transition dipoles would enlarge the EET rates by more than one order of magnitude; that is, the calculated EET would now become even too fast. However, the spatial extent of the charge distribution is non-negligible under these conditions and the point-dipole approximation may not be appropriate for EET modeling (Book et al., 2000). Moreover, the usual assumption of 700 fs for complete excited electronic state-thermalization in

BChl-B800 prior to EET, as a pre-condition for the validity of the Förster-based reasoning, remains to be confirmed (Ma et al., 1997). Results with dissolved BChl *a* (Book et al., 2000) suggest a cautious interpretation; possibly, the theory of intermediate EET (Kimura et al., 2000) is more appropriate for the EET process BChl-B800 → BChl-850.

EET from BChl-B850 of LH2 may occur either to another BChl-B850 or to BChl-B875 of LH1. For the latter process, a time constant of 4.6 ± 0.3 ps has been determined at room temperature in a mutant of *Rba. sphaeroides* lacking the RC. A second time constant of 26.3 ± 1.0 ps has been attributed to excitation migration in the LH2 pool preceding EET to LH1. Back transfer BChl-B875 → BChl-B850 has not been observed (Nagarajan and Parson, 1997). For a single LH2 → LH2 EET step, a calculated value of 10 ps still awaits experimental verification (Hu et al., 2002).

C. The Core Antenna Complex, Light Harvesting Complex 1

For BChl-B870 in LH1 of purple bacteria, a waterwheel-like closed circular arrangement has been assumed, analogous to that of BChl-B850 of LH2; however, it has a larger diameter and binds up to 34 pigments per RC all located in the center of the ring. This model is based on the low-resolution structure of LH1 (Karrasch et al., 1995) and of LH1-RC complexes from strains lacking the PufX protein (Walz et al., 1998). For such BChl arrangements, exciton spectra and dynamics can be expected which are largely comparable to B850. Indeed, the steady state spectroscopic properties of LH1 from *Rsp. rubrum*, in which up to 90% BChl *a* was replaced with Zn-BPhe, could be simulated by altering merely dipole strengths and maintaining nearest-neighbor interactions (400 cm^{-1}) and diagonal disorder (600 cm^{-1}) similar to those of LH2 (Wendling et al., 2002). The recent, somewhat 'spiral-shaped' structure of LH1 in a core complex still awaits theoretical interpretation, but like any deviation this is expected to influence the exciton level structure (Roszak et al., 2003).

A smaller unit size of 20 BChls has been determined for PufX-containing LH1 from *Rba. sphaeroide*s, in which a fraction of the native BChl *a* had been replaced by Ni-BPhe *a,* from 40 fs pump-probe experiments within the 875 nm band (Fiedor et al., 2000); this was also confirmed by fluorescence yield and decay measurements (Fiedor et al., 2001). This relatively small unit size agrees with the suggestion that PufX may interrupt ring formation (Cogdell et al., 1996). Remarkably, substitution of just one out of the twenty BChls *a* by Ni-BPhes is sufficient to induce a monoexponential 60 fs-ground state recovery, by-passing the fluorescent level which in native LH1 is populated within 750 fs after Q_y-excitation (Fiedor et al., 2000). In a similarly substituted LH1-RC system, the EET BChl-B875 → RC would be completely inhibited. Further, a single quencher pigment within a LH1-RC complex, such as a BChl cation radical (Law and Cogdell, 1998), would also suffice to prevent ISC. Varying oligomer sizes up to 10 or 11 αβ-heterodimers in LH1 from the PufX-containing M21 strain of *Rba. sphaeroides,* which lacks LH2, has only a minor effect on the Q_y absorption maximum (Westerhuis et al., 2002).

EET from LH1 to the RC occurs in about 25 ps at RT and, remarkably, the back transfer is about three times faster. Because the initial electron transfer step in the RC occurs in 3 ps, trapping and photoprotection of an already closed RC is efficient (Hu et al., 2002).

III. Excitation Energy Transfer in Light-Harvesting Complex II-type Complexes of Higher Plants

Higher plants possess complex light-harvesting antenna systems for both Photosystems I and II (PS I and PS II). Most abundant is the peripheral LHC II, which binds Chl *a* and *b*, and is associated mainly with PS II. LHC II consists of trimers of closely related proteins, Lhcb1-3, which are members of a large protein family also including the monomeric minor PS II antenna complexes CP29, CP26, CP24 (alternatively designated Lhcb4, Lhcb5 and Lhcb6), as well as Lhca1-4 of PS I, and the Chl *a/c* containing complexes from heterokont algae (Jansson, 1994). Recently the structure of pea PS I including the Lhca1-4 proteins has been solved to 4.4 Å, confirming the proposed structural similarities of these proteins to LHC II and their pairwise, Lhcb1/4 and Lhcb2/3 dimer-formation (Ben-Shem et al., 2003).

The extent of excitonic interactions between Chls and their significance for EET in these LHC is much less clear-cut than for those of purple bacteria: i) the arrangement of the chromophores (Kühlbrandt et al., 1994; Liu et al., 2004; Standfuss et al., 2005) is considerably less symmetric; ii) the previously

available resolution (3.4 Å) could not distinguish between Chls *a* or *b* (Kühlbrandt et al., 1994). An assignment, based on an assumed necessity of triplet quenching by the two central luteins (Kühlbrandt et al., 1994), was only partly verified by mutagenesis (Bassi et al., 1999; Remelli et al., 1999; Rogl and Kühlbrandt, 1999; Rogl et al., 2002; Chapter 26, Paulsen). As a further complication, promiscuous binding sites (occupied by Chl *a* or *b*) have been proposed (Bassi et al., 1999; Remelli et al., 1999; reviewed by van Amerongen and van Grondelle, 2001; but see also Rogl and Kühlbrandt, 1999; Rogl et al., 2002); iii) orientations of the Chl transition dipole moments remained unresolved in the 3.4 Å Kühlbrandt-model; and, iv) neither the site energies of the individual and/or coupled pigments are known, nor the refractive index of the pigment-surrounding medium at the respective binding sites (see below). Hence, calculations of excitonic interactions as well as EET rates between pigments have been controversial (Kühlbrandt et al., 1994; Voigt et al., 1996; Trinkunas et al., 1997; Gradinaru et al., 1998; Renger and May, 2000; Iseri and Gülen, 2001; van Amerongen and van Grondelle, 2001).

Excited state kinetics in LHC II are multiphasic with lifetimes ranging from a few 100 fs to several ns (Eads et al., 1989; Palsson et al., 1994; Bittner et al., 1994, 1995; Kleima et al., 1997; Gradinaru et al., 1998; summarized in Table 2). The fastest EET step (about 200 fs) occurs from Chl *b* to Chl *a* within the monomeric subunits (Kleima et al., 1997), but it has not yet been established whether its nature is excitonic or incoherent hopping-type (Leupold et al., 1999a). Close packing of the pigments and recent nonlinear laser-spectroscopic studies (Krikunova et al., 2002; Leupold et al., 2002; Schubert et al., 2002; Voigt et al., 2002) render strong excitonic interactions among certain Chls in LHC II and related complexes highly likely, but their extent is still controversial, as well as any consequences thereof for EET.

Most work on EET has been interpreted in the framework of the Förster-formalism. Simulations of ultrafast transient absorption in CP29 did not agree with the experimental data. Instantaneous bleaching in the spectral region of the pumped Chl *b* (640 nm) and, *simultaneously* of Chl *a*, can not be explained by Förster-type EET (Cinque et al., 2000). The ultrafast EET steps, observed in one- and two-color pump and probe experiments (Bittner et al., 1994, 1995), are now explained by excitonically coupled Chl *a/b* heterodimers (Renger and May, 2000).

Table 2. Experimentally observed EET time constants (in ps) in LHC II and CP29 (adapted from Gradinaru et al., 1998)

λ_{pump} [nm]	λ_{probe} [nm]	LHC II	CP29
640	678	0.3; 1	0.35
650	670–676	≤0.2, 0.5, 2–6	2.2
660–670	670–680	0.3–0.4	0.3
670	678	10–20	10–13

An early exciton calculation concluded that the lowest excited state in LHC II carries almost no excitonic character (Voigt et al., 1996): the calculated dipole strength was only 1.16 times that of monomeric Chl *a*, whereas that of the next higher state was twice as strong. Trinkunas et al. (1997) were able to model, by the Förster-formalism, the transient absorption data of Connelly et al. (1997) as well as steady state spectroscopic data obtained with LHC II. The latter was only possible if two Chl *a* (a1 and a2; Kühlbrandt et al., 1994) were swapped for Chl *b* (which is not in agreement with mutagenesis studies). More recently, it has been shown theoretically that the lowest excited state has significant excitonic character but with a dipole strength only 0.5 times that of Chl *a* (Renger and May, 2000). A somewhat larger value (0.8) was derived from hole-burning experiments (Pieper et al., 1999). Van Amerongen and van Grondelle (2001) used the pigment assignment of Remelli et al. (1999) to calculate excitonic interactions and EET rates, concluding that the lowest excited state is essentially localized on a single Chl *a*. Such a value (1.18) was corroborated in a study of super-radiance (Palacios et al., 2002). However, exciton delocalization is expected to be strongly time-dependent (Dahlbohm et al., 2001), and steady-state super-radiance measurements may yield only the final value after thermalization. From a two-pulse photon echo study it was also concluded that the long wavelength Chls *a* in LHC II are only weakly coupled (Hillmann et al., 2001).

Early experimental indications for strong excitonic interactions in LHC II and related complexes are based on the high optical activity (Ide et al., 1987; Hemelrijk et al., 1992). However, distortions of the Chl macrocycle may also lead to strong CD (Wolf and Scheer, 1973).

Recent non-linear absorption and intensity-dependent NLPF work favors strong excitonic interactions in LHC II: Both experiments indicated that a spectral form emitting at 682 nm has a dipole strength twice that of monomeric Chl *a* (Schubert et al., 2002).

The most obvious explanation for the enhancement is excitonic interaction between the Chl molecules forming the terminal emitter. These experiments could not distinguish between a homo- (Chl *a*/Chl *a*) or a hetero-dimer (Chl *b*/Chl *a*). A special variant of the NLPF-technique was employed to assess heterodimeric interactions in LHC II (Krikunova et al., 2002). NLPF-spectra are pumped in a low-energetic band, and probed in a (spectrally well separated) higher-energetic absorption band. Remarkably, Chl *a* excitation in the Q_y region resulted in a NLPF-response in the higher-energy Chl *b*-Soret-region, which appears to be explained only by strong excitonic coupling between certain Chls *a* and *b*. Strong Chl *a/b* interactions were also inferred from NLPF experiments with the structurally-related antenna complex, CP29 (Voigt et al., 2002). There are, nonetheless, marked differences between both complexes: whereas in LHC II the lowest energy Chl *a* (~678 nm) appears to be strongly coupled to Chl *b*, the red-most Chl-form in CP29 was attributed to a non-coupled Chl *a* (Pieper et al., 1999; Voigt et al., 2002). The strongly interacting pigments in CP29 appear to be a Chl *a* absorbing at 670 nm and a Chl *b* absorbing at 640 nm. These observations are consistent with the assignment of the longest wavelength band in LHC II to Chl a2 (Remelli et al., 1999; Rogl and Kühlbrandt, 1999; Rogl et al., 2002): Chl a2 is closest to Chl 'b2' at a binding site which is apparently lacking in CP29. The different character of the lowest-energy transition in LHC II and CP29 is corroborated by studies both at low (Pieper et al., 1999) and ambient temperatures (Leupold et al., 2002). Stepwise two-photon excitation with 100-fs pulses in the Q_y-region of Chl *a* and *b* elicits a weak 'blue' fluorescence of considerably different character (Leupold et al., 2002). The blue emission profiles of LHC II are virtually identical (peaking at about 475 nm) when exciting in the Chl *a* (680 nm) or Chl *b* (650 nm) range: this is consistent with strong Chl *a*/*b* coupling. By contrast, two different peaks are observed in CP29 upon excitation of Chl *a* (at 450 nm) and Chl *b* (at 475 nm).

From the above results and previous site-directed mutagenesis studies on LHC II (Remelli et al., 1999; Rogl and Kühlbrandt, 1999; Rogl et al., 2002), we suggested that Chl a2 (Kühlbrandt et al., 1994) is involved in the proposed excitonic pigment cluster (Fig. 2) (Schubert et al., 2002). The distance to the nearby Chl 'b2' (8 Å) was the closest of all mutual Chl-Chl distances determined in pea LHC II (Kühlbrandt et al., 1994).

Very recently the structure of spinach LHC II was solved by X-ray crystallography to <3 Å (Liu et al., 2004; Standfuss et al., 2005). The considerably refined structure confirmed many previously observed features (Kühlbrandt et al., 1994) but also revealed important hitherto unknown details: Two additional Chls (Chls *b* 601 and 605, in the nomenclature of Liu et al., 2004) were detected. All Chls *a* and *b* could be identified directly. Thus, two 'Chls *b*' (previously

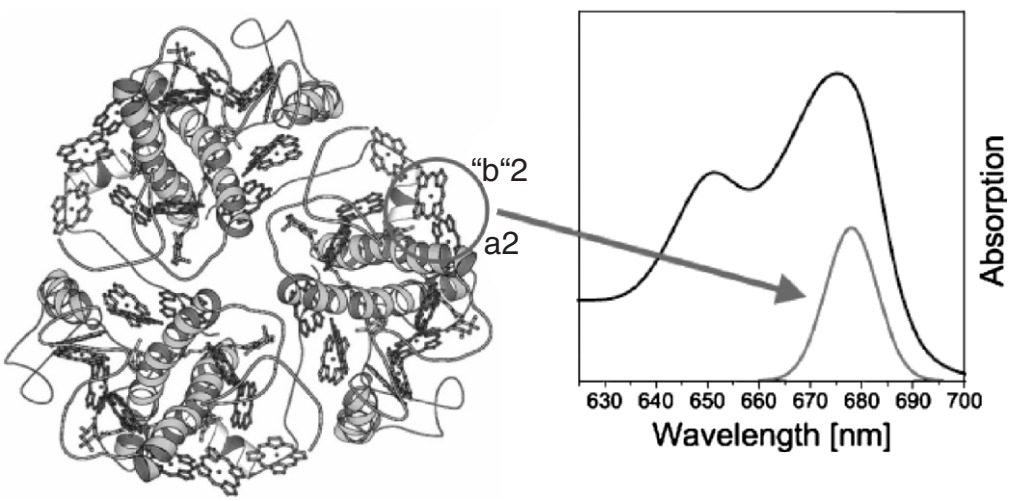

Fig. 2. Structure (left, adapted from Rogl et al., 2002) and absorption spectrum (solid line, right) of LHC II. The red-most excitonic transition (peaking at 678 nm, dashed line, right) can be assigned to a cluster involving the pigment binding sites a2 and 'b'2 in the structural model of LHC II (but compare also the recent, refined structures of Liu et al., 2004; Standfuss et al., 2005). See also Color Plate 7.

designated b2, now: 611 and b3 now: 614) had to be re-assigned as Chl *a*. One 'Chl *a*' (a7 now: 607) had to be swapped for Chl *b*. No indication of promiscuity of the binding sites was found. Orientations of the transition dipole moments of all Chl were identified. Thus, more reliable estimates of excitonic interactions strength between individual pigments could be given (Liu et al., 2004; see supplementary information): Strong excitonic coupling is inferred for Chl *a* 611/612 (a2/'b2') as well as at least two Chl *a/b*-pairs: Chl *a* 604 (a6)/*b* 611 (b6) and Chl *a* 603 (a5)/*b* 609 (b5). Thus, our predictions, from nonlinear laser-spectroscopic studies on excitonic interactions between Chls *a* and *a* as well as Chls *a* and *b* in LHC II, are confirmed by the structural data of Liu et al. (2004). Based on this refined, atomic level structure of LHC II much deeper insight into light harvesting in plants can be expected for the near future.

The Chl *a* 611/612 (a2/'b2') pair (possibly involving interactions with further nearby pigments), is located on the outer surface of LHC II, also in its trimeric form (Fig. 2). Its red-shifted absorption renders it a 'relay state' (for EET to neighboring complexes) of LHC II. Additionally, the enhanced dipole moment may 'attract' excitations from inside the complex to the surface. This would contribute to the efficiency of light-harvesting in an extended PS II antenna-network, because Chl a2 are the most closely spaced pigments in adjacent LHC II trimers.

IV. Excitation Energy Transfer in Chlorosomes

Chlorosomes occur in both green filamentous- (designated F-chlorosomes) and green sulfur-bacteria (S-chlorosomes). Among LHCs, these extremely large, extra-membranous structures are unique and their function, almost exclusively, appears to result from pigment-pigment interactions: the protein content of chlorosomes is generally very low (Olsen, 1998), and chlorosomes devoid of any protein exhibit nearly the same spectroscopic properties as those containing protein. However, the CD spectra of such isolates are quite variable (Griebenow and Holzwarth, 1989) and proteases induce distinct changes (Niedermeier et al., 1992); the function of the remaining proteins is therefore still unclear (Chapters 15, Frigaard et al., and 20, de Boer and de Groot). Chlorosomes consist of a core and an envelope. The core contains several thousand molecules of BChl *c, d* or *e* (depending on the species), which are organized in 10–30 (but see also Niedermeier et al., 1992) parallel tubular structures called rod elements (Blankenship et al., 1995; Olsen, 1998). Rod diameters and lengths are about 5 nm and 100 nm, respectively, for F-chlorosomes, or 10 nm and 180 nm, respectively, for S-chlorosomes (Olsen, 1998).

BChls within the rods are strongly excitonically coupled, but there is also non-negligible nearest-neighbor inter-rod interaction. Otherwise, a spectroscopic behavior would be expected that is comparable to that of the well-known J-aggregates (Buck and Struve, 1996; Bednarz and Knoester, 2001), with most of the dipole strength concentrated in the lowest transition. This, however, is not the case with chlorosomes: absorption spectra, the large Stokes-shift of fluorescence and hole-burning spectra all indicate that the lowest exciton band carries only a few percent of the total dipole strength of the Q_y transition, while transitions to higher exciton levels are strongly allowed. From pump-probe (Savikhin et al., 1998a) and temperature-dependent fluorescence spectra (Mauring et al., 1999), a tubular aggregate model has been developed for F-chlorosomes. The unit BChl *c* building block comprises 24 strongly coupled BChls *c*, arranged in six parallel chains of four BChls *c*: the maximum inter-chain interaction of 44 cm^{-1} is equal to about one tenth of intra-chain nearest-neighbor interaction energy (Yakovlev et al., 2002). For comparison, a cluster size of 16 BChls *c* has been derived from the EPR line width of partly oxidized F-chlorosomes (van Noort et al., 1997). The individual exciton wave functions are delocalized over 7–12 BChl *c* molecules, and the coherence size of the steady state exciton wave packet is 7.4 BChl *c* (Yakovlev et al., 2002; for definitions, see Fidder et al., 1991; Meier et al., 1997). Much larger delocalization lengths have been recently reported by Holzwarth and Prokhorenko (2002). Their model (Holzwarth and Schaffner, 1994; Prokhorenko et al., 2000; Chapter 20, de Boer and de Groot) has a higher pigment packing density (36 chains per rod of S-chlorosomes of *Chlorobium (Chl.) tepidum*) than the model of Yakovlev et al. (2002), resulting in high intra-stack (-chain) as well as inter-stack interaction energies (about 500 cm^{-1} and 200 cm^{-1}, respectively).

F-chlorosomes are attached to the cytoplasmic membrane via a baseplate containing monomeric BChl *a* (B795) which is essential for EET to the RC. Within the Q_y-band of F-chlorosomes, relaxation from

the high-energy exciton levels is multiphasic with times between sub-ps to several ps, probably reflecting faster intra-rod processes and slower inter-rod exchange. These processes are temperature-dependent, as is the final step from the lowest BChl *c* Q_y exciton-level to the base plate BChl *a*, which takes about 50 ps at low temperatures and 10–20 ps at RT (Prokhorenko et al., 2000 and references therein).

EET from S-chlorosomes to the RC also occurs via a base plate; however, these EET kinetics are dependent not only on temperature but also on redox potential. At high (positive) redox potential, the chlorosomal Q_y lifetime is shortened and EET to the base plate BChl *a* is strongly reduced. A similar redox dependence has been observed for the subsequent EET steps in green sulfur bacteria, thereby shortening, for example, the Q_y lifetime in the FMO complex (see reviews by Olsen, 1998 and Psencik et al., 1998)

V. Excitation Energy Transfer in the Fenna-Matthews-Olsen (FMO) Complex

The FMO complex of green sulfur bacteria is a trimeric, water-soluble pigment-protein complex carrying 7 BChl *a* in each monomeric subunit. In the EET chain, it links the chlorosome and the RC. The spatial arrangement of the 7 BChl *a* in the monomer, and the mode of their attachment to the protein matrix, are known at a resolution of 1.9 Å (Fenna and Matthews, 1975; Tronrud and Matthews, 1993; Li et al., 1997). Yet, only recently has a detailed picture of the structure-function relationship emerged. Both pigment-pigment and pigment-protein interactions contribute to the absorption band substructure and EET processes and, in particular, the latter are theoretically not well understood (Pearlstein, 1992; Savikhin et al., 1998b, 1999). The 7 BChl *a* in the monomeric subunit are 'irregularly' arranged (as in LHC II), with nearest neighbor Mg-Mg distances between 11 and 15 Å. Therefore, significant transition-dipole interaction can be expected, as reflected by a redistribution of oscillator strengths and energetic shifts of the 7 Q_y transitions of the BChls at the seven different sites and, also, by large CD signals (Savikhin et al., 1998b, 1999). The closest distance between BChls in different subunits of the trimer is about 24 Å, the maximum inter-monomer coupling strengths (10–20 cm^{-1}, depending on the model) are about one order of magnitude smaller than intra-monomer couplings (100–190 cm^{-1}) (Pearlstein, 1992; Vulto et al., 1998a; Iseri and Gülen, 1999; Wendling et al., 2002). It is expected, therefore, and largely confirmed, that the essential FMO structure-function relations are dominated by the properties of the monomer.

At room temperature, neither the Q_y-absorption (λ_{max} = 809 nm) nor the CD show fine structure. They become well-structured, however, at 77 K: Philipson and Sauer (1972) resolved 5 bands for FMO from *Prostecochloris (Ptc.) aestuarii*. Hole-burning studies at temperatures of a few K gave 8 excitonic components (Johnson and Small, 1991), which is one component more than expected for pure intra-monomer BChl interaction and strict C_3-symmetry with identical micro-environments for corresponding BChl sites in all three subunits. A further component has been resolved and the three lowest-energy components have been attributed to the lowest Q_y states in each of the three non-equivalent monomers (Rätsep et al., 1999). These data have been complemented by absorption, linear dichroism, CD and transient spectra (Savikhin et al., 1998b, 1999; Vulto et al., 1998a; Wendling et al., 2002)

Earlier simulations of the Q_y structure of FMO trimers from *Ptc. aestuarii* resulted in seven groups of exciton levels in the range between 775 and 825 nm (Pearlstein, 1992; Lu and Pearlstein, 1993). In each group, the excitation density is distributed (unevenly) over several BChls, but mostly localized at one or two sites ('mini-excitons'). Refined calculations reproduced distinctly different spectral characteristics between FMO from *Chl. tepidum* and *Ptc. aestuari*, in spite of largely identical pigment arrangements (Gülen, 1996; Louwe et al., 1997, Vulto et al., 1998a,b). Calculations have concentrated on monomers, yielding, consequently, seven exciton levels. They suggest, that spectral differences are due to different energies of the BChls at the seven binding sites, possibly related to differences in hydrogen bonding and planarity of the porphyrin rings (Vulto et al., 1998a,b). Unfortunately, these site energies are adjustable parameters in the calculations. They are, currently, neither available experimentally nor from quantum chemical calculations which take into account the protein micro-environment (the latter, however, has been obtained for BChl-B800 in LH2; Linnanto et al., 1999; see above). Other refinements, for example, the inclusion of broadening mechanisms, are already available and have given additional evidence for inter-monomer interactions (Wendling et al., 2002).

There seems to be consensus that after excitation to the highest exciton level, energy relaxation to the

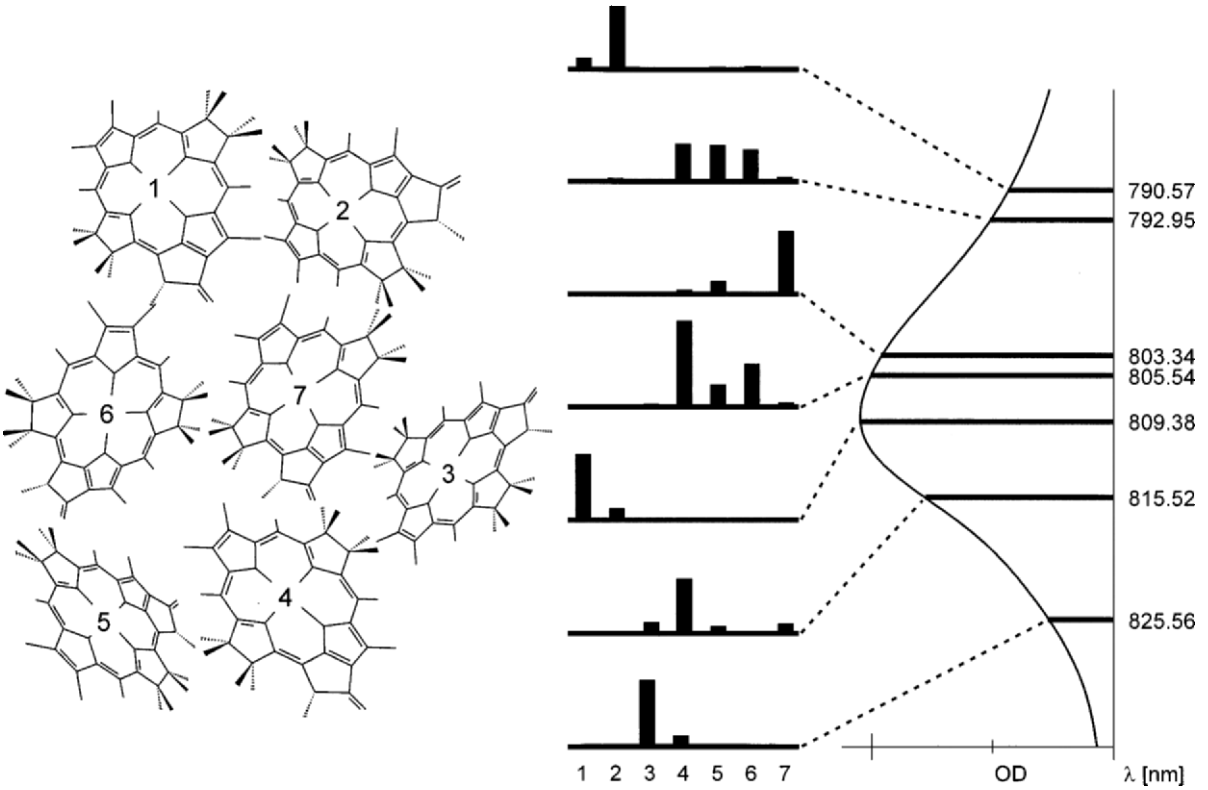

Fig. 3. Simplified projection of the BChl *a*-arrangement in the monomeric subunit of the FMO-complex (left). Room temperature absorption spectrum of the FMO-complex (Q_y-range, right). Exciton levels and corresponding excitation densities at the seven pigment sites (center) are adapted from Vulto et al. (1998a).

second-highest level in several tens of fs is the fastest process in a, possibly branching, cascade down to the lowest level, with time constants gradually increasing up to few ps (Savikhin et al., 1998b, 1999; van Amerongen et al., 2000). As the exciton levels in the relaxation cascade can be linked to defined pigment sites (mini-excitons), the fs/ps time course of EET can be represented in the structural picture as rapidly varying excitations of defined BChls (see Fig. 3 for a preliminary representation). There is an emerging consensus that the final site, preceding EET to the RC, is a BChl in the core of the subunit (site 3) (Vulto et al., 1998a; Owen and Hoff, 2001; Wendling et al., 2002).

Note Added in Proof

Recent experimental results with LH2 of purple bacteria highlight the contribution of exciton transitions to the 'blue absorbance tail' (at around 800 nm) of B850: Hole-burned absorption and line-narrowed fluorescence spectra at 5 K indicate that in *Rba. sphaeroides* more than 2/3 of this 'blue absorbance tail' are of excitonic nature, only the remainder belongs to dysfunctional BChl *a* (Rätsep et al., 2005). Whereas the exciton structure of the blue tail is interpreted by the authors as result of off-diagonal disorder, single-molecule spectroscopy (at 1.4 K) of B850 from *Rps. acidophila* led to the conclusion, that random and correlated diagonal disorder — rather than off-diagonal — dominates (Hofmann et al., 2004).

Structural features of LHC II (Liu et al., 2004) were confirmed at even higher (2.5 Å) resolution (Standfuss et al., 2005). The 2.72 Å data were used to generate a sophisticated excitonic model of EET in LHC II (Novoderezhkin et al., 2005) confirming the predicted excitonic clusters and their relevance for inter-complex EET.

FMO of *Chl. tepidum* was studied by femtosecond two-dimensional heterodyne-detected three-pulse photon echo spectroscopy at 77 K (Brixner et al., 2005). The theoretical analysis revealed the following non-cascading energy relaxation pathways between

the 7 excitonic levels (see also Fig. 3): 7→3→2→1; 6→5 and from level 5 two parallel channels (→4→2→1 and →2→1).

Acknowledgments

The authors gratefully acknowledge support by the Deutsche Forschungsgemeinschaft: SFB 429 TP A2, D.L. and H.L.; and SFB 533 TPA6, H.S.).

References

Bandilla M (1995) Rekonstruktion der Antennen B875 und B850 aus *Rhodobacter sphaeroides* 2.4.1. mit Eintausch chemisch modifizierter (Bacterio-)Chlorophylle. PhD Thesis, University of Munich

Bandilla M, Ücker B, Ram M, Simonin I, Gelhaye E, McDermott G, Cogdell RJ and Scheer H (1998) Reconstitution of the B800 bacteriochlorophylls in the peripheral light harvesting complex B800-850 of *Rhodobacter sphaeroides* 2.4.1 with BChl *a* and modified (bacterio-)chlorophylls. Biochim Biophys Acta 1364: 390–402

Bassi R, Croce R, Cugini D and Sandona D (1999) Mutational analysis of a higher plant antenna protein provides identification of chromophores bound into multiple sites. Proc Natl Acad Sci USA 96: 10056–10061

Bednarz M and Knoester J (2001) The linear absorption and pump-probe spectra of cylindrical molecular aggregates. J Phys Chem B 105: 12913–12923

Ben-Shem A, Frolow F and Nelson N (2003) Crystal structure of plant Photosystem I. Nature 426: 630–635

Bittner T, Irrgang KD, Renger G and Wasielewski MR (1994) Ultrafast excitation energy transfer and exciton-exciton annihilation processes in isolated light harvesting complexes of Photosystem II (LHC II) from spinach. J Phys Chem 98: 11821–11826

Bittner T, Wiederrecht GP, Irrgang KD, Renger G and Wasielewski MR (1995) Femtosecond transient absorption spectroscopy on the light-harvesting Chl *a/b* protein complex of PS II at room temperature and 12 K. Chem Phys 194: 311–322

Blankenship RE, Olsen JM and Miller M (1995) Antenna complexes from green photosynthetic bacteria. In: Blankenship RE, Madigan MT and Bauer CE (eds) Anoxygenic Photosynthetic Bacteria, pp 297–313. Kluwer Academic Publishers, Dordrecht

Book, LD, Ostafin AE, Ponomarenko N, Norris, JR and Scherer NF (2000) Exciton delocalization and initial dephasing dynamics of purple bacteria LH2. J Phys Chem B 104: 8295–8307

Brixner T, Stenger J, Vaswani HM, Cho M, Blankenship RE and Fleming GR (2005) Two-dimensional spectroscopy of electronic couplings in photosynthesis. Nature 434: 625–628

Buck DR and Struve WS (1996) Tubular exciton models for BChl *c* antennae in chlorosomes from green photosynthetic bacteria. Photosynth Res 48: 367–377

Cinque G, Croce R, Holzwarth A and Bassi R (2000) Energy transfer among CP29 chlorophylls: Calculated Förster rates and experimental transient absorption at room temperature. Biophys J 79: 1706–1717

Cogdell RJ, Fyfe PK, Barrett SJ, Prince SM, Freer AA, Isaacs NW, McGlynn P and Hunter CN (1996) The purple bacterial photosynthetic unit. Photosynth Res 48: 55–63

Connelly JP, Müller MG, Hucke M, Gatzen G, Mullineaux CW, Ruban AV, Horton P and Holzwarth AR (1997) Ultrafast spectroscopy of trimeric light-harvesting complex II from higher plants. J Phys Chem B 101: 1902–1909

Cory MG, Zerner MC, Hu X and Schulten K (1998) Electronic excitations in aggregates of bacteriochlorophylls. J Phys Chem B 102: 7640–7650

Dahlbohm M, Pullerits T, Mukamel S and Sundström V (2001) Exciton delocalization in the B850 light-harvesting complex: Comparison of different measures. J Phys Chem B 105: 5515–5524

Damjanovic A, Kosztin I, Kleinekathöfer U and Schulten K (2002) Excitons in a photosynthetic light-harvesting system: A combined molecular dynamics, quantum chemistry, and polaron model study. Phys Rev E 65 art. no. 031919

Eads DD, Castner EW, Alberte RS, Mets L and Fleming GR (1989) Direct observation of energy transfer in a photosynthetic membrane: Chlorophyll *b* to chlorophyll *a* transfer in LHC. J Phys Chem B 93: 8271–8275

Eichwurzel I, Stiel H, Teuchner K, Leupold D, Scheer H and Scherz A (2000) Photophysical consequences of coupling bacteriochlorophyll *a* with serine and its resulting solubility in water. Photochem Photobiol 72: 204–209

Fenna RE and Matthews BW (1975) Chlorophyll arrangements in a bacteriochlorophyll-protein from *Chlorobium limicola*. Nature 258: 573–577

Fidder H, Knoester J and Wiersma DA (1991) Optical properties of disordered molecular aggregates: A numerical study. Phys Rev E 95: 7880–7890

Fiedor L, Scheer H, Hunter CN, Tschirschwitz F, Voigt B, Ehlert J, Nibbering E, Leupold D and Elsaesser T (2000) Introduction of a 60 fs deactivation channel in the photosynthetic antenna LH1 by Ni-bacteriopheophytin *a*. Chem Phys Lett 319: 145–152

Fiedor L, Leupold D, Teuchner K, Voigt B, Hunter CN, Scherz A and Scheer H (2001) Excitation trap approach to analyze size and pigment-pigment coupling: Reconstitution of LH1 antenna of *Rhodobacter sphaeroides* with Ni-substituted bacteriochlorophyll. Biochemistry 40: 3737–3747

Fraser NJ, Dominy PJ, Ücker B, Simonin I, Scheer H and Cogdell RJ (1999) Selective release, removal and reconstitution of Bchl *a* molecules into the B800 sites of LH2 complexes from *Rhodopseudomonas acidophila* 10050. Biochemistry 38: 9684–9692

Georgakopoulou S, Frese RN, Johnson E, Koolhaas C, Cogdell RJ, van Grondelle R and van der Zwan G (2002) Absorption and CD spectroscopy and modeling of various LH2 complexes from purple bacteria. Biophys J 82: 2184–2197

Gradinaru CC, Özdemir S, Gülen D, van Stokkum IHM, van Grondelle R and van Amerongen H (1998) The flow of excitation energy in LHC II monomers: Implications for the structural model of the major plant antenna. Biophys J 75: 3064–3077

Griebenow K and Holzwarth AR (1989) Pigment organization and energy transfer in green bacteria. 1. Isolation of native chlorosomes free of bound bacteriochlorophyll *a* from *Chloroflexus aurantiacus* by gel-electrophoretic filtration. Biochim Biophys Acta 973: 235–240

Gülen D (1996) Interpretation of the excited-state structure of the Fenna-Matthews-Olsen pigment protein complex of *Prosthecochloris aestuarii* based on the simultaneous simulation of the 4K absorption, linear dichroism, and singlet-triplet absorption difference spectra: A possible excitonic explanation? J Phys Chem 100: 17683–17689

Hemelrijk PW, Kwa SLS, van Grondelle R and Dekker JP (1992) Spectroscopic properties of LHCII, the main light-harvesting chlorophyll *a/b* protein complex from chloroplast membranes. Biochim Biophys Acta 1098: 159–166

Herek JL, Fraser NJ, Pullerits T, Martinsson P, Polivka T, Scheer H, Cogdell RJ and Sundström V (2000) B800→B850 energy transfer mechanism in bacterial LH2 complexes investigated by B800 pigment exchange. Biophys J 78: 2590–2596

Hillmann F, Voigt J, Redlin H, Irrgang KD and Renger G (2001) Optical dephasing in the light-harvesting complex II: A two-pulse photon echo study. J Phys Chem B 105: 8607–8615

Hofmann C, Aartsma TJ and Köhler J (2004) Energetic disorder and the B850-exciton states of individual light-harvesting 2 complexes from *Rhodopseudomonas acidophila*. Chem Phys Lett 395: 373–378

Holzwarth AR and Prokhorenko V (2002) Exciton coupling and dynamics in chlorosomes and artificial aggregates. Book of Abstracts, ESF Workshop 'Femtochemistry and Femtobiology', Belek-Antalya, Turkey, 2002

Holzwarth AR and Schaffner K (1994) On the structure of bacteriochlorophyll molecular aggregates in the chlorosomes of green bacteria. A molecular modeling study. Photosynth Res 41: 225–233

Hu X, Ritz T, Damjanovic and Schulten K (1997) Pigment organization and transfer of electronic excitation in the photosynthetic unit of purple bacteria. J Phys Chem B 101: 3854–3871

Hu X, Ritz T, Damjanovic A and Autenrieth F (2002) Photosynthetic apparatus of purple bacteria. Quart Rev Biophys 35: 1–62

Ide JP, Klug DR, Kühlbrandt W, Giorgi LB and Porter G (1987) The state of detergent solubilized light-harvesting chlorophyll *a/b* protein complex as monitoed by picosecond time-resolved fluorescence and circular dichroism. Biochim Biophys Acta 893: 349–364

Ihalainen JA, Linnanto J, Myllyperkiö P, van Stokkum IHM, Ücker B, Scheer H and Korppi-Tommola JEI (2001) Energy transfer in LH2 of *Rhodospirillum molischianum,* studied by subpicosecond spectroscopy and configuration interaction exciton calculations. J Phys Chem B 105: 9849–9856

Iseri EI and Gülen D (1999) Electronic excited states and excitation transfer kinetics in the Fenna-Matthews-Olson protein of the photosynthetic bacterium *Prosthecochloris aestuarii* at low temperatures. Eur Biophys J Biophys Lett 28: 243–253

Iseri EI and Gülen D (2001) Chlorophyll transition dipole moment orientations and pathways for flow of excitation energy among the chlorophylls of the major plant antenna, LHCII. Eur Biophys J 30: 344–353

Jansson S (1994) The light-harvesting chlorophyll *a/b*-binding proteins. Biochim Biophys Acta 1184: 1–19

Johnson SG and Small GJ (1991) Excited-state structure and energy-transfer dynamics of the bacteriochlorophyll *a* antenna complex from *Prostheocochloris aestuarii.* J Phys Chem 95: 471–479

Jungas C, Rangk J, Rigaud J, Joliot P and Vermeglio A (1999) Supramolecular organization of the photosynthetic apparatus of *Rhodobacter sphaeroides*. EMBO J 18: 534–542

Karrasch S, Bullough PA and Gosh R (1995) The 8.5 Angstrom projection map of the light-harvesting complex 1 from *Rhodospirillum rubrum* reveals a ring composed of 16 subunits. EMBO J 14: 631–638

Kennis JTM, Streltsov AM, Vulto SIE, Aartsma TJ, Nozawa T and Amesz J (1997) Femtosecond dynamics in isolated LH2 complexes of various species of purple bacteria. J Phys Chem B 101: 7827–7834

Kimura A and Kakitani T (2003) Theory of excitation energy transfer in the intermediate coupling case of clusters. J Phys Chem B 107: 14486–14499

Kimura A, Kakitani T and Yamato T (2000) Theory of excitation energy transfer in the intermediate coupling case. II. Criterion for intermediate coupling excitation energy transfer mechanism and application to the photosynthetic antenna system. J Phys Chem B 104: 9276–9287

Kleima FJ, Gradinaru CC, Calkoen F, van Stokkum IHM, van Grondelle R and van Amerongen H (1997) Energy transfer in LHCII monomers at 77 K studied by sub-picosecond transient absorption spectroscopy. Biochemistry 36: 15262–15268

Knox RS and van Amerongen H (2002) Refractive index dependence of the Förster resonance excitation transfer rate. J Phys Chem B 106: 5289–5293

Koepke J, Hu X, Muenke C, Schulten K and Michel H (1996) The crystal structure of the light harvesting complex II (B800-850) from *Rhodospirillum molischianum*. Structure 4: 581–597

Koolhaas MHC, van der Zwan G, Frese RN and van Grondelle R (1997) Red shift of the zero crossing in the CD spectra of the LH2 antenna complex of *Rhodopseudomonas acidophila*: A structure based study. J Phys Chem B 101: 7262–7270

Koolhaas MHC, Frese RN, Fowler GJS, Bibby TS, Georgakopoulou S, van der Zwan G, Hunter CN and van Grondelle R (1998) Identification of the upper exciton component of the B850 bacteriochlorophylls of the LH2 antenna complex, using a B800-free mutant of *Rhodobacter sphaeroides*. Biochemistry 37: 4693–4698

Krikunova M, Voigt B and Lokstein H (2002) Direct evidence for excitonically coupled chlorophylls *a* and *b* in LHC II of higher plants by non-linear polarization spectroscopy in the frequency domain. Biochim Biophys Acta 1556: 1–5

Krueger BP, Scholes GD and Fleming GR (1998) Calculation of coupling and energy-transfer pathways between the pigments of LH2 by the ab initio transition density cube method. J Phys Chem B 102: 5378–5386

Kühlbrandt W, Wang DN and Fujiyoshi Y (1994) Atomic model of plant light-harvesting complex by electron crystallography. Nature 367: 614–621

Law CJ and Cogdell RJ (1998) The effect of chemical oxidation on the fluorescence of the LH1 (B880) complex from the purple bacterium *Rhodobium marinum*. FEBS Lett 432: 27–30

Leupold D, Stiel H, Teuchner K, Nowak F, Sandner W, Ücker B and Scheer H (1996) Size enhancement of transition dipoles to one-and two-exciton bands in a photosynthetic antenna. Phys Rev Lett 77: 4675–4677

Leupold D, Lokstein H and Hoffmann P (1999a) Structure-function relationships in the higher plant photosynthetic antenna complex LHC II as revealed by non-linear laser spectroscopy—the problem of 'chlorophyll forms.' Trends Photochem Photobiol 6: 43–52

Leupold D, Stiel H, Ehlert J, Nowak F, Teuchner K, Voigt B,

Bandilla M, Uecker B and Scheer H (1999b) Photophysical characterization of the B800-depleted light harvesting complex B850 of *Rhodobacter sphaeroides*. Implications to the ultrafast energy transfer 800 → 850 nm. Chem Phys Lett 301: 537–545

Leupold D, Voigt B, Beenken W and Stiel H (2000) Pigment-protein architecture in the light-harvesting antenna complexes of purple bacteria: Does the crystal structure reflect the native pigment-protein arrangement? FEBS Lett 480: 73–78

Leupold D, Teuchner K, Ehlert J, Irrgang K-D and Lokstein H (2002) Two-photon excited fluorescence from higher electronic states of chlorophylls in photosynthetic antenna complexes: A new approach to detect strong excitonic chlorophyll *a/b* coupling. Biophys J 82: 1580–1585

Li YF, Zhou WL and Blankenship RE (1997) Crystal structure of the bacteriochlorophyll *a* protein from *Chlorobium tepidum*. J Mol Biol 271: 456–471

Limantara, L, Sakamoto S, Koyama Y and Nagae H (1997) Effects of nonpolar and polar solvents on the Q_x and Q_y energies of bacteriochlorophyll *a* and bacteriopheophytin *a*. Photochem Photobiol 65:330–337

Limantara L, Fujii R, Zhang J-P, Kanuko T, Hara H, Kawamori A, Yagura T, Cogdell RJ and Koyama Y (1998) Generation of triplet and cation-radical bacteriochlorophyll *a* in carotenoidless LH1 and LH2 antenna complexes from *Rhodobacter sphaeroides*. Biochemistry 37: 17469–17486

Linnanto JM and Korppi-Tommola JEI (2000) Excitation energy-transfer in the LH2 antenna of photosynthetic purple bacteria via excitonic B800 and B850 states. J Chin Chem Soc 47: 657–665

Linnanto J and Korppi-Tommola JEI (2002) Theoretical study of excitation transfer from modified B800 rings of the LH II antenna complex of *Rps. acidophila.* Phys Chem Chem Phys 4: 3453–3460

Linnanto J, Korppi-Tommola JEI and Helenius VM (1999) Electronic states, absorption spectrum and circular dichroism spectrum of the photosynthetic bacterial LH2 antenna of *Rhodopseudomonas acidophila* as predicted by exciton theory and semiempirical calculations. J Phys Chem B 103: 8739–8750

Liu Z, Yan H, Wang K, Kuang T, Zhang J, Gui L, An X and Chang W (2004) Crystal structure of spinach major light-harvesting complex at 2.72 Å resolution. Nature 428: 287–292

Louwe RJW, Vrieze J, Hoff AJ and Aartsma TJ (1997) Toward and integral interpretation of the optical steady-state spectra of the FMO-complex of Prosthecochloris aestuarii. 2. Exciton simulations. J Phys Chem B 101: 11280–11287

Lu XY and Pearlstein RM (1993) Simulations of *Prosthecochloris* bacteriochlorophyll *a* protein optical spectra improved by parametric computer search. Photochem Photobiol 57: 86–91

Ma Y-Z, Cogdell RJ and Gillbro T (1997) Energy transfer and exciton annihilation in the B800-850 antenna complex of the photosynthetic purple bacterium *Rhodopseudomonas acidophila* (strain 10050). A femtosecond transient absorption study, J Phys Chem B 101: 1087–1095

Matsushita M, Ketelaars M and van Oijen AM (2001) Spectroscopy of the B850 band of individual light-harvesting 2 complexes of *Rhodopseudomonas acidophila*. II. Exciton states of an elliptically deformed ring aggregate. Biophys J 80: 1604–1614

Mauring K, Novoderezhkin V, Taisova A and Fetisova Z (1999) Exciton levels structure of antenna bacteriochlorophyll *c* aggregates in green bacterium *Chloroflexus aurantiacus* as probed by 1.8–293 K fluorescence spectroscopy. FEBS Lett 456: 239–242

Mauzerall D and Greenbaum NL (1989) The absolute size of a photosynthetic unit. Biochim Biophys Acta 974: 119–140

McDermott G, Prince S, Freer A, Hawthornthwaite-Lawless A, Pariz M, Cogdell R and Isaacs N (1995) Crystal structure of an integral membrane light-harvesting complex from photosynthetic bacteria. Nature 374: 517–521

Meier T, Zhao Y, Chernyak V and Mukamel S (1997) Polarons, localization, and excitonic coherence in superradiance of biological antenna complexes. J Chem. Phys 107: 3876–3893

Mostovoy MV and Knoester J (2000) Statistics of optical spectra from single-ring aggregates and its application to LH2. J Phys Chem B 104: 12355–12364

Nagarajan, V and Parson WW (1997) Excitation energy transfer between the B850 and B875 antenna complexes of *Rhodobacter sphaeroides.* Biochemistry 36: 2300–2306

Niedermeier G, Scheer H and Feick R (1992) The functional role of protein in the organization of bacteriochlorophyll *c* in chlorosomes of *Chloroflexus aurantiacus*. Eur J Biochem 204: 685–692

Novoderezhkin VI, Palacios MA, van Amerongen H and van Grondelle R (2005) Excitation dynamics in the LHCII complex of higher plants: Modeling based on the 2.72 Å crystal structure. J Phys Chem B 109: 10493–10504

Nowak, FR (1999) Beiträge der Nichtlinearen Polarisationsspektroskopie in der Frequenzdomäne zur Aufklärung ultraschneller Prozesse in photosynthetischen bakteriellen Pigment-Protein-Komplexen. PhD Thesis, University of Potsdam

Olsen JM (1998) Chlorophyll organization and function in green photosynthetic bacteria. Photochem Photobiol 67: 61–75

Owen GM and Hoff AJ (2001) Absorbance detected magnetic resonance spectra of the FMO complex of *Prosthecochloris aestuarii* reconsidered: Exciton simulations. J Phys Chem B 105: 1458–1463

Palacios MA, de Weerd FL, Ihalainen JA, van Grondelle R and van Amerongen H (2002) Superradiance and exciton (de)localization in light-harvesting complex II from green plants? J Phys Chem B 106: 5782–5787

Palsson LO, Spangfort M, Gulbinas V and Gillbro T (1994) Ultrafast chlorophyll *b*-chlorophyll *a* excitation energy transfer in the isolated light harvesting complex, LHC II, of green plants. FEBS Lett 339: 134–138

Papiz MZ, Prince SM, Hawthornthwaite-Lawless AM, McDermott G, Freer AA, Isaacs NW and Cogdell RJ (1996) A model for the photosynthetic apparatus of purple bacteria. Trends Plant Sci 1: 198–206

Pearlstein RM (1992) Theory of the optical spectra of the bacteriochlorophyll *a* antenna protein trimer of *Prosthecochloris aestuarii*. Photosynth Res 31: 213–226

Philipson KD and Sauer K (1972) Exciton interaction in a bacteriochlorophyll-protein from *Chloropseudomonas ethylica*. Absorption and circular dichroism at 77 K. Biochemistry 11: 1880–1885

Pieper J, Rätsep M, Jankowiak R, Irrgang KD, Voigt J, Renger G and Small GJ (1999) Q_y-level structure and dynamics of solubilized light-harvesting complex II of green plants: Pressure and hole burning studies. J. Phys. Chem. A 103: 2412–2421

Prokhorenko VI, Steensgaard DB and Holzwarth AR (2000) Exciton dynamics in the chlorosomal antennae of the green

bacteria *Chloroflexus aurantiacus* and *Chlorobium tepidum*. Biophys J 79: 2105–2120

Psencík J, Polívka T, Nemec P, Dian J, Kudrna J, Malý P and Hála J (1998) Fast energy transfer and exciton dynamics in chlorosomes of the green sulfur bacterium *Chlorobium tepidum*. J Phys Chem A 102: 4392–4398

Pullerits T, Hess S, Herek J and Sundström V (1997) Temperature dependence of excitation transfer in LH2 of *Rhodobacter sphaeroides*. J Phys Chem B 101: 10560–10567

Rätsep M, Blankenship RE and Small GJ (1999) Energy transfer and spectral dynamics of the three lowest energy Q_y-states of the Fenna-Matthews-Olsen antenna complex. J Phys Chem B 103: 5736–5741

Rätsep M, Hunter CN, Olson JD and Freiberg A (2005) Band structure and local dynamics of excitons in bacterial light-harvesting complexes revealed by spectrally selective spectroscopy. Photosynth Res 86: 37–48

Remelli R, Varotto C, Sandonà D, Croce R and Bassi R (1999) Chlorophyll binding to monomeric light-harvesting complex. J Biol Chem 274: 33510–33521

Renger T and May V (2000) Simulations of frequency-domain spectra: Structure-function relationships in photosynthetic pigment-protein complexes. Phys Rev Lett 84: 5228–5231

Robert B, Cogdell RJ and van Grondelle R (2003) The light-harvesting System of Purple Bacteria. In: Green BR and parson WW (eds) Light Harvesting Antennas in Photosynthesis, pp 169–194. Kluwer Academic Publishers, Dordrecht

Rogl H and Kühlbrandt W (1999) Mutant trimers of light-harvesting complex II exhibit altered pigment content and spectroscopic features. Biochemistry 38: 16214–16222

Rogl H, Schödel R, Lokstein H, Kühlbrandt W and Schubert A (2002) Assignment of spectral substructures to pigment-binding sites in higher plant light-harvesting complex LHC II. Biochemistry 41: 2281–2287

Roszak AW, Howard TD, Southall J, Gardiner AT, Law CJ, Isaacs NW and Cogdell RJ (2003) Crystal structure of the RC-LH1 core complex from *Rhodopseudomonas palustris*, Science 302: 1969–1972

Sauer K, Smith JRL and Schultz AJ (1966) The dimerization of chlorophyll *a*, chlorophyll *b*, and bacteriochlorophyll in solution. J Am Chem Soc 88: 2681–2688

Sauer K, Cogdell RJ, Prince SM, Freer A, Isaacs NW and Scheer H (1996) Structure-based calculations of the optical spectra of the LH2 bacteriochlorophyll-protein complex from *Rhodopseudomonas acidophila*. Photochem Photobiol 64: 564–576

Savikhin S, Buck DR, Struve WS, Blankenship RE, Taisova AS, Novoderezhkin VI and Fetisova ZG (1998a) Excitation delocalization in the bacteriochlorophyll *c* antenna of the green bacteria *Chloroflexus aurantiacus* as revealed by ultrafast pump-probe spectroscopy. FEBS Lett 430: 323–326

Savikhin S, Buck DR and Struve WS (1998b) Toward level-to-level energy transfers in photosynthesis: The Fenna-Matthews-Olsen-Protein. J Phys Chem B 102: 5556–5565

Savikhin S, Buck DR and Struve WS (1999) The Fenna-Matthews-Olsen protein: A strongly coupled photosynthetic antenna. In: Andrews DL and Demidov AA (eds) Resonance energy transfer, pp 399–434. John Wiley & Sons Ltd, Chichester

Scholes GD and Fleming GR (2000) On the mechanism of light-harvesting in photosynthetic purple bacteria: B800 to B850 energy transfer. J Phys Chem B 104: 1854–1868

Scholes, GD, Gould IR, Cogdell RJ and Fleming GR (1999) *Ab initio* molecular orbital calculations of electronic couplings in the LH2 bacterial light-harvesting complex of *Rps. acidophila.* J Phys Chem B 103: 2543–2553

Schubert A, Beenken W, Stiel H, Voigt B, Leupold D and Lokstein H (2002) Excitonic coupling of chlorophylls in the plant light-harvesting complex LHC II. Biophys J 82 1030–1039

Standfuss J, Terwisscha van Scheltinga AC, Lamborghini M and Kühlbrandt W (2005) Mechanisms of photoprotection and nonphotochemical quenching in pea light harvesting complex at 2.5 Å resolution. EMBO J 24: 919–928

Stiel H, Leupold D, Teuchner K, Nowak F, Scheer H and Cogdell RJ (1997) One- and two-exciton bands in the LH2 antenna of *Rhodopseudomonas acidophila*. Chem Phys Lett 276: 62–69

Sturgis JN and Robert B (1996) The role of chromatophore coupling in tuning the spectral properties of peripheral light-harvesting protein of purple bacteria. Photosynth Res 50: 5–10

Trinkunas G, Connelly JP, Müller MG, Valkunas L and Holzwarth AR (1997) Model for the excitation dynamics in the light-harvesting complex II from higher plants. J Phys Chem B 101: 7313–7320

Tronrud DE and Matthews BW (1993) Refinement of the structure of a water-soluble antenna complex from green photosynthetic bacteria by incorporation of the chemically determined amino acid sequence. In: Deisenhofer J and Norris JR (eds) The Photosynthetic Reaction Center, Vol I, pp 13–22. Academic Press, New York

van Amerongen H and van Grondelle R (2001) Understanding the energy transfer function of LHC II, the major light-harvesting complex of green plants. J Phys Chem B 105: 604–617

van Amerongen H, Valkunas L and van Grondelle R (2000) Photosynthetic Excitons. World Scientific Publishing, Singapore

van Noort PI, Zhu Y, LoBrutto R and Blankenship RE (1997) Redox effects on the excited-states lifetime in chlorosomes and bacteriochlorophyll *c* oligomers. Biophys J 72: 316–325

van Oijen AM, Ketelaars M, Köhler J, Aartsma TJ and Schmidt J (1999) Unraveling the electronic structure of individual photosynthetic pigment-protein complexes. Science 285: 400–402

Voigt J, Renger T, Schödel R, Schrötter T, Pieper J and Redlin H (1996) Excitonic effects in the light harvesting Chl *a/b*-protein complex of higher plants. Physica status solidi B 194: 333–350

Voigt B, Irrgang K-D, Ehlert J, Beenken W, Renger G, Leupold D and Lokstein H (2002) Spectral substructure and excitonic interactions in the minor Photosystem II antenna complex CP29 as revealed by non-linear polarization spectroscopy in the frequency domain. Biochemistry 41: 3049–3056

Vulto SIE, de Baat MA, Louwe RJW, Permentier HP, Neef T, Miller M, van Amerongen H and Aartsma TJ (1998a) Exciton simulations of optical spectra of the FMO complex from the green sulfur bacterium *Chlorobium tepidum* at 6 K. J Phys Chem B 102: 9577–9582

Vulto SIE, Neerken S, Louwe RJW, de Baat MA, Amesz J and Aartsma TJ (1998b) Excited-state structure and dynamics in FMO antenna complexes from photosynthetic green sulfur bacteria. J Phys Chem B 102: 10630–10635

Walz T, Jamieson SJ and Bowers CM (1998) Projection structures of the three photosynthetic complexes from *Rhodobacter sphaeroides*: LH2 at 6 Ångstrom, LH1 and RC-LH1 at 25 Ångstrom. J Mol Biol 282: 833–845

Wendling M, Przyjalgowski MA, Gülen D, Vulto SIE, Aartsma TJ, van Grondelle R and van Amerongen H (2002) The quantita-

tive relationship between structure and polarized spectroscopy in the FMO complex of *Prosthecochloris aestuarii*: Refining experiments and simulation. Photosynth Res 71: 99–123

Westerhuis WHJ, Sturgis JN, Ratcliffe EC, Hunter CN and Niederman RA (2002) Isolation, size estimates and spectral heterogeneity of an oligomeric series of light-harvesting 1 complexes from *Rhodobacter sphaeroides*. Biochemistry 41: 8698–8707

Wolf H and Scheer H (1973) Stereochemistry and chiroptic properties of pheophorbides and related compounds. Ann NY Acad Sci 206: 549–567

Wu HM and Small GJ (1997) Symmetry adapted basis defect patterns for analysis of the effects of energy disorder on cyclic arrays of coupled chromophores. Chem Phys 218: 225–234

Wu HM and Small GJ (1998) Symmetry-based analysis of the effects of random energy disorder on the excitonic level structure of cyclic arrays: Application to photosynthetic antenna complexes. J Chem Phys B 102: 888–898

Yakovlev A, Novoderezhkin V, Taisova A and Fetisova Z (2002) Exciton dynamics in the chlorosomal antenna of the green bacterium *Chloroflexus aurantiacus*: Experimental and theoretical studies of femtosecond pump-probe spectra. Photosynth Res 71: 19–32

Chapter 30

Mechanisms of Carotenoid-to-Bacteriochlorophyll Energy Transfer in the Light Harvesting Antenna Complexes 1 and 2: Dependence on the Conjugation Length of Carotenoids

Yasushi Koyama* and Yoshinori Kakitani
Faculty of Science and Technology, Kwansei Gakuin University,
2-1 Gakuen, Sanda, Hyogo 669-1337, Japan

Summary

This chapter summarizes the most recent results of investigations on carotenoid-to-bacteriochlorophyll (Car-to-BChl) singlet-energy transfer reactions. These reactions strongly depend on the number, *n,* of conjugated double bonds in the Car molecule. Subpicosecond time-resolved electronic-absorption data were analyzed by singular-value decomposition, followed by global-fitting based on a new energy diagram of the singlet and triplet excited states and also on a new scheme of singlet-to-singlet and singlet-to-triplet electronic conversions of Car molecules. The mechanisms and efficiencies of Car-to-BChl singlet-energy transfer varies from one Car to another depending on the conjugation length (*n*); in particular, a sudden drop in energy transfer when *n* is increased from 10 to 11 has been explained by the energetics and dynamics of Car excited states.

The chapter focuses on a comparison between the purple bacterial light harvesting antenna complexes 1

Note: Readers are encouraged to visit the website (http://epub.ub.uni-muenchen.de/archive/00000776/) for 'supplementary material,' where Figs. S1–S5 referred to in the text are posted.

*Author for correspondence, email: ykoyama@kwansei.ac.jp

Bernhard Grimm, Robert J. Porra, Wolfhart Rüdiger and Hugo Scheer (eds): Chlorophylls and Bacteriochlorophylls: Biochemistry, Biophysics, Functions and Applications, pp. 431–443.

and 2 (i.e., LH1 and LH2). Differences in the dynamics and efficiencies of singlet-energy transfer and of triplet generation is correlated with differences in the structures and physiological functions of these two complexes. The roles of the T_1 states of Car and BChl molecules in the excited-state reactions of the two antenna complexes are discussed.

I. Introduction

Carotenoids (Cars) in photosynthetic systems have an important function of light harvesting which includes the absorption of photons by Cars followed by transfer of their singlet energy to (bacterio)chlorophylls (BChls). The energy transfer reactions compete with rapid relaxation processes in Cars. Two excited states were well known until recently: the $1B_u^+$ state that strongly appears in the Car absorption spectra and the $2A_g^-$ state that does not and has, therefore, been called 'a dark state.' The mechanisms of singlet-energy transfer described by the use of those two electronic states have been reviewed (Frank and Cogdell, 1993; Frank and Christensen, 1995; Koyama et al., 1996; Sundström et al., 1999; Ritz et al., 2000; Hu et al., 2002).

Recently, a pair of new singlet states, i.e., the $1B_u^-$ and $3A_g^-$ states, have been discovered by measurement of resonance-Raman excitation profiles (Sashima et al., 1999, 2000; Furuichi et al., 2002). Furthermore, a singlet-to-triplet electronic conversion was identified, by subpicosecond time-resolved absorption spectroscopy, in addition to sequential singlet-to-singlet electronic conversions that follow the state ordering. Therefore, a completely new picture of the mechanisms of singlet-energy transfer needs to be proposed. Since the energies of the four singlet states vary depending on the conjugation length of the Car, the mechanism can vary from one Car to another.

Since the $1B_u^+$, $1B_u^-$, $3A_g^-$ and $2A_g^-$ states are energetically closely spaced, the singlet-to-singlet electronic conversions take place rapidly, in the 10 fs–10 ps time range. Also the singlet-to-triplet electronic conversion takes place in the 100 fs time range. In time-resolved absorption spectroscopy, we used ~100 fs pump and probe pulses. The pulse duration of the pump pulse allowed us to specifically excite the Car molecules to the $1B_u^+$ ($v = 0$) level. In order to enhance the time resolution, we used singular-value decomposition (SVD) followed by global-fitting of the time-resolved data matrices; this method enabled us to correctly determine the electronic-conversion and the energy transfer processes at a time resolution of ~10 fs.

We have applied the above method to the light harvesting complexes 1 and 2 (LH1 and LH2) whose structures are well defined, and succeeded in elucidating the roles of the newly-found $1B_u^-$ state in the singlet-to-triplet electronic conversion in Cars and in the singlet-energy transfer from Car to BChl.

Abbreviations: BChl(s) – bacteriochlorophyll(s); $1B_u^+$ – Car excited state directly accessible from G by single-photon excitation; $1B_u^-$, $2A_g^-$, $3A_g^-$ – hidden Car excited states that are generally not directly accessible from G by single-photon excitation; Car(s) – carotenoid(s); G – the ground state; LH1 – light harvesting complex 1; LH2 – light harvesting complex 2; n – the number of conjugated double bonds in carotenoid molecules; Q_y and Q_x – 1st and 2nd excited states of BChl. These terms generally refer to transitions, but have been used here to designate the respective states; *Rba. – Rhodobacter;* RC – reaction center; *Rps. – Rhodopseudomonas; Rsp. – Rhodospirillum;* SADS – species-associated difference spectra; S_n – a higher singlet-excited state; SVD – singular-value decomposition; T_1 – the first triplet-excited state; T_2 – the second triplet-excited state; T_n – a higher triplet-excited state

II. Intrinsic Properties of Carotenoids' Excited-States

A. Energy Levels of Singlet and Triplet States

Figure 1 shows an energy diagram for Cars having the number of conjugated double bonds, n = 9–13. The chemical structures of Cars relevant to the present article are shown in Fig. 2. The energies of the singlet states, including the $1B_u^+$, $3A_g^-$, $1B_u^-$ and $2A_g^-$ states, were determined by measurement of resonance-Raman excitation profiles for crystalline mini-9-β-carotene (n = 9), spheroidene (n = 10), lycopene (n = 11), anhydrorhodovibrin (n = 12) and spirilloxanthin (n = 13) (Sashima et al., 1999, 2000; Furuichi et al., 2002).

The electronic states with different symmetries (i.e., kB_u^+, lA_g^- and mB_u^-) originate from the approximate C_{2h} symmetry of the conjugated chain of all-*trans* Cars. A and B signifies 'symmetric' and 'antisymmetric' with respect to the 2-fold rotation, whereas g and u, with respect to the center of symmetry. The + and – symbols, used by Pariser (1956), indicate the symmetry of the electronic configuration (Callis et al., 1983). Optical transition (i.e., absorp-

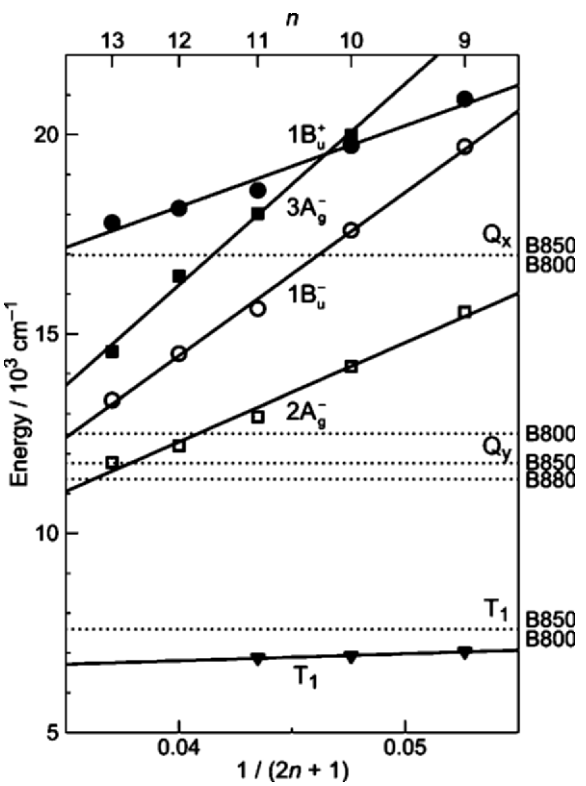

Fig. 1. The energies of the $1B_u^+$, $3A_g^-$, $1B_u^-$ and $2A_g^-$ singlet-excited states that were determined by measurement of resonance-Raman excitation profiles for crystalline mini-9-β-carotene ($n = 9$), spheroidene ($n = 10$), lycopene ($n = 11$), anhydrorhodovibrin ($n = 12$) and spirilloxanthin ($n = 13$) (Sashima et al., 1999, 2000; Furuichi et al., 2002), and those of the T_1 ($1B_u$) state that were determined by high-sensitivity emission spectroscopy for neurosporene ($n = 9$), spheroidene ($n = 10$) and rhodopin + lycopene ($n = 11$) bound to the LH2 complexes from *Rba. sphaeroides* G1C, *Rba. sphaeroides* 2.4.1 and *Rsp. molischianum* (Rondonuwu et al., 2004a). The Q_x, Q_y and T_1 energies of BChls in the LH2 and LH1 complexes, determined by conventional absorption spectroscopy, are also shown for comparison (flat dotted lines).

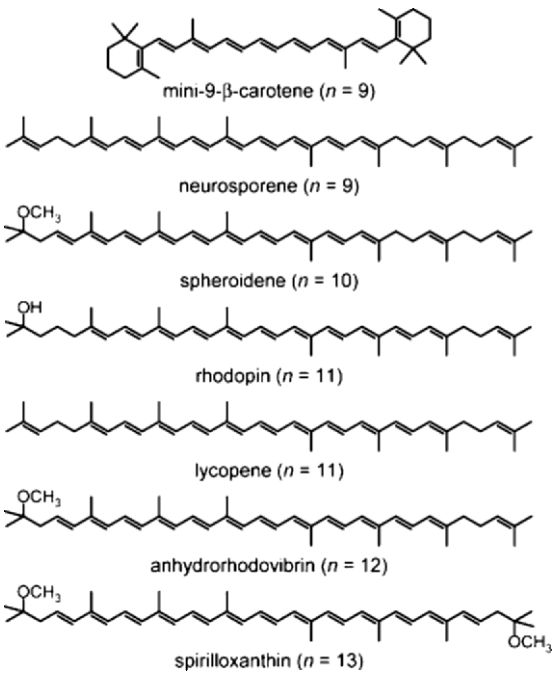

Fig. 2. The structures of typical bacterial Cars appearing in this chapter.

tion or fluorescence) is allowed between a pair of electronic states having different Pariser signs. The letters *k*, *l* and *m* label the singlet states having the same symmetry from the bottom to the higher-energy levels; the ground state is $1A_g^-$.

The uniqueness of the Car singlet states is that those electronic states, having different symmetries, are similar in energy. The absorptive transition from the $1A_g^-$ (ground) state to the $2A_g^-$, $1B_u^-$ or $3A_g^-$ state is symmetry-forbidden ('the dark states'). Consequently, the spectroscopic identification of these states has been delayed although their presence was theoretically predicted in shorter polyenes (Tavan and Schulten, 1986, 1987). On the other hand, the $1B_u^+ \leftarrow 1A_g^-$ absorption and the $1B_u^+ \rightarrow 1A_g^-$ fluorescence are strongly allowed. Due to the mixing with the $1B_u^+$ state, 'the dark states' become partially symmetry-allowed, and can be detected by either fluorescence (Fujii et al., 1998, 2001) or electronic-absorption spectroscopy (Wang et al., 2005).

Figure 1 also shows the T_1 ($1B_u$) energies, determined by phosphorescence spectroscopy (Rondonuwu et al. 2004a), of neurosporene ($n = 9$), spheroidene ($n = 10$) and rhodopin + lycopene ($n = 11$) bound to the LH2 complexes from *Rhodobacter* (*Rba.*) *sphaeroides* G1C, *Rba. sphaeroides* 2.4.1 and *Rhodospirillum* (*Rsp.*) *molischianum*, respectively. Here, the T_1 state of Cars was populated by energy transfer from T_1 BChl through the electron-exchange mechanism, described as T_1 BChl + S_0 Car $\rightarrow$ S_0 BChl + T_1 Car, although the direct $T_1 \leftrightarrow 1A_g^-$ in Car is spin forbidden.

B. Singlet-to-Singlet, Singlet-to-Triplet and Triplet-to-Triplet Electronic Conversions

As shown in the above energy diagram (Fig. 1), when the Car molecules are excited to the $1B_u^+$ state by absorption of photons, the next lower singlet state to electronically convert is the $1B_u^-$ state for $n = 9$ and 10,

Table 1. Dependence of the $1B_u^+$, $1B_u^-$ and $2A_g^-$ lifetimes (in ps) on the number of conjugated double bonds (n).

	neurosporene ($n = 9$)	spheroidene ($n = 10$)	lycopene ($n = 11$)	anhydrorhodovibrin ($n = 12$)	spirilloxanthin ($n = 13$)
$1B_u^+$	0.10	0.10	0.02	0.01	0.01
$1B_u^-$	0.24	0.23	–	–	–
$3A_g^-$	–	–	0.15	0.10	0.10
$2A_g^-$	24.0	8.9	3.9	2.2	1.4

whereas it is the $3A_g^-$ state for $n = 1$ –13. According to this expectation, different transient absorptions (i.e., one from the $1B_u^-$ state and the other from the $3A_g^-$ state) were identified by subpicosecond time-resolved absorption spectroscopy in the near-infrared region (Fujii et al., 2003).

Table 1 lists the lifetimes of the relevant states. These lifetimes show strong dependence on n.

(1) The lifetime of the $1B_u^+$ state is the shortest among all the singlet-excited states, and it decreases from 100 fs in $n = 9$ and 10 down to 20–10 fs in $n =$ 11–13. In the latter, the lower lying $3A_g^-$ state may shorten the $1B_u^+$ lifetime due to the accompanying $1B_u^+ \rightarrow 3A_g^-$ fluorescence.

(2) The $1B_u^-$ lifetime is in the 240–230 fs range for $n = 9$ and 10.

(3) The $3A_g^-$ lifetime is in the 150–100 fs range for n = 11–13. Here, the underlying $1B_u^-$ state may mediate the $3A_g^- \rightarrow 2A_g^-$ internal conversion, although the particular state was not seen in the near-infrared region.

In pump and probe absorption spectroscopy, the white-continuum probe pulse can cause stimulated emission in the downward symmetry-allowed electronic transitions. Therefore, the exact lifetimes of subpicosecond to picosecond duration can only be determined by fluorescence up-conversion spectroscopy, because the perturbation of the probe pulse is applied not to the excited-state molecule but to the emitted fluorescence.

Subpicosecond time-resolved absorption spectroscopy in the visible region could identify a transient absorption from the $1B_u^-$ state for the Cars with $n =$ 9–13 (Rondonuwu et al., 2003). Figure 3 shows the pathways of electronic conversions and the relevant time constants that were determined by SVD followed by global fitting of the time-resolved spectral data (Zhang et al., 2000). (The results of SVD and global-fitting are shown in Fig. S1 in the supplementary material.) This method will be briefly described later. Here, we identified:

(1) the sequential internal conversion of $1B_u^+ \rightarrow 1B_u^- \rightarrow 2A_g^- \rightarrow 1A_g^-$;

(2) the singlet-to-triplet conversion of $1B_u^- \rightarrow T_2$ ($1A_g$); and,

(3) the triplet-to-triplet conversion of $T_2 \rightarrow T_1$ ($1B_u$).

The T_2 state was found for the first time (Rondonuwu et al., 2003): we assumed that the T_2 energy is twice as high as the T_1 energy (Tavan and Schulten, 1987), the latter was evaluated by the use of the linear relation shown in Fig. 1. Interestingly, the time constant of the $1B_u^- \rightarrow T_2$ conversion becomes systematically shortened from 20 ps to less than 1 ps as n is increased from 9 to 13 in a manner which approximately follows the energy-gap law (Englman and Jortner, 1970). As a result, the yield of the T_2 state turned out to be 2.7, 5.1, 9.6, 17 and 26% in $n = 9$, 10, 11, 12 and 13, respectively. (The time constants of the $1B_u^- \rightarrow T_2$ conversion (in monodisperse solution) are shown in terms of an approximate energy-gap law in Fig. S2.)

III. Carotenoid-to-Bacteriochlorophyll Energy Transfer in Light Harvesting Complex 2

A. Excited-State Dynamics of Carotenoids and Bacteriochlorophyll

The overall singlet energy-transfer efficiencies from Car to BChl were determined by comparison of the fluorescence-excitation spectrum (the action spectrum of singlet-energy transfer) with the electronic-absorption spectrum of Car (reflecting the number

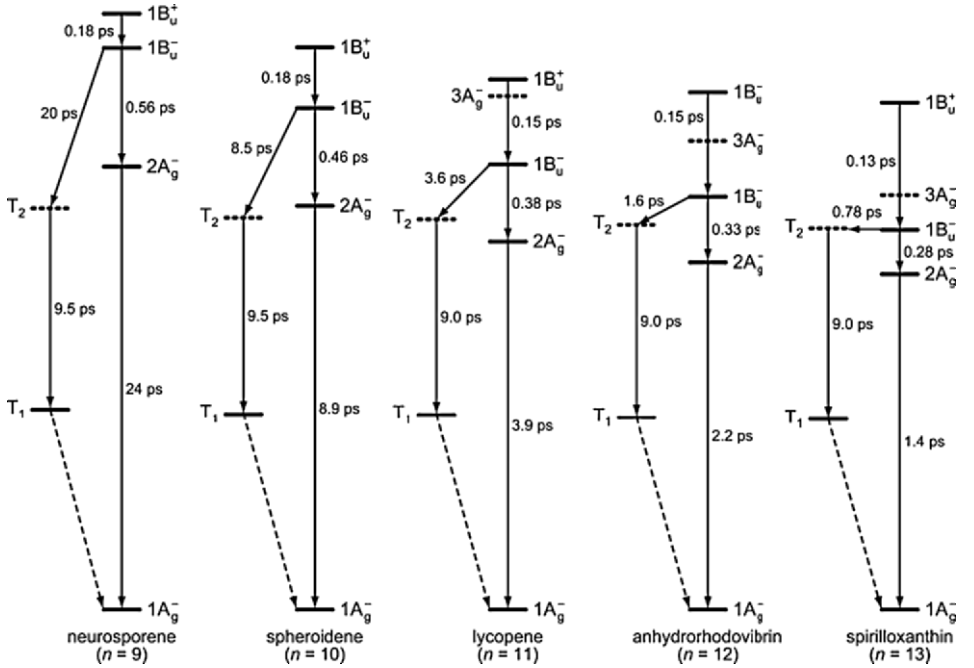

Fig. 3. Relaxation schemes, including singlet-to-singlet, singlet-to-triplet and triplet-to-triplet electronic conversions, that were determined by the SVD and global-fitting analyses of the data matrices obtained by visible, subpicosecond time-resolved absorption spectroscopy of neurosporene ($n = 9$), spheroidene ($n = 10$), lycopene ($n = 11$), anhydrorhodovibrin ($n = 12$) and spirilloxanthin ($n = 13$) in solution. (See Fig. S1 for the results of the SVD and global-fitting analyses.)

of photons absorbed by Car) after normalization at the Q_x peak of BChl (the absorbed photons by BChl should be emitted directly). These transfer efficiencies were determined for the LH2 complexes from *Rba. sphaeroides* G1C, *Rba. sphaeroides* 2.4.1, *Rsp. molischianum* and *Rhodopseudomonas* (*Rps.*) *acidophila,* which contained, respectively, neurosporene ($n = 9$), spheroidene ($n = 10$), rhodopin + lycopene ($n = 11$) and rhodopin glucoside ($n = 11$): the values obtained were 92, 89, 53 and 56%, respectively (Rondonuwu et al., 2004b; Macpherson et al., 2001). The sudden drop in the energy-transfer efficiency (from ~90% to ~55%) when n is increased from 10 to 11 motivated us to examine the detailed mechanisms of singlet-energy transfer. The question was: how can the above values of overall efficiency be explained in terms of the energetics and dynamics of Cars having the particular conjugation lengths?

Subpicosecond time-resolved absorption spectroscopy, in the visible and near-infrared regions, was used to probe the excited-state dynamics of Car and BChl molecules, respectively. Firstly, we applied SVD to the time-resolved spectral-data matrices to extract all components of physical significance. Secondly, we tried global fitting to the reduced data matrices to obtain the species-associated difference spectra (SADS) and time-dependent changes in their population, by interchanging (through trial and error) the various schemes of Car-to-BChl singlet-energy transfer. Since the least-square fitting did not allow us to determine all those time constants of internal conversion and singlet-energy transfer, we assumed that the time constants of singlet-to-singlet electronic conversions of $1B_u^+ \rightarrow 1B_u^- \rightarrow 2A_g^- \rightarrow 1A_g^-$ in each Car, and $Q_x \rightarrow Q_y \rightarrow$ ground in BChl, were not changed upon binding to the complexes (note that we use 'Q_x' and 'Q_y' to signify electronic states rather than the related electronic transitions). Then, we tried to determine the time constants for the three channels of Car-to-BChl singlet-energy transfer ($1B_u^+ \rightarrow Q_x$, $1B_u^- \rightarrow Q_x$ and $2A_g^- \rightarrow Q_y$) and for a channel of singlet-to-triplet electronic conversion within Car ($1B_u^- \rightarrow T_1$). The T_2 state was neglected because no indication of its presence was seen in the time-resolved spectra. Figure 4 shows the successful scheme chosen and the time constants of singlet-energy transfer determined by the SVD and global-fitting analyses.

Figure 5 shows the results of global fitting. The top four SADS panels clearly identify (from top to bottom):

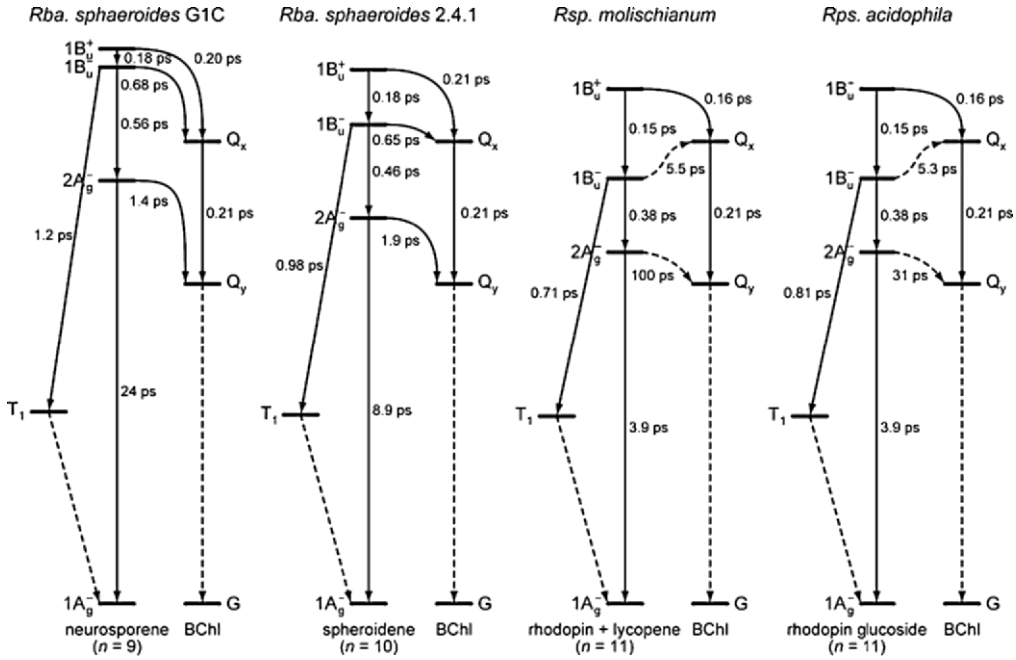

Fig. 4. Pathways and time constants of singlet-to-singlet and singlet-to-triplet electronic conversions in Cars, and those of singlet energy-transfer reactions from Car to BChl in the LH2 complexes from *Rba. sphaeroides* G1C, *Rba. sphaeroides* 2.4.1, *Rsp. molischianum* and *Rps. acidophila*. The time constants of singlet-to-singlet electronic conversions, within Car and BChl, were transferred from those determined in solution; then, the time constants of Car-to-BChl singlet-energy transfer through the $1B_u^+ \rightarrow Q_x$, $1B_u^- \rightarrow Q_x$, and $2A_g^- \rightarrow Q_y$ channels and those of the $1B_u^+ \rightarrow T_1$ singlet-to-triplet conversion in Car were determined by the SVD and global-fitting analyses (see Fig. 5). In this figure, a much slower energy-transfer pathway than the singlet-to-singlet electronic conversion, originating from the same state, is shown by a broken line.

(1) stimulated emission and transient absorption from the $1B_u^+$ state;

(2) broad transient absorption from the $1B_u^-$ state;

(3) sharp absorption from the $2A_g^-$ state; and,

(4) transient absorption from the T_1 state.

The strong stimulated emission was seen only in the optically-allowed $1B_u^+$ state, whereas the latter three 'dark states', instead, accompanied the bleaching of the ground-state ($1B_u^+ \leftarrow 1A_g^-$) absorption. The time-dependent changes in the population of the Car excited states (the middle panels) reflect the generation of both the $2A_g^-$ and the T_1 states from a common precursor, the $1B_u^-$ state. On going from $n = 10$ to $n = 11$, the amount of $1B_u^+$ decreases while that of $2A_g^-$ increases. The bleaching of the Q_y absorption (the bottom panels) reflects how the singlet energy was transferred to either the Q_x or the Q_y state of BChl. A slow bleaching component is seen in $n = 9$ and 10, but not in $n = 11$. All the above observations indicate a sudden change in the excited-state dynamics when n increases from 10 to 11, which is consistent with the closing of the $1B_u^- \rightarrow Q_x$ and $2A_g^- \rightarrow Q_y$ channels: the details of these closures will be described below. The set of reasonable SADS, reflecting the excited states involved, as well as the perfect agreement between the noisy observed curve and the smooth fitting curve in the time profiles of Cars and BChl (the middle and the bottom panels, respectively), prove that the global-fitting analyses were successful.

B. Mechanisms and Efficiencies of Singlet-Energy Transfer and Triplet Generation

The pathways of electronic conversion and energy transfer as well as the relevant time constants (Fig. 4) exhibit drastic changes in the mechanisms of singlet-energy transfer and triplet generation when n increases from 10 to 11. The changes can be characterized as follows:

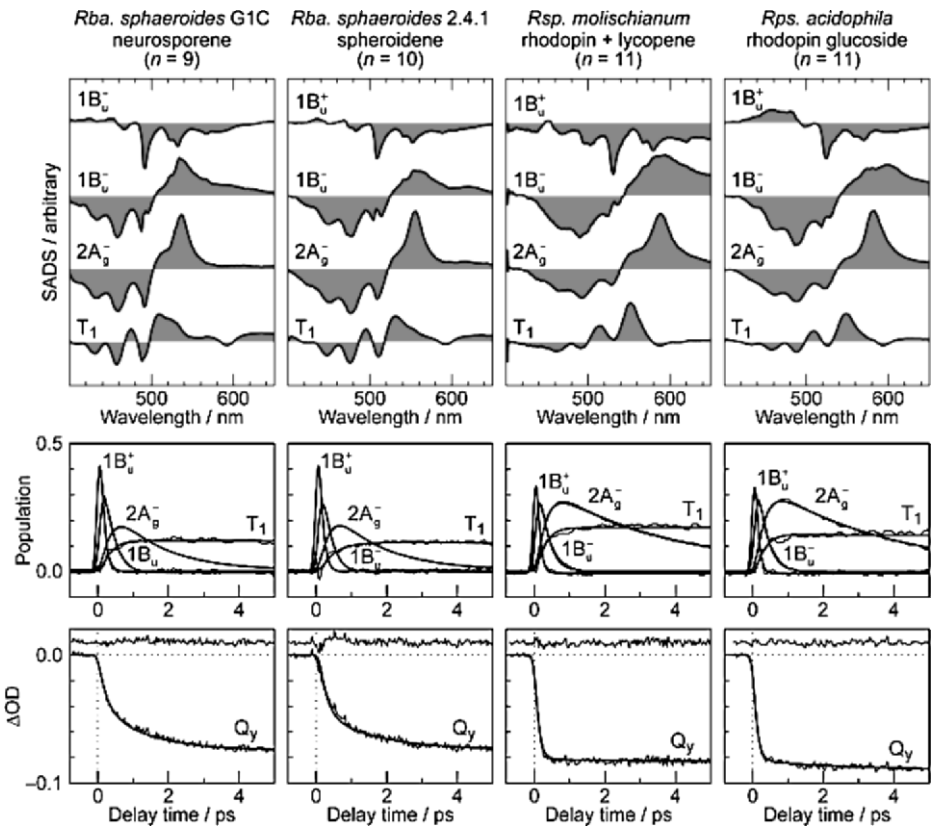

Fig. 5. The SADS (the top panels) and the time-dependent changes in population (the middle panels) for the $1B_u^+$, $1B_u^-$ and $2A_g^-$ singlet-excited states and the T_1 ($1B_u$) state of the Cars (see Fig. 4). The spectral data matrices, that were obtained by visible subpicosecond time-resolved absorption spectroscopy, were analyzed by SVD and global fitting by the use of a scheme shown in Fig. 4. The noisy curves show the observed time profiles, and the smooth curves show the fitting time profiles. Fitting to the bleaching profile of the Q_y absorption is shown in the bottom panels together with the residuals.

(1) The $1B_u^- \rightarrow Q_x$ channel of singlet-energy transfer substantially slows down and is practically closed because the $1B_u^-$ state becomes lower than the Q_x state, resulting in an up-hill energy transfer;

(2) The $2A_g^- \rightarrow Q_y$ channel of singlet-energy transfer is also practically shut down, although the $2A_g^-$ state is still higher than the Q_y state, possibly due to a poor Franck-Condon overlap between the $2A_g^-$ ($\nu = 0$) $\rightarrow 1A_g^-$ ($\nu = 0, 1, 2\cdots$) emission of Car and the $Q_y \leftarrow$ ground absorption of BChl; and,

(3) The generation of the T_1 state is strongly enhanced.

Table 2a lists the efficiencies of the Car-to-BChl singlet-energy transfer through the three channels and the efficiencies of triplet generation in Cars. The changes in the efficiencies can be characterized as follows:

(1) The energy-transfer efficiency through the $1B_u^+ \rightarrow Q_x$ channel is almost the same for all n = 9–11.

(2) The energy-transfer efficiencies through the $1B_u^- \rightarrow Q_x$ and the $2A_g^- \rightarrow Q_y$ channels are similar in n = 9 and 10, but both of them become practically zero in n = 11.

(3) As a result, the sum of the three channels proved to be 88, 84, 51 and 54% in Cars with n = 9, 10, 11 and 11, respectively; these values parallel nicely the overall efficiencies determined by fluorescence-excitation and electronic-absorption spectroscopies, i.e., 92, 89, 53 and 56%, respectively (Rondonuwu et al., 2004b).

Thus, the sudden drop in the Car-to-BChl singlet-energy transfer in the LH2 complex, on increasing n from 10 to 11, has been explained in terms of the

Table 2. Efficiencies (Φ in %) of Car-to-BChl singlet-energy transfer through the $1B_u^+$, $1B_u^-$ and $2A_g^-$ channels and those of the $1B_u^-$-to-T_1 singlet-to-triplet conversion in Cars, as determined by the SVD and global-fitting analyses of subpicosecond time-resolved, spectral data matrices. The overall efficiencies, determined by comparison of the fluorescence-excitation and electronic-absorption spectra, Φ(obs), are also shown.

(a) Native LH2 complexes

Carotenoid (*n*)	$\Phi(1B_u^+)$	$\Phi(1B_u^-)$	$\Phi(2A_g^-)$	Φ(sum)	$\Phi(T_1)$	Φ(obs)
neurosporene (9) [a]	48	19	22	88	10	92
spheroidene (10) [b]	46	18	20	84	12	89
rhodopin + lycopene (11) [c]	48	2	1	51	17	53
rhodopin glucoside (11) [d]	48	2	4	54	16	56

In the LH2 complexes from [a] *Rba. sphaeroides* G1C, [b] *Rba. sphaeroides* 2.4.1, [c] *Rsp. molischianum* and [d] *Rps. acidophila*

(b) Reconstituted LH1 complexes

Carotenoid (*n*) [e]	$\Phi(1B_u^+)$	$\Phi(1B_u^-)$	$\Phi(2A_g^-)$	Φ(sum)	$\Phi(T_1)$
neurosporene (9)	47	11	20	78	19
spheroidene (10)	47	9	19	75	20
lycopene (11)	41	2	3	46	27
anhydrorhodovibrin (12)	39	0	1	40	29
spirilloxanthin (13)	35	0	1	36	31

[e] Incorporated into the LH1 complex from *Rsp. rubrum* G9

energetics and dynamics of the bound Car molecules. The LH2 complexes from *Rsp. molischianum* and *Rps. acidophila,* containing rhodopin + lycopene and rhodopin glucoside, respectively, gave very similar results indicating that those energy-transfer parameters are mainly determined by *n*. On the other hand, the generation of the T_1 state is enhanced from 10–12% to 16–17%.

IV. Carotenoid-to-Bacteriochlorophyll Energy Transfer in Light Harvesting Complex 1

A. Excited-State Dynamics of Carotenoids and Bacteriochlorophyll

To compare the LH2 and LH1 complexes and to examine a wider range of Car molecules, neurosporene (n = 9), spheroidene (n = 10), lycopene (n = 11), anhydrorhodovibrin (n = 12) and spirilloxanthin (n = 13) were incorporated into the LH1 complex from *Rsp. rubrum* G9 (a carotenoidless mutant) and, then, the same spectroscopic and analytical methods were applied to examine the excited-state dynamics of Cars and BChl (Akahane et al., 2004).

Figure 6 shows the schemes used for the SVD and global-fitting analyses. For Cars with n = 9–11, exactly the same scheme was used as in the case of the LH2 complexes (Fig. 4). For Cars with n = 12 and 13, we found, by trial-and-error, that neither the $1B_u^- \rightarrow Q_x$ nor the $1B_u^- \rightarrow Q_y$ energy transfer was taking place. The time constants of singlet-to-singlet electronic conversions for the Car and BChl molecules were transferred from those determined in solution.

Figure 7 shows the results of the SVD and global-fitting analyses. A set of SADS patterns due to the $1B_u^+$, $1B_u^-$, $2A_g^-$ and T_1 states, that are similar to those in the LH2 complexes, were obtained (the top panels). The time-dependent changes in population (the middle panels) indicate increased contribution of the $2A_g^-$ and T_1 states when n increases. The time profiles of the bleaching of the Q_y absorption (the bottom panels) show that the contribution of the slower component decreases when n increases. These observations actually reflect the closure of the $1B_u^- \rightarrow Q_x$ and $2A_g^- \rightarrow Q_y$ energy-transfer channels in Cars n = 11–13, as occurs in LH2 complexes. The slow recovery of the Q_y bleaching in n = 12 and 13 can be ascribed to a singlet-triplet annihilation reaction (see Section V.B).

B. Mechanisms and Efficiencies of Singlet-Energy Transfer and Triplet Generation

The pathways of singlet-energy transfer and the relevant time constants (shown in Fig. 6) show that the LH1 complexes can be classified into two groups according to their mechanism of singlet-energy transfer. In Cars with n = 9 and 10, all the $1B_u^+ \rightarrow Q_x$,

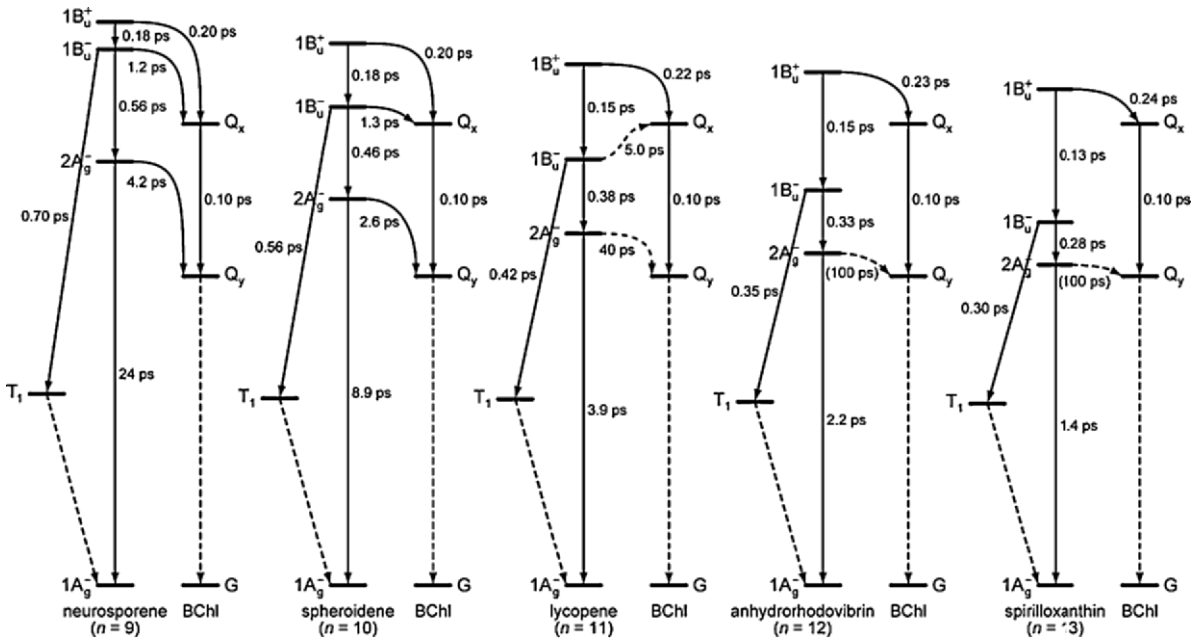

Fig. 6. The pathways and time constants of singlet-to-singlet and singlet-to-triplet electronic conversions in Cars and those of singlet-energy transfer from Car to BChl through different channels, in Cars incorporated into the LH1 complex from *Rsp. rubrum* G9. In determining the time constants of the Car-to-BChl singlet-energy transfer and singlet-to-triplet conversion in Cars, the same strategy as described in Fig. 4 was used. After trial fittings, some pathways were discarded. The results of the SVD and global-fitting analyses are shown in Fig. 7.

$1B_u^- \rightarrow Q_x$ and $2A_g^- \rightarrow Q_y$ channels are open, whereas in Cars with $n = 11 - 13$, the $1B_u^+ \rightarrow Q_x$ channel is open but the $1B_u^- \rightarrow Q_x$ and $2A_g^- \rightarrow Q_y$ channels are closed. Further, when n increases from 9 to 13, one observes a systematic but small deacceleration of the $1B_u^+ \rightarrow Q_x$ channel and a systematic but substantial acceleration of $1B_u^- \rightarrow T_1$ triplet generation.

Comparison of Fig. 3 with Fig. 6 shows that the T_1 state is generated by a direct pathway when Cars are bound to the LH2 and LH1 antenna complexes, whereas an indirect pathway via the T_2 state occurs in solution. Interestingly, both the $1B_u^- \rightarrow T_2$ singlet-to-triplet conversion in the latter, and the $1B_u^- \rightarrow T_1$ singlet-to-triplet conversion in the former, approximately follow the energy-gap law (Englman and Jortner, 1970), supporting the idea that both of them are direct transformations. (The time constants of the $1B_u^- \rightarrow T_1$ conversion when bound to the LH1 complexes are shown in terms of an approximate energy-gap law in Fig. S2 together with those of the $1B_u^- \rightarrow T_2$ conversion in solution (see above)). The direct $1B_u^- \rightarrow T_1$ transformation is probably due to the twisting of the conjugated backbone of Cars, when they are bound to the antenna complexes (see Section V.B).

Table 2b lists the efficiencies of the Car-to-BChl singlet-energy transfer through the three channels and those of triplet generation in Cars. As mentioned above, the $1B_u^-$ and $2A_g^-$ channels are closed in Cars with $n = 11$–13. As a result, the sums of the three channels were found to be 78, 75, 46, 40 and 36% for $n = 9$, 10, 11, 12 and 13, respectively (Akahane et al., 2004). Exact determination of the overall efficiencies, by means of fluorescence-excitation and electronic-absorption spectroscopies, was hampered by an excessive amount of Cars incorporated into the LH1 complexes, especially of neurosporene ($n = 9$) and of lycopene ($n = 11$) which have no methoxy groups.

V. Comparison between the Light Harvesting Complexes 1 and 2

A. Dynamics and Efficiencies of Singlet-Energy Transfer and Triplet Generation

Firstly, using Figs. 4 and 6, we compare the dynamics of the singlet-energy transfer and triplet generation between the LH2 and LH1 complexes, for Cars

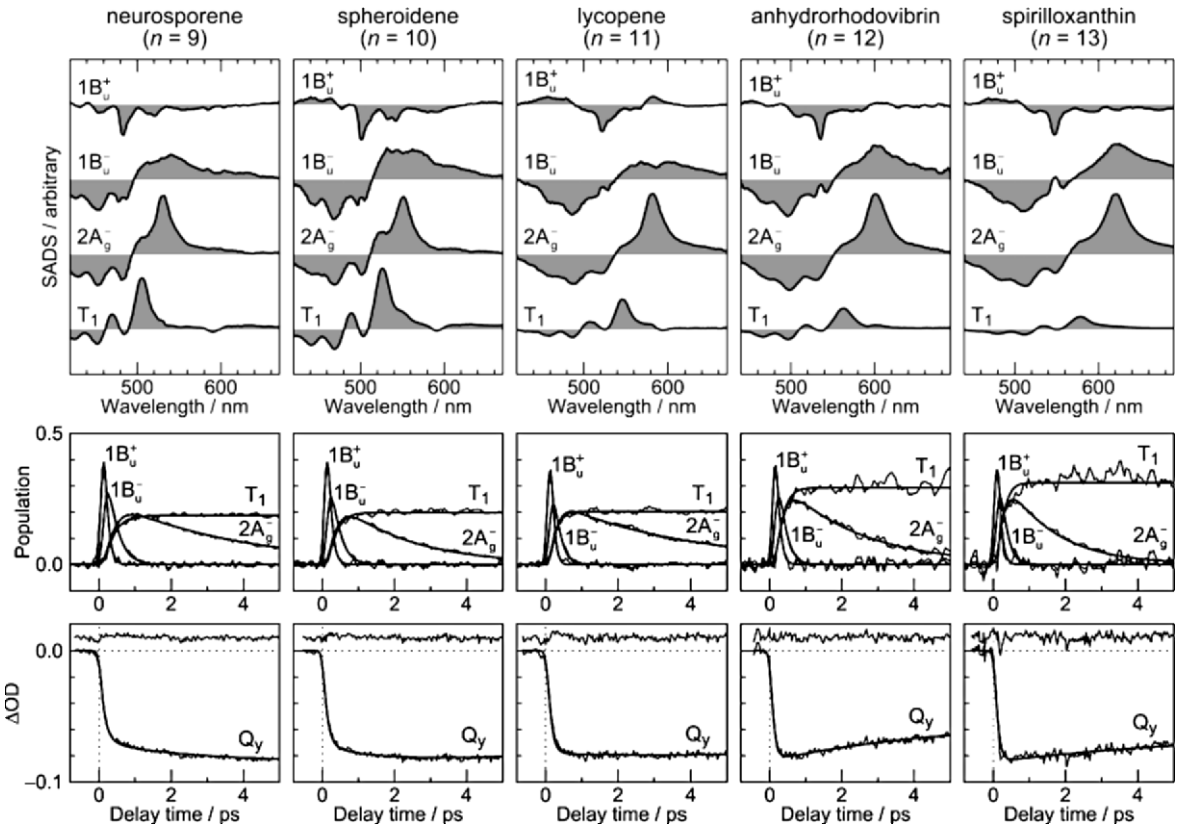

Fig. 7. The SADS (the top panels) and the time-dependent changes in population (the middle panels) for the $1B_u^+$, $1B_u^-$, $2A_g^-$ and T_1 states of the Cars (see Fig. 6). The spectral data matrices were obtained by visible, subpicosecond time-resolved absorption spectroscopy, and analyzed by SVD and global-fitting using the schemes shown in Fig. 6. Fittings to the time profiles of the Q_y bleaching (the bottom panels) that were recorded in the near-infrared region are also shown with the residuals.

with n = 9, 10 and 11. In the determination of the time constants of singlet-energy transfer and triplet generation in the antenna complexes, we assumed that the singlet-to-singlet electronic conversion time constants, within the Car and BChl molecules, were the same as in solution. Therefore, the time constants of singlet-energy transfer can be directly compared between the two antenna complexes as follows:

(1) The singlet-energy transfer through the $1B_u^+ \rightarrow Q_x$ channel is more or less similar in both antennas for Cars with n = 9 and 10, but it is definitely faster in LH2 than in LH1 for Car n = 11.

(2) The energy transfer through the $1B_u^- \rightarrow Q_x$ channel is much faster in LH2 than in LH1 for Cars with n = 9 and 10, where this channel is activated.

(3) The energy transfer through the $2A_g^- \rightarrow Q_y$ channel also is much faster in LH2 than in LH1 for Cars with n = 9 and 10. The natural LH2 complexes may be more refined for the light harvesting function than the artificial LH1 complexes that were reconstituted from Cars and carotenoid-less LH1.

(4) On the other hand, the triplet generation is much faster in LH1 than in LH2 for all the Cars n = 9, 10 and 11.

Next, using Table 2, we compare the efficiencies of singlet-energy transfer and triplet generation and note the following observations.

(1) The singlet-energy transfer through the $1B_u^+ \rightarrow Q_x$ channel is almost the same in the two antennas for Cars with n = 9 and 10, but it is more efficient in LH2 than in LH1 for Car with n = 11.

(2) Both the $1B_u^- \rightarrow Q_x$ and the $2A_g^- \rightarrow Q_y$ channels are closed for Car with n = 11.

(3) The singlet-energy transfer through the $1B_u^- \rightarrow Q_x$ channel is approximately twice as efficient in LH2 than in LH1 for Cars with $n = 9$ and 10.

(4) The singlet-energy transfer through the $2A_g^- \rightarrow Q_y$ channel is almost the same between the two complexes for Cars with $n = 9$ and 10.

(5) As a sum of all the three channels, the efficiencies of singlet-energy transfer are definitely higher in LH2 than in LH1.

(6) On the other hand, the triplet generation is much more efficient in LH1 than in LH2.

Thus, it can be concluded that the LH2 complexes are more efficient in singlet-energy transfer, and that the LH1 complexes are more efficient in triplet generation.

B. Relevance to the Structures and Functions of the Two Antenna Complexes

It is very likely that the above-mentioned higher efficiencies of singlet-energy transfer and of triplet generation, observed in the LH2 and LH1 antenna complexes, respectively, originates from difference in the intermolecular interactions between Cars and BChls and differences in the conformation of the conjugated chain of Cars in these two complexes. Stronger Car-to-BChl Coulombic interaction must facilitate more efficient Car-to-BChl singlet-energy transfer, while larger twisting of the conjugated chain must enhance triplet generation. We have already obtained some evidence consistent with these ideas, although they require final proof by evaluating known (McDermott et al., 1995; Koepke et al., 1996; Roszak et al., 2003) and forthcoming structures of both light harvesting complexes from X-ray crystallography studies.

Concerning the efficiencies of singlet-energy transfer, systematic differences in the Car and BChl electronic absorption spectra, between the two complexes, supports the above idea. Table 3 compares the wavelengths of the $1B_u^+ \leftarrow 1A_g^-$, $S_n \leftarrow 2A_g^-$ and $T_n \leftarrow T_1$ absorptions between the LH2 and LH1 antenna complexes. The absorption spectra in all four LH2 complexes binding Cars with $n = 9$–11 are, in general, *red-shifted* compared with those of the LH1 complexes that were reconstituted with the same Car, or with a different Car having the same conjugation length. The systematic red-shifts of the Car absorption spectra in LH2 strongly suggest a difference in the arrangement and, as a result, in the dispersive interaction between the conjugated systems of Cars and BChls: this would affect the electronic transitions from the ground and the excited states. It should be pointed out here that in the LH2 and LH1 complexes, the BChl molecules interacting with Car are ring-shaped aggregates that gives rise to a pair of common Q_y absorptions around 850 and 880 nm, respectively (Chapter 21, Köhler and Aartsma; Chapter 29, Leupold et al.). On the other hand, preliminary theoretical calculations have shown that the twisting of the conjugated backbone of Cars enhances the spin-orbit coupling and, as a result, the generation of the triplet states (H. Nagae, personal communication).

It is also likely that the above structural differences have been developed, during the evolution of purple photosynthetic bacteria, for slightly different functions of those antenna complexes. Since the LH2 complex is the major component in the membrane of most photosynthetic bacteria and is specialized for the light harvesting function, the efficiency of singlet-energy transfer should, therefore, be its most important role. On the other hand, in the central LH1 complex forming a 1:1 complex with the reaction center (RC), the photo-protective function may become as important as the light harvesting function.

Concerning the photo-protective function, it should be pointed out that the nearly isoenergetic T_1 states of Car and BChl (Fig. 1) are expected to be relevant. Here, we briefly discuss excited-state reactions in which the T_1 states are involved. (The detailed mechanisms of the following reactions, i.e., Eqs. 1 and 2, are depicted in Fig. S3.) The T_1 state of Car can be generated by the singlet-to-triplet conversion from the $1B_u^-$ state, as one of the intrinsic properties of Cars (see Sec. II). This reaction can function as a leak channel of the singlet energy harvested by Car.

The T_1 state of Car can quench the Q_y state of BChl through the (allowed) singlet-triplet annihilation reaction,

$$*\mathrm{BChl}(Q_y) + *\mathrm{Car}(T_1) \rightarrow \mathrm{BChl}(G) + *\mathrm{Car}(T_1) \quad (1)$$

The reactions can be regarded as a photo-protective function, when the harvested light exceeds the capacity of the RC. The delocalized Q_y state of BChl in the ring structures of B850 and B870 BChls of the LH2

Table 3. Comparison of the $1B_u^+ \leftarrow 1A_g^-$ (ground), $S_n \leftarrow 2A_g^-$ and $T_n \leftarrow T_1$ absorptions (in nm) of Cars in the LH2 complexes (as specified) with those of neurosporene ($n = 9$), spheroidene ($n = 10$) and lycopene ($n = 11$) incorporated into the LH1 complex from *Rsp. rubrum* G9.

	$1B_u^+ \leftarrow 1A_g^-$	$S_n \leftarrow 2A_g^-$	$T_n \leftarrow T_1$
Rba. sphaeroides G1C	491 / 483	537 / 531	509 / 505
neurosporene	459 / 452		475 / 470
($n = 9$)	432 / 425		444 / 438
Rba. sphaeroides 2.4.1	510 / 502	556 / 552	531 / 526
spheroidene	477 / 469		495 / 489
($n = 10$)	450 / 442		462 / 454
Rsp. molischianum	528 / 522	589 / 582	552 / 546
rhodopin + lycopene	492 / 486		515 / 507
($n = 11$)	466 / 458		480 / 471
Rps. acidophila	523 / 522	582 / 582	548 / 546
rhodopin glucoside	488 / 486		509 / 507
($n = 11$)	461 / 458		474 / 471

and LH1 complexes, has a good chance of colliding with the T_1 state of Car in close contact with each pair of the B850 and B870 BChls in the ring.

On the other hand, a triplet pair of BChl and Car can generate the Q_y state through the triplet-triplet annihilation reaction,

$$*\mathrm{BChl}(T_1) + *\mathrm{Car}(T_1) \rightarrow *\mathrm{BChl}(Q_y) + \mathrm{Car}(1A_g^-) \quad (2)$$

The resultant Q_y state of BChl can facilitate delayed singlet-energy transfer either from LH2 to LH1 or from LH1 to RC. Here, the T_1 state of Car, together with the T_1 state of BChl, can function as a transient energy reservoir that facilitates delayed singlet-energy transfer through the Q_y state of BChl. This reaction was observed in an LH2 complex at low temperature, where the BChl-to-Car triplet-energy transfer was not very efficient (Rondonuwu et al., 2004a). Actually, time-resolved phosphorescence spectroscopy at 25 K of the LH2 complex from *Rba. sphaeroides* G1C showed that the T_1 state of BChl, the T_1 state of Car and the Q_y state of BChl, all decayed, within the limit of experimental error, with the same constant (Fig. S4 shows their time profiles). This pathway of triplet-triplet annihilation followed by singlet-energy transfer may explain the *systematic* difference between the overall energy-transfer efficiencies determined by fluorescence-excitation and absorption spectroscopies and the sums of the singlet-energy channels determined by subpicosecond time-resolved absorption spectroscopy (see column Φ(obs) and Φ(sum) in Table 2a).

In summary, based on recent work from our laboratory, a scheme has been presented in this review concerning the state ordering and the electronic conversions in Car, and the singlet-energy transfer from Car to BChl in the antenna complexes from purple photosynthetic bacteria. It is concise and self-consistent, but should be regarded as a working hypothesis. The scheme needs to be established by further investigations. Consistency with the results from other laboratories needs to be critically examined.

As an extension of the present method, the next target is obviously to determine the roles of the $3A_g^-$ state. Much shorter pump and probe pulses are absolutely necessary to completely time-resolve the four singlet states. (The SADS of spirilloxanthin ($n = 13$) obtained by the SVD and global-fitting analyses of time-resolved absorption spectra that were recorded by the use of 5 fs pump-and-probe pulses is presented in Fig. S5, as an example.)

Acknowledgments

The authors thank Prof. Jian-Ping Zhang for reading the manuscript, and Prof. Hiroyoshi Nagae for stimulating discussion. This work has been supported by a grant from NEDO (New Energy and Industrial Technology Development Organization, 'International Joint Research Grant'), and a grant from the Ministry of Education, Culture, Sports, Science and Technology for an Open Research Center Project, 'A Research Center of Photo-Energy Conversion.'

References

Akahane J, Rondonuwu FS, Fiedor L, Watanabe Y and Koyama Y (2004) Dependence of singlet-energy transfer on the conjugation length of carotenoids reconstituted into the LH1 complex from *Rhodospirillum rubrum* G9. Chem Phys Lett 393: 184–191

Callis PR, Scott TW and Albrecht AC (1983) Perturbation selection rules for multiphoton electronic spectroscopy of neutral alternant hydrocarbons. J Chem Phys 78: 16–22

Englman R and Jortner J (1970) The energy gap law for radiationless transitions in large molecules. Mol Phys 18: 145–164

Frank HA and Christensen RL (1995) Singlet energy transfer from carotenoids to bacteriochlorophylls. In: Blankenship RE, Madigan MT and Bauer CE (eds) Anoxygenic Photosynthetic Bacteria, pp 373–384. Kluwer Academic Publishers, Dordrecht

Frank HA and Cogdell RJ (1993) The photochemistry and function of carotenoids in photosynthesis. In: Young A and Britton G (eds) Carotenoids in Photosynthesis, pp 252–326. Chapman & Hall, London

Fujii R, Onaka K, Kuki M, Koyama Y and Watanabe Y (1998) The $2A_g^-$ energies of all-trans-neurosporene and spheroidene as determined by fluorescence spectroscopy. Chem Phys Lett 288: 847–853

Fujii R, Ishikawa T, Koyama Y, Taguchi M, Isobe Y, Nagae H and Watanabe Y (2001) Fluorescence spectroscopy of all-*trans*-anhydrorhodovibrin and spirilloxanthin: detection of the $1B_u^-$ fluorescence. J Phys Chem A 105: 5348–5355

Fujii R, Inaba T, Watanabe Y, Koyama Y and Zhang J-P (2003) Two different pathways of internal conversion in carotenoids depending on the length of the conjugated chain. Chem Phys Lett 369: 165–172

Furuichi K, Sashima T and Koyama Y (2002) The first detection of the $3A_g^-$ state in carotenoids using resonance-Raman excitation profiles. Chem Phys Lett 356: 547–555

Hu X, Ritz T, Damjanović A, Autenrieth F and Schulten K (2002) Photosynthetic apparatus of purple bacteria. Q Rev Biophys 35: 1–62

Koepke J, Hu X, Muenke C, Schulten K and Michel H (1996) The crystal structure of the light-harvesting complex II (B800-850) from *Rhodospirillum molischianum*. Structure 4: 581–597

Koyama Y, Kuki M, Andersson PO and Gillbro T (1996) Singlet excited states and the light-harvesting function of carotenoids in bacterial photosynthesis. Photochem Photobiol 63: 243–256

Macpherson AN, Arellano JB, Fraser NJ, Cogdell RJ and Gillbro T (2001) Efficient energy transfer from the carotenoid S_2 state in a photosynthetic light-harvesting complex. Biophys J 80: 923–930

McDermott G, Prince SM, Freer AA, Hawthornthwaite-Lawless AM, Papiz MZ, Cogdell RJ and Isaacs NW (1995) Crystal structure of an integral membrane light-harvesting complex from photosynthetic bacteria. Nature 374: 517–521

Pariser R (1956) Theory of the electronic spectra and structure of the polyacenes and of alternant hydrocarbons. J Chem Phys 24: 250–268

Ritz T, Damjanović A, Schulten K, Zhang J-P and Koyama Y (2000) Efficient light harvesting through carotenoids. Photosynth Res 66: 125–144

Rondonuwu FS, Watanabe Y, Fujii R and Koyama Y (2003) A first detection of singlet to triplet conversion from the $1^1B_u^-$ to the 1^3A_g state and triplet internal conversion from the 1^3A_g to the 1^3B_u state in carotenoids: dependence on the conjugation length. Chem Phys Lett 376: 292–301

Rondonuwu FS, Taguchi T, Fujii R, Yokoyama K, Koyama Y and Watanabe Y (2004a) The energies and kinetics of triplet carotenoids in the LH2 antenna complexes as determined by phosphorescence spectroscopy. Chem Phys Lett 384: 364–371

Rondonuwu FS, Yokoyama K, Fujii R, Koyama Y, Cogdell RJ and Watanabe Y (2004b) The role of the $1^1B_u^-$ state in carotenoid-to-bacteriochlorophyll singlet-energy transfer in the LH2 antenna complexes from *Rhodobacter sphaeroides* G1C, *Rhodobacter sphaeroides* 2.4.1, *Rhodospirillum molischianum* and *Rhodopseudomonas acidophila*. Chem Phys Lett 390: 314–322

Roszak AW, Howard TD, Southall J, Gardiner AT, Law CJ, Isaacs NW and Cogdell RJ (2003) Crystal structure of the RC-LH1 core complex from *Rhodopseudomonas palustris*. Science 302: 1969–1972

Sashima T, Nagae H, Kuki M and Koyama Y (1999) A new singlet-excited state of all-*trans*-spheroidene as detected by resonance-Raman excitation profiles. Chem Phys Lett 299: 187–194

Sashima T, Koyama Y, Yamada T and Hashimoto H (2000) The $1B_u^+$, $1B_u^-$, and $2A_g^-$ energies of crystalline lycopene, β-carotene, and mini-9-β-carotene as determined by resonance-Raman excitation profiles: Dependence of the $1B_u^-$ state energy on the conjugation length. J Phys Chem B 104: 5011–5019

Sundström V, Pullerits T and van Grondelle R (1999) Photosynthetic light-harvesting: Reconciling dynamics and structure of purple bacterial LH2 reveals function of photosynthetic unit. J Phys Chem B 103: 2327–2346

Tavan P and Schulten K (1986) The low-lying electronic excitations in long polyenes: A PPP-MRD-CI study. J Chem Phys 85: 6602–6609

Tavan P and Schulten K (1987) Electronic excitations in finite and infinite polyenes. Phys Rev B 36: 4337–4358

Wang P, Nakamura R, Kanematsu Y, Koyama Y, Nagae H, Nishio T, Hashimoto H and Zhang J-P (2005) Low-lying singlet states of carotenoids having 8–13 conjugated double bonds as determined by electronic absorption spectroscopy. Chem Phys Lett 410 108–114

Zhang J-P, Inaba T, Watanabe Y and Koyama Y (2000) Sub-picosecond time-resolved absorption spectroscopy of all-*trans*-neurosporene in solution and bound to the LH2 complex form *Rhodobacter sphaeroides* G1C. Chem Phys Lett 331: 154–162

Chapter 31

Electron Transfer in Photosynthetic Reaction Centers

Josef Wachtveitl*
Institut für Physikalische und Theoretische Chemie, Goethe-Universität Frankfurt, 60439 Frankfurt, Germany

Wolfgang Zinth
Sektion Physik, Ludwig-Maximilians-Universität München, Oettingenstr. 67, 80538 München, Germany

Summary

The central importance of (bacterio)chlorophyll as a major photosynthetic pigment arises from its ability to both harvest the sunlight and perform ultrafast electron transfer (ET) reactions. The main function of the reaction center (RC) is to convert the photoexcitation in order to generate a trans-membrane potential in a series of ET steps. In bacterial RCs it is possible to relate molecular structure and biological function by exploring the early events after photoexcitation. In a series of ultrafast time resolved experiments with native and modified samples, the details of the primary photosy nthetic reactions become visible, information on the relevant electron transfer parameters (free energy, reorganization energy and electronic coupling) can be deduced. This leads to a better understanding of architectural principles in photosynthetic RCs and optimization strategies in photosynthesis.

*Author for correspondence, email: wveitl@theochem.uni-frankfurt.de

Bernhard Grimm, Robert J. Porra, Wolfhart Rüdiger and Hugo Scheer (eds): Chlorophylls and Bacteriochlorophylls: Biochemistry, Biophysics, Functions and Applications, pp. 445–459.

I. Introduction

The early events in photosynthesis are the absorption of a photon by the light harvesting antenna systems, followed by a rapid and efficient transfer of the excitation energy to the reaction center (reviewed in the preceding two chapters of this book), where the primary charge separation takes place. The general energy storage principle of the photosynthetic reaction center (RC) is to link electron transfer to directional proton transfer and thus generate a trans-membrane potential. The separation of electrons is established in (bacterio)chlorophyll ((B)Chl) containing pigment-protein complexes embedded in the photosynthetic membrane. A series of fast electron transfer (ET) reactions, along a chain of pigment molecules and across the photosynthetic membrane, stabilizes the electrochemical charge separation energy.

In oxygenic photosynthetic organisms, two photosystems (PS I and PS II) act in concert to transfer electrons from water to $NADP^+$. After the purple bacterial RC (Deisenhofer et al., 1984; Allen et al., 1987; Chang et al., 1991; Ermler et al., 1994; Stowell et al., 1997), PS I is the second type of photosynthetic RC for which the X-ray structure was solved with high resolution (Jordan et al., 2001; Ben-Shem et al., 2003). The structural data provide a detailed picture of the cofactor arrangement and, therefore, the basis for an assignment of the sequence of ET steps spectroscopically detected in PS I (Fig. 1, left) (Brettel and Leibl, 2001). The main experimental difficulty for time resolved optical spectroscopy is the fact, that PS I preparations are usually associated with their antenna systems, i.e., they contain approx. 100 chlorophyll molecules. Thus, the absorbance changes following photoexcitation contain both energy and electron transfer components, because both processes occur on the same time scale. Since the contribution of the antenna chlorophylls is approx. one order of magnitude larger (Savikhin et al., 2000), it is impossible to directly detect the first charge separated intermediate, $P700^+A_0^-$, in intact PS I preparations and the determination of the intrinsic time constants of primary reactions has to rely on indirect methods (Beddard, 1998; Brettel, 1997). Although for these reasons, the time constant for the formation of the first ET intermediate $P700^+A_0^-$ is not well established, values of a few picoseconds are reported in the literature (Byrdin et al., 2000; Savikhin et al., 2000). These ET rates can now be compared with the cofactor distances derived from the X-ray structure. An edge-to-edge distance of 13 Å between P700 and A_0 would lead to an estimated ET rate in the order of 10^7, i.e., 5 orders of magnitude slower than the one observed. This discrepancy can be overcome by assuming an active role for the chlorophylls eC-B2 (and/or eC-A2), located between P700 and A_0, as real electron transfer intermediate (reviewed in Brettel and Leibl, 2001). This discussion is reminiscent of the long standing debate concerning the role of the 'accessory' chlorophylls in bacterial RCs, which will be addressed in detail below.

Also, for PS II, electron and energy transfer processes are hard to disentangle. Although PS II reaction centers containing only six Chl molecules per complex can be isolated, the similar Chl couplings, and hence the lack of an isolated, low-lying excited state, complicate the assignment of the femto- and picosecond transients (Prokhorenko and Holzwarth, 2000). This supermolecular behavior can be described satisfactorily by a Multimer Model (Barter et al., 2003) that reproduces the experimental data in agreement with the medium resolution PS II structure (Jordan et al., 2001; Vasil'ev et al., 2001; Bibby et al., 2003).

In this chapter the discussion of primary electron transfer will be focused on purple bacterial RC. These systems can be prepared devoid of any antenna chlorophylls and show a largely unidirectional electron transfer. Thus, the integrated approach of structural analysis, ultrafast spectroscopy and protein (and/or pigment) modification allows a direct and detailed analysis of the early photosynthetic light reactions.

II. Dynamics and Energetics of the First Electron Transfer Reactions in Bacterial Reaction Centers

The experimental prerequisite for the time resolved observation of the fast ET dynamics within the RC is the synchronization of the reaction by an even faster external trigger. Femtosecond spectroscopy

Abbreviations: $B_{A/B}$ – sites of monomeric BChl in the RC (A and B refer to the position on the active and inactive branch, respectively); *Blc. – Blastochloris*; Cyt – cytochrome; ET – electron transfer; $H_{A/B}$ – sites of monomeric BPhe in the RC; P – primary electron donor; P_+P_- – upper/lower exciton band of P; P^+ – cation radical of P (note: in all ion radicals the dot is omitted, i.e., B^-, H^- instead of $B^{\bullet-}$, $H^{\bullet-}$; $Q_{A/B}$ – quinone sites; *Rba. – Rhodobacter*; RC(s) – reaction center(s); V – electronic coupling; ΔG – gain in free energy; λ – reorganization energy; λ_{pr} – probing wavelength

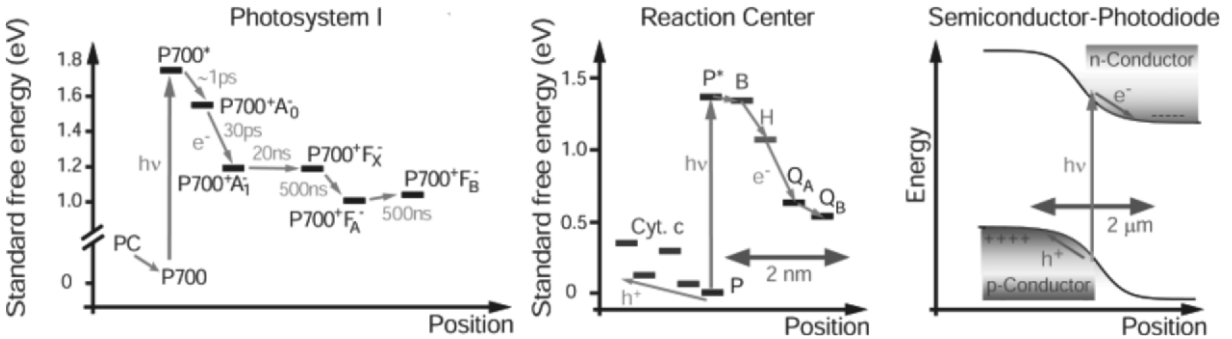

Fig. 1. Energetics of ET systems. left: PS I, middle: bacterial RC, right: semiconductor photodiode. For PS I the ET kinetics, electron pathways and energetics of ET intermediates are still under debate, the schematic arrangement and the energetic positions of the cofactors, as recently discussed in Brettel and Leibl (2001), is depicted on the left. The primary electron donor P700 is a dimer of Chl *a* and the chain of electron acceptors consists of a Chl *a* monomer (A_0), a phylloquinone (A_1) and three [4Fe-4S] clusters (F_X, F_A and F_B). The ET steps for purple bacterial RC from *Blc. viridis* (center) are discussed in detail in the text. The photoprocesses taking place in the reaction centers resemble those in a photodiode (right). In all systems light absorption is followed by fast charge separation processes involving both electron and hole transfer. See also Color Plate 6, Fig. 2.

with pulses in the range of a few 10 fs allows a direct observation (i) of the sequence of ET steps following the photoexcitation of the primary donor P in native and modified RC (Sections A and B) and (ii) of even initial nuclear motions via vibrational wave packet evolution (Section C).

A. The Primary Electron Acceptor, Energetics of the First Intermediate State $P^+B_A^-$

Since the successful resolution of the molecular structure of bacterial reaction centers (Deisenhofer et al., 1984; Allen et al., 1987), the individual chromophores within the protein can be directly related with the various primary photochemical events (Fig. 2). The RCs in purple bacteria consist of at least three protein subunits (L, M and H), four BChl and two BPhe molecules, one atom of non-heme ferrous iron and two quinone molecules. Most investigations on purple bacterial photosynthesis were carried out on *Rhodobacter* (*Rba.*) *sphaeroides, Rba. capsulatus* (which contain BChl *a* as tetrapyrroles) and *Blastochloris* (*Blc.*) *viridis* (which contain BChl *b*). The chromophores are arranged in two branches (termed A and B) with an approximate C_2-symmetry. Two BChl molecules are strongly coupled electronically and represent the primary electron donor P. Over the last two decades, the dynamics of the electron transfer steps following the light-induced generation of the excited electronic state P* has been studied by time-resolved spectroscopy. The most prominent kinetic component is the decay of the P*-state and the

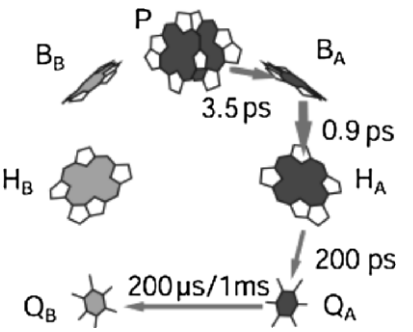

Fig. 2. Scheme of chromophore arrangement and reaction dynamics of primary electron transfer steps in the bacterial RC. ET proceeds via the active branch of electron carriers consisting of the special pair P, the BChl B_A, the BPhe H_A and the quinones Q_A and Q_B. The electron is transferred from P to Q_A within 200 ps, the $Q_A \rightarrow Q_B$ transition is approx. 10^6-fold slower. Recent FTIR-studies report that Q_B is not directly reduced by Q_A^-, but through an intermediary electron donor (Remy and Gerwert, 2003). According to these data, the main time constants are 150 µs for Q_B reduction and 1.1 ms for Q_A reoxidation.

formation of the product state $P^+H_A^-$ within ~ 3 ps at room temperature (Woodbury et al., 1985; Breton et al., 1986; Martin et al., 1986; Holzapfel et al., 1989, 1990; Dressler et al., 1991). Polarized spectroscopy on crystallized RCs (Zinth et al., 1983; Knapp et al., 1985) and time-resolved analysis based on spectral differences of H_A and H_B at low temperatures (Kirmaier et al., 1985; Michel-Beyerle et al., 1988) demonstrated that predominantly the A-branch is active in electron transfer. Advanced spectroscopic methods revealed details of the P* state, like the species-dependent degree of intradimer charge transfer character (of the type $P_L^+P_M^-$) (Lathrop and Friesner,

1994; Rautter et al., 1994) or the apparent deviations from a mono-exponential decay (Du et al., 1992; Hamm et al., 1993; Jia et al., 1993; Ogrodnik et al., 1994; Beekman et al., 1995).

Individual ET steps in the photosynthetic systems are often explained in the frame of Marcus theory (Marcus and Sutin, 1985; Moser et al., 1993). In the simplified description, four parameters control each reaction step: the electronic coupling V between the donor and acceptor molecules, the gain in free energy ΔG, the reorganization energy λ and the vibrational frequency ω, which is taken as a measure for the temporal modulation of the energy gap between donor and acceptor states induced by the molecular motion.

Inspection of crystallographic data and the effect of magnetic fields allowed exclusion of the direct reaction $P^* \rightarrow P^+H_A^-$, since the rate predicted by classical nonadiabatic Marcus theory would be several orders of magnitude too slow. Therefore, an active role of the monomeric chlorophyll B_A, either as virtual intermediate via a superexchange mechanism (Bixon et al., 1989, 1991), or as a real, transiently populated intermediate, appeared likely. A sequential electron transfer via B_A imposes not only restrictions on the energetics of the intermediate $P^+B_A^-$ (as will be discussed below), but also on its dynamics. The similar kinetics observed for P* decay and $P^+H_A^-$ formation requires that the decay of the intermediate, $P^+B_A^-$, must be significantly faster than its formation. Under that condition, only a small transient population of the $P^+B_A^-$ intermediate results (Marcus, 1987). This fact rendered the direct observation of the $P^+B_A^-$ state difficult; but, in a series of experiments, a distinct subpicosecond kinetic component could be identified (Holzapfel et al., 1989, 1990; Chan et al., 1991; Dressler et al., 1991; Arlt et al., 1993; Beekman et al., 1995). The amplitude of this component is especially pronounced in spectral regions with high BChl and $BChl^-$ absorption. The most suitable region for the unambiguous detection of the subpicosecond component is the near-IR absorption band of the monomeric BChl radical anion (in *Rba. sphaeroides* at 1020 nm (Fajer et al., 1975; Fujita et al., 1978)). Here, contributions from ground state absorption and stimulated emission are so small, that the transient absorption changes at early delay times can be modeled exclusively with a 0.9 ps time constant (Fig. 3, open circles). Photodichroism provides another critical test of the sequential reaction model. The transient absorption data in Fig. 3 reveal a change in the dichroic ratio $A_\parallel/A_\perp$ with delay time. This readily indicates that different intermediates with dissimilar direction of their transition dipole moments are involved in the electron transfer chain. The sequential model including a real $P^+B_A^-$ intermediate leads to an agreement within a few degrees between the spectroscopic data and the angle between the Q_Y transitions of P and B_A^- as predicted by the X-ray structure (Arlt et al., 1993; Wachtveitl et al., 1998).

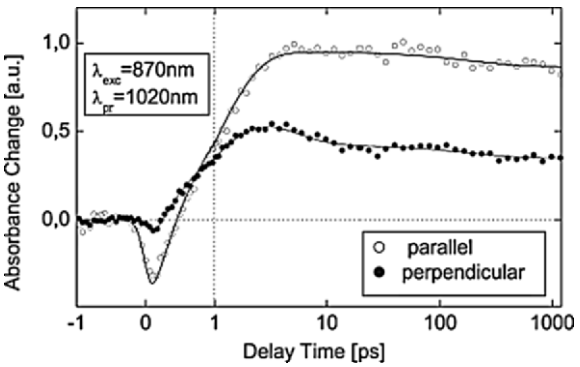

Fig. 3. Polarization dependent transient absorption kinetics in the BChl *a* radical anion band of native *Rba. sphaeroides* RCs. Open/filled circles: parallel/perpendicular polarization of pump and probe pulses. The model curves (lines) are calculated using time constants of 0.9 ps, 200 ps and infinity for parallel polarization and an additional 3 ps component for perpendicular polarization (modified after Wachtveitl et al., 1998). The time scale is linear for delay times $\tau_d < 1$ ps and logarithmic for $\tau_d < 1$ ps.

B. Specific Variation of Electron Transfer Parameters by Protein Engineering and Chromophore Modification

Since more than a decade, selective perturbations of the RC pigment-protein complex can be introduced by site-directed mutagenesis (Bylina and Youvan, 1988; Coleman and Youvan, 1990; Gray et al., 1990; Farchaus et al., 1993) or by pigment exchange (Struck and Scheer, 1990; Struck et al., 1990; Meyer and Scheer, 1995). The modifications allow us to address specific regions of the ET chain and result in a variation of the relevant parameters controlling ET dynamics.

1. The Primary Donor P

A series of mutants was designed to modify the environment of the primary electron donor P (Wachtveitl et al., 1993; Allen et al., 1996; Kuglstatter et al., 1999; Schenkl et al., 2002). It could be shown that a change

Table 1. Electron transfer properties for native and mutated *Blc. viridis* reaction centers at room and low temperatures

RC *Blc. viridis*	$\Delta U_{P/P}$+ [mV]	$\Delta\Delta G$ [cm^{-1}]	room temperature			low temperature 1) 30 K; 2) 50 K	
			τ_1 [ps]	τ_{1A} / τ_{1B} [ps]	$R = \frac{a(\tau_{1A})}{a(\tau_{1B})}$	τ_{1A} / τ_{1B} [ps]	$R = \frac{a(\tau_{1A})}{a(\tau_{1B})}$
WT	0	0	3.5 ± 0.4	1.8 / 7.4	1.4	1.1 / 37[1)]	2.9
L168HF	–80	–670	1.1 ± 0.2	0.8 / 3.8	4.8	0.25 / 1.7[1)]	1.9
M195YF	–45	–370	3.1 ± 0.3	1.5 / 5.4	0.8	1 / 3.5[2)]	3.3
L168HF/M195YF	–80	*	0.8 ± 0.2	0.6 / 3.2	3.0	–	–
M195YH	+20	+170	5.7 ± 0.5	3.5 /14.5	2.0	–	–
L181FY	–25	–210	1.7 ± 0.2	1.15/ 4.5	2.8	0.5 / 1.3[2)]	2.5
M208YF	+15	*	20 ± 3	8 /30	0.3	9 / 83[1)]	0.44
M208YL	+15	*	29 ± 5	11 / 50	0.5	–	–
L181FY/M208YF	–25	*	8.2 ± 1.5	4.5 / 16	2.3	–	–
L153HC	+2	+16	3.8 ± 0.4	2.5 / 10	3.0	–	–
L153HE	–	*	12 ± 1	7 / 40	2.0	–	–
L153HL	0	–1600	3.5 ± 0.4	3 / 43	4.0	–	–
L162YF	≈–5	–40	3.5 ± 0.4	2.7/ 16	>4.0	–	–
L162YG	+10	+80	5.4 ± 0.5	3.3/ 18	2.6	–	–

The P/P^+- redox midpoint potential ($\Delta U_{P/P}$+) is expressed as difference from the WT value of +520 mV (vs.NHE). This value together with the contribution arising from chromophore modification (e.g., BPhe *b* instead of BChl *b* at B_A position in L153HL RC) determines the change in free energy difference for the first electron transfer step. * $\Delta\Delta G$ cannot be calculated explicitly for these cases since additional changes are expected. The given decay constants result from a monoexponential (τ_1) or a biexponential (τ_{1A}, τ_{1B}) fit of the first electron transfer step $P^* \rightarrow P^+B_A^-$. R indicates the ratio of the respective amplitudes.

of the hydrogen bonding pattern between the two BChls constituting P and the protein is closely correlated to the oxidation potential of the primary donor (Lin et al., 1994; Wachtveitl et al., 1998). However, the altered driving force between donor and acceptor does not influence the ET rates in the way expected from the direct application of Marcus theory (Williams et al., 1992; Schenkl et al., 2002). This deviation was confirmed in fs-experiments on various mutant RCs at different temperatures (Huppmann et al., 2002). It is found, that different site specific mutant RCs can vary in their rate of the primary charge separation by more than one order of magnitude (Zinth et al., 1998; Huppmann et al., 2002). These results readily indicate that the kinetic picture is more complicated than a simple chromophore distance vs. log (k_{ET}) relationship (Moser et al., 1992). In Table 1 spectroscopic, redox and dynamic properties of native and mutated RC of *Blc. viridis* are compared. Under the often used assumption that the mutation predominantly influences the energetics of the primary electron transfer intermediates, the primary charge separation steps at room temperature can be modeled according to nonadiabatic ET-theory, if the single mode model is expanded and an additional high frequency mode (ω_h = 1500 cm^{-1}) is considered. This 'multi'mode treatment is necessary to explain the fast charge separation for mutant RCs, where the mutation pushes the primary reaction far into the Marcus inverted region (e.g., for L153HL). This procedure yields a value of 600 ± 200 cm^{-1} for the reorganization energy λ, an electronic coupling V = 37 ± 10 cm^{-1} and a free energy gap ΔG ranging from –600 to +800 cm^{-1} (Zinth et al., 1998; Huppmann et al., 2002, 2003). Interestingly, the primary reaction for native RCs appears to be slightly activated within this model (Huppmann et al., 2002). Consequently, several mutant RCs with a significantly accelerated primary reaction could be constructed (Table 1), especially by removing a hydrogen bond to the special pair P (L168HF, M195YF and L168HF/M195YF). Interestingly, such a strong acceleration was not observed for the corresponding mutants in *Rba. sphaeroides* (Murchison et al., 1993; Woodbury et al., 1994).

The classical Marcus treatment (Marcus and Sutin, 1985) results in a significant activation energy for

the primary ET reaction of native and some mutant RCs in *Blc. viridis* (e.g., $E_A \approx 180$ cm^{-1} for wild type RCs). Consequently, an Arrhenius-type temperature dependence, where the reaction slows down at reduced temperatures, is expected for these RCs. However in most RCs (except M208 mutants) an accelerated charge separation towards low temperatures (requiring negligible activation energies $E_A << \hbar\omega$) is found (Breton et al., 1988; Fleming et al., 1988; Lauterwasser et al., 1991; Huppmann et al., 2002). An improved description of ET in proteins therefore needs to consider not only different values for the energetics but also specific variations of other ET parameters upon mutation and temperature change. Especially the electronic coupling V is highly sensitive to subtle conformational changes and drastically affects the primary ET dynamics (McMahon et al., 1998; Zhang and Friesner, 1998; Kolbasov and Scherz, 2000). A modulation of the electronic coupling V with mutation is able to explain a number of observations. However, the strong acceleration of reaction rates upon cooling, found in many RC requires a different explanation. An increase of V upon cooling can consistently explain the fs data. Such a temperature dependence might even reflect more general dynamic properties of proteins: at high temperatures, protein motions have large amplitudes and cause local disorder, which results in a high entropic term and in large fluctuations of the donor/acceptor geometry away from the optimum required for fast ET. This may lead to relatively weak average electronic coupling. At low temperatures the protein is locked in a state with low entropy and high electronic coupling V leading to faster ET dynamics for the case of photosynthetic RCs.

In general, a quantitative description of the effect of a mutation or of the temperature dependence of the various ET-processes in photosynthetic reaction centers spanning a broad range cannot be obtained without a variation of the relevant ET parameters. A decrease in electronic coupling V with temperature is highly probable.

2. The Primary Acceptors B_A and H_A

Except for the BChl *a* dimer P, all tetrapyrroles in the *Rba. sphaeroides* RC are accessible to pigment exchange (Meyer and Scheer, 1995). With exchange rates as high as 90% or better, pigment-modified RCs are, therefore, especially suited to tune the

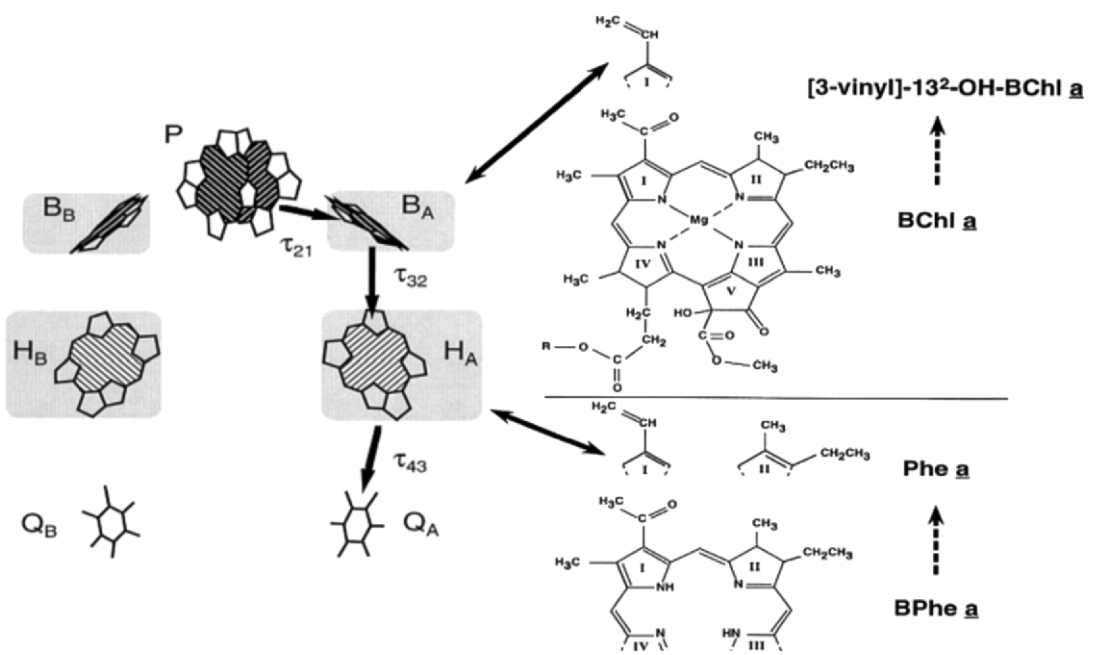

Fig. 4. Sites of pigment exchange (gray boxes) in the RC of *Rba. sphaeroides* (left) and structural differences between the native and the site-specifcally introduced modified pigments (right); modified after Spörlein et al. (2000). Rings I, II, III, IV and V are known as Rings A, B, C, D and E, respectively, in the IUB-IUPAC nomenclature system used elsewhere in this book. The 13^2-OH group in [3-vinyl]-13^2-OH-BChl *a* does ot interfere with electron transfer.

energy levels of the electron acceptors B_A and H_A without changes in the protein moiety (Fig. 4). The introduction of plant pheophytin (Phe *a*) into the H_A and H_B sites, replacing the BPhe *a* molecules, drastically alters the primary reaction dynamics (Shkuropatov and Shuvalov, 1993; Schmidt et al., 1994, 1995) and allowed the final proof of stepwise ET with the accessory BChl as a real electron carrier: a reduced quantum yield (Franken et al., 1997) and a long lived population of the $P^+B_A^-$ intermediate was observed (Fig.5). Since the redox potential of Phe *a* is considerably more negative (≈ 220 mV) than that of BPhe *a* (Geskes et al., 1995) the exchange results in an energetic proximity between the $P^+B_A^-$ and $P^+H_A^-$ intermediates. Forward and backward rates, according to the scheme depicted in Fig. 5 (top), are determined by the free energy difference ΔG of the different intermediate states and can be correlated by the principle of detailed balance (Schmidt et al., 1994, 1995). This procedure allowed the determination of the free energy difference between P* and $P^+B_A^-$ (ΔG ≈ 450 cm^{-1}). A similar value for the free energy difference was determined in recombination fluorescence measurements, where ΔG (P^*-$P^+B_A^-$) = 550 cm^{-1}

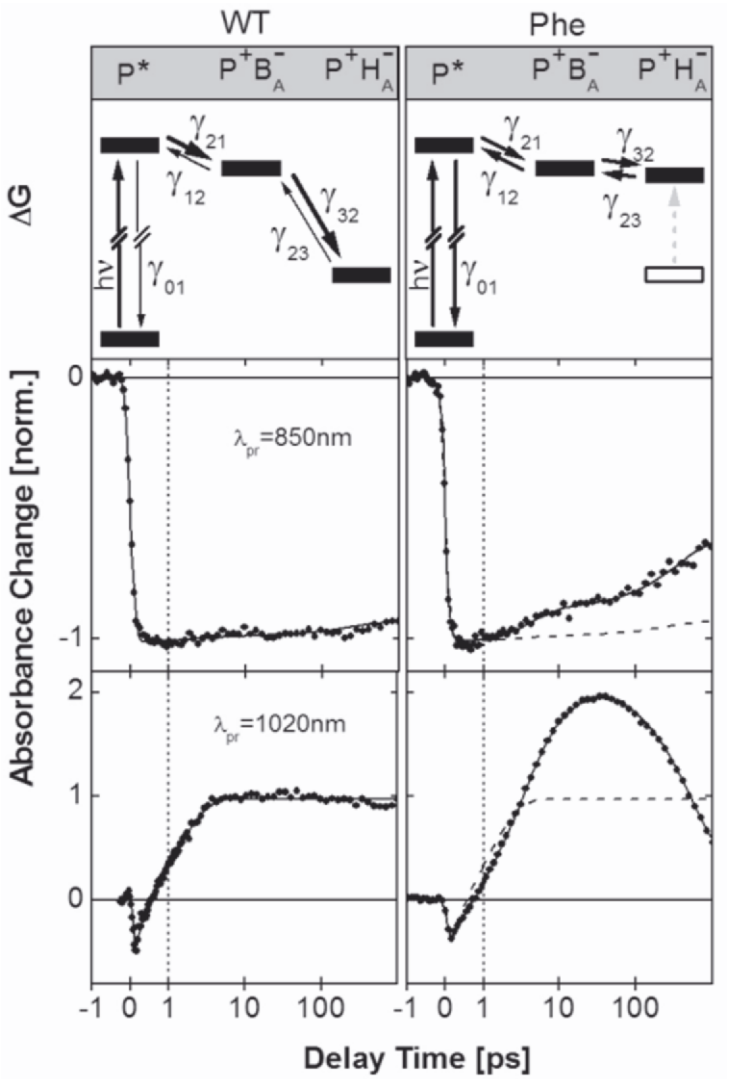

Fig. 5. Schematic representation of the energetic positions of the electron transfer intermediates and the corresponding microscopic time constants (top) for native (left) and Phe *a* containing RC. Transient absorbance changes for spectral regions with dominant contributions from ground state bleaching (middle) and BChl anion absorption (bottom).

(Shuvalov and Yakovlev, 2003). The temperature dependence of the charge separation in Phe *a* containing RC confirmed a ΔG (P^*-$P^+B_A^-$) value in this range; but, as discussed above, it also showed the necessity for an expansion of the simple Marcus picture by temperature-dependent parameters to consistently explain the low temperature data (Huber et al., 1998). As indicated in Fig. 4, BPhe *a* and Phe *a* differ in their chemical structures in two positions, that is the saturation of ring II (B) and the peripheral group at the C-3 position. The role of each variation can be addressed individually with RCs containing [3-vinyl]-BPhe *a* and [3-acetyl]-Phe *a* at the H_A and H_B positions. It was found that spectral and dynamic properties can be separated from each other in the sense, that the ring II (B) conjugation is responsible for the spectral shift between BPhe *a* and Phe *a*, whereas the C-3 substituent controls the efficiency of the primary reaction via optimization of the redox potential (Huber et al., 1995).

A systematic variation of the free energy could also be achieved for the primary electron acceptor B_A. The effect of an energetically elevated acceptor level, as expected for [3-vinyl]-BChl *a* RCs is, again, in accord with a stepwise electron transfer model: here, a slower and less efficient charge separation accompanied by a significant reduction of $P^+B_A^-$ population is found (Spörlein et al., 2000). This again underlines the fact that the ET chain in the bacterial RC represents a highly optimized system where alterations in pigment composition with the related changes of the energetics of the ET intermediates enhance the various loss mechanisms and, thus, reduce efficiency (Section IV).

C. Alternative Pathways and Vibrational Coherence

In a photosynthetic system, the RC is usually excited by energy transfer from the antenna system(s). The situation that P* is not directly produced by the incident light, but by energy transfer from other pigments, can be mimicked in isolated RCs by photoexcitation of the energetically higher lying states B*, H* or P^*_+ (upper exciton band of P). As expected, fast energy transfer to the lowest excited state P^*_- occurs within 50–200 fs and the electron transfer proceeds from there as described above (van Grondelle et al., 1994; Stanley et al., 1996; Vos et al., 1997). However, alternative electron transfer pathways also following B* and H* excitation (with laser pulses at 800 nm and 760 nm, respectively) — e.g., an intermediate with $B_A^+H_A^-$ character — were reported for mutant (van Brederode et al., 1997a,b) and wild type RCs (van Brederode et al., 1997b; Vos et al., 1997; S. Lin et al., 1998). Nevertheless, the lack of a $B_A^+H_A^-$ intermediate in a P-deficient mutant (Jackson et al., 1997) demonstrates the requirement for P for stable charge separation. The observation of the alternative reaction path may be of major importance for the understanding of photosynthesis in higher organisms, where the degeneracy of the Q_y transitions of the different pigments and the arrangement of the energy transducing Chl, prevent the predominant excitation of the special pair. Furthermore, the 'accessory' Chl in the active branch of the PS II core is suggested to act as the primary electron donor (Prokhorenko and Holzwarth, 2000; Barter et al., 2003).

Excitation of P with a fs laser pulse shorter than a vibrational period leads to a coherent excitation of vibrational nuclear motions. Quantum mechanically, this is described as a superposition of wavefunctions of several vibrational levels. Figure 6 illustrates the preparation and subsequent evolution of such a wave packet. Therefore, it is a quite common feature in ultrafast experiments that femtosecond kinetics are superimposed with oscillatory components (Rosker et al., 1986; Mokhtari et al., 1990; Wang et al., 1994). Thus, the first observations of vibrational coherence in photosynthetic reaction centers (Vos et al., 1991, 1993, 1994; Streltsov et al., 1997) immediately raised the question about a possible functional role of these coherent nuclear motions for photosynthetic electron transfer (reviewed in Vos and Martin, 1999). The first oscillatory components, with the strongest modes occurring in the <100 cm^{-1} region, were modulations of the stimulated emission from P* (Vos et al., 1991, 1993). Experiments probing the stimulated (Vos et al., 1994) and the spontaneous emission of P* (Stanley and Boxer, 1995) both gave similar results, and led to the assignment that the activated modes originate from the motion of a vibrational wave packet on the P* potential energy surface. The vibrational modes around 100 cm^{-1} are usually considered as chromophore vibrations or as chromophore driven protein motions. Molecular dynamics simulations (Warshel, 1980), and observations of similar low-frequency modes in other non-monomeric BChl assemblies (like antenna complexes) (Chachisvilis and Sundström, 1996; Joo et al., 1996; Monshouwer et al., 1997; Diffey et al., 1998), suggest a strong contribution from intradimer vibrational modes (Kumble et al., 1996).

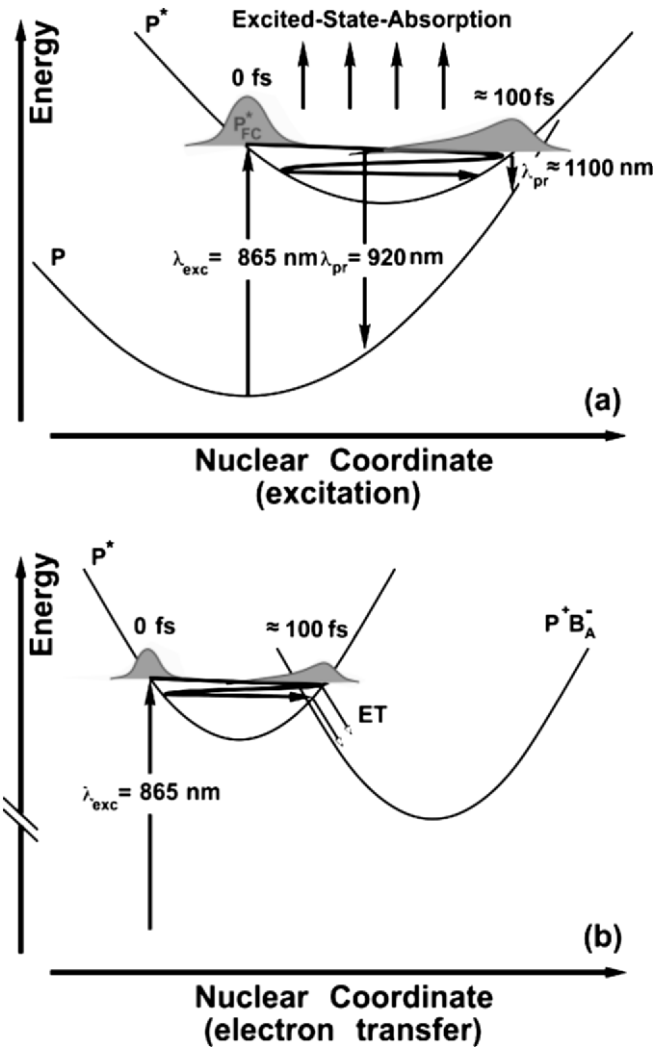

Fig. 6. Scheme to visualize oscillatory absorption changes via the modulation of stimulated emission (a) and modulated ET (b). (a) Wavepacket evolution on a one-dimensional representation of the excited state potential energy surface. The values given describe the energetic and dynamic properties in RCs from *Rba. sphaeroides*. After excitation (865 nm) from the ground state (P) in the Franck-Condon region of the excited state (P^*_{FC}), the created wavepacket moves on the potential energy surface P*. Since excited-state-absorption occurs as long as this state is populated, it is detectable instantaneously. After a few tens of femtoseconds the RC has reached the correct nuclear configuration to allow observation of stimulated emission. Oscillatory modulations of the transients due to the moving wavepacket are observed with different phases at both sides of the spectrum. At 1100 nm the signal of stimulated emission is measurable only for a short time of 250 fs, since at later times relaxation of the wavepacket by energy redistribution prevents the system from reaching this extreme nuclear configuration for a second time. (b) Simplified model for discontinuous electron transfer: after excitation, the wavepacket oscillates on the potential energy surface of P*. It is assumed that a considerable probability of transfer exists only in a small range of nuclear configurations. Each time the wavepacket reaches the intersection region of electron donor (P*) and acceptor ($P^+B_A^-$) there is a possibility to access the $P^+B_A^-$ surface. Therefore the P* state will be depopulated stepwise due to the wavepacket motion. The oscillations of the P* population should not change phase.

The question, if the dominant mode around 100 cm^{-1} is coupled to electron transfer, can be addressed experimentally in the spectral region covering both the electron donor and acceptor bands (Spörlein et al., 1998). Model calculations for the case of a stepwise depopulation of P* and a subsequent population of $P^+B_A^-$ (Fig. 6b), suggest a much stronger modulation of the $P^+B_A^-$ signal compared to the P* signal. In contrast to these expectations for a wave-packet-like modulation of the ET process, the features of the os-

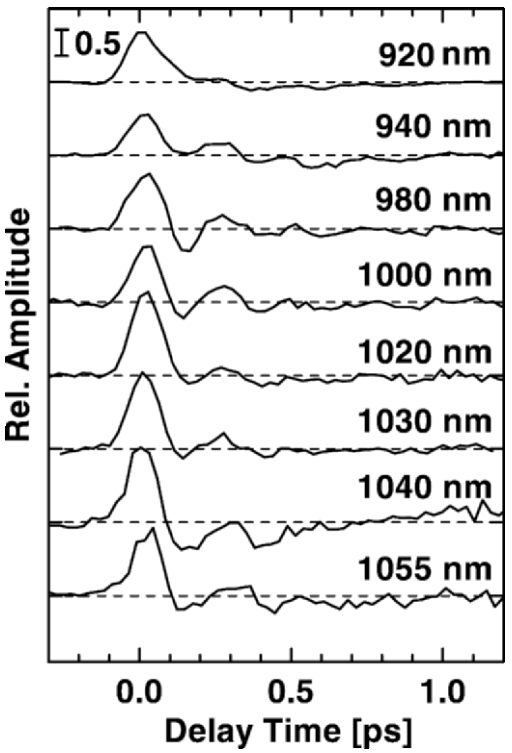

Fig. 7. Residuals from *Rba. sphaeroides* RCs obtained by subtracting a fit curve satisfying the exponential characteristics of the transients from experimental data. They reflect the nuclear motions in real time. The spectral range displayed covers both the stimulated emission band of P* and the absorption band of B_A^-. To allow a better comparison, the plotted graphs are normalized to the amplitude of stimulated emission, which decreases with probing wavelength (taken from Spörlein et al., 1998).

cillatory residuals (Fig. 7) do not change significantly within the B_A^--band (centered at 1020 nm). They can be readily explained by the motion of a vibrational wave packet on the excited state potential surface of the special pair P* and its effect on stimulated emission and excited state absorption, without employing a stepwise electron transfer (Spörlein et al., 1998). The spectral analysis of the residual signals revealed a dominant mode with 135 cm^{-1}, which is damped on the sub-ps time scale, and a weak 40 cm^{-1} mode for λ_{pr} <1030 nm. The involvement of such a low frequency (~30 cm^{-1}) mode in the coherent formation of $P^+B_A^-$ was previously suggested (as recently reviewed in Shuvalov and Yakovlev, 2003) and tentatively assigned to a rotation of water molecules bridging ET active chromophores by hydrogen bonds.

Also for *Blc. viridis* RC strong modulations of the kinetics in the region of a dominant stimulated emission signal with a Fourier spectrum similar to the one observed for *Rba. sphaeroides* could be obtained (Huppmann et al., 2003). Again these features cannot be taken as a direct proof for a coupling of coherent nuclear motion to primary electron transfer for the native RC at room temperature.

In conclusion, for the standard situation of non-adiabatic electron transfer reaction only a small transfer probability exists during a single vibrational period. In this case, the frequency ω influences the ET rate only at low temperatures. Theoretical simulations (Parson and Warshel, 1993; Xu and Schulten, 1994) and measurements of the temperature dependence place ω in the range of 70–200 cm^{-1} (oscillation periods in the 170–500 fs range). For these numbers it is apparent, that the first electron transfer step of room temperature RC occurs in the non-adiabatic regime. However, at cryogenic temperatures the nuclear motions become important for the secondary electron transfer from B_A^- to H_A and for the initial electron transfer reaction in mutated RC with an accelerated charge separation (Huppmann et al., 2003). Here adiabatic processes with medium control are involved in the electron transfer reaction.

III. Optimization of Photosynthesis

The photosynthetic RC is highly efficient in charge separation and electron transfer; for example, values as high as 97% have been reported for the quantum yield of $P^+Q_A^-$ formation (Trissl et al., 1990). The extremely high efficiency is closely related to the design of RC, which has to meet different requirements:

(i) Many photosynthetic bacteria inhabit ecological niches shaded by higher photosynthetic organisms. Therefore, they often must utilize light with wavelengths longer than 700 nm, motivating the usage of BChl instead of Chl. While most photosynthetic bacteria capture light between 750 and 870 nm, the antenna system of the bacterium *Blc.viridis* collects photons even at wavelengths beyond 1000 nm with its BChl *b*-containing antenna system.

(ii) The RC must efficiently collect the excitation coming from the antenna. In order to utilize the excitonic energy from the antenna the absorption of the primary donor—the special pair P of the bacterial RC — must be tuned to long wavelengths. This is achieved by proper selection of the type of bacterial chlorophyll (e.g., using BChl *b* in *Blc.*

viridis), the excitonic coupling of the two BChl molecules of the special pair, the arrangement of the chromophores and the interaction with the surrounding amino acids.

(iii) The excitonic excitation collected by the RC must be stored irreversibly in order to minimize back transfer to the antenna and loss by internal conversion in the antenna system. This demand is fulfilled in the bacterial RC, firstly by appropriate tuning of the energetic position of the excited electronic state of the primary donor (its absorption at the red end of the absorption of all chromophores in the RC) and the high excitonic coupling to other pigments. Secondly, the initial charge separation process is fast (≈ 3 ps), followed by an even faster (≈ 0.6 – 0.9 ps) secondary electron transfer step. In these two processes ≈2000 cm^{-1} of energy are dissipated which prevents a fast back reaction to the antenna.

(iv) The charge separation must be securely maintained before long-time energy storage reactions are accomplished by the later proton transfer processes. Here the RC must minimize the direct charge recombination via electron back transfer to the special pair. This is accomplished by the special design of the electron transfer pathway in the RC: the active branch of electron carriers (see Fig. 2) consists of the special pair P, the BChl B_A, the BPhe H_A and the quinones Q_A and Q_B, arranged in a linear chain. After initial charge separation between P and B_A within 3 ps, the electron travels over the pigment chain in stepwise fashion. The reaction speed decreases with distance from the special pair. The energy of the later intermediate states is also decreased. These two features enable the RC to fulfill the basic requirements for high quantum efficiency in a linear reaction chain: here, for each reaction step, the forward reaction rate must be faster than recombination. The individual optimization criteria are: (a) direct recombination is reduced by increasing the distance between the anion (P^+) and the cation (I^-), and by adjusting the forward reaction rate; and, (b) recombination via earlier intermediates is minimized by appropriate energy decrease for the different reaction steps.

These requirements, together with the standard parameters of the ET reaction in biological systems, determine the arrangement of the electron carriers, the number of intermediate states and the loss in free energy during the electron transfer. In this respect, it is interesting to compare the highly optimized wild type RC with mutated RC. The mutations change reactions rates, absorption properties and energetics of the RCs. In most cases, the reaction rates are reduced and the charge separation efficiency is lowered. In the situation of the mutant L168HF of *Blc. viridis*, where the initial charge transfer reaction is sped up, the absorption spectrum of the special pair is changed and energy transfer from the antenna is strongly reduced. Thus this mutation will not allow the organism to compete with wild type bacteria. It is interesting to note that many mutations lead to reduced quantum efficiencies while still maintaining electron transfer to some degree. This shows that evolutionary design criteria included not only highest quantum efficiency, but also robustness to point mutations and environmental changes.

IV. Concluding Remarks

The solar energy fixation, via charge separation in photosynthesis, is a process where the involved pigment protein complexes — the bacterial RC or the two photosystems PS I and PS II — work with highest efficiency. Structural analysis, ultrafast spectroscopy, site-directed mutagenesis and theoretical modeling have supplied information necessary to describe and to understand the function of the bacterial RC. Here, the interplay of the spatial arrangement and energetic tuning, yield highest quantum efficiency. Despite the elucidation of the molecular structures of PS I and the developing structure of PS II (Zouni et al., 2001; Ferreira et al., 2004), information on the two photosystems PS I and PS II is still incomplete. However, the high similarity of the core pigment arrangement implies that similar design principles are used, and should give some clues how an optimal solar energy converter is built.

References

Allen JP, Feher G, Yeates TO, Komiya H and Rees DC (1987) Structure of the reaction center from *Rhodobacter sphaeroides* R 26 — the cofactors. Proc Natl Acad Sci USA 84: 5730–5734

Allen JP, Artz K, Lin X, Williams JC, Ivancich A, Albouy D, Mattioli TA, Fetsch A, Kuhn M and Lubitz W (1996) Effects of hydrogen bonding to a bacteriochlorophyll-bacteriopheophytin dimer in reaction centers from *Rhodobacter sphaeroides*.

Biochemistry 35: 6612–6619
Arlt T, Schmidt S, Kaiser W, Lauterwasser C, Meyer M, Scheer H and Zinth W (1993) The accessory bacteriochlorophyll: A real electron carrier in primary photosynthesis. Proc Natl Acad Sci USA 90: 11757–11761
Barter LMC, Durrant JR and Klug DR (2003) A quantitative structure-function relationship for the Photosystem II reaction center: Supermolecular behavior in natural photosynthesis. Proc Natl Acad Sci USA 100: 946–951
Beddard GS (1998) Excitations and excitons in Photosystem I. Philos Trans Roy Soc Lond A 356: 421–448
Beekman LM, Visschers RW, Monshouwer R, Heer-Dawson M, Mattioli TA, McGlynn P, Hunter CN, Robert B, van Stokkum IH and van Grondelle R (1995) Time-resolved and steady-state spectroscopic analysis of membrane-bound reaction centers from *Rhodobacter sphaeroides*: Comparisons with detergent-solubilized complexes. Biochemistry 34: 14712–14721
Ben-Shem A, Frolow F and Nelson N (2003) The crystal structure of plant Photosystem I. Nature 426: 630–635
Bibby TS, Nield J, Chen M, Larkum AWD and Barber J (2003) Structure of a Photosystem II supercomplex isolated from *Prochloron didemni* retaining its chlorophyll *a/b* light-harvesting system. Proc Natl Acad Sci USA 100: 9050–9054
Bixon M, Jortner J, Michel-Beyerle ME and Ogrodnik A (1989) A superexchange mechanism for the primary charge separation in photosynthetic reaction centers. Biochim Biophys Acta 977: 273–286
Bixon M, Jortner J and Michel-Beyerle ME (1991) On the mechanism of the primary charge separation in bacterial photosynthesis. Biochim Biophys Acta 1056: 301–315
Breton J, Martin JL, Migus A, Antonetti A and Orszag A (1986) Femtosecond spectroscopy of excitation energy transfer and initial charge separation in the reaction center of the photosynthetic bacterium *Rhodopseudomonas viridis*. Proc Natl Acad Sci USA 83: 5121–5125
Breton J, Martin JL, Fleming GR and Lambry JC (1988) Low-temperature femtosecond spectroscopy of the initial step of electron transfer in reaction centers from photosynthetic purple bacteria. Biochemistry 27: 8276–8284
Brettel K (1997) Electron transfer and arrangement of the redox cofactors in Photosystem I. Biochim Biophys Acta 1318: 322–373
Brettel K and Leibl W (2001) Electron transfer in Photosystem I. Biochim Biophys Acta 1507: 100–114
Bylina EJ and Youvan DC (1988) Directed mutations affecting spectroscopic and electron transfer properties of the primary donor in the photosynthetic reaction center. Proc Natl Acad Sci USA 85: 7226–7230
Byrdin M, Rimke I, Schlodder E, Stehlik D and Roelofs TA (2000) Decay kinetics and quantum yields of fluorescence in Photosystem I from *Synechococcus elongatus* with P700 in the reduced and oxidized state: Are the kinetics of excited state decay trap-limited or transfer-limited? Biophys J 79: 992–1007
Chachisvilis M and Sundström V (1996) Femtosecond vibrational dynamics and relaxation in the core light-harvesting complex of photosynthetic purple bacteria. Chem Phys Lett 261: 165–174
Chan CK, DiMagno TJ, Chen LX, Norris JR and Fleming GR (1991) Mechanism of the initial charge separation in bacterial photosynthetic reaction centers. Proc Natl Acad Sci USA 88: 11202–11206
Chang CH, El-Kabbani D, Tiede D, Norris J and Schiffer M (1991) Structure of the membrane-bound protein photosynthetic reaction center from *Rhodobacter sphaeroides*. Biochemistry 30: 5352–5360
Coleman WJ and Youvan DC (1990) Spectroscopic analysis of genetically modified photosynthetic reaction centers. Annu Rev Biophys Biophys Chem 19: 333–367
Deisenhofer J, Epp O, Miki K, Huber R and Michel H (1984) X-ray structure-analysis of a membrane-protein complex — electron-density map at 3Å resolution and a model of the chromophores of the photosynthetic reaction center from *Rhodopseudomonas viridis*. J Mol Biol 180: 385–398
Diffey WM, Homoelle BJ, Edington MD and Beck WF (1998) Excited-state vibrational coherence and anisotropy decay in the bacteriochlorophyll *a* dimer protein B820. J Phys Chem B 102: 2776–2786
Dressler K, Umlauf E, Schmidt S, Hamm P, Zinth W, Buchanan S and Michel H (1991) Detailed studies of the subpicosecond kinetics in the primary electron transfer of reaction centers of *Rhodopseudomonas viridis*. Chem Phys Lett 183: 270–276
Du M, Rosenthal SJ, Xie X, Dimagno TJ, Schmidt M, Hanson DK, Schiffer M, Norris JR and Fleming GR (1992) Femtosecond spontaneous-emission studies of reaction centers from photosynthetic bacteria. Proc Natl Acad Sci USA 89: 8517–8521
Ermler U, Fritzsch G, Buchanan SK and Michel H (1994) Structure of the photosynthetic reaction-center from *Rhodobacter sphaeroides* at 2.65-Ångstrom resolution — cofactors and protein-cofactor interactions. Structure 2: 925–936
Fajer J, Brune DC, Davis MS, Forman A and Spaulding LD (1975) Primary charge separation in bacterial photosynthesis — oxidized chlorophylls and reduced pheophytin. Proc Natl Acad Sci USA 72: 4956–4960
Farchaus JW, Wachtveitl J, Mathis P and Oesterhelt D (1993) Tyrosine-162 of the photosynthetic reaction-center L-subunit plays a critical role in the cytochrome-c_2 mediated rereduction of the photooxidized bacteriochlorophyll dimer in *Rhodobacter sphaeroides*.1. Site-directed mutagenesis and initial characterization. Biochemistry 32: 12875–12886
Ferreira KN, Iverson TM, Maghlaoui K, Barber J and Iwata S (2004) Architecture of the photosynthetic oxygen-evolving center. Science 303: 1831–1838
Fleming GR, Martin JL and Breton J (1988) Rates of primary electron-transfer in photosynthetic reaction centers and their mechanistic implications. Nature 333: 190–192
Franken EM, Shkuropatov AY, Francke C, Neerken S, Gast P, Shuvalov VA, Hoff AJ and Aartsma TJ (1997) Reaction centers of *Rhodobacter sphaeroides* R-26 with selective replacement of bacteriopheophytin a by pheophytin *a*. 2. Temperature dependence of the quantum yield of $P^+Q_A^-$ and P_3 formation. Biochim Biophys Acta 1321: 1–9
Fujita I, Davis MS and Fajer J (1978) Anion radicals of pheophytin and chlorophyll *a* — their role in primary charge separations of plant photosynthesis. J Am Chem Soc 100: 6280–6282
Geskes C, Meyer M, Fischer M, Scheer H and Heinze J (1995) Electrochemical investigation of modified photosynthetic pigments. J Phys Chem 99: 17669–17672
Gray KA, Farchaus JW, Wachtveitl J, Breton J and Oesterhelt D (1990) Initial characterization of site-directed mutants of tyrosine M210 in the reaction centre of *Rhodobacter sphaeroides*. EMBO J 9: 2061–2070
Hamm P, Gray KA, Oesterhelt D, Feick R, Scheer H and Zinth W

(1993) Subpicosecond emission studies of bacterial reaction centers. Biochim Biophys Acta 1142: 99–105

Holzapfel W, Finkele U, Kaiser W, Oesterhelt D, Scheer H, Stilz HU and Zinth W (1989) Observation of a bacteriochlorophyll anion radical during the primary charge separation in a reaction center. Chem Phys Lett 160: 1–7

Holzapfel W, Finkele U, Kaiser W, Oesterhelt D, Scheer H, Stilz HU and Zinth W (1990) Initial electron transfer in the reaction center from *Rhodobacter sphaeroides*. Proc Natl Acad Sci USA 87: 5168–5172

Huber H, Meyer M, Nägele T, Hartl I, Scheer H, Zinth W and Wachtveitl J (1995) Primary photosynthesis in reaction centers containing 4 different types of electron accepters at site H_A. Chem Phys 197: 297–305

Huber H, Meyer M, Scheer H, Zinth W and Wachtveitl J (1998) Temperature dependence of the primary electron transfer reaction in pigment-modified bacterial reaction centers. Photosynth Res 55: 153–162

Huppmann P, Arlt T, Penzkofer H, Schmidt S, Bibikova M, Dohse B, Oesterhelt D, Wachtveitl J and Zinth W (2002) Kinetics, energetics, and electronic coupling of the primary electron transfer reactions in mutated reaction centers of *Blastochloris viridis*. Biophys J 82: 3186–3197

Huppmann P, Spörlein S, Bibikova M, Oesterhelt D, Wachtveitl J and Zinth W (2003) Electron transfer in reaction centers of *Blastochloris viridis*: Photosynthetic reactions approximating the adiabatic regime. J Phys Chem A 107: 8302–8309

Jackson JA, Lin S, Taguchi AKW, Williams JC, Allen JP and Woodbury NW (1997) Energy transfer in *Rhodobacter sphaeroides* reaction centers with the initial electron donor oxidized or missing. J Phys Chem B 101: 5747–5754

Jia YW, DiMagno TJ, Chan CK, Wang ZY, Du M, Hanson DK, Schiffer M, Norris JR, Fleming GR and Popov MS (1993) Primary charge separation in mutant reaction centers of *Rhodobacter capsulatus*. J Phys Chem 97: 13180–13191

Joo TH, Jia YW, Yu JY, Jonas DM and Fleming GR (1996) Dynamics in isolated bacterial light harvesting antenna LH2 of *Rhodobacter sphaeroides* at room temperature. J Phys Chem 100: 2399–2409

Jordan P, Fromme P, Witt HT, Klukas O, Saenger W and Krauss N (2001) Three-dimensional structure of cyanobacterial Photosystem I at 2.5 Ångstrom resolution. Nature 411: 909–917

Kirmaier C, Holten D and Parson WW (1985) Temperature and detection-wavelength dependence of the picosecond electron transfer kinetics measured in *Rhodopseudomonas sphaeroides* reaction centers resolution of new spectral and kinetic components in the primary charge-separation process. Biochim Biophys Acta 810: 33–48

Knapp EW, Fischer SF, Zinth W, Sander M, Kaiser W, Deisenhofer J and Michel H (1985) Analysis of optical-spectra from single-crystals of *Rhodopseudomonas viridis* reaction centers. Proc Natl Acad Sci USA 82: 8463–8467

Kolbasov D and Scherz A (2000) Asymmetric electron transfer in reaction centers of purple bacteria strongly depends on different electron matrix elements in the active-and inactive branches. J Phys Chem B 104: 1802–1809

Kuglstatter A, Hellwig P, Fritzsch G, Wachtveitl J, Oesterhelt D, Mäntele W and Michel H (1999) Identification of a hydrogen bond in the phe M197 -> tyr mutant reaction center of the photosynthetic purple bacterium *Rhodobacter sphaeroides* by X-ray crystallography and FTIR spectroscopy. FEBS Lett 463: 169–174

Kumble R, Palese S, Visschers RW, Dutton PL and Hochstrasser RM (1996) Ultrafast dynamics within the B820 subunit from the core LH-1 antenna complex of *Rs. rubrum*. Chem Phys Lett 261: 396–404

Lathrop EJP and Friesner RA (1994) Simulation of optical-spectra from the reaction-center of *Rhodobacter sphaeroides* — effects of an internal charge-separated state of the special pair. J Phys Chem 98: 3056–3066

Lauterwasser C, Finkele U, Scheer H and Zinth W (1991) Temperature-dependence of the primary electron-transfer in photosynthetic reaction centers from *Rhodobacter sphaeroides*. Chem Phys Lett 183: 471–477

Lin S, Jackson J, Taguchi AKW and Woodbury NW (1998) Excitation wavelength dependent spectral evolution in *Rhodobacter sphaeroides* R-26 reaction centers at low temperatures: The Q_Y transition region. J Phys Chem B 102: 4016–4022

Lin X, Murchison HA, Nagarajan V, Parson WW, Allen JP and Williams JC (1994) Specific alteration of the oxidation potential of the electron donor in reaction centers from *Rhodobacter sphaeroides*. Proc Natl Acad Sci USA 91: 10265–10269

Marcus RA (1987) Superexchange versus an intermediate bchl-mechanism in reaction centers of photosynthetic bacteria. Chem Phys Lett 133: 471–477

Marcus RA and Sutin N (1985) Electron transfers in chemistry and biology. Biochim Biophys Acta 811: 265–322

Martin JL, Breton J, Hoff AJ, Migus A and Antonetti A (1986) Femtosecond spectroscopy of electron transfer in the reaction center of the photosynthetic bacterium *Rhodopseudomonas sphaeroides* R-26 direct electron transfer from the dimeric bacteriochlorophyll primary donor to the bacteriopheophytin acceptor with a time constant of 2.8 plus or minus 0.2 picoseconds. Proc Natl Acad Sci USA 83: 957–961

McMahon BH, Muller JD, Wraight CA and Nienhaus GU (1998) Electron transfer and protein dynamics in the photosynthetic reaction center. Biophys J 74: 2567–2587

Meyer M and Scheer H (1995) Reaction centers of *Rhodobacter sphaeroides* R-26 containing C-3 acetyl and vinyl (bacterio)pheophytins at sites H_A, H_B. Photosynth Res 44: 55–65

Michel-Beyerle ME, Plato M, Deisenhofer J, Michel H, Bixon M and Jortner J (1988) Unidirectionality of charge separation in reaction centers of photosynthetic bacteria. Biochim Biophys Acta 932: 52–70

Mokhtari A, Chebira A and Chesnoy J (1990) Subpicosecond fluorescence dynamics of dye molecules. J Opt Soc Am B 7: 1551–1557

Monshouwer R, Abrahamsson M, vanMourik F and van Grondelle R (1997) Superradiance and exciton delocalization in bacterial photosynthetic light-harvesting systems. J Phys Chem B 101: 7241–7248

Moser CC, Keske JM, Warncke K, Farid RS and Dutton PL (1992) Nature of biological electron-transfer. Nature 355: 796–802

Moser CC, Keske JM, Warncke K, Farid RS and Dutton PL (1993) Electron-transfer mechanisms in reaction centers: Engineering guidelines. In: Deisenhofer J and Norris JR (eds) The Photosynthetic Reaction Center, pp 1–22. Academic Press, San Diego

Murchison HA, Alden RG, Allen JP, Peloquin JM, Taguchi AK, Woodbury NW and Williams JC (1993) Mutations designed to modify the environment of the primary electron donor of

the reaction center from *Rhodobacter sphaeroides*: Phenylalanine to leucine at l167 and histidine to phenylalanine at l168. Biochemistry 32: 3498–3505

Ogrodnik A, Keupp W, Volk M, Aumeier G and Michel-Beyerle ME (1994) Inhomogeneity of radical pair energies in photosynthetic reaction centers revealed by differences in recombination dynamics of $P^{+}H_{A}^{-}$ when detected in delayed emission and in absorption. J Phys Chem 98: 3432–3439

Parson WW and Warshel A (1993) Simulations of electron transfer in bacterial reaction centers. In: Deisenhofer J and Norris JR (eds) The Photosynthetic Reaction Center, pp 23–48. Academic Press, San Diego

Prokhorenko VI and Holzwarth AR (2000) Primary processes and structure of the Photosystem II reaction center: A photon echo study. J Phys Chem B 104: 11563–11578

Rautter J, Lendzian F, Lubitz W, Wang S and Allen JP (1994) Comparative-study of reaction centers from photosynthetic purple bacteria — electron-paramagnetic-resonance and electron-nuclear double-resonance spectroscopy. Biochemistry 33: 12077–12084

Remy A and Gerwert K (2003) Coupling of light-induced electron transfer to proton uptake in photosynthesis. Nat Struct Biol 10: 637–644

Rosker MJ, Wise FW and Tang CL (1986) Femtosecond relaxation dynamics of large molecules. Phys Rev Lett 57: 321–324

Savikhin S, Xu W, Chitnis PR and Struve WS (2000) Ultrafast primary processes in PS I from *Synechocystis* sp. PCC 6803: Roles of p700 and a(o). Biophys J 79: 1573–1586

Schenkl S, Spörlein S, Müh F, Witt H, Lubitz W, Zinth W and Wachtveitl J (2002) Selective perturbation of the second electron transfer step in mutant bacterial reaction centers. Biochim Biophys Acta 1554: 36–47

Schmidt S, Arlt T, Hamm P, Huber H, Nägele T, Wachtveitl J, Meyer M, Scheer H and Zinth W (1994) Energetics of the primary electron-transfer reaction revealed by ultrafast spectroscopy on modified bacterial reaction centers. Chem Phys Lett 223: 116–120

Schmidt S, Arlt T, Hamm P, Huber H, Nägele T, Wachtveitl J, Zinth W, Meyer M and Scheer H (1995) Primary electron-transfer dynamics in modified bacterial reaction centers containing pheophytin-a instead of bacteriopheophytin-*a*. Spectrochim Acta A 51: 1565–1578

Shkuropatov AY and Shuvalov VA (1993) Electron-transfer in pheophytin *a*-modified reaction centers from *Rhodobacter sphaeroides* (R-26). FEBS Lett 322: 168–172

Shuvalov VA and Yakovlev AG (2003) Coupling of nuclear wavepacket motion and charge separation in bacterial reaction centers. FEBS Lett 540: 26–34

Spörlein S, Zinth W and Wachtveitl J (1998) Vibrational coherence in photosynthetic reaction centers observed in the bacteriochlorophyll anion band. J Phys Chem B 102: 7492–7496

Spörlein S, Zinth W, Meyer M, Scheer H and Wachtveitl J (2000) Primary electron transfer in modified bacterial reaction centers: Optimization of the first events in photosynthesis. Chem Phys Lett 322: 454–464

Stanley RJ and Boxer SG (1995) Oscillations in the spontaneous fluorescence from photosynthetic reaction centers. J Phys Chem 99: 859–863

Stanley RJ, King B and Boxer SG (1996) Excited state energy transfer pathways in photosynthetic reaction centers .1. Structural symmetry effects. J Phys Chem 100: 12052–12059

Stowell MHB, McPhillips TM, Rees DC, Soltis SM, Abresch E and Feher G (1997) Light-induced structural changes in photosynthetic reaction center: Implications for mechanism of electron-proton transfer. Science 276: 812–816

Streltsov AM, Aartsma TJ, Hoff AJ and Shuvalov VA (1997) Oscillations within the B_L absorption-band of *Rhodobacter sphaeroides* reaction centers upon 30 femtosecond excitation at 865 nm. Chem Phys Lett 266: 347–352

Struck A and Scheer H (1990) Modified reaction centers from *Rhodobacter sphaeroides* R26 — exchange of monomeric bacteriochlorophyll with 13(2)-hydroxy- bacteriochlorophyll. FEBS Lett 261: 385–388

Struck A, Cmiel E, Katheder I and Scheer H (1990) Modified reaction centers from *Rhodobacter sphaeroides* R26 .2. Bacteriochlorophylls with modified c-3 substituents at sites B_A and B_B. FEBS Lett 268: 180–184

Trissl HW, Breton J, Deprez J, Dobek A and Leibl W (1990) Trapping kinetics, annihilation, and quantum yield in the photosynthetic purple bacterium *Rps. viridis* as revealed by electric measurement of the primary charge separation. Biochim Biophys Acta 1015: 322–333

van Brederode ME, Jones MR and van Grondelle R (1997a) Fluorescence excitation spectra of membrane-bound photosynthetic reaction centers of *Rhodobacter sphaeroides* in which the tyrosine M210 residue is replaced by tryptophan: Evidence for a new pathway of charge separation. Chem Phys Lett 268: 143–149

van Brederode ME, Jones MR, van Mourik F, van Stokkum IHM and van Grondelle R (1997b) A new pathway for transmembrane electron transfer in photosynthetic reaction centers of *Rhodobacter sphaeroides* not involving the excited special pair. Biochemistry 36: 6855–6861

van Grondelle R, Dekker JP, Gillbro T and Sundström V (1994) Energy-transfer and trapping in photosynthesis. Biochim Biophys Acta 1187: 1–65

Vasil'ev S, Orth P, Zouni A, Owens TG and Bruce D (2001) Excited-state dynamics in Photosystem II: Insights from the X-ray crystal structure. Proc Natl Acad Sci USA 98: 8602–8607

Vos MH and Martin JL (1999) Femtosecond processes in proteins. Biochim Biophys Acta 1411: 1–20

Vos MH, Lambry JC, Robles SJ, Youvan DC, Breton J and Martin JL (1991) Direct observation of vibrational coherence in bacterial reaction centers using femtosecond absorption spectroscopy. Proc Natl Acad Sci USA 88: 8885–8889

Vos MH, Rappaport F, Lambry JC, Breton J and Martin JL (1993) Visualization of coherent nuclear motion in a membrane protein by femtosecond spectroscopy. Nature 363: 320–325

Vos MH, Jones MR, Hunter CN, Breton J, Lambry JC and Martin JL (1994) Coherent dynamics during the primary electron-transfer reaction in membrane-bound reaction centers of *Rhodobacter sphaeroides*. Biochemistry 33: 6750–6757

Vos MH, Breton J and Martin JL (1997) Electronic energy transfer within the hexamer cofactor system of bacterial reaction centers. J Phys Chem B 101: 9820–9832

Wachtveitl J, Farchaus JW, Das R, Lutz M, Robert B and Mattioli TA (1993) Structure, spectroscopic, and redox properties of *Rhodobacter sphaeroides* reaction centers bearing point mutations near the primary electron donor. Biochemistry 32: 12875–12886

Wachtveitl J, Huber H, Feick R, Rautter J, Müh F and Lubitz W (1998) Electron transfer in bacterial reaction centers with an en-

ergetically raised primary acceptor: Ultrafast spectroscopy and ENDOR/TRIPLE studies. Spectrochim Acta 54: 153–162

Wang Q, Schoenlein RW, Peteanu LA, Mathies RA and Shank CV (1994) Vibrationally coherent photochemistry in the femtosecond primary event of vision. Science 266: 422–424

Warshel A (1980) Role of the chlorophyll dimer in bacterial photosynthesis. Proc Natl Acad Sci USA 77: 3105–3109

Williams JC, Alden RG, Murchison HA, Peloquin JM, Woodbury NW and Allen JP (1992) Effects of mutations near the bacteriochlorophylls in reaction centers from *Rhodobacter sphaeroides*. Biochemistry 31: 11029–11037

Woodbury NW, Becker M, Middendorf D and Parson WW (1985) Picosecond kinetics of the initial photochemical electron-transfer reaction in bacterial photosynthetic reaction centers. Biochemistry 24: 7516–7521

Woodbury NW, Peloquin JM, Alden RG, Lin X, Lin S, Taguchi AK, Williams JC and Allen JP (1994) Relationship between thermodynamics and mechanism during photoinduced charge separation in reaction centers from *Rhodobacter sphaeroides*. Biochemistry 33: 8101–8112

Xu D and Schulten K (1994) Coupling of protein motion to electron-transfer in a photosynthetic reaction-center — investigating the low-temperature behavior in the framework of the spin-boson model. Chem Phys 182: 91–117

Zhang LY and Friesner RA (1998) *Ab initio* calculation of electronic coupling in the photosynthetic reaction center. Proc Natl Acad Sci USA 95: 13603–13605

Zinth W, Kaiser W and Michel H (1983) Efficient photochemical activity and strong dichroism of single-crystals of reaction centers from *Rhodopseudomonas viridis*. Biochim Biophys Acta 723: 128–131

Zinth W, Huppmann P, Arlt T and Wachtveitl J (1998) Ultrafast spectroscopy of the electron transfer in photosynthetic reaction centres: Towards a better understanding of electron transfer in biological systems. Philos Trans Roy Soc Lond A 356: 465–476

Zouni A, Witt HT, Kern J, Fromme P, Krauss N, Saenger W and Orth P (2001) Crystal structure of Photosystem II from *Synechococcus elongatus* at 3.8 Ångstrom resolution. Nature 409: 739–743

Chapter 32

Chlorophyll Sensitizers in Photodynamic Therapy

Alexander S. Brandis[1], Yoram Salomon[2] and Avigdor Scherz[1]*
Departments of [1]Plant Sciences and [2]Biological Regulation,
The Weizmann Institute of Science, Rehovot, Israel

*Author for correspondence, email: avigdor.scherz@weizmann.ac.il

Bernhard Grimm, Robert J. Porra, Wolfhart Rüdiger and Hugo Scheer (eds): Chlorophylls and Bacteriochlorophylls: Biochemistry, Biophysics, Functions and Applications, pp. 461–483.

Summary

Photodynamic therapy (PDT) has proved to be a viable and interesting alternative to currently used less selective methods for palliative care of cancer and, in a limited number of cases, for curative treatment. Still, in spite of impressive progress and a few approvals for clinical applications, the great potential of PDT has not yet been fully realized because of current deficiencies of applied sensitizers and of applied treatment strategies. Introduction of chlorophyll- and bacteriochlorophyll-derived sensitizers is expected to markedly change this situation in the coming decade. In this and the following chapter we provide an updated summary of these new sensitizers, their syntheses, relevant characteristics and pharmaceutical activity in vitro and in vivo. The first chapter is focused on the general principles of photodynamic therapy with particular emphasis on the vascular-targeted approach to treatment. A general introduction is followed by a comprehensive description of chlorophyll based sensitizers. The following chapter (Chapter 33) is focused on the use of bacteriochlorophyll derivatives.

I. Introduction

A. Definition and Current Strategy of Photodynamic Therapy

Photodynamic therapy (PDT) of cancer is a relatively new method of treatment whereby non-toxic drugs (sensitizers) and non-hazardous visible and near infrared light (VIS/NIR) combine to generate cytotoxic reactive oxygen species (ROS) at a selected treatment site. The application of PDT in tumor care has been motivated by the quest for a treatment that is at least as effective but more selective than radio- and chemo-therapies, thus minimizing side effects. Current PDT aims at directly killing tumor cells and typically consists of five steps.

1. Administration of a photosensitizer, usually intravenously (i.v.).

2. A delay period that allows for retention or accumulation of photosensitizers in the target tissue.

Abbreviations: ALA – 5-aminolevulinic acid; AMD – age-related macular degeneration; BChl – bacteriochlorophyll; BChn – bacteriochlorin; BOLD MRI – blood oxygen level-dependent magnetic resonance imaging; BPP – bacteriopurpurin; BSA – bovine serum albumin; Chl – chlorophyll; Chl-Ser – chlorophyllide *a* L-serine ester; Chn – chlorin; CNV – choroidal neovascularization; EC_{50} – median effective concentration; HDL – high-density lipoprotein; HpD – hematoporphyrin derivatives; HPMA – N-(2-hydroxypropyl)methacrylamide; HPPH – [3-(1-hexyloxyethyl)]-pyropheophorbide; i.p. – intraperitoneally; i.v. – intravenously; IC_{50} – median inhibitory concentration; IgG – immunoglobulin G; ISC – intersystem crossing; LD_{50} – median lethal dose; LDL – low-density lipoprotein; NPe_6 – mono-L-aspartyl Chn e_6; PDT – photodynamic therapy; Pheide – pheophorbide; PP – purpurin; pyro-Pheide – pyropheophorbide; QSAR – quantitative structure-activity relationship; ROS – reactive oxygen species; TOOKAD® – [Pd]-bacteriochlorophyllide *a*; ϕ_Δ – quantum yield of singlet oxygen

3. Illumination of the target tissue (transcutanously or interstitially via optical fibers for inner organs) with consequent local generation of cytotoxic ROS.

4. Development of tumor necrosis and tumor eradication.

5. Tissue remodeling and healing.

New sensitizers have usually been designed to achieve preferential accumulation in the tumor cells while photoexcitation techniques have been developed to irradiate relatively deep tumor tissue thus expanding the usefulness and efficacy of PDT. Different porphyrinoids have been suggested as the preferred PDT sensitizers (Pandey and Zheng, 2000; Osterloh and Vicente, 2002), although cyclic and long-chain polyenes with a significant light absorption in the UV-VIS such as indocyanines and hypericin were also considered (Delaey et al., 2000; Chen et al., 2002; Kassab, 2002). For several decades, research and pre-clinical efforts have focused on hematoporphyrin derivatives (HpD) and other peripherally substituted porphyrins of (near) D_{4h} symmetry (Henderson and Dougherty, 1992; Dougherty et al., 1998; Bonnett, 1999; Pandey and Zheng, 2000; Ackroyd et al., 2001).

The preferential accumulation of hematoporphyrin derivatives in tumors relative to normal tissues, the formation of cytotoxic ROS, and necrotic or apoptotic processes that culminate in tumor eradication, were promising in early PDT development (Dougherty, 1987; Jori, 1992, 1996; Dougherty et al., 1998; Ronn, 1999); however, none of the clinically or pre-clinically used sensitizers have yet shown sufficiently high accumulation in the malignant tumor cells to enable optimally-selective and efficient treatment (Bonnett, 1999). In addition, the high attenuation of light in the UV-VIS domain, required for activation of tetrapyrrole senstitizers with D_{4h}-symmetry within animal tissues, has prevented treatment of massive tumors. Thus, the current clinical targets of PDT include relatively shallow malignant and benign tumors, choroidal neovascularization (CNV) in age-related macular degeneration (AMD), atherosclerotic lesions, as well as bacterial and viral infections. In addition, the photodynamic effect can be used as a subsidiary but method selectively for light-enhanced delivery of a drug to the body area/organ to be treated (Selbo et al., 2002).

Over the past decade, the use of PDT has increased significantly, mainly in cancer and AMD treatment. Protoporphyrin-based photosensitizers (tradenames: Photofrin®, Photosan®, Photoheme®, HpD®, Levulan®, Visudyne®) have been approved for clinical use, and successfully employed in PDT in many countries.

In spite of the impressive progress, the full potential of PDT has not yet been realized for the following reasons:

(1) the spectroscopic properties of the clinically used sensitizers only allow for sensitization of shallow tumors,

(2) the pharmacological properties of the current sensitizers (i.e., lack of sufficient specificity for the tumor cells) together with the treatment strategy result in eradication of both tumor and non-tumor tissues within the illuminated zone, and finally

(3) the retention of sensitizer in non-tumor tissues (e.g. skin) leads to prolonged cutaneous toxicity.

The disadvantages of currently-used drugs have long been known and have led to an extensive search for new sensitizers with superior spectroscopic properties.

As they were selected by evolutionary processes to perform VIS-NIR light-harvesting with consequent radical generation in photosynthesis, Chls and BChls have emerged as attractive alternative PDT sensitizers. However, because of their superior photophysics combined with a low chemical stability, Chls and BChls are rapidly degraded when exposed to light outside of their native and protective environment in the transmembrane proteins of light-harvesting complexes and photoreaction centers of chloroplasts. To overcome this limitation, major research efforts have focused on producing Chl- and BChl-like molecules that are sufficiently stable to enable light-induced radical generation deep within animal tissues and, preferentially, with higher selectivity for tumor cells than currently used sensitizers. Recently, an extensive description and screening of different Chl/BChl-based sensitizers has been published (Pandey and Zheng, 2000).

In this and the following chapter, we shall focus respectively on Chl- and BChl-derived PDT sensitizers. Each section will highlight features related to sensitizer preparation, its photochemical and

photophysical properties, in vitro screening and in vivo targets. The state of clinical development will be described at the end of each chapter.

Finally, we shall discuss current PDT treatment strategies and suggest an alternative approach made possible by new BChl-based sensitizers. The last review, dedicated to Chl and BChl sensitizers, was published more than a decade ago (Spikes and Bommer, 1991).

B. Guidelines for Selecting New Sensitizers

In searching for new and better PDT reagents, the following features have been generally accepted as criteria for optimal photosensitizers (Jori, 1996; Bonnett, 2000). These are especially relevant for PDT reagents synthesized from natural compounds such as Chl and BChl.

1. Chemical Purity

There is a consensus that new sensitizers should be chemically pure compounds unlike the composite sensitizer Photofrin®. A pure, single compound can be localized and targeted more efficiently and it is easier to estimate its sensitizing efficiency as well as its pharmacological and photochemical properties. Thus treatment protocols can be more rationally designed with readily identifiable quantitative structure-activity relationships (QSAR) (Dougherty et al., 1998; Pandey and Zheng, 2000; Macdonald and Dougherty, 2001 and refs. therein).

2. Significant Absorption at Long Wavelengths (>650 nm)

New sensitizers should preferably have strong electronic transition intensities in the range of 650–850 nm, where light penetration into animal tissue is maximized. At shorter wavelengths, endogenous pigments and light scattering substantially attenuate the photon flux to the tissue-impregnated sensitizers. At longer wavelengths, the energy transfer from the excited sensitizer becomes insufficient to transform oxygen into the excited singlet state (Moan, 1990). Further, the increased absorption of light by water molecules (λ >900 nm) reduces the effective dose of light and enhances thermalization (Macdonald and Dougherty, 2001).

3. High Quantum Yield of Reactive Oxygen Species

The type and quantity of ROS generated by an excited sensitizer determines its potential PDT efficacy. ROS generation is initiated from the triplet state of the excited sensitizer (^1T_S), which is populated by intersystem crossing (ISC) from the lowest excited singlet state (^1S_S) during its lifetime which is a few nanoseconds in the best cases. Energy or electron transfer from ^1T_S to molecular oxygen may result in:

(1) electron transfer from the excited sensitizer to the ground state oxygen, forming a superoxide radical (Type I processes) or

(2) relaxation of the sensitizer to the ground state ^0S_S with concomitant excitation of molecular oxygen to the excited singlet state (Σ^1O_2) (Type II processes) (Foote, 1968; Henderson and Dougherty, 1992; Pandey and Zheng, 2000; Macdonald and Dougherty, 2001).

The quantum yield for a particular ROS type depends on the nature of the sensitizer, the availability of oxygen, and the reaction environment. Heavy atoms and side groups increase the yield of the intersystem crossing and the amount of resulting singlet oxygen. The relative redox potentials of the excited sensitizer and concentrations of the molecular oxygen in the particular reaction environment determine the yield of electron transfer (Type I). The fate of the ROS and their cytotoxicity strongly depend on the site of their generation. This is mostly relevant to the oxygen radicals, which can be more reactive than $^1O_2$, and therefore possess a shorter lifetime than the excited singlet oxygen. Lipids, proteins and transition metals at low redox states may convert ROS to even more reactive forms that can initiate radical chain reactions (Halliwell and Gutteridge, 1990; Henderson and Dougherty, 1992). With most available sensitizers, Type II processes are generally believed to be the major pathway involved in tissue destruction, (Henderson and Dougherty, 1992; Pandey and Zheng, 2000; Bonnett, 2002); however, Type I processes may be highly relevant to PDT with Chl/BChl derived sensitizers.

4. No Dark Toxicity and No Undesired Phototoxicity in Skin, Eyes and Mucous Epithelia

Rapid clearance of the photosensitizer is desired, with no dark toxicity or mutagenic activity of the sensitizer or its degradation products. With a hydrophobic sensitizer, the carrier systems need to be clinically safe (Jocham, 1998).

5. Stability and Ease of Packaging

Before administration, the photosensitizer should have a long-term stability and shelf life; however, limited stability in vivo and under irradiation could be desirable to reduce the damage to normal tissue at threshold concentrations (Moan, 1986; Boyle and Potter, 1987; Svaasand and Potter, 1992). Water-soluble substances are favored.

6. Selectivity of Damage and Localization

Selectivity is important for PDT treatments which require the presence of light, sensitizer and oxygen to produce local cytotoxicity in the target tissue; thus a well-defined zone of destruction is provided while preferably maintaining differentiation between normal tissue cells and those of target tumor cells.

Tumor necrosis can be generally induced by: (i) direct cell killing; (ii) hypoxia caused by vascular shutdown, and (iii) immune effects. Here we shall briefly refer to the current status in PDT research.

(i) Current research is aimed at developing new PDT reagents that preferentially accumulate in tumor cells. Increasing the reagent's hydrophobicity is generally believed to enhance its accumulation in the neoplastic cells (Kozyrev et al., 1996a; Pandey et al., 1996c; Henderson et al., 1997; Pandey and Zheng, 2000). While better accumulation and higher efficacy of more lipophylic sensitizers was demonstrated in cultured tumor cells (Pandey et al., 1997a; Zheng et al., 2001b), no therapeutic benefit of these sensitizers was ever demonstrated in vivo. Indeed, the proven role of the antivascular effect of PDT (Henderson and Dougherty, 1992; Fingar, 1996; Regillo, 2000; Zilberstein et al., 2001; Schreiber et al., 2002; Koudinova et al., 2003) raises questions about the usefulness of such an approach.

(ii) The role of vascular shutdown in induction of tumor necrosis is now highly appreciated and suggests several new treatment approaches (Folkman, 1995; Schnitzer, 1998). Numerous experiments have indicated that tumor regression and cure after most PDT treatments involve occlusion and/or perforation of blood vessels (Boyle and Dolphin, 1996; Dougherty et al., 1998; Pandey and Zheng, 2000; Macdonald and Dougherty, 2001). This effect is more profound in treatment protocols that involve short intervals between drug administration and irradiation, and/or more hydrophilic sensitizers (Krammer, 2001). Further, relative response differences between the vascular bed of the tumorous and the normal tissue may provide the key for treatment selectivity as suggested by several recent studies (Ferrario et al., 1992; Roberts and Hasan, 1992; McMahon et al., 1994; Zilberstein et al., 2001; Dolmans et al., 2002a; Gross et al., 2003; Koudinova et al., 2003). Thus, the synthesis of specific vascular-directed PDT reagents may become an attractive option in future development of new sensitizers.

(iii) Systemic tumor response to PDT involving the immune system and other mechanisms that results in metastatic tumor regression has been reported by several laboratories (Canti et al., 2002; Schreiber et al., 2002). This may provide the basis for new PDT treatments that are no longer limited to the treatment of single local tumors. However, it is not yet clear how to design new sensitizers for such broader treatment strategies.

In the following sections, we shall review the Chl derivatives, highlighting the above-mentioned guidelines. BChl derivatives are treated in Chapter 33 (Brandis et al.).

II. Photosensitizers Derived from Chlorophyll *a*

A. Chlorophyll a

1. General Description and Chemistry

Natural Chl *a* (see formula in Chapter 1, Scheer) is a dihydroporphyrin with a fifth, isocyclic ring. Chl *a* can be extracted and purified with high yield and purity from practically inexhaustible plant and algal resources. Chl *a* without the admixture of

other chlorophylls can be obtained from biomass of the blue-green alga, *Spirulina*. Chl *a* has a high extinction coefficient at 660 nm ($\varepsilon \sim 10^5\ M^{-1}\ cm^{-1}$) and good singlet oxygen production ($\phi_\Delta = 0.57$ in CCl_4) (Krasnovsky Jr et al., 1990). However, Chl *a* is water-insoluble and very unstable, undergoing oxidative degradation in the presence of light, acid, bases and alcohols, and demetalation in the presence of acids. Therefore, Chl *a* is not suitable for pharmaceutical application but may provide a suitable source for the synthesis of new sensitizers that comply with the pharmaceutical requirements (for review see Spikes and Bommer, 1991). Such sensitizers should be derived by modifications that do not alter the π-electron system which provides the optical spectra. They should allow, on the other hand, modifications to the redox potential and the overall reactivity of the compound. Metal incorporation and modification of the C-3 vinyl substituent or the C-13[1] carbonyl on the isocyclic ring E will modify both the reactivity and stability of the Chls and should be carefully designed.

2. Pre-clinical Studies and Efficacy

No extensive studies have been conducted for determining the effectiveness of Chl *a* as a PDT agent.

B. Chlorophyllide a and Derivatives

1. General Description and Chemistry

Chlide *a* is a produced from Chl *a* by hydrolysis of the C-17[3] phytyl ester, which can be accomplished enzymatically with chlorophyllase. Enzymatic (Fiedor et al., 1992, 1996) and catalytic (Scherz et al., 1994) esterification of Chlide *a* as well as enzymatic (Fiedor et al., 1996; Scherz et al., 1994) and non-enzymatic transesterification (Scheer et al., 2001) of Chl *a* with different amino acids (e.g., serine, tyrosine), peptides and proteins significantly enhanced the pigment's hydrophilicity. The excited Chlide *a* generates singlet oxygen with a ϕ_Δ of about 0.3–0.4 (Fiedor et al., 1993).

Targeting. Further modification of the Chlide *a* propionic acid residue at C-17 via chemically activated amidation enabled conjugation with peptides, hormones and proteins as cell-specific ligands; for example, conjugation with melanocyte stimulating hormones for site-specific PDT of melanoma (Scherz et al., 1994).

2. Pre-clinical Studies and Efficacy

The L-serine derivative (Chl-Ser) showed 100-fold higher photocytotoxicity in M2R melanoma cell cultures than Photosan® (Rosenbach-Belkin et al., 1996). In vivo, the water-soluble Chl-Ser was excreted from the normal tissues within 72 h, but clearance was considerably and favorably retarded from tumor tissues (Rosenbach-Belkin et al., 1996), thus providing low skin phototoxicity. Its photodynamic activity, as tested in vivo on melanotic M2R melanoma tumors, was highly significant (Tregub et al., 1992; Scherz et al., 1994).

C. Pheophorbide a and Derivatives

1. General Description and Chemistry

Pheide *a* is the free-base analogue of Chlide *a*, easily obtained from Chl *a* by acidic elimination of the phytol side chain and central Mg. Its extinction coefficient near 660 nm is about 2/3 that of Chl *a,* but it has a higher dark- and light-stability, with ϕ_Δ of about 0.6 (Krasnovsky Jr et al., 1990; Fernandez et al., 1997). To examine the effect of pigment lipophilicity on the biological activity of Pheide *a*, three families of compounds with increasing n-octanol/water partition coefficients were synthesized: (a) 3-(1-alkoxyethyl) ether derivatives of Pheide *a* methyl ester (Pandey et al., 1991a); (b) esters with a longer alkyl chain (Wongsinkongman et al., 2002); and, (c) amides, in which the carboxylic group was linked to amino alkyls of various lengths and terminal functional groups (e.g. hydroxyl, amine, carboxyl, sulfonyl, sulfhydryl, and phosphoryl) (Dagan et al., 1995). It was found, in the presence of plasma, that the methyl esters of the tested 3-(1-alkoxyethyl) ether derivatives were susceptible to hydrolysis, probably by plasma esterases, whereas the ether bonds remained stable (Pandey et al., 1991a; Bellnier et al., 1993). Further, these compounds were found to slowly convert, at room temperature, into the more stable pyro-Pheides by cleavage of the methoxycarbonyl group at C-13[2] of the isocyclic ring (Pandey et al., 1996c). De-esterification of 3-(1-hexyloxyethyl) and 3-(1-heptyloxyethyl) ethers of the pyro-Pheide *a* methyl ester was carried out with LiOH-THF*(Pandey et al., 1996c). The ϕ_Δ remains at a value of 0.5 (Pandey et al., 1996c), close to that of the parent compound. The pyro-Pheide *a*

*LiOH-THF also promoted allomerization of pyro-Pheide (Kozyrev et al., 1998b).

derivative was further modified to determine the effect of steric hindrance, unsaturation and electron withdrawing capacity of introduced groups on the biologial activity of the parent compound. The tested substitutions included (a) 1-alkoxyethyl (secondary) and alkoxymethyl (primary) ethers of different chain lengths, formyl or ethyl instead of the vinyl group at C-3; (b) thiocarbonyl or methylene instead of the carbonyl at C-13^1; (c) 1-heptyloxyethyl ether instead of ethyl at C-8; (d) di-*t*-butyl aspartyl instead of methyl ester at C-17^3; and (e) the formyl group or alkoxymethyl (primary) ethers with different chain lengths at the C-20 position (Pandey et al., 1992c, 1996a,c). The replacement of the C-3 vinyl with the formyl group shifted the absorption maximum to 690 nm. The reduction of the C-13^1 oxo group in the pyro-Pheide *a* derivatives to CH_2 resulted in a blue shift to 648 nm (Pandey et al., 1996c), whereas the formation of alkyl ethers and pyro-compounds retained optical properties similar to those of the initial Pheide *a*.

Water-soluble derivatives of pyro-Pheide *a* were synthesized by substituting the vinyl with either the 2-carboxymethyl or 2-hydroxyethyl groups together with amidation of the propionic acid residue with glycine or aspartate. Being water-soluble (>5 mg kg^{-1} in 0.9% saline solution), these compounds underwent disaggregation with the addition of human serum albumin (Ando et al., 1991b). For testing the contribution of hydroxyl residues to Pheide hydrophilicity, the oxo, methoxycarbonyl and propionic acid groups of Pheide and pyro-Pheide were reduced to the corresponding mono-, di- and tri-ols. Although the resulting compounds were amphiphilic with opposing hydrophilic and lipophilic sites in the molecule, their water solubility was quite low (Bonnett et al., 1992, 1994). Recently, new water-soluble glucose and galactose derivatives of Pheide and pyro-Pheide were synthesized for use in PDT (Aksenova et al., 2000, 2001). Amidation of pyro-Pheide and its Zn complex with 2-trimethylammonium ethyleneamine led to cationic water-soluble photosensitizers, which efficiently induced DNA cleavage when irradiated at 690 nm: singlet oxygen and electron transfer mechanisms were invoked for the metal free compound and Zn complex, respectively (Mansouri et al., 1994). A similar cationic water-soluble compound was obtained by replacement of the C-17^3 carboxyl group with a NH_3Cl function (Fabiano et al., 1997). Aiming at mitochondrial localization within neoplastic cells, some water-soluble cationic vinyl-extended derivatives of pyro-Pheide and Chn e_6 methyl esters were prepared (Pandey et al., 1991b, 1992b). Nucleoside adducts of vinyl-substituted pyro-Pheide and Chn e_6 methyl esters were synthesized as potential anti-viral and anti-tumor drugs (Jiang et al., 1995, 1996).

Targeting. In an attempt to enhance the delivery and selectivity of the active ingredient, the Pheide was enclosed within β-cylcodextrin dimers (Roehrs et al., 1995), or was adsorbed either in monomer form on microcrystalline cellulose (Zeug et al., 2002) or as photodegradable dendrimer conjugates (Hackbarth et al., 2001).

2. Pre-clinical Studies and Efficacy

a. In Vitro Studies

Using Pheide as photosensitizer (IC_{50} 0.5–2.0 μM, 5 J cm^{-2}, 670 nm) on human pancreatic (Hajri et al., 1999) and colon (Hajri et al., 2002) carcinoma cells gave superior therapeutic results than with Photofrin®. The cyto-phototoxicity of Pheide *a* was 20-times higher than that of haematoporphyrin derivative (HpD) (Röder, 1998). The proposed phototoxic mechanism involved both type I and type II reactions (Tanielian et al., 2001). The Pheide was localized in the Golgi apparatus of OAT 75 lung carcinoma cells (Moser et al., 1992). Pheide and its methyl ester were far more phototoxic (EC_{50} 0.3–3 μM) than the esters with longer alkyl chains using a panel of human tumor cell lines. However, the butyl ester was more active than the ethyl, hexyl, octyl or benzyl analogues (Wongsinkongman et al., 2002). In a series of mono-, di-, and tri-ol derivatives of Pheide and pyro-Pheide, the mono-ol compound was the most effective for light-induced killing of mouse colon Colo26 cells (LD_{50} 0.35 μM), and possessed low dark toxicity (Bonnett et al., 1992; Bonnett et al., 1994). The photocytotoxicity observed in EMT-6 cells for Pheide amides with alkyl chain lengths of 4–6 carbon atoms, which terminated with OH or CH_3 groups, was three orders of magnitude higher than that of Photofrin®. A significant efflux of these drugs from cells, promoted by HDL and LDL lipoproteins, may account for their fast clearance from normal tissues and low phototoxicity side effects (Dagan et al., 1995).

The insertion of Zn as a central atom in 13^2-hydroxy-Pheide *a* and Chn e_6 methyl esters decreased phototoxic activity by a factor of 5–10, and increased the dark toxicity more than 40-fold (Wongsinkongman et al., 2002).

Targeting. To enhance both drug uptake by tumor cells and subsequent delivery to lysosomes, Pheide

was incorporated into liposomes coated with monoclonal antibodies. Phototoxicity (LD_{90}) toward human bladder tumor cells was about 0.8 μM (Bergstrom et al., 1994).

To target tumor cells over-expressing receptors to plasma LDL, pyro-Pheide was covalently linked by amide bonding with cholesteryl oleate as a double anchor for the LDL lipid core. The photosensitizer-LDL was successfully incorporated into human hepatoblastoma tumor cells (Zheng et al., 2002).

b. In Vivo studies

Twenty-four hours after i.v.-administration, the major target of Pheide *a* in rats carrying acinar pancreatic tumor was the reticuloendothelial system, with a very low level of Pheide in the skin. The ratio of tumor-tissue/surrounding-tissue partitioning of the drug was 6.7–13.5, resulting in PDT-induced (100 J cm^{-2}, 660 nm, 24 h after 9 mg kg^{-1} i.v.) selective necrosis of the tumor (66% cure, 120 days) (Aprahamian et al., 1993; Evrard et al., 1994). The higher selectivity and depth of sensitization provided by Pheide *a*, enabled more efficient PDT and better results than with 5-aminolevulinic acid (ALA)-induced protoporphyrin IX (100 J cm^{-2}, 670 nm, 24 h after 30 mg kg^{-1} i.p.) in treatment of a pancreatic tumor in mice (Hajri et al., 1999). However, the poor uptake and insufficient selectivity of Pheide in HT29 colon cancer implied that photodynamic treatment with this pigment is less safe than with Photofrin® which has better tumor uptake (Hajri et al., 2002).

The 3-(1-alkoxyethyl) ether derivatives of Pheide *a* methyl ester and the Chn e_6 trimethyl ester showed that hydrophobic ethers were more efficient photosensiters than the parental Pheide *a*, Chn e_6 methyl esters and Photofrin®, when tested on SMT/F tumors in mice. These findings suggested differences in localization and subcellular distribution of the different drugs. The new derivatives, in particular, had a shorter lifetime in normal tissues and were excreted within 5 days after injection, compared with weeks for Photofrin®. The 3-(1-hexyloxyethyl) ether of the Pheide methyl ester showed strong photodynamic efficiency (140 J cm^{-2}, 667 nm, 24 h after 1 mg kg^{-1} i.p.), providing 50% tumor response at day 30, which is much better than obtained with the related Chn e_6 derivative, in which the isocyclic ring E is cleaved (Pandey et al., 1991a).

Pyro-Pheide *a* derivatives provided even slightly higher efficiencies. The 3-(1-hexyloxyethyl) and 3-(1-heptyloxyethyl) ethers of pyro-Pheide *a* methyl ester and related 13^1-deoxy derivatives showed 50% tumor response at day 30 under lower drug dose (0.3 mg kg^{-1}), with only minor skin photosensitivity (Pandey et al., 1992c). In the authors' opinion, the shorter-chain pyro-Pheide ethers showed diminished activity due to rapid clearance from plasma and tissues. Introduction of a double bond into the hexyl side chain (the *cis*- and *trans*-3-hexenyl ethers) essentially negated the activity (Pandey et al., 1996c). [13^1-thione]- and [3-formyl]-pyro-Pheide and Pheide methyl esters were active when illuminated at 3 h, but not 24 h, post i.p.-injection (Pandey et al., 1991a, 1992c). The 3-(1-hexyloxyethyl) and 3-(1-heptyloxyethyl) ethers of pyro-Pheide carboxylate, prepared by saponification, were as efficient as the corresponding methyl esters. The low activity of the corresponding Chn e_6 ethers probably resulted from their enhanced hydrophilicity due to enzymatic de-esterification (Pandey et al., 1996c). The half-life time of [3-(1-hexyloxyethyl)]-pyro-Pheide (code name HPPH, see Fig. 1) in rat serum was 25 h (Lobel et al., 2001) and similarly 26.9 h in dogs (Payne et al., 1996), which is longer than in mice (bi-exponential decay: 0.69 h and 21 h) (Bellnier et al., 1993). Both direct effects on the tumor cells and indirect effects via vascular damage contributed to the overall PDT response (Bellnier et al., 1993; Henderson et al., 1997). HPPH-PDT was estimated in the rat model as a useful adjuvant treatment of malignant gliomas (Lobel et al., 2001), as an effective treatment of canine oral (McCaw et al., 2000), feline facial (Magne et al., 1997) and hamster cheek pouch (Furukawa et al., 1996) squamous cell carcinomas, but as an undesirable adjuvant therapy to surgery of canine hemangiopericytomas (McCaw et al., 2001). Photodynamic activity of the anionic pyro-Pheide derivatives was correlated with intracellular localization, which, in turn, was influenced by the aggregation state of the compound upon cellular uptake (Geze et al., 1993; Macdonald et al., 1999; Matroule et al., 1999, 2001; Kelbauskas and Dietel, 2002; Sun and Leung, 2002). Amphiphilicity could play a more dominant role than lipophilicity (Macdonald et al., 1999; Kelbauskas and Dietel, 2002). However, the optimal photodynamic activity could originate from the binding of the photosensitizer to mitochondrially-located peripheral benzodiazepine receptors (Dougherty et al., 2002).

PDT with Pheide 4-hydroxybutylamide (380 J cm^{-2}, 673 nm, 1 h after 2 mg kg^{-1} i.v.) reduced the time for doubling of tumor volume to ~12 days in

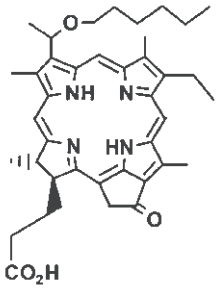

3^1-(1-hexyloxy)phytochlorin
Photochlor® (HPPH)

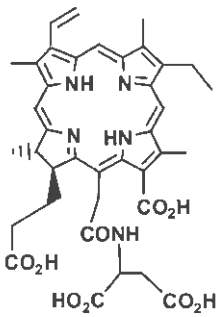

$3^1,3^2$-didehydro-rhodochlorin-15-(2-(N-2-succinyl)acetamide
NPe$_6$

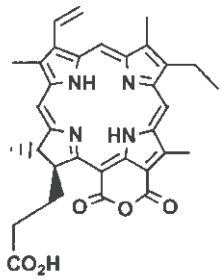

$3^1,3^2$-didehydro-15-carboxy-rhodochlorin-$13^1,15^1$-anhydride
PP *18*

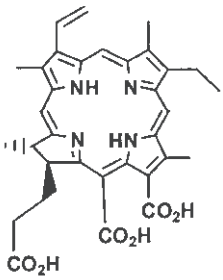

$3^1,3^2$-didehydro-rhodochlorin-15-carboxylic acid
Chn p_6

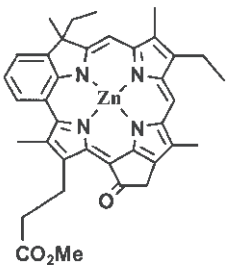

3-methyl-13^1-deoxo-13^2-oxo-benzo[*at*]-phytoporphyrinatozinc(II)
[Zn]-Benzochlorin derivative

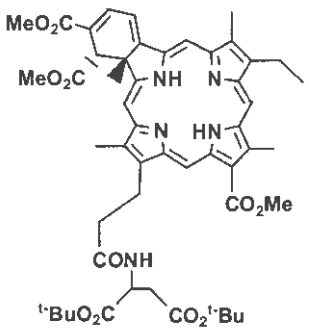

$2^1,2^2,13$-trimethoxycarbonyl-2-methyl-2*H*,2^1*H*-benzo[*b*]-pyrrochlorin 17^3-[2-succinato-di-*tert*-butyl ester]amide
2,3-Benzoporphyrin derivative

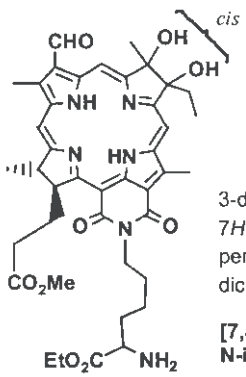

3-desethyl-3-formyl-7,8-*cis*-dihydroxy-7*H*,8*H*-N-(5-amino-5-ethoxycarbonyl-pentyl)pyrrochlorin-$13^1,15^1$-dicarboxamide 17-methyl ester
[7,8-*vic*-dihydroxy]-BPP *18* N-imide derivative

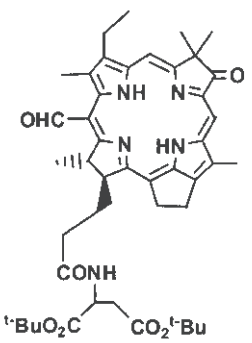

7-methyl-8-desethyl-8-oxo-13^2-desoxo-20-formyl-phytochlorin-17^3-[2-succinato-di-*tert*-butyl ester]amide
Keto-BChn derivative

Fig. 1. Structures of some Chl derivatives used as active photosensitizers (IUPAC-approved names are followed by the trade names or abbreviations)

mouse EMT-6 tumors (Morliere et al., 1998), probably by affecting the tumor vascular integrity (Chapman et al., 1994; Dagan et al., 1995; Gatt et al., 1996). When Pheide 4-hydroxybutylamide was used, photoinactivation of erythrocytes infected by transfusion-transmissible parasites was successful in whole blood with no side effects (Grellier et al., 1997).

Water-soluble carboxymethyl- and hydroxyethyl-substituted pyro-Pheide amides of glycine or aspartic acid exhibited fast clearance from normal organs and serum but were usefully retained in tumors for 24 h in hamsters with nitrosamine-induced pancreatic cancer (Ando et al., 1991b).

Targeting. Negatively charged phospholipid vesicles, used for solubilizing [3-(1-alkoxyethyl)]-Pheide methyl ester, decreased the possibility of occlusive vascular damage (Mayhew et al., 1993). On the other hand, PDT on murine mammary tumor, performed with a short light-drug interval (15 min) using the indium complex of pyro-Pheide methyl ester (code name MV6401) in cationically-charged egg yolk phosphatidylcholine emulsion (0.018-0.072 mg kg^{-1}, 5 J cm^{-2}, 664 nm), caused blood flow stasis and vascular hyperpermeability that became apparent 3 h later (Dolmans et al., 2002b). The plasma half-life of MV6401 was ~20 min, and the drug was confined to the vascular compartment during the first 15 minutes after administration. However, neovessel formation and tumor regrowth were observed 3 days after the treatment. Two equal MV6401 doses injected 4 h and 15 min before light exposure allowed the drug to localize in both vascular and tumor cell compartments: such double administration of drug before PDT resulted in a profound delay of tumor growth and a more extensive antivascular effect (Dolmans et al., 2002a).

Combining a PDT protocol, based on administration of ALA and a Pheide derivative, synergistically enhanced the inhibition of tumor growth (lymphoma and squamous cell carcinoma) in mice (Jin et al., 2000).

D. Chlorin e_6 and Derivatives

1. General Description and Chemistry

Chn e_6, formed by anaerobic alkaline hydrolysis of Pheide *a*, is a tricarboxylic water-soluble derivative absorbing light at 654 nm and has a ϕ_Δ of about 0.7 (Spikes and Bommer, 1993; Zenkevich et al., 1996; Fernandez et al., 1997). $[Sn]^{IV}$-Chn e_6 absorbs at 632 nm and generates singlet oxygen with ϕ_Δ equal to 0.83 (Spikes and Bommer, 1993). Amides of Chn e_6 at C-13[1] were regioselectively obtained by aminolysis of the isocyclic ring (Ando et al., 1991a, 1992; Gurinovich et al., 1992; Zhang and Xu, 1999; see also Ma and Dolphin, 1996; Belykh et al., 2002). Mono-L-aspartyl Chn e_6 (code name NPe_6, Fig. 1), obtained by amidation of the acetic acid residue of Chn e_6 with L-aspartic acid (Gomi et al., 1998), possessed an increased hydrophilicity (Boyle and Dolphin, 1996) and a ϕ_Δ of 0.77 (Spikes and Bommer, 1993).

2. Pre-clinical Studies and Efficacy

a. In Vitro Studies

A possible role for the acidic tumor microenvironment in the preferential uptake and retention of Chn e_6 has been reported (Zorin et al., 1996; Cunderlikova et al., 1999, 2000; Shevchuk et al., 2002). Higher accumulation of Chn e_6 dimethyl ester in leukemic cells caused their selective photocytolysis (Savitskiy et al., 2002). A glucosamine salt of Chn e_6 revealed high antifungal activity (Strakhovskaya et al., 2002).

NPe_6 (Fig. 1), localized in the lysosomes of murine hepatoma cells, caused photodamage by triggering the mitochondrial apoptotic pathway by releasing lysosomal proteases (Reiners et al., 2002). Serum components inhibited cellular uptake of NPe_6, and only free pigment was accumulated by murine leukemia cells and caused phototoxicity (Sheyhedin et al., 1998).

Targeting. Triacetoxymethyl ester of Chn e_6 (CAME) and acetoxymethyl ester of Pheide *a* (PAME) were synthesized as photosensitizers for lysosome-mediated PDT (Sahai et al., 1993). These lipophilic esters, reaching acidic lysosomes by endocytosis, were hydrolyzed by esterases into pH-sensitive amphipathic compounds. Contact with the neutral pH of the adjacent cytosol results in conversion of the hydrophobic drug to a more hydrophilic anionic species, presumably by allowing its diffusion into the lysosomal compartment and partitioning throughout the lipophilic and aqueous compartments of the cell. Brief incubation of murine leukemia cells with 10 mM CAME followed by irradiation, led to mitochondrial photodamage and apoptosis, whereas higher doses of CAME inhibited apoptosis, with cell death probably occurring via necrosis (Kessel and Poretz, 2000).

Immunoconjugates of Chn e_6 with anti-ovarian carcinoma murine monoclonal antibody were more

effective in the selective photochemical eradication of target cells than the free pigment (Goff et al., 1991, 1992).

Light-dependent killing of mammary adenocarcinoma cells was examined with a Chn e_6-transferrin conjugate, which was aimed at a corresponding receptor that is highly expressed in tumor cells (Cavanaugh, 2002).

Targeted delivery of $[Sn]^{IV}$-Chn e_6, conjugated to epidermal growth factor (EGF) through a carrier, showed increased phototoxicity to squamous carcinoma cells in relation to phototoxicity of the non-conjugated sensitizer, which express an increased number of EGF-receptors; however, the affinity of the conjugate was strongly dependent on the carrier used (dextran, polyvinyl alcohol or human serum albumin) (Gijsens and de Witte, 1998; Gijsens et al., 2000). $[Sn]^{IV}$-Chn e_6 linked to IgG selectively killed otherwise resistant strains of *Staphylococcus aureus* (Embleton et al., 2002).

The importance of positive charges on the sensitizer's periphery to the overall photodynamic activity was demonstrated by the killing of both gram-positive and gram-negative bacteria by cationic conjugates of Chn e_6 (Soukos et al., 1998; Hamblin et al., 2002b).

Conjugates for doubly-targeted delivery to both cell and nucleus were constructed using Chn e_6 together with BSA as a carrier, insulin as internalizable ligand and viral T-antigen within a β-galactosidase fusion protein as a nuclear localization factor. This molecular assembly demonstrated a 2400-fold higher photodynamic activity in human hepatoma cells (EC_{50} of 0.13 nM) compared to free Chn e_6 (Akhlynina et al., 1997). Co-incubation with adenovirus additionally increased the nuclear photosensitizing activity (Akhlynina et al., 1999). Chn e_6 was also attached to linear or branched peptides for guidance to both cytoplasmic and nuclear targets: such conjugates displayed 400- and 40-fold more phototoxicity in CHO and RIF-1 cells than Chn e_6 alone (Bisland et al., 1999).

b. In Vivo Studies

Photodynamic treatment of rat M-1 sarcoma with Chn e_6 (90 J cm^{-2}, 647 and 676 nm, 3 h after 5–10 mg kg^{-1} i.p.) induced tumor necrosis to a depth of 14–16 mm via simultaneously damaging both vascular stroma and malignant cells. The effect was potentiated by increasing the drug and light doses, but was attenuated with the extension of the drug-to-light interval (Kostenich et al., 1991): photoradiation of various transplantable rat tumors was far more effective 15 min after injection than after 24 h, leading to 100% cure on day 14 after the treatment of spindle cell fibrosarcoma and alveolar liver cancer (Kostenich et al., 1993). The regression was correlated with the morphological difference between the tumor microcirculatory bed, as the main target of photodynamic exposure, and the normal one (Kostenich et al., 1993). Pharmacokinetic studies revealed a maximum concentration of Chn e_6 in blood, internal organs and muscle 3 h after i.p.-injection, and in tumors after 12–18 h. Increased content and the relatively long clearance time of Chn e_6 (>72 h) in blood and tumor were attributed to its binding to and interaction with blood components including erythrocytes and transport proteins (Kostenich et al., 1994). Nevertheless, Chn e_6 demonstrated a high antitumor efficacy in colon carcinoma in mice with minimal damage to normal tissues (Orenstein et al., 1996). The efficient application of Chn e_6-PDT for treating rheumatoid arthritis has also been discussed (Tauraytis et al., 1992).

The water-soluble amide formed from Chn e_6 and ethylenediamine stimulated affinity for tumor cells and cellular membranes. The photodynamic effect, when the maximal concentration of sensitizer was reached in the tumor, was higher with the Chn e_6-amide than with Chn e_6, possibly due to preferential binding with lipoproteins (Gurinovich et al., 1992).

NPe_6 rapidly clears from the body (Ferrario et al., 1992). The maximal PDT effectiveness in murine mammary tumors, achieved following light treatment 2 h after drug injection, was correlated with the plasma, not tumor, levels of the photosensitizer (Ferrario et al., 1992) which possesses a selective affinity for proliferating neovasculature (Roberts and Hasan, 1992). In uterine cervical carcinoma the PDT effect using NPe_6 resulted from tumor necrosis secondary to the obstruction of blood vessels around the tumor (Nakamura et al., 2002). In rats bearing chondrosarcoma, the achieved tumor cure of 83%, with no regrowth for 21 days, was found after an optimal delay of 4 h between injection and illumination (i.e. 135 J cm^{-2}, 664 nm, 4 h after 10 mg kg^{-1} i.v.), when the effect of both vascular stasis and direct tumor cytotoxicity was maximal (McMahon et al., 1994).

Atherosclerotic plaques of abdominal aorta can be selectively degraded by NPe_6-PDT, as demonstrated in cholesterol-fed rabbits (50–200 J cm^{-2}, 664 nm,

6 h after 5 mg kg^{-1} i.v.) (Saito et al., 1998). Two main mechanisms might be complementary and synergistic in the photodynamic production of vascular lesions: endothelial cell damage and platelet aggregation (fibrin plugging) (Yamamoto et al., 1999).

Choroidal vessel occlusion was evident starting from 2.65 J cm^{-2} in pigmented rabbits and 0.88 J cm^{-2} in non-pigmented rabbits (2 mg kg^{-1} of NPe_6 i.v.). Lesion diameter decreased as the time between injection and irradiation increased from 5 min to 24 h (Kazi et al., 2000). NPe_6-PDT was found to have a lower threshold for choroidal vessel occlusion than for retinal vessels (Mori et al., 1999; Peyman et al., 2000a); thus, the PDT effect varied depending on the target characteristics (Peyman et al., 2000b).

Targeting. Both immunoconjugates of Chn e_6 with anti-ovarian carcinoma murine monoclonal antibody and non-conjugated photosensitizer reached peak tumor concentrations at 24 h but the absolute concentrations of the conjugate were always 2 to 3-fold higher. Also, after 24 h, the conjugate concentrations were 3.5- to 7.2-fold higher in tumor than in non-tumor cells. PDT with a single light exposure demonstrated a dose-dependent relationship with the fluence and the conjugate concentration. However, there was significant treatment-related toxicity at all light fluences tested (Goff et al., 1994).

A conjugate of Chn e_6 with BSA was efficiently taken up by a scavenger pathway, localized in areas of the intimal hyperplasia of the rat's abdominal aorta, and functioned as a PDT-sensitizer (Nagae et al., 1998). Covalently linked Chn e_6-albumin conjugate showed superior PDT-activated tissue sealing of scleral incisions than did non-covalent mixtures (Khadem et al., 1999).

Bio-distribution studies showed that the polyanionic conjugates of Chn e_6 with murine monoclonal antibody accumulated more selectively in liver tumors than corresponding polycationic conjugates or free Chn e_6. PDT with the polyanionic conjugates was more effective in eradicating liver tumors and resulted in better survival of normal tissue (Del Governatore et al., 2000b). Chn e_6-succinylated polylysine conjugate was used to activate the transforming growth factor P that modulates cartilage metabolism in osteoarthritis (Sullivan et al., 2002). A cationic poly-L-lysine conjugate of Chn e_6 to a Fab´ fragment of the murine monoclonal anti-human ovarian carcinoma antibody, showed a PDT response better than that of the anionic conjugate or free Chn e_6, with no systemic toxicity from the treatment (Molpus et al., 2000). The cationic conjugate, in combination with *cis*-platin chemotherapy ex vivo, displayed a synergistic effect (Duska et al., 1999). A comparison between the positively-charged polylysine- and negatively-charged succinylated polylysine-conjugates of Chn e_6 for PDT of rat orthotopic prostate tumor models indicated that both conjugates initially bind to the endothelium lining of the vasculature. However, the anionic compound extravasated faster into the tissue (Hamblin et al., 1999). Targeted cationic conjugates showed superior binding to human colon cancer cells (Del Governatore et al., 2000a). The use of cationic poly-L-lysine conjugate of Chn e_6 to control wound healing was shown in mice (Hamblin et al., 2002a).

The use of water-soluble N-(2-hydroxypropyl) methacrylamide (HPMA) polymer for anticancer drug delivery was intended to bypass some forms of multidrug resistance, to enhance preferential accumulation in tumor tissue by increased permeability and retention, and to take advantage of new targeting strategies such as polymerizable antibody fragments and synthetic receptor-binding epitopes (Kopecek et al., 2001). Combination therapy with the HPMA-anticancer drug containing doxorubicin and meso-Chn e_6 attached via an enzymatically degradable oligopeptide, cured tumors which could not be cured with either chemotherapy or PDT alone. HPMA-copolymer-bound drugs exhibited selective tumor accumulation in contrast to free drugs. Most effective was the combination of multiple chemotherapy with HPMA-copolymer-doxorubicin and multiple PDT with HPMA-copolymer-meso-Chn e_6, especially with the attachment of monoclonal antibodies to both copolymers. Reduced non-specific toxicity has been a constant advantage in all the preclinical studies (Kopecek et al., 2001).

E. Purpurin 18, Chlorin p_6, and Derivatives

1. General Description and Chemistry

Purpurin *18* (PP *18*, Fig. 1), having a 6-membered anhydride ring as a result of oxidative cleavage of isopentanone ring E, is easily prepared from Pheide *a* and its esters (Kenner et al., 1973; Hoober et al., 1988) or directly from a crude extract of Chl *a* (Mironov et al., 1993). PP *18* is lipophilic, has a strong absorption at 700 nm and ϕ_Δ of about 0.7 (Zenkevich et al., 1996). PP *18,* a stable intermediate, can be used for further chemical transformations. Alkaline cleavage

of the anhydride ring produces water-soluble Chn p_6 (Fig. 1), which absorbs at 656 nm and provides ϕ_Δ of about 0.6 in ethanol, the same as Chn e_6 (Zenkevich et al., 1996). The opening of the anhydride ring of the PP *18* methyl ester by L-lysine as a nucleophile yielded a water-soluble Chn p_6 13^1-lysylamide methyl ester (K. M. Smith et al., 1992; Lee et al., 1993). Replacement of the 3-vinyl group with the 1-hydroxyethyl and 1,2-dihydroxyethyl functions did not cause significant spectral changes, but substantially increased the hydrophilicity of the corresponding Chn p_6 derivatives. In contrast, the distinct bathochromic shift with vinyl oxidation to acetyl (25 nm) and formyl (35 nm) groups did not influence the amphiphilicity balance (Kozyrev et al., 1994; Pandey et al., 1994). The propionic acid residue of PP *18* was converted into corresponding amides with alanine and aspartic acid (Mironov et al., 1993).

Partial reduction transformed the anhydride ring of PP *18* into a δ-lactone. The mixture of the two products and their 3-(1-hydroxyethyl) and 3-acetyl derivatives displayed a higher stability toward acidic and basic cleavage; however, their spectral bands in the red region were blue shifted by 22–37 nm (Mironov et al., 1998).

PP *18* cyclic imides, isoimides, and the corresponding Chn p_6 derivatives with 1-hexylamine (Pandey et al., 1994; Kozyrev et al., 1996c) and N,N-dimethylethylenediamine (Kozyrev et al., 1997) instead of lysine, have also been synthesized. Following a similar QSAR-investigation approach as with Pheides, a set of lipophilic PP *18* N-imide derivatives was synthesized with various alkyl, aryl, and fluoroaryl substitutions at the C-3, C-8, C-20 and N-13 positions of the macrocycle: the main Q_y absorption band of this set of compounds was near 700 nm and they had ϕ_Δ values of 0.57–0.60 (Rungta et al., 2000; Zheng et al., 2000b, 2001b; Gryshuk et al., 2002).

PPs of increased hydrophiliciy, comprising cyclic imides with NH, N-substituted residues of C_2-C_4 aliphatic alcohols, carboxylic acids (C_1, C_5) or containing the N-OR group, where R is a hydrogen, alkyl or acyl residue, have their major absorption in the 706–718 nm domain. The replacement of the vinyl group by a formyl function resulted in a red shift to 750 nm (Mironov and Lebedeva, 1998; Mironov et al., 1999). A PP derivative with N-(3-hydroxypropyl) residue absorbs at 711 nm and has a ϕ_Δ value of 0.66 (Feofanov et al., 2002).

A positively charged PP was recently prepared by introducing a pyridinium group at the C-5 position of [Ni]-Chn p_6 trimethyl ester or at the C-12^1 position of [Ni]-PP *18* N-hexylimide methyl ester (Mettath et al., 2000).

2. Pre-clinical Studies and Efficacy

a. In Vitro Studies

The photodynamic efficacy of [3-formyl]-Chn p_6 and Chn p_6 were similar in causing necrotic death of A-549 human adenocarcinoma cells (IC_{50} about 4-8 μM), with the mitochondria as a primary target. The water-soluble Chn p_6 13^1-lysylamide methyl ester was found photocytotoxic against 9L glioma cells at concentrations 10 to 100-fold lower than Photofrin® (K. M. Smith et al., 1992; Lee et al., 1993). The Chn p_6 lysylamide was localized by endocytosis in the endosomal compartment, causing morphological damage in the mitochondria, Golgi apparatus, and rough endoplasmic reticulum (Leach et al., 1993).

A hydrophilic PP N-(3-hydroxypropyl)imide demonstrated photocytotoxicity on A549 human adenocarcinoma cells 60-fold higher than [3-formyl]-Chn p_6, with no dark cytotoxicity. Subcellular localization implied mitochondria and Golgi apparatus as the primary targets (Feofanov et al., 2002).

b. In Vivo Studies

PP *18* was found inactive, probably due to the instability of the anhydride ring in vivo (Zheng et al., 2000a). PDT on Ehrlich carcinoma in mice (90 J cm^{-2}, 696 nm, 5-10 mg kg^{-1} i.v.), performed 1-6 h after [3-formyl]-Chn p_6 administration, resulted in severe complications and light-induced deaths, whereas after 24 h it induced moderate suppression of tumor growth (Grichine et al., 2001).

PDT with Chn p_6 lysylamide on 9L glioma tumors in rats (100 J cm^{-2}, 664 nm, 4 h after 2.5 mg kg^{-1} i.v.) showed long-term inhibition of tumor growth. However, side effects in normal tissues, including severe skin necrosis, were observed (Leach et al., 1992). To prevent conversion of Chn p_6 lysylamide into PP imide, the C-15^1 acid residue was esterified (Lee et al., 1993). The Chn p_6 lysylamide esters were less efficient PDT sensitizers than the corresponding PP imide when tested on mammary adenocarcinoma in mice. However, these lysylamide agents caused a substantial direct toxicity with 5 mg kg^{-1} dose in contrast to NPe_6 (Kessel et al., 1995).

The tumorcidal ability of the 3-(1-alkoxyethyl)

ethers of PP *18* N-hexylimide methyl ester compared with that of the 17^3-alkylamide derivatives of PP *18* N-hexylimide was studied by Zheng et al. (2000b); the therapeutic response of RIF tumors in mice (135 J cm^{-2}, 705 nm, 24 h after 1 μmol kg^{-1}) was stronger with the ether derivatives, especially with the *n*-hexyl chain (100% tumor response on day 30), than with the amides. The location of alkylether substituents in alkylether analogues of meso-PP *18* N-hexylimide methyl ester and meso-PP *18* N-decylimide methyl ester is important for photosensitizing efficiency: the 3-(1-heptyloxyethyl is more efficient than 8-(1-heptyloxyethyl), 3-octyloxymethyl and 20-heptyloxymethyl derivatives (Rungta et al., 2000). Essential differences in tumor uptake, selectivity and PDT efficacy were observed among homologues of the PP-*18* imide methyl ester containing 3-(1-O-alkyl) and 13^2-N-alkyl substituents possessing similar lipophilicity and singlet oxygen production, suggesting differences in their pharmacokinetics and pharmacodynamics (Zheng et al., 2001b). Screening of PP *18* imide methyl esters, containing aromatic (3,5-dimethylbenzylic) or trifluoromethyl-aromatic substituents instead of O-alkyl or N-alkyl groups, indicated the superiority of the fluorinated purpurinimides, especially the N-fluoro-aryl derivatives (Gryshuk et al., 2002).

PDT in P-388 leukemia-bearing mice with hydrophilic PP N-(3-hydroxypropyl)imide (230 J cm^{-2}, >690 nm, 24 h after 25 mg kg^{-1}) halved the tumor growth rate (Mironov et al., 1999).

Targeting. Meso-PP *18* imide methyl ester, N-substituted with galactose or lactose via diene spacer, was designed for targeted delivery to the galectin-1 receptor, which is highly expressed by malignant cells. Preliminary studies have indicated the superiority of carbohydrate conjugates over non-conjugated photosensitizers (Zheng et al., 2001a).

F. Benzochlorin Derivatives

1. General Description and Chemistry

Benzoisobacteriochlorin, formed by the cyclization of a meso-acrolein to a β-pyrrolic position in the [20-(2-formylvinyl)-13^1-deoxypyro]-[Ni]-Pheide methyl ester (Vicente and Smith, 1991), was converted into benzochlorin, and then to 5-formyl, alkoxymethyl and cationic iminium salt derivatives (Pandey et al., 1995) and also to 13^1, 13^2-oxobenzochlorins (Fig. 1) (Mettath et al., 1998). These compounds have absorption maxima between 708-759 nm. Similarly, based on the PP *18* N-hexylimide methyl ester, 3-ethylidene-substituted isobacteriochlorins and fluorinated benzochlorin (λ_{max} 751 nm) were produced (Mettath et al., 1999).

G. Diels-Alder Adducts of Chlorins

1. General Description and Chemistry

When the 3-vinyl group of Pheide *a* was utilized as a diene component, isomerically pure 2,3-benzoporphyrin analogues (Fig. 1) were obtained (Pandey et al., 1993, 1996b; Ma and Dolphin, 1997). Also, by Diels-Alder cycloaddition, an 8-vinyl-meso-PP *18* methyl ester was transformed into 7,8-benzobacteriopurpurins, having an absorption at 760-795 nm (Zheng et al., 1996). Regioselective cycloaddition of diazomethane to pyro-Pheide and PP *18* N-methyl imide produced the corresponding 1′-pyrazolinyl-substituted derivatives, which were altered to cyclopropyl derivatives by pyrolysis (Kozyrev et al., 2003). However, with [13^2-oxo]-pyro-Pheide *a*, the primary target of diazomethane was the α-diketone ring, producing verdinochlorins with fused cyclohexenone rings and an absorption at 739–777 nm (Kozyrev et al., 1998a).

2. Pre-Clinical Studies and Efficacy

a. In Vivo Studies

In preliminary tests, a benzporphyrin derivative of rhodoporphyrin XV aspartyl amide (λ_{max} 668 nm) was a successful photosensitizer against SMT/F tumors in mice at 3 h but not 24 h after injection of 1 mg kg^{-1} (Pandey et al., 1996b).

H. Glycol- and Ketobacteriochlorin Derivatives

1. General Description and Chemistry

The reaction of non-vinyl derivatives of pyro-Pheide *a*, Chn e_6, PP *18* and its N-imides with osmium tetroxide yielded *vicinal 7,8*-dihydroxy-substituted bacteriochlorins (BChns, Fig. 1) with reduction of opposite pyrrole rings B and D: these compounds show significant spectral red shifts up to 754 nm for the 3-formyl-derivatives of pyro-Pheide *a* and Chn e_6 and 828 nm for the 3-formyl-derivative of

[Zn]-PP *18* (Pandey et al., 1992a,c, 1994, 1997b; K. M. Smith et al., 1992; Kozyrev et al., 1994, 1996a). By a similar approach, [Ni]-complexes of meso-Chn e_6 and meso-PP *18* methyl esters yielded *vicinal*-dihydroxy-substituted isoBChlns with reduction of adjacent pyrrole rings (Kozyrev et al., 1996a).

The pinacole-pinacolone rearrangement in *vicinal*-dihydroxy-BChns led to keto-BChns (Fig. 1). The migration of alkyl groups and the fluctuation of absorption maxima (711-786 nm) of the products obtained was influenced by the number and position of the electron-withdrawing groups (Pandey et al., 1992a, 1997b; Kozyrev et al., 1996b). The keto-BChn from [13^1-deoxo]-mesopyro-Pheide *a* provided a ϕ_Δ of 0.40 (Pandey et al., 1997a).

2. Pre-Clinical Studies and Efficacy

a. In Vivo Studies

BChn products derived from pyro-Pheide *a* and Chn e_6 were photodynamically inactive (135 J cm^{-2}, 702 nm, 3 h after 0.3 mg kg^{-1} i.p. or 4 and 24 h after 10 mg kg^{-1} i.v.) (Pandey et al., 1992c; Kessel et al., 1993). Among [3-formyl]-bacteriopurpurin (BPP) agents, however, the N-13^2-lysylimide and C-17^3-aspartylamide derivatives, irradiated 3 h post i.v.-injection (135 J cm^{-2}, 815 nm, 5 mg kg^{-1}), exhibited 100% tumor response on day 7, while the lysyl-free [3-formyl]-BPP was inactive (Pandey et al., 1994).

An isomeric mixture of keto-BChns, obtained from [3-acetyl-8-isobutyl]-pyro-Pheide *a* methyl ester, was successful in treating mice bearing the RIF tumor (135 J cm^{-2}, 5–10 mg kg^{-1}) when photoexcited at 4 h but not 24 h after i.v.-administration; however, some post-PDT toxicity was observed. The efficacy and cytotoxicity were correlated with plasma rather than with the tumor levels of the drug (Kessel et al., 1993). Similarly, keto-BChns from [13^1-deoxo-20-formyl]-mesopyro-Pheide *a* were photodynamically active on SMT/F tumors in mice (135 J cm^{-2}, 1–2.5 mg kg^{-1}), when illuminated 3 h but not 24 h after i.v.-administration, but post-PDT mortality was recorded. Di-tert-butylaspartic esters were more potent than the methyl ester derivative, probably due to esterase activity. Cutaneous phototoxic side effects were not observed from day 9 after keto-BChn injection. Photosensitizing efficacy was correlated with an affinity for the peripheral benzodiazepine receptor (Pandey et al., 1997a).

I. Dimeric and Oligomeric Structures

1. General Description and Chemistry

A number of Chl-based dimers and trimers with ether, amide and carbon-carbon linkages were prepared (Ando et al., 1991a, 1992; Brandis et al., 1992; Jaquinod et al., 1996; Pandey et al., 1996d; Zheng et al., 2000a) similar to Photofrin®, which consists of a mixture of dimers and higher oligomers with ether, ester and carbon-carbon linkages determining its biological activity (Pandey and Zheng, 2000; Macdonald and Dougherty, 2001). Dimers of pyro-Pheide *a*, Chn e_6 and PP *18* derivatives, linked with amide bonds via lysine and propylenediamine, had a $\phi_\Delta < 0.5$.

2. Pre-Clinical Studies and Efficacy

a. In Vivo Studies

Dimers of pyro-Pheide *a*, Chn e_6 and PP *18* derivatives, linked with amide bonds via lysine and propylenediamine, were evaluated in mice SMT/F tumors (135 J cm^{-2}, 665 nm, 24 h after 4 μmol kg^{-1} i.v.) and they generated weak antitumor activity relative to the related monomers (Pandey et al., 1996d; Zheng et al., 2000a), which contrasts with the enhanced effect of porphyrin dimers and trimers.

J. Chlorophyll Metabolites

1. General Description and Chemistry

Numerous metabolic derivatives of Chl, discovered in the last decade, exhibit biological activity as protective antioxidants or cellular signaling mediators (Ma and Dolphin, 1999). Some of them have potential in PDT. A hydrophobic Chl metabolite from silkworm excreta, 13^2-hydroxy-Phe *a*, generates singlet oxygen at a ϕ_Δ of 0.50 (Dai et al., 1992). Tolyporphin (see formula in Chapter 1, Scheer), extracted from the cyanobacterium *Tolypothrix nodosa*, has a structure similar to diketo-BChn photosensitizers: it possesses absorbance at 675 nm and has two sugar moieties, providing solubility in water (Prinsep et al., 1992).

2. Pre-clinical Studies and Efficacy

a. In Vitro Studies

Pheide *a* methyl ester isolated from *Garuga pinnata*

Roxb. leaves showed promising light-induced cytotoxicity against a number of human cancer cell lines including drug-resistant sublines (Wongsinkongman et al., 2002).

Tolyporphin was 6-, 70- and 5,000-fold more effective in photokilling EMT-6 tumor cells than Pheide *a* [4-hydroxybutylamide], [3-(1-hexyloxyethyl)]-pyro-Pheide *a* methyl ester and Photofrin®, respectively: this enhancement is probably due to permeation to different subcellular sites such as the endoplasmic reticulum and nuclear membrane and to reversal of multiple drug resistance (Morliere et al., 1998). Binding of tolyporphin to P-glycoprotein inhibited the transport of cytotoxic natural product drugs, enhancing the cytotoxicity of adriamycin or vinblastine in SK-VLB cells (C. D. Smith et al., 1994).

b. In Vivo Studies

PDT with tolyporphin (38 J cm^{-2}, 681 nm, 1 h after 2 mg kg^{-1} i.v.) appears promising as it delayed regrowth of mouse EMT-6 tumors by 20 days indicating that this sensitizer is 10-20 times more potent than Pheide *a* [4-hydroxybutylamide] or [3-(1-hexyloxyethyl)]-pyro-Pheide *a* methyl ester (Morliere et al., 1998). A very low level of the pigment in blood in contrast to elevated delivery to tumor 1 h after administration implied mutual direct (tumor cells) and indirect (vasculature) photokilling effect (Morliere et al., 1998).

III. Clinical Trials

PDT with HPPH (trade name Photochlor®) has entered Phase I/II clinical trials (Roswell Park Cancer Institute, Buffalo). Excellent results were reported in the treatment of five oesophageal cancer patients with no skin phototoxicity (Pandey, 2000). A recent study of the drug pharmacokinetics in humans demonstrated a bicompartmental clearance with short and long half lifetimes of 7.77 h and 596 h, respectively (Bellnier, 2003).

NPe_6-PDT entered a Phase I study (University of Louisville) on 11 patients with superficial cutaneous malignancies. Sixty six percent of the sites were tumor-free after 12 weeks (100 J cm^{-2}, 664 nm, 4 h after 2.5–3.5 mg kg^{-1} i.v.). At these drug doses, there was no apparent selectivity for destruction of tumor cells compared with normal skin cells, but only temporary generalized skin photosensitivity was noted (Taber et al., 1998) despite detection of the drug in the plasma for up to 6 weeks (Kessel, 1997). Phase II trials have commenced in Japan for use in endobronchial carcinoma; so far, thirty-nine lesions in 35 patients have been treated with an 85% response (33 lesions), out of which 29 patients (83%) showed a complete recovery (Furukawa et al., 2001).

Clinical trials with HPMA-copolymer-meso-Chn e_6 are also in progress (see Kopecek et al., 2001).

A clinical evaluation of PDT in different tumors with a water-soluble pigment mixture based on Chn e_6 and Chn p_6 (trade name Radachlorin®), is now being performed in Russia (RadaPharma, 2002).

Acknowledgments

A.S. is the incumbent of the Robert and Yadelle Sklare Professorial Chair in of Biochemistry, and Y.S. is the incumbent of the Tillie and Charles Lubin Professorial Chair in of Biochemical Endocrinology at The Weizmann Institute of Science, Rehovot, Israel. Work of the authors was supported in part by Steba Biotech NV, France.

References

Ackroyd R, Kelty C, Brown N and Reed M (2001) The history of photodetection and photodynamic therapy. Photochem Photobiol 74: 656–669

Akhlynina TV, Jans DA, Rozenkrants AA, Statsyuk NV, Balashova IY, Toth G, Pavo I, Rubin AB and Sobolev AS (1997) Nuclear targeting of chlorin e_6 enhances its photosensitizing Activity. J Biol Chem 272: 20328–20331

Akhlynina TV, Jans DA, Statsyuk NV, Balashova IY, Toth G, Pavo I, Rosenkranz AA, Naroditsky BS and Sobolev AS (1999) Adenoviruses synergize with nuclear localization signals to enhance nuclear delivery and photodynamic action of internalizable conjugates containing chlorin e_6. Int J Cancer 81: 734–740

Aksenova AA, Sebyakin YL and Mironov AF (2000) The synthesis of galactopyranosyl-substituted derivatives of pheophorbide. Rus J Bioorg Chem 26: 126–129

Aksenova AA, Sebyakin YL and Mironov AF (2001) Synthesis and properties of O- and S-glycosylated derivatives of pyropheophorbide alpha. Rus J Bioorg Chem 27: 124–129

Ando T, Irie K, Koshimizu K, Shingu T, Takeda N, Takemura T, Nakajima S and Sakata I (1991a) New photosensitizers for photodynamic therapy: Syntheses of chlorin e_6 dimer and trimer. Agr Biol Chem 55: 2441–2443

Ando T, Suzuki Y, Geka R, Irie K, Koshimizu K, Takemura T, Nakajima S and Sakata I (1991b) New water-soluble pyropheophorbide *a* derivatives as possible agents for photodynamic therapy of cancer. Tetrahedron Lett 32: 5107–5110

Ando T, Kazuhiro I, Koshimizu K, Nakajima S, Takemura T and

Sakata I (1992) A convenient synthesis of chlorin e_6 dimer and trimer. In: Spinelli P, Dal Fante M and Marchesini R (eds) Photodynamic Therapy and Biomedical Lasers, pp. 769–773. Elsevier Science Publishers B.V., Amsterdam

Aprahamian M, Evrard S, Keller P, Tsuji M, Balboni G, Damge C and Marescaux J (1993) Distribution of pheophorbide-*a* in normal tissues and in experimental pancreatic cancer in rats. Anticancer Drug Design 8: 101–114

Bellnier DA, Henderson BW, Pandey RK, Potter WR and Dougherty TJ (1993) Murine pharmacokinetics and antitumor efficacy of the photodynamic sensitizer 2-[1-hexyloxyethyl]-2-devinyl pyropheophorbide-*a*. J Photochem Photobiol B-Biol 20: 55–61

Bellnier DA, Greco WR, Loewen GM, Nava H, Oseroff AR, Pandey RK, Tsuchida T and Dougherty TJ (2003) Population pharmacokinetics of the photodynamic therapy agent 2-[1-hexyloxyethyl]-2-devinyl pyropheophorbide-*a* in cancer patients. Cancer Res 63: 1806–1813

Belykh DV, Karmanova LP, Spirikhin LV and Kutchin AV (2002) Synthesis of chlorin e_6 amide derivatives. Mendeleev Commun: 77–78

Bergstrom LC, Vucenic I, Hagen IK, Chernomorsky SA and Poretz RD (1994) In vitro cytophototoxicity of lysosomotropic immunoliposomes containing pheophorbide *a* with human bladder carcinoma cells. J Photochem Photobiol B-Biol 24: 17–23

Bisland SK, Singh D and Gariepy J (1999) Potentiation of chlorin e_6 photodynamic activity in vitro with peptide-based intracellular vehicles. Bioconjugate Chem 10: 982–992

Bonnett R (1999) Photodynamic therapy in historical perspective. Rev Contemp Pharmacother 10: 1–17

Bonnett R (2000) Chemical aspects of photodynamic therapy. In: Phillips D, O'Brien P and Roberts S (eds) Advanced Chemistry Texts, Vol 1, pp 129–147, Gordon and Breach Science Publishers, Amsterdam

Bonnett R (2002) Progress with heterocyclic photosensitizers for the photodynamic therapy (PDT) of tumors. J Heterocycl Chem 39: 455–470

Bonnett R, Grahn MF, Salgado A, Turkish M, Valles MA and Williams NS (1992) Amphiphilic chlorins derived from chlorophyll *a* for photodynamic therapy. In: Spinelli P, Dal Fante M and Marchesini R (eds) Photodynamic Therapy and Biomedical Lasers, pp 866–869. Elsevier Science Publishers B.V., Amsterdam

Bonnett R, Benzie R, Grahn MF, Salgado A and Valles MA (1994) PDT photosensitizers derived from chlorophyll *a*. Proc SPIE 2078: 171–178

Boyle DG and Potter WR (1987) Photobleaching Photofrin II as a means of eliminating skin photosensitivity. Photochem Photobiol 46: 97–101

Boyle RW and Dolphin D (1996) Structure and biodistribution relationships of photodynamic sensitizers. Photochem Photobiol 64: 469-485

Brandis A, Kozyrev AN and Mironov AF (1992) Synthesis and study of chlorin and porphyrin dimers with ether linkage. Tetrahedron 48: 6485–6494

Canti G, De Simone A and Korbelik M (2002) Photodynamic therapy and the immune system in experimental oncology. Photochem Photobiol Sci 1: 79–80

Cavanaugh PG (2002) Synthesis of chlorin e_6-transferrin and demonstration of its light-dependent in vitro breast cancer cell killing ability. Breast Cancer Res Treat 72: 117–130

Chapman JD, Stobbe CC, Engelhardt EL, Fenning MC, Brown DQ, Dagan A and Gatt S (1994) Exploitation of interstitial brachytherapy techniques for PDT. II. Novel photosensitizers for the treatment of solid tumors. Proc SPIE 2133: 128–139

Chen B, Roskams T and de Witte PAM (2002) Antivascular tumor eradication by Hypericin mediated photodynamic therapy. Photochem Photobiol 76: 509–513

Cunderlikova B, Gangeskar L and Moan J (1999) Acid-base properties of chlorin e_6: Relation to cellular uptake. J Photochem Photobiol B-Biol 53: 81–90

Cunderlikova B, Kongshaug M, Gangeskar L and Moan J (2000) Increased binding of chlorin e_6 to lipoproteins at low pH values. Int J Biochem Cell Biol 32: 759–768

Dagan A, Gatt S, Cerbu-Karabat S, Maziere J-C, Maziere C, Santus R, Engelhardt EL, Yeh KA, Stobbe CC, Fenning MC and Chapman JD (1995) Uptake by cells and photosensitizing effectiveness of novel pheophorbide derivatives in vivo. Int J Cancer 63: 831–839

Dai R, Shoemaker R, Farrens D, Han MJ, Kim CS and Song PS (1992) Characterization of silkworm chlorophyll metabolites as an active photosensitizer for photodynamic therapy. J Nat Prod 55: 1241–1251

Del Governatore M, Hamblin MR, Piccinini EE, Ugolini G and Hasan T (2000a) Targeted photodestruction of human colon cancer cells using charged 17.1A chlorin e_6 immunoconjugates. Br J Cancer 82: 56–64

Del Governatore M, Hamblin MR, Shea CR, Rizvi I, Molpus KG, Tanabe KK and Hasan T (2000b) Experimental photoimmunotherapy of hepatic metastases of colorectal cancer with a 17.1A chlorin e_6 immunoconjugate. Cancer Res 60: 4200–4205

Delaey E, van Laar F, De Vos D, Kamuhabwa A, Jacobs P and de Witte P (2000) A comparative study of the photosensitizing characteristics of some cyanine dyes. J Photochem Photobiol B-Biol 55: 27–36

Dolmans DEJGJ, Kadambi A, Hill JS, Flores KR, Gerber JN, Walker JP, Borel Rinkes IHM, Jain RK and Fukumura D (2002a) Targeting tumor vasculature and cancer cells in orthotopic breast tumor by fractionated photosensitizer dosing photodynamic therapy. Cancer Res 62: 4289–4294

Dolmans DEJGJ, Kadambi A, Hill JS, Waters CA, Robinson BC, Walker JP, Fukumura D and Jain RK (2002b) Vascular accumulation of a novel photosensitizer, MV6401, causes selective thrombosis in tumor vessels after photodynamic therapy. Cancer Res 62: 2151–2156

Dougherty TJ (1987) Photosensitizers: Therapy and detection of malignant tumors. Photochem Photobiol 45: 879–889

Dougherty TJ, Gomer CJ, Henderson BW, Jori G, Kessel D, Korbelik M, Moan J and Peng Q (1998) Photodynamic therapy. J Natl Cancer Inst 90: 889–905

Dougherty TJ, Sumlin AB, Greco WR, Weishaupt KR, Vaughan LA and Pandey RK (2002) The Role of the peripheral benzodiazepine receptor in photodynamic activity of certain pyropheophorbide ether photosensitizers: Albumin site II as a surrogate marker for activity. Photochem Photobiol 76: 91–97

Duska LR, Hamblin MR, Miller JL and Hasan T (1999) Combination photoimmunotherapy and cisplatin: Effects on human ovarian cancer ex vivo. J Natl Cancer Inst 91: 1557–1563

Embleton ML, Nair SP, Cookson BD and Wilson M (2002) Selective lethal photosensitization of methicillin-resistant *Staphylococcus aureus* using an IgG-tin(IV) chlorin e_6 conjugate. J

Antimicrob Chemother 50: 857–864
Evrard S, Keller P, Hajri A, Balboni G, Mensozaburgos L, Damge C, Marescaux J and Aprahamian M (1994) Experimental pancreatic cancer in the rat treated by photodynamic therapy. Br J Surg 81: 1185–1189
Fabiano A-S, Allouche D, Sanejouand Y-H and Paillous N (1997) Synthesis of a new cationic pyropheophorbide derivative and studies of its aggregation process in aqueous solution. Photochem Photobiol 66: 336–345
Feofanov A, Grichine A, Karmakova T, Pljutinskaya A, Lebedeva V, Filyasova A, Yakubovskaya R, Mironov A, Egret-Charlier M and Vigny P (2002) Near-infrared photosensitizer based on a cycloimide derivative of chlorin p6: 13,15-N-(3′-hydroxypropyl)cycloimide chlorin p_6. Photochem Photobiol 75: 633–643
Fernandez JM, Bilgin MD and Grossweiner LI (1997) Singlet oxygen generation by photodynamic agents. J Photochem Photobiol B-Biol 37: 131–140
Ferrario A, Kessel D and Gomer CJ (1992) Metabolic properties and photosensitizing responsiveness of mono-l-aspartyl chlorin-e_6 in a mouse-tumor model. Cancer Res 52: 2890–2893
Fiedor L, Rosenbach-Belkin V and Scherz A (1992) The stereospecific interaction between chlorophylls and chlorophyllase. Possible implication for chlorophyll biosynthesis and degradation. J Biol Chem 267: 22043–22047
Fiedor L, Gorman AA, Hamblett I, Rosenbach-Belkin V, Salomon Y, Scherz A and Tregub I (1993) A pulsed laser and pulse radiolysis study of amphiphilic chlorophyll derivatives with PDT activity toward malignant melanoma. Photochem Photobiol 58: 506–511
Fiedor L, Rosenbach-Belkin V, Sai M and Scherz A (1996) Preparation of tetrapyrrole-amino acid covalent complexes. Plant Physiol Biochem 34: 393–398
Fingar VH (1996) Vascular effects of photodynamic therapy. J Clin Laser Med Surg 14: 323–328
Folkman J (1995) Clinical applications of research on angiogenesis. New Engl J Med 333: 1757–1763
Foote CS (1968) Mechanisms of photosensitized oxidation. Science 162: 963–970
Furukawa K, Yamamoto H, Crean DH, Kato H and Mang TS (1996) Localization and treatment of transformed tissues using the photodynamic sensitizer 2-[hexyloxyethyl]-2-devinyl pyropheophorbide *a*. Lasers Surg Med 18: 157–166
Furukawa K, Kato H, Okunaka T, Sato M, Kuzunoki Y, Furuse K, Kawahara M, Furuoka M, Miyazawa T, Yana N, Matsui K, Okabayasi H and Horinoucti H (2001) Phase II clinical trial of PDT using ME2906 and diode laser in the treatment of central type early stage lung cancer in Japan. In: Clinical and Basic Applications of Photodynamic Medicine, p 84. IPA 8th World Congress of Photodynamic Medicine-Book of Abstracts, Vancouver
Gatt S, Dagan A, Santus R, Maziere JC, Chapman JD and Engelhardt EL (1996) Phorbine derivatives and their use in the diagnosis and therapy of cancer. US Pat 5,492,924
Geze M, Morliere P, Maziere JC, Smith KM and Santus R (1993) Lysosomes, a key target of hydrophobic photosensitizers proposed for photochemotherapeutic applications. J Photochem Photobiol B-Biol 20: 23–35
Gijsens A and de Witte P (1998) Photocytotoxic action of EGF-PVA-Sn(IV)chlorin e_6 and EGF- dextran-Sn(IV)chlorin e_6 internalizable conjugates on A431 cells. Int J Oncol 13: 1171–1177
Gijsens A, Missiaen L, Merlevede W and de Witte P (2000) Epidermal growth factor-mediated targeting of chlorin e_6 selectively potentiates its photodynamic activity. Cancer Res 60: 2197–2202
Goff BA, Bamberg M and Hasan T (1991) Photoimmunotherapy of human ovarian-carcinoma cells ex vivo. Cancer Res 51: 4762–4767
Goff BA, Bamberg M and Hasan T (1992) Experimental photodynamic treatment of ovarian-carcinoma cells with immunoconjugates. Antib Immunoconjug Radiopharm 5: 191–199
Goff BA, Hermanto U, Rumbaugh J, Blake J, Bamberg M and Hasan T (1994) Photoimmunotherapy and biodistribution with an Oc125-chlorin immunoconjugate in an in-vivo murine ovarian-cancer model. Br J Cancer 70: 474–480
Gomi S, Nishizuka T, Ushiroda O, Uchida N, Takahashi H and Sumi S (1998) The structures of mono-L-aspartyl chlorin e_6 and its related compounds. Heterocycles 48: 2231–2243
Grellier P, Santus R, Mouray E, Agmon V, Maziere JC, Rigomier D, Dagan A, Gatt S and Schrevel J (1997) Photosensitized inactivation of *Plasmodium falciparum*- and *Babesia divergens*-infected erythrocytes in whole blood by lipophilic pheophorbide derivatives. Vox Sang 72: 211–220
Grichine A, Feofanov A, Karmakova T, Kazachkina N, Pecherskih E, Yakubovskaya R, Mironov A, Egret-Charlier M and Vigny P (2001) Influence of the substitution of 3-vinyl by 3-formyl group on the photodynamic properties of chlorin p_6: Molecular, cellular and in vivo studies. Photochem Photobiol 73: 267–277
Gross S, Gilead A, Mazor O, Brandis A, Schreiber S, Machluf Y, Neeman M, Scherz A and Salomon Y (2003) Selective vascular and tumor responses to photodynamic therapy (PDT) with Pd Bacteriopheophorbide (TOOKAD®): Online and offline analyses. Proc AACR 44: 27
Gryshuk AL, Graham A, Pandey SK, Potter W, Missert JR, Oseroff A, Dougherty TJ and Pandey RK (2002) A first comparative study of purpurinimide-based fluorinated vs. nonfluorinated photosensitizers for photodynamic therapy. Photochem Photobiol 76: 555–559
Gurinovich GP, Zorina TE, Melnov SB, Melnova NI, Gurinovich IF, Grubina LA, Sarzhevskaya MV and Cherenkevich SN (1992) Photodynamic activity of chlorin e_6 and chlorin e_6 ethylenediamide in vitro and in vivo. J Photochem Photobiol B-Biol 13: 51–57
Hackbarth S, Horneffer V, Hillenkamp F and Röder B (2001) Photophysical properties of pheophorbide *a*-substituted diaminobutane polypropyleneimine dendrimer. Chem Phys 269: 339–346
Hajri A, Coffy S, Vallat F, Evrard S, Marescaux J and Aprahamian M (1999) Human pancreatic carcinoma cells are sensitive to photodynamic therapy in vitro and in vivo. Br J Surg 86: 899–906
Hajri A, Wack S, Meyer C, Smith MK, Leberquier C, Kedinger M and Aprahamian M (2002) In vitro and in vivo efficacy of Photofrin® and pheophorbide *a*, a bacteriochlorin, in photodynamic therapy of colonic cancer cells. Photochem Photobiol 75: 140–148
Halliwell B and Gutteridge JMC (1990) Role of free radicals and catalytic metal ions in human disease: An overview. In: Packer L and Glazer AN (eds) Methods Enzymol, Vol. 186, pp. 1–85. Academic Press, London

Hamblin MR, Rajadhyaksha M, Momma T, Soukos NS and Hasan T (1999) In vivo fluorescence imaging of the transport of charged chlorin e_6 conjugates in a rat orthotopic prostate tumour. Br J Cancer 81: 261–268

Hamblin MR, O'Donnell DA, Murthy N, Contag CH and Hasan T (2002a) Rapid control of wound infections by targeted photodynamic therapy monitored by in vivo bioluminescence imaging. Photochem Photobiol 75: 51–57

Hamblin MR, O'Donnell DA, Murthy N, Rajagopalan K, Michaud N, Sherwood ME and Hasan T (2002b) Polycationic photosensitizer conjugates: Effects of chain length and Gram classification on the photodynamic inactivation of bacteria. J Antimicrob Chemother 49: 941–951

Henderson BW and Dougherty TJ (1992) How does photodynamic therapy work? Photochem Photobiol 55: 145–157

Henderson BW, Bellnier DA, Greco WR, Sharma A, Pandey RK, Vaughan LA, Weishaupt KR and Dougherty TJ (1997) An in vivo quantitative structure-activity relationship for a congeneric series of pyropheophorbide derivatives as photosensitizers for photodynamic therapy. Cancer Res 57: 4000–4007

Hoober JK, Sery TW and Yamamoto H (1988) Photodynamic sensitizers from chlorophyll: Purpurin-18 and chlorin p_6. Photochem Photobiol 48: 579–582

Jaquinod L, Nurco DJ, Medforth CJ, Pandey RK, Forsyth TP, Olmstead MM and Smith KM (1996) Synthesis and characterization of bis(chlorin)s from the mcmurry reaction of formylchlorins. Angew Chem Int Ed Engl 35: 1013–1016

Jiang X, Pandey RK and Smith KM (1995) Synthesis of nucleoside adducts of porphyrins and chlorophyll derivatives. Tetrahedron Lett 36: 365–368

Jiang X, Pandey RK and Smith KM (1996) Nucleoside adducts of vinylporphyrins and vinylchlorins. J Chem Soc-Perkin Trans 1: 1607–1615

Jin ZH, Miyoshi N, Ishiguro K, Takaoka K, Udagawa T, Tajiri H, Ueda K, Fukuda M and Kumakiri M (2000) Photodynamic therapy based on combined use of 5-aminolevulinic acid with a pheophorbide *a* derivative for murine tumors. In vivo 14: 529–533

Jocham D (1998) Clinical experiences and expectations. In: Moser JG (ed) Photodynamic tumor therapy: 2nd and 3rd generation photosensitizers, pp. 213–225. Harwood, London

Jori G (1992) Low density lipoprotein-liposome delivery systems for tumor photosensitization in vivo. In: Henderson BW and Dougherty TJ (eds) Photodynamic Therapy, basic principles and clinical applications, pp. 173–187. Marcel Dekker, New York

Jori G (1996) Tumour photosensitizers: Approaches to enhance the selectivity and efficiency of photodynamic therapy. J Photochem Photobiol B-Biol 36: 87–93

Kassab K (2002) Photophysical and photosensitizing properties of selected cyanines. J Photochem Photobiol B-Biol 68: 15–22

Kazi AA, Peyman GA, Unal M, Khoobehi B, Yoneya S, Mori K, Moshfeghi D and Moshfeghi AA (2000) Threshold power levels for NPe6 photodynamic therapy. Ophthalmic Surg Lasers 31: 136–142

Kelbauskas L and Dietel W (2002) Internalization of aggregated photosensitizers by tumor cells: Subcellular time-resolved fluorescence spectroscopy on derivatives of pyropheophorbide-*a* ethers and chlorin e_6 under femtosecond one- and two-photon excitation. Photochem Photobiol 76: 686–694

Kenner GW, McCombie SW and Smith KM (1973) Pyrroles and related compounds. Part XXIV. Separation and oxidative degradation of chlorophyll derivatives. J Chem Soc-Perkin Trans 1: 2517–2523

Kessel D (1997) Pharmacokinetics of N-aspartyl chlorin e_6 in cancer patients. J Photochem Photobiol B-Biol 39: 81–83

Kessel D and Poretz RD (2000) Sites of photodamage induced by photodynamic therapy with a chlorin e_6 triacetoxymethyl ester (CAME). Photochem Photobiol 71: 94–96

Kessel D, Smith KM, Pandey RK, Shiau F-Y and Henderson B (1993) Photosensitization with bacteriochlorins. Photochem Photobiol 58: 200–203

Kessel D, Woodburn K, Gomer CJ, Jagerovic N and Smith KM (1995) Photosensitization with derivatives of chlorin p_6. J Photochem Photobiol B-Biol 28: 13–18

Khadem J, Veloso AA, Tolentino F, Hasan T and Hamblin MR (1999) Photodynamic tissue adhesion with chlorin e_6 protein conjugates. Invest Ophthalmol Vis Sci 40: 3132–3137

Kopecek J, Kopeckova P, Minko T, Lu Z-R and Peterson CM (2001) Water soluble polymers in tumor targeted delivery. J Control Release 74: 147–158

Kostenich GA, Zhuravkin IN, Furmanchuk AV and Zhavrid EA (1991) Photodynamic therapy with chlorin e_6. A morphological study of tumor damage efficiency in experiment. J Photochem Photobiol B-Biol 11: 307–318

Kostenich GA, Zhuravkin IN, Furmanchuk AV and Zhavrid EA (1993) Sensitivity of different rat tumor strains to photodynamic treatment with chlorin e_6. J Photochem Photobiol B-Biol 17: 187–194

Kostenich GA, Zhuravkin IN and Zhavrid EA (1994) Experimental grounds for using chlorin e_6 in the photodynamic therapy of malignant tumors. J Photochem Photobiol B-Biol 22: 211–217

Koudinova NV, Pinthus JH, Brandis A, Brenner O, Bendel P, Ramon J, Eshhar Z, Scherz A and Salomon Y (2003) Photodynamic therapy with Pd-bacteriopheophorbide (TOOKAD): successful in vivo treatment of human prostatic small cell carcinoma xenografts. Int J Cancer 104: 782–789

Kozyrev AN, Efimov AV, Efremova OA, Perepyolkin PY and Mironov AF (1994) New chlorin and bacteriochlorin-type photosensitizers for photodynamic therapy. Proc SPIE 2325: 297–305

Kozyrev AN, Dougherty TJ and Pandey RK (1996a) Effect of substituents in OsO_4 reactions of metallochlorins regioselective synthesis of isobacteriochlorins and bacteriochlorins. Tetrahedron Lett 37: 3781–3784

Kozyrev AN, Pandey RK, Medforth CJ, Zheng G, Dougherty TJ and Smith KM (1996b) Syntheses and unusual spectroscopic properties of novel ketobacteriochlorins. Tetrahedron Lett 37: 747–750

Kozyrev AN, Zheng G, Zhu C, Dougherty TJ, Smith KM and Pandey RK (1996c) Syntheses of stable bacteriochlorophyll-a derivatives as potential photosensitizers for photodynamic therapy. Tetrahedron Lett 37: 6431–6434

Kozyrev AN, Zheng G, Lazarou E, Dougherty TJ, Smith KM and Pandey RK (1997) Syntheses of emeraldin and purpurin-18 analogs as target-specific photosensitizers for photodynamic therapy. Tetrahedron Lett 38: 3335–3338

Kozyrev AN, Alderfer JL, Dougherty TJ and Pandey RK (1998a) Synthesis of verdinochlorins: A new class of long-wavelength absorbing photosensitizers. J Chem Soc-Chem Commun: 1083–1084

Kozyrev AN, Dougherty TJ and Pandey RK (1998b) LiOH promoted allomerization of pyropheophorbide *a*. A convenient

synthesis of 13^2-oxopyropheophorbide *a* and its unusual enolization. J Chem Soc-Chem Commun: 481–482

Kozyrev AN, Alderfer JL and Robinson BC (2003) Pirazolinyl and cyclopropyl derivatives of protoporphyrin IX and chlorins related to chlorophyll *a*. Tetrahedron 59: 499–504

Krammer B (2001) Vascular effects of photodynamic therapy. Anticancer Res 21: 4271–4278

Krasnovsky Jr AA, Neverov KV, Egorov SYu, Röder B and Lewald W (1990) Photophysical studies of pheophorbide a pheophytin *a*. Phosphorescence and photosensitized singlet oxygen luminescence. J Photochem Photobiol B-Biol 5: 245–254

Leach MW, Higgins RJ, Boggan JE, Lee SJ, Autry S and Smith KM (1992) Effectiveness of a lysyl chlorin p_6/chlorin p_6 mixture in photodynamic therapy of the subcutaneous 9L glioma in the rat. Cancer Res 52: 1235–1239

Leach MW, Higgins RJ, Autry SA, Boggan JE, Lee SJH and Smith KM (1993) In vitro photodynamic effects of lysyl chlorin p_6: Cell survival, localization and ultrastructural changes. Photochem Photobiol 58: 653–660

Lee SJH, Jagerovic N and Smith KM (1993) Use of the chlorophyll derivative, purpurin-18, for syntheses of sensitizers for use in photodynamic therapy. J Chem Soc-Perkin Trans 1: 2369–2377

Lobel J, Macdonald IJ, Ciesielski MJ, Barone T, Potter WR, Pollina J, Plunkett RJ, Fenstermaker RA and Dougherty TJ (2001) 2-[1-Hexyloxyethyl]-2-devinyl pyropheophorbide-*a* (hpph) in a nude rat glioma model: Implications for photodynamic therapy. Lasers Surg Med 29: 37–405

Ma LF and Dolphin D (1996) Nucleophilic reaction of 1,8-diazabicyclo [5.4.0]undec-7-ene and 1,5-diazabicyclo[4.3.0]non-5-ene with methyl pheophorbide *a*. Unexpected products. Tetrahedron 52: 849–860

Ma LF and Dolphin D (1997) Chemical modification of chlorophyll *a*: synthesis of new regiochemically pure benzoporphyrin and dibenzoporphyrin derivatives. Can J Chem 75: 262–275

Ma LF and Dolphin D (1999) The metabolites of dietary chlorophylls. Phytochemistry 50: 195–202

Macdonald IJ and Dougherty TJ (2001) Basic principles of photodynamic therapy. J Porphyr Phthalocya 5: 105–129

Macdonald IJ, Morgan J, Bellnier DA, Paszkiewicz GM, Whitaker JE, Litchfield DJ and Dougherty TJ (1999) Subcellular localization patterns and their relationship to photodynamic activity of pyropheophorbide-*a* derivatives. Photochem Photobiol 70: 789–797

Magne ML, Rodrigues CO, Autry SA, Edwards BF, Theon AP and Madewell BR (1997) Photodynamic therapy of facial squamous cell carcinoma in cats using a new photosensitizer. Lasers Surg Med 20: 202–209

Mansouri S, Gossauer A, Meunier B and Paillous N (1994) Pyropheophorbide-N,N-dimethylethylenediamine conjugates as new water-soluble photonucleases. New J Chem 18: 745–748

Matroule JY, Bonizzi G, Morliere P, Paillous N, Santus R, Bours V and Piette J (1999) Pyropheophorbide *a* methyl ester-mediated photosensitization activates transcription factor NF-kappa B through the interleukin-1 receptor-dependent signalling pathway. J Biol Chem 274: 2988–3000

Matroule JY, Carthy CM, Graville DJ, Jolois O, Hunt DWC and Piette J (2001) Mechanism of colon cancer cell apoptosis mediated by pyropheophorbide *a* methylester photosensitization. Oncogene 20: 4070–4084

Mayhew E, Vaughan LA, Panus A, Murray M and Henderson BW (1993) Lipid-associated methylpheophorbide-a (hexyl-ether) as a photodynamic agent in tumor bearing mice. Photochem Photobiol 58: 845–851

McCaw DL, Pope ER, Payne JT, West MK, Tompson RV and Tate D (2000) Treatment of canine oral squamous cell carcinomas with photodynamic therapy. Br J Cancer 82: 1297–1299

McCaw DL, Payne JT, Pope ER, West MK, Tompson RV and Tate D (2001) Treatment of canine hemangiopericytomas with photodynamic therapy. Lasers Surg Med 29: 23–26

McMahon KS, Wieman TJ, Moore PH and Fingar VH (1994) Effects of photodynamic therapy using mono-L-aspartyl chlorin e_6 on vessel constriction, vessel leakage, and tumor response. Cancer Res 54: 5374–5379

Mettath S, Shibata M, Alderfer JL, Senge MO, Smith MK, Rein R, Dougherty TJ and Pandey RK (1998) Synthesis and spectroscopic properties of novel benzochlorins derived from chlorophyll *a*. J Org Chem 63: 1646–1656

Mettath SN, Li G, Srikrishnan T, Mehta R, Grossman ZD, Dougherty TJ and Pandey RK (1999) Effect of substituents in directing the formation of benzochlorins and isobacteriochlorins in porphyrin and chlorin systems. Org Lett 1: 1961–1964

Mettath S, Zheng G, Zielinski T, Shibata M, Alderfer JL, Dougherty TJ and Pandey RK (2000) Effect of substituents in directing the regioselective synthesis of novel pyridinium chlorins. Tetrahedron Lett 41: 6289–6294

Mironov AF and Lebedeva VS (1998) Cyclic *N*-hydroxyimides in a series of chlorins and porphyrins. Tetrahedron Lett 39: 905–908

Mironov AF, Kozyrev AN and Brandis AS (1993) Sensitizers of second generation for photodynamic therapy of cancer based on chlorophyll and bacteriochlorophyll derivatives. Proc SPIE 1922: 204–208

Mironov AF, Lebedeva VS, Yakubovskaya RI, Kazachkina NI and Fomina GI (1999) Chlorins with six-membered imide ring as prospective sensitizers for cancer PDT. Proc SPIE 3563: 59–67

Moan J (1986) Effect of bleaching of porphyrin sensitizers during photodynamic therapy. Cancer Lett 33: 45–53

Moan J (1990) Properties for optimal PDT sensitizers. J Photochem Photobiol B-Biol 5: 521–524

Molpus KL, Hamblin MR, Rizvi I and Hasan T (2000) Intraperitoneal photoimmunotherapy of ovarian carcinoma xenografts in nude mice using charged photoimmunoconjugates. Gynecol Oncol 76: 397–404

Mori K, Yoneya S, Ohta M, Sano A, Anzai K, Peyman GA and Moshfeghi DM (1999) Angiographic and histologic effects of fundus photodynamic therapy with a hydrophilic sensitizer (mono-L-aspartyl chlorin e_6). Ophthalmology 106: 1384–1391

Morliere P, Maziere JC, Santus R, Smith CD, Prinsep MR, Stobbe CC, Fenning MC, Golberg JL and Chapman JD (1998) Tolyporphin: A natural product from cyanobacteria with potent photosensitizing activity against tumor cells in vitro and in vivo. Cancer Res 58: 3571–3578

Moser JG, Ruk A, Schwarzmaier H-J and Westphal-Frosch C (1992) Photodynamic cancer therapy: Fluorescence localization and light absorption spectra of chlorophyll-derived photosensitizers inside cancer cells. Opt Eng 31: 1441–1446

Nagae T, Louie AY, Aizawa K, Ishimaru S and Wilson SE (1998) Selective targeting and photodynamic destruction of intimal

hyperplasia by scavenger-receptor mediated protein-chlorin e_6 conjugates. J Cardiovasc Surg 39: 709–715

Nakamura H, Suzuki Y, Takeichi M, Saito T, Takayama M and Aizawa K (2002) Morphologic evaluation of the antitumor activity of photodynamic therapy (PDT) using mono-L-aspartyl chlorin e_6 (NPe_6) against uterine cervical carcinoma cell lines. Int J Gynecol Cancer 12: 177–186

Orenstein A, Kostenich G, Roitman L, Shechtman Y, Kopolovic Y, Ehrenberg B and Malik Z (1996) A comparative study of tissue distribution and photodynamic therapy selectivity of chlorin e_6, Photofrin II and ALA-induced protoporphyrin IX in a colon carcinoma model. Br J Cancer 73: 937–944

Osterloh J and Vicente MGH (2002) Mechanisms of porphyrinoid localization in tumors. J Porphyrins Phthalocyanines 6: 305–324

Pandey RK (2000) Recent advances in photodynamic therapy. J Porphyr Phthalocya 4: 368–373

Pandey RK and Zheng G (2000) Porphyrins as photosensitizers in photodynamic therapy. In: Kadish KM, Smith KM and Guilard R (eds) The Porphyrin Handbook, Vol. 6, pp 157–230. Academic Press, San Diego

Pandey RK, Bellnier DA, Smith KM and Dougherty TJ (1991a) Chlorin and porphyrin derivatives as potential photosensitizers in photodynamic therapy. Photochem Photobiol 53: 65–72

Pandey RK, Smith NW, Shiau F-Y, Dougherty TJ and Smith KM (1991b) Syntheses of cationic porphyrins and chlorins. J Chem Soc-Chem Commun: 1637–1638

Pandey RK, Shiau F-Y, Isaak M, Ramaprasad S, Dougherty TJ and Smith KM (1992a) Substituent effects in tetrapyrrole subunit reactivity and pinacol-pinacolone rearrangements: *vic*-dihydroxychlorins and *vic*-dihydroxybacteriochlorins. Tetrahedron Lett 33: 7815–7818

Pandey RK, Shiau F-Y, Smith NW, Dougherty TJ and Smith KM (1992b) Syntheses of water-soluble cationic porphyrins and chlorins. Tetrahedron 48: 7591–7600

Pandey RK, Shiau FY, Sumlin AB, Dougherty TJ and Smith KM (1992c) Structure/activity relationships among photosensitizers related to pheophorbides and bacteriopheophorbides. Bioorg Med Chem Lett 2: 491–496

Pandey RK, Jagerovic N, Ryan JM, Dougherty TJ and Smith KM (1993) Efficient syntheses of new classes of regiochemically pure benzoporphyrin derivatives. Bioorg Med Chem Lett 3: 2615–2618

Pandey RK, Shiau FY, Sumlin AB, Dougherty TJ and Smith KM (1994) Syntheses of new bacteriochlorins and their antitumor activity. Bioorg Med Chem Lett 4: 1263–1267

Pandey RK, Mettath SN, Gupta S, Potter WR, Dougherty TJ and Smith KM (1995) Regioselective syntheses and some in vivo properties of 'benzochlorin' analogues prepared from methyl 9-deoxymesopyropheophorbide. Bioorg Med Chem Lett 5: 857–860

Pandey RK, Constantine S, Goff BA, Kozyrev AN, Dougherty TJ and Smith KM (1996a) Chlorophyll-*a* derivatives in photodynamic therapy: Effect of position of heptyl ether side-chains on in vivo photosensitizing activity. Bioorg Med Chem Lett 6: 105–110

Pandey RK, Jagerovic N, Ryan JM, Dougherty TJ and Smith KM (1996b) Syntheses and preliminary in vivo photodynamic therapy of benzoporphyrin derivatives from phylloerythrin and rhodoporphyrin XV methyl esters and aspartyl esters. Tetrahedron 52: 5349–5362

Pandey RK, Sumlin AB, Constantine S, Aoudia M, Potter WR, Bellnier DA, Henderson BW, Rodgers MA, Smith KM and Dougherty TJ (1996c) Alkyl ether analogs of chlorophyll-*a* derivatives: Part 1. Synthesis, photophysical properties and photodynamic efficacy. Photochem Photobiol 64: 194–204

Pandey RK, Zheng G, Lee DA, Dougherty TJ and Smith KM (1996d) Comparative in vivo sensitizing efficacy of porphyrin and chlorin dimers joined with ester, ether, carbon-carbon or amide bonds. J Mol Recognit 9: 118–122

Pandey RK, Constantine S, Tsuchida T, Zheng G, Medforth CJ, Aoudia M, Kozyrev AN, Rodgers MAJ, Kato H, Smith KM and Dougherty TJ (1997a) Synthesis, photophysical properties, in vivo photosensitizing efficacy, and human serum albumin binding properties of some novel bacteriochlorins. J Med Chem 40: 2770–2779

Pandey RK, Isaak M, MacDonald I, Medforth CJ, Senge MO, Dougherty TJ and Smith KM (1997b) Pinacol-pinacolone rearrangements in *vic*-dihydroxychlorins and bacteriochlorins: Effect of substituents at the peripheral positions. J Org Chem 62: 1463–1472

Payne JT, McCaw DL, Casteel SW, Frazier D, Rogers K and Tompson RV (1996) Pharmacokinetics of pyropheophorbide-a-hexyl ester in the dog. Lasers Surg Med 18: 406–409

Peyman GA, Kazi AA, Moshfeghi D, Unal M, Khoobehi B, Yoneya S, Mori K and Rivera I (2000a) Threshold and retreatment parameters of NPe_6 photodynamic therapy in retinal and choroidal vessels. Ophthalmic Surg Lasers 31: 323–327

Peyman GA, Kazi AA, Unal M, Khoobehi B, Yoneya S, Mori K and Moshfeghi DM (2000b) Problems with and pitfalls of photodynamic therapy. Ophthalmology 107: 29–35

Prinsep MR, Caplan FR, Moore RE, Patterson GML and Smith CD (1992) Tolyporphin, a novel multidrug resistance reversing agent from the blue-green alga *Tolypothrix nodosa*. J Am Chem Soc 114: 385–387

RadaPharma (2002) (http://www.radapharma.ru/publications)

Regillo CD (2000) Update on photodynamic therapy. Cur Opin Ophthalm 11: 166–170

Reiners JJ, Caruso JA, Mathieu P, Chelladurai B, Yin XM and Kessel D (2002) Release of cytochrome *c* and activation of pro-caspase-9 following lysosomal photodamage involves bid cleavage. Cell Death Differ 9: 934–944

Roberts WG and Hasan T (1992) Role of neovasculature and vascular-permeability on the tumor retention of photodynamic agents. Cancer Res 52: 924–930

Röder B (1998) Pheophorbides. In: Moser JG (ed) Photodynamic tumor therapy: 2nd and 3rd generation photosensitizers, pp. 35–41. Harwood, London

Roehrs S, Ruebner A, Hartwich G, Scheer H and Moser JG (1995) Peripheral substitution of pheophorbides and bacteriopheophorbides to promote inclusion into inert carrier systems for PDT. Proc SPIE 2625: 333–338

Ronn AM (1999) Pharmacokinetics in photodynamic therapy. Rev Contemp Pharmaco 10: 39–46

Rosenbach-Belkin V, Chen L, Fiedor L, Tregub I, Pavlotsky F, Brumfeld V, Salomon Y and Scherz A (1996) Serine conjugates of chlorophyll and bacteriochlorophyll: Photocytotoxicity in vitro and tissue distribution in mice bearing melanoma tumors. Photochem Photobiol 64: 174–181

Rungta A, Zheng G, Missert JR, Potter WR, Dougherty TJ and Pandey RK (2000) Purpurinimides as photosensitizers: Effect of the presence and position of the substituents in the in vivo pho-

todynamic efficacy. Bioorg Med Chem Lett 10: 1463–1466
Sahai D, Lo J-L, Hagen IK, Bergstrom L, Chernomorsky S and Poretz RD (1993) Metabolically convertible lipophilic derivatives of pH-sensitive amphipathic photosensitizers. Photochem Photobiol 58: 803–808
Saito T, Hayashi J and Aizawa K (1998) Acute effects of photodynamic treatment on elastic fibre network in atherosclerotic plaques of rabbit aorta. Lasers Med Sci 13: 126–131
Savitskiy VP, Zorin VP and Potapnev MP (2002) Selective phototoxicity of chlorin-e_6 derivatives toward leukemic cells. Exp Oncol 24: 142–144
Scheer H, Kammhuber N, Scherz A, Brandis A and Salomon Y (2001) Synthesis and photodynamic activity of chlorophyll and bacteriochlorophyll esters. PCT Pat WO01/40232, 48 pp
Scherz A, Salomon Y and Fiedor L (1994) Chlorophyll and bacteriochlorophyll derivatives, their preparation and pharmacological compositions comprising them as photosensitizers for photodynamic therapy. EP Appl 584552, 32 pp
Schnitzer JE (1998) Vascular targeting as a strategy for cancer therapy. New Engl J Med 339: 472–474
Schreiber S, Gross S, Brandis A, Harmelin A, Rosenbach-Belkin V, Scherz A and Salomon Y (2002) Local photodynamic therapy (PDT) of rat C6 glioma xenografts with Pd-bacteriopheophorbide leads to decreased metastases and increase of animal cure compared with surgery. Int J Cancer 99: 279–285
Selbo PK, Hogset A, Prasmickaite L and Berg K (2002) Photochemical internalization: A novel drug delivery system. Tumor Biol 23: 103–112
Shevchuk IN, Chekulaeva LV and Chekulaev VA (2002) Influence of pH and glucose administration on the phototoxicity of chlorin-e_6 towards Ehrlich carcinoma cells. Exp Oncol 24: 135–141
Sheyhedin I, Aizawa K, Araake M, Kumasaka H, Okunaka T and Kato H (1998) The effects of serum on cellular uptake and phototoxicity of mono-L-aspartyl chlorin e_6 (NPe_6) in vitro. Photochem Photobiol 68: 110–114
Smith CD, Prinsep MR, Caplan FR, Moore RE and Patterson GML (1994) Reversal of multiple-drug resistance by topyporphyn, a novel cyanobacterial natural product. Oncol Res 6: 211–218
Smith KM, Lee S-J, Shiau F-Y, Pandey RK and Jagerovic N (1992) Syntheses of chlorin and bacteriochlorin-type photosensitizers for photodynamic therapy. In: Spinelli P, Dal Fante M andMarchesini R (eds) Photodynamic Therapy and Biomedical Lasers, pp. 769–773. Elsevier Science Publishers B.V., Amsterdam
Soukos NS, Ximenez-Fyvie LA, Hamblin MR, Socransky SS and Hasan T (1998) Targeted antimicrobial photochemotherapy. Antimicrob Agents Chemother 42: 2595–2601
Spikes JD and Bommer JC (1991) Chlorophyll and related pigments as photosensitizers in biology and medicine. In: Scheer H (ed) Chlorophylls, pp. 1181-1204. CRC Press, Boca Raton
Spikes JD and Bommer JC (1993) Photosensitizing properties of mono-L-aspartyl chlorin e_6 (Npe6): A candidate sensitizer for the photodynamic therapy of tumors. J Photochem Photobiol B-Biol 17: 135–143
Strakhovskaya MG, Belenikina NS, Ivanova EV, Chemeris YK and Stranadko EF (2002) The photodynamic inactivation of the yeast *Candida guilliermondii* in the presence of photodithazine. Microbiology 71: 298–301
Sullivan LG, Hasan T, Wright M, Mankin HJ and Towle CA (2002) Photodynamic treatment has chondroprotective effects on articular cartilage. J Orthop Res 20: 241–248
Sun X and Leung WN (2002) Photodynamic therapy with pyropheophorbide-a methyl ester in human lung carcinoma cancer cell: Efficacy, localization and apoptosis. Photochem Photobiol 75: 644–651
Svaasand LO and Potter WR (1992) The Implications of photobleaching for photodynamic therapy. In: Henderson BW and Dougherty TJ (eds) Photodynamic Therapy: Basic Principles and Clinical Applications, pp. 369–385. Marcel Dekker, New York
Taber SW, Fingar VH, Coots CT and Wieman TJ (1998) Photodynamic therapy using mono-L-aspartyl chlorin e_6 (Npe6) for the treatment of cutaneous disease: A phase I clinical study. Clin Cancer Res 4: 2741–2746
Tanielian C, Kobayashi M and Wolff C (2001) Mechanism of photodynamic activity of pheophorbides. J Biomed Opt 6: 252–256
Tauraytis VA, Shishporenok SI, Grubina LA, Sarzhevskaya MV, Gurinovich IF, Gurinovich GA and Matulis AA (1992) Estimation of possible applications of the photodynamic effect in rheumatology. Biofizika 37: 345–351
Tregub I, Schmidt-Sole J, DeJordy J, Rosenbach-Belkin V, Brumfeld V, Fiedor L, Salomon Y and Scherz A (1992) Application of chlorophyll and bacteriochlorophyll derivatives to PDT of malignant melanoma. In: Holick MF and Kligman AM (eds) Biologic Effects of Light, pp. 354–361. Walter de Gruyter, Berlin-New York
Vicente MGH and Smith KM (1991) Vilsmeier reactions of porphyrins and chlorins with 3-(dimethylamino)acrolein to give meso-(2-formylvinyl)porphyrins: New syntheses of benzochlorins, benzoisobacteriochlorins, and benzobacteriochlorins and reductive coupling of porphyrins and chlorins using low-valent titanium complexes. J Org Chem 56: 4407–4418
Wongsinkongman P, Brossi A, Wang HK, Bastow KF and Lee KH (2002) Antitumor agents. Part 209: Pheophorbide-*a* derivatives as photo-independent cytotoxic agents. Bioorg Med Chem 10: 583–591
Yamamoto Y, Shibuya H, Okunaka T, Aizawa K and Kato H (1999) Fibrin plugging as a cause of microcirculatory occlusion during photodynamic therapy. Lasers Med Sci 14: 129–135
Zenkevich E, Sagun E, Knyukshto V, Shulga A, Mironov A, Efremova O, Bonnett R, Songca SP and Kassem M (1996) Photophysical and photochemical properties of potential porphyrin and chlorin photosensitizers for PDT. J Photochem Photobiol B-Biol 33: 171–180
Zeug A, Zimmermann J, Röder B, Lagorio MG and San Roman E (2002) Microcrystalline cellulose as a carrier for hydrophobic photosensitizers in water. Photochem Photobiol Sci 1: 198–203
Zhang L and Xu DY (1999) Synthesis of chlorin e_6-6-amide derivatives. Chin J Org Chem 19: 424–430
Zheng G, Kozyrev AN, Dougherty TJ, Smith KM and Pandey RK (1996) Synthesis of novel benzobacteriopurpurins by Diels-Alder cycloaddition. Chem Lett: 1119–1120
Zheng G, Aoudia M, Lee D, Rodgers MA, Smith KM, Dougherty TJ and Pandey RK (2000a) Chlorin-based symmetrical and unsymmetrical dimers with amide linkages: Effect of the substituents on photodynamic and photophysical properties. J Chem Soc-Perkin Trans 1: 3113–3121
Zheng G, Potter WR, Sumlin A, Dougherty TJ and Pandey RK (2000b) Photosensitizers related to purpurin-18-N-alkylimides: A comparative in vivo tumoricidal ability of ester versus amide

functionalities. Bioorg Med Chem Lett 10: 123–127

Zheng G, Graham A, Shibata M, Missert JR, Oseroff AR, Dougherty TJ and Pandey RK (2001a) Synthesis of β-galactose-conjugated chlorins derived by enyne metathesis as galectin-specific photosensitizers for photodynamic therapy. J Org Chem 66: 8709–8716

Zheng G, Potter WR, Camacho SH, Missert JR, Wang G, Bellnier DA, Henderson BW, Rodgers MAJ, Dougherty TJ and Pandey RK (2001b) Synthesis, photophysical properties, tumor uptake, and preliminary in vivo photosensitizing efficacy of a homologous series of 3-(1′-alkyoxy)ethyl-3′-devinylpurpurin-18-*n*-alkylimides with variable lipophilicity. J Med Chem 44: 1540–1559

Zheng G, Li H, Zhang M, Lund-Katz S, Chance B and Glickson JD (2002) Low-density lipoprotein reconstituted by pyropheophorbide cholesteryl oleate as target-specific photosensitizer. Bioconjugate Chem 13: 392–396

Zilberstein J, Schreiber S, Bloemers MCWM, Bendel P, Neeman M, Schechtman E, Kohen F, Scherz A and Salomon Y (2001) Antivascular treatment of solid melanoma tumors with bacteriochlorophyll-serine-based photodynamic therapy. Photochem Photobiol 73: 257–266

Zorin VP, Mikhalovsky IS and Zorina TE (1996) The distribution of chlorin-e_6 derivatives in biological systems. Investigation of pH-effects. Proc SPIE 2625: 146–155

Chapter 33

Bacteriochlorophyll Sensitizers in Photodynamic Therapy

Alexander S. Brandis[1], Yoram Salomon[2] and Avigdor Scherz[1]*
Departments of [1]Plant Sciences and [2]Biological Regulation,
The Weizmann Institute of Science, Rehovot, Israel

*Author for correspondence, email: avigdor.scherz@weizmann.ac.il

Bernhard Grimm, Robert J. Porra, Wolfhart Rüdiger and Hugo Scheer (eds): Chlorophylls and Bacteriochlorophylls: Biochemistry, Biophysics, Functions and Applications, pp. 485–494.

Summary

Recent progress in the bioproduction and chemical manipulation of bacteriochlorophyll (BChl) *a* has opened the way for utilization of highly potent sensitizers in photodynamic therapy. Although less stable than their chlorin analogues in their native form, BChl derivatives provide a superior optical and biophysical profile for the generation of reactive oxygen species (ROS). In fact this pigment family probably represents the most efficient light collectors and radical generators in nature. Here we describe a recent development of this exciting family of drugs, with particular emphasis on vascular targeted therapy (VTP).

I. Introduction

The spectra, photophysics and photochemistry of native bacteriochlorophylls (BChls) have made them efficient sensitizers with optimal light-harvesting properties: they have clear advantages as sensitizers in photodynamic therapy (PDT) even when compared to their chlorophyll (Chl) counterparts. In particular, these molecules have very high extinction coefficients at long wavelengths (λ_{max} = 760–780 nm, $\varepsilon = (4–10) \times 10^4$ $M^{-1}cm^{-1}$), where light penetration into tissues is maximal (Pandey and Zheng, 2000). Moreover, they generate reactive oxygen species (ROS) at a higher quantum yield, depending on the central metal and, to some extent, on peripheral substituents (Musewald et al., 1998; Vakrat-Haglili, 2002). Unfortunately, BChls are much less stable than Chl analogues. In fact, the most common route of BChl degradation is by chemical or photochemical oxidation to their corresponding Chl form (Lindsay-Smith and Calvin, 1966; Henderson et al., 1991). Additionally, BChl biosynthesis usually requires light and anaerobic conditions: these are two major obstacles to large-scale production.

During the last decade, genetic manipulations (Ghosh, 2003), the development of illuminated flow-fermenters (Tsygankov et al., 1994, 1997) and especially the isolation of bacteria that grow vigorously under aerobic conditions in the dark while producing large concentrations of BChl *a* (Doi et al., 1991) have made BChl *a* a viable chemical precursor for the drug industry. In parallel, Smith et al. (1992) developed a chemical procedure that generates a BChl analogue from Chl *a*, thereby relieving, to a certain extent, the need for bacterial production of BChl *a*. Concurrently, several groups found ways to chemically modify BChls and purify the newly-formed chemical derivatives to the high degree required for pharmaceutical and chemical studies (Struck et al., 1992; Mironov et al., 1993; Scherz et al., 1994; Kozyrev et al., 1996). In view of this progress, BChl derivatives are expected to become principal participants in PDT during the coming decade. Among the more interesting properties of BChl-based photosensitizers is their relatively low redox potential (Watanabe and Kobayashi, 1991; Geskes et al., 1995; Noy et al., 1998) compared with other porphyrinoids. Thus, photoactivation of BChl and BChl derivatives under aerobic conditions is expected to enhance the production of superoxide and hydroxyl radicals that are significantly more potent sensitizers than singlet oxygen.

Tumor destruction generally results from direct cytotoxic effects, from hypoxia and starvation caused by vascular shutdown, and from the inflammatory response (Macdonald and Dougherty, 2001). Traditionally, PDT is thought to destroy tumor cells due to preferentially accumulated photosensitizers (Macdonald and Dougherty, 2001). However, early studies of BChl-based PDT (Henderson et al., 1991; Henderson and Dougherty, 1992) excluded the possibility of a direct BChl-PDT effect on the tumor cells because such BChl-based drugs were found ineffective when administered long before irradiation. Despite the superior optical properties and significant yield of ROS generation in vitro, no significant tumor regression was observed when irradiated for more than a few hours after administering the sensitizer. Soon, it was found that BChl derivatives act as antivascular drugs (van Leengoed et al., 1993; Zilberstein et al., 1997) which led to extensive developments towards a vascular targeted-PDT (VTP) approach (Scherz

Abbreviations: BChl – bacteriochlorophyll; BChl-Ser – bacteriochlorophyllide *a* L-serine ester; BChlide – bacteriochlorophyllide; BChn – bacteriochlorin; BOLD MRI – blood oxygen level-dependent magnetic resonance imaging; BPhe – bacteriopheophytin; BPheide – bacteriopheophorbide; BPP – bacteriopurpurin; Chl – chlorophyll; Chn – chlorin; HDL – high-density lipoprotein; i.v. – intravenously; IgG – immunoglobulin G; ISC – intersystem crossing; LD_{50} – median lethal dose; LDL – low-density lipoprotein; PDT – photodynamic therapy; PP – purpurin; ROS – reactive oxygen species; s.c. – subcutaneously; TOOKAD® – [Pd]-bacteriochlorophyllide *a*; VTP –vascular-targeted PDT; ϕ_Δ – quantum yield of singlet oxygen

et al., 1994, 2000, 2004). The research efforts and development programs of many groups, however, are still aimed at specifically attacking the tumor cells by ROS generation during illumination of cell-targeted BChl and BChl derivatives. In this chapter, we will present and discuss each group of the currently developed BChl-based sensitizers.

II. Photosensitizers Derived from Bacteriochlorophyll *a*

A. Bacteriochlorophyll a

1. General Description and Chemistry

BChl *a* (see formula in Chapter 1, Scheer) is a 7,8,17,18-tetrahydrophytoporphyrin structurally similar to the 17,18-dihydrophytoporphyrin, Chl *a*, in which the 3-vinyl group is replaced by an acetyl substituent. BChl *a* can be easily recovered from cultivated purple photosynthetic bacteria. As in Chl *a*, the optical spectrum, redox potentials, and overall reactivity of BChl *a* are mainly determined by the π electrons of the macrocycle and the incorporated metal. As a result, BChl *a* can be a potent photosensitizer with a strong absorption at 770–780 nm and high yield for ROS generation (quantum yield of singlet oxygen, ϕ_{Δ}, may reach 0.6, depending on the molecular environment). However, it easily undergoes isomerization, demetalation and oxidative degradation, including restoration of the 7,8-double bond (Lindsay-Smith and Calvin, 1966; Henderson et al., 1991). These disadvantages and the insolubility of BChl *a* in aqueous solutions limit its practical use. Metal substitutions in BChl modify the macrocycle's redox potentials, electronic transition energies (Chapter 2, Senge et al. and Chapter 34, Yerushalmi et al.), solubility and coordination properties; therefore, such modifications may dramatically affect the application of BChl as a photodynamic reagent. Furthermore, some of these modifications increase stability to harsher chemistry that could otherwise result in oxidation of the bacteriochlorin to the chlorin macrocycle with a consequent blue shift of the Q_y maximum absorption wavelength. Synthetic modifications of the BChl *a* periphery and metal replacement, aimed at higher stability and solubility, should facilitate its application as a PDT agent.

Targeting. A catalytic amount of photodegradable BChl-intruded liposomes containing encapsulated Ca^{2+} enabled release of a larger population of drug-loaded conventional liposomes using a Ca^{2+}-dependent lytic process (Wymer et al., 1998; Gerasimov et al., 1999).

2. Pre-Clinical Studies and Efficacy

a. In Vitro Studies

Photocytotoxicity of BChl *a* was tested against radiation-induced fibrosarcome (RIF) tumor cell lines and found to have only moderate and limited effectiveness due to rapid photobleaching of the sensitizer (Henderson et al., 1991).

b. In Vivo Studies

PDT with BChl *a* induced 80%-cure of spontaneous mouse mammary tumor (SMT-F) and RIF tumors on day 90 in mice, when irradiation (270 J cm^{-2}, 780 nm) was carried out for 2 h, but not 24 h, after intravenous (i.v.)-administration (5 mg kg^{-1}), which indicated rapid clearance and vascular shutdown (rapid or delayed) as the main factor in tumor necrosis. Normal skin tissue photosensitivity totally disappeared after 5 days, probably due to chemical instability of BChl in the biological milieu (Henderson et al., 1991).

B. Bacteriochlorophyllide a and Derivatives

1. General Description and Chemistry

Enzymatic hydrolysis or transesterification of BChl with amino acids as well as chemical amidation of the propionic side chain significantly increased its water-solubility (Scherz et al., 1994; Fiedor et al., 1996). Serine-conjugated bacteriochlorophyllide (BChlide) *a* seems to retain the photophysical properties of BChl (Eichwurzel et al., 2000). Significant generation of hydroxyl radicals in aqueous solutions has been reported (Katz et al., 1998). Unfortunately, like BChl *a*, BChlide *a* and its derivatives undergo fast photo-oxidation, demetalation in slightly acidic solutions, and biodegradation (Rosenbach-Belkin et al., 1996), preventing their wide application.

The replacement of the central Mg atom by Pd in BChlide *a* improved its stability and photodynamic reactivity (Scherz et al., 2000). The absorption band shifted to 763 nm, while maintaining its intensity. [Pd]-BChlide *a* was modified by esterification or amidation at the C-17 propionate residue (Scherz et

al., 2001) and by transesterification at the C-13[3] carboxylate residue (Scheer et al., 2001). These derivatives differed in their amphiphilicity. [Pd]-BChlide *a* underwent intersystem crossing (ISC) with quantum yield ~1. ROS generation with [Pd]-BChlide *a* was dependent on the molecular environment. The ϕ_Δ dropped from ~1 in hydrophobic solutions to ~0.5 in aqueous and micellar solutions, while the yields of hydroxyl and superoxide radicals increased to ~0.2%. Superoxide and hydroxyl radical generation by [Pd]-BChlide probably involves oxidation of the macrocycle that serves as both an electron and proton donor (Vakrat-Haglili, 2002).

Targeting. The conjugation of BChlide *a* with peptides, hormones and proteins as cell-specific ligands such as melanocyte stimulating hormones for site-specific PDT of melanoma, can be carried out via chemically-activated amidation of the BChlide *a* propionic acid residue at C-17 (Scherz et al., 1994).

[Pd]-BChlide *a* ethyl ester was modified to form inclusion complexes with dimeric cyclodextrins (Roehrs et al., 1995; Moser, 1998).

2. Pre-Clinical Studies and Efficacy

a. In Vitro Studies

BChlide *a* and BChl-Ser showed high antitumor activity in vitro in M2R mouse melanoma cells (median lethal dose (LD_{50}) of 0.2–0.5 μM) (Rosenbach-Belkin et al., 1996). Effective phototoxicity of the BChl derivatives, even under hypoxic conditions (L. Chen et al., 1998), probably occurs by the unusual mechanism of photosensitized oxidation by means of hydroxyl radicals (Katz et al., 1998). Substituting Pd for the Mg atom increased the photodynamic efficacy against M2R melanoma cells and other cell lines, decreasing the LD_{50} value to ~0.01–0.03 μM, with no dark toxicity (Scherz et al., 2001).

Targeting. BChlide *a*, conjugated to rabbit IgG, was 30 times more phototoxic in the inactivation of protein A-presenting *Staphylococcus aureus* compared to free BChl-Ser, indicating that site-specific generation of ROS can substantially increase the biological effect over that obtained by free sensitizer (Gross et al., 1997).

b. In Vivo Studies

Studies in mice, subcutaneously (s.c.) implanted with M2R mouse melanoma xenografts, displayed rapid (16 h) clearance of BChl-Ser from all tissues tested with only transient accumulation in the liver, which implied potential minimization of prolonged skin photosensitivity (Rosenbach-Belkin et al., 1996). Under the selected treatment protocol, when irradiated without delay after drug administration, the photodynamic effect (108 J cm^{-2}, 580–750 nm, shortly after 20 mg kg^{-1} i.v.) was predominantly conferred to the tumor vascular bed with vessel occlusion and complete blood stasis (Zilberstein et al., 1995, 2001). PDT with BChl-Ser resulted in a high cure rate (>80%) of pigmented melanoma in mice (Zilberstein et al., 2001) where sensitizing light penetration in the pigmented tumor was as deep as 0.9 cm (Zilberstein et al., 1997). BChl-Ser-PDT was also shown to be efficient against massive SD sarcoma xenografts in rats (Kelleher et al., 1999, 2003): here, PDT and hyperthermia were found to be synergistic when using BChl-Ser (Kelleher et al., 1999, 2003). When monitored with a tissue-inserted oxygen microsensor, the local photodynamic response of the tumor to BChl-Ser-PDT was associated with rapid light-dependent depletion of tumor oxygen levels, presumably due to ROS formation (Zilberstein et al., 1997).

[Pd]-BChlide *a* (trade name TOOKAD®, see Fig. 1) was found to have an exceptionally short clearance time with no skin phototoxicity in mice and rats (Scherz et al., 2000) and also in dogs (Hetzel F, private communication). High cure rates were demonstrated following TOOKAD®-PDT (90 J cm^{-2}, 770 nm immediately after 4 mg kg^{-1} i.v.) of massive s.c. human prostate cancer xenografts and bone metastases in mice (Koudinova et al., 2003).

Hemorrhagic necrosis of the entire prostate gland, accompanied by preservation of the urethra and urinal functions, was shown in dogs (200 J cm^{-2}, 763 nm after only 5 mg kg^{-1} i.v.): this demonstrated the expected benefit of the strong near infra red (NIR) excitation (763 nm) by inducing effective PDT to the depth of 2 cm from the optical fiber (Q. Chen et al., 2002a,b). PDT with TOOKAD®, aimed primarily at the tumor vasculature, efficiently eradicated solid C6 glioma tumors in mice, reducing the rate of groin and lung metastasis (Schreiber et al., 2002). Antivascular TOOKAD®-PDT also indiscriminately destroyed both multidrug resistant and wild type HT29 colon carcinoma tumors (Preise et al., 2003). Selective tumor eradication, with minimal damage to the surrounding tissue, probably resulted from the different responses of tumor- and normal-blood vessels

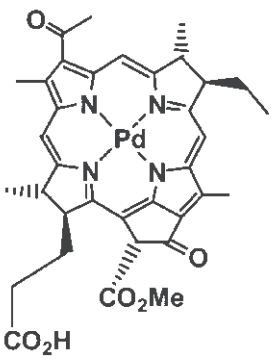

Palladium-Bacteriopheophorbide *a*

TOOKAD® (WST09)

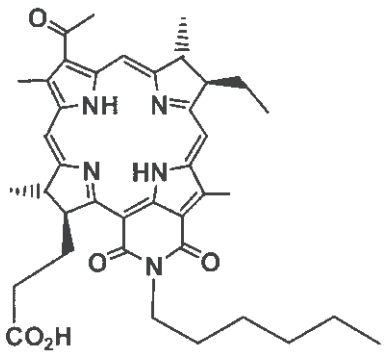

3^1-oxo-7,8-*trans*-dihydro-rhodochlorin-15-carboxy-13^1,15^1-N-hexylimide

BPP N-hexyl imide

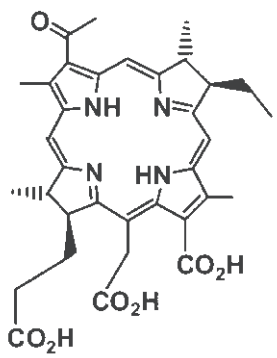

3^1-oxo-7,8-*trans*-dihydro-rhodochlorin-15-acetic acid

BChn *a*

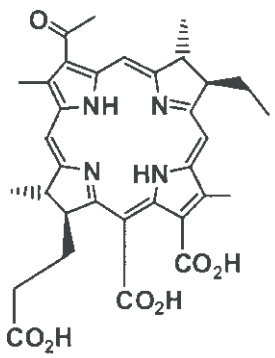

3^1-oxo-7,8-*trans*-dihydro-rhodochlorin-15-carboxylic acid

BChn p_6

Fig. 1. Structures of some BChl derivatives used as active photosensitizers (IUPAC-approved names are followed by the trade names or abbreviations).

(Mazor et al., 2002; Borle et al. 2003; Gross et al., 2003a). Massive photosensitization of TOOKAD® in the circulation was demonstrated with blood oxygen level-dependent magnetic resonance imaging (BOLD MRI), creating the possibility of online imaging of the photodynamic process and enabling accurate light guidance (Gross et al., 2003b).

C. Bacteriopheophorbide a and Derivatives

1. General Description and Chemistry

BPheide *a*, obtained from BChl *a* by acidic elimination of both Mg and the esterifying alcohol, either phytol or geranylgeraniol, has a lower extinction coefficient than BChl(ide) *a* near 760 nm, higher

dark and light stability and a ϕ_Δ value of about 0.6 (Krasnovsky Jr et al., 1990).

2. Pre-clinical Studies and Efficacy

a. In Vitro Studies

BPheide *a* and 13^2-hydroxy-BPheide *a* alkyl esters were efficient in treating several melanotic cell lines (Moser, 1993). These sensitizers were characterized by negligible threshold doses in comparison with Photofrin® and Pheide *a* (Moser et al., 1994b, 1995), with subcellular localization in the cytoplasm and Golgi apparatus (Moser et al., 1992, 1994a).

The photocytotoxicity observed with EMT-6 cells, using BPheide 4-hydroxybutylamide, was 2400 × higher than that of Photofrin®. Similar to Pheide analogs (see above), a significant efflux of the drug from the cells is promoted by high and low density lipoproteins (HDL and LDL, respectively), suggesting rapid clearance from normal tissue with low phototoxicity (Dagan et al., 1995; Gatt et al., 1996).

b. In Vivo Studies

Biodistribution and pharmacokinetics analysis of 13^2-hydroxy-BPheide *a* methyl ester in mice bearing Lewis lung carcinoma, revealed fairly rapid (4 h) clearance of the drug from the blood, but with a longer (up to 168 h) retention time in the internal organs and tumor, coupled with metabolic processes (Röder et al., 1994).

D. Bacteriochlorin a and Derivatives

1. General Description and Chemistry

Bacteriochlorin *a* (BChn *a*, Fig. 1), a structural relative of chlorin e_6 (Chn e_6), absorbs at 760 nm and generates not only singlet oxygen at relatively low ϕ_Δ value of 0.05 and 0.33 in phosphate buffer and liposomes, respectively (Damoiseau et al., 2001; Hoebeke and Damoiseau, 2002), but also produces superoxide and hydroxyl radicals, equal to the yield of singlet oxygen in buffer solution (Hoebeke et al., 1997). However, the preparation of BChn *a* as yet gives variable results (Post et al., 1996), and, being insoluble, its formulation is a suspension (Schuitmaker et al., 1991; van Leengoed et al., 1993; van Tenten et al., 2002), which complicates dose-response estimation (Post et al., 1996). BChn *a* amides and their metallocomplexes, however, are water-soluble: they were obtained recently from the corresponding BPheide *a* precursors by regioselective aminolysis and have proven to be efficient sensitizers for vascular targeted PDT (Scherz et al., 2004).

2. Pre-Clinical Studies and Efficacy

a. In Vitro Studies

BChn *a* in a serum-deficient medium was found to be an effective photosensitizer when tested on Chinese hamster ovary and T24 (human bladder) carcinoma cells, but ineffective in a (lipo)protein-rich cell culture medium. Association with lipoproteins (20% with LDL and 60% with HDL) is probably responsible for BChn *a* uptake by malignant neoplasms (Schuitmaker et al., 1995).

b. In Vivo Studies

BChn *a* induced complete necrosis of an isogeneic mammary tumor (100 J cm^{-2}, 760 nm, 0.25–1 h after 20 mg kg^{-1} i.v.) (van Leengoed et al., 1993) and a re-growth delay of both RIF tumors in mice (van Geel et al., 1995) and of model liver metastases in rats (using 10 mg kg^{-1}) (Rovers et al., 1998). Both vascular and direct tissue cell (mitochondrial) damage contributed to necrosis (Schuitmaker et al., 1991; van Leengoed et al., 1993).

PDT with BChn *a* for prevention of posterior capsule opacification after cataract extraction seemed promising (van Tenten et al., 2001; van Tenten et al., 2002).

A water-soluble derivative of [Pd]-BChn *a* showed rapid clearance from murine blood and all tissues within 30 min, with the hepatic clearance route having ~20 min half-life period: this suggests negligible diffusion of the pigment from the vasculature into organs other than liver, lungs and spleen. PDT (30 J cm^{-2}, 755 nm, immediately after 9 mg kg^{-1}) provided selective necrosis of solid M2R melanoma tumors in mice with a 70% cure on day 90 (Scherz et al., 2004). Even higher cure rates were found with HT29 colon carcinoma xenografts (Scherz et al, unpublished data).

E. Bacteriopurpurin 18, Bacteriochlorin p_6 and Derivatives

1. General Description and Chemistry

Bacteriopurpurin (BPP) *18*, obtained from a crude

extract of BChl *a* by a procedure similar to that used for preparation of purpurin (PP *18*), proved to be a stable compound with a strong absorption maximum at 818 nm (Mironov et al., 1993). Alkaline cleavage of the anhydride ring produced water-soluble BChn p_6 (Fig. 1), that absorbed at 766 nm (Mironov et al., 1993). Partial reduction transformed BPP *18* into a δ-lactone derivative with a 3-(1-hydroxyethyl) substituent, that was more stable towards acidic and basic cleavage, but the major absorption maximum shifted to 724 nm (Mironov et al., 1998). By opening the cyclic anhydride ring in BPP *18* with 1-hexylamine, the corresponding cyclic isoimide (λ_{max} 804 nm) and imide (λ_{max} 822 nm) derivatives (see Fig. 1) were obtained (Kozyrev et al., 1996). The more nucleophilic hydroxylamine provided [3^1-oxime]-BPP *18* N-hydroxyimide (λ_{max} 812 nm) in one reaction (Mironov et al., 2002).

2. Pre-Clinical Studies and Efficacy

a. In Vitro Studies

Targeting. Conjugates for doubly targeted delivery (cell and nuclear specific) were constructed using BChn p_6 and chimeric modular recombinant transporters, expressed in *Escherichia coli*. The transporters included an internalizeable ligand (α-melanocyte-stimulating hormone), a nuclear localization factor (viral T-antigen), a hemoglobin-like carrier protein and an endosomolytic factor (diphtheria toxin domain). The conjugates were 250-fold more photodynamically active in mouse melanoma cells than free BChn p_6 (Rosenkranz et al., 2003). Interestingly, the melanocyte-stimulating hormone was previously proposed to be used for in-situ PDT targeting of different BChl derivatives into melanoma cells (Scherz et al., 1994).

b. In Vivo Studies

Converted into a series of alkyl ether analogues, BPP *18* N-hexylimide derivatives showed similar in vivo efficacy in mice, but with notable differences in their activity in RIF tumors (135 J cm^{-2}, 785 nm, 24 h after 0.2 μmol kg^{-1} i.v.). The heptyl ether derivative was the most effective photosensitizer (80% tumor cure), with selective localization in mitochondria, but not via the peripheral benzodiazepine receptor (Y. Chen et al., 2002c).

III. Clinical trials

Steba Biotech, France, has recently accomplished Phase I/II clinical trials of TOOKAD®-PDT for prostate cancer therapy in 25 patients, with localized prostate cancer after radiation failure, using escalation of drug doses and irradiation fluence. Experiments conducted in two centers in Canada showed no severe adverse effects at the highest doses examined. The sensitizers were rapidly cleared from the circulation with no skin toxicity 3 h or less after administration to the patients. Local necrosis up to 3-cm diameter, induced by an interstitial diffuser-optic-fiber, was observed by MRI seven days after treatment (Elhilali, 2003; Trachtenberg J, personal communications). Early Phase II trials have already begun.

IV. Conclusions and Perspectives

PDT had already been proven to be a viable and interesting procedure for palliative and, in a limited number of cases, as a curative alternative to current, less selective treatment procedures for cancer. Yet, the application of PDT for first-line treatment is rare, and the authors of this review suggest that this delay in curative application of PDT reflects the search for and discovery of new sensitizers that may enable better targeting to the tumor cells. Vascular targeting, however, seems to us a more promising avenue for the future of PDT. Here, BChl derivatives with long wavelength absorption, high yield of ROS generation and fast clearance rates, together with simple diode lasers and sophisticated blood imaging procedures, may advance PDT into a 'key player' role in first-line tumor treatment. We believe that the concept of 'differential tissue response' rather than 'differential tissue uptake' may prove to be the major principle underlying selective PDT treatment and should become a key guideline in the future design of BChl- and Chl-based photosensitizers.

Acknowledgments

A.S. and Y.S. hold the Robert and Yadelle Sklare Professorial chair in Biochemistry and the Tillie and Charles Lubin Professorial chair of Biochemical Endocrinology, respectively, at The Weizmann Institut, Rehovot, Israel. Work of the authors was supported in part by Steba Biotech, France.

References

Borle F, Radu A, Fontolliet C, van den Bergh H, Monnier P and Wagnieres G (2003) Selectivity of the photosensitizer Tookad® for photodynamic therapy evaluated in the Sirian golden hamster cheek pouch tumour model. Br J Cancer 89: 2320–2326

Chen L, Gross S, Rosenbach-Belkin V, Brandis A, Scherz A and Salomon Y (1998) Photoinactivation of microorganisms by chlorophyll-serine, bacteriochlorophyll-serine and by targeted bacteriochlorophyll-IgG. In: Patrice T (ed) IPA-98 Proceedings, RC-41. Ispen Biotech, Nantes (CD-ROM)

Chen Q, Huang Z, Luck D, Beckers J, Brun P-H, Wilson BC, Scherz A, Salomon Y and Hetzel FW (2002a) Preclinical studies in normal canine prostate of a novel palladium-bacteriopheophorbide (WST09) photosensitizer for photodynamic therapy of prostate cancer. Photochem Photobiol 76: 438–445

Chen Q, Huang Z, Luck D, Beckers J, Brun P-H, Wilson BC, Scherz A, Salomon Y and Hetzel FW (2002b) WST09 (TOOKAD) mediated photodynamic therapy as an alternative modality in the treatment of prostate cancer. Proc SPIE 4612: 29–39

Chen Y, Graham A, Potter W, Morgan J, Vaughan LA, Bellnier DA, Henderson BW, Oseroff A, Dougherty TJ and Pandey RK (2002c) Bacteriopurpurinimides: Highly stable and potent photosensitizers for photodynamic therapy. J Med Chem 45: 255–258

Dagan A, Gatt S, Cerbu-Karabat S, Maziere J-C, Maziere C, Santus R, Engelhardt EL, Yeh KA, Stobbe CC, Fenning MC and Chapman JD (1995) Uptake by cells and photosensitizing effectiveness of novel pheophorbide derivatives in vivo. Int J Cancer 63: 831–839

Damoiseau X, Schuitmaker HJ, Lagerberg JWM and Hoebeke M (2001) Increase of the photosensitizing efficiency of the bacteriochlorin *a* by liposome-incorporation. J Photochem Photobiol B-Biol 60: 50–60

Doi M, Shioi Y, Gad'on N, Golecki JR and Drews G (1991) Spectroscopical studies on the light-harvesting pigment-protein complex II from dark-aerobic and light-anaerobic grown cells of *Rhodobacter sulfidophilus*. Biochim Biophys Acta 1058: 235–241

Eichwurzel I, Stiel H, Teuchner K, Leupold D, Scheer H, Salomon Y and Scherz A (2000) Photophysical consequences of coupling bacteriochlorophyll *a* with serine and its resulting solubility in water. Photochem Photobiol 72: 204–209

Elhilali M (2003) Palladium bacteriopheophorbide (WST09)—PDT in the treatment of prostate cancer: A phase I/II clinical study for recurrent prostate cancer after radiation therapy. In: Symposium-Steba-Biotech, the XVIII Congress of the European Association of Urology. Madrid, Spain

Fiedor L, Rosenbach-Belkin V, Sai M and Scherz A (1996) Preparation of tetrapyrrole-amino acid covalent complexes. Plant Physiol Biochem 34: 393–398

Gatt S, Dagan A, Santus R, Maziere JC, Chapman JD and Engelhardt EL (1996) Phorbine derivatives and their use in the diagnosis and therapy of cancer. US Pat 5,492,924

Gerasimov OV, Boomer JA, Qualls MM and Thompson DH (1999) Cytosolic drug delivery using pH- and light-sensitive liposomes. Adv Drug Deliv Rev 38: 317–338

Geskes C, Hartwich G, Scheer H, Maentele W and Heize J (1995) Electrochemical and spectroelectrochemical investigation of metal-substituted bacteriochlorophyll *a*. J Am Chem Soc 117: 7776–7783

Ghosh R (2003) New nucleic acid encoding geranylgeranyl-diphosphate synthase, and related cells, useful for preparation of farnesyl-bacteriochlorophyll *a*, for photodynamic therapy. DE10134103

Gross S, Brandis A, Chen L, Rosenbach-Belkin V, Roehrs S, Scherz A and Salomon Y (1997) Protein-A-mediated targeting of bacteriochlorophyll-IgG to *Staphylococcus aureus*: A model for enhanced site-specific phototoxicity. Photochem Photobiol 66: 872–878

Gross S, Gilead A, Mazor O, Brandis A, Schreiber S, Machluf Y, Neeman M, Scherz A and Salomon Y (2003a) Selective vascular and tumor responses to photodynamic therapy (PDT) with Pd bacteriopheophorbide (TOOKAD®): Online and offline analyses. Proc AACR 44: 27

Gross S, Gilead A, Scherz A, Neeman M, and Salomon Y (2003b) Monitoring photodynamic therapy of solid tumors online by BOLD-contrast MRI. Nature Med 9: 1327–1331

Henderson BW and Dougherty TJ (1992) How does photodynamic therapy work? Photochem Photobiol 55: 145–157

Henderson BW, Sumlin AB, Owcharczak BL and Dougherty TJ (1991) Bacteriochlorophyll-*a* as photosensitizer for photodynamic treatment of transplantable murine tumors. J Photochem Photobiol B-Biol 10: 303–313

Hoebeke M and Damoiseau X (2002) Determination of the singlet oxygen quantum yield of bacteriochlorin *a*: A comparative study in phosphate buffer and aqueous dispersion of dimiristoyl-L-alpha-phosphatidylcholine liposomes. Photochem Photobiol Sci 1: 283–287

Hoebeke M, Schuitmaker HJ, Jannink LE, Dubbelman TMAR, Jakobs A and van de Vorst A (1997) Electron spin resonance evidence of the generation of superoxide anion, hydroxyl radical and singlet oxygen during the photohemolysis of human erythrocytes with bacteriochlorin *a*. Photochem Photobiol 66: 502–508

Katz S, Vakrat Y, Brumfeld V, Weiner L, Brandis A, Gabelmann E, Paul A, Hild M, Lendt K, Leupold D, Norris JR, Scheer H, Moser J, Salomon Y and Scherz A (1998) Bacteriochlorophyll-serine generates only OH radicals under near-infra-red illumination (NIR). In: Patrice T (ed) IPA-98 Proceedings, RC-208. Ispen Biotech, Nantes (CD-ROM)

Kelleher DK, Thews O, Rzeznik J, Scherz A, Salomon Y and Vaupel P (1999) Water-filtered infrared-A radiation: A novel technique for localized hyperthermia in combination with bacteriochlorophyll-based photodynamic therapy. Int J Hyperthermia 15: 467–474

Kelleher DK, Thews O, Scherz A, Salomon Y and Vaupel P (2003) Combined hyperthermia and chlorophyll-based photodynamic therapy: Tumour growth and metabolic microenvironment. Br J Cancer 89: 2333–2339

Koudinova NV, Pinthus JH, Brandis A, Brenner O, Bendel P, Ramon J, Eshhar Z, Scherz A and Salomon Y (2003) Photodynamic Therapy with Pd-bacteriopheophorbide (TOOKAD): Successful in vivo treatment of human prostatic small cell carcinoma xenografts. Int J Cancer 104: 782–789

Kozyrev AN, Zheng G, Zhu C, Dougherty TJ, Smith KM and Pandey RK (1996) Syntheses of stable bacteriochlorophyll-*a* derivatives as potential photosensitizers for photodynamic therapy. Tetrahedron Lett 37: 6431–6434

Krasnovsky Jr AA, Neverov KV, Egorov SYu, Roder B and Lewald W (1990) Photophysical studies of pheophorbide *a* pheophytin *a*. Phosphorescence and photosensitized singlet oxygen luminescence. J Photochem Photobiol B-Biol 5: 245–254

Lindsay-Smith JR and Calvin M (1966) Studies on the chemical and photochemical oxidation of bacteriochlorophyll. J Am Chem Soc 88: 4500–4506

Macdonald IJ and Dougherty TJ (2001) Basic principles of photodynamic therapy. J Porphyr Phthalocya 5: 105–129

Mazor O, Brandis A, Gross S, Hami R, Vakrat Y, Koudinova N, Gladysh E, Kostenich G, Orenstein A, Salomon Y and Scherz A (2002) Pd-Bacteriopheophorbide (TOOKAD), a novel antivascular agent for photodynamic therapy of tumors: In vitro and in vivo studies. In: The 3rd Congress of the Federation of Israeli Societies for Experimental Biology (FISEB), p. 231. Book of abstracts, Eilat, Israel

Mironov AF, Kozyrev AN and Brandis AS (1993) Sensitizers of second generation for photodynamic therapy of cancer based on chlorophyll and bacteriochlorophyll derivatives. Proc SPIE 1922: 204–208

Mironov AF, Efremov AV, Efremova OA, Bonnett R and Martinez G (1998) Chlorins with an exocyclic δ-lactone ring and their derivatives. J Chem Soc-Perkin Trans 1: 3601–3608

Mironov AF, Grin M and Tsyprovskiy AG (2002) Synthesis of the first *N*-hydroxycycloimide in the bacteriochlorophyll *a* series. J Porphyr Phthalocya 6: 358–361

Moser JG (1993) Attempts to treat malignant melanoma by photodynamic therapy using bacteriopheophorbide ester as the sensitizer. Proc SPIE 1881: 116–125

Moser JG (1998) Bacteriochlorophyllides, bacteriochlorins and bacteriopheophorbides. In: Moser JG (ed) Photodynamic Tumor Therapy: 2nd and 3rd Generation Photosensitizers, pp. 43–49. Harwood, London

Moser JG, Ruk A, Schwarzmaier H-J and Westphal-Frosch C (1992) Photodynamic cancer therapy: Fluorescence localization and light absorption spectra of chlorophyll-derived photosensitizers inside cancer cells. Opt Eng 31: 1441–1446

Moser JG, Dembeck U, Hubert M, Spengler B, Bayer R and Wagner B (1994a) Subcellular storage compartments of bacteriopheophorbide sensitizers. Proc SPIE 2078: 532–538

Moser JG, Ostrowsky A, Gumusgadli M and Kleiber B (1994b) Bacteriopheophorbide esters: Photosensitizers without 'threshold dose'? Proc SPIE 2078: 193–204

Moser JG, Suchomski R, Danielowski T and Wagner B (1995) Significance of threshold doses for photodynamic therapy of melanotic and amelanotic tumors. Proc SPIE 2371: 178–186

Musewald C, Hartwich G, Pollinger-Dammer F, Lossau H, Scheer H and Michel-Beyerle ME (1998) Time-resolved spectral investigation of bacteriochlorophyll *a* and its transmetalated derivatives [Zn]-bacteriochlorophyll *a* and [Pd]-bacteriochlorophyll *a*. J Phys Chem B 102: 8336–8342

Noy D, Fiedor L, Hartwich G, Scheer H and Scherz A (1998) Metal-substituted bacteriochlorophylls. 2. Changes in redox potentials and electronic transition energies are dominated by intramolecular electrostatic interactions. J Am Chem Soc 120: 3684–3693

Pandey RK and Zheng G (2000) Porphyrins as photosensitizers in photodynamic therapy. In: Kadish KM, Smith KM and Guilard R (eds) The Porphyrin Handbook, Vol. 6, pp. 157–230. Academic Press, San Diego

Post JG, Poele JAM, Schuitmaker JJ and Stewart FA (1996) A comparison of functional bladder damage after intravesical photodynamic therapy with three different photosensitizers. Photochem Photobiol 63: 314–321

Röder B, Dressler C, Hagemann R, Fuchs B, Berlien H-P, Nowak C and Moser J (1994) The pharmacokinetics of 13^2-hydroxybacteriopheophorbide a methyl ester studied by fluorescence spectroscopy on Lewis lung carcinoma bearing mice. Proc SPIE 2078: 427–437

Roehrs S, Ruebner A, Hartwich G, Scheer H and Moser JG (1995) Peripheral substitution of pheophorbides and bacteriopheophorbides to promote inclusion into inert carrier systems for PDT. Proc SPIE 2625: 333–338

Rosenbach-Belkin V, Chen L, Fiedor L, Tregub I, Pavlotsky F, Brumfeld V, Salomon Y and Scherz A (1996) Serine conjugates of chlorophyll and bacteriochlorophyll: Photocytotoxicity in vitro and tissue distribution in mice bearing melanoma tumors. Photochem Photobiol 64: 174–181

Rosenkranz AA, Lunin VG, Sergienko OV, Gilyazova DG, Voronina OL, Jans DE, Kofner AA, Shumiantseva MA, Mironov AF and Sobolev AS (2003) targeted intracellular site-specific drug delivery: Photosensitizer targeting to melanoma cell nuclei. Rus J Genet 39: 259–268

Rovers JP, Schuitmaker JJ, Vahrmeijer AL, van Dierendonck JH and Terpstra OT (1998) Interstitial photodynamic therapy with the second-generation photosensitizer bacteriochlorin *a* in a rat model for liver metastases. Br J Cancer 77: 2098–2103

Scheer H, Kammhuber N, Scherz A, Brandis A and Salomon Y (2001) Synthesis and photodynamic activity of chlorophyll and bacteriochlorophyll esters. PCT Appl. WO01/40232, 48 pp

Scherz A, Salomon Y and Fiedor L (1994) Chlorophyll and bacteriochlorophyll derivatives, their preparation and pharmacological compositions comprising them as photosensitizers for photodynamic therapy. EP Appl. 584552, 32 pp

Scherz A, Salomon Y, Scheer H, Hartwich G and Brandis A (1997) Synthesis and bactericidal activity of metal-substituted bacteriochlorophyll derivatives for use in photodynamic therapy and as bactericides and virucides. PCT Appl. WO97/19081, 36 pp

Scherz A, Salomon Y, Brandis A and Scheer H (2000) Palladium-substituted bacteriochlorophyll derivatives and use thereof. PCT Appl. WO00/33833, 59 pp

Scherz A, Brandis A, Greenwald M, Rosenbach-Belkin V, Mazor O, Gross S, Hammi R, Vakrat Y, Simonneaux G, Scheer H and Salomon Y (2001) TOOKAD — a novel palladium-bacteriochlorophyll sensitizer for photodynamic therapy: Synthesis and characterization. In: Clinical and Basic Applications of Photodynamic Medicine, p. 79, IPA 8th World Congress of Photodynamic Medicine-Book of Abstracts, Vancouver, Canada

Scherz A, Brandis A, Mazor O, Salomon Y and Scheer H (2004) Water-soluble anionic bacteriochlorophyll derivatives and their uses. PCT Appl WO04/045492, 56 pp

Schreiber S, Gross S, Brandis A, Harmelin A, Rosenbach-Belkin V, Scherz A and Salomon Y (2002) Local photodynamic therapy (PDT) of rat C6 glioma xenografts with Pd-bacteriopheophorbide leads to decreased metastases and increase of animal cure compared with surgery. Int J Cancer 99: 279–285

Schuitmaker JJ, Vrensen GFJM, van Delft JL, de Wolff-Rouendaal D, Dubbelman TMAR and De Wolf A (1991) Morphological effects of bacteriochlorin *a* and light in vivo on intraocular melanoma. Invest Ophthalmol Vis Sci 32: 2683–2688

Schuitmaker JJ, Jannik JE and Dubbelman T (1995) Influence

of cell-culture medium on the photosensitizing effectiveness of bacteriochlorin-alpha. J Photochem Photobiol B-Biol 28: 143–148

Smith KM, Lee S-J, Shiau F-Y, Pandey RK and Jagerovic N (1992) Syntheses of chlorin and bacteriochlorin-type photosensitizers for photodynamic therapy. In: Spinelli P, Dal Fante M and Marchesini R (eds) Photodynamic Therapy and Biomedical Lasers, pp. 769–773. Elsevier Science Publishers B.V., Amsterdam

Struck A, Cmiel E, Katheder I, Schäfer W and Scheer H (1992) Bacteriochlorophylls modified at position C3: Long range intramolecular interaction with position $C13^2$. Biochim Biophys Acta 1101: 321–328

Tsygankov AA, Laurinavichene TV and Gogotov IN (1994) Laboratory-scale photobioreactor. Biotechnol Tech 8: 575–578

Tsygankov AA, Laurinavichene TV, Bukatin VE, Gogotov IN and Hall DO (1997) Biomass production by continuous cultures of *Rhodobacter capsulatus* grown in various bioreactors. Appl Biochem Microbiol 33: 485–490

Vakrat-Haglili Y (2002) Photophysical and photochemical processes in photodynamic therapy (PDT) Initiated by bacteriochlorophyll derivatives (Bchl-Der): Novel second generation sensitizers, PhD Thesis. The Weizmann Institute of Science, Rehovot, Israel

van Geel IPJ, Oppelaar H, Oussoren YG, Schuitmaker JJ and Stewart FA (1995) Mechanisms for optimizing photodynamic therapy — 2nd-generation photosensitizers in combination with mitomycin-C. Br J Cancer 72: 344–350

van Leengoed HLLM, Schuitmaker JJ, van der Veen N, Dubbelman TMAR and Star WM (1993) Fluorescence and photodynamic effects of bacteriochlorin *a* observed in vivo in 'sandwich' observation chambers. Br J Cancer 67: 898–903

van Tenten Y, Schuitmaker HJ, De Wolf A, Willekens B, Vrensen GFJM and Tassignon MJ (2001) The effect of photodynamic therapy with bacteriochlorin a on lens epithelial cells in a capsular bag model. Exp Eye Res 72: 41–48

van Tenten Y, Schuitmaker HJ, De Groot V, Willekens B, Vrensen GFJM and Tassignon M-J (2002) A Preliminary study on the prevention of posterior capsule opacification by photodynamic therapy with bacteriochlorin *a* in rabbits. Ophthalmic Res 34: 113–118

Watanabe T and Kobayashi M (1991) Electrochemistry of chlorophylls. In: Scheer H (ed) Chlorophylls, pp. 287–315. CRC Press, Boca Raton

Wymer N, Gerasimov OV and Thompson DH (1998) Cascade liposomal triggering: Light-induced Ca^{2+} release from diplasmenylcholine liposomes triggers PLA_2-catalyzed hydrolysis and contents leakage from DPPC liposomes. Bioconjugate Chem 9: 305–308

Zilberstein J, Scherz A, Bromberg A, Bendel P, Neeman M and Salomon Y (1995) Mechanisms involved in chlorophyll based photoinduced cell damage: Photodynamic therapy of melanoma. Proc Soc Magn Res 3: 1681–1682

Zilberstein J, Bromberg A, Frantz A, Rosenbach-Belkin V, Kritzmann A, Pfefermann R, Salomon Y and Scherz A (1997) Light-dependent oxygen consumption in bacteriochlorophyll-serine-treated melanoma tumors: On-line determination using a tissue-inserted oxygen microsensor. Photochem Photobiol 65: 1012–1019

Zilberstein J, Schreiber S, Bloemers MCWM, Bendel P, Neeman M, Schechtman E, Kohen F, Scherz A and Salomon Y (2001) Antivascular treatment of solid melanoma tumors with bacteriochlorophyll-serine-based photodynamic therapy. Photochem Photobiol 73: 257–266

Chapter 34

Metal-substituted Bacteriochlorophylls: Novel Molecular Tools

Roie Yerushalmi, Idan Ashur and Avigdor Scherz*
Department of Plant Sciences, The Weizmann Institute of Science, 76100 Rehovot, Israel

Summary

Chromophore molecules have fascinated scientists for decades. As early as 1903, chlorophylls were analyzed by chromatography, a newly introduced technique at that time (Tswett, 1906). Ever since, porphyrins and hydroporphyrins and their metal complexes, such as chlorophylls and bacteriochlorophylls, have been studied extensively in the context of their roles in photosynthesis, as biological model systems, and recently, as promising sensitizers for photodynamic therapy. When increasing ring saturation from the D_{4h} porphyrin macrocycle symmetry to the less symmetrical hydroporphyrins (together with an additional isocyclic ring), a wealth of possibilities for experimental observations of increasing complexity and detail became available. The synergistic link between theoretical and experimental approaches has advanced not only the understanding of various (bacterio)chlorophyll functions, but has also provided tools for exploring other complex electronic systems.

*Author for correspondence, email: avigdor.scherz@weizmann.ac.il

Bernhard Grimm, Robert J. Porra, Wolfhart Rüdiger and Hugo Scheer (eds): Chlorophylls and Bacteriochlorophylls: Biochemistry, Biophysics, Functions and Applications, pp. 495–506.

Here, three promising developments in (bacterio)chlorophyll chemistry are discussed: firstly, the application of metal-substituted bacteriochlorophyll complexes as versatile molecular tools that offer a unique look into the electronic structure and properties, which are usually concealed using conventional experimental techniques; secondly, the recent application of nickel bacteriochlorophyll in the context of testing theoretical and computational *ab initio* methods; and, thirdly, the role of metal-substituted bacteriochlorophylls in deciphering elementary steps of metal-centered enzymatic reactions.

I. Introduction

In this chapter, the first section provides a condensed historical survey highlighting the dual role of porphyrins, hydroporphyrins and their metal complexes in implementing and developing different theoretical and computational approaches for studying electronic structure. The second section focuses specifically on bacteriochlorophyll chemistry as a modular approach with particular emphasis on metal incorporation and the advantages of using metal-substituted bacteriochlorophylls for further development of semi-synthetic derivatives.

The third section describes the application of metal-substituted bacteriochlorophylls as molecular reporters and describes a prototype of a bacteriochlorophyll-based molecular tool. We outline the principles of measurement and give examples of the application of the 'molecular potentiometer' for evaluating quantum mechanical (QM) methods and for modeling certain aspects of metal redox activity in biological systems at various coordination states.

II. From Porphyrins to Bacteriochlorophylls: An Experimental Benchmark for Theoretical Approaches.

Chlorophyll (Chl) and bacteriochlorophyll (BChl) molecules may be regarded as derivatives of porphyrins (Por). The study of the electronic structure of (B)Chls has been intimately associated with advances in the study of the 'simpler,' more symmetrical and less chemically branched Por systems. Such a strategy is applicable since the electronic structures of (B)Chls may be considered in terms of a perturbed Por system (Streitwieser, 1961; Pople and Beveridge, 1970; Hanson, 1991). Thus, the Por framework offers a relevant, yet simpler benchmark for the development and testing of theoretical approaches. Furthermore, the study of Por and, in particular, hydroporphyrins (HPor) has been driven by their central role in electron and energy transfer processes. These classes of molecules have been extensively studied and used in both modeling elementary steps of charge transfer and as sensitive molecular reporters of their immediate molecular environment. These functions place the versatile class of Por, HPor and, in particular, the (B)Chls, as a link between theoretical approaches and experimental observations. Key players in these processes are the π-electrons in the frontier molecular orbitals (FMO), which participate in inter- and intramolecular electronic transitions.

Simpson (1949) provided a quantitative description for the observed electronic spectra of Por molecules, based on a physical model. This model was the first to predict the observed spectra using structural parameters obtained from cyclic polyene models. Later, Longuet-Higgins et al., (1950) introduced the first Linear Combinations of Atomic Orbitals-Molecular Orbitals (LCAO-MO) treatment of porphine. The quest of Platt (1950) and others to develop a theoretical approach capable of predicting the spectra of cyclic polyene molecules, originally motivated the development of the 'Four orbital model' by Gouterman (1959). Using Por molecules, Gouterman demonstrated that by including configuration interactions among different excited states (as suggested by Pariser and Parr (1953)) in LCAO calculations, the relative intensities of the electronic transitions could be predicted. The effects of metal on the Por spectrum were also considered, providing an assessment of the performance of the semi-empirical approach (Gouterman, 1959, 1961; Gouterman et al., 1963).

During that period, extended versions of 'electron in a box' models with various treatments for electron

Abbreviations: BPhe – bacteriopheophytin; Cat – catalase; EEP – electronegativity equalization principle; FMO – frontier molecular orbitals; HDFT – hybrid density functional theory; HPor – hydroporphyrin; [M]-BChl – metal substituted bacteriochlorophyll; [M]-BChlide – metal substituted bacteriochlorophyllide; [M]-Por – metal porphyrin; MCR – methyl coenzyme M reductase; [Mn]-SOD – manganese superoxide dismutase; [Ni]-BChl – nickel substituted bacteriochlorophyll; PDT – photo dynamic therapy; Por – porphyrin; QM – quantum mechanical; ROS – reactive oxygen species; RP – redox potential; TE – electronic transition

correlation effects were introduced to elucidate the observed electronic spectra (Kuhn, 1951; Försterling et al., 1967; Försterling and Kuhn, 1968). This approach was very useful and provided a physical model for understanding and predicting structural effects on the measured spectra in complex molecules (Scherz and Levanon, 1985). The development of modern computational methods enabled semi-empirical calculations with a large number of configurations (Scherer and Fischer, 1989; Thompson and Zerner, 1991; Thompson and Fajer, 1992). During the last three decades, *ab initio* calculations were gradually applied to larger systems with a lower symmetry including, in particular, Chls and BChls (Christoffersen, 1972; Petke et al., 1978, 1980a; Shipman, 1982; Edwards and Zerner, 1983; Facelli, 1998; Krueger et al., 1998; Zhang and Friesner, 1998; Scholes et al., 1999). Recently, hybrid Quantum Mechanics/Molecular Mechanics (QM/MM) methods were employed to consider solvation effects as well as the surrounding protein matrix (Mercer et al., 1999; Hughes et al., 2001). These studies illustrate the advantages and limitations of the more rigorous but computationally demanding quantum mechanical (QM) methods. Interestingly, the advances in *ab initio* approaches and computational techniques underscored the relevance of relatively simple and intuitive approaches such as Gouterman's model. Moreover, the progress in *ab initio* methods contributed to the resolution of Chl and BChl functions in light-harvesting and energy transduction. This includes detailed studies of energy and electron distribution in complex interacting systems containing several (B)Chl molecules (forming a 'supermolecule'), as well as the nearby amino-acid residues (Scherer and Fischer, 1990; Scholes et al., 1999). The computational results have been mainly used to resolve and assign experimental data such as electron transfer rates (Alden et al., 1996; Lubitz et al., 2002).

In subsequent sections we describe recent progress with BChls resulting in expansion of BChl studies in new directions beyond their long-established role in photosynthesis research. The novel approaches presented here have become practical in recent years because of recent developments in the chemistry of BChls and progress in computational methods for the treatment of large molecular systems.

III. Function-Oriented Chemical Modification of Bacteriochlorophylls

The development, in the recent decades, of various synthetic chemical modification techniques for (B)Chls has been mostly driven by the desire to understand their role in photosynthesis. In addition, another use for chemical modification is to provide engineered sensitizers for photodynamic therapy (Chapters 32 and 33, Brandis et al.). The fruitful developments in BChl chemistry, combined with their unique spectroscopic and redox properties, offer new uses for these semi-natural derivatives. In particular, the incorporation of Pd, Zn, Ni, Cd, Cu, Mn, Co and, more recently, Pt, Hg, and Fe into the (B)Chl macrocycle, combined with peripheral modifications, allow a rational, stepwise design of molecules with desired photophysical, photochemical, and coordination properties for applications monitoring microscopic details of various environments. This progress permits the building of BChl-based 'tools' for use as molecular spectroscopic probes, as model systems for studying elementary steps of enzymatic reactions and also as building blocks of supramolecular devices (Yerushalmi and Scherz, 2002; Yerushalmi et al., 2003).

When considering these systems as 'tools,' an important engineering aspect that emerges is the modular design strategy made possible by means of the various reactive sites present in the BChls (Fig. 1). Here we outline specific reactions of [M]-BChls relevant to their functioning as molecular probes. Comprehensive reviews concerning the chemistry of BChl peripheral modifications can be found elsewhere (Senge et al, Chapter 2; Hynninen, 1991; Scheer, 1991; Pandey and Zheng, 2000).

A. Metal Substitution

Direct metalation of bacteriopheophytin (BPhe) is generally difficult because enolization of the β-ketoester-system may lead to oxidation and/or isocyclic ring (E) opening. Oxidation of β- and meso- positions, as well as demetalation, is frequently encountered, although [M]-BChls are generally more stable towards demetalation compared to their Chl or Por analogues. As a result, the variety of [M]-BChls available is still limited compared with that of [M]-Por derivatives. Nevertheless, the structural complexity of the [M]-BChls compared with the simpler Por is the essence of their versatility. Initially, mild methods were devel-

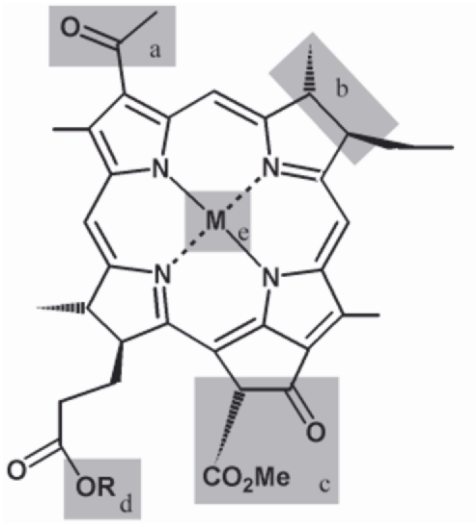

Fig. 1. BChl *a* molecule (R=Phytyl) with selected peripheral (*a-d*) and metal (*e*) sites amenable to chemical modification.

oped for replacing the Mg(II) atom by direct insertion of Zn(II), Cu(II), and Cd(II) into BPhe. Subsequently, a procedure was developed for transmetalation of [Cd]-BChl with other divalent metals, such as Co(II), Pd(II), Mn(II), and Ni(II) (Hartwich et al., 1998a; Scherz et al., 1998a,b). Later, direct metal incorporation into the BPhe macrocycle enabled Scherz and coworkeres to obtain different [M]-BChlides and their peripherally modified derivatives in a straightforward manner (Scherz et al., 2000, 2002). BChl, as well as [Zn]-BChl (Wakao et al., 1996), function as electron donors and acceptors, whereas BPhe functions as an electron acceptor in photosynthetic reaction centers (Michel-Beyerle, 1990; Farid et al., 1993). Variations at the central cavity of the molecule (site e, Fig.1) fine-tune its redox properties (Noy et al., 1998, 2000; Yerushalmi et al., 2002). Systematic studies of the spectroscopic and redox properties of [M]-BChls (Geskes et al., 1995; Hartwich et al., 1998a; Noy et al., 1998, 2000) revealed linear correlations between experimental data (e.g. electronic transition energy shifts) and factors related to the environment of the metal (e.g., the coordination state of the metal and charge density). It was found that the central metal [M] strongly affects the photophysical and photochemical behavior of the BChl molecule. For example, excited [Ni]- (with no axial ligation) and [Cu]-BChl undergo (non-radiative) relaxation into a lower metal-centered excited state within less than one tenth of a picosecond and show no photochemical activity; however, excited [Pd]-, [Mg]-, and [Zn]-BChls are highly photoactive (Teuchner et al., 1997). Knowledge of these properties is vital to design second-generation sensitizers for photodynamic therapy with better performance than the currently used first-generation compounds (Chapters 32 and 33, Brandis et al.). In the context of photosynthesis, the incorporation of [M]-BChls into the photosynthetic machinery enabled specific physical and chemical manipulation of electron and energy transfer in reaction centers and antennae, respectively (Hartwich et al., 1995, 1998b; Müller et al., 1999; Fiedor et al., 2001). Some metalated BChls, such as the [Pd] derivative, are significantly more stable at lower pH and/or under intense illumination than [Mg]- or [Zn]-BChls, enabling various peripheral modifications that require more aggressive conditions.

B. Macrocycle Modification

Four sites in the BChl macrocycle are readily amenable to chemical manipulation (see sites a–d in Fig. 1).

1. Site a: The 3-Acetyl Group

The 3-acetyl group can be reduced by $NaBH_4$ to yield [3-(1-hydroxy)-ethyl]-BChl *a*, followed by dehydration to [3-vinyl]-BChl *a* (Struck et al., 1992). Recently, Schiff's base formation was shown to be the result of an interaction of the 3-acetyl group with primary amines (Scherz et al., 2002). Further reduction with $NaCNBH_3$ transformed the Schiff's base into the corresponding secondary amine.

2. Site b: The 7,8-Double Bond

BChls are prone to spontaneous oxidation (dehydrogenation) to chlorin-type molecules (Seely, 1966; Brereton and Sanders, 1983; Hynninen, 1991). Selective chemical oxidation of BChl with dichlorodicyanobenzoquinone (DDQ) or by reactive oxygen species generated in the light by BChl, are well-known phenomena (Smith and Calvin, 1966; Vakrat et al., 1999). Transmetalation affects the tendency to undergo spontaneous oxidation since the metal strongly modifies the macrocycle redox potentials (Geskes et al., 1995; Noy et al., 1998) and photophysical behavior (Teuchner et al., 1997).

3. Site c: Isocyclic Ring E

The isocyclic ring of the BChls is amenable to various reactions: epimerization, hydroxylation, and demethoxycarbonylation reactions at C-13^2 occur because of the readily enolizable β-ketoester, as also occurs in the analogous Chls (for a comprehensive reviews see Hynninen, 1991; Woolley et al., 1998; Hynninen and Hyvarinen, 2002; Chapter 2, Senge). Alkaline hydrolysis of the isocyclic ring provides the basis for the synthesis of various bacteriochlorins, bacteriopurpurins, and bacteriopurpurinimides (Beems et al., 1987; Mironov et al., 1993; Kozyrev et al., 1996; Chen et al., 2002). Stable bacteriochlorin-6-amides obtained with a high yield by regioselective aminolysis of the isocyclic ring (Scherz et al., 2002), as occurs also in Chls (Pennington et al., 1967). Transesterification and transamination at the C-13^2 methoxycarbonyl group can modify the polarity and stability of native BChl. These reactions are of particular importance for pharmaceutical applications (Scheer et al., 2001). Again, transmetalation can broaden the scope of these reactions since the molecular framework becomes more stable with metals such as palladium.

4. Site d: The 17^3-Alcohol Group

Long-chain alcohols at C-17^3 in natural BChls can be *either* replaced by other alcohols through non-enzymatic (Scheer et al., 2001) or enzymatic transesterification (with chlorophyllase) (Fiedor et al., 1996; Rosenbach Belkin et al., 1996; Scherz et al., 1998a), *or* they can be removed by acid hydrolysis: to prevent isocyclic ring (E) opening, alkaline hydrolysis conditions are avoided. A free C-17 propionic acid residue can be further modified by dimethylaminopyridine-catalysed esterification followed by amidation after activation with N-hydroxysuccinimide (Fiedor et al., 1996) for coupling with biologically active molecules of interest.

IV. Applications

A major outcome of the extensive studies of the redox and spectroscopic properties of [M]-BChls (Geskes et al., 1995; Hartwich et al., 1995, 1998a; Noy et al., 1998, 2000; Yerushalmi et al., 2002) was the predictable response of the FMO energies to perturbations in the coordination sphere of the metal. This response, once characterized and calibrated, can be used as a reporting tool, a *molecular potentiometer*, described in the following section. Another possible application is the construction of molecular devices where the FMOs response reversibly regulates transitions between active and inactive states, as required in the action of molecular machines and switches (Yerushalmi and Scherz, 2002).

A. The Molecular Potentiometer

A simple empirical model was proposed to account for most of the observed variations in redox potentials and electronic transition energies (Geskes et al., 1995; Hartwich et al., 1998a; Noy et al., 1998), taking advantage of the splitting between the Q_y and Q_x bands in the *quasi* D_{2h} [M]-BChl symmetry. This model is based on the influence of electrostatic interactions between the electron densities of the FMOs and an effective positive charge at the molecular center. The latter was found to be a function of the electronegativity of the metal, χ_M, according to Mulliken's definition, and the covalent radius, r_M^c. Based on these guidelines, we introduced the *molecular potentiometer*, a molecular probe that can be used to measure microscopic molecular properties as well as thermodynamic indices (Yerushalmi, 1999; Noy et al., 2000; Yerushalmi et al., 2002, 2003).

1. Theoretical Insight

The application of [M]-BChl as a *molecular potentiometer* can be rationalized with reference to the 'electronegativity equalization principle' (EEP) (Sanderson, 1955, 1976). This approach stipulates that electron density flow between interacting chemical subsystems is proportional to the electronegativity difference, $\Delta\chi_o$, and is restrained by the sum of their hardness, η_o, which acts as a resistance (Pearson, 1988)

$$\Delta N = \frac{\Delta\chi_0}{2\eta_0} \quad \left\{\Delta\chi_0 \equiv \chi_a - \chi_b; \eta_0 \equiv \eta_a + \eta_b\right\} \qquad (1)$$

where ΔN is the amount of electron flow between sub-systems *a* and *b* on forming one chemical entity, using the properties (χ_o and η_o) of the isolated systems before the process of charge flow takes place.

A link between this intuitive approach and the QM formalism was introduced in the framework of the 'density functional theorem' (DFT), where Parr and co-workers identified the negative of the Lagrange

multiplier, μ_e, with χ (Eq. 2), and a QM proof for the Sanderson EEP was laid out (Parr et al., 1978):

$$\mu_e = -\chi = \left(\frac{\partial E}{\partial N}\right)_{v(\bar{r})} \quad (2)$$

where E is the total energy, N the total number of electrons, and *v(r)* is the external potential. μ_e is defined as the electronic chemical potential.

In 1983, Parr and Pearson reformulated the concept of hardness, η, as

$$\eta = \frac{1}{2}\left(\frac{\partial^2 E}{\partial N^2}\right)_{v(\bar{r})} \quad (3)$$

Thus, the electronic chemical potential, μ_e, as formulated in DFT formalism, provides a link between the intuitive chemical approach based on classical notions of electronegativity and the QM description. In particular, the concept of EEP and the subsequent mobilization of charge density on bond formation (Perdew et al., 1982; Cioslowski and Stefanov, 1993), which is not limited to the discrete charge unit of an electron, are of major importance. Experimental estimates of quantities such as fragmental charge flow (Perdew et al., 1982) and estimates of the electronic chemical potential in complex interacting systems may be useful in improving the treatment of theoretical approaches using physically valid methods and developing a new insight for the treatment of complex electronic systems.

2. The Principle of Measurement and Practical Outcomes

The pioneering studies of Gouterman (Gouterman, 1959, 1961; Gouterman et al., 1963) and the subsequent work by others (Zerner and Gouterman, 1966; Petke et al., 1980b; Warshel and Parson, 1987; Thompson and Fajer, 1992), showed that the four major electronic transitions of Por and related systems, Q_y, Q_x, B_x and B_y (in order of increasing energy), are determined by the energies of the lowest unoccupied molecular orbitals (LUMO and LUMO+1) and the relative energies of the highest occupied molecular orbitals (HOMO and HOMO-1). Whereas the D_4h symmetry of the [M]-Por macrocycle results in the pair-wise degeneration between the electronic transitions ($E_{Q_x} \approx E_{Q_y}$, $E_{B_x} \approx E_{B_y}$), the *quasi* D_{2h} BChl symmetry results in four non-degenerate electronic transitions. Hartwich et al. (1998a) and Noy et al. (1998) investigated the response of the FMO energies of [M]-BChl, as reflected in the UV-Vis-NIR electronic transition (TE) and redox potentials (RP), to changes in M (M = Mg, Zn, Cu, Ni, Pd, Cd, Mn, Co, and 2H). The experimental data could be quantitatively described by two physical parameters (Eq. 4):

$$\Delta E_{M,N} = l_{\chi,N} \cdot \Delta\chi_M + l_{r,N} \cdot \Delta r^c_M \quad (4)$$

where $l_{\chi,N}$ and $l_{r,N}$ are the loading coefficients obtained by target transformation, and N denotes a particular TE or RP.

Later, Noy et al. (2000) and Yerushalmi et al. (2002) used the loading coefficients obtained for the aforementioned series of metals to 'calibrate' the [Ni]-BChl system. This enabled an experimental estimate of charge density variations to be made at the metal core as a result of axial ligand coordination to [Ni]-BChl. The quantitative empirical estimates of charge donation and an increase in the metal's effective radius were supported by *ab initio* computational methods (Noy et al., 2000; Yerushalmi et al., 2002, 2003). Most importantly, the novel experimental method enables an estimate of the charge distribution of coordination complexes in solvent environments that cannot otherwise be resolved. Other methods such as NMR and IR spectroscopy provide experimental data that can be correlated with charge donation; however, they do not provide a direct and accurate gauge for monitoring fragmental charge flow. The combined experimental and theoretical studies provide the basis for the first BChl-based molecular tool: the 'molecular potentiometer.' This device can be visualized as possessing two components: one is the electronic π system of the BChl (or modified BChl derivative), with its FMO mainly delocalized over the macrocycle; the second component is a metal atom, chelated at the central core of the macrocycle by σ bonding to the four nitrogen atoms and functioning as an exchangeable 'probe.' To a first order approximation, the two components are independent of each other, except for electrostatic effects. Alterations in the effective radius of the metal or charge are monitored by changes in the energies of the π-electron system. The fragmental charge flow between the center of the metal and various axial ligands can be experimentally determined by measuring the energetic shift of the observed electronic transition energies among the FMO of the [Ni]-BChl frame. Because of orbital symmetry,

the Q_x and B_y spectroscopic bands are particularly sensitive to charge transfer and core size, since the B_y band involves primarily a transition from the a_{2u} to e_{gy} symmetry orbitals, and the Q_x band involves mainly a_{2u} to e_{gx} symmetries (Hanson, 1991). Importantly, Yerushalmi et al. (2003) showed, both experimentally and computationally, that fragmental charge flow (Perdew et al., 1982) between [Ni]-BChl and various axial ligands can be deduced from the Q_x band shift alone. This arises because the increase in core size is essentially constant when comparing the non-ligated low spin [Ni]-BChl and the various high-spin (S = 1) [Ni]BChl•L_n complexes, (where n = (1,2) and L is a ligand molecule) (Yerushalmi, 1999; Yerushalmi et al., 2002, 2003). This experimental gauge offers exceptional sensitivity and accuracy, independently verified by comparison with *ab initio* results and the small experimental error limits (±0.005 e^-). Notably, the Q_x band in [M]-BChl systems is readily resolved and has a relatively large oscillator strength (compared to the Chl or Por systems). This result enabled Yerushalmi et al. (2003) to look at fine details of the charge transfer processes between axial ligands and transition metals. In particular, the role of electron correlation effects on the charge transfer process could be resolved.

B. The Molecular Potentiometer: A Tool to Evaluate the Performance of Different Computational Methods

Since atomic charges cannot be directly measured, their theoretical determination depends on the computational scheme and the experimental data used to deduce them. This includes, for example, fitting point charges to dipole moments and integration of the computed density, or other population analyses. Since different molecular properties are used in various charge analysis schemes, different and occasionally contradictory charge distributions are obtained (Wiberg et al., 1991; Bergman and Hinze, 1996). The *molecular potentiometer* provided, for the first time, a direct experimental method with high sensitivity (±0.005 e^-) for evaluating the performance of different theories and related computational methods for atomic charge analysis. Yerushalmi et al., (2003) compared the experimentally observed fragmental charge flow between the chelated Ni(II) center and various axial ligands (as described in the previous section) with various computational methods. The low spin (S = 0) non-ligated [Ni]-BChl, as well as the mono-, and bi- ligated high spin (S = 1) complexes (16 structures) were fully optimized using various *ab initio* methods, including HDFT methods. The experimental results correlate well (R^2 = 0.99), for example, with the Natural Population Analysis (NPA) charge analysis results (Reed et al., 1988), whereas the Mulliken analysis fails to reproduce the experimental data. Notably, methods based on the electrostatic-fit (such as the Merz-Singh-Kollman (Besler et al., 1990), or Chelpg (Chirlian and Francl, 1987) schemes), while offering good performance when considering the charge distribution for mono-ligated complexes, perform poorly or even fail to describe the charge distribution for the bi-ligated complexes. This irregular behavior for a series of related complexes was not anticipated, and such a specific analysis has become possible due to the availability of precisely monitoring experimentally the fragmental charge flow. The experimental system also proved useful for resolving the contribution of electron correlation effects. The contribution of electron correlation effects to charge mobilization was studied by performing HF and post-Hartree-Fock calculations (second-order Møller-Plesset perturbation theory (MP2), DFT, and HDFT) and comparing the experimental data with the resulting populations across various levels of theory, as well as across different charge analysis schemes. It was found that electron correlation effects have a significant role in these processes (Yerushalmi et al., 2004).

C. Studying Elementary Steps of Enzymatic Catalysis

The BChl macrocycle can be regarded as a rather flexible chelator compared to the Por or Chl derivatives (Senge, 1992), yet it provides four coordination sites to different central metals. This structural flexibility enables accommodation of metals with different size and coordination geometries. The combination of structural flexibility with well-characterized and resolvable spectroscopic response to changes in the coordination sphere and redox conditions, has proved useful for studying certain aspects of enzymatic catalysis (Yerushalmi et al., 2002). In particular, it provides an opportunity to follow the dynamic coordination properties in a solvent environment (e.g., association and dissociation of axial ligands) without the need to crystallize or apply other drastic methods, and is fruitful in instances where these properties may be altered or where intermediates cannot be easily

isolated. We now provide two examples of such applications in the context of nickel and manganese redox proteins.

1. The Role of Axial Ligands in F-430: Model Studies with [Ni]-BChl

Crystallographic and spectroscopic data show a dynamic coordination sphere around the nickel center for the different states of the active site of methyl coenzyme M reductase (MCR). Recently, Telser et al. (2001) suggested that activation of the MCR F430 complex (Fig. 2) involves a reduction of Ni(II) to Ni(I) and partial dissociation of, at least, one axial ligand. This is supported by comparison with model compounds that have similar or even identical paramagnetic properties to those found for the cryogenically reduced MCR complex. It is still not clear from the extensive studies, however, which ligand is dissociated, or what is the nature of the intermediate coordination sphere of the Ni cation, especially when considering the significant changes in the Ni ionic radius when changing redox states. EXAFS and X-ray studies of low-spin Ni(II)-F430M and its 12,13-di-epimer showed short average Ni-N distances in both complexes of ~1.90A, with a slightly shorter distance for the di-epimer complex (Furenlid et al., 1990; Farber et al., 1991). The coordination of two axial ligands to the Ni(II) center in isolated F430 expands the Ni-N distance by ~0.2 Å to approximately 2.1 Å (Shiemke et al., 1989; Furenlid et al., 1990). A similar average Ni(II)-N distance was observed by X-ray crystallography at high resolution for F430 within the MCR protein (Grabarse et al., 2001). Yerushalmi et al. (2002) found that coordination of [Ni(II)]-BChl to one axial ligand is sufficient to bring the macrocycle to an essentially planar configuration, with an average Ni-N distance of 2.16 Å, compared with 1.97 Å in the non-ligated [Ni]-BChl complex.

Using the [Ni]-BChl system, Yerushalmi et al. (2002) showed: *firstly,* that axial ligands control the dimension of the central core and the planarity of the macrocycle as described above; and, *secondly,* that axial coordination modulates the electron density at the Ni center. Ultimately, these functions allow for efficient structural and electronic fine-tuning of the Ni center for alternate steps of reduction and substrate binding during the catalytic cycle. The increase of 0.19 Å, found for [Ni(II)]-BChl, compares well with the ~0.20 Å difference between the Ni-N average distance in ligated and non-ligated forms of the F430 models.

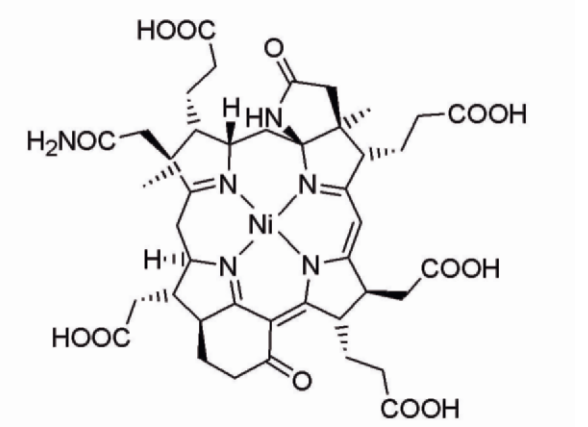

Fig. 2. Cofactor F430 found in the active site of methyl coenzyme M reductase.

Following these observations and related computations, Yerushalmi et al. (2002) suggested that even a weakly bound axial ligand might have a substantial effect on macrocycle conformation. For example, binding of the F430 cofactor to an axial glutamine residue, as suggested by the X-ray data (Grabarse et al., 2001), may have an important structural role in converting the complex to the reduced state. The coordinating environment in the MCR catalytic niche may be designed to ensure smooth adiabatic transitions between the different Ni redox states, where the structural modifications of the macrocycle are arranged before the reduction process. Moreover, the peripheral hydrogen-bonding network may have an additional structural influence on macrocycle conformation (Grabarse et al., 2001). Reduction is expected to be accompanied by partial dissociation of one of the axial ligands (either the glutamine residue or the thiol group) because of the accumulation of electron density at the metal core and the aforementioned electrostatic repulsion.

2. Axial Ligand Functions in [Mn]-Superoxide Dismutase: Modeling Catalytic Steps with [Mn]-BChl

Mn(II)/Mn(III) redox transitions play a key role in the regulation of reactive oxygen species (ROS) by Mn-containing enzymes. These include dismutation of the superoxide radical by mono and bi-centered [Mn]-SOD, decomposition of hydrogen peroxide to water and oxygen by catalase (Cat) and oxygen evolution by water oxidation in the Mn complex of PS II (OEC). The coordination sphere of the Mn center has been extensively characterized for some [Mn]-

SOD and Cat by X-ray crystallography (Dismukes, 1996; Christianson, 1997; Atzenhofer et al., 2002; Fluckiger et al., 2002). Various studies indicate that association and dissociation of a water molecule, hydroxyl anion, imidazole and carboxylic residues are cardinal to the catalytic cycle (Vance and Miller, 1998; Han et al., 2002; Whittaker, 2002). Still, the role of the ligand in the redox activity of Mn with the ROS or water molecules has remained an open question. Attempts to resolve this issue in vitro using Mn model systems, in particular Mn(II)/Mn(III) complexes with porphyrins and phthalocyanines, are extensively documented (Loach and Calvin, 1964; Boucher and Day, 1977; Lever et al., 1977; Uchida et al., 1978). More recently, other complexes with Mn at higher redox states were prepared and investigated as models for enzymatic activity in vivo (Dismukes, 1996; Christianson, 1997; Brunold et al., 1998). A major disadvantage of the studied complexes was the lack of robust reporters for the Mn redox states and redox state changes. Geskes et al. (1995) have correlated the electronic transitions of [Mn]-BChl with Mn(II)/Mn(III) transitions. Using spectro-electrochemical measurements, they related [Mn(II)]- and [Mn(III)]- BChl with Q_y transitions at 770 and 820 nm, respectively. Recently, Ashur et al. (2003) supported this assignment with electron spin resonance (ESR) studies. In this recent study, it was further shown that oxidation of the superoxide radical by Mn(III) is regulated by acetate and imidazole residues. Both ligands have a bi-functional role: in one capacity, they ligate to a [Mn(III)]-BChl(O_2H)(OH) complex and activate the bond cleavage of the bonded hydroperoxyl moiety (the $OOH^{\bullet}$ radical was trapped by DMPO to form a DMPO-OOH adduct and its ESR signal was shown to be a function of the ligand concentration); and, in its second capacity, the ligand functions as a general Brönsted base and ionizes the hydroperoxyl radical. The resulting superoxide radical undergoes oxidation by the [Mn(III)]-BChl•L complex, which remains inactive toward dioxygen. The overall reaction also involves the association and dissociation of hydroperoxyl radicals and dissociation of hydroxyl anion. Under certain conditions, the redox reaction leads to the dismutation of two hydroperoxyl radical molecules to hydrogen peroxide and dioxygen. Notably, the reaction rate of this process is faster by more than five orders of magnitude than the dismutation of two superoxide radical molecules and therefore it is much closer to the enzymatic catalytic rate for dismutation of [Mn]-SOD in vivo. These findings emphasize two aspects of the role played by ligands of the first coordination sphere in enzyme catalysis: controlling the binding affinity of the metal center to substrate molecules, and providing the driving force for a coupled electron-proton transfer. The [Mn]-BChl was recently introduced into synthetic protein maquettes (D. Noy, personal communication) and preliminary characterization of their redox chemistry is in progress.

V. Concluding Remarks

Modified [M]-BChl derivatives provide new tools for exploring fundamental issues of interest in chemistry and electronic structure, including elementary steps in metal-centered catalysis. The application of this class of molecules is also expected to advance new avenues for PDT (Chapters 32 and 33, Brandis et al.), and provide novel functional building blocks for constructing molecular devices. The exploitation of this prospect appears promising but requires further development and expansion of the available synthetic pathways.

Acknowledgments

We thank the Deutsche Forschungsgemeinschaft (SFB 533, TP A6) and the Avron-Minerva Center for Photosynthesis for their ongoing support of our research. A. Scherz is incumbent of the Yadelle and Robert Sklare Professional Chair for Biochemistry. The authors thank Dr. A. Brandis for fruitful discussions during the preparation of this article.

References

Alden RG, Parson WW, Chu ZT and Warshel A (1996) Macroscopic and microscopic estimates of the energetics of charge separation in bacterial reaction centers. In: Michel-Byerle (ed) Reaction Centers of Photosynthetic Bacteria: Structure and Dynamics, pp 105–116. Springer-Verlag, Berlin

Ashur I, Brandis A, Greenwald M, Vakrat-Hagalili Y, Rosenbach-Belkin V, Scheer H and Scherz A (2003) Control of redox transitions and oxygen species binding in Mn centers by biologically significant ligands; Model studies with [Mn]-bacteriochlorophyll a. J Am Chem Soc 125: 8852–8861

Atzenhofer W, Regelsberger G, Jacob U, Peschek GA, Furtmuller PG, Huber R and Obinger C (2002) The 2.0 angstrom resolution structure of the catalytic portion of a cyanobacterial membrane-bound manganese superoxide dismutase. J Mol

Biol 321: 479–489
Beems EM, Dubbelman TMAR, Lugtenburg J, Vanbest JA, Smeets MFMA and Boegheim JPJ (1987) Photosensitizing properties of Bacteriochlorophyllin-*a* and Bacteriochlorin-*a*, 2 derivatives of Bacteriochlorophyll-*a*. Photochem Photobiol 46: 639–643
Bergman D and Hinze J (1996) Electronegativity and molecular properties. Angew Chem Int Ed 35: 150–163
Besler BH, Merz KM and Kollman PA (1990) Atomic charges derived from semiempirical methods. J Comput Chem 11: 431–439
Boucher LJ and Day VW (1977) Manganese Schiff-Base complexes 5. Synthesis and spectroscopy of some anion complexes on N,N´ethylenebis(Acetylacetone Iminato)Manganese(III). Inorg Chem 16: 1360–1367
Brereton RG and Sanders JKM (1983) Bacteriochlorophyll *a* — Influence of axial coordination on reactivity and stability — design of an improved extraction procedure. J Chem Soc Perk T (I) 2: 431–434
Brunold TC, Gamelin DR, Stemmler TL, Mandal SK, Armstrong, WH, Penner-Hahn, JE and Solomon, EI (1998) Spectroscopic studies of oxidized manganese catalase and mu-oxo-bridged dimanganese(III) model complexes: Electronic structure of the active site and its relation to catalysis. J Am Chem Soc 120: 8724–8738
Chen YH, Graham A, Potter W, Morgan J, Vaughan L, Bellnier DA, Henderson BW, Oseroff A, Dougherty TJ and Pandey RK (2002) Bacteriopurpurinimides: Highly stable and potent photosensitizers for photodynamic therapy. J Med Chem 45: 255–258
Chirlian LE and Francl MM (1987) Atomic charges derived from electrostatic potentials: A detailed study. J Comput Chem 8: 894–905
Christianson DW (1997) Structural chemistry and biology of manganese metalloenzymes. Prog Biophys Mol Bio 67: 217–252
Christoffersen RE (1972) *Ab initio* calculations on large molecules. Adv Quant Chem 6: 333–393
Cioslowski J and Stefanov BB (1993) Electron flow and electronegativity equalization in the process of bond formation. J Chem Phys 99: 5151–5162
Dismukes GC (1996) Manganese enzymes with binuclear active sites. Chem Rev 96: 2909–2926
Edwards WD and Zerner MC (1983) Electronic-structure of model chlorophyll systems. Int J Quant Chem 23: 1407–1432
Facelli JC (1998) Density functional theory calculations of the structure and the N-15 and C-13 chemical shifts of methyl bacteriopheophorbide a and bacteriochlorophyll *a*. J Phys Chem B 102: 2111–2116
Farber G, Keller W, Kratky C, Jaun B, Pfaltz A, Spinner C, Kobelt A and Eschenmoser A (1991) Coenzyme F430 from methanogenic bacteria — complete assignment of configuration based on an X-ray-analysis of 12,13-Diepi-F430 pentamethyl ester and on NMR-spectroscopy. Helv Chim Acta 74: 697–716
Farid RS, Moser CC and Dutton PL (1993) Electron-transfer in proteins. Curr Opin Struct Biol 3: 225–233
Fiedor L, Rosenbachbelkin V, Sai M and Scherz A (1996) Preparation of tetrapyrrole-amino acid covalent complexes. Plant Physiol Biochem 34: 393–398
Fiedor L, Leupold D, Teuchner K, Voigt B, Hunter CN, Scherz A and Scheer H (2001) Excitation trap approach to analyze size and pigment-pigment coupling: Reconstitution of LH1 antenna of *Rhodobacter sphaeroides* with Ni-substituted bacteriochlorophyll. Biochemistry 40: 3737–3747
Fluckiger S, Mittl PRE, Scapozza L, Fijten H, Folkers G, Grutter MG, Blaser K and Crameri R (2002) Comparison of the crystal structures of the human manganese superoxide dismutase and the homologous *Aspergillus fumigatus* allergen at 2-angstrom resolution. J Immunol 168: 1267–1272
Försterling HD and Kuhn H (1968) Projected electron density method of pi-electron systems II. Excited states. Int J Quant Chem 2: 413–430
Försterling HD, Huber H and Kuhn H (1967) Projected electron density method of pi-electron systems. I. Electron distribution in the ground state. Int J Quant Chem 1: 225–241
Furenlid LR, Renner MW and Fajer J (1990) EXAFS studies of Nickel(II) and Nickel(I) factor 430 M. Conformational flexibility of the F430 skeleton. J Am Chem Soc 112: 8987–8989
Geskes C, Hartwich G, Scheer H, Mantele W and Heinze J (1995) An electrochemical and spectroelectrochemical investigation of metal-substituted bacteriochlorophyll *a*. J Am Chem Soc 117: 7776–7783
Gouterman M (1959) Study of the effects of substitution on the absorption spectra of porphyrin. J Chem Phys 30: 1139–1161
Gouterman M (1961) Spectra of porphyrins. J Mol Spectrosc 6: 138–163
Gouterman M, Wagniere GH and Snyder LC (1963) Spectra of porphyrins. Part II. Four orbital model. J Mol Spectrosc 11: 108–127
Grabarse W, Mahlert F, Duin EC, Goubeaud M, Shima S, Thauer RK, Lamzin V and Ermler U (2001) On the mechanism of biological methane formation: Structural evidence for conformational changes in methyl-coenzyme M reductase upon substrate binding. J Mol Biol 309: 315–330
Han WG, Lovell T and Noodleman L (2002) Coupled redox potentials in manganese and iron superoxide dismutases from reaction kinetics and density functional/electrostatics calculations. Inorg Chem 41: 205–218
Hanson LK (1991) Molecular orbital theory of monomer pigments. In: Scheer H (ed) Chlorophylls, pp 993–1014. CRC press, Boca Raton
Hartwich G, Friese M, Scheer H, Ogrodnik A and Michel Beyerle ME (1995) Ultrafast internal-conversion in 13(2)-OH-Ni-Bacteriochlorophyll in reaction centers of *Rhodobacter-sphaeroides* R26. Chem Phys 197: 423–434
Hartwich G, Fiedor L, Simonin I, Cmiel E, Schafer W, Noy D, Scherz A and Scheer H (1998a) Metal-substituted bacteriochlorophylls. 1. Preparation and influence of metal and coordination on spectra. J Am Chem Soc 120: 3675–3683
Hartwich G, Scheer H and Michel-Beyerle ME (1998b) Electron transfer in modified bacterial photosynthetic reaction centers. Abstr Pap Am Chem S 215: U217-U217
Hughes JM, Hutter MC, Reimers JR and Hush NS (2001) Modeling the bacterial photosynthetic reaction center. 4. The structural, electrochemical, and hydrogen-bonding properties of 22 mutants of *Rhodobacter sphaeroides*. J Am Chem Soc 123: 8550–8563
Hynninen PH (1991) Chemistry of chlorophylls: Modifications. In: Scheer H (ed) Chlorophylls, pp 145–209. CRC press, Boca Raton
Hynninen PH and Hyvärinen K (2002) Tracing the allomerization pathways of chlorophylls by O-18-labeling and mass spectrometry. J Org Chem 67: 4055–4061

Kozyrev AN, Zheng G, Zhu CF, Dougherty TJ, Smith KM and Pandey RK (1996) Syntheses of stable bacteriochlorophyll-*a* derivatives as potential photosensitizers for photodynamic therapy. Tetrahedron Lett 37: 6431–6434

Krueger BP, Scholes GD and Fleming GR (1998) Calculation of couplings and energy-transfer pathways between the pigments of LH2 by the *ab initio* transition density cube method. J Phys Chem B 102: 5378–5386

Kuhn H (1951) Elektronengasmodell zur quantitativen Deutung der Licht-absorption von organischen Farbstoffen II. Helv Chim Acta 34: 2371–2402

Lever ABP, Wilshire JP and Quan SK (1977) A Manganese Phthalocyanine-dioxygen molecular adduct. J Am Chem Soc 101: 3668–3669

Loach PA and Calvin M (1964) Oxidation states of manganese methyl phaeophorbide alpha in aqueous solution. Nature 202: 343

Longuet-Higgins HC, Rector CW and Platt JR (1950) Molecular orbital calculations on porphine and tetrahydroporphine. J Chem Phys 18: 1174–1181

Lubitz W, Lendzian F and Bittl R (2002) Radicals, radical pairs and triplet states in photosynthesis. Acc Chem Res 35: 313–320

Mercer IP, Gould IR and Klug DR (1999) A quantum mechanical/molecular mechanical approach to relaxation dynamics: Calculation of the optical properties of solvated bacteriochlorophyll-*a*. J Phys Chem B 103: 7720–7727

Michel-Beyerle ME (1990) Reaction centers of photosynthetic bacteria. In: Springer Series Biophysics, 6. Springer-Verlag, Berlin

Mironov AF, Kozyrev AN and Brandis A (1993) Sensitizers of second generation for photodynamic therapy of cancer based on chlorophyll and bacteriochlorophyll derivatives. In: Korppi-Tommola (ed) Laser Study of Macroscopic Biosystems, SPIE Proceedings, Vol 1922, pp 204–208. International Society for Optical Engineering

Müller P, Hartwich G, Ogrodnik A and Michel-Beyerle ME (1999) Novel multipulse saturation spectroscopy for quantum yield determination of charge separation in modified photosynthetic reaction centers. Chem Phys Lett 306: 239–248

Noy D, Fiedor L, Hartwich G, Scheer H and Scherz A (1998) Metal-substituted Bacteriochlorophylls: II. Changes in redox potentials and electronic transition energies are dominated by intramolecular electrostatic interactions. J Am Chem Soc 120: 3684–3693

Noy D, Yerushalmi R, Brumfeld V, Ashur I, Baldridge KK, Scheer H and Scherz A (2000) Optical absorption and computational studies of [Ni]-Bacteriochlorophyll-*a* provide a new insight into charge distribution between metal and ligands. J Am Chem Soc 122: 3937–3944

Pandey RK and Zheng G (2000) Porphyrins as photosensitizers in photodynamic therapy. In: KM Kadish, KM Smith and R Guilard (eds) The Porphyrin Handbook, pp 157–230. Academic Press, San Diego

Parr RG and Pearson RG (1983) Absolute hardness: Companion parameter to absolute electronegativity. J Am Chem Soc, 105: 7512–7516

Parr RG, Donnely RA, Levy M and Palke WE (1978) Electronegativity: The density functional viewpoint. J Chem Phys 68: 3801–3807

Pearson, RG (1988) Absolute electronegativity and hardness: Application to inorganic chemistry. Inorg Chem, 27: 734–740

Pennington FC, Boyd SD, Horton H, Taylor SW, Wulf DG, Katz JJ and Strain HH (1967) Reaction of Chlorophylls *a* and *b* with amines. Isocyclic ring rupture and formation of substituted chlorin–6-amides. J Am Chem Soc 89: 3871–3875

Perdew JP, Parr RG, Levy M and Balduz JL (1982) Density-functional theory for fractional particle number: Derivative discontinuities of the energy. Phys Rev Lett 49: 1691–1694

Petke JD, Maggiora GM, Shipman LL and Christoffersen RE (1978) Stereoelectronic properties of photosynthetic and related systems — *Ab initio* configuration interaction calculations on ground and lower excited singlet and triplet-states of magnesium chlorin and chlorin. J Mol Spect 73: 311–331

Petke JD, Maggiora GM, Shipman LL and Christoffersen RE (1980a) Stereoelectronic properties of photosynthetic and related systems.7. *Ab initio* Quantum-Mechanical characterization of the electronic-structure and spectra of chlorophyllide-*a* and bacteriochlorophyllide-*a* cation radicals. Photochem Photobiol 31: 243–257

Petke JD, Maggiora GM, Shipman LL and Christoffersen RE (1980b) Stereoelectronic properties of photosynthetic and related systems-VI. *ab-initio* configuration interaction calculations on the ground and lower excited singlet and triplet states of ethyl bacteriochlorophyllide *a* and ethyl bacteriopheophorbide *a*. Photochem Photobiol 32: 399–414

Platt JR (1950) Molecular orbital predictions of organic spectra. J Chem Phys 18: 1168–1173

Pople JA and Beveridge DL (1970) Approximate Molecular Orbital Theory. McGraw-Hill, New York.

Reed AE, Curtiss LA and Weinhold F (1988) Intermolecular interactions from a natural bond orbital, donor-acceptor viewpoint. Chem Rev 88: 899–926

Rosenbach Belkin V, Chen L, Fiedor L, Tregub I, Pavlotsky F, Brumfeld V, Salomon Y and Scherz A (1996) Serine conjugates of chlorophyll and bacteriochlorophyll: Photocytotoxicity in vitro and tissue distribution in mice bearing melanoma tumors. Photochem Photobiol 64: 174–181

Sanderson RT (1955) Partial charges on atoms in organic compounds. Science 121: 207–210

Sanderson RT (1976) Chemical Bonds and Bond Energy. Academic Press, New York

Scheer H (1991) Chemistry of Chlorophylls. In: Scheer H (ed) Chlorophylls, pp 3–30. CRC press, Boca Raton

Scheer H, Kammhuber N, Scherz A, Salomon Y and Brandis A (2001) Synthesis and photodynamic activity of chlorophyll and bacteriochlorophyll esters. PCT Int. Appl. WO/040232, 48 pp

Scherer POJ and Fischer SF (1989) Quantum treatment of the optical-spectra and the initial electron-transfer process with the reaction renter of *Rhodopseudomonas viridis*. Chem Phys 131: 115–127

Scherer POJ and Fischer SF (1990) Electronic excitations and electron transfer coupling within the bacterial reaction center based on an INDO/S-CI supermolecule approach including 615 atoms. Jerusalem Symposia on Quantum Chemistry and Biochemistry: pp 361–370

Scherz A and Levanon H (1985) Optical-transition energies of porphyrins - the application of Free-Electron Molecular-Orbital approach. Mol Phys 55: 923–937

Scherz A, Salomon Y, Fiedor L and Brandis A (1998a) Chlorophyll and bacteriochlorophyll derivatives, their preparation and pharmaceutical compositions comprising them. US Pat.

Application: No. 6147195
Scherz A, Salomon Y, Scheer H, Hartwich G and Brandis A (1998b) Synthetic metal-substituted bacteriochlorophyll derivatives and use thereof. PCT Int. Appl. WO/19081, 36 pp
Scherz A, Solomon Y, Brandis A and Scheer H (2000) Palladium-substituted bacteriochlorophyll derivatives and use thereof. PCT Int. Appl. WO/0033833, 59 pp
Scherz A, Brandis A, Mazor O, Salomon Y and Scheer H (2002) Water-soluble Bacteriochlorophyll derivatives and their pharmaceutical uses. PCT Int. Appl WO/045592, 36 pp
Scholes GD, Gould IR, Cogdell RJ and Fleming GR (1999) *Ab initio* molecular orbital calculations of electronic couplings in the LH2 bacterial light-harvesting complex of *Rps-acidophila*. J Phys Chem B 103: 2543–2553
Seely GR (1966) The structure and chemistry of functional groups. In: LP Vernon and GR Seely (eds) The Chlorophylls, pp 67–110. Academic Press, New York
Senge MO (1992) The conformational flexibility of tetrapyrroles — current model studies and photobiological relevance. J Photochem Photobiol *B* 16: 3–36
Shiemke AK, Kaplan WA, Hamilton CL, Shelnutt JA and Scott RA (1989) Structural and spectroscopic characterization of exogenous ligand-binding to isolated Factor-F430 and its configurational isomers. J Biol Chem 264: 7276–7284
Shipman LL (1982) Electronic structure and function of chlorophylls and their pheophytins. In: Govindjee (ed) Photosynthesis. Academic Press, New York
Simpson WT (1949) The theory of pi-electron system in porphines. J Chem Phys 17: 1218–1221
Smith JRL and Calvin M (1966) Studies on chemical and photochemical oxidation of Bacteriochlorophyll. J Am Chem Soc 88: 4500–4506
Streitwieser Jr A (1961) Molecular Orbital Theory for Organic Chemists. John Wiley, New York
Struck A, Cmiel E, Katheder I, Schäfer W and Scheer H (1992) Bacteriochlorophylls modified at position C-3 — long-range intramolecular interaction with position C-13.2. Biochim Biophys Acta 1101: 321–328
Telser J, Davydov R, Horng YC, Ragsdale SW and Hoffman BM (2001) Cryoreduction of methyl-coenzyme M reductase EPR characterization of forms, MCRox1 and MCRred1. J Am Chem Soc 123: 5853–5860
Teuchner K, Stiel H, Leupold D, Scherz A, Noy D, Simonin I, Hartwich G and Scheer H (1997) Fluorescence and excited state absorption in modified pigments of bacterial photosynthesis — A comparative study of metal-substituted bacteriochlorophylls *a*. J Lumin 72–4: 612–614
Thompson MA and Fajer J (1992) Calculation of bacteriochlorophyll *g* primary donors in photosynthetic heliobacteria. How to shift the energy of a phototrap by 2000 cm^{-1}. J Phys Chem 96: 2933–2935
Thompson MA and Zerner MC (1991) A theoretical examination of the electronic structure and spectroscopy of photosynthetic reaction center from *Rhodopseudomonas viridis*. J Am Chem Soc 113: 8210–8215
Tswett M (1906) Adsorptionanalyse und Chromatographiische Methode. Ber Deut Bot Ges 24: 384–393
Uchida K, Naito S, Soma M, Onishi T and Tamaru K (1978) New dioxygen complex of manganese phthalocyanine. J Chem Soc Chem Comm 6: 217–218
Vakrat Y, Weiner L, Brandis A, Mazor O, Hami R, Gross S, Schreiber S, Salomon Y and Scherz A (1999) Bacteriochlorophyll derivatives: Phototoxicity, hyrophobicity and oxygen radicals production. Free Radical Bio Med 27: S129-S129
Vance CK and Miller AF (1998) Simple proposal that can explain the inactivity of metal-substituted superoxide dismutases. J Am Chem Soc 120: 461–467
Wakao N, Yokoi N, Isoyama N, Hiraishi A, Shimada K, Kobayashi M, Kise H, Iwaki M, Itoh S, Takaichi S and Sakurai Y (1996) Discovery of natural photosynthesis using Zn-containing bacteriochlorophyll in an aerobic bacterium *Acidiphilium rubrum*. Plant Cell Physiol 37: 889–893
Warshel A and Parson WW (1987) Spectroscopic properties of photosynthetic reaction centers. 1. Theory. J Am Chem Soc 109: 6143–6152
Whittaker JW (2002) Prokaryotic manganese superoxide dismutases. Method Enzymol 349: 80–90
Wiberg KB, Hadad CM, Breneman CM, Laidig KE, Murcko MA and Lepage TJ (1991) The response of electrons to structural changes. Science 252: 1266–1272
Woolley PS, Moir AJ, Hester RE and Keely BJ (1998) A comparative study of the allomerization reaction of chlorophyll *a* and bacteriochlorophyll *a*. J Chem Soc Perk T(II) 8: 1833–1839
Yerushalmi R (1999) Effects of axial ligands on the electronic structure and redox potentials of nickel bacteriochlorophyll-*a*; the groundwork of a molecular potentiometer. M.Sc. thesis, The Weizmann Institute of Science, Rehovot, Israel
Yerushalmi R and Scherz A (2002) Synthetic Molecular Spring Device. WO/02073062
Yerushalmi R, Noy D, Baldridge KK and Scherz A (2002) Mutual control of axial and equatorial ligands: Model studies with [Ni]-Bacteriochlorophyll-*a*. J Am Chem Soc 124: 8406–8415
Yerushalmi R, Baldridge KK and Scherz A (2003) An experimental look into sub-electron charge flow. J Am Chem Soc 125: 12706–12707
Yerushalmi R, Scherz A and Baldridge KK (2004) Direct experimental evaluation of charge schemes performance by a molecular charge-meter. J Am Chem Soc 126: 5897–5905
Zerner M and Gouterman M (1966) Porphyrins IV. Extended Hückel calculations on transition metal complexes. Theo Chim Acta 4: 44–63
Zhang LY and Friesner RA (1998) Ab initio calculation of electronic coupling in the photosynthetic reaction center. Proc Natl Acad Sci USA 95: 13603–13605

Chapter 35

Chlorophyll Fluorescence as a Reporter on in vivo Electron Transport and Regulation in Plants

Ladislav Nedbal[1,2,*] and Michal Koblížek[2,3]
[1]Laboratory of Systems Biology, Institute of Landscape Ecology and [2]Institute of Physical Biology, Zámek 136, 37333 Nové Hrady, Czech Republic; [3]Laboratory of Photosynthesis, Institute of Microbiology, 379 81 Třeboň, Czech Republic

Summary

Transients of chlorophyll (Chl) fluorescence emission are widely used to estimate kinetics, yield and regulation of photosynthetic processes in intact plants. In this chapter, we introduce concepts and terms required for a qualified application of the technique. An overview of relevant processes that occur on different timescales, from picoseconds to organism lifetime, is provided as a reference framework for description of approximations and models connecting physiologically relevant photosynthetic parameters and the fluorescence data. Reaching beyond the conventional analysis, we also describe models including Photosystem II heterogeneity and short-living radicals that can affect plant-Chl fluorescence emission. Current state-of-the-art and future prospects for Chl-fluorescence instrumentation are described at the end of the chapter.

*Author for correspondence, email: nedbal@greentech.cz

Bernhard Grimm, Robert J. Porra, Wolfhart Rüdiger and Hugo Scheer (eds): Chlorophylls and Bacteriochlorophylls: Biochemistry, Biophysics, Functions and Applications, pp. 507–519.

I. Introduction

A rapid transition from dark to light elicits in plants a complex transient of fluorescence emission that was first reported in late 19th century by Müller (1874) and was then introduced to modern science more than 70 years ago by Kautsky and Hirsch (1931). At present, the dynamic changes in the chlorophyll (Chl) fluorescence emission are widely used as a reporter on photosynthetic activity and regulation in plants (Dau, 1994; Govindjee, 1995; Falkowski and Kolber, 1995; Kramer and Crofts, 1996; Strasser et al., 1998; Lazár, 1999; Krause and Jahns, 2002). The technique is well established in photosynthesis research with emerging applications in ecology, biotechnology and in precision farming (Bolhár-Nordenkampf et al., 1989; Mohammed et al., 1995; Lichtenthaler and Miehé, 1997; Jalink et al., 1998; DeEll et al., 1999; Nedbal et al., 2000).

Abbreviations: a – optical cross section; F_K, F_I, F_J, F_P – intermediate fluorescence levels of the fluorescence induction curve measured during a transition from dark adapted to light adapted state of a plant; F_0 – fluorescence emission of a dark adapted plant with the primary acceptor Q_A oxidized and non-photochemical quenching inactive; F_0' – fluorescence emission of a light adapted plant measured with the primary acceptor Q_A oxidized and non-photochemical quenching active ($F_0' < F_0$); F_M – fluorescence emission of a dark adapted plant exposed to a brief pulse of a strong light leading to a transient reduction of Q_A without induction of non-photochemical quenching; F_M' – fluorescence emission of a light adapted plant measured during a strong pulse of light with Q_A and the plastoquinone pool reduced and non-photochemical quenching active ($F_M' < F_M$); F_V, F_V' – variable fluorescence measured in dark-adapted ($F_V = F_M - F_0$) and in light-adapted plants ($F_V' = F_M' - F_0'$); Chl – chlorophyll; Cyt b_6f– cytochrome b_6f complex; *DCMU* – 3-(3,4-dichlorophenyl)-1,1′-dimethylurea; Fd – ferredoxin; FNR – ferredoxin-NADP$^+$ oxidoreductase; I – irradiance; J – parameter quantifying the inter-unit exciton transfer and the resulting sigmoidicity of the fluorescence induction curve ($J \equiv p/(1-p)$); k_P – rate constant of primary photochemistry in the reaction center of PS II; k_N – rate constant of non-radiative energy dissipation; k_F – rate constant of fluorescence emission; N – number of PS II units; *NPQ* – Stern-Volmer non-photochemical quenching parameter; p – probability that an exciton captured by a PS II antenna will migrate to antenna of a neighboring PS II reaction center; P680 – primary electron donor of Photosystem II; P700 – primary electron donor of Photosystem I; PC – plastocyanin; Phe – pheophytin; PS I – Photosystem I; PS II – Photosystem II; PS II^{open} – fraction of open reaction centers; PS II^{closed} – fraction of closed reaction centers; Q_A, Q_B – primary and secondary quinone acceptors of PS II; q_P – photochemical quenching; q_N – non-photochemical quenching parameter; S_n – oxidation states of manganese oxygen-evolving cluster; t – time; Y_z – tyrosine Z, secondary electron donor of PS II; Φ_p^{max}, $\Phi_p(t)$ – maximum and effective photochemical yield of PS II; $\sigma_{PS\,II}$ – functional cross section of PS II.

Plant Chl fluorescence originates predominantly from the lowest excited singlet state of Chl *a* adjacent to the Photosystem II (PS II) reaction center which, in turn, drives primary charge separation. Since the fluorescence emission competes with photochemistry for excitation energy, its measurement provides non-invasive and real-time insight into the dynamics of photosynthetic reactions.

The primary photosynthetic reactions are accomplished in a complex network of mutually coupled linear as well as cyclic processes that serve to transform light into chemical energy (Fig. l., reviewed in Ort and Yocum, 1996). The chemical energy, in the form of ATP and NADPH·H$^+$, is subsequently utilized in the dark phase of photosynthesis to assimilate inorganic carbon (Leegood et al., 2000). As in any complex metabolic system (Csete and Doyle, 2002), robustness of photosynthesis relies on a number of regulatory processes that sustain, coordinate and optimize its function in an uncertain dynamic environment. The complexity of forward redox reactions (Fig. l) combined with feedback regulations (Nedbal and Březina, 2002; Nedbal et al., 2003, 2005) is reflected in complex fluorescence transients occurring in response of plants to a light stimulus. The regulation makes the system-level response of photosynthesis non-linear with significant memory effects.

II. Time Scales

A. Before Photochemistry: In Hundreds of Picoseconds and Earlier

A photon of visible light has a wavelength comparable to the size of a thylakoid granum (Mehta et al., 1999) leading to increased scattering and optical path-length within the photosynthetic membranes. Photons cover the granum diameter in several femtoseconds (~10^{-15} s). If absorbed, its energy brings the pigment molecule to an initially de-localized excited singlet state, called an exciton. The exciton interacts with nuclear vibrations allowing thermal equilibration into the lowest excited singlet state of pigment molecule(s). The electronic dipole-dipole intermolecular interactions cause rapid movement of the molecular excited state towards Chl *a* in pigment-protein complexes of PS I or PS II (Fig. l). The equilibration within the Chl *a* pigment bed occurs effectively on a time scale comparable to the period of nuclear vibrations (~10^{-12} s), which makes the fate of

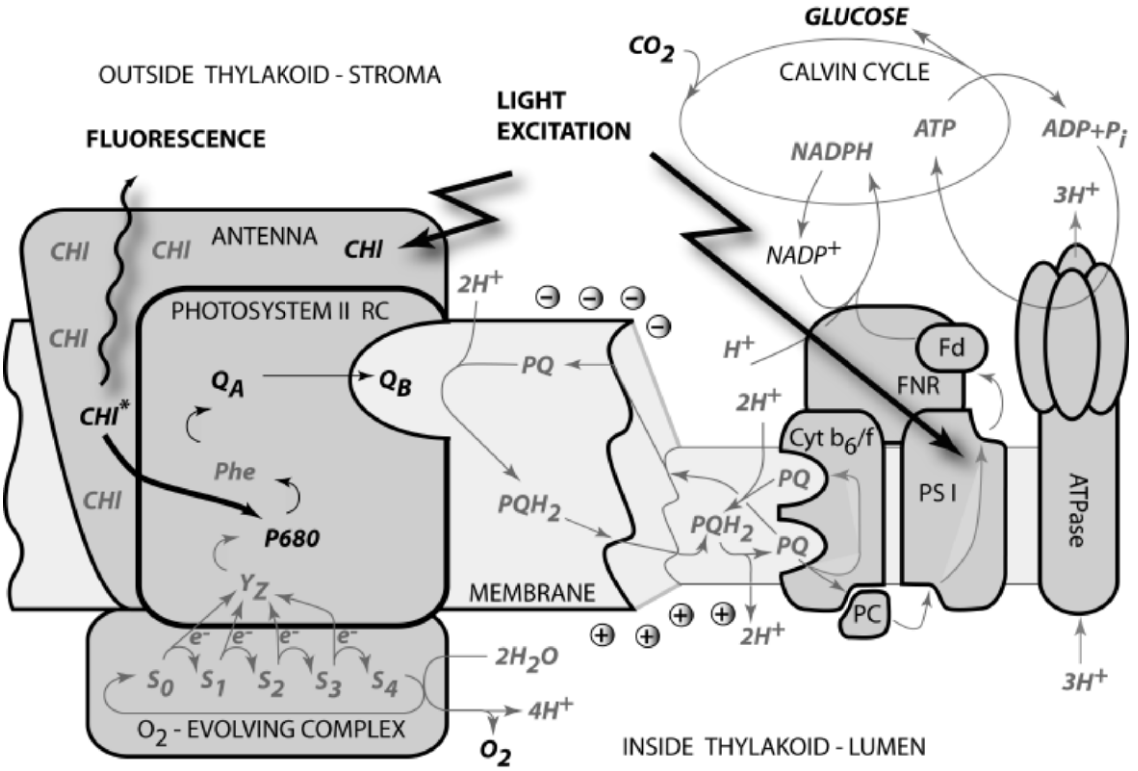

Fig. 1. Schematic presentation of a thylakoid membrane with key photosynthetic modules. Light is absorbed by antenna pigments of PS II (in front) and of PS I (at the back). The excitons generated in the antennae are rapidly transferred to the reaction centers where their energy serves to drive the primary charge separation. In PS II, the primary charge separation to $P680^{+\bullet}$-$Phe^{-\bullet}$ is followed by secondary charge transfer processes: the electrons are extracted by the oxidized primary donor $P680^{+\bullet}$ from water by the O_2-evolving complex and by the Y_Z donor. On the acceptor side, the electron is rapidly stabilized by a transfer from pheophytin ($Phe^{-\bullet}$) to the primary quinone acceptor Q_A. A mobile plastoquinone pool shuttles two electrons sequentially taken from $Q_A^{-\bullet}$ and two protons taken from the stromal side of the membrane to the lumenal side of cytochrome b_6f complex where the protons are released and electrons are sent to PS I. The PS I is using the excitonic energy to generate reductant $NADPH{\cdot}H^+$. The charge transfer reactions in the thylakoid membrane result in an accumulation of protons on the lumenal side and depletion on the stromal side of the thylakoid. The difference in electrochemical potentials is used by ATPase to generate ATP that is used together with $NADPH{\cdot}H^+$ in the Calvin-Benson cycle to assimilate inorganic CO_2 into sugars.

the excitation largely independent of the wavelength of the absorbed photons[1]. With the major fraction of the absorbed photons used for photochemistry in the reaction centers, only several percent are lost by fluorescence emission, thermal de-excitation or intersystem crossing (Latimer et al., 1956).

In higher plants at a physiological temperature, most of the total Chl fluorescence emission originates from PS II. At 683 nm, PS II contributes dominantly, with only a few percent of the total emission originating in PS I (Roelofs et al., 1992). The small fraction of Chl fluorescence that is emitted from PS I and from accessory pigment systems can be distinguished from the dominant PS II emission by its emission wavelength: PS II antenna emits fluorescence that is typically blue-shifted[2], and PS I emits fluorescence that is red-shifted relative to fluorescence from PS II core (Genty et al., 1990). The proportion of PS I fluorescence can increase several times in the long-wavelength range above 700 nm and at low temperatures.

[1] In contrast, fluorescence emission spectra depend on excitation wavelength in organisms such as cyanobacteria or red algae that have spectrally more widely spread peripheral antenna systems transferring excitonic energy less efficiently than the antennae of higher plants. Upon their excitation, the fluorescence emission occurs also from pigments with their singlet excited states higher than those of Chl.

[2] For an exception see Koehne et al., 1999.

B. Photochemistry and Soon Thereafter: From Nanoseconds to Seconds

Upon excitation of the primary donor P680 in the PS II reaction center (Fig. 1), a transient steady-state equilibrium is established between the excited state P680*-Phe and the radical pair state $P680^{+\bullet}$-$Phe^{-\bullet}$ (Schatz et al., 1988). The probability that the separated charges in $P680^{+\bullet}$-$Phe^{-\bullet}$ recombine is reduced in an open PS II reaction center by a rapid transfer of the electron from $Phe^{-\bullet}$ to the primary quinone acceptor Q_A (Fig. 1). The oxidized $P680^{+\bullet}$ accepts an electron from the tyrosine residue Y_Z that, subsequently, oxidizes the manganese cluster, advancing its redox state by one step from S_n to S_{n+1}. Photochemistry in the open PS II reaction centers shortens the excitation lifetime to hundreds of picoseconds, thereby lowering the fluorescence quantum yield to its minimum level F_0 — a phenomenon called photochemical quenching (Duysens and Sweers, 1963).

In contrast, the reduced primary quinone acceptor ($Q_A^{-\bullet}$) in closed PS II reaction centers hinders the primary charge separation by an electrostatic repulsive force (Schatz et al., 1988; Dau and Sauer, 1992), extending the excitation lifetime to several nanoseconds. The longer lifetime in the closed reaction centers leads to an increased fluorescence emission with maximal level F_M ($F_M \approx 5 \times F_0$). The variable part of fluorescence emission, $F_V = F_M - F_0$, reflects the limiting change in the photochemical quenching during transition from open to closed PS II reaction centers[3].

The closed reaction centers re-open with $Q_A^{-\bullet}$ oxidized by the plastoquinone molecule, Q_B, that is reversibly bound to the D1 protein of PS II, close to the stromal side of the thylakoid membrane (Fig. 1). The re-opened reaction center $Q_A/Q_B^{-\bullet}$ can undergo another stable charge separation resulting in $Q_A^{-\bullet}/Q_B^{-\bullet}$ and, eventually, in Q_A/Q_B^{2-}. By accepting two protons from the stroma, a neutral plastoquinol molecule Q_BH_2 is generated and released from PS II. This, in turn, is replaced by another molecule from the mobile plastoquinone pool Q_B. The plastoquinol migrates to the lumenal side of the Cyt b_6f complex where it is oxidized and protons are released. The electrons are transferred further through the chain of redox reactions, moved by another photochemical event in PS I towards the terminal acceptor $NADP^+$ reducing it into $NADPH{\cdot}H^+$.

On the donor side of PS II, the oxidative power of the manganese cluster increases with each turnover of the reaction center in $S_n \rightarrow S_{n+1}$ transitions until S_4 is reached. The S_4 state has oxidative potential capable of oxidizing water, which is split into protons and molecular oxygen, O_2. Four electrons return the manganese cluster to the S_0 state, and four protons add to the difference in the electrochemical potential between the stromal and lumenal sides of the thylakoid membrane. The electrochemical difference across the membrane drives phosphorylation of ADP into ATP. The ATP molecules combined with $NADPH{\cdot}H^+$ provide chemical energy and reducing power to the Calvin-Benson cycle assimilating inorganic CO_2 into sugars in C3 plants.

C. Regulation and Development: From Seconds to Lifetime?

The photochemical activities of both photosystems are coupled by the mobile plastoquinone pool, the Cyt b_6f complex and the soluble plastocyanine/cytochrome carrier. Multiple mobile redox elements make the entire system flexible and robust. PS II centers work in parallel so that damage to a small fraction of the centers has little effect on the overall performance (Behrenfeld et al., 1998). Also, temporal fluctuations and disharmony in the operation of the two photosystems are well buffered by the capacity of mobile carriers. Yet, the light environment of plants is highly dynamic and the long-term balance in the operation of both photosystems must be maintained by regulatory adjustments in optical cross section of their antenna systems or by redistribution of the excitation energy between the photosystems (Senger and Bauer, 1987; Wollman, 2001). Regulation also occurs when ATP and $NADPH{\cdot}H^+$ generated by the concerted operation of both photosystems cannot be effectively used by dark reactions of the Calvin-Benson cycle (Kanazawa and Kramer, 2002). This can be the case, for example, at limiting CO_2 concentrations or at supersaturating irradiance. Then, plants respond with multiple protective mechanisms that lower the excitonic flow to the reaction centers (Horton and Ruban, 1992). The reduction can be achieved by changes in leaf, cellular and thylakoid architectures, the decreased number of pigment-molecules or reaction centers or by quenching of excitonic states in the antenna systems. Either of these mechanisms is reflected in

[3] There is little or no variable fluorescence from PS I because its closed reaction center ($P700^+$) is quenching fluorescence as efficiently as an open reaction center (Nuijs et al., 1986, Dau, 1994).

a decrease of fluorescence emission conventionally called non-photochemical quenching.

The photosynthetic apparatus is also adapting to the biological changes during a cell cycle (Kaftan et al., 1999; Strasser et al., 1999) or during plant and leaf development in response to changing demand for assimilates (Maheswaran et al., 1987; Croxdale and Omasa, 1990; Huner et al., 1993) and the thylakoids are operating in different modes in source and sink leaves or leaf segments.

III. Analysis of Chlorophyll Fluorescence Transients

A. Flash of Light Removes Photochemical Quenching

The redox state of the PS II primary acceptor Q_A can be accurately manipulated by a short intense flash of light. Before the flash, reaction centers are open and have low fluorescence yield (i.e. minimal fluorescence F_0 in the interval 0–0.001s in Fig. 2) because the absorbed energy delivered by the dim measuring light is effectively used by photochemistry without perturbing the dark-adapted state of the plant. During the flash, which lasts typically no more than tens of microseconds, the acceptor Q_A is reduced in all reaction centers (single turnover). In the transiently closed centers, any absorbed energy from the dim measuring light cannot be used for photochemistry and contributes increasingly to fluorescence that is reaching its maximum, F_M (Fig. 2, 0.001 s). Neglecting PS I fluorescence, the limiting fluorescence levels, F_0 and F_M, can be expressed mathematically in relation to the number of PS II units N that are contributing to the measured fluorescence signal, local irradiance I, optical cross section a of PS II (Mauzerall and Greenbaum, 1989) and the rate-constants representing the three major pathways of de-excitation in PS II: k_P^{dark}, rate constant of PS II photochemistry; k_F, rate constant of PS II fluorescence emission; k_N^{dark}, rate constant of non-radiative dissipation which includes thermal dissipation, conversion to triplets and energy transfer outside the PS II reaction centers. The optical cross section of PS II is defined as the black-body area having identical frequency of photon capture with PS II antenna. The rate constant of PS II photochemistry k_P^{dark} is assumed to be negligible in closed reaction centers whereas the other rate constants and optical cross section are generally assumed to be invariant

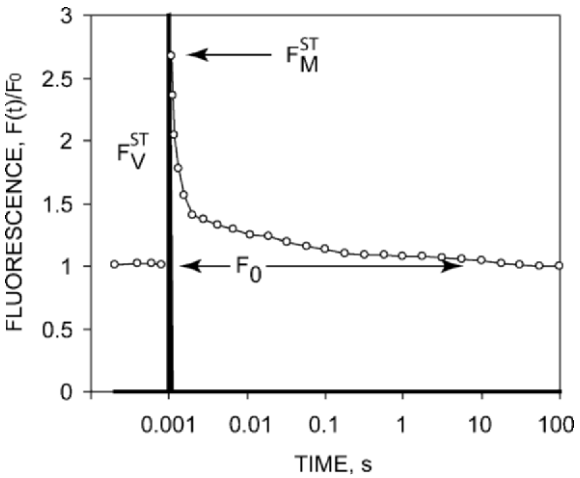

Fig. 2. Fluorescence transient induced in a suspension of the green alga, *Scenedesmus quadricauda,* by a single-turnover flash. The flash profile is schematically indicated by the heavy vertical line at 1 ms after starting the measurement. The irradiance during the flash reaches >0.1 mol (photons) $m^{-2}s^{-1}$ and the flash duration is typically less than 50 µs. Fluorescence was measured before and after the single-turnover flash using sufficiently weak excitation not altering the mean redox state of Q_A (Trtílek et al., 1997). First, 4 dim measuring flashes 250 µs apart were given to measure F_0. After the saturating flash at 1 ms, the dim measuring flashes were logarithmically spaced (4 measurements/decade) to increase the dynamic range of the data collection with very rapid sampling of the active centers in the initial phase and progressively slower sampling of inactive reaction centers in the final phase of the fluorescence transient.

in the measurements of F_0 and of F_M:

$$F_0 = (N \cdot I \cdot a)^{\text{dark}} \cdot k_F/(k_F + k_N^{\text{dark}} + k_P^{\text{dark}}) \quad (1)$$

$$F_M = (N \cdot I \cdot a)^{\text{dark}} \cdot k_F/(k_F + k_N^{\text{dark}}) \quad (2)$$

The maximum quantum yield of photochemistry, $\Phi_P^{\max}$, in open reaction centers is controlled by the same rate constants[4] and, thus, can be calculated from the measured fluorescence levels, F_0 and F_M (Malkin and Kok, 1966):

$$\Phi_P^{\max} = k_P^{\text{dark}}/(k_F + k_N^{\text{dark}} + k_P^{\text{dark}}) = (F_M - F_0)/F_M \equiv F_V/F_M \quad (3)$$

After the flash in Fig. 2, the Q_A acceptor is gradually oxidized by the plastoquinone Q_B, thereby restoring the charge separation capacity of the reaction center.

[4] This assumption may not be always true: k_N^{dark} constants may differ in open and closed reaction center (Koblížek et al., 1999)

Proportionately with the increasing number of re-opened reaction centers, the fluorescence drops as the photochemical quenching recovers (0.001–100 s in Fig. 2). The photochemical quenching, q_P, is frequently used to estimate the relative fraction of PS II reaction centers that are open at time t when the intermediate fluorescence levels, $F(t)$ are measured[5]:

$$q_P(t) \equiv (F_M - F(t))/(F_M - F_0) \approx [PS\,II^{open}/(PS\,II^{open} + PS\,II^{closed})](t) \quad (4)$$

The drop of fluorescence caused by the re-opening of the reaction centers after the flash proceeds with multiphase kinetics, that are usually resolved into three exponential phases, or, alternatively, into two exponentials and one hyperbolic phase (Vass et al., 1999). These are interpreted as reflecting heterogeneity of the acceptor side of PS II.

Product of the maximum quantum yield of photochemistry, Φ_P^{max} (see Eq. 3), multiplied by the fraction of open reaction centers measured by photochemical quenching, q_P (see Eq. 4) gives an estimate of the instantaneous quantum yield of photochemistry, $\Phi_P(t)$ (Paillotin, 1978):

$$\Phi_P(t) = \Phi_P^{max} \cdot q_P(t) = (F_M - F(t)) / F_M \quad (5)$$

Equations (4) and (5) link physiologically important parameters with the measured fluorescence signals.

B. Single-turnover Induction Reveals Antenna Functional Cross Section and Connectivity

The kinetics of the fluorescence transient from F_0 to F_M, induced by a single-turnover flash, reports on rates at which the light is captured and processed in PS II reaction centers (Kolber et al., 1998, Nedbal et al., 1999). The single-turnover transient is similar to that observed on a much longer time scale and in a weaker light when plants have the re-oxidation of $Q_A^{-\bullet}$ blocked by herbicides (e.g., DCMU). Simple models assuming uniform and isolated PS II (used in Eqs.4 and 5) predict a mono-exponential character of the transients. However, the measured induction transients in higher plants and green algae are typically sigmoidal (Joliot and Joliot, 1964; Koblížek et al., 2001). The sigmoidal kinetics can be explained assuming that an excitation generated in an antenna of a closed PS II reaction center can move to a neighboring PS II reaction center. The phenomenon of inter-unit excitation transfer is usually termed 'antenna connectivity.' With p being the probability of such a process, photochemical quenching can be related to the fraction of open reaction centers by Eq. (6a):

$$q_P \equiv (F_M - F_{(t)}) / (F_M - F_0) = \frac{PS\,II^{open}}{PS\,II^{open} + PS\,II^{closed} \cdot (1-p)} \quad (6a)$$

Equation (6a) is frequently re-formulated to show explicitly the hyperbolic relation between the photochemical quenching and the fraction of open reaction centers. To achieve that, a hyperbola constant C was introduced initially by Strasser (Strasser, 1978, 1981). Alternatively, the sigmoidicity parameter, $J \equiv p/(1-p)$ (Lavergne and Trissl, 1995), which is a numeric equivalent of the earlier Strasser's C is used dominantly in current literature to re-formulate Eq.(6a) into Eq.(6b):

$$q_P = \frac{PS\,II^{open}}{PS\,II^{open} + PS\,II^{closed}} \cdot (1+J) / (1 + J \cdot \frac{PS\,II^{open}}{PS\,II^{open} + PS\,II^{closed}}) \quad (6b)$$

The rate at which the PS II reaction centers are closed by irradiance I can be estimated from Eq. (7):

$$-\frac{d}{dt}\frac{PS\,II^{open}}{PS\,II^{open} + PS\,II^{closed}} = I \cdot \sigma_{PSII} \frac{PS\,II^{open}}{PS\,II^{open} + PS\,II^{closed}} (1+J) / (1 + J \cdot \frac{PS\,II^{open}}{PS\,II^{open} + PS\,II^{closed}}) \quad (7)$$

Numerical methods applied to Eqs. (6) and (7) can be used to find the sigmoidicity factor, J, and the PS II functional cross section, $\sigma_{PS\,II} = a \cdot \Phi_P^{max}$, that yield the best fit of experimental data by model kinetics. J values are typically found (Koblížek et al., 2001) in

[5] The estimate is based on an assumption of uniform and mutually isolated PS II. Corrections are necessary when other quenching mechanisms are present, PS II reaction centers are heterogeneous and the connectivity of antenna systems is considered.

the range from 0 (no connectivity, $p \approx 0$) to 1.5 (high connectivity, $p \approx 0.6$) with examples of fluorescence kinetics of extreme sigmoidicity shown in Fig. 3.

The introduction of connectivity does not perturb Eq. (5) which relates the instantaneous quantum yield of photochemistry $\Phi_P(t)$ with fluorescence data. Identical formula to Eq. (5) can be derived by combining Eqs. (6b) and Eq. (7).

C. Multi-turnover Induction Reflects Complexity

Plants, exposed to light of lower irradiance compared to that of a single-turnover flash, respond by a complex transient of fluorescence emission that is reflecting incoherent multiple-turnover transitions (Strasser et al., 1995; Lazár, 1999). The fluorescence transients consist of two major phases: the initial rise from the F_0 level to the fluorescence maximum labeled F_P (or F_M when Q_A is fully reduced) and the decline from F_P to the steady-state F_S (Fig. 4). The shape of the initial rise is polyphasic depending on the applied irradiance (Strasser et al., 1995; Kolber et al., 1998). In high irradiance, it consists of three (F_J, F_I, F_P in Strasser et al., 1995, alternatively, I_1-I_2-P in Neubauer and Schreiber, 1987) or, in heat stressed plants, four (F_K, F_J, F_I, F_P) phases, that are conveniently visualized on a logarithmic time-scale covering an interval from tens of microseconds to a second (Strasser et al., 1998).

The polyphasic fluorescence rise is characterized by the extreme emission levels F_0 and F_M (F_P), the initial rate of the rise, $(dF_V/dt)_{t\to 0+}$, the time integral,

$$\int_0^\infty (F_M - F(t))dt \,,$$

and by the independent amplitudes of the fluorescence rise phases, (F_{Vj}, F_{Vi}). A model was proposed (Strasser et al., 1998) to interpret the individual fluorescence characteristics on a molecular level. The parameters of the initial fluorescence rise are highly sensitive to the physiological state of the plant and may serve as an efficient screening tool (Strasser et al., 1998).

D. Non-photochemical Quenching Reflects Photoprotection

In a light-adapted plant, steady-state fluorescence, F_S, reflects a dynamic equilibrium between Q_A oxidation and reduction leading to a steady-state ratio of open and closed PS II reaction centers and, thus, to an intermediate level of photochemical quenching, q_P (see Eq. 6). Similar to the protocol described in Section III.A, the photochemical quenching can be transiently eliminated by a saturating flash to measure the maximum fluorescence, F_M', with all PS II centers closed (Fig. 4). F_M' measured in a light-adapted plant,

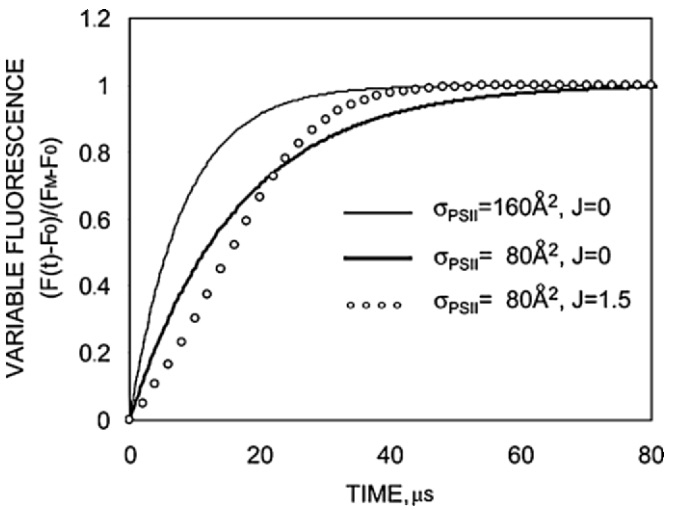

Fig. 3. Variable fluorescence calculated from Eqs. (6) and (7) for 3 types of PS II antenna systems. Isolated PS II antenna of a large functional cross section (thin line); isolated PS II antenna of a small functional cross section (heavy line); and, connected PS II antenna systems of a small functional cross section (open circles). The timescale corresponds to a light flux 0.1 mol (photons) $m^{-2}s^{-1}$ during a rectangular single-turnover flash of 650 nm.

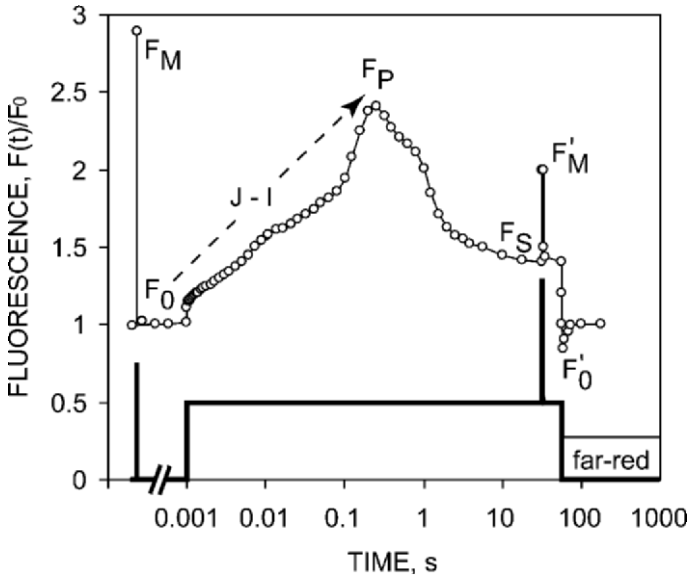

Fig. 4. Schematic presentation of a fluorescence transient based on a measurement with a suspension of the green alga, *Scenedesmus quadricauda*. The actinic light profile is schematically indicated by the heavy line at the bottom of the figure. The irradiance of the actinic light inducing the transient is typically in hundreds of μmol (photons) m^{-2} s^{-1}, whereas the irradiance of the saturating flashes (indicated by vertical lines) is typically stronger by one order of magnitude. After F_0 measurement, the saturating flash transiently reduced the plastoquinone pool to read F_M in dark-adapted cells. The F_0 emission was restored by a dark adaptation before actinic light was switched on (0.001s). The fluorescence rose to F_P level passing phases *J* and *I*. The decline to steady-state level reflected acclimation to the actinic irradiance. A second saturating flash was given to determine maximal fluorescence in the light-adapted plant F_M' that was diminished relative to F_M by non-photochemical quenching. The visible actinic light was replaced by far-red light at the end of the experiment to reveal the F_0' emission of the light-adapted plant.

is typically lower than the corresponding parameter F_M measured in the dark (Fig. 4)[6]. The difference between F_M and F_M' reflects non-photochemical quenching that is used by plants to cope with irradiance that is exceeding the photosynthetic capacity (Horton and Ruban, 1992). The non-photochemical quenching affects also the F_0' level. The F_0' fluorescence is measured in light-adapted plants after the visible light is switched off and replaced by a far-red irradiance that can rapidly oxidize the plastoquinone pool thus opening all PS II centers and maximizing the photochemical quenching (Fig. 4). In analogy to Eqs. (1) and (2), the following relations are derived for the limiting levels of fluorescence in light-adapted plants[7]:

$$F_0' = (N \cdot I \cdot a)^{light} \cdot k_F / (k_F + k_N^{\,\mathrm{light}} + k_P^{\,\mathrm{light}}) \qquad (8)$$

$$F_M' = (N \cdot I \cdot a)^{light} \cdot k_F / (k_F + k_N^{\,\mathrm{light}}) \qquad (9)$$

The non-photochemical quenching reducing F_M', F_0' relative to F_M, F_0 can be caused by increased non-photochemical dissipation $k_N^{light} > k_N^{dark}$ that is accompanied by corresponding shortening of the fluorescence lifetime (Dau and Hansen, 1990). Though terminologically incorrect, the term non-photochemical quenching is conventionally also used to describe the lowering of fluorescence due to lower light absorption ($I^{light}.a^{light} < I^{dark}.a^{dark}$) or a decrease in PS II numbers ($N^{light} < N^{dark}$). Lower light absorp-

[6] The prime symbol (e.g., in F_M', F_0' and F_V' and in Φ_P' and q_P') was introduced to indicate that the respective parameters were measured in a light-adapted plant. This 'prime' symbolism is, however, used inconsistently, e.g., *F(t)* is often used to represent fluorescence after *t* seconds of irradiance or F_S stands for steady-state equilibrium fluorescence reached after a long light exposure. Here, we combine the widely accepted 'prime' symbolism with explicit superscript labels 'light' and 'dark' wherever no historical precedent is known to us.

[7] Due to the homology between Eqs.8, 9 and Eqs.1, 2, the maximum quantum yield of PS II photochemistry ($\Phi_P^{\max}$), the instantaneous photochemical quenching $q_P(t)$ and the instantaneous quantum yield of PS II photochemistry $\Phi_P(t)$ can be quantified in light-adapted plants using Eqs.3-5 derived for dark-adapted plants. Only, F_M' and F_0' parameters must be used instead of F_M and F_0.

tion or a lower proportion of PS II centers preserves measured fluorescence lifetimes, and can thereby be distinguished from changes affecting the rate constant of non-photochemical energy dissipation, k_N.

In another classification, diverse types of non-photochemical quenching are distinguished by relaxation kinetics in the dark (Horton et al., 2000; Krause and Jahns, 2002). The fastest kinetics of relaxation (tens of seconds) is attributed to energy-dependent quenching mechanisms, $q_{N,E}$, that fade away with the difference in proton gradient across the thylakoid membrane (Briantais et al., 1979, 1980). The slower recovery kinetics (tens of minutes), $q_{N,T}$, is usually interpreted as reflecting detachment of an outer light harvesting antennae complex from PS II (Bennett et al., 1980; Wollman, 2001). Finally, the slowest phase is interpreted as recovery from photoinhibitory quenching, $q_{N,I}$, that is due to photodamage of PS II centers by high irradiance (Šetlík et al., 1990; Tyystjärvi and Aro, 1996).

The non-photochemical quenching is usually quantified using the difference between the maximum fluorescence measured in dark, F_M, and the one measured after a light exposure, F_M': $NPQ=(F_M - F_M')/F_M'$ (Bilger and Björkman, 1990)[8]. Assuming that the integral excitonic flow to reaction centers is constant, $(N.I.a)^{dark} \approx (N.I.a)^{light}$, and that the photoprotection is provided by an increase in the Stern-Volmer non-photochemical de-excitation rate, k_N^{light} relative to k_N^{dark}, NPQ can be used to measure light-induced changes in the concentration of the quencher. In the other limiting model case of reduced optical cross section or reduced number of contributing PS II units, NPQ quantifies the relative reduction in the integral flow of excitation to PS II centers that is caused by the light acclimation.

Assuming that the non-photochemical quenching is caused solely by change of k_N (i.e. no change in N, a or I), the relationship between the instantaneous yield of photochemistry, Φ_P', and the fluorescence parameters similar to Eq. (5) can be extended also to plants acclimated to light:

$$\Phi_P' = (F_M' - F_S)/F_M' \qquad (10)$$

Here, prime symbols indicate steady-state parameters measured in actinic light and F_S steady-state fluorescence. Eq. (10) is frequently used in plant physiology to estimate steady-state photosynthetic electron transport rates in conditions when primary photochemistry drives dominantly the linear photosynthetic electron flow. This relationship was experimentally verified in higher plants by Genty et al. (1989).

IV. Beyond the Conventional Analysis

A. Modulation by Redox Components

In a plant exposed to a strong nanosecond laser pulse, the fluorescence emission reaches its maximum only after a 35 μs delay once the Q_A acceptor is fully reduced (Mauzerall, 1972). The delay in reaching full F_M level is explained by a quenching of fluorescence due to transient appearance of oxidized PS II donor $P680^{+\bullet}$ (Sonneveld et al., 1979; Steffen et al., 2001) and of carotenoid triplets generated in the nanosecond flash (Breton et al., 1979).

Significant variability of F_M is also found with different techniques of Q_A reduction (Delosme, 1967; Kolber et al., 1998): F_M^{MT} measured in a multiple turnover pulse is typically higher than F_M^{ST} obtained using a single turnover flash. F_M^{DCMU} measured in presence of DCMU, the herbicide that inhibits Q_A reoxidation, is typically slightly lower than F_M^{MT} obtained in a multiple-turnover flash and higher than F_M^{ST} measured by the single turnover flash: that is, $F_M^{MT} > F_M^{DCMU} > F_M^{ST}$. Static quenching, by an oxidized plastoquinone pool directly interacting with the LHCII antenna chlorophylls during a single-turnover measurement, was proposed to account for the difference between F_M^{MT} and F_M^{ST} (Samson and Bruce, 1996; Vasil'ev and Bruce, 1998). Samson et al. (1999) tentatively explained the lowering of the single-turnover F_M^{ST} relative to F_M^{DCMU} by a quenching by the oxidized plastoquinone molecule bound in the Q_B pocket of herbicide-free PS II reaction centers.

Soon after the discovery of the sequential four-step mechanism of oxygen evolution by Joliot and Kok (Kok et al., 1970; Joliot et al., 1971), it was found that individual S-states of the water-splitting complex modulate both F_0 and F_M (Delosme, 1971; Joliot and Joliot, 1971; Zankel, 1973). Sonneveld et al. (1979) proposed that the life-time of $P680^{+\bullet}$ is S-state dependent, thereby affecting the F_M yield. However, this cannot explain the modulation of F_0 since it is

[8] Alternatively to the NPQ parameter, the photoprotective mechanisms are frequently quantified using light-induced reduction of variable fluorescence (van Kooten and Snel,, 1990: $q_N \equiv (F_V - F_V')/F_V$. The interpretation of q_N is more complex than with NPQ because it reflects not only non-photochemical quenching but also light-induced changes in photochemical rates.

measured on a time scale substantially exceeding the life-time of $P680^{+\bullet}$. Koblížek et al. (2001) showed that individual S-states differ in their photochemical yields, which suggests that the F_0 modulation by the S-states may be caused by the changes in the rate constant of the primary photochemistry, k_P.

B. PS II Heterogeneity

Uniform PS II units are expected to yield monophasic induction kinetics. However, the measured fluorescence transients consist frequently of multiple kinetically distinct components (Melis and Homann, 1975). Melis and Duysens (1979) interpreted such kinetics as reflecting the presence of two distinct sets of PS II units: PS II_α having large, mutually connected antenna systems and PS II_β with smaller isolated antenna systems. In higher plants, PS II_β typically account for about 30% of the total PS II having an optical cross section about half that of PS II_α (Lavergne and Briantais, 1996).

Another type of heterogeneity was found in the rates of $Q_A^{-\bullet}$ reoxidation. A substantial fraction of PS II reaction centers is unable to oxidize $Q_A^{-\bullet}$ at physiologically meaningful rates (Chylla et al., 1987). These inactive reaction centers are manifested in fluorescence induction in low light as the fastest kinetic component reflecting rapid accumulation of $Q_A^{-\bullet}$. In the fluorescence decline following the single-turnover flash, the inactive PS II reaction centers are responsible for the slowest component. The physiological role of the inactive reaction centers remains controversial (Lavergne and Briantais, 1996).

V. Prospects of the Technique and Instrumentation

Chl fluorescence measurements became widespread with the introduction of Pulse Amplitude Modulation fluorometers (PAM), separating fluorescence emission excited by measuring flashes from slowly changing background signals (Schreiber et al., 1986). Recently, the availability of high intensity light emitting diodes and the use of processor-controlled electronics made it possible to design a new generation of fluorometers which achieve time resolution in the microsecond range (Trtílek et al., 1997; Kolber et al., 1998; Strasser et al., 1998). The new light sources provide rectangular single-turnover pulses used for measurements of functional cross section and connectivity analysis (Kolber et al., 1998; Nedbal et al., 1999). Heterogeneity in Chl fluorescence emission over a plant surface can be mapped by kinetic fluorescence imaging (reviewed in Nedbal and Whitmarsh, 2004). The measured leaf or canopy area will be increased in the near future to facilitate applications of Chl fluorescence imaging in precision farming, a post-harvest quality control and in high-throughput mutant screening. Light Detection and Ranging (LIDAR) fluorometers resolving multiple kinetic parameters are being developed for applications in ecophysiology (Kolber et al., 2005). Substantial activity is emerging in the remote sensing of vegetation fluorescence detected in and near Fraunhofer lines and O_2 absorption lines in red and far-red bands (Theisen, 2002). At the other extreme, the resolution of the kinetic fluorescence imaging will be increased to optical diffraction limits to facilitate monitoring of photochemical activities within a single chloroplast (Küpper et al., 2000). Novel fluorescence techniques need to be designed to resolve regulatory processes that have, until now, escaped fluorescence detection because of their relatively slow kinetics (Nedbal and Březina, 2002, Nedbal et al., 2003, 2005).

Acknowledgments

This work was supported in part by the Czech Department of Education, Sports and Youth under Grant MSM6007665808, by the Institute of Landscape Ecology Grant AV0Z60870520 and by the Grant Agency of the Czech Republic GACR 206/05/0894 and 204/05/0307. Critical reading and helpful comments of Drs. Govindjee, Quigg, Strasser, Tsimilli–Michael and Trissl are gratefully acknowledged.

References

Behrenfeld M, Prášil O, Kolber Z, Babin M and Falkowski P (1998) Compensatory changes in Photosystem II electron turnover rates protect photosynthesis from photoinhibition. Photosynth Res 58: 259–268

Bennett J, Steinback K and Arntzen C (1980) Chloroplast phosphoproteins: Regulation of excitation energy transfer by phosphorylation of thylakoid membranes. Proc Natl Acad Sci USA 77: 5253–5257

Bilger W and Björkman O (1990) Role of the xanthophyll cycle in photoprotection elucidated by measurements of light-induced absorbance changes, fluorescence and photosynthesis in leaves of *Hedera canariensis*. Photosynth Res 25: 173–185

Bolhár-Nordenkampf H, Long S, Baker N, Öquist G, Schreiber U

and Lechner E (1989) Chlorophyll fluorescence as a probe of the photosynthetic competence of leaves in the field: A review of current instrumentation. Funct Ecol 3: 497–514

Breton J, Geacintov N and Swenberg C (1979) Quenching of fluorescence by triplet excited states in chloroplasts. Biochim Biophys Acta 548: 616–635

Briantais J, Vernotte C, Picaud M and Krause G (1979) A quantitative study of the slow decline of chlorophyll a fluorescence in isolated chloroplasts. Biochim Biophys Acta 548: 128–138

Briantais J, Vernotte C, Picaud M and Krause G (1980) Chlorophyll fluorescence as a probe for the determination of the photo-induced proton gradient in isolated chloroplasts. Biochim Biophys Acta 591: 198–202

Chylla RA, Garab G and Whitmarsh J (1987) Evidence for slow turnover in a fraction of PS II complexes in thylakoid membranes. Biochim Biophys Acta 894: 562–571

Croxdale JG and Omasa K (1990) Chlorophyll-*a* fluorescence and carbon assimilation in developing leaves of light-grown cucumber. Plant Physiol 93: 1078–1082

Csete M and Doyle J (2002) Reverse engineering of biological complexity. Science 295: 1664–1669

Dau H (1994) Molecular mechanisms and quantitative models of variable Photosystem II fluorescence. Photochem Photobiol 60: 1–23

Dau H and Hansen U (1990) A study on the energy-dependent quenching of chlorophyll fluorescence by means of photoacoustic measurements. Photosynth Res 25: 269–278

Dau H and Sauer K (1992) Electric field effect on the picosecond fluorescence of Photosystem II and its relation to the energetics and kinetics of primary charge separation. Biochim Biophys Acta 1102: 91–106

DeEll J, van Kooten O, Prange R and Murr D (1999) Applications of chlorophyll fluorescence techniques in post harvest physiology. Hort Rev 23: 69–107

Delosme R (1967) Etude de l'induction de fluorescence des algues vertes et des chloroplastes au debut d'une illumination intense. Biochim Biophys Acta 143: 108–128

Delosme R (1971) New results about chlorophyll fluorescence 'in vivo.' In: Forti G, Avron M and Melandri A (eds) 2nd International Congress on Photosynthesis Research, pp 187–195. Dr. W. Junk, The Hague

Duysens LNM and Sweers HE (1963) Mechanism of the two photochemical reactions in algae as studied by means of fluorescence. In*:* Studies on Microalgae and Photosynthetic Bacteria, Japanese Soc Plant Physiol, pp 353–372. University of Tokyo Press, Tokyo

Falkowski P and Kolber Z (1995) Variations in chlorophyll fluorescence yields in phytoplankton in the world oceans. Aust J Plant Physiol 22: 341–355

Genty B, Briantais J-M and Baker NR (1989) The relationship between the quantum yield of photosynthetic electron transport and quenching of chlorophyll fluorescence. Biochim Biophys Acta 990: 87–92

Genty B, Wonders J and Baker N (1990) Non-photochemical quenching of Fo in leaves is emission wavelength dependent—Consequences for quenching analysis and its interpretation. Photosynth Res 26: 133–139

Govindjee (1995) Sixty-three years since Kautsky: Chlorophyll *a* fluorescence. Aust J Plant Physiol 22: 131–160

Horton P and Ruban A (1992) Regulation of Photosystem II. Photosynth Res 34: 375–385

Horton P, Ruban A and Wentworth M (2000) Allosteric regulation of the light-harvesting system of Photosystem II. Phil Trans R Soc Lond B 355: 1361–1370

Huner N, Öquist G, Hurry V, Krol M, Falk S and Griffith M (1993) Photosynthesis, photoinhibition and low temperature acclimation in cold tolerant plants. Photosynth Res 37: 19–39

Jalink H, van der Schoor R, Frandas A, van Pijlen J and Bino R (1998) Chlorophyll fluorescence of *Brassica oleracea* seeds as a non-destructive marker for seed maturity and seed performance. Seed Sci Res 8: 437–443

Joliot A and Joliot P (1964) Etudes cinétique de la réaction photochimique libérant l'oxygène au cours de la photosynthèse. CR Acad Sci Paris 258D: 4622–4625

Joliot P and Joliot A (1971) Studies on the quenching properties of Photosystem II electron acceptor. In*:* Forti G, Avron M and Melandri A (eds) Proceedings of the 2nd international Congress on Photosynth Research, pp 26–38. Dr. W Junk NV Publishers, The Hague

Joliot P, Joliot A, Bouges B and Barbieri G (1971) Studies of System II photocenters by comparative measurements of luminescence, fluorescence and oxygen emission. Photochem Photobiol 14: 287–305

Kaftan D, Meszaros T, Whitmarsh J and Nedbal L (1999) Characterization of Photosystem II activity and heterogeneity during the cell cycle of the green alga *Scenedesmus quadricauda*. Plant Physiol 120: 433–441

Kanazawa A and Kramer D (2002) In vivo modulation of nonphotochemical exciton quenching (NPQ) by regulation of the chloroplast ATP synthase. Proc Natl Acad Sci USA 99: 12789–12794

Kautsky H and Hirsch A (1931) Neue Versuche zur Kohlensäureassimilation. Naturwissenschaften 19: 964

Koblížek M, Ciscato M, Komenda J, Kopecký J, Šiffel P and Masojídek J (1999) Photoadaptation in the green alga *Spongiochloris* sp. A three-fluorometer study. Photosynthetica 37: 307–323

Koblížek M, Kaftan D and Nedbal L (2001) On the relationship between the non-photochemical quenching of the chlorophyll fluorescence and the Photosystem II light harvesting efficiency. A repetitive flash fluorescence induction study. Photosynth Res 68: 141–152.

Koehne B, Elli G, Jennings R, Wilhelm C and Trissl H (1999) Spectroscopic and molecular characterization of a long wavelength absorbing antenna of *Ostreobium* sp. Biochim Biophys Acta 1412: 94–107

Kok B, Forbush B and McGloin M (1970) Cooperation of charges in photosynthetic O_2 evolution — 1. A linear four step mechanism. Photochem Photobiol 11: 457–475

Kolber Z, Klimov D, Ananyev G, Rascher U, Berry JA and Osmond CB (2005) Measuring photosynthetic parameters at a distance: Laser induced fluorescence transient (LIFT) method for remote measurements of PSII in terrestrial vegetation. Photosynth Res 84: 121–129

Kolber Z, Prášil O and Falkowski P (1998) Measurements of variable chlorophyll fluorescence using fast repetition rate techniques. I. Defining methodology and experimental protocols. Biochim Biophys Acta 1367: 88–106

Kramer D and Crofts A (1996) Control and measurement of photosynthetic electron transport in vivo. In*:* Baker N (ed) Photosynthesis and the Environment, pp 25–66. Kluwer Academic Publishers, Dordrecht

Krause G and Jahns P (2002) Pulse amplitude modulated chlorophyll fluorometry and its application in plant science. In: Green B and Parson W (eds) Light Harvesting Antennas, pp 373–399. Kluwer Academic Publishers, Dordrecht

Küpper H, Šetlík I, Trtílek M and Nedbal L (2000) A microscope for two-dimensional measurements of in vivo chlorophyll fluorescence kinetics using pulsed measuring light, continuous actinic light and saturating flashes. Photosynthetica 38: 553–570

Latimer P, Bannister T and Rabinowitch E (1956) Quantum yields of fluorescence of plant pigments. Science 124: 585–586

Lavergne J and Briantais J-M (1996) Photosystem II heterogeneity. In: Ort D and Yocum C (eds) Oxygenic Photosynthesis: The Light Reactions, pp 265–287. Kluwer Academic Publishers, Dordrecht

Lavergne J and Trissl H (1995) Theory of fluorescence induction in Photosystem II: Derivation of analytical expressions in a model including exciton-radical-pair equilibrium and restricted energy transfer between photosynthetic units. Biophys J 68: 2474–2492

Lazár D (1999) Chlorophyll *a* fluorescence induction. Biochim Biophys Acta 1412: 1–28

Leegood R, Sharkey T and von Caemmerer S (eds) (2000) Photosynthesis: Physiology and Metabolism. Kluwer Academic Publishers, Dordrecht

Lichtenthaler H and Miehé J (1997) Fluorescence imaging as a diagnostic tool for plant stress. Trends Plant Sci 2: 316–320

Maheswaran S, Popovic R, Colbow K and Vidaver W (1987) Chlorophyll fluorescence in leaves and cells of light-grown maize (*Zea mays*) during development. J Plant Physiol 130: 173–179

Malkin S and Kok B (1966) Fluorescence induction studies in isolated chloroplasts. I. Number of components involved in the reaction and quantum yields. Biochim Biophys Acta 126: 413–432

Mauzerall D (1972) Light induced fluorescence changes in *Chlorella*, and the primary photoreactions for the production of oxygen. Proc Natl Acad Sci USA 69: 1358–1362

Mauzerall D and Greenbaum N (1989) The absolute size of a photosynthetic unit. Biochim Biophys Acta 974: 119–140

Mehta M, Sarafis V and Critchley C (1999) Thylakoid membrane architecture. Plant Physiol 26: 709–716

Melis A and Duysens L (1979) Biphasic energy conversion kinetics and absorbance difference spectra of Photosystem II of chloroplasts. Evidence for two different Photosystem II reaction centers. Photochem Photobiol 29: 373–382

Melis A and Homann P (1975) Kinetic analysis of the fluorescence induction in DCMU poisoned chloroplasts. Photochem Photobiol 21: 431–437

Mohammed G, Binder W and Gillies S (1995) Chlorophyll fluorescence: A review of its practical forestry applications and instrumentation. Scan J Forest Res 10: 383–410

Müller N (1874) Beziehungen zwischen Assimilation, Absorption und Fluoreszenz im Chlorophyll des lebenden Blattes. Jahrb Wiss Bot 9: 42–49

Nedbal L and Březina V (2002) Complex metabolic oscillations in plants forced by harmonic irradiance. Biophys J 83: 2180–2189

Nedbal L and Whitmarsh J (2005) Chlorophyll fluorescence imaging of leaves. In: Papageorgiou G and Govindjee (eds) Chlorophyll *a* fluorescence: A Signature of Photosynthesis, pp 389–407. Kluwer Academic Publishers, Dordrecht

Nedbal L, Trtílek M and Kaftan D (1999) Flash fluorescence induction: A novel method to study regulation of Photosystem II. J Photochem Photobiol 48: 154–157

Nedbal L, Soukupová J, Whitmarsh J and Trtílek M (2000) Postharvest imaging of chlorophyll fluorescence from lemons can be used to predict fruit quality. Photosynthetica 38: 571–579

Nedbal L, Březina V, Adamec F, Štys D, Oja V, Laisk A and Govindjee (2003) Negative feedback regulation is responsible for the non-linear modulation of photosynthetic activity in plants and cyanobacteria exposed to a dynamic light environment. Biochim Biophys Acta 1607: 5-17

Nedbal L, Březina V, Červený J and Trtílek M (2005) Photosynthesis in dynamic light: Systems biology of unconventional chlorophyll fluorescence transients in *Synechocystis* sp. PCC6803. Photosynth Res 84: 99–104

Neubauer C and Schreiber U (1987) The polyphasic rise of chlorophyll fluorescence upon onset of strong continuous illumination: I. Saturation characteristics and partial control by the Photosystem II acceptor side. Z Naturforsch 42C: 1246–1254

Nuijs A, Shuvalov V, van Gorkom H, Plijter J and Duysens L (1986) Picosecond absorbance-difference spectroscopy on the primary reactions and antenna-excited states in Photosystem I particles. Biochim Biophys Acta 850: 310–318

Ort D and Yocum C (eds) (1996) Oxygenic Photosynthesis: The Light Reactions. Kluwer Academic Publishers, Dordrecht

Paillotin G (1978) Organization of the photosynthetic pigments and transfer of excitation energy. In: Hall D, Coombs, J and Goodwin TW (ed) Photosynthesis '77, pp 33–44. The Biochemical Society, London

Roelofs T, Lee C-H and Holzwarth A (1992) Global target analysis of picosecond chlorophyll fluorescence kinetics from pea chloroplasts. Biophys J 61: 1147–1163

Samson G and Bruce D (1996) Origins of the low-yield of chlorophyll-*a* fluorescence induced by single turnover flash in spinach thylakoids. Biochim Biophys Acta 1276: 147–153

Samson G, Prášil O and Yaakoubd B (1999) Photochemical and thermal phases of chlorophyll *a* fluorescence. Photosynthetica 37: 163–182

Schatz G, Brock H and Holzwarth A (1988) Kinetic and energetic model for the primary processes in Photosystem II. Biophys J 54: 397–405

Schreiber U, Schliwa U and Bilger W (1986) Continuous recording of photochemical and non-photochemical chlorophyll fluorescence quenching with a new type of modulation fluorometer. Photosynth Res 10: 51–62

Senger H and Bauer B (1987) The influence of light-quality on adaptation and function of the photosynthetic apparatus. Photochem Photobiol 45: 939–946

Šetlík I, Allakhverdiev S, Nedbal L, Šetlíková E and Klimov V (1990) Three types of Photosystem II photoinactivation. 1. Damaging processes on the acceptor side. Photosynth Res 23: 39–48

Sonneveld A, Rademaker H and Duysens L (1979) Chlorophyll *a* fluorescence as a monitor of nanosecond reduction of the photooxidized pripary donor P-680$^+$ of Photosystem II. Biochim Biophys Acta 548: 536–551

Steffen R, Christen G and Renger G (2001) Time-resolved monitoring of flash-induced changes of fluorescence quantum yield and decay of delayed light emission in oxygen-evolving photosynthetic organisms. Biochemistry 40: 173–180

Strasser R (1978) The grouping model of plant photosynthesis. In: Akoyunoglou G (ed) Chloroplast Development, pp 513–542. Elsevier, Amsterdam

Strasser R (1981) The grouping model of plant photosynthesis: Heterogeneity of photosynthetic units in thylakoids. In: Akoyunoglou G (ed) Photosynthesis III. Structure And Molecular Organisation of the Photosynthetic Apparatus, pp 727–737. Balaban International Science Service, Philadelphia

Strasser R, Srivastava A and Govindjee (1995) Polyphasic chlorophyll *a* fluorescence transient in plants and cyanobacteria. Photochem Photobiol 61: 32–42

Strasser RJ, Srivastava A and Tsimilli–Michael M (1998) The fluorescence transient as a tool to characterize and screen photosynthetic samples. In: Mohanty P, Yunus M and Pathre U (eds) Probing Photosynthesis: Mechanism, Regulation and Adaptation, pp 1–53. Taylor & Francis, London

Strasser B, Dau H, Heinze I and Senger H (1999) Comparison of light induced and cell cycle dependent changes in the photosynthetic apparatus: A fluorescence induction study on the green alga *Scenedesmus obliquus*. Photosynth Res 60: 217–227

Theisen A (2002) Detecting chlorophyll fluorescence from orbit: The Fraunhofer line depth model. In: Muttiah R (ed) From Laboratory Spectroscopy to Remotely Sensed Spectra of Terrestrial Ecosystems., pp 203-232. Kluwer Academic Publishers, Dordrecht

Trtílek M, Kramer D, Koblížek M and Nedbal L (1997) Dual-modulation LED kinetic fluorometer. J Luminesc 72-74: 597–599

Tyystjärvi E and Aro E (1996) The rate constant of photoinhibition, measured in lincomycin-treated leaves is directly proportional to light-intensity. Proc Natl Acad Sci USA 93: 2213–2218

van Kooten O and Snel J (1990) The use of chlorophyll fluorescence nomenclature in plant stress physiology. Photosynth Res 25: 147–150

Vasil'ev S and Bruce D (1998) Nonphotochemical quenching of excitation energy in Photosystem II. A picosecond time-resolved study of the low yield of chlorophyll *a* fluorescence induced by single-turnover flash in isolated spinach thylakoids. Biochemistry 37: 11046–11054

Vass I, Kirilovsky D and Etienne A-L (1999) UV-B radiation-induced donor- and acceptor-side modifications of Photosystem II in the cyanobacterium *Synechocystis* sp. PCC 6803. Biochemistry 38: 12786–12794

Wollman F-A (2001) State transitions reveal the dynamics and flexibility of the photosynthetic apparatus. EMBO J 20: 3623–3630

Zankel K (1973) Rapid fluorescence changes observed in chloroplasts: Their relationship to the O_2 evolving system. Biochim Biophys Acta 325: 138–148

Chapter 36

Meeting the Challenge of Monitoring Chlorophyll in the Ocean from Outer Space

André Morel
Laboratoire d'Océanographie de Villefranche, Université Pierre et Marie Curie, and CNRS, BP 8, 06238 Villefranche-sur-mer, France

Summary

Detecting and measuring, from space, the chlorophyll (Chl) content within the upper layer of the ocean, where the concentration is so low and the Chl-bearing phytoplanktonic cells are so small, can appear to be an impossible task. Further, a satellite-borne sensor directed towards the ocean captures the dominant atmospheric signal, due to light scattered by air molecules and aerosols, so that the marine signal must be extracted from this invasive background. Ocean color sensors, however, have been developed and now provide, on a daily basis, maps of the Chl distribution over the oceans of the world. This chapter explains how this challenge was faced and finally solved. These solutions involved the so-called 'bio-optical' properties of open ocean waters; namely, the existence in these waters of empirical relationships between the whole biogenic material, which governs the bulk optical properties, and a single component, the Chl content which can be detected and estimated from space by ocean color sensors. With newly developed sensors, it is now also possible to detect natural sun-stimulated Chl *a* fluorescence of phytoplankton which also provides a new promising approach to derive information about the physiological state of algal populations. The method of retrieving the marine signal and making the 'atmospheric correction' is briefly described. Paradoxically, this correction itself provides highly valuable information on the atmospheric aerosols, a crucial component of the radiative budget of our planet.

*Author for correspondence, email: morel@obs-vlfr.fr

Bernhard Grimm, Robert J. Porra, Wolfhart Rüdiger and Hugo Scheer (eds): Chlorophylls and Bacteriochlorophylls: Biochemistry, Biophysics, Functions and Applications, pp. 521–534.

I. Introduction

The determination of the chlorophyll (Chl) concentration within water bodies from space-based observation platforms could be deemed, a priori, as an impossibility for at least two reasons: Firstly, our planet as seen from space, is essentially blue as a result of its gaseous atmosphere that efficiently scatters back the incident solar radiation; consequently, information captured within the visible spectral range by any space-borne sensor directed at the ocean is largely dominated (> 90%) by this atmospheric signal. Secondly, the Chl concentration within the open ocean is rather low (approx. 0.20 mg Chl per m^3 of sea water, on average), making its detection a considerable challenge. Nevertheless, this challenge was accepted, and 'ocean color' measurements (through remote spectroscopy) were carried out from an airplane (Clarke and Ewing, 1974). The first ocean color satellite sensor, CZCS (Coastal Zone Color Scanner) was launched in 1978 and demonstrated the feasibility of such a technique. Currently, 'chlorophyll-maps' of the entire ocean are produced every day, thanks to new sensors such as SeaWiFS (Sea-viewing Wide Field-of-view Sensor), MODIS (Moderate Resolution Imaging Spectrometer), MERIS (Medium Resolution Imaging Spectrometer), and others. As Chls are the pigments ultimately responsible for photosynthesis and primary production, the determination of the concentration of the predominant Chl, Chl *a,* remains an essential research tool in biological oceanography, in marine ecology and in the study of bio-geochemical cycles, particularly of the carbon cycle.

From ancient times, mariners and fishermen have found significance in the changing color of the sea. From coastal turbid zones to open sea areas, the color evolves in a distinctive way. Also, in the open sea, the color may change from a dark deep green to intense blue as the observer moves from eutrophic waters with a high phytoplankton concentration to oligotrophic limpid waters with an extremely low phytoplankton content. This color shift has been an indication of food abundance for experienced fishermen and is the rationale for the detection and quantification of algal concentrations.

The physical translation of the human perception of color is the spectral reflectance, $R(\lambda)$, which is defined at each wavelength (λ) as the ratio of upwelling irradiance to downwelling irradiance just beneath the interface (denoted 0^-), so that the reflection of the skylight at the interface is ignored

$$R(\lambda) = E_u(0^-, \lambda) / E_d(0^-, \lambda) \quad (1)$$

The downward flux, $E_d(0^-, \lambda)$, originates from the (direct) solar radiation and the (diffuse) sky radiation. Its spectral composition depends on the zenith-sun angle and on the atmospheric properties (aerosol load and composition). The magnitude of the upward flux within the water body, $E_u(0^-, \lambda)$, is intuitively related to the two antagonistic processes of backscattering, which allows the downward photons to travel backwards, and of absorption, which annihilates photons and so cancels their chance of being backscattered. This heuristic approach translates into an expression of the following form:

$$R(\lambda) = f\,[b_b(\lambda)/a(\lambda)] \quad (2)$$

It involves the ratio of the backscattering-(b_b)- and the absorption-(a)-coefficients of the water body: these coefficients represent the probability of backscattering and absorption per unit length along the path of a beam, respectively (with the units m^{-1}). A more accurate approach uses the radiative transfer equation (RTE) which describes the radiance field within a scattering-absorbing medium, and relates radiation propagation to the inherent optical properties of the medium, namely, the absorption and scattering coefficients and the volume scattering function. Sophisticated computations using the RTE confirm, as expected, that the first determinant of $R(\lambda)$ is the ratio $[b_b(\lambda)/a(\lambda)]$.

These accurate computations also allow the assessment of the dimensionless factor, f, and the prediction of its variations which depends on wavelength (λ) and varies between approx. 0.3 and 0.5 dependent mainly on the solar angle. The backscattering coefficient includes the effects of both water molecules and suspended particles within the water body, while the absorption coefficient results from the water itself and from all the dissolved and particulate absorbing substances it contains. Herein lies the basis for remote

Abbreviations: Chl(s) – chlorophyll(s); [Chl] – chlorophyll *a* concentration; CZCS – Coastal Zone Color Scanner (NASA, launched 1978, stopped 1986); MERIS – Medium Resolution Imaging Spectrometer (ESA, launched 2002, in-flight); MODIS – Moderate Resolution Imaging Spectrometer (NASA, launched 2000, in-flight); NPP – net primary production; PAR – photosynthetically available radiation; RTE – radiative transfer equation; SeaWiFS – Sea-viewing Wide Field-of-view Sensor (NASA, launched 1997, in-flight); SST – sea surface temperature

sensing. Indeed, R(λ) will, to a first approximation, reflect in an inverse manner the absorption spectrum and would do so exactly if the backscattering (b_b) spectrum was perfectly flat. As the Chl pigments of the phytoplanktonic algae are extremely absorbing, they directly influence the shape of both the absorption and reflectance spectra.

Because of refraction and internal reflection, only about one half of the upward radiant flux (E_u) is able to emerge from the interface, and then to form the so-called 'water-leaving radiance' field. These exiting radiances, which carry information about the water content, propagate in all upward directions. They are partly attenuated (i.e., absorbed and scattered out) along their path through the atmosphere before reaching the orbiting sensor, whereas intense radiances, created by (multiple) scattering within the atmosphere, are added to the initial signal (see Fig. 1). The 'marine signal' is, therefore, 'nearly drowned' within a predominantly atmospheric signal.

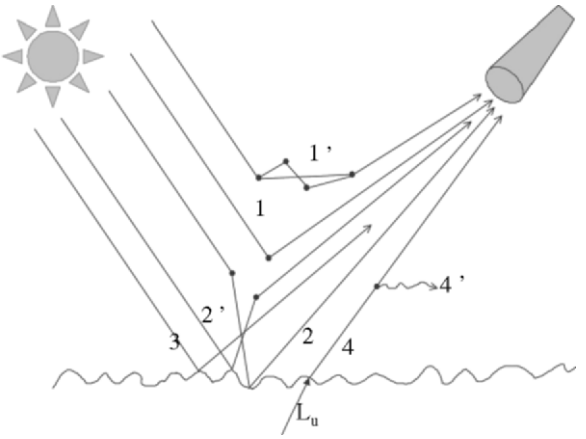

Fig. 1. Schematic representation of the various components forming the signal received by a satellite borne sensor directed at the ocean (wavy interface). Note that the sensor and the sun are generally not in the same vertical plane. The first component corresponds to solar photons scattered by atmosphere (i.e., by molecules or aerosols) toward the sensor; the path (1) describes a single scattering event, and (1′) double (or multiple) scattering events. Photons can be scattered and then reflected by the surface, or reflected and then scattered toward the sensor (paths 2 and 2′). The path (3) represents photons directly reflected back toward the sensor from the interface; if the sensor and the sun are in the same vertical plane and in symmetrical positions with respect to the zenith, the sensor aims at the specular image of the sun ('sun glint'); some sensors avoid this viewing angle (due to a tilt capability). Because of the presence of capillary waves, the sun glint is often much wider than the specular image. Finally, the in-water upward radiance L_u is the component which carries information: it propagates through the interface and forms the water-leaving radiance L_W (4); this radiance is partly attenuated (i.e., absorbed and scattered) by the atmosphere (4′), so that the radiance reaching the sensor is $t^* L_W$, where t^* represents the diffuse transmittance of the atmosphere (which depends on the aerosol load and ozone content).

II. Absorbing Substances in the Marine Environment

Two questions now arise. Are phytoplankters the only absorbers in the marine environment? Is chlorophyll the predominant absorbing pigment in phytoplankton? Both answers which, a priori, are 'no,' deserve some comments, since the determination of the chlorophyll concentration is the main goal.

In coastal areas, affected by river outflows, diversely colored sediments (inorganic and organic) are often abundant, and affect both the absorption and the backscattering processes. Absorbing dissolved substances, consisting of humic and fulvic acids, collectively called *'gelbstoff'* or yellow substance, are also brought to the sea by land drainage. These optically significant components generally vary independently of each other, and are independent of phytoplankton abundance. Such complex waters, categorized as 'Case 2 waters' (Morel and Prieur, 1977), are difficult to interpret, and the extraction of any chlorophyll 'signal,' interwoven with many others, remains difficult. In the open ocean, far from terrestrial influences, phytoplankton, and their co-existing retinue (virus, bacteria, other heterotrophs, as well as debris and dissolved organic substances) are recognized as the principal agents responsible for variations in optical properties (Morel and Prieur, 1977). In these so-called 'Case 1 waters,' which represent about 97% of the global oceans, the Chl concentration may span about three orders of magnitude (approx. 0.02 to 20 mg m^{-3}). The optical behavior of Case 1 waters is simpler and better understood than Case 2 waters, and thus their absorbing and scattering properties are more predictable as a function of the phytoplankton content. Below, emphasis will be put on these Case 1 waters; however, the specific problems raised by Case 2 waters have been examined in detail in a recent review (IOCCG, 2000).

In oceanic Case 1 waters, the absorption coefficient, a(λ), can be written as the sum:

$$a(\lambda) = a_w(\lambda) + a_{cdom}(\lambda) + a_p(\lambda) \quad (3)$$

where the subscripts w, cdom, and p represent water,

colored dissolved material, and particulate matter, respectively; this particulate matter consists of phytoplankton (subscript φ) and non-algal particles (subscript nap), thus, $a_p(\lambda) = a_\varphi(\lambda) + a_{nap}(\lambda)$.

The colored dissolved material is similar to the *gelbstoff* already mentioned, except that it is locally formed by excretion and/or decay of algal material. The non-algal particles essentially include debris and heterotrophic bacteria. Both $a_{cdom}(\lambda)$ and $a_{nap}(\lambda)$ exhibit a featureless spectrum characterized by an exponential increase towards the shorter wavelengths.

As an obvious consequence of Eq. 3, chlorophyll is not the only absorber. Even when considering the phytoplankton term, $a_\varphi(\lambda)$, a variety of absorbing accessory pigments, both photosynthetic and photoprotectant, are present in algal cells along with Chl *a*, or its derivative, [8-vinyl]-Chl *a* which has recently been found to be a major component in oceanic algae (Chapter 4, Kobayashi et al.). The pigment composition depends on species, and for a given species, often varies with such environmental conditions as light, depth and nutrients. In general, natural populations are mixtures of many species, although a single phytoplankton species may predominate in temporary 'bloom' conditions. These organisms encompass a wide size range, from >20 μm (diatoms, dinoflagellates) to ~ 0.5 μm (for abundant prokaryotes such as *Prochlorococcus*). The size of the individual cells has a strong influence on the effective absorption coefficient for a given internal pigment concentration. This physical phenomenon, termed the 'package effect' (Duysens, 1956), affects the relationship between the pigment content and the absorption coefficient (Morel and Bricaud, 1981). This effect, along with varying pigment compositions, explains that the 'Chl-specific' absorption spectra of phytoplankton (cultivated or natural) are far from being immutable (Fig. 2 a,b).

Nevertheless, all these spectra exhibit a sharp red peak near 675 nm, essentially due to Chl *a*, and a

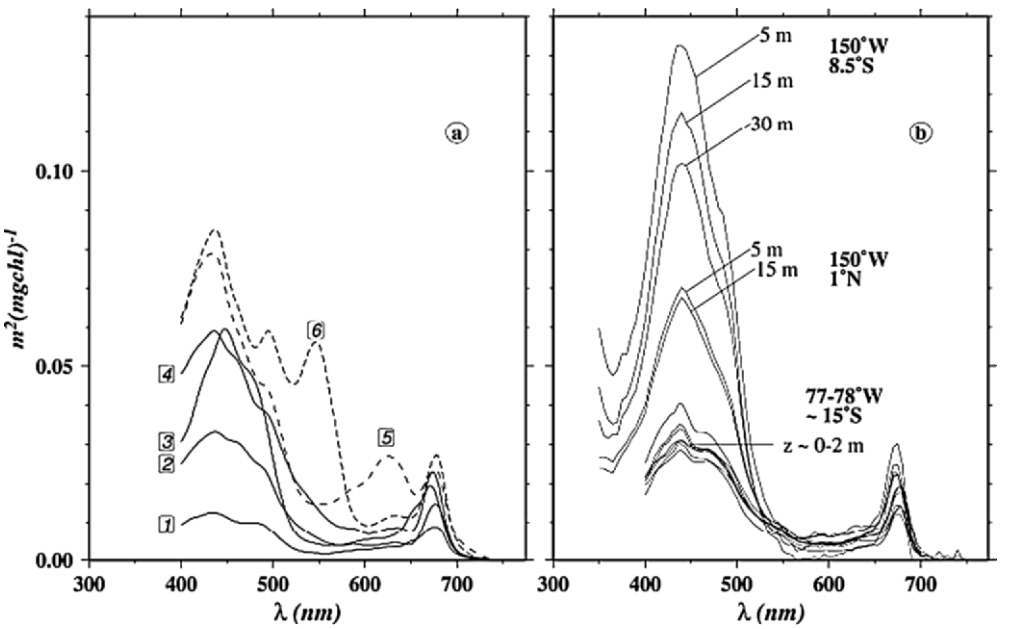

Fig. 2. (a) Examples of chlorophyll-specific absorption coefficients, aφ (λ), determined directly on suspensions of various phytoplankters grown in culture at moderate irradiance (see in Stramski et al. 2001); namely, 1 *Dunaliella bioculata*, 2 *Prymnesium parvum*, 3 *Chaetoceros curvisetum*, 4 *Prochlorococcus* sp. , 5 *Anacystis marina*, 6 *Synechococcus* sp. For the cyanobacteria (labeled 5 and 6), the presence of phycocyanin, phycoerythrin, and phycourobilin is indicated by the peaks at 630, 545, and 490 nm, respectively. Such prominent peaks, typical of monospecific cultures, are considerably smoothed in natural algal assemblages. (b) Examples of chlorophyll–specific absorption spectra for natural populations (determined using the in vitro filter technique) in three differing trophic regimes (all in the Pacific Ocean), namely: oligotophic situation in the southern gyre (8.5°S), mesotrophic conditions near the Equator (1°N), and eutrophic conditions within the Peruvian upwelling area: [Chl] are 0.13, 0.30, and 3 mg m^{-3}, respectively (see also Fig. 7); the sampling depths (m) are also indicated. Note that, in contrast to the data for pure cultures (panel a) , these spectra include the effect of accompanying non-algal particles and thus correspond to $a_p(\lambda)$ in Eq. 3.

broad absorption band in the blue 400–500 nm domain which peaks around 440 or 448 nm for Chl *a* or [8-vinyl]-Chl –*a*, respectively: these spectra are variously shaped as a result of changing pigment composition. The actual contribution of Chl *a* to the global absorption within this blue band largely varies between about 30 and 70%, and Chl *b*,*c* together with carotenoids, are responsible for the additional absorption. In the green 540–600 nm region of the spectrum, algal absorption is at its minimum, except when phycobilins are present, as in cyanobacteria. A second observation is the wide (~ten-fold) variation of the blue absorption per unit of Chl *a*, not only for an individual species (Fig. 2a), but equally for naturally-occurring mixed populations (Fig. 2b). In summary, the influence of other pigments, such as Chl *b,c* and various carotenoids, together with a more or less pronounced package effect, are responsible for the observed variability in total algal absorption, in so far as absorption has been normalized with respect to Chl *a* content.

These typical algal absorption spectra exhibit intense absorption in the blue region when compared with that of pure seawater (Fig. 4b), which, in contrast, shows extreme transparency in the blue and high absorption in the red. Therefore, even a trace of phytoplankton enhances the blue absorption and thus depresses blue reflectance. The red absorption peak which is essentially attributable to Chl *a*, however, remains indiscernible in the background water absorption, even in the presence of large algal concentrations. The green region of the spectrum, where algal absorption is minimal, is less sensitive to the presence of phytoplankton. Since the blue absorption cannot be attributed to Chl *a* alone, as already discussed, the capability of ocean color sensors for providing synoptic views of the Chl *a* distribution, based on the blue absorption, is necessarily limited.

Historically, only Chl *a* was routinely determined at sea, using either spectrophotometry or fluorometry. Consequently, its concentration, denoted [Chl], was the single index available when studying the so-called 'bio-optical' properties of water bodies (i.e., absorption, scattering, backscattering, diffuse attenuation and reflectance). These studies have resulted in empirical relationships between the bulk optical properties, which account for all pigments and substances, and the chlorophyll concentration alone. These relationships, established for Case 1 waters, remain fundamental for the algorithms which are presently applied to ocean color data to calculate [Chl]. This situation will change with the widening use of high performance liquid chromatography which allows many pigments to be quantified (see Chapter 8, Garrido and Zapata).

III. Bio-optical Relationships in Oceanic Waters and Chlorophyll Algorithms

The simplest approach consists of relating [Chl] directly to $R(\lambda)$, when both have been simultaneously measured at sea (Morel and Prieur, 1977; Smith and Baker, 1978). If statistically significant relationships exist between the two quantities, they can be used as algorithms. As the presence of algae strongly depresses the reflectance in the blue region of the spectrum and does not significantly affect the green reflectance, the strategy was to form a ratio of reflectances at two wavelengths, $R(\lambda_1)/R(\lambda_2)$, where λ_1 and λ_2 are located in the blue and green regions of the spectrum, respectively (see Table 1). Such ratios systematically decrease when [Chl] increases (Fig. 3). A polynomial fit to such data, within the log-log space, can be used to retrieve [Chl] from the reflectance ratios in Case 1 waters. Such algorithms (O'Reilly et al., 1998) are called 'purely empirical'.

'Semi-analytical' algorithms are derived from the use of Eq. 2 and on the additivity principle which applies to the backscattering and absorption coefficients. Various parameterizations of both these coefficients as a function of [Chl] have been proposed, leading to slightly different reflectance models (Lee et al., 1994). The total absorption coefficient (see Eq. 3), involves $a_{CDOM}(\lambda)$ and $a_p(\lambda)$. These partial coefficients can be related to [Chl] through empirical relationships (valid for Case 1) by measuring separately the absorption by both dissolved and particulate matter. For instance (Fig. 4a), the absorption coefficient a_p (at 440 nm) has been found to increase along with [Chl], but in a non-linear manner (Bricaud et al., 1998), as described by Eq. (4):

$$a_p(440) = 0.0520\ [\text{Chl}]^{0.635} \qquad (4)$$

On average, the partition of a_p between the non-algal and the algal compartment is about 30%–70%, respectively (see Fig. 4a). Expressions similar to Eq. 4 have been obtained for all wavelengths through regression analyses. In these expressions, the coefficient and the exponent are wavelength (λ) dependent so that the shape of the absorption spectrum changes

Table 1. Relevant information and main characteristics of several Ocean Color sensors (detailed information in IOCCG, 1998). These sensors are polar orbiting and sun synchronous with an equatorial crossing time between 10 am and noon (local time). Their altitude is about 700–800 km. With about 14 orbits per day, a total coverage of the earth is obtained within 3 days at the Equator, 2 days at mid latitude and in one day at high latitude. The spectral channels dedicated to ocean color and atmospheric correction (listed below) are 10 to 20 nm wide, except the narrower channels devoted to fluorescence detection. Note that the fluorescence channels are not centered on the maximum of the fluorescence peak (at 683 nm), because of the interference with an atmospheric absorption band due to O_2 (687–693 nm).

CZCS	SeaWiFS	MODIS	MERIS	Information retrieved
Channels (central wavelength [nm])				
	412	412.5	412.5	Gelbstoff detection
443	443	443	442.5	Phytoplankton absorption maximum
	490	488	490	Phytoplankton absorption
520	510	531	510	Hinge point for reflectance
550	555	551	560	Phytoplankton absorption minimum
670	670			Sediment detection
		667	665	Baseline for fluorescence detection
		678	681.25	Chlorophyll-a fluorescence detection
			709	Baseline for fluorescence detection
	765	748	779	Aerosol detection/quantification
	865	869.5	870	Aerosol detection/quantification
Swath (Km)				
1566	1800 (1200)*	2330	1150	*GAC mode (Global Area Coverage)
Resolution at nadir (Km),				in LAC (Local Area Coverage) mode
0.825	1.1 (4.4)*	1.0	0.3 (1.2)*	*for GAC mode

slightly and progressively with the concentration. Examples of spectra resulting from the sum $[a_w(\lambda) + a_p(\lambda)]$ are displayed in Fig. 4b. Several reasons for the natural non-linear, albeit regular, trend (expressed by Eq. 4) have already been identified. Among them, the changing mean cell size of unicellular algae is likely to be the most important (Bricaud et al., 2004). In oligotrophic waters ([Chl] <0.1 mg•m^{-3}), phytoplankton are dominated by minute species with a reduced package effect (i.e., maximal absorption per unit of Chl); in contrast, large species, with a more pronounced package effect (i.e., lesser absorption per unit Chl), prevail in eutrophic waters ([Chl] >1 mg•m^{-3}). In oligotrophic tropical waters, carotenoid-to-Chl ratios are often higher in the upper layer, where photoprotecting carotenoids are present in larger quantities in algal cells. Anyway, the carotenoids (both photoprotectant and light-harvesting pigments) contribute to the enhancement of algal absorption in the blue-green part of the spectrum. In summary, when [Chl] increases in the natural environment there is a progressive, rather regular, lowering of a_p*, the Chl-specific absorption coefficient (i.e., per unit of Chl, and expressed as m^2•mg^{-1}). With such a propitiously regular change of a_p* values, retrieval of [Chl] is possible: with random changes, retrieval would have been problematic.

The backscattering coefficient (Eq. 2) is the sum of the coefficients for pure water and for suspended particles, b_{bw} and b_{bp}, respectively. The contribution of water molecules is large; it is actually dominant for most oceanic waters (Fig. 5). The b_{bw} coefficient, varying as $\lambda^{-4.3}$ (Rayleigh-type scattering), thus strongly increases towards the shorter wavelengths, and accounts for the deep-blue color of clear oligotrophic waters. The parameterization of b_{bp} is generally performed in two steps. Firstly, based on regression analyses of field measurements in Case 1 waters (Gordon and Morel, 1983), the scattering coefficient, b_p, can be empirically related to [Chl]; again, non-linear relationships emerge as expressed in Eq. 5 (see Loisel and Morel, 1998):

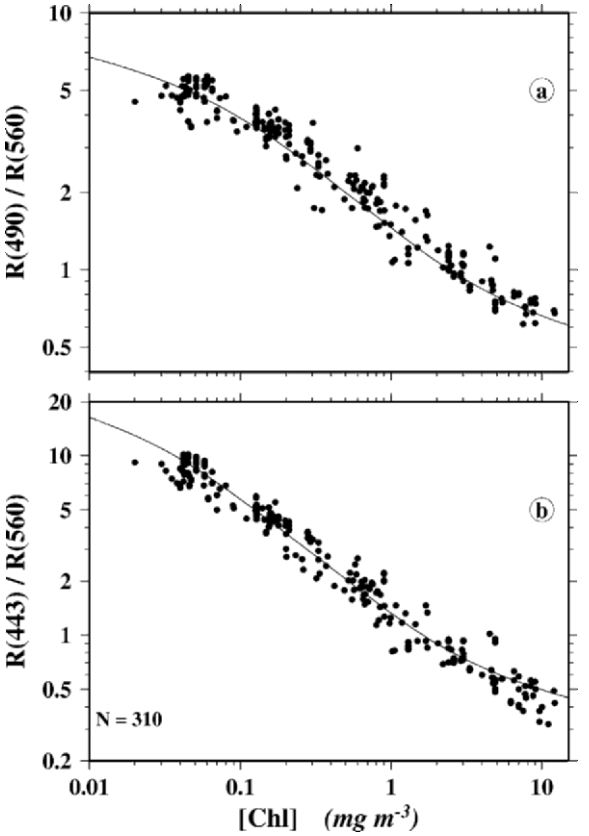

Fig. 3. Ratios of reflectance at two wavelengths (490–560 nm in a, and 443–560 nm in b), forming 'blue-to-green' ratios as a function of the chlorophyll concentration (log-scales). The curves have been produced via a predictive semi-analytical model (based on absorption and backscattering; see text and also Fig. 6a), whereas the dots are independently derived from paired measurements (N= 310) of reflectance and chlorophyll made in various parts of the world's oceans. Actually, the semi-analytical model and a purely empirical model (i.e., the best polynomial fit for the data) are very similar, as it can be guessed from these graphs.

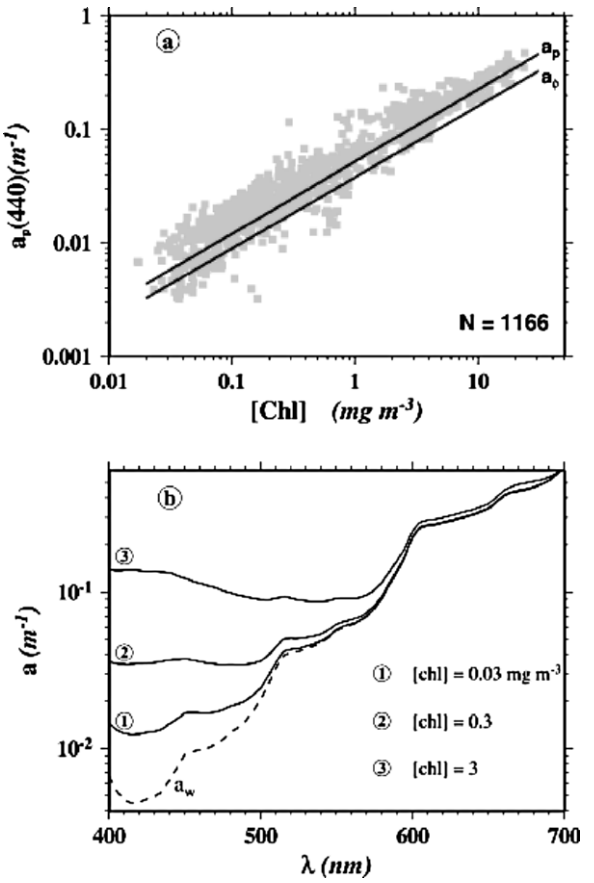

Fig. 4. (a) Simultaneous field measurements of the absorption coefficient at 440 nm by total particulate matter, a_p, (filter technique, Yentsch, 1962), and of the chlorophyll concentration (1166 couples of data, plotted with log-scales, as closed squares). The empirical straight line, denoted a_p, corresponds to Eq. 4. By extracting the pigments from the particles retained onto the filter (Kishino et al., 1985), and measuring the residual absorption, the non-algal and algal contributions to particle absorption can be separately assessed (Eq. 3). The line, denoted a_φ, is also obtained through regression analysis applied to absorption due only to phytoplankton (data not shown, but see Bricaud et al., 1995, 1998); note that the two lines are almost parallel. (b) Spectral absorption coefficients (log scale) for pure water, a_w (Pope and Fry, 1997), and as modeled for natural seawater with three chlorophyll concentrations. Note that the red absorption peak (675 nm) of chlorophyll (Fig. 2) is totally overwhelmed by water absorption. Therefore, this absorption capability of phytoplanktonic algae is irrelevant, in as much as there is no available red light in marine environments.

$$b_p(550) = 0.416\ [Chl]^{0.766} \qquad (5)$$

Based on other measurements and theoretical considerations, the spectral coefficient, $b_p(\lambda)$, is usually given a wavelength dependency according to λ^{-1} (Mie-type scattering).

The second step consists of adopting a value for the backscattering probability (i.e., of the ratio b_{bp}/b_p). In the absence of direct determinations, the resort to theoretical considerations is currently necessary, together with the inverted use of Eq. 2 (when both R and a have been measured, and f computed via the RTE). This ratio varies between about 1.5% in clear waters and 0.4% in Chl-rich waters. Clearly, some uncertainties still remain for this important parameter and, therefore, limit the capability of the semi-analytical approach.

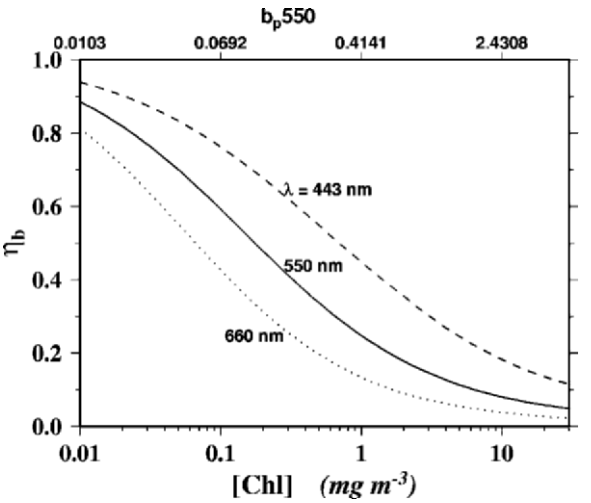

Fig. 5. Ratio $\eta_b = b_{bw} / (b_{bw}+b_{bp})$ of the backscattering by water molecules (Morel, 1974) to the total backscattering coefficient (molecules + particles), as a function of the chlorophyll concentration (log-scale), and at the three wavelengths as indicated.

IV. Reflectance of Oceanic Waters

With the parameterizations summarized above, and by using Eq. 2, a full spectral model for reflectance can be built (Fig. 6a). It accounts well for the spectral reflectance determined in the field (Fig. 6b). The ratio of two reflectances at two wavelengths, already shown in Fig. 3, is derived from this model, and is an example of a semi-analytical algorithm. When [Chl] increases, the reflectance in the blue part of the spectrum strongly decreases and a minimum develops around 430 nm (as a result of pigment absorption); meanwhile, the green reflectance increases (as a result of the increase in b_b), so that a maximum develops around 565 nm. In the red part of the spectrum (beyond 600 nm), R is always low (<0.2% in oligotrophic waters and <1% in eutrophic waters) whereas a relative maximum centered at 683 nm appears. This Gaussian peak (half height bandwidth ≅ 20 nm) corresponds to the sun-stimulated fluorescence emission of phytoplankton, which adds to the backscattered flux (Morel and Prieur, 1977; Gordon, 1979). This emission is separately modeled by computing the incident solar (400–660 nm) photons captured by algae by using $a_\varphi(\lambda)$, and by assuming a fluorescence quantum yield of 0.8% which is typical of cells inhabiting the well-lit oceanic upper layers (Maritorena et al., 2000; see also their Eq. 7 for the computation of the fluorescence emission). In this spectral domain, Raman scattering by water molecules, excited by shorter wavelengths, is not negligible. It may contribute about 10% to the reflectance observed beyond 600 nm in clear waters, and less when [Chl] increases. This emission has been measured, either directly (Sugihara et al., 1984; see also Fig. 6b), or via the Fraunhofer line filling method (see Hu and Voss, 1997), and can be accurately modeled.

V. Phytoplankton Distribution and Primary Production

Once the spectral radiances emerging from the water have been extracted from the total signal recorded above the atmosphere (see Section VII), blue-to-green ratios are calculated; then, with these ratios and by use of algorithms (i.e., the polynomial fit to curves as shown in Fig. 3), [Chl] is retrieved for each pixel in the scene. The [Chl] distribution in the world's oceans can thus be obtained (examples shown in Fig. 7). Such algorithms are valid only for oceanic Case 1 waters. When applied to complex Case 2 coastal waters (about 3% of the world ocean), such algorithms generally fail and lead to large overestimates of [Chl]. Consequently, locally-adapted algorithms, which are still being developed, are necessary for such coastal waters (IOCCG, 2000).

As the marine radiances originate only from the upper layer of the ocean, the exact significance of the retrieved [Chl] deserves examination. It has been shown (Gordon and McCluney, 1975) that 90% of the emerging photons originate from a layer having a thickness equal to the 'penetration depth' (the depth where the downward radiation is reduced to 1/e (i.e., 37%) of its initial value beneath the surface. This depth varies with [Chl], from about 20 m in clear oligotrophic waters to a few meters in eutrophic waters. Therefore, the estimated [Chl] can be considered as a weighed average of the chlorophyll concentration within this upper layer. Since phytoplankton can live and grow at a depth, known as the euphotic depth, where the PAR (photosynthetically active radiation) is reduced to only 1% (or even 0.1%) of its subsurface value, only a fraction (about one fifth) of the productive algal biomass is 'seen' by a remote sensor. This physical limitation is similar to that faced with terrestrial vegetation: the optical signal originates mainly from the canopy. This is an inescapable limitation when trying to assess the potential primary production of the entire biomass. Fortunately, however, rather robust statistical relationships exist between

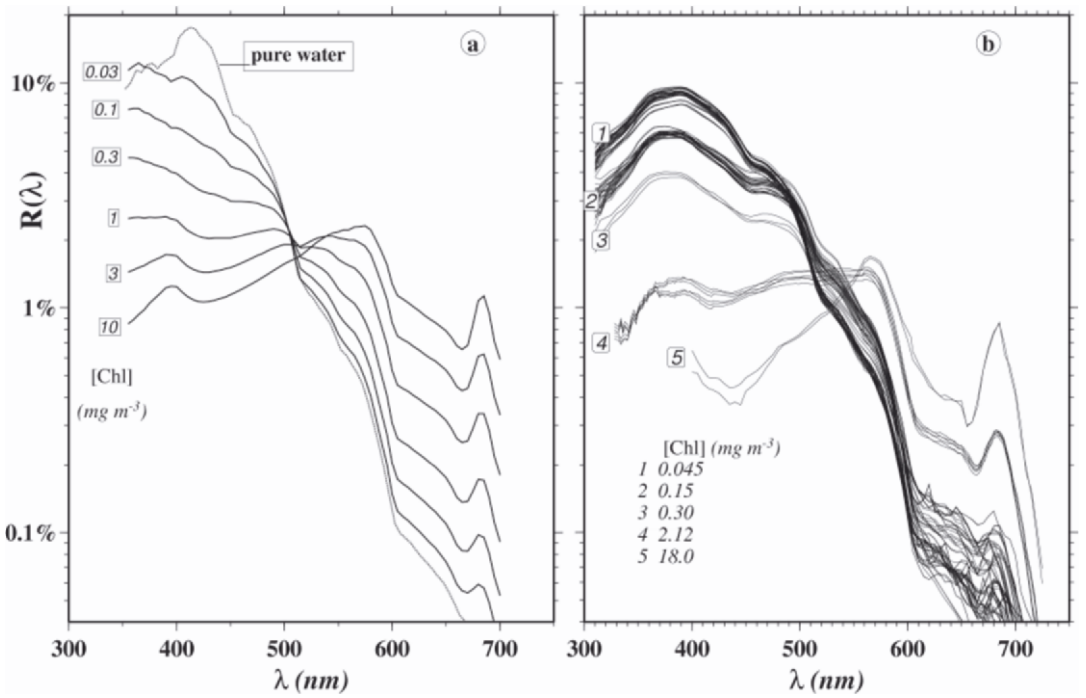

Fig. 6. (a) Reflectance spectra produced by a semi-analytical model (see text and Morel and Maritorena, 2001) for various chlorophyll concentrations. Note that these spectra account for Raman scattering and Chl *a* fluorescence (peak around 685 nm). The hypothetical reflectance spectrum computed for pure seawater is also shown. (b) Selected examples of reflectance spectra (Eq. 1), as determined at sea, in various locations with differing chlorophyll concentrations. Curves 1, 2, and 3 from the central Pacific, 4 from the Moroccan upwelling zone, and 5 from the Mauritanian upwelling zone.

the near-surface [Chl] and the vertical chlorophyll profile (Morel and Berthon, 1989); thus, in practice, this difficulty can be circumvented. The stability of the water column (depicted by the vertical profile of water density) is also involved in shaping the chlorophyll profile.

In essence, the prediction of the column integrated primary production is based on a triple integration (with respect to wavelength, time, and depth) of the instantaneous and local net photosynthesis equation (Morel, 1991). This equation involves the photo-physiological parameters derived from the production-irradiance curve (the so-called P-vs-E, curve), and a temperature dependency for the maximal, light-independent, production (the so-called P^{max} quantity). This equation is spectrally dependent through the algal absorption spectrum, $a^*(\lambda)$, combined with the spectral distribution of available light at any depth which is considered. When dealing with the global ocean and satellite information, the input parameters for the model are firstly, the day and latitude, which govern the day length together with the time course of photosynthetically available radiation (PAR) availability at the surface (computed via an atmospheric model) by assuming that the sky is clear; secondly, the cloudiness index, also derived from satellite data, which modulates PAR, and; thirdly, the sea surface temperature (SST), which is also detected from space. Knowing [Chl] in the surface layer (and the associated vertical chlorophyll profile), the computation consists of propagating PAR (and its spectral composition) throughout the water column, down to the euphotic depth, and then of entering the photosynthesis equation with the local [Chl]. Fortunately, these complex calculations can be made in advance for all possible cases thus providing lookup tables for practical use in conjunction with the time, date and latitude together with SST, cloudiness, and [Chl] information obtained from the satellite (Antoine and Morel, 1996). Various simplifications of the above scheme are also in use (e.g., Platt, 1986; Behrenfeld and Falkowski, 1997b). Parameterizing the photo-physiological response of algae remains a difficult and sensitive issue in comparison with the physical aspects of the problem,

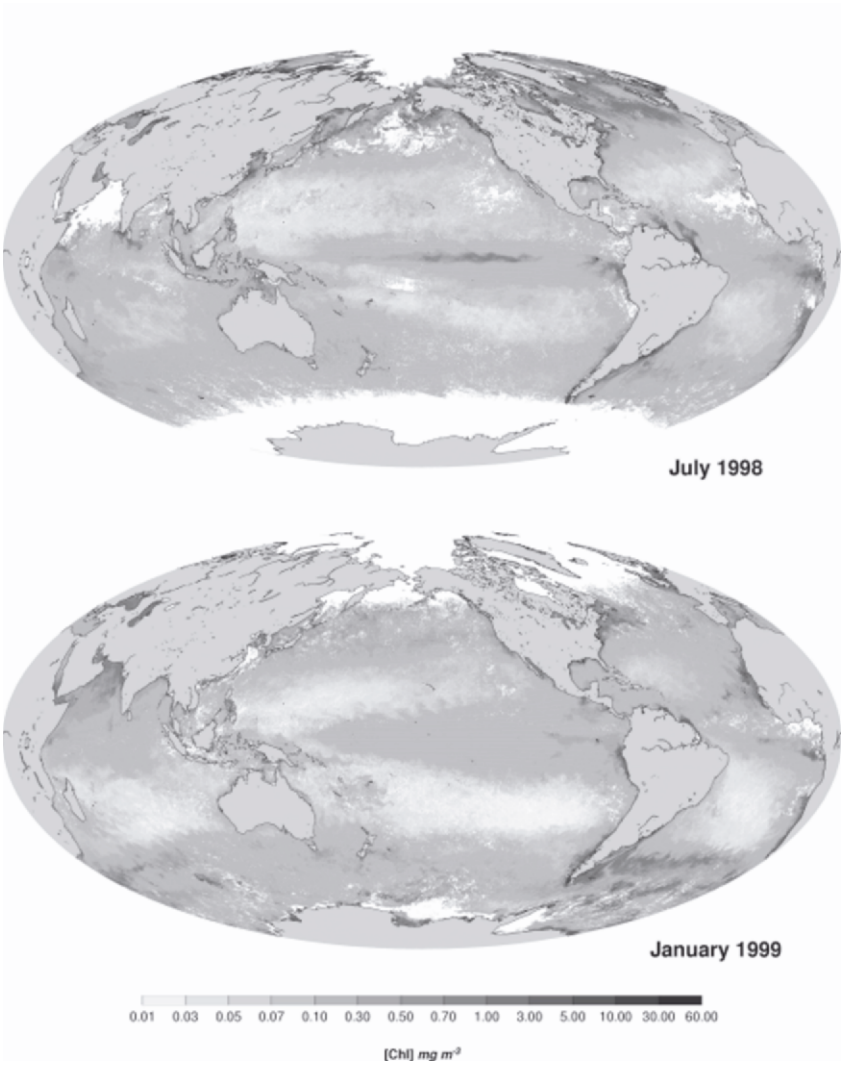

Fig. 7. Examples of global maps of chlorophyll concentration (color encoding indicated) within the oceanic upper layer, as derived from observations by the SeaWiFS sensor. Similar maps are produced on a daily basis; they are, however, incomplete, because of coverage limitations and presence of clouds. By merging daily maps, weekly, monthly, and yearly averages can be produced. Shown here are monthly averaged maps for two opposite seasons, July 1998 and January 1999. Even over one month, some areas remain unseen (clouds masked in white). The high latitude zones, alternatively in the Northern (January) or Southern (July) hemispheres, which are either ice covered,or too dark and in the polar night, are also masked in white. These maps show the permanence and extension of the oligotrophic deep blue subtropical gyres, and in-between, of the equatorial divergence which sustains an enhanced algal biomass. Spring-early summer blooms occur alternatively in both hemispheres at latitudes beyond 40°. The upwelling systems, induced by the trade winds, support high biomasses along the coasts of South Africa, Angola, Mauritania, Senegal, Chile, Peru. In the northeast Indian ocean sector, probably one of the most productive zones of the ocean, the situation is more complex because of the alternation of opposite monsoons in summer and winter. See also Color Plate 8.

which are more easily and safely modeled.

Global annual photosynthetic carbon fixation (called NPP, net primary production), as derived from previous space observation (CZCS), were converging around a value of 50 Pg C per year (Petagram = Pg = 10^{15}g) (Longhurst et al., 1995, Antoine et al., 1996, Behrenfeld and Falkowski, 1997a). Interestingly, with such a value, now confirmed by new estimates based on SeaWiFS imagery, the annual carbon fixation through marine photosynthesis appears to be similar to that realized by terrestrial vegetation (Field et al., 1998). Therefore, the average turnover time of the oceanic biomass is much shorter than for the terrestrial biomass (1 week vs. about 15 years),

because of their disproportionate sizes in terms of carbon biomasses (1 vs 700 Pg C approximately for the marine and terrestrial vegetation, respectively). Such a disproportion is obviously in keeping with the typical generation cycle time (i.e., years for terrestrial plants, and hours for unicellular algae). Geographic and seasonal variations in oceanic primary production can now be studied with an unprecedented amount of detail thanks to ocean color imagery: even if the absolute estimates of NPP become more accurate in the future, the errors currently incurred are probably small.

VI. Sun-stimulated Fluorescence

Algal biomass has been estimated at sea for more than 30 years using chlorophyll fluorescence, by means of active excitation techniques (Lorenzen, 1966). Passive (sun-induced) fluorescence has also been detected in reflectance spectra (Morel and Prieur, 1977). The use of this signal as a possible remote sensing technique for phytoplankton determination has been suggested (Neville and Gower, 1977) and sensors, such as MODIS and MERIS, now provide adequate spectral channels (Table 1). One narrow channel is centered on the red emission peak (683 nm), and two others, on each side of the peak, help to define a baseline permitting the fluorescence intensity to be quantified. In contrast to the conventional color ratio technique, fluorescence provides a specific signal, as it originates only from Chl *a* within the antenna of Photosystem II. This signal emitted in a narrow spectral band is added to the reflectance spectrum, and its amplitude is essentially unaffected by the presence of other optically active substances (at least when the turbidity is not too high). Therefore, a method based on its detection seems particularly useful in complex coastal Case 2 waters, where the color ratio technique generally fails. Further, there is no obstacle in extending it to Case 1 waters, at least when [Chl] exceeds 0.4 $mg \bullet m^{-3}$ (as occurs in about 10–20% of the world's oceans), which makes Chl fluorescence radiometrically detectable from space (Babin et al., 1996; Gower et al., 1999). There is, however, a serious disadvantage due to the strong water absorption in this spectral domain: the red signal which emerges, emanates only from the very upper water layer (about 1–2 m thick) thus only providing information about the near-surface [Chl].

The interpretation of fluorescence in terms of phytoplanktonic biomass is difficult. Indeed, the signal (the fluorescence line height) depends not only on [Chl] itself, but also on the intensity of the excitation, and on the realized fluorescence quantum yield, ϕ_f. Therefore, normalizing the fluorescence signal by the incident flux could provide an estimate of the biomass only if both the absorption capability of algae per unit of Chl *a* and ϕ_f were either invariant or easily derivable from other observable quantities. The absorption capability factor is known to be variable (Fig. 4b) and ϕ_f, the second factor, can also vary at least 5-fold depending on species, physiological state and radiation availability which rule the photochemical and non-photochemical quenching processes (Falkowski and Kiefer, 1985, Kiefer and Reynolds, 1992). Unfortunately, at a local level, the slopes of linear relationships between the fluorescence signal and [Chl] have been found to change widely with time and location (Gower et al., 1999). On the spatial and temporal scales involved in space observation, the possibility of reliably predicting ϕ_f, which would permit the fluorescence image to be readily transformed into quantitative chlorophyll maps, is still questioned. However, the comparison of fluorescence emission with the biomass, as derived through the conventional band ratio technique, could provide important information about the physiological state and photosynthetic performances of the algal crop. The relationship between fluorescence and photosynthesis, however, is not straightforward (Westberry and Siegel, 2003; Falkowski et al., 2004; Moya and Cerovic, 2004). Presently, the issue of non-photochemical quenching of fluorescence (an important source of variability) remains an obstacle in the comprehensive and systematic application of these fluorescence techniques.

VII. Concluding Remarks: The Atmospheric Correction

A reader, having learned in the first paragraph that the marine signal, to be interpreted in terms of chlorophyll concentration, represents a very small fraction of the signal captured by a satellite-borne sensor, will be curious to know how this problem is solved. This process is euphemistically called 'the atmospheric correction,' because the corrective term largely exceeds the desired variable (Gordon and Morel, 1983). For the sake of completeness, a brief overview of this corrective scheme follows.

For each spectral channel, the total radiance (λ omitted) recorded by a satellite-borne sensor at the top of the atmosphere, L_T (W m^{-2} $sr^{-1}\mu m^{-1}$), can be written in a simplified way as (see also Fig. 1)

$$L_T = L_R + L_A + L_{RA} + (L_F + L_G) + t^* L_W \quad (6)$$

To get the marine information, namely, $t^* \bullet L_W$, which represents the radiance leaving the water (L_W) modified by the atmospheric diffuse transmittance factor ($t^* < 1$), all other terms have to be estimated and then subtracted from L_T. The first three terms correspond to radiances generated by atmospheric scattering and reflection (sky reflection) at the interface (the paths 1, 1', 2, and 2', in Fig. 1); the subscripts R, A, and RA indicate the nature of the scattering events, which may occur only with air molecules (R for Rayleigh), or suspended aerosols (A), or both successively, via multiple scattering (the coupling term L_{RA}). These atmospheric terms depend on the geometry; namely, on the viewing angle and the zenith-sun angle, and involve the molecular (Rayleigh) and aerosol (Mie) scattering phase functions. They must be assessed by solving numerically the RTE, with the appropriate atmospheric input parameters. The two other terms to be subtracted are related to the local wind speed; namely, the additional radiance L_F, which is generated by the foam forming the white caps, and L_G (or 'glitter') which represents the sun radiation reflected by capillary waves, outside of the specular image itself (called the 'sun glint'). The knowledge of the wind field, associated with geometrical considerations, allows these terms to be estimated.

The above decomposition of the signal actually demonstrates that, besides [Chl], other unknowns appear in the ocean color remote sensing problem. The crucial additional unknown is the aerosol load (and nature), which governs the magnitude and the spectral behavior of the terms L_A and L_{RA}. Other unknowns, besides the wind speed, are the barometric pressure which reflects the number of air molecules and thus directly modulates Rayleigh scattering and the vertically integrated ozone content (an absorbing gas which influences t*). Ancillary data, derived from other satellite sensors or meteorological records, are used for estimating these three parameters and the corresponding corrections.

Regarding aerosols, however, there is no independent information that can be used. Therefore, an autonomous and co-located (i.e., pixel-by-pixel) solution must be found, based on the data provided by the sensor itself. In essence, the solution consists of using two well-founded assumptions: firstly, the Rayleigh scattering term can be computed with any desired accuracy at all wavelengths and, secondly, in the near infra-red (NIR), the ocean is black ($L_W = 0$), at least for Case 1 waters. Therefore, L_A and L_{RA} can be retrieved at two wavelengths in the NIR (see Table 1), assuming L_F and L_G can be constrained. The magnitude of L_A and L_{RA} is an indicator of the aerosol load (i.e., its optical thickness). The spectral dependency of these terms, as observed between the two wavelengths, is used for the identification of the nature of the aerosol and then for the extrapolation of aerosol scattering toward the visible part of the spectrum. These extrapolated values are subtracted to derive $t^* L_W$ in the visible part of the spectrum; then t* is computed, based on the aerosol optical thickness, and finally the quantities L_W can be retrieved. Such a correction scheme implies an extensive manipulation of the RTE for all possible geometrical configurations and for all possible aerosol 'models' (which differ by their phase functions and spectral behaviors). Pre-computed lookup tables are needed to speed up the processing of such data.

In spite of its complexity, this procedure has proven to be very efficient in most situations, but natural and computational limitations exist. Obviously, when the aerosol optical thickness becomes too high, the ocean signal vanishes, as also occurs in the presence of clouds. Some absorbing aerosols, such as soot from forest fires or industrial wastes or desert dust spreading over the ocean, are difficult to deal with. Also, the initial hypothesis of 'black' pixel in the NIR may fail, and often does, in coastal turbid areas, indicating that other techniques need to be employed. Interestingly, when the correction process works it provides extremely valuable information, as a by-product, about the aerosol distribution over the open ocean, which remains a crucial component of the radiation budget of our planet.

Acknowledgments

I thank H. Claustre, P. Falkowski, B. Genty, M. Lewis, J. Ras, and A. Sciandra for critically reading this manuscript, B. Gentili for the preparation of the figures, and the NASA Goddard-DAAC for providing the SeaWiFS data.

References

Antoine D and Morel A (1996) Oceanic primary production. 1. Adaptation of a spectral light-photosynthesis model in view of application to satellite chlorophyll observations. Global Biogeochem Cycles 10: 43–55

Antoine D, André J-M and Morel A (1996) Oceanic primary production. 2. Estimation at global scale from satellite (coastal zone color scanner) chlorophyll. Global Biogeochem Cycles 10: 56–69

Babin M, Morel A and Gentili B (1996) Remote sensing of sea surface sun-induced chlorophyll fluorescence; consequences of natural variations in the optical characteristics of phytoplankton and the quantum yield of chlorophyll *a* fluorescence. Int J Remote Sensing 17: 2417–2448

Behrenfeld MJ and Falkowski PG (1997a) Photosynthetic rates derived from satellite-based chlorophyll concentration. Limnol Oceanogr 42: 1–20

Behrenfeld MJ and Falkowski PG (1997b) A consumer's guide to phytoplankton primary productivity models. Limnol Oceanogr 42: 1479–1491

Bricaud A, Babin M, Morel A and Claustre H (1995) Variability in the chlorophyll-specific absorption coefficients of natural phytoplankton: Analysis and parameterization. J Geophys Res 100: 13321–13332

Bricaud A, Morel A, Babin M, Allali K and Claustre H (1998) Variations of light absorption by suspended particles with chlorophyll a concentration in oceanic (Case 1) waters: Analysis and implications for bio-optical models. J Geophys Res 103: 31033–31044

Bricaud A, Claustre H, Ras J, and Oubelkheir K (2004) Natural variability of phytoplanktonic absorption in oceanic waters: Influence of the size structure of algal populations. J Geophys Res 109: C11010,doi:10.1029/2004JC002419, 2004

Clarke GL and Ewing GC (1974) Remote spectroscopy of the sea for biological production studies. In: Jerlov NG and Steeman-Nielsen E (eds) Optical Aspects of Oceanography, pp 389–413. Academic Press, New York

Duysens LM (1956) The flattening of the absorption spectra of suspensions as compared to that of solutions. Biochim Biophys Acta 19: 1–12

Falkowski PG and Kiefer DA (1985) Chlorophyll *a* fluorescence in phytoplankton, relationship to photosynthesis and biomass. J Plankton Res 7: 715–731

Falkowski PG, Koblizek M, Gorbunov M and Kolber M (2004) Development of variable fluorescence techniques in marine ecosystems. In: Papageorgiou GC and Govindjee (eds) Chlorophyll *a* Fluorescence: A Signature of Photosynthesis, pp 757–778. Springer, Dordrecht

Field C, Behrenfeld M, Randerson J and Falkowski P (1998) Primary production of the biosphere: Integrating terrestrial and oceanic components. Science, 281: 237–240

Gordon HR (1979) Diffuse reflectance of the ocean: The theory of its augmentation by chlorophyll-*a* fluorescence at 685 nm. Appl Opt 18: 1161–1166

Gordon HR and McCluney WR (1975) Estimation of the depth of sun light penetration in the sea for remote sensing. Appl Opt 14: 413–416

Gordon HR and Morel A (1983) Remote Assessment of Ocean Color for Interpretation of Satellite Visible Imagery: A Review. Springer Verlag, New York

Gower JFR, Doerffer R and Borstad GA (1999) Interpretation of the 685 nm peak in water-leaving radiance spectra in terms of fluorescence, absorption and scattering, and its observation by MERIS. Int J Remote Sensing 20:1771–1786

Hu C and Voss KJ (1997) In situ measurements of Raman scattering in clear ocean water. Appl Opt 36: 6962–6966

IOCCG (International Ocean Color coordinating Group) (1998) Minimum Requirements for an Operational Ocean-Color Sensor for the Open Ocean. In: Morel A (ed) IOCCG Report No. 1, pp 46. Dartmouth NS, Canada

IOCCG (International Ocean Color Co-ordinating Group) (2000) Remote Sensing of Ocean Colour in Coastal, and Other Optically-Complex, Waters. In: Sathyendranath S (ed) IOCCG Report No. 3, pp 140. Dartmouth NS, Canada

Kiefer DA and Reynolds RA (1992) Advances in understanding phytoplankton fluorescence and photosynthesis. In: Falkowski PG and Woodhead AD (eds) Primary Productivity and Biogeochemical Cycles in the Sea, 155–174. Plenum Press New York and London

Kishino M, Takahashi M, Okami N and Ichimura (1985) Estimation of the spectral absorption coefficients of phytoplankton in the sea. Bull Mar Sci 37: 634–642

Lee Z, Carder KL, Hawes SK, Steward RG, Peacock TG and Davis CO (1994) Model for the interpretation of hyperspectral remote-sensing reflectance. Appl Opt 33: 5721–5732

Loisel H and Morel A (1998) Light scattering and chlorophyll concentration in case 1 waters: A reexamination. Limnol Oceanogr 43: 847–858

Longhurst A, Sathyendranath S, Platt T and Caverhill C (1995) An estimate of global primary production in the ocean from satellite radiometer data. J Plankton Res 17: 1245–1271

Lorenzen CJ (1966) A method for the continuous measurement of in vivo chlorophyll concentration. Deep-Sea Res 13:223–227

Maritorena S, Morel A and Gentili B (2000) Determination of the fluorescence quantum yield by oceanic phytoplankton in their natural habitat. Appl Opt 36: 6725–6737

Morel A (1974) Optical properties of pure water and pure sea water. In: Jerlov NG and Steeman-Nielsen E (eds) Optical Aspects of Oceanography, pp 1–24. Academic Press, New York

Morel A (1991) Light and photosynthesis: A spectral model with geochemical and climatological implications. Prog Oceanogr 26: 263–306

Morel A and Berthon J-F (1989) Surface pigments, algal biomass profiles, and potential production of the euphotic layer: Relationships reinvestigated in view of remote sensing applications. Limnol Oceanogr 34: 1545–1562

Morel A and Bricaud A (1981) Theoretical results concerning light absorption in a discrete medium, and application to specific absorption of phytoplankton. Deep-Sea Res 28, 1375–1393

Morel A and Maritorena S (2001) Bio-optical properties of oceanic waters: A reappraisal. J Geophys Res 106: 7163–7180

Morel A and Prieur L (1977) Analysis of variations in ocean color. Limnol Oceanogr 22: 709–722

Moya I and Cerovic ZG (2004) Remote sensing of chlorophyyll fluorescence: Instrumentation and analysis. In: Papageorgiou GC and Govindjee (eds) Chlorophyll *a* Fluorescence: A Signature of Photosynthesis, pp 429–445. Springer, Dordrecht

Neville RA and Gower JFR (1977) Passive remote sensing of phytoplankton via chlorophyll *a* fluorescence. J Geophys Res 82: 3487–3493

O'Reilly JE, Maritorena S, Mitchell BG, Siegel DA, Carder KL, Garver SA, Kahru M and McClain C (1998) Ocean color chlorophyll algorithms for SeaWiFS. J Geophys Res 103: 24937–24953

Platt T (1986) Primary production of the ocean water column as a function of surface light intensity: Algorithms for remote sensing. Deep Sea Res 33:149–163

Pope RM and Fry ES (1997) Absorption spectrum (380–700 nm) of pure water, II, Integrating cavity measurements. Appl Opt 36: 8710–8723

Smith RC and Baker KS (1978) The bio-optical state of ocean waters and remote sensing. Limnol Oceanogr 23: 247–259

Stramski D, Bricaud A and Morel A (2001) Modeling the inherent optical properties of the ocean based on the detailed composition of the planktonic community. Appl Opt 40: 2929–2945

Sugihara S, Kishino M and Okami N (1984) Contribution of Raman scattering to upward irradiance in the sea. J Oceanogr Soc Jap 40: 397–404

Westberry T K, and Siegel D A (2003) Phytoplankton natural fluorescence variability in the Sargasso Sea. Deep-Sea Res I, 50: 417–434

Yentsch CS (1962) Measurement of visible light absorption by particulate matter in the ocean. Limnol Oceanogr 7:207–217

Chapter 37

Geochemistry of Chlorophylls

Brendan J. Keely
Department of Chemistry, University of York, Heslington, York, YO10 5DD, U.K.

*Author for correspondence, email: bjk1@york.ac.uk

Bernhard Grimm, Robert J. Porra, Wolfhart Rüdiger and Hugo Scheer (eds): Chlorophylls and Bacteriochlorophylls: Biochemistry, Biophysics, Functions and Applications, pp. 535–561.

Summary

In spite of intensive studies over more than 70 years, the geochemistry of tetrapyrrole pigments still presents numerous challenges. Recent studies have focused on functionalized precursors of sedimentary porphyrins, making extensive use of developments in analytical capabilities. Many new structures have been characterized, confirming the Treibs hypothesis linking chlorophyll *a* to the major sedimentary porphyrin, deoxophylloerythroetioporphyrin, and revealing a number of alternative transformation pathways. Functionalized transformation products of chlorophylls *a*, *b*, and *c* and of bacteriochlorophylls *c* and *d* have all been recognized indicating that all primary producer communities are represented in the sedimentary record. It is evident that redox status, grazing pressure and secondary reactions can all influence the fate of chlorophyll, and that the variety of transformation products present in natural sedimentary environments contains a wealth of information pertaining to the conditions present at the time of sediment deposition. Several entirely novel pigment transformation products have been identified and others represent viable precursors for sedimentary porphyrin structures previously of uncertain origin. As a direct result of the advances in analytical methods it is now possible to perform on-line analysis at very high stratigraphic resolution. At cm and mm scale resolution pigment profiles can show a significant degree of variation, indicating that the pigments are highly sensitive markers of environmental change. Thus, in addition to providing information on the source organisms present in past environments, chlorophyll derivatives have great potential for use in a range of paleoenvironmental proxies.

I. Introduction

During the mid 1930s the German chemist Alfred Treibs presented two seminal papers in which he reported the presence of the alkyl metallo-porphyrins deoxophylloerythroetioporphyrin (DPEP; **1a**) and etioporphyrin III (**2a**) and their carboxylic acid counterparts (**1b, 2b**) in sediments (Treibs 1934, a,b). Treibs isolated the components by partitioning according to acid number and assigned structures, making extensive use of ultraviolet-visible (UV/Vis) spectroscopy. The structural similarity of DPEP to chlorophyll (Chl) *a* (**3**) and of etioporphyrin III to heme (**4**) led Treibs to suggest that these components represented precursor-product pairs (Treibs, 1936). Later, Corwin (1960) noted that sedimentary porphyrin distributions were more complex than Treibs' initial work had suggested and argued, on the basis of mass balance of the precursors, that the majority of porphyrins were derivatives of Chl. Within a few years, the application of mass spectrometry in the analysis of sedimentary porphyrins provided very clearly evidence that they are complex distributions of homologous components dominated by cycloalkanoporphyrins (CAPs) such as DPEP and etioporphyrins (Baker, 1966) such as etioporphyrin III. More recently, structural evidence for the origins of etioporphyrins from both heme (Bonnett et al., 1983) and from Chl (Fookes, 1985) has been reinforced by stable isotope analysis ($\delta^{13}C$ measurement) of sedimentary porphyrins (Boreham et al., 1989; Ocampo et al., 1989). The major pathway leading to etioporphyrins is likely to occur via oxidative cleavage of ring E of Chl as suggested by Baker et al. (1983, 1986).

Treibs' suggestion of a precursor-product relationship between biological tetrapyrroles and the ancient porphyrins present in sediments led to the development of the field of Organic Geochemistry. The precursor product relationship has since been extended to numerous classes of natural product and significant advances have been made in understanding the nature of, and controls on, the transformation reactions of natural products in the natural environment. A major part of this understanding can be linked directly to the pioneering work of Treibs in which the series of transformation reactions required to effect conversion of Chl to DPEP was proposed (Treibs, 1936). The viability of the Treibs hypothesis has been confirmed by the characterization, in three

Abbreviations: APCI – atmospheric pressure chemical ionization; BChl – bacteriochlorophyll; biCAP – bicycloalkanoporphyrin; BPheide – bacteriopheophorbide; BPyPhe –bacteriopyropheophytin; BVir – bacterioviridin; CAP – cycloalkanoporphyrin; CCE – chlorin carotenyl ester; Chl – chlorophyll; Chlide –chlorophyllide; Chlone – chlorophyllone; COSY – correlation spectroscopy; CSE – chlorin steryl ester; CyPheide – cyclopheophorbide; DPEP – deoxophylloerythreoetioporphyrin; LC-MS – liquid chromatography mass spectrometry; MS – mass spectrometry; MS/MS – tandem mass spectrometry; MS^n – multistage mass spectrometry; NMR – nuclear magnetic resonance; NP-HPLC – normal-phase high performance liquid chromatography; Phe – pheophytin; Pheide – pheophorbide; Py – pyro; PyPhe – pyropheophytin; PyPheide – pyropheophorbide; RP-HPLC – reversed-phase high performance liquid chromatography

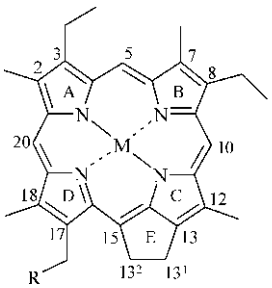

1a R=Me, M = Metal/2H
b R=CO_2H, M = Metal/2H

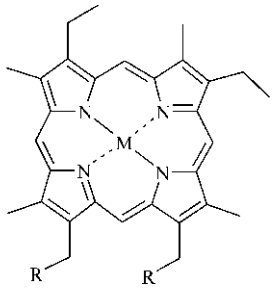

2a R=Me, M = Metal/2H
b R=CO_2H, M = Metal/2H

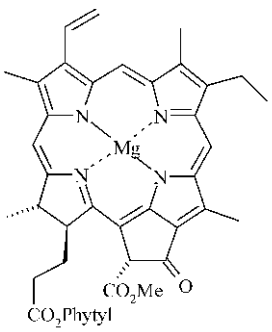

3

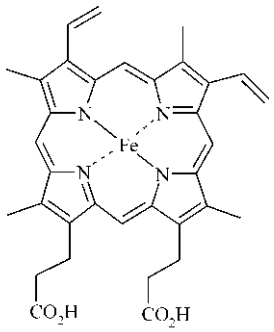

4

sediments, of the minimum number of intermediates required to complete the conversion of Chl *a* to DPEP (Keely et al., 1990). Thus, the Treibs Scheme (Fig. 1) provides an essential framework for understanding and interpreting the significance of sedimentary tetrapyrrole distributions.

A. Porphyrins in the Geological Record

Over the years, a number of comprehensive reviews have been published detailing the variety of porphyrin structures identified in sediments and oils (Baker and Palmer, 1978; Baker and Louda, 1986; Louda and Baker, 1986; Chicarelli et al., 1987; Ocampo et al., 1987; Callot et al., 1990; Callot, 1991; Callot and Ocampo, 2000). Accordingly, only the key features of sedimentary porphyrin geochemistry are presented here, sufficient to provide the essential context within which functionalized sedimentary tetrapyrrole structures must be viewed. Specifically, the issues discussed relate to the ability, or otherwise, to designate a particular biological source to individual sedimentary porphyrin structures, and the nature of the transformation pathways by which particular classes of sedimentary porphyrin are suggested to arise. Representative examples of porphyrin structures are included in this section: no attempt has been made to provide a comprehensive review. Sedimentary porphyrins occur mainly as Ni and VO complexes, though a variety of other metals have been observed in sediments, coals and oil. For detailed coverage, including the structures of the many homologues and isomers of the various classes of porphyrin discussed, the reader is directed to three excellent review articles (Chicarelli et al., 1987; Callot, 1991; Callot and Ocampo, 2000). Thorough and detailed discussion of the nature and distributions of metals in sedimentary porphyrins can be found in Filby and van Berkel (1987).

Sedimentary porphyrins identified to-date include many structures that could originate from two or more precursor Chls. Interestingly, although Chl *a* is almost certainly the major precursor of sedimentary porphyrins, no known sedimentary porphyrin structure can be linked exclusively to this precursor. Some porphyrins, however, do possess unique structural

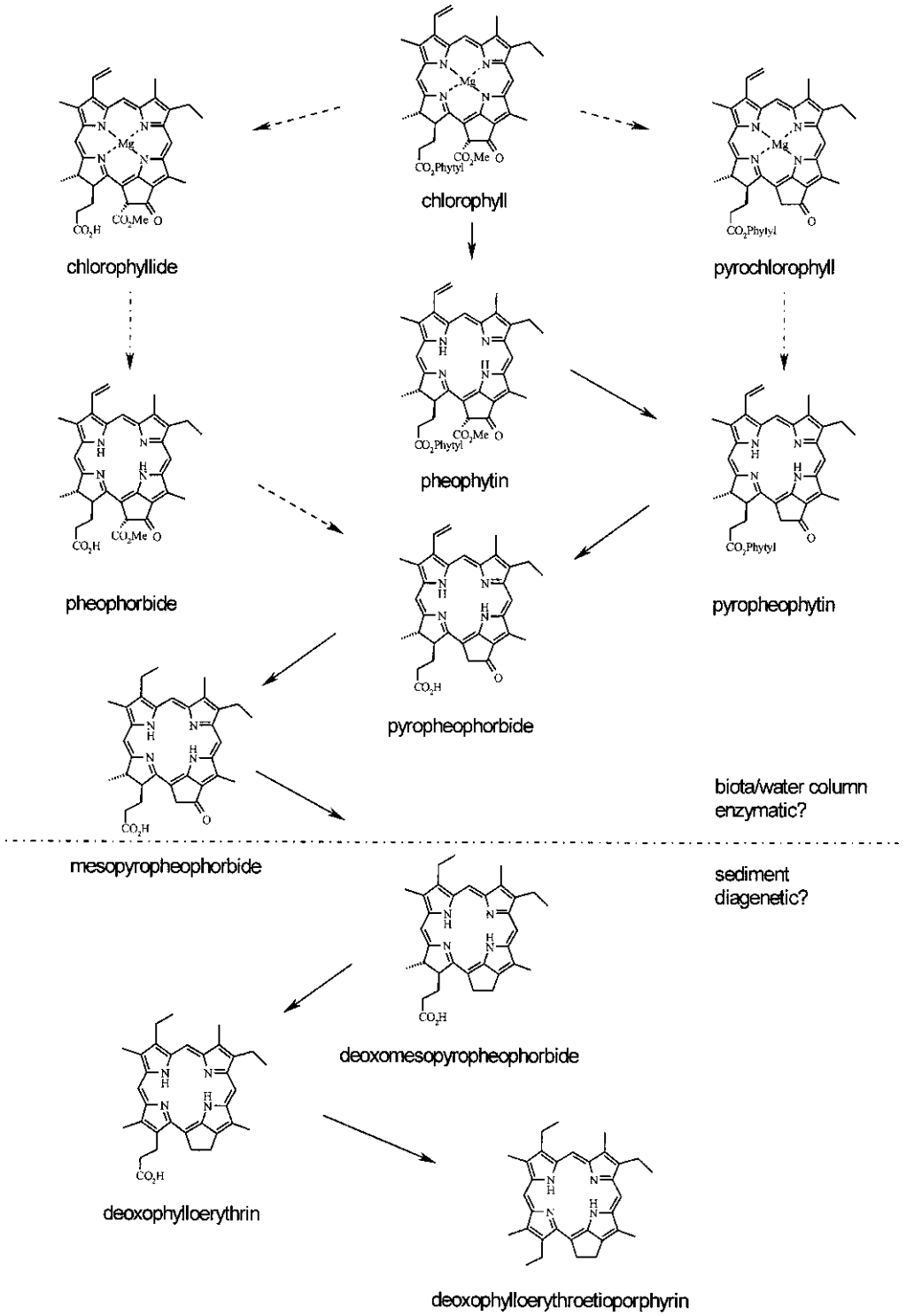

Fig. 1. Representation of the Treibs Scheme leading to cycloalkanoporphyrins, formulated for Chl *a*. The minimum number of intermediates required to effect conversion of Chl *a* to DPEP are connected by solid arrows, dotted arrows indicate variations in reaction order that are known to occur — many others are possible. Structures above the broken line can be formed within the water column or surface sediment, the timing of formation of those below the dotted line is uncertain (adapted from Keely et al., 1990).

features that permit an origin from a particular Chl to be recognized. Thus, as a result of the restricted occurrences of individual Chls among photoautotrophs, porphyrins can provide direct evidence for contributions to the sedimentary organic matter pool from specific groups of organisms.

1. Source Specific Porphyrins

The presence of a β-hydrogen at C-7 (see structure **1** for numering) was initially suggested to indicate that porphyrin (**5**) was a specific transformation product of Chl *b* (**6**; Chicarelli and Maxwell, 1984), implying an origin from Chlorophyta or from type II cyanobacteria, though the former are a more likely source based on relative abundance in nature. Subsequently, however, the discovery of Chl c_3 (**7c)** in a coccolithophorid alga (Fookes and Jeffrey, 1989) provided an alternative source. Consequently, there are no porphyrin structures known that can be assigned an origin exclusively from either Chl *a* or Chl *b*. The best candidates for source-specific porphyrins of algal origin are CAP structures (**8**; Ocampo et al., 1984; Verne-Mismer et al., 1988, 1990) derived from Chls *c* (**7**). These compounds can be recognized as Chl *c* derivatives by the unusual structural motif whereby a methyl- or ethanoic acid- substituted five-membered exocyclic ring exists between C-15 and C-17 and not between C-13 and C-15 as is usual in CAPs (cf **1**). The ring system originates from an acid catalyzed Michael-type addition reaction involving the acrylic acid side chain of the Chls *c* and the nucleophilic C-13^2 carbon atom of the ring-E ketoester system, with loss of the C-13^1 and C-13^3 carbon atoms by decarboxylation and decarbomethoxylation. The C_{31} derivative (**8a)** could arise from Chls c_1, c_2 or c_3 (**7a-c**) whereas the C_{30} derivative (**8b**) could only originate by C-7 decarbomethoxylation of Chl c_3 (**7c**).

Bacteriochlorophylls (BChls) *a* (**9**) and *b* of the purple bacteria also can not be linked to unique alkyl

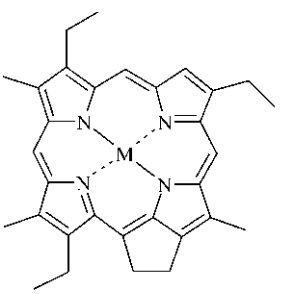

5 M = Metal

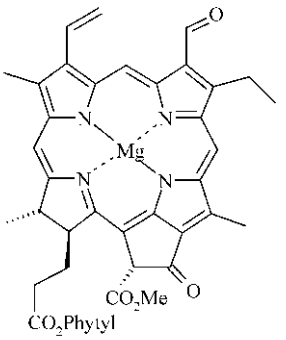

6

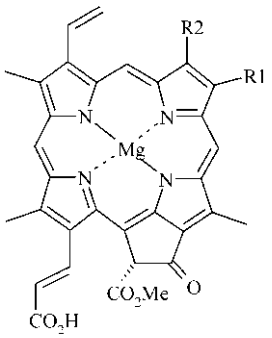

7a R1 = Et, R2 = Me
b R1 = Vinyl, R2 = Me
c R1 = Vinyl, R2 = CO_2Me

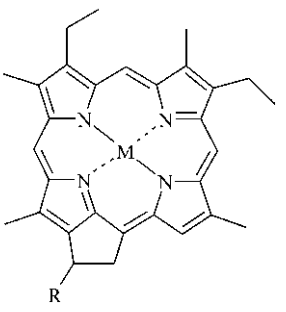

8a R = Me, M = Metal
b R = CH_2CO_2H, M = Metal

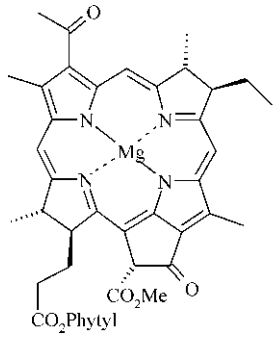

9

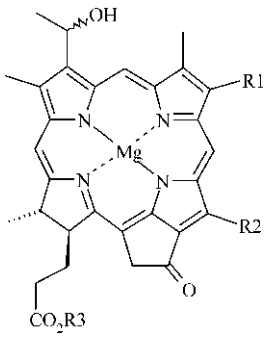

R1 = Et, *n*-Pr, *i*-Bu, *neo*-Pent
R2 = Et, Me
R3 = Alkyl (various)

10

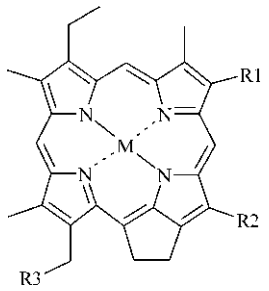

R1 = Et, *n*-Pr, *i*-Bu
R2 = Et, Me
M = Metal

11a R3 = CO_2H
b R3 = Me

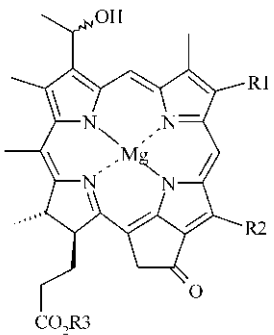

R1 = Et, *n*-Pr, *i*-Bu
R2 = Et, Me
R3 = Alkyl (various)

12

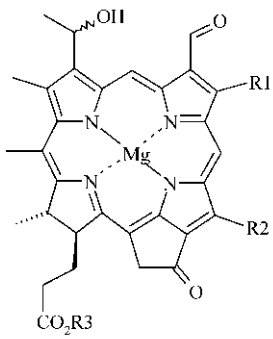

R1 = Et, *n*-Pr, *i*-Bu, *neo*-Pent
R2 = Et
R3 = Alkyl (various)

13

porphyrin structures: reduction of the C-3 methyl ketone and oxidation of the bond between C-7 and C-8 would lead to structures that could equally well arise from any of the Chls *a*, *b* and *c* or from the BChl *d* (**10**) homologues possessing the [C-8, C-12] alkylation pattern [Et, Me]. By contrast, BChl *d* from green sulfur bacteria can be recognized as the source of the porphyrin carboxylic acids (**11a**) and alkylporphyrins (**11b**) with the unique structural feature of extended alkylation at C-12 and/or C-8 (Ocampo et al., 1985; Keely and Maxwell, 1993; Gibbison et al., 1995). Similarly, partial structure analysis of a sedimentary porphyrin from the Oulad Abdoun oil shale of Morocco suggested the presence of a C-20 Me substituent, leading Callot et al., (1990) to suggest an origin from either BChl *c* (**12**) or *e* (**13**) of the green bacteria.

2. Unusual Porphyrin Structures

A number of sedimentary porphyrins possess ring structures that can only be rationalized as arising through modification of precursor Chls. In addition to the Chl *c*-derived porphyrins discussed above, these components include methylcyclohexano- (**14**; Chicarelli et al., 1984) and cycloheptano- (**15**; Fookes, 1983; Wolff et al., 1983) porphyrins, bicycloalkanoporphyrins (bi-CAPs, e.g., **16;** Prowse et al., 1987) and a 13^1-methyl-substituted bicycloalkenoporphyrin (**17**; Chicarelli and Maxwell, 1986), tetrahydrobenzo- (**18**; Verne-Mismer et al., 1987) and benzoporphyrins (**19**; Kaur et al., 1986). Plausible mechanistic pathways to the cyclohexanoporphyrin and bi-CAP structures have been suggested, involving condensation reactions between the C-17 propionic acid substituent and the $C\text{-}13^2$ carbon atom. Despite attempts to identify likely precursors, the origins of

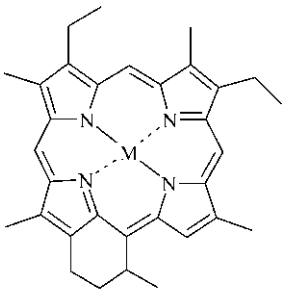

14 M = Metal

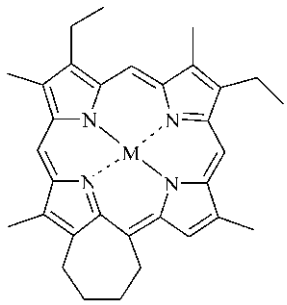

15 M = Metal

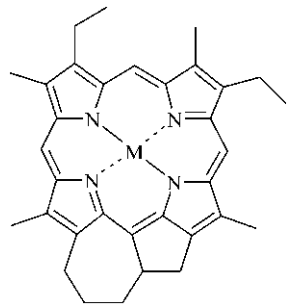

16 M = Metal / 2H

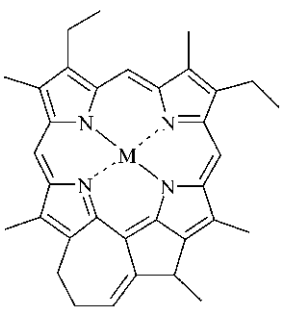

17 M = Metal

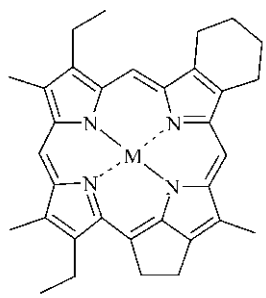

18 M = Metal

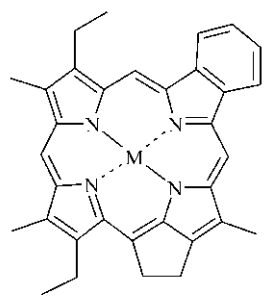

19 M = Metal

the 13^1-methyl-substituted component (**17**), tetrahydrobenzo- (**18**) and benzoporphyrins (**19**) remain uncertain, though a Diels-Alder reaction involving [8-vinyl]-Chl *a* (present in some type II cyanobacteria; Chapter 1, Scheer) has been suggested for the last two (May and Lash, 1992).

The brief review above illustrates the wide range of structural variations within natural porphyrin distributions, alludes to their complexity and shows that questions as to the origins of some structures remain to be answered. In order to provide insights into the origins of sedimentary porphyrins, recent work has largely focused on identification of functionalized derivatives in Recent sediments and on characterizing distributional differences within, and between, a range of depositional settings. These studies owe much to the early work of Baker and co-workers who identified functionalized tetrapyrroles in cores recovered under the Deep-Sea Drilling Project (for reviews see Baker and Louda, 1983, 1986; Louda and Baker, 1986). Owing to the limited capabilities of analytical instrumentation at that time, those studies were restricted in the extent to which structures could be confirmed. Over the last ten years, the considerable advances in development of analytical techniques and their application to identification of the functionalized precursor chlorins have allowed greater certainty in structure assignments and have revealed a number of novel components. During that time research activity in this area has been substantially greater than in the analysis of the corresponding sedimentary alkyl porphyrins. Major targets in the studies of functionalized precursors have been the identification of transformation products and the pathways by which they are formed, and the recognition of environmental- and source-specific markers. Accordingly, the main focus of this article concerns the functionalized precursors of sedimentary porphyrins, representing the earliest stages of transformation. Derivatives of all of the major Chls are included, encompassing dihydroporphyrins (chlorins, e.g., Chl *a*; **3**), tetrahydroporphyrins (bacteriochlorins, e.g., BChl *a*; **9**) and porphyrins (e.g., Chl *c*; **7**). A brief resume of the most widely used methods of analysis is presented, followed by discussion of the main transformation pathways, transformation products and uses in environmental assessment.

B. Analytical Methods

Sedimentary tetrapyrroles occur as complex distributions, necessitating chromatographic separation prior to analysis. The main spectroscopic methods employed in characterization are UV/Vis, mass spectrometry (MS) and nuclear magnetic resonance (NMR). Other techniques, including Raman spectroscopy and stable isotope ratio analysis, have also been applied but will not be considered further here. Owing to the chemical reactivity of many of the functionalized tetrapyrroles there is considerable opportunity for the formation of artifacts during extraction and workup. Hence, the methods used to extract and analyze the tetrapyrroles must be sufficiently mild and rapid so as to avoid reactions leading to such products.

1. Extraction

The sensitivity of Chl derivatives to oxidation reactions in alcoholic solutions was recognized around 100 years ago (Willstätter and Stoll, 1913). More recently, it has been established that these are facile autoxidation reactions that are specific to components possessing a carbomethoxy substituent at position C-13^2: they depend on the activation of the C-13^2 hydrogen atom provided by the β-ketoester system (Hynninen, 1991; Woolley et al., 1998). Accordingly, extraction of tetrapyrroles possessing this structural feature requires the avoidance of alcohols in the extraction medium. Acetone is the preferred extraction solvent and, as a precaution to avoid photo-oxidation, solutions are protected from exposure to strong light. In order to prevent autoxidation, which occurs only very slowly in acetone, rapid extraction methods such as sonication are employed (Keely et al., 1990; Airs et al., 2001a).

2. Reversed-phase High Performance Liquid Chromatography (RP-HPLC) Analysis

Several RP-HPLC methods have been developed for the analysis of functionalized tetrapyrroles (for examples, see the review by Roy, 1987). To be of maximum value in geochemical analysis the analytical methods need to give good resolution over a wide polarity range, encompassing highly polar derivatives such as Chls *c* through to highly apolar derivatives including chlorin steryl esters (CSEs; see later). The availability of photodiode array detectors for HPLC places an additional constraint on the mobile phase composition. In order to obtain spectral information of Chl derivatives and co-occurring carotenoids over a wide range, UV absorption by the mobile phase should be as low as possible. Thus, replacement of acetone (Eckardt et al., 1991; Verzegnassi et al., 1999; Zapata et al., 2000) by ethyl acetate (Wright et al., 1991) is favored. To achieve the combined goals of excellent chromatographic resolution, UV-transparency and compatibility with liquid chromatography mass spectrometry (LC-MS), a method was developed for the analysis of sedimentary tetrapyrroles (Method A; Airs et al., 2001a). Variants of the method were also developed, allowing flexibility according to the requirements of the analysis and the availability of instrumentation and preparative apparatus. Methylation of carboxylic acids by treatment with diazomethane is recommended in order to obtain the best chromatographic peak shape possible and to permit long term storage of extracts (Airs et al., 2001a and references therein).

3. Normal-phase High Performance Liquid Chromatography (NP-HPLC) Analysis

Chlorophyll autoxidation reactions lead to the formation of a range of products, some of which are not well resolved under RP-HPLC conditions. Better chromatographic resolution of Chl oxidation products can be achieved using NP-HPLC (Kuronen et al., 1993) and the compatibility of this approach with LC-MS analysis has been demonstrated for mixtures of Chl oxidation products formed in the laboratory (Jie et al., 2002).

4. Liquid Chromatography-Mass Spectrometry Analysis

Broad distinctions between different classes of Chl derivative can be made according to chromatographic elution order and on-line UV/Vis spectra, and further refinement is possible from co-elution with authentic standards. For rigorous assignment, however, it is necessary to obtain molecular mass and structural information by MS. The value of tandem MS (MS/MS) in assignment of functionalized sedimentary tetrapyrrole structures was demonstrated using fractions isolated by preparative HPLC and ionized using fast atom bombardment (Keely and Maxwell, 1990a). Fragment ions yielding structure-specific information were readily obtained, but the off-line analytical ap-

proach is laborious and places severe constraint on the number of samples that can be processed. For this reason, LC-MS, which enables on-line analysis, is now the method of choice for MS analysis of sedimentary tetrapyrrole distributions. Significant improvements in the ease and rapidity of MS/MS analysis result from use of the atmospheric pressure ionization techniques electrospray (Chillier et al., 1994) and atmospheric pressure chemical ionization (APCI; Airs et al., 2001a; Airs and Keely, 2002). APCI has been shown to give excellent response for production of radical anions (negative ion-mode) and of protonated molecules (positive ion mode) from functionalized free-base tetrapyrroles (Verzegnassi et al., 1999; Airs et al., 2001a). Combined with post-column addition of acid, to effect on-line demetallation of the Mg-containing derivatives (Airs and Keely, 2000), the technique also provides excellent response for the Mg-containing species (Airs et al., 2001a; Airs and Keely, 2002). The application of ion-trap mass spectrometry, with its unique multistage (sequential or MS^n) approach to MS/MS, has been of particular benefit in distinguishing between structurally similar Chl derivatives (Airs et al., 2001a; Airs and Keely, 2002; Squier et al., 2002; Wilson et al., 2003, 2004a). In APCI ion trap MS of Chl derivatives the precursor ion, the protonated molecule, is isolated within the trap and is subjected to resonance excitation, forming product ions by fragmentation induced by collision with the He bath gas in the trap. The product ion spectrum (MS^2) is generally dominated by one fragment ion. The process of isolation and fragmentation can be repeated on one of the MS^2 product ions and subsequently up to at least MS^7 (Airs and Keely, 2002; Wilson et al., 2003, 2004a). In this way, the detailed fragmentation behavior of a significant number of Chls and their derivatives has been determined and it is apparent that the derivatives follow systematic fragmentation pathways (Jie et al., 2002; Airs and Keely, 2002; Walker et al., 2003; Wilson et al., 2003, 2004a).

A study of BChls from green and brown bacteria exemplifies the need for the combined approach offered by LC-MS analysis. Bacteriochlorophylls from cultured organisms reveal highly complex distributions in which variations are evident both in the extent of alkylation at C-8 and/or C-12 and in the nature of the esterifying alcohol (Airs et al., 2001b). Within each of the BChl series (*c, d* or *e*), which can be assigned from the on-line UV/Vis spectra, the *m/z* value of the protonated molecule provides very limited structural information as a result of the large number of structural isomers possible for each molecular mass. The application of tandem MS allows designation of the esterifying alcohol to a restricted range of possibilities (Airs et al., 2001b; the exact structure of each can be determined by gas chromatography-mass spectrometry of the free alcohols after hydrolysis) and the total extent of alkylation at [C-8, C-12]. Detailed studies of the MS^n spectra of the (demetallated) Chls (Airs and Keely, 2002) or their corresponding pheophorbides (Pheides; Wilson et al., 2003, 2004a) allow assignment of the alkyl substitution patterns at each of the two positions. Notably, the use of MS^n analysis allowed contributions from co-eluting isobaric bacteriopheophorbides (BPheides) to be detected and the overlapping signals to be deconvoluted (Wilson et al., 2003, 2005), highlighting the necessity for mass spectral analysis as an essential tool in the determination of complex sedimentary pigment distributions.

Normal-phase LC-MS/MS has also been employed in the analysis of sedimentary alkyl porphyrins (Rosell-Melé et al., 1996, 1999; Mawson et al., 2004). In the later of these studies the complexity of the distributions, and lack of chromatographic resolution as a result of the preponderance of isomeric structures, precluded the isolation of individual components for NMR analysis. The application of LC-MS^n allowed assignment and quantification of many porphyrins, including structures exhibiting only partial chromatographic resolution (Mawson et al., 2004).

5. Nuclear Magnetic Resonance Analysis

Proton NMR analysis is one of the most rigorous methods for characterizing sedimentary tetrapyrroles: analysis of spin-spin interactions and through space connectivities determined from nuclear Overhauser enhancement allows full assignment of structures of individual components isolated from sediments and oils (Chicarelli et al., 1987; Callot et al., 1990; Callot and Ocampo, 2000). The application of two dimensional techniques (e.g., correlation spectroscopy, COSY; Keely and Maxwell, 1990b and COSY and rotating-frame Overhauser enhancement spectroscopy; Ocampo and Repeta, 1999) can lead to greater structural specificity by avoiding effects due to irradiation spill, and simplifies the analysis by alleviating the need to select individual irradiation positions in setting up the experiment. In the case of porphyrins, where the number of isomeric structures

is greatest, NMR is still required to discriminate some porphyrin structures and is the method of choice to confirm novel structures. By contrast, the majority of the more functionalized derivatives can be fully assigned using LC-MS/MS (e.g., Airs et al., 2001a; Squier et al., 2002; Wilson et al., 2004a), alleviating the need for isolation and purification for NMR analysis.

II. Chlorophyll Transformations

Geochemical interest in Chl derivatives relates both to their potential as sources of the porphyrin derivatives that occur in sediments and oils and their potential as indicators of specific environmental conditions and processes. Since the latter depends on an understanding of their origins, the following discussion considers Chl transformation products in the context of common transformation pathways. Transformation reactions of Chls that leave the macrocycle intact have been termed type I transformation reactions and ones that lead to cleavage of the macrocycle are termed type II (Hendry et al., 1987). In situations where the environment is oxygen-limited or oxygen-deficient (termed reductive below) type I reactions dominate. In environments where oxygen is readily available (termed oxidizing below) both type I and type II reactions can occur.

A. Regular Reductive Transformation Products

1. Products of Simple Type I Defunctionalization Reactions

The characteristic structural feature that identifies the products of reductive transformation reactions of Chls is the intact carbon skeleton of ring E. Structures including pheophytins (Phes), Pheides and their pyro- (Py) derivatives (Fig. 1) are formed by simple defunctionalization reactions that involve modifications of functional groups around the periphery of the macrocycle. Pheophytins, Pheides and their Py-counterparts are among the earliest derivatives produced in natural environments, being formed either through the processes of senescence (Schoch et al., 1981; Spooner et al., 1994a; Chapter 17, Kräutler and Hörtensteiner) or herbivory (Shuman and Lorenzen, 1975). Typically, they are among the major products in contemporary and Recent sediments (Keely et al., 1990; Villanueva et al., 1994a; Airs et al., 2001a; Squier et al., 2002; Airs and Keely, 2003; Squier et al., 2004a; Wilson et al., 2004a) and Py-pheoporphyrins (**20, 21**) derived from Chls c_1 and c_2 have also been detected (Harradine and Maxwell, 1998). Similar transformation products of BChl *a* have been identified (Villanueva et al., 1994b), indicating that the same transformation mechanisms affect the prokaryote and eukaryote communities. In the case of BChls *c, d* and *e*, the main derivatives identified in Recent sediments are the Phes (Squier et al., 2002, 2004a; Airs and Keely, 2003; Wilson et al., 2004a); the absence of a C-13^2 carbomethoxyl group in these BChls limits the variety of structures possible. Thus, the bacteriopheophytins (BPhes) *c, d* and *e* are structurally analogous to the Py-derivatives of Chls *a, b, c* and BChl *a*, but require one fewer reaction step in their formation. The presence of Phe derivatives of BChls and of bacteriopyropheophytin *a* (BPyPhe *a*) in sediments provides evidence that senescence is important in their formation. The major BChl-producing organisms are confined to dysoxic and anoxic regions of the water column (van Gemerden, 1983), hence grazing organisms can play only a minor role in the transformation reactions leading to their sedimentary derivatives.

Phes and PyPhes are also commonly found within fecal material (Burkill et al., 1987; Talbot et al., 1999a,b) where they are considered to be products of the grazing process. Clearly, however, the process of grazing itself can induce senescence reactions and the distinction between endogenous algal and exogenous (e.g., grazer) enzyme effects is unclear. For example, Spooner et al. (1994b) incubated lysed diatom cells in the dark and found that the rate of formation of chlorophyllide (Chlide), Pheides, Phe and PyPhe, produced by the actions of the algal enzymes, matched zooplankton gut clearance rates. High abundances of Pheides in marine environments have been suggested to be indicative of grazing (Shuman and Lorenzen, 1975). Although Pheides occur in high relative abundance in the fecal material of some grazers, they can also be produced by demetallation of Chlide formed by the actions of chlorophyllase, an active enzyme in certain diatoms (Jeffrey and Hallegraeff, 1987) and various other algae. Accordingly, caution must be exercised in the interpretation of Pheides in sediments. The occurrence of Pheides in a submerged microbial mat system from which grazers were absent (Villanueva et al., 1994a) attests to formation resulting from chlorophyllase activity. In that case, the enzyme appeared to have its origins in diatoms co-existing with the cyanophyta that comprised the main photoautotrophs in the mat.

Other Chl derivatives formed through reductive

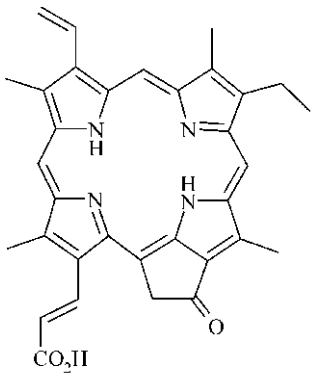

20

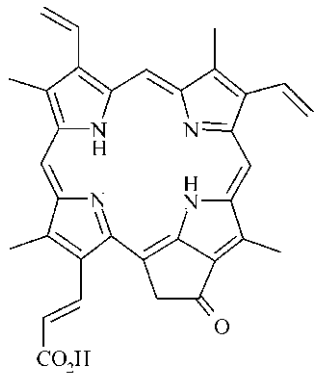

21

transformation pathways include the products of C-3 vinyl and C-13[1] ketone reduction, aromatization and decarboxylation (Keely et al., 1990, 1994). Notably, none of the derivatives formed by these reactions have been identified in the water column, though they have been identified in unconsolidated and thermally immature sediments from Maraú (Keely et al., 1990), Willershausen (Keely et al., 1994), Messel oil shale (Ocampo et al., 1992) and marls of the Vena del Gesso evaporitic sequence (Keely et al., 1995). Precedent for the C-3 vinyl reduction depending on microbial activity comes from the formation of mesoPyPheide *a* (Fig. 1) in laboratory microcosms in which algal cells were incubated in the presence of sulfate reducing bacteria (Spooner et al., 1995). The mechanisms leading to C-13[1] ketone reduction, aromatization and decarboxylation remain to be established, though it is evident, by the occurrence of derivatives in immature sediments, that the reactions are not exclusively thermal.

The occurrence, as the predominant BChl derivative in an Antarctic sediment, of BPhe a_{gg} in which the esterifying alcohol is geranygeraniol signifies an input from the aerobic purple bacteria, which are heterotrophs (Squier et al., 2004b). The recognition that such aerobic bacterial inputs can impart a dominant signature on the sedimentary pigment profiles indicates the caution that must be exercised in interpreting the presence of de-esterified counterparts of BChl *a*.

B. Oxidative Transformation Products

1. Products of Type II Reactions

Oxidation reactions of Chls follow two distinct mechanistic pathways. Photo-oxidation involves reaction with singlet oxygen and follows a pathway in which the initial attack of oxygen is at position C-5, generating products in which the macrocycle is cleaved (Mühlecker et al., 1993). Reactions involving cleavage of the Chl macrocycle are designated type II (Hendry et al., 1987) and produce linear tetrapyrrole products that are colorless or weakly-colored, and which are subsequently degraded to maleimides (monopyrrolic derivatives). Maleimides have been identified in sediments of the Kupfershiefer and the Serpiano shale, where the alkylation patterns of individual structures (e.g., **22, 23**) could be assigned an origin from BChls *c*, *d* or *e* (Grice et al., 1996). Isotopic signatures enriched in ^{13}C lend support to the proposed partial origin of **22** and origin of **23** from Chlorobiaceae (Grice et al., 1997). The characterization of maleimides, both as free components and following chromic acid oxidation of bound residues, has since been applied to marine sediments of Neogene age from the Shinjo basin (Kozono et al., 2001) and Cretaceous-Tertiary boundary sediments from Kawaruppu (Shimoyama et al., 2001). In those settings, 2-methyl-3-ethylmaleimide was the dominant component, occurring with lesser amounts of 2-methyl-3-*n*-alkyl derivatives (methyl to pentyl at C-3 in Shinzo and methyl to butyl in Kawaruppu). The extended *n*-alkylation up to C-5 at C-3 does not suggest a specific origin from pigments of green bacteria. Rather, it can only be rationalized as resulting from retention of carbon atoms C-13 to C-17, most likely from derivatives in which the C-13[1] ketone had been reduced. Lesser amounts of 2-methylmaleimide, benzomaleimide (**24**) and methylated homologues, and tetrahydrobenzomaleimide were also present. Marked differences in the distributions of the free and bound maleimides were attributed to the former being products of photo-oxidation of Chls and the latter being formed from bound porphyrins. Evidence for the formation of maleimides by oxidative trans-

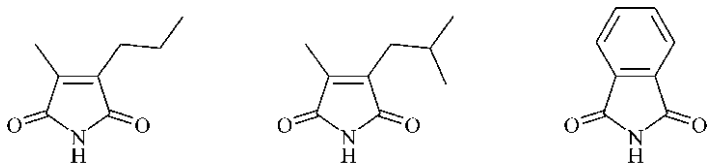

22 23 24

formation in the water column of a contemporary environment was provided by their recognition in the surface sediments of Tokyo Bay (Kozono et al., 2002). The benzo-derivatives in the ancient sediments were suggested to be products of oxidation of benzo- and tetrahydrobenzoporphyrins. Notably, evidence of maleimides with branched side chains was lacking (Kozono et al., 2001; Shimoyama et al., 2001), implying the absence of Chlorobiaceae at the time of sediment deposition. By contrast, clear evidence of photic zone euxinia associated with the major oceanic anoxic event of the Permian (Zechstein basin) was provided by recognition of maleimides with branched C-3 alkyl groups (Pancost et al., 2002), and later in sediments of Cenomanian-Turonian (North Atlantic), early Toarcian and early Aptian (Marche-Umbria, Italy) age, times also associated with oceanic anoxic events (Pancost et al., 2004).

2. Products of Regular (Type I) Reactions

Chlorophyll reacts with molecular oxygen (triplet oxygen) via type I reactions, leading to oxygen incorporation centered on ring E. A range of oxidation products form in alcoholic solution, including hydroxyl derivatives, lactones and ring-opened derivatives (Hynninen, 1991; Woolley et al., 1998). A number of related structures occur in natural sedimentary environments. The C-13^2 hydroxyl derivatives of Phe *a* (**25**) were identified in Loch Ness and Lake Baikal (Airs et al., 2000) and in Kirisjes pond (Walker et al., 2002), and corresponding C-13^2 hydroxyl derivatives of BPhe *a* and BPheide *a* in a coastal salt pond (Salt Pond) from the USA (Ocampo and Repeta, 2002, 2004). The ring-opened derivative purpurin-7 phytyl ester (**26**) was identified (as the dimethyl ester) in the sediments of Priest Pot, Loch Ness and Lake Baikal (Airs et al., 2000) and the anhydride derivatives purpurin-18 (**27a**) and its phytyl ester counterpart (**27b**) in Loch Ness and Lake Baikal (Naylor and Keely, 1998). The former anhydride was also found to occur in surface sediments of the Peru margin (Ocampo and Repeta, 1999). Derivatives formed by disruption of ring E with incorporation of oxygen are likely precursors of sedimentary etioporphyrins (Naylor et al., 1998; Airs et al., 2000). The presence of the hydroxyl and purpurin-18 derivatives in senescent algae (Louda et al., 1998, 2002) indicates viable mechanisms for formation within the water column. Clearly, therefore, parallels exist between laboratory oxidation products and the products of natural oxidation reactions. Although the main oxidation products found in the natural environment can be explained according to the autoxidation mechanism proposed by Hynninen (1991), a full treatment of the reaction mechanism remains to be performed.

Products of BChl *a* in which the 3-acetyl-tetrahydroporphyrin structure has been converted to a dihydroporphyrin (the so-called bacterioviridins, BVirs) have recently been identified in sediments where exposure to oxygen occurred. Specifically, the BVirs (**28a, b**) derived from BPhe *a* and BPheide *a* were identified (Wilson et al., 2004b), indicating breakdown of the dysoxic conditions required by the bacteria, leading to incursion of oxygen. It was not possible to determine if the ingress of oxygen occurred before, during or after deposition. Conversely, some environments containing BChl *a* derivatives do not contain BVirs (Villanueva et al., 1994b), consistent with their formation being dependent on the redox status of the environment. The BVir derivatives also have parallels in the laboratory oxidation of BChls (Woolley et al., 1998; Walker et al., 2003), indicating that oxygen penetration into the anoxic zone can impact on the bacterial community and leave a signature in the biological marker record.

Although it is not conclusive, evidence that water column redox status controls the presence and relative abundances of Chl oxidation products comes from the relative abundances of oxidation products in sediments. Thus, the highest levels of oxidation products have been observed in environments with long and more highly oxygenated waters (Naylor and Keely, 1998; Airs et al., 2000). Clear support

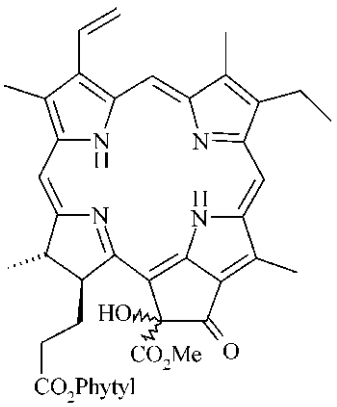

25

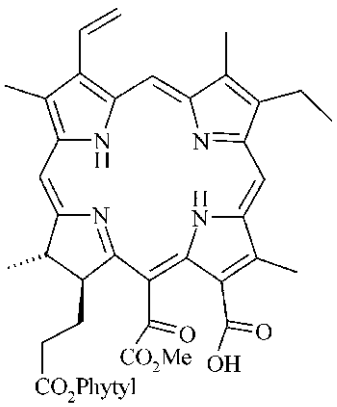

26

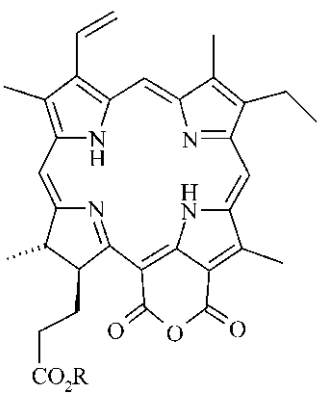

27a R = H
b R = Phytyl

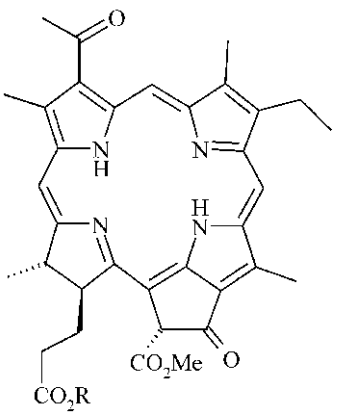

28a R = Phytyl
b R = H

for this hypothesis comes from the presence, in an Antarctic lake sediment, of Chl oxidation products during periods where algae were the main primary producers, and absence in regions of the sediment core deposited when anoxygenic bacteria dominated the primary producer community, but where algae were still present (Walker et al., 2002). Furthermore, a later study, examining distributions of Chls and their oxidation products during and following the Spring bloom in the Celtic Sea, found higher relative abundances of oxidation products during the later stages of the bloom (Walker and Keely, 2004). The timing of their formation indicates that these components are produced during overturn of the bloom, probably following exposure of the Chls as a result of cellular disruption associated with senescence. The presence of substantial amounts of Chl oxidation products in algal cultures subjected to senescence under oxidizing conditions (Louda et al., 1998, 2002) attests to their origins through autoxidation mechanisms, perhaps influenced also by the presence of peroxides released by the senescent algae (Merzlyak et al., 1993). Given that either route involves and depends on the availability of molecular oxygen, it is evident that Chl oxidation products have potential for use in paleoenvironmental proxies for the availability of molecular oxygen at the time of sediment deposition (see later). In order for this to be extended beyond a relative measure, the exact mechanism of oxidation needs to be determined, the role of peroxyl species defined, and the dependence on algal type examined.

C. Non-Regular Transformation Products

A number of non-regular Chl transformation products have been identified in which the normal functional group modifications are supplemented by reactions involving the coupling of non-Chl derived substituents or forming non-biosynthetic exocyclic ring structures. The departure from the typical degradative transformation reactions of Chls means that these components hold great potential as informative biological markers for specific processes affecting the primary producer community.

1. Chlorin Steryl and Triterpenoid Esters

Chlorin steryl esters (e.g., **29**), unusual components that were first identified in sediments (King and Repeta, 1991; Prowse and Maxwell, 1991), result from an esterification or transesterification reaction between a Chl derivative and a sterol. The major components found in sediments are derivatives of PyPheide *a* (Pearce et al., 1993), and there is much variety in the nature of the esterifying sterols (Harris et al., 1995a; Pearce et al., 1998). Lesser amounts of derivatives of PyPheide *b* and Pheide *a* have also been reported (Talbot et al., 1999b; Riffé-Challard et al., 2000). The sterols identified to-date represent typical algal sterols, though methyl sterols are under-represented compared with the free sterol distributions (Talbot et al., 2000). A significant overprint of the C_{27} sterol cholesterol from the grazing organism is apparent, and alterations to the sterol distribution can occur if the diet of the grazer is limited in cholesterol, in which case phytosterols are metabolized. The formation of CSEs has been observed during experiments in which diatoms were grazed by copepods (Harradine et al., 1996a; Talbot et al., 1999a). Their presence in high relative abundance in sediment traps (King and Repeta, 1994) and in the gut contents of marine salps, but absence in suspended particulate matter (King and Wakeham, 1996), has led to wide acceptance that CSEs are markers of herbivory. Similar derivatives, containing tetrahymanyl (**30**) or a hopanyl (**31**) in place of the steryl moiety, were identified in the sediments of Lake Valencia, Venezuela (Harradine et al., 1996b). The incorporation of tetrahymanol, which occurs in ciliates when dietary levels of sterols are low, together with hopanols was attributed either to zooplankton grazing a mixed diet comprising cyanophyta and ciliates or a direct effect of ciliates grazing cyanophyta (Harridine et al., 1996b).

Although high levels of CSEs in sediments have been attributed to their greater stability compared with free pigments, sediments of Lake Valencia and the Black Sea contain amounts of CSEs up to *c.* 20% of the pigment preserved in the sediment (Eckardt et al., 1992). Both are highly productive environments and grazing activity in the latter is confined to the surface waters (ca. 80 m), the water column being predominantly anoxic. Hence, the conditions are favorable to pigment preservation. Clearly, it is still necessary to reconcile the levels observed in natural environments with the lower levels observed in grazing experiments. Possible causes of these abundance differences include algal specificity and/or different extents of conversion by different grazers. Thus, for the CSEs to be employed as a quantitative measure, broader ranges of algae and grazing organisms need to be examined.

2. Chlorin Carotenyl Esters

Structures resulting from the esterification/transesterification of Chl derivatives with carotenol derivatives of fucoxanthin (e.g., **32**) were identified in sediments from the Southern California Bight, San Pedro and Santa Barbara Basins, Monterey Bay Canyon and Oman and Peru margins (Goericke et al., 1999). The assignments were made on the basis of HPLC retention times, on-line UV/Vis spectra and LC-MS^n analysis, and selected derivatives were prepared for comparison. Esters of both PyPheide *a* and Pheide *a* were detected and presumed to form in a manner analogous to CSEs. The apparent restriction of the carotenol source to fucoxanthin derivatives was suggested to reflect a specific grazing activity involving copepods and other crustaceans feeding on diatoms (Goericke et al., 1999). Studies of sediments from the Louisiana continental shelf also revealed CCEs to be restricted to fucoxanthinol derivatives, including novel structures in which dehydration of the carotenol had not occurred (Chen et al., 2003). In that study CCEs were also identified in fecal pellets collected from zooplankton trawled from surface waters (Chen et al., 2003).

3. Chlorophyllones and Cyclopheophorbide Enols

Chlorophyllones (Chlones, **33**) have been reported to occur in a wide range of sediments (Chillier et al., 1993; Harris et al., 1995b) and the structurally related

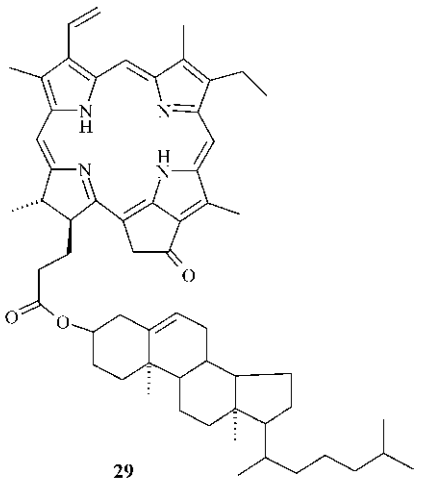

29

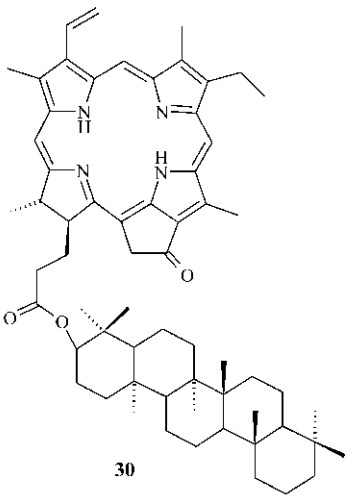

30

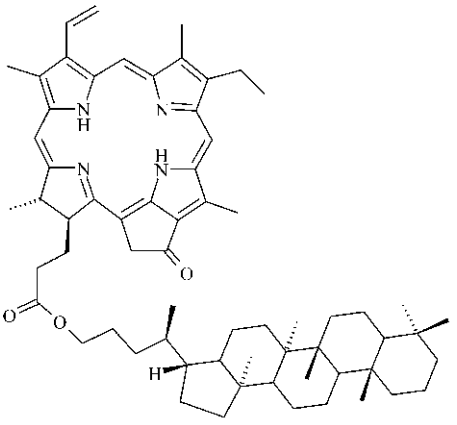

31

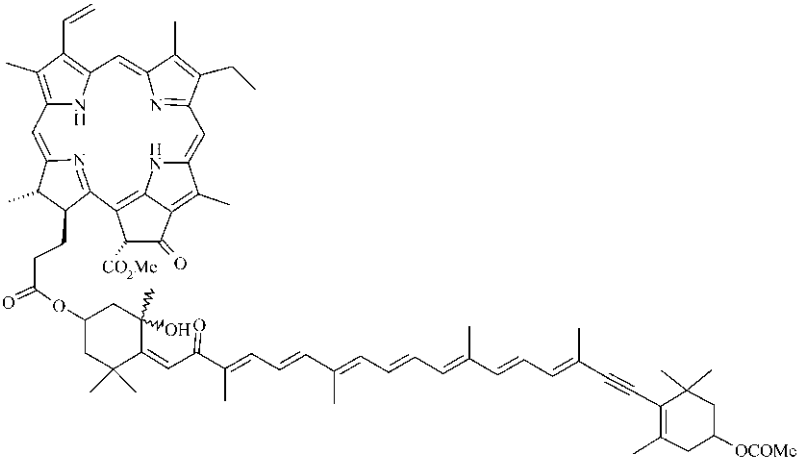

32

cyclopheophorbide (CyPheide) enols (**34**) have been identified in sediments (Ocampo et al., 1999; Louda et al., 2000) and in water column particulates (King and Wakeham, 1996; Ocampo et al., 1999). Both structural types exhibit features analogous to the bi-CAP porphyrins (e.g., **16**) and chlorin (**35**) found in older sediments. The enols were first identified in marine organisms including a sponge (Karuso et al., 1986), clams (Sakata et al., 1990; Yamamoto et al., 1992; Watanabe et al., 1993), and in the diatoms that comprised the diet of the latter (Watanabe et al., 1993). It was noted that the enols were unstable during chromatography (Ocampo et al., 1999) and in solvent in the presence of oxygen (Goericke et al., 2000), producing approximately 1:1 mixtures of the Chlone 15^1 (*R:S*) diastereomers and minor amounts of [13^2-oxo]-PyPheide *a* (**36;** Ocampo et al., 1999). It has been suggested that Chlone in sediments formed as a product of transformation of the enols during chromatography on silica (Louda et al., 2000). Recently, however, it was noted that Chlone in natural environments often occurs with the 15^1*S* diastereomer in vast excess and it was confirmed that alteration during chromatography leads to 1:1 mixtures of the two diastereomers (Aydin et al., 2003).

The Chlone and CyPheide enol structures represent Chl *a* derivatives that can be rationalized to form by a condensation reaction between the C-13^2 position in ring E and the C-17 propionic acid substituent, in a manner analogous to the Dieckmann condensation or Claisen condensation. Synthetic derivatives have been prepared by these methods (Falk et al., 1975; Ma and Dolphin, 1996, respectively), in both cases involving generation of a carbanion from the demethoxycarbonyl derivatives using a strong base. It is uncertain if the natural precursor requires the presence of a labile hydrogen at position C-13^2, *i.e.,* if the β-ketoester functionality that is present in the Chls *a*, *b*, and *c* and the BChls *a* and *b* is a pre-requisite for reaction. Consideration of the environments in which such condensation products have been identified, either as the functionalized derivatives or as the alkyl porphyrins, suggests that basic conditions may favor their formation, consistent with the mechanism involving deprotonation of a β-ketoester intermediate. Issues remaining to be addressed include: determination of a mechanistic basis for the formation of Chlones and structurally related species

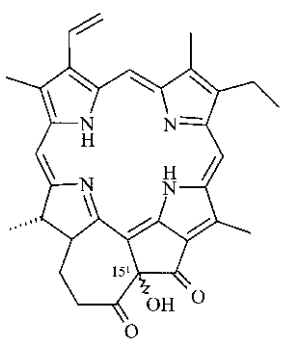

33

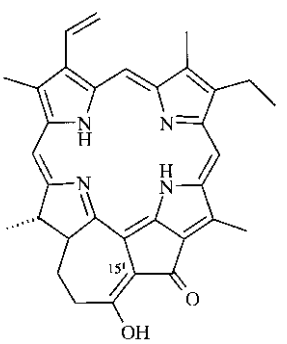

34

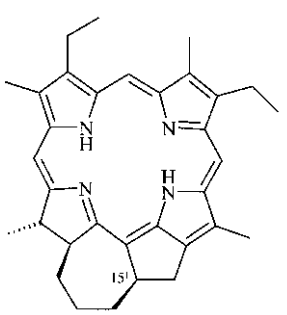

35

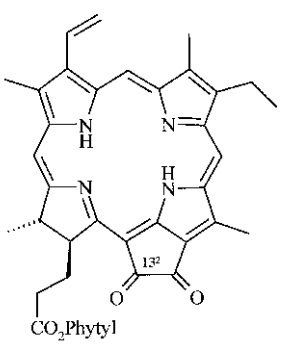

36

in nature; determining if the reactions are chemically- or biologically-mediated; determination of the quantitative significance of the derivatives in the sedimentary record; determination of the potential for formation from Chls other than Chl *a* that possess the β-ketoester functionality.

4. Alkyl Sulfides

An entirely novel series of transformation products has been identified in which a carbon-sulfur bond has been formed through diagenetic reaction. The derivatives identified comprise C-3[1] alkyl sulfides (e.g., **37**) containing between one and five additional carbon atoms and representative structures occur for the Chl and Phe counterparts (Squier et al., 2003, 2004a). Although the mechanism of formation remains to be established, it is evident that the derivatives are formed early during diagenesis and it appears likely that their formation involves reaction of the Chl derivative with an alkylthiol or alkylsulfide (Squier et al., 2004a). Notably, the derivatives were identified in a lake sediment in which BChls form a major component of the signature from the primary producer community, indicating the environment to have been one in which organosulfur species were likely to form. One significant feature of the presence of the Chl alkysulfide derivatives is that they provide evidence on the timing of sulfur incorporation into organic matter in general, as well as providing a rationale for the occurrence of sulfur cross-linked alkyl porphyrins (**38**), albeit linked at a different position in the structure (Schaeffer et al., 1993). The recognition of the alkysulfide derivatives raises many questions including: the nature of the mechanism of their formation; their environmental significance; their relevance as determinants of the extent of sulfur incorporation into sedimentary organic matter and the potential for tetrapyrroles to be cross-linked to macromolecular organic matter by a variety of different mechanisms.

III. Timing and Nature of Transformations

It is apparent that many of the transformation reactions of Chls in the natural environment take place during the very earliest stages of diagenesis. The majority of the early stage reductive transformation reactions can be linked to biological activity associated with senescence and/or herbivory. Others, such as oxidation and sulfur incorporation, most likely relate to secondary reactions that occur following release of the Chls into the environment as a result of cellular disruption. As such, it appears that reactions at least up to and including the formation of PyPheides (Fig 1) occur mainly within the water column or, particularly in the case of benthic communities, in the surface sediment. A number of the transformation steps appear to be later stage processes, possibly associated with burial of the sediments. These include reduction of the keto- groups, aromatization, decarboxylation and metallation. In spite of the long-standing interest in the geochemistry of tetrapyrroles, these later-stage reactions in the natural environment remain to be explained in full, both in terms of the reaction mechanisms and their causes and how the environmental conditions influence the product distributions.

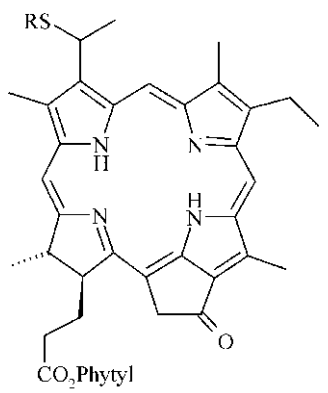

37 R = Me, Et, Pr, Bu, Pent

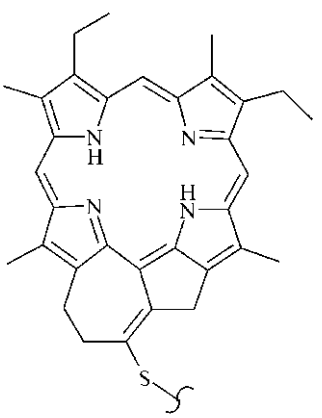

38

The transformation pathways of Chls in terrestrial environments differ significantly from those that operate in aquatic environments. This is partly the result of differences in cellular structure and organization but is also a reflection of the different environmental stresses to which plants are subjected in these two distinct regimes.

A. Terrestrial

Net Chl production in terrestrial environments has been estimated at 2.92×10^8 tons per annum (Hendry et al., 1987). The vast majority of that Chl is destroyed through the natural processes involved in autumnal senescence in leaves. These reactions involve oxidative cleavage of the macrocycle to generate weakly colored and colorless derivatives (Mühlecker et al., 1993). For this reason, the amount of Chl from higher plant sources that enters the long-term sedimentary reservoir, through preservation of structures with the macrocycle intact, can be assumed to be essentially zero. Accordingly, the absolute abundances of porphyrins in coals, the main terrestrial reservoir of sedimentary organic matter, are considerably lower than in accumulations originating from aquatic environments. In addition, the depositional environments in which coals that contain porphyrins accumulate are most likely to be stagnant deltaic settings in which algae and phototrophic bacteria are present and possibly serve as the main sources of coal porphyrins.

B. Aquatic

Net Chl production in aquatic environments has been estimated at 8.63×10^8 tons per annum (Hendry et al., 1987). Chlorophyll preservation in aquatic environments is strongly influenced by the redox conditions and depth of the water column. Under strongly oxidizing conditions Chl photo-oxidation reactions have been implicated in destruction of the macrocycle, leading to removal of most of the Chl before it reaches the anoxic conditions that exist either in the lower reaches of the water column or within the first few centimeters of the sediment. Under fully oxic and intermediate redox conditions, heterotrophic processes are highly favorable and utilize the high-energy pathways associated with the use of oxygen as the oxidant. By contrast, under reducing conditions Chls can be exceptionally well preserved with the carbon skeleton being structurally conserved. Under intermediate redox conditions, or darkness, the macrocycle can remain intact but with modification at the periphery through oxidation reactions centered on ring E (Naylor and Keely, 1998; Airs et al., 2000; Walker et al., 2002). The major Chls found in aquatic sediments typically comprise algal pigments, the most important being Chl *a*. In some situations, however, the major Chls comprise bacterial pigments originating from anoxygenic purple and green photosynthetic bacteria (Villanueva et al., 1994b; Squier et al., 2002, 2004a). These organisms require dysaerobic (purple bacteria) and anoxygenic (green bacteria) conditions, respectively, and can be quantitatively important components of the primary producer community (Hurley and Watras, 1991; Vila et al., 1998; Villanueva and Hastings, 2000; Chen et al., 2001). Owing to their intolerance to oxygen, these bacteria utilize H_2S as the electron donor in photosynthesis, leading to the production of elemental sulfur rather than molecular oxygen. Thus, the presence of bacterial Chls as the major components in sediments indicates the existence of anoxic and euxinic conditions within the photic zone, and prevalence of conditions favorable to the preservation of organic matter. Such conditions are often associated with highly productive lakes, where eutrophication leads to depletion of oxygen in the water column, or very steep-sided and deep lakes where wind mixing is minimal and the waters can become stratified, but can also occur in estuarine settings. The other fundamental requirement, the presence of H_2S, demands a significant activity among the sulfate reducing bacterial community. Sulfate reducers are heterotrophs that rely on relatively low energy-yielding oxidation reactions in which sulfate is the source of the oxidizing power. Thus, the relative abundances of Chl oxidation products versus indicators of reducing conditions reflect the redox status of the depositional environment and the prevalence of different communities of heterotrophic and autotrophic bacteria.

C. Water Column Studies

Temporal studies of contemporary lake and marine waters reveal the great variability in pigment composition that accompanies species succession in natural aquatic environments (Villanueva et al., 1994b; Walker and Keely, 2004). The duration of photosynthetic activity of individual species of primary producers varies, ranging from a matter of a few days for some microalgae through to several months or even years in the case of macroalgae. The

pigments provide a good means to monitor changes in the primary producer community, and changes in the nature and abundances of transformation products reflect the processes of senescence and grazing activity on the bloom. For example, the succession of transformation products during the overturn of a bloom in the Celtic sea commenced with demetallation, de-esterification and decarbomethoxylation reactions, followed by increasing extents of oxidation reactions with increasing exposure of the pigments to the oxidizing conditions within the water column (Walker and Keely, 2004). The oxidation reactions become increasingly important with duration of exposure within the water column and so appear, to some degree, to be dependent on the particle size, which exerts a strong influence on settling rate.

D. Sediment Studies

Early studies of pigment compositions in sediments largely focused on the identification of novel structures and the development of an understanding of the transformation pathways by which the original Chl derivatives are gradually converted into alkyl porphyrins. More recently, in the light of the increased knowledge of the structures and their significance, the focus has shifted towards characterizing the variability in conditions within depositional environments through development of detailed stratigraphic profiles of pigments. For example, Ocampo et al. (1992) examined changes in the distributions of alkyl porphyrins in the Messel shale and demonstrated that the distributions differ markedly over the timescale represented by the sediment core examined, reflecting the changes in depositional environment within the anoxic basin. Similarly, Keely et al. (1995) demonstrated changing profiles of porphyrins within a narrow time zone within the Miocene Vena del Gesso evaporitic sequence. In those studies the stratigraphic resolution that could be achieved was limited by the length and complexity of preparative stages prior to analysis. The development of on-line LC-MS approaches has allowed dramatic improvements in the stratigraphic resolution that can be achieved.

In an attempt to examine the extent to which pigment variations can be monitored over very short timescales, sediments have been examined at cm and sub-cm scale resolutions. The record of sedimentary pigments from an Antarctic lake was shown to exhibit dramatic shifts between a lacustrine and a marine influenced environment, which was evident with sampling at cm scale resolution (Squier et al., 2002; Walker et al., 2002). Furthermore, the profile within the marine section reveals subtle variations in pigment structure that probably relate to population shifts within the anoxygenic bacterial community (Wilson et al., 2004a). The studies demonstrate clearly that much detail on population changes, which are intrinsically linked to environmental conditions, is contained within the sedimentary pigment record. Through further examination of high-resolution stratigraphic records of pigments from appropriate sedimentary records (i.e., those in which bioturbation is absent), the significance of changes in pigment compositions in relation to variability within different depositional environments will become clear.

Ultra-high resolution studies of pigments in sediments were carried out in a microbial mat (Airs and Keely, 2003). Sampling at intervals of 2 mm demonstrated the feasibility of conducting pigment analysis at this scale and revealed that substantial changes in the pigment profiles are apparent at this stratigraphic resolution. Further ultra-high resolution studies of sediments from a range of depositional environments are warranted in order to determine the extent to which pigment profiles record short term variations in environmental conditions and the types of depositional environments in which variations are most marked.

IV. Transformation Scheme

It is evident that a much greater variety of reactions affect Chls than those recognized in the Treibs Scheme. In an attempt to reflect the number and nature of the reactions to which Chls are subjected a revised transformation scheme has been developed (Fig. 2). Although the scheme goes some way to addressing the complexity of processes in the natural environment, it is evident that there are still gaps in understanding. For example, it is not yet possible to include transformation reactions that would lead to the cleavage of the C-3 substituent to generate precursors for the C-3 Me or C-3 H porphyrins, structures that are evident in ancient sediments. Clearly, therefore, it must be recognized that the scheme is incomplete. It is hoped that it might serve as a stimulus to direct efforts towards identifying the missing links: increased understanding of the structures and the mechanistic basis by which sedimentary tetrapyrroles are formed is still needed in order to liberate the full potential of the pigment geochemical record.

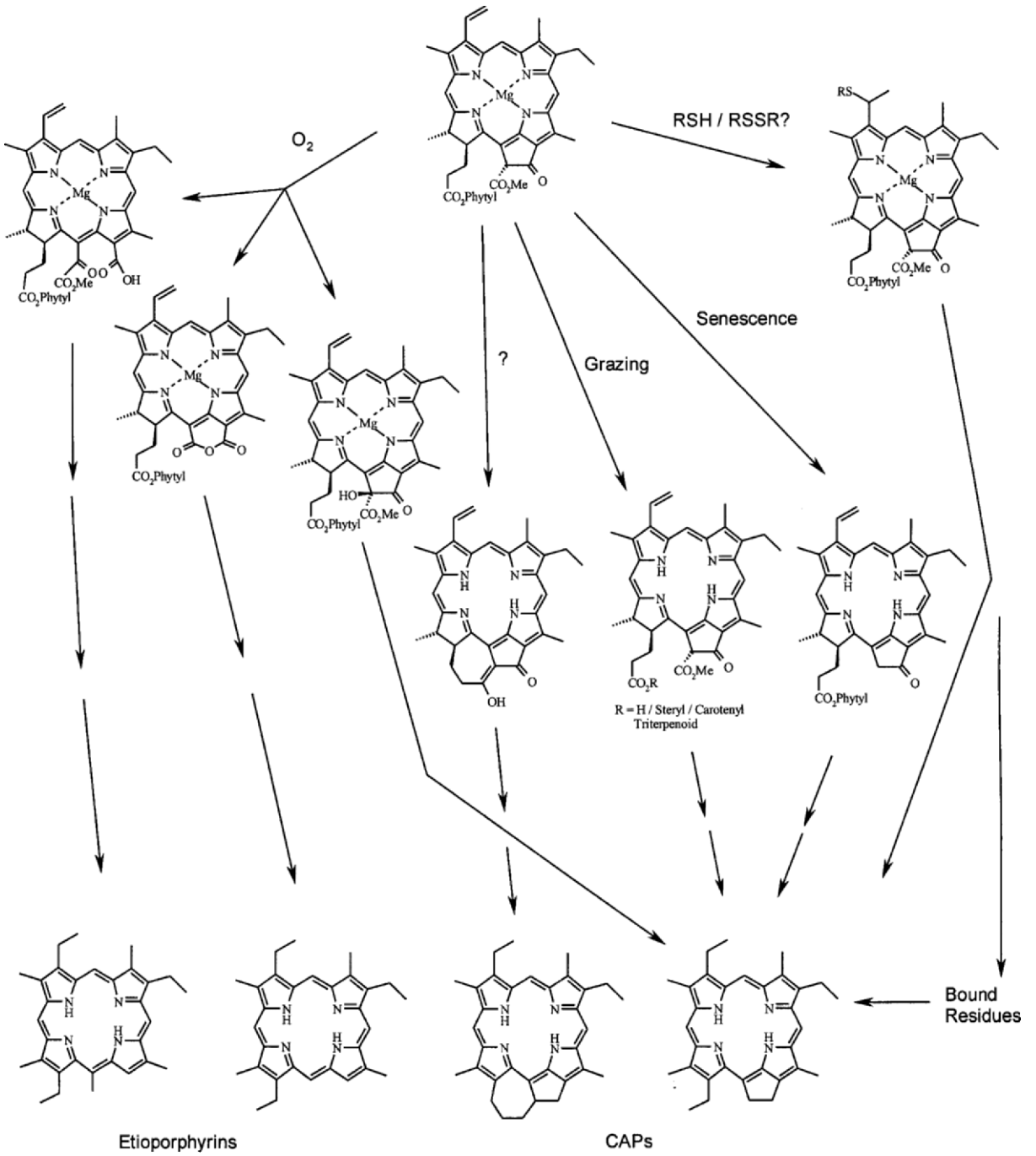

Fig. 2. Representation of various transformation reactions to show the expansion of the Treibs scheme as illustrated for Chl *a*. For simplicity, only one functionalized derivative and one potential product is shown in each case. The defunctionalization reactions leading to the alkylporphyrin products can be assumed to follow pathways such as those outlined in Fig. 1.

V. Applications

Development of applications to which the analysis of sedimentary pigment distributions is beneficial continues to be an active area. One of the most compelling reasons for an interest in the geochemistry of these derivatives is their origin in the primary producer community. Thus, their signatures provide informa-

tion about the most fundamental component of the food web, on which the vast majority of other forms of life depend. Some applications have already been realized and others have the potential for development in the future.

A. Realized

Specific Chl pigments act as biological markers for the presence of selected broad groups of organisms. Thus, Chl *b* indicates the presence of green alga (Chlorophyta) and Chl *c* indicates a contribution from one or more of a restricted range of algae including diatoms, dinoflagellates, and cryptophytes. The BChls are more specific: BChl *a* indicates an input from purple bacteria, the BChls *c* and *d* an input from Chloroflexaceae or from green strains of Chlorobiaceae, and BChl *e* indicates contributions from brown strains of Chlorobiaceae. Similarly, the absence of an accessory Chl pigment accompanying Chl *a* is suggestive of contributions from cyanobacteria or some cryptophytes. In addition to revealing contributions from specific primary producers, the algal pigments indicate regions of oxygenated waters whereas the bacterial pigments (with few exceptions) indicate photic zone anoxia and euxinia (see above). Where algal and bacterial pigments both occur, it is likely to suggest either stratified waters, or redox conditions alternating at a frequency higher than that represented by the stratigraphic resolution achieved by the sampling. The other main applications suggested for pigment geochemistry at the present time are the assessment of past productivity (Harris et al., 1996), the impact of grazers on the algal community from examination of CSE distributions and amounts (Dahl et al., 2004), and the indication of different relative extents of oxygen availability from the relative abundances of Chl oxidation products versus unaltered derivatives (Walker et al., 2002).

B. Outstanding Issues and Potential Developments

Further advances are required in order to develop the uses of pigments as rigorous proxies for environmental parameters. The potential applications include quantitative estimates of: grazing pressure; extent of senescence; oxygen availability; sulfur incorporation into sedimentary organic matter and photic zone anoxia and euxinia. It is evident that pigment abundances in sediments are influenced both by the productivity and by the extent of preservation: decoupling these two factors is an issue of importance to the assessment of carbon cycling as well as being of specific interest in the area of pigment geochemistry. In general, approaches required to develop pigment-based proxies will involve evaluation and validation of the proposed proxy against the parameter of interest both in controlled laboratory trials and in field trials. For BChls, where the distributions exhibit marked variation in response to different environmental conditions, studies need to be conducted in conjunction with controlled manipulation of bacterial cultures. In addition, the stabilities of components included in the proxies need to be established over the longer term.

One important issue that remains to be addressed fully is the determination of the controls on the metallation of sedimentary porphyrins. While it is clear that metallation is related to the availability of various metals in the depositional environment and their relative stabilities in the porphyrin macrocycle, the connection between metal availability and speciation remains to be translated from a theoretical consideration based on E_H pH stability fields (Lewan and Maynard, 1982, Lewan, 1984) to one based firmly on environmental measurements. The difficulty here is that transmetallated functionalized tetrapyrroles have not been observed in natural aquatic systems prior to deposition in sediments, hence it appears that sediments at the appropriate stage of diagenesis need to be examined.

C. Nature of Transformation Reactions

The exact nature of the reactions leading to a number of specific transformation products in the natural environment remain to be established. These include the reactions that yield the Chlone and CyPheide enol structures, reactions leading to the sulfur-containing Chl derivatives, reactions leading to CSEs and CCEs and the precise mechanisms leading to the formation of Chl oxidation products.

D. Quantifying Possible Links with Climate (Environmental Variability)

A major goal over the next few years is likely to be the establishment of links between the pigment distributions preserved in sediments and factors controlling climate. The primary producer community is undoubtedly strongly influenced by climatic changes

and it is highly likely that these influences are recorded within the pigment record either through changes in species composition (though this would be difficult to decouple from other forcing factors) or through changes in the specific nature and the abundances of various transformation products. Such influences on the pigment compositions are most likely to be revealed by studies in which other biological markers are evaluated in conjunction with the pigments, for example, carotenoids, UV screening pigments such as scytonemin (Squier et al., 2004c) and lipids are all possible candidates.

VI. Concluding Remarks

Since its development nearly 100 years ago, pigment geochemistry has evolved from a focus on the characterization and identification of individual compounds as biological markers to a field focused more on the examination of complex pigment distributions for the evaluation of past environments. This development reflects that the field is developing towards, but has not yet achieved, a mature status. The developments over the next few years are likely to arise from studies that involve combinations of laboratory and field studies aimed at revealing the factors that are of greatest importance in controlling pigment compositions and transformation reactions. It is likely that a variety of new analytical approaches will be developed and, through the use of rigorous methods to separate and identify components in complex mixtures, that further novel Chl transformation products will be identified. The ultimate goal might be to construct three dimensional maps from temporal and spatial distributions of pigments and to translate these to reconstruction of environmentally important parameters, for example intensity of primary productivity, heterotrophy and water column redox potential and the prevalence of euxinia in times past.

Note Added in Proof

The following notes summarize developments in the field that have been published since the writing of this chapter.

Grazing experiments with freshwater crustaceans examined the formation of CSEs from mixed phytoplankton sources, confirming a significant level of incorporation of cholesterol from the grazer into the CSEs along with the sterols of the dietary phytoplankton. Grazing of mixtures of algae containing sterols ranging from C_{27} to C_{29} revealed a bias towards incorporation of C_{29} sterols within the CSEs, attributed to easier metabolism of the lower carbon numbered species. The potential for under-representation of contributions from specific algal sources was noted (Soma et al., 2005).

Comparison of pigment decay rates in oxic and oxygen depleted sites in the Mississippi Delta led Chen et al. (2005) to conclude that sedimentation rate and lability of organic matter were more important than bottom water hypoxia in controlling the preservation of pigments, and organic matter in general, in sediments. Reuss et al. (2005) showed clear differences in pigment abundances and distributions between sites that exhibited significant differences in the environmental conditions and sedimentary regime and concluded that more work is required in order to assess the full potential of pigments as biomarkers in marine and estuarine environments.

Studies of older sediment sequences have examined variations in pigments over glacial-interglacial periods. Nara et al. (2005) showed distinct changes in algal-sourced pigments over glacial-interglacial cycles and suggested that changes in productivity had occurred as a result of increased fertilisation due to higher precipitation during the warmer climatic periods. Squier et al. (2005) similarly observed marked changes in pigment profiles and also detected periods of water column euxinia from the presence of BPhys *e,* markers of brown strains of green sulfur bacteria. Both studies demonstrate that extreme climate events can exert major influences on aquatic, resulting in clear signatures in the sedimentary pigment record. Another interglacial sediment also yielded BChl *e* derivatives indicative of photic zone euxinia (Mallorqui et al., 2005). The recognition of derivatives of BChl *e* in sediments means that the preservation of each of the BChls of green sulfur bacteria has now been demonstrated in the sedimentary record, further supporting the view that all of these BChls are possible precursors of sedimentary porphyrins.

It is also noteworthy that a marine cyanobacterium in which the major pigment has been shown to be Chl *d*, the 3-desvinyl-3-formyl derivative of Chl *a,* has been identified as a free-living and widespread organism that inhabits environments restricted in visible radiation but enriched in near infrared (Larkum and Kühl, 2005). The significance of this

observation lies in the potential for Chl *d* to be a major source of 3-methyl and 3-H porphyrins in the geological record. Thus, these porphyrins may have value as indicators of defined biological inputs and of specific environmental conditions. It will be of particular interest to try to relate environments that the contemporary Chl *d*-containing organisms inhabit with paleoenvironments in which the 3-methyl and 3-H porphyrins are prevalent.

Acknowledgments

My interests in chlorophyll geochemistry have been indulged, supported and extended by the efforts and enthusiasm of a number of excellent graduate students whom I have had the good fortune to supervise. They are Christopher Naylor, Jane Atkinson, Paul Woolley, Ruth Airs, Stuart Walker, Angela Squier, Michael Wilson and Deborah Mawson. Thanks are also due to my collaborators and friends, Rutger de Wit, Jesus Garcia-Gil and Carlos Borrego who helped us to start up the microbial cultures at York, Dominic Hodgson whose contribution in the studies of Antarctic lake sediments has been invaluable, and Carole Llewellyn for arranging my participation in the cruise in the Celtic Sea during 2002.

References

Airs RL and Keely BJ (2000) A novel approach for sensitivity enhancement in atmospheric pressure chemical ionization liquid chromatography/mass spectrometry of chlorophylls. Rapid Commun Mass Spectrom 14: 125–128

Airs RL and Keely BJ (2002) Atmospheric pressure chemical ionisation liquid chromatography/mass spectrometry of bacteriochlorophylls from Chlorobiaceae, characteristic fragmentation. Rapid Commun Mass Spectrom 16: 453–461

Airs RL and Keely BJ (2003) A high resolution study of the chlorophyll and bacteriochlorophyll pigment distributions in a calcite/gypsum microbial mat. Org Geochem 34: 539–551

Airs RL, Jie C and Keely BJ (2000) A novel sedimentary chlorin: Structural evidence for a chlorophyll origin for aetioporphyrins. Org Geochem 31: 1253–1256

Airs RL, Atkinson JE and Keely BJ (2001a) Development and application of a high-resolution liquid chromatographic method for the analysis of complex pigment distributions. J Chromatogr A 917, 167–177

Airs RL, Borrego CM, Garcia-Gil J and Keely BJ (2001b) Identification of the bacteriochlorophyll homologues of *Chlorobium phaeobacteroides* strain UdG6053 grown at low light intensity. Photosynth Res 70, 221–230

Aydin N, Daher S and Gulaçar F (2003) On the sedimentary occurrence of chlorophyllone *a*. Chemosphere 52: 937–942

Baker EW (1966) Mass spectrometric characterization of petroporphyrins J Am Chem Soc 88: 2311–2315

Baker EW and Louda JW (1983) Thermal aspects of chlorophyll geochemistry. In: Byoroy M (ed) Advances in Organic Geochemistry 1981, pp 401–421. Wiley, Chichester

Baker EW and Louda JW (1986) Porphyrins in the geological record. In: Johns RB (ed) Biological Markers in the Sedimentary Record, Methods in Geochemistry and Geophysics, pp 125–128. Elselvier, Amsterdam

Baker EW and Palmer SE (1978) Geochemistry of porphyrins. In: Dolphin D (ed) The Porphyrins Vol 1, pp 485–551. Academic Press, London

Bonnett R, Burke PJ and Reszka A (1983) Iron porphyrins in coal. J Chem Soc Chem Commun 1085–1087

Boreham CJ, Fookes CJR, Popp BN, and Hayes JM (1989) Origins of etioporphyrins in sediments: Evidence from stable carbon isotopes. Geochim Cosmochim Acta 53: 2451–2455

Burkill PH, Mantoura RFC, Llewellyn CA, and Owens NJP (1987) Microzooplankton grazing and selectivity of phytoplankton in coastal waters. Mar Biol 93: 581–590

Callot HJ (1991) Geochemistry of chlorophylls. In: Scheer (ed) Chlorophylls, pp 339–364. CRC Press, Boca Raton

Callot HJ and Ocampo R (2000) Geochemistry of porphyrins. In: Kadish KM, Smith KM and Guilard R (eds) The Porphyrin Handbook Vol I, pp 350–398. Academic Press, London

Callot HJ, Ocampo R and Albrecht P (1990) Sedimentary porphyrins: Correlations with biological precursors. Energy Fuels 4: 635–639

Chen NH, Bianchi TS, McKee BA and Bland JM (2001) Historical trends of hypoxia on the Louisiana shelf: Application of pigments as biomarkers. Org Geochem 32: 543–561

Chen NH, Bianchi TS and Bland JM (2003) Novel decomposition products of chlorophyll-alpha in continental shelf (Louisiana shelf) sediments: Formation and transformation of carotenol chlorin esters. Geochim Cosmochim Acta 67: 2027–2042

Chen N, Bianchi TS and McKee BA (2005) Early diagenesis of chloropigment biomarkers in the lower Mississippi River and Louisiana shelf: Implications for carbon cycling in a river-dominated margin. Mar Chem 93: 159–177

Chicarelli MI and Maxwell JR (1984) A naturally occurring, chlorophyll *b* related porphyrin. Tetrahedron Lett 25: 4701–4704

Chicarelli MI and Maxwell JR (1986) A novel fossil porphyrin with a fused ring system: Evidence for water column transformation of chlorophyll? Tetrahedron Lett 27: 4653–4654

Chicarelli MI, Wolff GA, Murray M and Maxwell JR (1984) Porphyrins with a novel exocyclic ring system in an oil shale. Tetrahedron 40: 4033–4039

Chicarelli MI, Kaur S and Maxwell JR (1987) Sedimentary Porphyrins: Unexpected structures, occurrence, and possible origins. In: Filby RH and Branthaver JF (eds) Metal Complexes in Fossil Fuels: Characterisation and Processing, ACS Symposium Series, 344, pp 40–67. American Chemical Society

Chillier XFD, Gülaçar FO and Buchs A (1993) A novel sedimentary lacustrine chlorin — characterization and geochemical significance. Chemosphere 27: 2103–2110

Chillier XFD, Van Berkel GJ, Gülaçar FO and Buchs A (1994) Characterization of chlorins within a natural chlorin mixture using electrospray ion-trap mass-spectrometry Org Mass Spectrom 29: 672–678

Corwin AH (1960) Petroporphyrins. In: Murphree, EV (ed) Proceedings of the 5th World Petroleum Congress, pp. 119–129.

Fifth World Petroleum Congress, New York
Dahl KA, Repeta DJ, Goericke R (2004) Reconstructing the phytoplankton community of the Cariaco Basin during the Younger Dryas cold event using chlorin steryl esters Paleoceanography 19: PA1006, doi:10.1029/2003PA000907, 2004
Eckardt CB, Keely BJ and Maxwell JR (1991) Identification of chlorophyll transformation products in a lake sediment by combined liquid-chromatography mass-spectrometry. J Chromatogr 557: 271–288
Eckardt CB, Pearce GES, Keely BJ, Kowalewska G, Jaffe R and Maxwell JR (1992) A widespread chlorophyll transformation pathway in the aquatic environment Org Geochem 19: 217–227
Falk H, Hoornaert G, Isenring H-P and Eschenmoser A (1975) Über enolderivate der chlorophyllreihe. Darstellung von 13^2,17^3-cyclophäophorbid-enolen. Helv Chim Acta 58: 2347–2367
Filby RH and van Berkel GJ (1987) Geochemistry of metal-complexes in petroleum, source rocks, and coals — an overview. ACS Symposium Series 344: 2–39
Fookes CJR (1983) Identification of a homologous series of nickel(II)-15,17-butanoporphyrins from an oil shale. J Chem Soc Chem Commun 1474–1476
Fookes CJR (1985) The etioporphyrins of oil shale — structural evidence for their derivation from chlorophyll. J Chem Soc Chem Commun 706–708
Fookes CJR and Jeffrey SW (1989) The structure of chlorophyll c_3, a novel marine photosynthetic pigment. J Chem Soc Chem Commun 1827–1828
Gibbison R, Peakman TM and Maxwell JR (1995) Novel porphyrins as molecular fossils for anoxygenic photosynthesis. Tetrahedron Lett 36: 9057–9060
Goericke R, Shankle A and Repeta DJ (1999) Novel carotenol chlorin esters in marine sediments and water column particulate matter. Geochim Cosmochim Acta 63: 2825–2834
Goericke R, Strom SL and Bell MA (2000) Distribution and sources of cyclic pheophorbides in the environment. Limnol Oceanogr 45: 200–211
Grice K, Gibbison R, Atkinson JE, Schwark L, Eckardt CB and Maxwell JR (1996) Maleimides (1H-pyrrole-2,5-diones) as molecular indicators of anoxygenic photosynthesis in ancient water columns. Geochim Cosmochim Acta 60: 3913–3924
Grice K, Schaeffer P, Schwark L, and Maxwell JR (1997) Changes in palaeoenvironmental conditions during deposition of the Permian Kupferschiefer (Lower Rhine Basin, northwest Germany) inferred from molecular and isotopic compositions of biomarker components. Org Geochem 26: 677–690
Harradine PJ and Maxwell JR (1998) Pyrophaeoporphyrins *c*(1) and *c*(2): grazing products of chlorophyll *c* in aquatic environments. Org Geochem 28: 111–117
Harradine PJ, Harris PG, Head RN, Harris RP and Maxwell JR (1996a) Steryl chlorin esters are formed by zooplankton herbivory. Geochim Cosmochim Acta 60: 2265–2270
Harradine PJ, Peakman TM and Maxwell JR (1996b) Triterpenoid chlorin esters: Water column transformation products of chlorophyll *a.* Tetrahedron 52: 13427–13440
Harris PG, Carter JF, Head RN, Harris RP, Eglinton G and Maxwell JR (1995a) Identification of chlorophyll transformation products in zooplankton fecal pellets and marine sediment extracts by liquid-chromatography mass-spectrometry atmospheric-pressure chemical-ionization. Rapid Commun Mass Spectrom 9: 1177–1183
Harris PG, Pearce GES, Peakman TM and Maxwell JR (1995b) A widespread and abundant chlorophyll transformation product in aquatic environments. Org Geochem 23: 183–187
Harris PG, Zhao M, Rosell-Melé A, Tiedemann R, Sarnthein M and Maxwell JR (1996) Chlorin accumulation rate as a proxy for Quaternary marine primary productivity. Nature 383: 63–65
Hendry GAF, Houghton JD and Brown SB (1987) The degradation of chlorophyll — a biological enigma. New Phytol 107: 255–302
Hurley JP and Watras CJ (1991) Identification of bacteriochlorophylls in lakes via reverse-phase HPLC. Limnol Oceanogr 36: 307–315
Hynninen PH (1991) Chemistry of Chlorophylls: Modifications. In: Scheer H (ed) Chlorophylls, pp 145–209. CRC Press, Boca Raton
Jeffrey SW and Hallegraeff GM (1987) Chlorophyllase distribution in 10 classes of phytoplankton—a problem for chlorophyll analysis. Mar Ecol Prog Ser 35: 293–304
Jie C, Walker JS and Keely BJ (2002) Atmospheric pressure chemical ionization normal phase liquid chromatography mass spectrometry and tandem mass spectrometry of chlorophyll *a* allomers. Rapid Commun Mass Spectrom 16: 473–479
Karuso P, Bergquist PR, Buckleton JS, Cambie RC, Clark GR and Rickard CEF (1986) 13^2,17^3-cyclophaeophorbide enol, the first porphyrin isolated from a sponge. Tetrahedron Lett 27: 2177–2178
Kaur S, Chicarelli MI and Maxwell JR (1986) Naturally occurring benzoporphyrins: Bacterial marker pigments? J Am Chem Soc 108: 1347–1348
Keely BJ and Maxwell JR (1990a) Fast atom bombardment mass spectrometric and tandem mass spectrometric studies of some functionalised tetrapyrroles derived from chlorophylls *a* and *b*. Energy Fuels 4: 737–741
Keely BJ and Maxwell JR (1990b) NMR studies of sedimentary tetrapyrroles. Energy Fuels 4: 716–719
Keely BJ and Maxwell JR (1993) The Mulhouse basin: Evidence from porphyrin distributions for water column anoxia during deposition of marls. Org Geochem, 20: 1217–1225
Keely BJ, Prowse WG and Maxwell JR (1990) The Treibs Hypothesis: An evaluation based on structural studies. Energy Fuels 4: 628–634
Keely BJ, Harris PG, Popp BN, Hayes JM, Meischner D and Maxwell JR (1994) Porphyrin and chlorin distributions in a late Pliocene lacustrine sediment. Geochim Cosmochim Acta 58: 3691–3701
Keely BJ, Blake SR, Schaeffer P and Maxwell JR (1995) Distributions of pigments in the organic-matter of marls from the Vena del Gesso evaporitic sequence. Org Geochem 23: 527–539
King LL and Repeta DJ (1991) Novel pyrophaeophorbide steryl esters in Black Sea sediments. Geochim Cosmochim Acta 55: 2067–2074
King LL and Repeta DJ (1994) Phorbin steryl esters in black-sea sediment traps and sediments — a preliminary evaluation of their paleooceanographic potential Geochim Cosmochim Acta 58: 4389–4399
King LL and Wakeham SG (1996) Phorbin steryl ester formation by macrozooplankton in the Sargasso Sea. Org Geochem 24: 581–585
Kozono M, Nomoto S, Mita H and Shimoyama A (2001) Detection of maleimides and their characteristics in Neogene sediments

of the Shinjo basin, Japan. Geochem J 35: 225–236
Kozono M, Nomoto S, Mita H, Ishiwatari R and Shimoyama A (2002) 2-Ethyl-3-methylmaleimide in Tokyo bay sediments providing the first evidence for its formation from chlorophylls in the present photic and oxygenic zone. Biosci Biotechnol Biochem 66: 1844–1847
Kuronen P, Hyvarinen K and Hynninen PH (1993) High-performance liquid-chromatographic separation and isolation of the methanolic allomerization products of chlorophyll-*a*. J Chromatogr A 654: 93–104
Larkum AWD and Kühl M (2005) Chlorophyll *d*: The puzzle resolved. Trends Plant Sci 10: 355–357
Lewan MD (1984) Factors controlling the proportionality of vanadium to nickel in crude oils. Geochim Cosmochim Acta 48: 2231–2238
Lewan MD and Maynard JB (1982) Factors controlling enrichment of vanadium and nickel in the bitumen of organic sedimentary rocks. Geochim Cosmochim Acta 46 2547–2560
Louda JW and Baker EW (1986) The biogeochemistry of chlorophyll. In: Sohn ML (ed) Organic Marine Chemistry, pp 107–125. American Chemical Society
Louda JW, Li J, Liu L, Winfree MN and Baker EW (1998) Chlorophyll *a* degradation during cellular senescence and death. Org Geochem 29: 1233–1251
Louda JW, Loitz JW, Rudnick, DT and Baker EW (2000) Early diagenetic alteration of chlorophyll *a* and bacteriochlorophyll *a* in a contemporaneous marl ecosystem; Florida Bay. Org Geochem 31: 1561–1580
Louda JW, Liu L and Baker EW (2002) Senescence- and death-related alteration of chlorophylls and carotenoids in marine phytoplankton. Org Geochem 33: 1635–1653
Ma L and Dolphin D (1996) Stereoselective synthesis of new chlorophyll *a* related antioxidants isolated from marine organisms. J Org Chem 61: 2501–2510
Mallorqui N, Arellano JB, Borrego CM and Garcia-Gil LJ (2005) Signature pigments of green sulfur bacteria in lower Pleistocene deposits from the Banyoles lacustrine area (Spain). J Paleolimnol 34: 271–280
Mawson DH, Walker JS and Keely BJ (2004) Variations in the distributions of sedimentary alkyl porphyrins in the Mulhouse basin in response to changing environmental conditions. Org Geochem 35: 1229–1241
May DA and Lash TD (1992) Porphyrins with exocyclic rings. 2. Synthesis of geochemically significant tetrahydrobenzoporphyrins from 4,5,6,7-tetrahydro-2H-isoindoles. J Org Chem 57: 4820–4828
Merzlyak MN, Hendry GAF, Atherton NM, Zhigalova TV, Pavlov VK and Zhiteneva OV (1993) Pigment degradation, lipid peroxidation, and free radicals in leaves during autumn senescence. Biochem Moscow 58: 129–135
Mühlecker W, Kräutler B, Ginsberg S and Matile P (1993) Breakdown of chlorophyll: A tetrapyrrolic chlorophyll catabolite from senescent rape leaves. Helv Chim Acta 76: 2976–2980
Nara F, Tani Y, Soma Y, Soma M, Naraoka H, Watanabe T, Horiuchi K, Kawai T, Oda T and Nakamura T (2005) Response of phytoplankton productivity to climate change recorded by sedimentary photosynthetic pigments in Lake Hovsgol (Mongolia) for the last 23,000 years. Quat Int 136: 71–81
Naylor CC and Keely BJ (1998) Sedimentary purpurins: Oxidative transformation products of chlorophylls. Org Geochem 28: 417–422
Ocampo R and Repeta DJ (1999) Structural determination of purpurin-18 (as methyl ester) from sedimentary organic matter. Org Geochem 30: 189–193
Ocampo R and Repeta DJ (2002) Isolation and structure determination of two novel C(13^2)-OH bacteriopheophytin *a* allomers from a coastal salt pond sediment. Org Geochem 33: 849–854
Ocampo R and Repeta DJ (2004) 13^2(S)–OH methyl bacteriopheophorbide *a* allomer in sedimentary organic matter. Org Geochem 35: 209–214
Ocampo R, Callot HJ, Albrecht P and Kinzinger JP (1984) A novel chlorophyll-*c* related petroporphyrin in oil-shale. Tetrahedron Lett 25: 2589–2592
Ocampo R, Callot HJ and Albrecht P (1985) Occurrence of bacteriopetroporphyrins in oil shale. J Chem Soc Chem Commun 4: 200–201
Ocampo R, Callot HJ and Albrecht P (1987) Evidence for porphyrins of bacterial and algal origin in oil shale. In: Filby RH and Branthaver JF (eds) Metal Complexes in Fossil Fuels; ACS Symposium Series Volume 344, pp 68–73. American Chemical Society, Washington
Ocampo R, Callot HJ, Albrecht P., Popp BN, Horowitz MR and Hayes JM (1989) Different isotopic compositions of C_{32} DPEP and C_{32} etioporphyrin III in oil-shale. Naturwiss 76: 419–421
Ocampo R, Callot HJ, Albrecht P and Bauder C (1992) Porphyrins from the Messel oil shale (Eocene, Germany): Structure elucidation, geochemical, and biological significance and distribution as a function of depth. Geochim Cosmochim Acta 56: 745–761
Ocampo R, Sachs JP and Repeta DJ (1999) Isolation and structure determination of the unstable 13^2,17^3-cyclopheophorbide *a* enol from recent sediments. Geochim Cosmochim Acta 63: 3743–3749
Pancost RD, Crawford N, and Maxwell JR (2002) Molecular evidence for basin-scale photic zone euxinia n the Permian Zechstein Sea. Chem Geol 188: 217–227
Pancost RD, Crawford N, Magness S, Turner A, Jenkyns HC and Maxwell JR (2004) Further evidence for the development of photic-zone euxinic conditions during Mesozoic oceanic anoxic events. J Geol Soc 161: 353–364
Pearce GES, Eckardt CB, Keely BJ, Harradine PJ and Maxwell JR (1993) Characterization of naturally occurring steryl esters derived from chlorophyll *a*. Tetrahedron. Lett 34: 2883–2886
Pearce GES, Harradine PJ, Talbot HM and Maxwell JR (1998) Sedimentary sterols and steryl chlorin esters: Distribution differences and significance. Org Geochem 28: 3–10
Prowse WG and Maxwell JR (1991) High molecular weight chlorins in a lacustrine shale. Org Geochem 17: 877–886
Prowse WG, Chicarelli MI, Keely BJ, Kaur S and Maxwell JR (1987) Characterisation of fossil porphyrins of the 'di-DPEP' type. Geochim Cosmochim Acta 51: 2875–2877
Reuss N, Conley DJ and Bianchi TS (2005) Preservation conditions and the use of sediment pigments as a tool for recent ecological reconstruction in four Northern European estuaries. Mar Chem 95: 283–302
Riffé-Chalard C, Verzegnassi L and Gülaçar FO (2000) A new series of steryl chlorin esters: Pheophorbide a steryl esters in an oxic surface sediment Org Geochem 31: 1703–1712
Rosell-Melé A, Carter JF and Maxwell JR (1996) High-performance liquid chromatography-mass spectrometry of porphyrins

by using an atmospheric pressure interface. J Am Soc Mass Spectrom 7: 965–971
Rosell-Melé A, Carter JF and Maxwell JR (1999) Liquid chromatography/tandem mass spectrometry of free base alkyl porphyrins for the characterization of the macrocyclic substituents in components of complex mixtures. Rapid Commun Mass Spectrom 13: 568–573
Roy S (1987) High performance liquid chromatography analysis of chloropigments. J Chromatogr A 391: 19–34
Sakata K, Yamamoto K, Ishikawa H, Yagi A, Etoh H and Ina K (1990) Chlorophyllone *a*, a new phaeophorbide *a* related compound isolated from *Ruditapes phillippinarum* as an antioxidative compound. Tetrahedron Lett 31: 1165–1168
Schaeffer P, Ocampo R, Callot HJ and Albrecht P (1993) Extraction of bound porphyrins from sulphur-rich sediments and their use for reconstruction of palaeoenvironments. Nature 364: 133–136
Schoch S, Scheer H, Schiff JA, Rüdiger W and Siegelman HW (1981) Pyrophaeophytin *a* accompanies phaeophytin *a* in darkened light grown cells of Euglena. Z Naturforsch 36c: 827–833
Shimoyama A, Kozono M, Mita H and Nomoto S (2001) Maleimides in the Cretaceous/Tertiary boundary sediments at Kawaruppu, Hokkaido, Japan. Geochem J 35: 365–375
Shuman FR and Lorenzen CJ (1975) Quantitative degradation of chlorophyll *a* by a marine herbivore. Limnol Oceanogr 20: 580–586
Soma Y, Rob N, Itoh N, Tani Y and Soma M (2005) Sterol composition of steryl chlorin esters (SCEs) formed through grazing of algae by freshwater crustaceans: Relevance to the composition of sedimentary SCEs. Limnol 6: 45–51
Spooner N, Keely BJ and Maxwell JR (1994a) Biologically mediated defunctionalisation of chlorophyll in the aquatic environment-I. Senescence/decay of the diatom *Phaeodactylum tricornutum*. Org Geochem 21: 509–516
Spooner N, Harvey HR, Pearce GES, Eckardt CB and MaxwellJR (1994b) Biological defunctionalisation of chlorophyll in the aquatic environment. 2. Action of endogenous algal enzymes and aerobic-bacteria. Org Geochem. 22: 773–780
Spooner N, Getliff JM, Teece MA, Parkes RJ, Leftley JW, Harris PG and Maxwell JR (1995) Formation of mesopyrophaeophorbide *a* during anaerobic bacterial-degradation of the marine prymnesiophyte *Emiliania-huxleyi* Org Geochem. 22: 225–229
Squier AH, Hodgson, DA and Keely BJ (2002) Sedimentary pigments as markers for environmental change in an Antarctic lake. Org Geochem 33: 1655–1665
Squier AH, Hodgson DA and Keely BJ (2003) Identification of novel sulfur-containing derivatives of chlorophyll *a* in a Recent sediment. Chem Commun: 624–625
Squier AH, Hodgson DA and Keely BJ (2004a) Structures and profiles of novel sulfur-linked chlorophyll derivatives in an Antarctic lake sediment. Org Geochem 35: 1309–1318
Squier AH, Hodgson DA and Keely BJ (2004b) Identification of bacteriophaeophytin *a* esterified with geranylgeraniol in an Antarctic lake sediment. Org Geochem 35: 203–207
Squier AH, Hodgson DA and Keely BJ (2004c) A critical assessment of the analysis and distributions of scytonemin and related UV-screening pigments in sediments. Org Geochem 35: 1221–1228
Squier AH Hodgson DA and Keely BJ (2005) Evidence of late Quaternary environmental change in a continental east Antarctic lake from lacustrine sedimentary pigment distributions. Ant Sci 17: 361–376
Talbot HM, Head RN, Harris RP and Maxwell JR (1999a) Distribution and stability of steryl chlorin esters in copepod faecal pellets from diatom grazing. Org Geochem 30: 1163–1174
Talbot HM, Head RN, Harris RP and Maxwell JR (1999b) Steryl esters of pyropheophorbide *b*: A sedimentary sink for chlorophyll *b*. Org Geochem 30: 1403–1410
Talbot HM, Head RN, Harris RP and Maxwell JR (2000) Discrimination against 4-methyl sterol uptake during steryl chlorin ester production by copepods. Org Geochem 31: 871–880
Treibs A (1934a) Über das vorkommen von chlorophyll-derivatenin einem Ölschiefer aus der oberen Trias. Liebigs Ann 509: 103–114
Treibs A (1934b) Chlorophyll- und häminderivate in bituminösen Gesteinen, Erdölen, Erdwachsen, und Asphalten. Liebigs Ann 510: 42–62
Treibs A (1936) Chlorophyll and hemin derivatives in organic materials. Angew Chemie Int Edition 49: 682–686
van Gemerden H (1983) Physiological ecology of purple and green bacteria. Ann Microbiol (Inst. Pasteur) 134: 73–92
Verne-Mismer J, Ocampo R, Callot HJ and Albrecht P (1987) Isolation of a series of vanadyl-tetrahydrobenzopetroporphyrins from Timhadit oil shale. Structure determination and total synthesis of the major constituents. J Chem Soc Chem Commun: 1581–1583
Verne-Mismer J, Ocampo R, Callot HJ and Albrecht P (1988) Molecular fossils of chlorophyll-*c* of the 17-nor-DPEP series-structure determination, synthesis, geochemical significance. Tetrahedron Lett 29: 371–374
Verne-Mismer J, Ocampo R, Callot HJ and Albrecht P (1990) New chlorophyll fossils from Moroccan oil shales — porphyrins derived from chlorophyll-c_3 or a related pigment. Tetrahedron Lett 31: 1751–1754
Verzegnassi L, Riffé-Chalard C, Kloeti W and Gülaçar FO (1999) Analysis of tetrapyrrolic pigments and derivatives in sediments by high performance liquid chromatography atmospheric pressure chemical ionization mass spectrometry. Fresenius J Anal Chem 364: 249–253
Vila X, Abella CA, Figueras JB and Hurley JP (1998) Vertical models of phototrophic bacterial distributions in the metalimnetic microbial communities of several freshwater North-American kettle lakes. FEMS Microbiol Ecol 25: 287–299
Villanueva J and Hastings DW (2000) A century-scale record of the preservation of chlorophyll and its transformation products in anoxic sediments. Geochim Cosmochim Acta 64: 2281–2294
Villanueva J, Grimalt JO, de Wit R, Keely BJ and Maxwell JR (1994a) Chlorophyll and carotenoid pigments in solar saltern microbial mats. Geochim Cosmochim Acta 58: 4703–4715
Villanueva J, Grimalt JO, de Wit R, Keely BJ and Maxwell JR (1994b) Sources and transformations of chlorophylls and carotenoids in a monomictic sulphate-rich karstic lake environment. Org Geochem 22: 739–757
Walker JS and Keely BJ (2004) Distribution and significance of chlorophyll derivatives and oxidation products during the spring phytoplankton bloom in the Celtic Sea April 2002. Org Geochem 35: 1289–1298
Walker JS, Squier AH, Hodgson DA and Keely BJ (2002) Origin and significance of 13^2-hydroxychlorophyll derivatives in sedi-

ments. Org Geochem 33: 1667–1674
Walker JS, Jie C and Keely BJ (2003) Identification of diastereomeric chlorophyll allomers by atmospheric pressure chemical ionisation liquid chromatography/tandem mass spectrometry. Rapid Commun Mass Spectrom 17: 1125–1131
Watanabe N, Yamamoto K, Ihshikawa H, Yagi A, Sakata K, Brinen LS and Clardy J (1993) New chlorophyll *a* related compounds isolated as antioxidants from marine bivalves. J Nat Prod Lloydia 56: 305–317
Willstätter R and Stoll A (1913) Untersuchungen über Chlorophyll. Methoden und Ergebnisse, pp 29–147. Julius Springer-Verlag, Berlin
Wilson MA, Md Saleh SR, Hodgson DA and Keely BJ (2003) Atmospheric pressure chemical ionisation liquid chromatography/multistage mass spectrometry of isobaric bacteriopheophorbide *d* methyl esters. Rapid Commun Mass Spectrom 17: 2455–2458
Wilson MA, Hodgson DA and Keely BJ (2004a) Structural variations in derivatives of the bacteriochlorophylls of Chlorobiaceae: Impact of stratigraphic resolution on depth profiles as revealed by methanolysis. Org Geochem 35: 1309–1318
Wilson MA, Airs RL, Atkinson JE and Keely BJ (2004b) Bacterioviridins: Novel sedimentary chlorins providing evidence for oxidative processes affecting palaeobacterial communities. Org Geochem, 35: 199–202
Wilson MA, Hodgson DA and Keely BJ (2005) Atmospheric pressure chemical ionisation-liquid chromatography/multistage mass spectrometry for assignment of sedimentary bacteriochlorophyll derivatives. Rapid Commun Mass Spectrom 36: 38–46
Wolff GA, Murray M, Maxwell JR, Hunter BK and Sanders JKM (1983) 15, 17-Butano-3,8-diethyl-2,7,12,18-tetrametylporphyrin — a novel naturally occurring tetrapyrrole. J Chem Soc Chem Commun: 922–924
Woolley PS, Moir AJ, Hester RE and Keely BJ (1998) A comparative study of the allomerization reaction of chlorophyll *a* and bacteriochlorophyll *a*. J Chem Soc Perkin Trans 2: 1833–1839
Wright SW, Jeffrey SW, Mantoura RFC, Llewellyn CA, Bjornland T, Repeta D and Welschmeyer N (1991) Improved HPLC method for the analysis of chlorophylls and carotenoids from marine-phytoplankton. Mar Ecol Prog Ser 77: 183–196
Yamamoto K, Sakata K, Watanabe N, Yagi A, Brinen LS and Clardy J (1992) Chlorophyllonic acid methyl ester, a new chlorophyll a related compound isolated as an antioxidant from short-necked clam, *Ruditapes philippinarum*. Tet Lett 33: 2587–2588
Zapata M, Rodriguez F and Garrido JL (2000) Separation of chlorophylls and carotenoids from marine phytoplankton: A new HPLC method using a reversed phase C-8 column and pyridine-containing mobile phases. Mar Ecol Prog Ser 195: 29–45

Index

B

C

D

E

F

G

H

I

J

K

L

M

N

O

P

Q

R

S

T

U

V

W

X

Y

Z

Advances in Photosynthesis and Respiration

Series editor: Govindjee, University of Illinois, Urbana, Illinois, U.S.A.

1. D.A. Bryant (ed.): *The Molecular Biology of Cyanobacteria.* 1994 ISBN Hb: 0-7923-3222-9; Pb: 0-7923-3273-3
2. R.E. Blankenship, M.T. Madigan and C.E. Bauer (eds.): *Anoxygenic Photosynthetic Bacteria.* 1995 ISBN Hb: 0-7923-3681-X; Pb: 0-7923-3682-8
3. J. Amesz and A.J. Hoff (eds.): *Biophysical Techniques in Photosynthesis*. 1996 ISBN 0-7923-3642-9
4. D.R. Ort and C.F. Yocum (eds.): *Oxygenic Photosynthesis: The Light Reactions.* 1996 ISBN Hb: 0-7923-3683-6; Pb: 0-7923-3684-4
5. N.R. Baker (ed.): *Photosynthesis and the Environment.* 1996 ISBN 0-7923-4316-6
6. P.-A. Siegenthaler and N. Murata (eds.): *Lipids in Photosynthesis: Structure, Function and Genetics.* 1998 ISBN 0-7923-5173-8
7. J.-D. Rochaix, M. Goldschmidt-Clermont and S. Merchant (eds.): *The Molecular Biology of Chloroplasts and Mitochondria in Chlamydomonas.* 1998 ISBN 0-7923-5174-6
8. H.A. Frank, A.J. Young, G. Britton and R.J. Cogdell (eds.): *The Photochemistry of Carotenoids.* 1999 ISBN 0-7923-5942-9
9. R.C. Leegood, T.D. Sharkey and S. von Caemmerer (eds.): *Photosynthesis: Physiology and Metabolism*. 2000 ISBN 0-7923-6143-1
10. B. Ke: *Photosynthesis: Photobiochemistry and Photobiophysics.* 2001 ISBN 0-7923-6334-5
11. E.-M. Aro and B. Andersson (eds.): *Regulation of Photosynthesis.* 2001 ISBN 0-7923-6332-9
12. C.H. Foyer and G. Noctor (eds.): *Photosynthetic Nitrogen Assimilation and Associated Carbon and Respiratory Metabolism.* 2002 ISBN 0-7923-6336-1
13. B.R. Green and W.W. Parson (eds.): *Light-Harvesting Antennas in Photosynthesis.* 2003 ISBN 0-7923-6335-3
14. A.W.D. Larkum, S.E. Douglas and J.A. Raven (eds.): *Photosynthesis in Algae*. 2003 ISBN 0-7923-6333-7
15. D. Zannoni (ed.): *Respiration in Archaea and Bacteria.* Diversity of Prokaryotic Electron Transport Carriers. 2004 ISBN 1-4020-2001-5
16. D. Zannoni (ed.): *Respiration in Archaea and Bacteria.* Diversity of Prokaryotic Respiratory Systems. 2004 ISBN 1-4020-2002-3
17. D. Day, A.H. Millar and J. Whelan (eds.): *Plant Mitochondria*. From Genome to Function. 2004 ISBN 1-4020-2399-5
18. H. Lambers and M. Ribas-Carbo (eds.): *Plant Respiration.* From Cell to Ecosystem. 2005 ISBN 1-4020-3588-8

Advances in Photosynthesis and Respiration

19. G. Papageorgiou and Govindjee (eds.): *Chlorophyll a Fluorescence*. A Signature of Photosynthesis. 2004 ISBN 1-4020-3217-X
20. Govindjee, J.T. Beatty, H. Gest and J.F. Allen (eds.): *Discoveries in Photosynthesis*. 2005 ISBN 1-4020-3323-0
21. B. Demmig-Adams, W.W. Adams III and A. Mattoo (eds.): *Photoprotection, Photoinhibition, Gene Regulation, and Environment*. 2005 ISBN 1-4020-3564-0
22. T.J. Wydrzynski and K. Satoh (eds.): *Photosystem II*. The Light-Driven Water: Plastoquinone Oxidoreductase. 2005 ISBN 1-4020-4249-3
23. R.R. Wise and J.K. Hoober (eds.): *The Structure and Function of Plastids*. 2006 ISBN 1-4020-4060-1
24. B. Grimm, R.J. Porra, W. Rüdiger and H. Scheer (eds.): *Chlorophylls and Bacteriochlorophylls.* Biochemistry, Biophysics, Functions and Applications. 2006 ISBN 1-4020-4515-8

For further information about the series and how to order please visit our Website
http://www.springer.com